Proceeding of the Seventeenth International Conference on Tailings and Mine Waste, 3-6 November 2013, Banff, Alberta, Canada

Tailings and Mine Waste ’13

Edited by

G. Ward Wilson
David C. Sego
Nicholas A. Beier
University of Alberta Geotechnical Center &
Oil Sands Tailing Research Facility (OSTRF)

University of Alberta Geotechnical Center Edmonton, Alberta, Canada

Copyright ©
All rights reserved. No part of this publication or the information contained herein may be reproduced, stored in a retrieval system of transmitted in any form or by any means, electronic, mechanical, by photocopying, recording or otherwise, without written prior permission from the publisher.

Although all care is taken to ensure the integrity and quality of this publication and the information herein, no responsibility is assumed by the publishers nor the author for any damage to property or persons as a result of operation or use of this publication and/or the information contained herein.

Published by: University of Alberta, Dept. of Civil & Environmental Engineering

ISBN: 978-1-55195-326-7

Printed in Canada

Forward

It is a pleasure and a privilege to host **Tailings and Mine Waste 2013** among the majestic Rocky Mountains in Banff, Alberta, and to mark the 17th conference of the series. Next year, the conference returns to Colorado, where it all began in 1978, originally as the "Uranium Mill Tailings Management Conference", thanks to visionaries like Dr. John Nelson of Colorado State University. Thirty-five years after the inaugural conference, Tailings and Mine Waste continues to provide a premium forum and meeting place for members of the mining community, researchers, engineers and scientists, regulatory groups and other interest groups concerned with environmental issues related to tailings and mine waste management. Presentations will cover an array of topics related to the engineering and management of tailings and mine waste, including case histories; the design, operation, and disposal for mine waste management; geotechnical considerations; mine waste/tailings modeling; liners, covers and barriers for waste control; acid mine drainage; reclamation and remediation of mine impacted sites; oil sands issues; surface water and groundwater management and geochemistry; and policies, procedures and public safety.

Special to this year's conference is an unprecedented industry presentation session by member companies of Canada's Oil Sands Innovation Alliance Tailings Environment Priority Area (COSIA Tailings EPA). As of 2011, over 850 million cubic meters of mature fine tailings are being stored in massive tailings ponds that are viewed nationally and internationally as an environmental blemish on the northern Alberta landscape as well as a significant environmental risk. This moderated panel presentation will provide the most recent developments in oil sands tailings and management, and how industry is responding to these major challenges.

We want to personally thank the Oil Sands Tailings Research Facility (OSTRF) and Dr. Norbert Morgenstern for their encouragement and support for the conference. The conference would not have been possible without the dedication of Nicholas Beier, Vivian Giang and especially Sally Petaske who provided so much assistance and leadership throughout the planning and execution of the conference.

A successful conference is only possible due to the presentations and the quality of the research presented in the manuscripts contained in the proceedings. The manuscripts become a lasting archival record and a snapshot of the state of knowledge in 2013. We want to thank our professional colleagues who willingly shared their experiences and insight with us. To all the authors, thank you for contributing your technical knowledge and for your efforts in submitting your manuscripts, especially in these extremely busy days when time is our most precious commodity. The proceedings contain information representing hundreds of years of collective experience. We know you will find insight and answers that will assist you in a better understanding of tailings and mine waste management.

David C. Sego & G. Ward Wilson
Co-Chairs, Tailings and Mine Waste 2013 Organizing Committee

ORGANIZATION

The Tailings and Mine Waste 2013 conference was organized by the Department of Civil and Environmental Engineering, University of Alberta, Edmonton, Alberta, Canada in conjunction with Colorado State University, Fort Collins, Colorado, and the University of British Columbia, Vancouver, British Columbia.

ORGANIZING COMMITTEE:

G. Ward Wilson (Co-Chair)	University of Alberta
David C. Sego (Co-Chair)	University of Alberta
Nicholas Beier	University of Alberta
Vivian Giang	University of Alberta
Sally Petaske	University of Alberta

SPONSORS:

A special thank you to ConeTec, BGC, DuPont, O'Kane Consultants Inc., WorleyParsons, COSIA, OSRIN, NorWest Corporation, MWH, and Robertson GeoConsultants Inc. for their invaluable sponsorship of the conference.

Thank you to the following sponsors for their support in making the17th International Conference on Tailings and Mine Waste a success:

























Table of Contents

Forward iii
Organization v
Sponsorship vii

KEYNOTE PRESENTATIONS

De-Licensing Oil Sands Tailings Dams – When Is A Dam No Longer A Dam? xvii
A. Küpper et. al.

Mine Waste Management @ RIME xxxi
M. Aubertin & B. Bussière

Oil Sands

ILTT and Thin Lift Dewatering

Dewatering And Shear Strength Performance Of In-Line Flocculated Mature Fine Tailings Under Different Depositional Schemes 5
A. Dummola, C. Côté, G. Freeman, D. Kolstad, J. Song & S. Masala

Mud Farming Of Fine Tailings - Application And Benefits Of Mudmaster® Technology 15
L.D. Munro & D. Smirk

The Role Of Desiccation And Rheology In Optimizing Operations For Polymer-Amended Fine Tailings Disposal 25
S. Soleimani, S. Mizani, P. Simms, W. Wilson , & A. Dunmola

Determination Of Geotechnical Properties Of In-Line Flocculated Fine Fluid Tailings For Oil Sands Reclamation 37
L. Kabwe, G.W. Wilson & R. Donahue

Properties and Behaviour

Influence Of Surface Cracking And Salinity On Evaporation In An Oil Sands Thickened Tailings 47
T. Innocent-Bernard, P. Simms, A. Sedgwick, H. Kaminsky & X. Yang

Chemistry And Geotechnical Properties Of Fluid Fine Tailings Treated By In-Situ Polymerization Of Silica 57
R.H. Moffett & J.L. Flatter

Properties Which Affect The Consolidation Behavior Of Mature Fine Tailings **69**
J.D. Scott, L.K. Kabwe, G.W. Wilson, A. Sorta , & S. Jeeravipoolvarn

Residual Bitumen And Flocculation: Do We Understand Its Effects? **91**
E. Santanach Carreras, N. Passade-Boupat, M. Bourrel, A. Sedgwick, X. Yang , & A. Junaid

Seepage Induced Consolidation Testing Of Mature Fine Tailings **101**
M. Estepho, D. van Zyl, D. Znidarčić *& A. Revington*

Stiffness And Deformation Characteristics Of The Compacted Lean Oil Sands Dykes **111**
K.W. SoeMoe, K.W. Blggar, G. Claypool & S. Martens

Geophysical Methods As An Aid To Planning, Monitoring, And Abandoning Tailings Facilities In The Alberta Oil Sands **123**
P. Bauman, D. Parker, B. Hansen & L. Pankratow

Chemical Amendments and Flocculation

Monitoring Of Agglomerating Mature Fine Tailings In Pipe Reactor Flow **127**
A. van der Spek & J. Viega

The Effects Of In-Line Static Mixer Flow Loop Operational Parameters On Flocculant Performance In Mature Fine Tailing Samples **137**
P.A. Gillis, J.S. Moore, M.K. Poindexter, C.A. Witham, W. Chen, H. Singh, C.E. Mohler & J. Atias

Understanding Dewatering Limits Of Polymer Flocculated Oil Sands Mature Fine Tailings **147**
T. Fenderson, S.G. Thakurta, A. Mahmoudkhani, P. Watson, K. Stewart & M. Nair

Modelling and Thickened Tailings

Evaluation Of Evaporation And Under-Drainage In Dewatering Oil Sands Tailings In Northern Alberta **157**
Q. Song & M. O'Kane

Observations Of Tailings Flow And Application Of The Mcphail Beach Profile Model To Oil Sands And Metal Mine Tailings **169**
L.E. Charlebois, G.I. McPhail, A. Revington & D. van Zyl

Predictive Model For Thick Lift Placement Of Silica-Treated Fluid Fine Tailings **181**
J.C. Sobkowicz, M. Pinheiro, T.W. Moore & R. Moffett

Tailings Treatment and Chemical Amendments

The Compatibility Of Geotextiles With Mature Fine Tailings **193**
M.J. Chappel & E. Blond

Mature Fine Tailings Treatment Using Inline Flocculation And Filtration **203**
C. Côté, K. Sibble, R. Heffel, K. Cafferata, A. Changara, W. Duttlinger & J. Knauer

Effect Of Coarse Solid Addition On The Dewatering Of Mature Fine Tailings **213**
S.G. Thakurta, T. Fenderson, A. Mahmoudkhani, K. Stewart & P. Watson

Waste Management

Improving Oil Sands Tailings Filterability By Reducing Capillary Forces In The Filtrated Cake Using Surfactants **225**
Y. Wu, K. Stewart, R. Tellakula, A. Mahmoudkhani, M. Nair, T. Fenderson & G. Subhayan

Experiences Relevant to ERCB Directive 074 **235**
H.K. Mittal & P.G. Landine

The Potential For Hydraulic Mining By Sluicing In The Oil Sands **245**
J. Boswell, R. Cooke & M. Kofoed

Oil Sands Process-Affected Water Inventory Management **255**
T. Hann & J. Lee

Cover System And Lysimeter Design To Demonstrate Site Specific Net Percolation Performance **263**
M. Phillip, G. Williams R. Shurniak & M. O'Kane

Tailings

Tailings Modelling

A Finite Strain Consolidation Model With Evaporation: Actual Evaporation And Unsaturation Correction Approach **277**
S. Jeeravipoolvarn, I. Gidley, T. Moore & D. Tran

The Development Of A Non-Newtonian Flow Model For Bounding The Beach Slope Angle Of High Density Tailings Stacks **287**
Y. Babaoglu & P. Simms

Modeling Strength Development And Distribution Within Hydrating Cemented Paste Backfill Structure **295**
M. Fall & O. Nasir

Modeling Soil-Fluid And Fluid-Soil Transitions With Applications To Tailings **305**
P.A. Vermeer, L. Sittoni, L. Beuth & Z. Wieckowski

Tailings

Designing Non-Segregating Tailings Pump And Pipeline Systems **319**
S. Bodtker & R. Cooke

Tailings Embankment Construction Material Alternative – Cyclone Sand Or Mined Rockfill **327**
J. FitzGerald, D. Friedman & K. Brouwer

Thickened Tailings Disposal System: Three Years Of Successful Operation **337**
J.P. Wu, L. Reshaw & Y. Che

Characterising Settling And Dewatering Of Slurries Of Commercial Clay-Rich Coal Tailings 347
D.J. Williams, T.M.A. Delport & M.S. Whitton

Geotechnical Fundamentals Of Uranium Tailings Management In Canada 357
H.K. Mittal & P.G. Landine

Dry Stack Tailings: Some Ideas 367
J.A. Caldwell & C.A. Crystal

Tailings Facilities

Field Deformations Compared To A Numerical Model For A Staged Centerline Raise – Cerro Corona Tailings Storage Facility, Peru 379
C. Krautmann, F. Torres, W. Vela Amoros, S. Abbaszadeh & J. Gutierrez

Liquefaction Assessments Of Tailings Facilities In Low-Seismic Areas 389
H. Rourke & C. Holmes

Factual And Foreseeable Reliability Of Tailings Dams And Nuclear Reactors: A Social Acceptability Perspective 399
F. Oboni & C. Oboni

Tailings Facility Failures In 2012 409
H. Rourke & C. Holmes

Dams

Dams and Liner Systems

State Of Practice Dynamic Analysis Of A Rock Fill Dam Subjected To High Seismic Earthquake Conditions 425
A.L. Dolezal, J.L. Castillo & A.J. Breitenbach

Seismic Deformation Analysis Of Cerro Corono Tailings Dams 435
Y. Babaoglu & P. Simms

Bituminous Geomembrane Failure At A Co-Disposal Tailings Storage Facility 447
P. Addis, B. Andruchow & I. Wislesky

Subaquatic Repairs Of A Hdpe Liner System By Using An Asphaltic Base Geosynthetic Material "El Valle-Boinas" Mine Asturias, Spain 457
P.A. Vermeer, L. Sittoni, L. Beuth & Z. Wieckowski

Mining

Mine Water Treatment

Coal Mine Effluents: Tackling The Selenium Issue **467**
L.R. Moore & J.R. Durand

Metal Chelation: Addressing The Concerns Of Nickel In Effluents **477**
L.A. Sanders, L.R. Moore, & J.R. Durand

Mine Water Treatment With Geotextile Tube System At Goldex Mine (Val d'Or, Qc, CANADA) **485**
J. Douhéret & A. Lister

Titanium Dioxide Mediated Removal Of Benzene-Like Compounds From Wastewater And Industrial Effluent **493**
S. Linley & F, Gu

Mine Waste Management

The Evolution Of Coal Mine Waste Management Practices In Western Canada **505**
F. Claridge, W. Fund & L. Martin

Treatment Options For Selenium Control In Mine-Site Runoff **515**
D.A. Jackson, A. Timmis & A. Bronsro

Water Quality Guidelines For Metals **525**
S. Dixit, T. El-Fityani & D. Spry

Development Of An Integrated Mine Waste Management Plan For The Mutates Gold-Silver Project, Durango And Sinaloa States, Mexico **533**
W.A. Cincilla, A. Breitenbach & J. Carrasco

Development Of A Mine Site-Wide Water Balance **543**
M. David, Z. Zurakowski & T. Alexieva

Mine Waste Modelling

Modelling Of Seepage Through Segregating Waste Rock **555**
M.D. Fredlund & R.C. Thode

Numerical Simulations Of Air Convection Cover For Mine Tailings Lupin Mine **569**
N.H. Pham & D.C. Sego

Model Analysis Of Differential Settlement For A Heap Leach Constructed On A Mine Waste Storage Facility **579**
S. Abbaszadeh, N. Haws, S. Taylor & C. Weber

Covers and Closure Planning

Distributed Temperature Observations Reveal The Scale Of Spatial Variability In Unsaturated Soil Covers **593**
L.K. Tallon, M. O'Kane, B.C. Si & S.L. Barbour

Case Study - Experimental Cells Complex In Permafrost **603**
J-F. St.-Laurent, Y. Jalbert, M. Paradis & A. Hébert

Toward Effective Closure Planning: From Progressive Reclamation To Sustainable Mining **615**
G. McKenna, R. An, E. Scordo & J. McGreevy

Regional Mine Closure Plans – The Next Improvement In Closure Planning **627**
J. McGreevy, G. McKenna, R. An & E. Scordo

Post-Closure Land Uses In The Athabasca Oil Sands Area **637**
K.N. Doran

Acid Mine Drainage

Co-Disposal of Coal/Biomass Fly Ash and Reactive Mine Tailings Under Neutral and Acidic Conditions **649**
K. Penney & E. Mohamedelhassan

Mobilization of Arsenic Under Reducing Conditions: A Case Study From The Delnite Mine Tailings Site **659**
D. Paktunc, . Thibault & B. Tisch

Keynote Presentations

De-licensing oil sands tailings dams – when is a dam no longer a dam?

A.G. Küpper, *BGC Engineering Inc. (formerly with AMEC)*, B. Hurndall, *BJH Engineering*, N. Morgenstern, *University of Alberta*, J. Sobkowicz, *Thurber Engineering Ltd.,* W. Abeda, *Canadian Natural Resources Ltd*., G. Baldwin, *Shell Canada Energy,* R. Cameron, *Syncrude Canada Ltd.*, N. Eenkooren, *Suncor Energy*, C. Grapel, *EBA, CDA Director for Alberta during part of this project*, S. Martens, *Shell Canada Energy (formerly with Klohn Crippen Berger)*, G. McKenna, *BGC Engineering Inc.*, Y. Mihiretu, *Alberta Energy Regulator*, W. Mimura, *Syncrude Canada Ltd.*, K. Parsons, *Alberta Energy Regulator*, S. Paz, *AESRD, CDA Director for Alberta*, T. Petersen, *Norwest Corp.*, A. Small, *AMEC, CDA Director for New Brunswick, CDA Mining Committee*, S. Tan, *Total E & P*, K. Wog, *Epcor (formerly with Alberta Environment), CDA Director for Alberta during part of this project*, S. Yazdanpanah, *Imperial Oil Resources*.

ABSTRACT: Some of the oil sands tailings dams, licensed under the Alberta dam safety regulations, have reached the end of their service life and under a responsible environmental stewardship should be closed and reclaimed. The path to closure and reclamation requires de-licensing of these structures, since dams require active intensive risk management programs. There is currently limited technical guidance on the requirements and on the process to de-license a tailings dam. This paper presents a de-licensing framework, based on a performance and risk-based approach, to take oil sands tailings dams to a stage such that they can be de-licensed as dams and considered as solid mine waste structures.

1 INTRODUCTION

1.1 *Background*

Oil sands open pit mines typically include large mining pits, tailings dams, overburden structures (mine waste dumps) and various industrial and operational plants. Once the use of these facilities is complete, the land will be reclaimed and ultimately returned to the Crown. Where practical, tailings facilities, mine waste dumps and mine pits may be closed and reclaimed progressively during operation to reduce the overall impact of the mining activities on the environment. Closure and final reclamation of oil sands mines and their associated tailings facilities are a commitment for operators, regulators, and stakeholders.

Oil sands tailings dams are licensed as dams by the Alberta Regulators. Oil sands dams are designed, built, monitored and operated under the precepts of Canadian Dam Association (CDA) Dam Safety Guidelines, as required by the Alberta Regulators. The Mining Association of Canada "Guide to the Management of Tailings Facilities" is also generally followed by the oil sands mine operators.

This regulatory environment includes intensive surveillance, monitoring, analyses, maintenance and extensive reporting. It is a standard risk management approach that is adopted worldwide for dams. Such a level of management, while essential and commendable for dams, is not compatible with the objectives of closure and reclamation. As the oil sands industry moves towards closure and reclamation of tailings ponds, it is necessary to develop a process by which tailings dams can be decommissioned, closed and de-licensed for final reclamation and certification.

The path to closure and reclamation of tailings facilities requires de-licensing of the dams. To be de-licensed, these dams need to be converted to structures that are no longer considered to be dams and that have acceptable risk levels in the absence of active intensive risk management programs. There is currently limited guidance in the literature and in the regulations, in Alberta and elsewhere, on the requirements and on the process to de-license a tailings dam.

This paper presents a process to take oil sands tailings dams to a stage such that they can be de-licensed as dams and considered solid mine waste structures. The de-licensing framework presented herein is founded on a performance and risk-based approach and outlines a process of identifying and implementing measures that would be required for a given oil sands tailings dam to transition to the status of a solid mine waste structure.

1.2 *Approach*

A working group ("Oil Sands Tailings Dam Committee") was formed in 2009 to outline a process whereby tailings dams could be transitioned to solid mine waste structures (or "waste dumps") and de-licensed as dams. The particular focus of the committee was to define the conditions that must be satisfied for a tailings dam to be no longer considered a dam.

The Oil Sands Tailings Dam Committee, whose members are the authors of this paper, was formed as a collaborative initiative among all Alberta regulatory agencies that have jurisdiction over oil sands tailings dams, all of the oil sands operating companies with active and/or planned tailings facilities, and the engineering design consultants primarily involved in oil sands tailings dam design. The committee representatives were senior professionals with experience in oil sands, and tailings dams in particular. The full report produced by the Oil Sands Tailings Dam Committee can be found at the Oil Sands Research and Information Network (OSRIN) site (http://www.osrin.ualberta.ca).

This work focuses on the structural aspects of the facility – geotechnical and hydrotechnical stability – for the final stages of its life cycle. Discussion of the environmental aspects is outside the scope of this document but remains a consideration when closing tailings dams.

The technical and risk management approach in this work is intended for the oil sands tailings dams of Alberta, but it contains elements that may be applicable to other jurisdictions and types of tailings dams with due consideration of their specific situation and special conditions. The collaborative approach adopted here by owners, regulators and consultants is also applicable to other places and industries.

2 LIFE CYCLE STAGES OF A TAILINGS FACILITY AND ADOPTED TERMINOLOGY

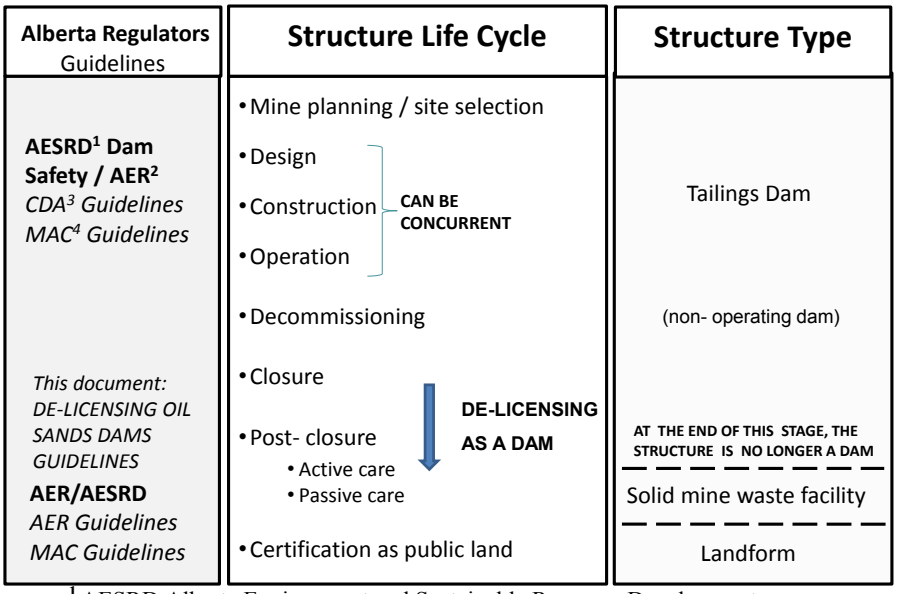
2.1 *Life cycle stages*

The life cycle stages of an oil sands tailings facility are summarized in Figure 1. This figure also indicates the type of structure for the various life cycle stages and the Alberta Regulators for each of the stages.

2.2 *Terminology*

Key elements of the terminology adopted to describe the various stages of the life cycle of an oil sands tailings facility are:

Operation - An operating (active) tailings dam receives liquids and/or tailings, and typically has water reclaiming facilities. It may still be under construction and not yet to final design height. An operating/active tailings dam requires active surveillance and monitoring and regular reporting of its structural and operational condition, including submission of yearly performance reports and scheduled independent dam safety reviews to the Regulator. After the impoundment final capacity is achieved, the dam can continue in operation as a settling basin and/or a recycle water reservoir, or it can be decommissioned from operation. In either case, the structure remains a dam, and thus continues to require regular reporting of its structural and operational condition to the Regulator.



[1] AESRD Alberta Environment and Sustainable Resource Development
[2] AER Alberta Energy Regulator
[3] CDA Canadian Dam Association
[4] MAC Mining Association of Canada
[5] AESRD not including Dam Safety Branch

Figure 1. Life Cycle of an Oil Sands Tailings Facility

Decommissioning - A tailings dam is considered a non-operating (inactive) or decommissioned dam when it is no longer receiving tailings or fluids other than natural precipitation and run-off. It may still have water reclaiming facilities to control its water level, and continues to require active surveillance and monitoring and regular reporting to the Regulator.

Closure - A non-operating dam that is to be reclaimed would go through a transitional stage when various measures are implemented to convert the tailings dam into a solid mine waste structure ("waste dump"). These measures may include removal of the impounded fluid, removal of soft and/or mobile tailings, removal of operational structures, breach of the containment structure, construction of outlet channels, and other risk mitigation measures. The closure period eventually involves reclamation of the facility such that it qualifies as a landform ready to receive a Reclamation Certificate.

De-licensing process - When sufficient measures have been implemented to meet the de-licensing criteria, the former tailings dam would become a solid mine waste structure that would qualify to be de-licensed as a dam. During the de-licensing process, a tailings facility transitions from a licensed dam to a de-licensed structure. During this process, it is necessary to demonstrate that the transition of a tailings dam into a solid mine waste facility has achieved its objectives, that the resulting facility no longer meets the definition of a dam and now poses only residual risks that are compatible with the risk level of the natural surrounding environment and hence it would qualify for a formal process of being de-licensed as a dam. Monitoring of the structure for some period may be required to help demonstrate that the structure now meets all the requirements for de-licensing. When the facility is de-licensed as a dam, regular reporting of the facility's structural and operational condition to the Dam Safety Regulator is no longer required. These facilities would then be regulated as a solid mine waste structure and not as a dam. After the structures go through final reclamation, they constitute landforms.

Post-closure – During the post-closure stage the solid mine waste facility is monitored by the mining operator. This stage would include two periods:

- Active Care: the period when monitoring and possibly minor active intervention is required to achieve a final sustainable stable form. De-licensing of the dam would occur during this period, as active care of the solid mine waste structure may still be required for a period.

- Passive Care: the period following active care, during which the performance of the solid mine waste facility is monitored to ensure its compliance with the closure objectives. This period has no time limit but can be defined as being necessary until the solid mine waste structure is considered to be physically, chemically, and ecologically stable, having a performance, and a residual risk level that are acceptable.

Certification of the landform as public land (relinquishment) - When the landforms that have been created during the closure process meet all provincial and federal closure and reclamation criteria, a Reclamation Certificate is issued by the Regulators. At this point, the landform is no longer under the jurisdiction of the mine ownership and it is transferred to the Crown.

2.3 *Modified definition of dam*

A dam is defined in the Alberta Water Act, Water (Ministerial) Regulation, Part 6, and in the 2007 Canadian Dam Association (CDA) Dam Safety Guidelines, as a barrier constructed for the retention of water, water containing any other substance, fluid waste, or tailings, that is capable of impounding at least 30,000 m^3 of fluid and is at least 2.5 m high. In the context of earth dams, the barrier may be constructed either by placing fill or by excavating native ground such that a pillar of in situ material is formed. CDA (2007) proposes that this definition be expanded to include smaller dams if the consequences of dam operation or failure are considered to be unacceptable. Fundamentally, the formal definition of a dam accounts for consequence of failure. The height of the barrier and the volume of fluid impounded are directly related to the potential consequence of failure.

Following the same fundamentals, the width of the structure could also be taken into account in the definition of a dam. It is possible to envisage a situation where the width of the barrier retaining fluid is so large that the barrier does not constitute a dam. Therefore, similar to CDA (2007) expanding the definition of a dam to include smaller dams if the consequences of failure are likely to be unacceptable, this paper proposes a limitation of the definition of a dam to exclude cases where the width of the barrier is so large that the residual risks associated with the barrier are negligible and a potential breach of the barrier, exposing contents, is not practically possible now or in the long term. This proposed limitation of the definition of a dam respects the fundamental principle of the current formal definition in its consideration of the potential consequences of failure.

3 DAM DE-LICENSING FRAMEWORK

3.1 *De-licensing objectives*

The objectives for the transformation of an inactive oil sands tailings dam into a solid mine waste facility that qualifies for de-licensing as a dam, are:

1. The structure should be modified in a manner that:
   a. it no longer meets the definition of a dam; and
   b. the probability of the facility ever reverting to a configuration that meets the definition of a dam is extremely low.
2. The resulting structure is considered to have a physical performance that, as a minimum, can be managed as a solid mine waste structure (waste dump) but that ideally is acceptable for eventual Reclamation Certification.

It is noted that the natural areas in the oil sands region, as in all other areas of the planet, undergo a geomorphic process of landscape evolution. As part of this natural process, slope instabilities, surface erosion, wave and river erosion, groundwater level fluctuation, fires, etc. are common in the region. It is also noted that the objectives listed above focus on the physical requirements to be met for a structure to qualify for de-licensing as a dam. Environmental and other requirements also need to be met so that a solid mine waste structure eventually qualifies for a Reclamation Certificate, but that topic is not considered in this paper.

3.2 *Acceptable risk*

Risk is defined as the probability of failure multiplied by the consequence of failure. It is the expectation of society that all dams pose acceptably low risk to people, the environment, and to cultural and economic values. During operations, the performance of each dam is monitored (to a degree consistent with the consequence-of-failure classification of the dam), and remedial measures are invoked as needed in order to maintain an acceptably low risk of failure. This applies to both operating and decommissioned dams, since they still maintain a dam status.

When the dam is converted to a solid mine waste facility for de-licensing as a dam, the risk is further mitigated by reducing both the consequences and the probability of failure. The closure measures designed and implemented to convert the dam into a solid mine waste facility need to reduce the risk such that eventually the facility has a level of risk that is compatible with the level of risk of the natural surrounding environment.

3.3 *Potential scenarios*

The current configuration of oil sands tailings dams and the various closure landscapes being considered by the oil sands industry could lead to the following scenarios relative to the de-licensing of oil sands dams:

Scenario 1 – No significant surface water or fluids in the solid mine waste structure

This scenario occurs when all water, fluid tailings and potentially mobile solids are removed from the former tailings dam, which then transitions basically to a typical mine waste dump. In this case, the final configuration of the solid mine waste structure would be such that there will be no future accumulation of water in the structure. This scenario could be developed, for example, by removing all fluids and potentially mobile solids and by completely infilling a tailings dam with solid waste to achieve a domed shape that will shed water even if some settlement occurs in the future. Scenario 1 would pose the least challenge for de-licensing the structure as a dam.

Scenario 2 - Minor surface water in the solid mine waste structure

In this case, the solid mine waste structure may have a small pond on the surface, designed as part of the closure landscape, to provide wildlife habitat and runoff controls. Such a pond would mimic naturally occurring water bodies in the region, and would be designed with measures to prevent excessive water accumulation. The pond would be set so that either its volume is less than the minimum volume in the definition of a dam, or its location is sufficiently far from an area of lower topography that the intervening material does not practically constitute a dam. An example of this scenario would be “ring dyke” tailings dam, common in the oil sands area, that has all fluid and most soft tailings removed and is breached at one location where an outlet is implemented. The original, typically massive, dam structure would still be there but it would not impound any significant amount of fluid in the present or the future, although a minor pond or wetlands area might be formed in its interior. An outlet channel that is sustainable in the long term is a critical element of this scenario.

Scenario 3 - Significant surface water or mobile solids in end-pit containment

Some closure landscapes of mined-out pits are envisioned where larger water bodies or deposits of potentially mobile solids are contained by barriers of constructed and/or in-situ materials. If the width of these barriers is sufficiently large that there is negligible risk of release, for all reasonably foreseeable present and future sets of circumstances that may act to modify the barrier, without the need for any ongoing intervention to maintain the barrier, that barrier would not be deemed to be a dam as per Section 2.3. The barrier dimensions needed to achieve these conditions would vary based on the nature of the contained materials, the properties of the barrier, and the potential external conditions that may affect it. Current in-pit dams may need to be modified to achieve the required conditions to qualify for de-licensing. It would be up to the Operator applying to de-license the structure as a dam to demonstrate that a suitably low level of residual risk is achieved by the structure to be de-licensed, using the risk based approach outlined in this document. An example of this scenario would be the end pit lakes that are being considered in some closure plans. A guide document to planning and design of end pit lakes was published by the Cumulative Environmental Management Association (CEMA) in 2012.

3.4 *Approach for de-licensing a dam*

The proposed approach for the de-licensing of an oil sands tailings dam is summarized in Figure 2. It involves decommissioning a facility, designing and implementing measures to modify the structure to meet the requirements for de-licensing and conducting a risk assessment to determine whether the resulting structure will meet or has, in fact, met all the requirements. If not, additional measures would be identified, designed and implemented until the de-licensing objectives are fulfilled. Typically a period of monitoring would be required to demonstrate the acceptable performance (and the residual risk level) of the modified structure. When this situation is achieved, the structure could be de-licensed.

The proposed approach for the de-licensing of an oil sands tailings dam involves the following specific steps:

1. Cease operation and decommission the tailings dam into a non-operating (inactive) facility.
2. Propose measures to modify the structure so that it meets the objectives in Section 3.2. The actual measures required will vary by structure and should be considered and assessed using a Failure Modes and Effects Analysis (FMEA) or similar approach.
3. Conduct a risk assessment to determine whether the proposed measures would lead to a residual risk that is compatible with the risks of the natural areas in the region for all reasonably foreseeable circumstances, including extreme weather events, seismic events, slope instability, channel or outlet instability, and erosion. If the residual risk is not acceptable, identify additional measures that are required to further reduce the risk. Re-run the risk assessment until the proposed measures result in an acceptable risk level.
4. Implement these measures and monitor the performance of the modified structure during implementation and then over a sufficiently long period to confirm that the performance target was achieved and the risk level is acceptable. The structure eventually should have a performance compatible with the performance of the natural areas in the region for all reasonably foreseeable circumstances.
5. When it can be demonstrated that the modified structure meets the de-licensing objectives, apply to the Regulators to de-license the structure as a dam.

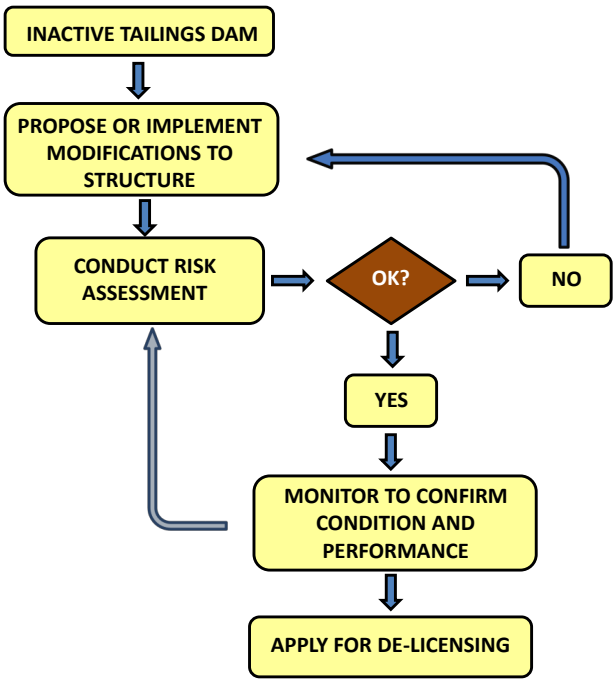


Figure 2. Summary of Proposed Approach for De-Licensing

The process for de-licensing a tailings facility, i.e., Steps 2 to 5 above, is described and discussed in below. Section 4 describes the risk assessment in the context of the de-licensing process. For de-licensing, the risk assessment is conducted to: a) demonstrate that the modified structure design will achieve or is achieving the requirements for de-licensing, , or to b) identify further modifications required to achieve this status at any time during design or implementation.

During the risk assessment, the design analyses should be updated to reflect the as-constructed conditions and projected to future conditions that may occur. The past performance history of the operating structure should be taken into account when assessing the expected future performance of the modified structure.

4 RISK ASSESSMENT FOR DE-LICENSING

4.1 *Introduction*

It is common in modern practice in the dam industry to incorporate risk-based approaches for design, operations and regulation. Extending the practice to dam de-licensing (and later closure and reclamation) is a logical step, and it is the approach adopted in this document. A risk-based approach in this context is a systematic assessment to identify the sources of risk and the magnitude of the risk within the system. The risk assessment should be undertaken by qualified and experienced professionals.

The risk-based approach for de-licensing of the structure follows the steps described in Section 3.4 and summarized in Figure 2. It includes the following components:

- *Hazard Identification and analyses.* During this stage the potential hazards and conditions that could lead to inadequate performance relative to dam safety or failure are identified along with their contributions to vulnerabilities of the system and the potential risks. All potential failure modes associated with these hazards are identified and analyzed.
- *Risk Reduction.* The structure is modified so that the incremental residual risk associated with its structural safety is negligible. During the early post-closure stage, it is assumed that some level of monitoring will be in place and maintenance would be done, if and as required. For the later post-closure and the reclamation certification stages, the incremental residual risk needs to be negligible with no maintenance.
- *Risk Assessment.* This component is used as a check that the proposed closure design for the facility will or has already transitioned into a structure that meets the requirements for de-licensing. If the risk assessment shows that the residual risk is still unacceptably high for de-licensing, additional risk reduction measures are identified / implemented and the process is repeated.
- *Risk Communication*. There needs to be communication among all stakeholders involved in the process of de-licensing a dam (owners, operators, regulators, public, and others, as applicable) relative to the residual risks associated with the structure. This includes clear statements of the values and philosophy of the Operator and the Regulators and clear description of nature of the risks and the magnitude of their potential consequences.

It is important to take into account some of the unique characteristics of the oil sands tailings structures when assessing their potential failure modes and the associated risks of the de-licensed structures. The flat slopes required due to weak foundation materials, combined with the large production of the oil sands mines and the use of large mining equipment for construction, lead to the massive size of most oil sands tailings dams. Several dams in the oil sands region are more than 100 m high, with the majority of them being higher than 50 m. Crest widths are typically 30 to 50 m, but can be up to several hundred metres including the beaches that are used for some dam types. Crest lengths range from several hundred metres to more than ten kilometres for some external tailings facilities. Base widths of these dams often approach or exceed 1000 m.

The relatively flat to undulating topography of the Athabasca oil sands area results in the tailings facilities either having a relatively small contributing watershed or being a ring dyke, where the watershed is only the facility itself. This fact, combined with the relatively dry climate of

the area, is also a significant aspect when considering the risks associated with the various life cycle stages of the facility.

4.2 *Hazard Identification and Potential Failure Modes*

The external and internal hazards and the potential failure modes for tailings dams and for solid mine waste structures are well understood as are methods for assessing risk for particular structures and for developing measures to reduce this risk. Most of the hazards and many of the failure modes used for dams also have direct application in assessing the failure risk for oil sands tailings structures being de-licensed.

Potential failure modes can be analysed using a Failure Modes and Effects Analysis (FMEA). FMEA is a method of identifying and analyzing the component failures and their associated consequences. For a tailings facility or a solid mine waste structure, a FMEA would incorporate a review of the system to identify the mechanisms through which the structure, its foundation, and any appurtenances could potentially fail under imposed loads or other external influences. For each structure, the process is site-specific, and relies on site data, design and construction aspects and information regarding the past behaviour of the structure, and it is calibrated by an understanding of the behaviour of similar structures.

Examples of failure modes to be included in de-licensing risk assessments are listed below. However, the Operators and the engineer-of-record are responsible for determining all the failure modes that may be specific to each structure. Failure modes could include: external or internal slope failure, failure of the drainage outlet leading to an increase in ponded water on the structure, consolidation of contents leading to settlement and a deeper existing pond or creation of a new pond, liquefaction failure, excessive erosion, outlet hydraulic instability, surface water erosion of slopes, slope failures blocking the outlet, and overtopping. All elements and conditions that could contribute to risk and vulnerabilities of the system need to be considered in the risk analysis.

4.3 *Risk Control/Reduction*

Risk reduction measures required for a structure to qualify for potential de-licensing as a dam vary for each structure and for the type of scenario (Section 3.3) that is the goal for that structure. A key risk reduction measure in the transition of a tailings dam to a solid mine waste structure is fluid removal and the related issue of creating a stable outlet that performs well during the life of the structure. Additional measures may be required to prevent significant future accumulation of water in the facility, so it does not revert to a fluid impoundment structure in the long term. Other risk reduction measures might be required to achieve a final structure that is sufficiently robust to meet the de-licensing objectives under all reasonable potential conditions that could occur during the life of the facility. Risk reduction measures can be incorporated during initial construction, during operation or in preparation for de-licensing.

The risk reduction measures to be taken in the process of converting a tailings dam into a solid mine waste structure vary from case to case depending on the specific details of each structure. Examples of some of the measures requiring consideration for the facilities include:

- *Remove fluids and soft tailings.* Most or all of the water and fluid fine tailings would generally be removed from the facility. A small pond may be allowed to form in the interior area provided its size is small compared to the overall area, it is located at a significant distance from the former containment structures and its depth is small compared to the vertical distance between the pond surface elevation and the elevation of the former containment structures. This small pond would have benefits relative to providing wildlife habitat and some attenuation of flows to the outlet facility.
- *Address potentially liquefiable or mobile solids.* Deposits that are assessed as being potentially liquefiable or mobile may be removed, treated (densification, consolidation, etc.) or kept at a location and to such a quantity that there is a negligible likelihood of this material ever leaving the facility or having any significant consequence in case of liquefaction or other type of event being triggered.
- *Breach the containment structure.* The containment structure would be breached so that it does not impound any significant amount of fluid even under the Probable Maximum

Flood (PMF) in the area. A breach section with more than one low spot, or more than one breach section may be considered in case one of the outlets becomes blocked by slope instability or beaver activity.

- *Build an outlet facility.* Design and build a very robust outlet system that is capable of conveying specified design events leading up to the PMF that are commensurate with the consequences of the failure. Oil sands tailings dams are generally designed to have no outlets or spillways during their operational/active period; excess water is usually pumped back to the plant site for re-use. Following decommissioning, a drainage outlet would be designed and implemented to prevent excessive accumulation of ponded water from precipitation and runoff from adjacent slopes. The geotechnical and hydraulic stability of the outlet facility is critical to a successful landform design. Geotechnical instability of slopes in the area of the outlet could lead to blockage of the outlet and impoundment of water in the former tailings area. Erosion of the outlet channel floor could be a significant risk if it leads to potential excessive erosion and deposition, outburst flooding, flow-slide of tailings deposits or instability of slopes due to down-cutting of the toe. The outlet generally should be founded on robust materials. The outlet channel should have a modest gradient and be geomorphologically stable. The outlet location and elevation should be selected prior to the start of re-shaping the area.
- *Re-shape area to promote drainage towards an outlet.* The configuration of the area should be designed to limit the potential for ponding water within prescribed distances from the landform crest. Re-shaping of the area can be done by excavating and/or by placing materials such as overburden or tailings beaches. Creation of a deep drainage valley system within the internal area using caps, hummocks, deep ditching and/or overall wedge sloping designs helps reduce the risk of excessive water ponding in the facility.
- *Address potential settlement.* Large areas that could potentially settle need to be densified, shaped, built up or otherwise designed into the drainage scheme to avoid significant settlements that could lead to excessively deep or large ponding of water on the facility.
- *Address slope stability issues.* Slopes should be designed for long-term geotechnical stability under all potential static and dynamic conditions such that their stability is compatible with the stability of natural analogues. Stability of slopes should not rely on a functional internal drainage system in the long term. The design seismic ground motions should have an Annual Exceedance Probability (AEP) that is in alignment with the magnitude, probability and consequence of the event. Deformation and stability under the relevant seismic loading should be evaluated using state of practice methods. Some deformation under extreme seismic loading is acceptable provided its effects do not lead to unacceptable consequences. Possible slope movements under static or dynamic conditions should be similar to those in natural slopes and should not result in significant progressive degradation of the overall structure integrity. The structure should perform acceptably without requiring maintenance or monitoring.
- *Address erosion issues.* Many of the active dams in the oil sands region experience some level of slope erosion due to overland flow of precipitation, snowmelt, and in some cases exiting seepage waters, leading to the formation of rills and to gully erosion. Such slope erosion is particularly acute where runoff water accumulates on benches, or is concentrated by ramps. Many of the materials used in dam construction and reclamation are highly erodible, especially tailings sand. Uncontrolled seepage can be particularly damaging to slopes, as salty tailings seepage water may degrade the vegetation designed to provide erosion protection. Slope erosion can lead to over-steepening of slopes, disruption of surface water drainage courses, sedimentation in ditches, creeks, and rivers at the toe of the slope, loss of soil and vegetative cover, and poor aesthetics. The potential risk that headward cutting of a large erosion gully could intersect potentially mobile materials behind the landform crest, leading to potential flow-slides, or a new unprotected outlet, needs to be addressed. Slope erosion risk reduction measures, if required, could include minimizing overland flow paths, limiting sub-watershed catchment sizes, capping slopes with reclamation material and dense vegetation, controlling phreatic surfaces to avoid spring sapping and soil salinization, creating large ‘bunds’ so that water cannot pond and exit plateaus over the slope, and armouring key areas. Particular attention should be placed on

erosion of slope toes as many of the existing active oil sands tailings dams have seepage control ditches at the toe and some active dams are adjacent to natural creeks or rivers.

- *Address future groundwater conditions.* Seepage assessments should be conducted for the design of the solid mine waste structure to determine that, under all potential seepage conditions, no future slope failure or mass movement could result that leads to unacceptable residual risks. Potential seepage conditions may include those resulting from degradation of internal seepage control systems (pipes and/or granular filters) that were included in the original dam structure, occurrence of Probable Maximum Precipitation (PMP) and PMF inflow conditions, and surface erosion. Seepage gradients must be sufficiently low under the worst reasonably foreseeable conditions to maintain an appropriately low residual risk level. Assessment of the seepage gradients should consider the potential for non-uniform materials and variable permeability along the flow path, even in material zones that were designed to be homogeneous. Future groundwater conditions may be improved by altering the facility content properties in place by using a combination of capping and drainage, densification, aggressive sloping of overall relief, allowing time for consolidation, internal dewatering, or other measures.

As mentioned earlier, the list of risk reduction measures above is an example only. Each facility will require specific risk mitigation measures that are appropriate for the particular situation of that facility and the proposed design for its de-licensing as a dam (discussed below).

4.4 *Risk assessment*

Risk assessments would be conducted at various stages, including (i) to evaluate proposed risk reduction measures to determine whether they would be sufficient to meet the de-licensing objectives; and (ii) to evaluate implemented measures in view of monitoring data to confirm they have met their objectives. The key purpose of the risk assessment is to confirm that the ongoing residual risks related to the solid mine waste structure are acceptable to the Regulators and to society. The objective is to eliminate the need for human intervention to maintain residual risk levels that are compatible with the risk levels in natural areas.

After risk reduction measures are implemented, the probability of a serious or catastrophic failure of a de-licensed structure should gradually become close to the probability of similar events in natural analogues. For example, slope instabilities occur naturally in the oil sands region due to the presence of various weak glaciated materials in the natural terrain, therefore slope failures of similar magnitude, frequenccy and consequence would be acceptable in the final landform created from a reclaimed tailings facility. The size of the affected area is used to describe the failure consequence, as it is a primary consideration.

The risk assessment process would start by determining all potential failure modes and submodes and their possible consequences by utilizing a Failure Mode and Effects Analyses (FMEA) or a similar technique. Assessment of the probability of each failure mode under various triggering events and appropriate risk categories must be determined using qualitative or semi-quantitative methods, using sound engineering principles and judgments, and signed off by recognized Geotechnical Engineering experts.

The level of residual risk achieved for the facility being de-licensed is assessed using a risk matrix that is described in detail in the next section. Should a facility not meet an acceptable residual risk category, additional risk reduction strategies should be considered and implemented to further reduce the consequence and/or probability of failure, until an acceptable risk category is achieved.

The process expanded in the next section examines the risks and provides a rational way of comparing those to proposed benchmarks. The tables in the next section establish limits on acceptable end conditions (as discussed in Section 3.3) for the structure to be de-licensed. The risk assessment carried out in this process determines whether the residual risk is significant enough to warrant additional risk control measures being implemented. It combines the analysis of a risk with the benchmark against which the risk is compared, to facilitate decision-making regarding future actions.

4.4.1 *Risk Category Determination*

The fundamental metrics of the risk assessment are given in Table 1. This table allows determination of the final risk category achieved for each failure mode, for each relevant cross-section or for the overall disposal area, and then its eligibility for de-licensing from a dam to a solid mine waste structure and eventually to a final landform. The risk category chart is shown on Table 1d. An example of the use of the risk categories shown in Table 1 and the overall risk assessment process is described in the next section.

4.4.2 *Risk Assessment Process*

Each landform component failure mode is tested using the risk matrix, to determine the final risk category and to document it. In case modifications are required, this process is used to support the need for these modifications. The recommended process of assigning a final risk category to a given failure mode is:

- Evaluate all potential failure events, with input from additional technical studies when required. Include failure size when applicable. The risk for different sizes of potential failures may need to be individually assessed, since small failures may have higher probabilities of occurring but will not lead to significant consequences, whereas larger failures may have much lower probability but have much more severe consequences. It is necessary to determine which combination of consequence and probability poses the highest risk. Consider cumulative failure mode effects.
- Determine the Consequence Event Rating for each failure mode or sub-mode using Table 1a. There are five consequence levels, which in decreasing order are: Very Serious, Serious, Minor, Limited, and Natural Analogue. The elements that determine the consequence are: loss of function of the structure, degree of human intervention required on the structure after an event occurs, population at risk and environmental impacts. These are similar to the CDA (2007) categories for consequence classification of active dams. One noticeable modification from the conventional categories is the element of human intervention. As these structures are future closure landforms, the intent is to reach a state of minimal or no human intervention in response to the consequences of various events.
- Determine the Probability of Occurrence of the event using Table 1b. This table has four probability categories:
  - i) Low (10% probability event could happen in 10 years),
  - ii) Unlikely (10% probability event will happen in 100 years),
  - iii) Remote/Highly Unlikely (10% probability event will happen in 1000 years), and
  - iv) Extremely Unlikely (1% probability the event will happen in 1000 years).
- The probability rating of each potential is to be evaluated by qualified engineers with input from additional technical studies, when required.
- Use the Consequence Event Rating and Probability from the previous two steps to look up the Risk Category in Table 1c (Probability and Consequence). The categories of risk in Table 1d are (listed from highest to lowest risk): Not Acceptable, Requires Further Review, and Acceptable. Record the results to document the evaluation.
- Repeat for all possible failure modes and combination of possible failure modes for all applicable cross-sections and for the overall tailings facility area (as applicable).
- The highest Risk Category determined governs, i.e., the worst ranking from any single event or combination of events, determines the overall ranking for the structure.
- The risk assessment process is complete when all potential failure modes and failure sizes, all relevant cross-sections and all overall disposal area considerations that could lead to unacceptable performance have been properly categorized, documented and pass through the risk category in Table 1d and are found to be "Acceptable".
- If a ranking from Table 1c falls in the Not Acceptable risk category, then further risk mitigation work is required on the structure. In essence, the structure would still be considered as a licensed dam based on its risk classification.
- If the ranking falls in the 'Requires Further Review' risk category, the dam may be deemed acceptable for de-licensing in principle, pending further review on a case-by-case basis by regulators applying site-specific regulatory evaluation.

- If the ranking falls in the 'Acceptable' risk category, adequate risk reduction measures have been employed, and the structure is considered a suitable candidate to be submitted to the regulatory agencies for consideration for de-licensing as a dam.
- All relevant information should be documented in a clear format for review internally and by regulatory agencies.

4.5 *Risk Communication*

The concept that the on-going residual risks associated with the closed solid mine waste structure are compatible to the risk level of natural landforms in the region is central to the closure strategy. This principle and the residual risks for each facility should be communicated to all stakeholders to establish clear and reasonable expectations for the long-term performance of de-licensed structures. The framework proposed in this document can facilitate comparisons of the close mine waste structures to other, similar structures, facilities and acceptable societal risks.

5 CONCLUSION

The performance and risk-based framework presented above provides technical guidance to owners and engineers to transform an oil sands tailings dam into a structure that could be de-licensed as a dam and managed as a solid mine waste facility. It provides a technical basis for the evaluation of the-licensing applications by the government Regulators who have authority over the approval process.

6 REFERENCES

AESRD 1998. Water Act, Water (Ministerial) Regulation, Part 6 Dam and Canal Safety. Alberta Environment and Sustainable Resource Development, Queen's Printer, Edmonton.

CDA 2007. Dam Safety Guidelines. Canadian Dam Association, Ottawa.

CEMA 2012. End Pit Lake Guidance Document, Cumulative Environmental Management Association, Fort McMurray, Alberta.

Oil Sands Tailings Dam Committee (2013). De-Licensing of Oil Sands Tailings Dams. Oil Sands Research and Information Network (OSRIN) (http://www.osrin.ualberta.ca).

Mining Association of Canada 2011. A Guide to the Management of Tailings Facilities, Second Edition. Mining Association of Canada, Ottawa.

Table 1 – Risk Assessment

Table 1a - Consequence Event

CONSEQUENCE EVENT RATING	DESCRIPTION OF EVENT		CONSEQUENCE OF EVENT	
	LOSS OF FUNCTION**	HUMAN INTERVENTION	POPULATION AT RISK (PAR)*	ENVIRONMENTAL ECONOMICS
Very Serious	Significant	Impracticable structure repair	Permanent within Area of Influence	Loss of contents beyond the original structure footprint is > 1km x 1km Significant water body and environmental impact for 100 years or more
Serious	Small Loss	Requires repairs or maintenance to maintain full function	Temporary or None	Loss of contents beyond the original structure footprint is < 1km x 1km Water and environmental impact expected to last < 100 years and to reduce over time
Minor	Insignificant Reduction	Overall structure integrity maintained No human intervention or maintenance required	None	Any loss of contents beyond the original structure footprint is localized to one area and is < 1km x 1km No significant impact on water body or surrounding environment
Limited	No Loss	Overall structure integrity maintained No human intervention or maintenance required	None	No movement of contents beyond the original structure footprint and represent a flow < 500 m x 500 m No significant impact on water body or surrounding environment
Natural Analogue	No Loss	Overall structure integrity maintained No human intervention or maintenance required	None	No movement of contents except through normal erosion processes No significant impact on water body or surrounding environment

*Definitions for Population at Risk (PAR applies to current land use only. Any future land use is under government regulatory control):

None - There is no discernable population at risk , so there is no possibility of loss of life other than through unforeseeable misadventure

Temporary - People are only temporarily in the consequence event area of influence. May need to be addressed case by case by a regulator ie current roadway risk may not be relevant to closure risk

Permanent - People must reside within the area of influence of the consequence event

**Loss of function means structure no longer maintains the ability to contain contents within original footprint from a rapidly occurring event.

Table 1b - Probability

PROBABILITY		
Low Likelihood	Event could happen in 10 years (10% probability in 10 years)	P < 0.01
Unlikely	Event could happen in 100 years (10% probability in 100 years)	P < 0.001
Remote / Highly Unlikely	Event could happen in 1000 years (10% probability in 1000 years)	P < 0.0001
Extremely Unlikely	Event probably won't happen in 1000 years (1% probability in 1000 years)	P < 0.00001

Probability of failure mode leading to consequence event.

P = annualized probability

Table 1c - Risk Matrix

RISK MATRIX						
PROBABILITY	Low Likelihood	Acceptable	Requires Further Review	Not Acceptable	Not Acceptable	Not Acceptable
	Unlikely	Acceptable	Acceptable	Requires Further Review	Not Acceptable	Not Acceptable
	Remote/ Highly Unlikely	Acceptable	Acceptable	Acceptable	Requires Further Review	Not Acceptable
	Extremely Unlikely	Acceptable	Acceptable	Acceptable	Acceptable	Requires Further Review
Risk = Consequence x Probability		Natural Analogue	Limited	Minor	Serious	Very Serious
		CONSEQUENCE				

Table 1d - Risk Category

RISK CATEGORY	
Not Acceptable	Not acceptable for de-licensing and requires further risk reduction by reducing consequence and re-testing in Risk Matrix
Requires Further Review	May or may not be acceptable for de-licensing. May or may not require risk reduction by reducing consequence and re-testing in Risk Matrix. This category can be de-licensed if further study allows, and the "Very Serious" consequence category may require a process as determined by the applicable regulatory agency
Acceptable	Acceptable for de-licensing with final case by case approval from regulators

Risk Category is qualitative but based on sound engineering principles

Mine wastes management @RIME

Michel Aubertin
Research Institute on Mines and the Environment, Polytechnique Montreal, QC, Canada

Bruno Bussière
Research Institute on Mines and the Environment, UQAT, Rouyn-Noranda, QC, Canada

ABSTRACT: This article summarizes the work that has been performed over the last few years by the Industrial NSERC Polytechnique-UQAT Chair on Environment and Mine Wastes Management. This Industrial Research Chair (IRC), which completed Phase II in December 2012, has lead to the creation of the Research Institute on Mines and the Environment -- RIME UQAT-Polytechnique -- officially launched in April 2013 in collaboration with mining companies. The work to be conducted by RIME over the next 7 years or so is also briefly described.

1 INTRODUCTION

Mining activities generate a variety of waste products that must be managed safely to protect the environment. In this regard, special attention must be given to the hydrogeotechnical and hydrogeochemical behaviour of mine wastes, particularly when they are reactive and prone to generate acid mine drainage (AMD) or contaminated neutral drainage (CND). The Industrial NSERC Polytechnique-UQAT Chair was created in 2001 to investigate issues related to the environment and mine wastes management. The research work, conducted under the Chair (held by the Authors as Chair and Associate Chair holders, respectively) aimed at developing tools and techniques that lead to improved practices for solid and liquid waste disposal, including waste rock from the mine, tailings produced by the mill, liquid effluents, and sludge generated by the water treatment plant. After a first term of five years, the Industrial Research Chair (IRC) was renewed for a second phase that ended in December 2012. The research program of this Phase II included 8 interrelated projects. The studies have been mainly conducted by graduate students (more than 100) trained through the Chair's program.

The following briefly summarizes the objectives and progresses made during this Phase II of the IRC (2006-2012). The line of work pursued by the Chair is continuing through the newly created Research Institute on Mines and the Environment - RIME UQAT-Polytechnique - that involves 2 universities and 5 mining companies (with additional participants to be announced shortly). The work being conducted by RIME is also described briefly in this invited article.

2 OVERVIEW OF THE INDUSTRIAL NSERC CHAIR'S PROJECTS

During Phase I (2001-2006), the IRC's work revolved around two broad themes identified as i) Waste management during mining operations, and ii) Closure and reclamation of disposal sites. During Phase II, the organization of the research program was reviewed to integrate mine closure aspects with actual mine operation issues. The program was then structured around eight main research projects, which are briefly described below. More details on these projects, including lists of individual student's projects and about 300 publications, have been presented in

a general report for this Phase II (Aubertin et al. 2010) and in a recent update prepared for NSERC (Bussière et al. 2013).

2.1 *Improved surface disposal of tailings*

Tailings produced from the milling of extracted ore from hard rock mines are made of finely ground rock flour (mainly silt size) with a relatively large surface area and water content. The classical methods for disposal of tailings as a slurry may raise some geotechnical and geochemical issues, particularly when they contain reactive minerals. This important project addressed various specific problems related to the physical and chemical stability of tailings and of their retaining structures. The project also included components on the desulphurization of tailings at the mill and on the behavior of paste tailings, which are considered as promising new means for better management of milling waste . The main progresses have been made in the following areas.

A) Predictive methods for hydrogeological properties: Extensions of the modified Kovács (MK) model, initially developed to predict the water retention curve (WRC) of stiff soils and tailings, have been formulated to describe (and in some cases predict): the WRC of compressible materials using the volumetric shrinkage curve (VSC); the unsaturated hydraulic conductivity function from the WRC; the hysteresis of the WRC of granular soils. The MK model parameters have also been related to those of well-known descriptive models (i.e. Brooks and Corey and van Genuchten) for granular soils (sand and silts, which include tailings). Additional work refined the testing procedure and interpretation method for assessing shrinkage (with or without cracking) of fine grained materials (including tailings and clayey soils).

B) Water budget and deep infiltration: Research conducted on the response of tailings under various climatic conditions includes an investigation of surface fluxes conducted with physical models (instrumented columns) combined with material characterisation, and numerical simulations. A good understanding of water movement is a critical parameter for mine site reclamation, especially when an elevated water table technique is used in the reclamation scheme (see Sect. 2.7), to favor the efficient of the reclamation scenario.

C) Mechanical/physical stability: An investigation was conducted on the liquefaction potential of mine tailings and on related control measures that can be used to minimise the associated risks. This work comprised shaking tests on a seismic table, cyclic tests on small scale samples, tensile tests on desiccated (unsaturated) tailings samples, in situ piezocone tests, and numerical simulations of various scenarios that include the geotechnical influence of reinforcement and draining columns made of waste rock (see Sect. 2.5).

D) Environmental desulphurization: Different materials that could beneficiate from a desulphurization stage before their disposal were investigated. The main objective was to reduce the environmental impact of tailings by concentrating problematic minerals using flotation of pyrite and arsenopyrite. This study also involved the development of criteria (in term of sulphide recovery) to characterize non problematic fractions (i.e. tailings that are non acid generating or not producing contaminated neutral drainage). The environmental and mechanical impact of using the sulphide concentrate from the desulphurization process in cemented paste backfill was also investigated.

E) Thickened and paste tailings: This component focused on the hydrogeochemical and geotechnical behaviour of surface paste tailings. It included an assessment of consolidation, evaporation, and desiccation. Colum tests were also installed to evaluate the evolution of the paste geotechnical properties and to study the influence of different deposition scenarios on these properties. A series of columns and an intermediate-scale physical model containing uncemented and cemented sulphidic paste tailings (homogeneous or with cemented layers) were used to assess the response of sulphide surface paste tailings to wetting (flushing) cycles. The results indicated that using cemented layers constitutes a promising approach to limit AMD production, at least in the short term. Results obtained were compared to hydrogeochemical numerical modelling using a code that combines fractured and porous media. In parallel, two experimental cells (with and without cement) were constructed in the field to further validate the laboratory and modelling results.

2.2 *Optimizing surface disposal of waste rock*

Waste rock piles often occupy a large area on the surface of mine sites. Such piles can have a significant impact on mine water quality, especially when they contain chemically reactive minerals. The geotechnical stability of piles can also be a source of concern. This project aimed at developing methods for the characterization of waste rock piles (in the lab and in situ) and developing models that can be used to assess their response. Another objective was to propose alternative disposal methods that could help minimize environmental impact. The main areas of progress have been in the following sub-themes:

A) Field characterization: Extensive field investigations with hydrogeological and geophysical methods have been conducted on two existing waste rock piles located in the province of Quebec: one from an underground mine and one on a large size waste rock piles from an open pit mine. The hydro-geophysical techniques developed during Phase I and the early part of Phase II on the smaller (acid-generating) waste rock pile have been modified to integrate the impact of the larger size of the pile and the different mineralogy of the (non-acidic) waste rock. Infiltration and other in situ characterization tests have been conducted.

B) Laboratory testing and predictive methods: This component focused on the measurement of hydrogeological and geophysical properties in large size columns. Saturated and unsaturated conditions have been considered in the various tests conducted. Migration of fine particles into waste rock and localized flow in macropores have been identified as important factors that affect hydrogeological testing results. Existing predictive models for the saturated hydraulic conductivity (k_{sat}) and the water retention curve (WRC) were modified to better represent the behavior of waste rocks with widely distributed grain size curves. These properties serve as input for numerical simulations (component C).

C) Hydrogeological modeling: A large number of numerical simulations have been conducted with various codes to simulate the unsaturated behavior of waste rock piles (based on actual field cases). The modeling work (see also hydro-geochemical issues below) included parametric analyses to interpret field tests and to investigate the effect of material properties (with deterministic and stochastic values), pile's internal structure and geometry, boundary (climatic) conditions, and alternative construction methods.

D) Modified disposal approaches: This component focused on two main aspects. The first one aimed at investigating (using numerical methods) actual and alternative pile configurations and construction methods in order to assess (and minimize) the risk of producing contaminated leachate (AMD or CND), and also to improve its geotechnical stability. Results showed that inclined layers of compacted material in the waste rock pile can help reduce deep water infiltration. When non problematic waste rock is available, it then becomes possible to channel water infiltration in zones where there is no contaminant generation; the same approach can also help control instability due to pore water pressure build up in some critical zones of the pile. The second aspect focused on the use of waste rock inclusions (as continuous fills) within impoundments to promote consolidation and higher liquefaction resistance of tailings.

2.3 *Disposal in mine openings*

The use of backfill has become a key component for many underground mining operations, favored in recent years by the development and general use of cemented paste backfill (CPB). The effect of backfill on the environment must also be assessed to make sure that returning mine wastes in mine stopes is safe. The main progress has been in the following areas.

A) Open pit backfilling: This investigation, which is complementary to a project on water covers (see Sect. 2.7), included a series of numerical analyses to evaluate the response of open pits filled with tailings or waste rocks. The simulations analysed the flow of water and contaminants around pits in fractured rock masses with various characteristics. Additional work was done to develop modelling tools to assess reactive transport in fractured media.

B) Behavior of backfill in underground stopes: Part of this work focused on the hydrogeotechnical properties of laboratory CPB samples (consolidated and unconsolidated). Results showed a significant evolution of CPB properties (hydraulic conductivity k_{sat}, air permeability, water retention curve WRC, consolidation parameters, microstructural properties, etc.) with cur-

ing. This work was complemented by a series of simulations (performed with different codes) to evaluate the stress and strain distribution and pore water pressures in backfilled stopes under a variety of situations and for different backfill properties. Analytical solutions were also developed to assess the stress state in backfilled stopes and the total and effective stresses on barricades.

C) Geochemical and environmental behavior of backfill: The risks of chemical instability of cemented paste backfill and hydraulic backfill due to the oxidation of sulphidic minerals were evaluated. Results showed that CPB is a better option than hydraulic fill for sulphidic tailings and that adding binders can help reduce the reactivity of the tailings. The project also includes an investigation of metal stabilization in arsenic rich CPB using various kinetic tests and geochemical modeling.

2.4 *Properties of AMD treatment sludge*

Treatment of acid mine drainage (AMD) is usually performed via chemical neutralization with lime, followed by precipitation of metals and solid-liquid separation. The sludge produced at the treatment plant must be disposed of and stored in a secure manner. The behavior of such sludge is poorly understood. The main objective of this project was to use new measurement methods (developed during Phase I and early Phase II) to characterize the hydro-geotechnical behavior of sludge during the sedimentation and consolidation stages. The main work can be summarized as follow.

A) Characterisation of sludge: Laboratory testing of sludge has been conducted to determine their sedimentation and consolidation properties. An improved experimental column set up was designed and used to measure the targeted properties of sludge. These results were used to develop models for the numerical simulations (see below).

B) Design of disposal areas: Simulations were conducted to analyse the column tests results (see A above), and to assess current disposal methods and develop new deposition schemes. The model relies on properties obtained from the laboratory measurements. The numerical analyses showed how to control and optimise consolidation of sludge upon disposal.

2.5 *Use of wastes on mine sites*

Improved approaches are being used by mines to reduce, recover, recycle and re-use the wastes produced on their site. This helps minimize the amount of final waste products and reduces the impact of the mine operation. The objective of this project was to explore various means to valorize mine wastes. The main progresses revolved around two main applications.

A) Use of low sulphide tailings as cover material: This work evaluated the performance of mono- and multi-layered covers made of low-sulphide tailings as oxygen barriers. A series of column tests with different configurations were performed in the laboratory on fresh or already oxidized tailings from different mines. The main parameters controlled (or monitored) include layers thickness and material properties (including sulphide content in the cover material), effect of pre-oxidation of the covered tailings, and the position of the phreatic surface (water table). Field measurements on mine sites and modeling work performed with different hydrogeological and hydrogeochemical codes complemented the laboratory testing program. The results showed, among other findings, that non acid generating tailings can be efficient in covers to reduce AMD, and that indirect oxidation may have a significant impact on the cover performance when placed over pre-oxidized tailings.

B) Co-disposal of waste rock in impoundments: Some of the work mentioned above refer to the placement of waste rock inclusions (as heaps and continuous fills) into tailings impoundments in order to add reinforcement elements and to favor drainage and consolidation of the tailings during and after deposition. When the coarse-grained waste rocks are acid generating, this approach also helps control water flow and oxygen availability (to prevent AMD). The concept was studied using laboratory tests, field data, and numerical modeling. The results showed that the addition of waste rock inclusions in the impoundment can improve significantly the geotechnical stability of tailings and dikes submitted to dynamic leadings, while accelerating the tailings consolidation within a zone of influence that depends on their properties and thickness.

2.6 *Water quality prediction*

To meet environmental standards, mine effluents must contain low contaminant concentrations and satisfy component-specific or toxicity tests. This project, which was at the core of the Chair's program, aimed to improve the experimental procedures for conducting characterization and predictive tests. Another key goal was to develop mathematical tools for the prediction and modeling of the hydrogeochemical response of mining wastes. This project was closely related to many others, and it lead to progresses along the following lines.

A) Mine wastes characterization: A new approach has been developed based on a computer program (SEM-XMAP) that combines X-ray dot mapping images acquired by SEM to identify (and quantify) the different minerals, including cementitious phases in cemented paste backfill (CPB). Complementary techniques, such as ATD-ATG, XANES and XAFS, were also used to characterize the materials. In addition, selective dissolution tests were used to better characterize mobility of metals and their stabilization in CPBs. The use of multispectral image analysis with optic microscopy was also investigated as an automatic means to quantify the mineralogy of mine wastes. Different sorption tests were used to evaluate the sorption potential of mine wastes with a CND potential. Additional work has also been performed to isolate the reaction rate parameters in sulphidic wastes (at various temperatures, including cold conditions).

B) Prediction of acid mine drainage (AMD): A project was dedicated to the modification of standard kinetic tests to obtain more reliable results. This includes a new humidity cell set-up that integrates oxygen consumption and water content measurements. A statistical analysis of a many column test results was also performed; the results showed that a good reproducibility can be achieved when a suitable set-up methodology and rigorous control of the boundary conditions are used. A comparison of interpretation methods to assess the long term AMD potential of low sulphide tailings has also been conducted; it showed that the method proposed in the ASTM standard (humidity cell test) often tends to overestimate the neutralization potential. In a complementary study, numerical and semi-analytical solutions have been developed to predict gas flux and oxygen consumption through partially saturated covers and reactive tailings.

C) Prediction of contaminated neutral drainage (CND): This project focused in part on the geochemical mechanisms behind Ni release and the influence of sorption on the generation of CND from waste rock samples (and pure minerals) from a mine located in eastern Québec. Also, comparisons were made on geochemical results from laboratory kinetic tests and in situ experimental cells, to assess the influence of scale and of other factors. This component also involved kinetic tests (columns and weathering cells) to evaluate CND generation of different rock types under normal and cold conditions. The main results showed that small scale lab tests often give reaction rates that are quite different from those obtained in experimental field cells, and that sorption affects significantly the CND from waste rock, especially in the relatively short term.

D) Numerical modeling of hydro-geochemical processes: Water flow and geochemical reactions in mine wastes are key components of numerical models developed to simulate the hydro-geochemical behavior of mine wastes. An existing (research oriented) code been applied (with some modifications) to simulate laboratory columns tests on reactive tailings with an elevated water table and also field conditions that include mono- and multi-layer covers (see Sect. 2.7). The same code was also used to simulate CND generating waste rock by adding a sorption component. A new model was developed to simulate transport behavior and geochemical evolution of acidic mine drainage (AMD) in discretely fractured porous media. A comparison of AMD evolution in different fracture networks showed that the plume evolution in a fractured medium can be significantly different from that obtained from an equivalent porous medium.

2.7 *Evaluation of cover systems*

Approaches to limit the generation of AMD from sulphidic mine wastes generally focus on eliminating one (or more) of the three main components of the acidification reactions: oxygen (air), water, and sulphide minerals themselves. The most common technologies involve the use of soil or water covers placed over the reactive wastes. This broad project investigated the behavior of various types of cover systems.

A) Single-layer cover and elevated water-table: This component aimed at evaluating the efficiency of single-layer covers to limit AMD generation from fresh or already oxidized tailings

(using samples from existing mine sites). Small and large columns have been installed with different configurations; some used natural soils while others used low sulphide tailings for the covers. Wetting and drying cycles with measurements of oxygen concentration, volumetric water content and suction were performed to analyse the hydrogeochemical behaviour of the different tailings-cover systems. Results showed that phreatic surface depth and evaporation protection are two critical parameters for the performance of such covers. It was also observed that indirect oxidation (in pre-oxidized tailings) can reduce the efficiency of the cover system. The investigation included a comparison between lab results and in situ measurements. Another component involved numerical simulations to develop a predictive approach to assess the efficiency of this (and related) technique, under different situations.

B) Multi-layer cover with capillary barrier effects (CCBE): The performance of CCBEs to limit water infiltration and/or O_2 ingress was evaluated using numerical modelling of fluid flow (water and oxygen migration) through horizontal and inclined covers, direct measurements within an actual layered cover on a mine site. The impact of different factors on cover performance was investigated including: inclination angle, length, material properties, and presence of a suction break. A geophysical investigation was performed in situ to assess the distribution of moisture (water content) in an inclined CCBE. An investigation of passive and active direct measurement methods for oxygen concentration was also conducted. In addition, the oxygen-consumption test was modified for use as a more reliable tool to quantify cover performance, considering different interpretation methods. A methodology to characterize the evolution of vegetation on CCBEs was developed and applied to a mine site. In parallel, in situ test plots have been constructed to investigate natural bio-intrusion barriers and evaluate the capacity of allelopathic plants (which can inhibit germination and growth of a certain species of plant) to limit long term degradation of CCBE caused by tree-roots invasion.

C) Water covers: The performance of a water cover placed over highly reactive tailings was investigated, using laboratory and field measurements on an existing site (i.e. flooded pit). Different scenarios were simulated in the lab, including stagnant water cover and fully aerated water cover with a without tailings resuspension. Another component involved seepage modelling (saturated and unsaturated) and contaminants transport for rock wastes and tailings disposed of in mine openings (pits and stopes) in fractured rock masses. This project did not directly address the use of man-made water covers (with engineered dikes), which are considered at high risk in the long term (as an alternative for closure and reclamation).

2.8 *Passive treatment systems*

Passive methods for AMD treatment can offer several potential advantages such as a high efficiency for metal removal at low pH, improved sludge characteristics, lower operation and maintenance costs, reduced use of chemicals, and minimal energy consumption. This project focused on the following two techniques.

A) Passive bioreactors: This project investigated passive treatment systems made with biofilters. The study included laboratory investigations on reactive mixtures, to assess metal removal mechanisms, ecotoxicity of treated effluents, and long term efficiency of treatment systems in the particular case of highly contaminated AMD. The results showed that biofilters can improve significantly water quality, although high concentrations of iron can reduce the system efficiency. The use of multi-stage treatment systems was also investigated using an in situ pilot treatment system (and laboratory tests). The results showed how a combination of treatment stages can treat highly contaminated mining effluents.

B) Limestone drain (LD): Limestone drains were simulated with column tests and with an intermediate scale physical model, for two different scenarios (oxygenated and anoxic drains) and various residence times. The effect of iron that tends to precipitate at the effluent, thus reducing the pH (typically from 6 to 3), was also addressed. In-situ measurements on two existing LDs were also performed to assess their efficiency for treating a highly contaminated acidic effluent. Column tests were also performed to evaluate the impact of the mineralogy and grain size of the limestone, and of the AMD quality, on the neutralization capacity. Numerical modeling of the flow inside LDs and in-situ tracer tests have also been conducted to better understand the hydraulic behavior of such systems.

3 OTHER IMPACTS FROM THE IRC

The above mentioned reports presented to NSERC, in 2010 and 2013, have shown that all the projects included in the proposal for Phase II of the IRC, submitted in 2005, have been completed. The advancement followed fairly closely the initial plan, although some components (often expanded) needed more time than initially planned (which explains the 18-month extension, from June 2011 to December 2012).

The projects described above show that the Industrial NSERC Chair has been working on a variety of issues that are important for a mining industry that represents a vital component of the Canadian economy. The Chair's research outcomes provide new or improved tools and techniques for the characterization, modeling, and evaluation of various mine wastes and of management and reclamation practices. The Chair was also very active in training highly qualified personnel (see below), who then become the much needed specialists that help the industry achieve its goals. In addition to its technical impact, it should also be recalled that the Chair (with its partners and collaborators) actively contributed to the mining engineering program at the Ecole Polytechnique de Montréal and at UQAT, and to the development of the Abitibi-Témiscamingue region (which depends mainly on natural resources). Because of the Chair, UQAT can now provide the local mining industry a unique expertise in mining environment and mine wastes management, which helps to maintain its high level of competitiveness.

The IRC has provided a critical mass of professionals, working on a variety of interconnected topics. The Chair's team has grown significantly since it was created in 2001. This expansion has led to a diversity of expertise, which covers areas such as hydrogeology, geotechnique, geochemistry, geophysics, mineral processing, and biochemistry, with strong components in lab and field characterization techniques, and numerical modeling. The basic team is formed by the Chair holders (M. Aubertin and B. Bussière) and the three main collaborators (Profs. G.J. Zagury, M. Mbonimpa, and M. Benzaazoua). They worked closely with full time researchers and with Professors from Polytechnique (Robert P. Chapuis, Richard Simon, Li Li, Michael James, and Michel Chouteau) and UQAT (Tikou Belem, Yves Bergeron, Carmen Neculita, and Francine Tremblay). The eight projects presented above have also involved several external collaborators (about 20) working for other research organizations in Canada and abroad (France, Belgium, Australia, Morocco, Algeria, Tunisia).

3.1 *Training*

Many students have been involved in the IRC's research program. During Phase I, more than 60 graduate students and 12 undergraduate students worked on projects directly related to the Chair's program, significantly exceeding the original goal (of 22 graduate students). During Phase II, 79 graduate students (i.e. 30 Ph.D., 42 Masters, 7 PDF) participated to the Chair's program, again largely exceeding the initial goal. Overall, more than 160 students have been trained through the IRC (see details in the above mentioned reports).

Most students conducted their project in collaboration with one or more industrial partner(s). They also participated in the preparation of many publications for conferences and for refereed journals, and many have presented their research results to the Chair's partners and during local and national technical meetings. These opportunities give them invaluable experience for communicating their expertise. The demand for their services is high; graduates have been hired as specialists in mine waste management, geotechnique, hydrogeology and related fields.

3.2 *Dissemination*

The Chair's main proponents worked hard to ensure that their results have been transferred to their Partners and to the related community. For this purpose, they published regularly in journals and conference proceedings. A list of more than 300 papers is presented in the latest Chair's report (Bussière et al. 2013). The production during Phase II (2006-2012) involved more than 120 Peer reviewed Journal papers, about 160 Conference papers (and presentations), and nearly 20 Technical Reports.

The Chair has also been actively contributing to a number of initiatives to promote technology transfer, by participating in various national and international gatherings. In addition to the presentations given during the IRC's Scientific Committee meetings, the 2008 and 2011 Symposia on *Mines and the Environment* were organized in collaboration with other groups (i.e. URSTM, CIM, MRNF, AMQ, MEND). A symposium on Modeling Tools for Improving Mine Waste Management was held in Quebec City in 2008, during a conference organized by GAC-MAC. Two specialty conferences (one on mine wastes management and the other one on Challenges related to mine site reclamation) were held during the ACFAS Congresses in 2010 and 2012. The Chair Holders have also participated to various organizing committees, such as the 2009 CLRA conference held in Quebec City and Paste 2010 held in Toronto. Also, a number of workshops, seminars, short courses, and graduate courses have been presented on different topics of interest, such as AMD prediction, cover technology, modeling techniques, underground waste disposal as backfill, surface disposal of densified/paste tailings, and reclamation methods. It is also worthwhile recalling that the Mineral Engineering Master Program of École Polytechnique is offered at UQAT as a formal extension (since 2004). Students are thus able to enroll directly in Abitibi and complete their entire program at UQAT. Several new courses were created as part of this extension. Some of these are offered by video transmission, thus allowing students at different locations (i.e. Montreal, Rouyn-Noranda, Val d'Or) to follow the course from their home town.

3.3 *Additional aspects*

Since the Chair was created in 2001, new laboratory facilities have been built at both Universities, and new equipment has been purchased with funds from the Chair's budget and with additional funds from other sources. A list of the main equipment was included in the reports mentioned above. These include, for instance, oxygen optic sensors, echo-log probes, hydrogeochemical instruments for wells and piezometers, LECO furnace, a SEM, roots digitizer, ionic chromatograph, mobile laboratory facilities, small loop-test, and column testing material. Additional (in kind) laboratory support was provided by both universities, as part of their contribution to the Chair's activities. These facilities have been used by the authors of this article and by the other collaborators of the Chair (and their students). The growth of the research team made the Chair one of the major players in the field of mine wastes management on the national and international scenes.

There have been many challenges since the Chair was set up in 2001. These included the organisation of the work between the 2 universities, fund management, and supervision of a large group of students. Nonetheless, the collaboration (at every level) between the two institutions has rapidly become very efficient, and a real team spirit has emerged. As stated above, the key milestones were realized as planned, with some being expanded using complementary funding. Care was taken to ensure a good coordination of the various projects. The main proponents involved also showed a strong commitment for the supervision of the many students involved in the Chair's projects. Another major challenge lied in the conduct of field work on mine sites, especially for the projects located in more remote areas. This required careful planning and regular exchanges with the local operations, including attention to health and safety issues. It should be emphasized here that the extensive collaboration from the Chair's Partners was of great help, and in many ways essential to the success of the IRC. Thanks to the interactions between the researchers, students, collaborators, and partners, the Chair was able to conduct elaborate research projects that involved fairly complex laboratory and field measurements and sophisticated modelling analyses.

4 ONGOING WORK AT RIME

As mentioned earlier, a new Research Institute on Mines and the Environment was created to pursue the work initiated by the IRC. RIME UQAT-Polytechnique targets the development of environmental solutions for the entire mine life cycle. The program will involve several mining industry partners: Agnico Eagle, Osisko Mining Corporation, IAMGOLD Corporation, Rio Tinto, Fer et Titane Inc., and Xstrata Nickel Raglan Mine. With a value of nearly $10 million provided over seven years by these companies, and with additional funds anticipated shortly, it can be expected that this innovative partnership will produce a top-notch research program and train a large number of highly qualified professionals.

It is worthwhile recalling here that Université du Québec en Abitibi-Témiscamingue (UQAT) and Polytechnique Montréal have pooled their expertise for over 30 years, by collaborating on various teaching and research projects. Created in 1983, UQAT offers some 100 undergraduate, master and doctoral programs; it holds 10 Research Chairs and operates 11 research units linked with the priority niches in its surrounding areas. Founded in 1873, Polytechnique Montréal is one of Canada's leading engineering teaching and research institutions. With over 40,000 graduates, Polytechnique has educated nearly one-quarter of the current members of the Ordre des ingénieurs du Québec through its 15 engineering specialties, By making the most of the existing research infrastructure, the experience of seasoned professors and researchers , and the successful partnerships established between Polytechnique, UQAT and the industry, RIME is positioning itself as a promising space for training and innovation, contributing to the mining industry's competitiveness and growth. In this perspective, the mining companies involved are active partners in this project. In addition to their financial contribution, they have participated enthusiastically in establishing the research program and they are providing personnel, with access to their sites and facilities for supporting the research work

RIME UQAT-Polytechnique is contributing to the development of environmental solutions for a mine's full life cycle, while consolidating training for the mining sector at the undergraduate, master and doctoral levels RIME's program includes a number of topics related to current industry issues, some of which are summarized very briefly below.

4.1 *Mine sites reclamation*

The objective in this component is to develop new technologies, or improve existing technologies, to reclaim mine waste disposal areas (tailings impoundments and waste rock piles) from hard rock mines. Mine site reclamation is becoming more and more crucial, even at the initial stage of a project when the community needs to be convinced that the proposed mine will not become an environmental problem at the end of the mine life. The proposed program is based on needs expressed by the industry and governmental agencies. As such, results will benefit mining companies, consulting firms, and society in general, by helping with the development of better mine site reclamation practices.

This broad theme involves a number of specific projects including the treatment of highly contaminated AMD with passive systems (focusing on Fe, Mn, As, Sb); reclamation of mine sites under Nordic conditions; using mining materials as components of reclamation scenarios; performance of geosynthetics in covers; reclamation techniques for CND generating sites; pit disposal and reclamation; water diversion on top and within waste rock piles to control water contamination; development of numerical tools to better predict the response of reclaimed mine sites; long term geotechnical stability of reclaimed sites; engineered covers (analysis, design and long term performance); revegetation ; influence of climatic changes on design requirements. As was the case for the work presented above, a combination of laboratory modelling, in-situ measurements, and numerical simulations will be used to meet the research objectives.

4.2 *Hydro-geotechnical behavior of wastes*

This component is closely related to the previous one. It will focus on the hydrogeological and geotechnical aspects of mine waste management. The program includes specific projects on issues of concerns for the industry and regulatory agencies, such as: the physical stability of tailings impoundments and waste rock piles; risks due to extreme rainfalls and seismic events; the use of probabilistic methods in stability evaluation; improved techniques for surface disposal such as the use of waste rock inclusions placed in tailings impoundments and the geotechnical behaviour of densified tailings.

4.3 *Other projects and closing remarks*

Other R&D priorities related to mines and the environment have been identified by the RIME team, including:

- Rheological behaviour of densified tailings and paste backfill;
- Geotechnical/geomechanical behaviour of cemented backfill in underground stopes;
- Stabilization of contaminants in cemented backfill;
- Optimization of backfill recipes and deposition sequences;
- Effect of consolidation, drainage, filling rate on stress state and bulkhead design for single and multiple stopes;
- New approaches for the design of waste rock piles, based on waste rock characterization, fluid flow and reactive transport modelling, to control their geotechnical and geochemical and stability;
- Tailings desulphurization (AsPy, Py, Po) and integrated management of mine wastes;
- Prediction of water quality (and modeling tools) with emphasis on As and Sb;
- Treatment of CND (Mn, As, Sb), mine water with cyanides, and other species.

As was the case for the IRC, RIME UQAT-Polytechnique will rely on the strong interactions between practitioners working in industry (i.e. mining companies and consulting firms), researchers in academia, and professionals working for regulators. In addition to the mining industry investment, funding for the projects mentioned above will also come from various governmental agencies such as NSERC, FQRNT, and provincial ministries (particularly Ministère des resources naturelles du Québec).

More information on the IRC and RIME can be obtained from the authors.

5 REFERENCES

Aubertin, M., Bussière, B., Benzaazoua, M., Mbonimpa, M., Zagury, G.J. 2010. *48 Months Report, Phase II,* Industrial NSERC Polytechnique-UQAT Chair Environment and Mine Wastes Management. 37 pages.

Bussière, B., Aubertin, M., Benzaazoua, M., Mbonimpa, M., Zagury, G. J. 2013. *Final Report, Phase II,* Industrial NSERC Polytechnique-UQAT Chair Environment and Mine Wastes Management. 53 pages.

Oil Sands

Oil Sands – ILTT and Thin Lift Dewatering

Dewatering and shear strength performance of in-line flocculated mature fine tailings under different depositional schemes

A. Dunmola, C. Côté & G. Freeman
Shell Canada Energy, Calgary, AB, Canada

D. Kolstad
Barr Engineering Co., Minneapolis, MN, USA

J. Song
O'Kane Consultants Inc., Calgary, AB, Canada

S. Masala
Barr Engineering and Environmental Science Canada LTD., Calgary, AB, Canada

ABSTRACT: A field trial comparing three depositional schemes in terms of tonnes of solids dewatered to minimum undrained shear strength of 5kPa in one year was initiated at Shell Canada's Muskeg River Mine in 2012 and continued in 2013. Three instrumented test cells (named Thin Multi-lift, Thick Multi-lift and Deep Stack), designed to hold eight 0.5m lifts, three 1 to 1.5m lifts and a single 5m lift, respectively, were poured to characterize dewatering and shear strength performance. Preliminary results showed that for all deposits, immediate water release from flocculated MFT was the most significant dewatering mechanism. For the multi-lift deposits, settlement occurred most rapidly in the first two weeks following deposition, coinciding with dissipation of excess pore-water pressure. Prior to the onset of desiccation, shear strength was found to increase with depth, indicative of consolidation. Placement of a fresh layer enhanced the strength gain of the upper portion of underlying layer as well as the lower part of the fresh layer for the Multi-lift deposits.

1 INTRODUCTION

Shell Canada Energy (Shell) is currently implementing in-line flocculation of mature fine tailings (MFT) at a commercial scale using the "Atmospheric Fines Drying (AFD)" process at the Muskeg River Mine (MRM) site. A description of the AFD process is provided in Kolstad et al. (2012). In general terms, the process is based on instantaneous water release from flocculated MFT followed by atmospheric drying with the ultimate aim of converting fluid fine tailings (FFT) into soft deposits that can be capped and reclaimed. The technology requires that several thin lifts (~ 30cm thickness per lift) of flocculated MFT be placed sequentially over the course of a dry season to maximize atmospheric dewatering. A fresh lift is placed once the old lift is sufficiently desiccated to provide the required bearing capacity for another layer. One of the challenges of in-line flocculation technology is the large footprint required for dewatering as well as the extent of operational efforts associated with repeated placement of limited tonnage of treated FFT as thin lifts into a given footprint.

As part of the continuous improvement efforts for the Shell AFD operations at MRM, a field test program was initiated in 2012 aimed at assessing various depositional strategies for in-line flocculated MFT in terms of maximizing the tonnage of fines that can be processed per unit footprint and minimizing associated operational efforts. Hence, the main objectives of the multi-year field test program was to evaluate various depositional schemes in terms of: (a) the tonnage of fines processed per unit footprint to a minimum undrained shear strength of 5kPa in 1 year, and (b) minimizing operational complexity in terms of the frequency of deposition, operating costs and need for re-handling. Secondary objectives for the technical program include the

evaluation of the: (c) relative contribution from flocculation, evaporation, consolidation and freeze-thaw to dewatering and strength gain, and (d) relative benefit of multi-layer deposition and deep stacking.

To this end, three instrumented test cells namely: Thin Multiple Lifts (Thin ML), Thick Multiple Lifts (Thick ML) and Deep Stacking (Deep Stack) were constructed at MRM's AFD operations site in summer 2012. Deposition into the test cells began in late summer 2012 and is currently on-going, with deposition planned to be completed in late summer 2013. Once completed, the three test deposits will be left in place, monitored and tested for a period of 1 year until late summer 2014. This paper presents the test methodology, instrumentation and monitoring design for the field test program. Also, some preliminary results from the test program, especially related to part of objectives (c) and (d) above are presented. Future publications providing updates on the assessment of the field performance of the test deposits as per the identified metrics (primary objectives (a) and (b) above) are anticipated.

2 FIELD TEST DESIGN

2.1 *Test plan: depositional schemes investigated*

Three test cells were constructed to represent a wide design envelope for possible depositional schemes for in-line flocculated MFT. The depositional configurations of the test cells are presented in Figure 1 and are described as follows:

- *Thin Multi-Lift (Thin ML)*: Two lifts of approximately 0.5m lift thickness deposited in 2012; six lifts of 0.5m thickness to be deposited in 2013, with a cycle time of about 1 month.
- *Thick Multi-lift (Thick ML)*: One lift of 1m thickness deposited in 2012; 2 lifts of 1.5m thickness to be deposited in 2013, with a cycle time of about 3 months.
- *Deep Stacking (Deep Stack)*: One 5m thick lift deposited in 2012 in one continuous pour.

2.2 *Test plan: Test cells' design, instrumentation and deposit in-situ sampling and testing*

The three test cells were constructed side by side within the existing footprint of the AFD commercial operations at MRM. The cells were designed to have similar height to footprint ratio in order to maintain comparable boundary condition, with a design base slope of 2%. After construction, the base slopes ranged between 1 and 2%. Each test cell had three primary instruments' posts and two ancillary instrument posts as shown in Figure 2. The installed instruments were designed for continuous monitoring of the pore-water pressures, temperatures (air, surface and profile), volumetric water contents, settlement, total stress, matric suction and surface albedo of the test deposits. Meteorological data used for the estimation of potential evaporation (PE) were also recorded at a station located within the AFD commercial operations site. Core samples of test deposits were collected periodically from monitoring stations located within the general vicinity of the primary instrumentation posts, with access provided by floating docks placed close to each primary instrumentation post. The sample cores were analyzed for profile solids contents, as well as ancillary geotechnical parameters (e.g. void ratio, degree of saturation, bulk wet and dry densities). In addition, in-situ vane shear testing was done periodically at the sampling locations to obtain profiles of peak and residual shear strengths.

2.3 *Test plan: deposition into test cells*

Lift 1 into the Thin ML and Thick ML was placed on August 27, 2012, while lift 2 of the former was placed on October 3, 2012, followed by continuous pouring into the Deep Stack on October 4, 2012. The average cumulative thicknesses of the lifts into the test cells are presented in Table

1. With the exception of the Thin ML deposits, the actual cumulative thicknesses of the test deposits were generally close to target. Lift 1 into the Thin ML was deliberately poured thicker (than planned) to ensure coverage of the footprint, thereby providing a steeper surface slope for subsequent lifts. Lift 2 was poured thinner than target to maintain 1m cumulative thickness for the first two lifts. The thicknesses of the test deposits immediately at the end of deposition are shown in Table 1. Additional deposition into the two multiple lift test cells is on-going at the time of preparing this paper and hence, results from the 2013 deposition events are not reported here. Apart from some settlement and pore-water pressure data, other performance data for the Deep Stack deposit are also not presented here as they are not available at this time.

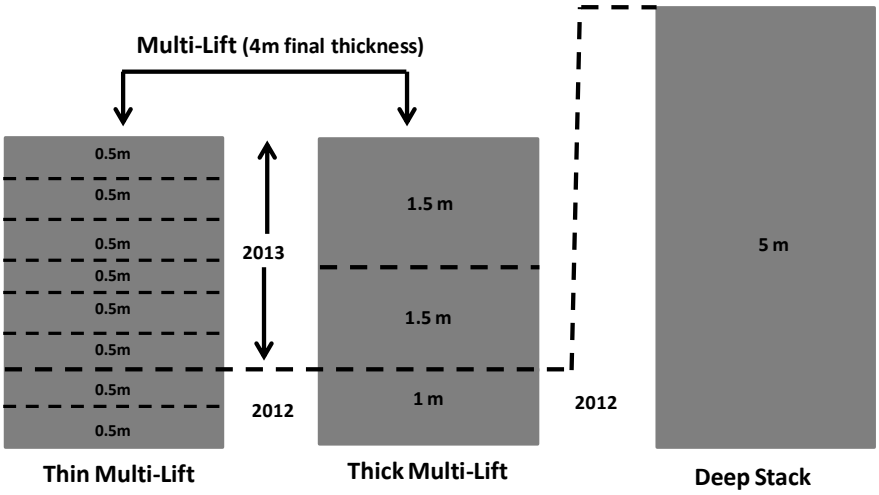


Figure 1. Depositional configurations for the Thin and Thick Multi-lift and Deep Stack Test Cells

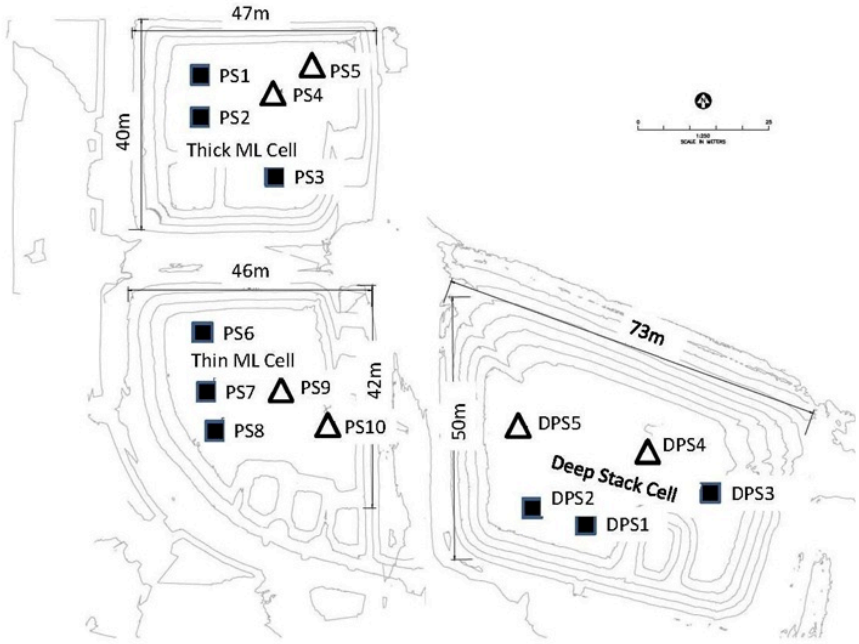


Figure 2. Layout of the Test cells showing the locations of the instruments posts for the Thin and Thick ML test cells (PS) as well as for the Deep Stack test cell (DPS).

Table 1. Cumulative thicknesses of in-line flocculated MFT deposited into the Test Cells in 2012. Results for thicknesses determined from graduated rulers at the primary instrumentation posts as well as from laser scanning are presented.

Deposit	**Target height (m)**	**Average height (m)-end of deposition at primary posts**	
		Graduated Ruler	Laser Scanning
Thin ML Layer 1	0.5	0.75	0.75
Thin ML Layer 2	1.0	0.92	0.92
Thick ML	1.0	1.05	1.05
Deep Stack	5.0	4.58	4.58

3 RESULTS AND DISCUSSION

3.1 *Flow behaviour of test deposits*

One of the sensitivities around the field deposition of in-line flocculated MFT is balancing the rheology (yield stress) of the material with uniform flow within the depositional footprint. The average yield stress for each depositional event in 2012 was in excess of 150Pa, resulting in deposits that are relatively uniformly distributed, with the ratio of deposit surface slope to bed slope ranging from 1 to 2. The two Thin ML deposits had the higher ratio (2) due to their relatively small thickness and the tendency for material to stack up higher closer to the discharge location. This is indicative of the comparatively bigger challenge of maintaining uniform lift thickness and optimum footprint utilization with thin-lift deposition. Current operational practice involves having sufficiently high base slopes (in excess of 2%) for the depositional cells to ensure uniformity of spread, or use mechanical means (equipment) to spread the deposited material. However, either of these options may potentially further add to the cost pressures for in-line flocculated MFT technology.

3.2 *Dewatering mechanism for test deposits*

The four main dewatering mechanisms identified for the test deposits include: initial water release from flocculation and resulting sedimentation; under-drainage through the cell base; evaporation; and, freeze-thaw dewatering. Since this paper mainly focuses on data obtained prior the test deposits freezing in 2012, an evaluation of the contribution of freeze-thaw to the dewatering of the test deposits is excluded. A number of alternative approaches were taken to quantify the contribution from each of the mechanisms as summarized below:

- *Initial Water Release*: this was quantified using: laser scanning of the test cells (difference in volumes of initial deposit scan immediately after deposition and after release water removal); metered pumping of the release water; in-situ sampling of the deposits followed by gravimetric analysis; and, volumetric water contents recorded by installed instrument-Time Domain Reflectometry (TDR) sensors.
- *Under-drainage*: this was quantified from: hydraulic gradients across the tailings base-cell floor interface recorded from vibrating-wire piezometers (VWP) installed just above and within the cell foundation using Darcy's Law; and, water balance from settlement, precipitation, water removal and actual evaporation (AE) data.
- *Evaporation*: PE was calculated from meteorological data recorded using the Penman's equation (Penman 1948), while AE was calculated from tailings surface temperature and albedo, as well as other meteorological data using the Modified Wilson-Penman equation (Wilson 1990).

Table 2 presents the contribution of individual dewatering mechanisms to the overall increase in solids content for the test deposits, covering the time period indicated. As expected, initial water release from flocculation was the most significant contributor to dewatering for the short duration under consideration. With the exception of the Deep Stack, evaporative drying was the

second most significant dewatering mechanism. The Deep Stack is sufficiently thick such that evaporative drying was minimal for the brief period considered, in addition to the evaporative demand at the time (Late Fall) being relatively low. The expectation is that for the Multi-lift deposits, evaporative drying will become more pronounced over time. For the Deep Stack, the relative contribution of evaporative drying and consolidation to dewatering in the longer term will be assessed in the future. Under-drainage being the least important dewatering mechanism for the majority of the test deposits is consistent with the low downward hydraulic gradient recorded at most locations within the test cells' foundation. As mentioned previously, the relative contribution of freeze-thaw dewatering will be assessed in subsequent publication(s).

Table 2. Contribution of individual dewatering mechanisms to test deposits' solids content (SC) gain. Numbers shown are the averages for data from all primary instrument post locations, all profile depths and different estimation approaches.

State		**Thin ML (Oct 6)**	**Thick ML (Oct 6)**	**Deep Stack (Nov 10)**
Initial	Initial SC (%)	35 (Ave. of 2 lifts)	36	35
Contribution to SC Change (%)	Initial Water Release	+7.5	+8.7	+7.1
	Under-drainage	+0.2	+1.2	+0.5
	Evaporation	+1.9	+2.8	+0.1
Final SC (%)	Water balance	45	49	43
	TDR	46	51	51
	Sampling	48	53	50

3.3 *Geotechnical characterization of test deposits: comparison of instrumentation and sampling results*

The geotechnical state of the test deposits is monitored over time from continuous record of their stress state as well as regular in-situ sampling of the deposits from the floating docks deployed close to the instrumentation posts. Geotechnical data from instrumentation and in-situ sampling is compared to ensure confidence in the field performance data reported for the test deposits. Presented in Figure 3 is a comparison of the profiles of total stress extrapolated from value recorded by the total pressure (TP) cell installed at the base of the Thick ML test deposit and the corresponding stress values calculated from measured profiles of wet densities on day 41 after deposition. Profiles of total stress measured and values from the instrument record show very good agreement. Also, comparison of the solids contents measured from gravimetric analysis of profile core samples obtained from the Thick ML test deposit and values obtained from TDR measurements is shown in Figure 4. Considering two depths (0.2m and 0.6m above the cell foundation), the two datasets are shown to be well correlated over the period in consideration. The values shown in Figure 4 are generally higher than the final solids contents previously presented in Table 2 as the latter are the averages for all instrument post locations, all profile depths, as well as all estimation approaches considered. The foregoing demonstrates a high degree of confidence in the functionality of the installed instruments as well as the accurate characterization of the geotechnical state of the test deposits as presented in the following subsections.

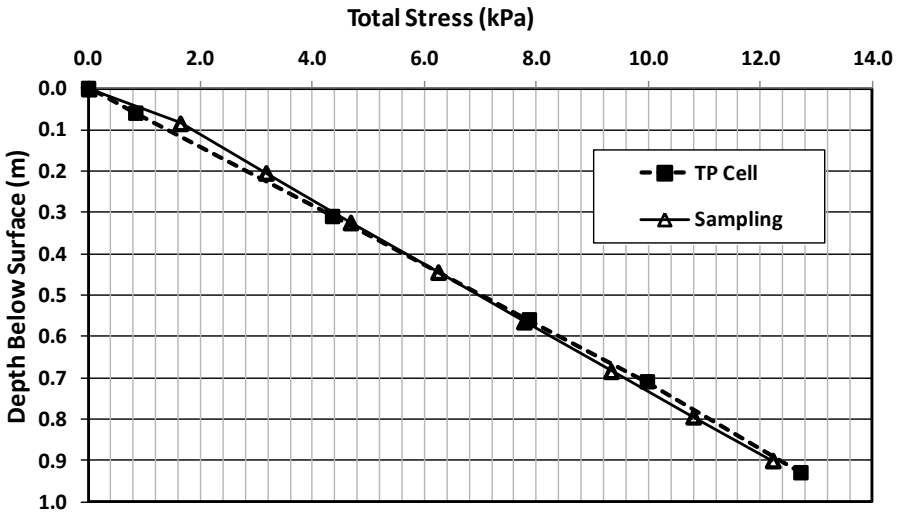


Figure 3. Comparison of profiles of total stress extrapolated from data recorded by the Total Pressure (TP) cell at cell base and sampling measurements made close to the corresponding primary instrumentation post (PS2) on day 41 for the Thick ML test deposit.

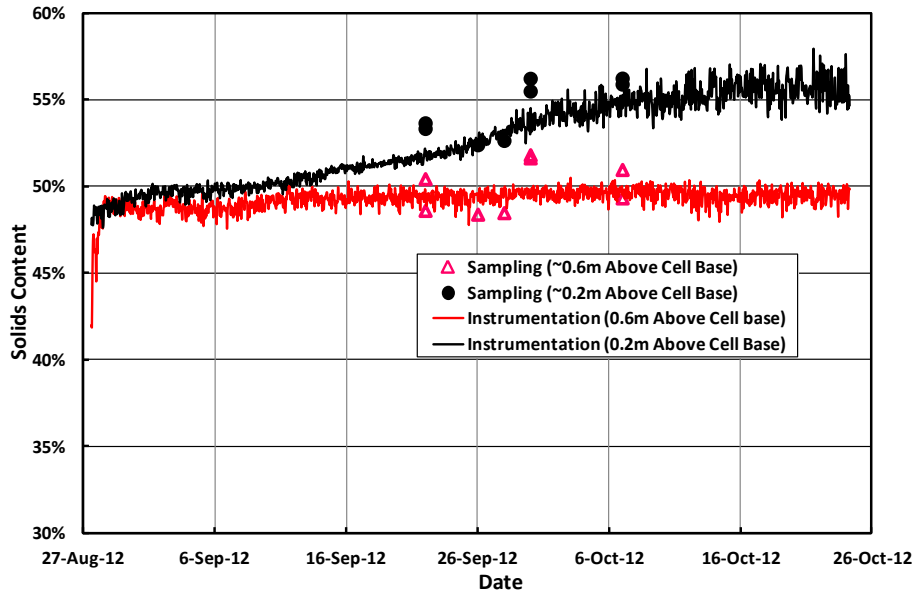


Figure 4. Comparison of solids contents measured over time from profile sampling and values calculated from installed TDR measurements at PS2 for depths of 0.2m and 0.6m above the cell base for the Thick ML test deposit.

3.4 *Geotechnical performance of test deposits: Settlement, desiccation and consolidation*

As shown in Figure 5, most of the settlement recorded for the test deposits in Fall of 2012 occurred within 4 weeks after deposition and generallly coincided with the dissipation of pore-water pressures (as indicated by red block arrows). Afterwards, the rates of settlement for the test deposits were much slower. The total settlements for the Thin ML (combined for the 2 lifts) and the Thick ML deposits were similar, being 34% and 32%, respectively, based on average deposit thickness from scan data. Desiccation is typically indicated by the development of negative pore-water pressure (matric suction) and/or the development of surface cracks as the deposit desaturates. Neither of these indicators was recorded for the test deposits for the limited period under consideration, hence desiccation was not observed in the Fall of 2012. The end of

primary consolidation, as indicated by the dissipation of excess pore-water pressure appeared rapid for layer 1 of the Thin ML deposit (between several days and 2 weeks after deposition; interference from rainfall responsible for the multiple points indicated by red arrows in Figure 5). In contrast, end of primary consolidation took a relatively longer duration (~ 3.5 weeks) for the Thick ML deposit. This pattern is indicative of a lower total stress and shorter drainage path for the first lift of Thin ML compared to the Thick ML deposit.

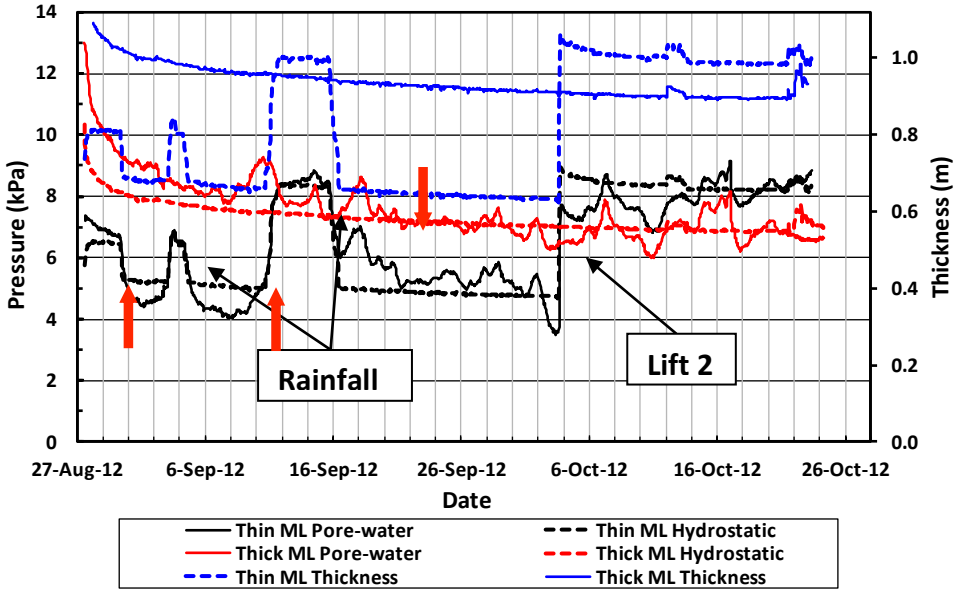


Figure 5. Pore-water recorded by instrument and hydrostatic pressures calculated at depth close to the cell base for Thin and Thick Multi-lift test deposits over time. Data shown for depth of 0.15m and 0.20m above the cell base for the Thin (PS 7) and Thick (PS2) ML test deposit, respectively. Spikes in pressures for the Thin ML due to rainfall / run-off and Lift 2 placement as indicated. Also shown is the respective test deposit thickness.

3.5 *Geotechnical performance of test deposits: Densification, shear strength gain and effect of multiple layering*

The profiles of solids content for the two lifts into the Thin ML and first lift into the Thick ML test cells are presented in Figure 6. After initial dewatering and primary consolidation (within the first 4 weeks after deposition), the solids contents for lifts 1 in both the Thin and Thick ML deposits are shown to rapidly increase. For both deposits, solids contents generally increased with depth, consistent with consolidation-driven densification of the test deposits. The top of the deposits having the lowest solids contents further confirms the previous observation that evaporative drying was not the most significant dewatering mechanism shortly after deposition. There were no profiles solids content data shown between day 0 and 26 in Figure 6 due to lack of access for in-situ sampling for this time interval. However, for both multi-lift cells, the highest rate of dewatering (as indicated by the profiles of solids content) seems to have been prior to Day 26 and 27 for the first lifts of Thin and Thick ML deposits, respectively. There was no significant difference in the profiles of solids contents for the first lifts into the Thin and Thick ML cells over the fourth week (Day 26 to 36) post deposition.

The corresponding profiles of peak shear strength for the multi-lift test deposits are shown in Figure 7. Consistent with the solids content profiles, for both test deposits, the shear strength rapidly increased within 4 weeks after deposition. The undrained shear strength profiles are generally linear, with little or no strength at the surface, indicating that evaporative drying and the development of negative pore-water pressure (suction) are not the primary mechanisms for

shear strength gain. Although the linear strength profile suggests that consolidation may be the primary driver for shear strength development, the magnitude of shear strength measured is higher than expected from the standpoint of the corresponding profile effective stresses. It is postulated that flocculation is responsible for this additional shear strength in excess of what effective stress development alone could account for. This additional shear strength enhancement resulting from flocculation has been noted by previous authors (Beier et al. 2012; Kolstad et al. 2012). This additional strength from flocculation is expected to become relatively less significant with additional increase in effective stress due to further consolidation.

Similar to the profiles for solids contents (Figure 5), the profiles of shear strength recorded for the Thick ML cell is not substantially different from the corresponding values for the first lift into the Thin ML cell (Figure 7). On one hand, this may be expected given the fact that the difference in average thickness of the Thin ML (first lift) and Thick ML deposits (0.75m versus 1.05m as per Table 1) was not as substantial as was designed (0.5m versus 1.0m). On the other hand, this may suggest that when evaporative drying is not the dominant dewatering mechanism, the sensitivity of in-line flocculated MFT deposit thickness to dewatering and shear strength performance in the short term may not be as pronounced, at least within the context of relatively "thin" (0.5 – 1.0m) deposits considered in this paper. This hypothesis will be further refined as more depositions into the multiple lift test cells are completed in 2013. As expected, the shear strength profiles follow the same pattern as the solids contents, increasing with depths, consistent with consolidation driving the densification of the test deposits.

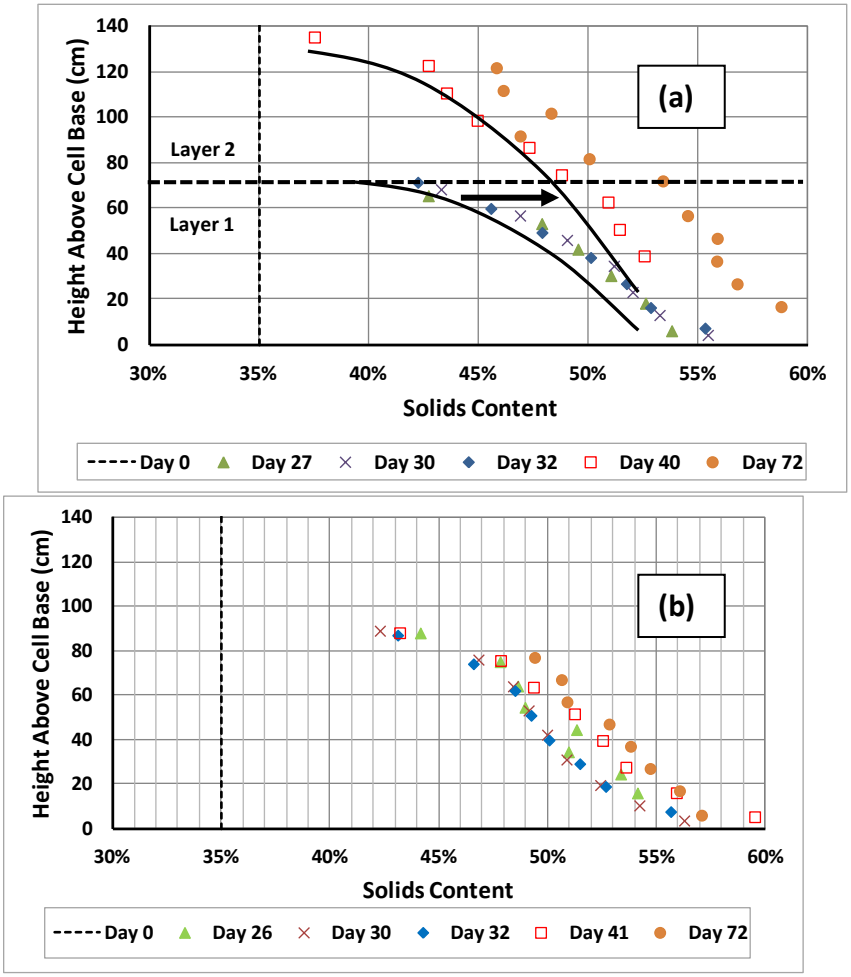


Figure 6. Profiles of solids contents for: (a) Layers 1 and 2 for the Thin ML; and, (b) Layer 1 for the Thick ML cells. Layer 2 for the Thin ML was placed on Day 37. Arrow depicts shift in profile solids content due to placement of layer 2.

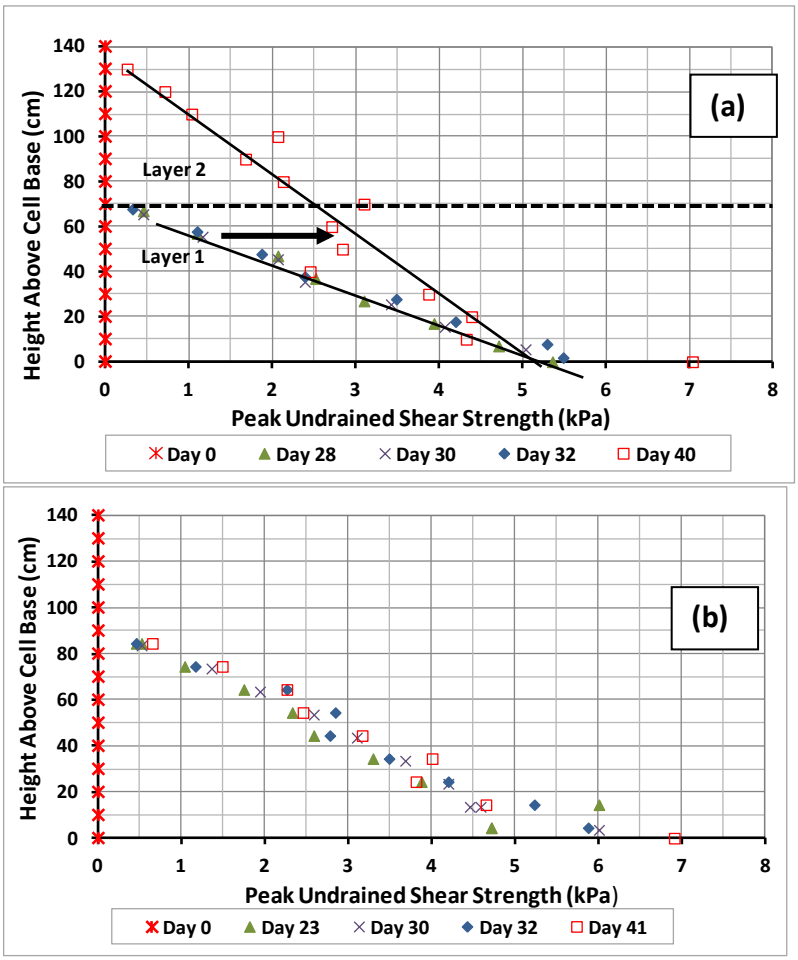


Figure 7. Profiles of peak undrained shear strength for: (a) Layers 1 and 2 for the Thin ML; and, (b) Layer 1 for the Thick ML cells. Layer 2 for the Thin ML was placed on Day 37. Arrow depicts a shift in profile undrained shear strength due to placement of layer 2.

It is noteworthy that immediately following the placement of the second lift into the Thin ML cell, both the solids contents and peak shear strength profiles of the upper portion of the underlying (previous layer 1) increased (Figures 6 and 7). This is indicative of increase in effective stress due to surcharge from the fresh layer on the previous layer accelerating the dewatering and shear strength gain of the upper portion of the former. Concurrently, the fresh layer (Layer 2) is observed to rapidly dewater and gain shear strength, especially at its lower portion (Figures 6 and 7). This is attributed to the inter-layer transmission of water from the upper (fresh) layer to the old (underlying) layer as previously reported by Fisseha et al. (2010). It is reasonable to expect that the re-wetting effect on previously desiccated layer will result in a substantial reduction in the solids contents and trigger a loss of shear strength for the lower layer. However, previous work by Fasking et al. (2012) on thickened tailings solvent recovery unit (TSRU) tailings suggests that any shear strength loss in underlying tailings layer due to re-wetting from a fresh lift is temporary and recoverable. Though the results and observations herein presented are preliminary and cover a limited time period, it seems that multiple layering exhibits the added benefit of enhancing further consolidation of the underlying layer as well as potential for increased rate of dewatering for the fresh lift. However, it is important to note that this benefit may gradually diminish as the number of layers increase and the drainage path for consolidation, evaporation and under-drainage becomes longer. This phenomenon will be assessed with additional deposition into the multiple lift test cells in 2013. Profiles of void ratio and dry density for the Thin and Thick ML test deposits follow the same trend as the solids contents and shear strength profiles, and are therefore not presented here.

4 SUMMARY AND CONCLUSIONS

Preliminary results from an on-going field pilot assessing the depositional scheme that maximizes the tonnage of MFT fines processed per unit footprint to target shear strength per year are presented. Three instrumented test cells (Thin ML, Thick ML and Deep Stack) were constructed and started to be filled in 2012. The test deposits generally exhibited fairly uniform spread across the footprint. For all test deposits, initial water release from flocculation and sedimentation was the most significant dewatering mechanism for the brief period considered. Settlement and dissipation of excess pore-water pressures in the multi-lift cells was rapid. Solids contents generally increased with depth, consistent with consolidation of the deposits induced by effective stress development. The same pattern was observed for shear strength profile, with additional shear strength enhancement than what effective stresses alone could account for, attributable to flocculation. For the Thin ML cell, placement of a fresh lift on previous layer enhanced the dewatering and shear strength gain of both layers.

Practical considerations for field deposition of in-line flocculated MFT should involve balancing the rheology of the product with deposit thickness as discussed in Kolstad et al. (2012). The higher the yield stress and thinner the design lift thickness, the more challenging it is to achieve efficient footprint use. The sensitivity of dewatering and shear strength gain performance of in-line flocculated MFT deposits to lift thickness may not be substantial if evaporative drying is not the significant dewatering mechanism. For the limited number of multiple lifts considered in this paper, there was no negative impact on dewatering and shear strength gain due to the placement of fresh tailings lift on an old layer. Deposition into the test cells and performance monitoring of the pilot deposits is on-going and updated results and observations vis-a-vis the identified assessment objectives will be provided on a go-forward basis.

5 REFERENCES

Beier, N., Sorta, A., Wilson, W., Sego, D. and Dunmola, A. 2012. Geotechnical aspects of flocculation-based technologies for dewatering mature fine tailings. *Proceedings, 64th Canadian Geotechnical Society Conference, Winnipeg, MB, 1-3 October 2012*.

Fasking, T., Dunmola, A., McKay, D., Masala, S., and Langseth, J. 2012. Bench-scale drying of multi-layered thickened TSRU tailings. In David Sego, Ward Wilson and Nicholas Beier (ed.), *Proceedings, 3rd International Oil Sands Tailings Conference Edmonton, AB, 2–5 December 2012*. University of Alberta Geotechnical Centre. pp 421-429.

Fisseha, B., Bryan, R. and Simms, P. 2010. Evaporation, unsaturated flow, and salt accumulation in multilayer deposits of a paste gold tailings. *J. Geotech. and Geoenviron. Eng.*. 136 (2): 1703-1712.

Kolstad, D., Dunmola, A., Dhadli, N. O'Kane, M., Song, J. and Masala, S. 2012. Towards the improvement in geotechnical performance of atmospheric fines drying (AFD) deposits at Shell's Muskeg River Mine. In David Sego, Ward Wilson and Nicholas Beier (ed.), *Proceedings, 3rd International Oil Sands Tailings Conference Edmonton, AB, 2–5 December 2012*. University of Alberta Geotechnical Centre. pp 411-420.

Penman, H.L. 1948. Natural evaporation from open water, bare soil and grass. *Proc. Roy. Soc.*. A193: 120-145.

Wilson, G.W. 1990. Soil evaporative fluxes for geotechnical engineering problems. PhD Thesis, University of Saskatchewan, Saskatoon, Canada.

Mud farming of fine tailings - application and benefits of MudMaster® technology

Leon D. Munro & David Smirk
Residue Solutions, Brisbane, Queensland, Australia

ABSTRACT: Effectively consolidating mature fine tailings (MFT) with predictable outcomes has led to extensive research by the Oil Sands industry to identify sustainable management practices that are both cost effective and in accordance with regulatory requirements. To date, the oil sands industry has investigated the application of mechanically assisted dewatering (mud farming) of flocculated MFT using conventional earthmoving equipment. Extensive research and development in the minerals industry elsewhere has proven mud farming with MudMasters® (specialized Archimedes screw tractors (AST's), also known as Amphirols) provides a low risk, predictable and sustainable management system capable of delivering cost-effective, high strength tailings. When implemented correctly, this process significantly accelerates the strengthening of tailings slurries through sustained dewatering, largely independent of weather, significantly reducing the size of the required management area.

Given the broad success of this technology in similar tailings to MFT, mud farming with MudMasters® has been trialed in MFT at two Alberta Oil Sands operations since 2011. Key outcomes of these trials include:

- Flocculated MFT placed in layers up to 1.0 m in depth are effectively dewatered in around 28 days with strength >20 kPa;
- Deposited profile solids content increased from <40% to >60% over the trial periods. Rainfall within this period did not impact the dewatering process;
- MFT volume reduced by approximately 20% due to water release and flocculation network collapse. No volume changes were observed in control (unfarmed) areas;
- Subsequent to the above outcomes, a new layer of MFT was deposited on top of farmed tailings and the process repeated, demonstrating sequential / cyclic operation.
- Performance was sustained over a range of flocculation dose rates, although higher dose rates required additional machine operation;
- No injuries or reportable safety events (with >3,000 hours operation).

On a commercial scale, mud farming with MudMasters® can be applied at an approximate cost of $1.50 (CAN/USD) per dry ton of MFT. The technology and process has proven itself capable of delivering dewatered MFT of high strength and reduced volume with significant cost savings over current practice.

1 INTRODUCTION

Mechanically assisted profile dewatering, or mud farming, is a process by which tailings or soft, over-saturated areas (swamps, dredge ponds etc) are actively managed in situ to accelerate the rate of densification enabling rapid and cost effective management. The effectiveness of mud

farming is dependent on the type of equipment used, the layout of the mud farming area and how the regime is implemented. This management system was born out of the inability of traditional earthmoving equipment to access (deep) marginal terrains in addition to the limited efficacy of these equipment to dewater these environments. The equipment and process used for true mud farming were first developed by the Dutch (Amphirols) in the 1960's, with subsequent reviews by the US Army Corp of Engineers of the equipment for transport in marginal terrain (USA TECOM, 1964) and the process for densification of dredge spoils (Johnson et al, 1977). At that time, densification was not considered to be viable with the equipment tested.

Renewed interest in the principles and process of mud farming occurred in the 1980's within the minerals industry, as increased capital costs and environmental pressures forced reassessment of tailings management practices. Whilst reductions in cost and area requirements were identified, predictable control and sustained performance of the dewatering process was not possible until large-scale, in-situ mechanical dewatering techniques could be further refined. In short, simply applying an AST/Amphirol to an oversaturated environment did not guarantee success.

Further research indicated that equipment needs to be configured to match fundamental material characteristics and applied within a suitable (and strictly adhered to) cyclic management strategy. This is a completely different management approach to the traditional method of striving to modify material properties to suit available equipment or striving to modify its behaviour to fit within a rigid design. With several decades of evolution this has led to the modern AST/Amphirol, otherwise known as the "MudMaster®" (Figure 1) and its application within the mud farming process.



Figure 1. A MudMaster® in MFT (Day 26, Pass 6).

Mud farming with AST's is now commonplace in the minerals industry with over 30 million dry tons of tailings currently managed annually and to a lesser extent, dredge reclamation operations. Given that many of these current mud farming applications have similar physical characteristics to flocculated MFT in addition to preliminary model outputs, a degree of confidence was built into the prediction of similar performance levels to be expected with MFT.

With minor reconfiguration to the (standard) MudMaster® design, MFT management was trialed at two operations commencing in summer 2011 and repeated in 2012. The aim of this paper is to provide a summary of the data acquired from the largest trial of mud farming using the MudMaster® in the Canadian Oil Sands to allow stakeholders to assess the viability of this management technology to meet regulatory requirements for full-scale, long-term MFT management.

1.1 *Mud Farming using the MudMaster®*

The first step in mud farming is to determine the settled density of the material to be farmed. This should be measured within 72 hours of deposition, although with highly flocculated MFT, 24 hours has been determined as sufficient due to rapid initial dewatering. This value is then used to match machine configuration with the resultant deposition depth to provide three important points:

- It ensures complete profile penetration to sustain traction whilst;
- Limiting the interaction with/reworking of the substrate and:
- Avoids re-pulping of the layer to be farmed.

The next step is deposition of the material at the required location at the required depth (nominally 1.0 m). Failure to adopt this approach can lead to deposition being too deep or too shallow. If the deposition is too deep the commencement of mud farming can be delayed with only the upper region developing strength and thus, strength stratification will result, potentially introducing some localized weakness within the tailings deposit. If the deposition is too shallow, mud farming can be executed to high strength very quickly, but this approach is inefficient due to higher fuel consumption and equipment wear rates and requires a heightened regime discipline through faster rotation sequences.

Once the tailings is deposited, repeated scrolling of (machine passes on) the surface begins on a staggered but strictly controlled basis to permit surface drain development and discharge of pore water out of and away from the deposited profile. This is monitored to ensure sustained progression of the dewatering process. Scroll pattern and timing is dependent on the layout of the tailings management area and the properties of the tailings; together these dictate the dewatering rate. Importantly, scrolling should be a planned and defined activity:

- Scroll too infrequently and the dewatering rate will not be optimized resulting in a longer dewatering cycle;
- Scroll too frequently and there will be higher operational costs and wear rates with little dewatering benefit.

When the dewatered tailing has reached their required strength and/or density, a new tailings layer is deposited as before and the cycle is repeated.

In applications where profile depth already exceeds equipment penetration capabilities (for homogenous strength development), mud farming can be applied over several weeks to months to develop the necessary upper-profile strength to sustain operations. This is generally referred to as a recovery phase and once complete normal (cyclic) mud farming operations can commence.

1.2 *Mud Farming Strategy*

A mud farming strategy ensures planned operations are followed and the system is managed through four key performance indicators:

- Tailings placement control – the right amount of tailings, of the right quality being placed in the right place at the right time;
- Sustained dewatering – ensuring no pooled water in any farmed area at any time and that scrolling is occurring where necessary, when necessary;
- Performance tracking – quantifying equipment coverage, strength and/or density development and operational efficacy;
- Forward planning – using the above information to forecast sustained performance and execute this plan in a cyclic operation.

The fifth, unquantifiable KPI is management resourcing to sustain the process. This is dependant on field operational staff closely monitoring performance and reporting the above aspects of mud farming to management to ensure timely and effective decision making and support.

2 APPLICATION IN OIL SANDS OPERATIONS IN ALBERTA

These aforementioned tailings management principles and techniques have been applied and proven in many mineral processing operations and locations around the world, although until now, had not been applied in the Oil Sands industry. Therefore, the mud farming trials undertaken in 2011 and 2012 with MudMasters® undertaken at two MFT operations in Alberta, Canada represent the first steps to determining the efficacy of this management regime to deliver the requirements of Directive 74 (ERCB, 2009) to the Oil Sands industry.

2.1 *Trial Parameters*

2.1.1 *Trial Areas*

The trials were undertaken in multiple compartments that each possessed multiple discharge points along the highest wall. The total area trialed for the results herein was >55 ha. Dewatering performance was assessed on a range of slopes from discharge to drainage collection.

2.1.2 *MFT Characteristics*

After recovery from storage dams, MFT slurry was pumped to each area and flocculated immediately prior to discharge. The slurry solids content ranged from approximately 21-26 wt% solids (density 1.16 – 1.20 t/m^3), was flocculated immediately prior to discharge at (up to 1,200 g/L) and deposited sequentially from the discharge wall, with each set of spigots being operated for approximately 24 hours.

2.1.3 *Depth control*

A match between MudMaster® configuration, substrate density and MFT settled density indicated that pour depth should be controlled at 0.8 – 0.9 m to ensure maximum efficiency. This was facilitated through the installation of depth markers at 25m and 50m from the centre of each set of four discharge spigots.

2.1.4 *Sampling and analysis*

Within the preliminary stage of the trial, sampling was only undertaken from the MudMaster® as no other access was possible. However, after several passes, samples were taken from both the machine and from walking access onto consolidated MFT.

Measurements taken included shear vanes along with moisture content, density and particle size distribution (PSD). Shear vane samples were taken from all areas of machine passage (beside, within and adjacent to scroll tracks). All samples collected for analyses were immediately double-bagged in plastic zip-lock bags with all air expelled and were not refrigerated.

2.1.5 *Equipment tracking*

Series V MudMasters® were utilized within the trials and tracked for daily coverage capacity, maximum speed, altitude telemetry, fuel consumption, torque output and propulsion efficiency.

3 RESULTS

Scrolling commenced 72 hours after deposition completion. Sampling was undertaken commensurate with the scrolling regime to track the impact of each machine pass.

The combination of the variable slope from discharge to drainage and high flocculent dose rates resulted in highly variable and difficult to control pour depths. Actual depths ranged from 0.3 – 1.4 m (Figures 2 & 3). Machine altitude telemetry and depth sampling indicated that approximately 40% of the cells were poured within the most efficient machine working depth (0.7 to 1.1 m), thus indicating that 60% of the cell was either too deep or too shallow for efficient mud farming. The ideal depth was found mostly in the upper, steeper-sloped regions of the cell, with the lower more gently sloped region displaying very shallow MFT deposition (<0.5 m).

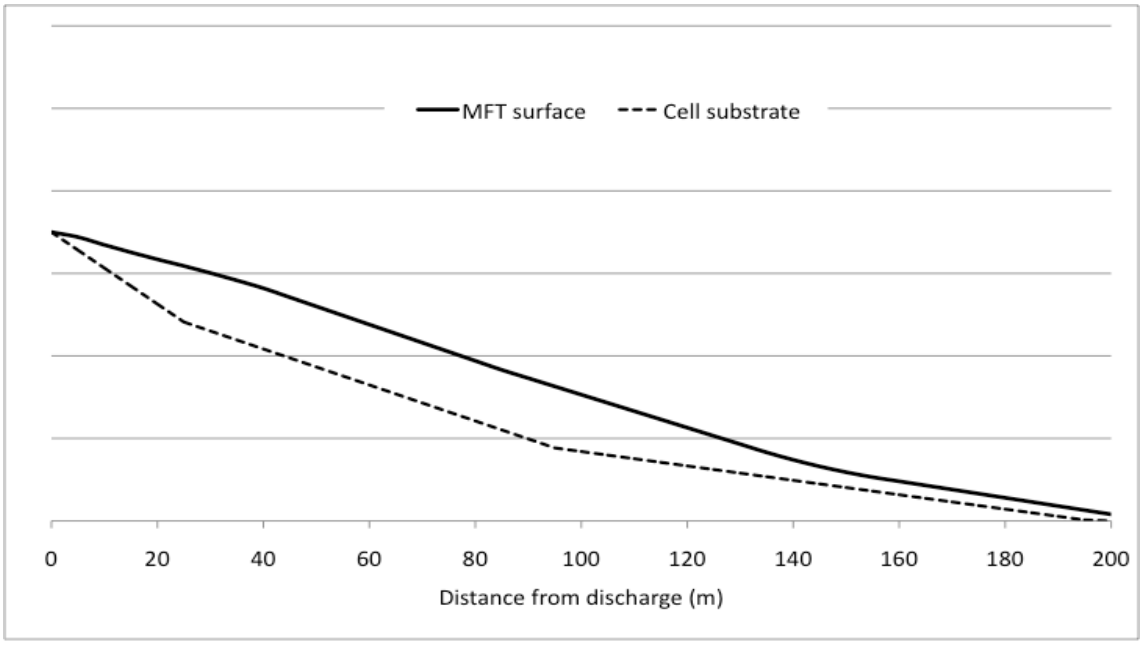


Figure 2. Deposition profile with exaggerated vertical axis.

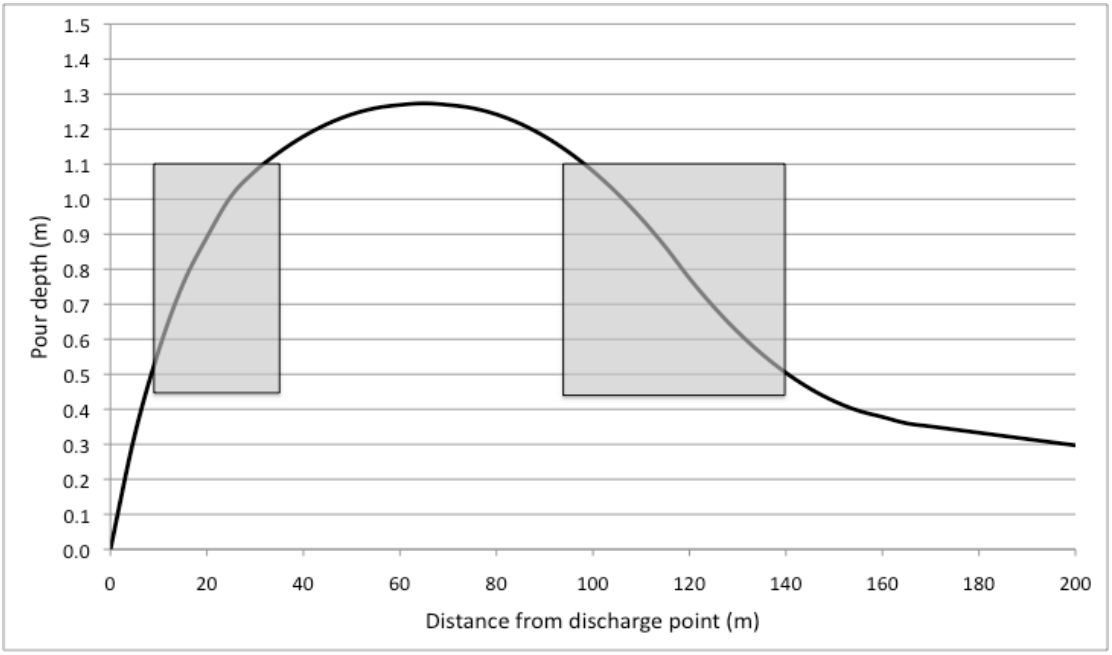


Figure 3. Average profile depth with respect to distance from discharge point. Shaded areas indicate region poured to target (optimum farming) depth.

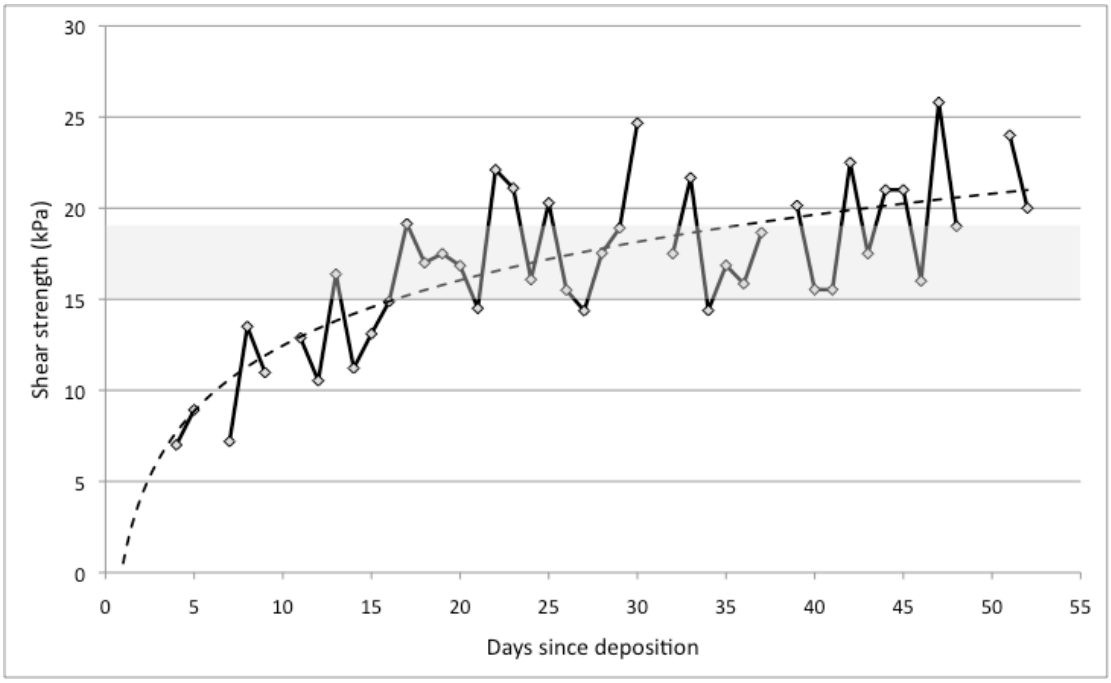


Figure 4. Strength development with respect to days since deposition. Shaded area indicates target strength minimum for sustained/cyclic farming.

Due to the variable deposition depth, shallow areas (<0.5 m) received as few as 2-3 scrolls to exceed 25 kPa, areas 0.5 to 1.1 m were worked with up to 10 scrolls to realize target strength and areas >1.1 m as many as 13 scrolls with highly variable results prior to redeposition. In short, the highly variable depth dictated a highly variable scrolling campaign and strength development.

Strength development results provided in Figure 4 are derived from >1,200 shear vane samples and indicate a rapid increase in shear strength up to around day 28, followed by a stagnation in further improvement. The rapid increase is attributed to the collapse of flocculent structure and interstitial water release, leading to increased density. Conversely, as the only areas being worked after 28 days were poured beyond recommended working depth, the limited evidence of further strength development in deep areas is consistent with equipment performance limitations.

Although highly variable, moisture content data indicated an overall improvement from <40 wt% to >60 wt% solids in the course of the trial. However, as expected, deeper areas retained more moisture for longer periods.

Redeposition was undertaken after 45 days and new scrolling campaigns were successfully implemented after 72 hours. This indicates that the MFT had gained sufficient strength to sustain cyclic MudMaster® operation.

4 DISCUSSION

The first and foremost KPI for effective mud farming is controlling residue placement depth. This not only directly impacts the required duration, but potentially the overall efficacy of the subsequent mud farming campaign. Overall adherence to planned pour depth was around 40% of the trial area and therefore adequate to provide a representative area for application of this management system. All areas poured up to the maximum effective working depth of the MudMaster® achieved high density and strength within 28 days of deposition, whereas areas poured beyond this depth required more time and farming intensity, and yielded variable results.

A significant contributing agent to MFT placement control in the trials was flocculent dosage. Flocculent addition applied in MFT management is a proven and extremely effective tool for rapid preliminary dewatering. However, its impacts on MFT flow properties can impart difficulty for operational staff to adhere to strict pour depth requirements. Within the trials, this led to highly variable depth, required management intensity and final strength / density. Mud farming of MFT may not be possible without flocculation, as this approach provides an ideal initial density for farming commencement and therefore, a better strategic approach to MFT management incorporating mud farming would be to investigate optimal flocculent dose rates that provide dewatering benefit without significantly contributing to placement depth variability.

Trial data indicated no observable difference of higher flocculent doses contributing to enhanced final strength. Furthermore, areas with dose rates >1,000 g/L imparted difficulty for equipment to traverse the MFT whilst shear strengths were <20 kPa. It has been recognized by the oil sands industry that the gel strength acquired through flocculation should not be misinterpreted as true (mechanical) strength, and may serve to inhibit mechanical strength development (COSIA, 2012). The culmination of the above suggests that research and/or control of flocculation levels <600 g/L are worthy of investigation.

Put simply, mud farming overcomes hindered settling and establishes and sustains drainage from tailing areas. Consistent with the above, drainage efficacy was sustained in all areas that possessed a slope towards the water recovery drains. However, in areas with slopes of <1.0% or with other depth/drainage issues (submerged/internal bunds, groundwater inflow etc), more intensive management was required, leading to the deep and/or poorly drained areas requiring more scrolls to achieve target. Conversely, areas at or below target depth with good drainage were easily managed to exceed minimum strength requirements for sustained/cyclic mud farming.

Equipment performance tracking indicated that machines were able to sustain required coverage capacity (>4.5 ha/dy) throughout the trial, but the efficacy of their coverage was dictated by material properties (i.e. high plasticity), the above shortcomings in pour depth control and drainage. More specifically, the quantifiable improvement in profile strength and density derived from each machine pass was clear and positive in areas poured at or below target depth with good drainage, but stagnated and variable in deep and/or poorly drained areas. Ultimately, a well-executed mud farming regime in MFT can plan to exceed 20 kPa in 28 days, beyond both Directive 74 (5 kPa) and minimum cyclic mud farming thresholds, and consistent with similar tailings under MudMaster® management elsewhere (Munro & Smirk, 2012 and Figure 5).

High strength (up to 35 kPa without accounting for evaporation) is an expected outcome of the mud farming process, and not an arbitrary target. While re-deposition could have occurred at a lower strength and still sustained farming, this would eventually compromise the operational intent, as material properties would inflict handling issues during the recovery phase. Therefore, MFT managers need to understand and clearly define what material properties best suit their long-term management plans so that further mud farming campaigns with enhanced controls can be matched to deliver them.

The efficacy of mud farming with MudMasters® in wet weather is sustained through the inability of rainwater to penetrate an already over-saturated, settled profile in addition to the provision of drainage channels for runoff. The process is therefore not reliant on evaporation for achieving target (although this is of additional benefit). In contrast, traditional earthmoving equipment, by way of action, repulp the profile which places greater reliance on evaporation for dewatering and leads to higher variability in performance. Furthermore, track driven equipment are not well suited to immersion in deep, mineral slurry profiles and will require extensive maintenance if applied in such conditions.

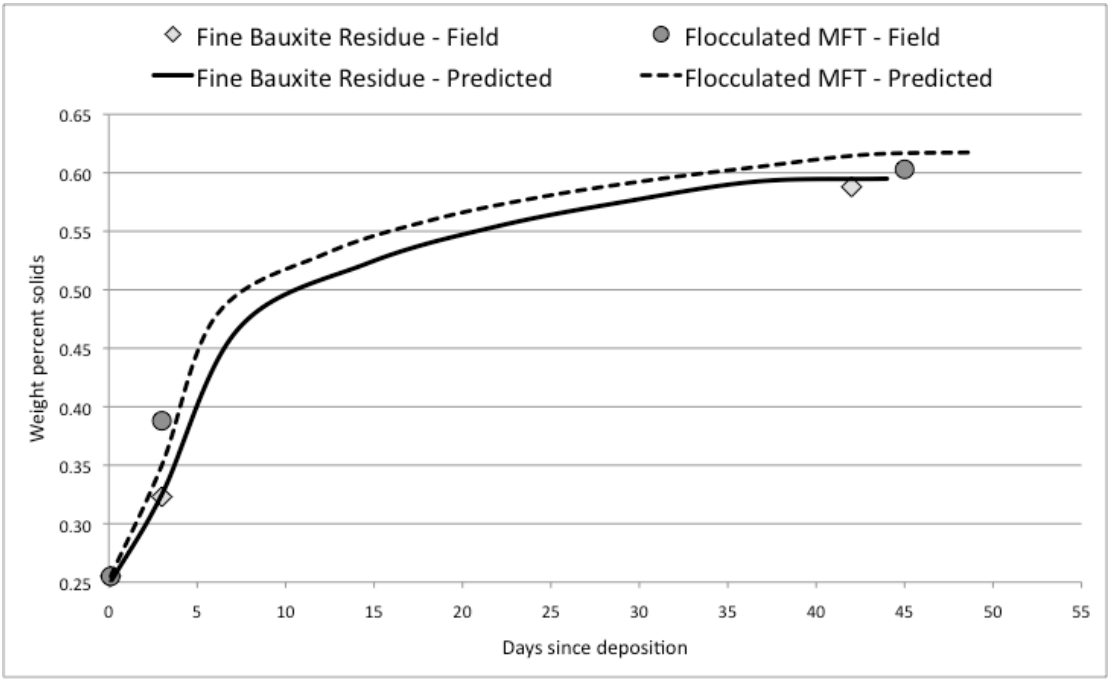


Figure 5 Comparative dewatering performance of MFT and fine bauxite residue under mud farming. Flocculation of MFT provides benefit to initial density, although both streams can be effectively managed to similar end-points in similar time frames.

5 CONCLUSIONS AND RECOMMENDATIONS

Mud farming with MudMasters® is a safe and complimentary tool to existing practices in large-scale flocculated MFT management that provides the additional benefit of reducing operational footprint. The combination of cost-effective operation, flexible configuration and ability to exceed regulatory targets supports this approach as a viable and low risk alternative to conventional earth moving equipment applied to this task.

The strength achieved through mud farming also provides opportunity to investigate the viability for each layer to remain in-situ for subsequent re-deposition if required, as is applied in other upstream embankment construction operations.

Trial results in MFT align well with the performance of mud farming operations using the MudMaster® in other tailings operations. This trial supports further investigations into improving deposition control and reducing costs through reduced application of traditional earthmoving equipment for MFT dewatering and lower flocculation dosage rates. Examples from other tailings operations (Figure 5) suggest that a similar performance level can be sustained at lower flocculation rates.

Although mud farming may not be ideally suited for all sites, the success displayed within these initial trials supports an expanded adoption of this technology on a larger-scale within the oil sands industry.

6 ACKNOWLEDGEMENTS

The authors would like to convey their gratitude to SRK Vancouver for their assistance in trial design, setup, sampling and analysis and to North American Construction Group for on-site support.

7 REFERENCES

United States Army Test & Evaluation Command, 1964. Final Report of Military Potential Test of Marsh Screw Amphibian (Plan A – M113). USA TECOM Project No. 7-5-0524-01-9.

Johnson, S. J., Cunny, R. W., Perry, E. B. and Devay, L., 1977. State of the Art Applicability of Conventional Densification Techniques to Increase Disposal Area Storage Capacity, Dredged Material Research Program, Technical Report D-77-4. Soils and Pavement Laboratory, U. S. Army Engineer Waterways Experiment Station.

Energy Resources Conservation Board, 2009. Directive 074: Tailings Performance Requirements for Oil Sands Mining Schemes. ERCB, Alberta, February, 2009.

Canadian Oil Sands Innovation Alliance, 2012. Technical Guide for Fluid Fine Tailings Management.

Munro, L. D. and Smirk, D., 2012. Optimising Bauxite Residue Deliquoring and Consolidation. Proceedings of the 9th International Alumina Quality Workshop. Perth, Western Australia, March 18-22, 2012.

The role of desiccation and rheology in optimizing operations for polymer-amended fine tailings disposal

S. Soleimani, S. Mizani & P. Simms
Carleton University, Ottawa, ON, Canada

W. Wilson
University of Alberta, Edmonton, AB, Canada

A. Dunmola
Shell Canada, Calgary, AB, Canada

ABSTRACT: Several oil sand operations have undertaken commercial scale demonstration of fine tailings dewatering technologies that utilize polymers. The application of polymer results in rapid water-release post-deposition or post-thickening. To meet regulatory requirements for shear strength development, however, such technologies all rely, to some degree, on post-deposition dewatering from desiccation, freeze-thaw, and/or consolidation. To maximize the contribution of desiccation, and to minimize drainage length, control over tailings deposit geometry is important. The goal of this study, which involves fieldwork at different demonstration trials for polymer-amended technologies, is to improve understanding of desiccation behaviour, how desiccation affects subsequent dewatering through consolidation, and how the rheology of polymer-amended tailings changes during deposition. The former will allow for optimization of lift geometry, while the latter will provide insight on how to improve control over such geometry. This paper reports preliminary field and laboratory work on polymer-amended tailings, which highlights the role of cracking in promoting evaporation, tracks how the materials densify during desiccation and subsequent consolidation, and provides information on how rheology of the tailings is influenced by polymer dosage, shearing and aging.

1 INTRODUCTION

The management of oil sands fine tailings (i.e., mature fine tailings) with current increasing volume of about 800 million m^3 is one of the key environmental challenges that need to be addressed by the industry (COSIA, 2012). In order to address this challenge, In 2009 the provincial oversight body (ERCB, 2009) introduced new regulations, Directive 74, to mandate that deposited tailings develop a shear strength of 5 kPa by one year after deposition, and be reclaimable within 5 years. Mature fine tailing (MFT) with a poor consolidation and settling behavior and approximate solid concentration of 35% remains practically the same for decades (Wells, 2011). Hence, operators examined different new technologies to reduce MFT inventory, enhance performance and reduce the cost of existing technologies. Some of these technologies currently being utilized are centrifugation, conventional thickening in a thickener, composite tailings or non-segregating tailings (recombining fine tailings with sands and flocculent) and in-line flocculation (COSIA 2012).

These viable technologies need some kind of post-deposition dewatering to promote dewatering through desiccation (evaporation, drainage, and/or freeze-thaw) and consolidation. The two most common tailings deposit type which is currently being utilized by operators are thin-layered and deep deposit. Initial dewatering for both deposit types relies on dewatering by chemical or mechanical treatment; however, the long-term dewatering is achieved by atmospheric evaporation and freeze thaw for thin-layered deposit and by consolidation and creep for

deep deposit (Fair, 2012). The site-by-site variable conditions such as the available area footprint, and the material characteristics defines the layer thickness and rate of deposit for thin-layered deposit. However, there is substantial room for optimization of layer thickness and drying time to improve sustainability of the operations and reduce footprints of tailings disposal areas. This project focuses on optimizing the deposition of flocculated MFT to enhance post-deposition drying and assess the relative contributions of desiccation and consolidation for varying deposition schemes.

Shell Canada's Atmospheric Fine Drying (AFD) technology, which involves the use of a chemical flocculent to improve settlement followed by bed drying, demonstrate potential application of MFT dewatering technology to enhance management of oil sands fine tailings at full scale production rates. Figure 1 illustrates in-line thickening operation at Shell Canada's Muskeg River Mines (MRM) where a rapid mixing of polymer occurs in a 17 ft pipeline. As it is shown in this figure, dewatering of the tailings starts rapidly during the deposition. Inline-flocculated MFT has usually about 40-45% solid few hours after discharge due to rapid initial dewatering. The understanding of initial dewatering mechanism of flocculated MFT and its relation with the flocculant dosage is important to improve operation and reduce costs. Hence in this study initially an attempt to quantify the mechanisms of water loss as it relates to the flocculant dosage was reported. This paper also details the improvement in understanding of the influence of cracking in promoting evaporation, and the effect of polymer dosage in slurry rheology and flow behavior. Also, preliminary field data obtained from pilot-scale inline-flocculated MFT deposition at Shell MRM are presented and recommendations to improve desiccation behavior are given.



Figure 1. In-line thickening operation at Muskeg River Mines (Shell Canada Energy)

2 MATERIALS AND METHODS

2.1 *Materials*

MFT and polymer used in this study were obtained from Shell Canada's Muskeg River Mine. The released water formed on top of MFT containers during the transportation were mixed thoroughly to bring them to their initial condition. The raw MFT had an initial solid content of 35.5% and sands to fines ratio of 0.27. The geotechnical of MFT is shown in Table 1. An anionic polymer, A3338, was used as the flocculant for fast dewatering of MFT samples. Flocculant Solution of 0.4% (w/w) were prepared by adding 4 gr of polymer to 996 gr of reclaimed water. Reclaimed water was also received from the Muskeg River Mines.

Table 1. Geotechnical properties of raw MFT

Property	**Value**
Specific gravity	2.50
Hydraulic conductivity (cm/s)	4.3×10^{-6}
D_{10}, D_{50}, D_{60} (microns)	0.8, 6.4, 11.1
Cu (D_{60}/D_{10})	14.1
Liquid limit (%)	83
Plastic limit (%)	28.7
Fines content (<44μm, %)	78.7

2.2 *Experimental methods*

2.2.1 *Column dewatering test*

Flocculated MFT were prepared using different dosages of polymer at 600, 725, 850, 1,000 and 1,200 g/ton to study the dewatering potential. To prepare flocculated MFT (polymer amended MFT) in the laboratory, Elite dual-speed mixer (VWR International) with four-blade impeller with radius of 8.5 cm was used at a fixed speed of 250 rpm. 1,800 g of MFT was mixed for 10 (s) with desired amount of 0.4% (w/w) flocculant solution based on the dosage. The performance of flocculation processes are usually evaluated using settling rate, supernatant turbidity or sediment compressibility (Hogg 2000). In the current study the release water and total solids of supernatant was measured as an indication of settling rate and supernatant turbidity, respectively. For this purpose, the flocculated MFT were poured in 500 mL graduated cylinders to a height of 0.3 m and covered to prevent evaporation. Measurement of released water was performed for longer time (i.e., 13 days) to investigate the dewaterability potential due to consolidation as well as sedimentation. Measuring total solid concentration of released water was performed on day 6 to evaluate the supernatant turbidity. Solid concentration was measured by oven drying of 15 mL of released water collected from the columns.

2.2.2 *Pilot -scale deposition of In-line Thickened Tailings*

To better understand how sequential layer deposition can improve dewatering and drying of in-line polymer amended tailings, a pilot-scale deposition was carried out at Shell atmospheric fines drying (AFD) site at Muskeg River Mine (MRM). For this purpose, two deposition cells with approximately 30 x 30 m dimension with a comparable height to area ratios were constructed. Tailings depositions started in August 2012 and will continue into the 2013 operational season (Figure 1). First deposition in both cells was carried out on 27th of August and second deposition in Thin-Lift cell was deposited on 3rd of October, 2012.

The focus of this test program was to compare geotechnical performance of the resulting deposits deposited in 0.5-0.7 m lift thickness with 1-1.5 m lift thickness. Hence, in 2012 two 0.5 m-lifts were deposited in the Thin-Lift cell and one 1 m-lift was deposited in the Thick-Lift cell. Schematics of deposition plan are shown in Figure 2. MFT collected from external tailings facility at Sell MRM was flocculated at 800 ppm in Thick-lift cell and at 845 and 900 ppm for the two deposited layers in Thin-Lift cell. The solid content of polymer amended MFT was increased instantly from 35.5% to 36.4% upon mixing of the polymer.

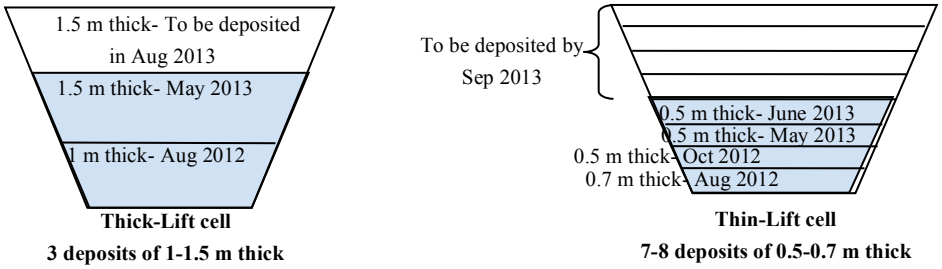


Figure 2. Schematics of deposition scheme for 2012-2013 depositions. The colored area shows the completed deposition so far.

2.2.3 *Sampling and Analysis*

Core and surface samples were collected after depositions for further analysis. Core samples were collected by a piston sampler. The samples were extruded at the site and cut into 7 cm pieces, waxed and placed inside the small jars for shipment to Carleton University. The core samples were used for determining the density, electrical conductivity (EC) and suction profile as well as some microstructural analysis.

To analyze the crack formation and their contribution to desiccation small amount of samples (~50 g) were collected from the surface of deposit at the crack edge, between the cracks and inside cracks. Surface samples were collected from top 2-3 cm of surface with a minimal disturbance during sampling.

EC was measured using saturation extraction method. In this method, tailing samples were mixed with a known amount of water for 20 minutes, then the water was extracted by centrifugation at 10000 rpm for 3 minutes. The measured EC of the effluent was extrapolated back to the tailing natural water content using the dilution factor (Fredlund, 2012). Total suction was measured using Chilled-mirror dew-point psychrometer, WP4 (Decagon Devices, Inc.).

3 RESULTS AND DISCUSSIONS

3.1 *Dewater-ability of flocculated MFT*

Flocculation effectiveness can be assessed based on the settling rate tests where the mud height over time is measured in large graduated cylinder (Mohler et al., 2012). The effects of flocculant dosages were investigated by measuring the release water from tailings prepared at different dosages. Figure 3 illustrates the water release and solid concentration as a function of flocculant dosages at different times. Although initially the dosage of 850 g/ton had the highest water release, dewaterabillity of the 725 g/ton started to exceed others after 6 days (Figure 3a). The same trend was observed for the solid content of flocculated materials over time (Figure 3b). This may be explained by the fact that at higher dosage, the floc structure may be stiffer and hence dewatering due to consolidation at this very low stress (5 kPa) is reduced. Jin et al. (2004) found that in wastewater sludge the dewaterability potential will be reduced by formation of bigger flocs and high viscosity of the material. It is also believed that high flocculant dosage increases the amount of free floc, consequently increases the negative charges.

Figure 4 shows the total solid concentration in the released water which is a representative of turbidity of the water and usually is used to evaluate flocculation performance. As shown in Figure 4, the most clear water was obtained at the flloculant dosage of 1,000 g/ton. Observation of high turbidity water can be explained by either inadequate flocculant dosage to provide particle neutralization for all the dispersed particles or improper mixing to break the formed flocs. Hence, it may be interpreted that at flocculant dosages of less than 1,000, the amount of flocculant was not enough to neutralize all the particle charges.

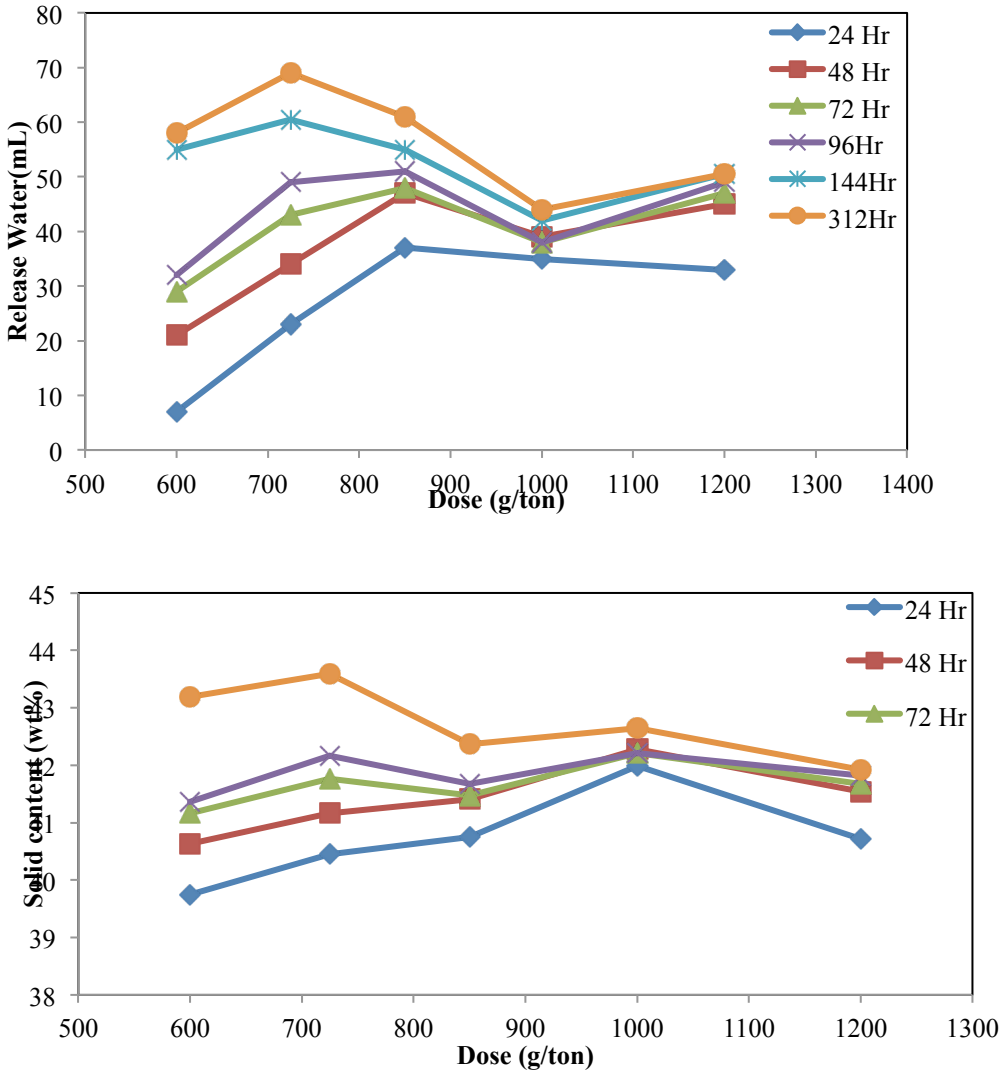


Figure 3. a) Solid concentration and, b) Water release as a function of flocculant dosage and time.

3.2 *Desiccation and Cracking*

Total suction and water content (presented as geotechnical gravimetric water content, GWC) was measured for surface sample collected at the crack edge (CE), between cracks (BC), inside crack (IC) and sites without any cracking (Figure 4). The results are further analyzed to obtain the average of the total suction, and water content at different sites of the tailings surface as shown in Table 2. According to this table higher suction and lower water content was observed where cracks were present. Also, the highest total suction of 626.7 kPa was observed on the crack edge where the highest evaporation might locally occur. The water content of tailings could significantly drop from 140% to 44 % due to the cracking (Table 2). It is impotent to note that for this material 55% GWC corresponds to 67% solids. Crack formation increased the desiccation rate rapidly. As shown in Table 2, after crack formation, it took only one week to reduce the average water content from 72% to 59% as the average total suction also increased by 74 % during this time.

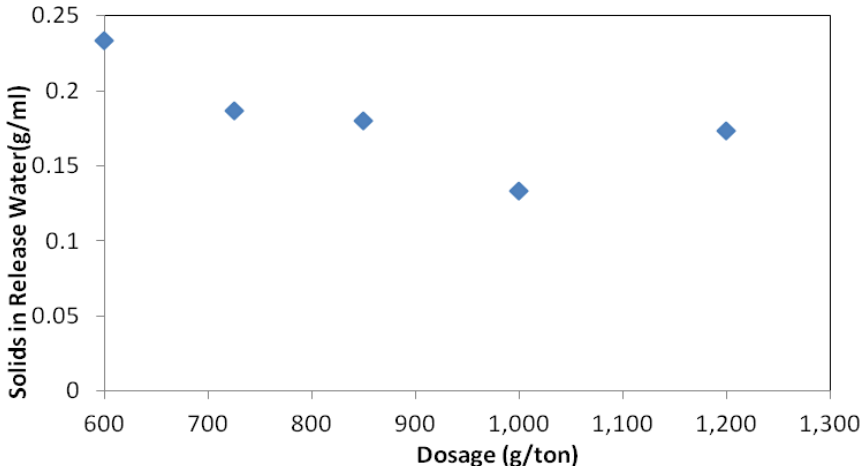


Figure 4. Total solid concentrations in released water as a function of flocculant dosage.

Table 2. Analyses of total suction and GWC at different sites of the tailing surface: where no cracks were present (no cracks), between cracks (BC) crack edges (CE) and inside cracks (IC).

		No crack	**BC**	**CE**	**IC**
After 42 days of deposition (2nd of Oct)	%Water content	111.9	55.2	56.8	64.3
	Suction (kPa)	80.0	174.0	152.0	195.0
After 48 days of deposition (8nd of Oct)	%Water content	87.8	45.6	44.1	54.3
	Suction (kPa)	281.7	510.8	626.7	370.0
2 days after the new deposition (5th of Oct)	%Water content	140.5	no cracks was formed		

The presence of dissolved ions in water decreases the soil vapor pressures, relative humidity, which then increases total suction. Osmotic suction which arises from the salt concentration in the soil pore water can be a significant portion of the total suction. Osmotic suction of tailing samples can be obtained by measuring the electrical conductivity of pore water. Electrical conductivity is related to osmotic suction using the USDA equation:

$$\pi(\text{kPa}) = 0.0191 * \left[EC \frac{microS}{cm}\right]^{1.074} \quad (1)$$

Table 3 presents the osmotic suction and conductivity values obtained from the surface samples at the crack sites. According to this table, the contribution of osmotic suction to total suction is significant. Relatively high local evaporation probably occurs initially at the crack edges, leading to the high accumulation of ions, and higher ionic conductivity. From both measurement dates, the highest osmotic suction was obtained at the crack edge. The relatively lower water content and EC inside the cracks comparing to the crack edge is due to the rainfall events causing the cracks to be filled with water.

3.3 *Ion Transport*

Measuring the electrical conductivity (EC) of the pore-water over the depth of core samples is helpful in understanding the movement of ions. The movement of ions is caused by the flow of water in the deposit; hence obtaining electrical conductivity profile is also helpful to identify the main mechanism of dewatering (i.e., evaporation, seepage drainage). Figure 5 shows the profile of electrical conductivities for the core samples collected from Thick and Thin-Lift cells. According to this figure, dewatering by evaporation is mainly happening at the top 20 cm of both samples as EC increases rapidly over the top 20 cm. also, water movement due to drainage is

mostly driven at the bottom 30-40 cm. As Figure 5 shows drainage caused a rapid increase of EC starting at the depth of 20 cm to 55 cm for Thin Multi- lift sample and from 75 to 95 cm deep for Thick lift sample. Through modelling, the EC data can be used as a tracer to resolve the contributions of evaporation and consolidation to dewatering.

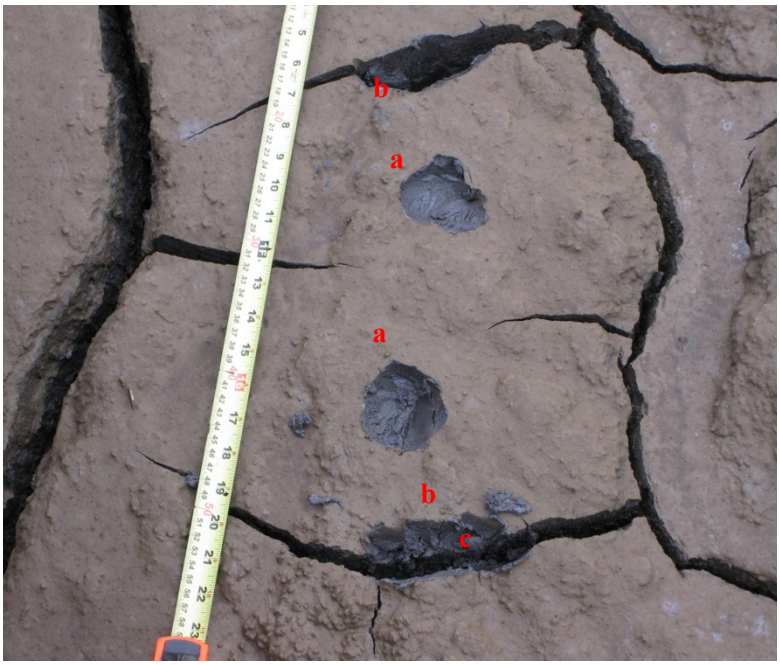


Figure 5. Surface of deposit showing the sampling areas; a) between cracks (BC), b) crack edge (CE), c) inside cracks (IC).

Table 3. Conductivity and Osmotic suction measurement of released water at different sites of the tailing surface: without any cracks, between cracks (BC) crack edges (CE) and inside cracks (IC). Data are average of measurement taken at two different days, 41 days after deposition(before the second deposition in Thin-Lift) and 48 days after deposition in Thick-Lift.

		No crack	**MC**	**CE**	**IC**
After 41 days of deposition (1st of Oct)	Total suction (kPa)	157.9	216.7	263.3	390.0
	EC (mS/cm)	2.5	3.6	5.2	2.5
	Osmotic (kPa)	83.4	126.9	187.2	86.7
After 48 days of deposition (8th of Oct)	Total suction (kPa)	281.7	510.8	626.7	370.0
	EC (mS/cm)	0.3	10.6	13.9	4.4
	Osmotic (kPa)	139.7	403.6	542.1	157.8

3.4 *Densification*

Density profiles of the two deposits with different lift thickness are shown in Figure 5. According to this figure slightly higher density was observed in the top and bottom portion of Thick-Lift deposits. The higher rate of density increase in the bottom of the deposits was likely due to self-weight consolidation (Figure 6).

Figure 5 illustrates the profile of solid content for Thin and Thick-Lift cell after approximately one month of deposition and slightly after the second deposition in Thin-Lift cell. After one month of drying, solid content was increased in the range of 45-59% and 46-58% for Thick and Thin-Lift deposit, respectively. The solid content was slightly higher for Thick-Lift deposit over the depth of the profile (Figure 7). Deposition of second layer of wet tailings immediately increased the solid content of the lower layer to some extent (Figure 7).

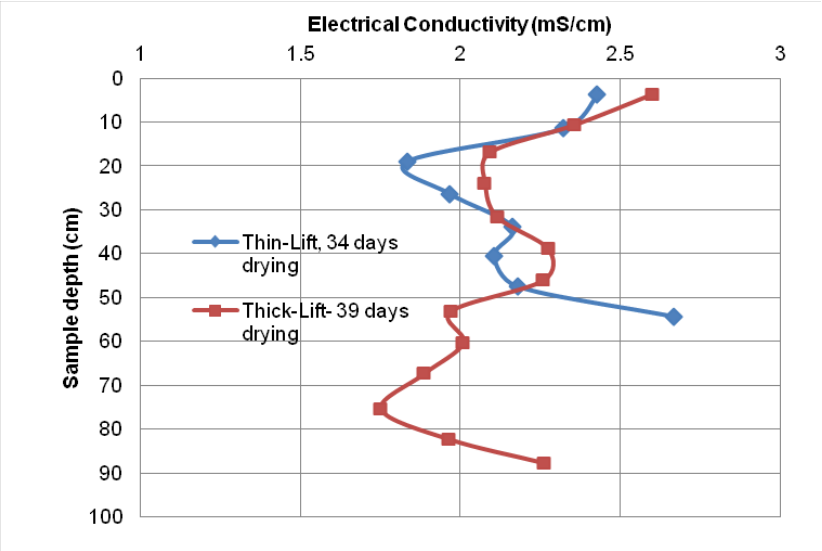


Figure 6. Profile of electrical conductivity of pore water for sample taken from Thick and Thin-Lift cells (sample taken on 1 and 5 of Oct, 2012 for Thin and Thick-Lift cell, respectively).

3.5 *Rheological behaviour*

The rheology of the flocculated MFT at different dosages was investigated using an Anton Paar Physica Rheometer by either stress growth technique with a constant shear rate of 0.1 (s^{-1}) or decreasing shear stress technique where a constant stress is applied for 30 seconds in a decreasing step. The measured yield stresses were then compared with yield stress obtained by slump test as shown in Table 4. Stresses obtained from the various techniques for dosages in the range of 600 to 1,200 g/ton are given in Table 4. As expected there is an increase in yield stress with increase in flocculant dosage. From the rheology measurements it can be seen that a closer agreement is obtained between the yield stress values measured from the slump and the decreasing shear stress test. That is due to the similarity of these two tests, where the yield stress is actually measured after shearing the material.

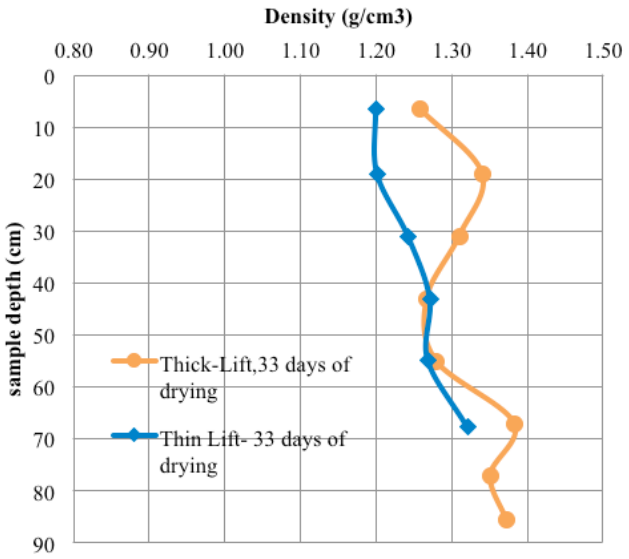


Figure 7. Density profile of deposit in Thick and Thin-Lift deposition cell after almost one month of drying (sample taken on 30 Sep, 2012).

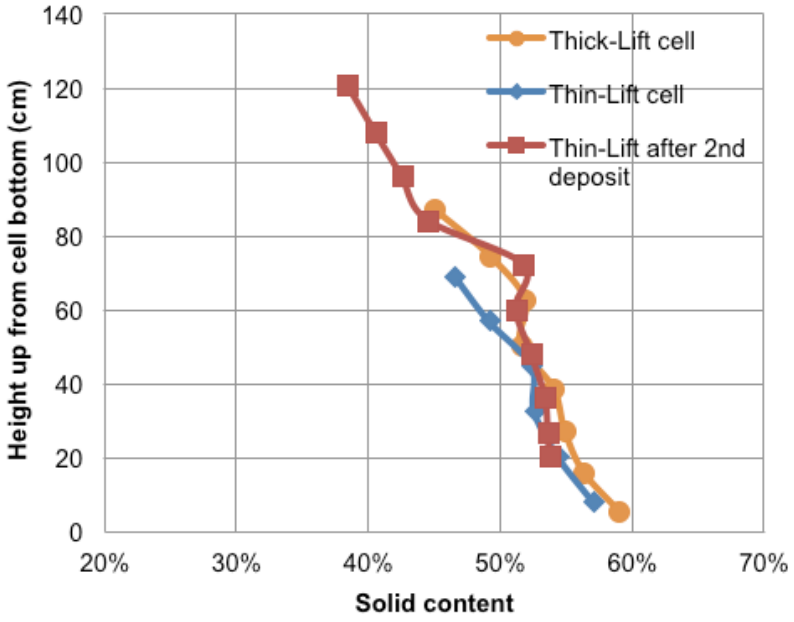


Figure 8. Profile of solid content in Thick and Thin-Lift deposition cell after almost one month of drying (sample taken on 30 Sep, 2012) and slightly after the second deposition in Thin-Lift cell (sample taken on 6 Oct, 2012).

Table 4. Yield stress measured from various techniques

Dosage (g/ton)	Slump (Pa)	Method of measurement: Stress growth Max stress(Pa)	Decreasing shear stress: Starting shear stress (Pa)	Decreasing shear stress: Interpreted yield stress (Pa)
MFT	-	28.0	100	10
600	92	207	200	50-100
725	125	323	450	50-100
850	154	510	700	50-100
1,000	163	1,020	1,000	250
1,200	187	1,180	1,300	-*

* Unable to detect yield stress due to high shear intensity and overflowing of tailings out of the measuring cup

Figure 8 illustrates the tailings profile deposited at one of the operational scale Shell Atmospheric Fine Drying cell during the Fall 2010 program. Total volume of tailings deposited in this cell was 7953 m3 with an average slope of 2.1%. Lubrication theory, a simplified form of the momentum and continuity equations, was used to model the steady state of tailings flow. The steady state profile of a Bingham fluid on inclined surface can be determined by Lubrication theory through (Liu and Mei 1990):

$$h' - h_0' + \ln(1 - h') = x' - x_0' \qquad (2)$$

Where h' and x' are defined as

$$h = h'\left(\frac{\tau_y}{\rho g \sin\theta}\right) and\ x = x' cot\theta \left(\frac{\tau_y}{\rho g \sin\vartheta}\right) \quad (3)$$

and ρ is the density, τ_y is the yield stress. h and x is the height and distance of the free surface and are measured vertically and horizontally from the discharge point, respectively.

In Figure 9, two different values of yield stress, 100 Pa and 240 Pa was used to fit Lubrication theory to the run-out curve. The first value is representative of yield stress measured by controlled stress rheometry with decreasing levels of stress (Mizani et al., 2013). The second value better predicts the maximum thickness of the deposit while the smaller yield stress value better predicts the maximum run-out. As the material is highly thixotropic over the timescale required for deposition (5 days), it is not surprising that a single yield stress value cannot capture the shape. The further shearing of the material as it flows down the beach cannot be ruled out as an explanation – this will investigated in further laboratory and field investigations.

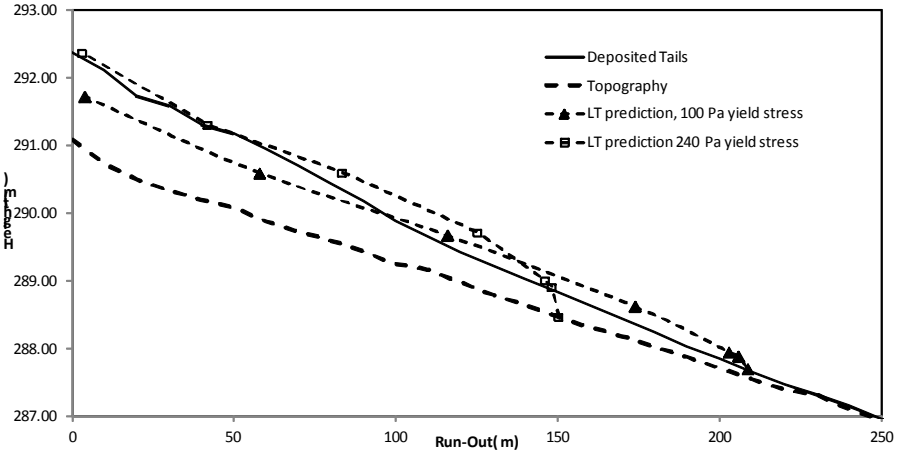


Figure 9. Tailings profile measured at Shell Atmospheric Fine Drying operation; predictions were modelled using lubrication theory (LT)

4 SUMMARY AND CONCLUSIONS

The oil sands operators have committed to commercially implement the necessary tailings management technologies to satisfy regulatory obligations. Polymer-amended tailings technology is one of these promising technologies which has been implemented or investigated by several operations. This project aims to help optimize such operations by undertaking field and laboratory investigations to examine the role of polymer on rheological, desiccation, and consolidation behaviour of polymer amended MFT. Preliminary field and laboratory studies reveal a number of interesting findings:

i) Identifying the proper concentration of polymer to achieve the optimized dewatering potential is essential to reduce costs and enhance rheology of the tailings. Dewaterability of the polymer amended MFT at different polymer dosage suggests that the increase in polymer concentration does not significantly enhance water release at high polymer dose. The highest water release was observed at polymer concentration of 725 g/ton.

ii) Surface measurements of total and osmotic suction suggest that the role of cracking may significantly influence the evaporative boundary condition. This will be further explored using simulations of multilayer deposition of AFD material in the laboratory in 1.5 m by 1.5 m plan area drying box tests (such as undertaken by Daliri et al. 2012).

iii) Osmotic suction is a substantial contributor to total suction at the surface. As evaporation is a function of total suction, the contribution of pore-water chemistry to the evaporative behaviour will be investigated further.

iv) Profiles of EC with depth show accumulation of ions near the surface and at the bottom of the deposits. While the former can be attributed to evaporation, the latter may be due to simply densification at the bottom of the layer. This data will be used as a target for coupled consolidation – mass transport numerical simulations, which will help resolve contribution of desiccation and consolidation to dewatering.

v) Investigation of rheology of the material and a simple analysis of deposit geometry illustrates the importance of properly characterizing both the shear history, and the evolution of the strength of the material immediately after it comes to rest. Future work aims to use CFD codes to account for thixotropic effects and investigating their applicability to the operational scale.

5 ACKNOWLEDGEMENTS

The authors would like to thank Shell Canada Research for providing access to Shell MRM site and Shell and Barr Engineering personnel for sampling support. This research is financially supported by NSERC and COSIA. Analysis of field samples was conducted at Carleton University with the assistance of laboratory technical staff and undergraduate student, Manuel Sanchez Sardon.

6 REFERENCES

COSIA 2012. Technical Guide for Fluid Fine Tailings Management, access online at http://www.cosia.ca/uploads/files/Projects/Tailings/Tech_Guide_Fluid_Tailings_Mgmt_30%20Aug%202012_COSIA.pdf

Daliri, F., Manlagnit, A. Dunmola, A., Simms, P. 2012., S. Sivathaylan. 2012 Laboratory simulation of desiccation, settling, and consolidation in variably thick multilayer deposits of high-density tailings The influence of desiccation on geotechnical stability of thickened tailings. In Proceedings of 2012 Canadian Geotecnical Conference in Winnipeg, Manitoba, September 2012.

ERCB 2009. Directive 074- Tailings Performance Criteria and Requirements for Oil Sands Mining- Energy Resources Conservation Board of Alberta.

Fair, A. 2012. Collaboration in Canada's oil sands: fluid fine tailings management. Third International Oil Sands Tailings Conference 2012, December 2-5, Edmonton, Alberta.

Fredlund, D. G., Rahardjo H., Fredlund M. D. 2012. Unsaturated soil mechanics in engineering practice Hoboken, N.J. : John Wiley & Sons, c2012..

Hogg, R. (2000) Flocculation and dewatering. International Journal of Mineral Processing, 58:223-236.

Jin, B., Wilén, B. M. and Lant, P. (2004) Impacts of morphological, physical and chemical properties of sludge flocs on dewaterability of activated sludge. Chemical Engineering Journal, 98(1), 115-126.

Mizani, S., Soleimani, S., Simms, P. 2013. Effects of polymer dosage on dewaterability, rheology, and spread-ability of polymer-amended MFT, paste and thickened tailings conference. 17-23 June, 2013, Brazil.

Mohler, C.E., Poindexter, M.K., Atias, J., Chen, W., Witham, C.A .(2012) Development of flocculants for oil sands tailings using high-throughput techniques. Third International Oil Sands Tailings, Edmonton, Canada

Wells, P.S. 2011. Long Term In-Situ Behaviour of Oil Sands Fine Tailings in Suncor's Pond 1A, Proceedings of Tailings and Mine Waste, Vancouver, BC, November 6 to 9, 2011

Determination of geotechnical properties of in-line flocculated fine fluid tailings for oil sands reclamation

Louis Kabwe & G. Ward Wilson
Civil & Environmental Engineering, University of Alberta, Edmonton, AB, Canada

Robert Donahue
Applied Geochemical Engineering Inc, Edmonton, AB, Canada

ABSTRACT: This paper describes large strain consolidation tests performed on in-line flocculated fine fluid tailings (ILF-FFT) thin lift deposits from Syncrude's Mildred Lake Settling Basin. Two important characteristics of the large strain consolidation test, compressibility and hydraulic conductivity (k), were measured directly. The compressibility plots (the void ratio - effective stress relation (e-σ')) of the ILF-FFT indicate an overconsolidation stress (i.e. e starts decreasing significantly only at σ' over 1 kPa). Therefore, σ' has to exceed 1 kPa for consolidation to take place. Results show that the k-e relation for the ILF-FFT thin lift deposits can be predicted with a power law mathematical equation, with a high correlation coefficient (R^2: 0.99). This information can provide an important tool in the evaluation of FFT consolidation behaviour.

1 INTRODUCTION

Syncrude and TOTAL E&P Canada conducted a large field trial for in-line flocculated fine fluid tailings (ILF-FFT) incorporating centrifugion and thin lift deposition of FFT from July 2010 to October 2010 at the Mildred Lake Settling Basin near Fort McMurray, Alberta (Wilson et al. 2011). The objective of the research was to evaluate these two methods of de-watering the FFT in order to increase the solids content and shear strength of the material during and following deposition. A sampling program was conducted March 22-23, 2010, to collect frozen cores from various cells for laboratory determination of ILF-FFT geotechnical properties at the Geotechnical Centre at the University of Alberta (UofA). This paper focuses mainly on evaluating the geotechnical properties of the ILF-FFT thin lift deposits core samples. Some of the mineralogical tests were carried out by AGAT Laboratories Ltd. in Calgary, Alberta, and results from AGAT Laboratories' report is presented in this paper.

2 MATERIALS AND METHODS

2.1 *In-Line Flocculated Fine Fluid Tailings (ILF-FFT)*

Samples of ILF-FFT were collected and transported to the UofA Geotechnical Centre during the field trial at the Mildred Lake Settling Basin to investigate their geotechnical properties. ILF-FFT involves the injection of flocculant into the pipeline at a given distance upstream from the discharge point to allow the required mixing and contact to take place within the pipe. Mixing and shear during transportation allow the formation of clay flocs. The slope of the depositional beach promoted immediate de-watering by ensuring that the decant waters rapidly drained to the

toe of the thin lift layer as the tailings settled. Further de-watering continued through drainage and evaporation, and continues today over the long term.

2.2 *Frozen Core Samples*

Frozen cores were collected from Cells 28, 29 and 32 at the Mildred Lake Settling Basin during March 22 and 23, 2010 (see Figure 1). Samples were delivered frozen to the UofA Geotechnical Centre and kept in a cold room prior to testing.



Figure 1. Frozen core sample collected from a cell at the Mildred Lake Settling Basin, Syncrude.

Frozen cores were machined (cut and trimmed) to a diameter of about 100 mm and to a height no less than 70 mm and no greater than 140 mm.

2.3 *Mineralogy*

The mineralogical analysis of the ILF-FFT was not conducted in this study. Results presented in this paper were collected from Syncrude in 2010.

2.4 *Bitumen Content*

The bitumen content on a total mass basis was determined on the ILF-FFT sample using a modified Dean Stark method (AGAT Laboratories Ltd.). The Dean Stark bitumen removal process requires driving off all the water from the sample as well as removing the bitumen by refluxing the sample with toluene in a modified Stark Extractor. This method uses a dispersant agent to separate the clay fraction.

2.5 *Particle Size Distribution (PSD) Measurements*

Dispersed and non-dispersed Hydrometer-Sieve tests were conducted on the ILF-FFT samples. The objective of the non-dispersed test is to not disperse the polymer flocculated FFT clay flocs any more than what they were in the 2010 field study. The non-dispersed test was also conducted to compare results with the methylene blue (MB) value. A modified ASTM Standard Hydrometer-Sieve Test Method was used to measure the PSDs of the ILF-FFT. The amount of fines (<45 μm) was determined by sieving, and the amount of clay-size (<2 μm) material was determined by hydrometer.

2.6 *Methylene Blue (MB) Test*

The MB adsorption value was determined by AGAT Laboratories Ltd. to assess the degree of dispersion of active clays. MB is a cationic dye that can be adsorbed on the exposed negatively charged surface of clays and is routinely used to measure exposed surface area of clays in soils.

2.7 *Atterberg Limits Measurements*

The liquid limit (w_L) and plastic limit (w_P) were determined for the ILF-FFT following the procedure outline in ASTM D 4318-05 (ASTM 2005a). The water content was lowered by evaporation to the liquid and plastic limit ranges, as suggested in the procedure. The tests were performed quickly to minimize the effect of thixotropy (as tailings are known to exhibit a very rapid thixotropic gain in strength).

2.8 *Large Strain Consolidation*

The large strain consolidation test directly measures two important characteristics: the compressibility and hydraulic conductivity of the slurry. Figure 2 shows the large strain consolidation test apparatus. The cell has a 140-mm inside diameter and can accommodate samples up to 200 mm in height. The wall friction is minimized by choosing the appropriate initial height of the samples so that the diameter to height ratio is acceptable when effective stresses develop. A multi-step loading test was used in the consolidation test. Specimen deformation under each stress increment, and the saturated hydraulic conductivity (k) was measured using a constant head test at the end of consolidation for each load increment.

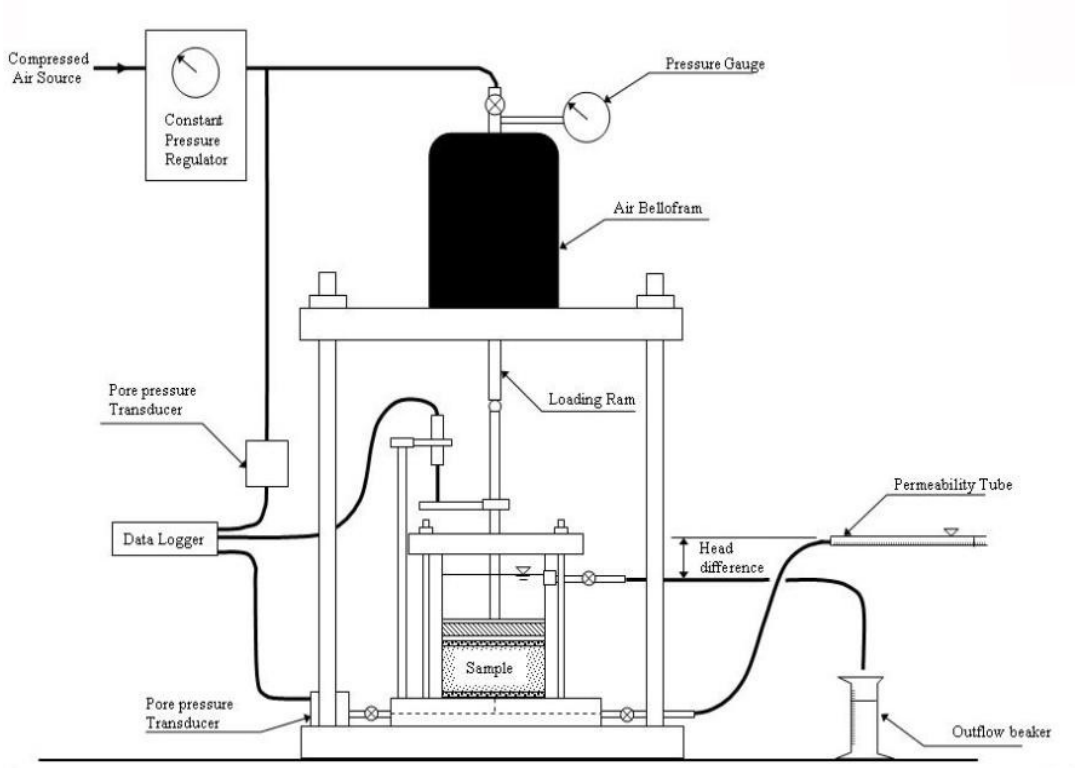


Figure 2. Schematic of the University of Alberta large strain consolidation test apparatus.

3 RESULTS AND DISCUSSIONS

3.1 *ILF-FFT Slurry Sample Testing*

3.1.1 *Mineralogy*

The FFT used in the 2010 field project had solids >70% (by weight) clay. The feed mineralogy consists of 28.1% kaolinite (K+S) and 1.0% illite (I+S). Other minerals present include anatase (3.0%), calcite (0.1%), rutile (3.0%), siderite (2.2%) and quartz (36.3%) (Syncrude 2010).

3.1.2 *Bitumen*

The bitumen content determined in the ILF-FFT sample by the Dean Stark method was found to be 1.22% based on total mass (AGAT Laboratories Ltd.).

3.1.3 *Particle Size Distribution (PSD)*

Figure 3 shows both the dispersed and non-dispersed Hydrometer-Sieve PSDs of the ILF-FFT samples. The amounts of clay-size (<2 μm) material determined by hydrometer for the dispersed and non-dispersed averaged 47% and 37%, respectively. The amounts of fine (<45 μm) material determined by hydrometer averaged 75% and 66% for the dispersed and non-dispersed samples, respectively. The comparison between the dispersed and non-dispersed hydrometer tests show a difference of 10% in the amount of clay-size (<2 μm) material. The remainder of the clay in the non-dispersed hydrometer must be in the form of peds and booklets coarser than 2 μm (Scott and Jeeravipoolvarn 2004), as not all clay peds are dispersed in this laboratory test procedure. The non-dispersed test should more accurately reflect the PSDs of the FFT as they were in the 2010 field studies. This ILF-FFT is mainly silt-clay with a sand to fine ratio (SFR) of about 0.6.

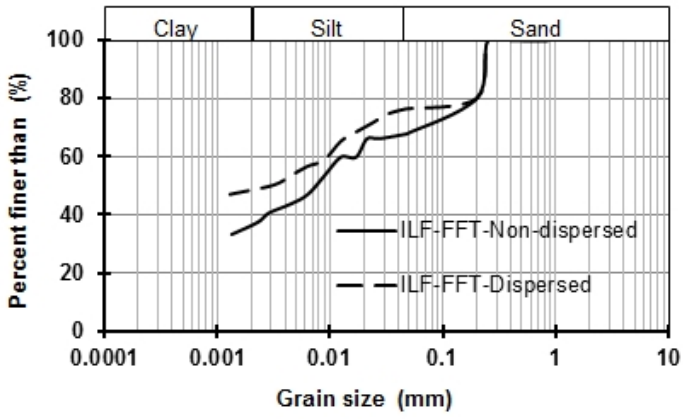


Figure 3. Particle size distributions (dispersed and non-dispersed) for the in-line flocculated fine fluid tailings samples.

3.1.4 *Clay Fraction by MB Test*

It should be noted that the MB test was conducted on a dispersed ILF-FFT sample (AGAT Laboratories Ltd.). The quantity of exposed clay mineral in the sample can be calculated using an empirical relationship developed for oil sands tailings (Morin 2008) given below:

$$\text{Clay mineral fraction (\%)} = [(0.006)(\text{MB value}) + 0.04]/0.14 \quad [1]$$

Results yield a value of 48% of clay fraction in the ILF-FFT sample. This value is very close to the value of 47% determined in the dispersed PSD curve in Figure 3.

3.1.5 *Atterberg Limits*

The w_L and w_P for the ILF-FFT tested were 51% and 24%, respectively, with a plastic index (I_P) of 26%. Thus, the ILF-FFT would be classified as a high plastic clay. It is known that the w_{Ls} of fine tailings are influenced by the water chemistry, clay mineralogy and bitumen content (Suthaker and Scott 1996). It should be noted that the polymer adsorbs water, so it increased the w_L of the sample by about 15%; as a result, the I_P increased. A kaolinite-dominated soil should plot as a low to medium plastic soil, but the addition of polymer artificially raised the liquid limit. Therefore, it plots as a high plastic clay, but does not exhibit any of the volume change characteristics of a high plastic clay.

3.2 *ILF-FFT Frozen Cores Samples Testing*

3.2.1 *Solids Content*

Table 1 shows the bulk densities and solids content of the ILF-FFT core samples measured by oven drying at 105°C for 24 h. For geotechnical purposes, solids content is defined as the mass of tailings solids (the nonwater portion of the tailings consisting of bitumen and mineral solids) divided by the total mass of the tailings. It should be noted that the bitumen is such a heavy hydrocarbon that there is negligible evaporation at 105°C. Solids content ranges from 43.55 to 56.94%. The data indicates that the solids contents were higher at the bottom of the deposits across the three cells. It should be noted that the solids content upon deposition of the ILF-FFT in Cell 32 (e.g. sample 32-A-3) on September 2, 2010, was about 32% (results not presented here). The solids content measured from the core sample had increased by 44% from its initial value of 32% to a value of 56.94%. Matthews et al. (2011) observed a similar trend in their field trial of thin lift deposition and suggested a consolidation mechanism with bottom drainage as the primary mechanism for densification in their studied cell.

Table 1: Measured bulk densities and solids content of selected thin lift frozen cores samples.

Sample ID	Bulk Frozen Density	Position	Solids Content
	(g/cc)		(%)
28-C-3	1.2	Top	44.93
		Bottom	47.60
29-A-2	1.29	Top	50.74
		Bottom	59.60
32-A-1	1.33	Top	59.44
		Bottom	64.06

3.2.2 *Large Strain Consolidation Tests*

The large strain consolidation test was used to directly measure the compressibility and hydraulic conductivity (the relations between e-σ‘ and k-e, respectively) of the ILF-FFT cores samples. One unloaded step (self-weight effective stress) and five load steps ranging from 1.25 to 50 kPa were performed. Cores samples were thawed in the consolidation cell at room temperature prior to the consolidation test.

Figures 4 and 5 show the compressibility plots from the large strain consolidation test plotted on normal and log scales, respectively, in order to more clearly visualize the curve trends. Since approximately one-half of the volume decrease of the consolidation specimens occurred during self-weight consolidation, it is important therefore to include this change in void ratio in the log effective stress versus void ratio relationship for the fine tailings (Miller et al. 2010). The log minimum σ’ was chosen at 0.01 kPa (Figure 5) as most of the self-weight consolidation data occurs at σ’ from 0.01 to 0.13 kPa. Figure 5 shows that the e does not change significantly with

increasing σ' up to 1 kPa. A significant σ' starts to develop at an *e* of about 2. This indicates an overconsolidation stress (Suthaker and Scott 1996; Jeeravipoolvarn 2005). The overconsolidation pressure of the fine tailings is believed to be caused by the high thixotropic gain in strength of the material (Scott et al. 2008). Therefore, the σ' has to exceed 1 kPa for consolidation to take place. At 50 kPa effective stress, the magnitudes of the consolidation for all the specimens become similar.

By fitting a power law mathematical equation (equation 2) to the data points (Figure 5),

$$e = A\,\sigma'^{B} \qquad [2]$$

where, *e* is the void ratio, σ' is the effective stress, and A and B are fitted parameters, it is found that this model cannot be utilized with a high coefficient of determination (i.e. $R^2 = 0.7$) for the thin lift ILF-FTT tested samples.

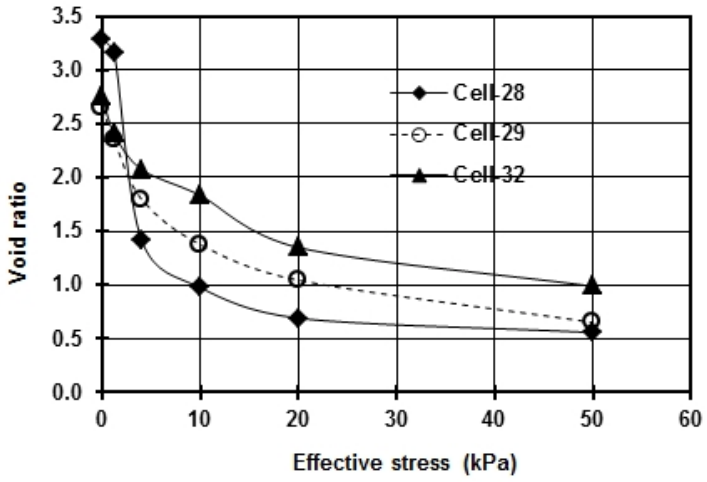


Figure 4. Effective stress (σ') versus void ratio (*e*) from the large strain consolidation test.

Other researchers (Jeeravipoolvarn et al. 2009) noted that the compressibility plot of oil sands fine tailings usually indicates an overconsolidation pressure and, therefore, the use of a Weibull function is more representative than the power function. The σ'-*e* relation in the form of Weibull function can be expressed as:

$$e = A - B\exp(-E\sigma'^{(F-1)}) \qquad [3]$$

where, *e* is void ratio, σ' is effective stress in kPa and A, B, E and F are fitted parameters.

A constant head, upwards flowing permeability step was performed after each load step. Figure 6 shows the relationship between k-*e*. The k decreases exponentially as *e* decreases. By fitting a mathematical equation to the data points, it is found that a power law model can be used to predict the change of k for the thin ILF-FFT samples tested:

$$k = A\,x^{B} \qquad [4]$$

where, k is the hydraulic conductivity, *e* is void ratio, and A and B are fitted parameters. The power law yields the prediction equations with high correlation coefficients for thin lift ILF-FFT samples tested:

$$k_{c28} = 4\text{x}10^{-09}\,e^{6.45};\ (R^2 = 0.997) \qquad [5]$$

$$k_{c29} = 4\text{x}10^{-09}\,e^{7.94};\ (R^2 = 0.903) \qquad [6]$$

$$k_{C32} = 2x10^{-10}\, e^{7.89};\ (R^2 = 0.903) \quad [7]$$

At *e* of about 2 where a significant σ' starts to develop, k is in the range of about 10^{-8} m/s.

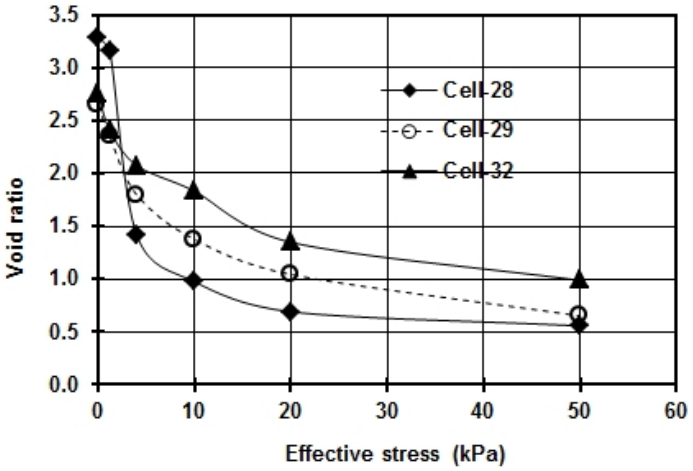


Figure 5. Void ratio (*e*) versus effective stress (σ') (log scale) from the large strain consolidation test.

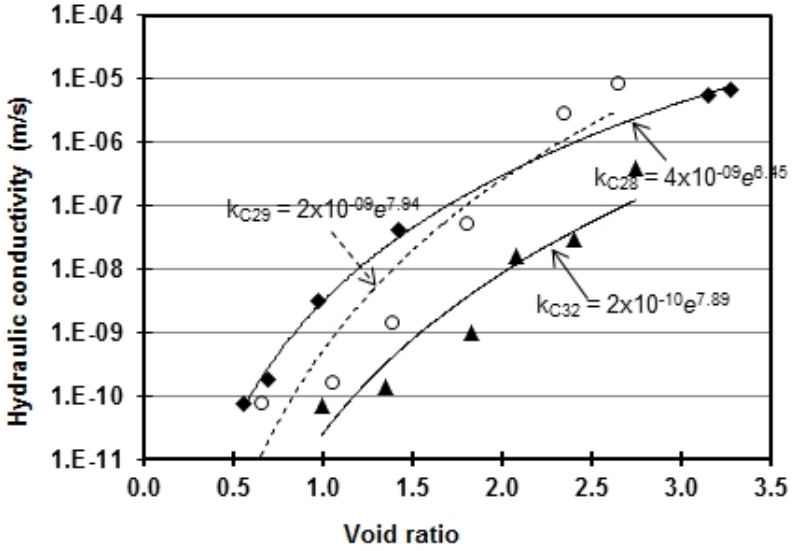


Figure 6. Hydraulic conductivity (k) versus void ratio (*e*) measured from the large strain consolidation test.

It is known that the k for the oil sands tailings is controlled by the fines content (Jeeravipoolvarn et. al. 2009). The difference in the slopes usually reflects the changes in the sand content in the samples.

In summary, results show that there is no significant change in *e* (i.e. *e* ~2.5) with increasing σ' up to 1 kPa and where the k value is large in the range of 10^{-8} m/s. However, at σ' over 1 kPa (i.e. from 1 to 50 kPa), both *e* and k start decreasing rapidly to their lowest values of 0.6 and 10^{-10} m/s, respectively.

4 CONCLUSIONS

The ILF-FFT frozen core samples tested indicate an increase of more than 40% in solids content over a period of five months including the winter period. The data also indicates that the solids content was higher at the bottom of the deposits, which suggest a consolidation mechanism with bottom drainage.

The compressibility plots (e-σ') indicate an overconsolidation pressure, where e does not change significantly with increasing σ'. But at σ' over 1 kPa, both e and k start decreasing rapidly to their lowest values.

It is found that a power law can yield the prediction equations of k-e with good correlation coefficients for the ILF-FFT tested.

It should be noted that the test results are only valid for ILF-FFT with the same mineralogy and flocculent type and dosage used during the pilot plant trial at the Mildred Lake Settling Basin between September and October 2010.

5 ACKNOWLEDGEMENTS

Funding for the field work was provided by Syncrude and TOTAL E&P Ltd. Thanks to Chenxi Zhang who assisted in the initial set up of the large strain consolidation test. Many thanks to Dr. J. Don Scott who reviewed this paper and provided some technical suggestions. Thanks to Vivian Giang who assisted in the editing and final preparation of this paper.

6 REFERENCES

Jeeravipoolvarn, S. 2005. Compression behavior of oil sands tailings. M.Sc. Thesis, Department of Civil and Environmental Engineering, University of Alberta, Edmonton, Alberta.

Jeeravipoolvarn, S., Scott, J.D. and Chalaturnyk, R.J. 2009. 10 m standpipe tests on oil sand tailings: long-term experimental results and prediction. *Canadian Geotechnical Journal*, 46: 875-888.

Matthews, J.G., Dhadli, N., House, P. and Simms, P. 2011. Field trials of thin-lift deposition of amended mature fine tailings at the Muskeg River Mine in Northern Alberta. *Proceedings of Paste 2011*, Perth, Australia.

Miller, W.G., Scott, J.D. and Sego, D.C. 2010. Effect of Extraction Water Chemistry on the Consolidation of Oil Sands Fine Tailings. *Canadian Institute of Mining, Metallurgy and Petroleum Journal*, 1(2): 113-129.

Morin, M. 2008. *AST methylene blue procedure: Sludge and slurries*. Ottawa, ON: Natural Resources Canada's Canada Energy Technology Centre, Advanced Separation Technologies, Tailings and Emulsions.

Scott, J.D., Jeeravipoolvarn, S. and Chalaturnyk, R.J. 2008. Tests for Wide Range of Compressibility and Hydraulic Conductivity of Flocculated Tailings, *Proceedings of the 61st Canadian Geotechnical Conference*, September 22-24, Edmonton, AB, pp. 738-745.

Scott, J.D. and Jeeravipoolvarn, S. 2004. Evaluation of Particle Size Distribution Test Methods for Albian Sands Tailings. Research Report prepared for Alberta Energy Research Institute, Albian Sands Energy Inc., and Canadian Natural Resources Ltd. April 12. Geotechnical Centre, Department of Civil & Environmental Engineering, University of Alberta, 12p.

Suthaker, N.N. and Scott, J.D. 1996. Measurement of hydraulic conductivity in oil sand tailings slurries. Canadian Geotechnical Journal, 33(4): 642-653.

Wilson, G.W., Kabwe, L.K., Donahue, R. and Lahaie, R. 2011. Field performance of in-line floccuilate fine fluide tailings using thin lift deposition. *Proceedings of Mine Closure 2011*, Lake Louise, Alberta, Canada.

Influence of surface cracking and salinity on evaporation in an oil sands thickened tailings

Tessa Innocent-Bernard & Paul Simms
Department of Civil and Environmental Engineering, Carleton University, Ottawa, ON, Canada

Andrea Sedgwick, Heather Kaminsky, & Xiaoli Yang
Total E&P Canada Ltd. – Calgary, AB, Canada

ABSTRACT: Evaporation in oil sands thickened tailings is a significant contributor to strength gain and volume change. However, it is affected by both pore water salinity and surface cracking. Salinity shuts down evaporation due to the precipitation of salts on the surface and by an increase in the total suction near the surface. Surface cracking facilitates drying through the exposure of wet underlying material with lower suction and provides a new path for water to evaporate from the tailings. This study tracks both phenomena using a multilayer deposition simulation in a sandbox sized (1 m by 0.7 m in plan) experiment. The presence of previously desiccated tailings accelerates both initial water loss and volume change in the fresh layer..

1 INTRODUCTION

In an effort to confront the poor consolidation of fine tailings produced from the surface mining of oil sands, and to meet regulated targets for undrained shear strength post-deposition (ERCB, 2009), Total E&P Canada Ltd.(referred as Total below), is piloting thickened tailings technology for dewatering the fine fraction of their tailings. With the aid of flocculants in a thickener, tailings are produced with a solids concentration ranging from 50 to 55%. To allow for reclamation within a reasonable time, Total is investigating tailings that will be deposited in lifts (<1m) where further dewatering and strength gain is expected through the processes of evaporation, freeze-thaw, and consolidation to allow for reclamation within a reasonable time. This study investigated dewatering in relatively thin (~0.2 m) lifts by evaporation and consolidation by simulating multi-lift deposition in 1 m by 0.7 m plan area experiment.

Evaporation is known to decrease with time as tailings (or soils) dewater, and is influenced by both salinity and crack surface crack dynamics (Chen 1992, Fujiyasu et al. 2000, Simms et al. 2007, Fisseha et al, 2010). This study attempted to quantify the influence of both these phenomena on evaporation from thickened fine oil sands tailings from Total E&P's pilot program.

1.1 *Background - Salinity and evaporation*

Water driven to the surface during evaporation in saline tailings (or soils) leaves behind the dissolved ions contained in it, contributing to increasing osmotic suction. Additionally, as the ion concentration near the surface approaches the solubility limit of constituent mineral phases, the salts precipitate along the pores, cracks and on the surface. Several authors (Chen 1992, Fujiyasu & Fahey 2000, Fujimaki et al. 2006, and Shimojima et al.1996) have shown that these solute driven phenomena can lower the evaporation rate by as much as 90%. The mechanisms that suppress evaporation may include an increase in albedo, the depression of the vapour pressure gradient due to increased osmotic suction at the surface, and the physical obstruction by salt precipitates to moisture flow (Fujiyasu & Fahey 2000, Simms et al. 2007, Fissheha et al. 2010, Dunmola & Simms 2010). Simms et al. (2007) reported that salts at the surface shut down

evaporation three (3) weeks after the start of a single layer field deposition trial at the Bulyanyulu mine in Tanzania. Although the authors measured an increase in albedo, they concluded that it was not the sole contributor. .Dunmola (2012) surprisingly found that for high total suctions (> 1 MPa), the osmotic to total suction ratio exceeded was the dominant contributor (> 60%) to total suction at high values of total suction (> 1 MPa) in a gold tailings. Dunmola (2012) also found that total suction can be capped in some saline soils or tailings by the solubility limit of precipitating minerals phases, but further drying beyond this limit, correlated with mineral precipitation, reduces the evaporation rapidly to a low residual value. Fujiyasu and Fahey (2000) observed a significant decrease in evaporation in a clayey tailings as a result of crust formation due to the rapid accumulation of salts at the tailings surface irrespective of the initial salt concentrations of the tailings under study.

This study sought to investigate the transport of solutes, their precipitation and their contribution to the reduction in evaporation for thickened fine oil sands tailings in a thin-lift deposition operation. The effect of albedo is not studied here as the tests were carried out in a controlled laboratory setting where the contribution of short-wave radiation to evaporation is negligible.

1.2 *Background – Surface cracking and evaporation*

Results from both laboratory and field tests conducted by Adams & Hanks (1964) suggest that cracks intensify water loss from soil. Once formed the cracks present a new network of macropores which play a major role in the infiltration of water into the soil during a rainfall event and also act as channels for water flow during evaporation, particularly in the case where surfaces become less permeable. Fujiyasu et al (2000), in a field investigation of evaporation from highly clayey (60% kaolinite, Liquid Limit (LL) of 96%) fresh water tailings, reported an increase in evaporation rates with the appearance of cracks. The authors noted that when the top of the tailings had a very low water content, evaporation from cracks contributed significantly to total water loss. Simms et al (2010), however, reported no significant increases in the evaporation rate as a result of surface cracking in laboratory drying tests on gold thickened tailings (Plasticity Index (PI) of 1- 3%). Obviously, the difference in size and frequency of cracks between these two studies was substantial. It was expected that the thickened oil sand tailings would exhibit behaviour somewhere between these two types of tailings.

2 MATERIALS AND METHODS

2.1 *Material*

The material tested was a fine grained oil sand thickened tailings of 50 % solids concentration (Product of Total's 2010 Tailings Thickening Pilot). The tailings had settled during shipping, forming a supernatant. Chemical analyses were performed on the supernatant and pore-water to assess composition. Results indicate major concentrations of sodium (650-689 mg/L), chloride (449-463 mg/L), bicarbonate (774-810) and sulphate (68-74) were present. Average electrical conductivity (EC) was 3.05 mS/cm. The tailings were remixed to a solids concentration of 50% and tested for basic geotechnical properties. Results are presented in Table 1.

From fixed-wall hydraulic conductivity tests, the hydraulic conductivity for samples with void ratios ranging between 2.0 and 2.3 were 6.7×10^{-8} m/s to 7.6×10^{-7} m/s. Clay speciation of the less than 2 micron fraction reveals 40% kaolinite and 60% illite. The illite has a 10 % smectite component, and trace amounts of layered chlorite-smectite. There were also trace amounts of mixed layers of chlorite-smectite and and kaolinite-smectite. The XRD tests were done at Activation Laboratories Ltd in Ancaster, Ontario: more details on the mineralogy are reported in Innocent –Bernard (2013). The tailings had a residual bitumen content of less than 2% and exhibited a fully sheared yield stress of 27 Pa (Slump Test as per Pashias et al. 1996).

Table 1. Characteristics of tested tailings

Characteristics (%)	Layer 1	Layer 2	Layer 3
Gravimetric water content	101	99.5	94.4
Solids Concentration	49.7	50.2	51.4
Liquid limit	27	35	25
Plastic limit	19.5	20	20
Shrinkage limit	17.5	18	17
Sands to fines ratio (SFR)	0.77	0.72	0.66

2.2 *Simulation of multilayer deposition tests*

A multilayer deposition test was simulated in the laboratory in a 0.7 m (W) x 1 m (L) x 1m (adjustable height) box. An initial lift thickness of 0.2 m was employed. The box was mounted on load cells (Figure 1) to directly measure water loss through evaporation and drainage. Drainage was measured using a tipping bucket placed at the base of the drainage port. Geotextile material was placed at the base of the box to prevent soil particle loss.

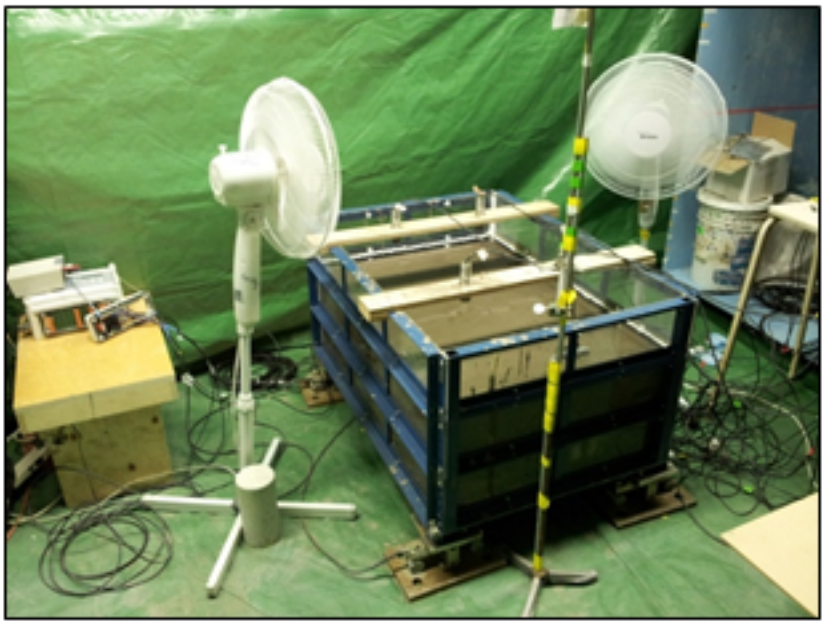


Figure 1. Multilayer Deposition Test

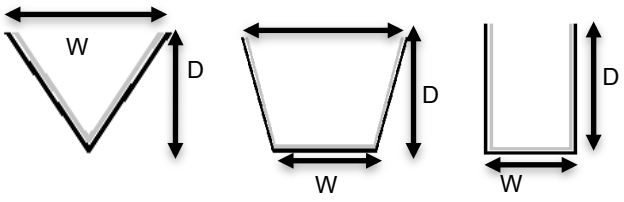
Above the box, four (4) ultrasonic non-contact distance sensors were placed to monitor the variation in height of the sample to estimate vertical volume change. T5 Tensiometers (UMS) were placed horizontally within 5 cm of the top layer and 10 cm from the surface of the tailings to measure matric suction. Six (6) volumetric water content sensors (Decagon) were also placed at the same heights where volumetric water content, temperature and bulk electrical conductivity of the sample were monitored hourly.

Above the soil surface, a Relative Humidity (RH) Easy Log USB sensor was placed to observe RH and temperature change. Two electrical standing fans, set at the lowest speed, were used to simulate wind. The box was placed in an area of the laboratory bound by tarpaulins and with no sunlight reaching the setup thus minimizing the effect of radiation.

The top 1 cm of the tailings surface was sampled daily to measure total suction using a Dewpoint Potentiameter (WP4-T, Decagon Devices Inc.), as well as to obtain samples for gravimetric water content and electrical conductivity measurement. Additionally, surface crack development was monitored by the measurement of crack dimensions to estimate surface area and

volume. Surface cracks were classified according to the shapes shown in Figure 2. Crack surface area on all planes (SA) and crack volume were then calculated based on these three geometries.

When the average water content of a given layer reached 18% (corresponding to the shrinkage limit), sections of the tailings was were removed and profiled for water content, total suction, and electrical conductivity with depth. The next layer was then deposited.



Perimeters are indicated in grey. W: Width; D: Depth

Figure 2. Crack Dimension and Measurement

Vane shear tests were conducted occasionally (to avoid sample disturbance) to estimate undrained shear strength.

2.3 *Measurement of relative evaporation and correlation with total suction*

The relative evaporation, RE, the ratio of Actual and Potential Evaporation rates, (AE/PE), was calculated using measured AE and PE rates. PE was calculated from the Penman-Monteith equation using relative humidity (RH) and temperature measurements, and back calculating the wind parameter assuming the evaporation during the first few hours was equal to the potential evaporation. The wind parameter was assumed to remain constant throughout the experiment. AE was determined directly from the load cell measurements, subtracting measured drainage.

The relative evaporation is often predicted within unsaturated flow codes (the soil-atmosphere boundary condition) as function of the total suction at the soil's surface. For example, Wilson et al.,(1997) defined relative evaporation as:

$$\frac{AE}{PE} = \frac{e^{-\frac{\psi W}{RT}} - RH_{air}}{1 - RH_{air}} \tag{1}$$

Where:
ψ – Soil suction or total suction, [kPa]
R – Universal (molar) gas constant, [8.314 J/mol K]
T – Absolute temperature, [K]
W – Molar volume of water [m3/kmol]
RH – Relative humidity

However, Fredlund et al., (2011) observed that substantial decreases in evaporation occurred at lower suctions than predicted by (1), and proposed that a correction factor to be applied to the total suction at the surface (Equation 2).

$$\psi_{adjusted} = \psi_{original} \times 10^{\delta} \tag{2}$$

The value of the empirical factor (δ) used in other studies (Fredlund et al. 2011) range from 0.5 to 2. Dunmola (2012) found that a value of 0.55 to 0.65 gave good results for a range of different drying tests on a gold tailings, for evaporation rates from 4 to 12 mm/day.

Fredlund et al. (2011) proposed that the empirical factor could correct for the effects of osmotic suction. Dunmola (2012), however, found that even when directly measuring total suction in the top 2 mm of a soil, a correction was still required to match Equation 1 to measured

AE values. Similar corrections to formulations equivalent to Equation 1 have been extensively reported in the soil science literature, purportedly to describe an increase in soil resistance to vapour flow at very low water contents (Daamen and Simmonds 1996) .

3 RESULTS AND DISCUSSION

3.1 *Water Loss*

The dewatering of individual layers is captured in the graphs of actual evaporation (Figure 3), gravimetric water content (Figure 4) and the average void ratio (Figure 5). Actual evaporation (AE) was measured during the test by using the change in mass (loading cells) less the drainage mass. Drainage was insignificant for all layers. AE ranged from 0.9 to 7.3 mm/day. When SA was considered, evaporation rates lowered to a range of 0.6 to 7 mm/day. AE showed pronounced oscillatory behaviour throughout the test.

In all three layers, a sharp decrease in evaporation was noted within the first 24 hours. This was a result of the rapid decrease in gravimetric water content at the surface (Figure 4) from an average of 98% to 32%, dwindling to about 11% by the end of the test. This decline in water content of the initial surface area of the tailings sealed off the rest of the tailings, shutting down evaporation. However, surface crack formation and development, caused the evaporation rates to increase again.

Once formed, cracks accounted for increased surface area in the tailings and accounted for up to 72% of total surface area (Figure 5). Along the full length of the cracks material of lower total suction, when compared to the remaining surface, was exposed. Figure 6 presents the total suction measured at the surface and along the crack profile and results show very low suctions for the cracks. From these low suctions, it can be inferred that the evaporation rate within the cracks was higher than at the original surfaces, which had higher suction. Evaporation rates eventually begin to decrease as crack surfaces become crusted with solute movement to the surface causing precipitation. However, the formation of secondary cracks and the propulsion of material from within the cracks (due to the weight of the overlying surface crust) exposed wetter underlying material, resulting in an increase in evaporation rate.

Potential evaporation ranged from 5.8 to 7 mm/day in layers 1 and 2, and at the beginning of layer 3, PE increased to 10.2 mm/day as the season changed towards the end of layer 3. The time required to reach 18% GWC was 28, 33 and 36 days for successive layers.

Void ratio was calculated using the heights of the sample provided by displacement sensors and assuming there was no swelling of previous layers. The void ratio decreased with decreasing water content and the lowest value recorded was 0.62 (Figure 7).

Water infiltration into underlying layers was detected by volumetric water content increase (Figure 8) to a value of 0.5 corresponding with a solids concentration of 74% and gravimetric water content of 34%. As a result of the infiltration, layers 1 and 2 showed faster settlement within the first few days (Figure 9). Infiltration into the underlying layers also enhanced crack development. Cracks were wider within the first 24 hours for layers 2 and 3 when compared to layer 1.

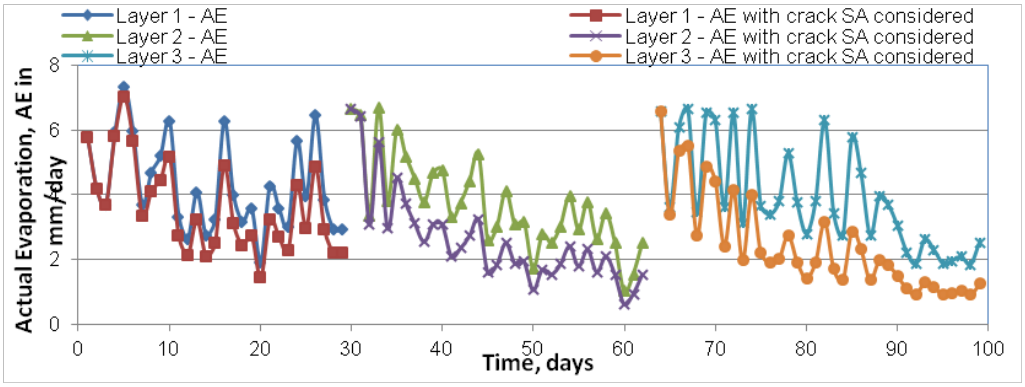


Figure 3. AE (with crack surface area (SA) consideration) in Layers 1-3

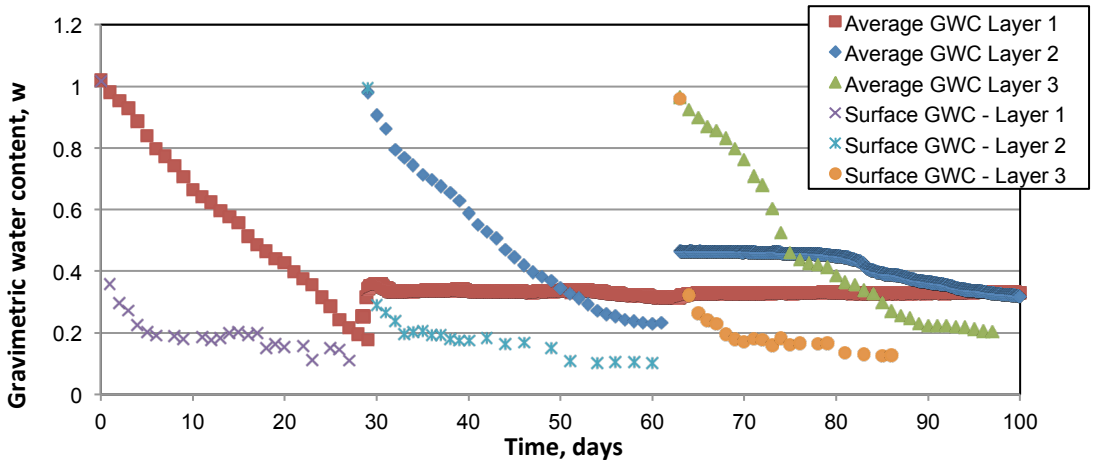


Figure 4. Surface (top 1 cm) and average GWC of top layer

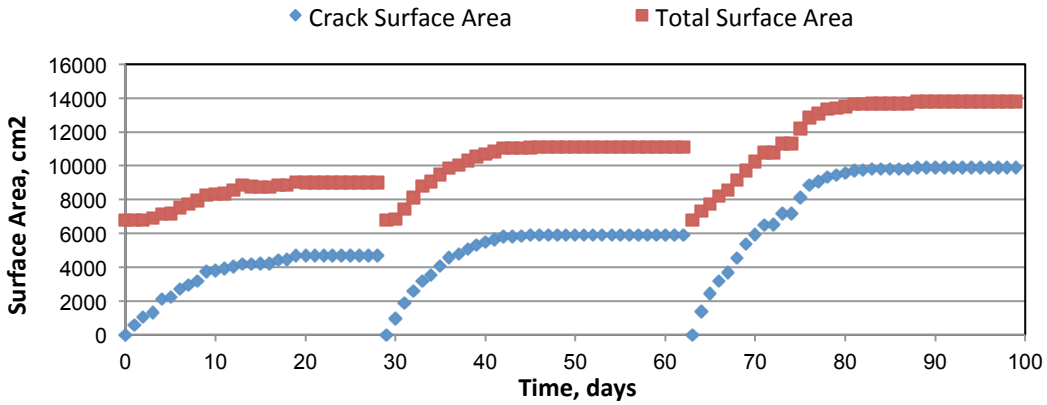


Figure 5. Total and crack surface area of top layer

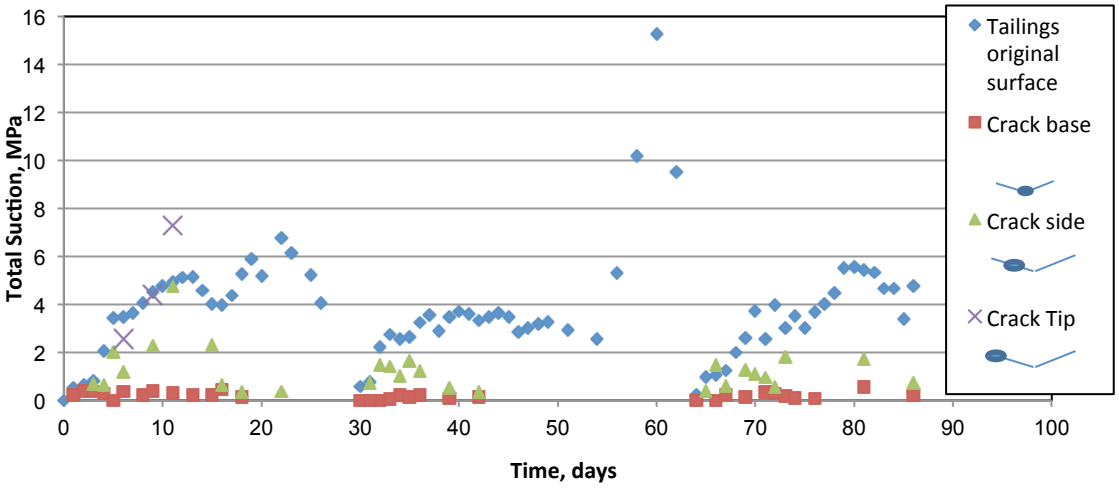


Figure 6 Total suctions measured at top surface (top 1 cm) and on crack surfaces

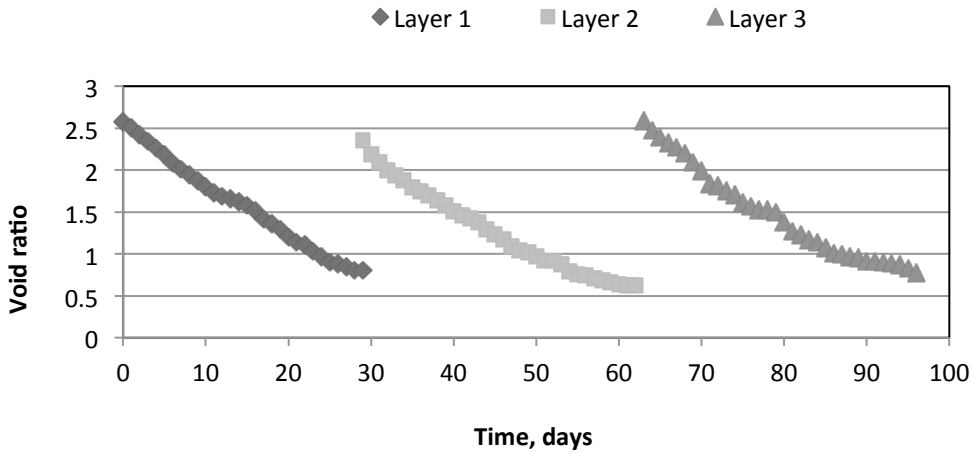


Figure 7. Void ratio in the top layer

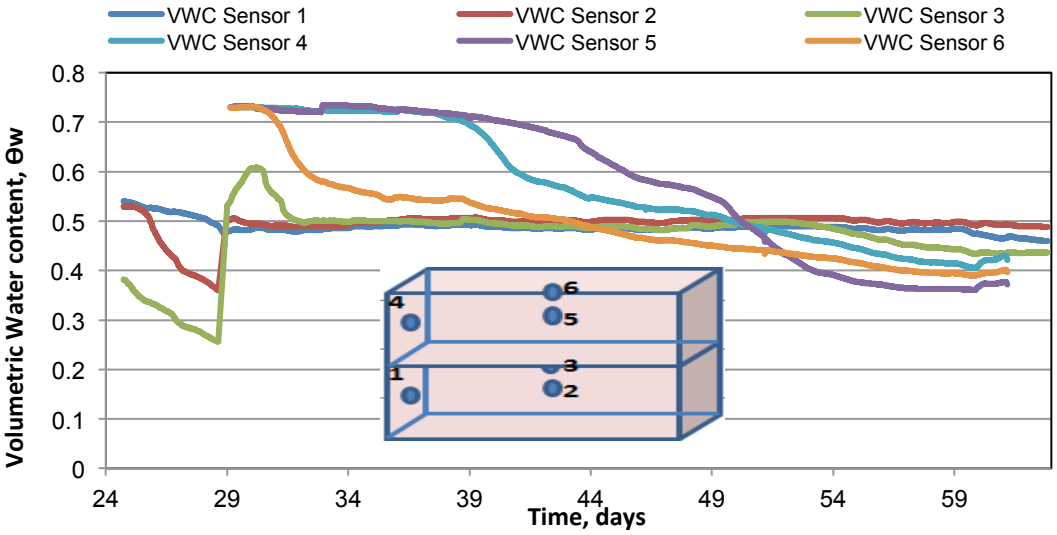


Figure 8. Volumetric water contents after deposition of Layer 2

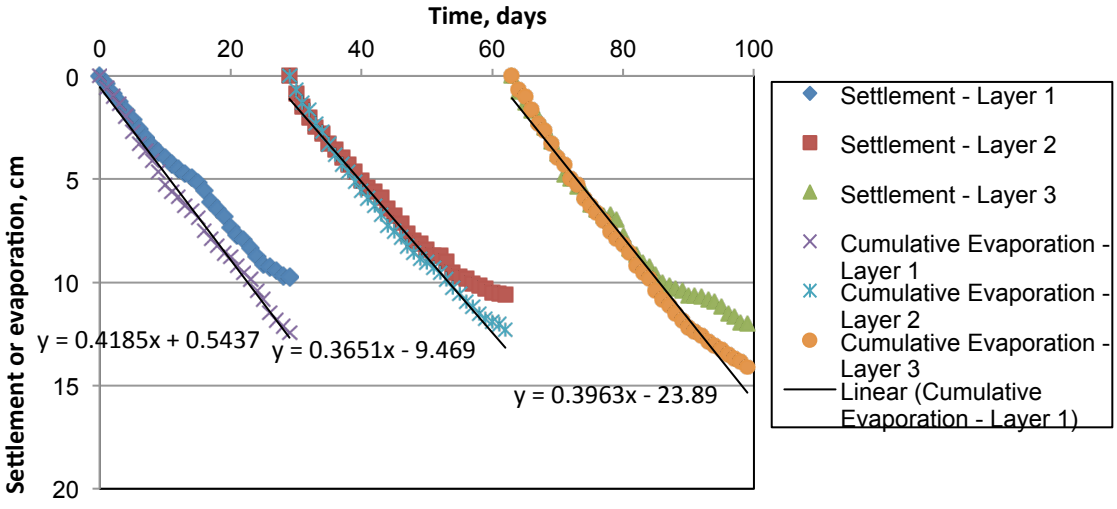


Figure 9. Cumulative evaporation and settlement

3.2 *Solute Transport*

The movement of salts to the surface was seen in the increasing values of electrical conductivity (EC) and total suction at the surface with time. The EC, when used to calculate the osmotic suction through Equation 4 (USDA, 1954), gave values greater than the total suction measured at the surface (See Figure 10 for EC and Suction values from Layer 2).

$$\text{Osmotic Suction, } \pi = 0.36 \times EC \times 101.35 \quad (4)$$

Where EC is the Electrical Conductivity in mS/cm and Osmotic Suction is given in kPa.

The apparently higher osmotic suctions are a result of the dissolution of precipitated salts during the measurement of EC, which employed dilution of the sampled tailings. A similar trend was observed in all three layers. These salt precipitates, were quite visible at the surface and during the soil sectioning exercise

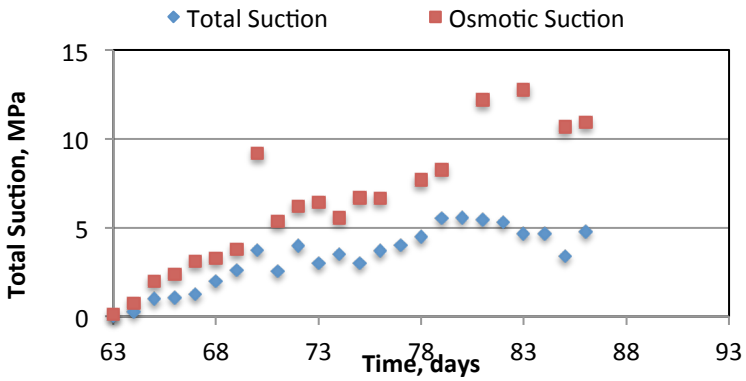


Figure 10 Total and apparent osmotic suction after deposition of layer 3

3.3 *Sectional analyses*

Undrained shear strengths measured at the end of each layer are presented in Table 2. Significant strength development was noted and progressively more uniform drying was observed in layers 2 and 3.

Table 2. Undrained shear strength measurements for soil profile

Layer	Depth (cm)	Peak Undrained Strength (kPa)	Residual Undrained strength (kPA)
Layer 1	3	24	10
	5	18	6
Layer 2	6	66	20
	12	16	12
	18	8	8
Layer 3	8	98	22
	12	18	9
	28	48	20
	32	22	12

The gravimetric water content and suction profiles at the end of each layer are presented in Figure 11. Apart from layer 1, dewatering was very uniform with successive layers with increased crack surface area contributing to increased dewatering.

3.4 *Predicting RE*

Due to the complexity of the evaporation behaviour, it is perhaps a meaningless exercise to use Equation 1 to model RE. Predicted values are shown in Figure 12, using total suction values measured at the surface, and for two different correction values of 1.3 and 1.5. The first value produces a match with the average evaporation rates, while the second matches the lower evaporation rates – the latter prediction might be more representative of evaporation from the top surface, which is where the total suction values were measured. Although a few oscillations were captured using Equation 1, most are not. Given that the total suction values are not uniformly distributed across the evaporating surfaces, and that substantial salt precipitation is observed, it is not surprising that the simple 1-D method cannot fully model the evaporation rate. Work is ongoing as to whether a new simple phenomenological relationship to capture evaporation can be used, or whether some form of 2-D or 3-D modelling is necessary to predict evaporation.

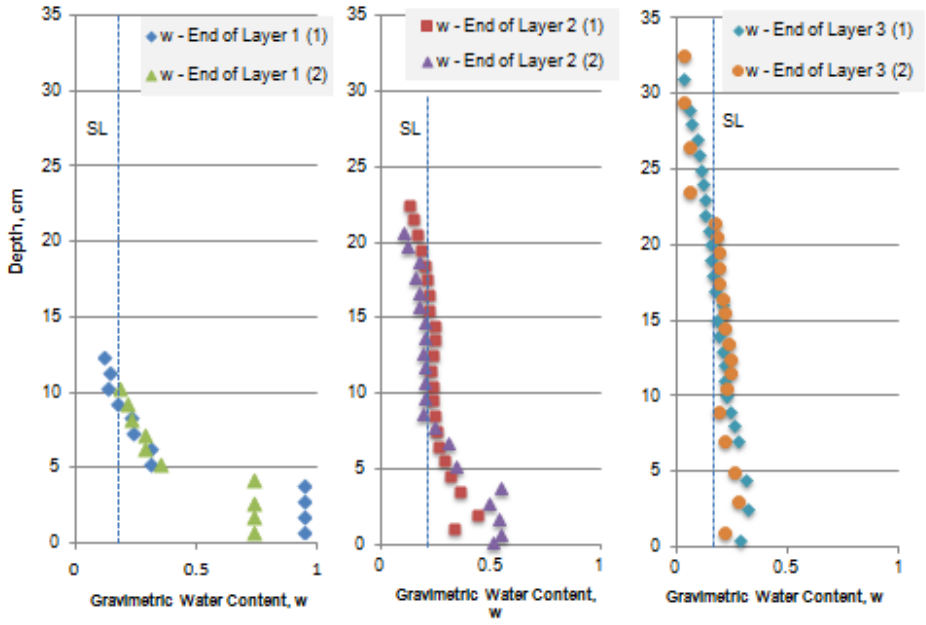


Figure 11. Gravimetric Water content profile at the end of each layer

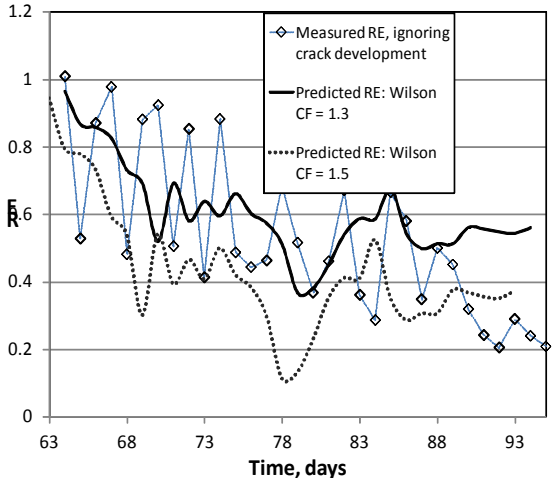


Figure 12 Predicted and measured AE in layer 3

4 CONCLUSIONS

The rapid decrease in the water content and accumulation of salts at the tailings surface rapidly suppressed evaporation at the surface. However, surface crack formation contributed significantly to an increase in the evaporation rate due to the exposure of relatively low suction surfaces. An average evaporation rate of 4 mm/day was seen across all three layers. Multilayer deposition of these thickened tailings promotes increased crack volume and also a more uniform profile of dewatering with depth.

5 ACKNOWLEDGEMENTS

The financial and technical support of Total E&P Canada Ltd. is gratefully acknowledged.

6 REFERENCES

USDA (1954). United States Department of Agriculture Handbook No. 60: Diagnosis and Improvement of Saline and Alkali Soils. Washington, D.C.: U.S. Goverment Printing Office.

Adams, J. E., & Hanks, R. J. (1964). Evaporation from soil shrinkage crack. Soil Science Soc. Am. J., 28, pp. 281-284.

Chen, X. (1992). Evaporation from a salt-encrusted sediment surface: Field and laboratory studies. Aust. J. Soil Res, 30, 429-442.

Daamen, C.C., & Simmonds, L.P. 1996. Measurement of evaporation from bare soil and its estimation using surface resistance. Water Resources Research, 32: 1393-1402.

Dunmola, A. (2012). Predicting evaporative fluxes in saline soil and surface-deposited thickened mine tailings. PhD Thesis. Ottawa: Carleton University.

Dunmola, A. S., & Simms, P. H. (2010). Coupled solule mass transport and evaporation in saline soil. In A. Gens (Ed.), Unsaturated Soils (pp. 1369-1374). CRC Press.

ERCB, E. R. (2009, February 3). Tailings Performance Criteria and Requirements for Oil Sands Mining Schemes. Retrieved from http://ercb.ca/directives/Directive074.pdf

Fissheha, B., Bryan , R., & Simms, P. (2010). Evaporation, unsaturated flow, and salt accumulation in multilayer deposits of “paste” gold tailings. Journal of Geotechnical Geoenvironmental Eng., 135(12), 1703-1712.

Fredlund, M. D., Zhang, J. M., Tran, D., & Fredlund, D. (2011). Coupling heat and moisture flow for the computation of actual evaporation. 2011 PanAm Conference CGS Geotechnical Conference. Toronto, ON.

Fujimaki, H., Shimano, T., Inoue, M., & Nakane, K. (2006). Effect of a Salt Crust on Evaporation from a Bare Saline Soil. VadoseZone Journal, 5, 1246-1256.

Fujiyasu, Y., & Fahey, M. (2000a). Experimental study of evaporation from saline tailings. Journal of Geotechnical and Geoenvironmental Engineering, 18-27.

Fujiyasu, Y., Fahey, M., & Newson, T. (2000b). Field investigation of evaporation from freshwater tailingsl engineering. Journal of Geotechnical and Geoenvironmental Engineering, 126(6), 556-567.

Innocent-Bernard, T. 2013. Evaporation, cracking, and salinity in a thickened oil sands tailings. MSc Thesis. Carleton University., Ottawa, Canada.

Shimojima, E., Yoshioka, R., & Tamagawa, I. (1996). Salinization owing to evaporation from bare-soil surfaces and its influences on evaporation. Journal of Hydrology, 178, 109-136.

Simms, P., Grabinsky, M., & Zhan, G. (2007). Modelling evaporation of paste tailings from the Bulyanhulu mine. Canadian Geotechnical Journal,44, 1417-1432.

Wilson, G.W. Fredlund, D.G., and Barbour, S.L. 1997. The effect of soil suction on evaporative fluxes from soil surfaces, Canadian Geotechnical Journal, 34, 144-155.

Chemistry and geotechnical properties of fluid fine tailings treated by in-situ polymerization of silica

Robert H. Moffett & Jessica L. Flatter
DuPont Chemicals & Fluoroproducts, Wilmington, DE, USA

ABSTRACT: The mining industry generates vast quantities of fluid fine tailings (FFT) throughout the world, and the management of these tailings is an on-going challenge. Long term impoundment of FFT has historically been a common practice in the mining industry but is no longer an option in many regions of the world. Mine operators are seeking novel technologies to accelerate FFT consolidation, and progress FFT to reclamation.

Various chemical and mechanical treatment alternatives have been proposed to help promote FFT from low solids slurries to geotechnically stable materials. Almost all methods focus on the solids fraction of the slurry, while the liquid phase typically represents a much larger fraction. Polymerization of silica within the liquid phase of the slurry offers a fundamentally different approach to FFT treatment. Establishment of a silica network throughout the water phase creates a synthetic soil structure which uniquely aids in dewatering, generation of higher yield strength and erosion resistance throughout the entire consolidation process allowing for faster reclamation.

Laboratory and field data have shown silica treatment to be effective over a wide range of FFT and thickened tailings compositions with varying solids concentrations, particle size distributions and mineralogy. The robust silica treatment process exhibits a low sensitivity to solids loading, mineralogy and process variabilities that plague other methods.

1 INTRODUCTION

Management of fluid fine tailings (FFT) remains an environmental challenge to the mining industry. For example the oil sand industry operating in Alberta Canada processes vast quantities of ore which is slurried in water to facilitate bitumen extraction. The residual solids (sand, clay, and minor amounts of bitumen) along with the added water have been traditionally placed into tailings ponds in an attempt to facilitate solids separation and allow for water recycle. Approximately 80% of the water used during the extraction process is recovered for reuse. Roughly 50% of the fine solids settle along with the coarse sand particles to form beaches. The remaining 50% of the fine solids are left dispersed in water. Over time the fine tailings dispersion will consolidate into what are termed mature fine tailings (MFT) having a solids content of 30-40 wt%. It is estimated it will take centuries for the MFT to reach the consistency of soft clay (Lord 1998).

Recently enacted environmental legislation (ERCB directive 074) requires oil sands operators to treat fluid tailings in a manner that creates trafficable deposits. These deposits must have a minimum undrained shear strength of 5 kPa within one year of deposition and 10 kPa within 5 years. Oil sands operators have investigated a number of different FFT treatment techniques in an effort to meet the ERCB directive. No single treatment has been identified as being acceptable to all operators. In-situ polymerization of silica has been recently proposed as an alternative tailings treatment approach to the more traditional use of flocculants to facilitate liquid-solids separation.

2 SILICA POLYMERIZATION

Ralph Iler in his classic book *The Chemistry of Silica* devotes an entire chapter to the subject of silica polymerization. Iler describes the polymerization process that occurs when the alkalinity of a soluble metal silicate is reduced. Polymerization follows a series of condensation reactions (Equations 1) to form primary silica particles approximately 1-2 nm in diameter.

Depending upon the reaction conditions chosen these primary silica particles can be enlarged in diameter while remaining as discrete particles, commonly known as colloidal silica. Or the primary particles can be linked together to form 3-dimensional chains and networks (Figure 1). In either case the atomic bonds are the same whether inter or intra-particle. That is Si-O-Si. The larger colloidal silica particles can also be caused to link together to form chained networks as shown in Figure 1.

Soil stabilization by injection and polymerization of either alkali metal silicate solutions or colloidal silica sols is a well-known and accepted geotechnical beneficiation process. Polymerization of the silica follows the same condensation reactions described above. In soil stabilization the goal is to fill voids between soil grains with silicate solution before the polymerization process takes place. Any water between the soil grains is desirably displaced by the silicate solution.

Recent work has shown that in-situ polymerization of silica within the water phase of fluid fine mine tailings (FFT) can vastly alter their rheological behavior and provide a novel approach to tailings treatment and consolidation (Moffett 2010).

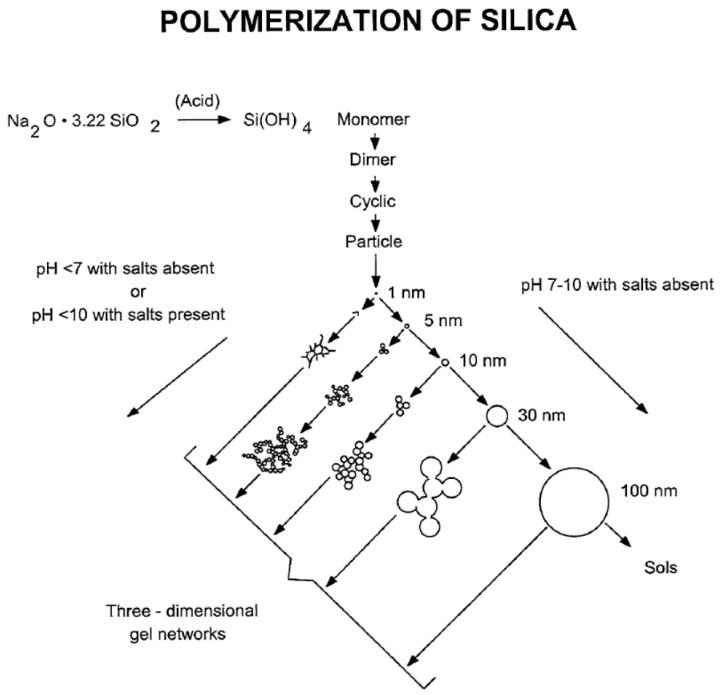


Figure 1. Polymerization of Silica. Iler (1979).

3 TAILINGS CHARACTERIZATION

Samples of fluid fine tailings were obtained from several mining companies. General physical properties of the tailings are shown in Table 1. Particle size distribution was determined by static light scattering using a Malvern Instruments Mastersizer 2000. For purposes of this paper, sand to fine ratio is defined as the volume ratio of particles > 44 micron in diameter relative to those particles < 44 microns. Tailings solids mineralogy was determined by XRD. Major cations dissolved within the pore water of the tailings were determined by ICP.

Table 1. Sample Characterization.

Sample	A	B	C	D
Tailings Type	Mature Fine Tailings	Thickened Tailings	Mature Fine Tailings	Mature Fine Tailings
Source	Alberta Oil Sands	Alberta Oil Sands	Alberta Oil Sands	Alberta Oil Sands
Wt% solids	30	35	40	36.7
pH	7.2	6.4	7.5	7.2
SpG (g/cc)	1.21	1.26	1.27	1.26
Particle Size Distribution (µm)				
D(0.1)	1.33	1.42	1.41	1.47
D(0.5)	6.44	7.44	8.1	7.8
D(0.9)	27.4	27.6	41.3	30.8
SFR	0.06	0.02	0.09	0.05
Solids Composition				
SiO2 (wt%)	50		50	50
Primary Clays (wt%)				
Kaolinite	30		30	30
Illite	15		7	15
Impurities	balance		balance	balance
Major Cations Dissolved in Pore Water (ppm)				
Ca	5	24	16	6
K	8	17	17	7
Mg	3	15	10	2
Na	418	755	602	431
S	12	56	46	9

4 PHYSICAL PROPERTY MODIFICATION

In-situ polymerization of silica within the water phase of FFT can have a dramatic effect on a number of physical properties of the tailings. Silica polymerization rate is a time dependent phenomena controlled by a number of variables. Sections 4.1 to 4.4 provide some details around the modification to the physical properties of MFT and thickened tailings.

4.1 *Chemical addition to tailings*

To assess the impact on FFT in-pipe viscosity, MFT "C" was diluted to 25 wt% solids and treated with 0.5% SiO2 as sodium silicate solution (relative to water concentration in the MFT). Silicate addition was followed by addition of sulfuric acid to reduce the tailings pH to 7. Viscosity was measured using a Brookfield rheometer equipped with a vane spindle rotating at 250 rpm. As shown in Figure 2, addition of alkaline metal silicate solution and acid to FFT causes a slight increase in viscosity initially but with continued agitation the viscosity rapidly decreases to a value slightly lower than that of the untreated FFT. This reduced viscosity can be maintained for extended periods of time if agitation (shear) is continued. When the agitation is stopped, yield strength will slowly begin to increase. This low viscosity can be advantageous in pumping of FFT.

4.2 *Build Rate of Yield Strength*

The rate at which yield strength increases is a function of a number of variables, including silica concentration, pH, solids and counter ion concentrations. For any given set of variables devel-

opment rate of yield strength can be decreased or increased as desired. To demonstrate this phenomena tailings sample "C" was treated with 0.5 wt% SiO2 (with respect to the water concentration in the tailings). After addition of the silicate solution pH of the MFT was adjusted to 7 with sulfuric acid and the sample was placed in a sealed container to prevent evaporation. This set of conditions was selected as the base case. Yield strength was measured intermittently over a 24 hour period using a Brookfield rheometer equipped with a vane spindle rotating at 0.1 rpm. The rheometer was interfaced to a PC utilizing Brookfield Rheocalc software. "Accelerated" development rate of yield strength was achieved by a small addition of magnesium sulfate. "Delayed" rate of yield strength development was achieved by a change in the order of chemical addition. Results (Table 2) show the yield strength can be essentially increased or decreased by a factor of 2x from the base case for at least an hour, but ultimate yield strength is largely unaffected.

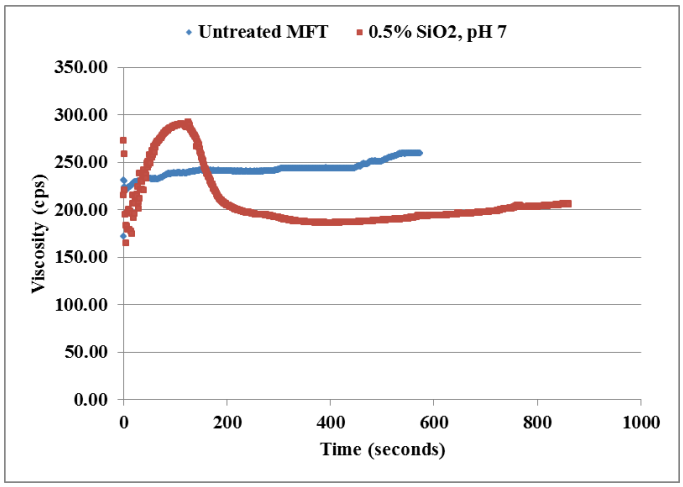


Figure 2. Viscosity of untreated and silica-treated FFT.

Table 2. Yield strength development rate as a function of treatment method.

	Yield Strength (Pa)		
Time (minutes)	Standard	Accelerated	Delayed
10	184	267	3
30	304	584	130
60	482	912	214
1440	1272	1264	1136

As previously discussed the on-set of yield strength development can be inhibited by continuing to mix (shear) the treated tailings after chemical addition. To assess the impact of extended shear times, two aliquots of MFT sample "C" were treated with 1 wt% SiO2 (relative to the water concentration in the tailings). pH was adjusted to 7 with sulfuric acid. The samples were subjected to shear via an overhead mixer for either 1 or 7.5 minutes after the addition of the acid. Figure 3 shows the extended shear time had essentially no impact on the yield strength development rate.

4.3 *Peak Wet Yield Strength*

The tailings samples listed in Table 1 were treated with various amounts of alkaline metal silicate (Figure 4). pH of the tailings samples were then reduced to the values shown by the addition of an acid. After chemical addition the samples were stored for 24 hours in sealed containers to prevent evaporation and allow the silica polymerization process to take place. Peak yield strength of the treated samples was measured 24 hours after chemical addition and compared to the untreated samples (Figure 4). The results show peak yield strength values can be increased

by more than an order of magnitude by the addition of 0.25% SiO_2 (relative to the water content in the tailings). Larger dosages of silica result in further increases in strength.

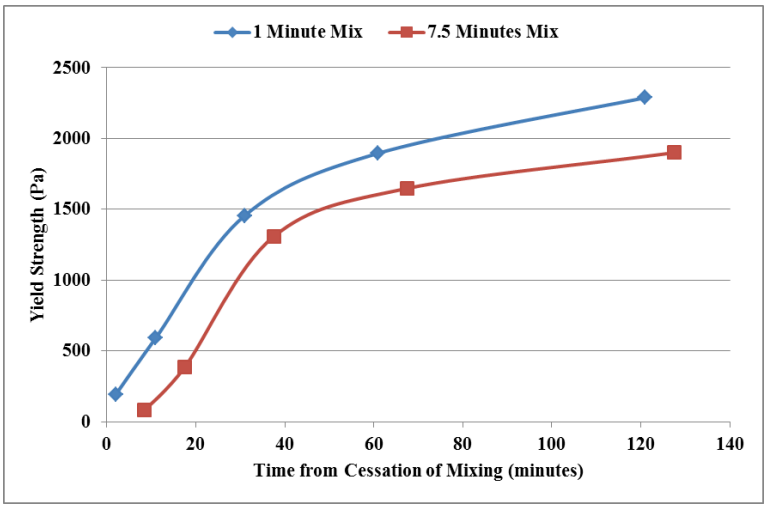


Figure 3. Effect of over-mixing on yield strength development rate.

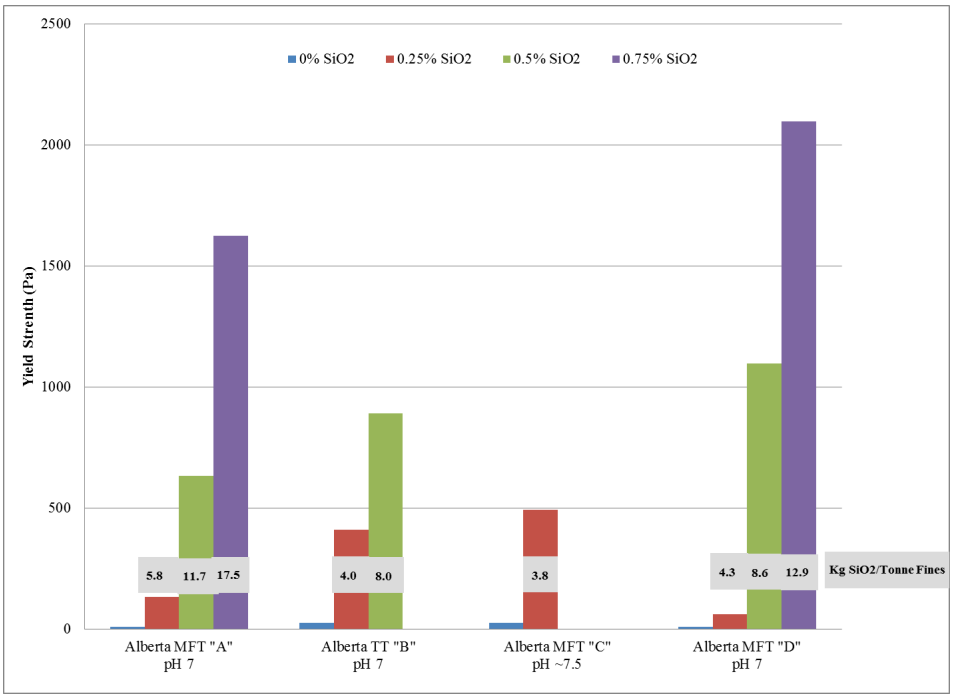


Figure 4. Peak yield strength of treated and untreated tailings.

4.4 *Alternative Silica Sources*

Silica derived from a number of different sources can be caused to polymerize. To assess the impact of silica from various sources MFT "D" was treated with various amounts of sodium silicate solution and a sol of 7 nm colloidal silica particles. pH of the MFT was adjusted to 7 with sulfuric acid after addition of the silica source. Additional samples of MFT "D" were also treated with various amounts of class C fly ash following the teachings in U.S. patent application publication 2013/0019780 (Karimi). After chemical treatment samples were placed in sealed containers to prevent water loss. Yield stress of the samples was measured over a number of days. The peak yield stress for each treatment is reported in Figure 5. Results show that the sodium silicate solution produced the highest yield strength at much lower silica concentrations.

This is because polymerization of the sodium silicate solution results in 1-2 nm particles being linked together to create the silica network as compared to the 7 nm particles from the colloidal silica. In the case of the fly ash a large percentage of the ash that is added is likely insolubilized and unavailable to participate in the polymerization process.

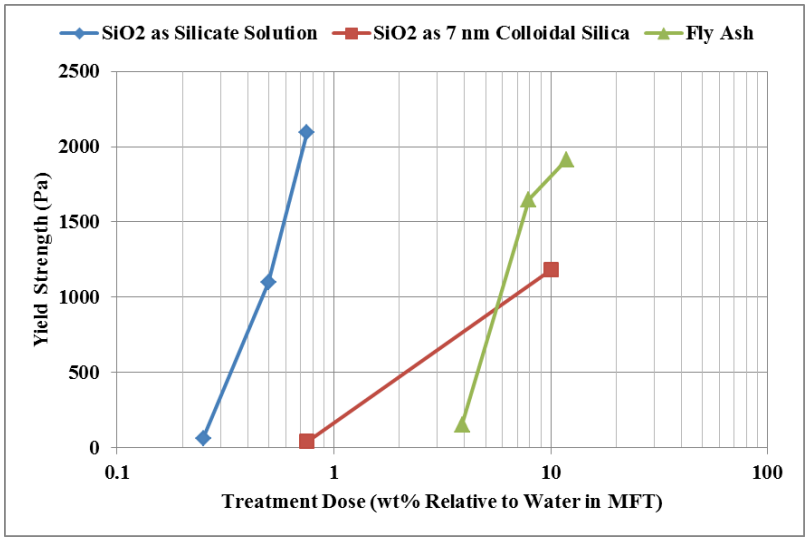


Figure 5. Comparative peak yield strength for various silica sources.

5 DEWATERING

To minimize its final storage volume, FFT needs to dewater as much as possible after treatment. Tailings treated by in-situ silica polymerization can be dewatered by a number of methods such as evaporative drying, self-weight consolidation and surcharge loading.

5.1 *Compressive Force Dewatering*

Dewatering by compressive force (e.g. self-weight or surcharge loading) is a simple, reliable technique that is particularly useful where climatic conditions do not favor evaporative drying of FFT. To assess the ability to dewater by compressive force large strain consolidometer tests were conducted on MFT "A". The consolidometer used in this test is 15 cm in diameter. Starting sample thickness was approximately 20 cm. The consolidometer is equipped to measure vertical displacement as well as pore pressure. Oil sands MFT sample "A" was treated with 0.25 and 0.5 wt% SiO_2 (relative to the water content of the tailings). Void ratio versus effective vertical stress is compared for the silica treated MFT samples to data reported in the open literature for untreated MFT (Figure 6). The results indicate that at very low effective stress the silica treated MFT resists compression more than untreated MFT. This is due to "stiffening" effect created by the silica networks formed in the water phase of the MFT. At higher effective stresses the silica network is no longer able to resist the compressive forces and the void ratio decreases to essentially the same level of those seen for untreated MFT.

Hydraulic conductivity plays an important role in compressive force dewatering. Hydraulic conductivity of silica treated FFTs have been found to be essentially unchanged from that reported for untreated FFTs (Moore). This is a result of the highly porous silica network formed during the polymerization process. Hydraulic conductivity values of approximately 10^{-7} m/sec have previously been reported for sand grouted with silicate solutions containing 14 wt% SiO2 (Krizek). It's interesting to note that hydraulic conductivity value of 10^{-7} m/s is approximately the same as that reported by Moore for untreated FFT having a void ratio around 5. Comparatively, acrylamides which are normally thought to release water quite well, when used to prepare grouted sand were reported to have much lower hydraulic conductivities values of $5x10^{-10}$ m/sec or nearly equivalent to untreated FFT having a void ratio of 1.

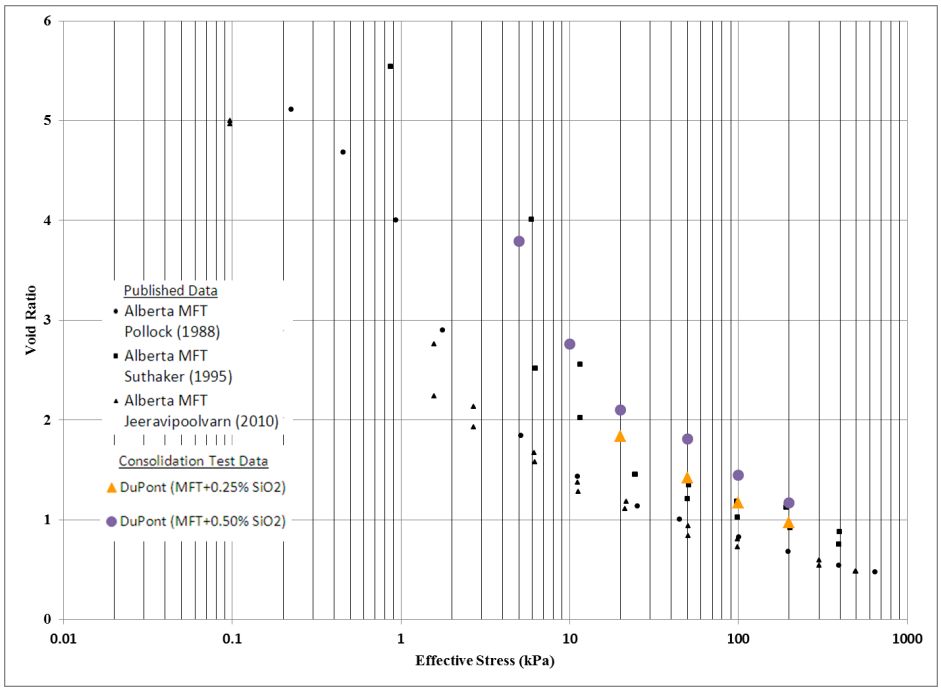


Figure 6. Compression curve for silica treated MFT.

Hydraulic conductivity in grouted sand will be controlled primarily by pore size of the silica (grout) network. Investigators (Munoz-Aguado) have determined that the average pore size in the silica network created during the polymerization of sodium silicate is approximately 50 nm. Pores of this size are sufficiently large enough to allow for relatively easy movement of water through the silica matrix and would be in agreement with high hydraulic conductivity values. A pore size of 50 nm is however small enough to entrap almost all FFT solids within the silica matrix. Analysis of release water from large deposits of FFT has shown suspended solids concentration of < 0.02 wt%, which would support the concept of solid particle entrapment.

5.2 *Evaporative Drying*

Evaporative drying can be a successful process to reduce water content in FFT when climatic conditions are favorable. Evaporative drying is generally employed with thin lift tailings deposition techniques. To assess the potential of evaporative drying of thin lifts, samples of treated oil sands tailings "A" were placed into 1 meter square pans. The pans were placed under lights to achieve a solar radiation input of 100 watts/m2 for 18 hours per day. Fans were used to provide a wind speed of 2 m/s across the surface of the samples. The drying pans were placed on load cells so water loss could be measured with time. An identical pan filled with water only was subjected to the same conditions and used as a reference to judge the evaporation rate from the tailings. The water pan had an evaporation rate of 4 mm/day. These conditions were selected to approximate the environmental conditions experienced at Fort McMurray, AB in the summer (Kolstad 2012).

Oil sands MFT "A" was treated by addition of 0.5 wt% SiO2 (relative to water content in the MFT). pH of the tailings was adjusted to 7 by addition of sulfuric acid.

As shown in Figure 7, rate of water loss from a 10 cm thick deposit of silica treated tailings was found to be equivalent to that of the reference water pan through the entire study whereupon the tailings had reached a solid concentration of > 70 wt%. Water evaporation rates from different thicknesses of silica treated FFT were also evaluated (Figure 8). At solids concentration < 70 wt% the results show essentially no difference in water evaporation rates with lift thicknesses between 2 and 30 cm. This data suggests the highly porous silica network formed within the water phase of the tailings does not significantly inhibit movement of the water to the surface of the tailings deposit.

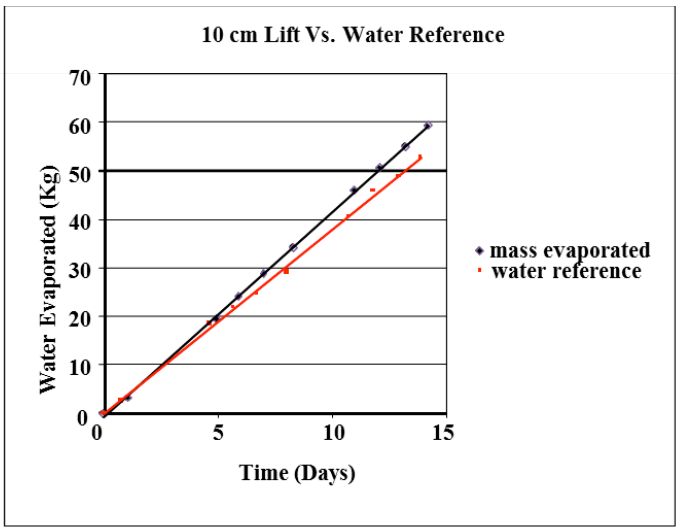


Figure 7. Evaporative drying rate of 10 cm thick silica treated MFT compared to water.

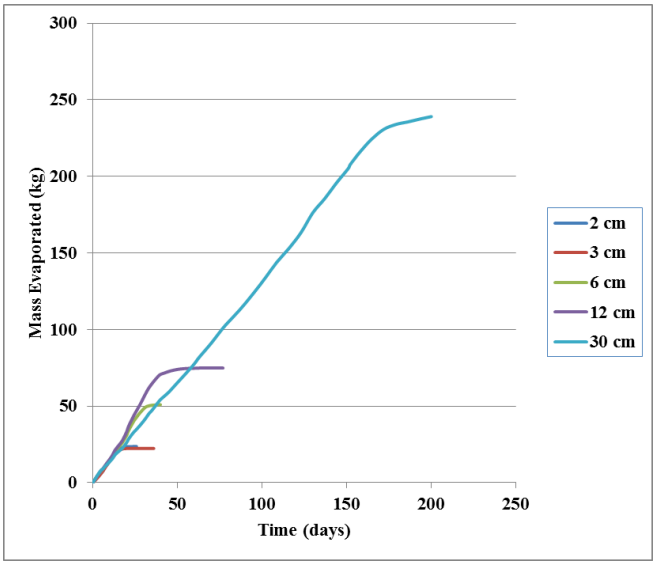


Figure 8. Evaporative drying rate of various thicknesses of silica treated MFT.

5.3 *Yield Strength with Water Loss*

Improvement in yield strength by silica treatment of FFT is maintained over the entire dewatering process. Figure 9 provides peak yield strength values as water concentration is reduced in the FFT samples. Silica dose in these experiments was 0.5 wt% relative to the initial starting water concentration of 27-30 wt% in the FFT.

6 FIELD TRIAL – COMPRESSIVE FORCE DEWATERING

A field demonstration of compressive force dewatering of silica treated MFT was conducted by applying a surcharge load on an enclosed volume of silica treated MFT. The MFT was compositionally similar to that reported for sample "A" having a solids concentration of approximately 30 wt%. The MFT was treated with 0.5 wt% SiO2 (relative to the water in the tailings) as it was being placed into a container of approximately 2.4m x 2.4m x 1.2m deep. The bottom of the container was covered with sand and a liner 0.4m smaller in cross section was inserted into the first box. The 0.2m annular space between the container and liner was filled with sand. The

liner had no top or bottom. After 24 hours the MFT was completely polymerized and the interior liner was removed from the outer container. A layer of sand was placed on top of the polymerized MFT followed by a floating plywood lid to protect the MFT during surcharging. Approximately 1.5 meters of soil was placed on top of the lid in order to simulate a surcharge loading condition of 12 kPa. Drain lines were connected to the bottom and sides of the outer box, emptying into 250 gallon totes for any water collection that would occur.

The height of the deposit was followed over approximately one year at which time the height of the sample was reduced by 42%. A 30% reduction in height was achieved in only 41 days (Figure 10). After one year core samples were removed from the box and analyzed for solids content and yield strength. The results in Table 3 show significantly higher solids content and yield strength than that seen for the starting material.

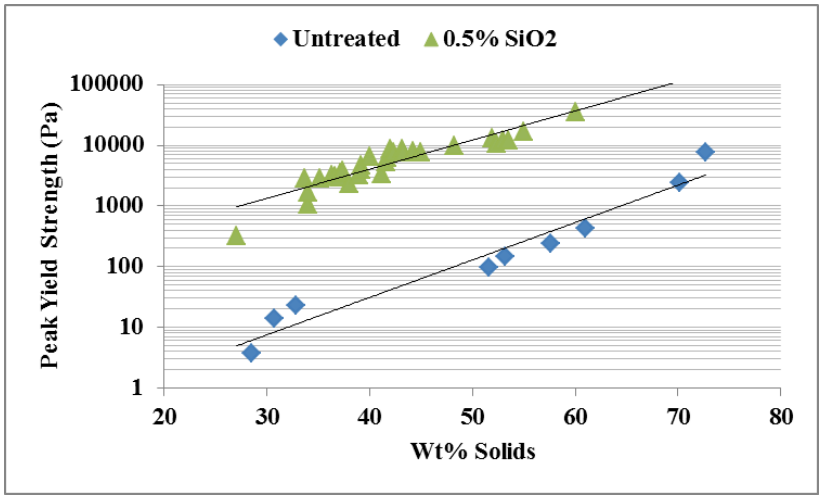


Figure 9. Yield strength of partially dewater MFT samples.

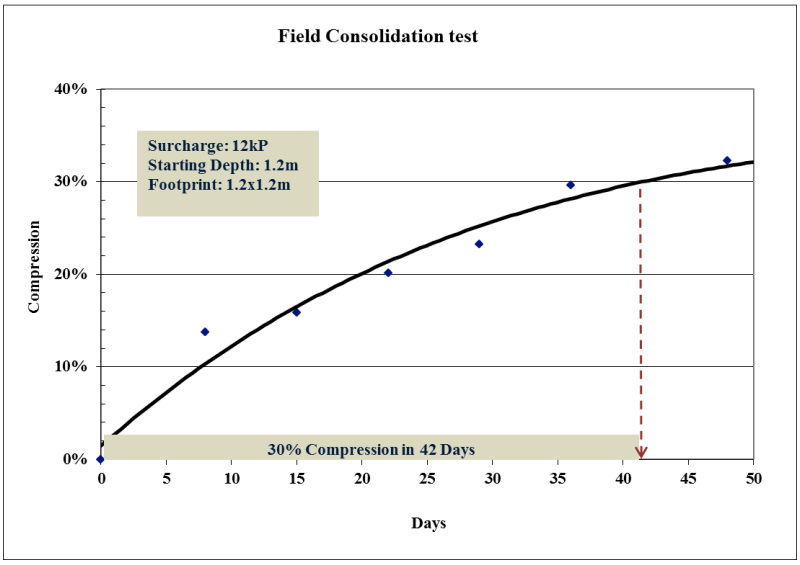


Figure 10. Consolidation of treated MFT over first 50 days.

7 FIELD TRIAL – EVAPORATIVE DRYING

Another field demonstration was conducted in northern Alberta to assess the potential for evaporative drying of silica treated MFT deposited in a relatively thin lift. Again the MFT was compositionally similar to that reported for sample "A" but having a solids concentration of 27 wt%. Treated MFT was deposited approximately 20 cm deep on top of an impervious clay base. Silica dose rate was 0.5 wt% (relative to the water content in the tailings). Core samples were taken over a 30 day period to determine solids concentration and yield strength at varying depths beneath the surface. Average potential evaporation during the test period was approximately 4.7 mm/day. Yield strength and solids concentration are seen to continually increase over the entire length of the study (Figures 11 and 12).

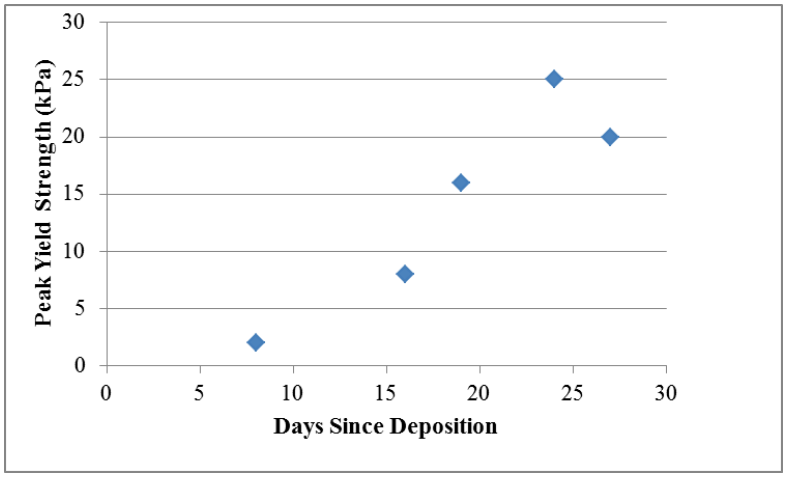


Figure 11. Peak yield strength of treated MFT after evaporative drying.

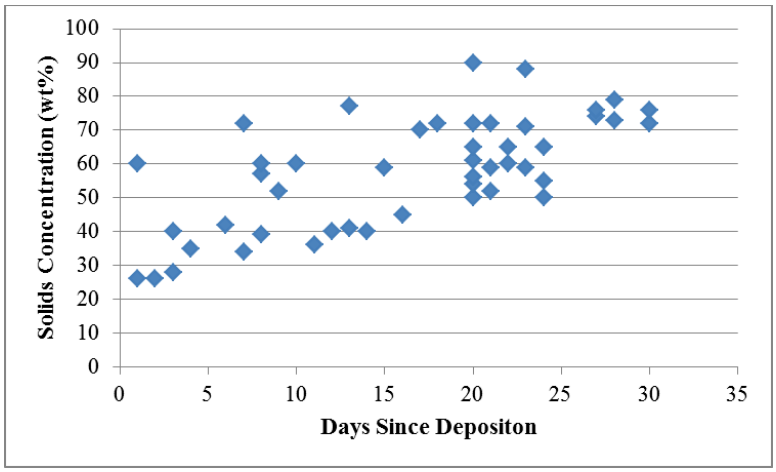


Figure 12. Solids concentration of treated MFT after evaporative drying.

Table 3. Solids content and peak yield strength after consolidation.

Depth (cm)	Solids Content Profile (wt%)				Peak Shear Strength (kPa)			
	SW	NW	NE	SE	SW	NW	NE	SE
1	68.1	61	62.9	45.1	6	4.4	7.5	6.9
10	42.5	44.7	46.2	44.3				
20	42.7	45.1	45.9	45.4	7.4	7.5	7.9	7.9
30	43.1	45	47.2	46				
40	43.5	46	48.1	46.4	7.9	6.3	8	8.1
50	44.5	46.8	48.2	46.9				
60	46.1	51.3	49.2	51.6	-	-	-	-

8 CONCLUSIONS

The in-situ polymerization of silica offers a unique approach for the management of thickened or fluid fine tailings. The chemistry is robust and relatively insensitive to the mineralogy of the tailings. The treated tailings at discharge have similar physical properties to the untreated. Entrained water in the treated slurry aids flow to maximize the placement options for low cost deposition into a disposal area with high land use density. Here, the silica polymerization creates a synthetic soil structure or fabric by the formation of silica networks throughout the water phase and significantly increases the stiffness or yield strength of the tailings. Unlike conventional chemistry treatments, these networks create a mechanism for the transmittal of stress from particle to particle, which makes self-weight consolidation possible. The networks are highly porous and readily release water after placement while entrapping fine solid particles.

Drying may be accomplished by evaporation and/or and compressive force dewatering (self-weight, and/or surcharge loading). Evaporation rates of the treated tailings are essentially equal to that of stand-alone water at the surrounding conditions. The strength of the silica treated tailings allows for surcharge loading to deliver compressive force to enhance dewatering in place. Additionally, the increased strength of the silica treated tailings will support the use of intermediate drainage layers in a thick deposit to further enhance drainage.

The use of in-situ polymerized silica in the treatment of either thickened or fluid fine tailings presents a uniquely different approach to tailings management with many combined benefits that deliver a simple, low cost solution with effective water recovery in the deposition area.

REFERENCES

Lord, E.; Liu, Y. 1998. Depositional and Geotechnical Characteristics of Paste Produced from Oil Sand Tailings, Fifth International Conference on Tailings and Mine Waste '98, Fort Collins Co, 1998: 147-157.

Iler, R. 1979 *The Chemistry of Silica*, John Wiley and Sons, New York, NY, USA

Kolstad, Dale 2012 *Towards The Improvement In Geotechnical Performance Of Atmospheric Fines Drying (AFD) Deposits At Shell's Muskeg River Mine*, International Oil Sands Tailings Conference.

Moffett, Robert H. 2010. U.S. patent application publication 2010/0104744 A1.

Karimi, Gholemhossein, et al. U.S. patent application publication 2013/0019780 A1.

Moore, Trempess, et al. Laboratory Investigation of the Large Strain Consolidation Behaviour of Oil Sands Fluid Fine Tailings Treated with DuPont Particlear™, Geo Montreal 2013 Conference proceedings.

Krizek, Raymond, et al. Permanence of Chemically Grouted Sands, Issues in Dam Grouting (Geotechnical Engineering Div., ASCE, New York, April 30, 1985)

Munoz-Aguado, Maria-Jose, et al. Sol-Gel Synthesis of Microporous Amorphous Silica from Purely Inorganic Precursors, Journal of Colloid and Interface Science 185, 459-465 (1977)

Properties which affect the consolidation behaviour of mature fine tailings

J. Don Scott, Louis K. Kabwe, G. Ward Wilson & Amarebh Sorta
Department of Civil & Environmental Engineering, University of Alberta, Edmonton, Alberta, Canada

Silawat Jeeravipoolvarn
Thurber Engineering Ltd., Calgary, Alberta, Canada

ABSTRACT: Oil sands tailings have been produced for 46 years and now cover an area of 176 km². The volume of mature fine tailings (MFT) now stored in tailings ponds is about 850 million m^3. Much research has been performed over the years to reduce the amount of MFT being produced, but the oil sands industry still has some problems meeting this objective. This paper discusses the MFT properties and suggests which properties are negatively affecting MFT consolidation and disposal. An in-depth review of a long-term large-scale self-weight MFT consolidation test at the University of Alberta then reports on the influence of these properties on the consolidation of the MFT. The test was a 10-m high, 1-m diameter standpipe filled with MFT, which was continuously monitored for 30 years. The MFT settled about 3.5 m during the 30 years. This settlement was defined as mainly creep, not consolidation, as the excess pore pressures had not dissipated greatly. The objective of the paper is to suggest to researchers and practitioners what MFT properties should be considered in research and design.

1 INTRODUCTION

The first oil sands mining project in the Athabasca oil sands deposit by the Great Canadian Oil Sands Company (now Suncor Energy Inc.) started production in 1967. As the tailings from the oil sands contain toxic products, the tailings water and the fluid fine tailings cannot be released and have to be stored in tailings ponds. In the ensuing 46 years, nine oil sands mining projects have been approved, and six of these are actively producing and storing fluid fine tailings. The tailings are predominately a medium-fine sand, but contain from 5% to 40% fine silt and clay and bitumen by mass. On tailings deposition, the solids in the tailings stream segregate with the sand forming dykes and beaches and about one-half of the fines and most of the water flowing into a tailings pond. Upon settling, these fluid fine tailings reach a solids content of around 30% and are then termed mature fine tailings (MFT). About 4% of the MFT solids are bitumen on a mass basis or 10% on a volume basis. By 2012, the volume of MFT held in above-grade containment dams had reached 850 million cubic meters (Fair and Beier 2012), and the land area covered by tailings ponds had reached 176 square kilometers (Weber 2013).

Concern about the growing volume of MFT resulted in the Energy Resources and Conservation Board (ERCB, now Alberta Energy Regulator, AER) setting out new requirements for oil sands fine tailings (ERCB 2009). These requirements were developed in consultation with the oil sands mining companies and were a staged approach which would be fully implemented in three years for existing fully operational mines by July 1, 2012, to June 30, 2013. The objective was to reduce the amount of fluid tailings being produced through 50% fines capture in dedicated disposal areas (DDAs). The oil sands mining operators have to submit their plans two years

prior to construction of the DDAs. Depending on the development of their plant and mine, different companies are at different stages in their three-year plan.

In June 2013, the ERCB reported on their assessment of the oil sands mining industry's tailings management performance in the previous two years (ERCB 2013). From July 1, 2011, to June 30, 2012, the four mining projects required to report only met from 0% to 73% of their required fines capture. Both the ERCB and the companies stated that it was "harder than first thought" (Weber 2013).

It is not as though no one has studied how to solve the oil sands tailings problem. Sobkowicz (2012) reports on the development of an oil sands tailings technology roadmap and action plan. In this project, 549 tailings technologies were identified that could have potential use in the oil sands industry. These were reduced to 101 unique technologies which have been discussed by McKenna et al. (2012). There are already 22 tailings technologies already in commercial use, many of which are mature and others in an advanced development stage (Sobkowicz 2012).

Why are oil sands MFT tailings so difficult to handle that 46 years of research has not come up with definite solutions? Why can it not be consolidated and disposed of similarly as other types of tailings? Mikula (2012) reviews some of the historical concepts of MFT behaviour and discusses what is important in determining MFT tailings behaviour. As it is necessary to fully understand MFT settlement/consolidation behaviour before solutions can be developed, this paper reviews MFT behaviour in a 30-year study of a 10-m tall standpipe filled with MFT. The formation and properties of the MFT are looked at to evaluate those, from a tailings disposal perspective, which are "good or benign" properties, those which are "bad or hostile" properties and those which are both. It is hoped this review will aid others in their research work on the oil sands tailings problem.

2 THE 10-METER STANDPIPE

In 1982, the need to understand the long-term consolidation behaviour of the MFT in the tailings ponds resulted in the establishment of large-scale self-weight consolidation tests at the University of Alberta (Jeeravipoolvarn 2005). These tests were continuously monitored for 30 years in two 10-m standpipes, and on-going results have been published by Jeeravipoolvarn et al. (2009) and upon decommissioning in 2012 by Kabwe et al. (2013).

The 10-m standpipes (Figure 1) have a 914 mm inside diameter and are 10.5 m in height. Pore-water pressure monitoring ports and sample ports are aligned at 0.5 m spacing down the sides of the standpipes. The standpipes were located in a laboratory that has a fairly consistent temperature of around 21^{o}C and were decommissioned in 2012. Tailings placed in the standpipes were MFT pumped from the center of Syncrude's Mildred Lake tailings pond from a depth of about 25 m (Jeeravipoolvarn et al. 2009). The MFT was placed in 72 barrels of approximately 200 L each and transported to the University of Alberta. The mixing and placement of the MFT were done by pumping from different barrels in a sequence to ensure a consistent material placement. The Standpipe 1 discussed in this study was filled to a 10 m height with 6.57 m^3 of MFT, after thoroughly mixing the MFT in barrels to achieve a uniform material. This standpipe was filled in October 1982 by pumping with a tremie hose discharging below the surface to prevent air entrainment. The second standpipe was filled with a mixture of MFT and sand and will not be discussed in this paper. The properties of MFT placed in Standpipe 1 in 1982 are shown in Table 1 (Jeeravipoolvarn et al. 2009). Table 1 also shows these same properties measured in 2012 just prior to the decommissioning of the standpipes. Because of the settlement of the MFT during these 30 years, the average void ratio has changed from 5.17 to 3.14. Most of the other properties reflect this change. Slight changes in fines content and specific gravity are within experimental error. The bitumen in the MFT is treated as part of the fines, and the properties are affected by this assumption. For instance, the low value for the specific gravity is caused by the bitumen only having an average specific gravity of about 1.03.

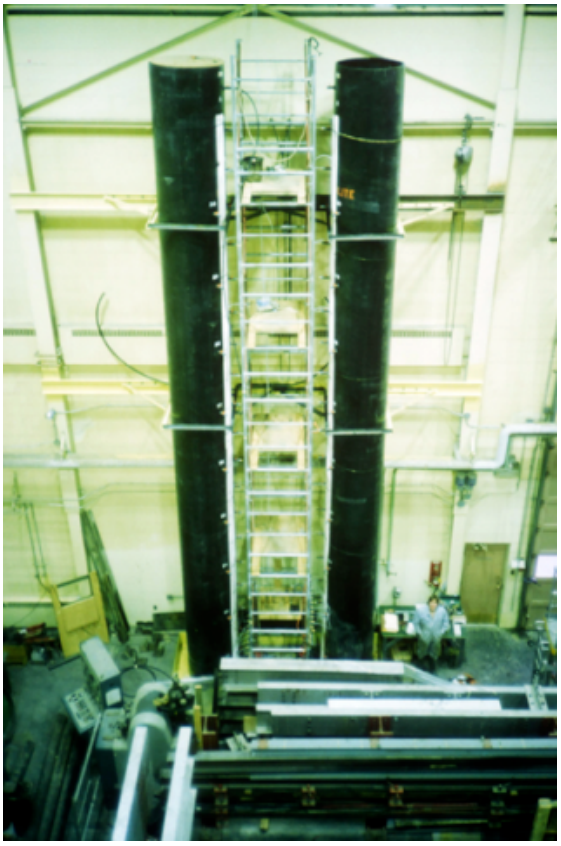


Figure 1. 10-m standpipes at the University of Alberta

Table 1. Average tailings properties in Standpipe 1

	1982	2012
Solids Content (%)	30.6	42.1
Water Content (%)	226.8	137.5
Sand Content (% by dry weight)	11	8
Fines Content (% by dry weight)	89	92
Bitumen Content (% by dry weight)	10.2	7.1
Bitumen Content (% by total weight)	3.1	3.0
Bulk Density (g/cm^3)	1.21	1.32
Void Ratio	5.17	3.14
Fines Void Ratio	5.8	3.41
Fines-Water Ratio (FWR)	28.2	61.4
Specific Gravity, Gs	2.28	2.33
Sand-Fine Ratio (SFR)	0.12	0.09

3 THE OIL SANDS ORE

The oil sands ore has properties, which are both benign and hostile. Over the 4,800 km² Athabasca oil sands mining area (Government of Alberta 2011) the properties of the ore can change substantially with (by mass) 55% to 80 % sand (>45 µm), 5% to 34% fines (<45 µm), 4% to 18% bitumen and 2% to 15% water. Typical deposits of average grade oil sands contain 72% sand, 12% fines, 11% bitumen and 5% water. Figure 2 shows a particle size distribution (PSD) of oil sands which contains almost no fines, and if the whole deposit was like this, it would be a benign property and there would be no fine tailings. Figure 2 also shows the PSD of a typical clay-shale seam in the oil sands McMurray Formation. The fines in the tailings come from these indurated clay-shale discontinuous seams and layers in the oil sands. Figure 3 is a photograph of a section in the Upper McMurray Formation showing typical clay-shale layers which are a hostile property of the ore. These dense but weak clay-shale materials are broken up during the mining process, and the larger more indurated pieces are screened out as reject material. In the bitumen extraction process, the clay-shale pieces are further broken down into clay lumps and aggregates, and some clay lumps are dispersed into small clay booklets and flakes. The amount of dispersion depends on the extraction process. The sodium hydroxide dispersing agent in the Clark Hot Water Extraction process used in the oil sands extraction plants effectively disperses much of the clay aggregates into clay flakes smaller than 2 µm, which have large active clay surfaces. Therefore the typical extraction process also results in a hostile property.

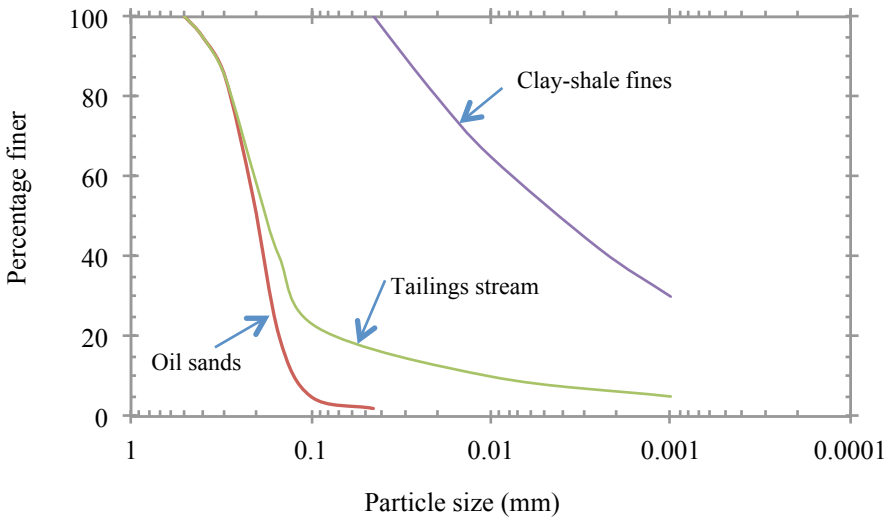


Figure 2. Particle size distribution of oil sands ore, clay-shale inclusions and resulting tailings stream.

4 THE TAILINGS STREAM

The mixing of the oil sands and the dispersed clay-shale seams results in the tailings PSD also shown in Figure 2. This PSD is the major hostile property of the tailings. There are only about 17% fines in the average tailings stream, although this can vary substantially. Morgenstern and Scott (1997) give the following description and history: the tailings are predominantly a mixture of uniform fine-grained sand and water, but also contain dispersed silt and clay as well as some residual bitumen. On deposition in a tailings pond, the sand fraction settles out to form dykes and beaches trapping about 50% of the fines (MacKinnon and Sethi 1993), and the remainder of the oily silt and clay fraction suspended in the water forms a sludge, called fluid fine tailings, that flows into the pond. All of these materials must be stored; however, most of the water in the pond is clean enough for re-use in the plant. The volume bulking factor of the tailings is about 1.4. The characteristics of segregating tailings noted above and the resulting large storage re-

quirements were not understood by the initial designers of the Suncor operation. The initial design of the out-of-pit storage contemplated a perimeter dyke about 12 m high along the Athabasca River. Tailings discharge was planned to be from the top of the adjacent valley wall, which was some 60 m above river level. The tailings sand was assumed to form a stable 8% slope. This facility would only have a three-year life. Construction of the retention dyke began in 1966. At this time, as a result of pilot studies, it also became clear that much of the fines would segregate from the sand, the 8% slope would not be realized and that the bulking factor had been underestimated.

This dyke, Tar Island Dyke, ultimately reached a final height of 98 m. 2.83" from margin; Lock anchor).

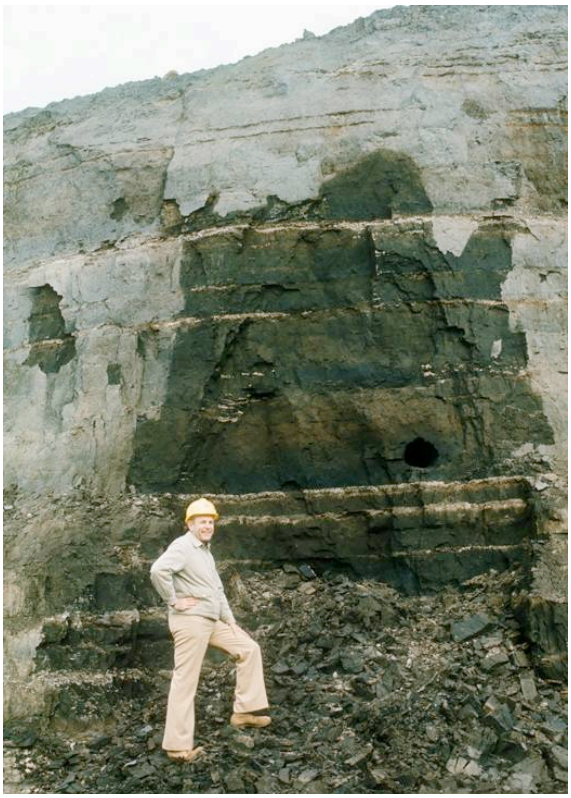


Figure 3. Section in the Upper McMurray Formation

5 PROPERTIES OF MFT

5.1 *Mineralogy*

MFT behaviour is directly related to the mineralogy and water chemistry of the MFT. Therefore, in 2000 and 2012 mineralogical tests (Table 2) were carried out by AGAT Laboratories Ltd. on the standpipe MFT. The mineralogy of the fine tailings reflects the average clay mineralogy of the parent material, the McMurray Formation, where kaolinite and illite are the dominate clay minerals. Trace amounts of mixed-layer clays, smectite, vermiculite and chlorite are also present (Kasperski 1992). The field fine tailings are characterized as dominantly kaolinite (55% to 65%) and illite (30% to 40%) with minute traces of mixed-layer clay minerals (Dereniwski and Mimura 1993).

Table 2. Mineralogy of MFT measured in 2000 and 2012

Year	Quartz and other rock-forming minerals	Clay Minerals	
		Kaolinite	Illite
	(%)	(%)	(%)
2012	36	42	22
2000	36	40	24

Quartz is the most abundant non-clay mineral. Minor amounts of siderite are found in all the fine tailings, while minor to trace amounts of plagioclase and K-feldspar are found in most samples. The mineralogy of fine tailings is not affected by the type of extraction process or the process water. It is a reflection of the mineralogy of the oil sands ore used to generate the fine tailing. The caustic hot water extraction process does not alter the clay mineralogy in the fine tailings (Scott, Dusseault and Carrier III 1985). As kaolinite and illite are not very active clays, the mineralogy properties can be considered a benign property. Unfortunately, the extraction process water chemistry and the organic content (bitumen) change the mineralogy to a hostile property.

Mikula and Omotoso (2004) reported that high specific surface areas typically observed in mature fine tailings can be attributed to smectite interstratification of kaolinite and illite. Amorphous oxides may also contribute to measured specific surface area. The discrepancy between calculated and measured specific surface areas for the fine tailings may be due to interstratification of kaolinite and illite with smectite that is not appreciated or readily apparent from X-ray diffraction (XRD) analysis and is reported as simply kaolinite or illite. As well, there may be incomplete dissolution of organics and residual bitumen during the test procedure. The influence of this smectitic interstratification on the geotechnical properties of the MFT requires examination.

5.2 *Atterberg Limits*

Table 3 includes the Atterberg Limits measured in 1982, 2003 and 2012 in the 10-m standpipe, and Table 4 shows the Limits with depth in 2012. The Atterberg Limits are plotted on a Plasticity Chart in Figure 4 which includes additional tests by Jeeravipoolvarn (2005). All of the samples are in the same range on the border between inorganic clays of medium plasticity and inorganic clays of high plasticity. These values are fairly typical for MFT, although some tailings from different geological ores have higher liquid limits. MFT with the bitumen removed generally shows lower liquid limits.

Figure 5 shows the liquid limits of the clay-shale inclusions in a vertical section of the McMurray Formation. They increase from 20 to 40 in the bottom of the formation to 30 to 50 in the top of the formation and are similar to the liquid limits in the MFT. The high values at the top of the figure are in the overlying Clearwater Shale Formation which is high in smectite.

The Atterberg Limits are similar to those of kaolinite and illite clay minerals. The Activity of MFT is about 0.57 while the Activities of kaolinite and illite are about 0.5 and from 0.5 to 1, respectively (Mitchell and Soga 2005). These values indicate that the smectitic interstratification noted by Mikula and Omotoso (2004) may only influence the clay mineral properties when the minerals are dispersed to very fine sizes, greater than the present dispersion in the bitumen extraction process.

5.3 *Bitumen Content*

MacKinnon and Sethi (1993) report on the bitumen content in the Syncrude and Suncor fine tailings. At Syncrude's Mildred Lake Settling Basin (MLSB), the average bitumen content through

the fine tailings zone was about 1.5% to 1.7%, while at Suncor it ranged from 2% to 4% in the majority of the fine tailings. These percentages are based on the total mass of the fluid fine tailings. In the oil sands industry, it is common practice to state the bitumen contents as a percentage of the total mass of the MFT. With this definition, however, a change in water content of the MFT will change the calculated % of bitumen. In geotechnical engineering, it is better to define the bitumen content as a % of the dry mass of the MFT when comparing different MFTs or changes with time. As a percentage of dry mass, the bitumen at Syncrude averaged about 4.5% and at Suncor about 8.6%. As the extraction plant processes have improved over the years, the amount of bitumen in the tailings has decreased below these values.

Table 3. Average index properties of the fine tailings

Year	1982	2003	2012
Average Water Content (%)	227	146	138
Liquid Limit (%)	46	52	47
Plastic Limit (%)	21	21	20
Plasticity Index (%)	25	31	27
Liquidity Index	8.24	4.03	4.37
Activity	0.53	0.53	0.57
Specific Gravity	2.28	2.28	2.33

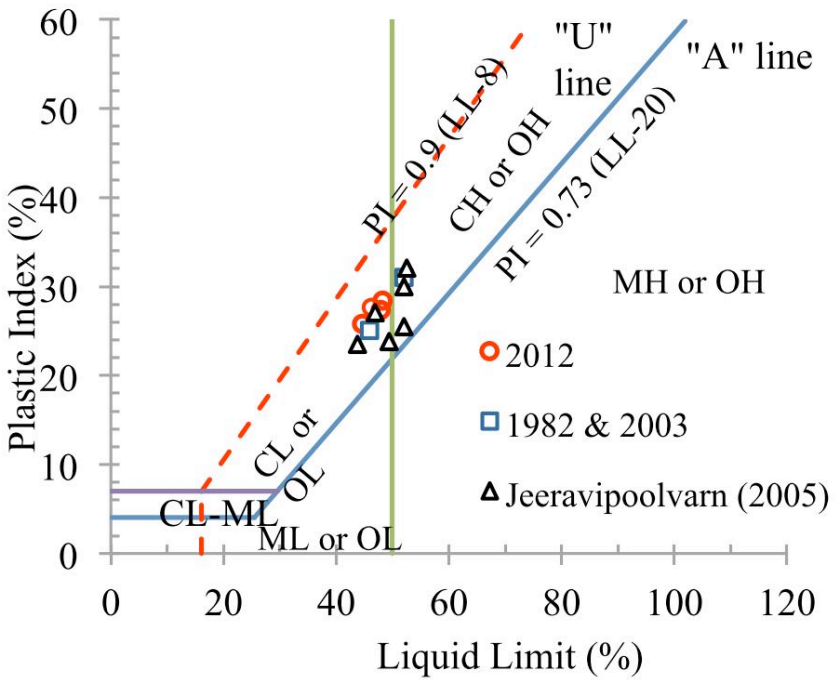


Figure 4. Plasticity Chart including 1982, 2003 and 2012 samples

Table 4. Specific Gravity and Atterberg Limits measured in 2012

Sampling Depth (m)	Specific Gravity	Liquid Limit (%)	Plastic Limit (%)	Plasticity Index
4	2.28	47.7	20.2	27.5
6	2.36	47.2	19.8	27.4
8	2.32	47.9	20.6	27.3
10	2.36	44.6	18.8	25.8

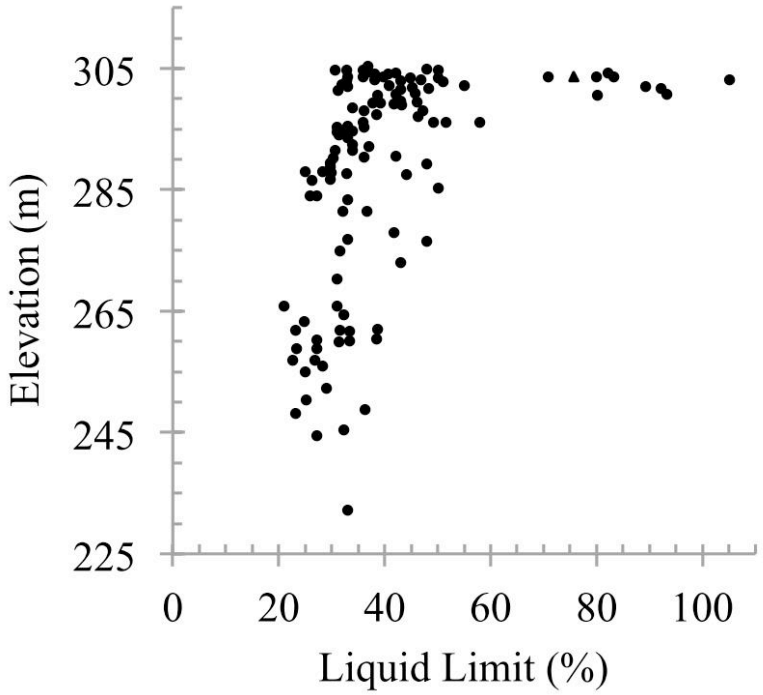


Figure 5. Liquid Limit of clay-shale inclusions in a vertical section of the McMurray Formation

Table 5 shows the average bitumen content in the 10-m standpipe in 1982 and 2012. In 1982, it was measured in all 41 drums of MFT, varying between 2.7% and 4.0% of the total mass with an average value of 3.1%. These measurements were done at the University of Alberta using a standard Dean Stark test. In 2012, the bitumen content by total mass was determined in three MFT samples from standpipe depths of 5 m, 7.5 m and 9.5 m by AGAT Laboratories Ltd. of Calgary using a modified Dean Stark method and averaged 3.0% (Kabwe et al. 2013). These values on a dry mass basis are 10.2% and 7.1%, respectively, which would indicate that there was less bitumen in the standpipe in 2012. No bitumen floated to the surface nor was removed in these 30 years, so the percentages on a dry basis should be the same. The difference could be the result of different test procedures.

Figure 6 shows the variation in bitumen content with depth in the standpipe measured with the Dean Stark method by the Department of Biological Sciences in 2012. The average is 3.2% on a total mass basis and 7.6% on a dry mass basis, which agrees with the AGAT tests in 2012. On a volume basis, this means that bitumen is 17% of the volume of the solids.

It should be noted that the amount of the bitumen is typically greater in finer tailings than coarser tailings. The Dean Stark bitumen removal process requires driving off all the water from the sample as well as removing the bitumen by refluxing with toluene in a modified Stark Extractor.

Table 5. Bitumen content dry mass basis measured in 2012 and in 1982

Year	Depth	Bitumen content
	(m)	(%)
2012	5.0	7.6
2012	7.5	6.9
2012	9.5	6.7
2012 (avg.)	-	7.1
1982 (avg.)	-	10.1

Generally, the bitumen is considered as a hostile property. It is messy, sticky and makes the MFT difficult to work with. For this reason, the bitumen is often removed by the Dean Stark method before MFT testing. Miller et al. (2010a) discuss the problems with this approach. Mikula (2012) reports that the Fine Tailings Fundamentals Consortium established that removing bitumen from the tailings only increases the initial settling rate and does not increase the clay to water ratio. Suthaker and Scott (1996) show that because of the bitumen an increase in hydraulic gradient in MFT will decrease the hydraulic conductivity. Such higher hydraulic gradients exist adjacent to wick drains and beneath surcharges. Penner and Foght (2010) suggest that bitumen may be an important carbon source to anaerobic microbial communities once other readily usable forms of carbon are no longer available, resulting in additional release of biogenic gas. No benign properties have been associated with the bitumen.

As the bitumen only has a specific gravity of about 1.03, it has a major influence on the specific gravity of the MFT. Table 4 shows the specific gravities with depth in the standpipe, and Table 3 includes its measured values in 1982, 2003 and 2012.

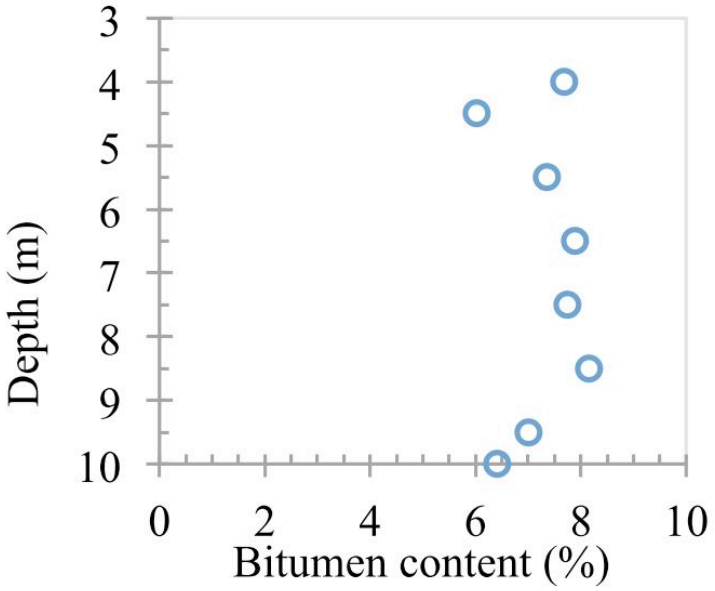


Figure 6. Bitumen content dry mass basis measured in 2012

5.4 *Pore Water Chemistry*

Only general pore water chemistry measurements are included in this paper. Presentation and discussion of the effects of the pore water chemistry on the properties of the MFT is beyond the scope of this paper. Pore water chemistry is variable depending on the ore and extraction process. Changes in pore water chemistry with time can also affect the potential consolidation of the MFT. Details on the chemistry are in a public domain report by Kasperski (2001).

Table 6 includes a water chemistry analysis of Syncrude oil sands ore connate water (Miller 2010a), Syncrude MFT water (MacKinnon and Sethi 1993) and average pore water from the 10-m standpipe (Jeeravipoolvarn 2005; Kabwe et al. 2013). Complete chemical analyses were performed on the standpipe pore water in 2000 and 2012, and only minor changes occurred during this period.

The major changes in the water chemistry of the ore connate water from the extraction process are increases in major cations, bicarbonate and heavy metals. Recycled tailings pond water and Athabasca River make-up water are used in the Clark Hot Water Extraction process. Sodium hydroxide is added in the extraction process as a dispersing agent and exists in the recycled pond water. Bicarbonate comes from the river water, the connate water in the ore and from the adsorption of CO_2 during aeration processes. Studies (FTFC 1995) on the effect of the composition of the tailings water concluded that the repulsive and attractive forces between the clay particles dominate the behaviour of the fine tailings water structure and the settlement of the MFT. This electro-kinetic behaviour is mainly caused by the presence of bicarbonate ions (Jeeravipoolvarn 2005).

Table 6. Pore water chemistry

Item	pH	EC* (mS/cm)	Cations (mg/L)				Anions (mg/L)			Others (mg/L)			
			Na	K	Mg	Ca	Cl	SO_4	HCO_3	Fe	Si	Al	NH_3/NH_4
Syncrude oil sands ore connate water	8.2	0.8	163	1.9	0	0	99.8	93.6	1.0	0	0.74	0	-
Syncrude MFT	8.2	1.3	480	12.3	2.9	5.0	135	6.0	940	0.17	3.8	0.44	7.1
Standpipe MFT	8.6	1.5	402	12.3	3.4	7.0	114	1.2	846	3.11	-	-	15.4

*EC= Electrical conductivity

5.5 *Thixotropy and Overconsolidation*

Figure 7 shows the measurements in several investigations of the thixotropic increase in shear strength of the MFT (Beier et al. 2012). The shear strength is plotted against liquidity index to take into account the initial water contents of the different samples. Miller et al. (2011) shows the thixotropic increase in shear strength during 365 days, and Suthaker and Scott (1997) shows the thixotropic increase during 450 days (Figure 8). Both references show an increase of about one order of magnitude during these elapsed times. Also shown are the shear vane strengths measured in the standpipe after 30 years. These shear strengths are higher than any others, being about two orders of magnitude increase assuming the initial shear strengths were similar to those in other MFT samples.

These shear strengths in the standpipe can be used to calculate the overconsolidation stress in the MFT. In natural sedimentary clay deposits, the undrained shear strength has been found to increase with depth and is proportional to the increase in effective stress with depth (Holtz and Kovacs 1981). A relationship between plasticity index and a ratio between undrained shear strength and effective stress, τ_u/σ'_{vo}, for normally consolidated clays was established by Bjerrum and Simons (1960). This relationship provides a τ_u/σ'_{vo} ratio of about 0.25 for oil sands fine tail-

ings with plasticity index of about 30. However, the large strain consolidation test results show that this ratio is not constant at all fines void ratio, but increases linearly with fines void ratio (Figure 9) (Jeeravipoolvarn 2010). The large values at high void ratios are indicative of the strong thixotropic bonds between the clay particles. As the clay particles are compressed during consolidation, the thixotropic bonds break and lose strength.

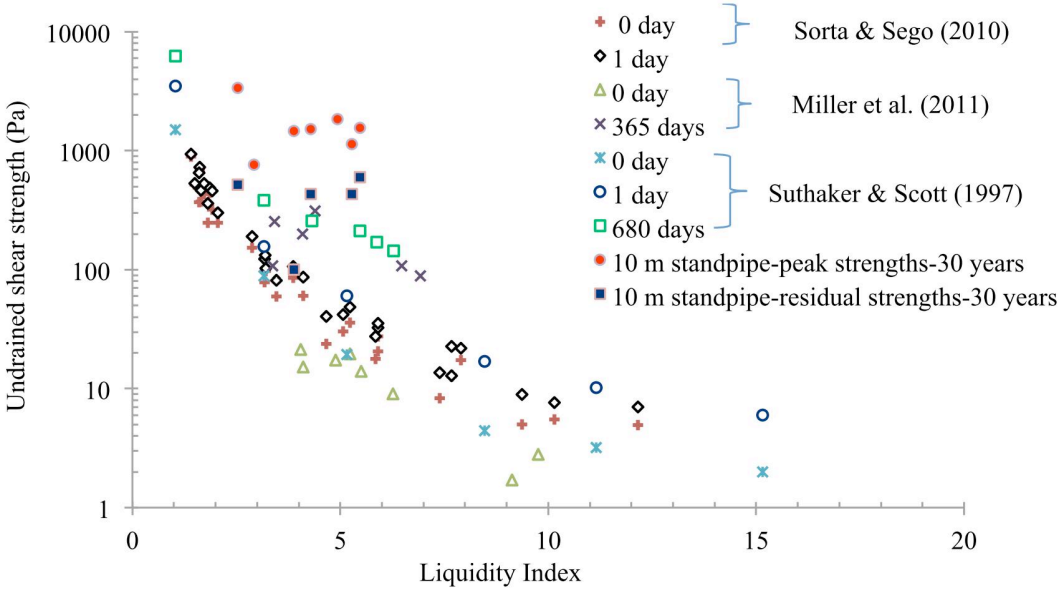


Figure 7. Undrained shear strength vs. liquidity index

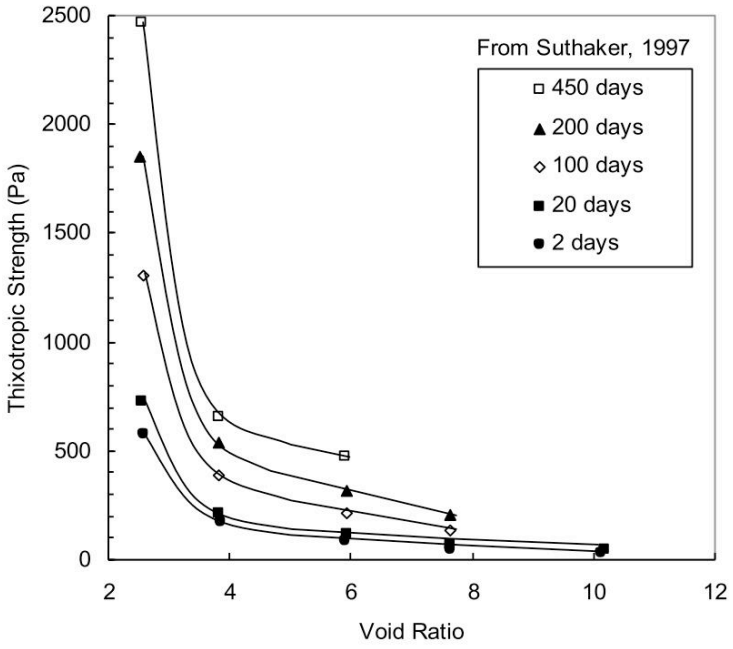


Figure 8. Thixotropic strength with time for cavity expansion tests.

The average total void ratio of the MFT in the standpipe in 2012 was 3.14. From Figure 9, then $\tau_u/\sigma'_{vo} = 0.50$. For an average shear strength of 1,400 Pa in the standpipe (Figure 7), then $\sigma'_{vo} = 2.8$ kPa. Therefore, the vertical effective stress has to exceed 2.8 kPa for consolidation to take place. As the vertical effective stress in the standpipe was less than this over most of its full height during the 30 years, no or little consolidation could take place, and creep was the main volume decrease mechanism. Self-weight consolidation progresses from the bottom up if there is no bottom drainage; therefore, most of the material is left at zero effective stress for a very long time. During this time, creep and thixotropic action can take place. The MFT in the tailings ponds is behaving similarly and is the reason why consolidation in the tailings ponds takes so long to become significant. As the void ratio decreases from creep, the hydraulic conductivity decreases, further slowing consolidation.

5.6 *Biogenic Gas*

All tailings ponds containing MFT generate gas from microbial action. Yong et al. (1982) reported on gas from microbial activity in the Suncor ponds, and Foght et al. (1985) studied the gas-producing microbial activity in the Syncrude MLSB. Figure 10 is a photograph of gas release from Syncrude's Mildred Lake Tailings Basin. Although the occurrence of gas in MFT has been studied, not all MFT tailings ponds have been investigated by biological researchers for possible diverse methanogenic communities. The only tailings pond that has undergone geotechnical research to determine the geotechnical implications of biogenic gas is Syncrude's MLSB (Guo et al. 2004). Both field and laboratory research on gas generation show increased water drainage from the MFT, an increase in solids content and an increase in shear strength as the gas bubbles to the surface.

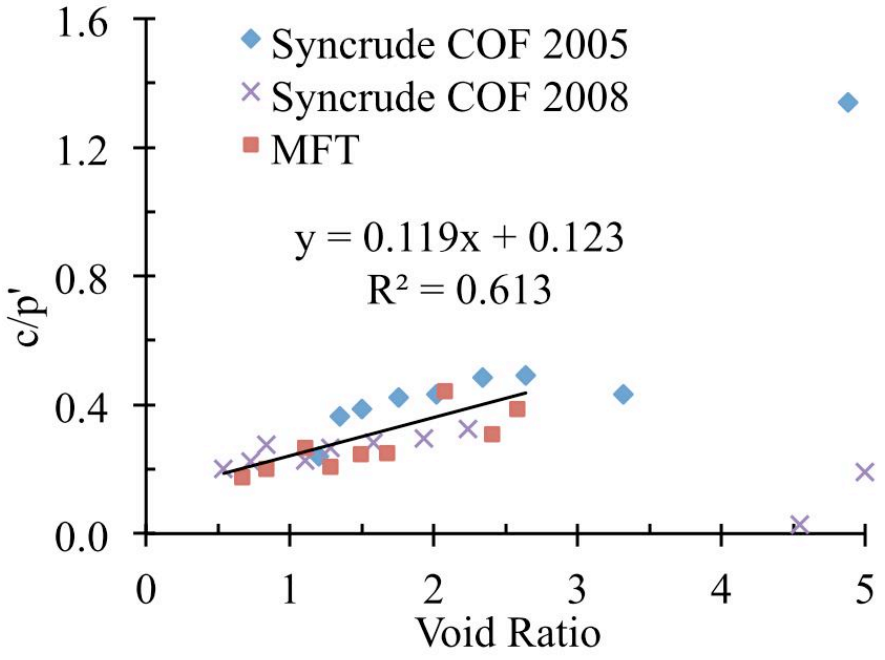


Figure 9. Undrained shear strength effective stress ratio



Figure 10. Photograph of gas release from Syncrude's Mildred Lake Tailings Pond

As the gas, which is mainly methane, bubbles upwards, it creates flow channels which greatly assist in water drainage and a fairly rapid increase in solids content takes place. This increase in solids content is usually considered as consolidation. However, there are other effects which must be considered. Although consolidation of tailings materials is usually considered as a decrease in volume, there are other mechanisms of volume decrease. The term "consolidation" should only be applied when there is a decrease in excess pore pressure resulting in an increase of effective stress. When gas bubbles exist in MFT, drainage of water resulting in an increase of solids content may not reduce excess pore pressure. As water drains out, the excess pore pressures tend to decrease, but a reduction in pore water pressure results in an expansion of the bubbles which can slow the excess pore pressure from dissipating and retards consolidation. Also, when excess pore pressures do decrease, more gas will come out of solution further retarding a decrease in volume.

Therefore, an increase in solids content does not necessarily mean the volume of MFT is smaller; it may be larger. Changes to MFT from gas generation must be evaluated by measuring both solids content and bulk density. Gas generation is then a benign property as it expels water from the MFT and increases its shear strength, but it is also a hostile property as it keeps excess pore pressures high.

6 MEASUREMENTS IN STANDPIPE

6.1 *Interface Settlement*

Figure 11 shows the settling behaviour of the MFT interface with time in the standpipe (Kabwe et al. 2013). The settlement of the MFT had reached approximately 3.5 m after 30 years. This settlement is not only the result of consolidation, as the excess pore pressures have not dissipated greatly during this period and remain close to the total stress in the top 65% of the MFT. As volume decrease at a constant effective stress (about 2 kPa in this case) is defined as creep, Figure 2 mainly shows the creep rate of the MFT.

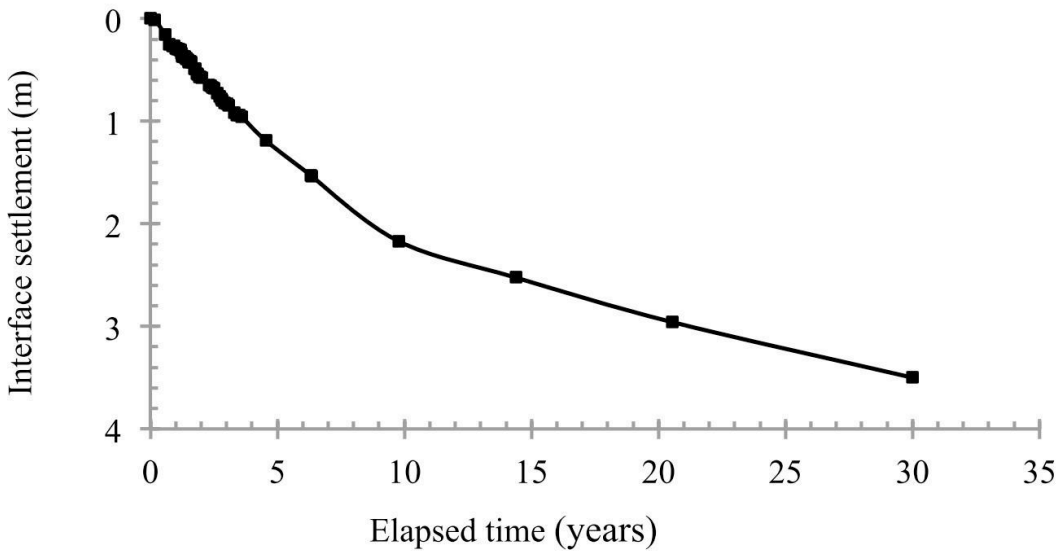


Figure 11. Interface settlement of the MFT in Standpipe 1

The settlement curve exhibits two settling rates: from Day 1 to Year 10 and from Year 10 to Year 30. It is postulated that the decrease in rate of settlement was the result of the thixotropic gain in strength of the MFT. The increase in strength is the result of the interparticle bonds increasing. These bonds increase the resistance to shearing as the MFT settles and slows the rate of creep.

6.2 *Particle Size Distributions in Standpipe 1 (from Kabwe et al. 2013)*

In the tailings ponds, segregation of the sand and fine tails slowly takes place. At a void ratio around 5, the fine particles are far enough apart that sand grains settle through the fines matrix. Therefore, the sand content increases with depth (MacKinnon and Sethi 1993).

In the oil sands industry, the sand-silt boundary is defined as being at 0.045 mm, which can be determined using the metric 45 μm sieve. The increase in sand content with depth results in a decrease in total void ratio (mass of solids/mass of water) with depth, which often is interpreted as consolidation taking place. However, the fines void ratio (mass of fines/mass of water) is relatively constant with depth indicating a lack of consolidation similar to the action in the standpipe. To guard against segregation taking place in the standpipe, the sampling depth of the MFT in the tailings pond for the standpipe tests was chosen where little sand remained. Monitoring for possible segregation in the standpipe was performed by measuring the particle size distribution with depth by the ASTM hydrometer-sieve test procedure (ASTM D422-63).

Figure 12 shows PSD results in 2012 at six depths: 4 m, 4.5 m, 6 m, 8 m, 9.5 m and 10 m. The PSDs in Figure 12 are very constant showing no increase in particle size with depth. Similar testing was performed in 1985 and 2003. The PSDs in those tests were also constant with depth and the same as the 2012 measurements (Jeeravipoolvarn 2005). As the particle size profiles do not show a significant change and are within the range of experimental error, it is concluded that no segregation took place during the 30-year history of the standpipe.

6.3 *Gas in the Standpipe*

As the MFT in the standpipe came from Syncrude's Mildred Lake Tailings Pond, the possibility of gas generation and gas bubbles forming in the standpipe MFT has been monitored. In 1997, 2003 and 2012, MFT samples have been taken to determine whether gas bubbles had formed. In the sampling procedure, the pore pressures with depth were first measured. A sampling tool was

developed where the sampling syringe could be first pressurized to the in situ pore pressure. A MFT sample was then slowly pulled into the syringe under the in situ pore pressure and kept under this pore pressure while its volume and mass were determined. This procedure was necessary to prevent any gas bubbles from expanding or gas coming out of solution during sample extraction and measurements. The degree of saturation of the samples could then be calculated.

Figure 13 shows the degrees of saturation with depth in 1997, 2003 and 2012. These are approximately 100% in all three sampling programs. No gas bubbles have developed in the standpipe MFT during its 30-year life. In 2012, a microbial investigation of the MFT (Foght 2012) did determine the existence of residual naphtha and viable microbial cells, including methanogens, but they were not the right microbes to anaerobically degrade naphtha hydrocarbons.

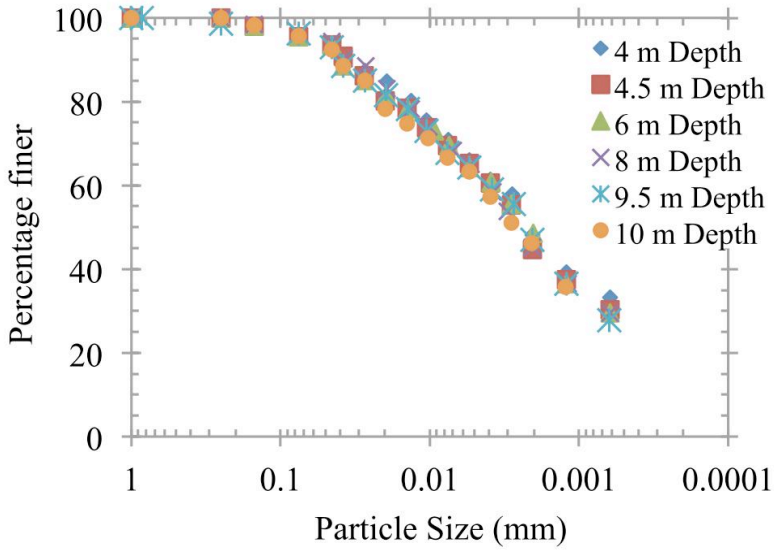


Figure 12. Particle size distribution of MFT in Standpipe 1 at different depths measured in 2012

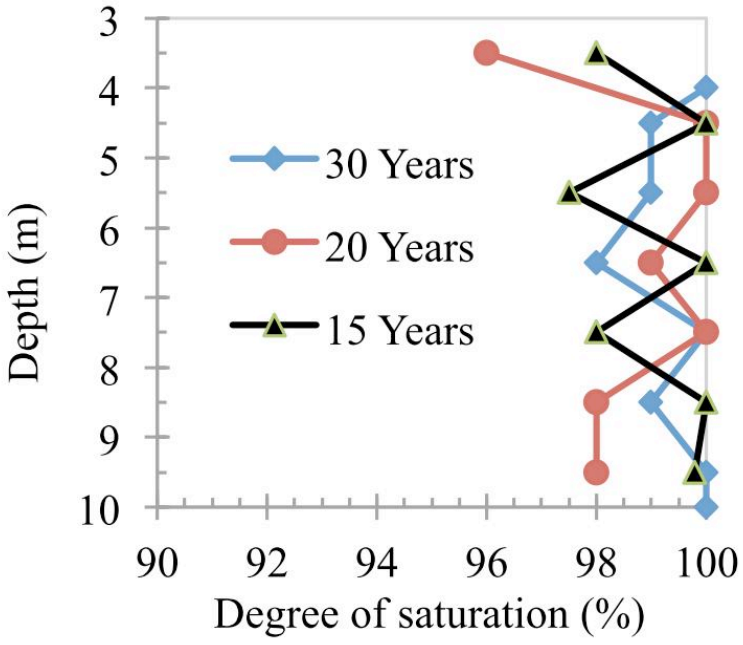


Figure 13. Degree of MFT saturation in Standpipe 1

6.4 *Adjusted Total Stress*

Generally, in geotechnical engineering, the percent consolidation and the magnitude of the effective stress are calculated by comparing the total vertical stress and total pore pressure. In low density slurry deposits where the water surface is at or above the water - fine tailings interface, the hydrostatic water column (the hydrostatic pore pressure) makes up a high portion of the total vertical stress and total pore pressure. A clearer picture of the increase in percent consolidation and development of effective stress is shown when the hydrostatic pore pressure is subtracted from both the total stress and the total pore pressure and the adjusted total stress and excess pore pressure are compared (Miller et al 2011).

Pore pressures in standpipes or tailings ponds can be measured with manometers, piezometers or pore pressure probes. Total stress, on the other hand, must be determined by measuring the slurry density changes with depth by direct sampling at a number of depths or by geophysical density probes. A problem with standpipe testing therefore arises in that every time a pore pressure profile is measured, a density profile should also be measured. If density samples were taken often, this would affect the volume of tailings in the standpipe. For this reason, density samples were only taken about once a year.

The adjusted total stress at other times has been approximated by taking advantage of the properties of low density slurries. At the interface, the adjusted total stress is always zero, and at the bottom of a standpipe, it is constant at the initial value. A straight line between these two points will approximate the adjusted total stress with only a small error. The actual adjusted total stress is calculated from density samples taken at 1-m intervals in the standpipe. Figure 14 shows void ratios calculated from density samples taken on the initial deposit and at 10 years and 30 years. The actual adjusted total stress calculated from these void ratio profiles is plotted in Figure 15. The approximated adjusted total stress is also plotted in Figure 15 for comparison. There is little difference in the two methods for determining the adjusted total stress. The approximation works when the solids contents of the tailings is small; changes in solids contents from creep and some consolidation have little effect on the density of the MFT, as the MFT is mainly water.

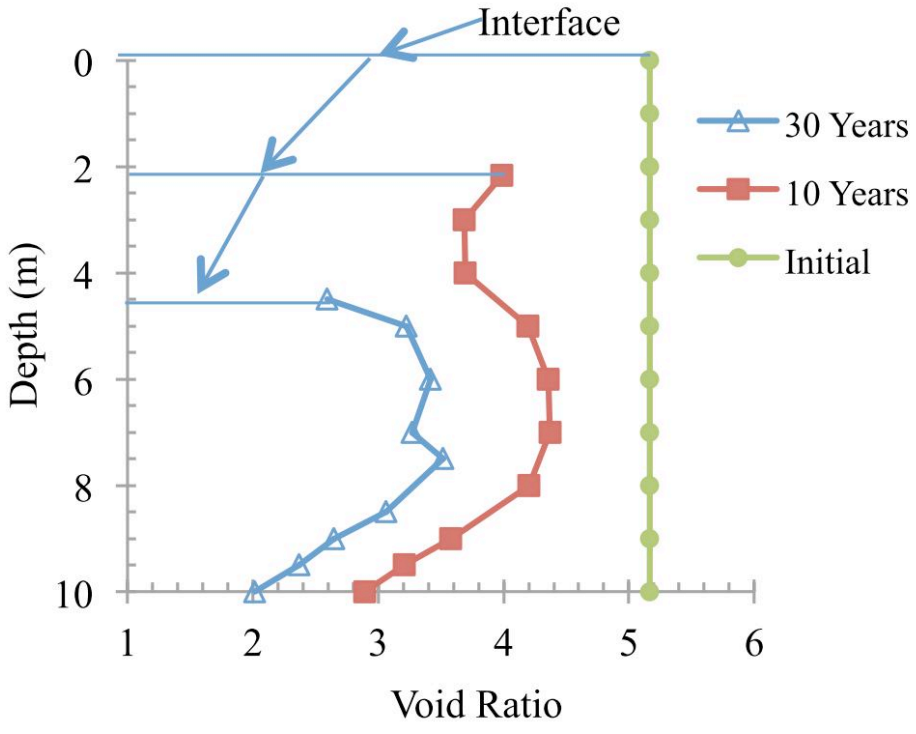


Figure 14. Void Ratio profiles

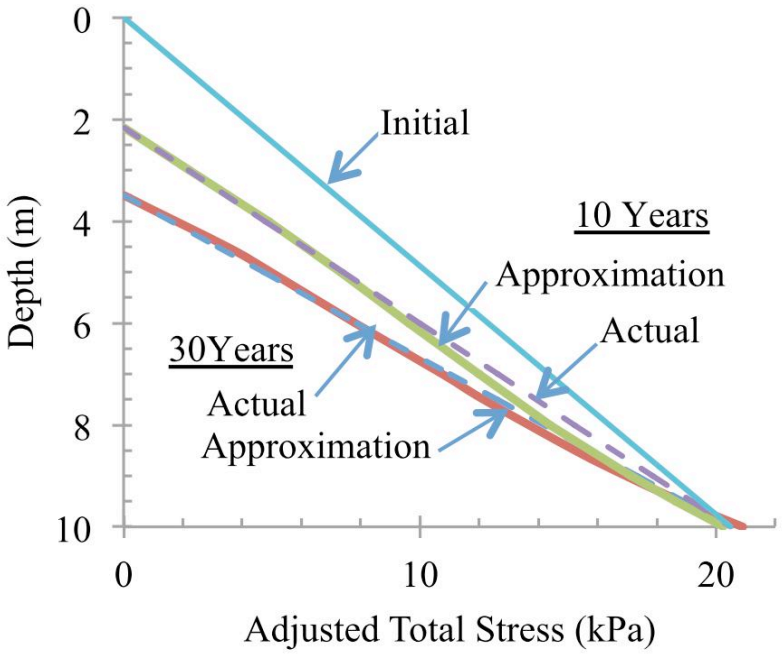


Figure 15. Actual and approximate adjusted total stress profiles

6.5 *Development of Effective Stress in the Standpipe*

6.5.1 *The First 900 Days*

The interface settlement and changes in effective stress in the first three years are instrumental in showing the effect of thixotropic strength in the MFT. Figure 16 shows the interface settlement in the first 900 days. During the first 50 days, little settlement took place. This behaviour is common for tests on MFT (Miller et al. 2010b). A standpipe test on a high water content slurry progresses through three stages. When the standpipe is filled with the slurry, a flocculation period or induction time may elapse during which no measurable settlement takes place. Following this period, settlement in the form of hindered sedimentation will occur, and then eventually long-term consolidation settlement continues until the excess pore pressures are fully dissipated. The 10-m standpipe had an induction period of about 50 days, and significant creep settlement did not commence until after about 100 days.

Figure 17 show the excess pore pressures in the standpipe in the first 900 days at four depths: 1 m, 4 m, 7 m and 10 m. Excess pore pressures were measured at 11 depths in the standpipe, and the changes were constant with depth. Only four depths are shown here for simplicity; all depths can be seen in Jeeravipoolvarn (2005).

In the first 70 days, the excess pore pressures dropped about 2 kPa throughout the 10 m height, although no significant interface settlement had occurred. The excess pore pressures then increased about 1 kPa over the next 60 days as interface settlement took place. After this period, a slow decrease in excess pore pressures occurred in parallel with the interface settlement. The decrease of 2 kPa in excess pore pressure is attributed to a 2 kPa thixotropic strength increase. Creep settlement caused shearing of the thixotropic bonds resulting in the 1 kPa increase in excess pore pressure. The long-term decrease in excess pore pressure was not caused by an increase in effective stress, but by the total stress decreasing as the interface moved downward.

6.5.2 *Thirty Years of Measurements*

Figure 18 shows the development of effective stress at eight different times over the 30-year history of the standpipe. Initially, the excess pore pressure was equal to the adjusted total stress. At 78 days, an effective stress of about 2 kPa had developed over the full height of the standpipe

from thixotropy. At 115 days, this effective stress had decreased to about 1 kPa over the full height of the standpipe from settlement shearing of the thixotropic bonds. At three years, the thixotropic bonds did not change much. From 10 years to 20 years, the thixotropic bonds were present in the lower half of the MFT and consolidation had occurred in the bottom meter. At 30 years, some consolidation had occurred in the bottom 2 meters, and a 2 kPa thixotropic bond had re-established in the top 4.5 meters.

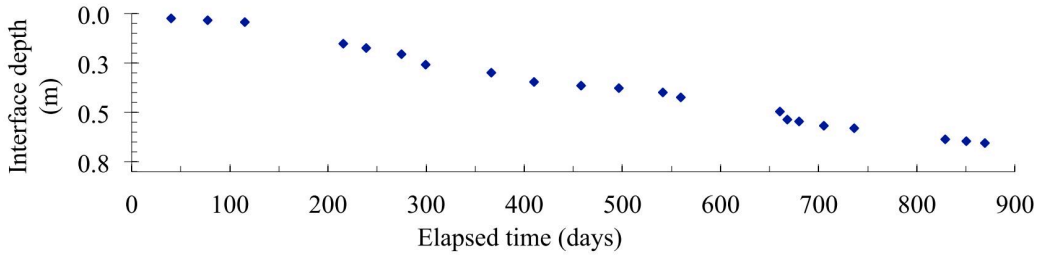


Figure 16. Interface settlements in the standpipe in the first 900 days

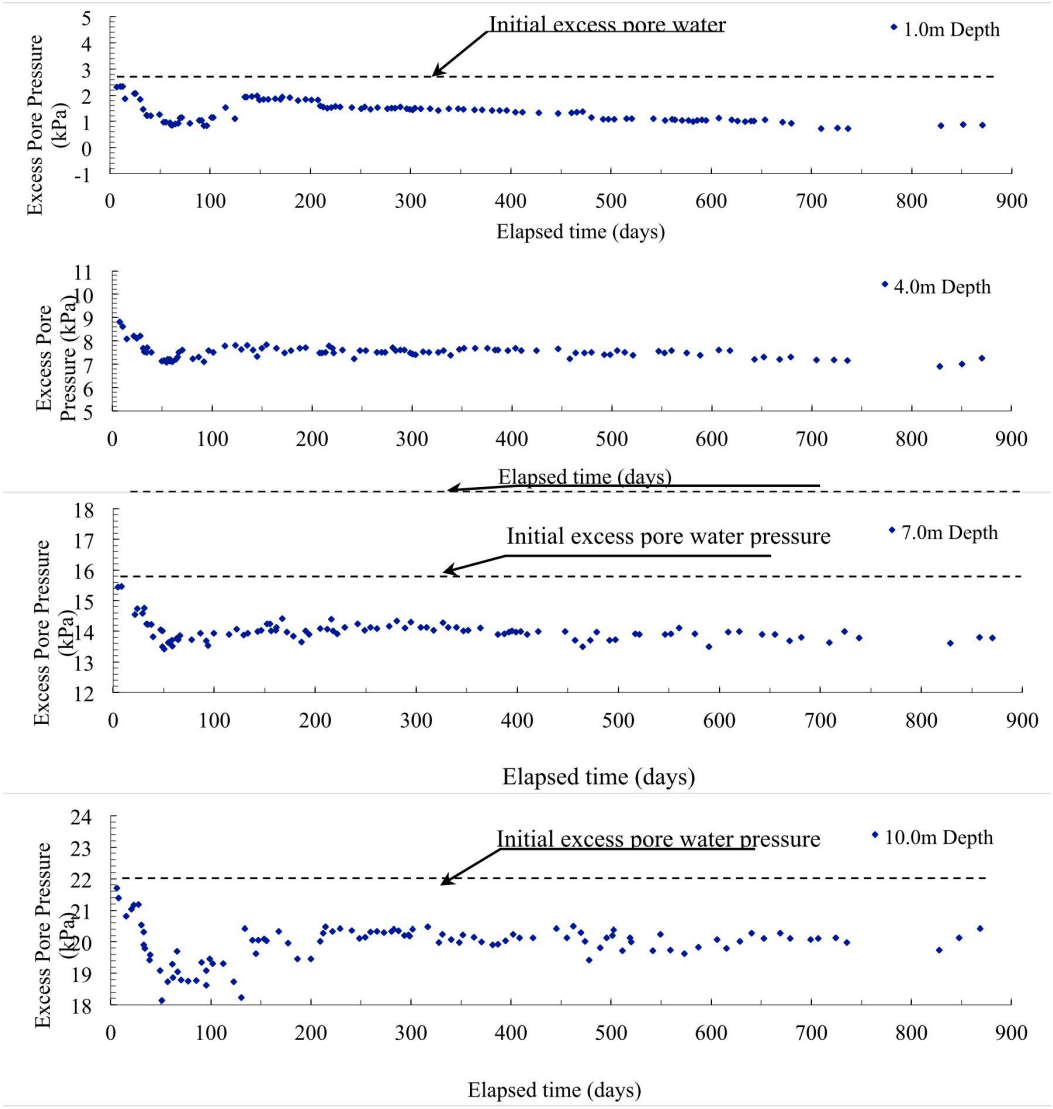


Figure 17. Excess pore pressures in the standpipe in the first 900 days

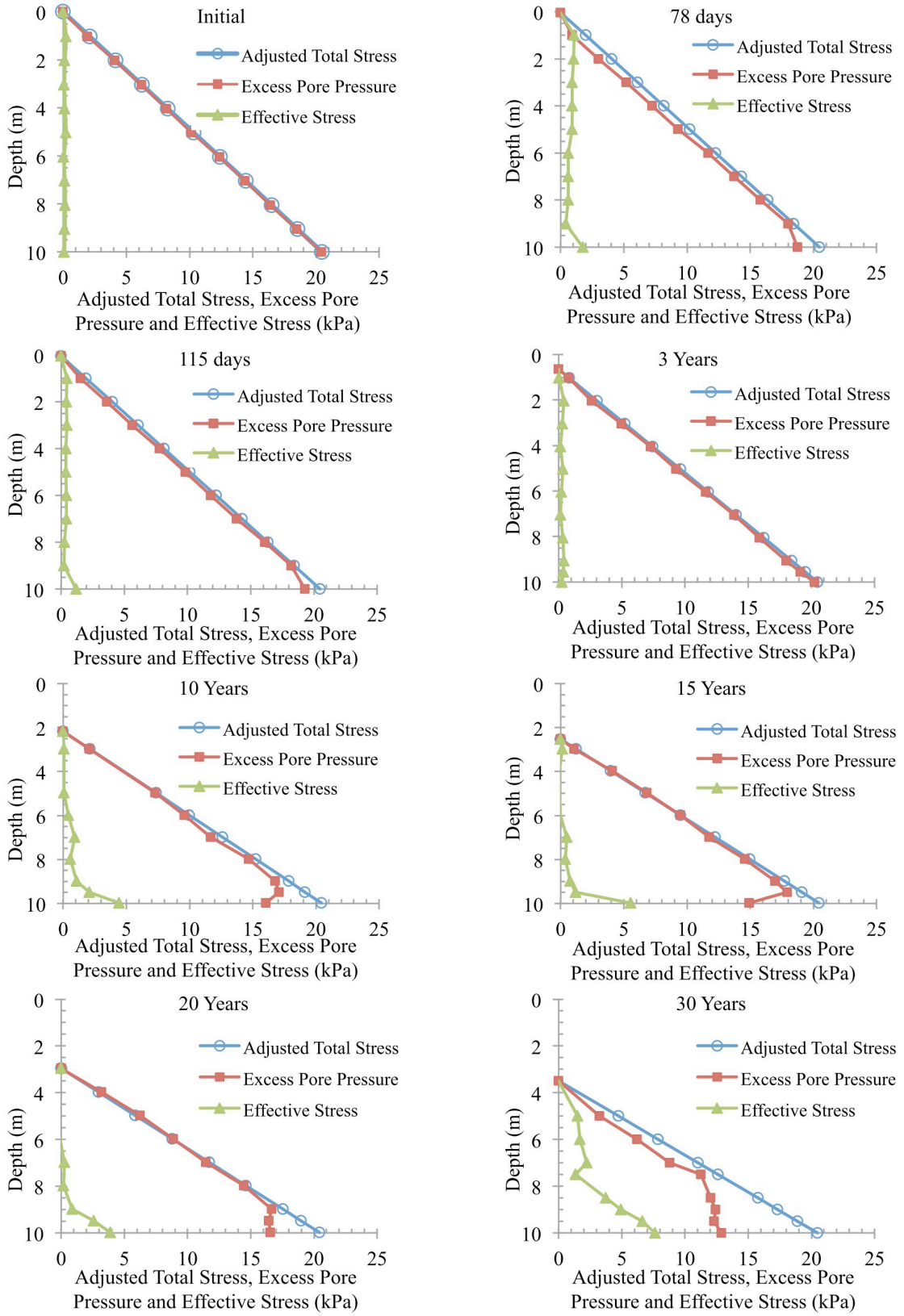


Figure 18. Effective stresses in the standpipe from the initial deposit to 30 years

7 SUMMARY AND CONCLUSIONS

Much research is underway to find ways to dispose of oil sands fine tailings in an acceptable manner. The first part of this paper reviews the properties of MFT and suggests which properties cause difficulties in disposal plans and hinder the consolidation of the tailings. The second part of the paper reviews the 30-year performance of a 10-m high standpipe containing MFT to evaluate these difficult properties. The main purpose of this review is to suggest to others what MFT properties have to be considered in research on MFT management and disposal.

The properties of the fine fluid tailings are the result of the amount and mineralogy of the clays, the amount and chemistry of the pore water and the amount and chemistry of the bitumen. Although considerable research has successfully identified these parameters, the resulting interactions which determine the geotechnical properties are still open for discussion. Research on these interactions has to carefully model the dispersion of the clays in the tailings ponds.

The dispersed fines are the major hostile property of the tailings. The fines in the tailings mainly come from clay-shale inclusions in the oil sands McMurray Formation. Too often the clay-shale aggregates and clay booklets are dispersed considerably more in research projects then that which occurs in the mining, extraction and tailings disposal processes resulting in unsubstantiated conclusions.

The fine tailings are characterized as dominantly kaolinite and illite. As kaolinite and illite are not very active clays, the mineralogy properties can be considered a benign property. The extraction process water chemistry and the organic content (bitumen), however, change the mineralogy to a hostile property.

The role of bitumen is not well understood and too often is not considered. Defining the amount of bitumen as a percent of the mass of tailings leads to an under appreciation of its influence. Defining the amount of bitumen as a percent of the volume of the solids in the tailings is a better definition. As the bitumen usually forms about 15% to 20% of the volume of solids in MFT, its influence on compressibility and hydraulic conductivity requires more study.

The effect of biogenic gas in the MFT tailings ponds is generally not studied. The oil sands tailings technology roadmap and action plan only mentions gas in a minor role. As the gas is mainly methane, its role in total greenhouse gas release at the oil sands mining projects is important. Often the solids content of the MFT is used to define its properties, which tacitly assume the MFT is 100% saturated. As well as measuring solids content, the bulk density at in situ pore pressure should also be measured to determine the amount of gas which is present. The existence of viable microbial cells, including Methanogens and the hydrocarbons which feed them, should be standard measurements in MFT tailings ponds to evaluate whether gas is being generated or may be in the future.

All tailings ponds containing MFT generate gas from microbial action. As the gas bubbles upwards, it creates flow channels which greatly assist in water drainage and a fairly rapid increase in solids content takes place. Gas generation is then a benign property as it expels water from the MFT and increases its shear strength, but it is also a hostile property as it keeps excess pore pressures high.

No gas bubbles have developed in the standpipe MFT during its 30-year life, as the 1982 standpipe MFT did not contain the right microbes to anaerobically degrade naphtha hydrocarbons.

An interesting conclusion from the property review and standpipe performance is that thixotropy overconsolidates the MFT and retards consolidation until effective stresses are large enough to overcome the overconsolidation stress. During this period, the MFT settles by a creep process which reduces the hydraulic conductivity and further hinders the consolidation process. As both thixotropy and consolidation are void ratio and time dependent, considerable time is required for a vertical effective stress to overcome thixotropic strength.

The particle size distribution profiles of MFT in the 10-m standpipe have not show a significant change during the 30-year history, and it is concluded that no segregation has taken place during this period.

8 ACKNOWLEDGEMENTS

A number of faculty and staff members, postdoctoral fellows and graduate students at the University of Alberta assisted in various aspects of this research program. Thank you to Vivian Giang who assisted in the editing and final preparation of this paper.

9 REFERENCES

Bjerrum, L. and Simons, N.E. 1960. Comparison of Shear Strength Characteristics of Normally Consolidated Clays, *1st PSC, ASCE*, 711-726.

Beier, N., Sorta, A.R, Wilson, W., and Sego, D.C. (2012). Challenges with meeting regulatory compliance in the oil sands industry. *Geotechnical News, Waste Geotechnics, 30(1):36-39.*

Dereniwski, Y. & Mimura, W. 1993b. Sand layering and enrichment to dispose of fine tails. *In Oil Sands-Our Petroleum Future Conference, April 4-7: Paper F20.*

ERCB, 2009. Directive 074: Tailings performance criteria and requirements for oil sand mining schemes. *Energy Resources Conservation Board of Alberta*, Calgary, February 3, 13 p.

ERCB, 2013. 2012 Tailings management assessment report, oil sand mining industry. *Energy Resources Conservation Board of Alberta*, Calgary, June, 11 p.

Fair, A. E. and Beier, N. A., 2012. Collaboration in Canada's Oil Sands: Fluid Fine Tailings Management. *Proceedings of the Third International Oil Sands Tailings Conference*, University of Alberta Geotechnical Centre, Edmonton, AB, 2-5 December, 3-12.

FTFC (Fine Tailings Fundamentals Consortium). (1995). Fundamental properties of fine tails basis for control of fine tailings behavior. *In Advances in Oil Sands Tailings Research*: Vol III (pp. 9-13). Edmonton: Alberta Department of Energy, Oil Sands and Research Division.

Foght, J. M., Fedorak, P. M., Westlake, D. W. S. and Boerger, H., 1985. Microbial content and metabolic activities in the Syncrude tailings pond. *AOSTRA J. of Research*, 1(3), 139-146.

Foght, J. M. 2012. Personal Communication.

Government of Alberta, 2011. About the resource. www.oilsands.alberta.ca/resource.html.

Guo, C., Chalaturnyk, R.J., Scott, J.D. and MacKinnon, M., 2004. "Densification of Oil Sands Tailings by Biological Activity", *Proceedings of the 57th Canadian Geotechnical Conference*, October 24-27, GeoQuebec2004, Quebec City, pp. 30-37.

Holtz, R.D. and Kovacs, W.D. 1981. An Introduction to Geotechnical Engineering. Prentice-Hall, Englewood Cliffs, NJ, 733 p.

Jeeravipoolvarn, S., 2005. Compression Behaviour of Oil Sands Tailings. *MSc Thesis*, University of Alberta, Edmonton, Alberta, Canada, 232 p.

Jeeravipoolvarn, S., 2010. Geotechnical Behavior of In-Line Thickened Oil Sands Tailings. PhD Thesis in Geotechnical Engineering, Department of Civil and Environmental Engineering, University of Alberta, Edmonton, Alberta, Canada, 431p.

Jeeravipoolvarn, S., Scott, J.D., and Chalaturnyk, R.J., 2009. "Three Ten Meter Standpipes: Experimental and Prediction", *Canadian Geotechnical Journal,* August, v 46, pp 875-888.

Kabwe, L.K., Scott, J.D, Sorta, A.R, Wilson, W., Kone, M., and Ulrich, A., 2013. Geotechnical characteristics of the mature fine tailings in a 30-year10-m standpipe experiment, Paper accepted for presentation at the GeoMontreal2013, Montreal, September 29 to October 3, 2013.

Kasperski, K.L., 1992. A review of properties and treatment of oil sand tailings. *AOSTRA Journal of Research*, 8, 11-53.

Kasperski, K.L., 2001. Review of research on aqueous extraction of bitumen from mined oil sands. Division Report CWRC 01-17 (CF), *Natural Resources Canada*, CANMET-WRC, May, 208p.

MacKinnon, M.D. & Sethi, A., 1993. A comparison of the physical and chemical properties of the tailings ponds at the Syncrude and Suncor oil sands plants. In *Oil Sands-Our Petroleum Future Conference*, April 4-7: Paper F2. Edmonton.

McKenna, G., Dawson, R., Hyndman, A., LeSueur, P. And Sobkowicz, J., 2012. The oil sands tailings technology roadmap and action plan: oil sands tailings state of practice overview. *Proceedings of the Third International Oil Sands Tailings Conference*, University of Alberta Geotechnical Centre, Edmonton, AB, 2-5 December, 205-212. Edmonton.

Mikula, R. J. and Omotoso, O. E., 2004. High surface areas caused by interstratification of kaolinite and illite in Athabasca oil sands. *Applied Clay Science*, vol. 25, no. 1, pp 37-47.

Mikula, R., 2012. Evaluation of off the shelf and off the wall tailings treatment technologies: a cautionary tale. . *Proceedings of the Third International Oil Sands Tailings Conference*, University of Alberta Geotechnical Centre, Edmonton, AB, 2-5 December, 231-236.

Miller, W.G**.,** Scott, J.D. and Sego, D.C., 2010a**. "**Influence of the Extraction Process on the Characteristics of Oil Sands Fine Tailings", *Canadian Institute of Mining, Metallurgy and Petroleum Journal*, v 1, n 2, pp 93-112.

Miller, W.G., Scott, J.D., & Sego, D.C., 2010b. "Influence of Extraction Process and Coagulant Addition on Thixotropic Strength of Oil Sands Fine Tailings". *Canadian Institute of Mining, Metallurgy and Petroleum Journal*, v 1,n 3, 197-205.

Miller,W.G., Scott, J.D., & Sego, D.C., 2011. Effect of Extraction Water Chemistry on the Self-weight Consolidation of Oil Sands Fine Tailings. *Canadian Institute of Mining, Metallurgy and Petroleum Journal*, v 2, n 1, pp 40-54.

Mitchell, J.K. & Soga, K. (2005). Fundamentals of Soil Behaviour, Third Edition. New York: John Wiley and Sons, Inc.

Morgenstern, N. R. and Scott, J. D., 1997. Oil Sand Geotechnique. *Geotechnical News*, Special Edition, 102-109.

Penner, T. J. and Foght, J. M., 2010. Mature fine tailings from oil sands processing harbour diverse methanogenic communities. *Can. J. Microbiology* 56, 459-470.

Scott, J.D., Dusseault, M.B. & Carrier III, W.D., 1985. Behavior of the clay/bitumen/water sludge system from oil sands extraction plants. *Applied Clay Science*, vol. 1, no. 12, pp 207-218.

Sobkowicz, J., 2012. The oil sands tailings technology roadmap and action plan: introduction and key recommendations. Proceedings of the *Third International Oil Sands Tailings Conference*, University of Alberta Geotechnical Centre, Edmonton, AB, 2-5 December, 13-22.

Sorta, A.R. and Sego, D.C. (2010). Segregation related use of Centrifuge in Oil Sands Tailings. *63rd Canadian Geotechnical Conference*, Calgary, Alberta, 656-664.

Suthaker, N.N. and Scott, J.D., 1996. "Measurement of Hydraulic Conductivity in Oil Sand Tailings Slurries". *Canadian Geotechnical Journal,* 33 (4), 642-653.

Suthaker, N. N., and Scott, J. D., 1997. "Thixotropic Strength Measurement of Oil Sand Fine Tailings." *Canadian Geotechnical Journal*, 34(6), 974-984.

Weber, B., 2013. Regulator, industry find oilsands cleanup harder than first thought. *The Canadian Press*, June 11.

Yong, R. N., Sheeran, D. E., Sethi, A. J. and Erskine, H. L., 1982. The dynamics of tar sand tailings. *Proceedings of the Sixth Symposium on Engineering Applications of Mechanics,* Calgary, AB.

Residual bitumen and flocculation: do we understand its effects?

E. Santanach Carreras, N. Passade-Boupat, & M. Bourrel
Pôle d'Etudes et Recherches de Lacq, Total SA, Lacq, France

A. Sedgwick, X. Yang, and A. Junaid
Total E&P Canada Ltd., Calgary, Alberta, Canada

ABSTRACT: Thickening of tailings is gaining importance as a way of treating the fines generated from oil sands bitumen extraction. During the extraction process, some residual bitumen is left with the tailings. It is not well understood whether the presence of this residual bitumen is beneficial or detrimental to the flocculation of the tailings. In this study, we investigated the effect of residual bitumen attached to the fines on flocculation. We found an optimal residual bitumen concentration. Despite the limited data, it seems that the optimal ratio of residual bitumen to solids is in the vicinity of 0.01. The physical meaning of this ratio is yet to be understood.

1 INTRODUCTION

Thickening of tailings through flocculation, coagulation, or a combination of both is a technique widely used in mining operations to accelerate consolidation of the solids before their disposal in order to maximize the reuse of water. The use of thickening agents does not only impact the water usage but also improves the stability and safety of tailings storage, and minimizes the potential for environmental damage and land footprint of operations.

For sustainability of the oil sands mining industry, the importance of tailings disposal areas is very high, as they are one of the long-term legacies of mining operations (Tacey and Hart, 2006). For the industry, it is necessary not only to have a managing plan for the future tailings, but also to take care of the tailings inventory accumulated over the years. Without an effort made in this direction, the stake-holders of the oil sands industry will be challenged by the increasing social and environmental standards. Thickening of tailings seems to be gaining acceptance within the industry.

Oil sands tailings have one particularity as described in the mid 80s by Scott *et al.* (1985). During the extraction process some residual bitumen is left within the tailings. Typically, the amount of this residual bitumen is in the order of a few tenths of a percent with respect to the solids. Scott *et al.* (1985) claimed in their work that this residual bitumen, a portion of which is attached to the mineral solids particles and the rest is in the form of free droplets, is beneficial for the initial settling of the tailings. The free bitumen droplets are supposed to act as a coagulant by coalescing with residual bitumen patches attached to different solid particles. On the other hand, at longer time scales, following some consolidation and with an increased volume fraction of the dispersed phase, the bitumen will hinder further compaction as it reduces the relative permeability through water. Results on the effect of the residual bitumen on the settling of tailings have been reported in different studies since then (Majid and Sparks 1991, Thompson 2011, Klein *et al.* 2013). However, clear conclusions have not been established to date.

A recent study published experimental results on the effect of residual bitumen on the flocculation of mature fine tailings (MFT) (Klein *et al.* 2013). Three protocols were used in this work

to obtain samples with residual bitumen amounts varying between 0.08-0.45 wt%. Their results showed that the process used for bitumen removal plays a critical role on the subsequent performance of the flocculant. Particularly for MFT with low residual bitumen content, initial settling rates differed by a factor of 5 for different bitumen removal processes. Two regimes were identified—one at low bitumen content that is mineralogy dominated and the other at high bitumen content dominated by the presence of bitumen. In the bitumen dominated regime, increasing residual bitumen content hinders the initial settling rate.

Despite some progress (Mikula 2012) made over the years on investigation ofthe effect of residual bitumen on flocculation, some vital questions remain open. For example, to date the published works do not distinguish between the impacts of different types of residual bitumen. It is reasonable to think that the effect of residual bitumen on settling and on the flocculation process may vary depending on its form. Referring back to the work of Scott *et al.* (1985), two different possibilities are pictured: free bitumen droplets and residual bitumen attached to mineral solids. Free bitumen may act as a coagulant to facilitate settling. Attached bitumen, on the other hand, could prevent interactions between the flocculant and the mineral solids, inhibiting the flocculation process and hence reducing the settling rate for a given dosage of polymer, given all other parameters kept constant.

The aim of this work is to investigate the role of each type of residual bitumen. To attain this aim, fines samples extracted from ores in a laboratory batch extraction unit (BEU) cell were used. Methods similar to those used by Klein *et al.* (2013), namely different flotation times and solvent washing of fines, were used to produce samples with different amounts of bitumen. Measurements were carried out to differentiate the amounts of residual bitumen that is free and that is attached to the mineral solids. Knowing that the mineralogy of the samples can be affected by these sample preparation methods, experiments were conducted with a model kaolinite clay sample in addition to the oil sands tailings. Since a single type of minerals was used in this set of experiments, the mineralogy of the solids was the same across different experiments within the set. These experiments allowed us to illustrate both the effect of the free residual bitumen and the residual bitumen that is strongly attached to the mineral solids without being impacted by any mineralogical difference.

2 MATERIALS AND METHODS

2.1 *Ore samples and model fines*

A low grade and an average grade ore sample were procured from the Joslyn North Mine (JNM) for this study. In addition, a kaolinite sample was used as the model fines. The compositions of all samples with respect to bitumen, solids, and water contents are shown in Table 1. The choice of these ores was based on the amount of fines to limit the number of BEU extractions required to produce sufficient samples for the settling experiments.

Table 1. Principal compositional characteristics of the ores and fines used in this study.

Sample ID	Grade	Bitumen (wt%)	Water (wt%)	Solids (wt%)	Fines (wt%)	MBI (meq/100g)	Primary recovery (%wt)	Total recovery (%wt)
S2	Low	5.9	11.3	82.2	28	2.9	9	26
#5	Average	9.1	5.8	85.3	13.6	2.3	83	89
K	-	-	-	-	100	-	-	-

The mineral solids from these ores were recovered by floating the bitumen using a BEU cell. The flotation process was carried out at 50 °C using synthetic process water with pH adjusted to 8.3 prior to use. For each batch, 500 g of ore was initially mixed with 150 g of synthetic process water for 10 minutes at 600 rpm while injecting air through the impeller. An additional 1000 g of synthetic process water was then added, the air flow was shut off, and mixing was continued for 10 more minutes at 600 rpm. At this point the entire froth, which corresponds to the primary

recovery, is skimmed with a spatula, weighted and characterized. The air flow is then opened and the impeller speed is set to 750 rpm for 5 minutes. Any additional froth generated by this, termed as secondary recovery, is skimmed, weighted, and characterized. By choosing a low grade but high fines ore, the BEU procedure could be modified to ensure more or less bitumen was kept with the solids.

The water, mineral solids, and residual bitumen were recovered from the cell. Both coarse and fine tailings were present in this tailings and required separation. To achieve this, simple elutriation was conducted for 5 minutes. A diffraction laser granulometer, Mastersizer 2000 (Malvern), was used to verify that the mineral solids used for settling tests were below the 44 µm limit for fines. Figure 1 shows the cumulative particle size distribution for the fines obtained from each of the two ores and the model fines.

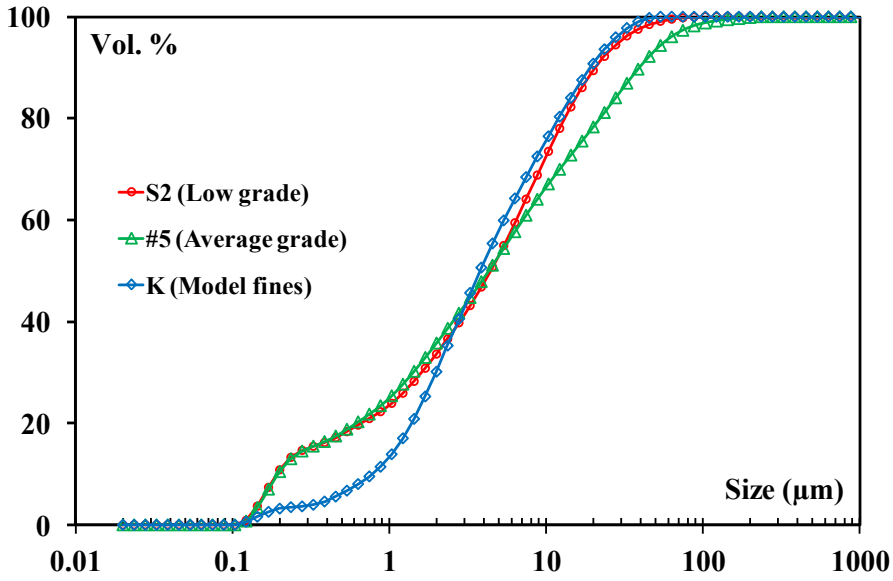


Figure 1. Particle size distribution of the fines extracted from a low grade (S2) and an average grade (#5) ore as well as the model fines used in this study.

For all three types of fines used, we see that nearly 100% of the particles have characteristic size below 44 µm as expected. Hence our experiments were carried out in the limit of Solids (> 44 µm) to Fines (< 44 µm) Ratio (SFR) ~ 0. The mean size of the main population was within the range of 6-10 µm. We observed that all three samples contained a small portion of particles that are ultra fines and have characteristic sizes of about 100-200 nm. This was more important for the fines generated from the ore than the model solids. These particles were small enough so that thermal and gravitational effects were comparable. Their settling would have occurred at time-scales much longer than the length of our experiments, especially when no flocculant was added. For tests with flocculant use, the settling of these ultra fines would be favored through direct interaction, or via entrainment within the flocs.

2.2 *Sample Preparation and characterization.*

Mixing of dispersed bitumen and mineral solids is a simple way to modify the residual bitumen content. An ultrasonic probe (Branson Sonifier 250) was used at 50% power output and on a 50% duty cycle to disperse purified bitumen extracted from the oil sands ores using a Dean-Stark apparatus. The bitumen was dispersed in synthetic process water for 10 minutes. The resulting bitumen droplets had a mean diameter of 1 µm and 99% of them had a characteristic size of <4 µm.

The amounts of residual bitumen on tailings were controlled by different degrees of toluene wash of BEU extracted tailings. This controlled the amount of residual bitumen attached to the

fines. Residual bitumen was added by mixing the fines sample with the dispersed bitumen as free droplets.

To quantify the amount of residual bitumen in the sample, a novel method based on the use of tetrahydrofurane (THF) and a spectrophotometer working in the UV-Visible range was used (Bourrel and Gras, 2012). THF is a good solvent of both the oil and aqueous phases. It forms a single liquid phase when mixed with the tailings. Extra heavy oils and bitumen from oil sands show a characteristic absorption peak at 406 nm where the absorbance by water is negligible. This peak corresponds to the presence of porphyrin complexes containing the vanadyl group VO^{2+} (Doukkali *et al.*, 2002; Evdokimov and Losev, 2006).

2.3 *Flocculation tests*

Settling tests were carried out in 500 mL graduated cylinders for the tailings samples generated from the JNM ores. Graduated cylinders of 100 mL were used for the settling experiments with the model fines. AF 309, a high molecular weight (14 MDa), highly branched and partially hydrolyzed polyacrylamide flocculant procured from SNF was the only polymer used for flocculation. A stock polymer solution of 1000 ppm concentration was used for all settling experiments. The flocculant was added stepwise to the graduated cylinder followed by a 2 minute settling test after each step. Each step represented 25 g of AF309 addition per ton of solids, which corresponds to 625 µL of stock polymer solution addition for the tests with the 500 ml graduated cylinders at 5 wt% solids. The sample was homogeneized with a plunger that was moved up and down in the graduated cylinder 10 times. The position of the mud line was followed for 2 minutes after homogenization. Addition steps were carried out as necessary to ensure the polymer dosage was above the optimal one. Typically, between 10 and 20 addition steps were carried out for each sample.

3 RESULTS

3.1 *Fines extracted from JNM ores*

Following the experimental procedures described above, batch settling tests were carried out for samples containing a constant amount of solids (5 wt%) and a varying amount of bitumen (ranging from 66 - 20,000 ppm). Care was taken to characterize the free and attached portions of bitumen in the samples.

Figure 2 reports the mud line height normalized by the total height as a function of time for a series of step additions. For clarity, data from all the steps had not been plotted; nevertheless the figure represents typical experimental results. The initial settling rate (ISR) was calculated as the initial slope (0-30 s) of the curve for the time slot specific to an addition step as schematically shown in the figure. The ISR for each step was then plotted as a function of the cumulative polymer dosage used. A typical curve is shown in the inset of the figure. Two distinct regions can be depicted in the inset. At the beginning (time scale of minutes) the settling rate is negligible, which is attributed to the small size of the fines in absence of any floc formation. With polymer addition floc formation occurs and the ISR increases until an optimum point is reached as indicated by the arrow in the inset. In the second part of the curve, the settling rate decreases. When the flocculant is overdosed, the flocs no longer grow with polymer addition. They may be too fragile and break-down during homogenization of the sample prior to settling. The excess flocculant can actually induce steric stabilization of the broken-down flocs. Although this particular example demonstrates a sharp decrease, the ISR can also remain constant following the optimal dosage as seen in other cases.

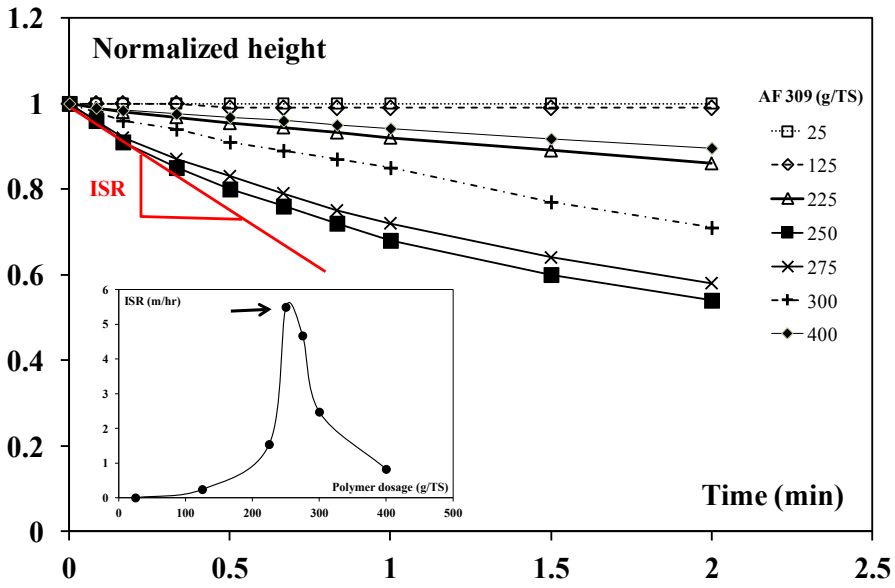


Figure 2. Typical experimental data obtained during batch settling tests with step-wise addition of AF 309 flocculant. This particular example was based on an average grade ore (Sample #5). Each curve shows the data obtained at different cumulative dosages of flocculant. For the curve corresponding to 400 g/ts (■), the straight line tangent to the experimental curve at the origin illustrates the calculation of ISR for that particular step. The inset shows the ISR as a function of polymer dosage and clearly shows an optimum in terms of ISR.

Figure 3 shows ISR values at optimal dosage as a function of the amount of attached residual bitumen (B_R) in the sample normalized by the amount of fines (S). The attached residual bitumen was considered only since free bitumen is expected to simply hinder the settling through hydrodynamics effects. In principle, the B_R/S normalization will allow comparison of data obtained from different residual bitumen and mineral solids concentrations. Let us first consider the data obtained with sample #5. The data point at B_R/S=0.017 and an ISR=4.5 m/hr corresponds to tailings suspension obtained from the BEU test. Despite a great variability in results, when the residual bitumen is decreased, the ISR will increase up to a point. The maximum average ISR obtained in our experiments is in the order of 9 m/hr at a $B_{R/S}$=0.008. An additional data point was generated for a sample with extended bitumen removal; the amount of attached residual bitumen left in the test graduated cylinder was 66 ppm. In this case, at B_R/S~ 0.0013, a significantly lower ISR is seen, and after 2 minutes no effect of the flocculant was observed for polymer dosages as high as 500 g per ton of fines. Finally, an experiment with the addition of 1000 ppm of free bitumen was carried out. In this case the ISR remained comparable to the reference one determined with the tailings sample as obtained from the BEU test (B_R/S=0.017).

Data obtained with the low grade sample showed a similar trend. In this case the reference sample, as obtained from the BEU, is the right-most data point. The ISR values tend to increase with significant bitumen removal. However, the window for increasing ISR is quite narrow and a maximum can be expected somewhere in the vicinity of a B_R/S in the order of 0.008.

Trying to understand the magnitude of the maximum ISR is well-beyond the objective of this study given the limited amount and variability of data. Nevertheless, a significant improvement is observed when some of the residual bitumen is removed, and a weight ratio B_R/S~0.01 is reached.

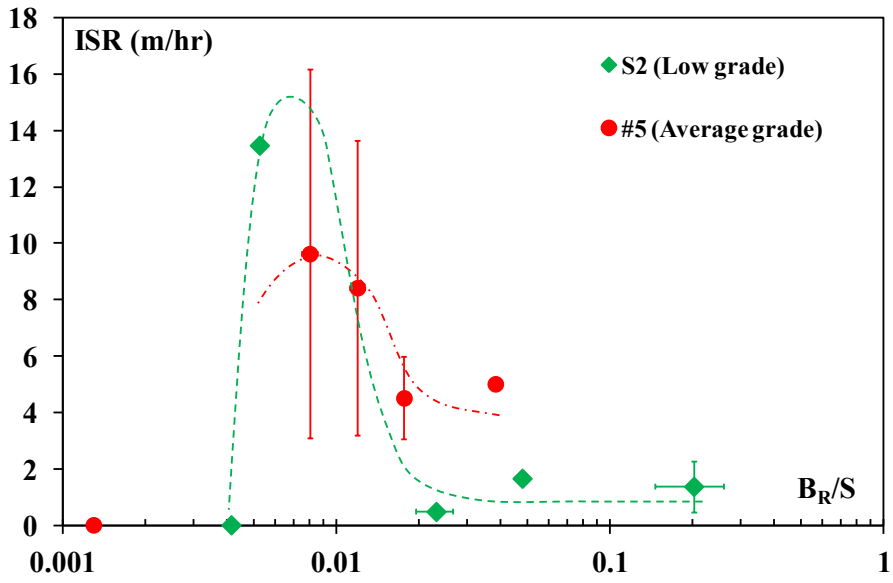


Figure 3. ISR at optimal flocculant dosage as a function of residual bitumen normalized by fines content for the different samples considered.

3.2 *Experiments with model fines*

Use of model fines can provide insight on the role of residual bitumen on the settling of fine tailings. Model fines allow better control of the sample preparation as the nature of the solids remains constant. Additionally, it provides a clean reference state free of any solvents used to wash and remove residual bitumen on the solids obtained from the BEU process.

The model samples in this study were prepared by adding a bitumen emulsion into a suspension of clean model fines. The first thing examined in this process was how the bitumen interacted with the dispersed solids even in the absence of any flocculant. It should be noted that at the pH of the experiments (8.3), the free bitumen droplets were not very stable—they tend to coalesce and cream at the free air-liquid interface. For the model fines experiments the creamed free bitumen was removed prior to the flocculation tests. Hence, for the results presented in this section, it can be considered that only attached residual bitumen, B_R, was present. Figure 4 shows the amount of residual bitumen attached to the fines as a function of the total amount of bitumen added to the sample. If all the added bitumen were to attach to the clean model fines, the data points would have aligned with the dashed line representing a 1:1 slope. It was observed that above a bitumen concentration of ~0.05% approximately 55-60% of the added bitumen remained as residual bitumen attached to the solids.

Figure 4 demonstrates that different amounts of bitumen can be added into the model fines suspensions in a controlled manner. The next step in the study was to determine the effect of this bitumen onto the model fines in absence of any flocculant. For this, fines suspensions at 5 wt% with different amounts of residual bitumen were prepared and batch settling tests were carried out. The ISR were determined and are reported as a function of B_R/S in Figure 5. The dashed line in the figure is only a suggested data trend if additional experiments were carried out at intermediate bitumen concentrations. When the fines were allowed to settle freely without the addition of any polymer the ISR was 0.20 m/hr. The actual experimental bitumen concentration data cannot be plotted on the graph as a logarithmic scale is used. The ISR increases with the increase in the amount of residual bitumen present in the sample with the addition of bitumen. Since an increase in the amount of dispersed free bitumen would have resulted in increased hydrodynamic hindering, this can only be attributed to the interactions between the bitumen and fines. As depicted By Scott *et al.* (1985), the initially free bitumen droplets will attach to the fines creating small clusters. The mean size of these clusters will increase with increasing bitumen concentration and hence the settling will be faster. The range of residual bitumen was limited to $B_R/S<0.012$ at which the mud line was no longer detectable. One last data point was ob-

tained with a sample containing $B_R/S=0.1$. To achieve such a high ratio it was necessary to soak the fines in a bath of bitumen diluted with toluene. The toluene was then allowed to evaporate and the remaining mixture of fines and bitumen was then washed of any excess bitumen with water, mixing, and flotation. The ISR determined for this data point is slightly higher (0.25 m/hr) compared to that of the clean fines (0.2 m/hr) and significantly lower than the maximum value (~1 m/hr). Hence, the model study conforms to the facts that there is an optimum B_R/S ratio for settling with additional bitumen and that is within the vicinity of 0.01.

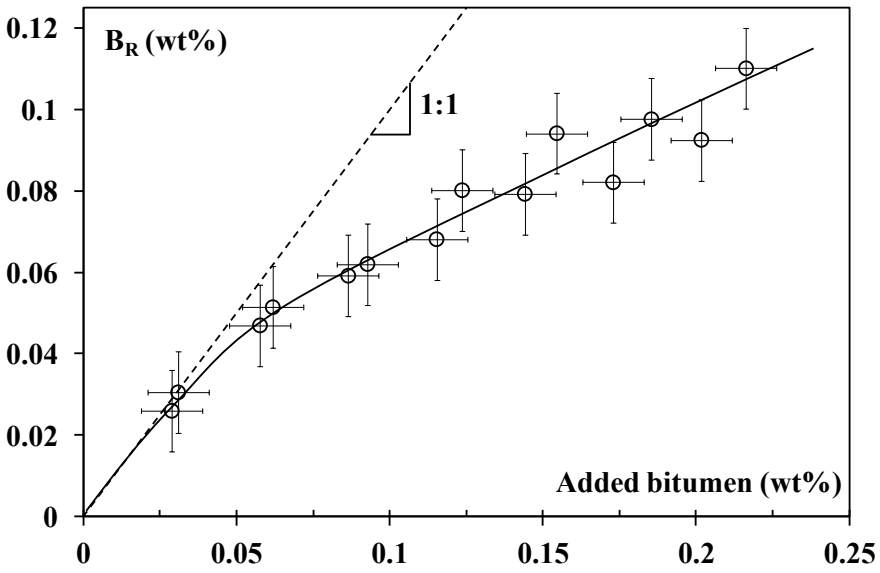


Figure 4. Residual bitumen, B_R, as a function of the added bitumen for the model fines tests.

With the flocculant free baseline data it was possible to study the effect of the flocculant on the settling performance of model fines with different levels of residual bitumen. Experiments with four different B_R/S ratios were carried out and the ISR determined for each at the different polymer dosages are reported in Figure 6. For model fines without any residual bitumen (presented by circles in Figure 6), the ISR is initially ~0 m/hr, which, with the stepwise addition of flocculant and floc growth, increases until an optimum point is reached. Up to this point this is similar to what we observed for the JNM ore sample (Figure 2). However, for the model system, this optimal ISR value remains constant despite overdosage of flocculant in contrast to our observations for the JNM ore sample, which shows decrease in ISR values with overdosage (Figure 2). This is attributed to the floc size and structure in the model system. Most possibly the size of the flocs remains constant despite overdosage of flocculant and their structure inhibits any shear induced effect on their size or ability to rebond when broken during homogenization.

Increasing the amount of residual bitumen shows an improvement on the ISR in general while maintaining similar trend. At $B_R/S=0.006$ the ISR at the optimal polymer dosage is ~8 m/hr, compared to the ~5.4 m/hr at $B_R/S=0$. Further increasing the residual bitumen content increases the ISR albeit less significantly. The ISR determined at a $B_R/S=0.011$ is ~9 m/hr. This is nearly a 2-fold increase compared to the clean fines and can be considered significant.

Increasing the amount for residual bitumen further, up to $B_R/S=0.1$, results in a significant decrease in ISR at the optimal polymer dosage. It is noteworthy to mention that that defining an optimal polymer dosage for this experiment in particular was not trivial since the settling rate kept increasing with the polymer dosage. Nevertheless, the ISR for this case is always significantly lower than the ISR for the clean model fines.

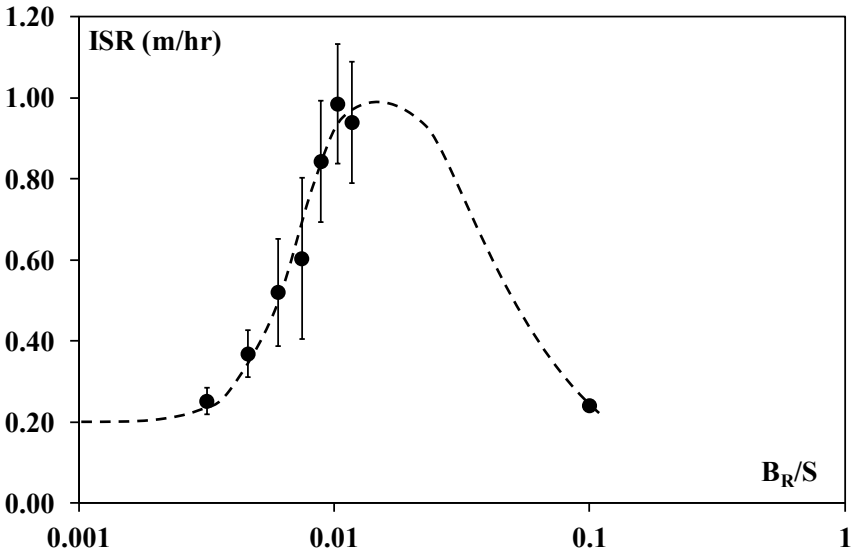


Figure 5. ISR determined as a function of residual bitumen normalized by the fines concentration (B_R/S) for batch settling tests without flocculant using model fines. The dashed line is only an expected trend including intermediate bitumen concentrations not tested in this study.

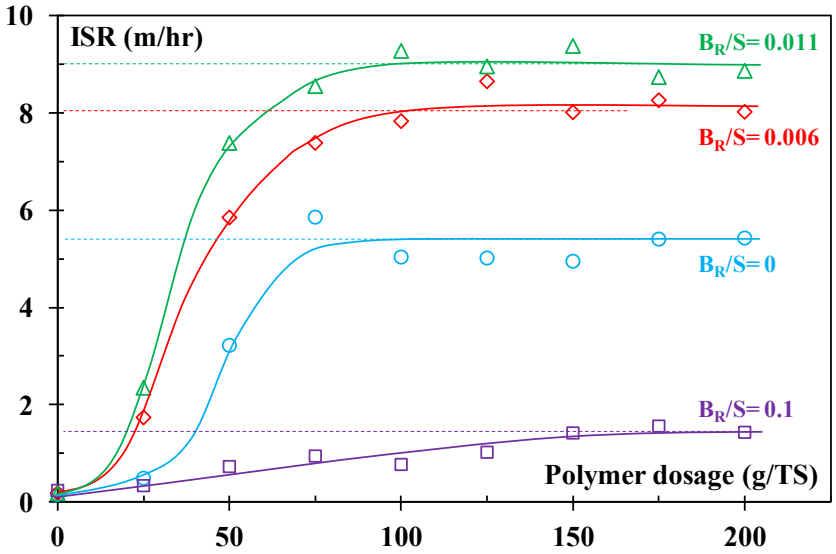


Figure 6. ISR for model fines settling as a function of polymer dosage for four different B_R/S ratios: 0 (○), 0.006 (◇), 0.011 (△), and 0.1 (□). The solid lines represent possible trends based on observation of data. The dashed lines show the ISR values at optimal (the lowest amounts necessary to achieve these values) polymer dosages.

The ISR values at optimal polymer dosage are presented in Figure 7 as a function of B_R/S. The black dashed line represents the ISR baseline at optimal polymer dosage for fines without bitumen. The data points clearly show that ISR will pass through a maximum value as illustrated by the projected red dotted-dashed line. This is demonstrated as an expected trend only since other volcanic shapes can be traced through these data points. But in all cases a maximum value can be expected at $B_R/S \sim 0.01$. In this plot, we have included data from Klein *et al.* (2013). To plot their data, we have normalized the bitumen concentrations by the amount of solids in their tests which is 10 wt%. Despite the differences between these two studies, from the nature of the samples to the preparation and flocculation procedures, we observe that the optimal residual bitumen concentrations are within the same ballpark range and show a maximum in the vicinity of $B_R/S=0.01$. It should be noticed that Klein *et al.* (2013) did not specify the differences between

free residual bitumen and attached residual bitumen (B_R). With the distinction in bitumen types, the data is expected to shift towards lower B_R/S ratios, closer to the 0.01 value observed for the samples used in this study. It is important to notice that Klein *et al.* (2013) observed a high ISR when the samples were toluene washed. Interestingly, in this study the ISR values at low residual bitumen concentrations are low. Klein *et al.* (2013) described a transition between a mineralogy dominated regime for low residual bitumen content to a bitumen dominated regime at high bitumen content. The optimum ISR observed in this study at B_R/S ~0.01would seem to be this transition. However, the specificity of this B_R/S ~0.01 is not well understood and further investigation is required to establish its universality as well as its response to other parameters such as the particle size ratio of bitumen droplets and fines.

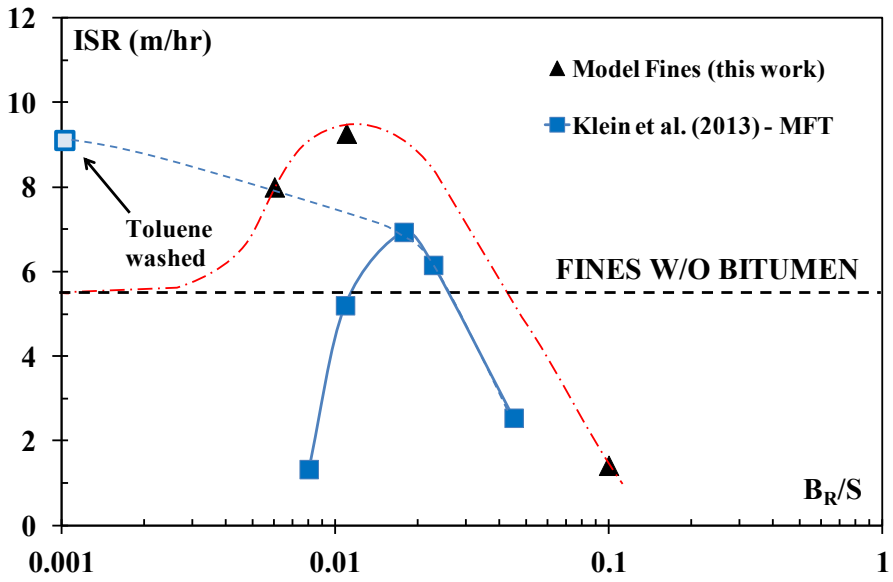


Figure 7. ISR at optimal flocculant dosage as a function of B_R/S ratio. The black dotted horizontal line in the graph corresponds to the experiment with clean model fines (baseline ISR at B_R/S~0). The red dotted-dashed line is a possible trend for the data with the ISR passing through a maximum between B_R/S=0.01 and 0.1. However, the exact value cannot be predicted with this limited number of data points. Data from Klein *et al.* (2013) has been reworked and incorporated in the figure.

4 CONCLUSIONS

The objective of the work was to gain insight on the effect of residual bitumen on the flocculation of fine tailings generated from oil sands. Specifically, the study investigated the impact of attached and free bitumen on solids settling. Studies were conducted using tailings samples from an average grade and a low grade ore from the Joslyn North Mine site and using model fines (Kaolinite).

The main conclusions from this work are:

- An optimal attached residual bitumen-to-solids-ratio (B_R/S) exists that increases the initial settling rate (ISR) at optimal polymer dosage significantly for all three samples used in this study. At least a two-fold increase in the ISR was observed for these samples. The ISR values were in agreement with the prior experimental work on MFT by Klein *et al.* (2013).
- The optimal B_R/S is in the order of 10^{-2} irrespective of the sample/system (tailings from oil sands ore vs. model system vs. MFT).

It is important to understand whether the range of the residual bitumen and solids used in this study can be considered general. The results from the samples used in this study seemed to be in agreement, but the number of data points was limited. More experiments with both model and real samples are necessary, especially to understand the physical significance of the optimum B_R/S value.

5 ACKNOWLEDGMENTS

The authors would like to thank G. Birade, A. Delaboissière, and P. Michaud for their contribution to the laboratory experiments.

6 REFERENCES

Bourrel, M. & Gras, J-M. 2012. *Method for metering hydrocarbons.* WIPO Patent, WO/2012/093111

Doukkali, A., A. Saoiabi, A. Zrineh, M. Hamad, M. Ferhat, J.M. Barbe, R. Guilard, 2002. Separation and identification of petroporphyrins extracted from the oil shales of Tarfaya: geochemical study. *Fuel*, 81, 467-472.

Evdokimov, I.N. and A.P. Losev. 2007. Potential of UV-Visible absorption spectroscopy or characterizing crude petroleum oil. *Oil and Gas Business*.

Klein, C. & Harbottle, D. & Alagha, L. & Xu, Z. 2013. Impact of fugitive bitumen on polymer-based flocculation of mature fine tailings. *The Canadian Journal of Chemical Engineering*, 9999, 1-6.

Majid, A. & Sparks B.D. 1991 Settling behavior of syncrude sludge pond tailings after removing residual organics and oils phase solids by an agglomeration technique. *Proceeding of the 5th UNITAR Conference on Heavy Crude and Tar Sands*, 4, 389.

Mikula, R. A cautionary tale of off the shelf and off the wall tailings treatment technologies. Proceedings of the Third International Oil Sands Tailings Conference. 231-235.

Scott, J.D. & Dusseault, M.B. & Carrier, W.D. 1985. Behaviour of the clay/bitumen/water sludge system from oil sands extraction plants. *Applied Clay Science.*1, 207-219.

Tacey, W. &Hart, B. 2006. Making Tailings disposable sutainable: a key business issue. In R.J. Jewell and A.B. Fourie (eds.), *Paste and Thickened Tailings – A Guide, Second Edition*, Nedlands: Australian Center for Geomechanics.

Thompson, T.E. 2011. Hydrocarbon recovery from waste streams of oil sands processing. Master Thesis. Universtiy of Alberta.

Seepage induced consolidation testing of mature fine tailings

Mathiew Estepho & Dirk van Zyl
Mining Engineering, University of British Columbia, Vancouver, Canada

Dobroslav Znidarčić
University of Colorado, Boulder, USA

Adrian Revington
Suncor, Calgary, Canada

ABSTRACT: This paper presents the development of equipment for consolidation testing of Mature Fine Tailings (MFT) at the University of British Columbia (UBC). The Seepage Induced Consolidation Test (SICT) was first developed at the University of Colorado, Boulder (CU) for testing phosphate slurries. The SICT equipment allows seepage induced loading at low equivalent normal stresses (less than 1kPa) as well as step load testing at higher normal stresses. The hydraulic conductivity of the sample can also be directly measured at each loading condition. With the financial support of Suncor a SICT setup was developed and implemented at UBC. Several benchmark tests were initially performed on kaolinite clay and compared with the CU tests as well as with published consolidation data. The results of these tests compared well and help build confidence in the SICT at UBC. Several tests have been performed on MFT and are shown to be in agreement with previous testing at CU. The tests results show that the SICT is repeatable and provide improved understanding of the consolidation behavior of these high void ratio materials.

1 INTRODUCTION

The consolidation of oil sands tailings is extremely slow which make standard step load consolidation testing procedures inadequate. The Seepage Induced Consolidation Test (SICT) has been successfully used for the last two decades to accurately determine consolidation parameters of soft slurries such as mine tailings and dredged soils. This test is suitable for very soft compressible slurries with low permeability such as Mature Fine Tailings (MFT). This paper outlines the construction of a SICT at the University of British Columbia (UBC), which is modeled after the SICT developed at the University of Colorado (CU) constructed over 20 years ago. The use of a flow pump to produce seepage forces to trigger the consolidation process allows for minimal disturbance during the low stress range (< 1kPa) and allows for the direct measurement of the hydraulic conductivity of a soil sample. Several benchmark tests were performed on kaolinite clay and show comparable results with CU testing as well as with published consolidation data. The results in terms of compressibility and permeability relationships of MFT are also presented and shown to be in agreement with published data.

2 SEEPAGE INDUCED CONSOLIDATION TEST OVERVIEW

The SICT is an experimental procedure used for determining the compressibility and permeability relationships of soft slurries. The test involves a three step procedure:

1. Determine void ratio at zero effective stress, e_0
2. Measure sample height to obtain compressibility and permeability characteristics at low effective stress range (< 1 kPa)

3. Measure sample height to obtain average void ratio and permeability at high effective stress range (> 150 kPa)

In the first step, e_0 is defined as the average void ratio of a short column of slurry which is allowed to settle due to self weight in which the effective stress is near zero, or the void ratio when the soil is formed and the consolidation theory (as opposed to the sedimentation theory) applies (Znidarcic, et al., 2011).

In the second step, the soil sample is placed inside a modified triaxial cell and allowed to settle due to self-weight and a small buoyant weight (about 0.10 kPa). The buoyant weight consists of a loading piston and a Linear Variable Differential Transducer (LVDT) rod. Once the sample stops settling, a small flow rate is imposed on the sample with a flow pump to trigger the consolidation process using seepage forces. Steady state settlement and pore pressure measurements are recorded in this phase of the test.

In the third step, the soil sample is consolidated to a desired maximum pressure using step loading on the loading piston, usually greater than 150 kPa. Then an imposed flow rate, usually one tenth of the flow rate imposed in step two, is used to obtain the average void ratio and permeability at this higher effective stress. The sample is then oven dried to determine the solids content.

The analysis of the test is performed using the software program SICTA (Seepage Induced Consolidation Test Analysis) (Abu-Hejleh & Znidarcic, 1994). The analysis involves inputting the final data from step three into the finite strain nonlinear consolidation theory to back calculate the measured data from steps one and two. The SICTA outputs five parameters A, B, Z, C and D used in the two compressibility and permeability relations below:

$$e = A(\sigma' + Z)^B \tag{1}$$

$$k = Ce^D \tag{2}$$

Both steps two and three provide a data point each for the above two equations but it is important to note that any number of data points can be measured by loading to intermediate effective stresses and imposing known flow rates. These extra data points are not necessary but provide a useful check on the results obtained from the SICTA.

3 SICT CONSTRUCTION

A schematic of the SICT constructed at UBC is shown in Figure 1. The UBC SICT is very similar to that of the one constructed at the CU laboratory but there are several key differences between the two and those differences are listed below:

- Larger diameter sample size: 6 inches vs. 3 inches
- LVDT rod placed through cell cap: allows for continuous settlement measurement
- Digital encoder placed on Flow Pump: allows for automatic pump resets

The larger diameter sample size allows for a lower flow rate across the sample for the same imposed discharge velocity from the flow pump. This results in significantly shortening the consolidation process because there will be smaller pore pressure build up due to the lower flow rates. The larger diameter sample also requires a larger sample chamber and load cell.

The LVDT rod for the UBC SICT was placed through the cell cap to allow for continuous measurement of the sample settlement. The disadvantage of this setup is that the water reservoir must be placed so that the water is level with the top of the SICT chamber (see Figure 1) to prevent water from leaking through the LVDT cap connection. This results in a lower back pressure than that of the CU SICT which has the water reservoir several meters above the SICT. Having a high back pressure provides better control of pore pressures measured across the sample in terms of having constant reference pressures. This modification has not been shown to affect the SICT results. Another result of having the LVDT rod through the cell cap is that it is now applying a small load to the sample that must be quantified. The buoyant weight determined for the UBC tests produces a seating stress on the sample of about 0.03 kPa.

A digital encoder is installed onto the flow pump, which allows for direct measurement of the distance that the flow pump piston has travelled and this allows for automatic resetting of the flow pump piston during testing whenever the maximum volume of water has been removed from the sample. In contrast, without an encoder to accurately measure where the flow pump piston is, it is required that the pump be manually reset.

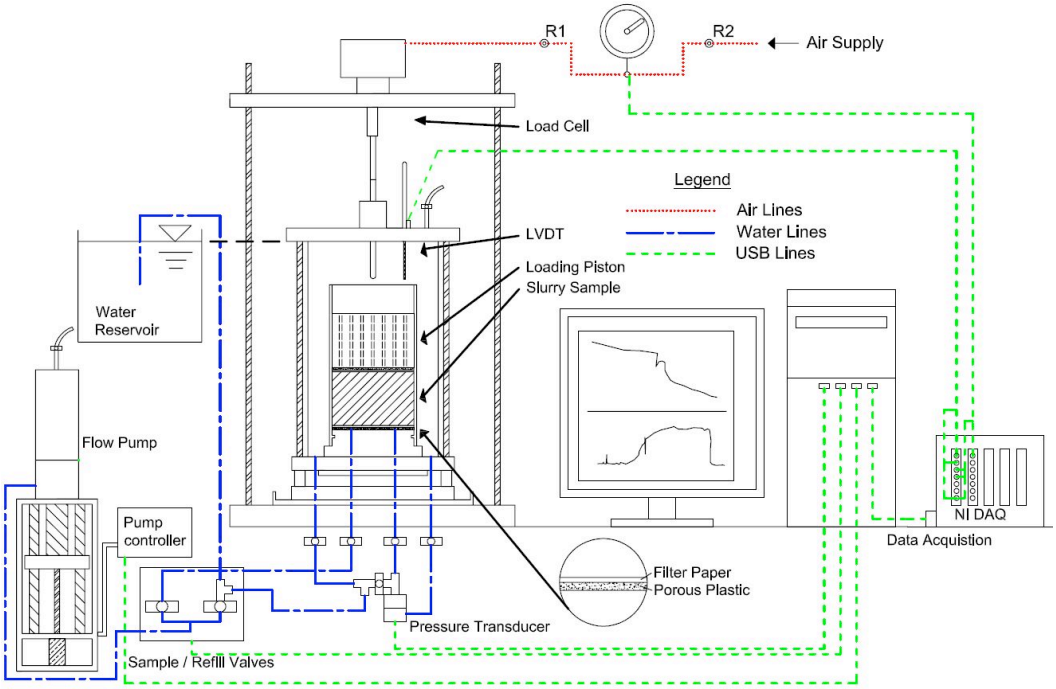


Figure 1. SICT Schematic

3.1 *Loading Piston Dimensions*

The loading piston is used to ensure that the sample settles uniformly. The piston is made of clear cast acrylic and is 6 inches in diameter and the height is selected to be 3.6 inches based on the empirical ratio shown in Equation 3 below.

$$0.6 = \frac{Height\ of\ Piston}{Diameter\ of\ Piston} \tag{3}$$

This ratio was subjectively determined during the piston design and construction process because it minimizes the effects of uneven settlement as compared to a thinner piston while at the same time minimizing the weight of the piston.

The loading piston weighs 1.55 kg and has 54 holes of a diameter of 5/16 inches drilled through the height of it to allow for drainage at the top of the piston while maintaining uniform sample settlement and minimizing weight. It has a buoyant weight of 128 grams, producing a seating stress of about 0.07 kPa on the sample Thus when accounting for the 0.03 kPa stress increase due to the buoyant weight of the LVDT rod, the total load on the sample due to the piston and the LVDT rod is about 0.10 kPa.

A plan view of the piston is shown in Figure 2. It is important to provide a balance between the area of holes versus the area with no holes to ensure adequate drainage and uniform settlement.

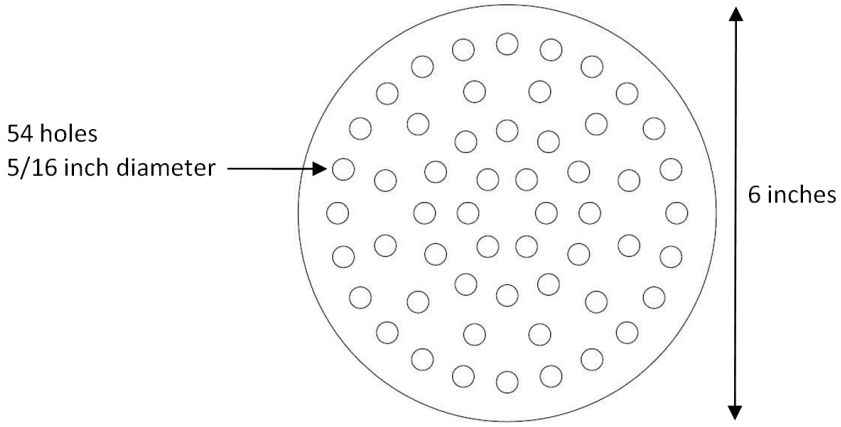


Figure 2: Loading Piston Top View

3.2 *Load Cell Setup*

The step-wise vertical load is applied through a Marsh Bellofram air pressure cylinder and regulator. The cylinder has a 9 -inch effective cross sectional area and a 3-inch stroke. The regulator can regulate a maximum air pressure of 100 psi and this translates to a maximum pressure of 200 kPa on a 6-inch diameter slurry sample.

3.3. *Data Acquisition System*

Data is collected with a National Instruments (NI) data acquisition system, which includes a NI CompactDAQ analog input and output controller and is programmed with the NI Labview graphical programming software. Data collected include the settlement measured with the LVDT, pore pressure, vertical load pressure readings as well as the flow pump position and velocity. Labview has good integration with the data acquisition instruments and the visual programming abilities allow for quick modifications to any new equipment requirements. It also allows for remote control of the testing in progress.

4 BENCHMARK TESTS ON KAOLINITE CLAY

Several benchmark tests were conducted with the SICT at UBC on kaolinite clay and compared with testing at CU. Kaolinite samples were prepared by mixing dry kaolinite clay with an adequate amount of water for a desired solids content. Solids contents ranged from 25 to 45% by mass and affect the starting point of the compressibility relationship (see Figure 3). The void ratio corresponding to the desired solids content must be modified to obtain the void ratio at zero effective stress, e_0. As stated earlier e_0 is the void ratio at which the sedimentation process ends and consolidation begins (Znidarcic, et al., 2011). A column of the kaolinite slurry is allowed to settle due to self-weight and the volume drop is used in obtaining e_0. The results of UBC versus CU tests are shown in Figures 3, 4 and Table 1.

Table 1: Compressibility and Permeability Relationships for CU and UBC Kaolinite Tests

Test Number	Compressibility ($e = A(\sigma'+Z)^B$)	Permeability (m/s) ($k = Ce^D$)
CU Boulder – Kaolin	$e = 2.332(\sigma'+0.075)^{-0.181}$	$k = (5.9 \times 10^{-10})e^{4.22}$
UBC kaolin 3	$e = 2.563(\sigma'+0.195)^{-0.143}$	$k = (6.6 \times 10^{-10})e^{3.89}$
UBC kaolin 4	$e = 2.759(\sigma'+0.518)^{-0.179}$	$k = (4.4 \times 10^{-10})e^{4.25}$
UBC kaolin 5	$e = 2.548(\sigma'+0.199)^{-0.202}$	$k = (7.6 \times 10^{-10})e^{3.91}$
UBC kaolin 6	$e = 2.368(\sigma'+0.357)^{-0.176}$	$k = (8.3 \times 10^{-10})e^{4.10}$

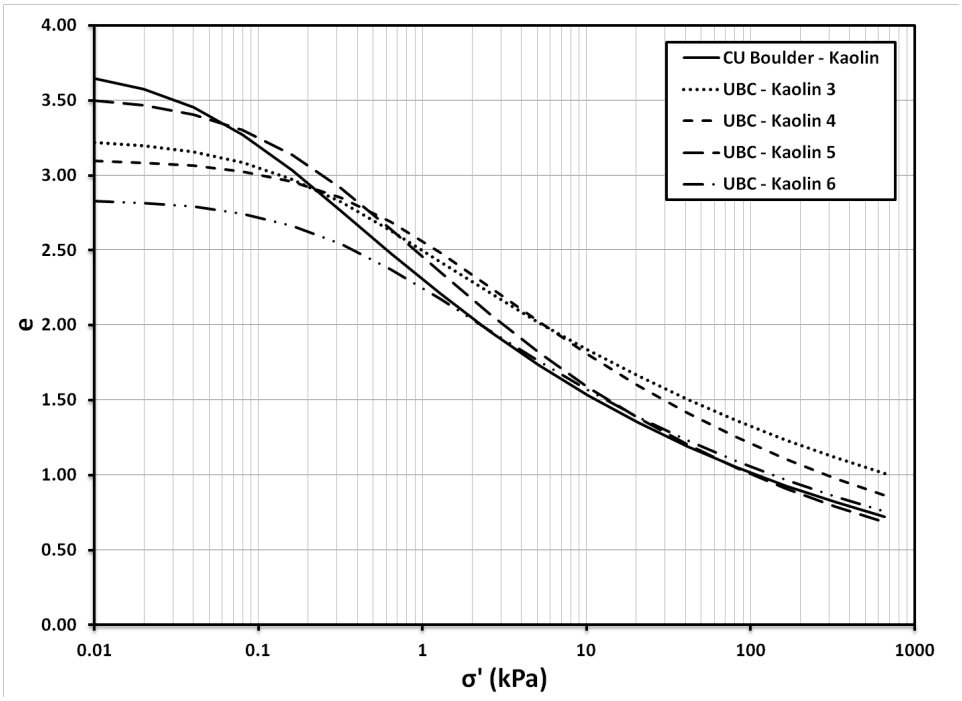


Figure 3: Compressibility of kaolinite clay: UBC SICT vs. CU SICT

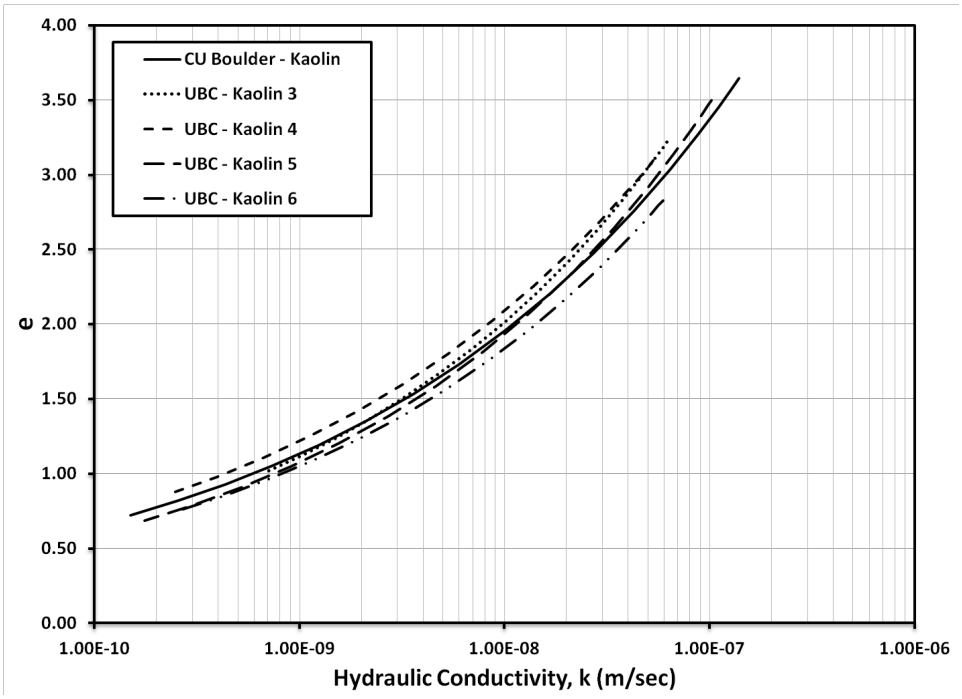


Figure 4: Permeability of kaolinite clay: UBC SICT vs. CU SICT

The results of the benchmark tests show that tests using the SICT at UBC are repeatable and show very similar results with the test at CU in both compressibility and permeability.

The results of the UBC SICT were compared with the results of a desktop centrifuge test (Reid & Fourie, 2012). The samples for the desktop centrifuge tests were prepared similar to that of the SICT except the void ratio at zero effective stress was not defined. Figures 5 and 6 show the compressibility and permeability of both the UBC SICT and the desktop centrifuge test.

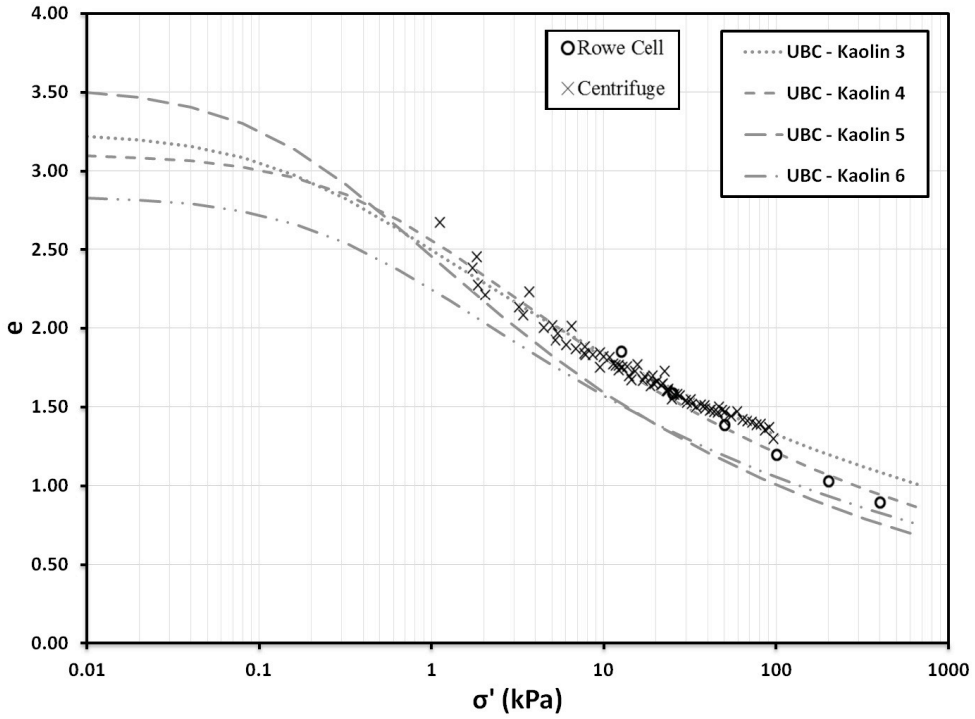


Figure 5: Compressibility of kaolinite clay: UBC SICT vs. Desktop Centrifuge

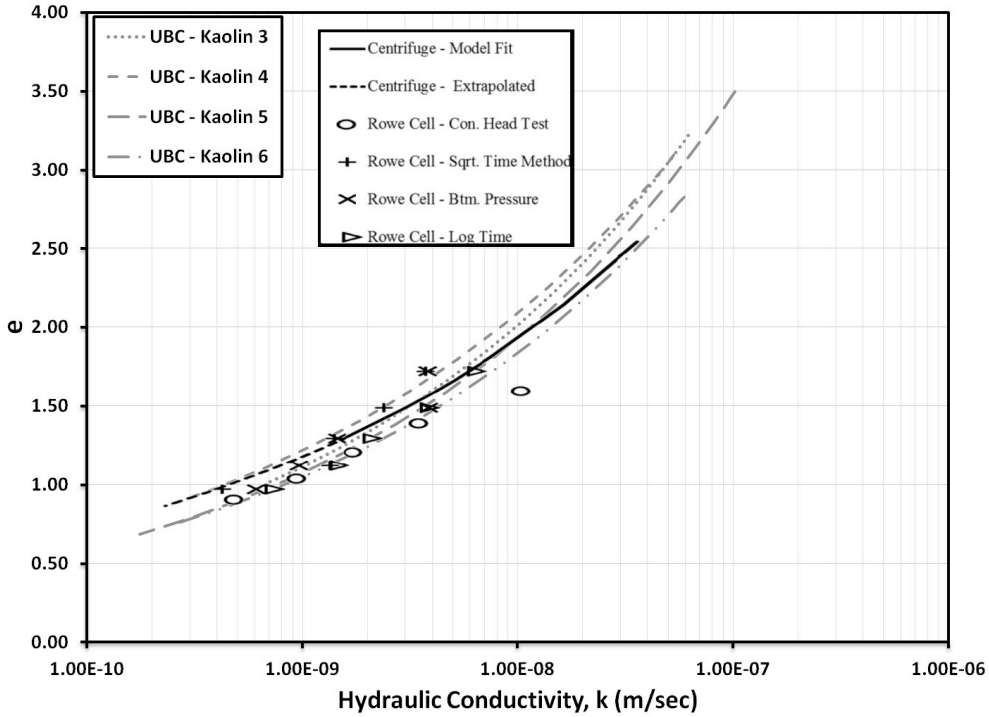


Figure 6: Permeability of kaolinite clay: UBC SICT vs. Desktop Centrifuge

The results of the tests performed at UBC compare well with those obtained from the desktop centrifuge. This further confirms the reliability of the testing apparatus and provided added confidence to undergo testing on MFT.

5 MFT SAMPLE PREPARATION

Suncor provided an MFT sample for testing. The sample averaged 97% fines and 90% clay activity by methylene blue. Further characterization testing is underway.

Mature fine tailings demonstrate thixotropic behaviour in which it gains shear strength when it is allowed to settle and behaves like a gel but when it is disturbed it loses strengths and becomes water like in consistency (Jeeravipoolvarn, 2005). In order to provide consistent samples for testing it is important to first shear the MFT samples with a rotating blade mixer until it loses most of its shear strength under the time frame of several hours of mixing. For MFT of about 31% solids content shearing for about 3 hours yields a shear strength of 2 pa. Testing at the UBC laboratory shows that the shear strength increases significantly due to small increases in solids content; about 3 pa increase in shear strength for each percent increase in solids content. It is important to note that MFT samples tested between 2 and 7 pa shown comparable consolidation results. The vane shear test as outlined by Fisher et al(2007) was used to evaluate the shear strength of the MFT.

5.1 *MFT Sample Height Selection*

The selection of the sample height used in the SICT is very important because it controls the duration of a test, which could be over a month long. The first test conducted at UBC on MFT involved using a sample height of 70 mm and took about two months to complete the SICT. The second test was performed on a sample with a height of 40 mm and the test took about one month while still obtaining two more compressibility and permeability data points than the first test. A sample height should be selected to yield a height of solids of 5mm to shorten testing time while ensuring that test results are not significantly affected due to small losses of MFT smearing on the piston side-walls during step loading.. This corresponds to a sample height of 32 mm for a MFT sample of 33% solids.

5.2 *Removing residue bitumen*

Prior to testing it is very important to remove visible residue bitumen that has risen to the top of the MFT sample. This is to prevent the bitumen from attaching to the filter paper and thus acting as a seal, which prevents upwards drainage. The residue bitumen can easily be removed by lightly placing a paper towel over the top of the sample and removing it after it “absorbed” the bitumen.

5.3 *MFT Cleanup*

Experience on this project has shown that the household cooking oil spray PAM works very well in cleaning up bitumen stains on all surfaces including cleaning hands covered with bitumen. Other professionals have reported similar experience informally. PAM is edible and thus makes it a safe alternative to cleaning MFT as opposed to harmful chemical cleaners such as Toluene.

6 MFT RESULTS AND COMPARISON WITH CU TESTING

Two tests were performed on MFT at the UBC laboratory and are compared with published data from the CU laboratory (Znidarcic, et al., 2011). The results in terms of compressibility and permeability are shown in Figures 7, 8, and Table 2.

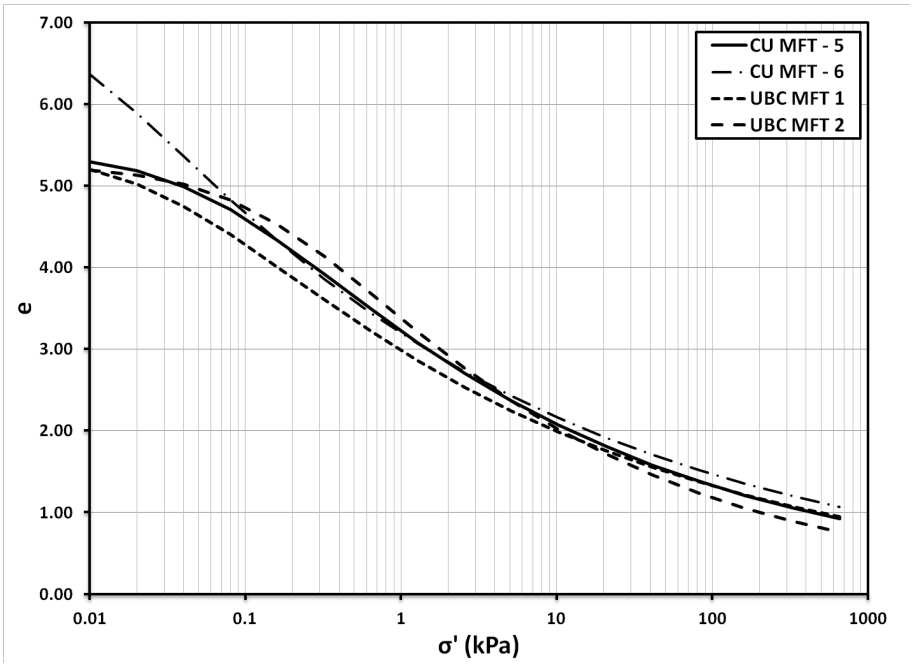


Figure 7: Compressibility of MFT: Void Ratio vs. Effective Stress

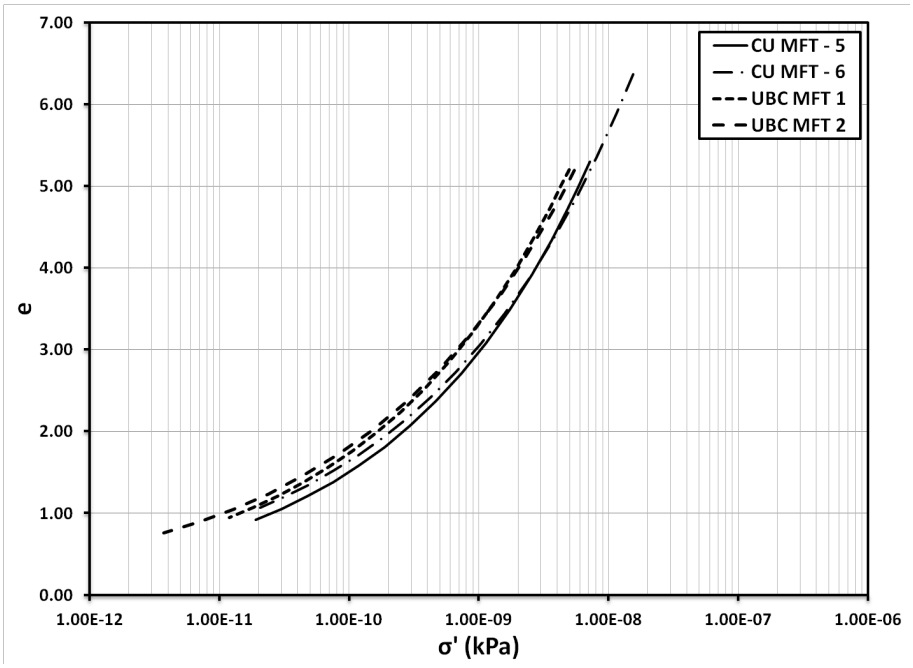


Figure 8: Permeability of MFT: Void Ratio vs. Hydraulic Conductivity

Table 2: Compressibility and Permeability Relationships for CU and UBC MFT Tests

Test Number	Compressibility ($e = A(\sigma'+Z)^B$)	Permeability (m/s) ($k = Ce^D$)
CU MFT 5	$e = 3.27(\sigma'+0.074)^{-0.195}$	$k = (2.5x10^{-11})e^{3.39}$
CU MFT 6	$e = 3.20(\sigma'+0.007)^{-0.169}$	$k = (1.6x10^{-11})e^{3.71}$
UBC MFT 1	$e = 3.00(\sigma'+0.035)^{-0.177}$	$k = (1.4x10^{-11})e^{3.55}$
UBC MFT 2	$e = 3.52(\sigma'+0.181)^{-0.236}$	$k = (1.1x10^{-11})e^{3.79}$

The results are comparable for both CU and UBC tests. These results, along with previous tests on kaolinite clay, further confirmed the validity of the UBC SICT. Also it is important to note that the MFT tested at UBC had a fines content of about 99% in which 90% of the fines were clay minerals. This extremely high fines content helps explain why the results show that the UBC tests have permeabilities slightly less than the CU tests.

7 CONCLUSIONS

The SICT constructed at UBC follows the design of the SICT developed at CU but several equipment modifications to shorten the consolidation time while allowing continuous monitoring of sample settlement. The construction of the SICT as well as the testing procedure involves experience and utilizing several rules of thumbs, which were outlined in this paper. Benchmark testing on kaolinite clay showed UBC SICT test results to be in agreement with tests performed at CU and published data from desktop centrifuge tests. The benchmark testing show the UBC SICT is repeatable and helps build confidence in the performance of the testing equipment. MFT results show that testing with the UBC SICT results in comparable compressibility and permeability relations with CU testing.

REFERENCES

Abu-Hejleh, A. N. & Znidarcic, D., 1994. Estimation of the Consolidation Constitutive Relations. *Computer Methods and Advances in Geomechanics, Siriwardane & Zaman (eds) Balkema, Rotterdam,* pp. 499-504.

Fisher, D. T., Clayton, S. A., Boger, D. V. & Scales, P. J., 2007. The bucket rheometer for shear stress-shear rate measurement of industrial suspensions. *Journal of Rheology,* October, 51(5), pp. 821-831.

Gibson, R. E., England, G. L. & Hussey, M. J. L., 1967. The theory of one-dimensional consolidation of saturated clays: 1. Finite non-linear consolidation of thin homogeneous layers. *Geotechnique,* Volume 17, pp. 261-273.

Jeeravipoolvarn, S., 2005. *Compression Behaviour of Thixotropic Oil Sands Tailings,* Edmonton, Alberta: MASc Thesis, University of Alberta.

Reid, D. & Fourie, A., 2012. *Accelerated consolidation testing of slurries using a desktop centrifuge. Proceedings of the Tailings and Mine Waste Conference 2012,* Keystone, Colorado, pp. 17-28.

Znidarcic, D. et al., 2011. *Consolidation Testing of Oil Sand Fine Tailings.* Proceedings of the Tailings and Mine Waste Conference 2011, Vancouver, British Columbia.

Stiffness and Deformation Characteristics of the Compacted Lean Oil Sands Dykes

K.W. SoeMoe, K.W. Biggar,
BGC Engineering Inc., Edmonton, Alberta, Canada

G. Claypool
BGC Engineering Inc., Calgary, Alberta, Canada

S. Martens
Shell Canada Limited, Calgary, Alberta, Canada

ABSTRACT: This paper summarizes the stiffness and deformation characteristics of the compacted dyke fill from several investigations completed at Shell's Muskeg River Mine. In order to determine the stiffness of the compacted dyke fill, moduli from both field and laboratory investigations were deduced and discussed. Time dependent deformation characteristics of the dyke fill was presented using data from oedometer tests. Utilizing available stiffness data, the elastic deformation of the dyke fill was predicted using a finite element program. The outcome of the predicted deformation was compared with the deformation data from the instrumentation program, and reasonable agreement was observed.

1 INTRODUCTION

Surface oil sands mining operations produce large quantities of tailings as a result of bitumen extraction processes. At Alberta's surface oil sands mines, fluid tailings are stored in above ground structures and within the mined out pit contained by In-Pit Dykes (IPDs). These tailings containment structures, constructed with available mine waste materials and coarse sand tailings, are designed following Canadian Dam Association guidelines (CDA, 2007).

Shell Canada Energy (SCE) operates Muskeg River Mine (MRM), one of the surface oil sands mining operations located about 70 km north of Fort McMurray. Several in-pit tailings storage cells are being constructed at MRM. The first storage cell, Cell 1 is bounded by IPDs 1 and 2 and the pit wall. Cell 1 is separated by a temporary separator dyke, IPD 1i (now submerged), which connects IPD 2 and the south pit wall. The second storage cell, Cell 2a is bounded by the IPDs 2, 2i, 3s and the pit wall (Figure 1). Further storage cells are also being constructed.

At MRM, IPDs are constructed using lean oil sand wastes obtained from the mining operation. Fill materials are divided into different types depending on the properties of sandy and clayey facies located at the shovel face. Several field and laboratory investigations have been conducted at MRM to determine the geotechnical properties of the fill materials (BGC 2008, Norwest 2010). In 2010, an extensive field and laboratory investigation program was conducted to characterize the fill materials used for dyke construction. Field investigations included Cone Penetration Tests (CPTs), downhole geophysical logging, hydraulic fracturing and pressuremeter tests as wells as obtaining intact core samples for visual logging and

subsequent laboratory testing. Laboratory testing included index tests, direct shear tests, oedometer tests and triaxial tests (BGC 2011).

This paper presents the stiffness and deformation characteristics of the compacted dyke fill from several investigations programs. In order to determine the stiffness of the dyke fill, moduli from both field and laboratory investigation were determined. Time-dependent deformation characteristics of the dyke fill are presented using data from oedometer tests. Utilizing available stiffness data, the lateral and vertical deformation of the dyke fill was predicted using a finite element program. The outcome of the predicted deformation was compared with the deformation data obtained from slope inclinometers and magnetic extensometers.

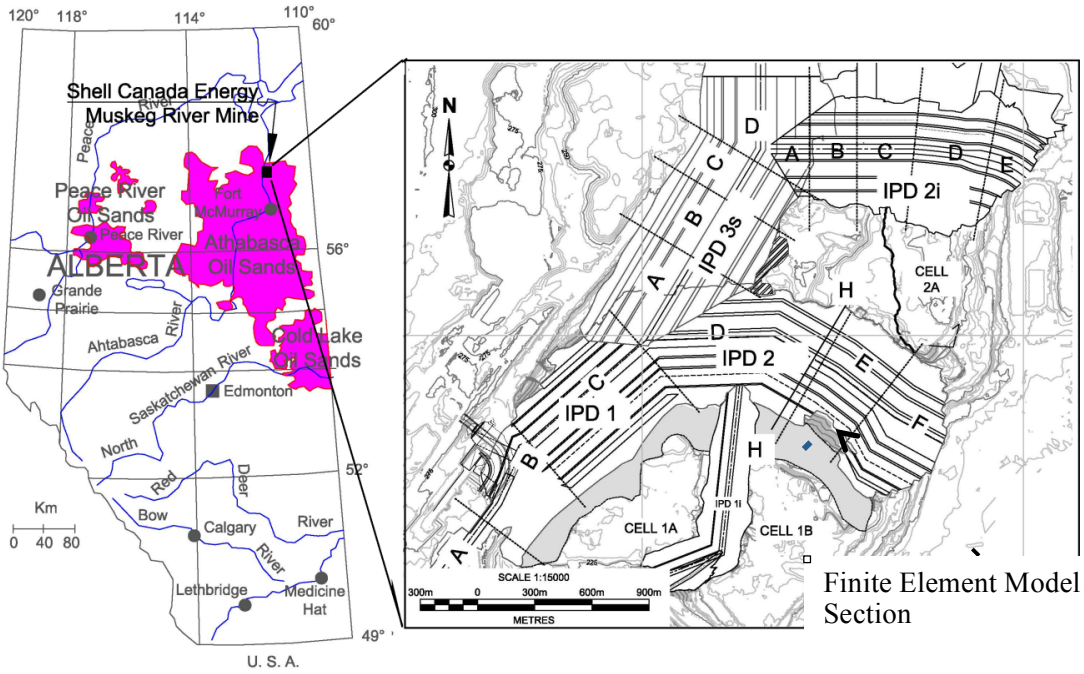


Figure 1. Plan view of the study area

2 GEOLOGIC SETTING

The recent soil cover at MRM comprises Holocene and Pleistocene units including glacial till, glacio-fluvial, glacio-lacustrine and most recently fluvial and peat deposits.

The recent soils are underlain by the Cretaceous McMurray Formation containing layers of shale, sandstone, and bitumen rich sands formed by river and ocean processes. The McMurray Formation has been divided into three members; Upper McMurray (UM), Middle McMurray (MM) and Lower McMurray (LM). These members reflect rising sea level during deposition, grading upwards from a continental-fluvial, tidal/estuarine to near-shore marine environment. The Middle and Lower McMurray are further divided into sub-members: MM1 and MM2, and LM1 and LM2, respectively. The ore body at MRM extends through all three McMurray Formation members. Although bitumen has been observed in each of the McMurray members, porous, clean sand deposits typically have the highest bitumen content. Water-bearing sands typically occur at the base of the Lower McMurray (LM1w) and are usually devoid of bitumen due to water saturation occupying the sand pore space. The waste units in each member are used as fill sources for dyke and other site construction.

The McMurray Formation is separated from the underlying calcareous shale and limestone of the Devonian Waterways Formation (DW) by a sub-Cretaceous unconformity. In some areas, the uppermost surface of the DW has weathered to a softened, high plasticity clay commonly referred to as a Paleosol. Prior to dyke construction, overburden materials and most of the McMurray Formation were removed during the mining operation except for the abutments, and

waste islands where large bodies of ore-poor deposits are left in place. Otherwise, IPDs are usually founded on the LM1w unit or DW formations. The base of pit elevations generally ranged from 200 to 230 m above sea level (masl) with the original ground elevation of 290 to 300 masl. To satisfy the varying foundation condition, IPDs are divided into sectors with similar foundation conditions, as shown in Figure 1.

3 FILL TYPE CLASSIFICATIONS

The fill materials used for dyke construction are: lean oil sand (containing less than 7% volume bitumen), clayey facies, and mixed facies that include bitumen rich layers that are too thin to isolate from the surrounding clays. Fill materials were initially divided into seven types depending on the amount of sand and clay facies involved. In July 2009, a field and laboratory testing program was completed to better understand the fill properties (Norwest, 2010). Following the results of the 2009 fill study program, fill classification was modified in 2009 and 2010.

For the dykes discussed in this paper, the fill materials are divided into three Types. Type 1 fill is a waste material with lower fines contents and a limit on the maximum clay content. As a result, Type 1 material is a sandier fill with a higher friction angle. Type 2 fill is a waste material with a higher fines content and less stringent limit on the amount of clay content. It tends to be much siltier than Type 1 and can sometimes be blocky depending on the facies source. Any fill material sourced from the clay-rich LM2 unit is classified as Type 5. Type classifications along with the minimum fluid content requirements and rut performance criteria for the various zones in the dykes are provided in Table 1. Within each fill Type, the engineering properties vary largely with the bitumen content, grain size, natural fluid content (defined as the ratio of mass of fluids (bitumen and water) to the mass of solids) and dry density to which the fill is compacted. The dyke is divided into core, shell, and toe berm zones, with each zone having different material properties (Figure 2).

Table 1. Fill type definition

Zone	Allowable Material Type	Maximum Lift Thickness (m)	Min. Dry Density (kg/m^3)	Min. Fluid Content (%)	Maximum Rut (mm)
Core	Type 1, 2	1.0	1675	10	200
Shell	Type 1, 2	1.0	1700	8	100
Toe Berm	Type 1, 2, 5	1.5	1650	-	300

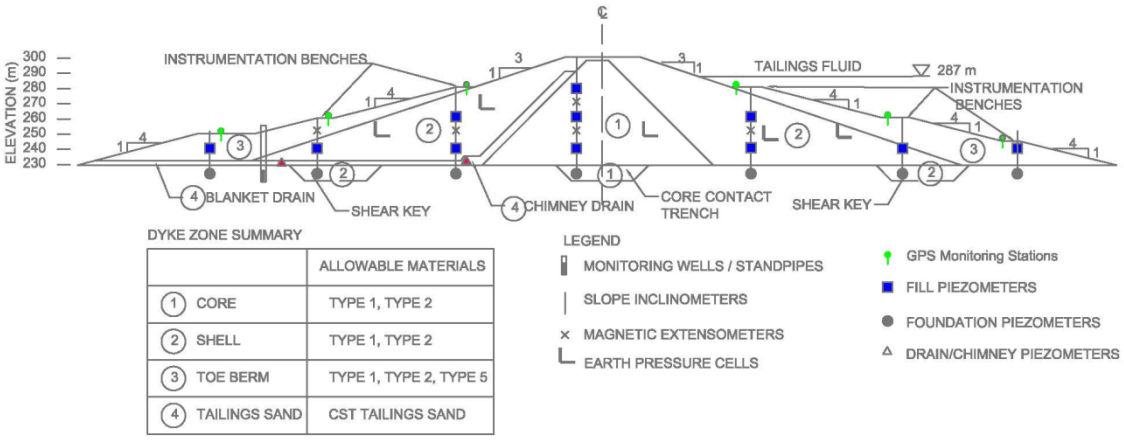


Figure 2. Typical cross section of IPD with instrumentation plan

4 STIFFNESS AND COMPRESSIBILITY CHARACTERISTIC DETERMINATION

The stiffness and deformability characteristics of the dyke fill materials have been assessed using both laboratory and in-situ programs completed at MRM since 2008. The various investigations and test methods used to assess the stiffness and deformability characteristics are summarized below:

- 2010 Fill Characterization Program (BGC, 2011)
  - Pressuremeter Testing
  - Consolidated Undrained (CU) Triaxial Testing on core samples
  - Odeometer Testing on core samples
- 2009 MRM Material Suitability Study (Norwest (2010)
  - CU tests on Standard Proctor compacted samples
- 2008 High Pore Pressures Study (BGC, 2009)
  - CU tests on core samples

4.1 *Index Properties of Fill Materials*

Index testing was conducted on core samples collected from the dyke fills during various investigation programs. Index testing included Oil-Water-Solid (OWS) determination, geotechnical water and fluid content determination, Atterberg Limits tests, density determination, sieve analyses and hydrometer tests. The results of the OWS tests were used to determine geotechnical water and fluid content (by solid mass) of the fill. A summary table of index testing results is presented in Table 2. The average degree of saturation of the dyke fill samples was calculated to be approximately 88%, suggesting that the majority of the dyke fill is unsaturated. The average bulk density from the core samples compares reasonably to the average density of 2130 kg/m^3 from 6077 downhole geophysical measurements in Dykes 1, 2, 3s and 1i.

Table 2. Summary of Index Properties of Fill Materials

	Bitumen	Water	Solids	Water Content	Fluid Content	Bulk Density	Dry Density
	(% Total Mass)			(% Solids)		(kg/m^3)	
Maximum	13.4	15.3	91.0	18.0	25.3	2325	2102
Minimum	0.1	5.0	79.7	5.7	9.5	1762	1519
Average	4.1	10.2	85.6	11.9	16.7	2081	1785

Note: Based on 128 core samples

Due to the sandy nature of the fill material, only samples with enough fines content were tested for Atterberg Limits. The Atterberg Limits results indicate that the fine grained layers in the waste comprising the Type 1 and Type 2 fills can be classified as low to intermediate plasticity with an average Liquid Limit of approximately 28%. The average Liquidity Index of the dyke fill materials was observed to be negative showing the fill is generally unsaturated and below its Plastic Limit. Grain size distribution analysis testing results suggest that the fill is primarily fine-grained, with combined silt and clay contents generally exceeding 65%. The average clay content of all of the samples was approximately 13%. A grain distribution curve of fill material is presented in Figure 3a and dry density versus geotechnical fluid content plot of the core samples is presented in Figure 3b.

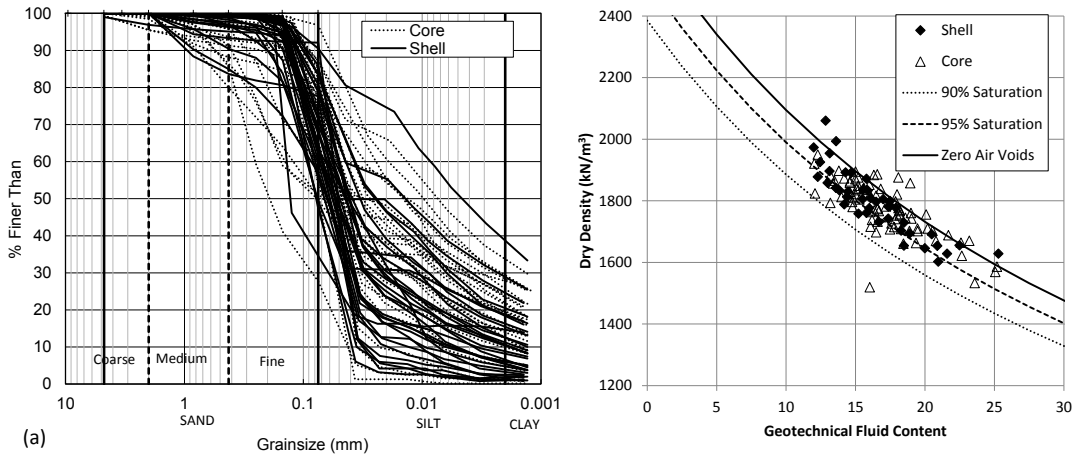


Figure 3. (a) Grain Size Distribution Curve (b) Dry Density versus Geotechnical Fluid Content

4.2 *Elastic Stiffness of Fill Materials*

Elastic deformation properties of fill materials were deduced from CU triaxial tests with pore pressure measurement, and pressuremeter tests. CU tests from the 2008 and 2010 programs were conducted on core samples and CU tests from 2009 were conducted on Standard Proctor reconstituted samples. Example plots of deviator stress versus axial strain and induced pore pressure versus axial strain at three different effective cell pressures (250 kPa, 500 kPa, 1000 kPa) are presented in Figures 4a and b. As shown in the figure, the deviator stress increased with the axial strain until it reached the peak strength after which only a small decrease in strength was observed up to 15% to 20% strain. The Young's modulus, E, is the ratio of stress to strain and obtained from the slope of deviator stress versus axial strain curve. The small strain initial tangent modulus, E_i, was determined from the slope of the deviator stress versus axial strain curve at approximately 0.1% strain. The mid-strain tangential elastic modulus, E_T, was determined from the slope of the deviator stress versus axial strain curve at approximately 50% of the maximum deviator stress. The secant modulus, E_S was determined from the slope of a straight line drawn between the origin of the plot and the point on the deviator stress versus axial strain curve corresponding to 50% of maximum deviator stress. An example of elastic modulus determinations is presented in
Figure 4a.

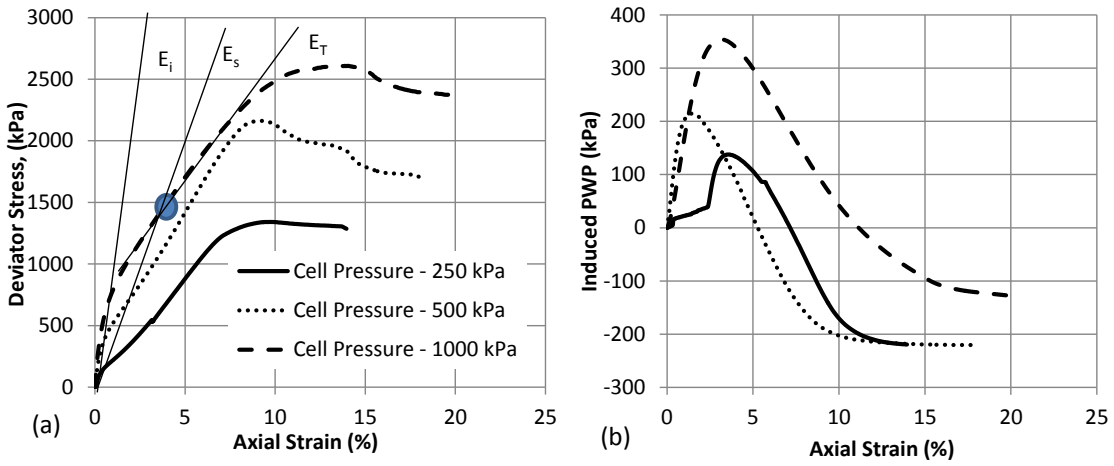


Figure 4. Example (a) Deviator stress versus axial strain, (b) Induced pore water pressure versus axial strain from CU testing on LOS core

The moduli deduced from various investigations are presented in Figure 5. Figure 5a shows the plot of initial tangent modulus versus effective confining pressure.

5b shows the tangent and secant moduli plotted against the effective confining pressure. The figure shows significant variation in moduli at each effective confining pressure but overall, the

moduli increase with increases in effective confining pressure. E_i values are generally higher than the E_T and E_s values. Similar ranges of moduli are obtained for E_T and E_s. The values of E_i ranged from 13 to 250 MPa for the effective confining pressure range of 250 to 2000 kPa. The values of E_T and E_S ranged from 13 to150 MPa for the effective confining pressure range of 250 to 2000 kPa. No noticeable difference was noted between the elastic moduli from the shell and core zones of IPDs, suggesting that there is minimal difference in the stiffness properties of the shell and core zones of the IPDs.

Twenty five strain-based pre-bored pressuremeter tests were conducted in three boreholes during 2010 fill investigation program. Membrane expansion was controlled by the flow of compressed nitrogen, increasing the pressure in small steps until the average strain of the wall was greater than about 1.5%, then the pressure was reduced and increased for the first unload-reload cycle. The pressure was then advanced in steps until the strain increased an additional 3% before completing a second unload-reload cycle. The shear modulus, G, of fill was determined from the slope of the unload/reload loops of the pressure versus radial displacement plots (Figure 6a). Once the shear modulus was determined, Young's modulus values could be deduced by using elastic theory as shown in Equation 1, and assuming a Poisson's ratio, μ, of 0.33 for the fill.

$$E = 2(G)(1+ \mu) \quad [1]$$

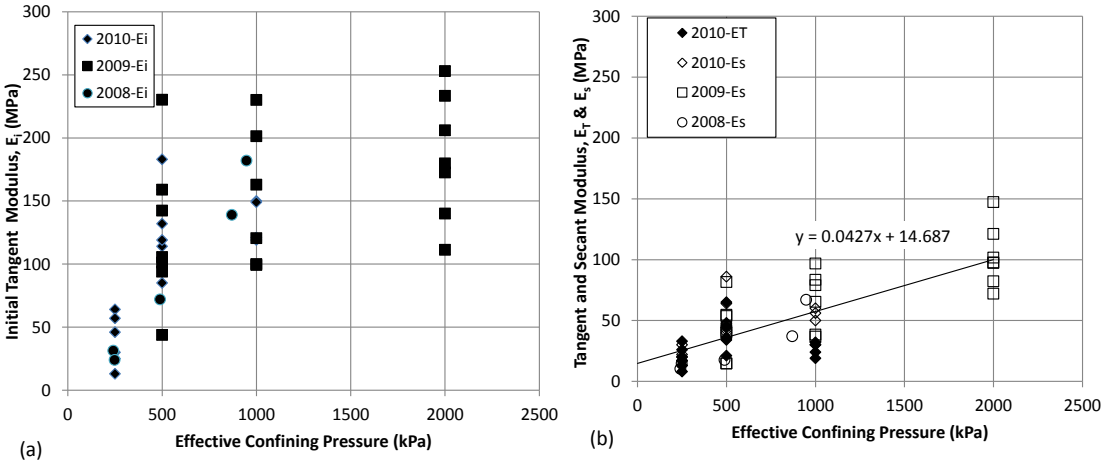


Figure 5. (a) Initial Tangent Modulus versus Effective Confining Pressure, (b) Tangent and Secant Modulus versus Effective Confining Pressure

Young's moduli determined from the pressuremeter tests are presented in Figure 6b against the test depths. The results varied throughout test depths and no relationship between E and test depths were observed. Young's moduli from pressuremeter tests ranged from 60 to 260 MPa for the test depths of 10 to 34 m. The elastic moduli from the pressuremeter tests were in a similar range as initial tangent moduli obtained from CU tests at similar confining pressures. The pressuremeter data did not show as low values at low confining stresses, likely indicating that at lot test pressures the lab results were affected by sample disturbance.

4.3 *Consolidation Characteristics of the Fill Material*

The time dependent deformation characteristics of the dyke fill materials were assessed from the oedometer tests. The oedometer tests were completed on 10 core samples collected during the 2010 fill characterization program. Prior to testing, the initial swelling pressure was determined by measuring the load that was required to prevent swelling of the test specimen following inundation. The initial normal load applied to the sample was approximately equivalent to twice the swelling pressure. Measured initial swelling pressures ranged from 0 to 62 kPa and the initial void ratio, e_o, ranged from 0.21 to 0.39. Following the consolidation of the sample under

the initial loading, the load was increased incrementally to a maximum load of 2150 kPa. After the consolidation under maximum load was complete, the loads were reduced in four increments, back to the initial swelling pressure. Each testing increment was typically run for 24 to 48 hours.

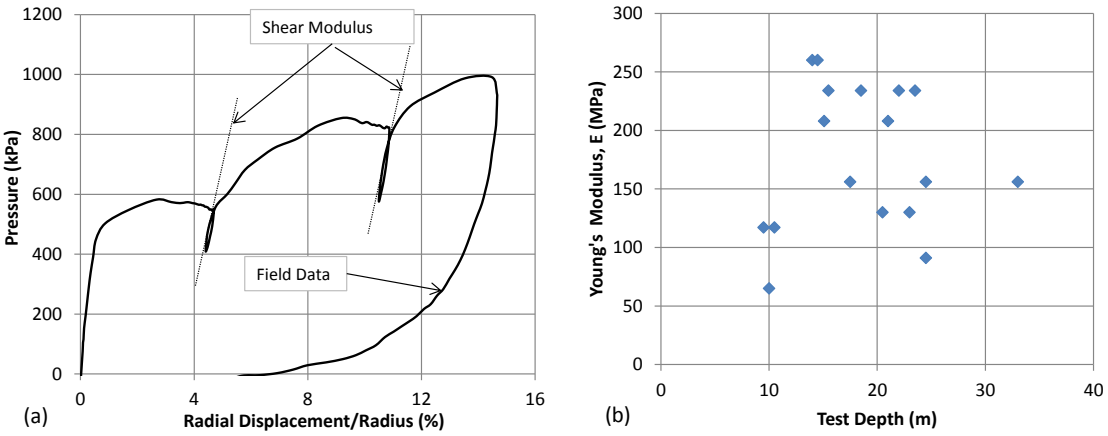


Figure 6. (a) Pressuremeter test – BGC-2010-INPIT-42, Depth 10.0 m, (b) Young's Modulus from pressuremeter tests

Figure 7a presents the plots of void ratio, e, versus effective stress, σ'_v, for various fill samples. As shown in the figure, e versus σ'_v plots did not show clear virgin compression curves within the maximum $\sigma`_v$ used in the oedometer tests. The difficulty in achieving a virgin compression curve is likely related to predominantly silty samples with some clays, which thus behaved as a granular soil rather than a clay. Therefore, the pre-consolidation pressure could not be determined from the plots.

Compression Index, C_c, values were determined from the slope of e versus σ'_v curve. Recompression Index, C_s, values were calculated from the unloading portion of e versus σ'_v curves. The calculated C_c values ranged from 0.03 to 0.11 and calculated C_r values ranged from 0.004 to 0.052 (Figure 7b). The C_c and C_s values show a weakly increasing trend with increase in initial void ratios.

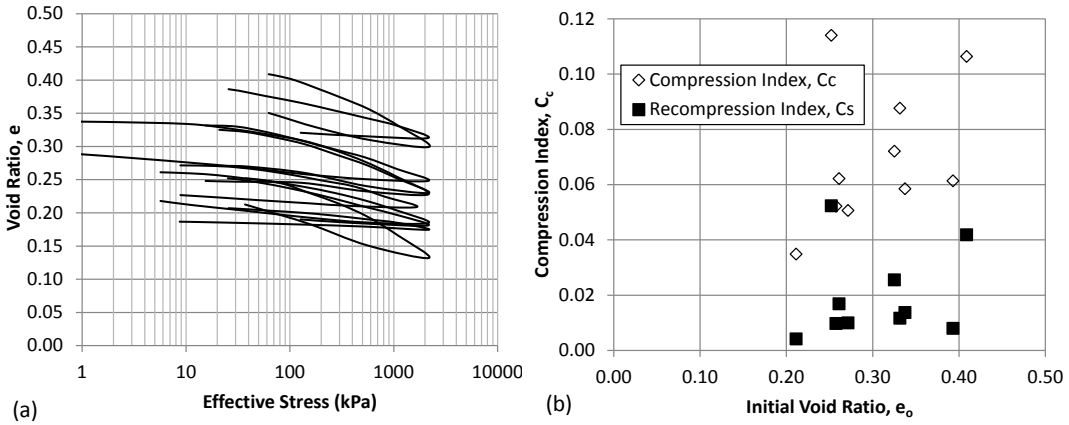


Figure 7. (a) Void ratio versus Log Effective Stress, (b) Compression Index versus Initial Void Radio

Coefficient of compressibility, a_v, and constrained modulus, D (equal to $1/m_v$), were determined from the oedometer tests. The value of a_v was determined by dividing the change in void ratio by the change in in effective stress. The value of D was determined by dividing the vertical effective stress by the vertical strain of the sample. The values of a_v ranged from 4.3 x 10^{-4} to 9.7 x 10^{-6} kPa^{-1} and the values of D ranged from 2.6 MPa to 103 MPa for the effective

stress range of 10 to 2100 kPa. As shown in the figure, both a_v and D values showed stress dependent behaviour.

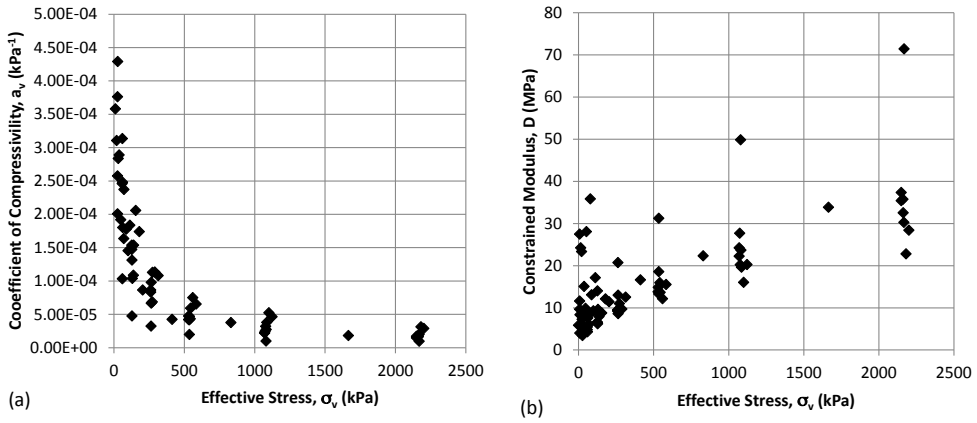


Figure 8. (a) Coefficient of Compressibility versus Effective Stress, (b) Constrained Modulus versus Effective stress

5 FIELD OBSERVATION

IPDs are constructed based on mine and tailings planning requirements and the waste material availability. Depending on fill material availability, the annual vertical construction rate of IPDs can range from 10 to 20 m. Due to the large amount of fill involved, IPD construction takes several years to complete. As a part of construction control and monitoring, an extensive instrumentation program is implemented at MRM including the installation of Vibrating Wire Piezometers (VWPs), Slope Inclinometers (SIs), Magnetic Extensometers (MEs), Earth Pressure Cells (EPCs) and Water Standpipes (WSPs). For each dyke, instruments are installed across a section of the dyke, usually at 200 to 300 m intervals along the dyke's alignment. A typical IPD section with instrument locations is presented in Figure 2.

Lateral deformation of the dyke fill is monitored using SIs. The base of SIs is seated in the stable foundation materials, usually in the DW Formation. Vertical deformation of the dyke fill and foundation material is monitored using MEs. An example of lateral deformation monitored from an SI during the dyke construction is presented in Figure 9. The left figure shows the cumulative movement of the inclinometer at two different times and the right figure shows the lateral displacement (mm) and dyke elevation versus time for the zone of movement (elevation 210 to 235 m). As shown, very little movement is observed when there was no nearby dyke construction, however the rate of movement increased once the dyke construction started in the area. The rate of movement reduced dramatically when the construction moved away from the area. No deformation was observed in the foundation material.

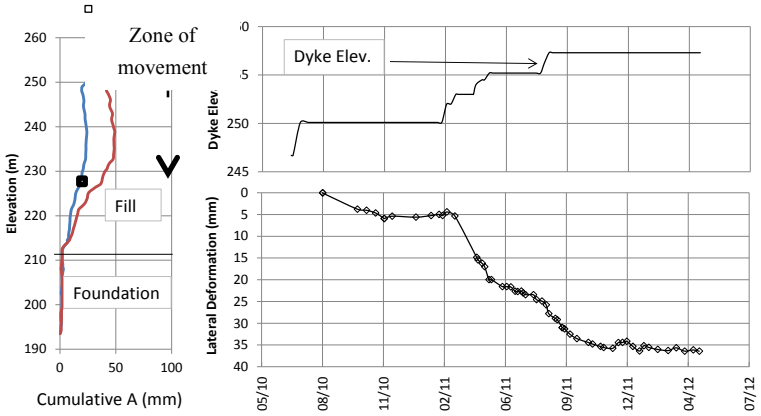


Figure 9. Observed lateral deformation due to dyke construction

For the IPDs, most of the observed movements are associated with the dyke construction. As the dyke construction moves away from the area, rate of movements start to slow down and eventually stop. Most of the observed lateral movements ranged from 0.01 to 0.07 mm/day. However, during the active nearby dyke construction, movement rates have gone up to 0.2 to 3.0 mm/day. The majority of movement is associated with shear strains distributed over 30-40 m thick zones in the dyke fill. The strain in the fill zone shown in Figure 9 was approximately 0.2%, much less than the typical shear strain to failure in the triaxial tests of 7 – 10%.

To monitor the settlement, 37 MEs were installed throughout the dyke fill and DW Formation. MEs were installed together with SIs and the datum magnet was installed in firm foundation material usually in DW. To monitor the settlement, the changes in vertical distance from the datum to MEs were measured using a readout unit. Since the installation of MEs, the fill placement throughout IPDs ranged from 0 to 15 m and the observed settlement ranged from 0 to 22 cm. At the time of writing, no deformation in the foundation was observed from the MEs installed in the foundation materials.

6 FINITE ELEMENT MODELLING

The elastic deformation of the dyke fill due to the dyke construction was predicted using the two-dimensional finite element software SIGMA/W (Geo-Slope, 2012). For the model, a well instrumented section located in IPD 2 Sector B was selected. The section location is presented in the plan view (Figure 1) and the section developed for numerical analysis is presented in Figure 10. To account for the incremental construction, the finite element model was developed with 10 horizontal layers, 10 m thick for each layer. For simplicity, the foundation was considered as a non- compressible layer. The Young's modulus for the fill material was deduced from the linear relationship obtained from E_T and E_s values presented in
Figure 5b. The range of moduli vary from 15 MPa to 100 MPa for the total vertical stress range of 0 to 2000 MPa. The same elastic parameters were used for the core and shell materials since no observable difference was found in the 2010 investigation program. A summary of parameters used for the finite element model is presented in Table 3.

Table 3 Summary of parameters used in the analysis

	Unit Weight (kN/m^3)	**Young's Modulus (MPa)**	**Poisson's Ratio**
Foundation	21	10,000,000*	0.25
Upstream and Downstream Shell/Core	19.5	$E=0.043\sigma_v + 14.7$	0.34

*Assumed non-compressible foundation layer

In order to account for the dyke construction with a series of lifts, analyses were completed in stages. Stage 1 involved determining the foundation stress condition before placing any fill. Stage 1 is followed by ten stages where each lift-stage represents the placement of 10 m of fill. Two scenarios were analyzed. The first scenario was for the dyke condition at elevation 260 m, which is the condition associated with the current SI and ME data. The second scenario was for the full height of the dyke with the final elevation of 290 m. The lateral deformations obtained from the finite element model were compared with deformation from two SIs located in the upstream slope of IPD 2 as shown in Figure 10. IN-0903 is located at the 235 m instrumentation bench and IN-1011 is located at the 260 m bench. Both SIs showed lateral bulk deformation during the dyke construction. The foundation in this section comprises of LM1w and DW and no deformation was observed in the foundation up to the dyke elevation of 260 m as shown in Figure 11.

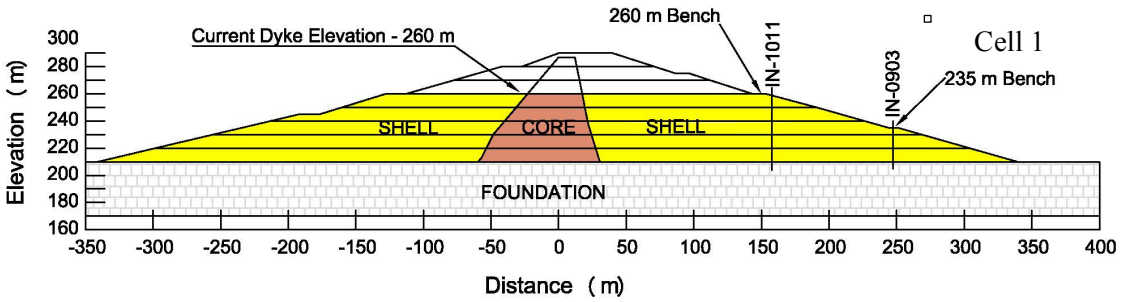


Figure 10. Finite Element Model Geometry

The predicted lateral deformation obtained from SIGMA/W is compared to the measured deformation from the SIs in Figure 11. As shown, the deformation for the dyke constructed to elevation 260 m obtained from the finite element model is in very good agreement with the field monitoring data from IN-0903. For IN-1011, higher deformation is predicted from the finite element model than was observed from the field monitoring data. However, IN-1011 was installed when the dyke elevation was around 240 m and was thus not able to capture the initial dyke deformation, so the true deformation is more than measured. The result of the predicted deformation for dyke elevation 290 m is also presented in Figure 11. As shown, most of the deformation at IN-0903 is already completed after dyke was constructed to 260 m and only 10 mm of further deformation is predicted when the dyke reaches to final elevation of 290 m. In contrast, significantly more deformation will occur at the IN-1011 location when dyke elevation reaches to 290 m; another 70 mm of lateral deformation are predicted at IN-1011.

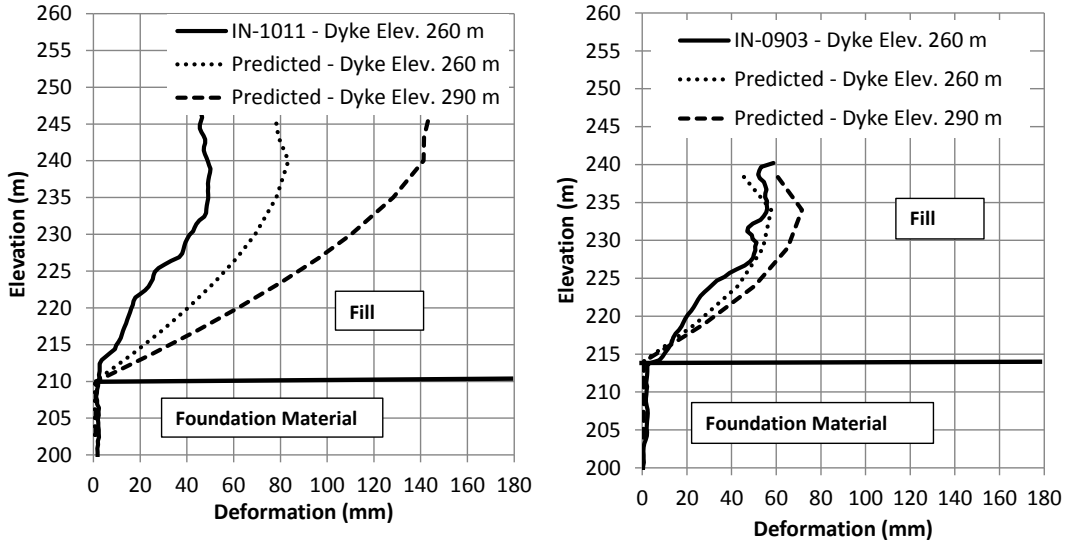


Figure 11. Measured and predicted lateral deformation of the dyke fill

The elastic settlement of the dyke was also predicted using the finite element model. The analysis indicates that the maximum settlement of the dyke fill will occur at the center of the dyke fill. The predicted elastic settlement for dyke elevation of 260 m ranged from 0.2 to 0.4 m whereas measured settlement from MEs ranged from 0 to 0.2 m. MEs were installed when the dyke elevations was around 240 to 250 m and was not able to capture deformation prior to ME installation.

7 CONCLUSIONS

Stiffness and deformation characteristics of the dyke fill material are presented using field and laboratory testing results. The CU moduli show some variation but overall, values increase with

increase in effective cell pressure. The moduli deduced from the pressuremeter tests are comparable with the initial tangent moduli from CU tests, and no correlation with depth was discernible.

The predicted elastic deformation from finite element modelling is compared with the field monitoring data. Reasonable agreement is observed from the predicted and monitored lateral deformations. The outcome elastic deformation from the finite element modelling could be used to predict future dike deformations as a quality control measure to ensure deformations are not excessive. As more data becomes available these modeled results could be field calibrated for improved accuracy.

8 ACKNOWLEDGEMENTS

The authors acknowledge the management of Shell Canada Energy for permission to publish this paper.

9 REFERENCES

Canadian Dam Association (CDA). 2007. Dam safety guidelines.

BGC Engineering Inc. 2009. In Pit dykes high pore pressures within embankment fills, Issued to Shell Canada Energy July 31, 2009.

BGC Engineering Inc. 2011. In Pit dykes 2010 fill characterization program factual site investigation report. Issued to Shell Canada Energy May 31, 2011.

Geo-Slope International Ltd. 2012. Stress-deformation modeling with SIGMA/W

Norwest Corporation (NW). 2010. Muskeg River Mine In-pit Dyke Material Suitability 2009 Lab Program Findings Report (Draft). Issued to Shell Canada Energy Ltd. April 15, 2010.

Geophysical methods as an aid to planning, monitoring, and abandoning tailings facilities in the Alberta oil sands

Paul Bauman, Dan Parker, Brad Hansen & Laurie Pankratow
WorleyParsons, Calgary, AB, Canada

ABSTRACT: Both surface and borehole geophysical techniques have a wide range of cost-effective applications to all stages of oil sands tailings management. When siting tailings impoundments, surface geoelectical methods are particularly effective in delineating Quaternary channels that, if not fully and accurately mapped, may provide pathways for off-site leachate migration. Rapidly applied waterborne geophysics has already been applied in much of the Athabasca watershed to establish baseline conditions before pond construction, especially flow conditions resulting in naturally occurring discharge zones from deep seated Devonian brines. During the life of a tailings pond, surface techniques can be used for imaging the accumulation of underlying "beach" sands, the varying thickness of stratified layering within tailings, and the accumulated thickness of capping material. Borehole geophysical sondes can be logged directly into tailings ponds for monitoring physical properties. Where tailings sand impoundments are being reclaimed, a wide variety of surface geoelectric methods can be used to image salt migration and groundwater flow; this is particularly relevant as high salinity discharge zones often function as primary controls of revegetation. While not a replacement for intrusive methods, surface geophysical surveys can greatly reduce the magnitude of intrusive sampling programs, provide a conceptual basis to designing such programs, and assist in interpolating between intrusively sampled points or borings. Numerous examples will be provided to illustrate the above applications of geophysical methods.

1 INTRODUCTION

Generally, characterization of sites associated with tailings is largely done by intrusive methods. Dikes for impoundments are generally sited with drill hole information. Seepage zones in the Athabasca are identified by surface observations or very sparse and somewhat random, and usually temporal piezometer placements. Consolidation information from tailings ponds is gathered by a relatively few laboratory tested grab samples and cone penetrometer tests.

Borehole data are sparsely spaced. Lithology descriptions are often highly qualitative. Even when boreholes are drilled for geotechnical characterization, geophysical logging of boreholes is unusual. The characterizations of groundwater recharge into large river systems is much too large a problem to be attempted with a limited number of piezometers or mini-piezometers placed to very shallow depths. CPT logging on tailings ponds, while being quantitative and effective, is expensive. Furthermore, while high confidence can be placed in the CPT data, only a relatively small volume of any single tailings pond can be practicably sampled.

2 CHARACTERIZATION OF FOUNDATIONS FOR TAILINGS DIKES

Often, tailings ponds are sited in locations poorly suited to such structures as they are often underlain by Quaternary channels. Sand and gravel channels may provide short circuiting of fluids from inside the structures to outside the dikes. Numerous geophysical techniques are well suited to imaging and characterizing such channels in 2-D and 3-D. Such techniques include:

1. Electrical resistivity tomography (ERT), which images subsurface materials based on their electrical properties. Granular material will be highly resistive, while clay till and Clearwater Shale will be highly conductive.
2. Seismic Reflection, which images subsurface materials based on their density and acoustic properties. Seismic reflection is particularly well suited to defining the bottom contacts of channels incised into bedrock.
3. MASW, or multi-channel analysis of surface waves provides a cross-section of the subsurface in terms of the shear wave velocity. As shear wave velocity is related to stiffness, overburden material and bedrock are easily differentiated. In addition, shear wave velocities provide a good understanding of consolidation in fill materials.

The above data sets, once collected, can then be used for siting geotechnical boreholes for more detailed lithologic characterization. The drilled boreholes can be used for borehole geophysical logging for constraining the surface geophysical data sets.

3 CHARACTERIZATION OF SEEPAGE INTO THE ATHABASCA RIVER AND ITS TRIBUTARIES

Seepage zones into the Athabasca River watershed are characterized by elevated electrical conductivity due to increased salinity of waters sourced from the Devonian, or seepage from tailings ponds or other impoundments. As such, these seepage zones are readily mapped and imaged in cross-section using a variety of different geoelectical techniques including electromagnetic conductivity mapping and ERT. Such techniques are well suited to being deployed from small boats or larger jet boats where river conditions require. Many kilometers of river reach can be surveyed on a daily basis. This data can then be used to site well placed piezometers for direct subbottom connate water sampling.

4 CHARACTERIZATION OF TAILINGS PONDS

Using ERT, sonar, and geophysical logging techniques, cost-effective geophysical techniques can provide considerable characterization on active tailings ponds. Waterborne resistivity surveys with a towed streamer can provide near 3-D characterization of a tailings pond in terms of approximate solids content, bottom depth, and beach sands delineation. Low frequency sonar surveys can readily determine the thickness of the layer of low total suspended solids (recycled) water, though sonar is not able to penetrate layers of total suspended solids in the tens of thousands of ppm. Density logging directly into ponds provides a direct measure of consolidation. Temperature, conductivity, neutron porosity, and natural gamma logging all provide other additional physical properties characterization of any given point at any given location with depth.

5 CONCLUSION

Geophysical techniques provide cost-effective means of characterizing and monitoring tailings impoundments, the foundations of such impoundments, as well as seepage from tailings impoundments. Generally, such non-intrusive surveys should be combined with drilling, sampling, cone penetrometer testing, or other intrusive studies in order to increase confidence and provide detailed information on lithologies, chemistry, and other physical properties.

Oil Sands – Chemical and Amendments Flocculation

Monitoring of agglomerating mature fine tailings in pipe reactor flow

Alex van der Spek
ZDoor BV, Rotterdam, ZH, The Netherlands

John Viega
CiDRA Oil Sands, Wallingford ,CT, USA

ABSTRACT: The rheology of fluids is described by a constitutive equation which relates (wall) shear stress to (wall) shear rate. Polymer induced agglomerating of Mature Fine Tailings (MFT) will result in a varying relation between shear stress and shear rate as the reaction progresses. A velocity profiling method to monitor shear stress and shear rate in real time was developed and implemented on a field scale pipe reactor. Results indicate very little difference in the shape of the velocity profile between the turbulent flow of agglomerating MFT and the laminar flow of MFT in its native Bingham plastic state.

With the change in the rheology a different mechanism of energy dissipation will evolve. In laminar flow the pressure gradient required to drive the flow is linearly related to the rate of flow. In fully developed turbulent flow the pressure gradient is quadratically related to the rate of flow. A method is described to monitor the rate of energy dissipation per unit volume from array velocity measurements.

The spectrum of energy distribution over a variety of length scales is measured and compared to the Kolmogorov 5/3 law. Deviations from the latter indicate non turbulent or partially turbulent flow. Partial implementation on a field scale was accomplished using the same instrumentation as used in the velocity profiling method. Results from a field experiment show that periods of laminar and turbulent flow can easily be identified.

1 INTRODUCTION

Mature Fine Tailings (MFT) is a rheological fluid characterized by a non-Newtonian constitutive equation. Often a Bingham model or a Herschel-Bulkley model is applied to model the rheological behavior of MFT. Bingham fluids exhibit a yield point. Wall shear stresses below the yield point will not result in flow. Otherwise the shear stress increases linearly with the shear rate. Herschel-Bulkley fluids also exhibit a yield point but the shear stresses increase either super-linearly or supra-linearly with the shear rate. Herschel-Bulkley fluids are therefore capable of modeling dilatant or pseudo-plastic behavior. A comparison of the various constitutive equations for MFT is given in Figure 1. This figure is to scale and representative values for MFT were used. For reference the black line represents water at room temperature, water being a purely Newtonian fluid.

Dewatering of MFT can be accomplished by a variety of means. Evaporative drying, polymer assisted floccing and mechanical separation are all being used. The economic viability and technical complexity of these techniques is very different. It is fair to state that all means of MFT dewatering would benefit in some form or measure from an on-line measurement of the rheological parameters of the MFT. To date an instrument to do so is not available. The requirements for an on-line measurement of rheology of MFT will depend on the dewatering technique chosen. The method of control, feed-forward or feed-backward, will bring additional requirements.

In evaporative drying, for instance, the yield point of the MFT is of prime importance as this quantity determines the minimum shear stress for positive flow and thereby dictates the slope of the land on which the MFT is deposited. Obviously, a form of feed-back control is not practical in this case.

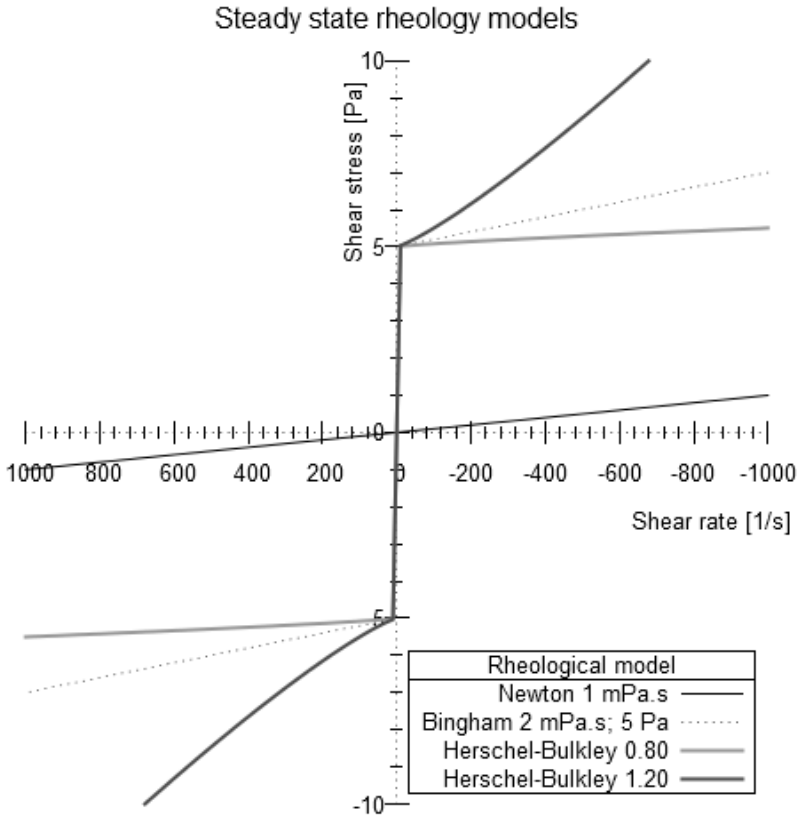


Figure 1. Comparison of various rheological models.

In mechanical drying, similarly, the MFT's plastic viscosity will determine size of and the required power of the drying machinery.

In polymer assisted floccing however; it is important not to shear newly formed flocs apart and hence a measure of the mixing intensity or the energy dissipated at length scales comparable to the flocs is important. In case the chemical reaction occurs in a pipe reactor, feed-back control on the flow rate and chemical dosing may be implemented using a measured quantity related to mixing intensity. In case the polymer is injected just upstream of the drainage points to the drying cells only feed-forward control based on the rheology of the untreated MFT is practical.

It appears, therefore, that two different sets of measurements may be necessary. Rheological parameters such as yield point and plastic viscosity which are commonly determined by laboratory determination of the shear stress to shear rate relation. Furthermore, flow parameters such as the average rate of shear, the mixing intensity or the power dissipation specific to the length scale of the flocs are important for feed-back control of chemically assisted dewatering.

1.1 *Rheological parameters*

The wall shear stress is an important quantity in pipe flow of any rheological fluid. An integral momentum balance across a control volume inside the pipe shows that the wall shear stress, τ_R, is easily determined from a measurement of the pressure gradient in the line (Bird, 1960):

$$\tau_R = \frac{R}{2}\frac{dp}{dx} \tag{1}$$

Here R is the inside radius of the pipe and dp/dx is the pressure gradient along the axial dimension of the pipe. The shear stress at the wall is the maximum shear stress that can occur. In laminar flow of MFT the profile of the shear stress is linear as the momentum balance equation is of first order.

The wall shear rate is much more difficult to determine in any on-line instrument as it requires the measurement of a velocity profile in the line. The resolution of the velocity profile must be sufficient to extract the gradient of the velocity profile at the pipe wall.

Alternatively we may assume that the flow is of a particular type, e.g. Bingham plastic flow. For such a type of flow the velocity profile may be calculated (Bird, 1960) and hence the velocity gradient at the wall and thereby the wall shear rate is known.

When the type of flow is unknown but it is known that the flow is laminar the shear rate at the wall may still be evaluated from a cross plot of the flow rate and the pressure gradient. This is an application of the Rabinowitsch-Weissenberg (Bird, 1960) equation and is standard practice in many rheological problems. The technique is not well suited to real-time control as historical data is required to evaluate the slope of the flow rate versus pressure gradient plot.

1.2 *Flow parameters*

The rate of energy dissipation per unit mass determines mixing intensity and average shear rate. In pipe flow the rate of energy dissipation per unit mass, ε, can be expressed as:

$$\varepsilon = \frac{1}{\rho} V \frac{dp}{dx} \tag{2}$$

Here ρ is the density of the fluid, V the velocity and dp/dx the pressure gradient. The above equation (2) does not, however, specify any particular scale of length at which energy is dissipated. As long as energy is dissipated on scales much larger or much smaller than a representative dimension of flocs, such flocs will not be affected. Compare this to the stirring of a large vessel. Even though a lot of power is dissipated, the stirring may not be effective in dispersing small pockets of material concentration because only small amounts of power are dissipated at this scale.

The theory of homogenous isotropic turbulence by Kolmogorov predicts that energy is dissipated only at certain, small, length scales. At length scales much larger than this smallest scale the spatial distribution of power is given by a 5/3 power law in the inverse of the wavenumber k. It is of interest here to determine the fraction of the total power that is effective at the length scale of flocs.

1.3 *Field experiment*

We present field data taken on a pipe reactor of length L1 where Mature Fine Tailings (MFT) is treated by polymer flocculent in order to release water and allow the MFT to dry. All three of the instruments on the pipe reactor are capable of measuring volumetric flow rate, a velocity profile and spectra of the energy dissipated. Differential pressure data was not available.

2 VELOCITY PROFILING

A segmented array of strain sensitive elements attached to the outside circumference of a pipe may be used as a velocity profile meter (Rothman, 2009). The velocity profile is thus obtained at 5 different positions in the pipe from the top to the bottom. Such velocity profiles are measured at three locations in the pipe reactor as indicated in Figure 2.

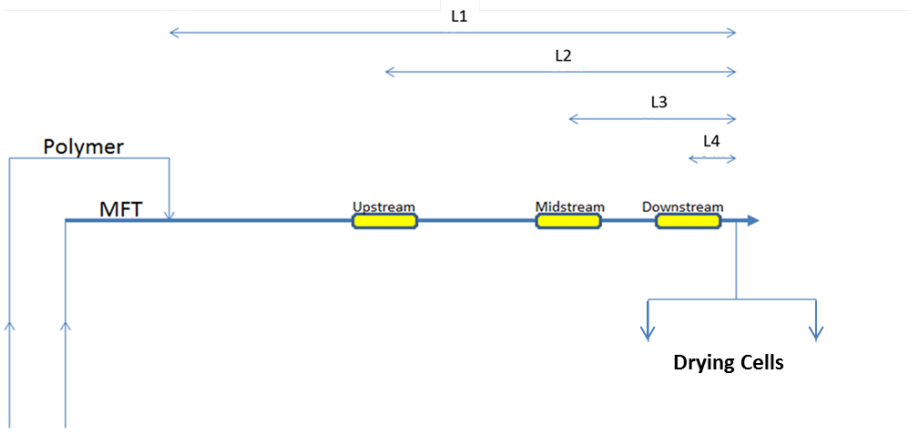


Figure 2. Schematic of the field set up.

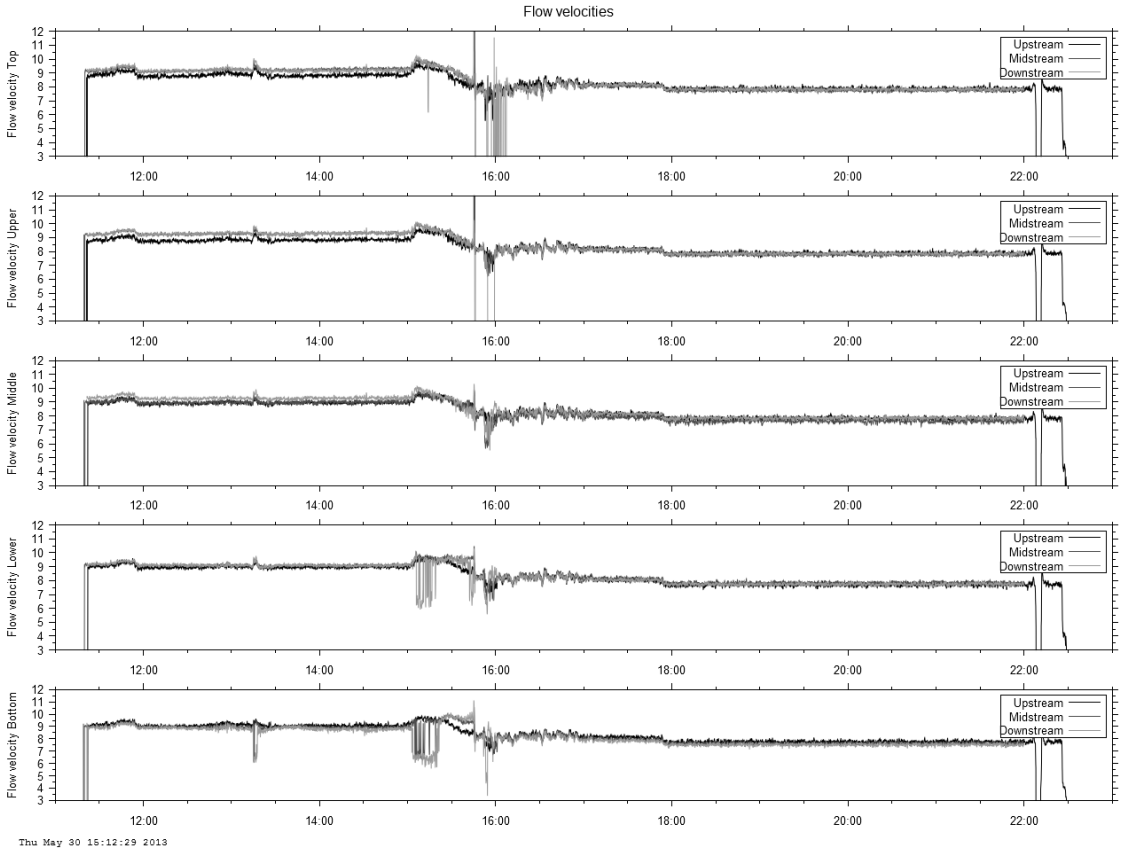


Figure 3. Velocity profiling data.

Around 16:00 the line was switched over from one drying cell to the next. Consequently before 16:00 there was chemical flocculent present in the line and after 16:00 there was none. Therefore the data shown here represents the velocity profile in both treated and untreated MFT, the latter presumably flowing in laminar state.

In Figure 3 the velocity data is shown from top to bottom in 5 different panels, as it would occur in the pipe. The three lines in each panel represent the upstream, midstream and downstream meter respectively. Thus it is easy to compare how the velocity profile progresses downstream as the reaction between MFT and chemical occurs.

First and foremost there does not appear to be any dramatic difference between the velocity profile of untreated MFT (after 16:00) and treated MFT (before 16:00). It is also apparent that

the magnitude of the velocity is about the same for all positions in the pipe. This indicates that the velocity profile is almost uniform. A rectangular flow profile is expected for both turbulent flow and for Bingham type flow. The former may well be present in the treated MFT where water is being released upon floccing. The latter is almost certainly present in untreated MFT as a result of the high yield point.

Observe that the upstream meter's top and upper velocity are slightly below the same for the midstream and downstream meter in the period before 16:00. This is the law of mass conservation in action. As there is a tendency of the MFT flocs to settle the velocity in the lower parts of the pipe is slightly lower there. As a result the top and upper velocity must be slightly larger.

The tendency of the MFT flocs to settle may be substantiated by the two periods of time visible at around 13:15 and 15:00. There the bottom and lower velocity for the downstream meter show a steep, sudden decrease which is associated with bedding of solid material. Bedding is an unwanted phenomenon in a pipe reactor. Fortunately only two periods of short duration were found.

In order to derive a representative gradient of the velocity at the wall from a measured velocity profile it is necessary to find in the measured 5 velocity points an appreciable variation in velocity towards the wall. If that were the case an approximate profile may be constructed by interpolation from which a gradient can be obtained. It goes without saying that the measured velocity profiles do not lend themselves to such a procedure.

3 ENERGY DISSIPATION

The same segmented array of strain sensitive elements as is used for velocity profiling may also be used to infer a quantity closely related to the dissipation of energy in the flow. The way velocity is extracted from array sensors is explained in detail elsewhere (O'Keefe, 2009). The fundamental result however is a map of frequency versus wavenumber for any form of coherent power propagating through the array of sensors. If such power is found to be concentrated on a line (termed a 'ridge' in array processing) of constant slope then that slope itself is inversely proportional to a velocity. The magnitude of the power is not given further consideration.

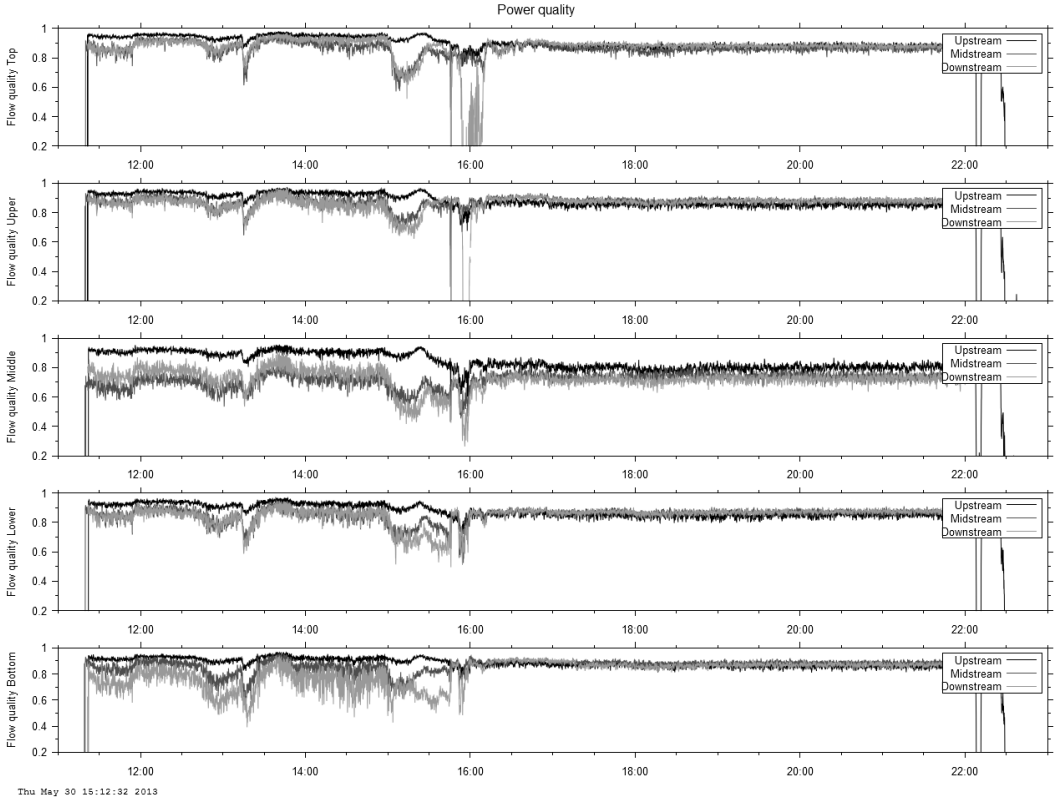


Figure 4. Power quality data.

In Figure 4 above we plot, in the same manner as the velocity data in Figure 3, a measure of the actual (normalized) power of a constant velocity ridge along the line of constant slope. Thus the above Figure 4 complements Figure 3.

Observe that contrary to the velocity data, i.e. the slope of the ridge, there now appears a dramatic difference between the period before 16:00 and the period of time after 16:00. This difference is visible in all positions, top, upper, middle, lower and bottom sensor array and it is visible in all three locations, upstream, midstream and downstream. The difference manifests itself in both the magnitude of the power quality as well as in the fluctuation thereof.

The transition in flow around 16:00 from treated to untreated MFT, presumably being paired with a transition of the flow from turbulent and settling to laminar is very easily observed. It should be noted that the upstream meter, being located upstream of the "T-off" valve shows little effect. Apparently about half way down from the point of chemical injection (equivalent to about 10 s of reaction time at the prevalent flow velocity) the floccing and settling of MFT is not yet occurring.

Contrariwise, downstream of the upstream location, at the midstream position a significant change in the power quality has occurred. This is evident from the changes in the value as well as in the range and the fluctuations occurring. By binning the power quality data in representative time periods of 2 hours it is easier to visualize the change in the power quality progressing down the line through the reaction zone where MFT forms flocs and settles. Such binning is shown in Figure 5, below.

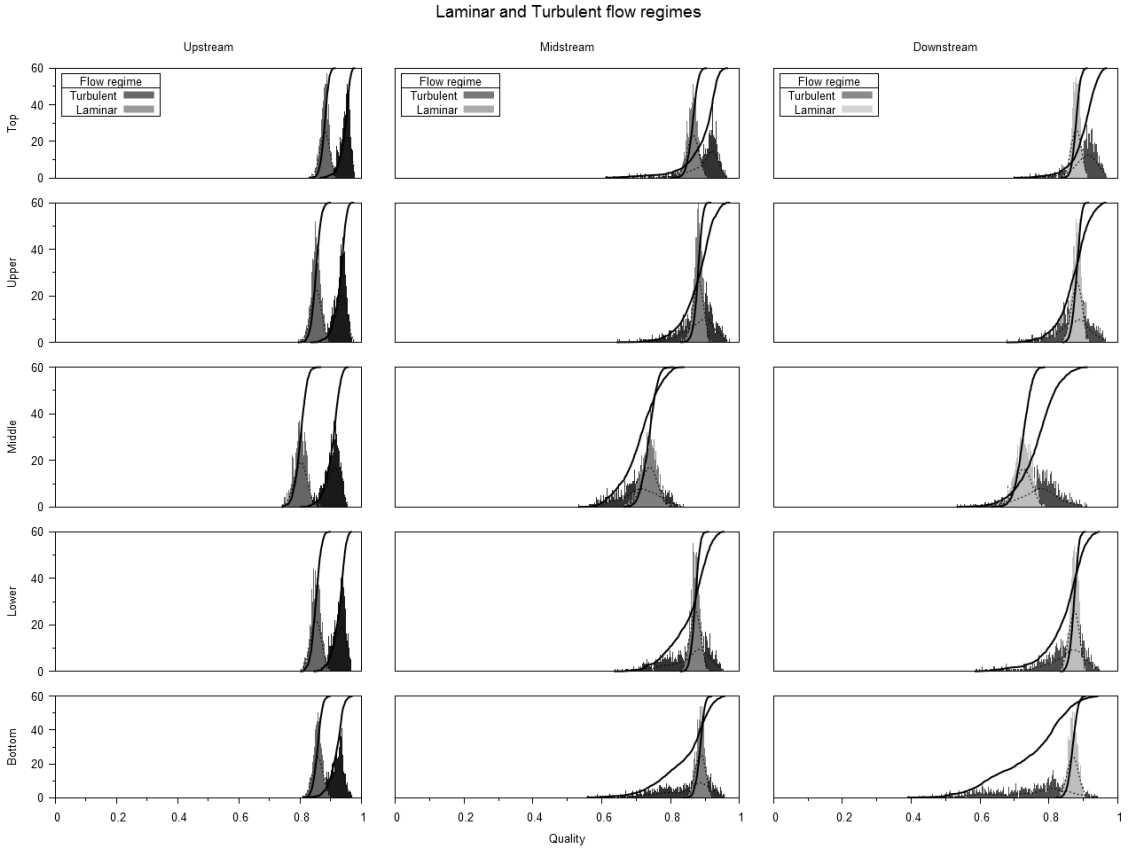


Figure 5. Histograms of power quality.

Note that the horizontal axes are all on the same scale of 0 to 1 in normalized power quality. Likewise all left hand vertical scales run from a 0 count to a count of 60. All right hand vertical scales are from 0 to 1 to indicate the cumulative as given by black lines.

Observe how the middle sensor array consistently results in somewhat smaller power qualities. This occurs irrespective of the location of the meter on the pipe reactor and irrespective of the flow regime. It is not understood why this is the case.

In the flow periods termed 'laminar' both the location and the width of the binned power

quality data does not appear to change much either by meter location or by sensor array position. Contrariwise, in the flow period termed 'turbulent' the change is dramatic and occurs on both the midstream and downstream meter.

4 INTERPRETATION

The results obtained in the field trial were contrary to expectation. It was expected to find little to no variation in the power quality between periods of flow of treated and untreated MFT. It was expected to see larger variation in the velocity profiles between the two periods. A beginning of an interpretation may be found in the Kolmogorov theory of homogenous isotropic turbulence (Davidson, 2009). According to this theory the important scales for length, time, velocity and shear rate (the inverse of the time scale) are given by simple formulae in terms of the kinematic viscosity of the fluid υ and the rate of energy dissipation per unit mass ε. For representative values of MFT in this work the scales are given in Table 1, below.

It is concluded that the Kolmogorov length scale is much larger than the typical particle sizes of the fines (< 44 μm) that make up MFT. It is only when such fines are flocculated that the Kolmogorov length scale may be approached. In the case that the particles are smaller than the length scale at which energy is dissipated such particles do not influence the energy dissipation in any way or form.

Table 1. Kolmogorov scales

	Formula	*Value*	*Unit*
Length	$\sqrt[4]{(\nu^3/\epsilon)}$	0.2	mm
Time	$\sqrt{(\nu/\epsilon)}$	5	ms
Velocity	$\sqrt[4]{\nu\epsilon}$	4	cm/s
Shear rate	$\sqrt{(\varepsilon/\nu)}$	200	1/s

It is also concluded that the Kolmogorov length scale is much smaller than the length scale to which a sensor array with a spacing of 61 mm is sensitive too. Apparently measured power spectra by an array of sensors are thus not affected by either the small scale eddies nor by the large scale effects which are on the order of the pipe diameter.

It is precisely in this range that the shear rate as given by the formula in Table 1 may be used as a representative value of the average rate of shear. However, what is of more interest is the spatial distribution of rate of shear or in other words the variation thereof with length scale.

By way of example in Figure 6 the spectra of vertical eddies in turbulent flow are given for a range of pipe sizes but at a constant velocity (left hand panel) and for a range of velocities (right hand panel) but at a constant pipe diameter. The graphs shown here are measured using similar array type sensors albeit without segmentation as this is only required for velocity profiling. The data originates from calibrations done in a high accuracy flow loop. As such there is no connection with the MFT field experiments reported here. Yet the graphs help to interpret the power quality data resulting from the MFT field experiment. It should be noted here that the "peaks" appearing in the spectra are a well understood artifact of array processing.

The Kolmogorov theory of homogenous isotropic turbulence predicts that the latter should all fall on the same curve when the power is scaled by the rate of energy dissipation as is seen to be the case. The theory also predicts that the spectra should collapse to the same curve when the wavenumber is scaled to the pipe diameter. With the exception of the 24 inch pipe this is indeed the case. The relation between the rate of energy dissipation per unit mass ε, wave number k and the power spectrum P(k) is given by Kolmogorov's celebrated 5/3's law:

$$P(k) = c\varepsilon^{2/3}k^{-5/3} \tag{3}$$

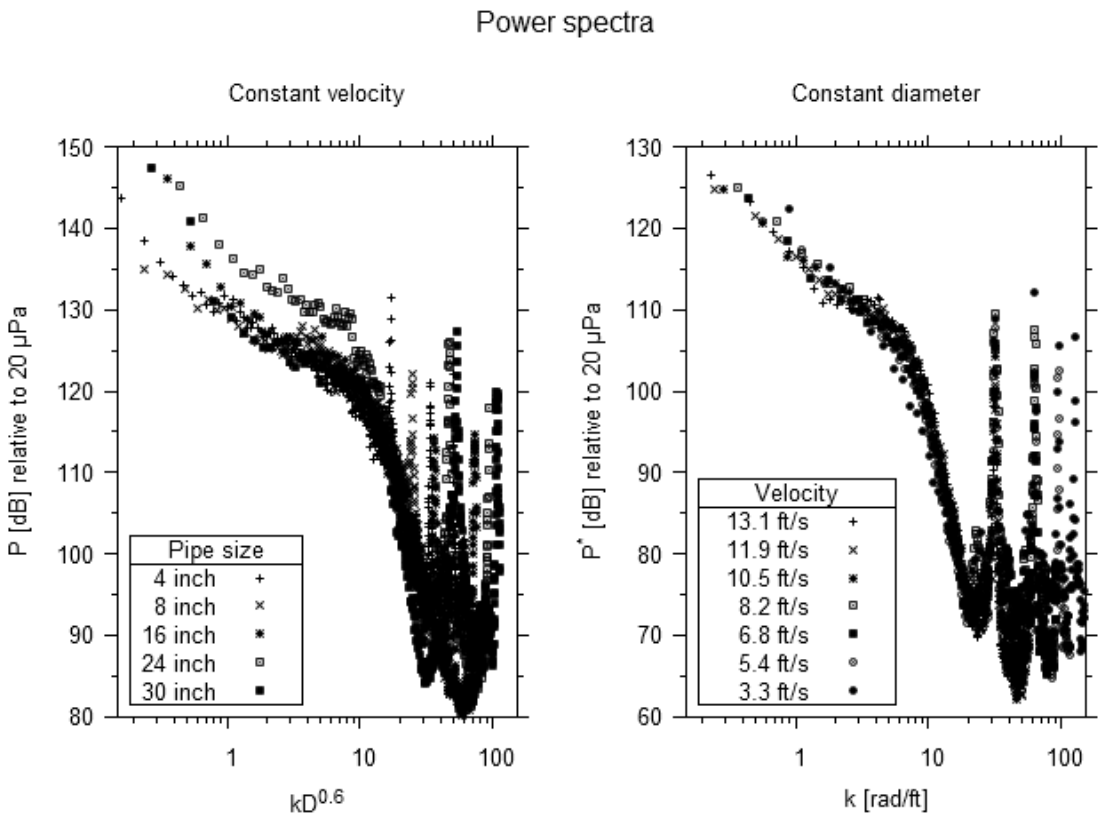


Figure 6. Vortical power spectra in turbulent flow of water.

Here c is a universal, dimensionless coefficient. The formula links the length scale to the energy dissipation rate per unit mass. Length scale should here be taken as the inverse of the wavenumber. The power quality as given in the Figures 4 and 5 is a normalized sum of P(k) between two bounds. The lower bound being the length scale corresponding to the pipe diameter. The upper bound being given by the distance between the individual sensors of an array.

The power quality is therefore a not just a measure of the amount of dissipated power but also, whenever such power is dissipated at length scales between the upper and lower bound of the (inverse) wavenumber of the length scale itself. It may be postulated that when flocs of MFT are of similar size as this length scale, i.e. the size of "eddies" in turbulent flow significant effects occur. In such cases that this leads to breaking down of the flocs by shear action should be taken to prevent this.

5 CONCLUSIONS AND RECOMMENDATIONS

Regardless of the dewatering methodology, on-line instrumentation for the measurement of the rheological parameters of MFT is necessary to control the process and to cope with the variations in the properties of MFT.

Measured velocity profiles in pipe flow of MFT show a nearly uniform velocity profile as is expected for flow of a Bingham plastic. MFT which is flocking and releasing water after treatment with polymer also show a nearly uniform velocity profile as is expected for turbulent flow.

The size of fines in MFT is much smaller than the Kolmogorov length scale in typical flows of MFT. The hydraulic power in the flow is therefore dissipated without being influenced by the fine particulate material. Flocs of MFT, formed by polymer injection will grow to sizes comparable to the length scale at which hydraulic power is dissipated.

Sonar based array processing techniques are sensitive to any form of (coherent, hydraulic) wave power propagating through the sensors making up the array at length scales dictated by the

distance of the sensors. Power quality is a measure derived from sonar based array sensing which responds to both the magnitude of and the length scale at which energy is dissipated.

Measured values of (normalized) power quality in agglomerating MFT show large fluctuations and cover a wide range whereas in native MFT power quality shows narrow distributions centered at one particular value.

In the pipe reactor the agglomeration of MFT under the influence of polymer is not noticeable in the beginning of the line. Only in the second half of the pipe reactor does normalized power quality indicate the formation of flocs of length scales much larger than the Kolmogorov length.

There is virtually no tendency of such flocs to settle into a bed. Measured velocity profiles show only short, intermittent periods of bedding. At times that bedding is suspected the normalized power quality shows lower values on average. The latter indicates that power dissipation is significantly affected on length scales comparable to the distance between sensors.

Normalized power quality is neither a direct measure of the amount of energy being dissipated nor is it directly indicative of the precise length scale at which hydraulic power is dissipated. Development of a measure that does both is possible using Kolmogorov theory and detailed array processing quantities. Average rate of shear may then be calculated at a different length scales. The rheology of agglomerating MFT may then be characterized at a multitude of scales.

6 REFERENCES

Bird R Byron, Stewart Warren E., Lightfoot Edwin N, 1960, *Transport phenomena*, John Wiley & Sons.

Davidson, P.A., 2009,*Turbulence*, An introduction for scientists and engineers, Oxford University Press.

Rothman Paul, O'Keefe Christian, Thomas Aaron, 2009, *Application of Unique Sonar Array Based Process Monitoring Measurement Equipment for Minerals Processing Applications*, CiDRA Corporation, white paper, http://www.cidra.com/sites/default/files/document_library/BI0407_Application_of_Unique_SONAR_7-15-09_Final.pdf.

Maron Robert J., Fernald Mark, O'Keefe Christian, Viega John, Bailey Tim, 2008, *New Applications of sonar-based technology in the minerals processing industry: Velocity profile measurement and pipe wall wear monitoring -in hydrotransport lines*, MAPLA 2008.

O'Keefe, Christian, Maron Robert, Fernald Mark, Bailey Timothy, Van der Spek, Alex, Davis, Michael, 2009*, New developments in flow and pipe management capabilities through new velocity profile measurement and pipe wall wear monitoring instrumentation*, SME 2009.

O'Keefe C.V., Maron R.J., Rothman P.J., Poplawski J., 2008, *Description of non-intrusive sonar array-based technology and its application to unique and difficult slurry and paste flow measurements*, PASTE 2008, Kaskane Botswana, May 2008.

The effects of in-line static mixer flow loop operational parameters on flocculant performance in mature fine tailing samples

P.A. Gillis, J.S. Moore, M.K. Poindexter, C.A. Witham, W. Chen, and H. Singh
The Dow Chemical Company, Freeport, Texas, USA

C.E. Mohler
The Dow Chemical Company, Midland, Michigan, USA

J. Atias
The Dow Chemical Company, Calgary, Alberta, Canada

ABSTRACT: Government regulations and growing environmental concerns are driving the need to remediate tailings produced by bitumen extraction from surface mining of Canadian oil sands. The remediation of the tailings is challenging due to the geological variations between mining operations and the inherent colloidal stability of the clay particles. Chemical flocculants are frequently used to aid the various dewatering processes for mature fine tailings (MFT). Flocculant mixing is critical to performance. Several mixing processes occur at different spatial and temporal scales during this flocculation process. For example, sufficient blending is needed to homogenize the additive with the MFT, but excessive shear can break up flocculated particles. The MFT treatment process has been traditionally studied with laboratory-scale impeller agitated tank systems.

In-line static mixer configurations allow for a greater understanding of the interaction of the key mixing parameters. Specially, the contributions of blending, floc formation kinetics, and shear rate can be independently varied and quantified. Experiments were conducted with static mixers positioned within a flow loop to show the effect of mixing on flocculant-aided MFT dewatering. These experiments quantify how the intensity and duration of blending, loop recirculation time, shear rate, and flocculant dosage affect dewatering by gravity settling. This study included several MFT sources and flow loops at various scales. A new developmental flocculant was shown to increase dewatering and perform effectively through a broad range of operating conditions.

1 INTRODUCTION

1.1 *The opportunity*

One of the most abundant forms of fossil fuel is bitumen (Dusseault 2001). This abundance, coupled with the globally increasing demand and value of petroleum, has fueled the development of the oil sands industry, particularly in western Canada. The high recovery of mined bitumen in the extraction process (88-95%, Masliyah et al. 2004) offers further advantages with this production method. However, one of the byproducts of the water bitumen extraction process is a tailings waste stream containing fine clay particles that are particularly challenging to remediate (Kasperski 1992). Since the opening of the first commercial oil sands mining operation in 1967, almost 1 billion cubic meters of mature fine tailings have accumulated (Houlihan & Haneef 2008). Furthermore, the volume of MFT in the tailings ponds is expected to increase in the future (Houlihan & Haneef 2008). Government regulations are now in place requiring the remediation of tailing ponds.

There are a number of methods being developed to remediate the tailings, including tailing thickening, chemical treatments, and centrifugation (Sobkocwicz & Morgenstern 2009, Mikula

et al. 2009, Wells et al. 2011). Extensive summaries of various remediation methods have recently been published (BGC 2010, Oil Sands Tailings Roadmap, 2012). A key class of methods for tailings remediation involves the addition of a chemical agent(s) to cause coagulation/flocculation (Watson et al. 2011, Mohler et al. 2012, Mahmoudkhani et al. 2012, Stewart et al. 2012). The performance requirements for these high molecular weight flocculants are significant. The additive must flocculate a significant amount of clay fines to enable rapid dewatering. In addition, the flocs must withstand the shearing forces experienced in the tailings treatment, transport, discharge, and deposition systems.

Mixing plays a critical role in the use of flocculants to aid in the dewatering of oil sands tailings. Historically, lab-scale tests have been performed using 2 L and smaller agitated vessels. However, due to capital costs, it is unlikely that stirred flocculation tanks will be implemented on an industrial scale. In-line systems, which might include a static mixer, are more suited to the continuous treatment of large volumes of MFT.

1.2 *Previous Work*

Laboratory studies have shown that optimal dewatering of flocculated tailings requires a sufficient but not excessive amount of mixing (Yao 2012). Some existing chemical additives are limited by the effect of both mixing and dosage on their performance. Commercial MFT treatment operations will encounter process variability, and it is desirable that the chemical additive is effective over a broad range of clay types, clay concentrations, solids loadings, water chemistry, and residual bitumen.

The focus of this effort is on using in-line static mixer systems to study the effect of operational parameters on flocculant performance for dewatering MFT. Demoz and associates have been studying MFT treatment mixing for a number of years. They showed (Demoz & Mikula 2010) a clear dewatering peak as a function of mixing time in an agitated 2 L vessel for an anionic high-molecular-weight polymer flocculant. It was further concluded (Demoz et al. 2010) that the "payback of proper mixing is as much as selecting an effective flocculant." Both capillary suction time (CST) and water release by gravity settling were used to quantify performance.

In 2012, this work expanded to encompass static mixer systems (Demoz 2012). Once-through in-line flocculant addition experiments were conducted to determine appropriate scaling parameters. Velocity, Reynolds number (Re), and mixing energy density were evaluated as scaling parameters. Mixing energy density is a variation of the common mixing scaling parameter power per unit mass (kJ/kg); it is typically used to scale multi-phase contacting, solids suspension, and reactive flow problems (Harnby et al. 1985). Demoz observed that additional static mixers lowered the velocity requirements to reach peak dewatering performance. The study concluded that "mixing energy density can be used to scale flocculation mixing."

1.3 *Mixing and Flocculation*

The word "mixing" is generally used to describe a wide range of physical mechanisms including phenomena associated with the adjacent fields of fluid mechanics and rheology. In order to minimize confusion, the general term "mixing" will be avoided and the discussion will focus on more specific mixing terminology. Mixing mechanisms are typically classified by the scale upon which they occur (Buckhorn et al. 2010). The most common mixing concept is macro-mixing or blending; this refers to increasing homogeneity through large scale fluid motion. Micro-mixing relates to small scale phenomena such as molecular interactions, multi-phase interactions, and Kolmogoroff scale eddies (Hinze 1959).

Prior to prescribing a mixing solution, an understanding of the basic physics is required. Oftentimes, processes contain multiple mechanisms with conflicting mixing requirements. MFT flocculation involves at least three distinct physical mechanisms (Dobias 1993). First, the flocculation agent must be blended with the tailings stream. Second, some molecular transport and alignment is required for the floc formation. Finally, the floc must be protected from excessive shear rates, which could destroy the floc structure. Although these mechanisms are primarily sequential, the shear environment can simultaneously affect each step.

These separate mixing phenomena are listed in Table 1, which includes mixing measures, dewatering penalties, and the relationship of these phenomena to the experimental apparatus that

will be described in the next section. There are clear conflicting mixing objectives; high shear rates improve blending at the expense of floc stability. Additive contacting can be quantified as the time needed to reach a specific level of mixture homogeneity. This blending is needed to insure the capture of the clay fines in the flocs. Once the flocculant is dispersed in the tailings stream, a finite amount of time is required for the floc formation. If this time is not achieved, fines will remain unbound. Excessive shear is known to break up the flocs and release the clay particles. In order to quantify each of these phenomena, an experimental apparatus needed to be developed where these mechanisms can be varied independently.

Table 1. Critical phenomena in the flocculation process and their relationship to mixing.

Step	Additive Contacting	Floc Formation	Floc Stability
Mixing Need	Blending	Growth Kinetics	Shear Environment
Mixing Measure	Homogeneity	Time	Shear Rate
Dewatering Penalty	Free (clay) Fines	Unbound Fines	Fines Release
Mixer Loop Measure	Mixer Element Passes	Post-Blend Time	Velocity

2 EXPERIMENTAL

2.1 *Apparatus*

A static mixer flow loop was built to evaluate the effects of chemical additives and operational parameters on MFT flocculation and dewatering. The apparatus allowed the independent variation of blending (through modifying the type, size, and number of mixing elements), additive injection rate, and post-blend time (flow loop recirculation time after additive addition). This device was constructed at several scales: 100 mL, 500 mL, 1 L, and 2 L. The key differences between the scales were the tubing lengths and diameters, mixer diameters, and pump capabilities. The smallest apparatus facilitated the generation of numerous data points without consuming large amounts of MFT. Over 1,000 run conditions have been evaluated on the 100 mL scale. In contrast, the larger rigs can produce sufficient treated MFT quantities for consolidation and drying tests.

A diagram of the static mixing loop is shown in Figure 1. This apparatus consists of three primary sections: the surge tank (which can be quickly connected and disconnected), the flocculant injection system, and the pump/static mixer section. The surge tank provides a means for rapidly opening the flow loop, either for the initial introduction of the MFT or to pump the treated loop contents into a settling cylinder. Furthermore, the vessel provides flexibility in the total system volume which is needed due to the introduction of the flocculant stream. The system fluid volume is adjusted to prevent air from being drawn into the flow loop from the bottom of the surge tank.

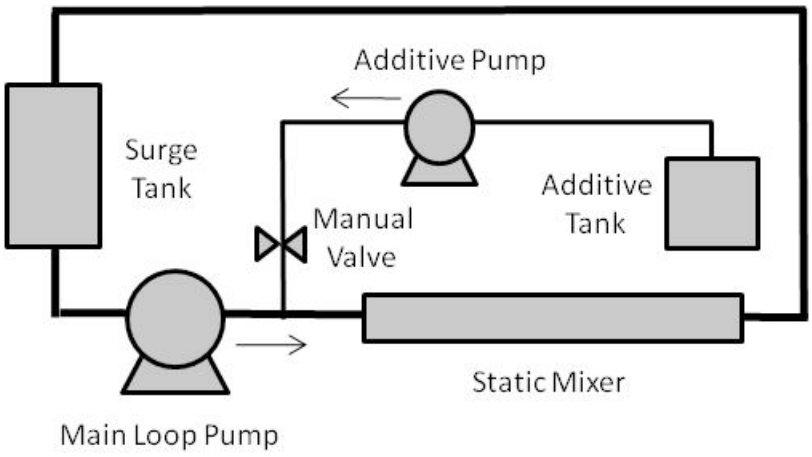


Figure 1. Diagram of static mixer loop experimental apparatus

The chemical additive is introduced through a separate line. The flocculant is pumped from a vessel into the flow loop. The inlet line is isolated from the main flow loop with a manually operated valve. On the 100 mL flow loop, the additive is introduced in a T-junction. A variety of static mixer geometries has been evaluated. By varying the number of mixer elements, the effect of blending can be separated from floc formation kinetics (injection and blending time) and shear rate. The various sections of the apparatus are connected by tubing.

2.2 *Procedure*

This section describes the experimental procedure used to generate performance data.

1. Flocculant is mixed to the desired weight percent in process water. The industry standard for this is 0.4 wt%.
2. Prior to the initial experiment, the polymer addition line is cleaned and filled with fresh polymer solution. The manual valve is closed.
3. A quantity of MFT is weighed out and diluted to a set weight percent solids using process water. The mixture is agitated to ensure proper blending and solids suspension.
4. The static mixer loop is flushed with water and drained.
5. MFT is poured into the surge tank and the loop pump is run slowly to allow the static mixer to fill.
6. The surge tank inlet feed line is connected to close the mixing loop.
7. The loop pump is set to the desired flow rate and the recirculation flow is started.
8. The manual valve is opened and the flocculant addition pump is set to the desired flow rate. The flocculant is added for a predetermined amount of time, after which the additive pump is stopped, and the valve closed.
9. The main loop pump is run for an additional predetermined amount of time and then shut off.
10. The surge tank connection is opened and the upper line is allowed to drain into the surge tank.
11. The surge tank contents are poured into a graduated cylinder. The system is drained initially by gravity. The loop pump is run slowly in reverse to empty the system.
12. The graduated cylinder is set aside so that the settling can be monitored.
13. The procedure is repeated (beginning from step 3) for each additional experiment.

3 RESULTS AND DISCUSSION

3.1 *Performance quantification*

The ultimate goal in treating MFT is to reclaim the land occupied by the tailings ponds. This requires removing sufficient water so that the remaining solids are trafficable (ERCB 2009). Different processes are under development to meet these objectives. However, most methods include a couple key steps, namely, dewatering and consolidation. Although one of the purposes for the static mixer flow loop was to prepare treated MFT samples for consolidation and drying tests, this paper will focus solely on the dewatering by gravity settling.

Two common measures of dewatering are the capillary suction time and water release through gravity settling. Previous studies (Scholz 2006, Demoz 2012) have shown that these techniques correlate well with each other. Short capillary suction times correspond to high water releases; both methods quantify water mobility within the floc structures. The experimental apparatus was configured so that the contents of the flow loop could be easily pumped directly into a graduated cylinder. The cylinders are left to settle and the mud line height is monitored (either manually or through time-lapse photography) over time. Figure 2 show a series of treated MFT sample that have settled for 20 hours. This figure shows significant differences in mud line height (due to varying pump speed) as well as distinct levels of water clarity. The amount of water release does not appear to be related to the turbidity of the released water. It was hypothesized that water clarity is related to floc stability.

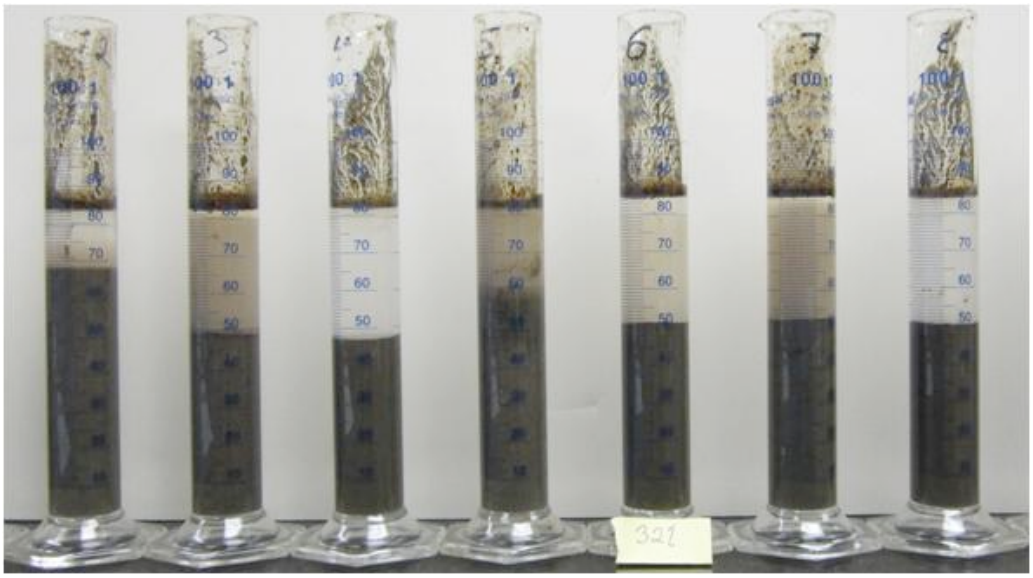


Figure 2. Water clarity and solids volume (mud line) variations after 20 hours of settling

For this study, both the diluted Net Water Release (dNWR) and neat Net Water Release (nNWR) are metrics of interest. The later measure (nNWR) is defined as the percent of the water released that was part of the original MFT sample. This does not include water added to dilute the MFT for treatment or the water that accompanies the chemical additive. Neat NWR will be negative until all the dilution water is separated. Diluted NWR is a less effective performance measure as higher values are associated with greater initial MFT dilution; dNWR is determined by dividing the released water by the sum of the water from the original MFT and the water associated with dilution(s).

Probably the best measure of dewatering performance is the average solids weight percent (of the suspension below the mud line). This calculation requires knowledge of the solids and liquid densities. The volume and mass of four components of the system need to be quantified: solids in the original MFT sample, water in the original MFT sample, dilution water, and flocculant addition water. Furthermore, some of the treated MFT material is left in the apparatus. This is due to surface coating and the percentage of lost material increases (up to 15%) at smaller scales. This material must be accounted for in the performance calculations.

Figure 3 shows settling curves for mud line percent, nNWR, and solids weight percent for a single flocculant experiment. The solid line denotes the drop in the mud line from 100% to below 50% over time. The neat Net Water Release reaches 0% at approximately one hour. A log scale is used for settling duration to account for the diminishing changes over time. Very little improvement is seen past 1000 minutes. The solids weight percent dashed line shows the gradual increase in this variable. This line shows that initial dilution (both dilution water and additive water) dropped the solids loading below 30%. Furthermore, the solids wt% corresponding to the 0% nNWR indicates that the original MFT has a solids weight percent of approximately 45%. These lines are fairly smooth, and a specific set time period was chosen to report solids weight percent. Although 24 hours is the normal settling time reported, a duration of ~20 hours was chosen to facilitate the daily experimental turnaround associated with laboratory operation.

3.2 *Variability*

An important consideration is the experimental repeatability and the factors that influence this variation. For these MFT flocculation tests, an important source of variability was found to be the MFT sampling. Care was taken to maintain a uniform solids suspension in the MFT source containers and to insure uniform extraction of MFT samples for each flow loop experiment.

Furthermore, the static mixer flow loop was developed in part to create a more repeatable small-scale system for quantifying flocculant performance.

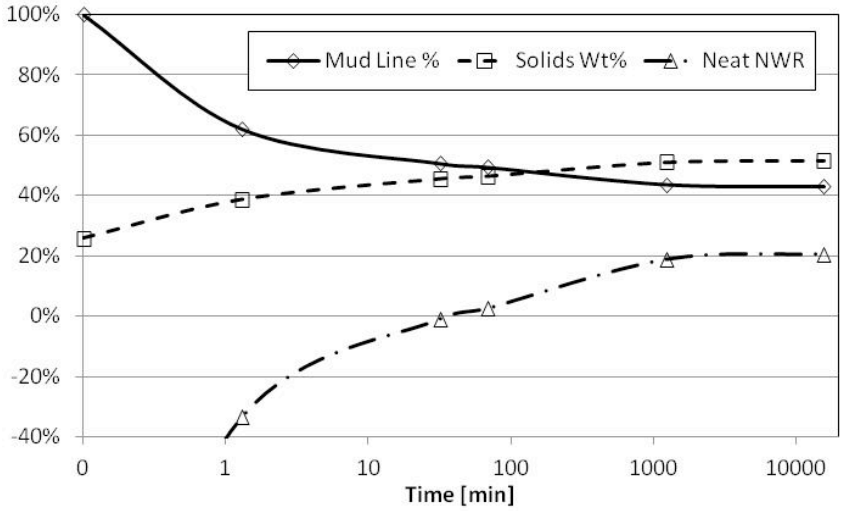


Figure 3. Comparison of parameters for evaluating settling performance

Initially, a 15 mL stirred cell system was used to evaluate flocculants. One purpose of these experimental tools is the screening of different additives and mixing conditions. These systems constitute the next progression following the high-throughput methods employed in the initial additive screening (Mohler et al. 2012). Figure 4 compares the CST variation typically seen with the 15 mL stirred cell (first 5 values) to the 100 mL static mixer flow loop runs (measurements labeled 6–10) for the same flocculant and dosage. The static mixer flow loop apparatus produces both lower variability and lower CST values (probably due to improved flocculant blending). The CST was compared when the water front moved 15 cm. Errors associated with each mean are 1 standard deviation.

It is also important to understand the variation in the performance measure chosen by this study, namely, the solids weight percentage after ~20 hours of settling. Figure 5 contains data for six experimental runs. Each run of 10 data points (a sweep of pump speeds ranging from 7% to 80%) was generated on a different day over a period of 3 weeks. For the most part, the solids weight percentage deviated from the mean (denoted by the lines) by less than 2% (absolute values). The one exception is the high data point (open square, solids wt% of 43%) at the pump speed of 16%.

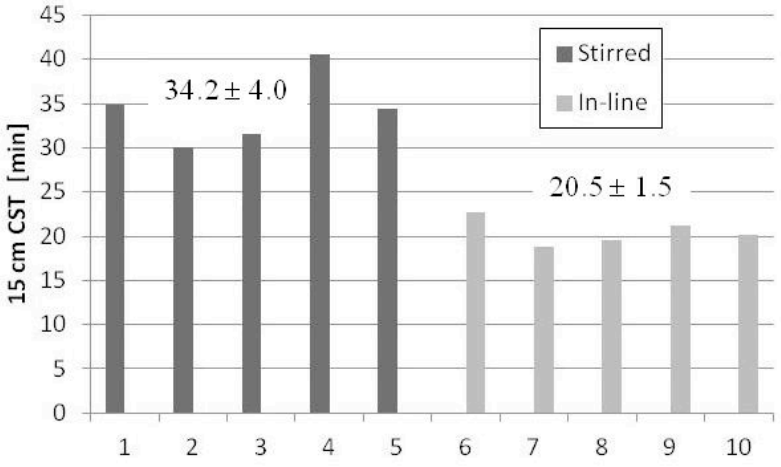


Figure 4. Comparison of CST variability for two small scale (100 ml or less) experiments

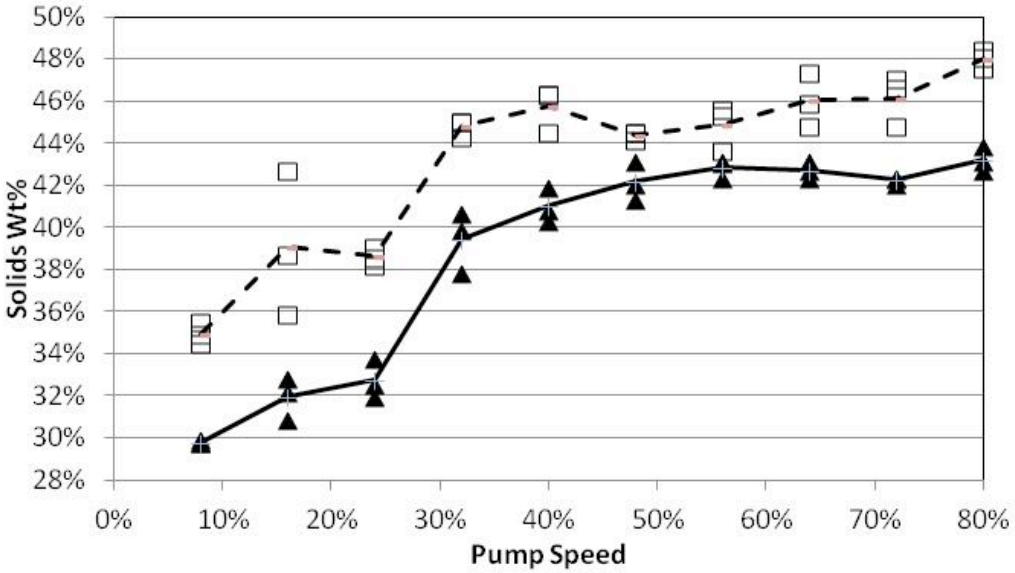


Figure 5. Variability illustrated through three repeated sweeps for two MFT dilutions

3.3 *Additive Performance*

When comparing different flocculating agents, it is important to understand that the blending requirements, floc formation kinetics, and shear sensitivity of the chemicals can vary significantly. Improved flocculants could be inaccurately evaluated if they are judged solely by their performance based on operational parameters optimized for a different additive. Furthermore, these new chemical agents could possess important commercial-scale characteristics (such as improved shear rate stability) that can only be demonstrated by subjecting the treated MFT samples to a wide range of hydrodynamic conditions.

The static mixer flow loop previously described was used to evaluate the performance of a variety of chemical additives from several MFT sources. Two representative cases will be presented which compare the performance of two flocculants on two MFT samples. The two additives evaluated are Chemical H (a commonly used polymer in the oil sands tailing industry) and a developmental flocculant (denoted as Chemical X in the figures).

Figure 6 contains 40 data points showing the performance of these two flocculation agents on a particular MFT initially diluted to a 28% solids level. The dashed lines and filled makers denote the Chemical H results; solid lines and open markers are used for the Chemical X. The shading of the lines and marker symbolize the concentration of additive (as a ratio to the initial solids). Chemical H dewatering performance peaks in a narrow range around a pump speed of 15%. At these low pump speeds, compound X produces less relative dewatering. However, as the pump speed increases, the performance of Chemical X exceeds that of Chemical H, with the exception of the lowest concentration of the additive (open circles). It is noteworthy to observe that the higher shear rates at the higher pump speeds do not appear to affect the dewatering performance of Chemical X.

A similar set of data was generated for a different MFT (Fig. 7). An equivalent format was used to depict the data (dashed lines for Chemical H and with line shading denoting flocculant loading). As in previous figures, no effort has been made to filter the data and remove outlining or unexplainable data points. Analogous trends are seen for the second MFT. The Chemical H data shows that performance for the two chemical loading levels track one another. The higher concentration of the Chemical H degrades the performance indicating a strong sensitivity to both concentration and hydrodynamics (blending extent, floc formation time, and shear forces).

Chemical X shows superior performance (higher dewatering) for pump speeds greater than ~25%. A slight improvement in solid weight percentage is seen for increased levels of polymer X. In contrast to Figure 6, the lower loading level of Compound X ('X-low', which represents the same ppm level in both graphs) results in good dewatering.

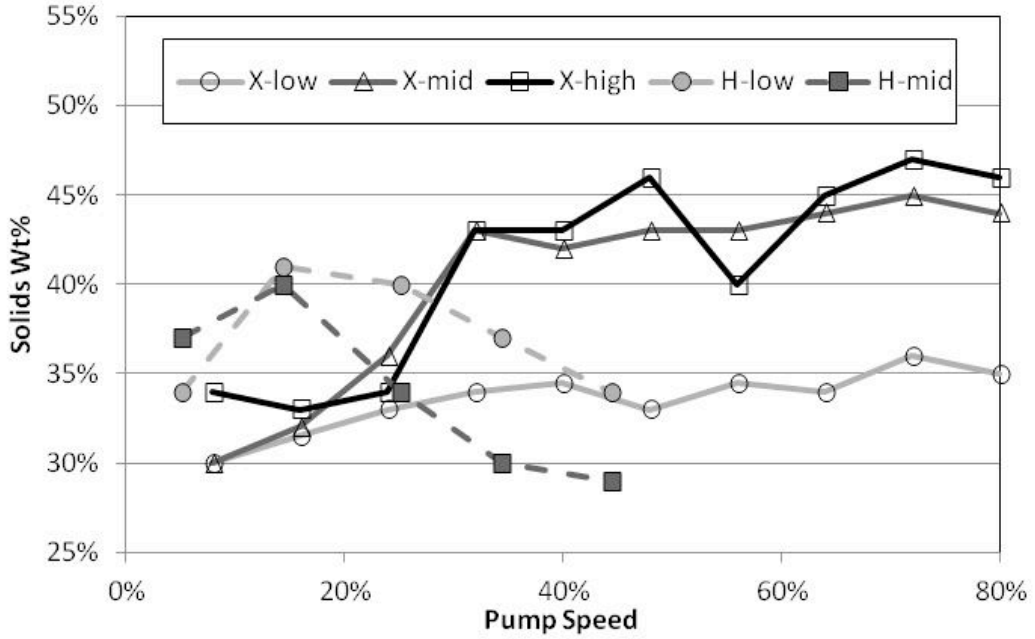


Figure 6. Dewatering performance as a function of chemistry (X or H) and loading for the first MFT

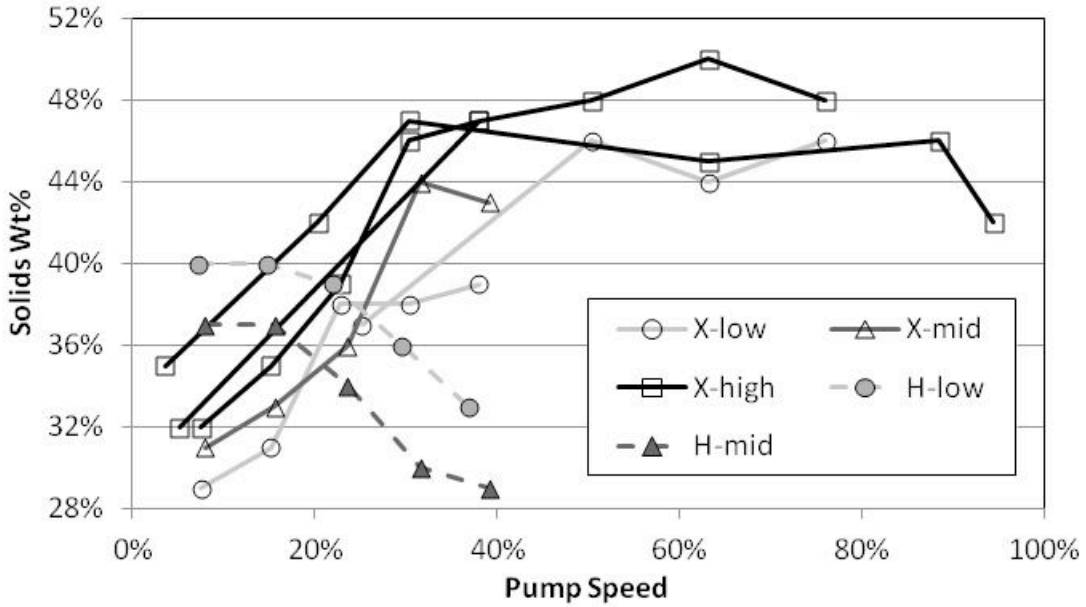


Figure 7. Dewatering performance as a function of chemistry (X or H) and loading for the second MFT

It appears that at the highest pump speed (approaching 100%), the effect of excessive shear rates might be beginning to degrade the performance of Compound X. The peak performance difference for this MFT is more significant than the MFT evaluated in Figure 6. Another benefit of Compound X is that performance does not degrade with excessive loadings as seen in Compound H.

This data indicates that flocculant performance can vary according to the hydrodynamic environment. Compound X appears to require higher pump speeds to achieve peak performance. Compound H appears to be more shear sensitive, and performance degrades at the optimal conditions for Compound X. It is also evident that different MFTs might require different polymer concentrations and even different blending, floc formation times, and shear rates.

4 CONCLUSIONS

Copious quantities of mature fine tailings exist, and future volumes are projected to increase even further. An effective treatment process is needed to remediate the tailings ponds. The majority of prior work on flocculant performance has focused on laboratory stirred tanks. In order to evaluate flocculants and mixing conditions for field applications, a static mixer flow loop was developed. This apparatus allows for the independent study of blending, floc formation kinetics, and floc shear stability. Performance is measured by determining the solids weight percent after ~20 hours. This static mixer setup was shown to reduce experimental variability compared to a small-scale stirred cell.

This study demonstrates that flocculant performance can vary according to the hydrodynamic environment. The performance of two flocculating agents was evaluated over a range of additive concentration, degree of blending, floc formation times, and shear rates. The height and breadth of the peak dewatering performance depend on the flocculant selection, concentration, and the hydrodynamic environment (blending extent, floc formation time, and shear forces). Due to the variation that is expected in commercial scale operations, it is desirable to use flocculating agents that exhibit peak performance over a wide range of concentrations and hydrodynamic conditions.

5 REFERENCES

BGC Engineering Inc. 2010. Oil Sands Tailings Technology Review. Oil Sands Research and Information Network, University of Alberta, School of Energy and the Environment, Edmonton, Alberta. OSRIN Report No. TR-1.

Buckhorn, H., Mewes, D., Peukert, W. & Warnecke, H.J (ed). 2010. *Micro and Macro Mixing: Analysis, Simulation and Numerical Calculation*, Berlin: Springer-Verlag.

Demoz, A. & Mikula, R.J. 2010. Role of Mixing Energy in the Flocculation of Mature Fine Tailings*, J. Environ. Eng.* ASCE, 138(1), 129-136.

Demoz, A., Munoz, V. & Mikula, R. 2010. Optimizing MFT Dewatering by Controlling Polymer Mixing, *Second International Oil Sands Tailing Conference*, Edmonton, Alberta.

Demoz, A. 2012. Mixing Energy Density Criterion for Peak Dewatering Flocculation by Static Mixers, *Third International Oil Sands Tailing Conference*, Edmonton, Alberta.

Dobias, B. 1993. *Coagulation and Flocculation: Theory and Applications.* New York: Marcel Dekker.

Dusseault, M.B. 2001, Comparing Venezuela and Canadian Heavy Oil and Tar Sands, Canadian International Petroleum Conference, Calgary, Alberta, Paper #61.

ERCB (Energy Resources Conservation Board) 2009, Tailing Performance Criteria and Requirements for Oil Sands Minig Schemes, Directive 074.

Harnby, N., Edwards, M. & Nienow, A. 1985. Mixing in the Process Industries. Oxford: Butterworth-Heinemann.

Hinze, J.O. 1959. *Turbulence*. New York: McGraw-Hill.

Houlihan, R. & Haneef, M., 2008. Oils Sands Tailings: Regulatory Perspective, *First International Oil Sands Tailings Conferenc*e, Edmonton, Alberta.

Kasperski, K. 1992, A Review of Properties and Treatment of Oil Sands Tailings, *AOSTRA J. Res*. 8, 11.

Mahmoudkhani, A., Tellakula, R., Watson, P., Fenderson, T., Stewart, K. & Yw, Y. 2012. Consolidation of Oil Sands Process Tailing by Enhanced Coagulation-Flocculation, *Third International Oil Sands Tailing Conference,* Edmonton, Alberta.

Masliyah, J., Zhou, Z., Xu, Z., Czarnecki, J. & Hamza, H. 2004, Understanding Water-Based Bitumen Extraction from Athabasca Oil Sands, *Canadian J. Chem. Eng*. 82, 628.

Mikula, R.J., Muoz, V.A. & Omotoso, O. 2009. Centrifugation Options for Production of Dry Stackable Tailings in Surface-Mined Oil Sands Tailings Management, *J. Can. Petro.Tech*., 48(9), 19.

Mohler, C., Poindexter, M., Atias, J., Chen, W. & Witham, C. 2012. Development of Flocculants for Oils Sands Tailings Using High-Throughput Techniques. *Third International Oil Sands Tailing Conference*, Edmonton, Alberta.

Oil Sands Tailings Technology Deployment Roadmaps. 2012. Report to Alberta Innovates – Energy and Environment Solutions. Volume 1 Project Summary.

Scholz, M. 2006. Revised capillary suction time (CST) test to reduce consumable costs and improve dewaterability interpretation. *J. Chem. Technol. Biotechnol*. 81, 336-344.

Sobkowicz, J.C. & Morgenstern, N.R. 2009. A Geotechnical Perspective on Oil Sands Tailings. *Tailing and Mine Waste 2009*, Banff, Alberta.

Stewart, K., Fenderson, T., Mahmoudkhani, A., Watson, P., Wu, Y. & Nair, M. 2012. A Study of Environmentally Friendly Chemical Aids for Consolidation of Oil Sands Tailings, *Third International Oil Sands Tailing Conferenc*e, Edmonton, Alberta.

Watson, P., Farinato, R., Fenderson, T., Hurd, M., Macy, P. & Mahmoudkhani, A. 2011. Novel Polymeric Additives to Improve Oil Sands Tailings Consolidation, SPE 141398.

Wells, P.S. & Revington, R. & Omostso, O. 2011. Mature Fine Tailings Drying – Technology Update. *Proc. 14th Int'l Seminar of Paste and Thickened Tailings*. Perth: Australian Centre for Geomechanics.

Yao, Y. 2012. The Effect of Flocculant on the Geotechnical Properties of Mature Fine Tailings: An Experimental Study, *Third International Oil Sands Tailing Conference*, Edmonton, Alberta.

Understanding dewatering limits of polymer flocculated oil sands mature fine tailings

T. Fenderson & S.G. Thakurta
Kemira Chemicals Inc. Edmonton, Alberta, Canada

A. Mahmoudkhani, P. Watson, Y. Wu, K. Stewart, & M. Nair
Kemira Chemicals Inc. Atlanta, Georgia, USA

ABSTRACT: The path to land reclamation for the oil sands mining process in Alberta, Canada involves making trafficable deposits out of the tailings which are generated. A major obstacle in this process is managing the mature fine tailings (MFT), which are a colloidal suspension of fine particles that have reached a gel-like state over time. While some commercial success has been made by chemically treating the MFT with polymer flocculants, there are limits to the final degree of dewatering which can be achieved by this method. In order to surpass this limit, a better understanding of the controlling factors on dewaterability needs to be established. While the <0.3 μm clay fraction is believed to be primarily responsible for many of the difficulties in MFT, separating and analyzing several specific size fractions can aid in determining the role of each on dewatering and also optimize polymer selection. The purpose of this work is to determine how bitumen and fine particles affect the polymer flocculant selection, dosage, and overall dewatering of the treated system.

In this study, the 10-45 μm size fraction from an MFT sample was targeted for treatment with polymer flocculants. The effect of charge density and molecular weight were determined and compared to the effects observed on unfractionated MFT. The dewaterability was established by following capillary suction time and final compaction of the treated samples. Supernatants and flocculated beds after centrifugation were measured for suspended and dissolved solids content. The results demonstrate that a detailed understanding of the particle size present in MFT can play a significant role in determining polymer selection and dosage for proper dewatering of MFT.

1 INTRODUCTION

As commercial processes such as centrifugation and thin lift evaporative drying are implemented for oil sands mature fine tailings (MFT) remediation, surpassing current dewatering rates is still desired and it is not understood how to achieve it, or even clearly all the factors which prevent it. In each remediation scheme mentioned, mechanical separation is coupled with a pretreatment of polymer flocculant. With centrifugation, as the treated MFT stream is released into designated disposal areas, they can reach solids levels of 55-60 wt% and yield strength levels of approximately 2 kilopascals (Mikula et al. 2009). Given months or in some cases years, the treated MFT is expected to reach requirements set forth by Alberta Energy Regulator (AER, formerly ERCB) Directive 074, but with current quantities of MFT at approximately 830 million m^3 (Alberta ESRD, 2010), there is still a significant benefit from reducing the timescale of the dewatering.

One of the factors responsible for keeping water bound in the MFT dispersed state, and potentially in the flocculated state, are the ultra-fine materials < 0.3µm. This fraction, which is found in MFT at concentrations of 3-4 weight percent, have been found to be the controlling factor in formation of MFT, and only a small concentration of ultra-fines is needed to produce the gel-like state (Kotylar et al. 1998). It has been shown that the ultra-fines have higher viscoelastic properties than the larger solids in MFT (Adeyinka et al. 2009), which can compound the issue of attempting to release water which is held in the system by capillary action.

An attribute that differentiates MFT from other mineral extraction tailings is the presence of adsorbed organic matter. The ultra-fines exist as hydrophilic or bi-wetted solids which have organic matter coatings <4 and 40 atomic percentage, respectively (Darcovich et al. 1989). It has been demonstrated that due to the presence of bitumen, MFT can be 10 to 100 times less permeable than a similar system without bitumen (Scott et al. 1985). The presence of this organic matter also increases the already high viscoelastic properties of the ultra-fines (Adeyinka et al. 2009). It is important to understand how the addition of chemicals is impacted by the presence of organic matter, which can vary between MFT samples.

In activated sludge treatment, free water in a system will behave as pure water and separate easily by thickening or the addition of force (centrifugation, pressure filtration, etc.), but the bound water will be more difficult to remove and can be held by physical, mechanical, or chemical means (Colin & Gazbar. 1995). It has been found that floc formation increases the amount of free water, but there exists a point where it also contributes to the amount of bound water in the floc (Jin et al. 2003). In these instances, larger flocs are not necessarily better in terms of short-term dewatering. This has relevance to MFT, where polymer flocculants provide significant benefits in creating free water from MFT, but there may be an inherent level of bound water that comes with flocculation of the fine particles. It is possible that this is one of the limiting factors in obtaining dewatering without lengthy periods of atmospheric drying. Gains can be made by proper polymer flocculant selection and dosage in creating large amounts of free water combined with a lower tendency to hold bound water.

2 EXPERIMENTAL

2.1 *MFT fractionation*

MFT for this work was received from an oil sands producer in Alberta, Canada. The sample (MFT-1) was analyzed by dean-stark extraction to determine oil/water/solids composition. Additional samples were prepared by mechanical separation of residual bitumen and ultrafine solids from MFT-1. To separate the ultrafine solids, centrifugation speeds were adjusted to 2500 relative centrifugal force (rcf) in a Sorvall GLC-2B centrifuge until a centrate was present that contained majority <10 µm solids. The centrifugation also separated a significant layer of bitumen above the centrate. In order to evaluate the changes occurring from the separation of this bitumen layer, a sample set was made where the bitumen layer was removed, and then centrate and settled solids were recombined into a homogenous MFT sample (MFT-2). For the next set, the MFT was centrifuged and both the bitumen layer and centrate were removed while the settled beds were retained for flocculation experiments (MFT-3).

The approximate wettability of these three fractions was calculated by use of an oil-water partition test, described in detail elsewhere (Dang-Vu et al. 2009). Approximately 1 gram of MFT solids was placed in a vial with 10 mL of deionized water, shaken, and sonicated to disperse. Light mineral oil in the amount of 10 mL was then added to the sample, and shaken mildly for 5 minutes to allow contact time for the solids with both liquids. The sample then rested 5 minutes as more hydrophobic solids partitioned into the oil-phase, hydrophilic solids settled to the bottom aqueous phase, and partially hydrophobic or bi-wetted solids rested at the oil-water interface. The vial was then gently flooded with water in order to displace the oil phase out of the vial along with the hydrophobic and bi-wettable solids. The vial was then dried in order to determine the percent solids with preference for the aqueous phase.

2.2 *Flocculation experiments*

Descriptions of the four commercial polymer flocculants (Kemira) used in this study are presented in Table 1. The flocculants were used as 0.5 wt% solutions in oil sands process-affected water (OSPW).

Table 1. Polymer flocculant characteristics

Polymer	Anionic charge density (mol%)	Relative molecular weight
A	1	High
B	20	Very high
C	40	Very high
D	100	Medium

For the flocculation experiments, MFT was combined with OSPW in order to obtain a 20 weight percent (wt%) solids slurry. The diluted MFT (100 g) was homogenized by mixing with a three-bladed propeller stirrer at 500 rpm for 2 minutes. Polymer solution was then added at 250, 500, 750, or 1000 grams / dry ton of MFT solids (g/t) over a 1 minute period, followed by an additional 30 seconds of mixing to homogenize the flocculated material. The solution was added as close to the impeller as possible to prevent localized over-flocculation. Treated samples were transferred into a tube for centrifugal separation or a sampling bottle for capillary suction time measurements. The tubes were then centrifuged for 5 min at 1200 rcf. The resulting centrate and settled bed were measured for solids content by oven drying at 105 °C.

2.3 *Particle size distribution*

To demonstrate the size of material being removed from the MFT by centrifugation, a Beckman Coulter LS230 particle size analyzer was used for measuring the size distribution based on the angular dependence of scattered light (mainly in the forward direction). Tailings samples were dispersed in the fluid module containing water and were recirculated through the instrument which applies both Mie and Fraunhofer theories of light scattering. For the optical constants, a complex refractive index of 1.5295, 3.00i, was used for the solids and a real refractive index of 1.3300 used for the continuous water phase. Samples were measured each minute until a steady-state distribution was obtained. For in-line flocculation experiments, once a steady-state was reached, polymer flocculant was introduced into the fluid module and the resulting change in distribution was followed over time until a steady-state was achieved.

2.4 *Capillary suction time (CST)*

The dewatering properties of materials excised from settled beds of treated tailings were measured using a capillary suction time method as described in Standard Method APHA 2710 G (APHA, 1999). CST measurements were carried out using a CST instrument from Venture Innovations Inc. (California, USA). The CST is the time interval it takes an aqueous solution to traverse between two radial positions in a filter paper (Whatman No. 5) under the influence of capillary suction, shown schematically in Figure 1. A low CST value implies good dewatering; i.e. the water from the sample releases quickly with little impediment. Each measurement was conducted in triplicate and the average presented.

3 RESULTS AND DISCUSSION

The centrifugation protocol did not completely remove <10 µm solids from the MFT, but reduced the fraction by approximately 6 volume percent in MFT-3 as given in Table 2. Once the majority of bitumen and a portion of the <10 µm solids are removed, there is a significant increase in the weight percent of water-wet solids in sample MFT-3. The effect is apparent when attempting gravity settling experiments at 20 wt% solids for each MFT sample with no polymer

addition. After 2 hours, a clear supernatant is observed in MFT-3 while the other samples remain well-dispersed as shown in Figure 2a. Oven dried samples also showed residual bitumen for MFT-1, while much less was seen for MFT-3 as shown in Figure 2b. This clearly demonstrates the change in solid characteristics.

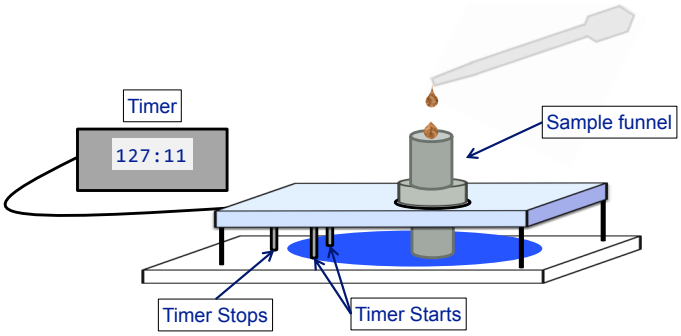


Figure 1. Capillary suction timer

Table 2. MFT Characteristics

Sample	Bitumen (wt%)	Water (wt%)	Solids (wt%)	<10.8µm (vol%)	Water-wet solids (wt%)
MFT-1	2.6	56.8	40.1	42.4	69.7
MFT-2	1.3	58.3	40.4	-	87.3
MFT-3	0.3	36.5	63.2	36.5	94.8



Figure 2. Gravity settling after 2 hours (a) and appearance of oven-dried solids (b)for MFT 1, 2, and 3, from left to right.

3.1 *Centrifugation*

Solids content in the centrate and bed solids as a function of flocculant dosage are shown in Figures 4 and 5. A general trend is observed in each MFT treatment where a decrease in centrate solids, i.e. better fines capture, resulted in a decreased bed compaction and thus lowers bed solids. This trend has even been observed in field trial applications for MFT treatment (Mikula et al. 2009). Polymers B, C and D demonstrate this effect by capturing fines in MFT-1 and MFT-2 with a reduction in bed solids compaction at higher dosages. When adding polymer A to each MFT, instead of forming individual flocs as observed with other flocculants, very large, viscous globules are formed. A photograph of these flocs attached to the impeller after a flocculation test is shown in Figure 3. Even with slow addition rates, localized over-flocculation made it dif-

ficult for polymer A to contact all of the MFT. This typically results in lower fines capturing and therefore higher bed solids compared to other flocculants.



Figure 3. Large, viscous floc formed with Polymer A

The removal of bitumen to form MFT-2 appears to further reduce fines capture for polymer A, indicating that some of its function may be related to the polymer-bitumen interactions. Bitumen is negatively charged and would therefore have the lowest repulsive interaction with polymer A compared to the other negatively charged flocculants. In MFT-1, the increased presence of bitumen may assist Polymer A in attaching to hydrophobic solids associated with bitumen, resulting in higher fines capture. An attachment to bitumen may also help to explain the viscous, globule-like aggregates only observed with polymer A. The removal of bitumen has the largest impact on Polymer A and a diminishing impact as the charge of the polymer increased. When MFT-2 is compared to MFT-1, the average increase in bed solids for polymers A, B, and C was 10.0, 3.5, and 0.8 wt%, respectively.

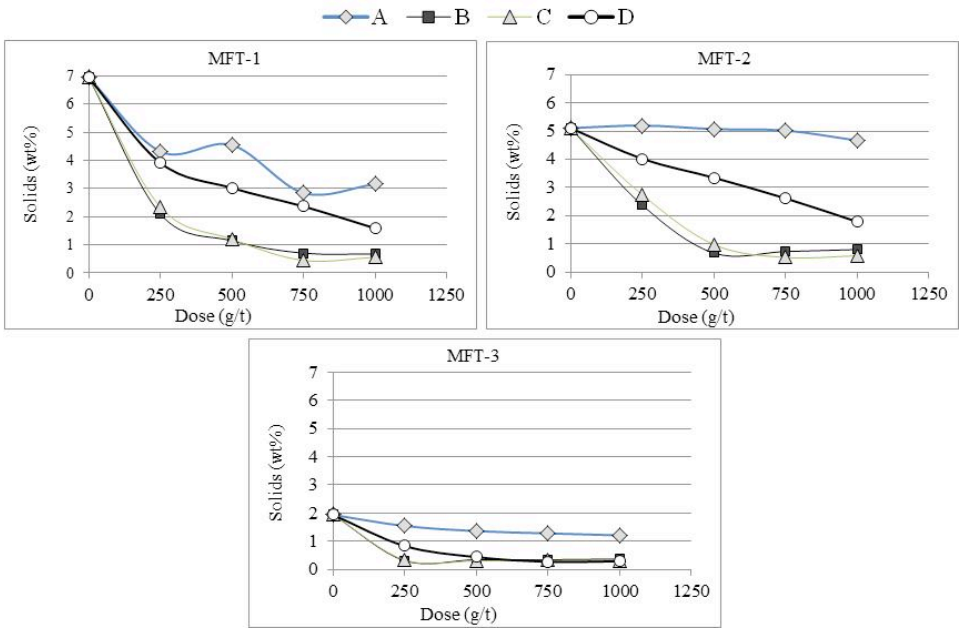


Figure 4. Centrate solids content as a function of polymer dosage

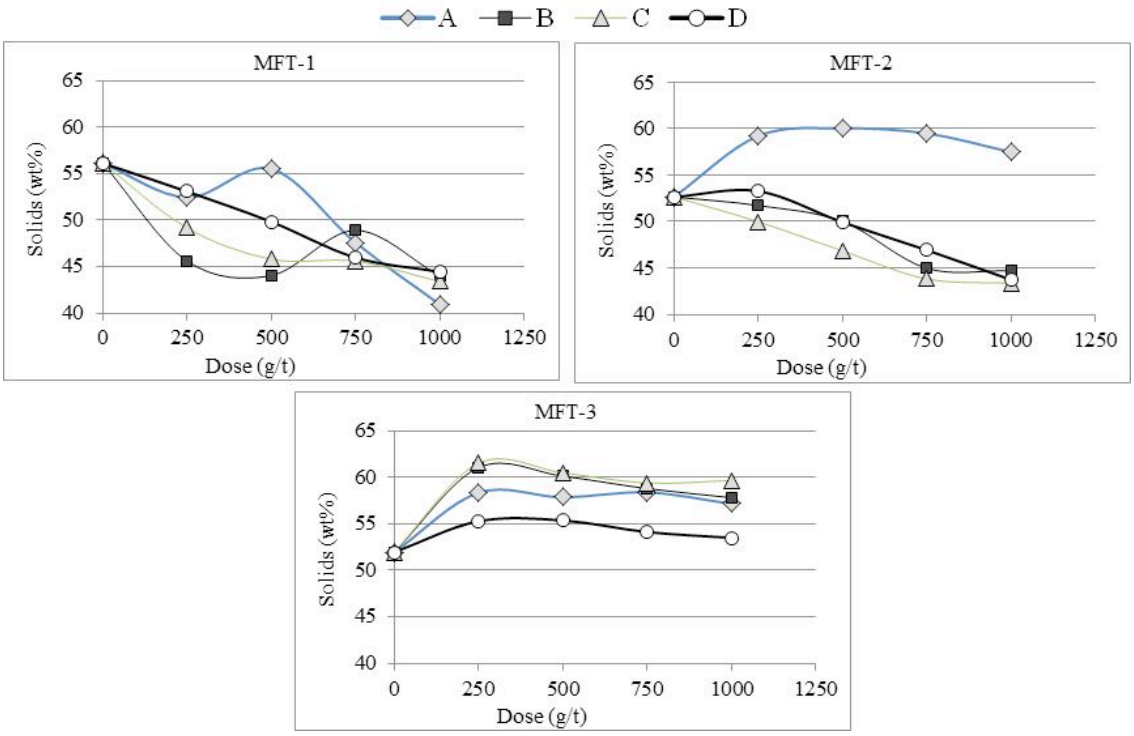


Figure 5. Centrifuged bed solids content as a function of polymer dosage

For MFT-3, the untreated sample contains 2 wt% centrate solids, down from 7 wt% for MFT-1, while the bed solids are down to 52.0 (for MFT-3) from 56.1 wt%, (for MFT-1). The reduction in fines did not alone increase bed solids, but improved the polymer flocculation of the system. In MFT-1, even at the lowest dose the addition of each polymer reduced bed solids compared to the untreated sample. In MFT-2, the same effect is observed except for polymer A. In MFT-3, the addition of each polymer increased the bed solids when compared to the untreated sample. Polymers B and C were able to produce the lowest centrate solids and also the highest bed solids, an effect that goes against published results (Mikula et al. 2009) of polymer addition to MFT and highlights the role of ultra-fine solids. The reduction of fine solids <10 µm allowed the flocculants to create a maximum bed solids content of 61.5 wt%, compared to the maximum of 56.1 wt% observed in MFT-1, which occurred without the addition of any flocculant. The flocculants limiting contribution to the compaction of the settled bed is closely tied to the packing of the flocculated solids.

3.2 *Capillary Suction Time*

CST measurements in Figure 6 reveal that the removal of fine (<10 µm) solids lowers the optimal flocculant dosage. For polymer C, the lowest CST times for MFT-1, 2, and 3 are obtained at dosages of 750, 500, and 250 g/t, respectively. The results for MFT-3 also demonstrate that polymer D can achieve faster dewatering times than polymers B and C, but it occurs at a higher dose that is not evident until testing with MFT-3. This demonstrates that if the composition of the MFT can be modified, significant benefits to dewatering may be obtained by proper adjustments not only to polymer dose, but also polymer composition. CST measurements also reveal the issue of polymer overdosing, as dewatering times increase with a dose above a certain level. In the case of polymer C and D treatment of MFT-3, when the dose is more than 500 g/t, flocs quickly settled to produce a clear supernatant and large amounts of free water released, yet the CST for these experiments is higher than even the control experiment without polymer. This may be explained by increases in viscosity of water due to the excess polymer, which makes it more difficult to remove as capillary forces hold water in the suspension. This has also been demonstrated in sludge dewatering where an increase in viscosity increases the CST (Abu-Orf et al. 2003). This illustrates the need for more considerations in polymer selection. Polymer D has a broader operating dosage range than polymers B and C. While B and C perform very well at a

specific dose, it could lead to undesirable dewatering if the MFT composition changes and excess polymer is applied.

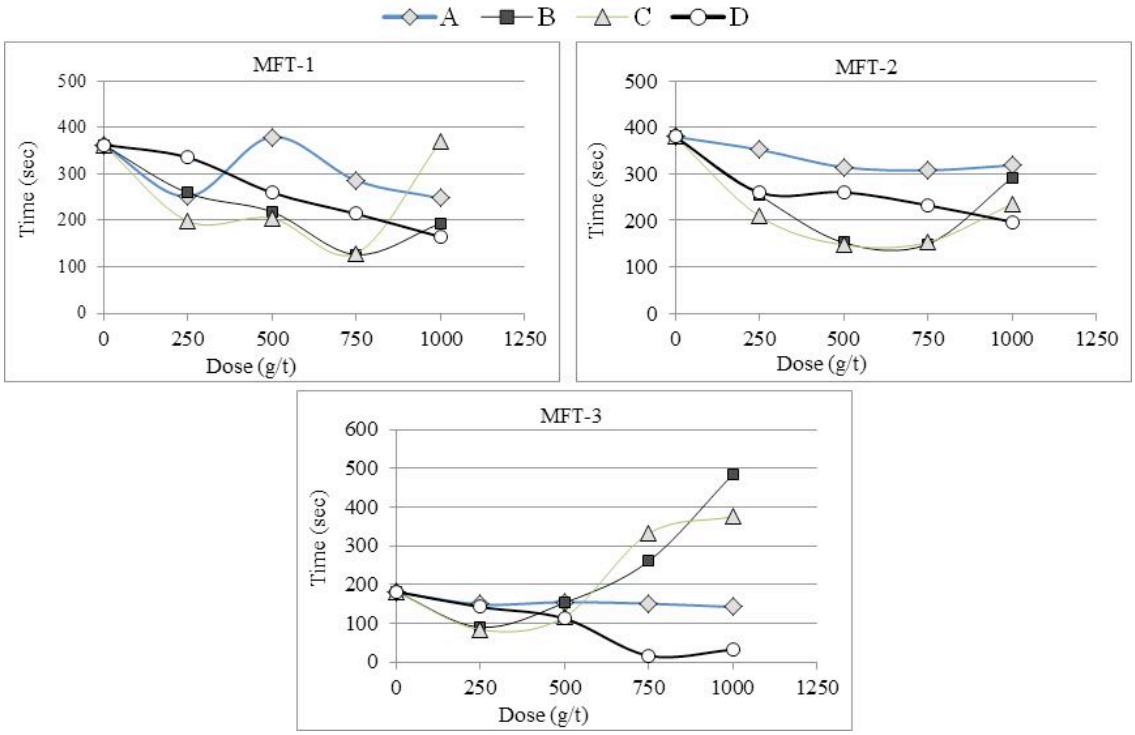


Figure 6. Capillary suction time as a function of polymer dosage

3.3 *In-Line Flocculation*

The change in particle size with the addition of flocculant for MFT-1 and MFT-3 is demonstrated in Figure 7. Polymer A forms the largest flocs in the dynamic measurement, followed by polymer C, while polymer D shows a distribution that is very similar to the original MFT. The removal of bitumen and <10 µm solids had a slight impact on the size distribution of the flocs, but no significant increase in distribution was observed for any of the flocculants due to the change in MFT composition.

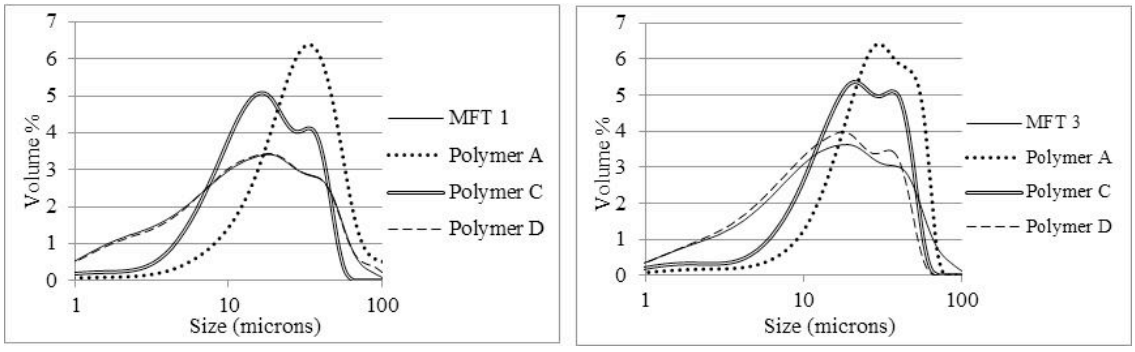


Figure 7. Comparison of particle size distributions for flocculated MFT

4 CONCLUSIONS

In this study, several factors which control dewatering and consolidation of treated MFT were examined. Reduction in bitumen content had little impact on higher charged flocculants, but has a pronounced influence on low charge flocculants. Removing fine (<10 μm) solids reduces the amount of flocculant necessary to capture fines and provide optimal dewatering. It has also been demonstrated that a highly charged flocculant, such as polymer D, can provide the highest level of dewatering under the correct conditions. The size distribution of solids in MFT was the dominant factor observed in limiting dewatering and compaction, and it directly impacted the performance ability of the flocculant.

An overdose can occur for certain polymers if the MFT composition is altered, resulting in reduction in dewaterability. Additional understanding of how each type of polymer is affected by the different fines can lead to proper flocculant selection and dosage so that a broader operating window can be utilized in commercial operations.

5 ACKNOWLEDGEMENTS

The authors would like to thank the management of Kemira for permission to publish this research.

6 REFERENCES

Abu-Orf, M., Walker, C., Dentel, S. 2003. Centrate viscosity for continuous monitoring of polymer feed in dewatering applications. *Advances in Environmental Research* 7: 687-694.

Adeyinka, O., Samiei, S., Xu, Z., Masliyah, J. 2009. Effect of particle size on the rheology of Athabasca clay suspensions. *The Canadian Journal of Chemical Engineering* 87: 422-434.

Alberta Environment and Sustainable Resource Development. http://environment.alberta.ca/apps/osip/

Alberta Energy Regulator. 2009. Directive 074: Tailings performance criteria and requirements for oil sands mining schemes.

Colin, F. & Gazbar, S. 1995. Distribution of water in sludges in relation to their mechanical dewatering. *Wat. Res.* 29(8): 2000-2005.

Dang-Vu, T., Jha, R., Wu, S., Tannant, D., Masliyah, J., Xu, Z. 2009. Wettability determination of solids isolated from oil sands. *Colloids and Surface A: Physico. Eng. Aspects* 337: 80-90.

Darcovich, K., Kotylar, L.S., Tse, W.C., Ripmeester, J.A., Capes, C.E., Sparks, B.D. 1989. Wettability study of organic rich solids separated from Athabasca oil sands. *Energy and Fuels* 3: 386.

Jin, B., Wilen, B.M., Lant, Paul. 2003. Impacts of morphological, physical and chemical properties of sludge flocs on dewaterability of activated sludge. *Chemical Engineering Journal* 98: 115-126.

Kotylar, L.S., Sparks, B.D., Woods, J.R. 1998. Effect of particle size on the flocculation behavior of ultrafine clays in salt solutions. *Clay Minerals* 33: 103-107.

Mikula, R., Dang-Vu, T., Omotoso, O. 2009. Dry stackable tailings as a tailings management option: Preliminary laboratory and field experience using centrifuges. *Canadian International Petroleum Conference; Proc. Calgary, Alberta, 16-18 June 2009.*

Scott, J.D., Dusseault, M.B., Carrier, W.D. 1985. Behaviour of the clay/bitumen/water sludge system from oil sands extraction plants. *Applied Clay Science* 1(2): 207-218.

Standard methods for the examination of water and wastewater. (20th ed.) 1999. American public health association, American water work association, Water environment federation, Washington, D.C.

Oil Sands – Modelling and Thickened Tailings

Evaluation of evaporation and under-drainage in dewatering oil sands tailings in northern Alberta

Q. Song & M. O'Kane
O'Kane Consultants Inc., Calgary, Alberta, Canada

ABSTRACT: The oil sands mining industry in northern Alberta is in the process of addressing recent changes to fine tailings deposition requirements put forth by the Alberta Government. This paper presents evaporation and under-drainage contribution to dewatering mature fine tailings (MFT) in northern Alberta, Canada. Evaporative dewatering for tailings consolidation is evaluated on the basis of a >100-year climatic database. Achievable tailings deposition thickness for the required shear strength changes from month to month depending on available evaporation for tailings dewatering. Under-drainage controlled by tailings permeability decreases with tailings consolidation. Incorporating under-drainage to the calculation of achievable MFT deposition thickness due to evaporation provides better understanding of fine tailings management in the northern Alberta area. Using the developed method, oil sands industry operators can determine the potential MFT deposition thickness achievable in their climate.

1 INTRODUCTION

Alberta Energy Resources Conservation Board (ERCB) issued Directive 074 (ERCB 2009) to regulate tailings management in order to reduce containment of fluid tailings and create a trafficable landscape at the earliest opportunity to facilitate progressive reclamation. Directive 074 requires the reduction of fluid tailings through fines captured in dedicated disposal areas (DDAs). The deposited fluid tailings in DDAs each year must achieve a minimum undrained shear strength of 5 kPa within one year of deposition. Challenged with this requirement, oil sands owners and operators are evaluating several opportunities for tailings dewatering. One approach being considered to reduce water content of fluid oil sands tailings is by taking advantage of environmental evaporation and under-drainage.

Evaporative drying technology takes advantage of the evaporation potential, following tailings deposition, to assist with dewatering tailings. The evaporative drying rate of fluid tailings is affected by environmental factors, characteristics of the tailings, and tailings depositional conditions / processes. The environmental factors include solar radiation, air temperature and relative humidity, wind speed, and precipitation intensity and duration. Characteristics of the tailings include salt concentration in the pore-fluid in the tailings and potential to form a crust (Simms et al. 2009) as well as tailings hydraulic characteristics. The factors associated with tailings deposition processes / conditions include tailings filling rates (i.e. deposition lift thickness and frequency), capillary barrier effects, and under-drainage conditions (Boswell & Sobkowicz 2010).

Both the foundation material in a tailings storage facility (TSF) and deposited tailings in the TSF can influence tailings dewatering through under-drainage. If the hydraulic conductivity of the foundation material is greater than the deposited tailings hydraulic conductivity, the deposited tailings could be a dominant factor to determining under-drainage flux. Alternatively, the

foundation could be a dominant factor to controlling under-drainage if the hydraulic conductivity of the tailings is greater than that of the foundation material. Consequently, determination of under-drainage in the field is a complex issue due to the facts that (i) TSF foundations are usually not homogeneous and (ii) the tailings hydraulic conductivity at the base will decrease with tailings consolidation caused by under-drainage. It is the authors' experience that under-drainage from mature fine tailings (MFT) is controlled by the MFT's hydraulic conductivity when MFT is deposited over a sand beach.

Whether or not the tailings deposition thickness satisfies a particular requirement (e.g. ERCB-D 074) is a function of the tailings dewatering rate and tailings initial and target states (i.e. solids content or void ratio). For a given thickness of tailings deposit, evaporative drying and under-drainage can affect each other during tailings dewatering. Although thin lifts (typically less than 20 cm) have substantial benefit in regards to consolidation through self drainage and desiccation (e.g. Boswell 2009), a general description of thin lifts do not satisfy the demands of tailings deposition management due to varied climates.

Tailings management with evaporative drying includes determining the tailings filling rate (achievable tailings deposition thickness) and then maximizing utilization of environmental evaporation. Seneviratne et al. (1996), at a site in Western Australia, found that a threshold filling rate is 5.3 m/yr for a clayey silt tailings (initial void ratio 4.6) for an annual potential evaporation (PE) rate of approximately 3000 mm. The threshold filling rate for a given PE is the fastest rate that the tailings should be deposited while still allowing evaporation to have its full effect. Northern Alberta has a humid continental climate with long, cold winters and warm, short summers. The average annual precipitation is approximately 460 mm, which, in general, is evenly distributed between winter and summer. PE is in the range of 500 - 700 mm per year. As a result, it is anticipated that the threshold filling rate in northern Alberta should be much smaller than that in Western Australia for a similar deposit. Including the contribution of under-drainage to tailings dewatering will enhance the tailings deposition thickness compared to only considering evaporation.

This paper presents a simplified methodology to determine MFT tailings deposition thicknesses, in the context of the exceedance probability of achieving the desired solids content (and hence undrained shear strength), for different times of the year. Firstly, the MFT deposition thicknesses are calculated based on only PE. A 100-year climate database developed for northern Alberta was used to calculate PE based on Penman's equation (Penman 1948). Secondly, under-drainage is considered to dewater tailings, which can increase the tailings deposition thickness. Under-drainage is calculated using Darcy's Law with an assumption of unit hydraulic gradient. The achievable tailings deposition thickness satisfying the requirement of solids content (and resultant undrained shear strength) in a given timeframe is the result that the removed water from the tailings due to evaporation and under-drainage exactly makes the filled tailings to obtain the required solids content. Based on the achievable tailings filling rate, evaporation and under-drainage contributions are discussed. The achievable tailings deposition thicknesses obtained in this paper provide guidelines for oil sands tailings management in the northern Alberta area.

2 MATERIAL AND METHODS

2.1 *Mature fine tailings material*

Oil sands plants produce large volumes of tailings consisting of sand, clay, water, and residual bitumen. Tailings discharged from an extraction plant are a segregating type due to different densities of components. The fines (<45 μm size) that are not captured or retained in the tailings sand deposits usually flow into a tailings pond in suspension to form fluid fine tailings. MFT is a stable suspension of fluid fine tailings, having about 33% solids content which is almost all fines (Scott & Ozum 2010). Further densification of MFT is a very slow process; therefore, MFT is usually further treated with flocculants to form flocculated MFT to accelerate water release from fines. Accumulation of MFT is considered an environmental liability; both oil sands industry and government regulatory agencies have committed to reduce the production of MFT.

The flocculated MFT investigated in this paper has the following properties:

- Specific gravity (G_s): 2.3;
- Solids content after initial dewatering (sc_1): 43%;
- Void ratio after initial dewatering (e_1): 3.0;
- Solids content when achieving undrained shear strength of 5 kPa (sc_2): 70%;
- Void ratio when achieving undrained shear strength of 5 kPa (e_2): 1.0; and
- Hydraulic conductivity (k) vs. void ratio (e) relationship: $k=3.3 \times 10^{-4} e^{1.378}$ (m/day).

2.2 *Evaporation from MFT*

The Penman equation (Eq.1) (Penman 1948) is employed in this study to calculate potential evaporation (PE) from the tailings surface. The parameters used in the Penman equation are meteorological data in a 100-year (1908-2012 inclusive) climatic database developed specifically for northern Alberta. Detailed development of the 100-year climatic database is referred to in Song et al. (2011). In the present paper, PE is calculated with measured net radiation and other climatic parameters (e.g. temperature, relative humidity, wind speed):

$$E = \frac{H\Delta + E_a\gamma}{\Delta + \gamma} \quad (1)$$

where:

E = potential evaporation;
H = net radiant energy available at the evaporating surface;
γ = psychrometric constant (γ = 0.27, in °F and mm.Hg units);
Δ = slope of the saturation vapour pressure versus temperature curve at the mean temperature of the air;
E_a = $(e_a - e_d)f(u)$;
e_a = saturation vapour pressure in the air;
e_d = saturation vapour pressure at the dew point in the atmosphere above; and
f(u) = a function of the horizontal wind velocity.

2.3 *MFT deposition thickness due to evaporative dewatering*

The tailings deposition thickness due to evaporative dewatering is calculated based on the following equation (Eq. 2).

$$H_1 = T_{wr} + H_2 \quad (2)$$

where:

H_1 = tailings deposition thickness due to evaporation;
T_{wr} = thickness of released water from the tailings due to evaporative drying; and
H_2 = tailings thickness after evaporative drying and at which vertical effective stress is 20 kPa in the tailings.

The tailings deposition thickness (H_1) was obtained through a trial and adjustment method. H_1 was first assumed and its state (void ratio and solids content) was set as the tailings state after initial dewatering. The flocculated MFT solids content after initial dewatering usually increases by 5-8% compared to the tailings solids content at a discharge point. After water removal (T_{wr}) due to evaporative drying, the tailings thickness changed toward the final state at which vertical effective stress is 20 kPa in the tailings. H_1 is adjusted if the specified vertical effective stress in the tailings deposit is not achieved after water removal. During the calculation, the mass of solids in tailings was maintained unchanged.

The tailings final state was determined to have a vertical effective stress of 20 kPa because the tailings at this state can most likely achieve an undrained shear strength of 5 kPa if a minimum coefficient of 0.25 (the ratio of undrained shear strength over vertical effective stress) is applied (Hyndman and Sobkowicz 2010). It should be noted that tailings consolidation (void ratio – vertical effective stress relationship) may vary depending on the tailings 'type' and solids content. Therefore, characterization of the site-specific consolidation characteristics of the mate-

rial is crucial for tailings deposition and settlement analysis. Figure 1 illustrates water removal (T_{wr}) and tailings height change from H_1 to H_2 due to evaporative drying.

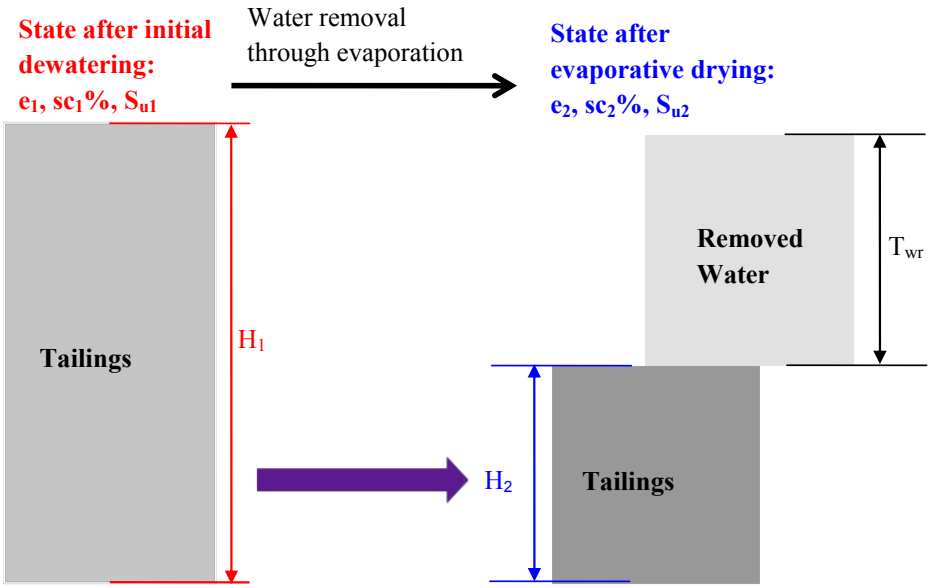


Figure 1. Illustration of MFT deposition thickness calculation method due to evaporative drying.

2.4 *Under-drainage from MFT*

Under-drainage through the base of a MFT deposit would occur during MFT deposition. However, it is challenging to accurately calculate the amount of under-drainage. A number of factors can affect the under-drainage occurring through the base of a MFT deposit, including permeability and saturation of the TSF foundation, pore-water pressure conditions in the TSF foundation, and permeability of the MFT deposit. In order to investigate the contribution of under-drainage to the tailings deposition thickness, the under-drainage calculation is simplified in this paper. Specifically, it is assumed that the under-drainage is dominated by the MFT material (especially the permeability of the MFT deposit) and can be calculated with Darcy's law. The hydraulic gradient near the tailings base is assumed to be a unit gradient. The cumulative under-drainage can be calculated with the following equation (Eq. 3).

$$Q = \int_0^T k_t \, IA dt \tag{3}$$

where:
Q = cumulative under-drainage;
k_t = MFT hydraulic conductivity at time t;
I = hydraulic gradient near the MFT deposit base (assumed to be 1.0 in this paper);
A = area of MFT deposit;
dt = infinitesimal increment of t; and
T = time period for under-drainage occurring.

The MFT hydraulic conductivity is changing against time because the tailings volume changes along with pore-water flowing out of the tailings deposit through under-drainage. When only under-drainage is considered, under-drainage can be calculated in a Microsoft Excel spreadsheet with the following steps:

Step 1: Calculate k at Day 1 based on the tailings hydraulic conductivity versus void ratio relationship (the tailings initial state must be known);
Step 2: Calculate under-drainage at Day 1 by assuming one day integration in Eq. 4;

Step 3: Obtain the tailings settlement at Day 1 by assuming that the settlement equals the under-drainage flow over a unit area;
Step 4: Calculate the tailings void ratio after Day 1 (i.e. void ratio at Day 2);
Step 5: Repeat Steps 1 to 4 until the specified tailings final void ratio is achieved or other constraints are reached; and
Step 6: The cumulative under-drainage is sum of daily under-drainage calculated above.

2.5 *MFT deposition thickness due to evaporation and under-drainage dewatering*

When under-drainage is considered for contributing to MFT deposition thickness, Equation (2) can be re-expressed as the following equation (Eq. 4).

$$H_1' = T_{wr} + T_u + H_2' \tag{4}$$

where:
H_1' = tailings deposition thickness due to evaporation and under-drainage;
T_u = thickness of water removal from the tailings due to under-drainage; and
H_2' = tailings thickness after evaporation and under-drainage and at which vertical effective stress is 20 kPa in the tailings.

Similarly, the calculation process of MFT deposition thickness can be illustrated in Figure 2.

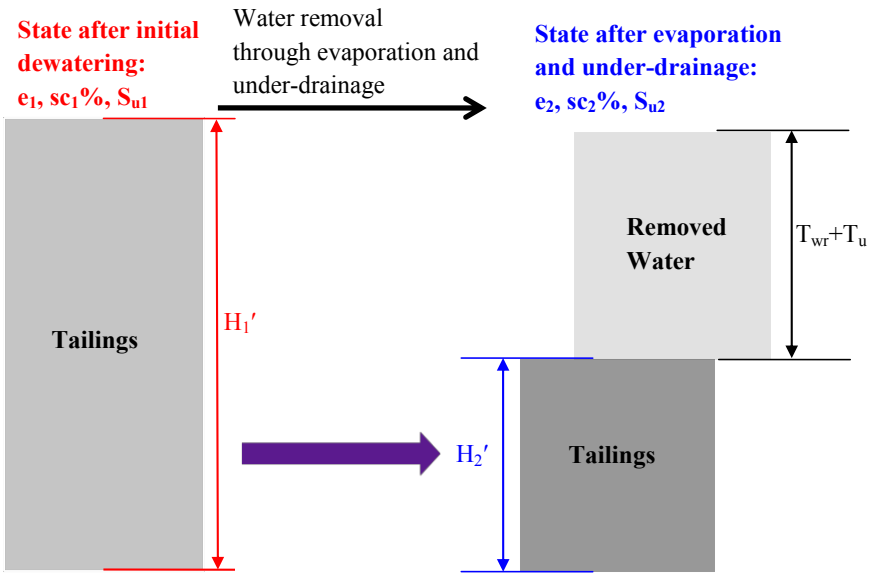


Figure 2. Illustration of MFT deposition thickness calculation due to evaporation and under-drainage.

The calculation of water removal due to under-drainage would be a bit more complicated when considering both evaporation and under-drainage than just under-drainage. Under the situation having both evaporation and under-drainage in a MFT tailings, the tailings settlement at a certain day is expected to be a result caused by both evaporation and under-drainage; that is, the tailings settlement in Step 3 in Section 2.4 should be modified to be the sum of evaporation and under-drainage (expressed in water thicknesses). Once water removal due to under-drainage is available, the MFT deposition thickness can be obtained based on Equation (4).

An alternative method for the calculation of entire MFT deposition thickness due to both evaporation and under-drainage is to calculate MFT deposition thicknesses due to evaporation and due to under-drainage separately; then the entire MFT deposition thickness is obtained from the sum of the calculated thicknesses due to evaporation and the thickness due to under-drainage. The same initial state (state after initial dewatering) and final state (state evaporation and under-drainage) are applied to the both evaporation and under-drainage situations. All cal-

culations are based on monthly MFT deposition thickness. This method was checked with the method presented in Equation (4) and the same entire MFT deposition thicknesses were obtained for both methods.

2.6 *Exceedance probability*

Exceedance probability is the probability that a certain value is going to be exceeded. The following equation (Eq. 5) is used to calculate exceedance probability of tailings deposition thickness.

$$E_p = \frac{R}{N+1} \tag{5}$$

where:
Ep = exceedance probability;
R = rank of the value (deposition thickness); and
N = total number of values (i.e. 105 in the present paper)

The calculated tailings deposition thickness for each month over the 100 years modelled is first ordered from the largest to smallest, then the rank of each deposition thickness is found and the exceedance probability corresponding to the deposition thickness is calculated.

3 RESULTS

3.1 *Potential evaporation*

The calculated PE values between February and October in the context of exceedance probability are presented in Figure 3. PE values in January, November, and December are negligible and not shown. The Penman equation (Penman 1948) was used in PE calculation. All parameters are meteorological data. The annual PE is approximately 540 mm with an exceedance probability of 80%. The maximum monthly PE occurs in July, 122 mm with an exceedance probability of 80%.

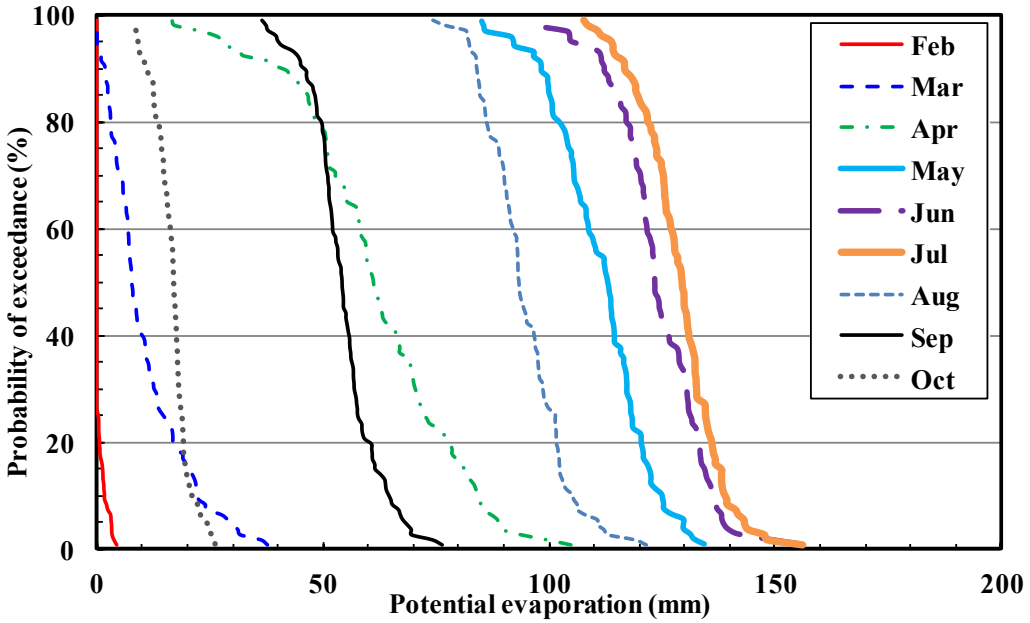


Figure 3. Potential evaporation obtained from the meteorological database.

Table 1 presents average PE in each month. The average annual PE is approximately 600 mm in the area. The major period in which PE occurs is the months between April and September, while almost no PE occurs in the winter months between November and February during which air temperatures are less than 0°C. June and July have average PE values close to approximately 125 mm.

Table 1. Average potential evaporation in each month in northern Alberta.

Month	Jan	Feb	Mar	Apr	May	Jun	Jul	Aug	Sep	Oct	Nov	Dec
PE (mm)	0	0	10	62	111	124	129	95	55	17	0	0

3.2 *MFT deposition thickness due to potential evaporation*

When only PE is considered to dry the MFT deposit, the calculated MFT deposition thicknesses in between February and October are presented in Figure 4. With an 80% probability of exceedance, the MFT deposition thicknesses in March and October are less than 5 cm in order to achieve undrained shear strength of 5 kPa. The achievable MFT deposition thicknesses are about 10 cm in April and September with an 80% probability of exceedance. The largest MFT deposition thicknesses are close to 23 cm and 24 cm with an 80% probability of exceedance, occurring in June and July, respectively. As expected, the MFT deposition thickness (Fig. 4) has similar distribution shape as PE (Fig. 3).

Figure 4 indicates that the entire MFT deposition thickness in a year is approximately 107 cm with an 80% probability of exceedance in order to achieve undrained shear strength of 5 kPa. The MFT deposition thickness can increase to 118 cm when the exceedance probability decreases to 50%.

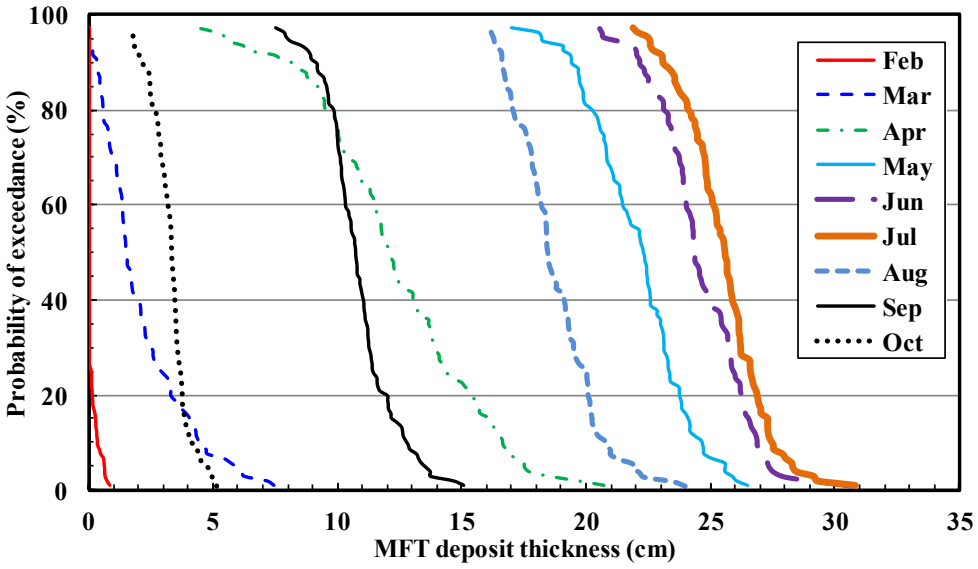


Figure 4. MFT deposition thicknesses to reach undrained shear strength of 5 kPa due to potential evaporation.

3.3 *MFT deposition thickness due to potential evaporation and under-drainage*

The MFT deposition thickness resulting from the contribution of under-drainage is approximately 4.5 cm in each month based on the applied MFT hydraulic properties. Accordingly, approximately 23 mm of water is removed from the MFT deposit during the dewatering process of under-drainage. The MFT deposition thicknesses with an exceedance probability of 80% in each month due to PE and under-drainage are presented in Figure 5.

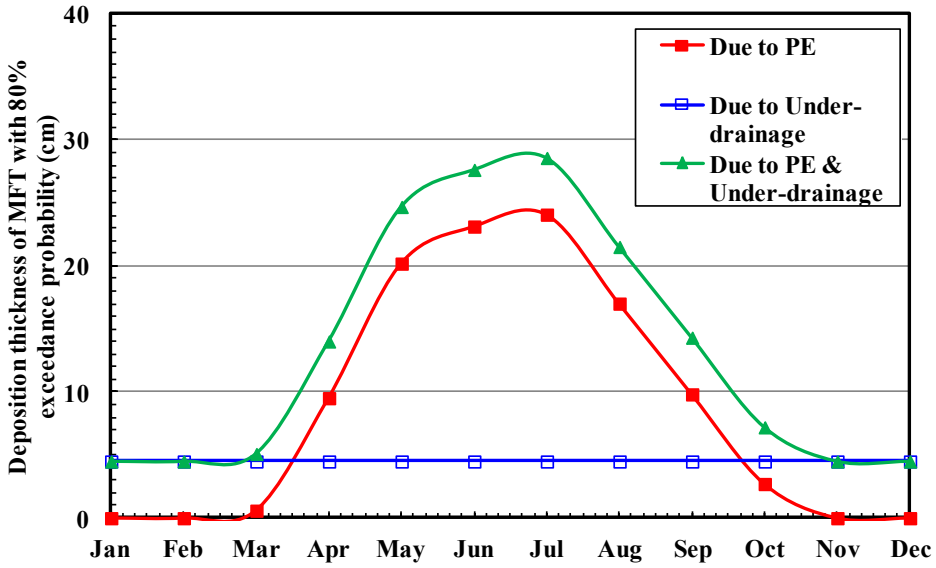


Figure 5. MFT deposition thicknesses due to both potential evaporation and under-drainage.

Figure 5 indicates that under-drainage is the dominant dewatering mechanism for MFT in the winter months (January, February, March, October, November, and December) in the northern Alberta area, while PE is the dominant dewatering mechanism in the summer months from May to August. The entire MFT deposition thickness in a year is approximately 160 cm (assuming 80% probability of exceedance) when both PE and under-drainage are considered to dewater the MFT deposit.

The annual MFT deposition thickness resulted from under-drainage is approximately 54 cm, which accounts for almost half of the annual MFT deposition thickness (107 cm as presented in Fig. 4) resulting from PE. The removed water amount (272 mm in a year) due to under-drainage is also approximately half of the annul PE capacity (542 cm) based on the same 80% exceedance probability.

4 DISCUSSION

Surface water management is important when evaporation is used to dewater MFT deposits. Figure 6 compares average PE and precipitation in each month in northern Alberta. PE can be larger than precipitation only between April and September. It can be imagined that the ponded water due to spring melt could 'consume' lots of evaporative energy if no measures were taken to remove ponded water over the MFT deposit surface.

As part of the sensitivity analyses, Figure 7 presents effective evaporation obtained with consideration of various precipitation impacts on consumption of potential evaporation. "No precipitation impact" means that the calculated PE with Penman equation is the entire effective evaporation that can be used to dry the MFT deposit. "Slight precipitation impact" means that a small part of the calculated PE was used to balance out a specified precipitation (i.e. a threshold value for precipitation at a 'wet' day). Here the threshold of 0.5 mm/day is used to determine the evaporative energy available for tailings evaporative drying. This value was determined by considering the MFT's saturated hydraulic conductivity and general duration of rainfall in northern Alberta. The effective evaporation on a given day is assumed to be the calculated PE of the day less the precipitation threshold (i.e. 0.5 mm/day) on that day. Any daily precipitation greater than the threshold value is assumed to report as surface runoff, which is removed from a MFT deposit facility and does not 'consume' evaporation energy. "Substantial precipitation impact" means that all precipitation will 'consume' evaporation energy. Figure 7 indicates that only June and July have effective evaporation for MFT drying if there is no surface water removal from a MFT facility. The effective evaporation does not have substantial difference from the calculated

PE when a precipitation threshold of 0.5 mm/day is considered to produce influence on the calculated PE.

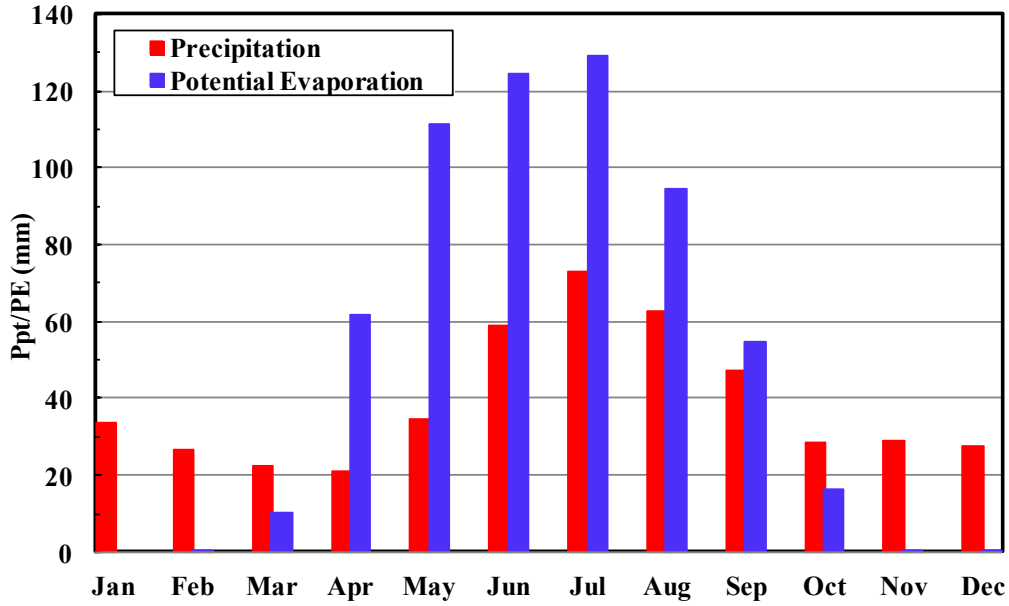


Figure 6. Average monthly precipitation and potential evaporation in the northern Alberta.

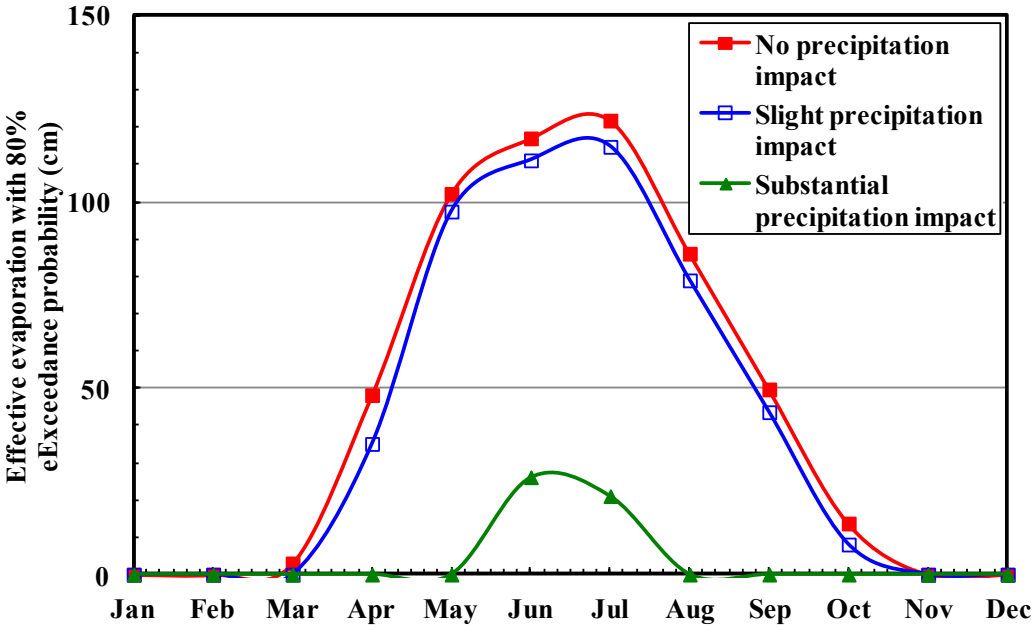


Figure 7. Monthly effective evaporations applicable for MFT drying when considering various precipitation impacts. "No precipitation impact" means the entire calculated PE is applicable for MFT drying; "Slight precipitation impact" considers a precipitation threshold of 0.5 mm/day will impact evaporation energy; "Substantial precipitation impact" means that all precipitation will 'consume' evaporation energy.

In addition to the impact of precipitation, effective evaporation is also affected by tailings albedo, residual bitumen content, pore-water salinity, and crust development at the MFT surface. Song et al. (2011) reported that the MFT deposition thickness obtained with the modified PE (calculated with net radiation that was calculated with the measured tailings albedo values) was 25% larger than that obtained with the normal PE (calculated with net radiation that was meas-

ured from meteorological sensors). Kabwe et al. (2013) investigated influence of residual bitumen content on actual evaporation from flocculated MFT. The authors concluded that at low solids content the residual bitumen in the MFT deposit forms a film on the tailings surface that significantly reduces actual evaporation in the early stage of drying. Accumulation of salts and crust development at a tailings surface can also reduce evaporation from the tailings deposit. Therefore, it is challenging to accurately determine effective evaporation (also even PE) that can be used for MFT drying.

The presented MFT deposition thickness in the current paper is based on the MFT properties specified in Section 2.1. When the MFT properties change, the achievable deposition thickness will change. For example, a higher solids content of MFT at pouring will lead to a larger MFT deposition thickness because the required water removal from the tailings decreases when obtaining the same undrained shear strength of 5 kPa (Song et al. 2011). The change of MFT properties will also affect contribution of under-drainage to the MFT deposition thickness. Sensitivity analyses on the MFT hydraulic conductivity indicate that under-drainage will be a dominant dewatering mechanism in all months when the MFT hydraulic conductivity increases by an order of magnitude (compared to the values in Section 2.1), while the contribution of under-drainage to MFT deposition thickness is negligible when the MFT hydraulic conductivity decreases by one order of magnitude (compared to the values in Section 2.1). A relatively large hydraulic conductivity may mostly occur in coarser-textured tailings, but not likely in the oil sands MFT material. The MFT hydraulic conductivity decreases with increase of tailings settlement and consolidation (hence increase of the tailings solids content). This implies that a consolidated old MFT layer could prevent seepage from an overlying fresh MFT layer.

The uncertainty of the under-drainage calculation is also associated with the assumption of the unit hydraulic gradient in the MFT deposit. Field measurements of pore-water pressures in MFT deposits and calculated hydraulic gradients indicate that the hydraulic gradients are not a constant. The hydraulic gradients in MFT deposits change with the tailings consolidation process (i.e. dissipation of excess pore-water pressure). Again, it is challenging to accurately predict under-drainage from MFT deposits. A good prediction of under-drainage requires detailed characterization of the MFT deposit, the foundation material over which the MFT is poured, and the pouring process. However, the under-drainage calculation in the current paper may help to demonstrate its relative contribution to the MFT deposition thickness compared to PE.

5 SUMMARY

The methodology presented in this paper provides a simple and quick approach to calculate potential MFT deposition thickness due to evaporative drying and under-drainage in a year in the northern Alberta area. This method is on the basis of measured meteorological data and tailings consolidation behavior. Based on the specified MFT properties and evaluated potential evaporation, under-drainage accounts for approximately one third of the entire MFT deposition thickness (assuming 80% exceedance probability) resulting from both potential evaporation and under-drainage. This result implies that water removal through under-drainage is approximately 23 mm in each month. Under-drainage would be a dominant dewatering mechanism from MFT deposits during the winter months while evaporation would be a dominant dewatering mechanism during the summer months. The developed method can serve oil sands industry operators and MFT deposition management in northern Alberta, Canada and may also be helpful for fine tailings deposition management in other areas.

6 REFERENCES

Boswell, J.E.S. 2009. Strategies for dealing with fine fluid tailings and suspended fines: some international perspectives. In D.Sego, M. Alostaz and N. Beier (eds), *Proceedings of the Thirteenth International Conference on Tailings and Mine Waste '09*:171–184. Banff, 1–4 November 2009.

Boswell, J.E.S. & Sobkowicz, J.C. 2010. Environmental assistance for tailings disposal. In *Proceedings of the 63rd Canadian Geotechnical Conference and 6th Canadian Permafrost Conference:* 665 –669. Calgary, 12 –16 September 2010.

ERCB 2009. *Tailings performance criteria and requirements for oil sands mining schemes*. Directive 074, Energy Resources Conservation Board (ERCB), Edmonton, Canada, 14 p.

Hyndman, A. & Sobkowicz, J. 2010. Oil sands tailings: reclamation goals & the state of technology. In *Proceedings of the 63rd Canadian Geotechnical Conference and 6th Canadian Permafrost Conference*: 642-655., Calgary, 12 –16 September 2010.

Kabwe, L.K., Kone, M., Sorta, A., Wilson, W.G., Scott, D., & Ulrich, A. 2013. Measurements of unsaturated soil properties of old and new mature fine tailings MFT. In *Proceedings of Mine Closure 2013*, Cornwall, 14-22 September 2013.

Penman, H.L. 1948. Natural evapotranspiration from open water, bare soil and grass. *Proceedings of the Royal Society of London, Series A, Mathematical and Physical Sciences* 193: 120–146.

Scott, J.D. & Ozum, B. 2010. Oil sands tailings: What needs to be done. *Mining.com Magazine.* September 2010.

Simms, P., Dunmola, A. & Fisseha, B. 2009. Generic predictions of drying time in surface deposited thickened tailings in a "wet" climate. In D.Sego, M. Alostaz and N. Beier (eds), *Proceedings of the Thirteenth International Conference on Tailings and Mine Waste '09*: 749-757. Banff, 1–4 November 2009.

Seneviratne, N.H., Fahey, M., Newson, T.A. & Fujiyasu, Y. 1996. Numerical modelling of consolidation and evaporation of slurried mine tailings, *International Journal for Numerical and Analytical Methods in Geomechanics* 20: 647–671.

Song, Q., O'Kane, M., Dhadli, N., & Matthews, J. 2011. Deposition thickness and evaporative drying for oils sands tailings in Northern Alberta. In A.B. Fourie, M. Tibbett and A. Beersing (eds.), *Proceedings of Mine Closure 2011*: 373-382. Lake Louise, 18-21 September 2011. Perth: Australian Centre for Geomechanics.

Observations of tailings flow and application of the McPhail beach profile model to oil sands and metal mine tailings

L.E. Charlebois
Robertson GeoConsultants, Vancouver, B.C., Canada

G.I. McPhail
SLR Consulting, Perth, W. Australia

A. Revington
Suncor Energy, Calgary, Alberta, Canada

D. van Zyl
University of British Columbia, Vancouver, B.C., Canada

ABSTRACT: In this paper, we present two case studies embodying the state of the art in tailings management with respect to managing the overland flow behaviour of engineered mine tailings and the resulting sub-aerial tailings beaches. In the first example, we highlight the role of rheology in dictating the beach forms associated with a new, complex mine waste material – polymer-flocculated Oil Sands tailings in Canada's north. In the final case study, we describe the application of rheology and deposit modelling for an Australian copper-gold mine transitioning from conventional to thickened tailings discharge. The two case studies are linked by the application of the McPhail stream power approach to beach profile modelling.

1 INTRODUCTION

The flow behaviour and beach formation processes associated with mine tailings often manifest as multi-phase, non-Newtonian, non-linear, time-dependant, rate-dependant, hysteretic, and chaotic challenges for tailings facility designers and operators. Yet, over the years, engineers and scientists have observed, documented, sampled, analyzed, and modelled these complex behaviours with success through empiricism. Accordingly, the state of the art has progressed from haphazard 'slimes' discharge to the precisely-tuned management of 'engineered tailings' at operations the world over.

As mine operators are presented with operational opportunities (improved waste and water storage, water recovery, etc.) and regulatory pressure (environmental, reclamation, and closure requirements), the significance of engineered tailings and the need for management thereof is on the rise.

This paper summarizes two case studies embodying the state of the art in tailings management with respect to the overland flow behaviour of engineered mine tailings and the resulting sub-aerial tailings beaches. By most definitions, the tailings discussed in this paper would classify as slurry and thickened tailings; however, it should be noted that depending on the imposed discharge conditions and material conditioning it is observed that they may demonstrate a spectrum of flow behaviours.

2 CASE STUDY 1: SUNCOR OIL SANDS TAILINGS REDUCTION OPERATIONS, ALBERTA, CANADA

2.1 *Background*

Suncor's Tailings Reduction Operations (TRO) has been commercially implemented at the Steepbank/Millenium Mine, located 26 km north of Fort McMurray, Alberta, since 2010. In the first two seasons of commercial operation, the TRO process successful dewatered and dried approximately 5.3 million tonnes of clay and silt fines derived from the Mature Fine Tailings (MFT) inventory at a peak rate of 30,000 tonnes of fines processed per day (during the available drying season – approximately May to October).

The TRO process involves extracting MFT from an existing source pond, flocculating the MFT using an anionic polymer solution, conditioning the flocculated product during hydrotransport, and sub-aerially depositing the product on a sloping beach. The flocculated MFT undergoes a rapid dewatering phase, followed by drainage and evaporative drying to the desired soil condition (Fig. 1).



Figure 1. A typical commercial-scale MFT drying cell used for performance research at Suncor's Tailings Reduction Operations near Fort McMurray, Alberta, Canada (Robertson GeoConsultants, 2012).

In 2012, Suncor completed one billion dollars of infrastructure improvements to expand TRO, enabling Suncor to cancel plans for building five conventional fluid tailings storage facilities. Robertson GeoConsultants has been involved in the beaching, water balance, and facility design aspects of the TRO project since 2010.

2.2 *Sub-aerial flow behaviour of flocculated oil sands tailings*

2.2.1 *General*

During the initial phases of commercial implementation, the sub-aerial flow behaviour of flocculated MFT was studied at the field-scale to better understand the flow and beach development processes associated with this new tailings material (Charlebois, 2012b). The field investigations carried out by Robertson GeoConsultants during the 2011 season included:

- Visual observation and classification of flow behaviours
- In-stream rheology
- In-stream sampling for evidence of sedimentation / segregation
- Beach profile measurement

Unprecedented access to the deposition cells via simple and safe scaffolding structures ("catwalks") allows for monitoring the changes in flow behaviour and stream characteristics along

the length of the deposit and within active streams and deposition fronts. The structures are also used for parallel water balance monitoring.



Figure 2. Scaffolding ("catwalk") access within a typical MFT drying cell to allow for detailed tailings flow monitoring, water balance study, and instrumentation maintenance (Robertson GeoConsultants, 2012).

2.2.2 *Classification of flow*

Visually, the tailings flows can be classified into four distinct regimes:

- Stacking flow
- Sheet flow
- Laminar/tranquil channel flow
- Turbulent channel flow

Stacking flows are characterized by a lobate morphology (Fig. 3a) that progress downslope at a relatively low velocity, and may grow vertically at a rate faster than the rate of horizontal elongation. These lobes are generally derived from a high viscosity tailings product discharged with little momentum (low kinetic energy). This flow behaviour is rare, but can be deleterious to operations if not corrected.

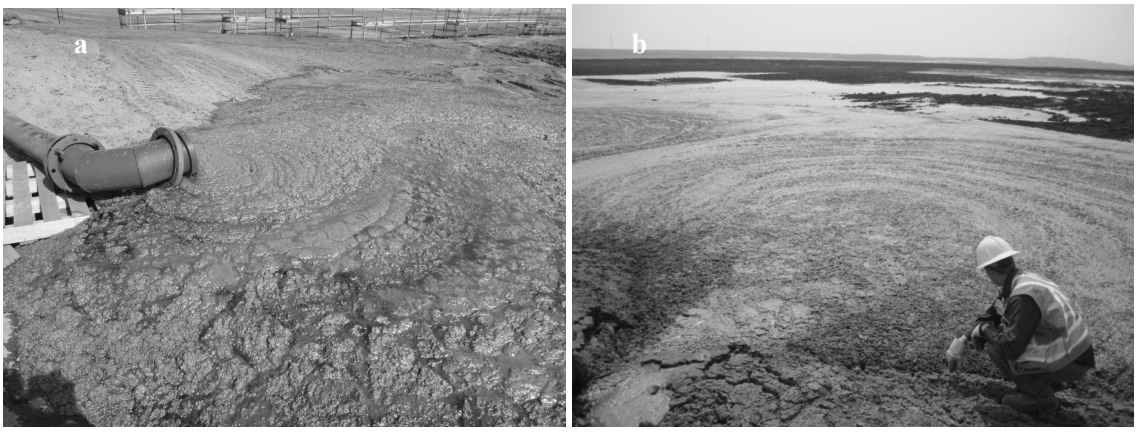


Figure 3. (a) A rare instance of stacking flow, forming a lobe immediately downstream of the discharge spigot and (b) an example of sheet flow in which the flocculated MFT advances downslope as a uniform layer (Robertson GeoConsultants, 2011).

Sheet flows are characterized by a coating flow, of generally uniform thickness, that progress downslope at a relatively low velocity (Fig. 3b). The consistency of the tailings product capable of supporting sheet-like flow behaviour will be of a viscosity generally lower than that of a

stacking material. The kinetic energy of the flow will be generally low, and dominated by gravity flow on the slope. Sheet flows, while able to provide effective deposition cell coverage, may be practically very difficult to maintain in a commercial operation.

Channel flow behaviours are by far most common in flocculated MFT, and may manifest in one or both of two forms: laminar or turbulent. For the purposes of this field study, the use of laminar and turbulent are used qualitatively as detailed measurements of the channel velocity profiles were not practical, nor necessary for this study. The laminar (or tranquil) flow descriptor was used to describe flow patterns in which there was little vertical mixing observed, and in which there were no obvious surface waves or disturbances along the flow length and width (Figure 4).

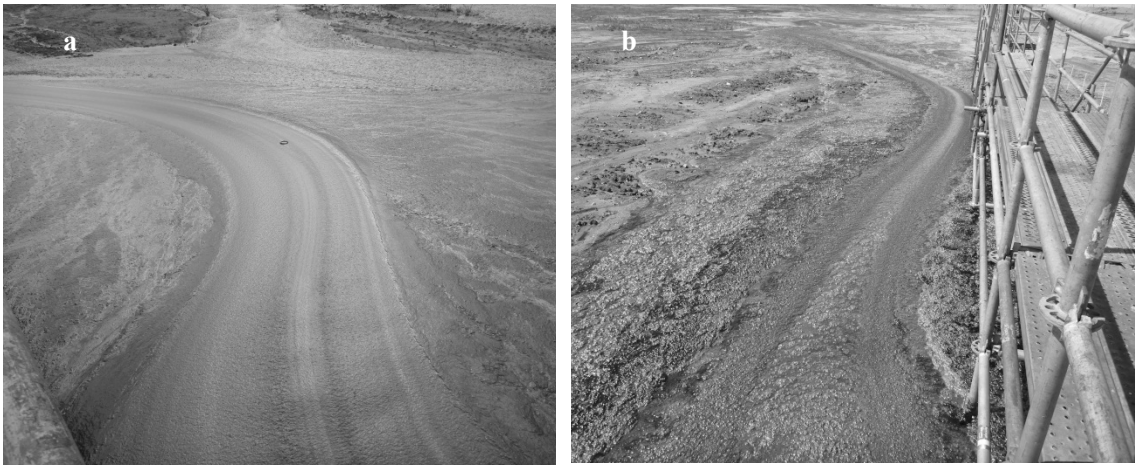


Figure 4. Two examples of laminar flow behaviour in naturally formed, flocculated MFT channels. The active flow widths are typically between 400 (a) and 300 mm (b) (Robertson GeoConsultants, 2011/2012).

Through field measurement, a conceptual model ("flow map") was developed to describe the range of observed flow behaviours and transitions therein (Figure 5). The details of this conceptual model formulation are provided in Charlebois, 2012b. The conceptual model distinguishes flow behaviours as a function of the tailings rheology and the kinetic energy of the flow.

The kinetic energy is defined as the *unit volume kinetic energy* (E_k) and calculated in Equation 1:

$$E_k = \frac{\rho V^2}{2} \tag{1}$$

where ρ is the slurry density (kg/m^3) and V is the bulk flow velocity (m/s).

The behavioral state of the material will transition left on the flow map as kinetic energy is consumed and the tailings flow loses velocity. The behaviour may shift vertically if the consistency changes along the flow path (e.g. due to shear thinning, sedimentation, floc degradation, etc.).

2.2.3 *In-stream rheology*

The flow behaviour of the flocculated MFT product was evaluated using basic field measurement principles including the modified slump cylinder (Pashias & Boger 1996) and (rotational) shear vane testing in a simplified "infinite bucket" rheometer (Fisher *et al.* 2007).

Rheology was assessed in order to translate numerical boundaries to the conceptual flow map (Figure 6) and to assess the degree to which the flocculated structure was altered during beach flow. Monitoring revealed that distinct changes in rheology due to fluctuations in the process and resultant product were a key determinant of beach flow behaviour. Rheological monitoring of active streams also indicated that the yield stress of the flocculated tailings could be reduced when the flows sustained high kinetic energy on the beach (Figure 7).

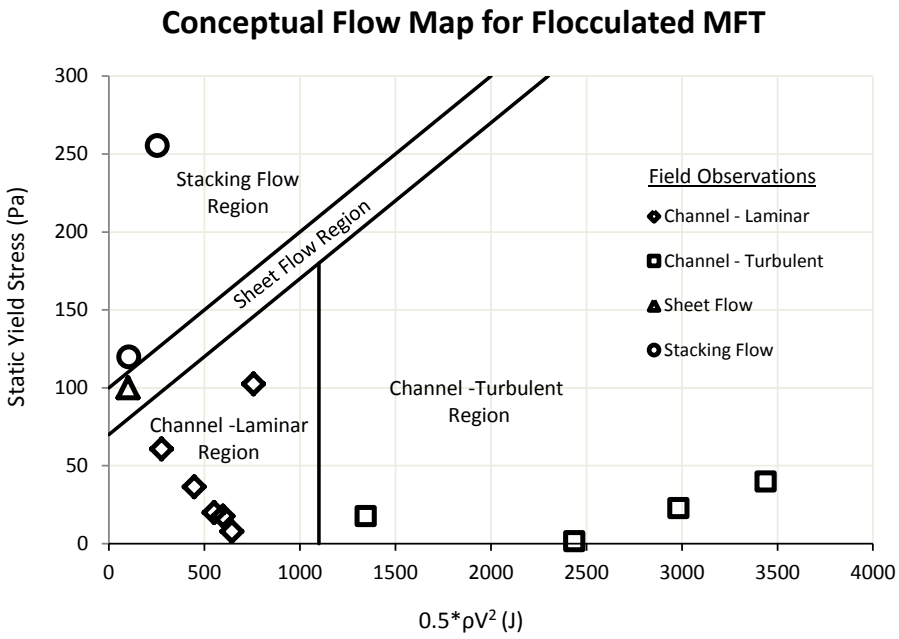


Figure 5. Conceptual "flow map" for flocculated MFT. Select field observations plotted for reference, indicative of relative frequency of observed behaviours. (Charlebois, 2012b).

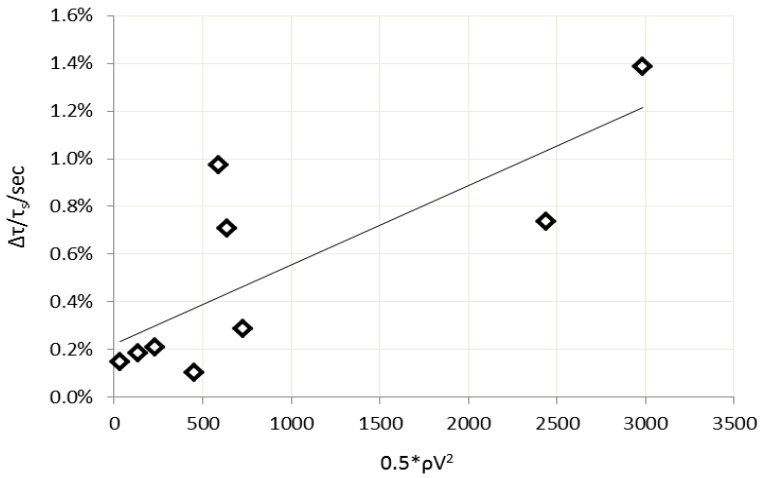


Figure 6. Degradation of flocculated MFT yield stress (change in yield stress, τ, per second of channel flow) as a function of the energy of the flowing stream.

2.2.4 *Sedimentation and segregation in flocculated MFT channels*

Previous research in conventional and thickened tailings deposition has shown the processes of sedimentation and segregation to be paramount in beach formation (McPhail 1995, Fitton 2007). In parallel with rheological monitoring, in-stream sampling was conducted in channel flows accessible from the catwalk structure. In all instances, there was no appreciable sedimentation or segregation (down-slope fining) observed; however, sampling of the active stream was limited to approximately 80 metres from the point of discharge (of a total deposit length of >200 metres) due to the limits of the scaffolding access. Subsequent sampling across the entire beach length at other test sites indicates little evidence of segregation across the beach.

While in the upper reaches of the beach there was no evidence to suggest that solids were lost to the channel bed during transport, post-discharge elevation surveys indicate that the beach did indeed aggrade in these areas. Video and time-lapse photography revealed that the flow rate of

the tailings would fluctuate as a result of variable rheology and fluctuations in the plant throughput. These fluctuations resulted in a frequent overbanking behaviour (Charlebois 2012a), as is typical of river systems with unsteady flows. During the overbanking process, fluid and solids are lifted out of the main channel and over the leveed banks where the flow width increases, the velocity decreases, and solids are deposited. It is suggested that this overbanking phenomenon is a key deposition mechanism for flocculated MFT in an unsteady flow scenario.

2.3 *Beach Profiles*

Numerous beach profiles were obtained during the 2011 field season by laser level profiling and ground-based LIDAR surveys. The profiles were obtained from full-scale deposition cells ranging in length from 150 to 270 metres in length (downslope), 80 to 100 metres in width (across slope) and with initial foundation grades ranging from <1% to approximately 3.5%. Comparison of the Suncor TRO beaches using normalized horizontal and vertical axes reveals a reasonable level of agreement between profiles (representative profiles shown in Figure 7). This generalized beach form may be used for correcting storage estimates traditionally calculated using average beach slopes. The range of concavity observed in the field was shown to account for as much as 14 to 20% overestimate of storage capacity versus an assumed monotonic average beach slope.

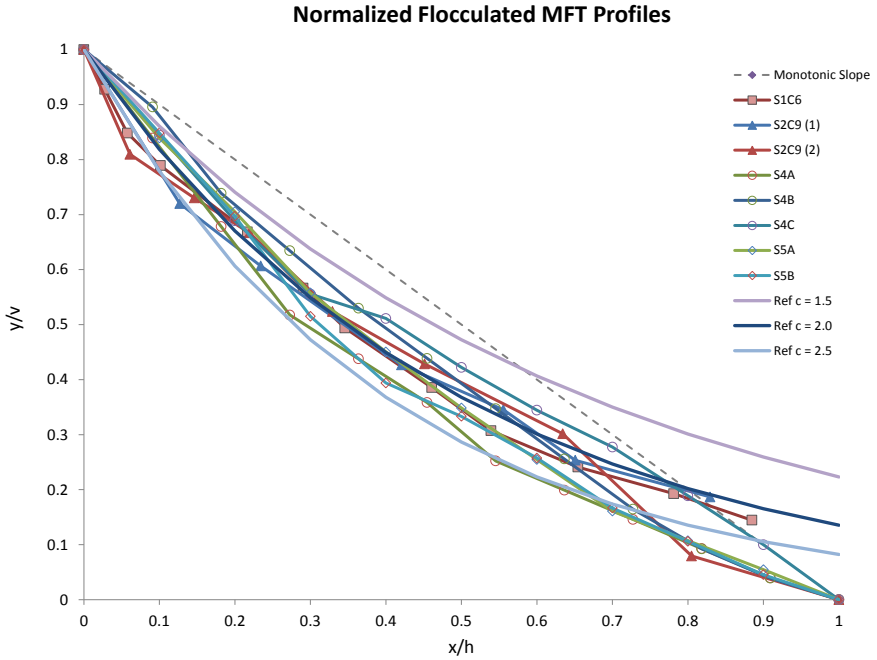


Figure 7. Flocculated MFT beach profiles (normalized) compared to a monotonic slope and concave reference profiles.

The McPhail stream-power entropy approach was adopted to model and predict flocculated MFT beach profiles. A comparison of back-analyzed beach profiles and laboratory and field rheology data indicated that the model was appropriate for simulating deposits formed by the agglomerated flocs transported downslope in naturally formed channels. Figure 8 shows a McPhail model-fitted profile for a full-scale flocculated MFT beach.

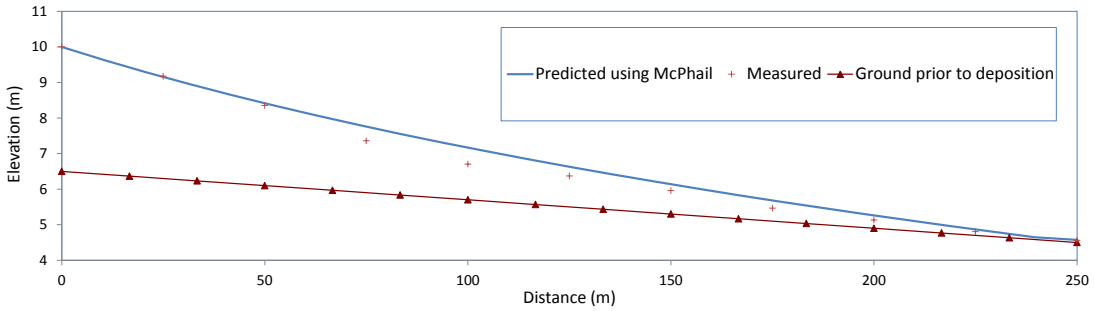


Figure 8. Measured flocculated MFT beach profile with predicted McPhail stream power-entropy slope profile for a 250 metre long beach in a Suncor TRO production cell.

3 CASE STUDY 2: OSBORNE COPPER-GOLD MINE, QUEENSLAND, AUSTRALIA

3.1 *Background*

The Osborne mine in Northern Queensland, Australia is an underground copper-gold operation that has been active since 1996. The operation is located in an arid environment with an average annual rainfall of 335 mm (McPhail *et al.* 2004). Thickened tailings were identified by the operator as a potential means of achieving water savings and reducing costs associated with raising perimeter embankments of the existing TSF (via steepened tailings beaches). The data on the Osborne tailings presented below represents an update on the analysis of data presented in McPhail 2008 and incorporates improvement in the analysis methods that have been developed over the ensuing 5 years.

3.2 *Tailings characteristics*

Osborne tailings comprise mostly magnetite and has a particle specific gravity of 3.6. The tailings are relatively fine grained with a P80 of 0.15mm and 55% passing the 75 micron sieve. Figure 9 shows particle size distributions for the Osborne tailings. The tailings are non-plastic and fines comprise rock flour.

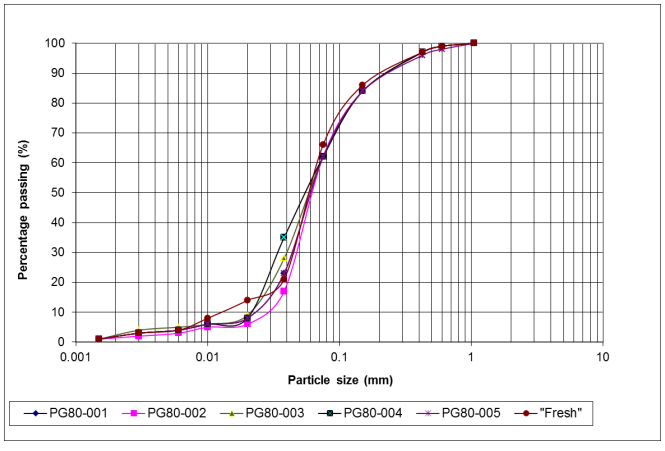


Figure 9. Particle size distribution of Osborne tailings

3.3 *Rheological assessments*

Laboratory viscometer testing was undertaken on the Osborne tailings at a range of solids contents. It was found that even at high percent solids the tailings settled in the viscometer so that the viscometer results were unreliable. Figure 10 below shows the flow curves obtained.

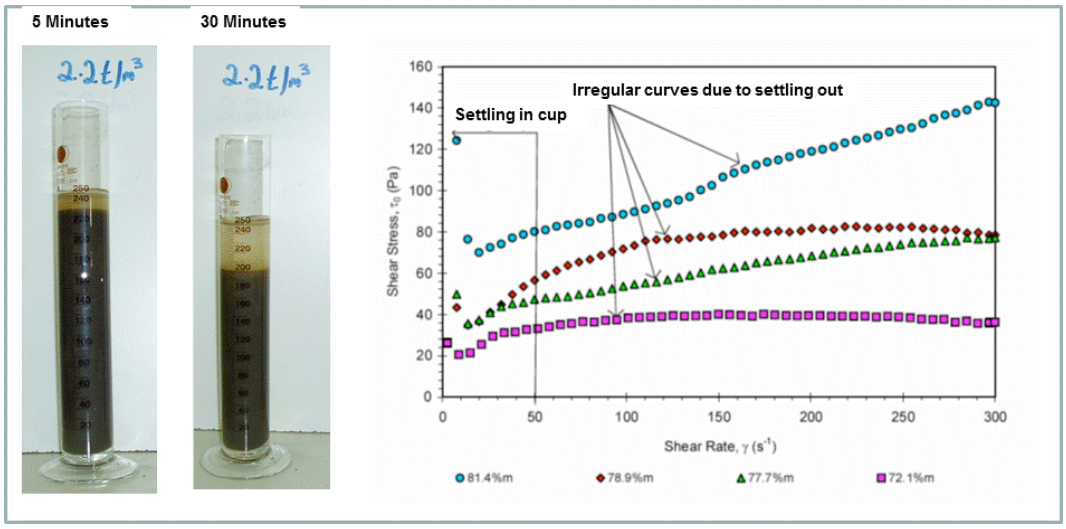


Figure 10. Rheological testing results on Osborne tailings

The flume results have been re-analyzed using the latest analytical methods to determine shear rates and shear stresses at points down the beach formed in the flume. Particular emphasis was placed on estimating the yield stress. The results of the analyses are presented in Figure 11 below.

Slurries settling on a beach do so at shear rates that are generally less than $10s^{-1}$ and since the flow curves were particularly unreliable in the low shear rate zone it was necessary to abandon the use of the laboratory rheological measurements. Since the problem relates to settling out of the solids it was decided to set up rheological measurement test that would work with the settling out. To this end, small scale flumes were selected as described in the next section.

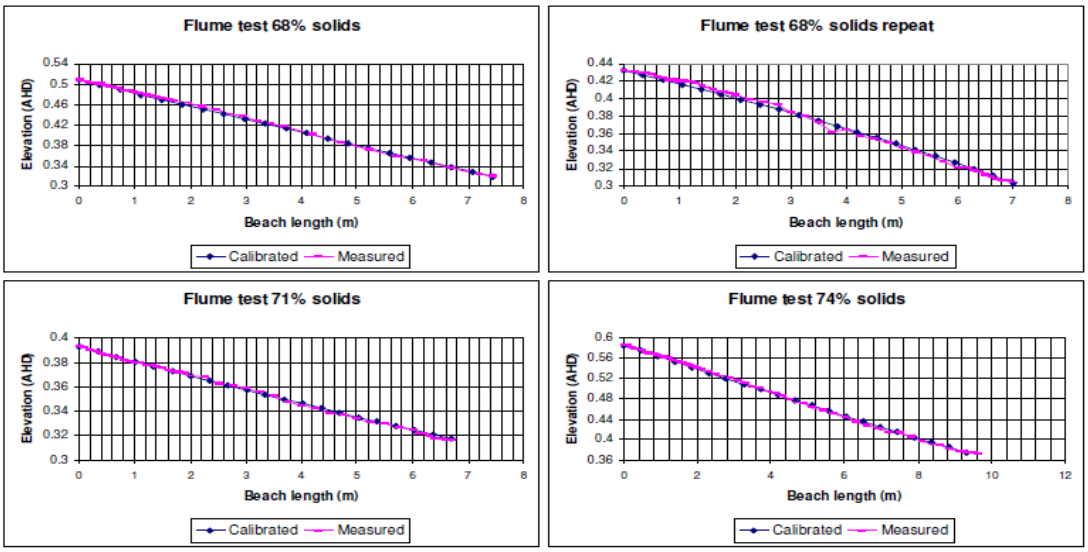


Figure 11. Results of flume testing and calibration of the McPhail stream power-entropy model for the Osborne thickened tailings at a range of solids concentrations (68% to 74% SBW).

3.4 *Flume testing*

The Osborne tailings were deposited at a rate of 0.8 L/s into a flume measuring 7 metres long by 0.5 metres wide (McPhail 2008). Figure 12 shows the resultant beaches of slurry deposited into the flumes at a range of solids concentrations (68 to 74% SBW) along with corresponding post-calibration profiles from the McPhail model.

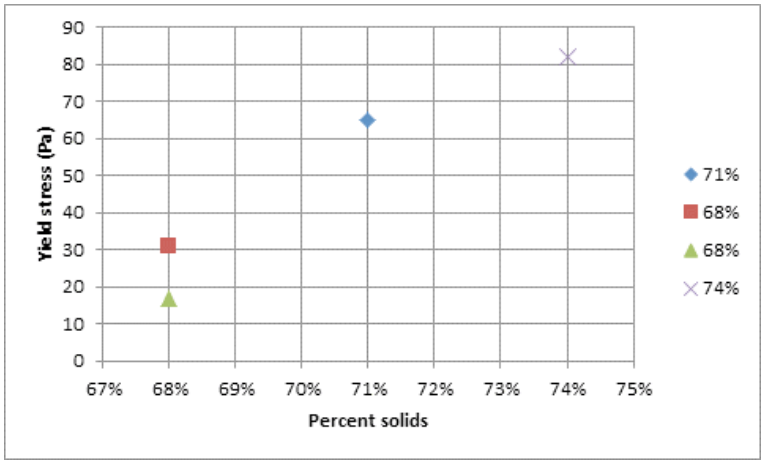


Figure 12. Yield stresses from the small scale flume tests

3.5 *Full-scale beach profiles on TSF1*

The flume tests provided a theoretical basis for proceeding with full scale trials. These were conducted as improvements to the thickening technology were developed (McPhail et al 2004) over a period of almost 2 years with the first step-up in percent solids from 55% to 65%. The deposition at 65% solids, and subsequently at 68% solids, took place as part of routine operations on TSF1 while the initial earthworks for TSF2 were being constructed.

Beach modeling on these two beach profiles was used to compliment the flume tests and provide improved data on which to ultimately justify carrying out further process plant modifications to raise the percent solids beyond 68%. Measurements of percent solids were from a density meter in the processing plant and it was subsequently found that this instrument could be out by 2% to 3% solids either way due, it is suspected, to the magnetite rock characteristics. The density readings have, nonetheless, been applied throughout the assessments in this paper.

The McPhail model was used to analyze the original 55% solids beach as well as the two full scale operating beaches formed at 65% and 68% solids on TSF1. Figure 13 shows the measured and calibrated profiles.

Evaluation of the beaching analyses has been repeated with current methods of analysis which now permits the backward construct of representative flow diagrams for the tailings. More importantly, the understanding of the role of rheology in controlling the beaching behavior has been refined and incorporated into the analyses. The yield stresses have been back calculated from the full scale beach profiles and added to the table of yield stresses from the flume testing. Figure 13 shows the resulting plot. It is evident from Figure 13 that the flume test results for 68% solids are outliers from the trend of the other results. These have therefore been excluded and the best fit line from the results other than those for the 68% flume is indicated on Figure 154

On the basis of the full scale and flume beach profiles, additional modifications were made to the thickener in the processing plant (McPhail et al 2004) to maximize the percent solids that could be achieved for the tailings. This was established to be in the range of 71% to 77% solids. The best fit yield stress curve indicated in Figure 1 has, for this paper, been used to back analyze three full scale trials conducted at a range of percent solids within the target range.

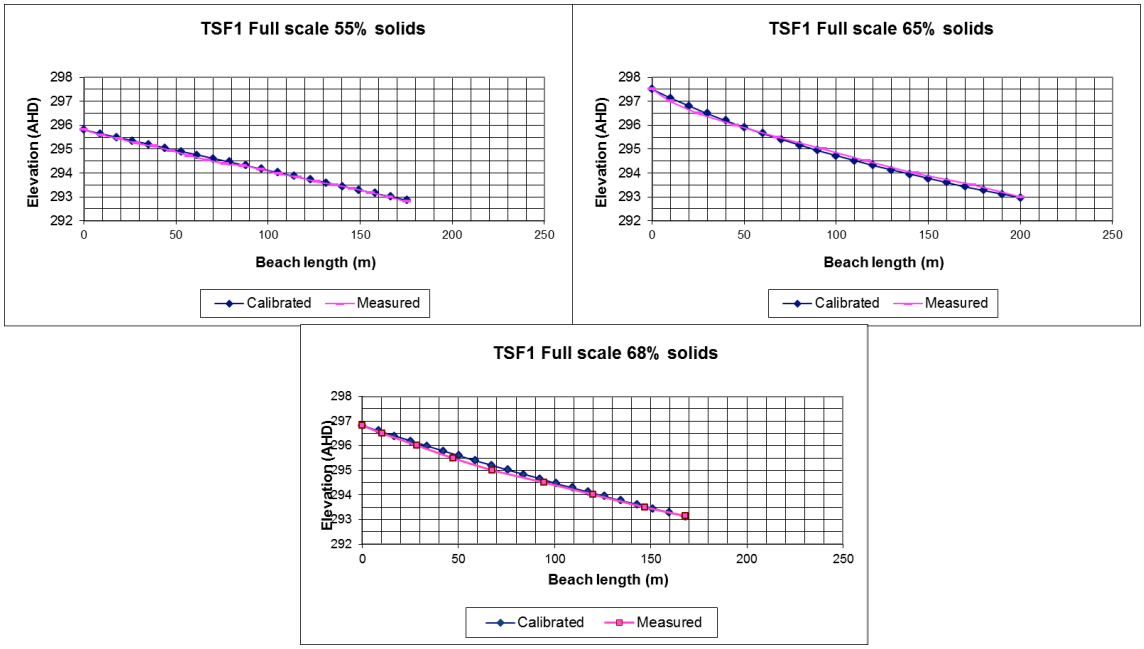


Figure 13. Beach profile predictions (using the calibrated model) and measure full-scale beaches formed by conventional Osborne tailings (55% SBW) and by thickened Osborne tailings (66.5, 68, and 74% SBW).

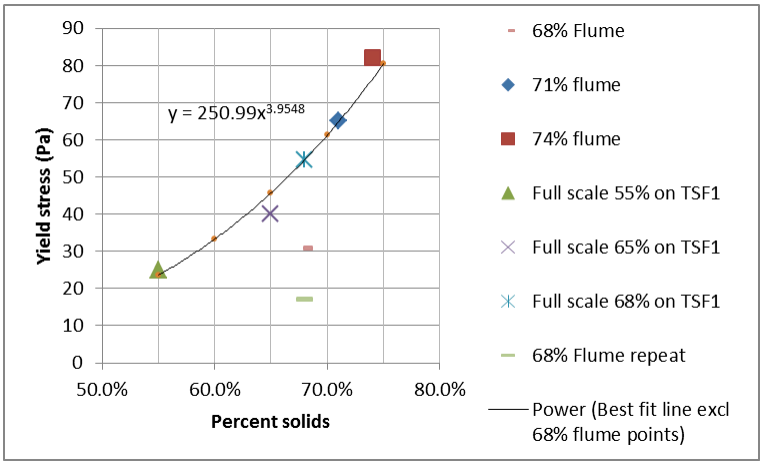


Figure 14. Yield stresses from the flume and full scale trials on TSF1

3.6 *Full-scale beach trials on TSF2*

TSF2 was commissioned in May 2002 ahead of the final modifications to the thickener circuit and at percent solids in the range 65% to 68% solids and using conventional ring main deposition from the toe starter embankment discharging in towards a decant. During 2002 the final modifications to the thickener circuit were completed and a set of three trials at the target percent solids range of 71% to 77% were carried out over a period of 18 months. Figure 15 shows the beach profiles measured from these trials as well as the averaged percent solids over the trial deposition period. Also indicated on Figure 15 are the calibrated beach profiles obtained using the McPhail beach model.

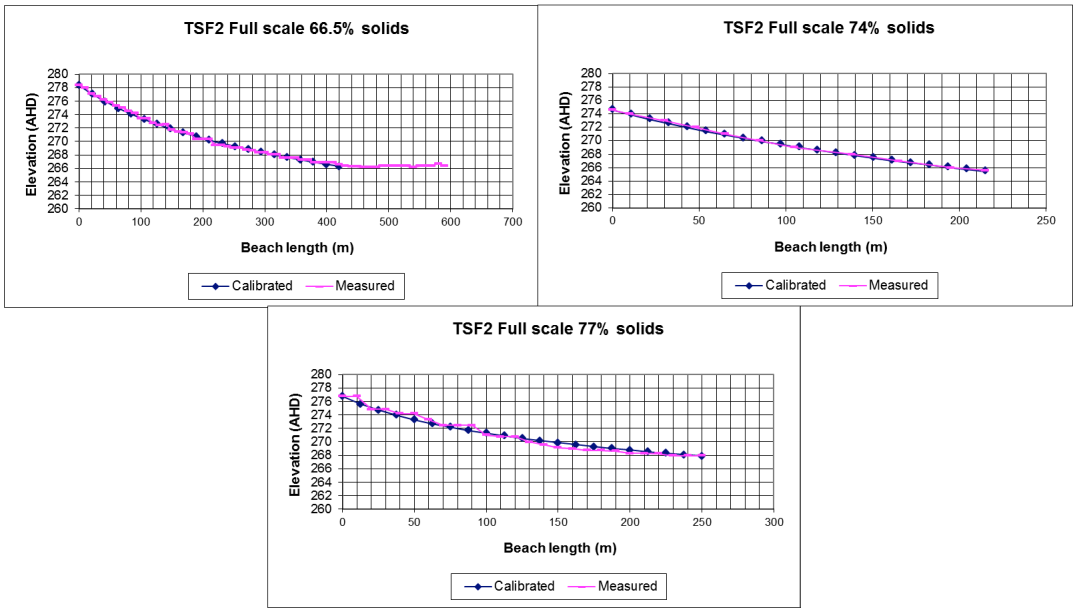


Figure 15. Full scale beach profiles from trials on TSF2

Using the principle that the tailings flowing down the beach needs to satisfy the constraints imposed by the flow rate, available energy/stream power and the rheology, the beach models have been iteratively run using the yield stress-percent solids relationship from Figure 16 to back calculate Herschel-Bulkley parameters which can be used to describe the flow diagrams applicable to slurries over the target range and at low shear rates. Figure 16 shows the resulting flow diagrams. In carrying out the back calculation, the Mooney Rabinowitsch correction to derive true shear rate parameters from the bulk shear rates has been applied.

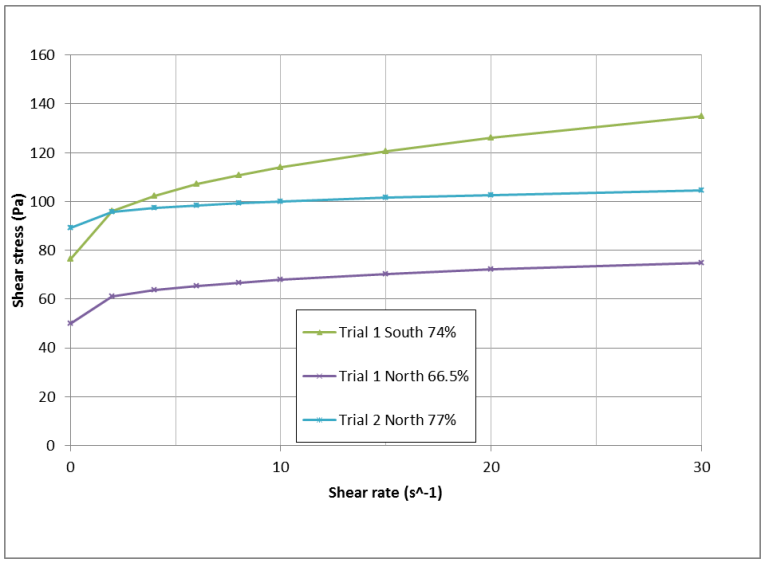


Figure 16. Flow diagrams based on back-calculated and calibrated Herschel-Bulkley parameters

The above flow diagrams are plotted together with the flow diagrams from the laboratory rheological testing in Figure 17.

It is evident from Figure 17 that the laboratory testing has significantly underestimated the shear stresses in the slurry as a result of settling out of the tailings in the rheometer. Moreover, the estimates of the rheology in the low stress range are more reliable.

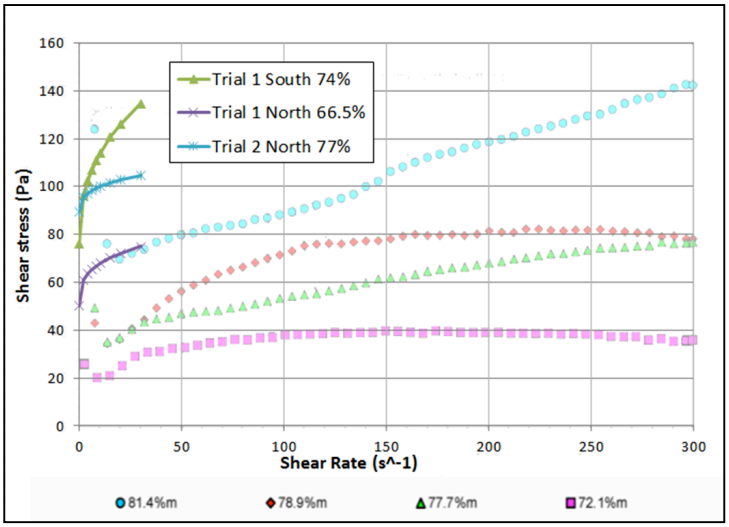


Figure 17. Co-plot of the laboratory and the back-calculated flow diagrams

4 CONCLUSIONS

Despite the complex behaviours of concentrated mineral suspensions, including oil sands and metal mine tailings, this paper has shown that an empirical approach combined with energy-based modelling can facilitate the thoughtful design and successful operation of sub-aerial tailings storage facilities. The McPhail method of beach profile prediction has been proven effective in both metal mine and oil sands applications, covering a broad spectrum of tailings characteristics and flow behaviours.

The paper has also highlighted a problem with the laboratory testing of mine tailings to determine flow diagrams. Many, if not most, mine tailings slurries will tend to settle out to some degree in the rheometer and the numbers obtained from laboratory testing may significantly underestimate the rheological characteristics of the slurry especially at low shear rates where the speed of rotation of the viscometer is insufficient to keep the coarser particles in suspension. In such instances, small scale flume testing complemented with pilot and, where practicable, full scale beaching trials are the only practical method of representatively estimating the rheological parameters.

5 REFERENCES

Charlebois, L.E. 2012a. Pahoehoe to paste: Rheological field methods for characterizing overland tailings flow behaviour. Proceedings of Tailings and Mine Waste 2012: 559-567

Charlebois, L.E. 2012b. On the flow and beaching behaviour of sub-aerially deposited, polymer-flocculated oil sands tailings: A conceptual and energy-based model. *MASc thesis*. University of British Columbia. Available at http://hdl.handle.net/2429/43761

Fisher, D.T., Scales, P.J., Boger, D.V. 2007. The bucket rheometer for the viscosity characterization of yield stress suspensions. *Journal of Rheology* 51(5): 82.

Fitton, T. 2007. Tailings beach slope prediction. *PhD dissertation*. RMIT University.

Pashias, N. & Boger, D.V. 1996. A fifty-cent rheometer for yield stress measurement. *Journal of Rheology* 40(6), 1179.

McPhail, G.I. 1995. Prediction of beaching characteristics of hydraulically placed tailings. *PhD dissertation*. University of Witwatersrand.

McPhail, G.I. 2008. Prediction of the beach profile of high density thickened tailings from rheological and small scale trial deposition data. Proceedings of the 2008 International Seminar on Paste and Thickened Tailings. Kasane, Botswana.

McPhail, G.I., Noble, A., Papageorgiou, G., Wilkinson, D. 2004. Development and implementation of the thickened tailings discharge at Osborne Mine, Queensland, Australia. Proceedings of the 2004 International Seminar on Paste and Thickened Tailings. Cape Town, South Africa.

Predictive model for thick lift placement of silica-treated fluid fine tailings

J.C. Sobkowicz, M. Pinheiro & T.W. Moore
Thurber Engineering Ltd., Calgary, Alberta, Canada

R.H. Moffett
DuPont Chemicals and Fluoroproducts, Wilmington, Delaware, USA

ABSTRACT: One desirable method of storing fluid fine tailings is in a deep pit, as it occupies a small footprint and has a relatively low conveyance and storage cost. The challenge with this type of deposit is that it relies on sedimentation and consolidation to cause dewatering, which is a long process: 5 to 10 years for capping; 30 to 50 years for most of the consolidation to occur. Dewatering is necessary to transform the fluid fine tailings into a solid that can be capped, reclaimed, and become part of a closure landscape.

Fluid fine tailings treated with nanometer silica particles develop a synthetic soil structure that has a similar hydraulic conductivity after treatment as before (as a function of void ratio; Moore et al., 2013). However, the treated material develops strength quicker at lower solids content, which means it is possible to place intermediate drainage layers, if desired. It is also stiffer and thus consolidates in a shorter time and in a more uniform manner than its untreated cousin. This paper summarises the improved properties of silica-treated fluid fine tailings, and shows examples of how it might be employed to reduce time to capping and to final closure of deep deposits of fluid fine tailings. The behaviour of the deep deposit is predicted using a finite strain consolidation model and comparisons are made between silica-treated and untreated tailings. Examples are given for "thickened tailings". Improvements that might be seen when using intermediate drainage layers for both untreated and treated cases are also shown.

1 INTRODUCTION

One desirable method of storing fluid fine tailings is in a deep pit, as it occupies a small footprint and has a relatively low conveyance and storage cost. The challenge with this type of deposit is that it relies on sedimentation and consolidation to cause dewatering, which is a long process: 5 to 10 years for capping; 30 to 50 years for most of the consolidation to occur. Dewatering is necessary to transform the fluid fine tailings into a solid that can be capped, reclaimed, and become part of a closure landscape.

This paper discusses a novel method of treating the fluid fine tailings with nanometre-size silica particles, which increases the material stiffness and strength, without significantly impacting permeability. The benefits that can be realized from this treatment, in terms of reduced consolidation time, are also presented.

2 SILICA TECHNOLOGIES

Silica technologies use nanometre-sized particles. The concept behind this chemical additive is very different from that of either flocculants or coagulants (Moffett, 2010a, 2010b). Fluid fine tailings are dosed with nano-sized silica particles, based on the water content and not the solids content or mineralogy. These silica particles form their own network within the water phase and,

in the process, solid particles get trapped within the network while water can move through the void space as freely as it would do otherwise in the absence of the silica. In essence, the silica network forms a weak, synthetic soil structure, which develops its own strength and stiffness.

These technologies have also been used in both water clarification and ground stabilisation. Laboratory and pilot tests have been performed with a commercial version of this technology, Particlear™, to investigate its potential benefits for fluid tailings dewatering at one oil sands mine (Sobkowicz, 2013). Alternate sources of this technology might be available in the form of fly ash, a waste product in the cement industry, although there are issues with particle size, product consistency, and long term sourcing.

3 MODELLING FRAMEWORK

The behaviour of the deep fine fluid tailings deposit is predicted using the one-dimensional finite strain consolidation model originally formulated by Gibson et al. (1967), and later reformulated by Somogyi (1980). This model accounts for large variations in compressibility and hydraulic conductivity of the material, and thus describes well the behaviour of both untreated and silica-treated fluid fine tailings. Constitutive equations representing these variations have been expressed in various forms, as described by Bartholomeeusen et al. (2002) and Jeeravipoolvarn (2010). Here, the following constitutive equations are used:

$$\frac{\sigma}{\sigma_1} = \left(\frac{e}{e_1}\right)^n \tag{1}$$

$$\frac{k}{k_1} = e^m \tag{2}$$

where σ is the vertical effective stress, e is the void ratio, k is the hydraulic conductivity, σ_1 is equal to 1 kPa for dimension consistency, e_1 is the void ratio at σ_1, k_1 is the hydraulic conductivity when e = 1.0, and n and m are best-fitting exponents. These equations are just a variant of those employed by Jeeravipoolvarn (2010).

The peak undrained shear strength of the tailings material, as a function of void ratio, or solids content, is estimated based on the following equation, which is analogous to Eq. (1):

$$\frac{s_u}{s_{u1}} = \left(\frac{e}{e_{s1}}\right)^{n_s} \tag{3}$$

where s_u is the undrained shear strength, s_{u1} is equal to 1 kPa for dimension consistency, e_{s1} is the void at s_{u1}, and n_s is a best-fitting exponent.

4 THICKENED TAILINGS DESCRIPTION

This work focuses on thickened tailings (TT), one of the various forms that fluid fine tailings can take. TT is produced by the concentration of solids from a solid-liquid suspension by the action of gravity sedimentation in a high rate thickener (Sobkowicz, 2012). Typical thickening of the fines improves solids content (based on total weight) from 10-20% (in the cyclone overflow) to 45-55% (in the thickener underflow). Thickening is aided by the use of flocculants to encourage gravity settling within the thickener.

The following subsections describe some of the mechanical and hydraulic properties of the TT studied here. Both untreated and amended conditions will be considered. Chemical amendment was completed using silica, dosed at 0.25% (by mass) of the water component. The equipment and the procedure used to test and characterise the TT material are described in Moore et al. (2013). Comparison with other thickened tailings materials, as well as mature fine tailings (MFT), is also presented.

4.1 *Characterisation*

Table 1 lists some relevant index properties of the TT under investigation and compares them with those of the Albian Sands TT reported in Jeeravipoolvarn et al. (2008). Figure 1 shows particle size distribution (PSD) curves for these two tailings. The different laboratory techniques used to obtain the PSD curves of the tailings specimens are noted in the legend. The TT used in this study has a higher solids content and more fines (esp. clays) but a lower bitumen content than Albian Sands TT. This explains its higher specific gravity and unit weight.

Table 1. Index properties of untreated TT

	Study	Shell
Saturated unit weight, γ [kN/m^3]	14.1	12.7
Specific gravity, G_s [dimensionless]	2.60	2.44
Initial void ratio, e_0 [dimensionless]	2.65	3.82
Solids content, by mass, SC [%]	50.0	39.0
Bitumen content, by mass, b [%]	1.3	4.6
Fines content (< 44 µm), f [%]	68.0	54.0
Sand content (> 44 µm), s [%]	32.0	44.0
Clay content (< 2 µm), c [%]	30.0	21.0
Sand to fines ratio, SFR [%]	0.60-0.80	0.81

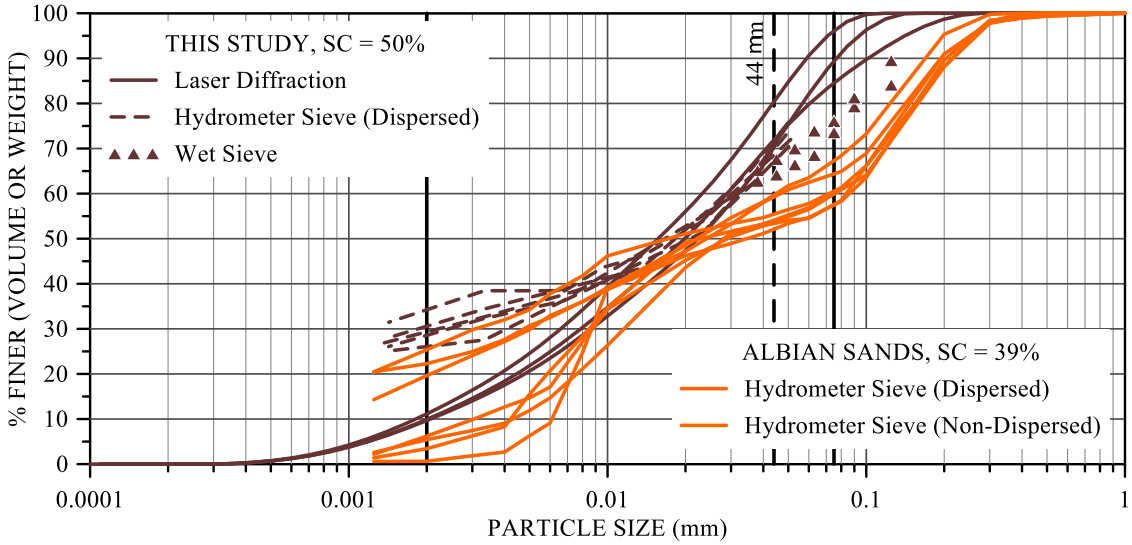


Figure 1. Particle size distribution curves for two TT materials

4.2 *Mechanical behaviour*

Figure 2 compares the vertical effective stress versus void ratio response of untreated and silica-treated TT (at a Particlear™ dose of 0.25%) and that of other fluid fine tailings (including Albian Sands) reported in the literature (Yong, et al., 1983; Pollock, 1988; Suthaker, 1995; Proskin, 1998; Wong, et al., 2008; Scott, et al., 2008; Shaw, et al., 2010; Jeeravipoolvarn, 2010). These results show that, starting from a fixed void ratio (e.g., for TT, about 3), the network of silica particles stiffens the TT material, making it less compressible (i.e., the treated TT undergoes a smaller void ratio change while consolidating from its initial state to a specified vertical effective stress, than the untreated TT).

Figure 3 presents peak undrained shear strength vs. void ratio data for untreated TT, silica-treated TT and other fluid fine tailings. The silica network is responsible for higher values of peak undrained shear strength for the treated versus the untreated TT. For example, at the initial void ratio of 2.65, chemical amendment with silica boosted the peak undrained shear strength from 0.025 kPa to 0.4 kPa. Strength gain at denser states, i.e. lower solids content, is not as high but still significant, which means it is possible to place intermediate drainage layers and speed

up ever further the consolidation process, as discussed in Section 6.3. This is true even when taking into account the different void ratios of treated and untreated material, when consolidated to the same vertical effective stress. For example, comparing the two sets of dashed lines on Figures 2 and 3, consolidated under a vertical effective stress of 5 kPa, the untreated TT would have a void ratio of 1.1 and the treated TT of 1.5. The corresponding peak undrained shear strengths for these materials would be 1.5 and 3-5 kPa (untreated and treated TT, respectively).

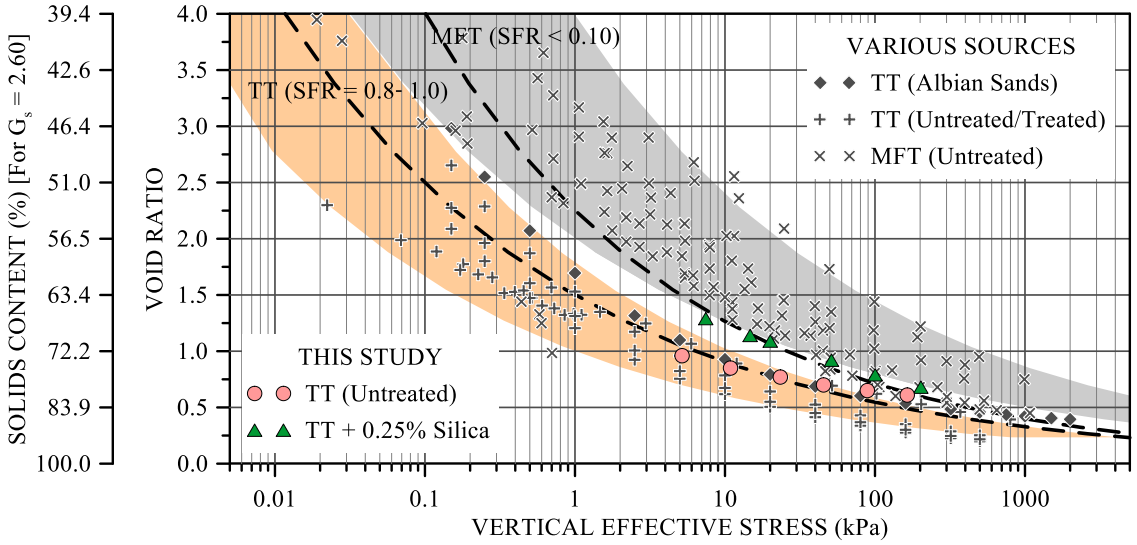


Figure 2. Compressibility data for various TT and MFT materials

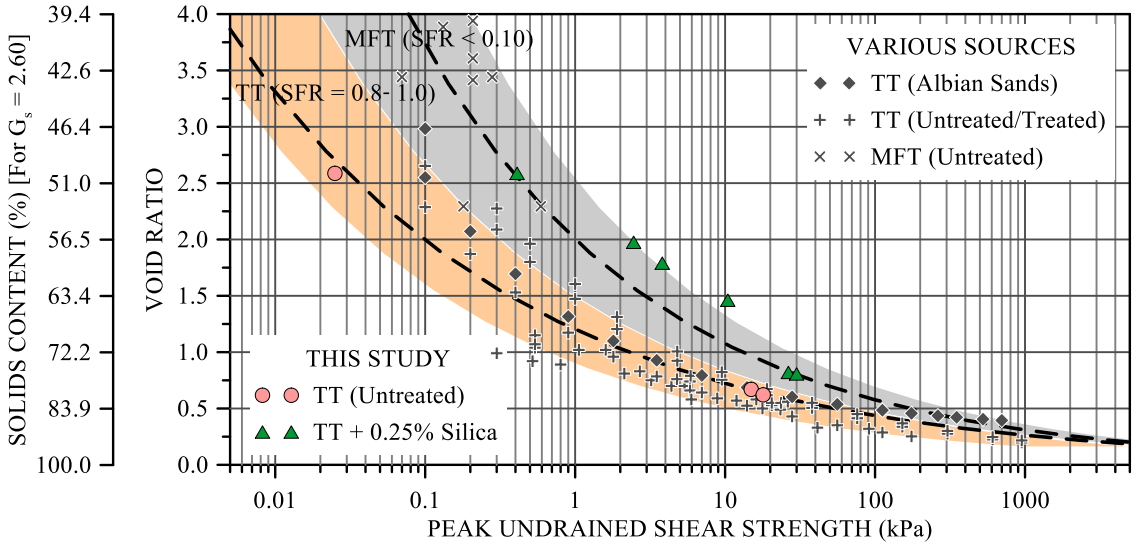


Figure 3. Undrained shear strength data for various TT and MFT materials

4.3 *Hydraulic behaviour*

Figure 4 compares the hydraulic conductivity versus void ratio response of both untreated and silica-treated TT (at a Particlear™ dose 0.25%) and that of other TT and MFT materials reported in the literature (*op. cit.*). The figure shows that silica does not affect the permeability of TT. As explained earlier, the silica particles form their own network within the water phase, but still allow water to move through the network as freely as it would do otherwise in the absence of the

amendment. The results also reveal that permeability is highly dependent on SFR, i.e. the greater the sand to fines ratio, the more permeable the tailings material is.

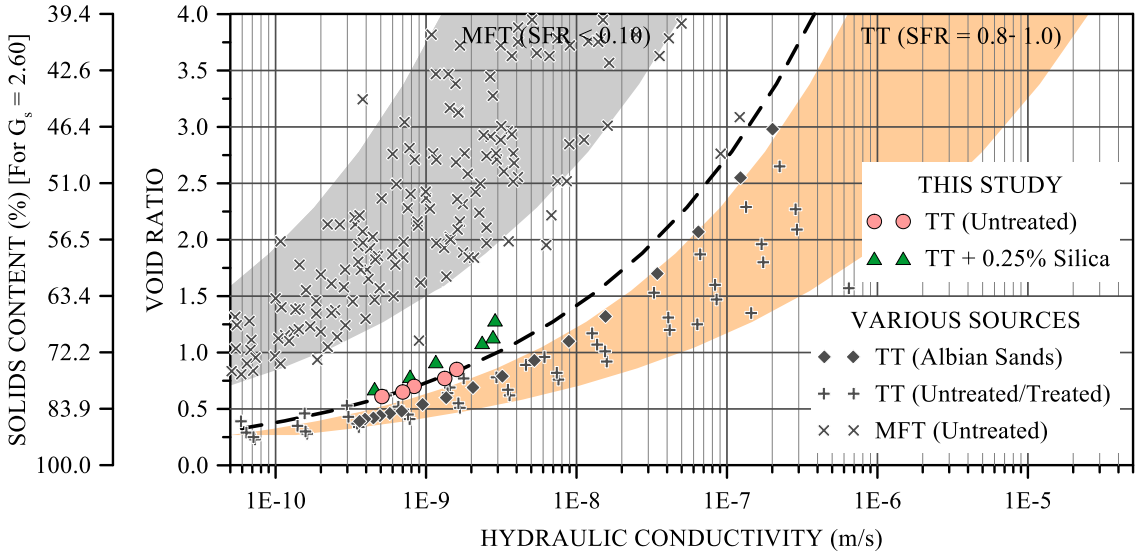


Figure 4. Hydraulic conductivity data for various TT and MFT materials

5 ANALYSIS

In the following subsections, three studies are carried out to identify some practical implications associated with silica as an amendment for fluid fine tailings. In particular, the time required to capping and final closure of deep deposits of thickened tailings is investigated, as well as the potential improvements associated with intermediate drainage layers.

5.1 *Study 1: Parametric Study – Time Required to Achieve 98% Consolidation*

A simple parametric study was conducted to analyse the effects of deposit thickness and sand cap on the time required for a TT deposit to achieve 98% consolidation. Assumptions and modelling conditions are as follows:

- Instantaneous TT deposition (deposit thickness = 1 m, 10 m and 50 m).
- Instantaneous sand cap deposition (sand cap thickness = 5 m, modelled as a 25 kPa load).
- Double drainage boundary condition.
- Silica dosages = 0.00% (untreated TT) and 0.25%.

5.2 *Study 2: Deep Deposit – Constant TT Filling Rate*

The second study compares the consolidation performances between untreated TT and silica-treated TT for a 47 m thick deposit filled over a 7-year period, at a constant filling rate. Assumptions and modelling conditions are as follows:

- Instantaneous sand cap deposition (sand cap thickness = 5 m, modelled as a 25 kPa load).
- Single and double drainage boundary conditions.
- Silica dosages = 0.00% (untreated TT) and 0.25%.

5.3 *Study 3: Intermediate Drainage Layers*

The last study investigates the role of interlayering sand, as a way to shorten the time for consolidation and final closure of the deposit. This study is also based on a 47 m thick deposit filled over a 7-year period, at a constant filling rate. Assumptions and modelling conditions are as follows:

- Instantaneous sand cap deposition (sand cap thickness varies according to the cases presented below).
- Double drainage boundary condition. Intermediate sand layers are modelled as free drainage boundaries.
- Silica dosages = 0% (untreated TT) and 0.25%
- Sand interlayering cases as shown in Table 2:

Table 2. Sand interlaying cases

	Case 1	Case 2	Case 3
Number of sand interlayers	0	1	2
Year of deposition	7.0	3.5	2.3 / 4.6
Interlayering sand thickness [m]	0.0	2.0	1.0 / 1.0
Sand cap thickness [m]	7.0	5.0	5.0

5.4 *Material Parameters*

The constitutive parameters assumed for the untreated TT and the silica-treated TT at dosage 0.25% are listed in Table 3. The dashed curves in Figures 2-4 were plotted based on these material parameters.

Table 3. Modelling parameters for untreated TT and silica-treated TT at dosage 0.25%

		Silica	
		0.00%	0.25%
Compressibility (Eq. 1)	e_1 [dimensionless]	1.50	2.25
	n [dimensionless]	0.22	0.25
Hydraulic conductivity (Eq. 2)	k_1 [m/s]	3.0E-09	3.0E-09
	m [dimensionless]	3.50	3.50
Undrained shear strength (Eq. 3)	e_{s1} [dimensionless]	1.20	2.00
	n_s [dimensionless]	0.22	0.27

6 RESULTS AND DISCUSSION

6.1 *Study 1: Parametric Study – Time Required to Achieve 98% Consolidation*

Figure 5 shows the results of the parametric study, which reveal that treatment of TT with as little as 0.25% of silica can reduce the time to 98% consolidation by as much as 40 to 50%. The results also show that the thinner the deposit thickness, the more effect dosage has on improving the rate of consolidation. Surprisingly, sand capping of the thicker deposit (i.e. 10 m, 50 m) did not seem to have much of an impact on the consolidation time as compared to the uncapped counterpart. Although sand capping helps drive water away from the deposit and speed up the consolidation process, its placement generates further excess pore water pressure, which in turn adds time to the consolidation process.

6.2 *Study 2: Deep Deposit – Constant TT Filling Rate*

Table 4 summarises the results of the consolidation analyses involving a deep TT deposit filled at a constant rate over a period of 7 years.

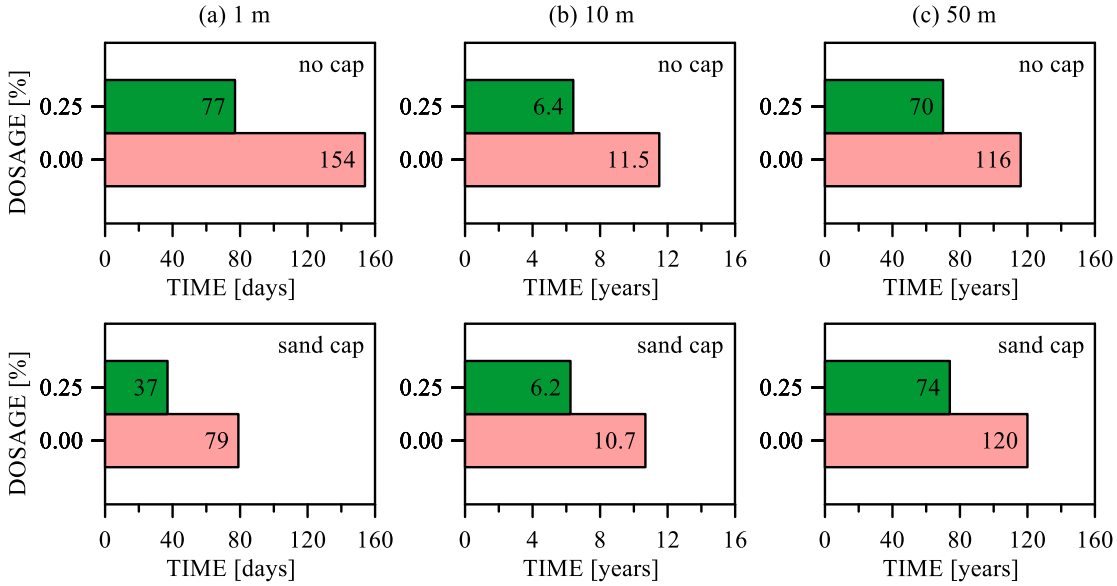


Figure 5. Length of time required to achieve approximately 98% consolidation for "no cap" and "sand cap" conditions and various deposit thickness (a) 1 m [*in days*], (b) 10 m [*in years*], and (c) 50 m [*in years*]. No effects of drying or freeze thaw were assumed for any of the cases.

Table 4. Summary of the analyses for study 2: deep deposit – constant TT filling rate

	Silica Dosage			
	0.00%		0.25%	
	Drainage		Drainage	
	Double	Single	Double	Single
TT thickness at end of deposition (i.e. at Year 7) [m]	36.3	37.1	34.0	35.2
TT thickness at 98% consolidation (not including cap) [m]	17.5	< 17.9[(1)]	19.4	< 19.5[(1)]
Remaining settlement 30 years after end of deposition [m]	1.6	3.0	0.6	2.0
Top boundary (approx..) flux during filling [m/yr/m^2]	2	2	2	2
Bottom boundary (approx.) flux during filling [m/yr]	0.2	0	0.2	0
Time after end of deposition for TT to reach 98% consolid. [yr]	101	>> 100	60	>> 100
Time after end of deposition for TT to reach s_u = 10 kPa [yr]	never[(2)]	never[(2)]	20	26
Time when top boundary flux is ≤ 0.25 m/year [yr]	23	23	20	22

[(1)] Values at 100 years after end of deposition are shown. Time to 98% consolidation is much greater than 100 years.
[(2)] A 5-m sand cap is insufficient to drive the upper 20 cm of untreated TT to a void ratio necessary for s_u = 10 kPa.

The following findings can be drawn from these results:

- The silica-treated TT requires less storage space compared to the untreated material at the completion of filling.
- The silica-treated TT reaches 98% consolidation much sooner than the untreated material.
- The silica-treated TT is able to achieve the minimum undrained shear strength of 10 kPa, although not strictly within the timeframe required by the Directive 074 (ERCB, 2009). The untreated material could not achieve this minimum strength throughout the deposit, even with placement of a 5-m sand cap. Note that the analyses presented here did not account for strength gain due to evaporation and freeze-thaw.

The results also show that, during the first seven years of filling, approximately 14 m of water is released from the deposit per square meter. After that, seepage rates decrease exponentially, eventually dropping to below 0.25 m/year/m^2 within 25 years.

6.3 *Study 3: Intermediate Drainage Layers*

Figure 6 shows the results of study 3, which examined the effect of intermediate drainage sand layers on the consolidation time and strength gain of thick untreated and silica-treated TT deposits.

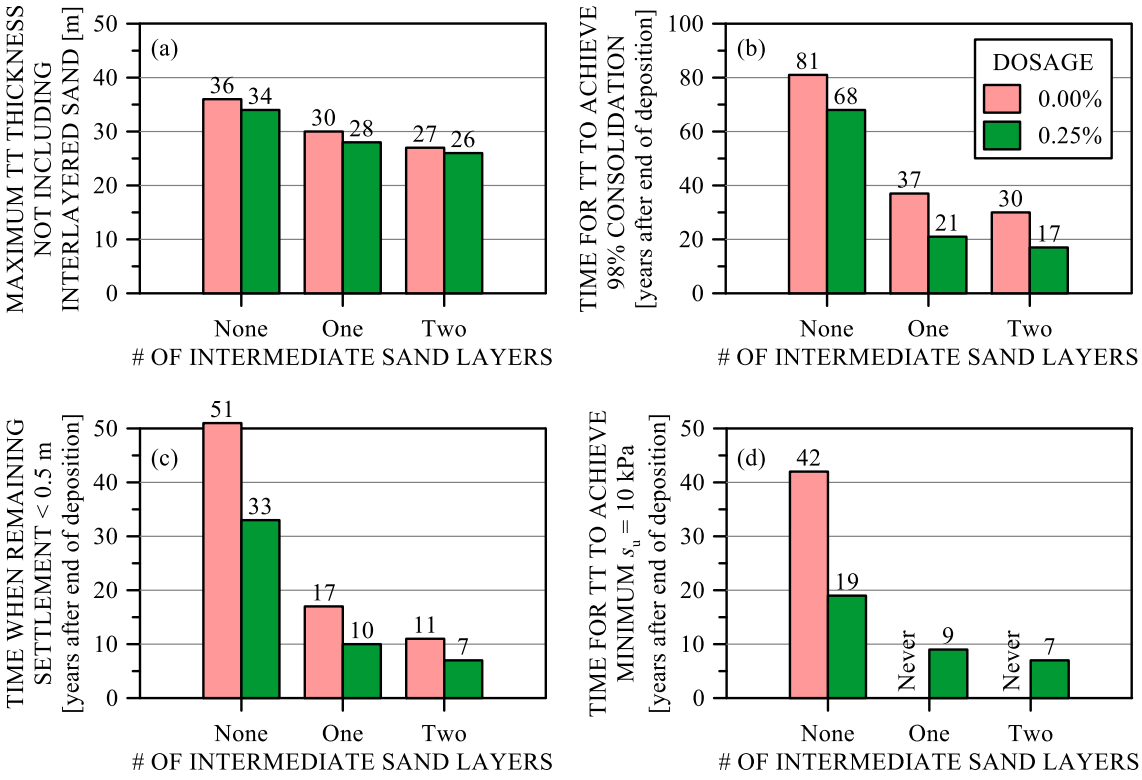


Figure 6. Effect of intermediate sand layers and silica amendment on consolidation performance

The results reveal that placement of intermediate drainage sand layers reduces even further the storage required to house the thickened material (Fig. 6a). They also reveal that the intermediate drainage layers shorten significantly the time required to consolidate the deposit (Fig. 6b) and achieve a minimum s_u = 10 kPa throughout the deposit (Fig. 6d). Note that the untreated TT never achieves this minimum strength throughout the deposit for the "one" and "two" intermediate sand layer cases, in which a 5-m sand cap is used.

7 FINAL REMARKS

This paper summarises the improved properties of silica-treated, thickened tailings, and shows examples of how silica might be employed to reduce time to closure. The behaviour of the deep TT deposit was predicted using a finite strain consolidation model and comparisons were made between untreated and silica-treated tailings. It was found that the silica-treated TT has a similar hydraulic conductivity profile (with varying void ratio) as the untreated material, but it is much stiffer and thus consolidates faster under a particular applied load. A perceived implication of this technology is the higher strength gain at moderate solids contents, allowing early placement of intermediate drainage layers to increase the rate of consolidation and/or of a final cap and reclamation material. Improvements that might be seen when using intermediate drainage layers for the treated case are also shown.

This technology has advanced as far as pilot testing for thin lift deposition. Some technical issues are yet to be addressed as the process is scaled up through prototype testing to full commercial operation (Sobkowicz, 2013). One of these is determining the silica dose to obtain the

right stiffness and strength at various levels in a deep deposit, and to develop sufficient erosion resistance to allow hydraulic placement of intermediate drainage layers or the final sand cap.

8 ACKNOWLEGMENTS

The authors would like to acknowledge DuPont Chemicals and Fluoroproducts (DuPont) for allowing the publication of the data, and Thurber Engineering Ltd. (Thurber) for allowing the preparation and presentation of this paper. Appreciation is expressed to all individuals involved in the careful execution of the laboratory tests at Thurber and DuPont. The authors also would like to thank Silawat (Song) Jeeravipoolvarn for the various fruitful discussions and valuable suggestions we had during execution of the consolidation analyses presented herein.

9 REFERENCES

Bartholomeueusen, G., Sills, G.C., Znidarcic, D., van Kesteren, W., Merckelbach, L.M., Pykes, R., Carrier III, W.D., Lin, H., Penumadu, D., Winterwerp, H., Masala, S. & Chan, D. 2002. Sidere: numerical prediction of large-strain consolidation. *Geotechnique*, 52(9): 639-648.

Energy Resources Conservation Board, ERCB. 2009. *Directive 074: Tailings Performance Criteria and Requirements for Oil Sands Mining Schemes*. February 3, 2009.

Gibson, R.E., England, G.L. & Hyssey, M.J.L. 1967. The theory of one-dimensional consolidation of saturated clays. *Geotechnique*, 17: 261-273.

Jeeravipoolvarn, S. 2010. *Geotechnical Behavior of In-Line Thickened Oil Sands Tailings*, PhD Thesis, University of Alberta, Edmonton, AB, Canada.

Jeeravipoolvarn, S., Scott, J.D., Chalaturnyk, R.J., Shaw, W. & Wang, N. 2008. Sedimentation and consolidation of in-line thickened fine tailings. In: *1st Intl Oil Sands Tailings Conference*, Edmonton, AB, December 7-10, 2008, pp. 209-223.

Moffett, R.H. 2010a. Treatment of fluid fine tailings with silica. In: *Proc. 14th Annual Conference on Tailings and Mine Waste*, Vail, Colorado, October 17-20, 2010, pp. 347-353.

Moffett, R.H. 2010b. Treatment of oil sands mature fine tailings with silica. In: Proc. 2nd Intl Oil Sands Tailings Conference, Edmonton, Alberta, December 5-8, 2010, pp. 383-391.

Moore, T., Zhang, C. & Sobkowicz, J. 2013. Laboratory investigation of the large strain consolidation behaviour of oil sands fluid fine tailings treated with DuPont Particlear™. In: *GeoMontreal 2013, 66th Canadian Geotech. Conference*, Montréal, Quebec, September 29 - October 3, 2013, 7p (*in press.*)

Pollock, G.W. 1988. *Large Strain Consolidation of Oil Sand Tailings Sludge*. MSc Thesis, University of Alberta, Edmonton, AB, Canada.

Proskin, S.A. 1998. A Geotechnical Investigation of Freeze-Thaw Dewatering of Oil Sands Fine Tailings. PhD Thesis, University of Alberta, Edmonton, AB, Canada.

Scott, J.D., Jeeravipoolvarn, S. & Chalaturnyk, R.J. 2008. Tests for wide range of compressibility and hydraulic conductivity of flocculated tailings. In: *61st Canadian Geotechnical Conference*, Edmonton, AB, Canada, pp. 738-745.

Shaw, B., Hyndman, A. & Sobkowicz, J. 2010. Consolidation projections for thickened tailings. In: *2nd Intl Oil Sands Tailings Conference*, Edmonton, AB, Canada, pp. 209-223.

Sobkowicz, J.C. 2012. *Oil Sands Tailings Technology Deployment Roadmaps*. Report to Alberta Innovates – Energy and Environment Solutions, June 19, 2012.

Sobkowicz, J.C. 2013. Developments in treating and dewatering oil sand tailings. In: R.J. Jewell, A.B. Fourie, J. Cadwell & J. Pimenta, *Paste 2013*, *16th Intl. Seminar on Paste and Thickened Tailings*, Belo Horizonte, Brazil, June 17-20, 2013. Keynote Paper, 16p (*in press.*)

Somogyi, F. 1980. Large Strain Consolidation of Fine Grained Slurries. In: *Canadian Society for Civil Engineering Conference*, Winnipeg, Manitoba, May 29-30, 1980.

Suthaker, N.N. 1995. *Geotechnics of Oil Sand Fine Tailings*, PhD Thesis, University of Alberta, Edmonton, AB, Canada.

Wong, R.C.K., Mills, B.N. & Liu, Y.B. 2008. Mechanistic model for one-dimensional consolidation behavior of nonsegregating oil sands tailings. *Journal of Geotechnical and Geoenvironmental Engineering*, 134(2): 195-202.

Yong, R.N., Siu, S.K.H. & Sheeran, D. 1983. On the stability and settling of suspended solids in setting pone. Part I. Piece-wise linear consolidation analysis of sediment layer. *Canadian Geotechnical Journal*, 20: 817-826.

Oil Sands – Tailings Treatment and Chemical Amendments

The compatibility of geotextiles with mature fine tailings

M.J. Chappel, E. Blond
CTT Group, St-Hyacinthe, QC, Canada

ABSTRACT: Geotextiles have been used in civil engineering applications since the 50's as a means to compensate for the lack of quality soils or to reduce costs in reinforcement, soil separation and filtration applications. Geotextiles are increasingly being used in mining for the same reasons (i.e. reinforcement for tailings dams), and for similar applications, including dewatering tailings. Although these has been some experience in oil sand tailings dewatering, their use remain relatively limited, in particular because of the very specific properties of oil sands mature fine tailings (MFT) and the difficulty to filter/dewater them. In order to investigate opportunities for geotextiles in MFT management or treatment, the characteristics of nine geotextiles have been investigated. Geotextiles studied includes nonwoven polyester, nonwoven polypropylene, and woven polyester monofilament. The laboratory tests focused on the physical characteristics of the geotextiles, including pore size measurement, permeability, mass per unit area, grab tensile peak melting temperature and thickness.

In addition to standard tests, the compatibility of the geotextiles with MFT was considered. MFT properties were characterized with a literature review, and a synthetic tailings formulation was developed and used in a gradient ratio test in conjunction with a geotextile, to evaluate the geotextile-soil combination, with the geotextile not demonstrating any blinding or piping effects. A chemical immersion test was also conducted on the geotextiles, using chemicals and the pH range that is normally found in MFT. After immersion, the grab tensile, mass per unit area and thickness were compared to the original geotextiles. The geotextiles were not significantly affected by the two month immersion.

1 INTRODUCTION

Geotextiles have many uses in civil engineering, including reinforcement to add strength to soil, separating soils with different grain sizes, and filtering water from soil. Their use for mining applications is growing, but the more complex and aggressive environment requires additional investigation and design.

The study outlines important considerations for geotextile product choice for tailings applications, specifically for filtration. Tests included the grab break strength, gradient ratio, filtration opening size, pore size, permeability, mass per unit area, thickness, polymer type and a chemical immersion test for durability.

Effective filters retain their designed flow throughout their service life, hold in place most of the soil particles, and are not damaged during installing or long term stress (Wolski and Mlynarek 2000). In this case, stress includes physical, thermal and chemical factors. There are currently many geotextiles with different fiber formulations and types, and manufacturing processes (most significantly woven or nonwoven, but also the thermal, mechanical or chemical

bonding process for nonwoven). All of these differences affect the pore size distribution, and therefore filtration properties (Bhatia and Smith 1996).

The objective of this paper is to outline the process for geotextile selection to match the requirements of MFT, as well as other tailings applications.

2 BACKGROUND

2.1 *Geotextile Filtration: Mechanisms Involved and Relevant Materials Properties*

Geotextile filters are used between a relatively fine grained soil and a material with larger pores, including filtering soil from entering the core of a drainage geocomposite. Geotextile filter requirements include particle retention, water permeability, clogging prevention, and resistance to both installation damage and long term chemical exposure. These properties are all specific to the intended application and site conditions.

It has been found that a geotextile in soil creates a more complex physical barrier which prevents small particles from passing through the pores (Figure 1). Initially, a thin layer of particles that are too large to move into the geotextile pores builds up on the surface of the geotextile. At the same time, a small amount of finer particles within this zone pass through the geotextile pores (Lafleur et al. 1989). This thin layer adjacent to the geotextile becomes the long term filter, not the geotextile itself (Mlynarek and Lombard 1997). This soil filter layer should prevent the migration of fines, and allow water to pass through. The best filter performance occurs when both the hydraulic conductivities of the geotextile and the geotextile-soil system are higher than the hydraulic conductivity of the soil to be filtered (Giroud 1996).

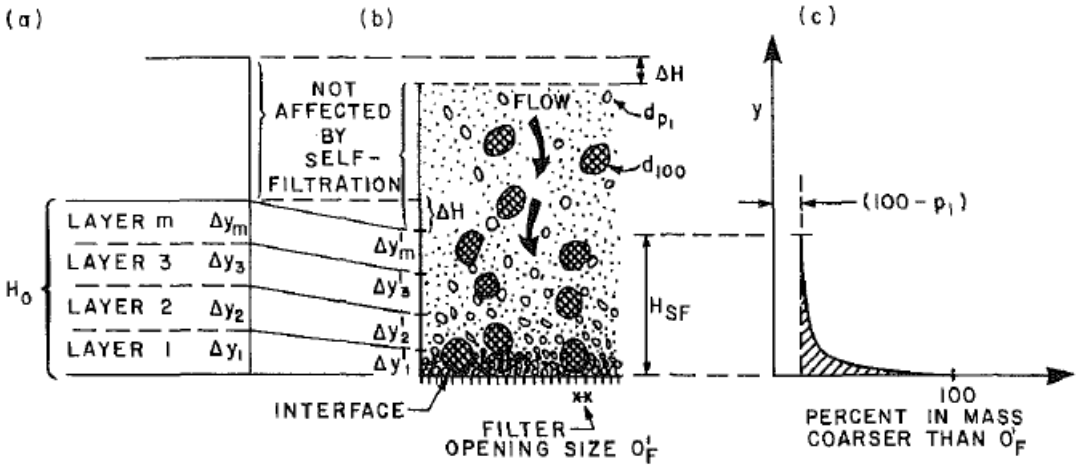


Figure 1. Soil filter created above a geotextile under downward flow: (a) before flow at initial soil height; (b) steady-state condition after the smallest particles have moved through the filter and larger particles have formed a filter layer over the geotextile; (c) particle distribution coarser than filter opening size (O'_F) (After Lafleur et al. 1989).

There are several mechanisms that prevent this balance of retention and passage. If fine particles block the pores of the filter soil layer located immediately upstream of the geotextile and block the passage of water, then the geotextile is blinded. Geotextile clogging is when particles are retained in the pores of the geotextile, or if there is chemical deposition in the geotextile pores that lead to a significant reduction of the permeability of the geotextile. Piping is the excessive migration of fines out of the protected soil, up to a point where the self-filtering structure cannot develop (Mlynarek and Lombard 1997). Therefore, optimal filter performance is a balance between a greater hydraulic conductivity of the geotextile and geotextile-soil filter than the original soil, and the elimination of piping after a short initial period of piping of small particles very close to the geotextile (Mlynarek and Lombard 1997). Thus, geotextile filters should be

chosen with a range of opening sizes that is small enough to retain an adjacent soil filter, but large enough to allow a small volume of adjacent fines to initially pass through the geotextile in order to create a self-filtering soil structure. This system is considered to be in equilibrium and effective (Mlynarek and Lombard 1997).

Although other filtration design criteria exist, it is recommended that Mlynarek (1998) is used due to its broad scope, which has three steps: determining the conditions of the site, such as the hydraulic conditions, chemistry, and the layout of the site. The second step is a soil investigation of basic properties (i.e., grain size analysis, Atterberg Limits, dispersion potential). From this information, the third step is selecting a suitable geotextile filter, which may include testing the geotextile-soil compatibility in the laboratory or the field.

In tailings filtration applications, a high percentage of the tailings particles are smaller than 2μm, therefore determining the percent dispersion of the soil is the next step in the decision making process. The percent dispersion is completed by comparing the sedimentation in water by double hydrometer, and by hydrometer using a mechanical agitation and a dispersing (ASTM 2005, ASTM 2007). If the dispersion is less than 50%, then it is recommended that the FOS of the geotextile should be greater than 50 μm. If the dispersion is greater than 50%, then a layered geotextile is suggested with a corresponding filtration test. The most relevant filtration test is Standard Test Method for Measuring the Filtration Compatibility of Soil-Geotextile Systems (ASTM 2012).

Filtration Opening Size (FOS) as measured by CAN-CGSB 148.1 No.10 is considered to be the most relevant geotextile filtration test to this application because it is measured using a technique that reflects actual field conditions, with soil particle movement initiated by dragging force generated by water flow.

Challenging soil environments for geotextiles include non-cohesive silt and dispersive clay, which accurately describe the type of particles found in mature fine tailings. When a specific soil is used in a unidirectional flow path (such as to dewater tailings), the Standard Test Method for Measuring the Filtration Compatibility of Soil Geotextile Systems can be used to measure particle retention and flow capacity in the system (ASTM Standard D5101 2012a). The soil of interest is placed over a candidate geotextile in a rigid wall permeameter, and a hydraulic head is applied over the system. Manometers located above and below the geotextile measure water pressure. The ratio between the hydraulic gradient at the soil-geotextile boundary to the hydraulic gradient further away, in a location considered to represent the undisturbed soil is reported as the gradient ratio. A gradient ratio of about 1 is an indication that the geotextile does not change the hydraulic conductivity of the soil. If the gradient ratio is greater than 1, the geotextile may be blinded or clogged. If the gradient ratio is less than 1 or decreasing, there may be excessive fines piping out of the system (ASTM Standard D5101 2012a). A very small gradient ratio can also indicate that the hydraulic conductivity of the system is extremely low.

2.2 *Polymer Compatibility*

Different physical, chemical and temperature environments have different effects on polymers. Degradation is a result of many processes, including oxidation and hydrolysis (Kay 2004). The main conditions that degrade geotextiles are: particle size distribution of the soils and granular angularity; pH of the surroundings; the presence of metal ions and/or oxygen; water content; organics; temperature; and microorganisms (Kay 2004).

Two common polymers used in geotextiles are polyester (PET) and polypropylene (PP). Polyester (PET) has a low rate of creep as well as good mechanical properties, and is thus widely used for reinforcement applications. However, it is sensitive to alkaline environments, especially under load (Rahman and Alfraro 2004). PP is generally resistant to acids, bases and many solvents. It also has a high tensile strength and stiffness (Rollin 2004).

Oil sands tailings are typically relatively neutral, with pH in the range of 8-8.5, but also have some hydrocarbons and may also include other chemicals used during the oil extraction process and/or components of the natural oil sands. The temperature of the tailings ranges depending on their depth and the season. The chemical composition and the potential effects on PET and PP are outlined below.

3 INVESTIGATION OF THE SUITABILITY OF NINE GEOTEXTILES FOR THE FILTRATION OF MFT

Figure 2 shows images of the geotextiles taken using a scanning electron microscope (SEM) and Table 1 shows the geotextile labels, their structures, and the geotextiles that are related by product line (and therefore manufactured by the same company). Note that there is one SEM image for each product line in Figure 2. These images show that the porosity of nonwoven geotextiles is greater than woven. In addition, the structure of the openings is different, with woven geotextiles have a slot-shaped opening, and the nonwoven geotextiles have open spaces with individual yarns creating complex obstacles for particle passage. The internal geometries may generate very different filtration behavior and therefore different design criteria.

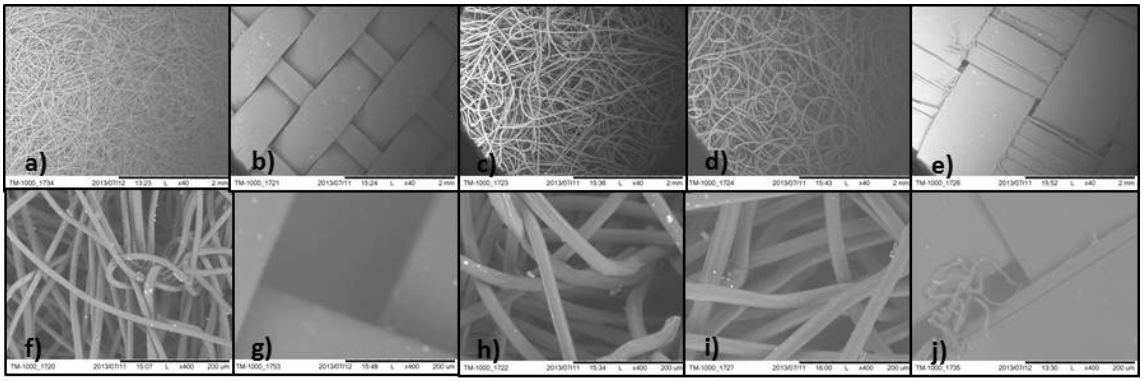


Figure 2. SEM images of geotextiles at 40x magnification: a) A; b) C; c) G, d) H; and e) I. SEM images of geotextiles at 400x magnification: f) A; g) C; h) G, i) H; and j) I.

The geotextiles in Table 1 were tested using the standard tests listed in Table 2. The method used to evaluate their chemical compatibility with the chemical environment typically found in MFT is outlined below. The grain size distribution of a sample of MFT was found and compared to the geotextiles using the criteria outlined by Mlynarek (1998).

3.1 *Chemical Compatibility Experimental Design*

When designing an immersion test to quantify compatibility, the chemicals, pH and temperature of the environment are considered. If desired, long term projected behavior can be modeled by completing the test at three or more elevated temperatures and using the Arrhenius equation to project behavior to the future, because polymer reactions depend on both temperature and time. In this case, long term behavior was not taken into account at this time.

Table 1. Geotextiles investigated.

Geotextile	Structure	Product Line/Manufacturer
A	Nonwoven, needlepunched	1
B	Nonwoven, needlepunched	1
C	Woven, monofilament	2
D	Woven, monofilament	2
E	Woven, monofilament	2
F	Nonwoven, needlepunched	3
G	Nonwoven, needlepunched	3
H	Nonwoven, needlepunched	4
I	Woven, multifilament	5

Table 2. Standard test conducted on geotextiles.

Test	Standard
Standard Test Method for Grab Breaking Load and Elongation of Geotextiles	ASTM D4632
Filtration Opening Size	CAN-CGSB 148.1 No.10
Standard Test Methods for Water Permeability of Geotextiles by Permittivity	ASTM D4491
Standard Test Method for Measuring Mass per Unit Area of Geotextiles	ASTM D5261
Standard Test Method for Measuring the Nominal Thickness of Geosynthetics	ASTM D5199
Standard Test Method for Melting And Crystallization Temperatures By Thermal Analysis	ASTM E794
Standard Practice for Immersion Procedures for Evaluating the Chemical Resistance of Geosynthetics to Liquids	ASTM D5322

The test was conducted in accordance with ASTM D5322 Standard Practice for Immersion Procedures for Evaluating the Chemical Resistance of Geosynthetics to Liquids. The first step to determining chemical compatibility is to find the common chemicals in the service environment, through a literature search or chemical analysis. The chemical concentration of tailings process water was found in Allen (2008) and presented in Table 3. Next, the general compatibility between the polymer resin and the chemicals was reviewed (Table 3). Note that this reference book reports 100% concentrations or an aqueous analyte dissolved to saturation, which is much greater than the reported concentrations in tailings.

The composition of the immersion solution was based on the amount of the chemical reported in the MFT, and its reported chemical compatibility (Pruett 2000). It was determined that the slightly caustic environment (pH=8 to 8.5), with ammonium hydroxide, calcium carbonate, naphthenic acid and sodium chloride may cause physical or mechanical changes in the polymer. The concentrations were: 14 mg/L ammonium; 2500 mg/L carbonate; 70 mg/L naphthenic acid and 700 mg/L sodium. The pH of the solution was controlled using 0.1M solutions of hydrochloric acid or 0.1M solutions of sodium hydroxide, as required.

Several chemicals were not tested that Allen (2008) reported and could potentially degrade the polymers (from Pruett 2000): VOCs (benzene and toluene), creosol, and bitumen. VOCs and creosol were not tested due to health concerns, and the very small concentrations in the tailings. Bitumen is not soluble in water so it would not be possible to mix with available equipment. In addition, PP and PET geotextiles have been used in the construction of asphalt roads since the 1970s, so bitumen and geotextiles are most likely compatible for the quantities of bitumen present in the MFT.

Since space in the immersion tanks was limited, only five representative geotextiles were tested; A, C, G, H, and I. The remaining products were manufactured by the same companies and are similar products to the ones tested. The temperature of the test was 21°C. The immersion test will be run for 4 months, and results are presented for the first month. The solutions were stirred using a peristaltic pump, and strategically placing the tubes in the tanks. The pH of the solution was measured once a week. If the pH was less than 8, then an appropriate volume of 0.1M solution of sodium hydroxide was added (the volume was determined by titration).

4 RESULTS

A range of geotextiles with different properties have been tested and compared to the conditions they may be exposed to in MFT. The melting peak temperature, mass per unit area, thickness, filtration opening size and permittivity are in Table 4. The peak melting temperature of samples A and B were characteristic of PET, and the melting temperatures of the remaining samples were characteristic of PP. The grab break results are presented in Table 5.

Table 3. Chemical concentrations measured in tailings process water from Allen (2008) and chemical compatibility for saturated solution or 100% chemical for immersion time periods of 1 month to 1 year. Data was collected from multiple sources, so the answers may not be consistent (Pruett 2000).

Chemical/Element	Concentration (mg/L)	Resistance of PET	Resistance of PP
Ammonia	0.03-14	Excellent resistance to 21°C Not recommended at 60°C	Excellent resistance up to 85°C
Asphaltenes	-	No data	No data
Benzene	0.6-6.3	Good to excellent chemical resistance/ not recommended at 21°C	Not recommended at 21°C Excellent chemical resistance up to 27°C
Bitumen	-	Probably good to excellent resistance	Good to excellent resistance to 21°C
Carbonate	200-2500	Good to excellent resistance to calcium carbonate	Good to excellent resistance to calcium carbonate to 120°C
Creosol M+O+P	-	Not recommended at 21°C	A 50-100% solution is not recommended for up to 66°C
Fulvic acid	-	No data	No data
Humic acid	-	No data	No data
Naphthenic acid	40-70, up to 130	Good to excellent resistance to 38°C	Good to excellent resistance to 38°C
Phenols	0.008	No data	No data
Sodium	100-660	Good to excellent resistance to sodium chloride	Excellent resistance up to 107°C, no stress, Excellent resistance up to 82°C, stressed
Toluene	1-3	Not recommended to good at 21°C	Not recommended to excellent at 21°C, slow degradation
Aluminum	0.07-0.5	No data	No data
Arsenic	0.006-0.015	No data	No data
Chromium	0.003-2	No data	No data
Copper	0.002-0.9	No data	No data
Iron	0.8-3	No data	No data
Lead	0.04-0.19	No data	No data
Nickel	0.006-2.8	No data	No data
Zinc	0.01-3.2	No data	No data

4.1.1 *Pore Size Compatibility with Grain Size Distribution*

The FOS (Table 4) is often used to determine if the geotextile is compatible with the soil (i.e., Mlynarek 1998). The FOS of the geotextiles ranged from 51 to 258 μm. Using Mlynarek's criteria, the MFT would require the installation of a multilayer geotextile filter. This may be a future step if necessary, after determining the gradient ratio (ASTM D5101) and observing MFT-geotextile behavior.

Geotextile A was tested with synthetic MFT (similar composition and properties to average MFT). A gradient ratio in the range of 0.13 was measured with a MFT-geotextile system hydraulic conductivity of 1.8×10^{-5} cm/s and a negligible amount of soil piped through the geotextile. The low gradient ratio was thought to be related to the very low hydraulic conductivity of the MFT, and the difficulty to obtain a planar, uniform flow through the soil in a downward direction. Although this system had satisfactory performance, different geotextiles perform differently depending on structure, mass per unit area, thickness, etc., and therefore more testing is required using a revised test method to better understand the filtration behavior.

Table 4. Results of standard tests conducted on geotextiles.

Geotextile (structure)	Melting Peak Temperature (°C)	Mass/Unit Area (g/m²)	Thickness (mm)	Permittivity (s^{-1})	Filtration Opening Size (µm)
A (NW)	249.5	298	2.14	0.55	51
B (NW)	249.3	520	3.52	0.25	73
C (W)	164.4	206	0.71	2.8	291
D (W)	163.9	271	0.80	0.37	220
E (W)	164.1	211	0.39	0.40	258
F (NW)	164.1	523	4.73	0.83	75
G (NW)	163.9	342	3.56	1.4	84
H (NW)	162.9	300	3.56	1.6	89
I (NW)	163.2	158	0.51	0.16	247.8

Table 5. Geotextile grab break results.

Geotextile	Machine Grab Break Strength (N)	Machine Elongation (%)	Cross Grab Break Strength (N)	Cross Elongation (%)
A (NW)	873	73	862	84
B (NW)	1434	75	1414	90
C (W)	1904	32	961	12
D (W)	1768	20	1749	9
E (W)	1919	22	1110	18
F (NW)	2080	83	2633	82
G (NW)	1408	71	1513	74
H (NW)	1131	94	1040	100
I (NW)	1041	22	1150	14

4.1.2 *Chemical Compatibility*

After an immersion period of 1 day, one month, and two months, the product thickness, mass per unit area, and elongation at break and strength at break were measured to test for changes in the samples. The student t-test was used to assess whether the geotextile properties have changed or remained the same from the initial properties. The results for the change in the maximum breaking load and elongation, thickness and mass per unit area are shown in Figure 3. Samples A and I are so far the most robust products. Only the elongation decreased in A, and Sample I experienced some swelling, but the other properties were consistent with the initial values. There were no changes in the mass per unit area of any of the geotextiles. The elongation in the machine and cross directions for samples A, C, G and H all decreased. There were generally no significant differences between the behavior of the one PET sample (A) and the remaining PP samples. In general after 2 months, the geotextiles are compatible with the immersion fluid.

4.2 *Investigation of MFT*

Grain size analyses were performed on MFT using the hydrometer methods in ASTM D422 and D4221 to determine the percentage of particles that are smaller than 2 µm, and the percent dispersion (Figure 5). It can be observed from Figure 5a that 72% of the particles are in the clay size range, i.e. < 0.045 mm (in the tailings terminology, clay size is smaller than in the Unified Soil Classification System (USCS)). This value is lower than the 90% value generally reported for MFT (Jeeravipoolvarn 2010), which highlights the necessity of either designing for a range of grain sizes, or installing different geotextile filters in different areas of the tailings storage area. The dispersion potential is 120% which indicates a dispersive soil. A sieve grain size analy-

sis was not performed because the soil grains behave differently when aggregated in flocs in water, and when the soil is dried.

The Atterberg Limits were tested using the ASTM Standard Test Methods for Liquid Limit, Plastic Limit, and Plasticity Index of Soils (ASTM 2010a). The liquid limit was measured to be 68%, the plastic limit was measured to be 31% and the plasticity index was 38%, which is a highly plastic soil, a characteristic of clay.

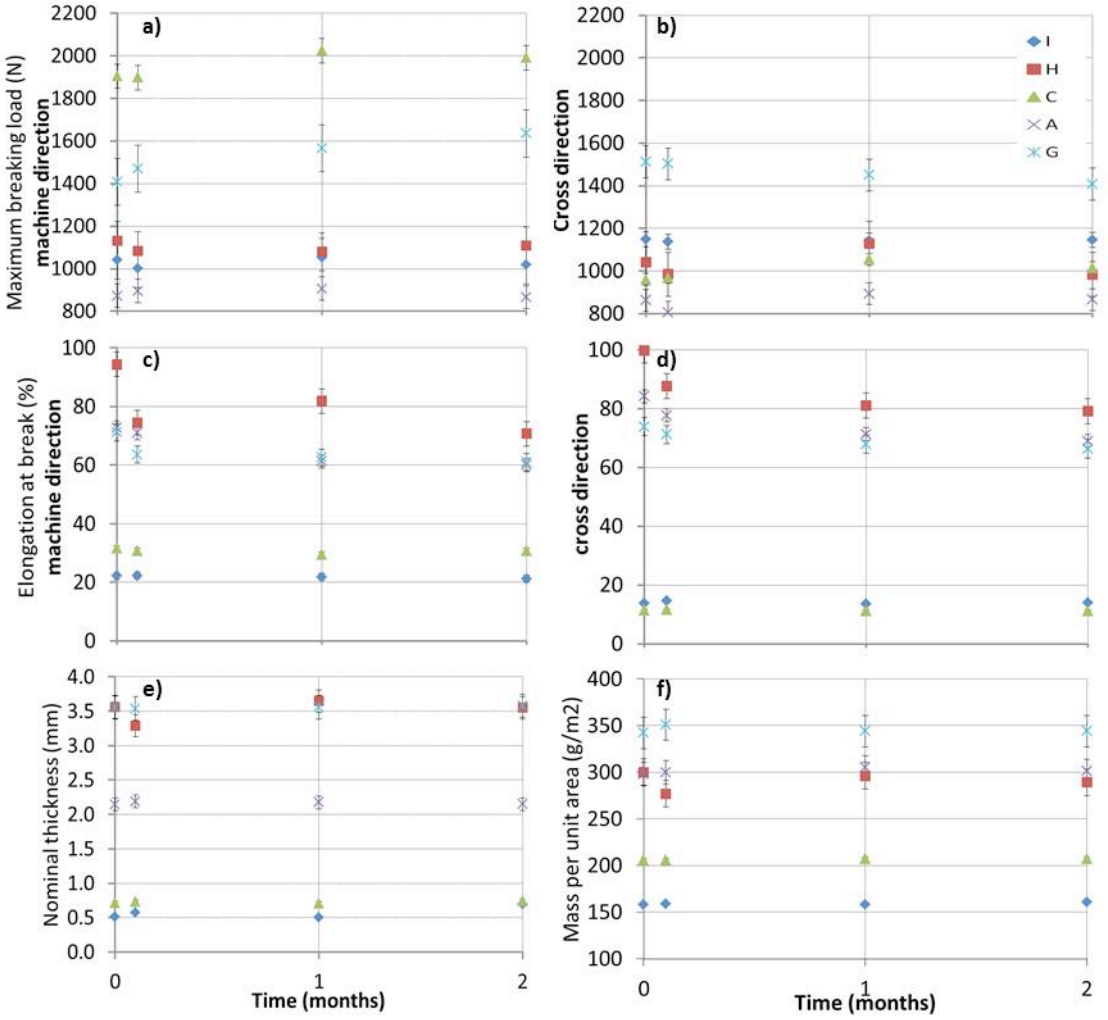


Figure 3. Measured geotextile properties over time: a) maximum break load in machine direction; b) maximum break load in cross direction; c) elongation at break in machine direction; d) elongation at break on cross direction; e) thickness; and f) mass per unit area.

5 DISCUSSION AND CONCLUSIONS

There are a wide variety of geotextile products with different structures on the market for various purposes. For tailings applications, there is a variety of site-specific requirements that may also change with time depending on how consistent the tailings properties are.

Filtration behavior of the tailings-geotextile system may vary from one geotextile to the other, and is difficult to measure with standard ASTM soil/geotextile filtration tests due to the low hydraulic conductivity of the tailings. On the other hand, the one geotextile that was tested had satisfactory filtration performance using a standard test. Therefore, further laboratory and field investigation is necessary to determine if a new filtration test is required for use with MFT and geotextiles.

Other geotextile design criteria for design that must be considered include seam strength and installation requirements (season of installation, are specialized installation methods necessary, etc).

The expected chemical environment does not seem to significantly affect the material properties of any of the geotextiles.

As a preliminary observation, filtration seems to be the most important concern to address when selecting a geotextile for dewatering MFT.

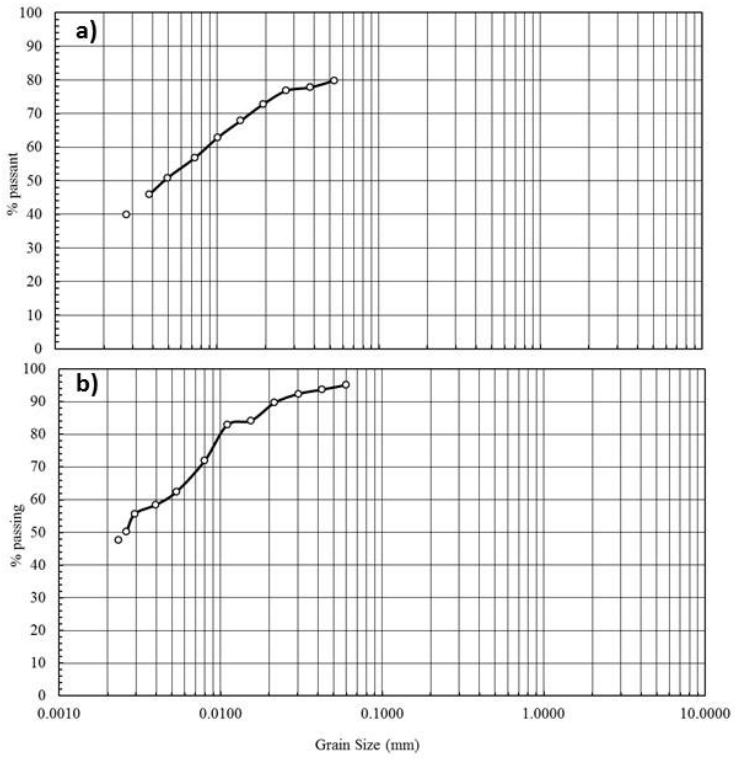


Figure 4. a) ASTM D422 hydrometer grain size analysis of MFT sample and b) ASTM D4221 grain size analysis

6 ACKNOWLEDGEMENTS

The authors would like to express appreciation for the testing completed by technicians at the CTT Group. Marianne Leroux assisted with conducting the one day immersion test and the analysis of the immersion test results.

7 REFERENCES

Allen, E.Q. 2008. Process water treatment in Canada's oil sands industry: I. Target pollutants and treatment objectives. Journla of Environmental Engineering and Science. 7:123-138.

ASTM Standard D422, 2007. "Standard Test Method for Particle-Size Analysis of Soils". West Conshohocken, PA, USA, 2007.

ASTM Standard D4221, 2005. "Standard Test Method for Dispersive Characteristics of Clay Soil by Double Hydrometer". West Conshohocken, PA, USA, 2005.

ASTM Standard D4318, 2010a. "Standard Test Methods for Liquid Limit, Plastic Limit, and Plasticity Index of Soils". West Conshohocken, PA, USA, 2010.

ASTM Standard D4491, 2009a. "Standard Test Methods for Water Permeability of Geotextiles by Permittivity". West Conshohocken, PA, USA, 2009.

ASTM Standard D4632, 2013. “Standard Test Method for Grab Breaking Load and Elongation of Geotextiles” . West Conshohocken, PA, USA, 2013.
ASTM Standard D5101, 2012a, “Standard Test Method for Measuring the Filtration Compatibility of Soil-Geotextile Systems” ASTM International West Conshohocken, USA, 2012.
ASTM Standard D5199, 2012b. “Standard Test Method for Measuring the Nominal Thickness of Geosynthetics”. West Conshohocken, PA, USA, 2012.
ASTM Standard D5261, 2010b. “Standard Test Method for Measuring Mass per Unit Area of Geotextiles”. West Conshohocken, PA, USA, 2010
ASTM Standard E794, 2012c. “Standard Test Method for Melting And Crystallization Temperatures By Thermal Analysis”. West Conshohocken, PA, USA, 2012.
ASTM Standard D5322, 2009b. “Standard Practice for Immersion Procedures for Evaluating the Chemical Resistance of Geosynthetics to Liquids”. West Conshohocken, PA, USA, 2011.
Bhatia, S.K. and Smith, J.L., 1996. Geotextile Characterization and Pore-Size Distribution: Part I. A Review of Manufacturing Processes”, Geosynthetics International, Vol. 3, No. 1, pp. 85-105.
Blond. 2005. Geotextile Opening Size Measurement techniques: AOS, FOS, O90, BBP…. TC221 / ASTM D 35 – Workshop: Geosynthetics in Hydraulic Applications, Wednesday, November 02, 2005
Giroud, J.P. 1996. “Granular Filters and Geotextile Filters.” Proceedings of Geofilters ‘96, Montreal, Quebec, Canada, 565-680.
Jeeravipoolvarn, S. 2010. Geotechnical behaviour of in-line thickened oil sands tailings. PhD thesis. University of Alberta, Edmonton, Canada.
Lafleur, J., Mlynarek, J., and Rollin, A. 1989. Filtration of Broadly Graded Cohesionless Soils. Journal of Geotechnical Engineering., 115(12), 1747–1768.
Mlynarek, J. 1998. Designing geotextile filters part I: Soil Filtration. Proceedings of the 51st Canadian geotechnical Conference, Edmonton, Canada.
Mlynarek, J. and Lombard, G. 1997. Significance of percent opening are (POA) in the design of woven geotextile filters. Proceedings of Geosynthetics ’97 Long Beach, USA.
Pruett, K.M. 2000. Chemical Resistance Guide for Plastics. Compass Publications La Jolla, USA. 680p.
Rahman, M. and Marolo, A. 2004. Degradation of polyester geotextiles in alkaline solutions under applied load. Proceedings of 57th Canadian Geotechnical Conference. Montreal, Canada.
Rollin, A. L. 2004. Long Term Performance of Geotextiles. Proceedings of 57th Canadian Geotechnical Conference. Montreal, Canada.
Vermeersch, O.G., Mlynarek, J., Desrochers, J.-F. 1997. Pore size distribution of non-woven geotextile filters under compression stress. Geosynthetics 1997, IFAI, Long Beach, USA.
Wolski, W., and Mlynarek, J. 2000. Geo Drains and Geo Filters – Retrospective and Future Trends. From Filters and Drainage in Geotechnical and Environmental Engineering Wolski, W. and Mlynarek, J. Eds. Rotterdam, p. 27-47.

Mature fine tailings treatment using inline flocculation and filtration

Cynthia Côté
Shell Canada Energy, Calgary, Alberta, Canada

Kristen Sibbel
Teck Resources Limited, Calgary, Alberta, Canada

Rory Heffel & Kevin Cafferata
Ledcor Environmental Solutions Ltd., Vancouver, British Columbia, Canada

Anoop Chengara & William Duttlinger
NALCO Champion., Naperville, Illinois, USA

Jochen Knauer
NALCO, Leiden, Netherland

ABSTRACT: The management and treatment of Mature Fine Tailings (MFT) from oil sands tailings facilities are of interest to the industry as a means to provide a valuable source of reclaimed water and dewatered fine solids. Filtration technology has often been dismissed for the treatment of MFT because of technical challenges including cloth blinding due to the bitumen residue. Flocculation of MFT prior to a filtration cycle, have shown the process to be viable. Ledcor Nalco Services (LNS) successfully demonstrated this with a trial plant that paired an inline flocculation system and a small scale TH Filter press. The results showed that inline flocculation produced cakes that were significantly higher in solids with significantly higher shear strength. Also found was that filter cloths would not foul over extended cycles when both cationic and anionic polymers were used in combination with periodic, in place, front cloth washing.

1 INTRODUCTION

The filterability of the oil sands tailings has often been overlooked because of the residual bitumen and the high fines material resulting in premature filter blinding and poor efficiency. However, it has been shown that coagulation and flocculation can improve the filterability of the MFT by increasing the hydraulic conductivity, particle sizes and permeability/porosity of the flocs. These are key success factors in applying pressure filtration to MFT dewatering.

Pressure filtration has often been placed in the high capital and operating costs category. However, filter presses have been successfully deployed at a large scale for use in treating mine waste at a cost that is competitive with alternative technologies. Pressure filtration is an appealing option for the oils sands industry considering the simplicity of the process and its ability to meet Energy Resources Conservation Board (ERCB) requirements regarding strength.

There is some documentation in the literature of filter press testing, but most of the reported results were utilizing a bench-scale filter press, in the order of a few liters per press only.

2 BACKGROUND AND OBJECTIVES

In the fall of 2012, Shell Canada Energy and Teck Resources Limited joined efforts with Ledcor Nalco Services to validate the effectiveness of using inline flocculation and pressure filtration to dewater MFT. The MFT samples were provided by Shell from the Atmospheric Fines Drying (AFD) site. The MFT were pumped from the Muskeg River Mine (MRM)'s External Tailings Facilities (ETF) with the same dredge used to feed the AFD plant.

The test program was based on two major components, the APN5 filter press from Technicas Hydraulicas (Figure 1) and the inline mixer Flocmaster™ V3 (Figure 2). The TH APN 5 press has two chambers that are 0.47m x 0.48m x 0.042m thick, for a total volume of approximately 19 liters.

Figure 2 shows a view from inside the pipe as well as a view of the complete device. The polymer solutions are fed through the impeller of the mixer.



Figure 1. TH APN 5.

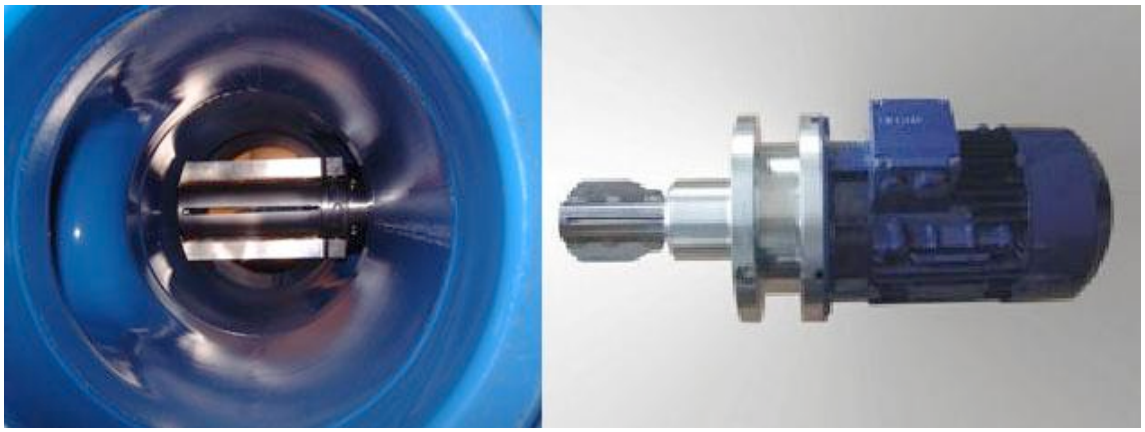


Figure 2. View of the FlocMaster™ V3 mixer blades showing slits for polymer injection (left) and the motor and paddle arrangement (right).

The three month experiment measured the effect of process variables had on the key performance indicators. The evaluation of the process parameters were first made with batch flocculated MFT. The Nalco Flocmaster™ was then evaluated separately to determine proper operating parameters to achieve adequate flocculation on a scale that is relevant for commercial scale-up. Once complete, the batch flocculation was replaced with inline flocculation and the filter press tests were re-run. Due to a substantial mismatch in throughput, it was not possible to feed the press directly with MFT flocculated inline using the Nalco Flocmaster™. Instead the MFT was flocculated inline and re-directed through a flexible hose to a second vessel connected to the press, where it was then pumped into the filtration chambers.

The primary objectives of this test program were to:

- Demonstrate the viability of using pressure filtration to dewater MFT,
- Demonstrate the benefit of using a dual flocculant program (anionic and cationic) over an anionic flocculant alone,
- Demonstrate the dynamic inline flocculation ability of the Nalco Flocmaster™,

– Demonstrate the benefit of combining these two technologies.

The process utilized to meet the objectives is shown in Figure 3 below as a block flow diagram.

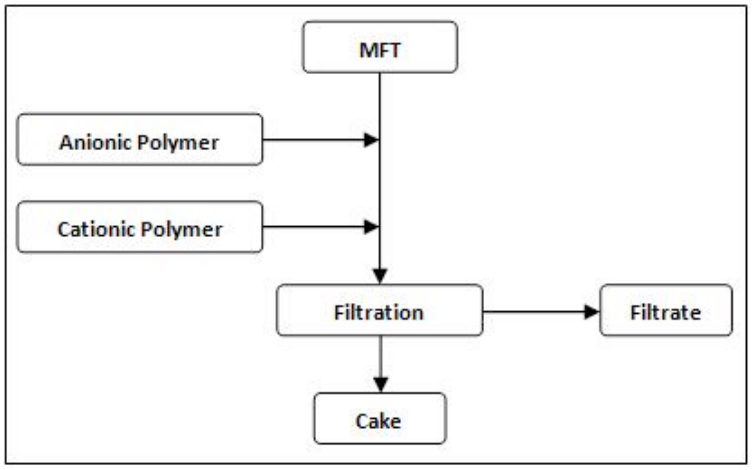


Figure 3. MFT flocculation and filtration block flow diagram.

Demonstrating the viability of using pressure filtration to dewater MFT required proving that the MFT could be dewatered to a trafficable state out of the press without additional drying or treatment and that the process was repeatable. For the first part of the test program batch flocculation was used. The MFT was mixed at 200rpm with an anionic polymer in a dosage range of 0.4-0.5kg of actives/dry tonnes of solids in a tank for 45 seconds. Upon completion of that cycle a cationic polymer was similarly introduced and mixed, in a dosage range of 0.2-0.3kg of actives/dry tonnes of solids. The addition of the cationic polymer increased size and integrity of the flocs and clarified the separated water by capturing fine particles, both properties being critical to minimize cloth blinding during the pressure filtration. The flocculated MFT was then pumped into the closed chambers of the filter press via a positive displacement pump. The pump fed the filter press continuously at a constant pressure of 10bar for a pre-determined press time. To demonstrate repeatability the process was repeated multiple times using a variety of press parameters.

For ease of polymer make-down, inverse emulsion polymers were used instead of dry polymers. The flocculation process works equally well using dry polymers, as separate jar tests have shown.

To demonstrate the dynamic inline flocculation ability of the Nalco Flocmaster™ tests were first done with the inline mixer only to identify the parameters needed for proper floc formation. The MFT was pumped through a 3 inch pipeline with the two inline mixers 4 meters apart. While the Nalco Flocmaster™ V3 is rated for flow rates from 2-100m^3/h, only the flow of 2m^3/h was tested due to the limited MFT supply at the test site. The first inline mixer added anionic polymer and the second added the cationic polymer. The flocculated MFT was piped to a retention tank for evaluation. Parameters were then adjusted until the desired floc was achieved.

To demonstrate the benefits of using inline flocculation in combination with pressure filtration the inline flocculated MFT was diverted to a holding tank via a 15m flexible 1.5” diameter hose. From there the flocs were pumped into the press. The same process parameters for the filter press and cake quality metrics that were utilized during the batch mixing study were applied.

3 RESULTS AND DISCUSSION

This section describes the parameters that were tested and the results obtained, it also shows some pictures of the process and products.

3.1 *Filter press process parameters with chemical batch mixing*

Below is the list of the filter press process parameters studied during the first part of the experiment and a summary of the results obtained.

3.1.1 *Cycle time*

The cycle time is the total amount of time between the filling of the filter press chambers and the chambers opening prior to the cake dropping. The filling time of the chambers is approximately 40 sec prior to the press time. The cycle time parameter was varied between 5 and 60 minutes.



Figure 4. Filter press cakes obtained from various cycle times.

The 10 minute cakes have a softer center which makes the cakes collapse on themselves when they drop from the press. As the cycle time is increased, the middle portion of the cake becomes more and more firm, as seen on the 30 and 60 minute cakes kept their form off the press. All cakes develop an outside crust that is very similar between the different cycle times.

Figure 5 shows the cake solids as a function of the cycle times and cloth permeability. Two different cloths with permeability of 60 and 120 cubic feet of air per minute per square foot (cfm) were compared. Results showed that cloth permeability does not affect dewatering performance, particularly when the filtration time is sufficient. The remainders of the tests were performed with the 60 cfm cloth.

Another key performance indicator is the strength of the cakes. Figure 6 below shows the correlation between the strength of the cakes and the cycle times. Cake strength was measured with a hand vane. While efforts were made to limit the measurement error there was a large degree of variation in the measurements depending on the shear history of the sample and the fault lines in the packing of the cake in the measurement cell. However, despite that there is still a clear trend towards increased shear strength with increased press time.

3.1.2 *Cloth life*

Cloth life is crucial to estimate the viability of the technology as it has a substantial impact on the operating and maintenance costs. To test the cloth life, the filter press was operated repeatedly using a 30min press time without any cleaning. After 36 cycles the filtration rate decreased due to fines plugging the cloth pores and cake release from the cloth needed manual assistance.

The cloths were then washed with water using a pressure washer for 1min without removing them from the press. The press continued on for another 24 cycles without any signs of degradation. The test demonstrated that front cloth washing is a viable means to remove fines from the pores of the cloth to increase the cloth life. Time limitations did not allow for testing cloth life to the point of irrecoverable failure. In other pressure filtration applications it is typical for cloths to last 600 to 1000 cycles before replacement.

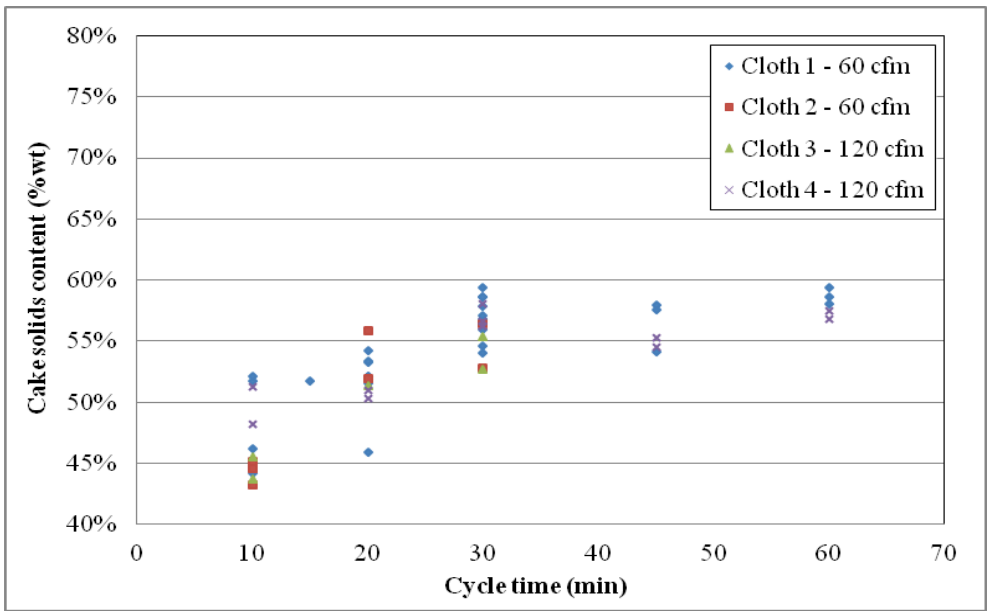


Figure 5. Cake solids content vs cycle time for the batch polymer mixing tests.

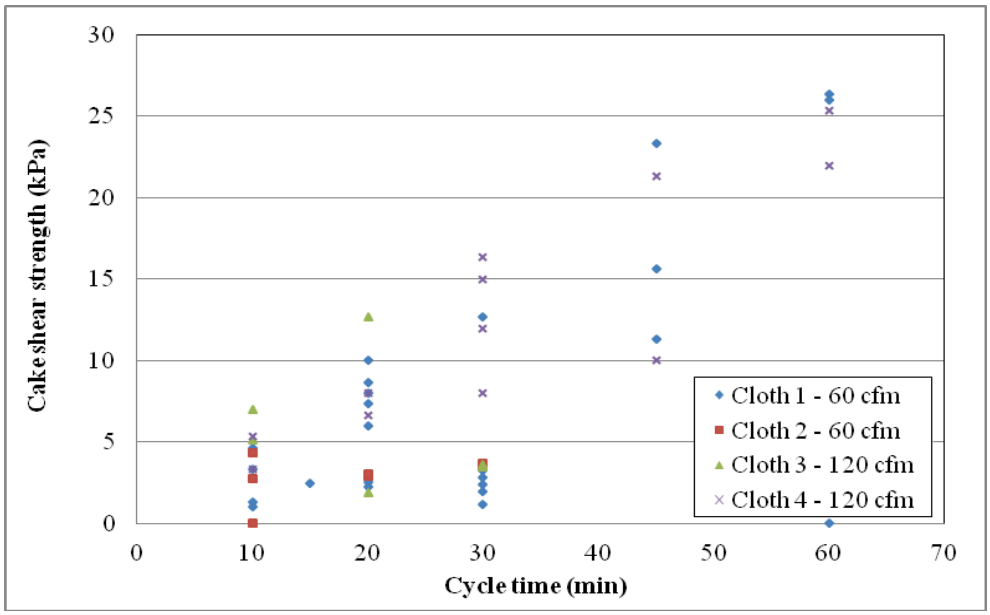


Figure 6. Cake shear strength vs cycle time for the batch polymer mixing tests.

Figure 7 and Figure 8 show how the solids content of the cake remained high and stable while the total suspended solids in the filtrate stayed low all through the cycles. The cake strength was relatively noisy; however this was most likely due to the limitations in the hand vane measurement. There was no overall trend evident.

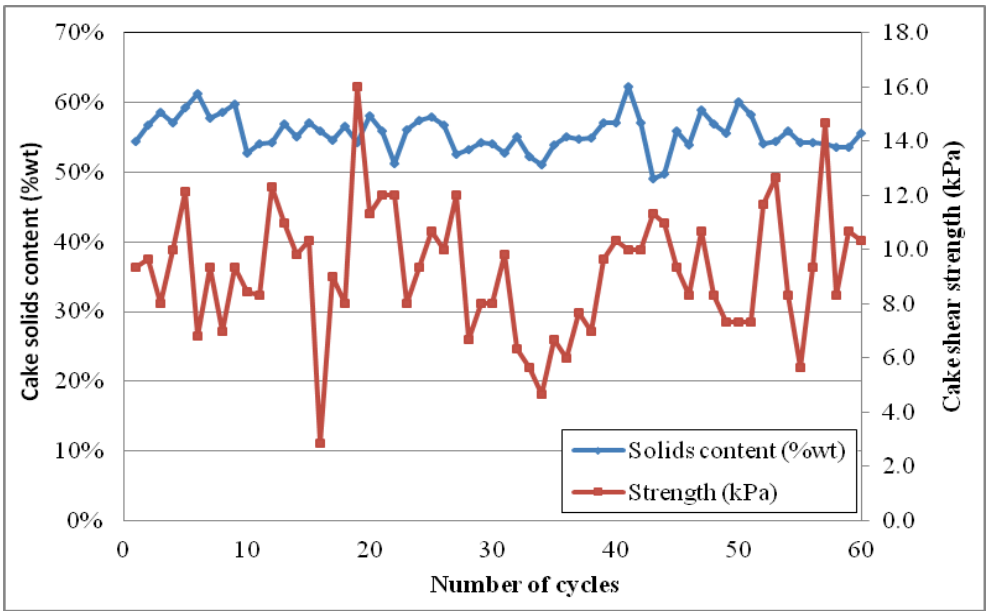


Figure 7. Cake solids content vs number of cycles using batch polymer mixing.

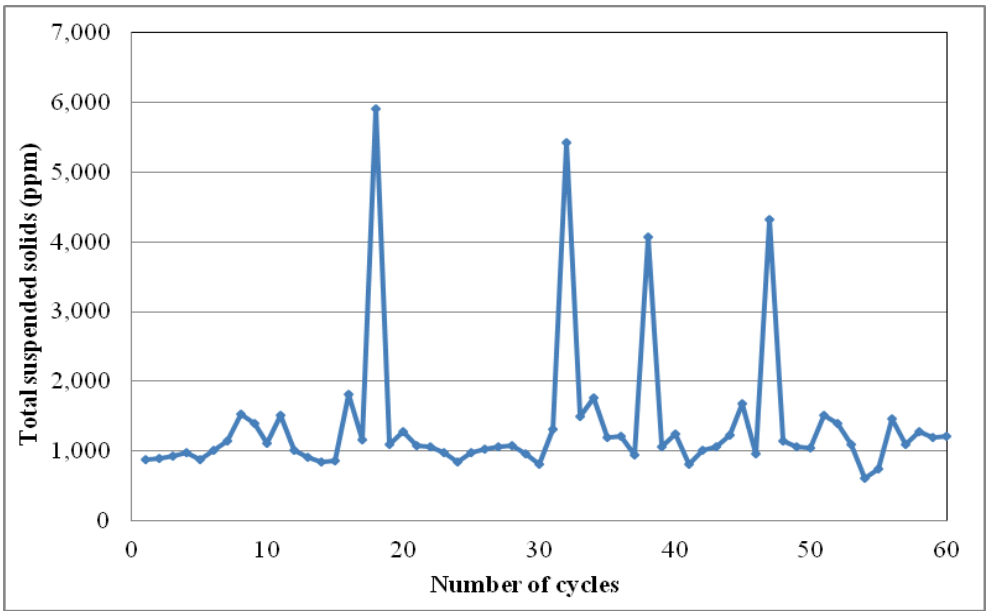


Figure 8. Total suspended solids in the filtrate vs number of cycles.

Figure 9 shows the state of the cloth after 60 presses, the bitumen migrated through the cloth and built up between the cloths and plates without negatively impacting dewatering.

3.1.3 *Anionic only polymer dosing*

To demonstrate the important role the cationic polymer plays, several runs were made using only anionic polymers. While a cake of acceptable solids content was produced, the release properties were substantially worse than cakes that used cationic polymer. As shown in Figure 9, the filter cloth fouled after only 6 presses.



Figure 9. Picture of cloths, plate side after 60 presses and after 6 presses without cationic polymer.

3.1.4 *Cake water release*

Often a second stream requires re-handling, which is the water released from the deposits after deposition. Some cakes were monitored over a period of 15 days, the solids content of the cake went from 58 to 75%wt without any water release. All the water that could be recovered by mechanical means from the cake had been released during the filtration cycle; further dewatering occurs by evaporation only.

3.2 *Inline flocculation*

The process parameters investigated with the Nalco Flocmaster™ were impeller rotation speed, polymer dosage, polymer concentration and the downstream pipe length. The operating parameters for the anionic dosing Flocmaster™ were adjusted first until the desired floc quality was achieved. The impeller speed was varied between 300-1200rpm for each mixer. The polymer dosages were varied between 440-1350g of dry polymer/dry tonnes of solids (g/t) for the anionic polymer and between 220-550g/t for the cationic polymer. Both emulsion polymers were made-down at 0.5 and 1%wt concentrations on a product basis for these tests, although the Flocmaster™ mixing capability has been proven even as high as 1.5-2%wt concentration in other commercial applications involving dry polymers of similar charge density and molecular weights. In commercial application, this capability is of great use in reducing the water requirement for polymer activation. Optimum flocculation conditions were observed to be 440-550g of dry anionic polymer/dry tonnes of solids, 220-330g of dry cationic polymer/dry tonnes of solids and between 600-700rpm of impeller speed for the MFT flow regime tested.

3.3 *Filter press parameters with chemical inline mixing*

The same process parameters studied using batch mixing were re-evaluated for pressing Flocmaster™ produced floc. The cake thickness was also increased from 36mm to 42mm, below are the results:

As was seen with batch mixed MFT, the solids content vs cycle time plot for the inline mixing shows solids content increasing with cycle time. However, Figure 13 shows that solids content was significantly higher for the same cycle time with the Flocmaster™ inline mixers than with a batch mode of flocculation. Figure 13 also shows that the solids content seems to reach a plateau after approximately 30 minutes.



Figure 10. Inline flocculation installations and flocculated MFT through clear pipe.



Figure 11. Filter press cakes obtained from various cycle times.

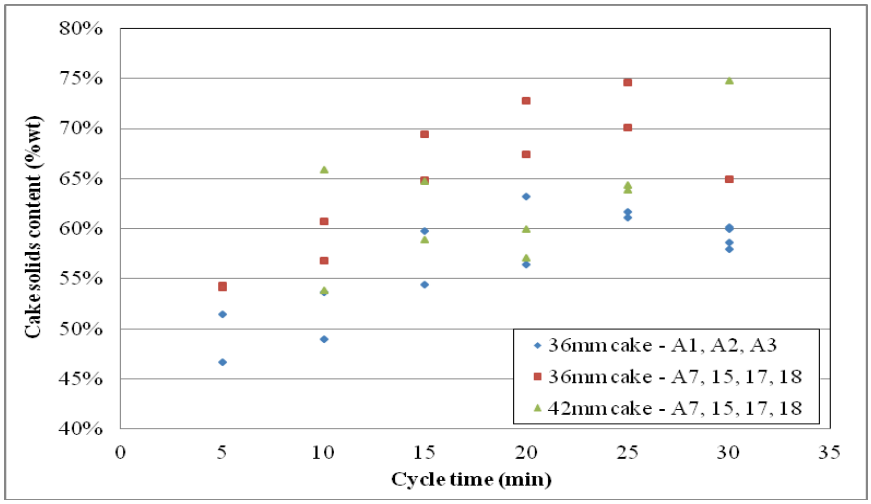


Figure 12. Cake solids content vs cycle time for the inline polymer mixing tests.

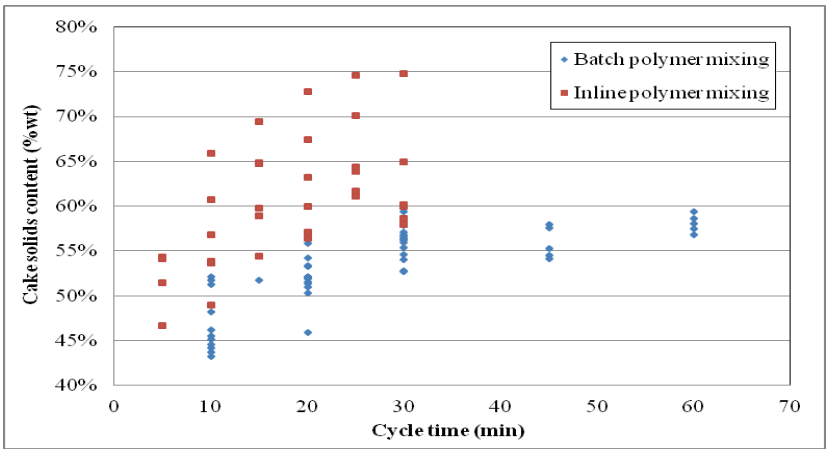


Figure 13. Comparison of cake solids content vs cycle time between polymer mixing options.

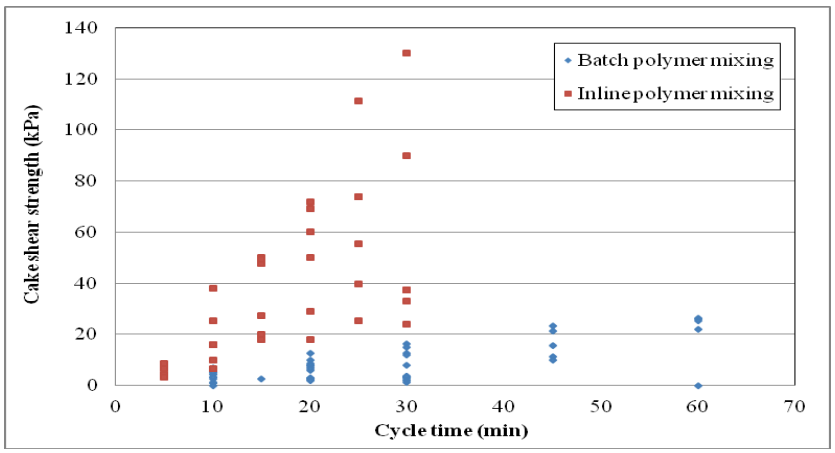


Figure 14. Comparison of cake strength vs cycle time between polymer mixing options.

Cake strength for Flocmaster™ formed flocs also followed the same trend as with batch mixing, but at significantly improved values for the same cycle time as seen in Figure 14.

To analyze the effect of remolding, some cakes were sheared with a hand held impeller for approximately 20 minutes at 550 rpm. The solids content was quantified and a rheometer was used to measure residual strength in the mixture. Figure 15 and Table 1. Cake process parameters and strengthTable 1 summarize the comparisons between the strength measurements. The cakes sheared were pressed under the same conditions.



Figure 15. Filter press cake before and after shearing.

Table 1. Cake process parameters and strength.

Sample ID	Cycle time	Anionic	Cationic	Unsheared	Sheared
	min	g/t*	g/t*	kPa	kPa
CK-IM-04-02	30	542	405	24.0	0.783
CK-IM-04-06	5	542	405	3.3	0.083
CK-IM-04-07	10	542	405	6.7	0.207
CK-IM-04-10	15	542	405	20.0	0.645
CK-IM-04-12	20	542	405	29.0	0.834
CK-IM-04-14	25	542	405	25.3	0.761
CK-IM-05-02	30	650	0	23.7	0.927
CK-IM-05-04	20	650	0	28.0	0.660
CK-IM-05-06	10	650	0	10.0	0.218
*grams of dry polymer/tonnes of dry solids.					

4 KEY FINDINGS

1. The performance of the small scale system used in this trial and the proven nature of both inline flocculation and pressure filtration at a large scale, give a high level of confidence that this process will work at full scale.
2. Filter press cakes exceed shear strength limit set in Directive 074, immediately upon release. This results in a substantial saving of pond reclamation time.
3. For pressure filtration, flocs produced using the Nalco Flocmaster™ produces flocs that outperform those generated using batch mixing.
4. Cationic polymer is critical to fines capture and cloth life. Anionic and cationic polymer used sequentially significantly improves filterability compared to anionic polymer alone.
5. Blinding of the cloth by fines can be avoided with appropriate MFT flocculation and periodic front cloth washing.

5 REFERENCES

January 2013. *Filtered, Paste and Thickened Tailings Course*. Golden. Colorado School of Mine.

BGC Engineering Inc., 2010. *Oil Sands Tailings Technology Review*. Oil Sands Research and Information Network, University of Alberta, School of Energy and the Environment, Edmonton, Alberta. OSRIN Report No. TR-1. 136 pp.

Xu, Yuming. Filterability of oil sands tailings. *Process Safety and Environment Protection* (86 (2008)): 268-276.

Alamgir, Aurangzeb. Al-PAM assisted filtration system for abatement of mature fines tailings. *Chemical Engineering Science* (80 (2012)): 91-99.

Heffel, Rory. Ledcor Nalco Services (LNS). *Shell Pilot Project Report.* November 23, 2012.

Effect of coarse solid addition on the dewatering of mature fine tailings

S.G. Thakurta & T. Fenderson
Kemira Chemicals Inc, Edmonton, AB, Canada

A. Mahmoudkhani, K. Stewart & P. Watson
Kemira Chemicals Inc, Atlanta, GA, USA

ABSTRACT: Dewatering of mature fine tailings (MFT), clay and silicate particles measuring less than 44 μm in diameter, is one of the major concerns of the oil sands mining industry. There are several technologies available for capturing MFT and dewatering the agglomerated particles, and one such family of treatments involves the use of polymeric flocculants. Once flocculated, MFT dewatering can be accelerated through mechanical processes like centrifugation or filtration. However, the properties of mature fine tailings are extremely variable from site to site, and even pond to pond. For example, the MFT may contain a high concentration of ultrafine particles with diameters below 1 μm, or a high clay content, factors which further complicate an already difficult dewatering process. This paper deals with the treatment of MFT samples with a very high concentration of fine clay particles, which is estimated from a high methylene blue index.

Addition of coarse particles has been examined in treating these MFT samples. In this study we show that in order to effectively dewater MFT by centrifugation or filtration it is important to choose the right combination of flocculants and coarse solids. It was observed that when nonionic polymers and coarse solids are added, a very low moisture residue is obtained after centrifugation. However, the centrate quality is poor, showing that the treatment is not effective in capturing fines. When a low-charge high molecular weight polymer and medium sand are used instead, the centrate solids are very low and the moisture content in the centrifuge cake is also improved. Similar dewatering enhancements are also observed in filtration of the MFT sample.

1 INTRODUCTION

1.1 *Background*

During bitumen extraction from oil sands through mining, large amounts of water are slurried with ore to release bitumen. As bituminous froth is collected, coarse sand settles to the bottom of the separation vessel and the middlings, which contain fines and residual bitumen, go to a secondary flotation process. The slurry remaining after this step is pumped into large tailings ponds where the larger particles settle rapidly are used to build dykes (FTFC, 1995). Initially, the finer solids sediment and a layer of clear water forms at the top of the pond. When the fines concentration below the water layer exceeds 15% by weight, the settling becomes hindered and the settling rate is greatly diminished. When the suspension solids concentration reaches at least 30% by weight, the suspension is termed as mature fine tailings (Masliyah et al. 2004), and sedimentation becomes almost nonexistent. Managing this tailings stream is the biggest challenge in the oil sands mining process.

In 2009, Alberta Energy Regulator (AER, formerly ERCB) set certain guidelines for management of oil sands tailings through Directive 074. The Directive requires reduction of fine tailings through fines capture in dedicated disposal areas. The other important requirement in the Directive is the conversion of tailings into trafficable deposits which will be ready for reclamation within five years of deposition. There are several remedies were introduced for tailings

treatment, e.g. different additives like gypsum, lime, are carbon dioxide are added to the tailings, to produce "dry tailings" for stacking and dewatering of mature fine tailings (Xua et al, 2008). Centrifugation is also a viable technology for tailings dewatering and land reclamation (Mikula et al. 2009). However, these strategies are yet to be commercialized in industry.

In finely divided suspensions like mature fine tailings, solid-liquid separation is often facilitated by a chemical treatment like flocculation (Swaska et al. 2000). In flocculation the suspended fine solids are destabilized and aggregates of fines are formed that increase the settling rate and improve dewatering. However, the dewatering is also dependent on the structure of aggregated particles. In tailings, water is tied up in the pore spaces of the sand, silt and clay. The objective is to remove the trapped water from the interstitial spaces so that the dewatered tailings are dry and stackable and can be transformed into reclaimable land.

It has been observed that during tailings treatment with flocculants the dewatered solids have a limiting moisture content remnant in them. Somasundran et al. (1973) have shown improvement in the dewatering properties of phosphate slimes with addition of coarse solids. The coarser particles create fissures and channels in the slurry structure for faster dewatering (Rao, 1980). Preliminary flocculation studies show that addition of flocculant improves the clarity of the supernatant and reduces the solid concentration in the supernatant. However, the moisture content in the centrifuge residue only is decreased marginally.

In this study coarse solids are used as extenders during flocculation of mature fine tailings in order to improve dewatering and consolidation of the tailings. Additionally, coarse solid addition is investigated as an option to improve the moisture content in the dewatered tailings obtained from centrifugation.

1.2 *Materials used*

Samples of mature fine tailings (MFT-1) and oil sands process affected water (OSPW) were received from a major oil sands producer in the Athabasca region. The MFT-1 sample was analyzed for bitumen-solids-water (BSW) content and its methylene blue index was determined for relative clays content.

Table 1. Characteristics of MFT sample used in this study.

Bitumen Content wt%	**Solids Content wt%**	**Water Content wt%**	**MBI meq/100g**	**Calculated Clay Content wt%**
0.64	18.00	81.36	16	100

Particle size determination revealed the MFT-1 sample having higher fine content, with D_{90} of 13.9 micron, than other MFT samples, with D_{90} of about 44 micron, previously tested (see Figure 1). The MFT sample was further diluted to 10% solids using OSPW and the resulting slurry was used for experimentation. Various grades of sands (quartz) were used as extenders to improve MFT dewatering upon flocculation. Particle size distributions of the solids were determined and graphically presented in Figure 2.

The polymer flocculants used for treatment of MFT samples were of commercial grade (Kemira) with characteristics given in Table 2.

Table 2. Characteristics of anionic flocculants used in this study.

Flocculant	**Description**
Polymer A	No charge, high molecular weight
Polymer B	Low charge, ultra high molecular weight
Polymer C	Medium charge, very high molecular weight
Polymer D	High charge, medium molecular weight
Polymer E	Medium charge, high molecular weight

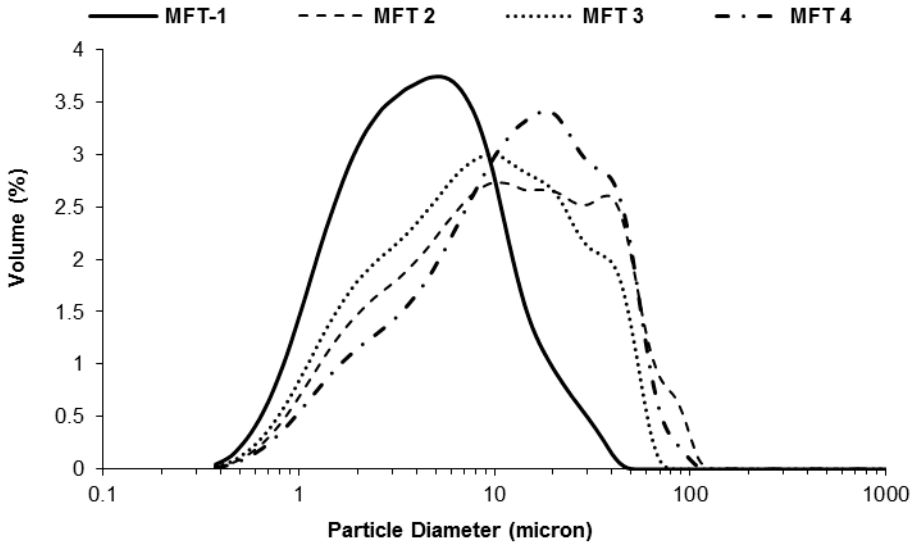


Figure 1. Particle size distribution of MFT sample used in this study (MFT-1) compared to other MFT samples.

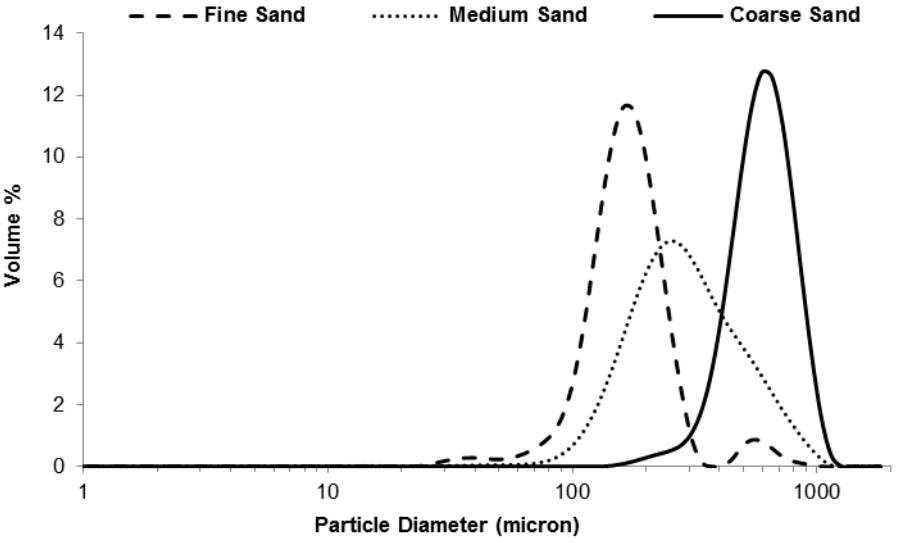


Figure 2. Particle size distribution of sand samples used in this study.

1.3 *Methods*

In order to determine consolidation and dewatering of tailings, the MFT samples were treated with anionic polymeric flocculants listed in Table 2 in presence and absence of coarser solids. The samples were centrifuged using a SORVALL GLC-2B centrifuge. The solids content in the supernatants and the moisture content in the settled beds were measured by oven drying at 105ºC. The dewatering properties of the treated tailings samples were determined by capillary suction time method described in Section 2.2.1 and the particle size distributions of coarse solid samples used were measured using the method delineated in Section 2.2.2.

1.3.1 *Capillary Suction Timer*

The dewatering properties of the treated and untreated tailings samples were measured using capillary suction time (CST) method. The method followed is described in Standard Method APHA 2710 G. CST measurements were performed using a capillary suction timer (Venture Innovations, California, USA). The CST is defined as the time taken by the water in the sample to traverse between the two radial positions of a Whatman No. 5 filter paper due to capillary suction. The samples having better dewatering properties will have lower CST value. Each measurement was conducted in triplicates and the mean value of the measurement is reported as the CST value for that particular sample.

1.4 *Particle size distribution*

Particle size distributions (PSD) were determined with a Beckman Coulter LS 230 laser diffraction particle size analyzer, which measures the angular dependence of scattered light (mainly in the forward direction). Samples were dispersed in the fluid module of the unit without additional chemical dispersants. Particle size distributions were computed as equivalent-sphere size distributions based on Mie scattering and Fraunhofer diffraction formalisms applied to the scattering data.

The optical constants used for these computations were a complex refractive index of 1.5295, 3.000i for the solids and a real refractive index of 1.3300 for the continuous phase. Measurements were taken during each test at 60, 120, 180, 240, and 300 seconds after addition of the sample to the diluent under continuous agitation. This procedure allowed us to assess whether a steady-state size distribution had been achieved. Typically we used the size distributions after 180 sec of mixing for comparisons, since steady state was achieved by this time.

1.5 *Pressure Filtration*

The effect of coarse solids addition on pressure filtration of MFT was also evaluated. MFT was first slurried with coarse solids and followed by the addition of flocculant and a coagulant (to improve filtrate clarity). The slurry was passed through a filter cloth at a pressure of 16 bar for a maximum pressing time of 40 minutes. The resulting filtrate and filter cake were analyzed for moisture content by oven drying at 105 °C and compared to experiments without treatment.

2 RESULTS AND DISCUSSIONS

2.1 *Effect of flocculation on the centrifugation of mature fine tailings sample*

During preliminary screenings, a dosage of 1500 ppm of polymer flocculant was applied in order to obtain highest supernatant clarity. MFT was treated with flocculants and centrifuged. Four different polymer flocculants as described in Table 2 are used for this experiment. Figure 3 demonstrates the total solids content in the centrate and centrifuge bottoms. These results serve as benchmarks to determine whether an improvement can be achieved upon addition of coarser solid additives.

Polymer D has higher charge than A, B and C, while polymer A having the minimum charge. It is observed that the polymer A with the lowest charge provides highest solid content in the centrifuge bottoms but has a poor centrate quality due to residual solids. Higher centrate clarity was only obtained when MFT was treated with polymer B and C.

2.2 *Dewatering properties of polymer treated tailings*

The dewatering properties of the polymer treated and untreated tailings determined by Capillary Suction Timer (CST) method and data are summarized in Table 3. It was observed that treatment with polymer A and C showed faster dewatering properties than with polymer B and D. This may be attributed to differences in flocs structure and viscosity of released water. Denser solids packing and higher water viscosity can significantly reduce dewatering rate.

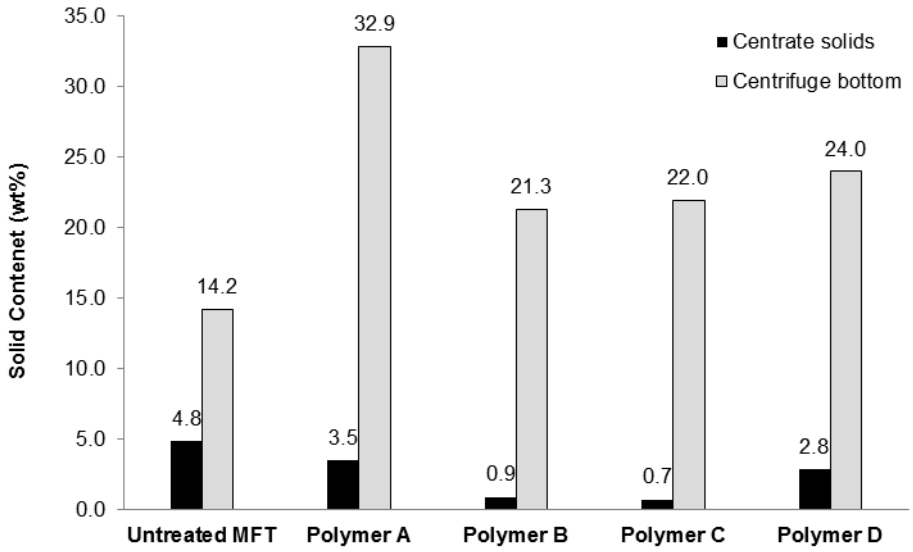


Figure 3. Solids content in the centrate and centrifuge bottom for untreated and treated MFTs.

Based on charge density and structure of the polymer, it's electrostatic and dipole-dipole interactions with solid surface determine the floc geometry and packing of flocculated solids. When excess polymer is used (overdosing), non-adsorbed polymer remains in water phase and increases its viscosity. It is therefore necessary to determine optimal dosage for each flocculant by which faster dewatering can be achieved. For polymer C, faster dewatering was obtained using 1000 ppm of flocculant (see table 4).

Table 3. CST values for untreated and treated MFT

Samples	Untreated	Polymer A	Polymer B	Polymer C	Polymer D
CST (sec)	414.3	294.7	593.9	246.3	406.8

Table 4: CST values for MFT treated with polymer C

Polymer Dosage	500 ppm	750 ppm	1000 ppm	1250 ppm	1500 ppm
CST (sec)	282.8	172.2	135.6	256.2	246.3

2.3 *Effect of coarse solids addition on dewatering of flocculant treated tailings*

The effect of different coarse particles on the centrifugation of the mature fine tailings were observed by comparing the total solids and CST data with those for polymer flocculated tailings. The fine, medium and coarse sands were added at different ratios to the MFT samples before treatment using polymer flocculants. The sand to fine ratio was varied from 0.25:1 to 1:1 while flocculant dosage was kept at 1500 ppm for simplicity.

2.3.1 *Addition of Coarse Sand*

In a set of experiments, the MFT-1 sample was mixed with coarse sand (with D_{50} of 629 micron) at varied proportions (by weight of dry solids) and flocculated with polymers A, B, C and D and the flocculated tailings were centrifuged. The percentages of solids in the centrate and bottom product obtained after centrifugation were measured using oven-drying method at 105 ºC. Figures 4 and 5 show the variation of percentage solids in the centrifuge bottom and centrate with the variation in the ratio at which the coarse sand was mixed with MFT-1 samples. For treatments with polymer A, solid content in the centrifuge bottom were improved, however, centrate quality reduced at higher sand loadings. It was also found that, with coarse sand the centrifuge bottom was not improved when polymer B, C and D were used for flocculation. The coarse sands might be too large to allow the complete adherence of the fines by flocculation and there were no major interactions of the polymer to the surface of the sand.

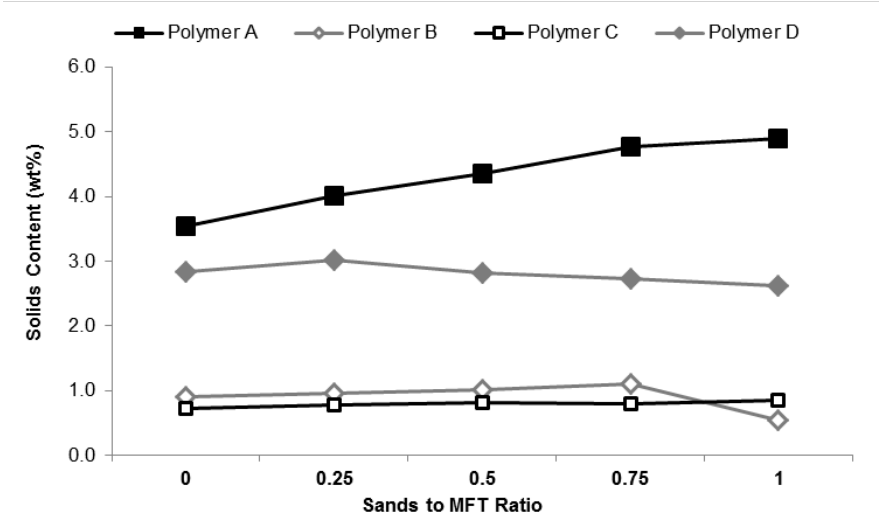


Figure 4. Percent of solids in centrate from centrifugation of MFT treated with different polymer flocculants and coarse sand.

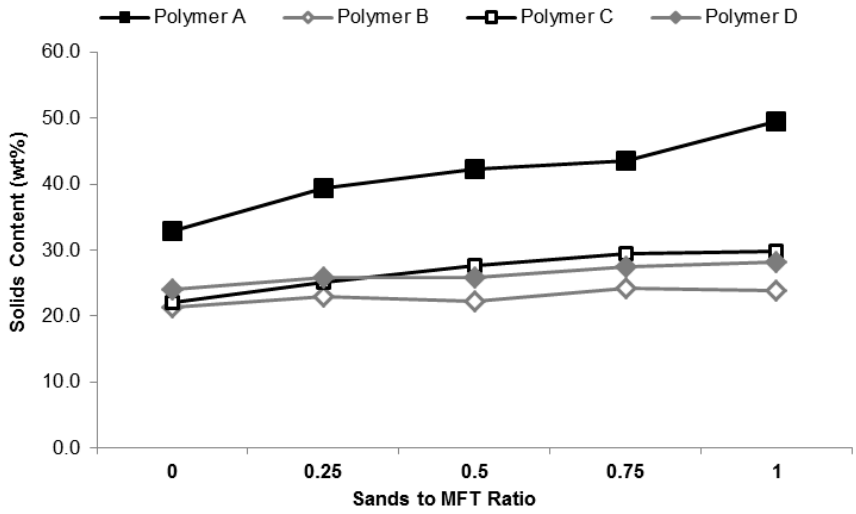


Figure 5. Percent of solids in the settled bed obtained from centrifugation of MFT treated with different polymer flocculants and coarse sand.

2.3.2 *Addition of Medium Sand*

Medium sand (with D_{50} of 291 micron) at varied proportions (by weight of dry solids) was added along with a specific dosage of polymer flocculant to the MFT sample and the mixture was centrifuged. The percentages of solids in the centrate and bottom product obtained after centrifugation were measured using oven-drying method at 105 ºC. The percentage solids in the centrate and bottom were plotted as a function of sands to MFT ratio in Figures 6 and 7.

It was observed that the percentage solids in the centrifuge bottom have increased after addition of medium sand. However, the percentage solids in the centrate did not change for all combination of polymers and medium sand ratios. It was interesting to observe that the non-ionic polymer A has a limiting effect on the centrate solids. Centrate clarity was reduced with polymer A in combination with medium sand sand when compared to no sands added. Anionic polymers and medium sand show improvement in the solid content in the centrifuge bottom and while centrate clarity remained unaffected. The best results are obtained with polymer C which has medium charge and high molecular weight. Polymer D with very high charge improves the solids content in the bottom but does not improve the centrate quality to a great extent. The

trend observed with different polymers and medium sand in centrifugation is that the anionic polymers, both high molecular weight and medium charge, provide best results in combination with medium sand in improving the solid content in the centrifuge bottom.

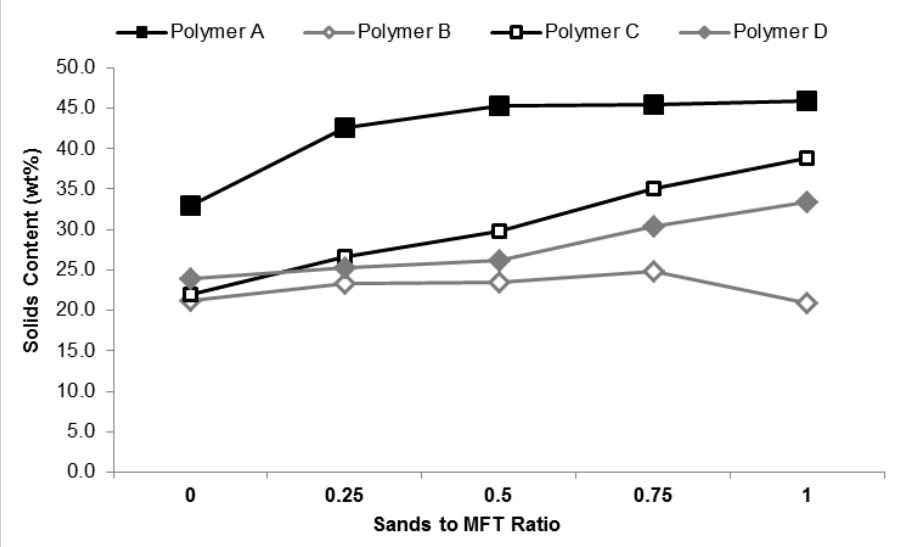


Figure 6. Percent of solids in the settled bed obtained from centrifugation of MFT treated with different polymer flocculants and medium sand.

2.3.3 *Addition of Fine Sand*

In order to prove our hypothesis that the sands do not have strong interactions with the polymer flocculant and clay fines, we chose the best performing flocculant, polymer C, and use fine sands separated from hot water extraction experiments which has a smaller particle size distribution (D_{50} of 174 micron) than the medium sand. We observed similar results as medium sands with the fine sands combined with polymer C. There was an improvement in the centrifuge bottom solids with addition of fine sands but at slightly higher ratio of 0.75:1 or 1:1. Despite the improvement in centrifuge bottom solids there was no significant effect on the centrate quality with the fine sands as shown in Figures 8 and 9.

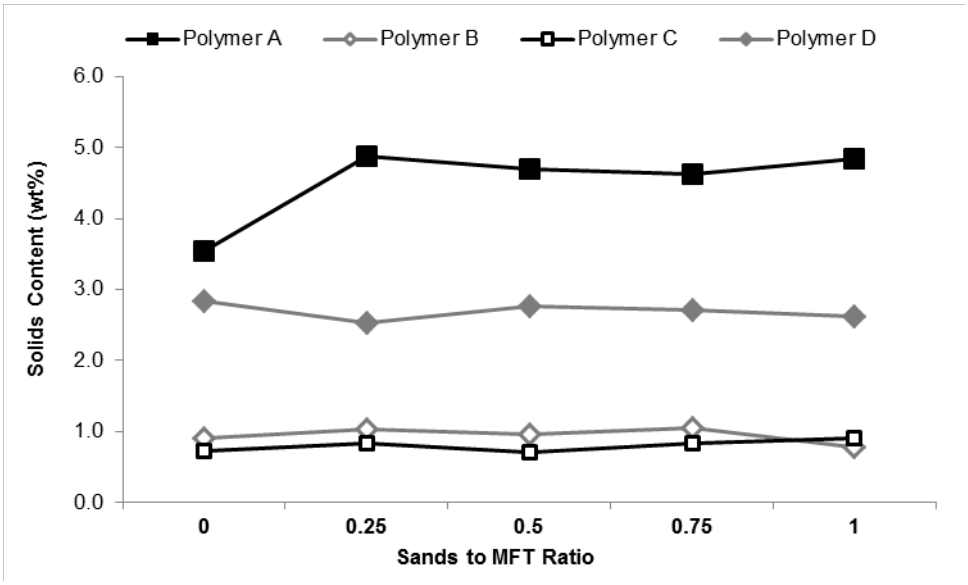


Figure 7. Percent solids in centrifuged tailings treated with different polymeric flocculants and medium sand.

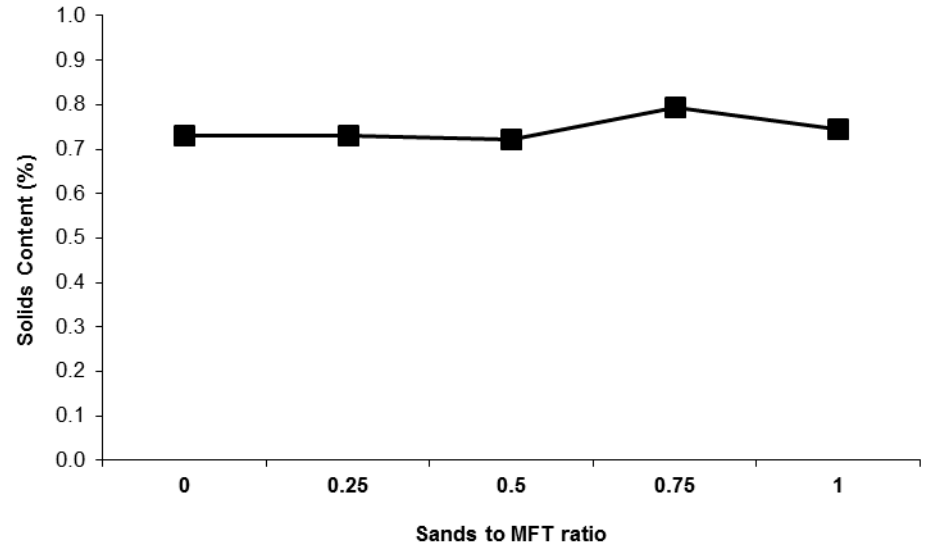


Figure 8. Percentage of solids in the centrate obtained from centrifugation of mature fine tailings with fine sands and polymer C.

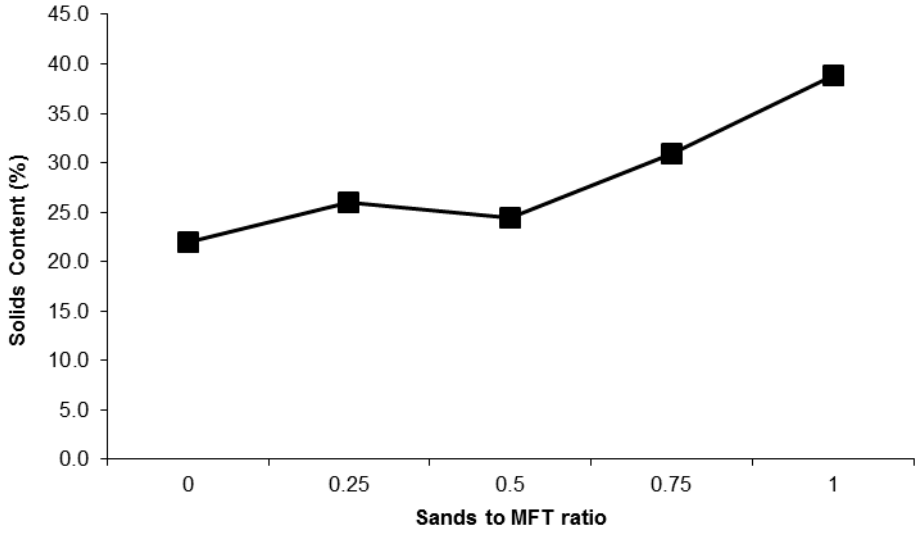


Figure 9. Percentage solids in the settled bed obtained from centrifugation of mature fine tailings with fine sands and polymer C.

2.4 *Filtration of MFT with flocculants and coarse solids*

The results in Table 3 demonstrate that pressure filtration alone is not a viable option for separating untreated MFT as the slow filtration rate (58 L/m^{2}h) produced a filter cake with very high moisture (55%) and high filtrate solids (15.6%). The addition of polymer C without sand addition significantly improved the filtration rate which decreases the moisture content of the cake, but only marginally improves the filtrate solids.

Sand addition without flocculant has different effects depending on the particle size. The coarse sand, of larger particle size, creates a cake bed that helps bring moisture close to 20 %, but most fine solids pass through this network at a slow filtration rate. The medium sand, of smaller particle size, creates a more favorable cake bed for filtration as the rate rose significant-

ly, but has very poor retention of fine solids producing high filtrate solids. When polymer C is added in combination with coarse sand the filtrate contained only 12.2% solids and a cake moisture below 10%, but the floc structure prohibited easy passage of water and the filtration rate is low.

Adding polymer E to medium sand and MFT-1 produces a floc structure that allows easy passage though the filter cloth with high retention of fine solids, as the filtration rate was the highest observed, and filtrate solids the lowest. Cake moisture was still at a favorable level below 20%. The results demonstrate that the addition of coarse particles to this MFT sample can significantly improve the solid-liquid separation when combined with a flocculant, and the particle size of the solids plays a significant role in determining performance.

Table 3. Pressure filtration results for MFT combined with sand and flocculant

Sand	Polymer	Polymer dose (g/t)	Filtrate solids (wt%)	Cake moisture (wt%)	Filtration rate (L/m^2h)
None	None	0	15.6%	55.3%	58
None	Polymer C	1000	14.7%	15.4%	172
Coarse sand	None	0	14.2%	22.2%	25
Medium Sand	None	0	19.6%	2.3%	149
Coarse sand	Polymer C	1500	12.2%	7.4%	46
Medium Sand	Polymer E	1500	6.6%	17.2%	259

3 CONCLUSIONS

The possibility exists that during field operations an MFT sample will be completely devoid of solids >44 µm. This study looks into the performance enhancement of flocculation of the tailings samples which have very high clay content. In order for centrifugation/flocculation treatments to be effective in such samples it is important to introduce coarse particles into the system. However, the particle size distributions of the coarse particles are extremely important in order to have a positive effect on the centrifugation results. The largest particles like coarse sand may not interact with the polymer well and hinder the flocculation of the fines in the MFT. Thus, particle size distributions similar to medium sand and fine sand are recommended for coarse addition in the treatment of MFT samples with high percentage of clay content in them.

In the case of pressure filtration, addition of coarse solids contributes to better cake compaction and a very low moisture content is observed in the residual cake. However, in this case if the right combination of polymers is not selected then the filtrate quality may be adversely affected just as observed in centrate during centrifugation.

4 ACKNOWLEDGEMENTS

The authors would like to thank the management of Kemira for permission to publish this research.

5 REFERENCES

Abu-Orf, M., Walker, C., Dentel, S. 2003. Centrate viscosity for continuous monitoring of polymer feed in dewatering applications. *Advances in Environmental Research* 7: 687-694.

FTFC (Fine Tailings Fundamentals Consortium), 1995 “Vol I, Clark Hot Water Extraction Fine Tailings” In: Advances in Oil Sands Tailings Research, Alberta Department of Energy, Oil Sands and Research Division.

Masliyah, J., Zhou, Z. Xu, Z., Czarnecki, J. and Hamza, H. 2004. Understanding Water Based Bitumen Extraction from Athabasca Oil Sands, *Can. J. Chem. Eng* 82: 628-654.

Ramachandra Rao, S, 1980, Flocculation and dewatering of Alberta oil sands tailings, International Jounal of Mineral Processing 7: 245 – 253.

Somasundaran, P., Smith, E.L., Harris, C.C. 1973. Effect of coarser solids on the settling characteristics of phosphate slimes. *Proc. 1st Int. Conf. on Particle Technology* Chicago, IL: 144-150.

Sworska, A., Laskowski, S., Cymerman, G. 2000. Flocculation of the Syncrude fine tailings Part I. Effect of pH, polymer dosage and Mg^{2+} and Ca^{2+} cations. *Int. J. Miner. Process* 60: 143–152.

Xua, Y., Dabrosa, T., Kanb, J. 2008. Filterability of oil sands tailings. *Process safety and environment protection* 86: 268–276.

Oil Sands – Waste Management

Improving oil sands tailings filterability by reducing capillary forces in the filtrated cake using surfactants

Y. Wu, K. Stewart, R. Tellakula. A. Mahmoudkhani & M. Nair
Kemira Chemicals Inc., Atlanta, Georgia, USA

T. Fenderson & G. Subhayan
Kemira Chemicals Inc., Edmonton, Alberta, Canada

ABSTRACT: In order to find alternatives to current methods of mine waste disposal, companies are investigating different methods to produce dry, stackable tailings. One method to achieve dry tailings is filtration, which is becoming an increasingly common process for tailings management. Filtration of tailings can take place using pressure or vacuum force.

In addition to nature of the tailings, it has been reported the following factors are important when considering filtration: (1) Fines content plays a critical role in filtering the oil sands tailings. Filtration is applicable for tailings with less than 4% fines. (2) Pre-flocculation with polymers can improve tailings filterability significantly; (3) Polymer dosage has an effect on the filtration resistance and filter cake moisture content.

In our previous work on improved tailing dewatering, it has been found that tailings viscosity can be reduced significantly with addition of suitable surfactants, which act to accelerate particle settling velocities and improve tailings dewatering. In filtration, as the flocculated particles accumulate and create a filter cake, many small channels and porous structures are formed inside the cake. As the filtration continues, the tailings cake condenses and the diameters and pore sizes of the channels shrink. As a result, the capillary forces increase, and a much higher pressure is required to maintain the same filtration rate. With addition of surfactant at very low dosage, this capillary force can be reduced significantly.

We intend to show that the use of surfactants can significantly improve tailings filterability. Some preliminary results show a decrease in specific resistance to filtration, a standard method for assessing the filterability and an increase in the filtration rate, with the addition of surfactant when compared to untreated tailings.

1 INTRODUCTION

In order to find alternatives to current methods of mine waste disposal, companies are investigating different methods to produce dry, stackable tailings. One method to achieve dry tailings is filtration, which is becoming an increasingly common process for tailings management. Filtration of tailings can take place using pressure or vacuum force. Below is a summary of current technologies used in the filtration processes to separate the solids from tailings (see reference list for details).

1.1 *Filtered Whole Tailing:*

This technology consists of filtering the whole (unaltered) tailings stream. Filtration is one of the most traditional methods for solid-liquid separation. It has been widely used in other industries. Filtering can take place using pressure or vacuum force. Drums, horizontally or vertically stacked plates and horizontal belts are the most common filtration plant configurations. Pressure

filtration can be carried out on a much wider spectrum of materials though vacuum belt filtration is probably the most logical for larger scale operations.

1.2 *Cross-flow Filtration of Whole Tailings:*

In cross-flow filtration, the feed is passed across the filter membrane (tangentially) at positive pressure relative to the permeate side. A proportion of the material which is smaller than the membrane pore size passes through the membrane as permeate or filtrate; everything else is retained on the feed side of the membrane as retentate. With cross-flow filtration the tangential motion of the bulk of the fluid across the membrane causes trapped particles on the filter (cake) surface to be rubbed off. This means that a cross-flow filter can operate continuously at relatively high solids loads without blinding.

1.3 *Filtered Coarse Tailings:*

This technology consists of filtering and dry stacking of the coarse fraction, cyclone underflow tailings (CUT) of the tailings slurry. Variants include adding some fines to the mix prior to filtration. CUT are usually stripped of some fines and water and are not too dissimilar, although somewhat more variable, in composition than composite/consolidated tailings. Development of large capacity vacuum and pressure filter technology has presented the opportunity for storing tailings in an unsaturated state, rather than as conventional slurry or in a paste consistency associated with thickened tailings.

1.4 *Filtered Thickened Fines Tailings:*

This technology includes filtration and dry stacking of thickener underflow (predominantly fines). Other fine tailings streams may include centrifuge fine tailings and MFT. This technology has been proposed but it seems impractical due to the high fines content. The fines content of fine tailings can be as high as 96%. Bench-scale tests have demonstrated that filtering flocculated fine tailings with fines content greater than 18% are very challenging and perhaps impractical at large-scale.

Filter cake is produced at sufficiently high solids content to truck or convey to a reuse or final disposal site. Placement in the facility can be done by a conveyor radial stacker system or trucks depending upon the application and the design criteria. As with most mechanical dewatering systems the need for settling basins, return water systems, and containment area reclamation, as well as the piping and pumps to the settling area is minimized or eliminated.

In filtration, as the flocculated particles accumulate and create a filter cake, many small channels and porous structures are formed inside the cake as shown in Figure 1 below. As the filtration continues, the tailings cake condenses and the diameters and pore sizes of the channels shrink as shown in Figure 2. As a result, the capillary forces increase, and a much higher pressure is required to maintain the same filtration rate.

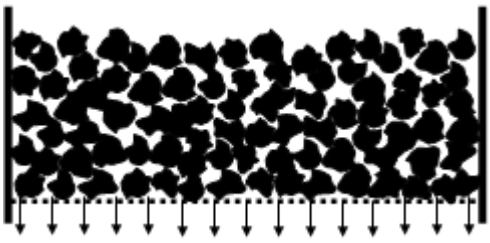


Figure 1. In filtration, a filter cake is created and many small channels and porous structures are formed.



Figure 2. As the filtration continues, the cake condenses and the diameter and pore size of the channels become smaller.

Capillary Pressure and Capillary Force: they are generated where interfaces between two immiscible fluids (or gas) exist in the pores (capillaries) of the reservoir rock. It is usual to consider one phase as a wetting phase and the other as a non-wetting phase. However, intermediate cases occur which can greatly complicate the picture. The drainage case, i.e. a non-wetting phase displacing a wetting phase applies to hydrocarbon migrating into a previously brine saturated rock. Imbibition data is the opposite to drainage, i.e. the displacement of a non-wetting phase by a wetting phase. Thus, the drainage data can usually be used to predict non-wetting fluid saturation at various points in a reservoir, and the imbibition data can be useful in assessing the relative contributions of capillary and viscous forces in dynamic systems. The basic relationship (Figure 1) between capillary pressure, interfacial tension, contact angle and pore radius is given by the equation 1 below:

$$P_c = \rho g h = A \cdot \frac{2\gamma \cos\theta}{R} \tag{1}$$

where:

P_c = capillary pressure (psi)
ρ = density of water (g/cm^3)
g = standard gravity (9.8 m/s^2)
h = height of the meniscus (cm)
γ = interfacial tension (mN/m)
θ = contact angle of water (degrees)
R = pore radius (microns)
A = 0.145 (constant to convert to psi)

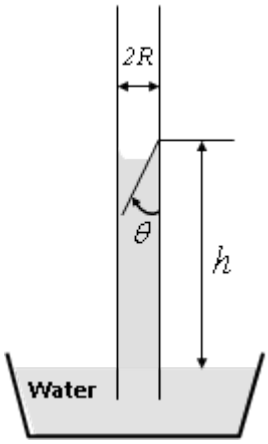


Figure 3. Capillary pressure

Interfacial tension (IFT) between water and nonpolar organic fluids is usually high. For example, interfacial tension between water and *n*-decane is 52.0 mN/m, between water and *n*-dodecane is 52.8 mN/m, which result in a high capillary pressure when diameter of the capillary is small. However, with addition of proper surfactant even at very low dosage, such high IFT between water and oils can reduced significantly to very low level. As a result, the capillary force and pressure can be reduced remarkably.

In the equation (1), it should be noted that there are two cases for θ, contact angle of water: $\theta < 90°$ and $\theta > 90°$. The former indicates the capillary surface is hydrophilic or water-wet; the later means the surface is hydrophobic or oil-wet. In this case, the meniscus in the capillary will be lower than the water surface outside the capillary. Up to date, there is no experimental data

available for the water contact angle on the original tailings particle surface. Based on our previous work on the wettability study of the dried tailings particle surface, water contact angle on the glass square coated with tailings and dried in oven is about 40 °. This indicates the tailings particle surface is hydrophilic or water-wet in a certain extent.

Surfactants used in this experiment include five sugar-based alkyl polyglucoside (APG) surfactants and one sorbitan laurate SPAN® 20. In order to investigate the synergistic effect on the interfacial reduction, several mixtures of the APG surfactant and the SPAN® 20 surfactant were also used in the experiment. Molecular structure and relevant product information are shown below:

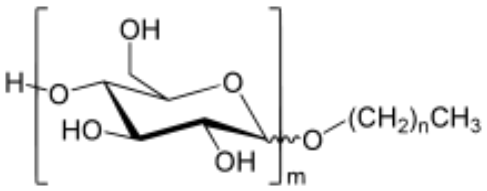


Figure 4 Molecular structure of alkyl polyglucoside surfactants. *m*: degree of polymerization; *n*: hydrocarbon chain length.

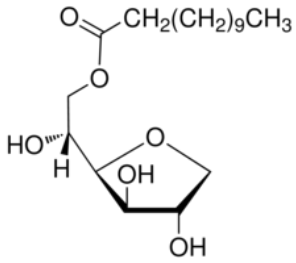


Figure 5. Molecular structure of SPAN® 20, sorbitan mono-laurate. M.W. 346.5; Solids content ~98%.

Table 1. Product Information of Simulsol® SL Surfactants by SEPPIC

Product Name	Solid Content (wt.%)	Chemical Description	Degree of Polymerization	Molecular Weight
Simulsol® SL-4	49 ~ 51%	Butyl polyglucoside (*n* = 3)	*m* = 1.2-1.45	300
Simulsol® SL-8	58 ~ 62%	Octyl polyglucoside (*n* = 7)	*m* = 1.2-1.45	347
Simulsol® SL-10	53 ~ 57%	Decyl polyglucoside (*n* = 9)	*m* = 1.2-1.45	365
Simulsol® SL-11W	52 ~ 67%	Undecyl polyglucoside (*n* = 10)	*m* = 1.2-1.45	374
Simulsol® SL-55	52 ~ 57%	Undecyl and Lauryl polyglucoside	*m* = 1.2-1.45	385

2 EXPERIMENTAL

2.1 *Preparation of synthetic brine and the surfactant solutions using the brine*

In order to make our screening test under the conditions similar to the real case, a synthetic brine was prepared following the compositions and the recipe based upon its compositions. Both the compositions and the recipe are listed in Table 2 below. TDS (total dissolved solids) in the synthetic brine is 3,200 ppm.

Surfactant solutions were prepared at 1,000 ppm (0.10 wt.%) based on the solids content in the surfactant samples. For mixtures, each individual surfactant concentration is 500 ppm, the total concentration will be 1,000 ppm once two individuals are placed together for possible synergistic effect in the interfacial tension reduction.

Table 2. Compositions and recipe of the synthetic brine

Brine Compositions		Recipe to Make Synthetic Brine		
Na^+	1225.7 ppm	Salt	Molecular Weight	Amount (g)
Ca^{2+}	12.70 ppm	NaCl	58.44	3.111
Mg^{2+}	5.20 ppm	$CaCl_2 \cdot 2H_2O$	147.01	0.046
K^+	12.20 ppm	$MgCl_2 \cdot 6H_2O$	203.30	0.044
Sr^{2+}	1.30 ppm	KCl	74.55	0.023
SO_4^{2-}	3.90 ppm	$SrCl_2 \cdot 6H_2O$	266.62	0.004
Cl^-	1938.9 ppm	Na_2SO_4	142.04	0.006
TDS	3200.0 ppm	Distilled H_2O	18.02	996.766

2.2 *Interfacial Tension Measurement*

To evaluate performance of the individual surfactants and their mixtures in interfacial reduction, two organic compounds, *n*-decane and dodecane model oil phase. Dodecane is a liquid alkane hydrocarbon with the chemical formula $CH_3(CH_2)_{10}CH_3$, an oily liquid of the paraffin series. It has 355 isomers. The interfacial tension was measured using a spinning drop tensiometer SITE100 from KRÜSS with the large volume method. That means the interfacial tension was measured directly by use of fresh oil and aqueous samples without a pre-equilibrium. The results obtained by this method may be higher than that obtained by the pre-equilibrium method, particularly for the systems with a low or ultralow interfacial tension. An image of one oil drop in the spinning tube displayed on the computer screen for measuring the interfacial tension is shown in the Figure 6, in which diameter of oil drop was measured to be 0.97 mm, and the interfacial tension was calculated to be 2.91 mN/m by the computer based on the experimental parameters, e.g. spinning rate 6000 RPM (rotation per minute); density of oil phase and aqueous phase, etc.

2.3 *Filtration Test*

Samples of mature fine tailings (MFT) and oil sands process affected water (OSPW) were obtained from a major oil sand producer in Alberta, Canada. The MFT were diluted to 20 wt% using OSPW and flocculant-grade anionic polymer solutions were prepared at concentrations of 0.4 wt% using OSPW. An OFITE Low Pressure Filter Press was used to obtain filtration behavior measurements. The base cap was fitted with a screen and appropriate sized filter paper (9 cm), with a pore size of 2.7 μm to remove any particles from the filtrate, and attached to the test cell. 200 g of the 20 wt % MFT solution was dosed with the appropriate treatment and gently mixed by cupping back and forth. The flocculated tailings were then dosed with surfactant and again gently cupped to mix the slurry. This treated slurry was then transferred to the test cell and covered with the attached cap to seal. The test cell was secured by a T-screw and 100 PSI of pressure of air was applied. A clean graduated cylinder was placed under the filtrate tube to measure and collect the filtrate. Measurements were recorded at 10 minute intervals over a 30 minute time period. As the filtration progressed to approach the breakpoint, the filtration rate decreased sharply and approached zero to indicate completion of capillary filtration. In this study, filtration continued for 30 min, after which the filter cake was dried in an oven at 105 °C to a constant weight for moisture content analysis.

3 RESULTS AND DISCUSSION

3.1 *Calibration of the Spinning Drop Tensiometer*

To ensure high accuracy of the interfacial tension data measured by the spinning drop tensiometer, it was calibrated by measuring the interfacial tension for distilled water/n-decane and distilled water/dodecane at relatively high spinning rate, e.g. 9,000 RPM. The calibration results are listed in Table 3.

Table 3. Calibration Results of the Spinning Drop Tensiometer

Oil Phase and density	Aqueous Phase and density	Experimental Results	Results in literatures	Experimental Error
n - Decane, (0.732 g/cm^3)	Distilled water (0.998 g/cm^3)	51.8 mN/m	52.0 mN/m	-0.4%
Dodecane, (0.751 g/cm^3)	Distilled water (0.998 g/cm^3)	47.5 mN/m	52.8 mN/m	-10.0%

From data in the table, it can be found that the calibration result for *n*-decane is in a high agreement with the data in the published papers, the experimental error is only 0.4%. However, experimental error with dodecane is high and up to 10%. The reason is probably that the published result was obtained with *n*-dodecane. Our experimental results were obtained with an industrial sample of dodecane, which contains all possible isomers as many as 355 different molecular structures with the same chemical formula, which result in a quite different interfacial tension against water surface. Based on these calibration results, it can be concluded that our spinning drop tensiometer is in an excellent work condition.

3.2 *Interfacial Tension of the Individual Surfactants*

IFT results of individual surfactants at 1,000 ppm in the synthetic brine are listed in Table 4. In the table, it can be found that for the alkyl polyglucoside surfactants, the interfacial tension decreases with the increase in the hydrocarbon chain length of the surfactant molecules for both *n*-decane and dodecane, but for all the surfactants tested at the concentration of 1,000 ppm, the interfacial tension is higher than 1 mN/m.

Table 4. Interfacial Tension of Individual Surfactants

Surfactant and Concentration	Interfacial Tension (mN/m)	
	n-Decane	Dodecane
Simulsol SL-4 (1000 ppm)	41.8	32.7
Simulsol SL-8 (1000 ppm)	8.83	8.54
Simulsol SL-10 (1000 ppm)	3.85	3.56
Simulsol SL-11W (1000 ppm)	1.16	1.14
Simulsol SL-55 (1000 ppm)	1.97	1.95
SPAN® 20 (1000 ppm)	7.45	6.68

Compared to the interfacial tension with distilled water, it has just been reduced by about one order of magnitude. This reduction is significant but still not enough. We need to formulate the

surfactants by proper mixing them to get more reduction through synergistic effect in the surfactant mixtures.

3.3 *Interfacial Tension of the Surfactant Mixtures*

IFT results for the surfactant mixtures at total concentration of 1,000 ppm in the synthetic brine are listed in Table 5. Compared with the data in Table 4, it can be found in Table 5 that except for mixture of Simulsol SL-10 and SPAN® 20, the other three mixtures exhibited strong synergistic effect on the interfacial reduction. Among them, the mixture of Simulsol SL-11W and SPAN® 20 shows the strongest effect in the IFT reduction. For oil phase of *n*-decane, the interfacial tension against water can be reduced by three orders of magnitude from 51.8 mN/m to 0.05 mN/m. For oil phase of dodecane, the interfacial tension against water can be reduced by 2~3 orders of magnitude from 47.5 mN/m to 0.22 mN/m. The synergistic effect in the surfactant mixtures are shown in the Figure 6.

Table 5. Interfacial Tension for the Surfactant Mixtures at 1000 ppm Total

Surfactant Mixtures and Concentration			Interfacial Tension (mN/m)	
			n-Decane	Dodecane
1	Simulsol SL-4 (500 ppm)	SPAN® 20 (500 ppm)	6.15	9.66
2	Simulsol SL-8 (500 ppm)	SPAN® 20 (500 ppm)	1.47	2.24
3	Simulsol SL-10 (500 ppm)	SPAN® 20 (500 ppm)	4.58	7.27
4	Simulsol SL11W(500 ppm)	SPAN® 20 (500 ppm)	0.05	0.22
5	Simulsol SL-55 (500 ppm)	SPAN® 20 (500 ppm)	not soluble	not soluble

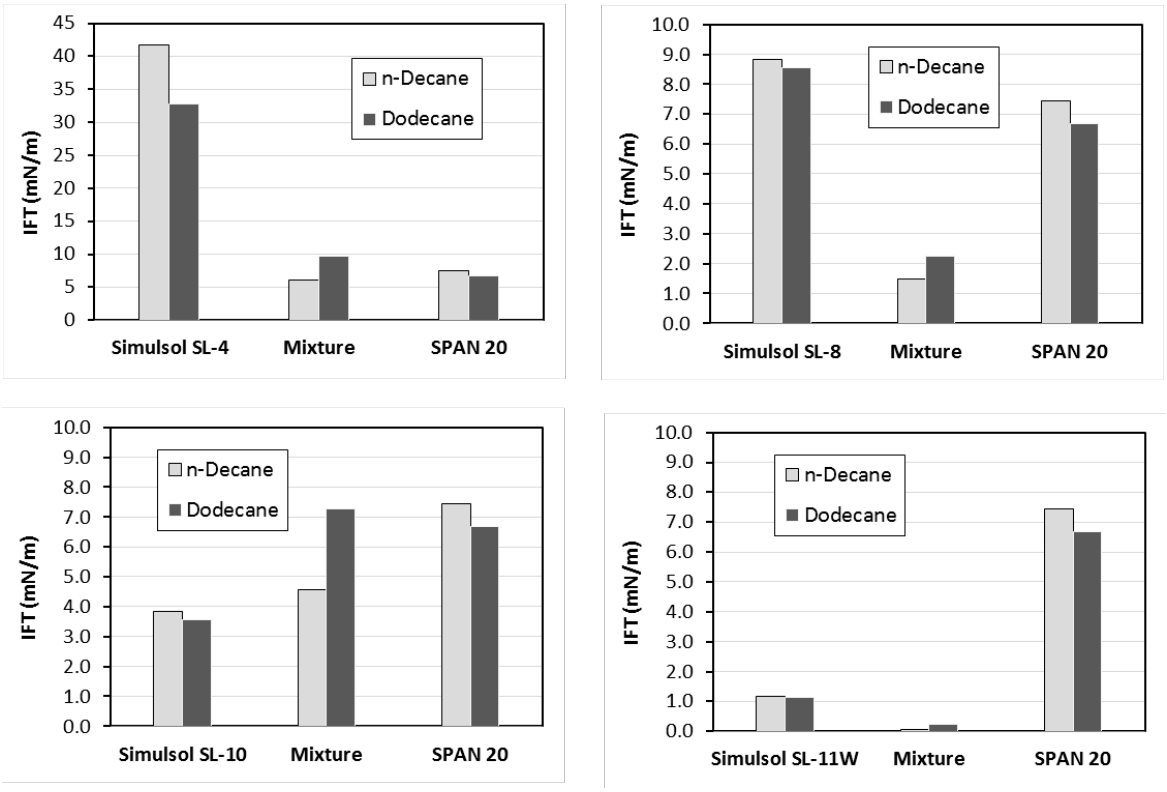


Figure 6. Synergism of surfactant mixtures in interfacial (IFT) reduction

3.4 *Filterability of Mature Fine Tailings in the Presence of Surfactants*

The data represented by Table 6 shows a significant increase in dewatering upon flocculation of MFT tailings. Addition of surfactants to the tailings slurry was evaluated for treatments with an anionic polymer or anionic polymer + coagulant. An increase in the amount of filtrate was found with addition of some surfactant mixtures. For anionic flocculant treatments, an increase in filterability were noted as seen in Table 6. Surfactant 5 showed the greatest percent increase in total filtrate with an almost 12 % increase in filtrate volume. Lastly, the coagulation-flocculation process was examined and data are reported in Table 6. Most cases showed an increase in total filtrate, with a significant percent increase in filtrate of 16 % by adding Surfactant 5.

Table 6. Changes in the amount of total filtrate (mL) when various surfactants are added to MFT flocculated by a polymer blend.

Chemical Treatment	**10 min (mL)**	**10 min (mL)**	**10 min (mL)**	**Total Filtrate (mL)**	**Increase in Total Filtrate (%)**
None	5	2.5	1.4	9.4	-
500 ppm Polymer A	12.8	6.2	4.6	23.6	
500 ppm Polymer A + Surfactant Mix 1	14.6	6.2	4.8	25.6	+7.8
500 ppm Polymer A + Surfactant Mix 2	13	5.6	4.2	23.2	No Improvement
500 ppm Polymer A + Surfactant Mix 3	12.8	5.8	4.6	23.2	No Improvement
500ppm Polymer A + Surfactant Mix 4	14	6.4	5	25.4	+7.1
500 ppm Polymer A + Surfactant Mix 5	15.4	6.4	5	26.8	+11.9
250 ppm Polymer A + 500 ppm Coagulant 1	10	4.5	4	18.5	
(250 ppm Polymer A + 500 ppm Coagulant 1) + Surfactant Mix 1	8.8	3.8	3.4	18.2	No Improvement
(250 ppm Polymer A + 500 ppm Coagulant 1) + Surfactant Mix 2	11.2	5	4	20.2	+8.4
250 ppm Polymer A + 500 ppm Coagulant 1) + Surfactant Mix 3	10.2	4	3.6	18.1	No Improvement
(250 ppm Polymer A + 500 ppm Coagulant 1) + Surfactant Mix 4	15.4	6	4.8	18.7	No Improvement
(250 ppm Polymer A + 500 ppm Coagulant 1) + Surfactant Mix 5	12.6	5.2	4.3	22.1	+16.3

4 CONCLUSION

Improvement in tailing filterability requires removal of the fine particles and pre-flocculation of the remaining tailings slurry. To further improve oil sands tailings filterability, the addition of surfactants is necessary to lower the capillary forces, thus increasing the amount of filtrate and dryness of filter cake. Surfactant systems used in this study are biodegradable and environmentally friendly and were selected to have no negative effect in downstream operation. Future work will continue looking into other polymers of various charge densities and molecular weight for flocculation as well as the chemical addition treatment order.

5 ACKNOWLEDGEMENTS

The authors would like to thank the management of Kemira for permission to publish this research.

6 REFERENCES

Beier, N. and Sego, D. 2008. *Dewatering of oil sands tailings using cross-flow filtration*. IN: GeoEdmonton '08 - 61st Canadian Geotechnical Conference, Edmonton, Alberta. Canadian Geotechnical Society.

Ifill, R.O., Beier, N.A., Zhang, C. and Sego, D. 2010. Crossflow filtration: An option towards compliance with Directive 074. Geotechnical News 28(2), 30-33.

Wang, X. and Masliyah, M. 2008. *Polymer aids for settling and filtration of oil sand tailings*. IN: First International Oil Sands Tailings Conference, Edmonton, Alberta.

Wu, Y., Sanders, L., Stewart, K., Fenderson, T., Watson, P., Mahmoudkhani, A. and Nair, M. 2012. A Novel Method to Improve Tailings Dewatering. IN: Third International Oil Sands Tailings Conference, Edmonton, Alberta.

Xu, Y., Dabros, T. and Kan, J. 2008. Filterability of oil sands tailings. Process Safety and Environmental Protection 86(4), 268-276.

Experiences relevant to ERCB Directive 074

H.K. Mittal,
H.K. Mittal and Associates Ltd., Saskatoon, Saskatchewan, Canada

P.G. Landine
Cameco Corporation, Saskatoon, Saskatchewan, Canada

ABSTRACT: In 1984, Rabbit Lake pit was converted into the first in-pit disposal facility in Canada to receive chemical-rich uranium mill tailings. Initially, filtered tailings were hauled, dumped and dozed into place at this facility. Pre- filtering of tailings had to be abandoned after few months due to trafficability problems on the tailings surface. Tailings preparation has since consisted of pre-thickening of tailings slurry to a density of 35 to 40% solids prior to pipeline transport to the disposal site.

With the current disposal practice, uranium tailings are expected to reach a high degree of self-weight consolidation leading to deposits that are ready for cover construction within 5 to 10 years after cessation of tailings deposition (consistent with a significant goal of DR074). Contrary to another requirement of DR074, pre-stiffening/thickening of material beyond that needed to prevent particle size segregation is not required for these deep tailings deposits. Surface trafficability for cover construction is gained through surface desiccation and by placing the initial lift of cover material in late winter while the surface layer is frozen.

1 INTRODUCTION

It is understood that in order to ensure the timely decommissioning of oil sand tailings deposits, the Energy Resources Conservation Board (ERCB) of Alberta issued Directive 074 (DR074) on February 3, 2009. The main geotechnical requirements of DR074 are that a significant portion of oil sand tailings be deposited in designated disposal areas (DDAs) with geotechnical performance criteria based on the undrained strength (Su) of the tailings deposit as follows.

(i) Tailings in DDAs must achieve an Su of 5 kPa within one year of deposition; and
(ii) The DDAs must be ready for reclamation within 5 years after active deposition has ceased with a trafficable surface having an Su of 10 kPa.

There is available experience with disposal of chemical-rich uranium tailings in Saskatchewan, Canada, indicating that tailings deposits can be generally ready for cover placement within about 5 to 10 years following cessation of active deposition. No pre-conditioning of uranium tailings, beyond that needed to prevent particle size segregation during pipeline transport and/or deposition of tailings at the disposal sites has been found to be necessary.

2 TAILINGS DEPOSITION AT RABBIT LAKE IN-PIT FACILITY

The mined-out Rabbit Lake pit, at Cameco Corporation's uranium mine in Northern Saskatchewan (Figure 1), was converted into the first in-pit tailings management facility in late 1984. The design of the Rabbit Lake In-Pit Tailings Management Facility (RLITMF) includes a pervious

surround drainage system consisting of a base drain at the bottom of the pit and a perimeter drainage system along the pit walls (Figure 2). The drainage system is provided for collection of ground water and tailings seepage water during operation and diversion of ground water around the tailings deposit after closure.

The original design at the RLITMF called for sub-aerial deposition of dewatered tailings (by filtration). The filtered tailings were hauled and deposited using scrapers and a wide-track dozer for spreading on a trial basis in November to December, 1984, and then in November, 1985 until mid-June, 1986. During this period, the tailings were deposited as a filter cake with an approximate density of 50 percent solids by weight. However, the tailings surface became untrafficable for the scrapers and dozer operation during the warmer (summer) season. This forced a change-over to slurry discharge on June 19, 1986 with a target minimum slurry density of 35 to 40% solids by weight.

Initially, the thickened slurry discharge was achieved by modifying the filter plant to receive only the neutralized raffinate and then combine the filter cake with neutralized leach residue in a small mixing box at the output of the filter plant; tailings were then transported by pipeline down the pit ramp for sub-aerial deposition on a tailings beach within the pervious surround of the RLITMF. Since 1995, tailings slurry has been thickened in a conventional cone thickener at the mill. Sub-aerial deposition resulted in the build-up of extensive frozen layers within the tailings mass which has hindered consolidation of the tailings deposit. Between 1999 and 2012, tailings were intermittently injected at depths of up to 70 m below the surface to help thaw existing frozen layers and mitigate frost build-up in new tailings. However, deep injection of tailings slurry was found to be only partially successful for frost mitigation purposes. Beginning in 2012, to mitigate further frost build-up, thickened tailings slurry is discharged sub-aqueously below a water depth of approximately about 1 to 3 m. Additional details are presented in an accompanying paper to this conference (Mittal & Landine, 2013).

3 UNDRAINED STRENGTH OF FILTERED TAILINGS

While undrained strength (Su) was not defined as a criterion for performance of deposited dewatered (filtered) tailings at Rabbit Lake, it is of interest to provide an estimate for comparison with the requirements of Directive 074 for oil sand tailings. The Su of normally consolidated clays can be typically shown to vary with overburden stress as follows.

$$\frac{Su}{p'} = \frac{\sin\phi'}{1+(2A-1)\sin\phi'} \quad (1)$$

where

Su = undrained shear strength
p′ = effective overburden stress
ϕ' = effective angle of shearing resistance
A = pore pressure parameter (Bishop & Henkel, 1962)

Assuming a ϕ' of 30°, Su/p′ can be computed to be equal to 0.33 for normally consolidated clays and 0.28 for normally consolidated marine clays with A=1.0 and 1.3 for these materials respectively (Bishop & Henkel, 1962).

Results from cone penetration testing in the slimes pond at the Rabbit Lake Above-Ground Tailings Management Facility (RLAGTMF) performed in 1987 are shown in Figure 3. Tailings slurry (without pre-thickening) was previously discharged at this facility between 1975 and 1985 by the conventional sub-aerial deposition method resulting in particle size segregation with coarse tailings beaches and a slimes pond containing fine-grained tailings.

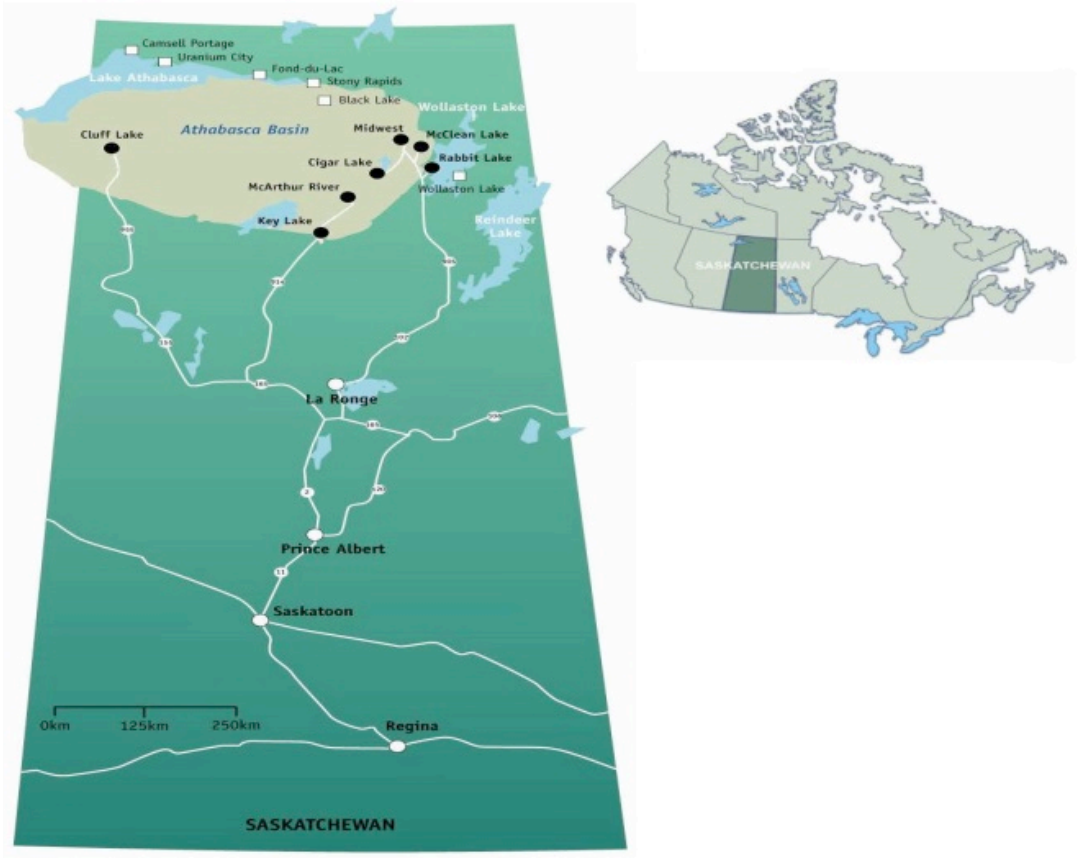


Figure 1 - Location of Rabbit Lake Mine Site

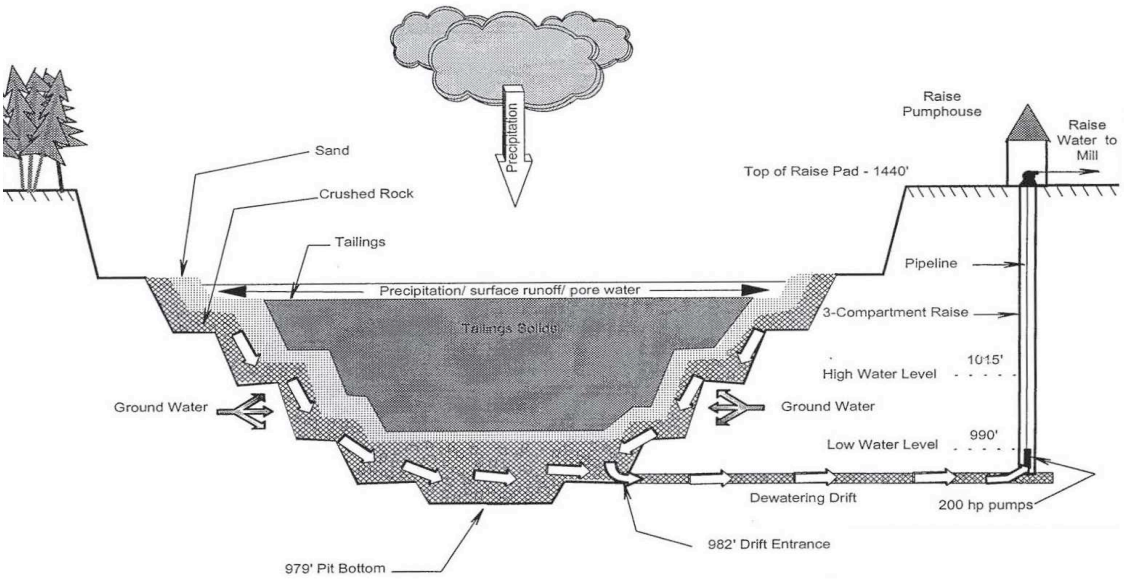


Figure 2. Conceptual design - RLITMF

The test results, in Figure 3, indicate a lower Su/p´ value of about 0.2 for the fine-grained

uranium tailings. This might be due to the highly sensitive nature of the uranium tailings deposits with much higher "A" values in undrained loading.

A best-fit e/log p′ relationship for the thickened slurry/filtered tailings in the RLITMF, based on bore hole data, is shown in Figure 4. Pre-consolidation pressure for the filtered tailings of 10 kPa can be estimated from Figure 4 at 50 percent solids (void ratio 2.74, at S.G.=2.74), suggesting an Su of filtered tailings to be about 2 to 3 kPa.

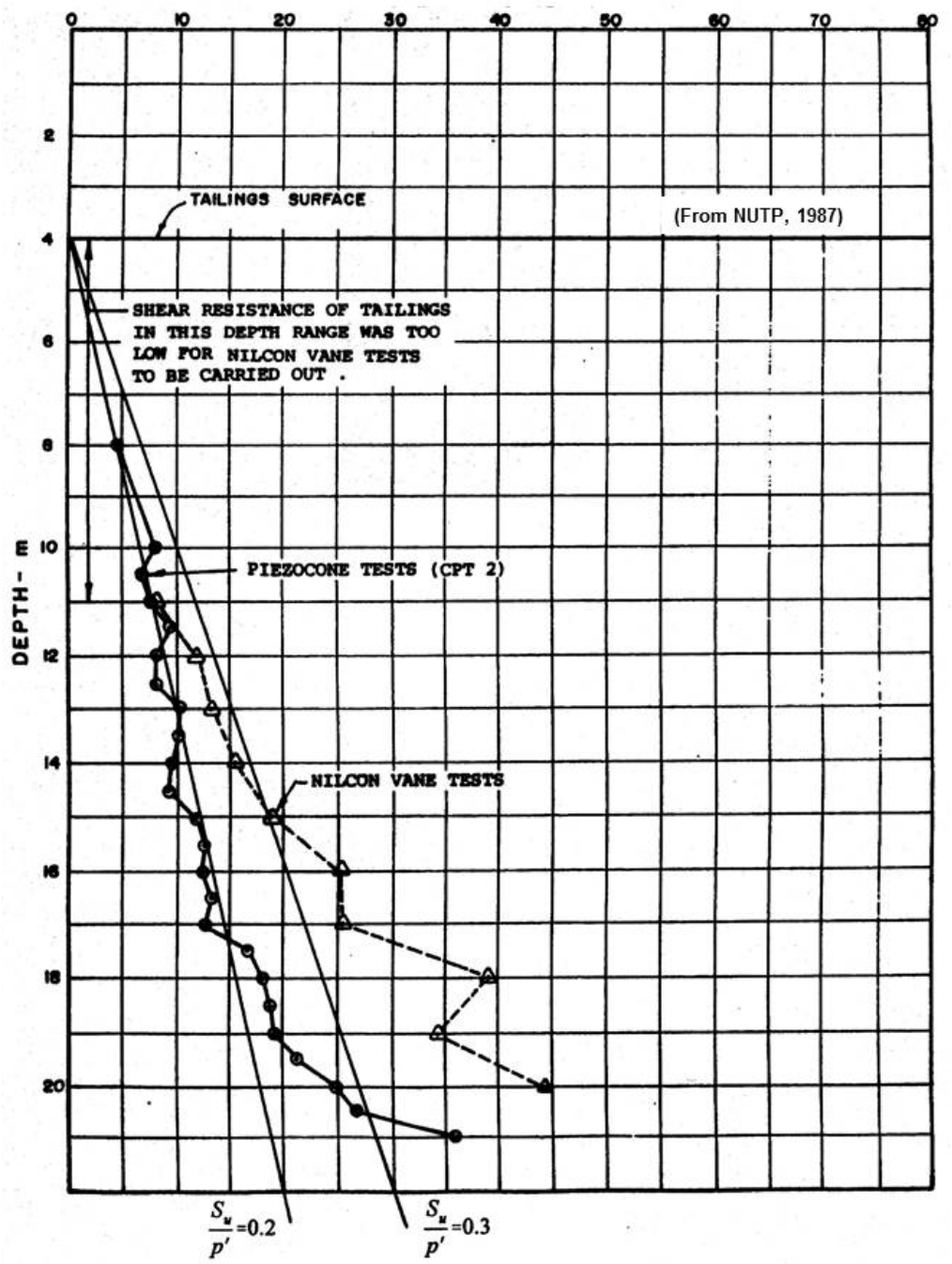


Figure 3. Undrained strength of uranium tailings – RLAGTMF (Slimes Pond)

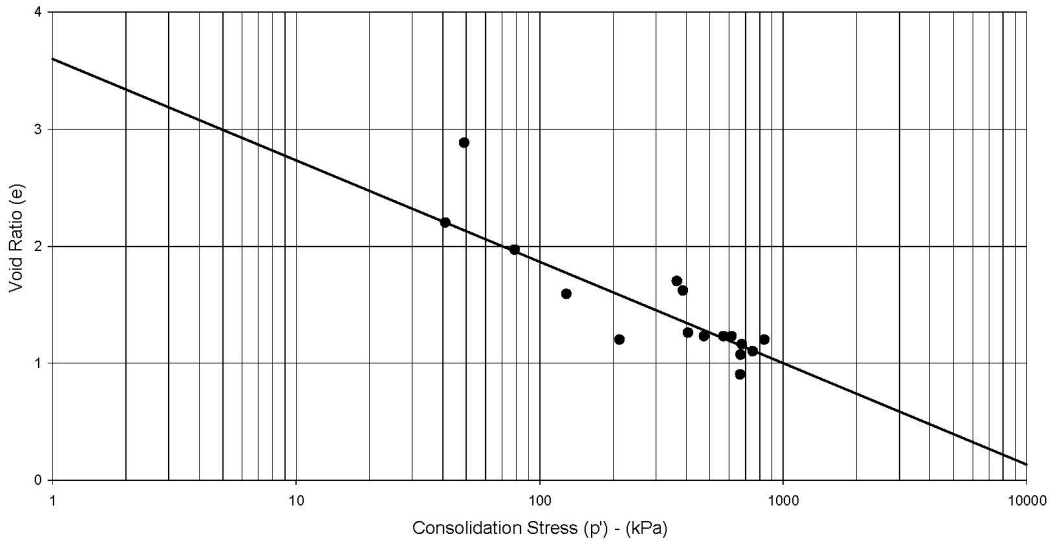


Figure 4. Void ratio vs effective stress for B-Zone tailings from bore hole/piezometer data - RLITMF

4 TYPICAL GEOTECHNICAL PROPERTIES OF URANIUM MILL TAILINGS

Based on laboratory geotechnical testing, uranium mill tailings can be classified as compressible silts. The typical geotechnical properties can be described as follows.

(i) The as-discharged fines contents (<0.075 mm) of these tailings has been found to range from about 50 to 65 percent by mass of dry solids. Some uranium tailings have been found to contain up to 20 to 25 percent clay minerals, as well as up to about 25 to 30 percent chemical precipitates from the milling process. The chemical precipitates consisting of gypsum and metal hydroxides are included in the fines content.

(ii) Consolidation tests in relatively large slurry consolidometers have been performed for the various uranium mill tailings. Constant head (or constant flow) hydraulic conductivity determinations have been performed in conjunction with the slurry consolidation tests. Compressibility characteristics (e/log p´) and hydraulic conductivity determinations, based on back analyses, have been performed on several uranium mill tailings deposits using data from bore hole investigations and monitoring instrumentation.

(iii) The compressibility data can generally be characterized using linear void ratio (e) versus log of effective stress (p´) relationships. Therefore, the compressibility results can be discussed in terms of a void ratio (e_1) at an effective consolidation pressure of 1 kPa and compression indices (Cc) for comparison purposes. e_1 has been found to vary between about 2.2 and 5.0, and the compression indices (Cc) between 0.4 and 1.07 for the unsegregated uranium tailings.

(iv) Hydraulic conductivity (k) of non-segregated uranium tailings is found to vary approximately between 10^{-7} to 10^{-8} m/s. Hydraulic conductivity values in this range lead to timely consolidation during operation and following cover placement, while, at the same time being low enough to minimize migration of contaminants from the facilities after closure.

5 CURRENT DISPOSAL PRACTICE

Current practice of uranium mill tailings disposal in Northern Saskatchewan has evolved based on cumulative experiences gained from various tailings disposal facilities over the last 40 years. The following are the main highlights of the current tailings disposal practice and the expected results during operations and following closure.

(i) To provide permanent physical containment, in-pit disposal is the current method of choice. This approach, in combination with a permeable surround and a low permeability tailings deposit, also results in minimal migration of contaminants from the tailings to the downstream environment following closure.

(ii) Tailings slurry is pre-thickened to 35 to 40 percent solids to minimize particle size segregation during deposition ensuring a relatively uniform (non-segregated) tailings deposit.

(iii) To prevent freezing of slurried tailings from sub-aerial deposition during winter season, as experienced in all of the older facilities, the preferred method of tailings deposition is by sub-aqueous discharge beneath a water cover of sufficient depth to prevent freezing of the tailings surface during the winter.

(iv) The in-pit tailings deposition facilities are designed with adequate drainage systems to facilitate a high degree of consolidation of the tailings slurry during deposition and a timely closure within about 5 to 10 years after cessation of active tailings deposition. A man-made pervious surround drainage system is provided to divert ground water flow around the tailings deposit after closure, unless a naturally permeable strata exist around the facility, as is the case at the Key Lake Deilmann and McClean Lake facilities.

(v) Dry cover construction is feasible in most cases. After an initial period of surface desiccation, staged loading commencing in late spring when the tailings surface is still frozen has proven successful. This is based on experience gained from preload fill placement over fine-grained uranium tailings in the "slimes pond" area of the Rabbit Lake Above-Ground Tailings Management Facility (RLAGTMF), as part of the decommissioning plan for that facility (Mittal et al. 2000). This fill placement project can be briefly described, as follows.

A general layout of the RLAGTMF is shown in Figure 5. Preload fill placement over the slimes pond at the RLAGTMF was initiated in 1995 with the construction of one hectare test fill. Based on the outcome of the test fill program, full-scale implementation of the fill placement (over the slimes pond) was initiated in 1997 with placement of a 0.7 m fill layer over an area of 14 hectares. This was followed by additional fill placement in stages to a maximum fill thickness of 6 m in the deepest part of the valley. A brief description of the test fill program is presented below in the next section.

6 TEST FILL PROGRAM

An approximately 2 ½ m thick test fill was placed in 1995 over a (50 m x 200 m) selected area near the southeast edge of the slimes pond at the RLAGTMF (Fig. 5).

The objectives of the test fill program were as follows.

(i) To confirm the validity of the proposed method of fill placement which consisted of placement of an initial thin lift of fill (up to 1000 mm) over the frozen tailings surface commencing at the end of winter in about mid-March to mid-April. After a suitable period for settlement or consolidation and pore water pressure dissipation, additional lifts of fill could be placed. Specifically, the following procedure was followed.

- Snow was cleared from the frozen tailings surface with a wide track D6 dozer;
- Woven filter cloth (type #200ST, from Armtec) was placed over the cleared tailings surface;
- An initial 500 mm tick lift of sandy till was placed over the geomembrane in the last week of April, 1995. Construction equipment was only permitted on the fill surface during this period;
- Geotechnical instruments (settlement plates and piezometers) were installed at the surface of the fill and in the tailings , respectively;
- A further 500 mm of rock fill was placed in the first week of August, 1995 allowing construction traffic only on the surface of the new fill; and
- (ii)Finally 1.5 m of rock fill was placed between September 19 and 26, 1995.

(ii) To confirm material properties used during design for estimation of settlements.

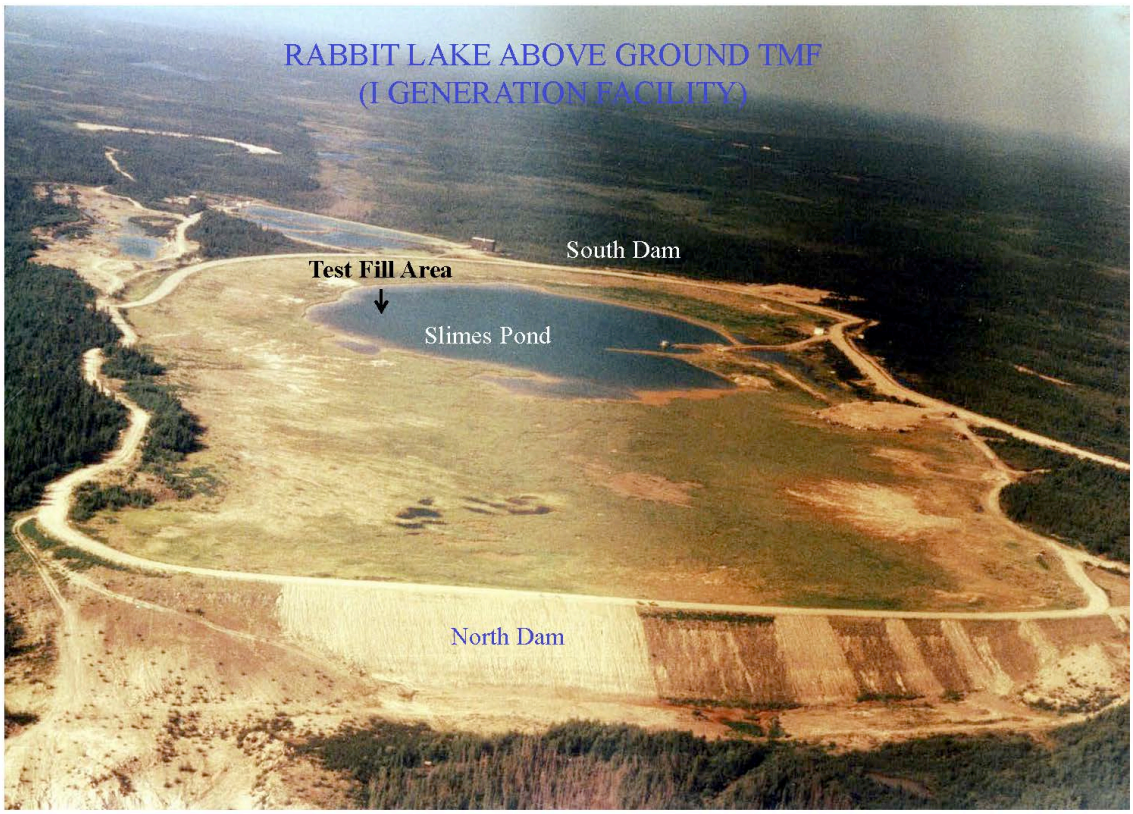


Figure 5. General Layout of Rabbit Lake Above-Ground TMF

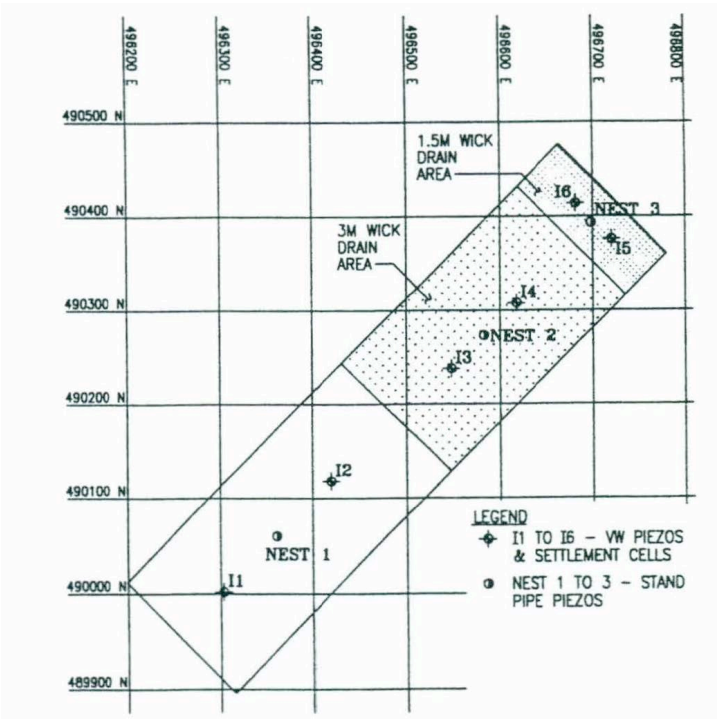


Figure 6. Test fill site details and instrument locations

(ii) To assess possible use of prefabricated wick drains. For this purpose, wick drains "Alidrain type DC" were installed over the full depth of tailings (about 17 m) at 1.5 m and 3.0 m spacings in portions of the test fill site as shown in Figure 6. The sequence of fill placement at the test fill site, typical time settlement plots and pore water pressures measured at mid-depth in the tailings are shown in Figure 7.

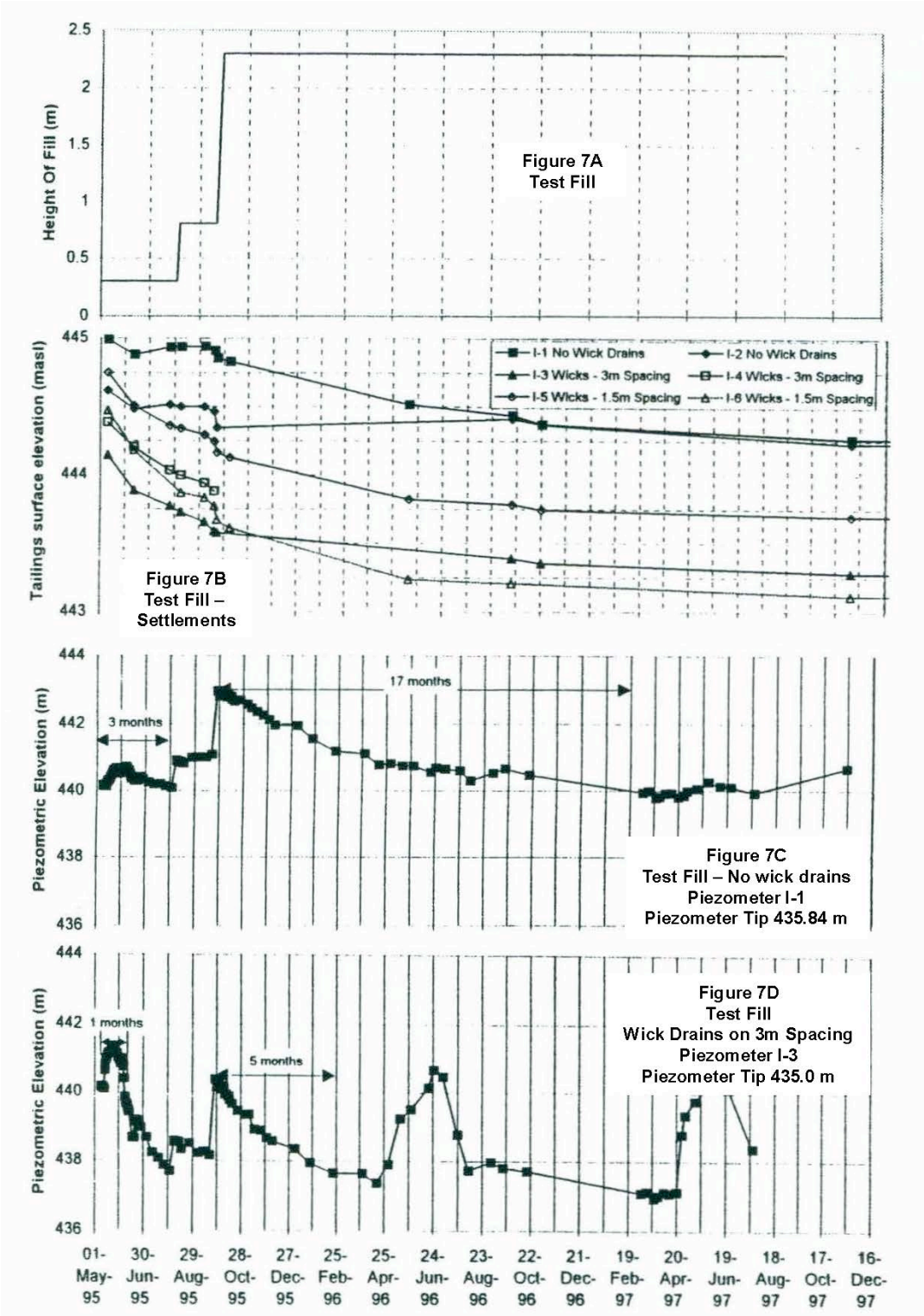


Figure 7. Test fill loading history and typical monitoring data

While, as shown in Figure 7, the wick drains provided accelerated rates of consolidation by a factor of about 3, the consolidation rates in the area without wick drains were considered to be adequate to meet the proposed decommissioning schedule of the RLAGTMF. Therefore, no wick drains were installed in the full-scale fill placement. Following successful completion and analysis of the test fill, general fill placement over the slimes pond area was commenced in 1997. The construction procedures used were similar to those applied at the test fill site.

7 DISCUSSION AND COMMENTS

The experiences with uranium mill tailings described in this paper may also be applicable to oil sand tailings. However, caution is advised in making use of the information in this paper for application to the behavior of oil sand tailings. Further comments are presented below.

(i) The difficulties related to transporting and/or spreading of dewatered (filtered) uranium tailings at the disposal site would probably be expected for oil sand tailings treated to meet the required minimum strength criteria of ERCB Directive 074.

(ii) The favourable experiences with timely consolidation of uranium tailings slurries (during active disposal or after closure) can be generally attributed to the silty nature of the uranium tailings with hydraulic conductivity (k) of 10^{-7} to 10^{-8} m/s. It is understood from Caughill et al. 1993, that oil sand tailings (full particle size range) suitably treated to minimize particle size segregation, are expected to have a similar range of hydraulic conductivity (10^{-7} to 10^{-8} m/s). Therefore, unsegregated oil sand tailings might be expected to have similar consolidation behavior to that of unsegregated uranium mill tailings.

(iii) In contrast, oil sands mature fine tailings (MFT) is expected to have k of about two orders of magnitude lower (Caughill et al. 1993). Therefore, it should be expected that MFT, treated to meet the criterion of ERCB DR074, but without improved hydraulic conductivity, would experience large on-going settlements after initial cover placement.

8 ACKNOWLEDGEMENTS

The authors are grateful to Cameco Corporation for encouragement and permission to publish data presented in this paper.

9 REFERENCES

Bishop, A.W. & Henkel, D.J. 1962. *The measurement of soil properties in the triaxial test*. Second edition, Edward Arnold (publishers) Ltd.

Caughill, D.L., Morgenstern, N.R. & Scott, J.D. 1993. Geotechnics of non-segregating oil sand tailings. *Canadian Geotech Journal*. Vol. 30, pp. 801-811.

ERCB Directive 074. 2009. Tailings performance criteria and requirements for oil sands mining schemes. *The Energy Resources Conservation Board of Alberta*. February 3, 2009.

Mittal, H.K. & Landine, P.G. 2013. Geotechnical fundamentals of uranium tailings management in Canada. *Tailings and Mine Waste*, Banff, 3-6 November 2013. Alberta, Canada.

Mittal, H.K., Holl, N. & Landine, P.G. 2000. Two uranium tailings management facilities. *Uranium 2000;Proc. intern. symp. on the Process Metallurgy of Uranium*, Saskatoon, 9-15 September 2000. Saskatchewan, Canada.

NUTP. 1986. Uranium tailings program consolidation of uranium mill tailings – final report – Part A (review modeling methods & examples). July 1986. DSS File No. 15 SQ-23241-5-1708.

NUTP. 1987. National uranium tailings program consolidation of uranium mill tailings – final report – Part B (field investigations – Rabbit Lake). February 1987. DSS File No. 15 SQ-23241-5-1708.

The potential for hydraulic mining by sluicing in the Oil Sands

Jeremy Boswell
Thurber Engineering Ltd., Calgary, Alberta, Canada.

Robert Cooke
Paterson & Cooke Ltd., Denver, Colorado, United States

Morgan Kofoed
Previously with Thurber Engineering Ltd., Calgary, Alberta, Canada.

ABSTRACT: The hydraulic transport of ore and tailings is a well-established technology in the Oil Sands. While hydraulic mining (the use of high pressure water jets to produce slurry-at-face) has been employed for many decades in the international mining and tailings industries, it has not been adopted at full scale in the Oil Sands. Recent technology scouting and screening studies have reconsidered the potential for hydraulic mining by sluicing in the Oil Sands.

The hydraulic mining of ore and tailings is a similar but competing technology to dredging, and holds some useful features and distinct benefits, which the authors describe in the paper. The paper briefly traces the history of the development of hydraulic mining of tailings and ore around the world.

1 INTRODUCTION

Hydraulic mining is a unique technology which holds potential to be applied in Oil Sands mining operations instead of the more conventional truck and shovel mining techniques. Although the technology has been used for many decades around the world, the application of hydraulic mining and sluicing to extract bitumen reserves would represent a step change in Oil Sands mining technology. The transfer of this method to the modern mining operations in Fort McMurray could present an economic opportunity.

There is a strong collaborative effort to innovate and improve upon current industry standards in Oil Sands mining, bitumen extraction, and tailings management. This paper on sluicing is presented for consideration: in the words of Confucius, "*I see and I forget; I hear and I remember; I do and I understand.*"

Hydraulic mining has been used in several different roles since its initial conception in the 19th century; this paper provides a brief overview of hydraulic mining technology, a history of the development of this technology, the current status of hydraulic mining, and the potential for application in the Oil Sands.

2 OVERVIEW OF THE TECHNOLOGY

Hydraulic mining, also known as hydraulicking, water jetting, or jet piercing, is a form of mining historically applied to surface deposits with limited application in underground mines. Hydraulic mining uses high pressure jets, also known as hydraulic monitors, of water to erode or dislodge material and sediment. The resulting slurry formed from the combination of the pressurized water and sediment is then moved through a network of trenches to a series of sluice

gates, and the desired ore is extracted through additional processes. Typically, hydraulic mining has been used for gold, kaolin, anthracite, coal, and more recently to re-mine and relocate tailings stockpiles in various industries (Summers, 2002). Engels (2013) created a simplified diagram to display the hydraulic mining process as applied to re-mining of tailings, reproduced below in Figure 1. Figure 2 illustrates a typical tailings re-mining operation.

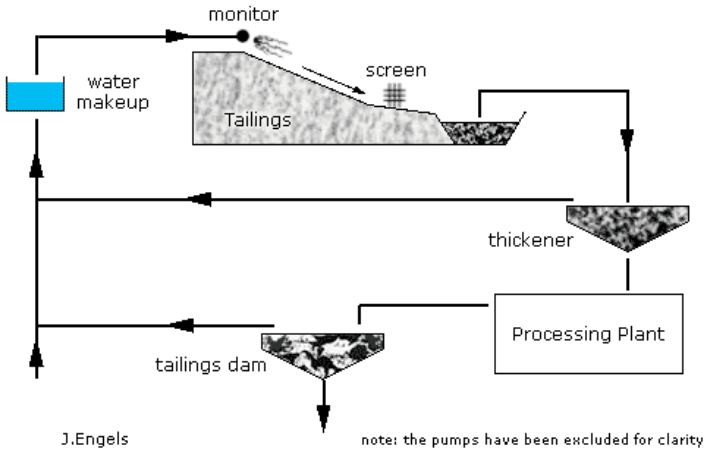


Figure 1. Simplified Diagram Showing Application of Hydraulic Re-mining of Tailings (Engels)



Figure 2. Typical tailings re-mining operation

The technology may be applied in a variety of configurations. Some mines use track mounted monitors controlled remotely from off site to minimize risk to workers and maximize operational efficiency. The more traditional hands-on approach requires operators to be in control of the monitors at all times, to direct the water jet flow from them to optimize production and maintain a safe site (Garling, 2010). The selected monitors need to be small, mobile, adaptable and robust equipment suited to their application as shown in Figure 3.



Figure 3. Mobile small scale monitor arrangement

Historically, hydraulic mining has been used to wash away alluvial deposits, operating with pressures ranging from 1 to 4 MPa (Garling, 2010). Recent developments operate within a narrow band of pressures, typically 2.8 to 4 MPa as required by the material being eroded. Pressure ranges are specific to the material, and the application of the monitor. For example, softer materials may be mined using long range, lower pressure monitors (Engels, 2010).

The slurry mixture of water and sediment can be guided and optimized to flow through the network of trenches on the mine floor, minimizing requirements for pump stations and associated costs. Any pump stations used should be designed to be simple, mobile, and located on skids to ensure quick adaptability as the mine develops. *Figure 4* illustrates a typical collection sump with integral pump arrangement.

2.1 *Important Considerations*

When reviewing the applicability of hydraulic mining for the Oil Sands, it is important to focus on several characteristics of interest, specifically the ones that will have a controlling influence in the performance of the technology. Several characteristics of interest are listed below:

- Relative density.
- Pressure requirements.
- Trenching control.
- Cut slope angle.
- Energy requirements.



Figure 4. Collection sump and pump arrangement

Holland (1942) provides an overview of some of the important background information and considerations required prior to mining a gold deposit with hydraulicking; some of which would be considered transplantable to the Oil Sands:

- Area and depth of the deposit, average grade per cubic yard, distribution and nature of the mineral content.
- Supply of water available and the attainable pressure head. These values will form a basis for mine plan estimations.
- Total length of high pressure water pipelines, flumes and slurry channels required.
- The nature and grade of the bedrock as well as depth from the surface.
- Elevation and area available for disposal of tailings.

In a review of requirements for hydraulic mine planning, Engels notes that the main conditions governing the use of hydraulic methods include:

- Geological properties.
- Climate.
- Physical-mechanical properties of the tailings such as,
    - Density, porosity.
    - Moisture content.
    - Shear strength and plasticity.

The planning process for a hydraulic mine should consider a wide array of items to reduce operational complexity and the occurrence of unforeseen items.

2.2 *Layout Optimization*

The use of a water jet relies on the impact with the rock, tailings, or sediment in order to effect a change in the material properties. Resulting increases in the capillary pressure can cause changes to the physical properties of the material, decreasing the shear strength. The penetration of the pressurized water into the cracks and crevices of the soil formation cause the cracks to grow to a point where they start to disintegrate the material, causing it to fall into a slurry collection

trench. To optimize excavation rates, the geometry of the material faces must be tightly controlled, providing tighter control of the slurry flow paths. The two primary methods of approach to mining the surface are: bottom up mining where the jets are applied from below the face, and top down mining, when the monitor is located above the deposit, and cuts in a downward direction.

The applied direction of the hydraulic jet can be combined with different slurry trench configurations to create four primary mining scenarios (Engels, 2010):

1. Water jet application and slurry flow out is in the same direction. The jet is applied from above the deposit, and the slurry flows in the direction of the applied water in a trench. An advantage of this method is that the pipeline and monitors remain on a dry surface; facilitating maintenance. This method results in reduced efficiency caused by the sharp impact angle of the water with the deposit, and usually slightly lower slurry relative densities.
2. Water jet application and slurry flow out are not in the same direction. The jet is applied from above the deposit. This method requires a trench to be placed along the entire section to be mined prior to excavation.
3. Water jet application and slurry flow out is in the same direction. The jet is applied from below the deposit. The impact angle of the jet from below the deposit will increase the efficiency of the operation and result in rapid material excavation. A trench is required prior to commencing hydraulicking operations. Slurry relative densities tend to be higher.
4. Water jet application and slurry flow out are not in the same direction. The jet is applied from below the deposit. This is the most commonly used method of hydraulic mining as it requires no site preparation prior to material excavation. The impact angle of the water jet with the material surface will increase the operation efficiency.

Use of hydraulic sluice mining in the gold industry typically produces 500 tons/hour of material removed for processing and relocation, but has been known to achieve production levels of up to ten times that amount (ERGO operations, East Rand, South Africa). Full scale testing specific to Oil Sands would have to be carried out to formulate a better understanding of rates applicable to Oil Sands.

2.3 *Background References*

Several of the items outlined above have been studied and well described by a number of researchers. Excellent background information on some of the progress made with hydraulic mining can be found in the following references:

- A general history is given by Holland (1942).
- General reference is given by Engels et al (2004).
- A discussion of previous studies in the Oil Sands is given by Tannant et al (2001).
- A brief case history is recounted in Engels (2011).
- Governing factors can be found in several different papers, including Engels (2004) & Holland (1942).

3 HISTORY OF THE TECHNOLOGY

3.1 *Early History*

Although pressurized water monitors have been used for different applications throughout history, the first recorded mining use occurred in the gold fields of California during the 1850's (Holland, 1942). The use of the monitor has been attributed to Edward Mattison, who in 1853 was responsible for creating the first monitor from a rawhide nose, and a wooden nozzle (Sierra, 2009). The original purpose of hydraulicking was to direct a jet of highly pressurized gravity fed water at an embankment to excavate and wash the gravel side hills into a sluice where the gold would settle into flumes and could be retrieved (Holland, 1942). However, the application of hydraulic mining was short lived in the Californian gold fields. The uncontrolled disposal of sediment resulted in impacts to farming communities downstream (Alpers, 2000), and in 1883 a

justice passed a decision effectively ending hydraulic mining of the gold fields (Summers, 2002).

Following the advent of hydraulic mining in the 19th century, mechanical powered hydraulic sluice mining was implemented in several countries over the course of the 20th century, including Prussia, the Soviet Union, and Germany. Initial trials were completed in the Ural Mountains to test hydraulic mining in underground coal mines. The trials proved sufficient to convert a second mine to hydraulic mining. A five year mine plan for 1956 to 1960 was orchestrated that identified 60 underground coal mine units that would increase production from 250,000 tons in 1955 to 12.5 million tons in 1960. During the trial period, limitations on hydraulic mining production rates became apparent; with the original mine unable to surpass 1500 tons per annum in contrast to the planned output of 900,000 tons per annum. The inability to meet the production scale requirements slowed further implementation of hydraulic mining (Summers, 2002).

In the late 1950's the British investigated the impact of different shaped nozzles on process efficiency at different pressure rates; conclusions from this study directed later research into the base design of nozzles across several different industries. Changing market conditions slowed further investigations and research in the 1970's.

Concurrent to these developments, hydraulic mining was used in New Zealand to mine coal reserves that were thought to be previously unrecoverable. A brief historical discussion of hydraulic mining in New Zealand is presented by Whittall (2006) and Duncan (1998) who discuss some modern applications of hydraulic coal mining in New Zealand.

3.2 *Timeline for development*

Salient events in hydraulic mining (sluicing) development are listed below:

- First used in the California Gold Fields in the 1850's.
- Cessation of hydraulic mining in California in 1883.
- Implementation of mechanical powered mining in the 20th century.
- Trials for underground coal mining in Germany, Prussia and the Soviet Union.
- Planning for 60+ underground coal mines.
- Hydraulic Mine clearing of overburden and coal extraction in New Zealand.
- 1950's research by the British into different nozzle types and the efficacy.
- Used sporadically worldwide for different purposes throughout the late 20th century.
- Initial trials in the Oil Sands were completed in the 1980's.

3.3 *History in the Oil Sands*

Several previous efforts have considered the application of hydraulic mining to the Oil Sands, and are summarized below from Tannant et al (2001):

In 1984, a series of field trials was initiated by Syncrude to assess the effectiveness of using a high pressure water jet to excavate oil sands. A range of water pressures (2 to 30 MPa) and standoff distances (0.5 to 6 m) were tested using a hydraulic jet with exit diameters ranging from 6 to 25 mm. The trials were conducted to ascertain whether it would be more efficient to apply the hydraulic jets aerially, or subaqueously.

Test results showed that using a pressure of 30 MPa applied from a nozzle diameter of 13 mm, the water jet could penetrate 2.5 m into the oil sand in five minutes aerially, or 27 minutes when submerged. Bitumen extracted using this method was at an ambient temperature of 15°C, created in a bitumen froth with ~ 56% bitumen.

A second trial was conducted where a water jet with 24 MPa of applied pressure through a 19 mm diameter nozzle cut through 20 m of oil sands. In the trials, it was observed that the Oil Sands material would readily cave downwards after an initial void space was created underneath the bulk of the material; the cave in would occur over several days.

Following initial tests by Syncrude, Imperial Oil conducted borehole mining field trials in the Clearwater Lake oil sand formation near Cold Lake in 1990 and 1991. High pressure water jets were inserted into vertical borehole and used to make a cavern 40 m thick, approximately 480 m below ground surface. A combination of water jets and cavern fluid pressure changes were used as "active" excavation tool to bring the bitumen and sand to the surface in the space between the casing and the jetting string (Tannant, 2001).

It is important to note that the aforementioned testing of hydraulic jet cutting of Oil Sands was conducted prior to the integration of hydrotransport into operations. In other words, hydraulic mining of Oil Sands ore was considered and abandoned (perhaps prematurely), prior to the advent of hydrotransport (of Oil Sands ore), and would therefore not have considered the concomitant benefits of the use of water in mining, transport, extraction and tailings management. This alone is a key factor in considering future applications.

A practical approach to the potential for hydraulic mining of Oil Sands might be to mine and size the material with the water jets, followed by a hydrotransport line to the extraction plant. The principal application of hydraulic mining would be initial excavation and transportation of the material. The required energy for operation of the hydraulic monitors and hydrotransport lines would have to be compared with the energy requirements of conventional truck and shovel operations for a more comprehensive evaluation. International experience elsewhere suggests that the economic benefits may be substantial.

4 CURRENT DEVELOPMENT STATUS

Current applications of hydraulic mining have evolved through innovation over a series of technology refinements. Some of the improvements have included decreased fuel consumption of the mechanical systems, and a reduction in the dust and particle migration left by the application of the jets. Several companies believe that hydraulic mining by sluicing could improve productivity, allowing mining to proceed up to 400% faster than dredging or conventional mining (Allen, 2013). Technological development has increased the viability of hydraulic mining application for several projects.

Garling et al (2010) identified several benefits associated with hydraulic mining including:

- Reliability (proven technique and technology).
- Safety.
- Low cost.
- Water and resource efficiency.
- Flexibility.

5 FEATURES AND BENEFITS

From previous experience by one of the authors (Boswell), in the planning, design and operation of sluicing operations in tailings recovery, the following benefits were realized in the gold, copper and diamond tailings industries:

- Substantially lower cost than conventional mechanical mining methods.
- Reliable 24 hour production of a high relative density (RD) slurry (a typical contract would specify a slurry RD of 1.55, with penalties applying if the RD dropped below 1.5 for any significant period of time, and bonuses applicable if the RD was held above 1.6).
- Rock and heavy waste was left as a residue on the mining site, and not entrained in the slurry.
- Light waste and debris (plant material, wood, etc.) was screened through trommel screens and other screening systems.
- Low maintenance effort required.
- Satellite and remote operation was readily achieved (for example, the Los Bronces contract was conducted in the 1990's at over 3500m in the Chilean Andes).
- High reliability. Attention to detail was required for the high pressure water pumping and pipeline systems.
- Low field complexity. The simplicity of operation and absence of moving parts meant that with a moderate duty of care, a system was not difficult to operate.
- High safety record.

In addition, sluicing was found to offer benefits and advantages over dredging in certain applications:

- Higher slurry relative densities.

- Substantially lower water inventory.
- Rapid start-up and shut-down, if required.
- Remote, satellite and small or isolated applications.
- Simultaneous operation of multiple sites, for increased contingency, at low cost.
- Reduced infiltration to groundwater.

6 UNKNOWNS, RISKS AND RESEARCH AREAS

When considering a technology for a new application there are always a multitude of unknowns to be resolved during the early stages of application. Without first trying the technology, it may be nigh on impossible to identify the full potential of the technology, or the areas that warrant further attention.

Early testing completed by Syncrude (Tannant et al, 2001) identified that hydraulic mining has the potential to be used in the Canadian Oil Sands. Some of the current needs to progress the technology might include:

- Mine planning and control of mine development.
- Research into the logistics of commencing and operating a hydraulic mine.
- Environmental impact.
- Safety of operations.
- Process optimization.
- Cost of operation and cost of introduction or retrofit.

The first step would be to take a small patch of land, and pilot the method. From preliminary results, further information about the practicality of the process may be learned and integrated into additional developments. A more formal process of technology development for the Oil Sands is described by Gidley et al (2013).

7 CONCLUSIONS

The notion of hydraulic mining by sluicing has been presented as an established international technology in mining and tailings engineering. The salient aspects of the technology are described, with a brief history over the past 150 years.

Opportunity exists for further consideration of hydraulic mining in the Oil Sands, with the prospect of the benefits as described in the paper, including substantially lower cost, reliable feed characteristics and sound maintenance, environmental and safety features.

8 REFERENCES

Allen, N. 2013. Hydraulic Mining: Not Your Everyday Pressure Washer. InfoMine. Retrieved May 10, 2013. URL: http://technology.infomine.com/articles/1/8617/hydraulic.hydraulicking.hydromining/hydraulic.mining.not.aspx

Bowie, A.J. 1877. Hydraulic Mining in California. Read at the Wilkes-Barre Meeting, May, 1877. 79 p.

Bowie, A.J., 1905. A practical treatise on hydraulic mining in California: New York, Van Nostrand, 313p.

Duncan, G.J. 1998. Hydraulic coal mining developments in New Zealand. Coal Operators' Conference, University of Wollongong & the Australasian Institute of Mining and Metallurgy. 333 -342.

Engels, J. et al. 2004. Tailings Management Facilities – Intervention Actions for Risk Reduction. A European Research and Technological Development Project. http://www.tailsafe.com. 152 p.

Engels, J. 2013. Hydraulic Mining of Tailings. Retrieved May 7 2013 from http://www.tailings.info/technical/hydraulic.htm.

Garling, R. & Prentice, D. 2010. Hydraulic Mining: A proven and cost effective way to Re-Mine Tailings for Plant Feed and Sustainable Relocation. Presentation given at Cobar Mining Seminar on August 8, 2010. 26 slides.

Gidley, I. & Boswell, J. 2013. A Model for Technology Development in the Oil Sands. Proc Paste 2013, Belo Horizonte, Brazil.

Gray, I. 2011. Hydraulic Sluiced Longwall Mining without Supports. 11th Underground Coal Operators'

Conference, University of Wollongong & the Australasian Institute of Mining and Metallurgy. 16-21.
Holland, S.S. 1942. Hydraulic Mining Methods. Victoria, B.C.: British Columbia Department of Mines Bulletin No. 15.
Hydraulic Coal Mining – Seddonville. URL:http://www.nzhistory.net.nz/culture/seddonville/hydraulic-mining, (Ministry for Culture and Heritage), updated December 20, 2012.
2009. Monitors – Water Cannons of Hydraulic Mining. Journal of Sierra Nevada History & Biography. Spring 2009. Vol. 2 No. 1. Retrieved May 7 2013 from http://www.sierracollege.edu/ejournals/jsnhb/v2n1/monitors.html.
Summers, D. 2002. Hydraulic Mining from California to British Columbia the long way. Mining History: The Bulletin of the Peak District Mines Historical Society. Volume 15, Nos. 4/5. 111-114.
Tannant, D.D., Martin, C.D., Regensburg, B. (2001). Hydraulic underground mining of oil sands – the next big step? CIM Bulletin, 94(1054), 63-66.
Whittall, P. 2006. Pike River Coal – Hydraulic Mine Design on New Zealand's West Cost. Coal Operators' Conference, University of Wollongong & the Australasian Institute of Mining and metallurgy, 155 – 163.

Oil sands process–affected water inventory management

Tom Hann & Jonathon Lee
WorleyParsons Canada, Edmonton, Alberta, Canada

ABSTRACT: Directive 074 of the Alberta Energy Resources Conservation Board (ERCB) has intensified oil sands' industry focus on treating mature fine tailings (MFT) with various technologies so as to create trafficable surfaces. Today, tailings ponds have process–affected water (PAW) layered on top of MFT, and this PAW is recycled for bitumen extraction. As MFT volumes are converted to trafficable surfaces, inventory management of PAW will be increasingly important. This paper provides a basis for determining MFT production when processing oil sands, which extends to identifying inventory maintenance water associated with three MFT tailing treatment methods. The integrated tracking of fines through bitumen recovery and tailings operations is expected to lead to improved management of PAW inventories.

1 INTRODUCTION

The Athabasca area in northeastern Alberta contains an estimated 1.3 trillion barrels of bitumen in place. About 10 % to 15 % of the estimated bitumen in place is amenable to surface mining techniques, and current mining and processing technologies facilitate recovering the mineable bitumen resources. Currently five mineable oil sands operators produce approximately 1.5 million barrels of bitumen and, in addition to on-going production increases by existing operators, three other operators are planning mineable oil sands lease developments.

The scale of mineable oil sands operations is large and involves disturbing an area of 781 km^2. Each produced bitumen barrel involves processing about 2 tonnes of oil sand. Each tonne of oil sand uses about 1 tonne of water for bitumen recovery and hydraulic transport of the oil sands mineral faction from ore preparation through to the tailings disposal area. When the mineral fractions are deposited in tailings disposal areas either as sand deposits or fluid tailings, the PAW is recovered in a tailings pond for recycling in a closed-loop to the bitumen recovery process. In some operations, the process water that is recycled also provides heat recovery from other process facilities.

At the current scale of mineable oil sands operations, tailing areas involve an area of 182 km^2 (Ramcharita 2013) which satellite imagery clearly displays to both industry and public at large. To reduce the accumulation of fluid tailings, the Alberta Energy Conservation Board (ERCB) set out Directive 074 in 2009, for tailing operations associated with mineable operations. The performance criteria set out by the regulations direct operators to capture mature fine tailings (MFT) in dedicated disposal areas (DDA). Operators may use a suite of technologies to meet the directive requirements.

This paper outlines a model to predict MFT production volumes and establish "inventory maintenance water". The term "inventory maintenance water" refers to water retained in the fi-

nal deposits of sand and/or fine tailings. This term is used in lieu of make-up or import water and represents water consumed in processing oil sands and depositing tailings.

In PAW inventory management, inventory maintenance water represents the system water demand. This demand would draw down PAW inventory over time if no make-up or import water is added to the system. As each mineable oil sand operation involves unique make-up or import water options which may include water streams such as mine drainage, basal depressurization water, condensed steam, water streams from other process operations, the scope of this paper is limited to only identifying the inventory maintenance water demand.

2 MINEABLE OIL SANDS BITUMEN PRODUCTION PROCESS

General block flow diagram Figure 1 shows schematically unit operations for processing mineable oil sands. It is important to recognize this as a schematic. In specific mineable oil sands flow sheets, portions of both unit operations: bitumen recovery and tailing operations may overlap or share common equipment.

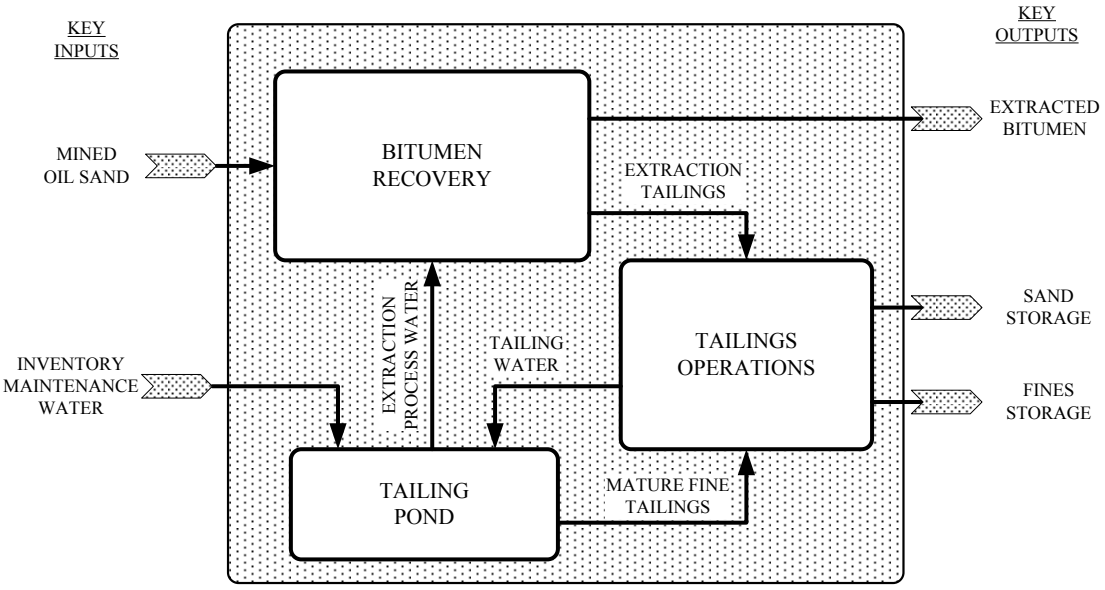


Figure 1. Mineable Oil Sands Block Diagram

2.1 *Bitumen Recovery*

Bitumen recovery unit operation involves the following steps:

- Shovels load trucks to transport oil sands from the mine face to the ore preparation plant.
- Crushers break large rocks and oil sands lumps in the mined oil sands for downstream processing, generally under 150 mm.
- Crushed oil sands are mixed with hot process water as hydrotransported slurry conditions and transports oil sands to primary separation vessels.
- Bitumen separates in the separation cell and flotation cells as bitumen froth leaving primary tailings pumped to tailings operations.
- Bitumen froth is diluted with diluent to establish a density differential for separating froth water and minerals from the hydrocarbon phase, which is the bitumen product.
- Froth water and minerals are stripped of diluent prior to pumping to tailings operations.

2.2 *Tailing Operations*

2.2.1 *Conventional Tailing Operations*

Conventional tailing operations in mineable oil sands projects create dyke structures to impound fluid tailings and the inventory the tailing pond with PAW. Conventional tailing disposal operations involve the following steps:

- Sand in primary extraction tailings is deposited in cells on the dyke structure or beaches between the dyke and tailings pond and water with fines gravity drains into the tailing pond.
- In the tailing pond fines settle into MFT in the bottom of the pond freeing PAW for recycle for bitumen recovery.

2.2.2 *Non-Segregating Composite Tailings*

Non-segregating composite tailings operations combine MFT and sand with gypsum as a process aid to create non-segregating tailings. To accelerate the production of MFT, some mineable oil sands operators use thickeners to concentrate extraction fine tailings. Non-segregating composite tailings operations involve the following steps:

- Cyclones concentrate sand in extraction tailings
- MFT is blended with cyclone underflow sand stream and pumped to the tailings disposal area.
- The non-segregating composite tailings compact and release residual water to the tailings pond.

2.2.3 *MFT drying*

MFT drying operations involve the use of polymers to aid the release of water from fluid MFT. The MFT drying operations involve the following steps:

- Polymer is injected into MFT
- Thin lift deposits or centrifuges permit the separation of water from MFT and the dried MFT is deposited directly in DDAs.
- The released MFT water is directed to the tailings pond.

2.3 *Tailings Pond*

Tailings pond operations involve pumping of PAW to bitumen recovery operations with inventory maintenance water provided by a variety of import streams.

3 PRODUCING MFT

MFT are fines in the tailing operations with a suspended solids concentration at least 30% by mass. The oil sands industry defines “fines” as any particle less than 44 μm by particle size distribution (psd). The small particle diameters of fines result in slow settling rates. The fines originate in oil sands and are dispersed into the aqueous phase of the bitumen recovery process. Without chemical additions to flocculate fines as employed in thickeners, the long retention time in a tailing pond permits fines to settle to MFT.

Linking produced MFT to mined oil sands requires considering the facies characteristics of oil sands and their implication on bitumen recovery. A field guide to the facies characterization for Athabasca oil sands are described in EUB Special Report 13 2001.

An early production model for MFT was disclosed by Camp 1977. This model applied a simplified material balance model to predict fluid tailing accumulations generated by bitumen recovery from oil sands during the initial GCOS (Great Canadian Oil Sands—now Suncor Energy) plant operations to the observed the accumulation rates of sludge (now referred to as MFT) in Tar Island pond. The material balance algorithm tracked clay as particles less than 4 μm from mined oil sands to the tailings pond using actual operating plant data. However, the process simplifications in the model together with the clay particle algorithm restricted its applicability. Clay as particles in oil sands and bitumen recovery operations is not routinely tracked.

The model discussed in the current paper tracks fines in oil sands from the mined oil sands through all process streams in the bitumen recovery ultimately to sand or fine deposits products of tailing operations.

3.1 *Characterizing Oil sands*

Athabasca oil sands is a three component mixture of bitumen, water, and minerals with the mineral fraction sub-divided between sand and fines. Components are schematically represented in Figure 2 schematically represents the components. Bitumen in mineable grade oil sands is over 7 wt% and typically averages about 11 wt%. Water in mineable oil sands is from 3 wt% to 6 wt% which wets the sand and recovery of bitumen by aqueous processes. While the mineral fraction is relatively constant, ranging between 84 wt% and 86 wt%, the fines content in the mineral fraction while typically about 15 wt% of the mineral fraction may range to 30 wt% (Masliyah et al. 2007).

The representation of oil sands in Figure 2 is schematic. While fines are assumed as dispersed particles in oil sands, this current paper considers that a significant proportion of the fines in oil sands deposits is associated mudrock lenses as schematically presented in Figure 3. While frequently referenced in literature on oil sands as clay lenses, the term mudrock refers to all silisiclastic sedimentary rocks composed by particles less than 65 μm deposited in a sedimentary environment. Mudrock includes rocks such as siltstone, mudstone, claystone, and shale originating from sedimentary deposits. Due to the geologic history and environment, the physical properties of mudrock are highly variable.

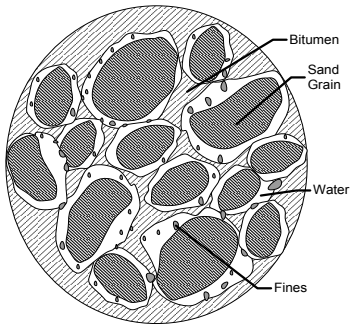


Figure 2. Schematic arrangement of oil sands

In oil sands formations, inter-bedding of mudrock layers can range from simple individual layers to highly complex depositional structures (EUB Special Report 13, 2001). The thickness of mudrock layers can range from under 5 mm to above 3 m. ERCB Directive 82 classes mudrock lenses less than 3 m thick as ore and over 3 m as waste which by can be excluded from mined oil sands.

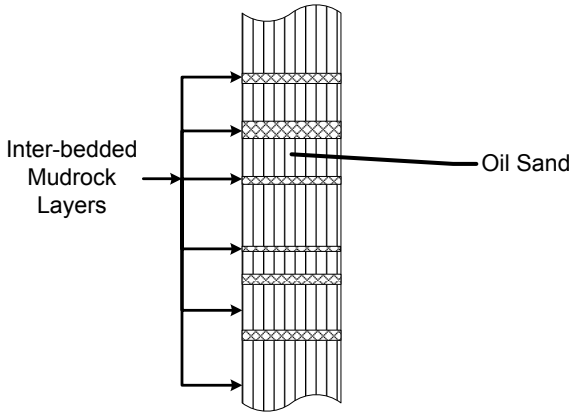


Figure 3. Schematic representation of oil sands deposits

Investigations of oil sands mudrock formations are limited. Most oil sands research is directed at processing oil sands for bitumen recovery. The test procedures in most research use oil sands with maximum particles sizes smaller than the equipment used in commercial plant operations. Either screening or crushing oil sands with mudrock layers introduces uncertainty in projecting small scale pilot test results to commercial operations. The data in Camp (1977) reflect commercial plant operations and is the forerunner of todays' large scale operations.

3.2 *Processing Mudrock*

The mining of oil sands involves excavating ore from the formation and transporting the material to the ore preparation facility. The energy intensively of these operations is important with respect to processing mudrock. In the downstream bitumen recovery operations, dispersed fines behave as individual particles while un-dispersed mudrock (UDMR) is similar to sand or gravel in sedimentation behavior. The MFT production model splits the fines at the ore preparation plant as either dispersed or UDMR which are tracked through to the tailing deposits.

Suncor historical mining operations described by Camp (1977), differs in two ways from current oil sands practice. Firstly, bucket-wheeled excavators and conveyors transported the mined oil sands to bitumen recovery. Openings in the bucket wheel and transfer system limited maximum rock sizes in the ore delivered to ore preparation. Secondly, ore preparation used rotating conditioning drums to mix oil sands with hot water and steam prior to screening. While slurry in the conditioning drum had a nominal 4 minute retention time, drum advancers and retarders in the drums retained rocks to semi-autogenously reduce oil sands lumps in the conditioned slurry. Slurry pump materials require screening particles greater than 10 mm from the conditioned slurry which resulted in an oversize reject stream that was typically 5 wt% of the oil sands feed and contained about 50% fines. The oversize stream both as a % of oil sands and fines level reflected the inter-bedded mudrock characteristics of the operating bucket- wheel excavators.

The downstream bitumen recovery operations with separation and flotation cells for primary bitumen recovery and froth treatment in Camp (1977) were similar to current operations when bitumen recovery is coupled to conventional tailings disposal. Primary tailings stream discharges about 50% mineral to the dyke structure for hydraulic placement of sand and UDMR. The void space in the deposited sand/ UDMR deposit is saturated by water and an associated proportion of dispersed fines. The water and dispersed fines that are not captured in the dyke structure discharge to the tailings pond. The UDMR and trapped dispersed fines results in the dyke mineral deposits over 5 wt% fines in Camp (1977) data. The dispersed fines in the de-sanded tailings stream discharge to the pond where dispersed fines are allowed to sediment from extraction water and concentrate into MFT.

A review of Suncor bitumen recovery commercial operating data presented in the Camp 1977 indicated the total fines dispersed was 43%. Alternately 57% of fines were contained in the oversize reject stream or behaved in sedimentation as UDMR.

Technological improvements in the early 1990s introduced truck/ shovel operations for oil sands mining and oil sands hydro transport for ore preparation, thus reducing energy intensity of mineable oil sands. Large scale truck/ shovel methods currently used for mining oil sands deliver significantly larger materials to ore preparation. While ore preparation currently crushes mined oil sands to feeder breakers, particles over 100 mm are permitted by the current generation of slurry pumps. The feeder breakers only slurries oil sand and the conditioning times are provided during the hydro transport of the oil sand to the bitumen separation facility. These technological changes suggest that UDMR could be in the range of 60 to 80% of the total fines. Esposito (2012) identified fines capture in dyke sand deposits at Muskeg River at 65% which is consistent with UDMR in hydro transported oil sands slurry. The implications of this range of UDMR on MFT production is illustrated on Figure 4.

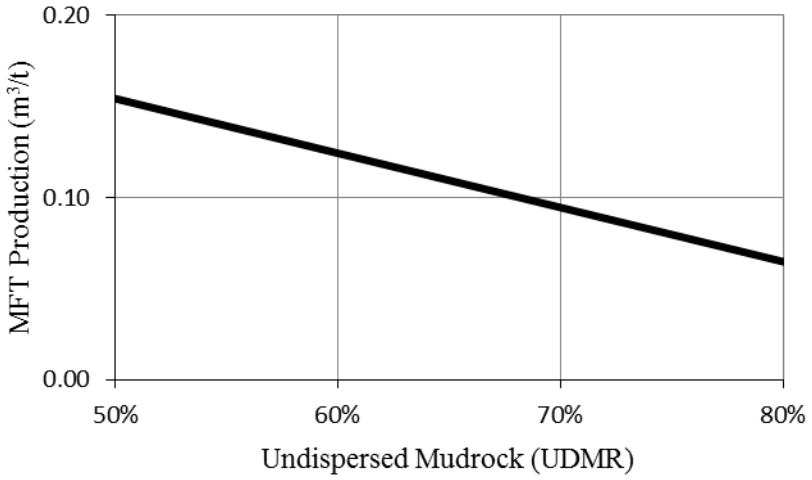


Figure 4. MFT Production Sensitivity to UDMR

Directionally higher UDMR produces less MFT for a specific bitumen recovery operation. The reduced level of dispersed fines in oil sand slurries is important for tailing disposal.

4 INVENTORY MAINTENANCE WATER DEMAND

The material balance model requires the inclusion of all water streams through the bitumen recovery process to track the flow of either dispersed fines or UDMR. This loop identifies the inventory maintenance water requirements associated with various tailing disposal methods.

Figure 5 identifies the relative sand, fines and total volumes of tailings for three tailing operations in mineable oil sands. Each case is based on the same bitumen extraction operation. The conventional tailings deposits sand and UDMR in a sand structure and contains MFT as a fluid within a containment structure. The conventional tailings with dried MFT has the fluid MFT processed using polymer aids to release water and create a trafficable surface landscape. The non-segregating composite tailings mixes MFT with sand and gypsum which is placed within a structure and over time consolidates to a trafficable surface landscape. While both conventional tailings with dried MFT and the non-segregating composite tailing total volumes are similar the distribution between sand deposits and fine deposits is significant.

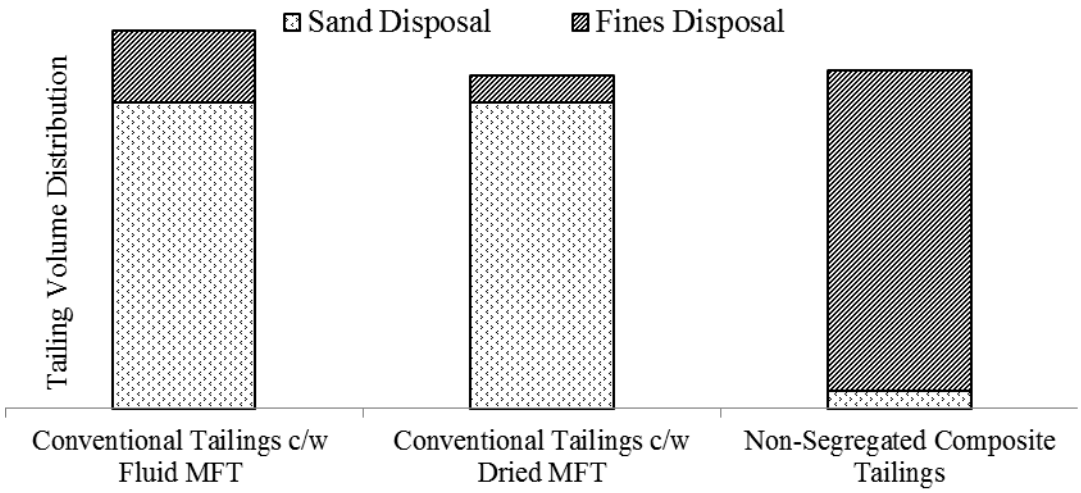


Figure 5. Volume of tailings for three tailing operations

The water content of sand and fines deposits is shown in Figure 6.

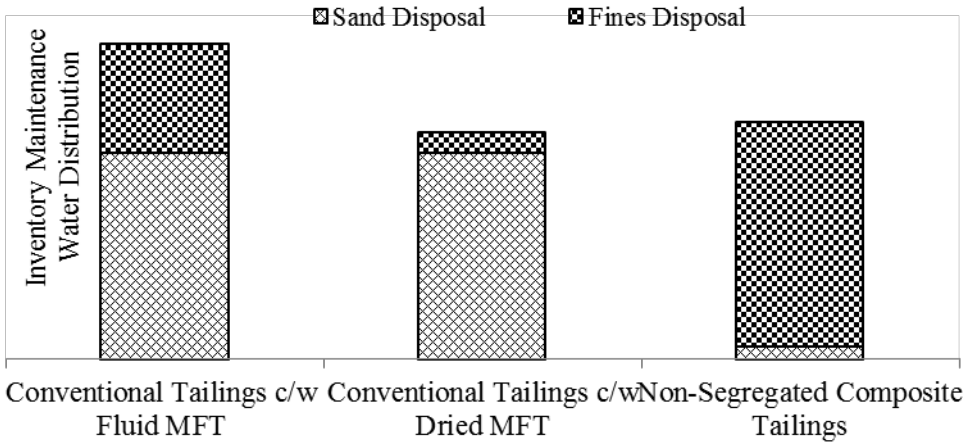


Figure 6. Distribution of inventory maintenance water for 3 tailing operations

Sand deposits are relatively permeable. The MFT production model considers that seepage water either naturally drains to the tailings pond or is collected in drains and returned to the tailings pond.

Fine deposits are relatively impermeable. Process affected water retained in fine deposits is essential locked within the deposit.

For either conventional tailings with dried MFT or non-segregating composite tailings, Figure 6 indicates reduced inventory maintenance water requirements relative to conventional tailings with fluid MFT. While the inventory maintenance water volumes appear similar in Figure 6, variations in the oil sands characteristics and process configuration can result in differences between the two MFT treatment options. Understanding the inventory maintenance water requirements between various tailing operations is important in the long term inventory of PAW.

5 CONCLUSIONS

The UDMR concept improves the understanding of MFT production. Mudrock lenses in the oil sands deposits are fines. The mining and ore preparation process steps in mineable oil sands operations determine the level of mudrock that are not dispersed into producing MFT. The current mining and ore preparation technologies have projected UDMR levels in the range of 60 to 80% of fines in mineable oil sands.

An improved understanding of MFT production enhances the understanding of inventory maintenance water requirements associated with various tailings operations. Inventory maintenance water requirements are important when implementing MFT technologies and managing long term inventories of PAW. The integrated tracking of fines through bitumen recovery operations and tailings operations is thus expected to lead to improved management of PAW inventories.

6 REFERENCES

Camp, F. W. 1977. Processing Athabasca tar sands – tailing disposal, *Can. J. Chem.Eng*. 55: 581-591, doi:10.1002/cjce.5450550516

ERCB Directive 074: Tailings Performance Criteria and Requirements for Oil Sands Mining Schemes February 2009

ERCB Directive 082: Operating Criteria: Resource Recovery for Oil Sands Mine and Processing Plant Operations, February 2013

Esposito, G. 2012. High Fines Capture at MRM North Pool Beach, IOSTC 2012

EUB Special Report 13: A comprehensive Field Guide for Facies Characterization of the Athabasca Oil Sands , Northeast Alberta.
Masliyah, Jacob, Gray, and Murray 2007, Extraction and upgrading of oilsands bitumen: Intensive short course notes, June 2007.
Ramcharita, R. 2013. Tailing and policy government perspective, 2013 Tailings technology development and commercialization, NAIT Center for Green Chemistry & Engineering Mar 19, 2013

Cover system and lysimeter design to demonstrate site specific net percolation performance

Mark Phillip
O'Kane Consultants USA, Anaconda, MT, USA

Grant Williams
J.R. Simplot, Afton, WY, USA

Robert Shurniak & Mike O'Kane
O'Kane Consultants Inc, Calgary, AB, Canada

ABSTRACT: The J.R. Simplot Smoky Canyon Mine received approval to expand operations in a 2008 Record of Decision (ROD). In addition, the ROD approved the Deep Dinwoody cover system, which was designed to meet site specific net percolation requirements to reduce selenium mass loading to groundwater. A condition of the approval was to construct a large-scale lysimeter on a 3H:1V slope to demonstrate performance of the Deep Dinwoody cover system. This paper is a case study of cover system design and performance monitoring, focusing on cover design numerical modeling and evaluation of lysimeter designs, field characterization and compaction trials of cover material, and lysimeter installation.

1 INTRODUCTION

1.1 *Site description*

Simplot operates the Smoky Canyon Mine (SCM) (42º40'N, 111º07'W); a phosphate mine in mountainous terrain located in Caribou County, Idaho, approximately 16 km west of Afton, Wyoming, and 38 km east of Soda Springs, Idaho (Fig. 1). The proposed "F" and "G" Panels expansion is located immediately south of the active mining operations. The mine is located at approximately 2130 m elevation, with annual average precipitation and potential evaporation of 795 mm and 840 mm, respectively.

1.2 *Cover system design, conditional approval & implementation*

The Deep Dinwoody cover system was designed in 2006 as part of the Environmental Impact Statement (EIS) process. The US Bureau of Land Management, US Forest Service, and the Idaho Department of Environmental Quality approved the 'Deep Dinwoody' cover system design in the 2008 Record of Decision (ROD) described as Alternative D in the Smoky Canyon Panels F and G Final Environmental Impact Statement. The ROD required construction of a large-scale lysimeter for measuring net percolation through the Deep Dinwoody cover system constructed on a 3H:1V slope of ROM material. The EIS and ROD were litigated and the design assumptions and modeling parameters used were determined to be adequate.

Dinwoody field compaction trials commenced in 2009 and completed in 2011. Lysimeter design modeling and lysimeter installation were performed in 2010, the same year mining commenced. The Deep Dinwoody cover system was installed and the field performance study area was completed in 2012.

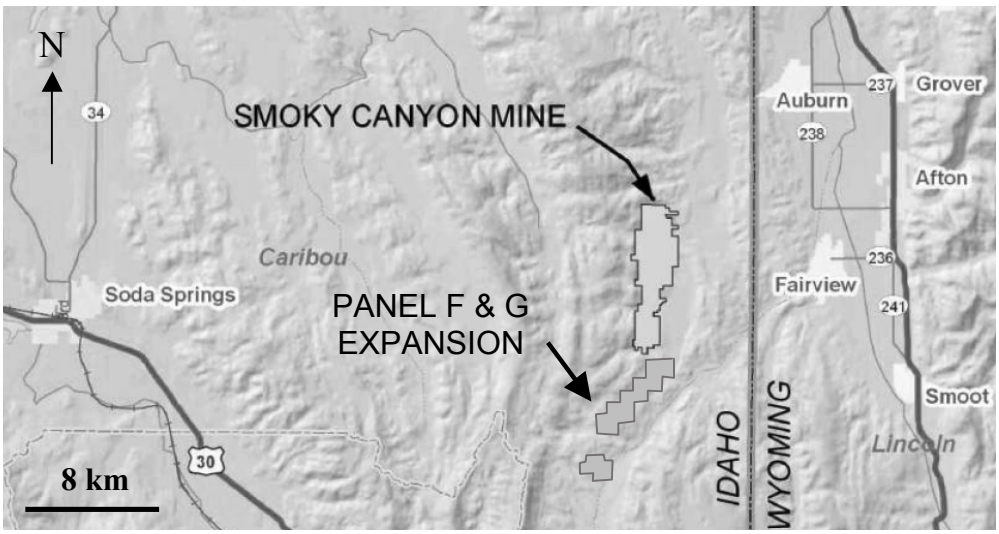


Figure 1. The J.R. Simplot Smoky Canyon mine in southeast Idaho, US.

1.3 *Cover system materials*

The cover system is comprised of topsoil, Dinwoody material, and chert, over run of mine (ROM) waste material that contains seleniferous center waste shale. The topsoil is salvaged during mining operations and has a fines content of approximately 65 to 70% (passing the 0.75 mm sieve). Dinwoody material is weathered siltstone with an average fines content of 58%. The chert and ROM are coarse material with 68% and 82%, respectively, retained on the 4.75 mm sieve.

2 COVER DESIGN MODELING

The cover system is designed with the goal of minimizing net percolation into ROM. From top to bottom the proposed cover system is comprised of 30 cm of topsoil, 30 cm lifts of Dinwoody material, 60 cm of chert overlying ROM. Two lifts of Dinwoody material, Upper and Lower, were originally evaluated; modeling demonstrated the need for a third lift Dinwoody material, referred to as the Deep Dinwoody. All results in this paper refer to the Deep Dinwoody cover system with three individual 30 cm lifts, for a total Dinwoody thickness of 90 cm.

2.1 *Modeling software*

One-dimensional (1D) and two-dimensional (2D) soil-atmosphere-plant numerical modeling of the cover system was originally completed using Vadose/W. Additional project modeling utilized current versions of Vadose/W and Seep/W.

2.2 *100-year climate database*

A 100-year climate database was developed for the project, providing input values for air temperature, relative humidity, average wind speed, precipitation and net radiation. The nearby Slug Creek, Idaho weather station, located approximately 13 km from SCM and at a similar elevation, was chosen as the station of record. To augment the limited Slug Creek data, eight additional weather station sites in the region were compared to overlapping Slug Creek data and adjusted for air temperature and precipitation. Relative humidity and wind speed were obtained from Pocatello, Idaho. Net radiation and potential evaporation values accounted for different slope aspects, specifically south, west and north-facing slopes.

2.3 *Material properties*

Material properties required for model input were obtained through laboratory analysis: particle size distribution (PSD), saturated hydraulic conductivity (k_{sat}), porosity (n), and moisture retention curves (MRCs). Hydraulic conductivity functions (k-functions) were estimated using the k_{sat} value and the van Genuchten (1980) method.

All Dinwoody lifts will be placed at a k_{sat} of $1x10^{-6}$ cm/s, but that the Upper and Lower lifts will weather (wetting/drying, root development, possible freeze/thaw) to $1x10^{-4}$ cm/s and $1x10^{-5}$ cm/s, respectively. Similar evolution of material properties have been observed in mine reclamation cover system material at Equity Silver and Syncrude Mildred Lake sites (O'Kane Consultants 2003) and documented at landfills as part of the Alternative Cover Assessment Program (Benson *et al* 2007)

The Deep Dinwoody k_{sat} is assumed to remain unchanged. Topsoil, chert and ROM have k_{sat} values of $8.9x10^{-5}$ cm/s, $3x10^{-2}$ cm/s, and $2.6x10^{-2}$ cm/s, respectively.

2.4 *Vegetation properties*

Two vegetation scenarios were modeled based on possible reclamation outcomes. A grass-dominant scenario is based on standard reclamation seed mix use. A tree-dominant scenario is based on the possibility of tree-planting in reclaimed areas. LAI and root distribution function were based on expected vegetation species. Rooting depth was limited to a maximum of 90 cm.

2.5 *One and two dimensional modeling results*

Both 1D and 2D modeling were completed for the cover system design. The complete 100-year climate database was run in the 1D model for each of the three slope aspects. Average annual net percolation rates for the north, west and south aspects are 18 mm, 15 mm, and 15 mm, respectively. Depending on mine site location, the net percolation results were below the minimum net percolation target of 20 mm.

Interflow, or lateral flow within the 2D cover system, is likely with the cover system design, both on the surface of the Dinwoody in the topsoil, and within the Dinwoody. The 5-year portion of the 1D modeling that produced the greatest net percolation was selected for evaluation in a 2D west slope Vadose model, to assess the cover system design in greater detail and compare with 1D results. The 1D and 2D net percolation results for this wetter 5-year period (average annual precipitation is 1,054 mm) were 53 mm and 48 mm, respectively. The similar nature of the results shows the 1D results to be conservative, and supports use of the results from the 100-years of 1D modeling.

2.6 *Deep Dinwoody cover system design and approval*

The Deep Dinwoody cover system, approved in the 2008 ROD, is comprised of:

- 30 cm topsoil;
- 30 cm Upper Dinwoody;
- 30 cm Lower Dinwoody;
- 30 cm Deep Dinwoody; and
- 60 cm chert.

The approval was conditional on a demonstration of performance. The Dinwoody material is required to have a geometric mean k_{sat} of $1x10^{-6}$ cm/s or less following placement and compaction. Construction of a cover system study area requires familiarity of proper Dinwoody compaction technique, and lysimeter design.

3 DINWOODY MATERIAL COMPACTION FIELD TRIALS

Prior to the F & G expansion, Dinwoody material was not present to any appreciable extent at the SCM, and was not previously used for mine reclamation. While samples of Dinwoody were obtained by excavation in the F & G Panel expansion area during the EIS process, compaction

field tests were necessary to select a compaction method that would produce both the required placed k_{sat} of $1x10^{-6}$ cm/s, and an opportunity to develop a reliable quality control surrogate test such as nuclear densometer readings. Compaction field trial work began in 2009 and concluded in 2011.

3.1 *Testing methodology*

Test pads were created to assess various compaction equipment and the necessary number of passes. Individual test sections were approximately 8 m by 67 m, allowing for full-scale construction. Ten measurement/sampling locations were evenly spaced in each test section. Dinwoody lifts were created by spreading material with a D9 Caterpillar dozer, followed by compacting the material with multiple passes of a Caterpillar 825 soil compactor, a Caterpillar 637G scraper, Caterpillar CP-63 vibratory padfoot, and the WRT PT-15 pull-type pneumatic roller.

Adjacent to each planned permeability test location, density readings were collected with a nuclear densometer; samples were collected with each reading to determine oven-dry moisture content and a corrected dry density. Following the permeability test, the wetted bulb was excavated for PSD analysis and determination of Atterberg limits.

A constant head permeameter test (ASTM D 6391-11, Method C) is used to determine the temperature-corrected field k_{sat}.

3.2 *Material variability*

Once Dinwoody material began to be recovered during the mining process, the Dinwoody was found to possess a wider range of properties than expected from the EIS characterization that was performed by excavator trenching. The EIS identified that coarse cobbles may be present in the Dinwoody, but these were believed to occur in discrete layers that could be easily excluded from reclamation material. Once mining began, however, cobbles were found to be at times more widely distributed and a challenge to identify. In addition, the Dinwoody at the bottom of the stratum was found at times to be a less weathered and blockier material. With training, staff were able to identify these changes in material properties and selectively deliver the desired Dinwoody material.

3.3 *Field trial results*

All compaction equipment except the soil compactor produced a geometric mean k_{sat} of $1x10^{-6}$ cm/s or less. The soil compactor was unable to successfully navigate a 3:1 slope. While other equipment may be used, for reasons of efficiency the WRT PT-15 pneumatic roller is the standard compaction device; with four passes the pneumatic roller produced a geometric mean field trial k_{sat} of $4.3x10^{-7}$ cm/s.

The field trial results were utilized to develop a Construction Quality Control document, providing the basis for the testing and frequency to be performed during reclamation operations. Even after trying to correct for PSD results, a relationship between nuclear densometer readings (such as dry density) and k_{sat} were not established. It is believed that the heterogeneity of the Dinwoody material is responsible for the lack of a surrogate test. Nuclear densometer readings are still collected to serve as a screening tool, but borehole permeameters are used at a frequency of one test per 0.4 ha to determine if the compacted Dinwoody material in that area is acceptable.

4 LYSIMETER DESIGN

Demonstrating the performance of the Deep Dinwoody cover system requires a lysimeter to measure net percolation. Because the presence of the lysimeter can influence its readings (O'Kane and Barbour 2003), the lysimeter design is critical to performance monitoring.

4.1 *Lysimeter design evaluation method*

All lysimeter designs were evaluated by comparison of their lysimeter collection ratio (LCR). The LCR is defined as the ratio of net percolation that would be measured by a lysimeter, as predicted by the model, to the net percolation predicted for outside the confines of the lysimeter (O'Kane and Barbour 2003). 2D designs were evaluated with Geo-Slope Seep/W. Vadose/W was used to model the 2D system and provide a comparison to confirm Seep/W results.

The 100-year climate database was evaluated to determine the most representative 20-year period for the site. The twenty years of 1976 to 1995 were chosen because it starts and ends with average or near average five-year precipitation periods and includes the wettest 5-year period within the database followed by the fourth driest five-year period on record. A synthetic average climate year was created and run repeatedly for five years at the start of the model to reduce the subjectivity of initial conditions for the 20-year climate period.

4.2 *Design options*

The first design option concerns the general size and number of lysimeters necessary to provide an accurate net percolation value. ROM, and cover material to a lesser degree, are heterogeneous materials that can influence results if scale is not taken into account. In addition, the 2D system will result in increased net percolation as the slope toe is approached. It may be possible to install dozens of Gee lysimeters or a few tank, or barrel, lysimeters (approximately 2.5 m diameter) to capture the net percolation variability. Similar to the lysimeter footprint of the Alternative Cover Assessment Program (ACAP), one large lysimeter 10 m x 20 m was selected because it was believed sufficiently large to encompass material heterogeneity (Benson *et al* 2001).

The optimum slope location of the lysimeter will be evaluated to ensure that the measured net percolation is indicative of the average net percolation along the slope. Design considerations include the depth of the lysimeter base; and, use of an open system with wall height to be determined, or a closed system similar to the ACAP study with sidewalls coming the surface.

4.3 *Modeling results*

The lysimeter size was first modeled, evaluating the 20 m slope length and lysimeters of greater length. The modeling showed that lengthening the lysimeter along the slope (i.e., greater than 20 m) does not necessarily improve performance and would likely increase the lag time between percolation events and readings. The modeling also showed that the 20 m lysimeter collects an average per unit length flux rate that is essentially the same unit flux rate of the full monitoring area slope without a lysimeter; therefore, the net percolation collected by a properly located 20 m lysimeter will be representative of the net percolation across a full slope.

A series of steady-state simulations were conducted to investigate side wall height and base depth; vertical side walls, a 20 m slope length and a surface flux rate representing 1% of annual average precipitation were standard (see Table 1). The results show that the base of the lysimeter needs to be below the chert/ROM interface to maximize the LCR. However, there is little additional increase in LCR for base depths 0.5 m below the chert/ROM interface. It is a subjective decision that is likely project specific, but concern for construction safety was balanced with a desire for lysimeter accuracy and a base depth of 1 m below the interface was used of the remainder of the design models.

Table 1. LCR results for initial model simulations

	Lysimeter Base Depth (distance below chert/ROM interface)				
Side Wall Height	0.0 m	0.5 m	1.0 m	1.5 m	2.0 m
Surface	0.94	0.97	0.98	0.99	0.99
Topsoil/Dinwoody Interface	0.94	0.97	0.98	0.99	0.99
Dinwoody/Chert Interface	0.93	0.97	0.98	0.99	0.99
Chert/ROM Interface	N/A	0.82	0.92	0.95	0.96

With the depth of the lysimeter base set at 1 m below the chert/ROM interface, a series of five 20-yr transient simulations were conducted to assess various vertical wall heights. Table 2 shows the cumulative transient LCR results for the five simulations.

Both Simulations 2 and 3 are influenced by the Dinwoody/chert interface. Either by direct contact (greatest influence) or even at a sufficiently close 15 cm distance, moisture is able to utilize the overlying Dinwoody layer to wick out of the lysimeter.

Simulation 5 is also influenced by an interface. With the wall height reaching to the chert/ROM interface, the sidewalls do not extend high enough to overcome the influence of the wetter conditions at the base of the lysimeter and wicking of moisture occurs because the wall height is not sufficient.

Table 2. Cumulative 20-year transient LCR results

Simulation	Side Wall Terminus Height	Terminus Depth (cm)	LCR
1	Surface (Closed System)	0	0.99
2	Dinwoody/chert Interface	122	0.72
3	15 cm below Dinwoody/chert Interface	137	0.86
4	Chert mid-point	152	1.06
5	22 cm above chert/ROM Interface	161	0.75

Simulation 4 with a wall height terminus in the middle of the chert layer, appears to be the most appropriate chert-related design. The sidewalls extend sufficiently above the base in Simulation 4 while minimally influencing pore-water pressure conditions in the Dinwoody and topsoil layers.

The Simulation 1 lysimeter with sidewalls to the surface, or a closed system (CS) lysimeter initially appears to function best (i.e. has an LCR closest to 1.0). However, extending the sidewalls to the surface isolates the lysimeter from the dynamics of the surrounding slope (e.g. lateral flow) and further examination raised concerns with this design. Figure 2 shows three pore-water pressure cross sections of the slope under a wet climate condition: no lysimeter, with a CS lysimeter (Simulation 1) and the chert mid-point lysimeter (Simulation 4). The no lysimeter case clearly shows the nature of 2D interflow moving down the slope in the Dinwoody and topsoil material, which is not replicated by the CS lysimeter.

At the downslope location of the CS lysimeter, suctions are lower in the Dinwoody and topsoil material than that modeled with no lysimeter present. This is due to accumulation of moisture at the downslope wall, which has moved laterally within the cover materials to this location. At the upslope location the opposite effect occurs (i.e. suctions are higher within the CS lysimeter as compared to that modeled assuming no lysimeter is present) due to the upslope wall limiting lateral flow.

The net effect of the different pore-water pressure conditions is complex (i.e. will the presence of the CS lysimeter result in a higher, or a lower, net percolation measured, in comparison to if the lysimeter were not present). It will depend on the magnitude of the difference in suction conditions at different locations within the lysimeter, but also on the flux conditions at the surface. For example, at the downslope location within the CS lysimeter, storage capacity of the near surface cover materials would be less than that for the no lysimeter condition. In addition, the infiltration capacity of the near surface material would be higher. Hence, the net effect of a rainfall event for the two different conditions will differ. Depending on the rainfall intensity, there may be more, or less, surface runoff, and less time for the near surface conditions to result in saturated overland flow (due to the reduced storage capacity of the near surface cover materials). Overall, these different responses will result in a different net percolation rate. There are multiple other scenarios that can be envisioned; however, the key point is that the CS lysimeter will not result in measurement of a net percolation rate that is representative of those that should be measured without the presence of the lysimeter.

The lysimeter footprint is a portion of the cover system study area, which has the goal of evaluating nearly all water balance components. A CS lysimeter relies on berms at the lysimeter crest and toe to prevent runon and allow collection of runoff generated within the lysimeter footprint. However, runoff generated over a 20 m distance will be vastly different than for the

entire study area slope. For these reasons, the CS lysimeter was not selected and the mid-point of the chert layer was selected as the side wall terminus (LCR = 1.06).

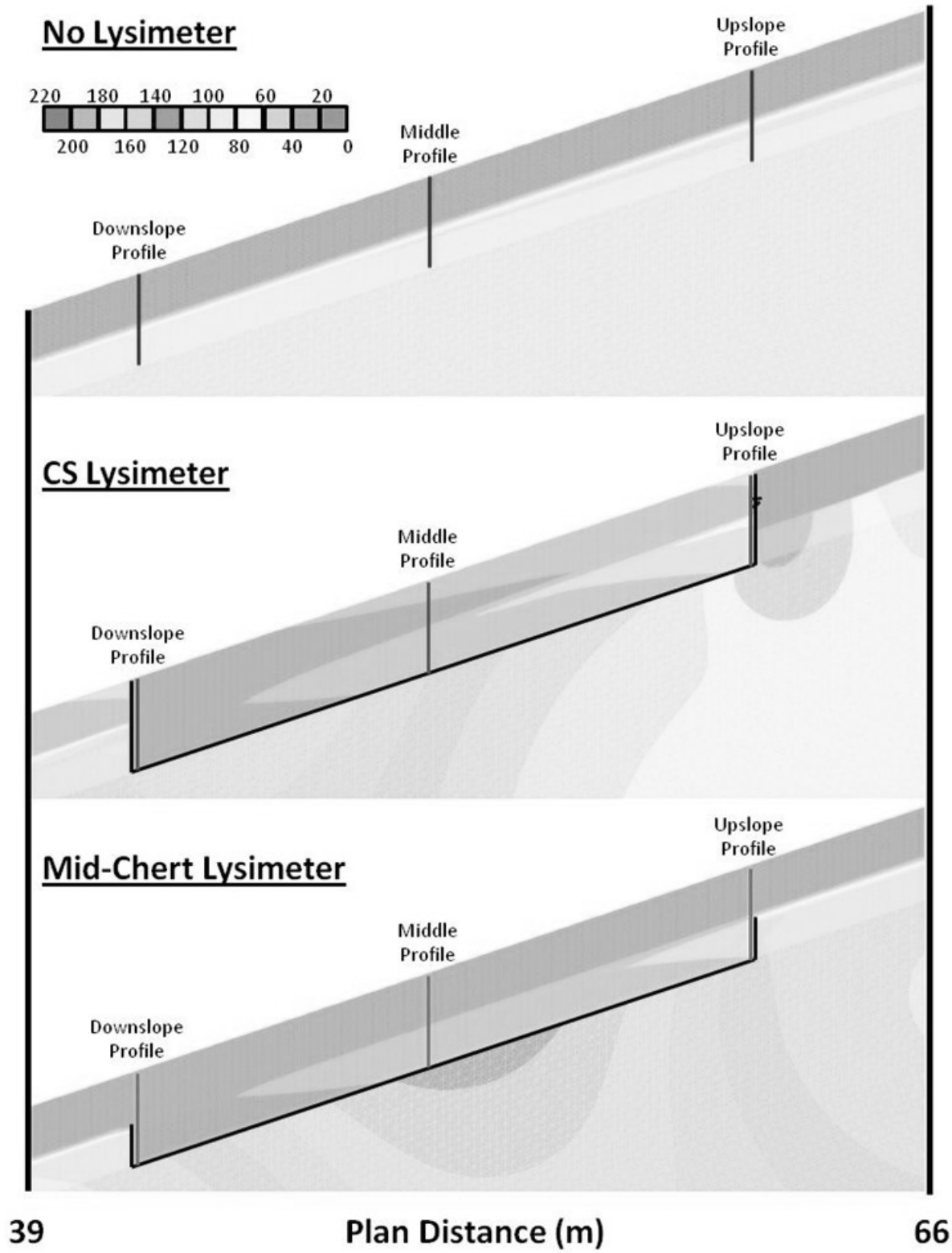


Figure 2. Wet climate condition suction contour cross-section for no lysimeter, CS and mid-chert lysimeters (kPa).

5 DEEP DINWOODY COVER SYSTEM STUDY AREA CONSTRUCTION

5.1 *Lysimeter installation*

Lysimeter construction began in 2010. The ROM was excavated to the depth of the lysimeter base. Density measurements of the ROM were collected to provide compaction targets during backfill. Prefabricated wood wall panels were assembled to support the lysimeter LLDPE liner, a base of sand was spread within the walls to protect the liner from the coarse ROM. The LLDPE liner (60 mil) was welded and trimmed *in situ* within the wood support wall dimensions, and welded to the drain boot. Geosynthetic drainage net was placed on the lysimeter base and approximately 30 cm up the walls. Geosynthetic clay liner sections were secured vertically inside the lysimeter walls to protect the LLDPE from the coarse ROM and chert.

All backfilled materials were placed in the lysimeter with a Caterpillar 320BL excavator, and then compacted using a Caterpillar CVP110 vibratory plate compactor. Alternating lifts of material were placed and compacted inside and outside the lysimeter. Material samples from each lift were collected for sensor calibration, and PSD and moisture content analysis. Once the lysimeter was buried, the remaining 30 cm of chert was placed with Caterpillar D9 dozers.

At various depths within all materials, paired volumetric water content and matric potential sensors were installed at six profiles: three profiles inside the lysimeter at toe, mid-lysimeter, and crest; and, at the same three locations outside the lysimeter.

With the lysimeter installed and buried, study area construction paused for the completion of the Dinwoody compaction field trial. All *in situ* automated sensors, as well as a weather station, were temporarily commissioned to monitor site conditions. Net percolation drainage was temporarily routed to a dosing siphon. The pause in construction was favorable from the expectation that the bare chert and ROM would be exposed to unmitigated precipitation, thereby consuming any moisture storage and priming the lysimeter for net percolation measurement once the cover system was constructed.

5.2 *Cover system installation*

The Deep Dinwoody cover system was installed in 2012 following completion of the 2011 compaction field trials. To eliminate any question of vegetation establishing roots in the lysimeter and drawing out net percolation, a root barrier of non-woven geotextile impregnated with trifluralin, a root inhibitor, was installed on the chert surface above the lysimeter footprint.

Prior to placing any Dinwoody material, the base of the interflow collection and runoff channel was constructed of chert material rising above the final surface of the chert layer. In profile the chert base is double-peaked, with the runoff channel in the middle, and the height of the uphill side of the base equal to cover system layer thickness to be placed in 2012. A single section of LLDPE was unrolled down the length of the runoff channel with the uphill side of the liner continuing downward on the chert base surface before curving uphill and terminating just under the chert surface. A geofabric-wrapped perforated pipe lies on the liner within the chert to collect Dinwoody interflow. While installing the liner prior to Dinwoody placement was a necessity because of the interflow collection system, it did present the liner as a target for any objects rolling down the hill when cover material was placed. Visual screening of objects (woody debris, significant rocks) was made when cover materials were delivered, for the dual purpose of construction quality control and runoff/interflow liner protection. The liner was inspected throughout the construction process and patches were made as needed.

Dinwoody lifts were placed and compacted with four passes of the pneumatic roller. Survey lift thickness, nuclear densometer readings, moisture content samples and borehole permeameter measurements were collected as quality control measures.

Topsoil was spread across the site, but terminated approximately 6 m above the runoff channel as a measure to minimize topsoil erosion from entering the runoff channel. Erosion control matting was installed along the bottom of the topsoil, and coarse gravel was placed between the topsoil and runoff channel with the goal of both protecting the Upper Dinwoody layer and filtering runoff sediment.

A topsoil interflow collection system is located approximately 2 m above the topsoil termination. The topsoil interflow is collected in a geofabric-wrapped slotted pipe within a continuous length of HDPE liner that is keyed into the Upper Dinwoody lift across the slope.

6 DEEP DINWOODY COVER SYSTEM STUDY AREA MONITORING

The study area monitoring goal is to measure as many water balance components as possible. The water balance equation that governs the study area can be written as:

$$\Delta S = P - RO - AET - IF - NP, \text{ where} \quad (1)$$

ΔS is the change in moisture storage, P is precipitation, RO is runoff, AET is actual evapotranspiration, IF is interflow (lateral percolation), and NP is net percolation. AET is the only water balance component not measured, which will be solved for and compared to the calculated potential evaporation (PE). Automated data acquisition systems and most sensors are sourced from Campbell Scientific.

6.1 *Meteorology*

The study area has a complete climate station monitoring air temperature, relative humidity, wind speed and direction, net radiation, snow depth, and precipitation (both tipping bucket rainfall, and weighing gauge precipitation). Both precipitation gauges feature wind screens. The variety of climate data allows for the calculation of PE. Snow surveys compliment the precipitation measurements.

6.2 *Moisture storage*

Moisture storage conditions are monitored in the six profiles in the cover system and ROM, three in the lysimeter and three adjacent in the buffer area. Automated monitoring is performed with paired volumetric water content and matric potential sensors.

6.3 *Cover saturation and temperature*

In addition to the temperature values provided by the matric potential sensors, two distributed temperature sensing (DTS) fiber optic cables are buried, one each at the top of the Deep Dinwoody and Lower Dinwoody layers. The DTS cables wind their way up and down the slope in the buffer area, providing a temperature measurements every 1 m of cable length, and therefore an areal view of temperature differences in the cover system. At two locations on the slope, two water levels sensors are buried at the bottom of the topsoil and in the Deep Dinwoody, to monitor for saturated conditions that may occur in response to snow melt and/or lengthy precipitation events.

6.4 *Net percolation, interflow and runoff*

Water balance flows are routed for redundant quantification to a heated and partially-buried monitoring station located at the end of the runoff channel and Dinwoody interflow collection. Runoff enters the station, passes through a u-trap, a 5 cm Parshall flume (high flow), and then a 1 L tipping bucket (low flow) and 10 cm Rissy/Orenco flout (low to moderate flow).

Interflow and net percolation are redundantly quantified in the monitoring station. Each of the three flows passes through a 100 mL sealed tipping bucket, followed by a 5 cm Rissy/Orenco flout. Flume and flout flow is determined with water level sensors.

Quantification of net percolation flow prior to the cover system placement was attempted with a dosing siphon; however, flow bypass occurred in the bell and quantification failed. The Rissy flout is also a dosing device, but the flout is a floating outlet on a flexible arm; when the flout reaches it maximum height, it infills with water, sinks through the water column allowing

drainage, and then resets. Following initial adjustments all flouts have performed without incident.

7 CONCLUSIONS

This paper describes a six-year process of reclamation cover system development, from numerical modeling cover design to construction of a full-scale field performance monitoring reclamation study area to demonstrate cover system performance. The project originated as a component of an EIS for a mine site expansion.

This process began with numerical modeling to design a cover system that would achieve a target net percolation during evaluation with a site-specific 100-yr climate database. The modeling assumed that cover material would weather over time and lead to the inclusion of a third layer of compacted Dinwoody material, and ROD approval of the Deep Dinwoody cover system.

Cover system approval was conditional on demonstrating field performance. Compaction trials were conducted to select a compaction methodology that would produce a final Dinwoody lift with a geometric mean k_{sat} of $1x10^{-6}$ cm/s or less. The compaction trials also served to train mine staff on construction, testing and sampling methodologies, and allowed for the development of a construction quality control plan.

Demonstrating cover system performance requires a lysimeter to measure net percolation. Numerical modeling of lysimeter design was performed to assess a variety of design aspects, and select the optimal design and location. A large-scale lysimeter with a 10 m by 20 m footprint was selected, with a base 1 m below the ROM surface, and sidewalls terminating at the mid-point of the chert layer. Lysimeter performance was sensitive to the location of the sidewall terminus within the chert layer. A closed system lysimeter was not selected due to the distortion of slope interflow.

Cover system study area construction was completed in 2012 using full-scale equipment. A largely automated monitoring system captures soil moisture data from six profiles and a weather station. Redundant measurements of interflow, net percolation and runoff are collected in a monitoring station. The study area is currently completing its first year of monitoring.

8 REFERENCES

ASTM D 6391-11. Standard Test Method for Field Measurement of Hydraulic Conductivity Using Borehole Infiltration.

Benson, C.H., T. Abichou, W.H. Albright, G.W. Gee, A.C. Roesler. 2001. Field Evaluation of Alternative Earthen Final Covers. International J. of Phytoremediation, 3:1, 105-127.

Benson, C., Sawangsuriya, A., Trzebiatowski, B., and Albright, W. 2007. Pedogenic Effects on the Hydraulic Properties of Water Balance Cover Soils. J. of Geotech. and Geoenv. Engr, 133:4, p. 349-359.

O'Kane Consultants. 2003. Evaluation of the Long-Term Performance of Dry Cover Systems, report for the International Network for Acid Prevention.

O'Kane, M. and Barbour, S.L. 2003. Field performance of lysimeters used to evaluate cover systems for mine waste. *In* Proceedings of the Sixth International Conference for Acid Rock Drainage, Cairns, Qld., Australia, July 12-18, pp. 327-339.

van Genuchten, M.T. 1980. A closed form equation for predicting the hydraulic conductivity of unsaturated soils. Soil Science Society of America Journal, 44: 892-898.

Tailings

Tailings Modelling

A finite strain consolidation model with evaporation: actual evaporation and unsaturation correction approach

Silawat Jeeravipoolvarn, Iain Gidley & Trempess Moore
Thurber Engineering Ltd, Calgary, AB, Canada

Dat Tran
University of Alberta, Edmonton, AB, Canada

ABSTRACT: This paper examines the use of an actual-potential evaporation correlation and saturated-unsaturated constitutive relationships to simulate tailings consolidation behavior during drying. This is achieved by incorporating an experimentally based actual-potential evaporation correlation into an evaporative flux boundary condition of the finite strain consolidation model. The model is corrected for unsaturation using saturated-unsaturated constitutive relationships. The developed model was compared with experimental data and other numerical model for thickened oil sands tailings. Qualitatively good agreements were obtained.

1 INTRODUCTION

High water content tailings undergoing drying are primarily affected by large strain self-weight consolidation and evaporation. Large strain self-weight consolidation is a reduction of soil volume due to the dissipation of excess pore water pressure induced by the soil mass. Evaporation occurs at the soil surface due to the difference in vapor pressure between the soil surface and the layer of air in contact with the soil. To predict the consolidation process, a finite strain consolidation theory (Gibson et al., 1967) is typically used, due to its ability to capture large strain behavior. For soil evaporation, a coupled soil-atmospheric model such as SoilCover (Wilson et al., 1994) can be applied. In tailings materials, modeling the combination of these two phenomena can be challenging due to:

- Large change in soil properties accompanying the large volume change.
- Lack of a measurement or an accurate approximation of unsaturated flow behaviour.
- Complex soil-atmospheric interaction.

Several modeling techniques have been proposed to combine consolidation and evaporation. This generally involves the implementation of an upward evaporative flux at the top boundary (Seneviratne et al., 1996; Abu-Hejleh and Znidarčić, 1997; Yao and Znidarčić, 1997; Meulen et al., 2012). The evaporative flux causes negative pore water pressure to develop at the boundary resulting in water flow and volume change. This approach is generally limited to a certain void ratio, where it can be assumed that the material is still at a saturated condition and that potential evaporation (*PE*) equals the actual evaporation (*AE*). However, this method becomes inaccurate once the soil surface begins to dry and becomes unsaturated.

Alternatively, soil-atmospheric models such as SoilCover and SoilVisions' SVFlux may be modified to include large strain consolidation theory. One example of this approach is presented by Stianson et al. (2012) who developed software based on SVFlux to have the capability to analyze saturated/unsaturated seepage, large strain consolidation, and an atmospheric boundary condition.

In this paper, to improve the evaporative flux boundary technique and provide an alternative to the soil-atmospheric model, a model was developed by considering the first two of three factors important to soil evaporation, as stated by Wilson (1990) that:

- The supply and demand of water are controlled by atmospheric conditions.
- Ability of the surface to transmit water is a function of the hydraulic conductivity and storage characteristics of the soil.
- The consumption of water through root uptake.

This paper discusses the development of a consolidation model that includes evaporation and accounts for unsaturated soil behaviour. Also presented is validation of the model with experimental data and outputs from other relevant model.

2 FINITE STRAIN CONSOLIDATION MODEL WITH EVAPORATION

Finite strain consolidation theory was used as the basis for the model. Evaporation was included through the application of actual evaporation as a boundary condition. The unsaturated soil behaviour is expressed through saturated-unsaturated constitutive relationships. Interactions between these modeling elements are illustrated in a flow diagram shown in Figure 1. The following subsections describe each component of the model.

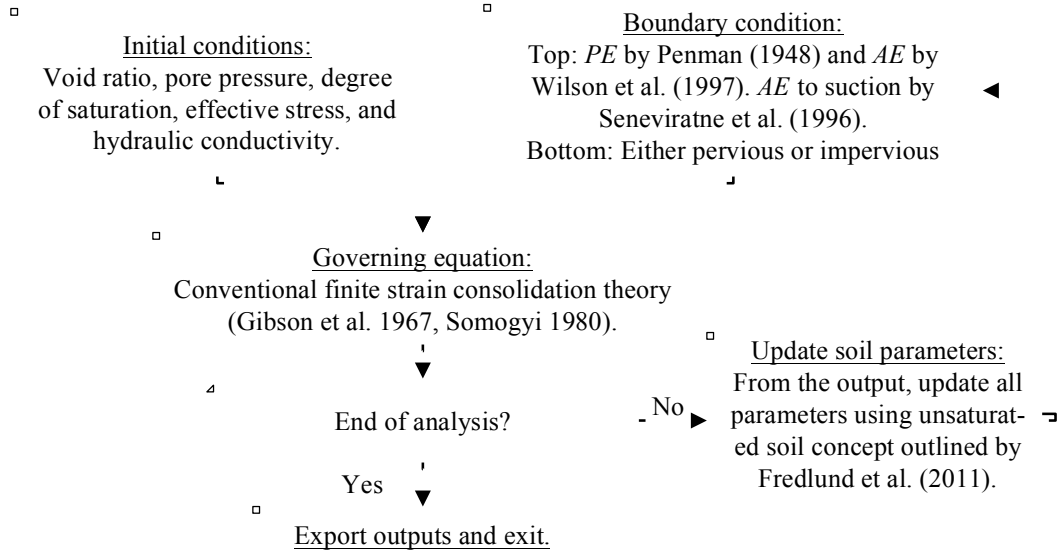


Figure 1 Finite strain consolidation model with evaporation framework

2.1 *Finite Strain Consolidation Framework*

Gibson et al. (1967) proposed a finite strain consolidation theory using a large strain derivation relating the soil volume change under the effective stress with the Darcy-Gersevanov's flow law. The governing equation proposed by Gibson et al. (1967) was reformulated in terms of excess pore water pressure by Somogyi (1980) as expressed in Equation 1.

$$\frac{\partial}{\partial z}\left[-\frac{k}{\gamma_w(1+e)}\frac{\partial u}{\partial z}\right]+\frac{\partial e}{\partial \sigma'}\left[(G_s-1)\gamma_w\frac{d(\Delta z)}{dt}-\frac{\partial u}{\partial t}\right]=0 \quad (1)$$

where e is the void ratio, σ' is the effective stress, u is the excess pore water pressure, G_s is the specific gravity of solids, k is the hydraulic conductivity, γ_w is the unit weight of water, z is the material co-ordinate, and t is time.

To solve Equation 1, Somogyi proposed that non-linear compressibility and hydraulic conductivity for saturated soils can be described by a power law function as:

$$e = A\sigma'^{B} \tag{2}$$

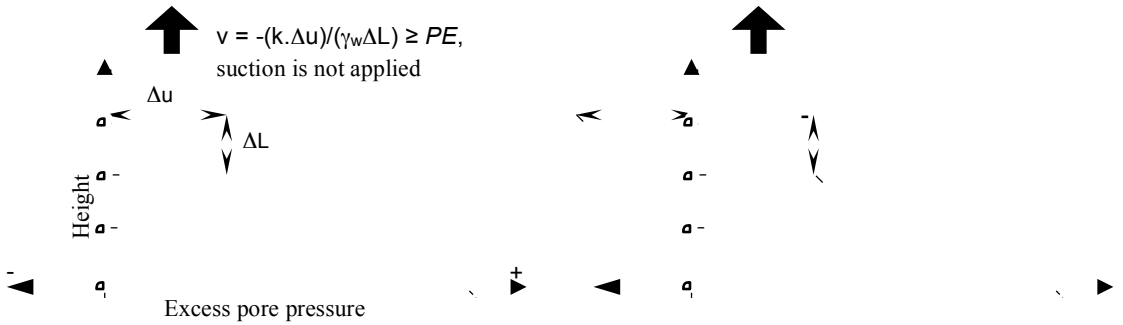
$$k = Ce^{D} \tag{3}$$

where A, B, C and D are curve-fit constants.

Using Equations 2 and 3, a model based on the excess pore water pressure formulation (Equation 1) was developed by using the finite difference numerical method.

2.2 *Evaporation Boundary Condition*

A method to implement evaporation into the tailings consolidation analysis was proposed by Seneviratne et al. (1996). This method was selected for the current study due to its direct relationship between soil suction pressure and potential evaporation. This evaporative flux boundary condition is illustrated in Figure 2.



a) When the top flux, v, is larger than *PE* b) When the top flux, v, is less than *PE*

Figure 2. Evaporation boundary condition at the top nodes

In Figure 2, it can be seen that:

a. If the upward seepage flux due to consolidation is larger than the seepage flux due to the potential evaporation, suction will not occur, and
b. As the seepage flux due to consolidation becomes smaller than that due to potential evaporation, suction is developed to satisfy the potential evaporation demand.

Potential evaporation can be calculated by using Penman's equation (Penman, 1948) or it can be obtained from a Class A evaporation pan experiment. This boundary condition can be expressed by Equation 4.

$$u_{top} = \begin{cases} u_{top} & ; \quad v = -k\dfrac{\Delta u}{\gamma_w \Delta L} \geq PE \\ u_{top+1} - \dfrac{PE.\Delta L.\gamma_w}{k} & ; \quad v = -k\dfrac{\Delta u}{\gamma_w \Delta L} < PE \end{cases} \tag{4}$$

where u_{top} and u_{top+1} are the excess pore water pressures at the top node and at the next node from the top, v is the top upward flux and ΔL is the soil element thickness.

2.3 *Actual Evaporation Correlation*

The relationship to estimate the actual soil evaporative flux by using the total soil suction is given by Wilson et al. (1997) as shown in Equation 5. This relationship was developed from drying test results of thin soil sections with an assumption that the air, water, and soil are at the same temperature.

$$\frac{AE}{PE} = \left[\frac{\exp\left(\frac{\Psi g W_v}{RT} \right) - h_a}{1 - h_a} \right] \tag{5}$$

where Ψ is the total suction in the liquid water phase expressed as the equivalent matric suction (as a negative value), W_v is the molecular weight of water (0.018 kg/mol), R is the universal gas constant (8.314 J/(mol.K)), T is absolute temperature (K), g is acceleration of gravity (m/s^2), h_a is the relative humidity of the air above the evaporating soil and water surfaces, and the term $\exp(\Psi g W_v/RT)$ is relative humidity in the soil voids.

For the new model, it is assumed that the soil-atmospheric interaction can be simulated using this relationship and that the assumptions used to develop this correlation apply. To use this relationship, soil suction is calculated from the boundary condition (Equation 4) and the relative humidity in the soil voids is calculated using the thermodynamic equilibrium relationship between the relative humidity and the total suction given by Edlefsen and Anderson (1943). The relative humidity of the air can be measured and Equation 5 can then be used to calculate *AE*. Once *AE* is obtained, the new flux boundary condition is calculated using *AE* instead of *PE*.

2.4 *Unsaturated Soil Property Corrections*

Evaporation involves saturated and unsaturated stages. The finite strain consolidation, even though developed for a saturated porous media, can be modified to approximate an unsaturated case using constitutive relationships.

To implement both saturated and unsaturated conditions for hydraulic conductivity, the hydraulic conductivity of tailings at various suction pressures must be established. A method outlined by Fredlund et al. (2011) was adopted for the current modeling approach where the degree of saturation (*S*) is used to develop an unsaturated hydraulic conductivity and total suction relationship.

To examine this concept, thickened oil sands tailings data given by Stianson et al. (2012) was used. An example of the hydraulic conductivity correction is shown in Figure 3a. Obviously the hydraulic conductivity can no longer be represented by Equation 3 when the soil becomes unsaturated. Alternatively, one may express the hydraulic conductivity in terms of suction as shown in Figure 3b. With this alternative, the hydraulic conductivity constitutive relationship becomes Equation 6.

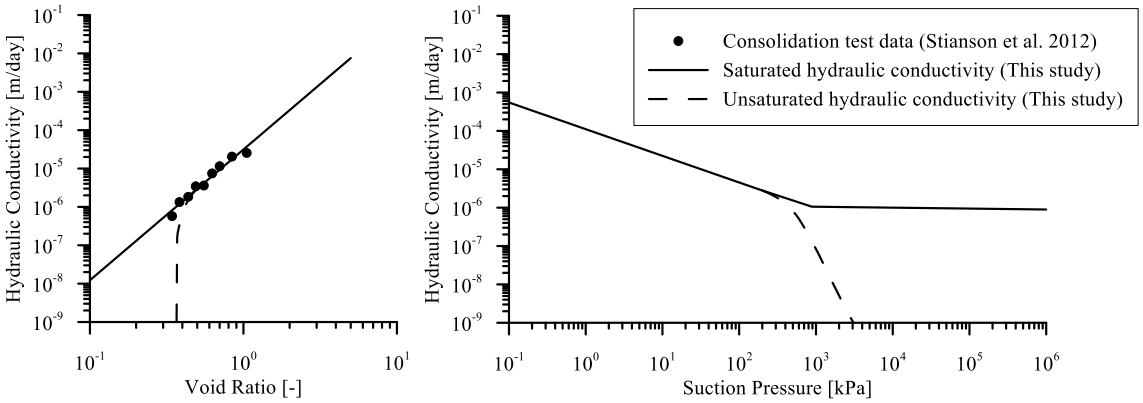
$$k = \begin{cases} C_1 e^{D_1} & ; e \geq e_k \\ C_2 \sigma'^{D_2} & ; e < e_k \end{cases} \tag{6}$$

where C_1, C_2, D_1 and D_2 are curve-fitting constants and e_k is the transition void ratio between a saturated state and an unsaturated state (i.e. a boundary between $S = 1$ and $S < 1$ or an air entry value).

For the compressibility, void ratio and suction pressure can be correlated using data from the soil water characteristic curve shown in Figure 4. Similar to the hydraulic conductivity, a single power law expression, given in Equation 2, is no longer appropriate to describe the relationship between void ratio and total suction. To maintain the conventional power law approach, Equation 7 is used.

$$e = \begin{cases} A_1 \sigma'^{B_1} & ; \sigma' < \sigma'_c \\ A_2 \sigma'^{B_2} & ; \sigma' \geq \sigma'_c \end{cases} \tag{7}$$

where A_1, A_2, B_1, B_2 are curve-fitting constants, and σ'_c is the suction pressure to connect the two functions.



a) Void ratio vs. hydraulic conductivity b) Suction vs. hydraulic conductivity

Figure 3. An example of hydraulic conductivity function correction

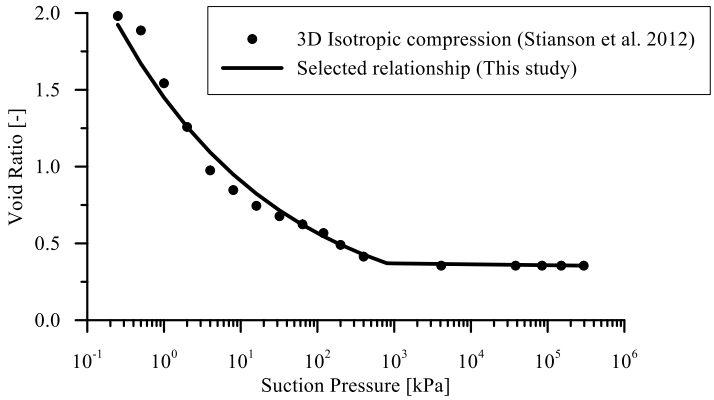


Figure 4. An example of compressibility function correction

To create the new consolidation-evaporation model, the finite strain consolidation model, the actual evaporation correction, and the saturated-unsaturated soil constitutive relationship modification were combined.

3 MODEL VALIDATION

To validate the model, laboratory and modeling results for thickened oil sands tailings presented by Junqueira et al. (2011) and Stianson et al. (2012) were selected. The thickened tailings was made from oil sands tailings with a fines content (<44 μm) of 55% and a specific gravity of 2.61. The initial solids content of the thickened tailings was 55%. Compressibility and hydraulic conductivity data for the tailings are given by Stianson et al. (2012) as shown in Figures 3 and 4.

The consolidation-evaporation experiment by Junqueira et al. (2011) used clear acrylic pipes with a diameter of 15.24 cm and heights varying from 20 to 120 cm. The tailings were poured into the columns at different heights and with different drainage conditions to investigate the consolidation and evaporation behaviour of the tailings. The tests were performed in a laboratory with an average temperature of 18.7°C, an average relative humidity of 33.5%, and an average potential evaporation of about 1.6 mm/day.

Three experiment cases presented by Junqueira et al. (2011) and Stianson et al. (2012) were selected to validate the new model: a 40 cm column with evaporation and no under-drainage; and 20 cm and 100 cm columns with evaporation and under-drainage at the base. Using the constitutive relationships provided in the model description (Figures 3 and 4), predictions were

made using the average properties described above.

The comparison between the predicted and measured data for the 40 cm column is shown in Figures 5 and 6 for interface height and final water content profile, respectively. The results of the new model compare well with the experimental results for both interface height (Figure 5) and water content profile (Figure 6a). The output from the model in this study also appears to be qualitatively similar to the other model by Stianson et al. (2012) (Figure 6b).

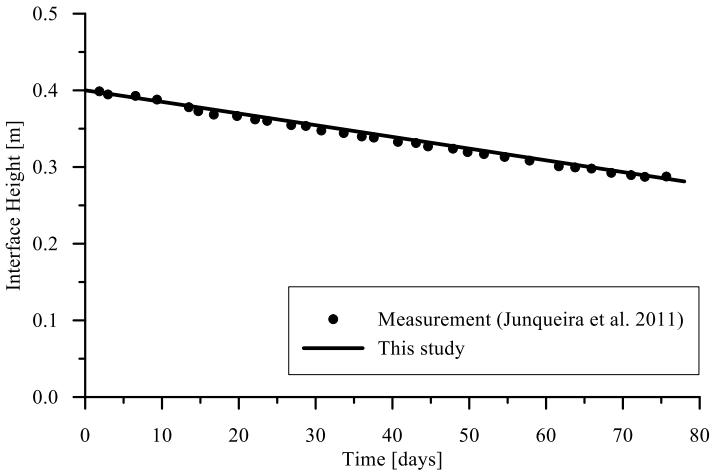
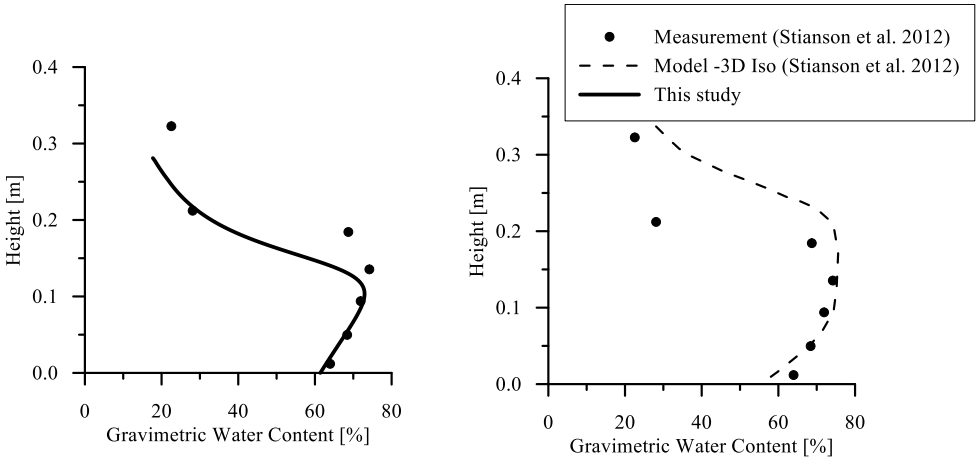


Figure 5. Interface height comparison for the 40 cm column test



a) Comparison between the new model and the experimental result

b) Comparison between the experimental result and a model by Stianson et al. (2012)

Figure 6. Water content profile comparison for the 40 cm column test at 78 days

Comparison of the predicted behaviour with the measured data for the 100 cm column is shown in Figures 7 and 8. In general, similar conclusions to the 40 cm column comparison can be made, with the proposed model showing a good correlation to the measured data. However, there is a noticeable difference between the predicted and experimental interface heights for both the proposed and comparison models. Upon closer examination it appears that the change in interface height slows down after 45 days of drying. Without additional data and observation from the laboratory, it is unclear whether the discrepancy is caused by three-dimensional shrinkage of the material close to the top, an over approximation of the unsaturated hydraulic conductivity, the bitumen migration which might have affected the hydraulic conductivity, or an overestimation of *AE*.

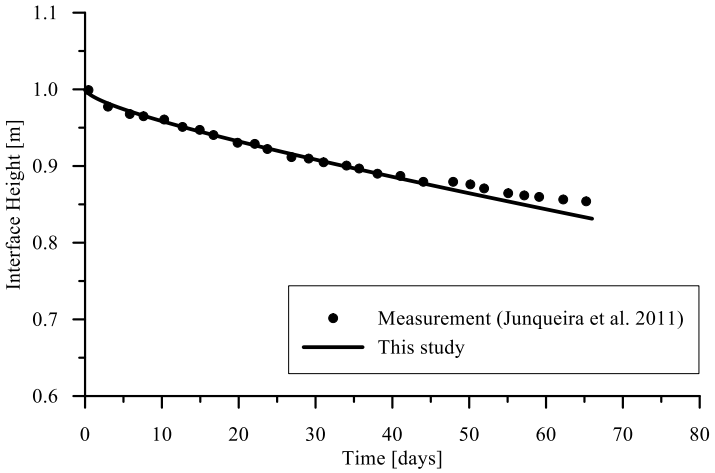
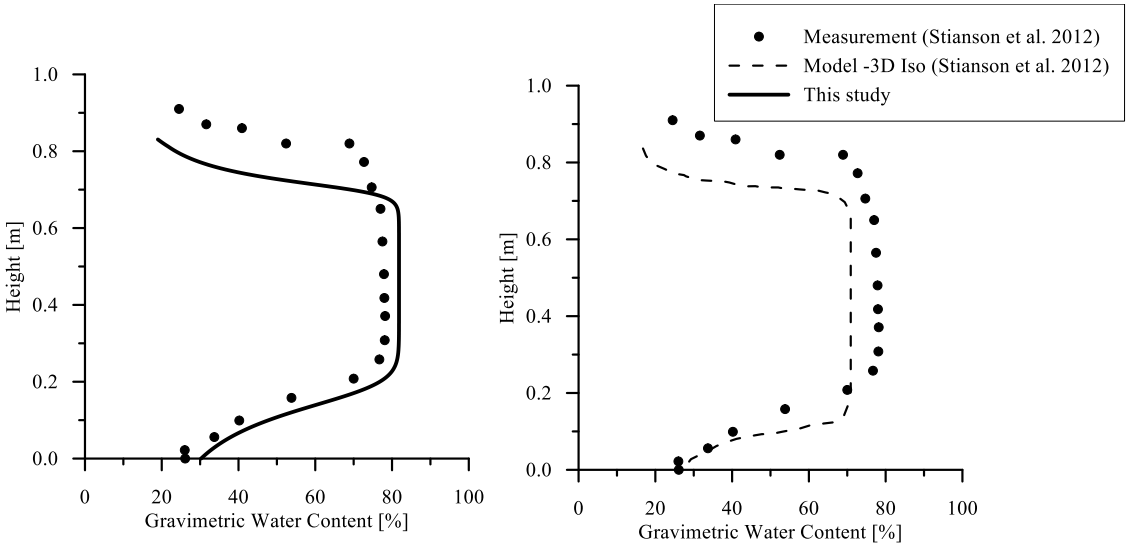


Figure 7. Interface height comparison for the 100 cm column test



a) Comparison between the new model and the experimental result

b) Comparison between the experimental result and a model by Stianson et al. (2012)

Figure 8. Water content profile comparison for the 100 cm column test at 66 days

Comparison of the predicted versus measured interface heights for the 20 cm column is shown in Figure 9. Similar to the 100 cm results, a discrepancy between the predicted and measured results can be observed. The model and the measurement appear to be initially similar but they start to diverge after 5 days. Interestingly, the final measured interface height is close to the predicted height from the model. It may be possible that since average atmospheric parameters were used in the model that the discrepancy is due to fluctuations in atmospheric parameters during the test. Further investigation of this particular experiment will be required to address this discrepancy.

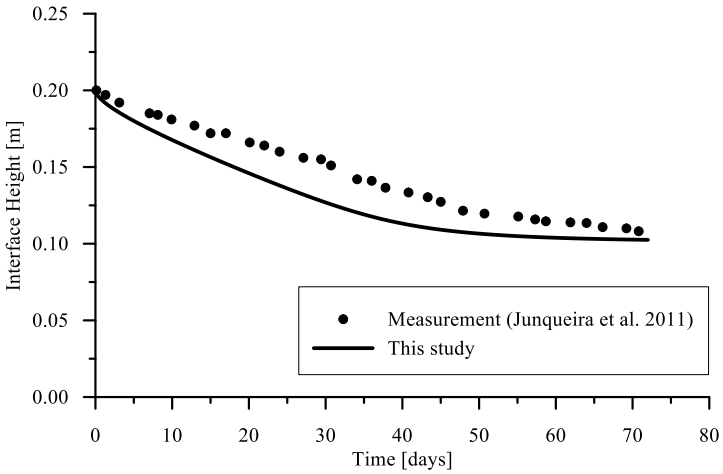


Figure 9. Interface height comparison for the 20 cm column test

4 DISCUSSION

The developed model is an attempt to surpass the limitations of the evaporative flux modeling approach by using an actual evaporation correlation and unsaturated constitutive relationships. These modifications allow the hydraulic conductivity to change significantly as the material begins to lose saturation and account for a reduction in the rate of evaporation as the suction pressure increases. Without these modifications there can be significant overestimation of the rate of drying, which can impact any environmental drying tailings disposal strategies.

The new model was compared to the laboratory experiments on thickened oil sands tailings. The predicted behaviour generally showed good agreement with the measured data. The slight discrepancy observed between the predicted and measured data is likely the result of the following four factors: three dimensional shrinkage; overestimation of unsaturated hydraulic conductivity; overestimation of AE; and bitumen migration impacting the hydraulic conductivity.

Three dimensional shrinkage would cause both vertical and lateral deformations. This could cause the interface height to decrease at a slower rate. Three dimensional shrinkage can be implemented into the current model by using the desiccation theory described by Abu-Hejleh and Znidarčić (1997). This concept uses a modified compressibility constitutive relationship to characterize vertical and lateral deformations when the soil cracks. The correction for the effect of cracks is currently under investigation by the authors of this article.

The approximation of the unsaturated hydraulic conductivity in this article was achieved by using a relationship between the degree of saturation and soil suction with the consideration of void ratio change under the suction pressure. However, it is required that this approach be validated with actual measurement of the unsaturated hydraulic conductivity of tailings. This can be further complicated due to the presence of bitumen and salt, which due to consolidation and evaporation can be concentrated near the surface. It may require that Figures 3 and 4 be developed for a range of initial bitumen and salt ion concentrations to adequately describe the changes in flow regime.

The actual evaporation correlation used in this paper is based on drying tests conducted on thin layers of natural soil. For tailings material with complex compositions, other phenomena, such as salt crusting, has been reported to suppress the actual rate of evaporation (Newson and Fahey, 2003; Simms et al., 2007). This may result in the need to develop an actual evaporation correlation specific to oil sands tailings to account for the observed changes in actual evaporation due to high salt concentrations in the pore water.

Finally, it is encouraged that evaporation experimental results such as provided by Junqueira et al. (2011) and Stianson et al. (2012) be published. This would provide an excellent opportuni-

ty to validate and/or calibrate any existing numerical models aimed at predicting water loss through evaporation under different field conditions.

5 CONCLUSIONS

A finite strain consolidation with evaporation model was developed by considering actual evaporation and an unsaturated soil property correction. The model represents an evolutionary step with regards to coupling large strain consolidation, evaporative drying, and unsaturated behavior. As such this model has been simplified from its fundamental roots. Continued effort to refine the model in the areas of three dimensional volume change and unsaturated hydraulic conductivity are required. The overall performance of the model is promising and it merits further calibration and validation with laboratory and field data sets. Further development will also need to consider a sensitivity analysis investigating the effect that certain parameters will have on the model results.

6 ACKNOWLEDGEMENTS

The author would like to acknowledge the financial support from Thurber Engineering Ltd., the review by Dr. Mauricio Pinheiro and Chenxi Zhang of Thurber Engineering Calgary, and the initial modeling inputs and discussion provided by Dr. Gord McKenna and Mr. Andy Jamieson of BGC Engineering Inc.

7 REFERENCES

Abu-Hejleh, A.N., and Znidarčić, D. 1995. Desiccation Theory for Soft Cohesive Soils. Journal of Geotechnical Engineering, 121(6): 493-502.

Edlefsen, N.E. and Anderson, A.B.C. 1943. Thermodynamics of soil moisture. Hilgardia, 15(2):31-298.

Fredlund, D.G., Stone, J., Stianson, J., and Sedgwick, A. 2011. Determination of water storage and permeability functions for oil sands tailings. Proceedings Tailings and Mine Waste 2011, Vancouver, BC, November 6 to 9. 15p.

Gibson, R.E., England, G.L. and Hussey M.J.L. 1967. The Theory of One-dimensional Consolidation of Saturated Clays. I. Finite Non-linear Consolidation of Thin Homogeneous

Layers. Géotechnique, 17(3): 261–273.

Junqueira, F.F., Sanin, N.V., Sedgwick, A. and Blum, J. 2011. Assessment of Water Removal from Oil Sands Tailings by Evaporation and Under-drainage, and the Impact on Tailings Consolidation. Proceedings Tailings and Mine Waste 2011. Vancouver, BC, Novermber 6-9, 2011.

Newson, T.A. and Fahey, M. 2003. Measurement of evaporation from saline tailings storages. Engineering Geology, 70: 217-233.

Meulen, J., Tol, F., Paassen, L. and Heimovaara, T. 2012. Numerical Modeling of Drying and Consolidaiton of Fine Sediments and Tailings. Third International Oil Sands Tailings Conference. December 2-5, 2012. Edmonton, Alberta, Canada. pp. 399-409.

Penman, H.L. 1948. Natural evaporation from open water, bare soil, and grass. Proceedings, Royal Society, London 193, pp. 120-146.

Seneviratne, N.H., Fahey, M., Newson, T.A., and Fujiyasu, Y. 1996. International Journal for Numerical and analytical Methods in Geomechanics, 20, 647-671.

Simms, P., Grabinsky, M. and Zhan, G. 2007. Modeling evaporation of paste tailings from the Bulyanhulu mine. Canadian Geotechnical Journal, 44: 1417-1432.

Somogyi, F. 1980. Large Strain Consolidation of Fine Grained Slurries. Presented at the Canadian Society for Civil Engineering, Winnipeg, Manitoba, May 29-30.

Stianson, J., Fredlund, D.G., Junqueira, F., Sedgwick, A. 2012. Formulation and solution of a numerical model for oil sands tailings from slurry to desiccation. Third International Oil Sands Tailings Conference. December 2-5, 2012. Edmonton, Alberta, Canada. pp. 381-389.

Wilson, G.W., Fredlund, D.G., and Barbour, S.L. 1997. The effect of soil suction on evaporative fluxes from soil surfaces. Canadian Geotechnical Journal 34: 145-155.

Wilson, G.W. 1990. Soil evaporative fluxes for geotechnical engineering problems. PhD thesis. University of Saskatchewan.

Yao, D.T.C., and Znidarčić, D. 1997. User's Manual for Computer Program CONDES0. Prepared for Florida Institute of Phosphate Research. Department of Civil, Environmental and Architectural Engineering, University of Colorado, Boulder, CO. 130p.

The development of a non-Newtonian flow model for bounding the beach slope angle of high density tailings stacks

Y. Babaoglu, & P. Simms
Carleton University, Ottawa, ON, Canada

ABSTRACT: Beach slope prediction remains a challenge for the design of thickened tailings impoundments. While a number of methods exist that can claim some degree of success, it is fair to say such success is not universal. This is probably due to the many different phenomena that could control tailings deposition. This paper describes preliminary work on investigating aspects of high density tailings flow behaviour using a numerical model that employs the smooth-particle hydrodynamics,(SPH) technique. The SPH technique is described. At present, the SPH based model is now able to replicate flows of tailings in flumes, and compares well with lubrication theory based analytical predictions of the final static profile. Ongoing and future development of the model and its applicability to provide insight on beaching behaviour is discussed.

1 INTRODUCTION

The flow of thickened tailings away from the deposition point and the estimation of stack geometry are important for the management of tailings facilities. These properties have an influence on the determination of the storage capacity and geotechnical stability of the stack. For example, if the overall slope angle is too steep; then it promotes erosion and decreases the geotechnical stability of the stack. On the contrary, if the angle is too small, impoundment footprint is increased as a result, or dyke construction volume must be substantially increased. The uncertainty associated with beach slope is a major impediment to wider application of high density tailings technology.

A variety of theories are used by consultants for predicting equilibrium beach profiles (Simms et al. 2011). Fitton's beach slope method and McPhail's stream power method are most commonly used. Though both these methods have different premises and assumptions, both link the final beach slope profile to the self-eroding behaviour of channelized flows. However, some evidence in the geomorphological literature suggests that this kind of analysis provides one bound on the overall slope of sediment deposits. Nor does this analysis provide information on the geometry of the individual layers of high density tailings, which either develop at the deposition point during early deposition, or at the terminus of channels. Lubrication theory based equation for static profiles of yield stress fluids have been used to describe individual layer geometries generated by spreading flows at the bench and pilot scales, however, these equations do fail once the overall stack angle reaches some critical value (Mizani et al. 2013). Additionally, it has been reported by operators that thickened tailings stacks do undergo slope stability type failures during deposition.

Given this complexity, a more fundamental investigation of high density tailings flows might be warranted. The motivation of this research is to investigate the possibility of using CFD techniques to analyze certain aspects of thickened tailings flow behaviour, for example, at what point do channels form during stack evolution. Though not advocated as a tool that would be used in consulting, it is hoped that this type of research would provide insights that would lead to more reliable beach slope prediction.

In recent years, significant progress has been achieved by using several numerical methods to study non-Newtonian fluid flows (Bovet, et al. 2007; Dean, et al. 2007; Glowinski 2011; Yuhi and Mei 2004). The present work aims to simulate the deposition of thickened or paste tailings using Smoothed Particle Hydrodynamics (SPH) method. SPH is originally introduced by Gringold & Monaghan (1977) and Lucy (1977) to solve astronomical problems and later extended to solve free surface problems by (Monaghan 1994). Other researches contributed to the method by solving non-Newtonian fluid problems using SPH method. Hosseini et al. (2007) used a three-step algorithm, fully explicit in time, to solve incompressible non-Newtonian fluid problems. Capone et al. (2011) simulated submarine landslides as a non-Newtonian fluid using Smoothed Particle Hydrodynamics method. The advantage of SPH for our problem is that it is a particle-based method, in which the free surface is implicitly defined by the location of the particles

This paper represents some preliminary results on the simulation of thickened tailings as a non-Newtonian fluid using SPH method. Open-source SPHYSICS program (Gómez-Gesteira, et al. 2012) is used for the simulations. The program is originally developed for Newtonian fluids; hence some adjustment had to be made which are explained in the upcoming section in detail. The applicability of the proposed algorithm is tested using flume test simulations. The simulated fluid is deposited from a pipe onto the flat surface similar to flume tests. The results are then compared with analytical equations derived from lubrication theory. This is a first step to develop an SPH method to simulate more complex flows.

2 BACKGROUND AND THEORY

SPH is a purely Lagrangian method where the equations of fluid dynamics are applied to a set of particles to obtain an approximate solution. Particle properties are interpolated to obtain the equations of motion and the future properties of these particles are determined from continuum equations of fluid dynamics. SPH method does not require a grid or connectivity. Also, field variables are defined for each particle hence it is an advantageous method for simulating free surface flows.

2.1 *Governing Equations*

The governing equations for the simulation of free surface flow problems consist of conservation of mass and momentum equations. Lagrangian forms of these equations, with regard to fluid particles, are defined as;

$$\frac{1}{\rho}\frac{d\rho}{dt} + \nabla \cdot \underline{\mathbf{u}} = 0 \tag{1}$$

$$\frac{d\underline{\mathbf{u}}}{dt} = -\frac{1}{\rho}\nabla P + \underline{g} + \frac{1}{\rho}\nabla \cdot \underline{\tau} \tag{2}$$

where ρ is the fluid density, g is the gravitational acceleration, t is time, P is pressure and τ is the shear stress tensor. Conservation of mass (Equation 1) defined above is in the form of weakly compressible flow to avoid solving Poisson' equation at each time step. The conservation of momentum equation consists of three driving force terms; forces due to the divergence of shear tensor, pressure gradient and the body force. These SPH equations must be solved for every particle in every time step. Equation (2), with its current form, is applicable for both Newtonian and non-Newtonian fluids. In the next section, application of the method to non-Newtonian fluid is briefly explained.

2.2 *Rheological Model*

The fluid is treated as a Bingham plastic; fluid at rest is capable of resisting any shear below the yield stress. The constitutive equation of generalized Newtonian fluid has to be referred to define Bingham fluid (Eq. 5). The shear stress τ is a function of shear rate tensor **D** (Vola, et al. 2004).

$$\mathbf{D}=\frac{1}{2}(\nabla\mathbf{v}+\nabla\mathbf{v}^{\mathrm{T}}) \tag{3}$$

The viscosity of the fluid is dependent on the second invariant of shear strain rate, $|\mathbf{D}|$ is calculated as;

$$|\mathbf{D}| = \sqrt{\sum_{ij}\mathbf{D}_{ij}\mathbf{D}_{ij}} \tag{4}$$

The constitutive relationship for Newtonian fluids is defined as (Vola, et al. 2004);

$$\tau = \mu(|\mathbf{D}|)\mathbf{D} \tag{5}$$

which demonstrates the relationship between the viscosity μ and shear strain **D**.

For a Bingham fluid, there is no deformation below the critical yield stress. Above this level, the material behaviour is Newtonian fluid. For ease of simulation, however, a 'bi-viscosity model' is often used in SPH codes to approximate behaviour of a Binghamm fluid (Beverly and Tanner 1992; Hosseini, et al. 2007). The main difference between the classical model and this model is that the viscosity is defined in the un-yielded region as well. Instead of defining no deformation below the critical zone, greater viscosity values are presented to the fluid. As a result, the transition between these two zones is smoother. The constitutive relationship can be defined as:

$$\begin{aligned} |\mathbf{D}| &\le \frac{\tau_y}{2\alpha\mu} \rightarrow \tau \quad 2\alpha\mu\mathbf{D} \\ |\mathbf{D}| &> \frac{\tau_y}{2\alpha\mu} \rightarrow \tau = (\frac{\tau_y}{|\mathbf{D}|} + 2\mu)\mathbf{D} \end{aligned} \tag{6}$$

where τ_y is the yield stress, μ is the viscosity, α represents the coefficient that gives a greater viscosity value in the un-sheared zone. D is the shear rate tensor and |**D**| is the second invariant of the shear strain rate. An effective viscosity term is added in the momentum equation to define the Bingham fluid (Capone, et al. 2010; Hosseini, et al. 2007).

$$\frac{d\mathbf{v}_a}{dt} = -\sum_b m_b(\frac{P_a}{\rho_a{}^2} + \frac{P_b}{\rho_b{}^2} + \prod_{ab}{}^{eff})\nabla_a W_{ab} \tag{7}$$

where m is the mass of the particle, P is the pressure, ρ is the density, d/dt refers to the material derivative and $\nabla_a W$ is the gradient of kernel. Effective viscosity term in the equation is represented as;

$$\Pi_{ab}^{eff} = \frac{K^{eff} v_{sig} \mathbf{v}_{ab} \cdot \mathbf{r}_{ab}}{\rho_{ab} |\mathbf{r}_{ab}|} \tag{8}$$

K^{eff} coefficient depends upon the second invariant of the stress tensor defined in Equation 6. The shear rate tensor **D** (equation 3), is calculated by the first derivative of velocity in SPH context is shown below.

$$(\nabla \cdot \mathbf{v})_a = \sum_b \frac{m_b}{\rho_b} (\mathbf{v}_b - \mathbf{v}_a) \cdot \nabla W_{ab} \tag{9}$$

The signal velocity, ν_{sig}, is defined by (Monaghan 2005)

$$v_{sig} = c_a + c_b - 4 \frac{v_{ab} \cdot r_{ab}}{|r_{ab}|} \tag{10}$$

Where c is the speed of sound values for particle a and d.

$$\frac{d\rho_a}{dt} = \sum_b m_b \mathrm{r}_{ab} \nabla_a W_{ab} \tag{11}$$

The fluid in SPH is treated as a weakly compressible fluid to avoid solving Poisson's equation for each time step. However, compressibility has to be adjusted to make sure that the time step is reasonable. The density variations in the program should be less than 15, in order to provide this condition, the speed of sound selected must be about ten times faster than themaxiumum fluid velocity.

$$P = B \left[(\frac{\rho}{\rho_0})^7 - 1 \right] \tag{12}$$

Where $B = (c_o^2 p_o)/7$, p_o is the the reference density and c_o is the speed of sound at the reference density.

3 MODEL APPLICATION

3.1 *Analytical benchmark: lubrication theory*

In order to understand the SPH code' applicability to simulate flowing thickened tailings, the results are compared with Lubrication theory. Lubrication theory has been previously applied to model lava and mud flows (Coussot and Proust 1996; Liu and Mei 1990). Several assumptions have to be made to simplify the continuity and momentum equations such as; the fluid is homogeneous, ratio of thickness to length is small and in order to eliminate the ratio of inertia to viscous forces from the equations, the velocity of the fluid is assumed to be very small (Liu and

Mei 1990). The lubrication theory equations have been used with success to describe layer geometries at the bench and the pilot scale for hard rock tailings (Mizani et al. 2013, Henriquez and Simms 2009). Here we use the equation for a single 2-D layer flowing away from a deposition point:

$$\tau_y(x - x_o) = \frac{\rho g}{2}(h_o^2 \quad h^2) \tag{13}$$

Where x_o and h_o are initial run-out distance and height respectively.

3.2 *Simulation of flow in a flume, where tailings are deposited out of a pipe*

The 2-D flume (infinite width) simulated in this model is 0.8 metres long and 2.1 metres high. The boundaries are represented by particles fixed in space. However, they follow conservation of momentum and continuity equations defined in the previous section (Eq. 1-2). When a particle approaches the boundary, the density of the fixed particle increases; resulting in a pressure increase. Hence, the force exerted of the particle increases due to the pressure term. This generates a repulsion mechanism and a repulsive force is applied to nearby particles, which generally keeps them from passing the boundary. This boundary condition can be tested by simulating a static tank of material and seeing if generated pressures are hydrostatic (Gómez-Gesteira, et al. 2012).

The fluid is initially positioned in a pipe and let it flow through onto the flat surface with time. Figure 1 represents the geometry of the flume and initial position of the fluid particles. Total of 3177 particles are used to define the boundaries and the fluid. Initial spacing of the particles is 0.005 metres in both directions. The initial thickness of the fluid in the pipe is set to 10.0 mm, and the height is 1.5 m. The density of the particles and the yield stress are set as 1823.8 kg/m^3 and 45 Pa respectively. The viscosity of the fluid is 0.8 Pa.s. These values are chosen as they pertain to material parameters of the tailings being used in bench scale tests, that will be the next target for simulation.

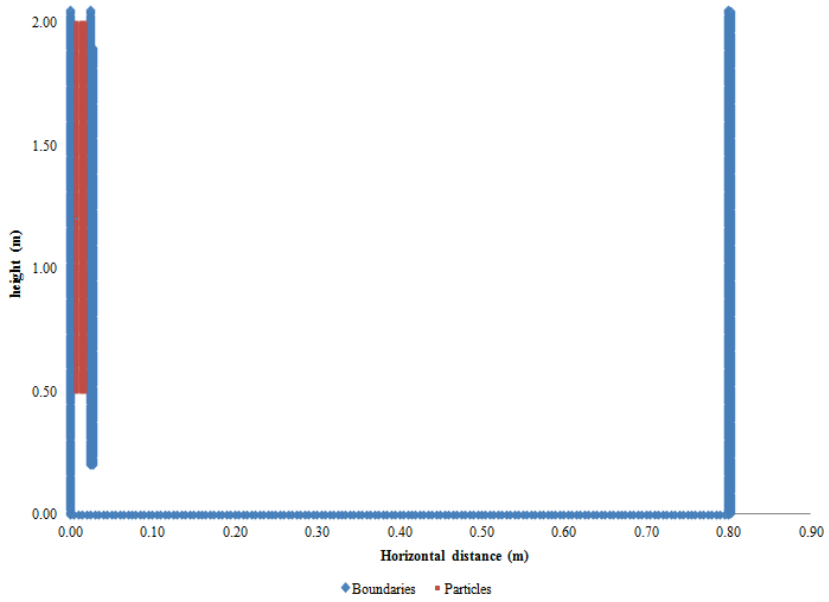


Figure 1. Initial position of the particles

4 RESULTS AND DISCUSSIONS

The fluid was completely out of the pipe at 0.93 seconds; however it reached its freezing profile at 7.52 seconds (as defined by stresses in the tailings falling below the yield stress). This final profile is then compared with the Lubrication theory predictions of Eq. 13 . The simulation was found to be sensitive to the value of α (Eq. 6) – this relates to the smoothness of the transition between low and high viscosity regimes. In literature, the most common α value is 100 (Beverly and Tanner 1992; Hosseini, et al. 2007); however, smaller values give better results in our simulations. Figure 2 demonstrates that a close agreement is observed between the Lubrication theory and computational results (α=40.0). In general, alpha values between 50 and 20 gave reasonable agreement with the lubrication theory prediction. Figure 3 shows the evolution of the profile with time. The runout does not vary much between 4 and 7 seconds, as the tailings transition from the low to high viscosity regimes.

This method is now being tested against bench scale 3-D multi-layer deposition tests, similar to those described in Mizani et al. (2013). Initially, particles will be deposited as per the flume test, and the position of each particle will be recorded in the simulations. Simulated top layers will be deposited on the topography defined by the final profile of the previous layer. Channelized flow was observed in these multilayer deposition tests, and the objective of the simulation will be to determine if SPH can replicate channel formation. It is hoped that this information will be beneficial for operators to improve control over stack geometry and ultimately geotechnical performance.

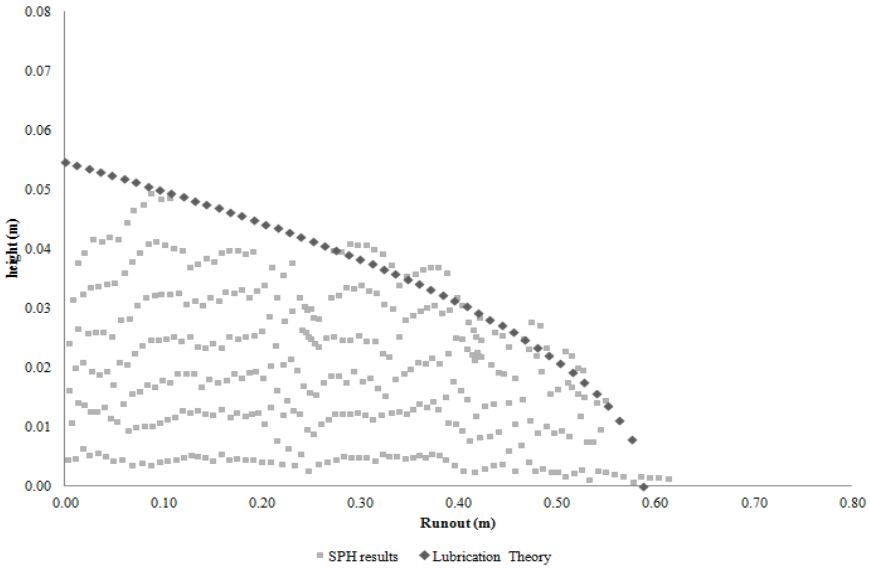


Figure 2. Final position (freezing profile) of the particles.

5 SUMMARY AND CONCLUSIONS

This paper uses a bi-viscous rheological model in the SPH algorithm for the simulation of a high density tailings flows on the beach. The numerical model has been developed to the point where it could simulate the equilibrium profile observed in single layer flume tests. Results demonstrated that the proposed method provides a close agreement with analytical equation derived using lubrication theory. Work is ongoing on applying this model to analysis of physical 3-D deposition simulations conducted at the bench scale on gold tailings.

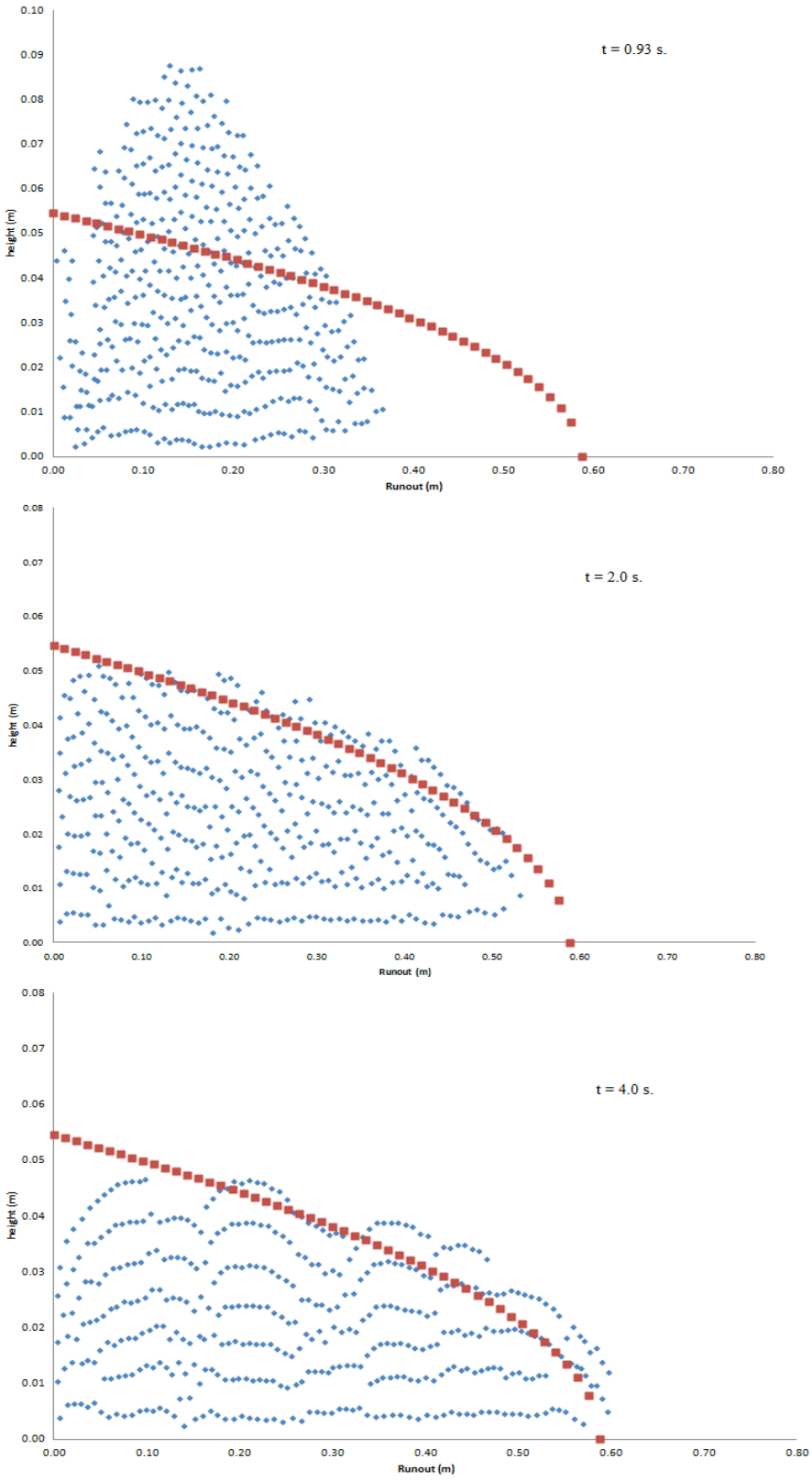


Figure 3. Surface profiles at various times

6 REFERENCES

Beverly C, Tanner R. 1992. Numerical analysis of three-dimensional Bingham plastic flow. Journal of non-newtonian fluid mechanics 42(1):85-115.

Bovet E, Preziosi L, Chiaia B, Barpi F. The level set method applied to avalanches; 2007. p 321-325.

Capone T, Panizzo A, Monaghan JJ. 2010. SPH modelling of water waves generated by submarine landslides. Journal of Hydraulic Research 48(S1):80-84.

Coussot P, Proust S. 1996. Slow, unconfined spreading of a mudflow. Journal of geophysical research 101(B11):25217-25,229.

Dean EJ, Glowinski R, Guidoboni G. 2007. On the numerical simulation of Bingham visco-plastic flow: old and new results. Journal of non-newtonian fluid mechanics 142(1):36-62.

Glowinski RW, A. 2011. On the numerical simulation of Viscoplastic flows. . In: P.G. Ciarlet RG, J. Xu, editor. In Handbook of Numerical Analysis. Amsterdam: North-Holland. p pp. 483-719.

Gómez-Gesteira M, Crespo A, Rogers B, Dalrymple R, Dominguez J, Barreiro A. 2012. SPHysics-development of a free-surface fluid solver-Part 2: Efficiency and test cases. Computers & Geosciences.

Hosseini S, Manzari M, Hannani S. 2007. A fully explicit three-step SPH algorithm for simulation of non-Newtonian fluid flow. International Journal of Numerical Methods for Heat & Fluid Flow 17(7):715-735.

Liu K, Mei C. 1990. Approximate equations for the slow spreading of a thin sheet of Bingham plastic fluid. Physics of Fluids A: Fluid Dynamics 2:30.

Mizani S, He X, Simms P. 2013. Application of lubrication theory to modeling stack geometry of high density mine tailings. Journal of Non-newtonian fluid mechanics.

Monaghan JJ. 1994. Simulating free surface flows with SPH. Journal of computational physics 110(2):399-406.

Simms P, Williams M, Fitton T, McPhail G, Jewell R, Fourie A. Beaching angles and evolution of stack geometry for thickened tailings-a review; 2011. p 5-7.

Vola D, Babik F, Latché J-C. 2004. On a numerical strategy to compute gravity currents of non-Newtonian fluids. Journal of computational physics 201(2):397-420.

Yuhi M, Mei CC. 2004. Slow spreading of fluid mud over a conical surface. Journal of Fluid Mechanics 519(25):337-358.

Modeling strength development and distribution within hydrating cemented paste backfill structure

Mamadou Fall & Othman Nasir
University of Ottawa, Ottawa, Ontario, Canada

ABSTRACT: A key parameter for the design of cemented paste backfill (CPB) structure is its strength; namely, unconfined compressive strength (UCS). Knowing the time at which the CPB reaches its reasonable strength is very important for reducing the mining cycle and ensuring the safety of mine workers. In this paper, a numerical model is developed (and implemented into FLAC software) for predicting UCS development and distribution of undrained hydrating CPB structure, taking into account the coupled effects of temperature (thermal factor) and binder hydration (chemical factors). The validation tests show good agreement between the predicted and experimental results. The developed tool is then used to simulate the strength development within CPB structures in several practical cases. The developed tool can contribute to more cost-effective and safer design of CPB structures.

1 INTRODUCTION

Financial revenues generated by the mining industry are essential for the economy of many countries including Canada. However, mining produces a huge quantity of solid waste, such as tailings. The disposal of tailings can create serious geotechnical and environmental problems (e.g., failures of tailings dams, acid mine drainage) (Fall et al. 2010). One of the most successful and innovative tailings management strategies to tackle these issues related to tailings disposal is the development of cemented paste backfill (CPB, a mix of tailings, water and binder). CPB is a vital component of underground mine operations. Its key functions are the mechanical stabilization of underground mine openings, and the maximization of safe and economic ore recovery. In addition, the maximum underground disposal of tailings and decreased acid generation represent significant environmental benefits.

Once placed into underground openings, a CPB structure should have enough strength to guarantee its mechanical stability, which will ensure the safety of miners who are working on adjacent stopes (Fall et al. 2010). In order to evaluate the mechanical stability of a CPB structure, the most direct and common method is to assess its uniaxial compressive strength (UCS) (Grice 2001). In general, the required UCS for CPB in a typical underground mining operation is 0.7–2 MPa (Brakebusch 1994; Nasir and Fall 2009). However, this UCS value can be very variable, depending on several factors, such as the function of the CPB, geomechanical and mining characteristics, and CPB structure size. One of the most significant factors that can affect UCS is the curing temperature. Recent studies (e.g. Fall et al. 2010) reveal that the curing temperature can significantly increase the early age strength gain rate and strength of CPB. This has significant practical applications. A high rate of early backfill strength gain achieved in an economical manner is the target for all stages in the mining operations. Early strength gain is of particular importance for the opening of barricades, scheduling extraction of adjacent stopes and

thus, diminution of the mining cycle time, hence increasing mining efficiency and production (Fall et al. 2010). This is clearly associated with economic benefits for mines (Wu et al. 2012). The most significant source of heat in CPB structures is the heat generated by binder hydration. The main chemical processes that affect the CPB strength development are binder hydration as well as precipitation of hydrated phases from the pore fluid of CPB. The hydration of tricalcium silicate (C_3S) and dicalcium silicate (C_2S) results in precipitation of hydration products (e.g., calcium silicate hydrate (CSH), calcium hydroxide (CH), and ettringite) in the cemented matrix of the CPB, thereby causing refinement of the pore structure and reduction in the porosity of the CPB (Ghirian et. 2011). This binder hydration is also significantly affected by the temperature; i.e. there is a coupled thermal-chemical effect on the strength development of CPB.

From the facts presented above, it is clear that this coupled effect of temperature and binder hydration has to be considered in the prediction of the evolution and distribution of strength within a CPB structure. Therefore, in this paper, a coupled thermo-chemical-mechanical model is developed to predict and analyze the evolution and distribution of strength within CPB. The model is implemented into FLAC software. The model and its validation against field and laboratory results will also be presented as follows. After that, the model will be applied to simulate some practical and relevant problems in backfilling operations.

2 DEVELOPMENT OF THE NUMERICAL MODEL

2.1 *Modeling Approach*

FLAC (Itasca 2005) was used for the numerical studies. "FLAC is a two-dimensional explicit finite difference program for engineering mechanics computation. Materials are represented by elements, or zones, which form a grid that is adjusted by the user to fit the shape of the object to be modeled". By using FLAC, a model based on the coupling of the thermal processes (T, heat generation and transfer, thermal properties), binder hydration processes (C) and the development of uniaxial compressive strength, UCS (M, mechanical factor), was developed (Figure 1). The CPB was considered as a fully saturated porous medium and subjected to undrained conditions. These assumptions are conservative with regards to the mechanical stability of CPB structure. Figure 1 provides a schematic representation of the coupled modeling approach adopted and the main coupled processes considered in the model development. The processes include:

- thermal processes (T); the thermal (temperature) process mainly involves heat generation (cement hydration) and heat transfer (heat transfer between the fresh CPB and its surrounding environment, such as rock and the mine atmosphere). The temperature has significant effects on the rate of binder hydration and the amount of cement hydration products generated within the CPB.
- chemical processes (C); they express and capture the binder hydration (which is a chemical reaction) that occur in CPB structures. The binder hydration is controlled by the coupled thermal (heat generation and transfer) and chemical (chemical reactions) processes. The binder hydration, and quantity and quality of the cement hydration products generated within the CPB will also be influenced by the chemical interactions between the tailings, mixing water (fresh, mine processing waters) and cement (various types of cement); The binder hydration rate and progress will significantly affect the temperature and the strength of CPB.
- mechanical processes (M) (limited to undrained and unconfined compressive strength in this paper); they express and predict the uniaxial compressive strength (UCS) development and distribution within the CPB structures. The UCS is the key parameter for the design of CPB structures from a mechanical stability point of view; and
- CPB filling processes (F); to take into account the effect of the CPB filling rate on the thermal, binder hydration and mechanical processes. From a numerical point of view, this backfilling rate is converted by a simple calculation into the rate of increase in the height of the backfill structure, and then to a change in the element properties (Nasir and Fall, 2009).

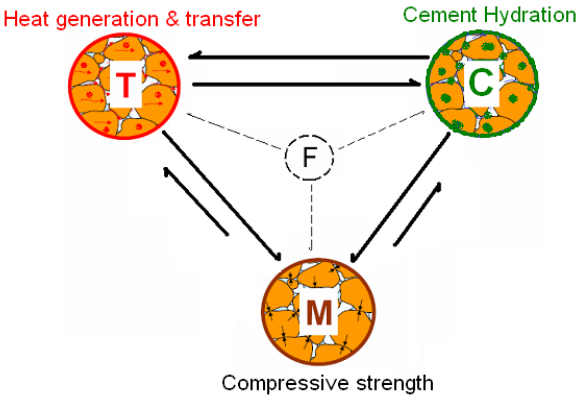


Figure 1. Schematic representation of the main coupled TCM factors in the hardening CPB structure considered in this study. F: Filling rate of the CPB; long arrow: strong coupling; short arrow: weak coupling; dashed arrow: one way effect

2.2 *Mathematical statement*

The main components of the developed model are shown in Figure 2, whereas the detailled description of the model equations (Eq. 1, 2 and 3) is given in Nasir and Fall (2009). The following model (eq. 1) proposed by Bents (2006) is adopted in this study to evaluate the degree of binder hydration (symbol α in Figure 2). This model takes into account the water-to-cement ratio (w/c) in the hydration process.

$$\frac{\partial \alpha}{\partial t} = A\frac{(B-\alpha)^2(1-\alpha)}{(C-\alpha)} \qquad A = \frac{k_3\left(f_{\exp}+\rho_{cem}CS\right)^2}{f_{\exp}\left[1+\rho_{cem}(w/c)\right]^2} \tag{1}$$

with:

$$B = \frac{\rho_{cem}}{f_{\exp}+\rho_{cem}CS}\left(\frac{w}{c}\right)$$

$$C = \frac{\rho_{cem}}{f_{\exp}}\left(\frac{w}{c}\right)$$

where:
α: degree of hydration
t: time
k_3 : constant (= 0.061 for sealed curing conditions)
$f_{\exp}$: volumetric expansion coefficient for the solid cement
ρ_{cem}: specific gravity of cement
CS: chemical shrinkage per gram of cement
w/c : water to cement ratio
The effect of temperature (θ) on the hydration process is introduced into Equation 1 by means of Arrhenius law.

To express the the relationship between the degree of hydration and compressive strength the following equation (eq. 2 in Figure 2) developped by Zelic et al. (2004) is adopted.

$$\frac{\alpha}{1-\alpha} = k_{fc2}\left(\frac{fc}{fc_{\infty} - fc}\right) + k_{fc3} \tag{2}$$

where:

k_{fc2} and k_{fc3} are constant (Zelic et al. 2004)

The effect of the temperature on the UCS of CPB is introduced by the constant k_{fc2} in Equation 2. The constant k_{fc2} is temperature dependent, and can be modified by the following equation:

$$k_{fc}(T) = k_{fc2}(50°C) - \beta(50 - T) \tag{3}$$

where:

$k_{fc}(T)$: temperature $(T°C)$ dependent constant to be used in Equation 6.

$k_{fc2}(50°C)$: reference value (at 50°C)

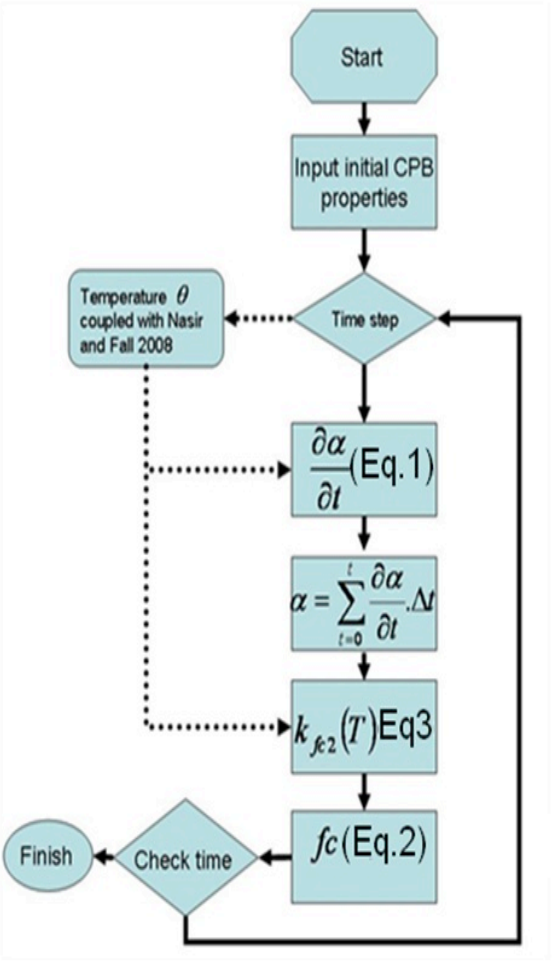


Figure 2. Flow chart for the model of UCS development in CPB.

2.3 *Modeling backfilling rate*

The rate of backfilling can be defined as the rate of the pumping of paste into the stope. This rate is strongly dependent on the size of the stope for a given backfill pumping capacity. Moreover, according to some field conditions, such as the stope size, the requirements for opening the barricades and the preparation rate of CPB, the backfilling rate may vary at different stages of a mine. The rate of placing CPB into stope could influence the thermal and chemical processes (thus the strength) that occur within the CPB. Therefore, the backfilling rate is coupled to the models that capture the thermal, chemical (binder hydration) and mechanical (strength) processes. This rate is given by the following equation:

$$\frac{\Delta H}{\Delta t} = \frac{\Delta p / \Delta t}{\gamma . A_r} \tag{4}$$

where:

H : height of backfill,

$\Delta p / \Delta t$: pumping rate (tonne/hour), and

A_r: cross section area of the stope.

2.4 *Model validation*

In order to test and verify the ability of the developed TCM model to predict the strength development within a CPB, the model was applied to simulate heat and strength development within CPB, and the simulation results were validated against the results obtained by field and laboratory investigations. The validation results have shown that there is good agreement between the results obtained from laboratory and field investigations, and those predicted. Two examples of validation results are illustrated by Figures 3 and 4. Figure 3 shows a comparison of the temperature history between the current study model and the field data from a selected example in the Lucky Friday mine (Williams et al., 2001). Figure 4 depicts a comparison between the UCS values of the CPB predicted by the TCM model and those experimentally obtained.

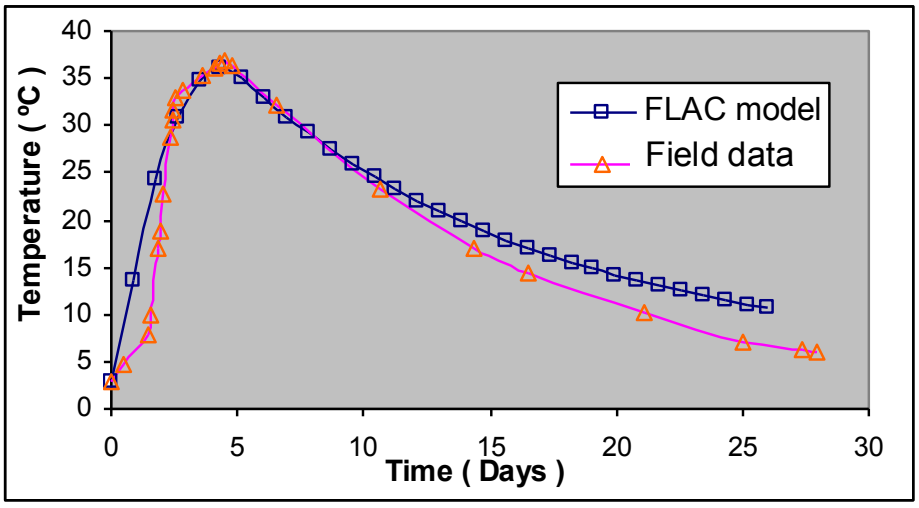


Figure 3. Comparison between the predicted and measured temperature development within the CPB structure in the field (Lucky Friday mine)

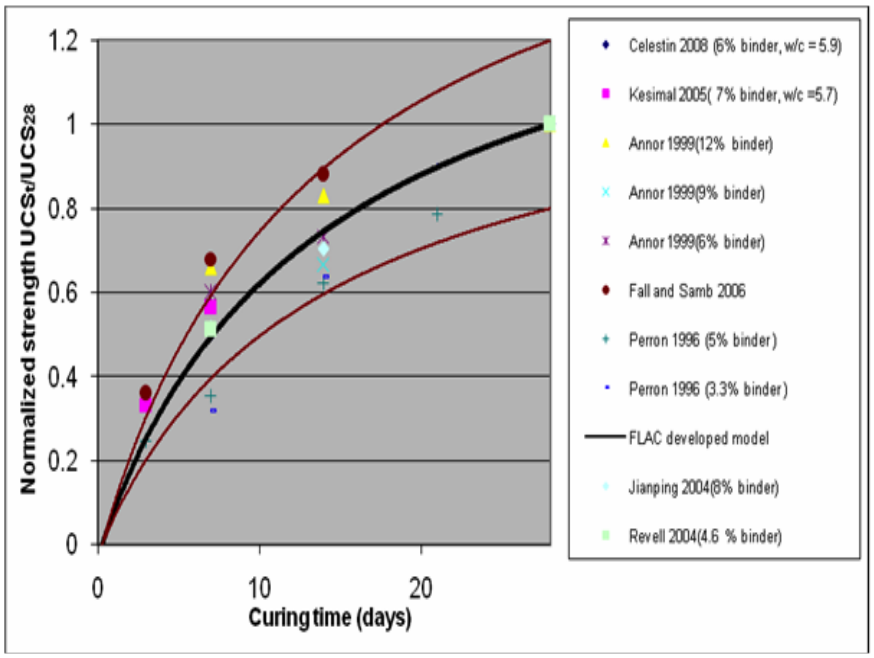


Figure 4. Comparison between the predicted and experimental UCS.

3 APPLICATION EXAMPLES

After the successful validation of the developed model against different experimental laboratory and field data, the model was applied to simulate the strength development and distribution within a CPB structure in underground mine openings and the different factors affecting it. The simulation focused on some practical problems that a mine operator or engineer has to face when backfilling a stope. The factors were chosen to assess the influence of stope geometry (size, shape, angle and height), rate of backfilling, initial CPB and rock temperatures, curing time, CPB mix components (e.g, tailings types, binder content) and rock thermal properties on the UCS development and distribution. Some samples of simulation results are presented and discussed below.

3.1 *Effect of stope size on the strength development within CPB structures*

Figures 5 shows both the strength development and distribution within stopes of different sizes. Strength is represented by the percentage gained of ultimate strength. Results reveal that the size of the backfilled stope significantly affect the strength development and distribution within a CPB structure. Increasing the stope size results in an increase in the strength developed, especially at the lower part of the stope, while with a smaller size, the strength will be lower and more homogenous. This is due to the fact that increasing the size will delay the heat transfer from the hydrated CPB to the surroundings, which leads to the accumulation of heat and increase in temperature, which then leads to increase in strength.

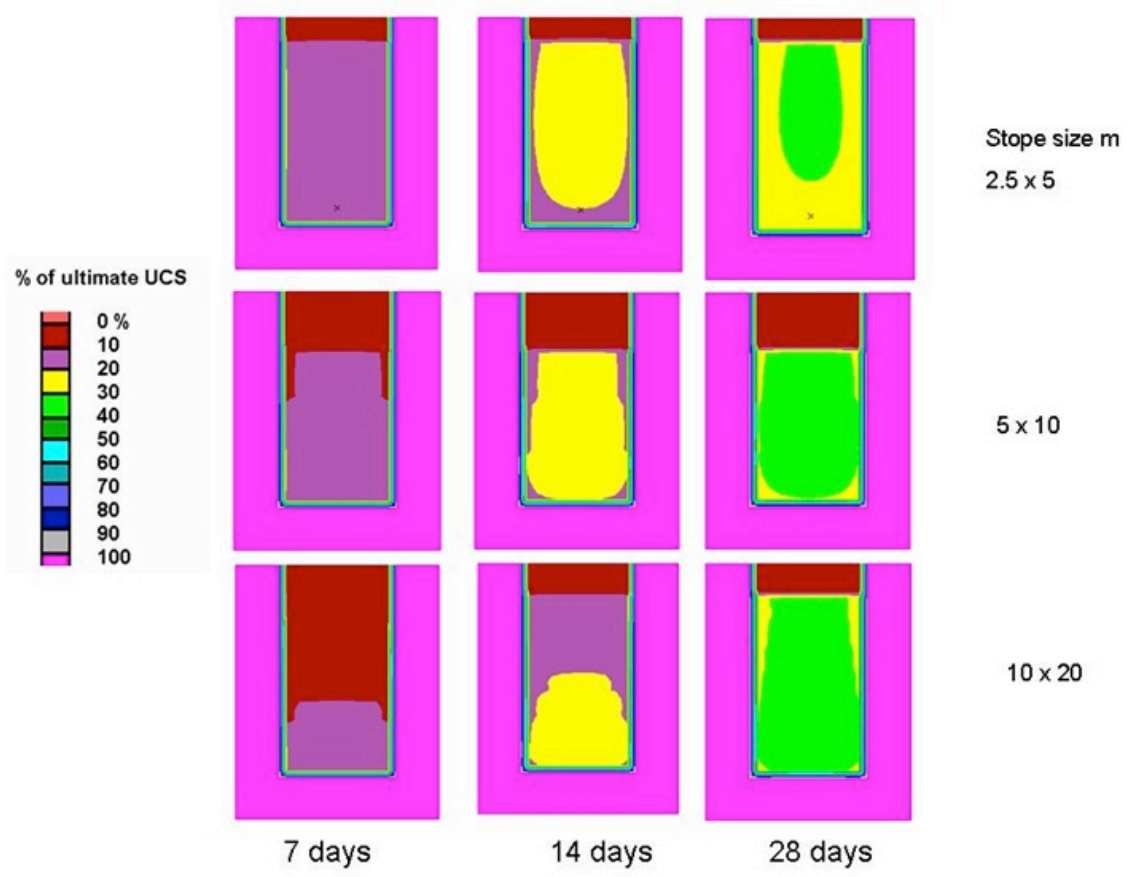


Figure 5. UCS development for different stope sizes (mix characteristics per Celestin (2008).

3.2 *Effect of the initial temperature on CPB on its strength development and distribution*

The initial temperature of CPB varies from one site to another, as well as from one season to another. Since CPB is a mixture of binders, water and tailings, its initial temperature is strongly affected by the initial temperatures of tailings and water (Wu et al. 2012). In addition, when preparing CPB, moderate heat could be added to attain a high early strength (Fall et al. 2007). Furthermore, the increase of the temperature in fresh backfill can happen during its transport in pipes from the surface to the underground working areas of a production section (Fall et al. 2010). These variable initial temperatures of fresh CPB make it necessary to study the effect of initial CPB temperatures on the heat developed within the CPB (Wu et al. 2012). In this study, a range of initial CPB temperatures of 0°C, 20°C and 30°C with a stope size of 10x20 m is chosen to study the effect of initial CPB temperatures on the strength development of CPB. Figures 6 and 7 show the effect of the initial temperature on the strength development and strength distribution within the CPB structure. Results show that increasing the initial CPB temperature from 0°C to 20°C will increase the strength by 60% as shown in Figure 8. The effect of the initial CPB temperature is obvious mainly during the very early ages (7 days). The strength increase with temperature can be attributed to two reasons. First, the accelerated reaction, and hence, higher hydration, resulting in a higher strength.

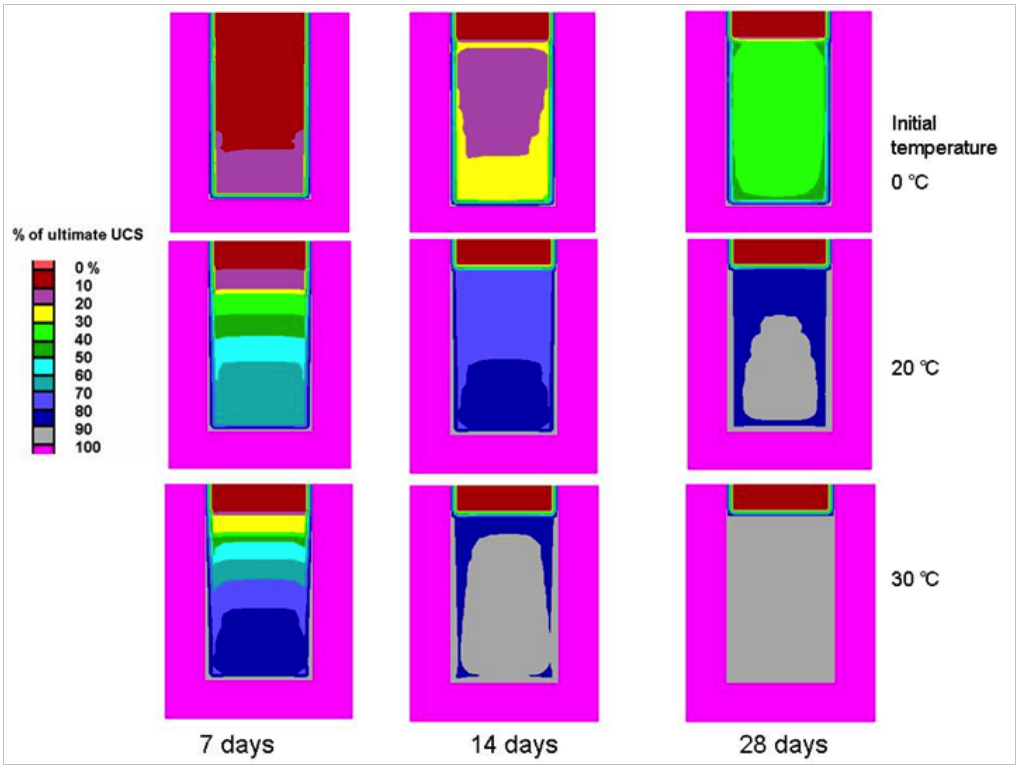


Figure 6. UCS development for different initial CPB temperatures (mix characteristics per Fall and Samb [5f]).

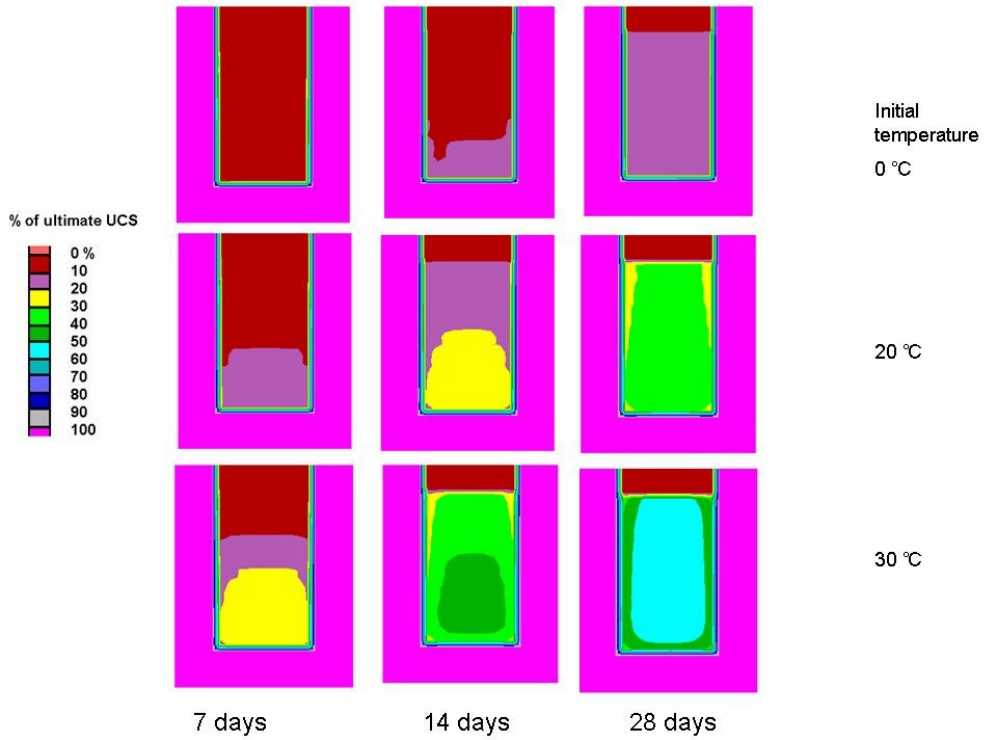


Figure 7. UCS development for different initial CPB temperatures (mix characteristics per Celestin, 2008).

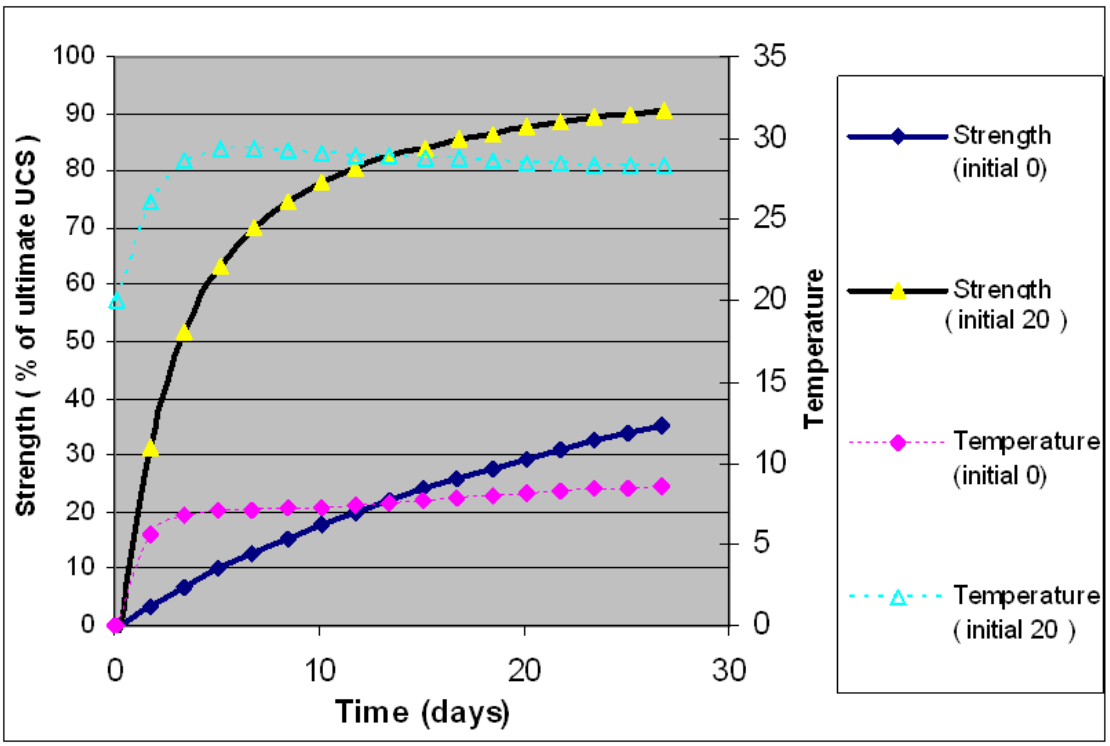


Figure 8. UCS development for different initial CPB temperatures

4 CONCLUSIONS

In this paper, a numerical model for predicting the UCS of the CPB is developed. Strength development is coupled with temperature and degree of hydration. For validation purposes, the predicted values were compared with laboratory and field results. The results show a good agreement between the predicted and measured values. The simulation results have shown that, binder content, stope size and initial CPB temperature have a significant effect on the strength development and distribution within CPB structures. Moreover, the results indicate that different mixes have different strength development, taking into consideration the temperature. The results gained in this study and the proposed model can be useful for backfilling practices in the field by providing important information on the design of the stope geometry, reducing the cost of preparing CPB (including decrease in the binder consumption), dealing with mine climatic situations, adjusting the backfilling rate, choosing a suitable backfilling strategy, controlling overly high maximum temperatures in CPB structures, and better understanding early age strength gain in CPB structures that is crucial to the opening of barricades. Despite the results obtained in this study, it is also clear that some influencing factors (e.g., confinement, and consolidation, stress) should be taken into account in the model to capture the development of the behavior of CPB in any situation. This is the topic of ongoing work.

5 REFERENCES

Brakebusch, FW (1994). Basics of paste backfill systems. Mining Engineering 46: 1175-1778.

Bentz, DP (2006). Influence of water-to-cement ratio on hydration kinetics: simple models based on spatial considerations. Cement and Concrete Research, 36: 238-244.

Célestin JC (2008) Geotechnical properties of CPB and tailings liners: Effect of mix components and temperature. Master (M.A.Sc.) Thesis (2008), University of Ottawa, 222p.

Fall M, Celestin JC, Pokharel M, Touré M (2010). A contribution to understanding the effects of curing temperature on the mechanical properties of mine cemented tailings backfill. Engineering Geology, 114(3-4): 397-413.

Fall, M, Nasir, O., and Celestin, JC (2007). Paste backfill responses in deep mine temperature conditions. *In* 9th Intern.Symposium of mining with backfill. Montreal, Canada, CD-Rom.
Ghirian A., Fall M., Tchantchou JP (2011). Coupled Thermo-Hydro-Mechanical-Chemical Evolution of Cemented Paste Backfill in Column Experiments. Pan.Am CGS Geotechnical Conference, CD rom.
Grice T (2001). Recent mine developments in Australia. Proceeding of the 7th international symposium on mining with backfill (MINEFILL); 351-357.
Itasca Consulting Group (2005). FLAC v.5.0, Fast Lagrangian Aanalysis of Continua, 3rd Ed..
Nasir O, Fall M (2009). Modeling the heat development in hydrating CPB structures. Computer and Geotechnics, 36(7): 1207-1218.
Nasir O, Fall M., 2010. Coupling binder hydration, temperature and compressive strength development of underground cemented paste backfill at early ages. Tunnelling and Underground Space Technology 25(1), 9-20.
Samb S.S. (2005). Experimental investigations of the effect of temperature on the mechanical and durability properties of cemented backfill. Master 2005 – Lausane, Switzerland.
Williams, TJ, Denton DK, Larson MK, Rains RL, Seymour JB, and Tesarik DR (2001). Geomechanics of Reinforced Cemented Backfillin an Underhand Stope at the Lucky Friday Mine, Mullan, Idaho. U.S. department of health and human services. 2001.
Wu D, Fall M, Si-Jing C (2012). Coupled modeling of temperature distribution and evolution in cemented tailings backfill structures that contain mineral admixtures. Geotechnical and Geological 30: 935-961.
Zelic J, Rusic D, Krstulovic R (2004). A Mathematical Model for Prediction of Compressive Strength in Cement-Silca Fume Blends. Cement and Concrete research, 34: 2319-2328.

Modeling soil-fluid and fluid-soil transitions with applications to tailings

Pieter A. Vermeer, Luca Sittoni, Lars Beuth
Deltares, Delft, The Netherlands

Zdzisław Więckowski
Łódź University of Technology, Poland

ABSTRACT: While geotechnical engineers concentrate on soil with a grain skeleton which is subject to effective stresses, hydraulic engineers concentrate on fluids and fluidized mixtures. Similarly, researchers in geomechanics may focus on soft soils, leaving fluidized materials to researchers in computational fluid dynamics. Hence, for a long time the transition from a soil skeleton to a fluid with soil particles, and vice versa, remained unsolved. Recently, a breakthrough was created by modeling this transition. The theory is summarized in this paper, even if the focus is on numerical applications. Before addressing the modeling of transition, the employed numerical method, the so-called material point method, is applied to sand capping problems and a collapsing water column for the purpose of validation. Afterwards, the collapse of an underwater slope is treated. Here, breaching is considered which occurs in case of steep slopes in dense dilative sand. Whereas classical finite element analyses tend to stop at the onset of a failure, the analysis with the material point method gives also results for post-failure flow and re-sedimentation.

1 INTRODUCTION

The deposition of tailings in ponds extending across several square kilometers with depths of up to 50 meters represents a demanding engineering problem that requires efficient and safe solutions. Typical tailings generally feature low strengths making it difficult to seal off tailings through sand capping. Once the sand cap is in place, it exhibits a very slow consolidation process and thus a very slow increase of strength with time. Clearly, such a material, tailings-related problems such as the installation of a sand cap respectively, require consideration of a two-phase material of soil and water including the transition from water-saturated soil to soil grains suspended in water.

The material point method (MPM) has been applied in recent years to large-deformation problems of granular flow and soil mechanics such as silo discharge, anchor pull-out, slope failure, pile jacking and driving (Więckowski et al. 1999, Więckowski 2004, Coetzee et al. 2005, Beuth et al. 2011, Beuth 2012, Al-Kafaji 2013). Recently, the consideration of large deformation processes involving mixtures of soil and fluid has been incorporated (Więckowski 2013). The latter allows considering problems such as consolidation of saturated soil, flow of water through porous media as well as erosion and sedimentation processes.

In this paper, numerical analyses with MPM are presented that involve soil and fluid as well as mixtures of both materials to demonstrate the applicability of the method to tailings-related problems.

In the following, firstly, numerical analyses involving *undrained soft soil behavior* are presented. Validation of the method is provided through comparison of results with an analytical

solution for the problem of placing a sand ridge onto tailings. Furthermore, placing of a heap of sand onto tailings is treated. Section 3 deals with the *modeling of fluids* with MPM. Validity of the fluid formulation is demonstrated by means of the problem of a collapsing water column. The extension of MPM to *soil-fluid mixtures* is treated in Section 4. Its application is demonstrated by means of the problem of breaching.

2 MATERIAL POINT METHOD FOR UNDRAINED SOFT SOILS

MPM can be considered as an extension of the classical updated Lagrangian finite element method (UL-FEM). For the UL-FEM, a body is discretized by finite elements that follow the deformations of the body. In case of large deformations of a body, the finite element mesh might eventually experience severe distortions, which lead to numerical inaccuracies and can even render the calculation impossible.

In MPM, a body is discretized by a cloud of material points that moves through a fixed finite element grid. Thereby, the material points capture the arbitrary large deformations of the body without the occurrence of severe deformations of finite elements. Material and state parameters of the body as well as applied loads are stored and transported in material points whereas the mesh does not store any permanent information.

For MPM, the underlying finite element mesh is used (as with UL-FEM) to solve the system of equations of motion. Once displacements, stresses and strains are computed at locations of material points, the mesh is usually reset into its original state. However, it might also be changed arbitrarily.

For further information on MPM the reader is referred to (Sulsky 1994, Więckowski 1999, Więckowski 2004, Al-Kafaji 2013). A detailed description of the method would exceed the scope of this paper.

In this section on undrained behavior of tailings, water-saturated soil will be considered as a single-phase material. This allows for a validation of the code on the basis of boundary value problems with an analytical solution, as will be done in Section 2.1.

As usual in soil mechanics, undrained material behavior is modeled on the basis of a so-called total stress analysis, in which shear stresses are limited by the introduction of undrained shear strength, being generally denoted as s_u. On performing numerical analyses, the undrained shear strength is embedded in an elastic-plastic material model. Both, the so-called Von Mises yield criterion and the resembling Tresca yield condition can be applied. In this study the latter is used.

2.1 *Validation for sloping sand cap on tailings*

The creation of a sand cap on top of tailings will inevitably involve a spatial variation of the thickness of this cap. No doubt, tailings will be able to carry such a cap as long as these spatial variations are small, but the bearing capacity of soft tailings will not allow for strong variations. Hence, analyses will have to be performed to assess the bearing capacity of tailings with respect to thickness variations of the sand cap. Considering soft tailings, pre-failure squeezing will be considerable, causing significant geometry changes of the sand-tailing interface even well before collapse. No doubt, the analysis of such large-deformation problems requires an advanced numerical analysis. On the other hand, small-deformation based analytical solutions remain important for the validation of numerical approaches such as MPM. In this section, this method will be validated by focusing on the bearing capacity of soft tailings under a ridge of sand, as illustrated in Figure 1a.

For soft tailings, the sand-ridge problem is of special interest as Davis & Booker (1973) published an analytical solution for the bearing capacity of soil layers in which the undrained shear strength increases linearly with depth. As their solution is restricted to small-deformation problems without geometry changes, this will also be assumed in the present numerical MPM analysis. Indeed, once this method has been validated for quasi-static small-deformation analyses, it can be applied with some confidence to dynamic large-deformation problems.

Material parameters roughly reproducing those of typical soft tailings are listed in Table 1. At the top of the tailings the undrained shear strength is taken to be 100 [N/m^2]. A significant in-

crease with depth is considered by adding 500 [N/m^2] for each meter of depth. The shear modulus also increases with depth and is assumed to be a hundred times larger than the undrained shear strength. At the surface this implies a shear modulus of 10 [kN/m^2] and its increase with depth is 50 [kN/m^2] per meter of depth. For undrained conditions, tailings cannot be compressed and this is modeled by taking the undrained Poisson ratio nearly equal to 0.5. For numerical reasons, a nearly incompressible material is modeled by adopting a value of 0.495.

Table 1. Soft tailings material parameters.

Undrained shear strength at top	$s_{u,top}$	100	[N/m^2]
Increment of undrained shear strength with depth	$s_{u,increment}$	500	[N/m^2/m]
Shear modulus at top	G_{top}	10	[kN/m^2]
Increment of shear modulus with depth	$G_{increment}$	50	[kN/m^2/m]
Undrained Poisson ratio	ν_u	0.495	

Placement of a long sand ridge with a total cross-sectional width of 2 [m] on top of tailings is considered, which yields a plane-strain symmetrical problem. A symmetrical half is shown in Figure 1a. As a full 3D code is used in this study, a slice of tailings of 0.2 [m] width is shown. This slice is divided into 4-noded tetrahedral finite elements. The thin sand fill is modelled by the application of a distributed load at the surface of the finite element mesh, as also shown in Figure 1a. Considering a tailings pond with a water level well above the tailings the submerged weight of the sand cap is applied. During the calculation, the slope of the sand cap is stepwise increased. In Figure 1b, the applied slope is plotted against resulting settlements at the center of the sand cap. For a slope inclination of 1:8, a 'run-away' failure is computed.

Davis & Booker (1973) present an analytical solution for the bearing capacity of clay taking into account an increase of strength with depth. For the considered sand ridge, they predict a maximum sand height at the foot of the slope of 5.7 [cm] and at the head of the slope of 16.7 [cm], corresponding to an inclination of 1:9. Ultimate sand heights of 6.3 and 18.2 [cm] and a slope inclination of 1:8 result from the numerical analysis. The good agreement with the analytical solution gives confidence in the used MPM.

Figure 2 indicates that a rather shallow failure mechanism evolves. At failure, only the upper 50 [cm] of the tailings material experience deformations.

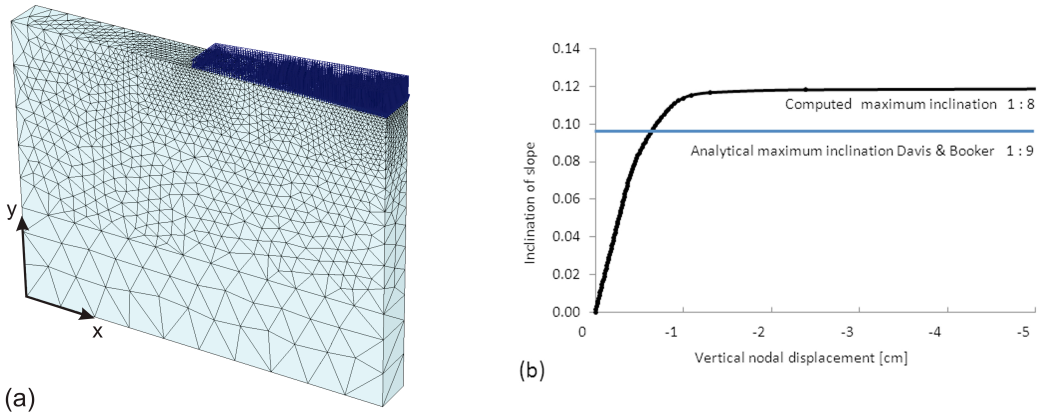


Figure 1. (a) Geometry and mesh of the discretized sand ridge and applied distributed load; (b) slope of the ridge plotted against the settlements at the center of the sand cap.

2.2 *Preliminary study of axisymmetric sand heap on tailings*

In addition to the installation of a sand ridge, the case of a sand heap with a radius of 1 [m] on tailings is considered in the following. The sand cap is modeled as in Section 2.1 by a distributed load. The same material parameters were used for the tailings material. Large deformation ef-

fects are not considered. The placement of a sand heap is treated as an axisymmetric problem. Only a slice of 20 [°] with a radius of 2 [m] and a height of 1 [m] is discretized. The geometry and discretization of the problem are shown in Figure 3a. The same finite element discretization as in the analysis described above is used.

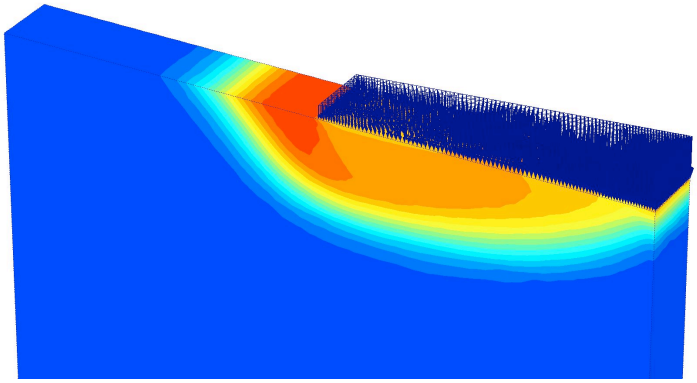


Figure 2. Relative magnitude of velocities at failure for sand ridge.

In Figure 3b, the applied slope is plotted against resulting settlements at the center of the sand cap. To the authors' knowledge, no analytical solution exists to this problem. The analysis renders a maximum thickness of the sand layer at the foot of the slope of 6.2 [cm] and a maximum thickness at the head of the slope of 21.7 [cm] which corresponds to an inclination of 1:7. As expected, a steeper slope can be realized compared to the plane strain problem, as the load is distributed with increasing distance from the center across a larger area. Obviously, as can be seen in Figure 4, failure of the tailings material involves progressive mobilization of its shear strength across a wider failure surface compared to the sand ridge. Likewise, in the numerical analysis a rather shallow failure mechanism is predicted reaching at failure a depth of only approximately 50 [cm], as indicated in Figure 4.

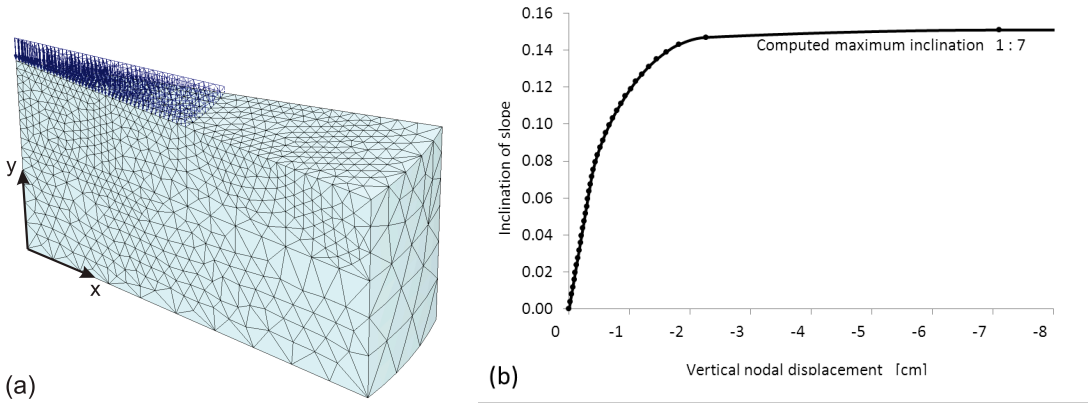


Figure 3. (a) Geometry and mesh of the discretized sand heap and applied distributed load; (b) slope of the heap plotted against the settlements at the center of the sand cap.

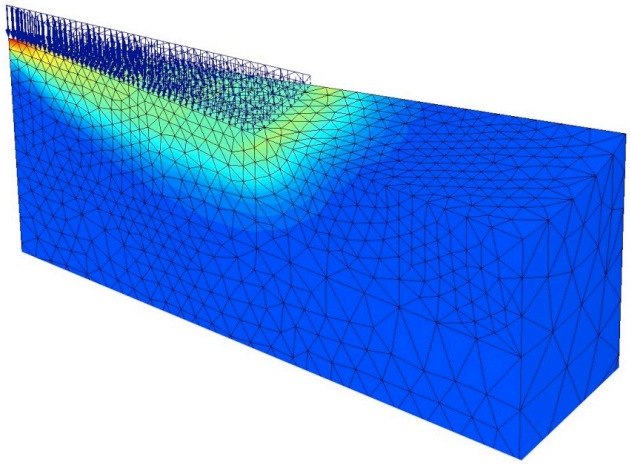


Figure 4. Relative magnitude of velocities at failure for sand heap.

3 MATERIAL POINT METHOD FOR FLUIDS

While solid mechanics problems are generally solved with Lagrangian methods such as UL-FEM, Eulerian methods such as the finite volume method are applied to problems of fluid flow. With the latter, basically, fluid velocities are computed at fixed points in space, for example the nodes of a stationary mesh, rather than at material points of the fluid.

MPM which can also be considered as a mixed Lagrangian-Eulerian approach is well suited for both types of problems. In fact, fluid simulations with MPM go back to its very beginnings in the 1950's when it was developed by Harlow under the name of particle-in-cell method (Harlow 1964). Since then it has been applied successfully to various problems of fluid flow and fluid-structure-interaction (Guilkey 2007).

As in the analyses of Section 2, a fluid is discretized by a cloud of material points that moves through a background finite element mesh. The equations of motion are assembled and solved at the nodes of the mesh, stresses and strains are computed at the location of material points. Contrary to Section 2, the equations of motion are now based on the Navier-Stokes equations which describe the motion of fluids.

Obviously, modeling fluids forms a prerequisite for considering soil-fluid mixtures. In the following, the application of MPM to the problem of a collapsing water column is presented for validation purposes.

Water is modeled as a viscous liquid. As with the previous analyses, a slight compressibility is considered for numerical reasons.

3.1 *Validation for collapsing water column*

A column of water is released from a box by suddenly removing one of its sides. The surfaces of the box are assumed to be smooth. The water spreads out onto a flat smooth surface. The problem has been investigated experimentally by Martin & Moyce (1952) and numerically by Zienkiewicz et al. (2005).

The geometry of the problem is shown in Figure 5. The water column initially has a height H_0 of 7 [m] and a width W of 3.5 [m]. A dynamic viscosity μ of $0.8905 \cdot 10^{-6}$ [kN/m^2·s], a bulk modulus K of $2.1284 \cdot 10^6$ [kN/m^2] and a mass density ρ_f of 1,000 [kg/m^3] are used.

The position of a water particle located initially at the top right corner of the column has been traced. In Figure 6, the relative column height computed from the particle's vertical position and the initial column height H_0 is plotted versus time. Clearly, good agreement is obtained with the experimental results of Martin & Moyce (1952).

This problem can also be solved by the finite element method formulated in the purely Lagrangian format even though severe mesh distortions occur. The purely Lagrangian solution of

the considered problem has been shown by Zienkiewicz et al. (2005). Comparison of the results in Figure 7 shows good agreement between the two numerical analyses.



Figure 5. Geometry and mesh of the water column in its initial state and extend of discretized space.

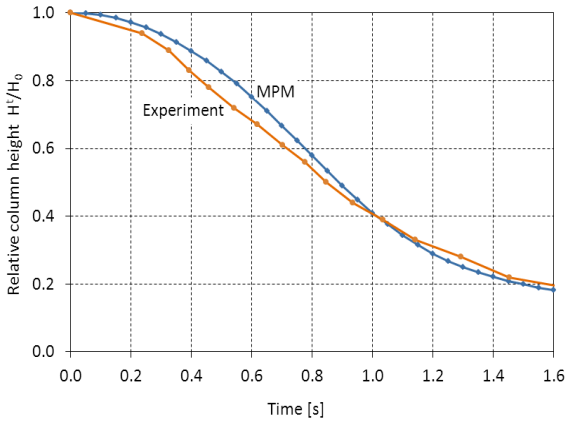


Figure 6. Relative column height plotted versus time.

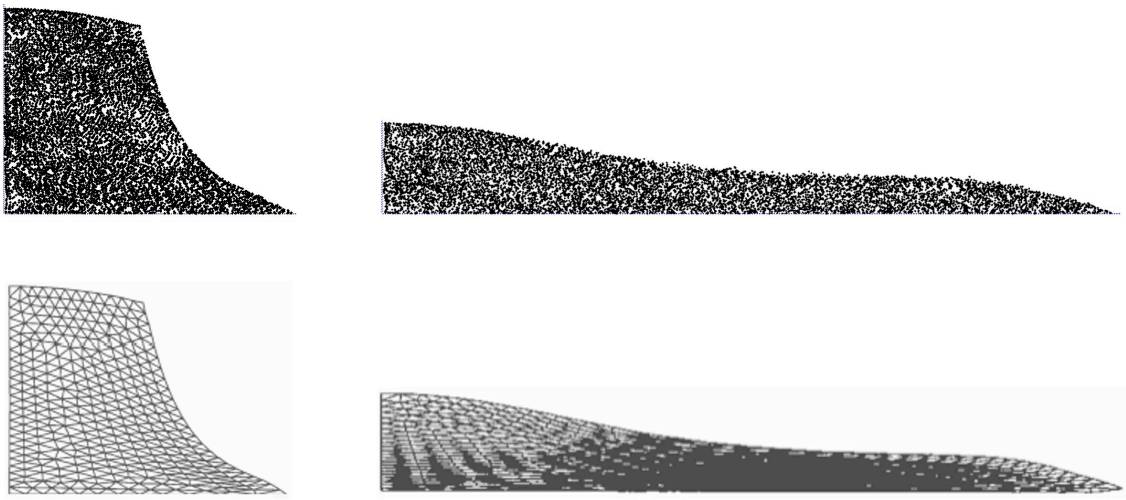


Figure 7. At top, collapsing water column computed with MPM. At bottom, UL-FEM computation (Zienkiewicz 2005). Results at t = 0.65 [s] and 1.60 [s] are shown.

4 MATERIAL POINT METHOD FOR TWO-PHASE TRANSITION PROBLEMS

This novel extension of the MPM has been recently developed by one of the co-authors, Z. Więckowski, in the frame of the EU-FP7 Geo Fluid project. The details of the problem formula-

tion and numerical model are shown in (Więckowski 2013).

In order to analyze state transition problems for a porous saturated body like fluidization and sedimentation, a two-phase formulation with two sets of material points representing solid and fluid is introduced into MPM. Now, instead of one set of equations of motion as in Sections 2 and 3, equations of motion for both, solid and fluid phases are solved, rendering separate velocity fields for solid and fluid. The equations of motion for both the media can be stated as follows:

$$(1 - n)\,\rho_s\,\partial v_i/\partial t = \sigma'_{ij,j} - (1 - n)\,p_{,i} + f_{di} + (1 - n)\,\rho_s\,g_i \tag{1}$$

$$n\,\rho_f\,\partial w_i/\partial t = -n\,p_{,i} + n\,s_{ij,j} - f_{di} + n\,\rho_f\,g_i \tag{2}$$

where v_i and w_i are the velocity vectors for the solid and fluid, respectively. n denotes the porosity of the soil defined as the ratio of void volume with respect to reference volume. ρ_s and ρ_f denote the mass density of the soil skeleton and of the fluid, respectively. σ'_{ij} is the effective stress tensor, p is the pore pressure of the fluid, s_{ij} the deviatoric part of the stress tensor, g_i the vector of acceleration of gravity. f_{di} denotes the drag force exerted by the fluid on the unit volume of the solid. The tortuosity of the fluid flow path is not taken into account in Equations 1 and 2.

Stresses are computed from the following constitutive relations for the soil:

$$\overset{\nabla}{\sigma'}_{ij} = f_{ij}\left(\sigma'_{pr}, d_{rs}\right) \tag{3}$$

and for the fluid:

$$\partial p/\partial t = -K_f\,\partial \varepsilon_f^{vol}/\partial t \tag{4}$$

$$s_{ij} = 2\,\mu_e\,d_{ij} \tag{5}$$

where $\overset{\nabla}{\sigma'}_{ij}$ is the objective rate of stress tensor, d_{rs} is the rate of deformation tensor and ε_f^{vol} denotes the volumetric strain for the fluid phase. The viscosity is considered to depend on the volume fraction of solid particles suspended in the fluid according to, for example (Beenakker 1984):

$$\mu_e = \mu\,(1 + 5/2\,\phi + 5.2\,\phi^2) \tag{6}$$

where ϕ denotes the volume fraction of the particles suspended in the fluid. This formula is derived for a fluid with spherical particles suspended in it.

The interaction between solid and fluid phase is described by means of Ergun's law (Ergun 1952):

$$f_{di} = n^2\,[\,\mu / \kappa\,(w_i - v_i) + n\,\rho_f\,F / \kappa^{1/2}\,|\,\mathbf{w} - \mathbf{v}\,|\,(w_i - v_i)\,] \tag{7}$$

Here, κ is the permeability of the soil and F Forchheimer's coefficient. These coefficients are defined as:

$$\kappa = \frac{n^3 d_p^2}{a(1 - n)^2} \qquad F = \frac{b}{\sqrt{a}\;n^{3/2}} \tag{8}$$

where d_p denotes the average particle size of the solid, a = 150, and b = 1.75.

The material can take on one of two states which are identified by means of the material's porosity. In the *low porosity state*, the grains of the soil skeleton are in contact and liquid flows

through the pores, the effective stresses in the soil are non-zero. In the *high porosity state*, the solid material is fluidized and there is no direct contact between its (suspended) grains inside the liquid, the effective stresses are zero. The cases of dry soil and pure fluid represent limits of these two states. The case of partially saturated soil can be considered as a case of low porosity.

Consideration of the solid phase: In the process of the soil-fluid mixture changing from a saturated to a liquefied state, the effective mean stress of the soil skeleton tends towards zero, while the porosity of the soil is increasing. The moment when the effective mean stress is zero, the soil can be considered as liquefied. In the reverse process of sedimentation, the porosity of the soil is decreasing. However, it cannot be controlled by tracing the effective mean stress. Therefore, a threshold porosity, n_0, is introduced at which the onset of contact between solid grains and thus non-zero effective stresses are assumed. The change of porosity is computed using the distribution of solid material points.

Consideration of the fluid phase: The fluid volume fraction is traced in order to detect the creation of voids inside the fluid due to the deformation process. When the fluid (locally) becomes a cloud of separated drops, the pressure and other stress components of the fluid vanish. Once the amount of voids diminishes, the mass concentration of the fluid reaches a threshold value and the non-zero stresses of the fluid are computed by means of Equations 4 and 5.

4.1 *Example of state transition analysis*

State transition phenomena like fluidization and the onset of sedimentation are analyzed considering the problem of a collapsing sand column submerged in a water reservoir. The example is described in detail in (Więckowski 2013). A cross-section through the reservoir and the initial configuration of the sand column are shown in Figure 8. Considering the symmetry of the problem, only half the region is discretized. The reservoir is discretized by a regular structured 2D mesh of triangular elements.

It is assumed that the sand is fully saturated. It is modeled by means of an elastic-viscoplastic material model using the Drucker-Prager yield condition (Więckowski 2004). The material parameters of the sand and water are listed in Tables 2 and 3. The bulk modulus of the fluid is chosen 100 times smaller than for water in order to increase the speed of the computation.

Figure 9 shows the soil mass concentration at the stated real times of the collapse process. Only the position of material points representing the solid phase is shown.

The fluidization phenomenon and subsequent flow of the liquefied sand along the column surface can be clearly seen. This kind of flow which takes place along vertical or steep submerged slopes is known as breaching and is purposely induced in some engineering processes such as dredging of a river or sea bed. In Figure 10, later stages of the flow process are shown. After 50 [s], when the column is almost “dissolved” in water, the onset of the sedimentation process can be noticed.

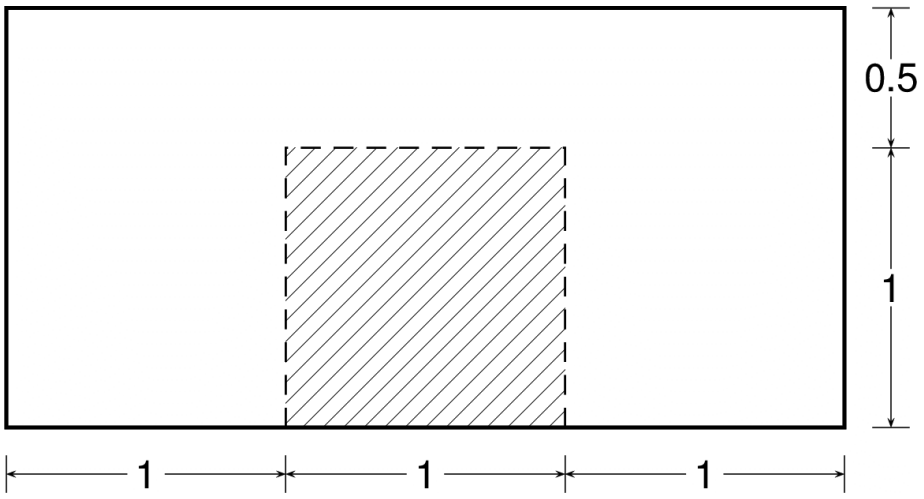


Figure 8. Initial configuration of submerged soil column. Dimensions are in [m].

Table 2. Sand material parameters.

Mass density	ρ_s	2,850	[kg/m^3]
Initial mass concentration	ρ_{so}	1,500	[kg/m^3]
Young's modulus	E	1,000	[kN/m^2]
Poisson ratio	ν	0.3	
Internal friction angle	φ	30	[°]
Viscosity	γ	10^{-3}	[1/s]
Index of power law	N	1	
Grain diameter	d_p	0.2	[mm]
Threshold porosity	n_0	0.5	

Table 3. Water material parameters.

Mass density	ρ_f	1,000	[kg/m^3]
Viscosity	μ	$8.905 \cdot 10^{-7}$	[kN/m^2·s]
Bulk modulus	K	$2.128 \cdot 10^4$	[kN/m^2]

5 CONCLUSIONS

In this paper, the feasibility of advanced numerical analyses on the cutting edge between geomechanics and hydromechanics has been demonstrated. Considering sediments, an important novelty is the modeling of state transitions in assemblies of solid particles, e.g. the erosion-type transition of a soil into a sediment suspension or inversely the sedimentation-type transition followed by consolidation. Near-surface consolidation is also of utmost importance for sand capping. Indeed, in this paper the immediate undrained response of loading tailings has been considered, but as yet we did not address resulting excess pore pressures. A proper evaluation of these pressures is needed for assessing the increasing shear strength of tailings during consolidation. On using relatively simple elastic-plastic soil models, excess pore pressures in soft tailings tend to be underestimated by a factor 0.5 and consequently more advanced models will have to be used (Beuth 2012). Subsequently, such constitutive models will have to be applied in consolidation analyses. Meanwhile, we began to do such analyses in the framework of dissertation studies. First results of such studies were published by Al-Kafaji (2013).

The treatment of mine waste in the form of tailings poses a demanding engineering problem. It requires knowledge and experience in both, geo- and hydromechanics. MPM is therefore proposed here as a powerful numerical tool to bridge the gap between the two disciplines, opening new paths to innovative solutions to this field of engineering.

6 ACKNOWLEDGEMENTS

The financial support from the European Community's Seventh Framework Program (Marie Skłodowska-Curie Intra European Fellowship) through grant PIEF-GA-2010-274335 (Geo Fluid) is gratefully acknowledged by Z. Więckowski, a co-author of this paper.

The research leading to these results has received further funding from the European Community's Seventh Framework Program FP7/2007-2013 under grant agreements n° PIAG-GA-2009-230638 (Geo-Install) as well as n° PIAG-GA-2013-324522 (MPM-Dredge).

The authors would like to thank Issam Al-Kafaji from Shell Global Solutions International for his contribution to the research efforts leading to this publication and Alexander Rohe from Deltares for his kind contribution to this publication.

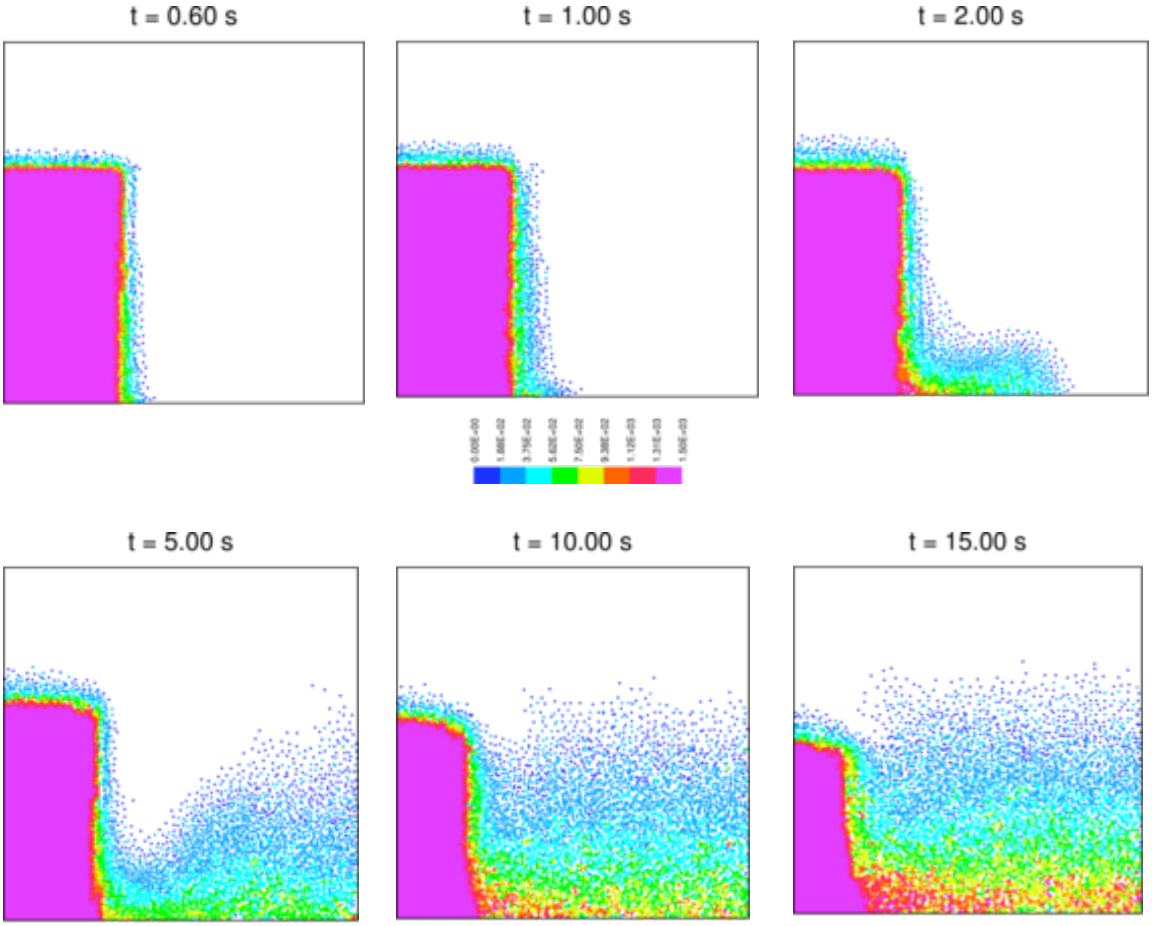


Figure 9. Soil mass concentration for some deformation phases of collapsing column.

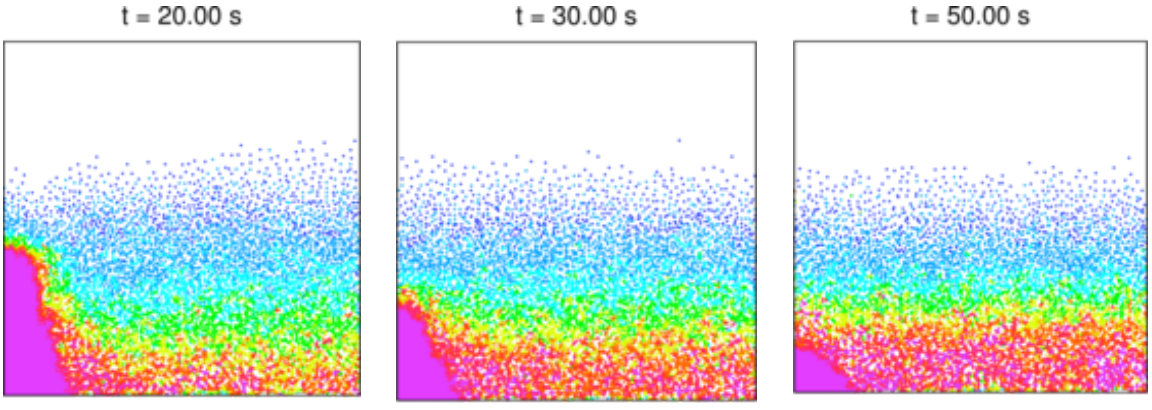


Figure 10. Soil mass concentration for some later deformation phases of collapsing column.

7 REFERENCES

Al-Kafaji, I.K.J. 2013. Formulation of a Dynamic Material Point Method (MPM) for Geomechanical Problems. Ph.D. thesis, University of Stuttgart.

Beenakker, C.W.J. 1984. The effective viscosity of a concentrated suspension of spheres (and its relation to diffusion). *Physica* 128(A): 48-81.

Beuth, L., Więckowski, Z. & Vermeer, P. 2011. Solution of quasi-static large-strain problems by the material point method. *International Journal for Numerical and Analytical Methods in Geomechanics*

35(13): 1451-1465.
Beuth, L. 2012. Formulation and Application of a Quasi-Static Material Point Method. Ph.D. thesis University of Stuttgart.
Coetzee, C., Vermeer, P. & Basson, A. 2005. The modelling of anchors using the material point method. *International Journal for Numerical and Analytical Methods in Geomechanics* 29(9): 879-895.
Davis, E.H. & Booker, J.R. 1973. The effect of increasing strength with depth on the bearing capacity of clays. *Géotechnique* 23(4): 551-563.
Ergun, S. 1952. Fluid flow through packed column. *Chemical Engineering Progress* 48: 89-94.
Guilkey, J.E., Harman, T.B., Banerjee, B. 2007. An Eulerian-Lagrangian approach for simulating explosions of energetic devices. Computers and Structures 85(11-14): 660-674.
Harlow, F.H. 1964. The particle-in-cell computing method for fluid dynamics. *Methods in Computational Physics* 3: 319-343.
Jassim, I., Stolle, D. & Vermeer, P. 2012. Two-phase dynamic analysis by material point method. *International Journal for Numerical and Analytical Methods in Geomechanics*, In Wiley Online Library, DOI: 10.1002/nag.2146.
Martin, J.C. & Moyce, W.J. 1952. An experimental study of the collapse of liquid columns on a rigid horizontal plane. *Philosophical Transactions of the Royal Society London A* 244: 312-324.
Sulsky, D., Chen, Z. & Schreyer, H. 1994. A particle method for history-dependent materials. *Computer Methods in Applied Mechanics and Engineering* 118(1-2): 179-196.
Więckowski, Z., Youn, S. & Yeon, J. 1999. A particle-in-cell solution to the silo discharging problem. *International Journal for Numerical Methods in Engineering* 45(9): 1203-1225.
Więckowski, Z. 2004. The material point method in large strain engineering problems. *Computer Methods in Applied Mechanics and Engineering* 193: 4417-4438.
Więckowski, Z. 2013. Enhancement of the Material Point Method for Fluid-Structure Interaction and Erosion, *Report on EU-FP7 research project Geo Fluid PIEF-GA-2010-274335*.
Zienkiewicz, O.C., Taylor, R.L., Nithiarasu, P. 2005. The Finite Element Method for Fluid Dynamics 6th Edition, Elsevier, Butterworth-Heinemann, Amsterdam.

Tailings

Designing non-segregating tailings pump and pipeline systems

S. Bodtker
Paterson & Cooke Canada Inc., Calgary, Alberta, Canada

R. Cooke
Paterson & Cooke USA Ltd., Denver, Colorado, USA

ABSTRACT: The design of non-segregating tailings (NST) pump and pipeline systems presents many challenges. This is primarily due to the non-Newtonian characteristics of the NST combined with the broad particle size distribution of the mixture. This paper reviews engineering design considerations for NST delivery systems, focusing on the following aspects: laminar and turbulent flow behaviour, selecting appropriate operating velocities, and predicting pipeline hydraulic gradients. The paper also identifies areas of ongoing research to reduce the uncertainty associated with the design of NST delivery systems.

1 INTRODUCTION

1.1 *Non-segregating Tailings*

Canadian Natural Resources Limited (CNRL) has developed a process for its Horizon Oil Sands Project, which produces non-segregating tailings (NST) by combining the following waste streams (Chu *et al*, 2008):

- The flotation tailings are dewatered in high rate thickeners (with the addition of polymer flocculent to aid settling of the fine particles) to create a concentrated thickener underflow which has a yield stress.
- The primary separation cell (PSC) underflow tailings are dewatered using two stages of classifying hydrocyclones to produce two concentrated coarse waste streams.

Following mixing of the above streams in a pump box, carbon dioxide is added prior to pumping the tailings to the in-pit disposal site. The carbon dioxide lowers the pH of the tailings mixture (through the formation of carbonic acid) further increasing the yield stress.

The yield stress supports the coarse particles creating a mixture which is stable under static conditions and effectively non-segregating during deposition.

The benefits of NST are (Chu *et al*, 2008):

- Reduced tailings pond capacity, leading to lower costs and a smaller environmental footprint.
- Accelerated pond site reclamation.
- Reuse of warm process water (thickener overflow), resulting in less natural gas used to heat water (reduced greenhouse gas emissions) and less fresh water pumped from the river.
- Bitumen is recovered by the tailings dewatering processes.

1.2 *Pump and Pipeline Transport of NST*

The flow properties of NST create unique challenges for the design of pump and pipeline transport systems compared with conventional oil sand tailings:

- Conventional tailings pipeline design relies on turbulence to suspend coarse particles and thereby prevent deposition of particles on the pipeline invert. The standard tailings pipeline design approach is to ensure that the operating velocity exceeds the deposition velocity under turbulent conditions by an appropriate margin (typically about 0.3 m/s).
- The yield stress of NST mixtures suppresses turbulence. The pipeline velocity required to achieve turbulent flow increases with increasing yield stress. The designer is faced with two choices:
  - Operate at the higher velocities required to achieve turbulence (and accept the higher friction losses and energy requirements)
  - Design the pipeline to operate in laminar flow. However, coarse particles settle when conveyed in a laminar flow. While there are tailings pipelines which successfully operate laminar flow, the science and engineering of these systems in not currently well understood.
- The yield stress also complicates the selection of suitable pumps for the system (higher pressures required and less certainty regarding the pump suction requirements).

1.3 *Paper Scope*

This is the first of two papers, which critically review the current state of practice for the design of pump and pipeline systems transporting non-segregating tailings. This paper deals with pipeline flow and the second paper will cover pump equipment selection.

2 NST PROPERTIES

2.1 *Rheology*

NST mixtures are considered mixed regime slurries and contain a wide range of particle sizes. The fine (clay and silt) particles form floc structures (enhanced through the addition of flocculants) which interact creating non-Newtonian flow properties including a yield stress. The flow behavior of NST mixtures can be characterized using the Bingham plastic model; the mixture rheology is defined by the Bingham yield stress and the plastic viscosity.

2.2 *Sensitivity of rheology to shear*

The rheology of NST slurries is reduced when exposed to shear; which can occur in the pump box, through the pump train and in the pipeline due to the turbulent nature of the flow. This shear effect is particularly important for the design of thickener underflow pumping systems.

2.3 *Sensitivity of rheology to chemistry*

The introduction of additives such as lime, gypsum or carbon dioxide to a NST mixture can have a significant effect on its rheology. It is important that the chemistry is considered when establishing the basis of design for a NST pumping system.

2.4 *Stability envelope*

As stated in the introduction, NST is a combination of thickened flotation tailings and concentrated coarse waste streams. NST is a mixture dependent on the right blend of coarse solids, fines, water and amendments. There is a range of sand-to-fine ratios (SFR), fines over fines plus water (FOFW), solids contents and chemical dosages where the mixture is stable (non-segregating) for effective disposal.

2.5 *Segregation Boundaries*

Through a series of lab tests conducted by the SRC it was learned that a yield stress of 5 Pa was sufficient to provide non-segregating behaviour in static storage of a NST mixture with a SFR of 3:1 and a solids content of 66%. A somewhat higher yield stress of 8 Pa was required for non-segregating behaviour for a mixture with a SFR of 4:1 and a solids content of 62% (Gillies et al 2006).

Hedblom & Solseng et al 2012 note that NST segregation boundaries are non-linear and dependent on SFR as well as FOFW due to increasingly hindered settling of coarse and fine tailings with increasing concentrations.

3 PIPELINE FLOW OF NST MIXTURES

3.1 *Pipeline Flow Behaviour*

Figure 1 presents a plot of pipeline pressure gradient versus flow velocity for two tailings mixtures in a 20 inch pipe loop (Gillies, *et al* 2006). The two mixtures have approximately the same solids content and sand to fines ratio; the rheology of the first mixture has not been amended, while gypsum[1] has been added to significantly enhance the rheology of the second mixture (thereby creating non-segregating tailings). The following observations are made:

- The flow is laminar for low flow velocities; as the velocity is increased the flow transitions to turbulent flow.
- The difference in rheology for the two mixtures has a significant impact on the laminar flow pressure gradients, but there is little impact in turbulent flow (where the friction losses are dominated by the mixture density).
- The transition velocity from laminar to turbulent flow increases significantly with increasing mixture rheology.

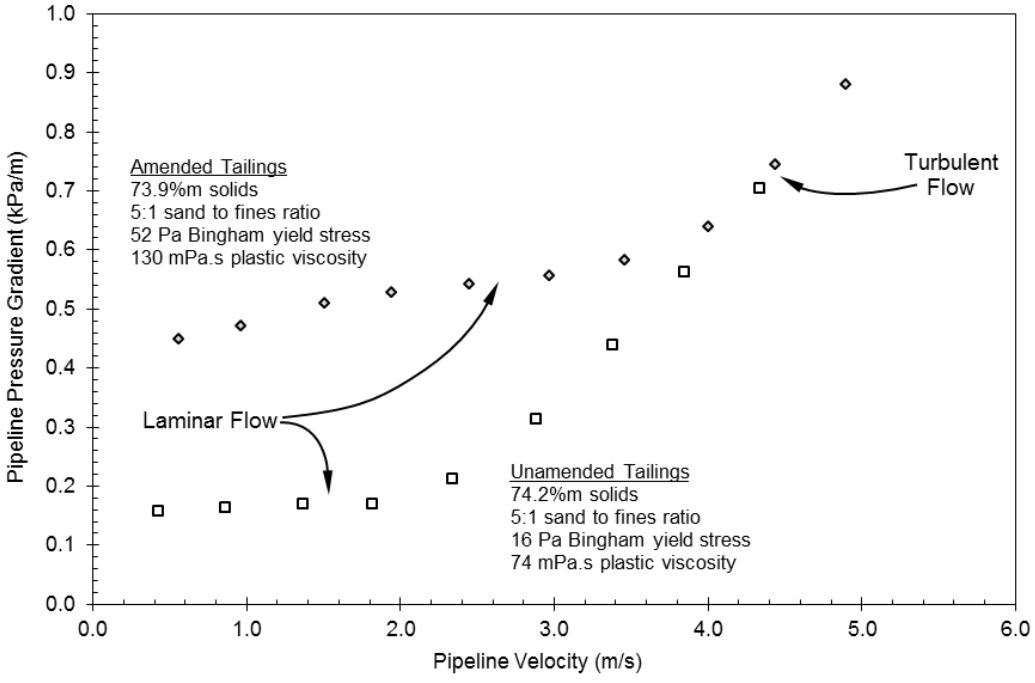


Figure 1. Tailings pipeline flow behaviour: pressure gradient versus velocity (Gillies, et al 2006)

[1] The rheology augmenting effect of adding gypsum is similar to carbon dioxide addition.

Figures 2 and 3 compare local velocity and concentration distributions for laminar and turbulent flow conditions for the test data presented in Figure 1. In turbulent flow, the velocity profile is reasonably symmetrical and the solids concentration is relatively uniform across the pipe section. In laminar flow, the velocity profile is asymmetric and there is an increase in solids concentration towards the pipe invert. The laminar flow measurements provide evidence of coarse particle segregation which has been reported previously by a number of authors: e.g. Gillies *et al* (2002), Pullum *et al* (2010) and Cooke (2002).

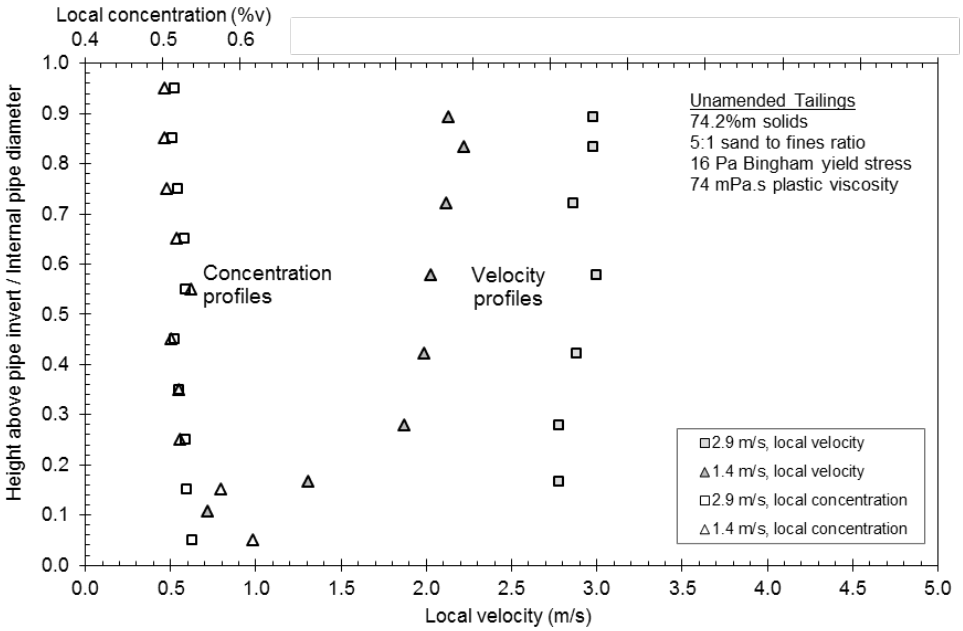


Figure 2. Tailings pipeline flow behaviour: velocity and concentration profiles (Gillies, et al 2006)

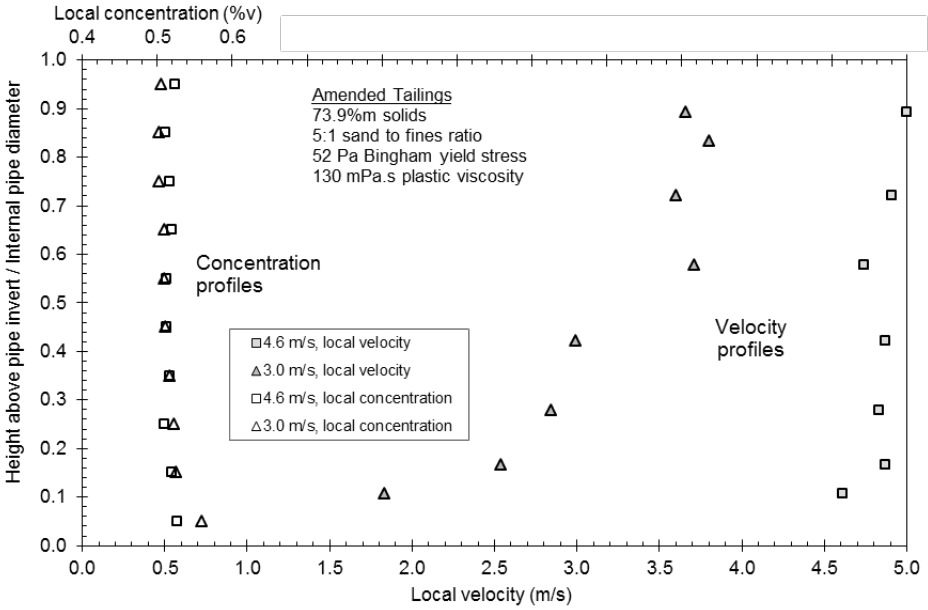


Figure 3. Tailings pipeline flow behaviour: velocity and concentration profiles (Gillies, et al 2006)

3.2 *Laminar Flow Pipeline Operation*

It is well accepted that mixtures which have a sufficiently large yield stress to support coarse particles under quiescent conditions will segregate when sheared in laminar flow conditions[2]. What is not well understood, however, is the impact of laminar flow segregation on the operation of slurry pipelines. The following remarks are made based on the authors' experience with laminar flow slurry pipeline operation:

- Coarse particles gradually settle[3] towards the pipe invert under laminar flow conditions. It is likely that only coarse particles in the sheared zone settle; coarse particles in the un-sheared zone in the central part of the pipe cross section are expected to be supported by the mixture yield stress.
- As coarse particles migrate towards the pipe invert, they increase the local solids concentration and mixture rheology. This migration of coarse particles continues until an equilibrium condition is reached; the physics governing this equilibrium condition are not yet well understood and it is a topic of current research.
- While coarse particles may form a stationary bed on the pipe invert, it appears that this generally does not occur for slurries with moderate yield stresses (above 20 Pa). Rather an asymmetric velocity profile develops with the local velocity gradually increasing from the pipe invert to a maximum velocity at the (un-sheared zone which is displaced to above the pipe axis) as discussed in the previous section.
- Due to the non-homogenous nature of the flow and the asymmetric velocity distribution, the *in situ* concentration is greater than the delivered concentration and the friction losses are greater than for homogeneous laminar flow.
- The non-homogeneity, with the consequent flow asymmetry and increase in in situ concentration, results in laminar flow pipeline friction loses which are greater than the friction losses for a homogenous mixture where the in situ concentration matches the delivered concentration.
- Following a period of laminar flow operation, a higher velocity is required to achieve turbulent flow due to the increased friction loss due to non-homogeneity compared with homogenous laminar flow; i.e. non-homogeneity increases the laminar to turbulent transition velocity.
- The non-homogeneity which results from laminar operation is dependent on the slurry rheology, coarse particle characteristics and pipe diameter. For high yield stress mixtures in relatively small pipelines (such as in paste backfill systems[4]), there is no evidence of laminar flow segregation and non-homogeneity. Operating experience with a 14 inch pipeline conveying thickened tailings (approximately 50 Pa yield stress, with 1 mm top size coarse particles) indicates pipeline pressure gradients about 50% greater than for homogeneous laminar flow.

The Saskatchewan Research Council's Pipe Flow Technology Centre (SRC) is currently investigating the laminar flow of yield stress slurries containing coarse particles as part of a multi-client research project. The findings of this work have not yet been published but it is expected that the research will provide new insights into the behaviour of laminar flow in pipelines.

3.3 *Pipeline Operating Flow Regime*

Conventional slurry pipeline design practice is to ensure compliance with both the following conditions:

- Operation in turbulent flow.
- The operating velocity must exceed the turbulent deposition velocity.

[2] In turbulent flow, there is sufficient mixing to counteract the settling tendency of coarse particles.
[3] The rate of settlement is likely governed by the particle properties (size, density and shape), the carrier fluid properties (density and plastic viscosity) and the local concentration of coarse particles.
[4] Pipe size sizes typically smaller than eight inches, yield stress generally greater than 250 Pa.

For long distance slurry pipelines, the particle size distribution, rheology and solids concentration are optimized to ensure these two conditions occur at roughly the same operating velocity for the selected pipe diameter.

High operating velocities are required to achieve turbulent flow for slurries with moderate yield stresses (as shown in Fig 1, 4.1 m/s is required to achieve turbulent for 52 Pa yield stress NST in a 20 inch pipeline). These high operating velocities significantly increase the pumping system energy requirements and so there is interest in designing pipelines to operate in laminar flow. However, as discussed in the previous section, there are significant uncertainties regarding laminar flow pipeline operation (primarily the equilibrium pressure gradient which will be achieved under laminar flow conditions).

Until definitive research findings or operational experience is available to provide guidance for designing laminar flow pipelines, our recommendation is that pipelines transporting NST mixtures are designed to operate in turbulent flow as per conventional design practice. However, there are opportunities to optimize the NST rheology for optimum pipeline operation:

- The solids concentration and carbon dioxide addition should be tailored to achieve only the yield stress required to optimize the non-segregating characteristics of NST required during deposition.
- Consideration should be given to adding carbon dioxide closer to the deposition point, so that the benefits of increased yield stress are achieved on during deposition without incurring the penalty during pipeline transport.

3.4 *Turbulent Flow Deposition Velocity and Pressure Gradient Prediction*

The SRC Pipe Flow model is the established and proven tool for turbulent flow deposition velocity and pressure gradient predictions for oil sand settling slurry pipelines. SRC PipeFlow 10.2 is the latest version publically available (to attendees of a SRC training course). This version does not accommodate yield stress carrier fluids and so the model should be used with caution for the design NST pipelines.

An earlier version (2006.4[5]) of the SRC Pipe Flow Model was developed specifically for slurries with carrier fluids which have a yield stress. This version makes provision for an increased viscous sub-layer thickness due to the non-Newtonian rheology as suggested by Thomas and Wilson (2007).

The SRC is currently engaged in the development of an improved pipe flow model as part of a multi-client research project.

The following remarks are noted regarding the use the SRC Pipe Flow Model:

- The SRC model divides the solids into fine particles (which mix with the water to form the carrier fluid) and coarse particles. Historically the SRC has considered the 74 μm particle size[6] as division between fine and coarse particles; it is recommended that this distinction is maintained when using the SRC model for oil sands projects.
- The rheology of the carrier fluid must be measured as there is no method available for predicting the rheology based on the fines and water properties.
- The model ascribes a single particle size to the coarse particles; the d_{50} of the particles coarser than 74 μm. This is probably the most significant weakness of the current SRC pipe flow models and is being addressed through the current multi-client project.
- The CNRL Horizon tailings contain five inch "lumps" which need to be considered in the design of the NST pipelines. Counter intuitively, the deposition velocity is dictated by particles around the 500 μm size range and so the lumps do not need to be considered in establishing the minimum pipeline operating velocity. However, the lumps do contribute to the pipeline friction losses (through added Coulombic friction) and so typically a correction is made for the lumps. Expert guidance[7] should be sought when mak-

[5] The 2006.4 version of the Pipe Flow model is proprietary and is only available for use by oil sand companies which sponsored the development of model.

[6] Note that the 44 μm particle size is used by the Oil Sands industry as the standard to differentiate between fines and sand. Accordingly care must be taken to avoid confusion between the SRC and standard oil sands definition for fines.

[7] i.e. Dr Randy Gillies of the Saskatchewan Research Council.

ing this correction. The SRC pipe flow model version being developed currently will allow the coarse particles to be represented as multi sizes and specific gravities and so will address this issue.

- The volume fraction of coarse solids in the settled bed is an important parameter (especially for higher concentrations slurries); this value needs to be measured in a laboratory test.

4 SUMMARY

Pump and pipeline transport of NST is a challenging endeavor given the large range in particle sizes and the variation in the properties of the mixture. Ideally, NST should be delivered at the minimum yield stress sufficient for optimum deposition behaviour at a velocity that minimizes power consumption.

5 REFERENCES

Chu, A., T. Paradis, V. Wallwork and J. Hurdal 2008. Non Segregating Tailings at The Horizon Oil Sands Project. Proc. !st Int. Oil Sands Tailings Conference, Edmonton, Canada, 7-10 Dec.

Cooke, R. 2002. Laminar flow settling: the potential for unexpected problems. Proc. 15th Int. Conf. on Hydrotransport, Bannf, Canada, 3-5 June.

Gillies, R., R. Sun, J. Schaan and C.A. Shook 2002. Pipeline flow of oilsand consolidating tailings slurries. Proc. 15th Int. Conf. on Hydrotransport, Banff, Canada, 3-5 June.

Gillies R., R. Sun and R. Tipman 2006. Flow testing of oil sand NST mixturies n a 500 mm diameter pipeline. Saskatchewan Research Council confidential report 12005-2C06.

Hedblom, E. and P. Solseng 2012. Non-Segregating Tailings (NST) Deposition Study Part 2. Canadian Natural Report No. 24P-RPT-TA-0001-00 by .

Pullum, L., L. Graham and J. Wu 2010. Bed establishment lengths under laminar flow. Proc. 18th Int. Conf. on Hydrotransport, Rio de Janeiro, Brazil, 22-24 September.

Thomas A.D. and K.C. Wilson 2007. Rough-wall and turbulent transition analyses for Bingham plastics. Proc. of 17th Int. Conf. on Hydraulic Transport of Solids, BHR/SAIMM, Cape Town, South Africa, p. 77-86.

Tailings embankment construction material alternative – cyclone sand or mined rockfill

Jeff FitzGerald, Daniel Friedman & Ken Brouwer
Knight Piésold Ltd., Vancouver, BC, Canada

ABSTRACT: The choice of construction material for the staged development of a tailings embankment is an important decision that should be based on careful evaluation of economic factors, constructability, operational flexibility, environmental/permitting challenges, mine closure planning and social acceptance. In many instances, the sandy fraction of hard rock tailings materials can be used for ongoing staged expansions of tailings embankments and is often considered to be the most cost-effective construction material when compared to earthfill or rockfill. An evaluation of actual costs from mining operations suggests that the overall costs for construction, operations, management and closure of cyclone sand tailings impoundments can actually be significantly greater than for an equivalent facility that utilizes earthfill or rockfill materials, particularly if open pit overburden and waste rock are geochemically benign and within a reasonable haulage distance. Large open pit mines often use large haul trucks that can efficiently deliver waste rock to the tailings embankments for an incremental haulage cost. The cost typically depends on the 'overhaul distance', which is the additional haulage beyond the waste haul required for disposal in dumps.

Knight Piésold Ltd. (KP) has evaluated actual costs for the implementation and the ongoing construction of a large cyclone sand tailings embankment at a large open pit mining operation in Canada. The cost information included capital expenditures and operating costs relating to manpower, equipment, electrical power and fuel, contractor support, water management, reclamation and environmental controls. Additional comparative cost information was also obtained from several other mining operations in Canada and in South America. These data have been used to evaluate the economic sensitivity of cyclone sand operations to the variations in labour and power costs that are often seen between different locations. The results of the analysis demonstrated that the cyclone sand construction method may not be the most cost effective approach for all mine operations.

A recent alternatives assessment for the Tailings Storage Facility (TSF) at a proposed 30,000 tpd tungsten project in New Brunswick, Canada initially indicated that mine waste rock was a more cost effective construction material than cyclone sand. However, ongoing waste characterization studies suggested that the waste rock was potentially acid generating and hence was not suitable for embankment construction. The construction materials evaluation was subsequently extended to consider a trade-off between more expensive quarried rockfill and cyclone sand. The study included detailed quarrying cost information obtained from a specialist mining consultant and input from a separate consultant with extensive experience in cyclone sand system design. This evaluation indicated comparable life-of-mine costs, but identified significant technical, operational, environmental and social considerations that resulted in the selection of quarried rockfill as the primary construction material for the embankment shell.

1 INTRODUCTION

1.1 *General*

Capital and operating costs for mine tailings storage are essential considerations when assessing the overall economic viability for a mining project. Embankments are typically constructed to create or enhance the storage capacity of the impoundment for a Tailings Storage Facility (TSF). The choice of an embankment construction material is an important decision that should be based on careful evaluation of economic factors, constructability, operational flexibility, environmental/permitting challenges, mine closure planning and social acceptance.

In many instances, the sandy fraction of hard rock tailings materials can be used as embankment fill and has often been considered to be the most cost-effective construction material compared to earthfill or rockfill. An evaluation of actual costs from mining operations suggests that the overall costs for construction, operation, management and closure of cyclone sand tailings impoundments can actually be significantly more than for an equivalent facility constructed using earthfill or rockfill, particularly if open pit overburden and waste rock are geochemically benign and located within a reasonable haulage distance of the embankment. If it is possible to integrate the TSF into the overall waste dump design, overhaul costs may be small to insignificant.

An appropriate embankment design is essential to minimize not only the embankment construction costs but total waste and water management costs throughout the mine life and into closure. Total peripheral waste and water management design costs beyond unit fill placement costs need to be taken into consideration when designing an embankment and appropriate trade-off studies should be performed to determine the optimal approach for the site.

1.2 *Cyclone Sand Basics*

Cyclone sand embankment fill can be produced by processing mine tailings through a hydrocyclone that separates the coarse sandy fraction of the tailings from the fine silt and clay sized particles. The coarser underflow fraction can be used as an embankment fill material while the finer overflow fraction is disposed within the TSF impoundment. Hydrocyclone systems are designed to provide a suitable sandy underflow product that meets the embankment material specifications (*e.g.* particle size gradation, drainage, geochemical characteristics). Hydrocyclone systems are sensitive to the characteristics of the tailings 'feed' and can require adjustment if variation in ore type and metallurgical processes result in changes to the tailings characteristics over time.

The key criteria that must be met to allow embankment constructions with cyclone sand are:

- Split of the tailings feed material to produce sufficient quantity of underflow
- Suitable quality of underflow product (geotechnical and geochemical)
- Underflow must be sufficiently permeable and must act as a filter for the tailings slurry being deposited upstream
- Density and solids content of the underflow (can be too wet or too dry depending on placement methods)

Two embankment construction methods that are typically used with cyclone sand are Direct Discharge and the Hydraulic Cell Placement method.

Direct discharge involves gravity flow of cyclone sand underflow discharged down the downstream slope of the embankment from multiple points along the embankment crest. Additional manipulation of the direct discharge tailings may be required depending on the design specifications; this may include compaction and spreading with a dozer traversing the slope.

An alternative construction method utilizes hydraulic placement of the sandy underflow into cells and involves constructing containment dykes to capture the sandy cyclone underflow where it is also spread and compacted using low ground pressure bulldozers. This method allows for point source deposition of cyclone underflow, controlled compaction to reduce the potential for liquefaction, and requires external collection of decant and seepage water. Both placement methodologies require water management systems to collect and manage excess water from seepage and from the hydraulic transport of the cyclone sand. Excess fine silty particles may be present in runoff water from the hydraulic cells and from erosion during surface runoff events. Suitable sediment capture and disposal systems may be necessary to manage the-

se fine sediments and can include dredge and pumping systems for return to the TSF impoundment.

1.3 *Rockfill Basics*

Rockfill embankments can be constructed using either non-acid generating (NAG) mine waste rock or NAG materials from nearby borrow areas or quarries. The advantage of using NAG waste rock from the mine is that the costs required to drill, blast, excavate, load, and partially haul the material are already accounted for under mining operations, and only the overhaul costs and spreading and compaction need to be included in the TSF embankment construction cost. Overhaul is the additional haulage required beyond the designated waste dump as shown on Figure 1. Construction costs for rockfill can be significantly reduced by using an overhaul approach and appropriately sized mine equipment, particularly as the larger mining equipment fleets can offer significant economies of scale. Larger equipment reduces unit placement costs ($/tonne) by reducing total overhead, maintenance, labour and fuel consumption per tonne of material moved. An advantage of utilizing rockfill instead of cyclone sand is that it is independent of the mill operation; therefore plant downtime, changing ore characteristics or other process changes that can influence the suitability of the cycloned tailings underflow product do not affect the fill material availability as illustrated on Figure 2.

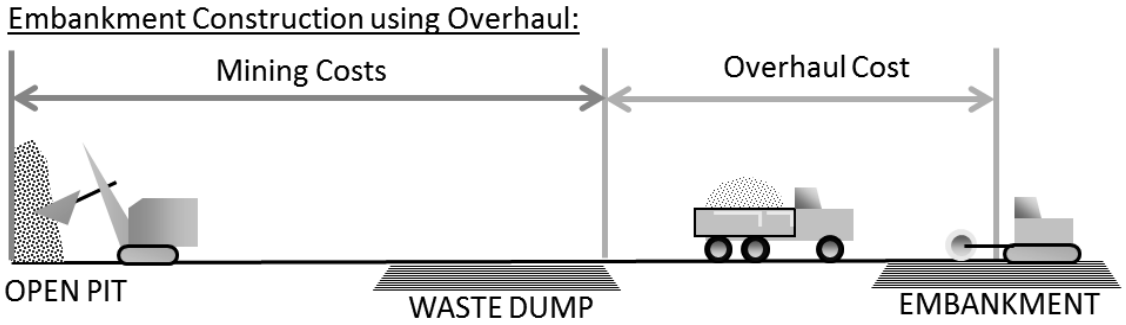


Figure 1. Simplified schematic illustrating Overhaul costs

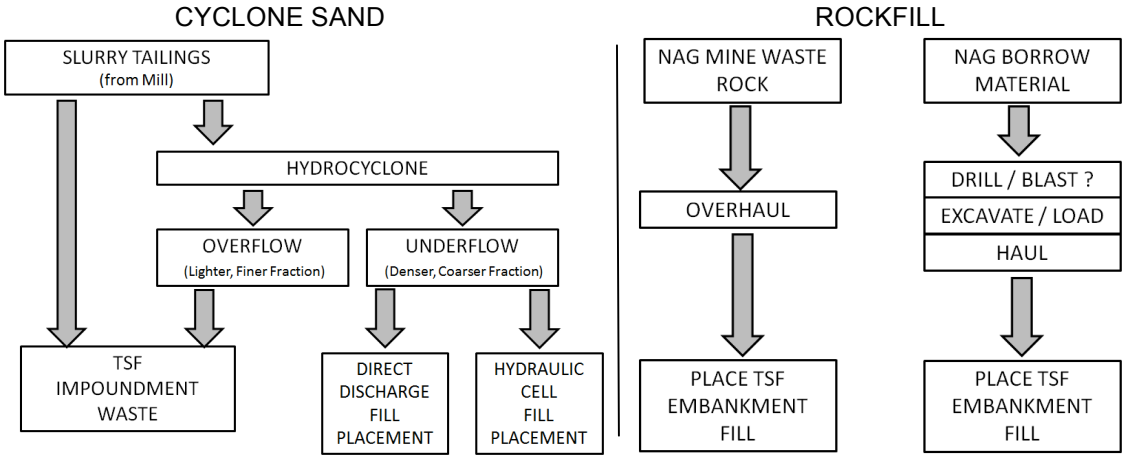


Figure 2. Simplified Schematics for Embankment Material Fill Placement (Cyclone Sand and Rockfill)

2 DESIGN CONSIDERATIONS

The design of a tailings embankment and the selection of the most appropriate fill material requires careful consideration of geotechnical, water management, construction, operational, envi-

ronmental, social, closure and economic factors. A summary of the key design considerations that apply to cyclone sand and rockfill is presented in the table below.

3 ECONOMIC CONSIDERATIONS

The economic assessment includes consideration of the project capital (initial and sustaining), total operational costs, closure and reclamation bonding requirements, and the time value of money. A net present value analysis may favor a design with higher lifetime capital and operating costs if the upfront capital requirements are substantially lower than an alternative with lower lifetime costs. A summary of the key economic considerations for cyclone sand and rockfill embankment construction options is presented in the table below.

Table 1. Design Considerations

Design Consideration		**Cyclone Sand**	**Rockfill**
Geotechnical	Flatter Embankment Slope	□	
	Typically Larger Embankment Fill Volume	□	
	Slightly Higher Embankment Elevation as sandy tailings also impounded		□
	Liquefaction Potential of Fill Material	□	
	Additional Drainage Control/Collection Measures	□	
	Variability in Ore or Metallurgical Processes Influence Fill Characteristics	□	
Water Management	Increased Drainage	□	
	Additional Drainage Zones and Pipeworks Required	□	
	Additional Pumping Requirements	□	
	Retention of Sediment From Run-Off (Dredging Requirements)	□	
Construction and Operational	Fill Material Availability	□	□
	Seasonal Restrictions in Cold Climates	□	
	Operational Complexity - Integration of Mine Schedules and Equipment		□
	Operational Complexity - Additional pumping/piping and movement of infrastructure (labour)	□	
Environmental and Social	Project footprint (dam, pipeline corridors, quarry, haul routes)	□	□
	Increased Wind and Water Erosion Control Measures	□	
	Seepage and Sediment Control	□	
	Public Perception of Good Seismic Stability		□
	Noise (blasting, hauling, cyclone operation)	□	□
	ML/ARD properties of Fill Material	□	□
	Sensitivity to Metallurgical Process or Ore Type and Tailings Geochemical Characteristics	□	
Closure Design	Additional Footprint of Borrow Areas		□(?)
	Steep downstream slopes may need re-grading for closure and reclamation	□	□
	Additional wind & water erosion control measures	□	
	Closure Bonding Requirements and NPV	□	□

Table 2. Economic Considerations

Economic Consideration		Cyclone Sand	Rockfill
Capital Cost	Additional Equipment Purchases (trucks, loaders, dozers)		□
	Quarry / Borrow Source Development and Permitting		□
	Additional Haul Road Development (unless treated as a waste dump)		□
	Cyclone Sand Plant EPCM	□	
	Additional Cost for New Pipeworks or the Incremental Costs to Existing Pipeworks	□	
	Hydraulic Cell Drainage Collection System, Sludge and Slime Ponds, and Dredging Equipment	□	
	Incremental Foundation Preparation for a larger dam footprint	□	
	Low Ground Pressure Dozer Purchase for Hydraulic Cell Placement	□	
	NPV Analysis – Time Value of Money (Amount of Upfront Capital)	□	□
Operational Cost	Regional Factors (Labour, Power, Fuel , Altitude and Water availability)	□	□
	Contractor, Specialist Firm or Mine Fleet performing work	□	□
	Drilling and Blasting		□
	Load, Haul, Place, Spread, Compact		□
	Incremental Tailings Pumping Costs	□	
	Slimes and Drainage Pumping Costs	□	
	Pond Dredging, Slimes and Water Management, Erosion Control Costs	□	
	Movement of cyclone system and pipelines	□	
	Sand Placement, Spreading and Compacting	□	

4 KEMESS MINE CALIBRATION CASE

4.1 *Project Background*

The Kemess Mine is a gold and copper open pit mine located in Northern BC as shown on Figure 3. The mine operated from 1998 through 2011 with a mill throughput of 56,000 tpd. Tailings were deposited in a surface TSF that included a 1.4 km long and 150 metre high embankment as illustrated in Photo 1. The TSF embankment was identified as one of the larger capital cost items during on-going operations, which led to an evaluation of opportunities for cost reduction.

The original TSF dam design incorporated a downstream fill zone constructed from local borrow sources. The use of NAG waste rock that would be hauled approximately 7 km from the open pit was also considered. An alternative embankment construction option using cyclone tailings sands hydraulically placed and compacted in sand cells was estimated to be less expensive and was subsequently developed (Rasmussen, 2009). Construction with tailings sand required a two-stage cyclone system combined with an intermediate pyrite separation circuit; a simplified schematic of the sand plant is shown on Figure 4.

4.2 *Kemess Cyclone Sand Embankment Construction*

The sandy underflow product was hydraulically deposited in the sand cells where it was redistributed with low ground pressure dozers. This placement strategy was required to densify and compact the sandy tailings in order to reduce the potential for liquefaction and enhance the embankment stability. Modifications to the placement methodology, containment berm construction, cell sizing and underflow solids content were made throughout operations to optimize placement and compaction. Some interruptions to sand placement were noted as a result of sand

plant downtime, equipment downtime, and extreme cold weather events in the months of December and January (minimal).

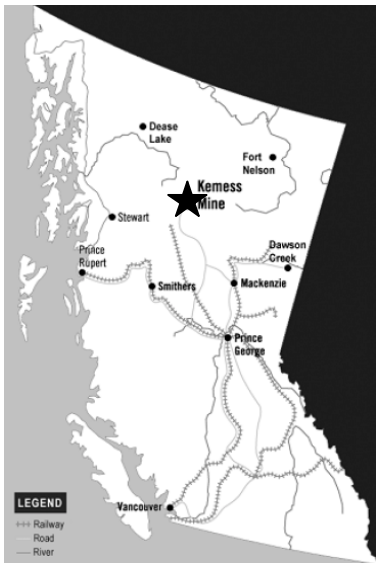


Figure 3. Kemess Mine Location.



Photo 1. Kemess Mine TSF

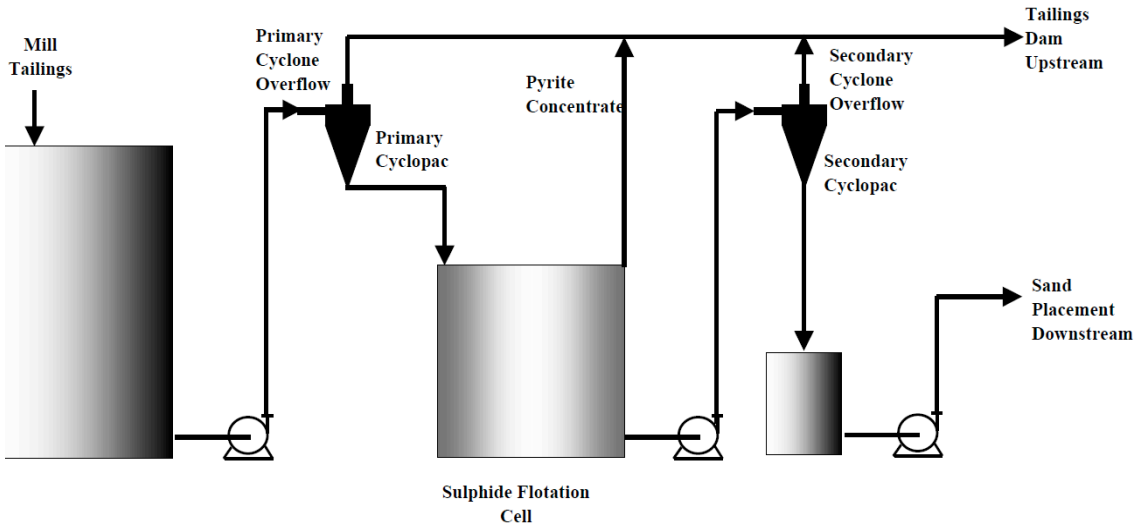


Figure 4. Kemess Mine Sand Plant Flowsheet

4.3 *Post Operations Cost Analysis*

The cost estimates presented by "Ramussen et al. 2009." indicated that the rockfill placement cost would average approximately 4.75 $/m^3 (2009 Canadian Dollars) and a cyclone sand placement cost of approximately 1.00 $/m^3. The cyclone sand placement cost comprised 0.25 $/m^3 to operate the sand plant and 0.75 $/m^3 for placement and operation of a rubber-tired tractor. These low operating costs provided a basis for justifying the capital expenditures required for a central sand plant (approximately $7 million prorated to 2009 dollars) situated adjacent at the abutment of the ultimate embankment. The cyclone sand costs did not account for items such as erosion control, sludge and slimes management, incremental slurry pumping costs, and the incremental power costs associated with increased pumping for sand cell drainage, collection and recycle.

Knight Piésold Ltd. conducted an updated cost analysis of the cyclone sand operations using actual capital and operating cost data provided by mine personnel. The goal of the analysis was to develop a more comprehensive cost estimate of cyclone sand embankment development that considered the additional items not included in previous estimates in order to develop an 'apples to apples' comparison to the alternative rockfill embankment construction materials option. The results of the cost analysis indicated that the operational placement costs for the cycloned sand construction materials was approximately \$4.20/ m^3; approximately four times higher than the initial estimate. A graphical representation of the perceived and actual costs is shown on Figure 5.

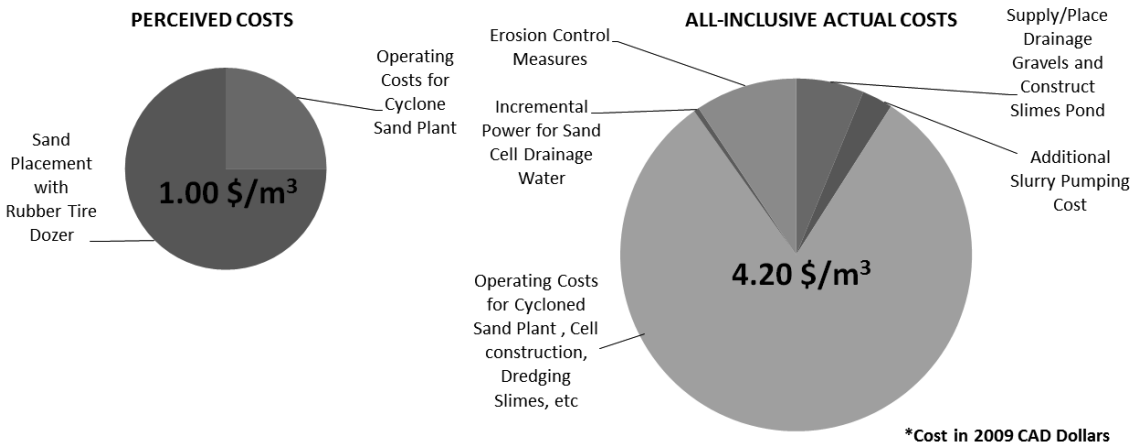


Figure 5. Perceived versus Actual Costs Cyclone Sand Embankment Construction Costs

4.4 *Kemess Calibration Study Results*

The Kemess calibration study illustrates the significant additional costs that may be incurred for cyclone sand embankment construction. Total cost accounting in trade-off studies is critical to perform a relevant comparison between the alternatives. The costs previously stated are operational costs only; however, when the capital cost of the sand plant is factored into the cyclone unit rate, the rate climbs to approximately 5.10 \$/m^3, which is higher than their estimated waste rock placement costs of 4.75 \$/m^3. On this basis, waste rock placement costs would have been an economically competitive alternative, especially if haul routes were optimized, and if overhaul was incorporated to avoid double handling of NAG rockfill material and allow for direct placement of waste rock sourced from on-going open pit stripping operations.

5 SISSON PROJECT

5.1 *Project Background*

The Sisson Project is a proposed tungsten and molybdenum open pit mine in west-central New Brunswick. The project will operate at a nominal 30,000 tpd mill throughput over a 27 year mine life producing 281 Mt of tailings, 193 Mt of PAG waste rock and 17 Mt of mid-grade ore. A feasibility study was completed in early 2013 by Northcliff Resources Ltd.

The TSF site consists of rolling hills and broad valleys at an average elevation of 290 to 400 masl. The TSF is located in a natural depression surrounded by a main embankment on the north, east and south sides, and a saddle embankment on the west side. The embankment is approximately 8 km long and has a maximum height of approximately 90 metres. The climate in the project area is relatively wet with an estimated mean annual precipitation of 1350 mm, with 75% of the annual precipitation falling as rain and the remainder as snow. The annual average potential evapotranspiration for the project site was estimated to be 500 mm.

Assessments to determine the best TSF site location and tailings deposition technology were undertaken that resulted in selection of a TSF adjacent to the open pit using conventional slurry tailings deposition. The project location and mine site layout are shown on Figures 6 and 7, respectively.



Figure 6. Sisson Project Location.

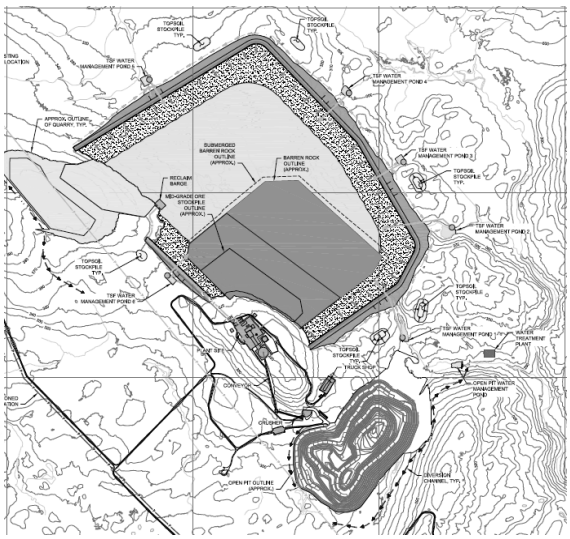


Figure 7. Sisson Project Site Layout

5.2 *TSF Embankment Fill Alternatives*

During preliminary engineering studies it was assumed that the TSF embankments could be constructed of NAG waste rock from mining operations; however, additional geochemical work during the feasibility study indicated that mine waste rock may be unsuitable due to the potentially acid generating (PAG) nature of some of the waste rock. A revised plan was developed to co-dispose and submerge all mine waste rock in the TSF to inhibit acid generation and simplify site water management. A trade-off study was carried out to compare cyclone sand and quarried rock as the primary embankment construction material.

A preliminary embankment design was completed for each alternative. The key differences in the design for the two alternatives are illustrated on Figure 8; these include: fill volumes, downstream slopes, embankment height, crest widths, and embankment under-drainage details. The fill volume for the cyclone sand alternative is higher as a result of the flatter downstream slope when compared to the rockfill embankment, which can be made steeper. The cyclone sand section has a lower elevation as a result of less tailings being disposed of in the impoundment since the coarse tailings are being used to build the embankment. The rockfill embankment section required a wider crest for the haul truck traffic. The cyclone embankment required additional under drainage works for managing the large quantity of water that needs to be collected during hydraulic fill placement.

5.3 *Cyclone Sand Considerations*

The key design considerations for a cyclone sand embankment were the tailings characteristics, tailings availability, sediment control and water management, and capital and operating costs.

The tailings characteristics are a critical input to the cyclone sand system design. The proposed design for the Sisson Project consisted of portable cyclones on the dam crest to allow downstream hydraulic cell placement. There was still some uncertainty around the mill process at the time of the trade-off study including ongoing refinement of the grind size and the resulting tailings particle size distribution. A secondary cyclone may have been needed to meet the geotechnical design specifications for embankment fill depending on the final tailings particle size distribution. The assessment was eventually completed assuming that only a single stage cy-

clone would be required based on the best available data at the time. However, this was identified as a potential capital cost risk given that a two-stage cyclone system would be more expensive that the simpler single-stage design.

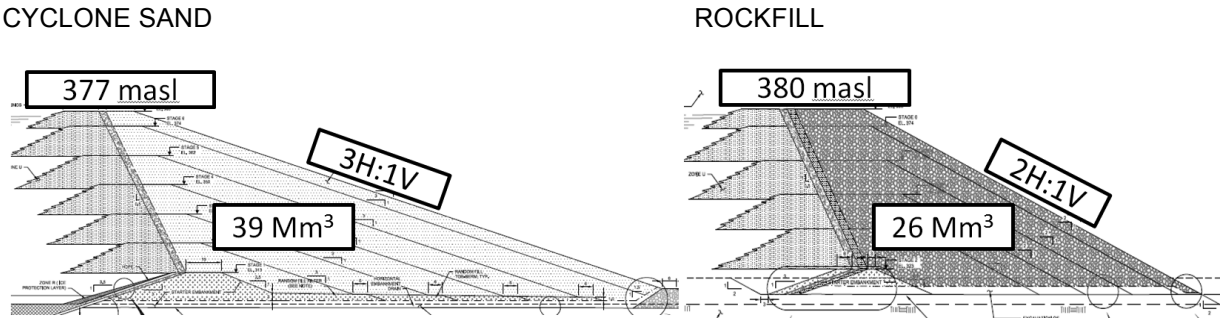


Figure 8. Sisson Project – Embankment Sections for Alternatives Assessment

Cyclone sand production capacity using mine tailings was found to be insufficient in the later years of the mine life due to increasing annual fill volume requirements. As a result, construction with cyclone sand for the Sisson TSF would require overbuilding the embankment in the initial years of the mine life to ensure that the embankment could be raised to the required height in later years and maintain the necessary storm storage and freeboard capacities.

Sediment control and water management were important considerations at Sisson as Atlantic Salmon and other fish species are present near the project. Comprehensive sediment and erosion control measures would be required to minimize downstream effects from construction of the embankment.

The upfront capital costs included the sand plant and its associated civil, mechanical systems and electrical systems; additional under drainage systems and larger sediment collection ponds; and overbuilding the embankment in the early years of the mine life to meet the ongoing staging requirements.

5.4 *Quarried Rock Considerations*

Key design considerations for rockfill were the borrow source location and the potential requirement to purchase additional mining equipment for quarrying operations.

The most effective borrow source was determined to be a quarry located in the northwest corner of the TSF. The location minimizes haul distances between the quarry and the TSF and allows the mine equipment to be integrated into quarrying operations given the close proximity to the open pit. A disadvantage of the quarry location is that it requires relocating an existing transmission line; this needed to be factored into the capital cost estimate.

5.5 *Sisson Cost Analysis*

Capital and operating cost estimates were developed for both the cyclone sand and quarried rockfill alternatives. Cyclone sand plant capital and operating costs were provided by Paterson and Cooke and cost for slimes management, erosion control and cell construction were developed either from first principles or from recent reference projects. Quarry development, drilling and blasting, haul, and placement costs were developed with input from Moose Mountain Technical Services who were responsible for the feasibility study mine plan and mining cost estimates.

The results of the cost analysis summarized in Table 7 indicated a lower total cost for a rockfill embankment even though the unit rate for cyclone sand was lower; this was because the rockfill embankment required less total volume. Applying a discount rate to account for the time value of money over the mine life further increased the relative difference in life-of-mine costs.

Table 3. Sisson Cost Analysis Results

Fill Material	Quantity (Mm^3)	Non-Discounted		Discounted @ 5%	
		Unit Rate ($/$m^3$)	Cost ($Million CAD)	Unit Rate ($/$m^3$)	Cost ($Million CAD)
Quarried Rockfill	26	$4.79	**$124**	$2.19	**$57**
Cyclone Sand	39	$3.42	**$134**	$1.76	**$69**

It should be noted that the costs are very similar when considering the level of detail in the study and the design assumptions made in developing the estimates. Neither alternative is clearly favored based on the total costs alone; however, looking at the NPV of the two alternatives highlights the reduced upfront capital costs associated with rockfill, as illustrated in the discounted cash flow on Figure 9.

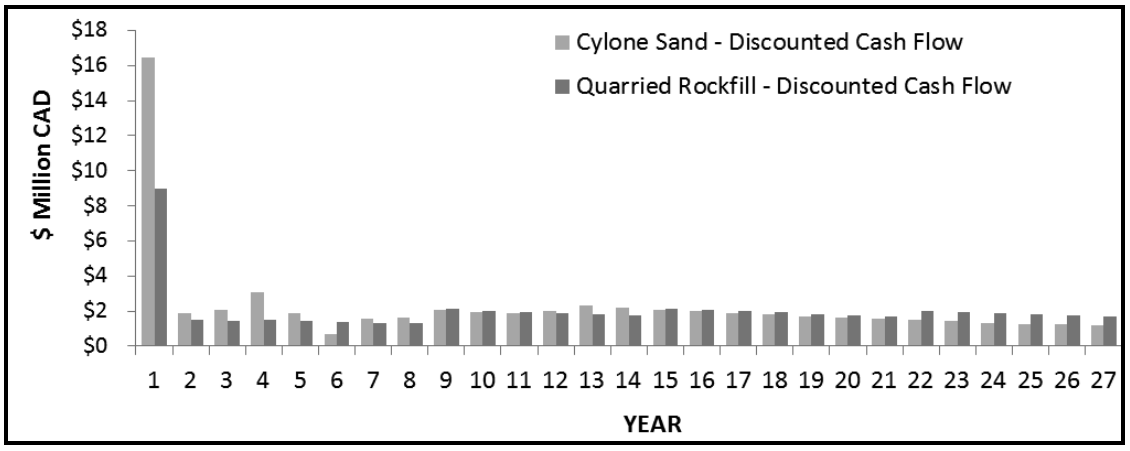


Figure 9. Sisson Project – Cyclone Sand versus Rockfill Discounted Cash Flow

5.6 *Sisson Case Study Results*

Quarried rockfill was selected as the preferred alternative for the Sisson Project based on the following key considerations:

- A rockfill operation has less operational complexity and offers more flexibility since it is not tied to mill processes.
- There are fewer downstream environmental concerns and reduced wind and water erosion control requirements, and
- A lower upfront capital cost.

6 CONCLUSIONS

A comprehensive embankment alternatives assessment needs to consider site wide design implications and total cost accounting. Total cost accounting should consider initial and sustaining capital, operating expenses, and closure costs for the site wide waste and water management plan. Regional factors such as power costs, fuel costs, water costs and labor costs play a significant role in the economics of each alternative. The embankment design should only be selected following a rigorous assessment of the viable alternatives on a project by project basis.

7 REFERENCES

Lysay, Georgia. McConnachie, Jennifer. Johns, Carolyn. & Evans, Jordan. 2009. Kemess South Mine Reclamation and Closure.: 1-11.

Rasmussen, Greg. Hoffert, John. Tucker, Greg. Kinch, Jeremy. Colwell, Darren. 2009. The Kemess Mines Ltd. Tailings Dam Construction Using Tailings Construction Sand.: 1-28.

Thickened tailings disposal system: Three years of successful operation

Jianping "JP" Wu, & Loel Renshaw
Ausenco, Concord, California, USA

Yueguang Che, P.E.
Ausenco, Beijing, China

ABSTRACT: A large iron mine is located 150 kilometers (km) north of Baotou City, the capital of Inner Mongolia, China. The mine has a thickened tailings system with a design capacity of 7 million metric tons per annum (MTA) and a project life of 13 years. Tailings from the process plant are fed into a deep cone paste thickener, which generates 70 to 73 weight percent (wt%) solids of thickened tailings. The thickened tailings are pumped to the tailings storage facility (TSF) for disposal.

Ausenco's team in Beijing, China was tasked by the mine owner to design and start-up the thickened tailings system, which includes thickening facilities, pipeline transport and distribution systems, and the storage facility.

Since the system became operational in 2010, Ausenco has provided continuous support to the owner by fine tuning the system operation and resolving some of the technical challenges they experienced during the first 2 years of operation. This paper summarizes the design of the thickened tailings system, including the various assumptions, slurry characteristics and laboratory tests, tailings thickening pilot tests, thickener selection, as well as challenges experienced during commissioning and operation.

1 INTRODUCTION

1.1 *Overview*

Mines are increasingly moving toward thickened or paste tailings disposal due to advantages such as water savings and decreased environmental risk (seepage and water spills). Advances in thickener design and thickening technology in recent years have made it possible to produce high density tailings at a reasonable cost.

A large iron mine is located approximately 150 km from Baotou City, in China's Inner Mongolia province. Since 2010, the West Mine has expanded the existing facilities, which produces 7 MTA.

In 2007, Ausenco was requested by the owner to provide a feasibility level study for a new tailings system. Upon review, Ausenco discovered that there was a strong economic incentive to minimize water usage as it is required to be transported by pipeline from 150 km away to the concentrator, which required maximizing the tailings dewatering. Ausenco performed a trade-off (re-screening) study to determine the optimal system configuration. Three design options were studied: conventional tailings (C_w = 50%), thickened tailings (C_w = 70%), and high density tailings dry stack (C_w = 85%). Due to the high cost of water, the thickened tailings option offered a significant cost advantage over the other options. Under the owner's direction, Ausenco's team in Beijing completed the design and start-up of the thickened tailings system, which included thickening facilities, the pipeline transport and distribution system, and the storage facility.

Since the system became operational in 2010, Ausenco has provided continuous support to the owner by fine tuning the system operation and resolving some of the technical challenges

they experienced during the first years of operation. The design of the thickened tailings system, including the various assumptions, slurry characteristics and laboratory tests, tailings thickening pilot tests, thickener selection, as well as challenges experienced during commissioning and operation are summarized in this paper.

1.2 *Design Challenges and Considerations*

1.2.1 *Water Conservation*

As part of the iron mine development, Ausenco also designed a 130 km, 915 mm water pipeline transporting 2,500 m^3/h of fresh water from the Yellow River to the mine site for the mine operations. The high pressure water pipeline uses only one pump station to lift water 520 meters across an arid region in support of both the mine operations and the livelihood of nearby communities.

Due to the high cost of the process water and the high evaporation in the TSF, there is a strong economic incentive to retain water within the plant and minimize water usage by increasing the tailings density.

1.2.2 *Tailings Containment*

The area of the tailings impoundment site is relatively flat and covers approximately 2.7 km^2. Use of the thickened tailings system would minimize the extent of perimeter embankments required and increase the mass of tailings stored on the given footprint. The thickened tailings can be deposited at a slope that increases the capacity of tailings storage.

1.2.3 *Dust Control*

The area of the tailings impoundment site is relatively flat and very windy. The design of the tailings pipeline and its operation must take specific actions to minimize dust and movement of dried tailings downwind as much as possible.

1.2.4 *Cold temperature*

During winter months, local temperatures range from approximately +40°C to -40°C. Thus, specific attention is required in designing the tailings pipeline to prevent freezing.

1.2.5 *Thickener Underflow*

The thickener underflow from the deep cone thickeners (DCTs) must be controlled to ensure reliable tailings pipeline operations and tailings deposition. The concentration of the thickener underflow must be maintained within a fairly narrow operating range. As shown in the tailings rheology charts, minimal wt% increase in the solids concentration may cause significant uprising in the slurry rheology. Higher slurry yield stress will result in higher transition velocity in the pipe and the tailings pipeline may operate in laminar flow. The viscosity and yield stress of thickened tailings can be quite high and it may not be possible to transport them in turbulent flow at reasonable velocities.

2 SYSTEM DESIGN

2.1 *Tailings System Design Throughput*

The tailings system design throughput is 7 MTA, with a system availability of 8,000 hours per year. The system hourly throughput is 875 metric tons per hour (mtph). The tailings system has a design life of 13 years, upon which the TSF reaches its maximum storage capacity.

2.2 *Tailings Properties and Slurry Characteristics*

Slurry samples of the mine tailings tested in Ausenco's laboratory yielded tailings properties and the slurry characteristics as follows:

Table 1. The summary of climatologic data at mine site

Parameters	Amount
Concentrator Elevation, mASL	1620
DCTs Elevation, mASL	1614
TSF Initial Embankment Elevation, mASL	1600
TSF Ultimate Embankment Elevation, mASL	1630
Annual Rainfall, mm	370
Annual Evaporation, mm	2400
Maximum Temperature, ^{o}C	+40
Minimum Temperature, ^{o}C	-40
Mean Freezing Days	120

Table 2. Tailings particle size distribution (PSD)

Tyler Mesh	Size in Microns	Cumulative Percent Passing
60	250	94.37
100	147	87.35
150	104	80.80
200	74	72.74
270	54	63.34
325	44	57.91
400	37	54.94

The solids specific gravity (SG) is 3.229

The tailings slurry rheology is illustrated in the Figures 1and 2 below.

2.3 *Site Conditions*

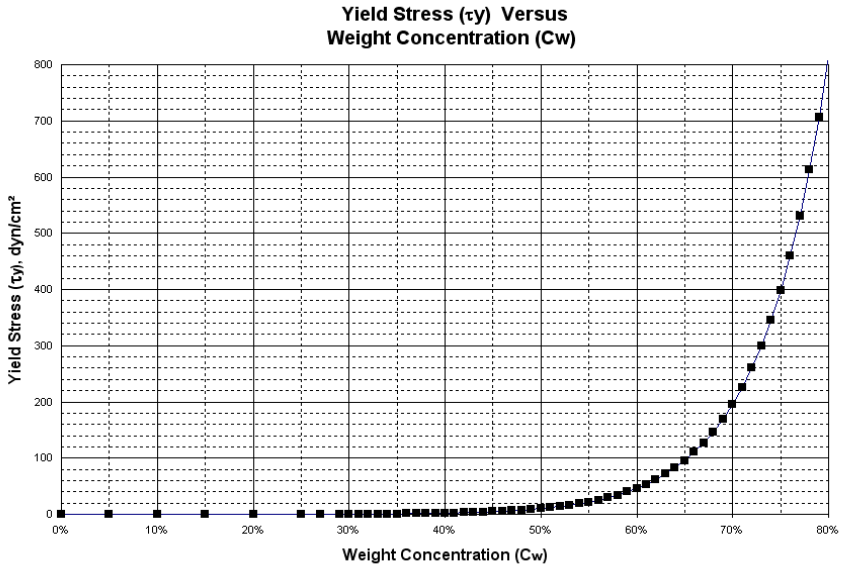


Figure 1. Yield stress vs. weight concentration.

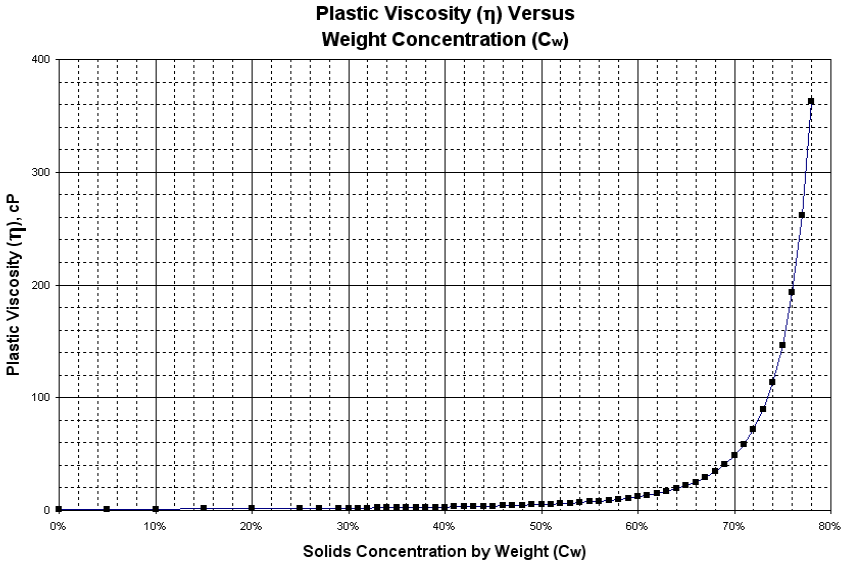


Figure 2. Plastic viscosity vs. weight concentration.

2.4 *System Description*

The thickened tailings system consists of two thickening stations: one at the process plant, and the other at the TSF. A 45 m diameter thickener at the first stage thickening station receives iron tailings from the concentrator at a 9% solids concentration by weight and dewaters the tailings to 45% to 50% solids by weight. The thickener underflow is pumped using two 14x12 centrifugal slurry pumps (one operating and one standby) through a 560 mm diameter high density polyethylene (HDPE) standard dimension ratio (SDR) 11, 2.9 km long pipeline to feed two 20 m diameter, 18 m height DCTs at the second thickening station near the TSF. A shearing pump is provided in each DCT to reduce the slurry yield stress and increase the pumpability of the thickened tailings underflow. The underflow of 70% solids by weight from the DCTs is then pumped through a 400 mm diameter steel pipe to the TSF and distributed through either 2 km or 1 km deposition pipelines on the northern or western embankments, respectively.

Tailings water seepage and rainwater within the TSF is collected in the collection sump located downstream of the TSF. The water collected in the sump is pumped back to the overflow tank at the DCTs through 220 mm diameter 3.1 km steel pipe. The water in the overflow tank at the DCTs is pumped back to the concentrator through a 400 mm diameter, 3 km steel pipeline.

2.5 *Hydraulic Design*

The tailings underflow from the conventional thickener operates in a settling slurry flow pattern in the 560 mm diameter HDPE SDR 11 pipe. The deposition and transition velocities are 1.5 and 0.24 meters per second (m/s), respectively. The operating velocity for the design throughput is 2 m/s, which is above both the deposition and transition velocity.

For the system design throughput and the design range of the solids concentration, the thickened tailings from the DCTs operate under the laminar flow pattern in the 400 mm diameter steel pipe.

The following figure depicts pressure gradients in both the 560 and 400 mm diameter pipes under various operating velocities. Pressure gradients for the thickened tailings in the 400 mm diameter pipe operating under the laminar flow were assumed without solids settling. When significant amounts of particles are larger than 20 microns, the larger particles will settle out during laminar flow. The pressure drop required to keep the settled solids moving must be added to the

laminar flow friction loss (Cook, 2002). Based on a loop test (Gilles, 1999) it is believed that a pressure gradient of 1 to 2 kPa/m was required to transport solids in laminar flow.

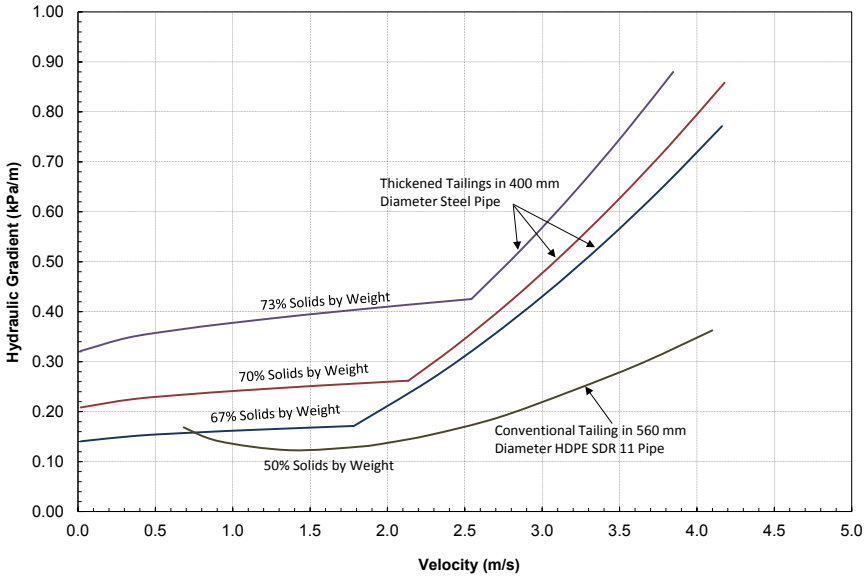


Figure 3. Tailings Pressure Gradient

2.6 *TSF Design*

The tailings TSF is an enclosed facility that consists of four dams: the south, west, north, and east. The tailings impoundment area is approximately 2.7 km^2 and it has 13 years of tailings storage capacity. Figure 4 shows a general plan view of the TSF. A typical dyke section is shown in Figure 5.

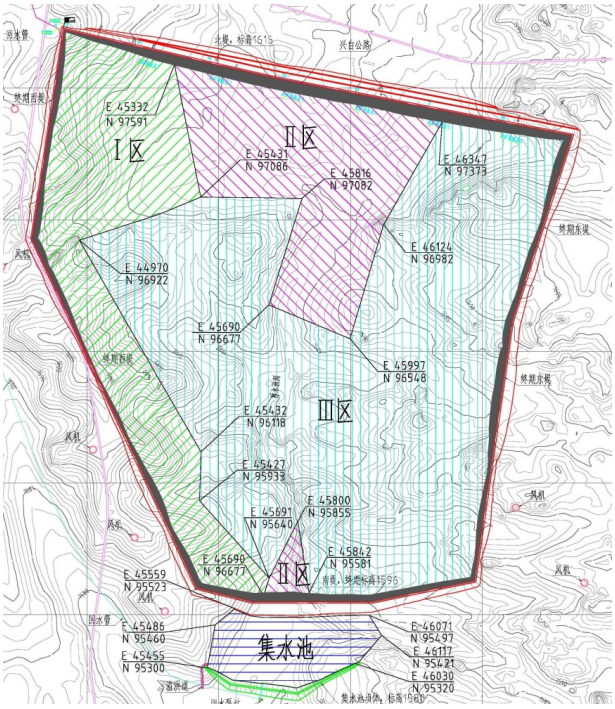


Figure 4. TSF general arrangement.

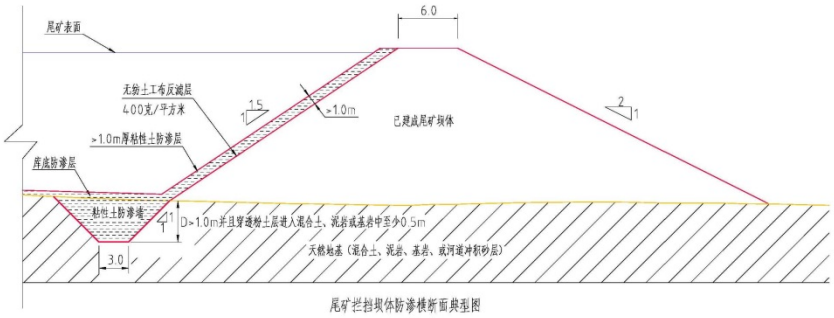


Figure 5. Typical dyke section.

The north starter dam has a crest elevation at 1616 mASL. East and west starter dams are less than 15 m high and 500 and 700 m long, respectively. No starter dams are required in the initial year for the south sides of the tailings impoundment. The east, west and south dams are raised in phases. The ultimate crest elevation of the south dam will be 1596 mASL and the west and east dams are connected with the north and south dams to form an enclosed impoundment. After the initial 5 years of tailings deposition from the north and the north-west sides of the impoundment, the disposed tailings will fill up to the crest of the north dam and will extend to the south side of the impoundment. In year 6, a 2 m height of dyke will be built 100 m south of the north dam and the thickener tailings will be distributed through spigots along the north dyke. Each 2 m dyke will last for one year of operation before it is full. Another 2 m dyke will be built 100 m south of previous dyke. A total of 7 dykes will be built during the 13 year project life. A small collection pond will be built outside of the south dam to collect the runoff and seepage water from the impoundment.

3 PILOT TEST

3.1 *Deep Cone Thickener Pilot Scale Tests*

In 2008, a 1-m diameter DCT pilot unit was shipped from Peru to the mine site for pilot-scale thickening tests, as show in Figure 6 below. The pilot unit was operated under various conditions to evaluate design parameters of the thickener, including feed rate, feed characteristics, mud residence time and bed depth, and flocculent dosage, etc. The test results were also used to select operating conditions to produce the thickened tailings underflow for deposition and pumping studies. The pilot-scale field testing successfully demonstrated the simultaneous production of a thickened underflow tailings product and a clear overflow water stream. The highest solids content in the thickened tailings was 74% with 25 g/t flocculent dosage. To treat 875 tph iron tailings at the design solids concentration of 73%, two 18 m diameter DCTs were needed. Figure 6 shows the pilot unit of deep cone thickener used in the pilot tests.

3.2 *Slump Tests*

The slump test is used to estimate the yield stress and viscosity of thickened tailings. The slump height measured via the slump test is generally used as the control parameter. For this project the effects of solids concentration on the deposition slope and slurry yield stress were investigated under different conditions. Experimental results indicated that the slope percentage increased significantly with increasing solids concentration. The slurry shearing reduced the slurry yield stress significantly, which is helpful for slurry transportation by pumping, but significantly reduced the deposition slopes. Results of slump tests are shown in Figure 7.



Figure 6. DCT pilot unit.

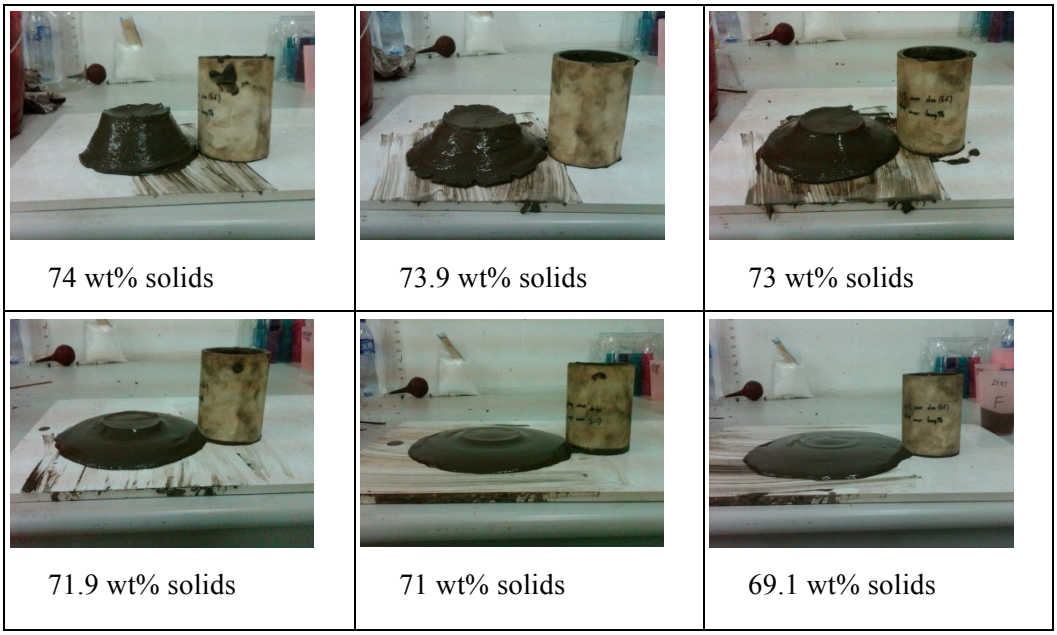


Figure 7. Cylinder slump photos.

3.3 *Deposition Tests*

Flume tests were performed during the on-site pilot-scale thickening study. The objectives of the tests were to determine the beach slope that could be achieved with the tailings at predetermined

solids concentration, the effectiveness for beach formation of selected deposition procedures, and the variation with time of the dry density, moisture content and degree of saturation of the tailings beach. In the flume tests, the thickened tailings were deposited into two 1 m wide 10 m long test flumes at the upper end of the test flume through a vertical drop pipe. The slurry was sampled at the start of each deposition to check the tailings properties. The tailings levels were measured on stakes fixed near the head, the middle, and the top of the flumes at various times before and after deposition in order to determine the variation in layer thickness. For the fully sheared, 70% solids by weight concentration tailings, 2.5% to 3% beach slope was achieved, without any solids segregation. Figure 8 shows the flume tests that were performed during the on-site pilot tests.



Fresh tailings @70% solids	After 1day and 2 nights	After one week

Figure 8. Flume tests.

4 SYSTEM COMMISSIONING AND OPERATION

Since undergoing commissioning in 2010, the thickened tailings system has been operating successfully.

4.1 *Tailings Deposition Plan*

The tailings disposal system consists of two tailings distribution headers, one on the north dam and the other on the west dam. Both headers are 400 mm diameter, API 5L bare steel pipe. The north header is 2 km in length and is divided into two sections for the two tailings disposal zones. Three 200 mm disposal pipes connected to the header in each zone, with a 280 m interval between the disposal pipes. The west header is 1 km in length with 4 single point discharge pipes. Each disposal pipe has 25, 2 inch diameter tailings spigots with a 2 m interval between each one. During summer operations, the thickened tailings are discharged through those spigots to form a layer of evenly distributed tailings beach as shown in Figure 9. The single point discharge is used in winter operation to avoid freezing.

4.2 *Tailings Underflow Control*

Although the high solids concentration was obtained with a reasonable flocculent dosage during the pilot-scale tests, the design solids concentration of 73% could not be achieved without a high dosage of flocculent. In the last three years of operation, the 69% to 70% solids concentration thickened tailings were achieved with 20 g/t. A 1.5% to 2% beach angle was achieved with the thickened tailings underflow, which satisfied the tailings impoundment design criteria. The tail-

ings samples in the tailings impoundment were taken near the discharge points, 50 m and 100 m from the discharge point. The particle size distribution data indicated that there are no solids segregation occurred.



Figure 9. Thickened tailings disposal in summer months.

4.3 *Dust Control*

After several years of successful operation, it is agreed that dust is not an issue in the thickened tailings surface disposal, at least not in this particular mine operation. On the contrary, dust was blown off the existing conventional tailings impoundment, which was adjacent to the new thickened tailings impoundment area and was used for dumping the 50% tailings when the DCTs were out of service.

5 CONCLUSIONS

The thickened tailings system is vital to the success of this mine development and subsequent operation. The most important advantage of the system is higher water recovery. For the same footprint of the disposal area the tailings storage capacity increases significantly.

6 REFERENCES

Gillies, R.G. Hill, K.M., etc. 1999. Solids Transport by Laminar Newtonian Flows, J. Powder Technology.

Cooke, R. 2002. Laminar Flow Settling: The Potential for Unexpected Problems, *Proc.15th intern. Conf. on Hydrotransport, Banff, 3–4 October 2002*.

Characterising settling and dewatering of slurries of commercial clays and clay-rich coal tailings

David J. Williams & Timothy M.A. Delport
The University of Queensland, Brisbane, Australia

M Stuart Whitton
Mechanical Advantage, Brisbane, Australia

ABSTRACT: Coal mining activities in Australia are proceeding into new resource areas; west into the Surat and Galilee Basins in Queensland, and into the western Hunter Valley Coalfields in New South Wales, in Australia, where clay-rich inter-burdens and multiple thin seams are frequently encountered. The resulting tailings slurries are clay-rich, and hence display poor settling and dewatering behaviour, making them difficult to manage and rehabilitate. It has proven difficult to achieve a settled solids concentration much better than 25% solids by mass on settling slurries of the clay-rich tailings. In an effort to better understand the settling behaviour of these clay-rich tailings, slurries of several commercial clays and two typical clay-rich coal mine tailings have been subjected to settling column testing from a range of initial solids concentrations, in two process waters with various concentrations of metal salts. The settling and dewatering of slurries of the commercial clays has shed light on the behaviour of clays in a more pure form. From this, the settling and dewatering of tailings containing a mixture of clay minerals and non-clay minerals may better be interpreted. The implications of the results are that clay-rich coal mine tailings will require dewatering by filtration and/or by desiccation on deposition to maximise process water recovery and achieve an acceptable tailings consistency.

1 INTRODUCTION

Researching and managing clay-rich coal mine tailings involves gaining an understanding of their behaviour across two scales:

- macro-behaviour; including settling, filtration, consolidation, desiccation and loading (on capping); constituting soil mechanics; and
- micro-behaviour; including clay mineral interactions with water, metal salts, coagulants and flocculants; constituting soil science.

This paper focuses on settling macro-behaviour and micro-behaviour affected by the water used, plus the effect of added metal salts. Metal salts are relevant due to their presence in the raw water typically available to mines for the processing of coal.

The problematic clays found in clay-rich coal mine tailings can range from bentonite (or smectite or montmorillonite) to kaolinite-dominant clays, plus minor non-clay minerals and amorphous material. The bentonites comprise a number of sub-species, classified by the dominant cation present, such as sodium (Na^+), calcium (Ca^{2+}), potassium (K^+), and aluminum (Al^{3+}), with Na and Ca species being particularly prevalent. As the clay and cation variations contribute significantly to the behaviour of the resulting tailings, commercial clays with identified dominant clays and cations (sodium bentonite, calcium bentonite and kaolinite) were sourced for testing as controls. From the behaviour of commercial clays, the behaviour of the tailings containing a range of clay species may better be understood.

2 SAMPLE CHARACTERISATION

The testing described in this paper involved a number of commercial clay samples, and two clay-rich coal mine tailings, conducted using either deionised water or simulated Surat process water, plus known additions of various metal salts. The metal salts used are relatively readily available, and were assessed for their ability to aid the settling and dewatering of slurries of commercial clays and clay-rich coal tailings.

2.1 *Solid samples*

The solid samples sourced for tested included six commercial clays, and two typical clay-rich coal mine tailings samples collected from a mine in the Surat Coalfields of south-central Queensland (symbol S/01/05) and from a mine in the Upper Hunter Valley Coalfields of New South Wales (symbol H/01/02), in Australia. Table 1 gives the sources of the commercial clays.

Table 1. Sources of commercial clays.

Supplier	Bentonite Products	Bentonite Products	Australian Pacific Coal	Arump	Amcol	Eckalite
Description	Sodium Bentonite	Calcium Bentonite	Sodium Bentonite	Sodium Bentonite	Sodium Bentonite	Kaolinite
Symbol	COM/01/01	COM/01/02	COM/02	COM/03	COM/04	COM/05

The commercial clays and the two typical clay-rich coal mine tailings samples were subjected to X-ray diffraction (XRD) analyses. Sample preparation involved grinding a 1.5 g sub-sample 10 min in a McCrone micronising mill under ethanol. Due to the presence of swelling clay minerals, the samples were twice Ca-saturated using 1 molar (1 M) $CaCl_2$, followed by washing in water then ethanol, before oven-drying at 60°C. The samples were centrifuged at 6,000 rpm following each step. The oven-dried samples were thoroughly mixed with an agate mortar and pestle before being lightly back pressed into stainless steel sample holders to achieve a random orientation of the mineral particles for XRD analysis.

XRD patterns were recorded with a PANalytical X'Pert Pro Multi-purpose Diffractometer using Fe-filtered Co-Ka radiation, auto-divergence slit, 2° anti-scatter slit and fast X'Celerator Si-strip detector. The patterns were recorded in steps of 0.016° 2 theta with a 0.4 s counting time per step, and were logged to data files for analysis. Quantitative analysis was performed on the XRD data using the commercial package SIROQUANT from Sietronics Pty Ltd. The results included estimates of unidentified or amorphous materials.

Table 2 summarises the results of XRD analyses of the commercial clays, while Table 3 summarises the XRD results for the two typical clay-rich coal mine tailings samples.

Table 2. XRD results for commercial clays, in terms of estimated % by mass of various clay and other minerals.

Symbol	COM/01/01	COM/01/02	COM/02	COM/03	COM/04	COM/05
% Kaolinite	11	15	-	2	4	99
% Anatase	< 1	< 1	< 1	< 1	<1	<1
% Bentonite	78	70	67	69	78	-
% Quartz	6	5	2	9	10	1
% Microcline/Orthoclase	-	-	-	1	-	-
% Albite/Anorthite	1	1	-	7	8	-
% Calcite	1	2	-	-	-	-
% Dolomite/Ankerite	3	5	-	-	-	-
% Siderite	< 1	< 1	-	-	-	-
% Amorphous	-	2	31	12	-	-
Total % non-clay	11	15	33	29	18	1

Table 3. XRD results for typical clay-rich coal mine tailings, in terms of estimated % by mass of various clay and other minerals.

Symbol	S/01/05	H/01/02
% Kaolinite	12	6
% Anatase	-	-
% Bentonite	83	73
% Quartz	< 1	15
% Microcline/Orthoclase	-	1
% Albite/Anorthite	-	3
% Calcite	-	-
% Dolomite/Ankerite	-	< 1
% Siderite	-	1
% Amorphous	5	1
Total % non-clay	5	21

The XRD analyses showed that the bentonite-dominated commercial clays COM/01/01, COM/01/02, COM/02, COM/03 and COM/04 were relatively pure, but contained 11 to 33% non-clay minerals by mass, comprising mostly Kaolinite, Quartz, Albite/Anorthite and/or Amorphous material, most of which would not be expected to influence the settling behaviour of slurries made from these bentonite-dominated clays. The Kaolinite-dominated commercial clay COM/05 was almost pure kaolinite. The Surat Coalfields clay-rich coal mine tailings sample (S/01/05) was bentonite-dominated at 83%, with 12% Kaolinite and 5% Amorphous material. The Hunter Valley Coalfields clay-rich coal mine tailings sample (H/01/02) was also bentonite-dominated at 73%, but with 6% Kaolinite and 21%non-clay minerals, dominated by Quartz at 15%.

The physical characterisation of the commercial clays and clay-rich coal mine tailings samples included Atterberg limit testing in accordance with AS 1289, and specific gravity testing using a helium pycnometer. The results are given in Table 4. From the Atterberg limit results, the Unified Soil Classification (UCS) is assigned, as indicated in Table 4. All of the samples classify as clays of intermediate to high plasticity.

Table 4. Physical characterisation of commercial clays and tailings samples reported.

Sample	COM/01/01	COM/01/02	COM/02	COM/03	COM/04	COM/05	S/01/05	H/01/02
Liquid Limit (%)	81	78	59	49	74	43	46	54
Plastic Limit (%)	30	19	22	24	20	27	14	17
Plasticity Index (%)	51	59	37	24	53	16	32	37
UCS	CH	CH	CH	CI/CH	CH	CI	CI	CH
Specific Gravity	2.42	2.51	2.50	2.21	2.31	2.48	2.05	2.32

Typical particle size distributions of the Surat (S/01) and Hunter Valley (H/01) Coalfields clayey run-of-mine (ROM) feed to the coal washery and of the washery thickener underflow are shown in Figure 1. The clayey ROM feed to the washery is representative of the natural clay-rich waste materials prior to beneficiation of the coal, while the washery thickener underflow is representative of the fine-grained waste from the washery following the addition of coagulants and flocculants and thickening to produce a tailings slurry that is then pumped to the tailings storage facility. The particle size distributions were obtained using sieving and hydrometer analyses carried out in accordance with AS 1289. Dispersant was added to the samples prior to wet sieving of the coarse-grained fraction and hydrometer analysis of the fine-grained fraction.

The two ROM samples are seen in Figure 1 to have more coarse-grained particles and a higher apparent clay content (finer than 0.002 mm) than the corresponding thickener underflow samples. This result is to be expected, since passage through the washery would be expected to break down the coarse-grained particles, while the addition of coagulants and flocculants in the thickener would agglomerate the clay particles, making them appear coarser-grained.

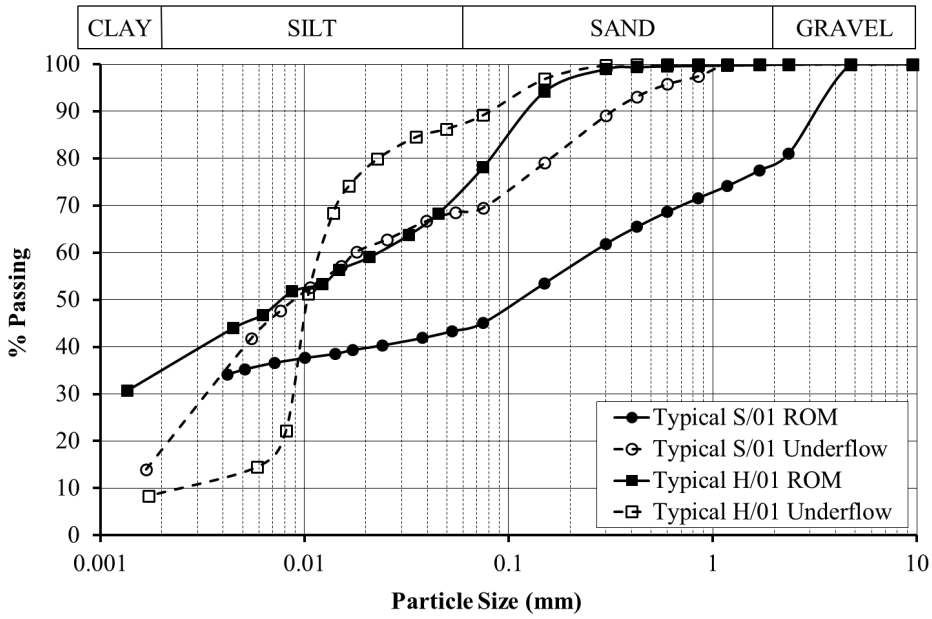


Figure 1. Typical particle size distributions of Surat (S/01) and Hunter Valley (H/01) Coalfields run-of-mine feed to coal washery and washery thickener underflow.

2.2 *Water samples*

Two water samples were used in the settling column testing: (i) deionised water, as a control, and (ii) simulated Surat process water, representing realistic process water quality. The pH, EC and TDS values of the deionised water used are given in Table 5. The waters available for processing in both the Surat and Hunter Valley Coalfields are somewhat saline and reasonably similar. The simulated Surat process water was designed to represent the chemistry of typically available process water, and comprised 3.13g/l NaCl (sodium chloride) and 4.6g/l $NaHCO_3$ (sodium bicarbonate), achieving the pH, electrical conductivity (EC) and total dissolved solids (TDS) values given in Table 6.

Table 5. Chemistry of deionised water, plus added equivalent ionic concentrations of metal salts, used for testing.

Parameter/Sample	Deionised water	NaCl	$CaCl_2$	$MgCl_2$	KCl	$CaSO_4$	$Al_2(SO_4)_3$
pH	7.71	8.32	7.55	7.96	8.13	6.18	3.74
EC (µS/cm)	414	1,515	1,058	1,190	1,637	527	1,111
TDS (ppm)	217	841	579	655	914	280	609

Table 6. Chemistry of simulated Surat process water, plus added equivalent ionic concentrations of metal salts, used for testing.

Parameter/Sample	Process water	NaCl	$CaCl_2$	$MgCl_2$	KCl	$CaSO_4$	$Al_2(SO_4)_3$
pH	7.96	8.20	7.71	8.07	8.17	7.65	7.55
EC (µS/cm)	2,123	994	877	903	962	898	863
TDS (ppm)	1,200	572	527	544	580	541	518

Metal salts were added to both the deionised water and the simulated Surat process water to assess their effectiveness in aiding settling. The metal salts selected for testing were based on mine site preferences, their availability and their cost. Sodium and calcium-based metal salts are prevalent in clays found in the coalfields, and hence are readily available and cheap. Magnesium and potassium-based metal salts were identified as a potential aid to the settling of clay-rich slurries, since they would allow ionic exchange to take place. Alum, which is widely-used in

sewage treatment, was also identified as a potential aid to settling. Alum is an industrial waste product, and hence relatively available and cheap.

In order to be able to compare the effect of the added metal salts on the same basis, an equivalent ionic concentration (EIC) of each salt was added, requiring different molar concentrations of the different salts. The EIC was based on a reference of 0.01 M NaCl (sodium chloride). Matching molar concentrations of the other metal salts were 0.0033 M $CaCl_2$ (calcium chloride), 0.0033 M $MgCl_2$ (magnesium chloride), 0.01 M KCl (potassium chloride), 0.0025 M $CaSO_4$ (calcium sulphate), and 0.0007 M $Al_2(SO_4)_3$ (aluminium sulphate, or Alum). The pH, EC and TDS values of the deionised water and the simulated Surat process water with metal salts added at the EIC are given in Tables 5 and 6, respectively.

In addition to settling column testing carried out using deionised water and simulated Surat process water with metal salts added at the EIC, selected tests were also carried using 5 times the EIC and 10 times the EIC; that is, equivalent to 0.05 M NaCl and 0.1 M NaCl.

3 SETTLING COLUMN TESTING METHODOLOGY

The settling behaviour of clay-rich coal mine tailings slurries is dependent on inter-clay reactions and clay-water reactions. While these reactions take place at the micro-scale, they can be investigated at the macro-scale by means of settling tests. Ideally, the settling behaviour of clay-rich coal mine tailings slurries, delivered to a storage by pipeline, would best be investigated under field conditions. However, this is impractical. Instead, investigations are conventionally carried out in the laboratory using column settling tests.

3.1 *Rationale for settling column testing*

Typically, laboratory settling tests are carried out in a graduated, 1,000 cc measuring cylinder. However, such a cylinder is tall and slender, unlike the shape of a typical tailings storage, which is flat and shallow, with sides so widely-spaced that they play a negligible part in the settling of the tailings slurry. The ratio of the volume of slurry to the surface area of the cylinder affects the resulting sedimentation and consolidation as a slurry settles (Williams and Morris, 1988). A relatively high surface area aids initial sedimentation due to enhanced flow along the wall of the cylinder, while it hinders subsequent consolidation as the sediment becomes soil-like due to the development of friction along the wall.

3.2 *Test methodology*

The settling column test methodology involved the following steps:

1. Adding the required mass of the selected commercial clay or clay-rich coal mine tailings to the specified water to make up 1,000 cc at an initial solids concentration of 5%, 10% or 20%.
2. Mechanically stirring the mixture at about 1,200 to 1,500 rpm for approximately 3 min, or until a consistent slurry is achieved.
3. Pouring the slurry into the 1,000 cc measuring cylinder, adding the cap, and upending the capped cylinder to produce a uniform suspension.
4. .Setting the cylinder on a level surface, and recording the level of the settling solids at 1, 2, 5, 10, 15, 30, 45, 60 min and regularly thereafter for a total of 72 hours, keeping the cap in place to prevent evaporation.
5. Calculating and plotting % solids versus time.

Settling column testing was carried out on slurries of commercial clays at various initial solids concentrations, in deionised water and simulated Surat process water, without and with added metal salts. Settling column testing was also carried out at various solids concentrations on slurries of the two typical clay-rich coal mine tailings samples S/01/05 and H/01/02 in simulated

Surat process water from 5% solids by mass initially. A photograph of some typical settling column tests is shown in Figure 2.

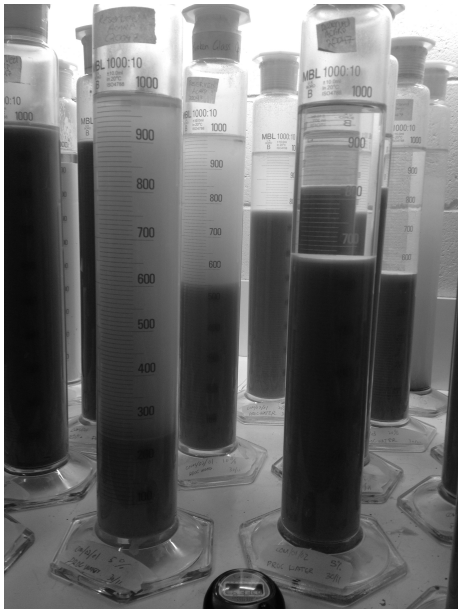


Figure 2. Photograph of some typical settling column tests.

4 SETTLING COLUMN RESULTS

The settling column test results are summarised in a series of figures in the following sections.

4.1 *Testing of commercial clays in deionised or process water alone*

Figure 3 shows the final versus the initial % solids for the commercial clays in deionised water alone and simulated Surat process water alone.

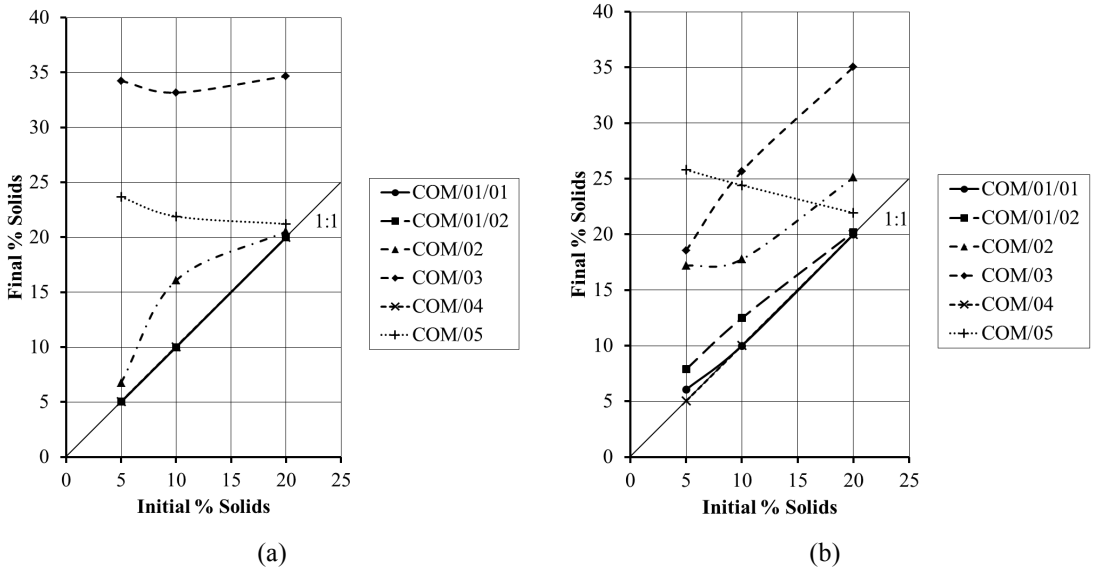


Figure 3. Final versus initial % solids for the commercial clays in: (a) deionised water alone, and (b) simulated Surat process water alone.

Commercial clays COM/02, COM/03 (in particular) and COM/05 (at low initial % solids) showed significant settling in deionised water, while COM/01/01, COM/01/02 and COM/04 did not settle from their initial % solids in deionised water. In simulated Surat process water, COM/02 settled better than in deionised water, COM/03 settled less well at low initial % solids, COM/05 settled slightly better, and COM/01/02 settled somewhat.

4.2 *Testing of commercial clays with added metal salts*

Figure 4 shows the final settled % solids, from 5% solids initially, for the commercial clays in deionised water, with and without different metal salts added at the EIC. In general, COM/01/01 did not settle, even with the addition of metal salts, although the addition of Alum had a minor beneficial effect. COM/01/02 showed some enhanced settling with the addition of $CaCl_2$ and $MgCl_2$. COM/02 showed substantially improved settling with the addition of metal salts, with the addition of $CaCl_2$ being most beneficial. COM/03 settled best among the commercial clays, and most well in deionised water alone. COM/04 did not settle, apart from with the addition of Alum. COM/05 settled second best of the commercial clays tested, in all cases, and best with the addition of $MgCl_2$.

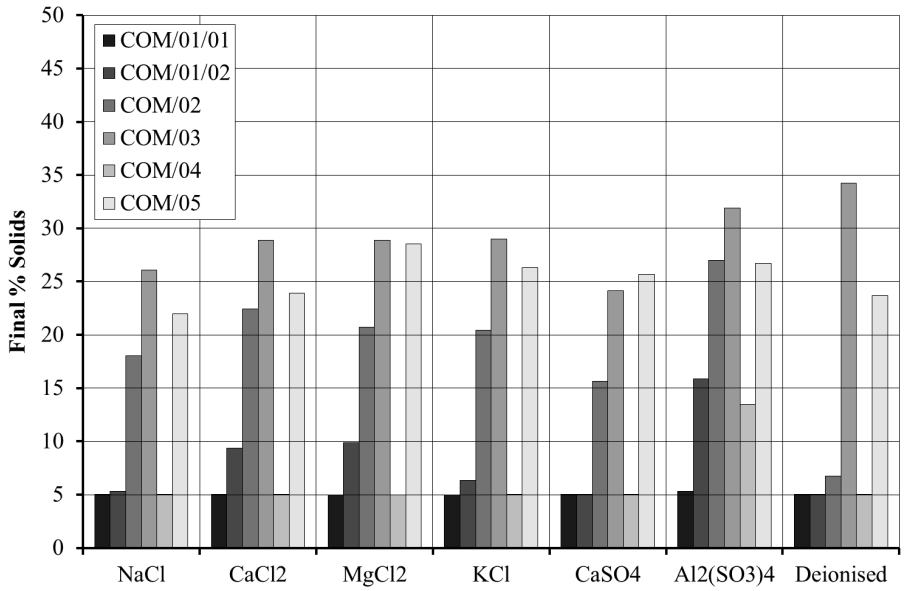


Figure 4. Final settled % solids, from 5% solids initially, for commercial clays in deionised water, with and without different metal salts added at EIC.

Figure 5 shows the final settled % solids, from 5% solids initially, for the commercial clays in simulated Surat process water, with and without different metal salts added at the EIC. The settling of COM/01/01 was slightly improved by the addition of KCl. The settling of COM/01/02 was improved by the addition of metal salts, particularly Alum, $MgCl_2$ and $CaCl_2$, in decreasing order. The settling of COM/02 was reasonable in simulated Surat process water, and largely unaffected by the addition of metal salts. The settling of COM/03 was reasonable in simulated Surat process water, and improved by the addition of Alum and $MgCl_2$, in decreasing order. COM/04 did not settle, apart from with the addition of a\Alum. COM/05 generally settled best among the commercial clay slurries, as would be expected, and largely irrespective of the metal salts added. Overall, the addition of Alum improved the settling behaviour most.

Focusing on the best-performing commercial clay COM/05, Figure 6 shows the final versus the initial % solids (10%, 20% and 30%), for COM/05 in simulated Surat process water, in deionised water, and in relatively high 0.1 M concentrations of various metal salts. In general, COM/05 slurries at low initial % solids settled relatively more than slurries at higher initial % solids, suggesting that water recovery is not necessarily improved by increasing the initial % solids. Of the metal salts tested, $CaSO_4$ improved settling the most.

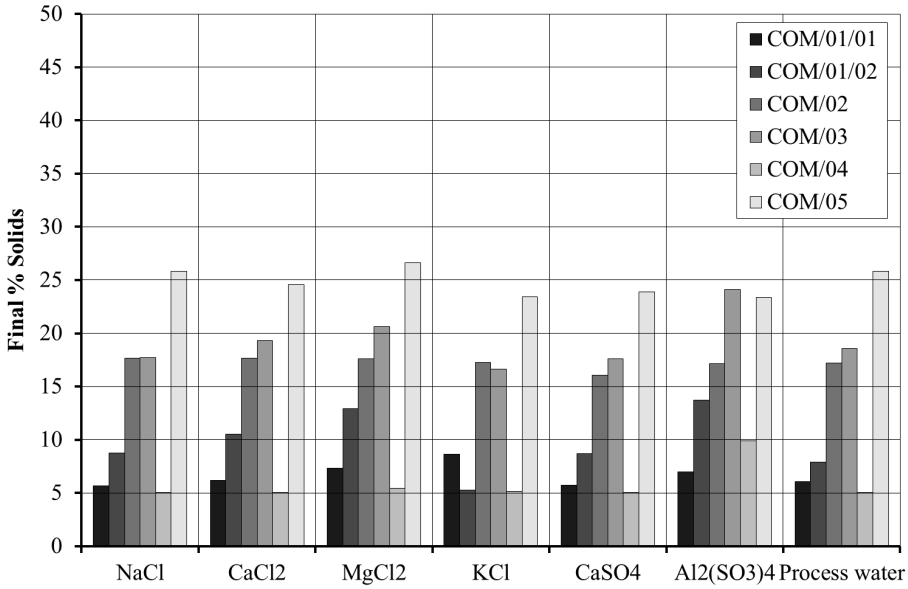


Figure 5 Final settled % solids, from 5% solids initially, for commercial clays in simulated Surat process water, with and without different metal salts added at EIC.

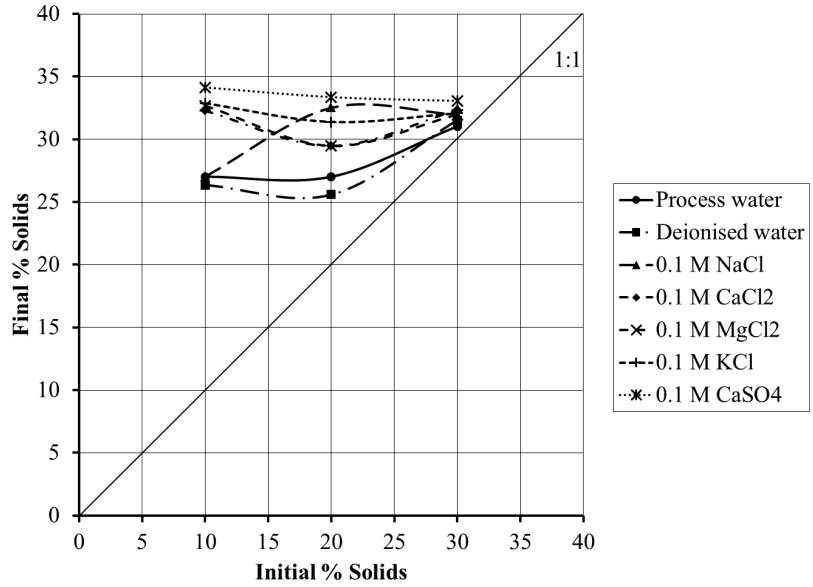


Figure 6. Final versus initial % solids, for commercial clay COM/05 in simulated Surat process water, deionised water, and 0.1 M concentrations of various metal salts.

Figure 7 shows the final settled % solids, from 5% solids initially, for commercial clay COM/02 in simulated Surat process water, with different salts added at the EIC, 5 x ECI, and 10 x EIC, to assess the effect of increasing the dosage of metal salts. In general, there was some improvement in settling, up to a certain metal salt concentration, which varies with the particular metal salt. However, for NaCl, the best settling behaviour was achieved at the EIC, and the final % solids achieved with NaCl was the lowest. The highest final % solids achievable for most metal salts was about 22 to 23%.

Figure 8 shows the final settled % solids, from 5% solids initially, for Surat clay-rich coal mine tailings sample S/01/05 in simulated Surat process water, with different salts added at the EIC, 5 x ECI, and 10 x EIC, to assess the effect of increasing the dosage of metal salts. In general, there is some improvement on settling, up to a certain metal salt concentration, which varies with the particular metal salt. NaCl performed the worst. The highest final % solids achieved was about 26.5% for $MgCl_2$, followed by Alum and $CaCl_2$ at about 24.5%.

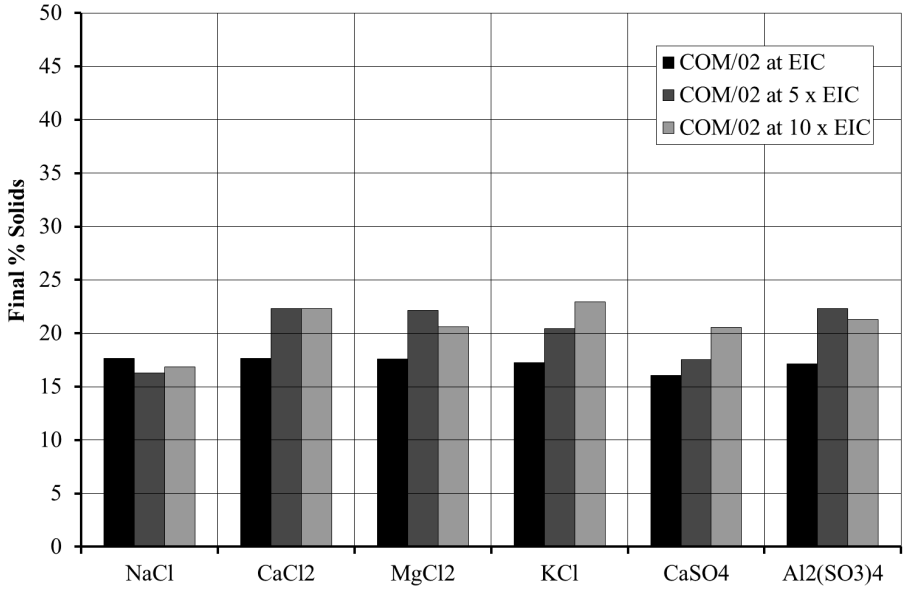


Figure 7. Final settled % solids, from 5% solids initially, for commercial clay COM/02 in simulated Surat process water, with different salts added at EIC, 5 x EIC and 10 x EIC.

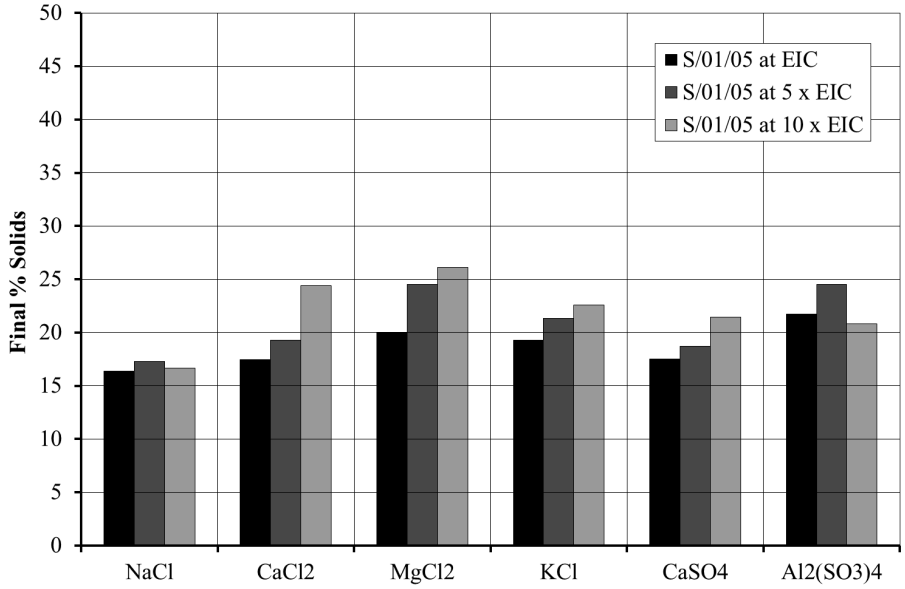


Figure 8. Final settled % solids, from 5% solids initially, for Surat tailings S/01/05 in simulated Surat process water, with different salts added at EIC, 5 x EIC and 10 x EIC.

Figure 9 shows the final settled % solids, from 5% solids initially, for Hunter Valley clay-rich coal mine tailings sample H/01/02 in simulated Surat process water, with different salts added at the EIC, 5 x ECI, and 10 x EIC, to assess the effect of increasing the dosage of metal salts. In general, there is some improvement on settling, up to a certain metal salt concentration, which varies with the particular metal salt. The highest final % solids achieved was about 24.5% for $MgCl_2$ and $CaCl_2$.

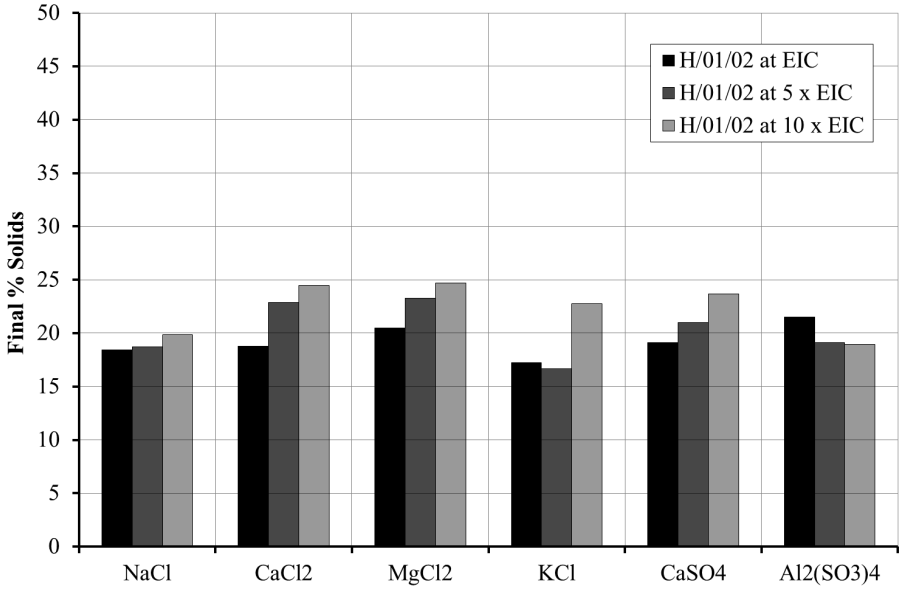


Figure 9. Final settled % solids, from 5% solids initially, for Hunter Valley tailings H/01/02 in simulated Surat process water, with different salts added at EIC, 5 x EIC and 10 x EIC.

5 CONCLUSIONS

The results presented in this paper highlight the complexity of the settling behaviour of slurries of commercial clays and typical clay-rich coal mine tailings. This is due to the complex behaviour at the micro-scale, due to interactions between clay minerals, and between the clay minerals and the metal salts contained in the water used.

Increasing the concentration of metal salts in the water used to form the slurries of commercial clays and clay-rich coal mine tailings samples tested, generally improved their settling behaviour, up to a concentration that varied with the clays and with the metal salts.

It is clear that slurries of commercial bentonite clays are unlikely to settle under their self-weight in a measuring cylinder to better than about 30% solids by mass, and even kaolinite is unlikely to settle to better than about 35% solids by mass, regardless of the metal salts added to the water. Slurries of the two clay-rich coal mine tailings tested settled to no better than about 25% solids by mass, implying a massive entrainment of water of at least 75% by mass or at least 85% by volume, which would be lost.

6 ACKNOWLEDGEMENTS

The research on which this paper is based is part of Australian Coal Association Research Program (ACARP) Project C20047 on improved dewatering, management and rehabilitation of problematic, clay-rich coal mine tailings. The funding provided by ACARP is gratefully acknowledged, as is the cooperation of participating coal mines and commercial clay suppliers in providing samples for testing. The authors also acknowledge the very able assistance with the testing provided by Timothy Vangsness, Michael Connors, Zoe Herbert, and Benjamin Duthie.

7 REFERENCES

AS 1289. Testing Soils for Engineering Purposes. Standards Australia.

Williams, D.J. and Morris, P.H. 1988. Properties of slurried coal tailings. *ASCE Geotechnical Specialty Conference on Hydraulic Fill Structures, Denver, USA, August 1988*, 410–429.

Geotechnical fundamentals of uranium tailings management in Canada

H.K. Mittal
H.K. Mittal and Associates Ltd., Saskatoon, Saskatchewan, Canada

P.G. Landine
Cameco Corporation, Saskatoon, Saskatchewan, Canada

ABSTRACT: Uranium tailings are compressible silts with a high percentage of chemical precipitates. Typical material properties include: C_c ranging from 0.4 to over 1.0; initial void ratios of up to 5.0; and permeability ranging from approximately 10^{-7} to 10^{-8} m/s. Physical containment of tailings solids is inherently assured, with in-pit disposal, which is the current method of choice in Canada. Therefore, containment of dissolved contaminants is the only critical design consideration. In the current disposal practice, tailings are placed within a high capacity drainage system (or pervious surround) surrounding the tailings deposit on all sides unless natural pervious strata are found to be satisfactory for site specific conditions. This in combination with low permeability of the tailings causes ground water to bypass around the facility, with a minimum of flow through the tailings deposit.

The first implementation of the above design system included sub-aerial deposition which resulted in creation of frozen layers in the tailings deposit. Subsequent implementations of the concept have included a water cover and sub-aqueous tailings deposition to prevent freezing. The system is designed to achieve a high degree of self-weight consolidation during operation with the deposit expected to be ready for cover placement within about 5 to10 years of cessation of tailings deposition.

1 INTRODUCTION

Canada is the second leading producer of uranium in the world, accounting for approximately 15% of annual global U_3O_8 production. At present, all Canadian uranium production is from Northern Saskatchewan. There are currently two operating mines (McArthur River, and Eagle Point at Rabbit Lake), and one mine under construction (Cigar Lake (Figure 1)). The current method of choice for tailings disposal is in mined-out or purpose-built open pits. At present, there are three operating in-pit tailings management facilities at McClean Lake, Key Lake, and Rabbit Lake mine sites. All three of these facilities are converted mined-out pits. A fourth in-pit tailings disposal facility is currently proposed at the Rabbit Lake mine site to be located in a purpose-built open pit. Physical containment of uranium tailings solids is inherently assured in these in-pit tailings disposal facilities. Since, with in-pit disposal, tailings reside within the ground water regime, containment of dissolved chemicals is the driving design criterion to minimize contaminant release from the tailings deposit into the ground water system.

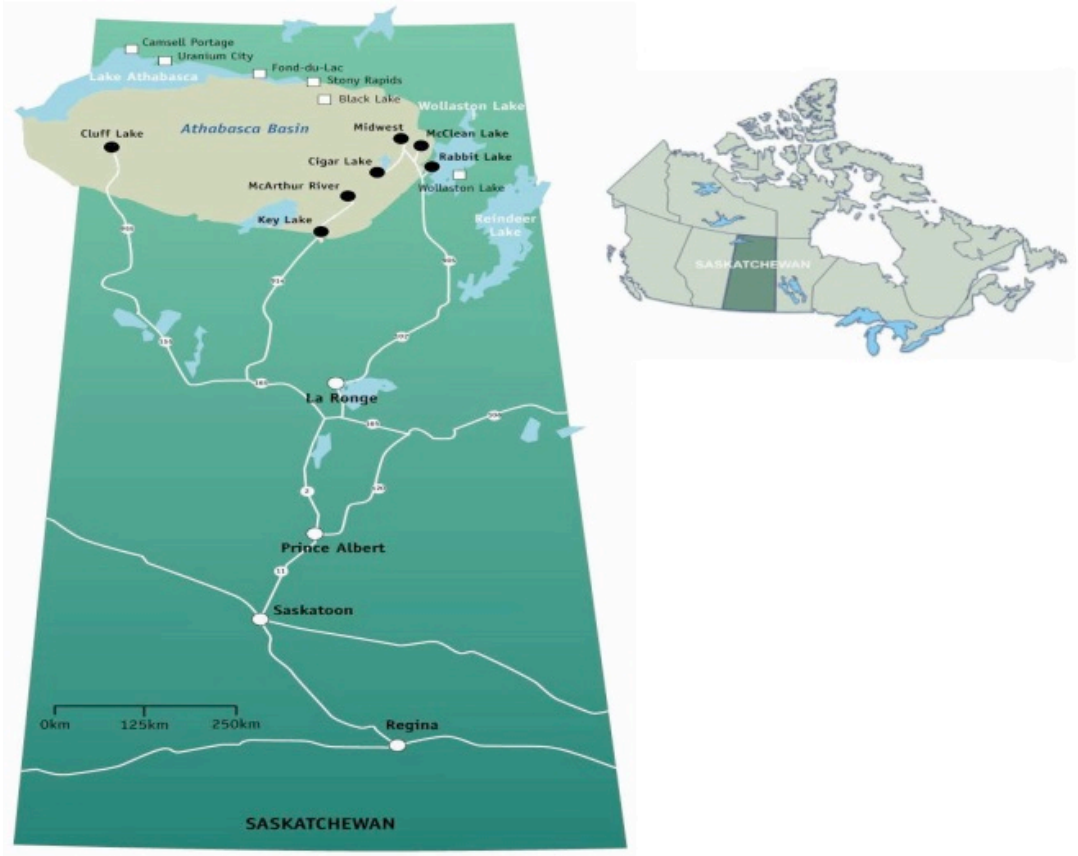


Figure 1. Location Map of Uranium Mine Sites in Saskatchewan

2 GEOTECHNICAL PROPERTIES OF URANIUM TAILINGS

A large number of laboratory geotechnical tests have been performed on uranium mill tailings from several sources in Saskatchewan over the last 30 years. Based on these testing results, uranium mill tailings can be generally described as compressible silts with fines contents (<0.075 mm) ranging from about 50 to 65 percent by mass of dry solids. Some of the uranium mill tailings have been found to contain up to 20 to 25 percent clay minerals, as well as, up to about 25 to 30 percent chemical precipitates from the milling process. The proportions of precipitates and clay size particles are governed primarily by the characteristics of the ore; ores with high uranium content or high impurities (other metals) will have more precipitates, while clays in the tailings are derived directly from the ore. The milling process can also have an effect on the proportion of chemical precipitates which primarily consist of gypsum and metal hydroxides.

Consolidation tests in relatively large slurry consolidometers have been performed for uranium mill tailings from several ore and mill sources. Hydraulic conductivity has been determined by constant head (or constant flow) tests in conjunction with the slurry consolidation tests. Some of the results from several testing programs are summarized in Table 1. Compressibility and hydraulic conductivity functions (e/log p´ and e/log k) have been determined for many of the uranium mill tailings deposits from back-analyses, based on borehole investigations and monitoring data. These results are also summarized in Table 1 and Figures 2 and 3.

Table 1. Compressibility data of various Northern Saskatchewan uranium tailings

Mine	Description	Ore Grade % U	Method of Stripping	Void Ratio at 1 kPa	Compression Index C_c	Source
B-Zone ore Rabbit Lake	unsegregated slurry tailings (4 tests)	0.32-0.67	Strong Acid	3.4	0.75	laboratory testing 1986
B-Zone ore Rabbit Lake	representaive undisturbed samples Rabbit Lake In-Pit TMF (4 tests)	0.32-0.67	Strong Acid	2.6-3.7	0.54-0.93	laboratory testing 1987
B-Zone ore Rabbit Lake	Segregated deposited tailings Rabbit Lake In-Pit TMF (9 tests)	0.32-0.67	Strong Acid	2.6-7.3	0.52-1.7	laboratory testing 1986
B-Zone ore Rabbit Lake	Tailings deposit in the RLITMF	0.32-0.67	Strong Acid	3.6[1]	0.87[1]	Back analysis From Bore Hole Data 2006
Eagle Point ore Rabbit Lake	Representative slurry sample	1.1-2.6	Strong Acid	2.05	0.42	Laboratory Tests 2005
	Tailings in RLITMF	1.1-2.6	Strong Acid	2.15[1]	0.40[1]	Back Analysis 2012
Rabbit Lake Pit ore	RLAGTMF Slimes Pond	0.37	Ammonium Sulphate	4.3[1]	1.2[1]	NUTP,1987
Rabbit Lake Pit ore	RLAGTMF Beach aAea	0.37	Ammonium Sulphate	2.4[1]	0.4[1]	NUTP,1987
Rabbit Lake Pit ore	RLAGTMF Intermediate Area	0.37	Ammonium Sulphate	3.8[1]	0.9[1]	NUTP,1987
Key Lake Deilmann ore	Neutralized Raffinate (1 test)	2.3	Ammonium Sulphate	6.5	1.1	HKM, 1993 Deilmann EIS
Key Lake Deilmann ore	Neutralized Leach Residue	2.3	Ammonium Sulphate	1.85	0.35	HKM, 1993 Deilmann EIS
Key Lake Deilmann ore	Neutralized to pH 10.5 Total Tailings Slurry (4 tests)	2.3	Ammonium Sulphate	3.9-5.0	0.8-1.0	HKM, 1993 Deilmann EIS
Key Lake Deilmann ore	neutralized to pH 4.0 total tailings slurry (1 test)	2.3	Ammonium Sulphate	3.8	0.90	HKM, 1993 Deilmann EIS
Cigar Lake	Slurry tTilings	N/A	N/A	4.9	1.03	Clifton, 1988
Cigar Lake	Slurry tTilings with gypsum removed	N/A	N/A	4.6	0.80	Clifton, 1988
Key Lake Tailings	Tailings Deposit in DTMF	2.3	Ammonium Sulphate	4.6[1]	1.07[1]	Back Analysis 2005
Blended McArthur River ore	Tailings Deposit in DTMF	4.0	Ammonium Sulphate	4.6[1]	1.07[1]	Back Analysis 2011

[1] Back-calculated from field sampling and instrumentation data

The compressibility data can generally be represented by linear void ratio (e) versus log of effective stress (p′) relationships for most uranium tailings. Therefore, the results are presented in terms of an initial void ratio (e_1) at an effective consolidation pressure of 1 kPa and compression indices (C_c) in Table 1 for comparison purposes.

Samples with a high e_1, and a high C_c generally suggest highly compressible tailings slurry which would be expected to have relatively high void ratios and consequently low average dry density even after consolidation is complete. The following general observations can be made from the results in Table 1.

(i) Void ratios at 1 kPa consolidation pressure are generally less than 5.0 for all unsegregated tailings. Higher values are generally associated with segregated slimes or chemical precipitates.

(ii) Compression index (C_c) generally varies from about 0.4 to 1.07 for most unsegregated tailings. Higher values are generally associated with segregated slimes or chemical precipitates.

(iii) Combined tailings (chemical precipitates and leach residues) derived from the relatively high grade Key Lake and blended McArthur River ores are at the high end of the range with e_1 of 4.6 and C_c of about 1.07.

(iv) Key Lake chemical precipitates alone, have the highest initial settled void ratio (e_1=6.5), and the highest compression index (C_c = 1.1).. In contrast, the neutralized leach residue from Key Lake ore has the lowest initial settled void ratio and the lowest compression index of e_1 = 1.85 and C_c = 0.35 respectively. Given the relatively high initial void ratio and high compressibility of combined tailings it can be seen that while chemical precipitates constitute a relatively small portion of the tailings (approximately 25 to 30% by weight) they appear to have a significant effect on the settling and consolidation characteristics of the tailings.

(v) Lower values of e_1 of 2.15 and C_c of about 0.4 at the low end of the range are associated with Eagle Point tailings. It should be noted that Eagle Point ore is generally devoid of any other metals which results in a lower precipitate content of 7 to 10%.

(vi) The results from Clifton (1988) for Cigar lake tailings with gypsum removed by washing, is of interest in that the remaining sample of the tailings (devoid of gypsum) still showed a relatively high initial void ratio and high compression index of e_1 = 4.6 and C_c = 0.8, respectively. The original sample contained about 27% gypsum. It would appear from these results that the settling and compressibility characteristics of uranium tailings may also be significantly affected by the metal hydroxides and not only the gypsum in the tailings. The above sample indicated an inclusion of about 15% clay size particles but the material had low plasticity (plasticity index of 11%) suggesting that the clay sized particles would not have significantly contributed to the initial high void ratio and the high compression index.

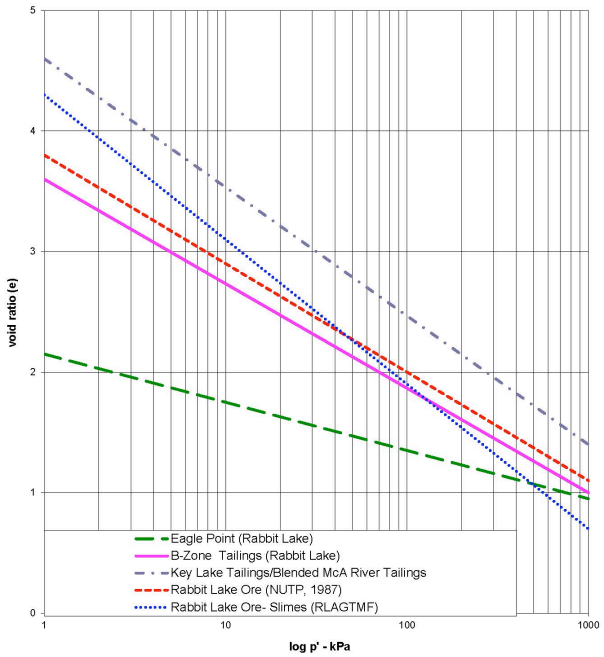


Figure 2. e/log p' functions - some uranium tailings (from back analyses)

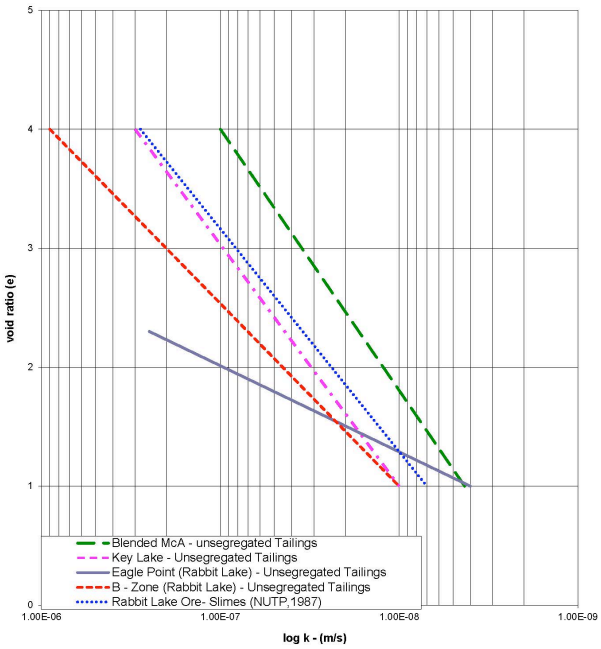


Figure 3. e/log k functions – some uranium tailings (from back analyses)

There are two competing requirements with respect to permeability of uranium tailings. First, the permeability must be sufficiently high to achieve timely consolidation during operations and following the closure process. Second, the tailings must have low enough permeability after closure to minimize advective migration of contaminants into the ground water system. It should be noted from Figure 3, that the permeability of uranium tailings after closure is expected to be 10^{-7} to 10^{-8} m/s or lower, especially near the base of thick deposits. This range of permeability has been found to meet both requirements reasonably well.

3 TYPICAL IN-PIT TAILINGS MANAGEMENT DESIGN

The mined-out Rabbit Lake open pit was the first to be converted into a tailings management facility in the early 1980's. The design of this facility includes a pervious surround drainage system for collection of ground water and tailings seepage water during operation and diversion of ground water following closure.

The design of the pervious surround drainage system at the Rabbit Lake In-Pit Tailings Management Facility (RLITMF) consists of a 3-layered base drain at the bottom of the pit and a continuous 2-layered side drain along the walls of the mined-out pit. The bottom drain consists of an approximately 4 m thick select rockfill layer, and, a two-layer graded filter for a total thickness of 7 m. The side drain consists of a coarse rock layer along the pit walls and a filter sand layer on the inside against the tailings. The original drainage system was designed to operate with a sub-aerial tailings deposition. Therefore, the bottom drain and pervious surround are maintained in a dewatered condition via a lateral drift and a raise pump house (Figure 4).

As of 2012, the design has been adjusted to permit sub-aqueous deposition of tailings under a shallow (1 to 3 m) water cover above the tailings. This has required a modification to the pervious surround design in that the filter zone has been changed from sand to sand-till with a reduced permeability to allow temporary ponding of water above the tailings surface.

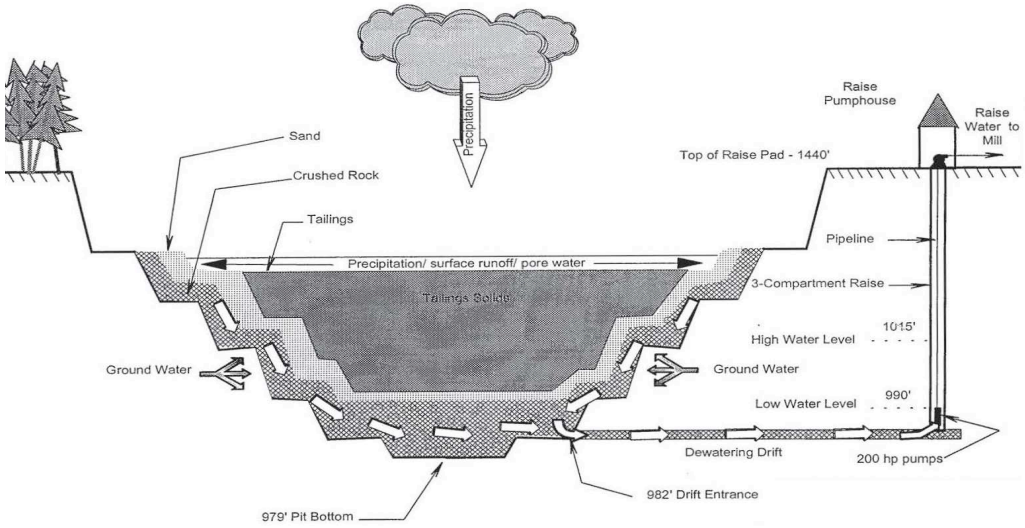


Figure 4. Conceptual design - RLITMF

A similarly designed pervious surround drainage system has been recently proposed in conjunction with sub-aqueous deposition at a future purpose-built tailings disposal facility at the Rabbit Lake site north of the existing facility.

Another variation of the in-pit tailings disposal concept is located in the mined-out Deilmann pit at Cameco Corporation's Key Lake mine site. At the Deilmann Tailings Management Facility (DTMF), a partial pervious surround drainage system in the lower portions of the facility was found to be adequate to meet the defined design objectives for the facility. The following site-specific conditions at the DTMF have contributed to the design at this facility.

- Relatively low ground water gradients across the TMF area after closure;
- Relatively high conductivity of surrounding overburden materials, to accommodate by-passing of groundwater flow; and
- A relatively uniform and low hydraulic conductivity (<10^{-7} m/s) of the tailings deposit.

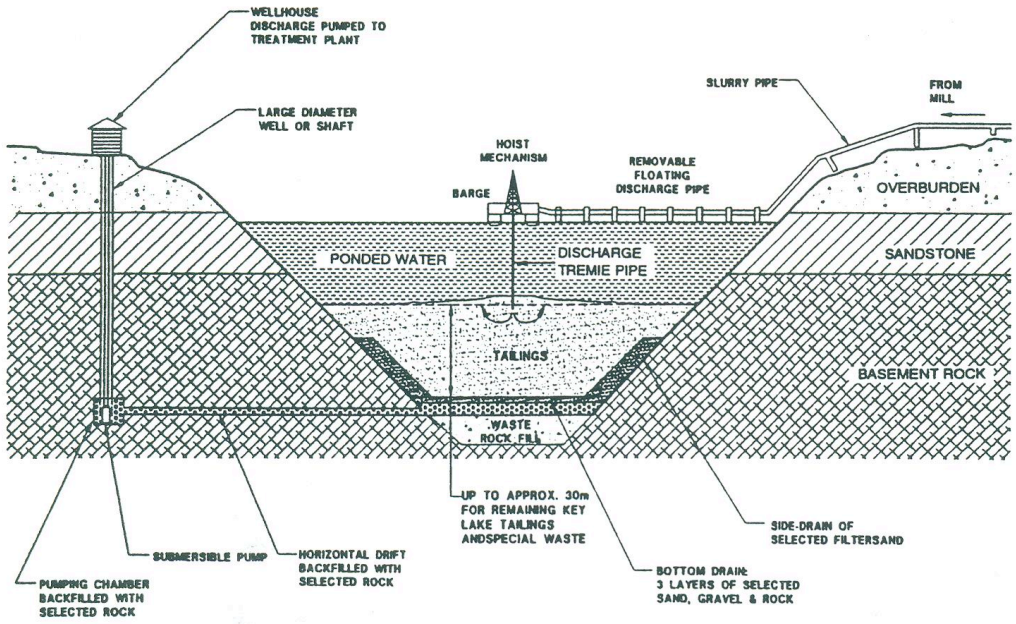


Figure 5. Conceptual design of Deilmann In-Pit TMF

Design details at the DTMF (Fig. 5) have been presented in a previous paper (Mittal et al. 2000). A similar design approach to that at the DTMF was followed at the Jeb Pit TMF at McClean Lake, owned and operated by Areva Resources Inc.

4 TAILINGS DEPOSITION METHODS

4.1 *Sub-Aerial Method*

The original design at the RLITMF included sub-aerial deposition of tailings consistent with the prevailing practice at that time. However, to minimize particle size segregation upon tailings deposition, the original design included deposition of filtered tailings cake with a density of about 50% solids. Deposition of the filter cake began in the fall and winter months of 1984/85 using conventional scrapers to haul and a dozer for spreading the filtered tailings material. However, the tailings surface became untrafficable for the scraper and dozer operation during the warmer (summer) season. This forced a change-over to thickened slurry discharge on June 19, 1986.

Continuously between June 19, 1986 and 1999 and intermittently from 1999 to 2012 tailings were deposited into the RLITMF sub-aerially by pipeline discharge of thickened slurry to about 35 to 40 percent solids.

It was noted that frozen tailings layers were being incorporated into the tailings deposit due to sub-aerial deposition during the winter months. These frozen layers have been determined to contain relatively high water contents and due to their lateral continuity were found to be impeding drainage from the tailings and hence consolidation of the tailings deposit. As of December, 2012, approximately 25 to 30% of the tailings deposit is determined to be in a frozen state. It is anticipated that active thawing of frozen tailings will be required prior to closure of the disposal facility. Based on a 2006 borehole investigation results, a typical section along the long axis of the tailings deposit is shown in Figure 6.

Other methods of tailings deposition have been implemented to mitigate frost build-up in the uranium tailings deposits as described below.

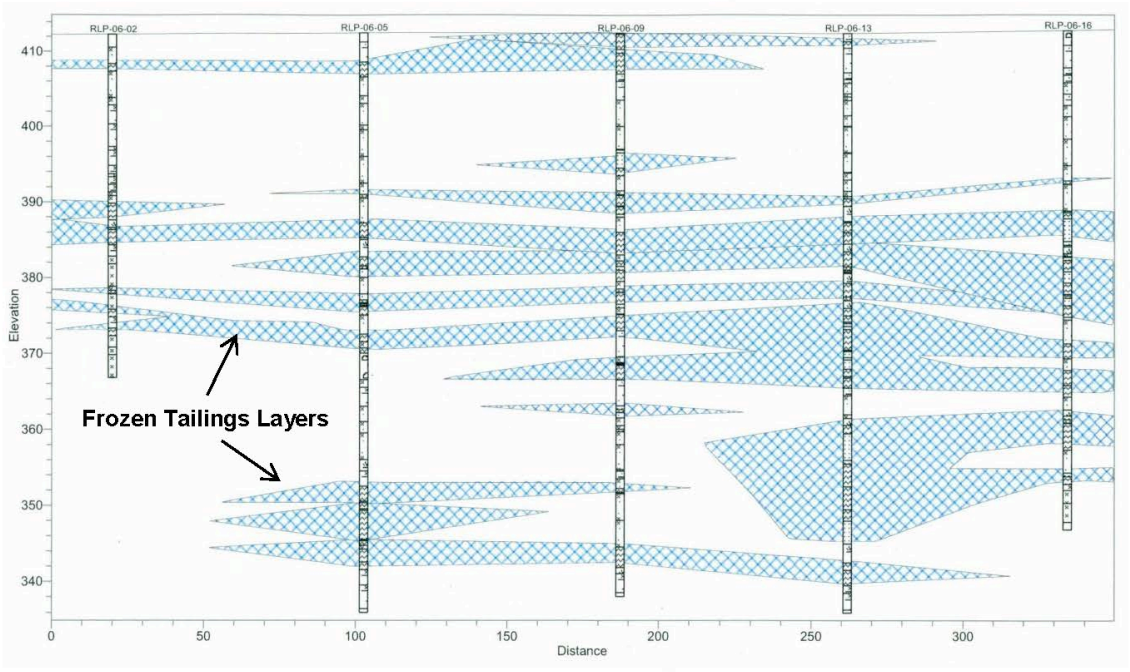


Figure 6. Frozen tailings layers in the RLITMF

4.2 *Deep Injection Method*

Tailings were deposited into the RLITMF intermittently between 1999 and 2012 by deep injection method. The pre-thickened slurry was injected via angled injection wells at depths of up to 70 m below the tailings surface. The objective of the deep injection program was to capture heat from the incoming tailings stream for melting of existing frozen layers. Deep injection of the slurry was partially successful in minimizing new frozen layers and only marginally successful in melting previously frozen tailings.

4.3 *Sub-Aqueous Deposition*

Sub-aqueous deposition is the current method of choice for disposal of uranium tailings. In this method, pre-thickened tailings slurry is deposited below a water cover above the tailings deposit. The sub-aqueous method of uranium tailings disposal was pioneered at the DTMF at the Key Lake mine site. In addition to the frost mitigation aspects, the sub-aqueous tailings disposal was perceived to provide the following advantages at the DTMF.

(i) Reduced radon exposure from the tailings surface to work force in the area; and
(ii) Reduced dewatering costs from the site dewatering program.

Sub-aqueous tailings deposition method has been used since 2000 at the DTMF. The thickened tailings slurry is deposited through a "tremie" pipe system from a barge or from open-ended pipe laterals sunk on to the tailings surface. The end of the "tremie" pipe is submerged about 2 m below the tailings surface to prevent free fall of thickened tailings slurry through the water column. To provide even distribution of tailings and minimize particle size segregation during deposition, discharge locations are frequently changed. Bathymetric surveys are conducted of the tailings surface annually; only minor mounding of the tailings surface is found at the discharge locations. Borehole investigation results show only minor localized particle size segregation at the discharge locations estimated to consist of about 10 to 12 percent of the tailings deposit by volume by the end of tailings deposition. For all practical purposes, the tailings deposit in the DTMF is anticipated to be relatively uniform without any significant adverse particle size segregation effects at the time of closure.

5 TYPICAL DESIGN ANALYSES

Extensive computer modelling and analysis are performed for the design of a uranium tailings management facility to assess regional ground water flow, contaminant migration, and consolidation of tailings deposit. The highlights of the modelling results are presented below.

(i) While a detailed discussion of the regional ground water flow and contaminant migration modelling results is beyond the scope of this paper, it suffices to state that a uniform (non-segregated) tailings deposit with an average permeability in the range of 10^{-7} to 10^{-8} m/s in combination with favourable site conditions and/or a purpose-built pervious surround drainage system is generally found to be adequate to meet the design objectives..
(ii) Consolidation modelling for the uranium tailings disposal facilities is generally performed with large strain non-linear consolidation computer codes. Computer code "ACCUMV" has been widely used in consolidation modelling for Cameco Corporation's tailings facilities. Consolidation modelling results for the proposed to be purpose-built in-pit TMF at the Rabbit Lake mine site are shown in Figures 7-8. It is noted that the modelling results predict a high degree of self-weight consolidation during tailings deposition and a potential for cover placement over the deposit within about 5 years of end of tailings deposition.

6 CURRENT DISPOSAL PRACTICE

The preferred management practice for uranium tailings disposal in Northern Saskatchewan has evolved from cumulative experiences gained from various tailings disposal facilities over the

last 40 years. The following are the main highlights of the current tailings disposal practice and the expected results during operations and following closure.

(i) To provide permanent physical containment, in-pit disposal is the current method of choice. Given that the tailings surface lies below the surrounding terrain, erosion of the surface is not a concern.

(ii) Since tailings reside within the ground water system, mechanisms are required to minimize ground water flow through the tailings deposit. These mechanisms include: a highly permeable zone (pervious surround) around the tailings to limit gradients across the tailings and a low permeability of the tailings deposit itself.

(iii) Tailings slurry is pre-thickened to 35 to 40 percent solids to minimize particle size segregation during deposition from pipeline discharge. A uniform non-segregated tailings deposit is essential to the design.

(iv) To prevent freezing of slurried tailings during winter season, as experienced in all of the older facilities due to sub-aerial deposition, the currently preferred deposition method is underwater (sub-aqueous).

(v) The in-pit tailings deposition facilities are designed with adequate drainage systems to facilitate a high degree of consolidation of the tailings slurry during deposition and a timely closure within about 5 to 10 years after cessation of active tailings deposition.

(vi) At closure, the tailings surface is drained and allowed to desiccate for a period of about 2 years. After this period, the placement of suitable cover fill in staged lifts may commence in late winter while the tailings surface is frozen. This method is based on experience gained from cover placement over fine-grained uranium tailings in the "slimes pond" area of the Rabbit Lake Above-Ground TMF in conjunction with decommissioning of that facility, (Mittal et al. 2000).

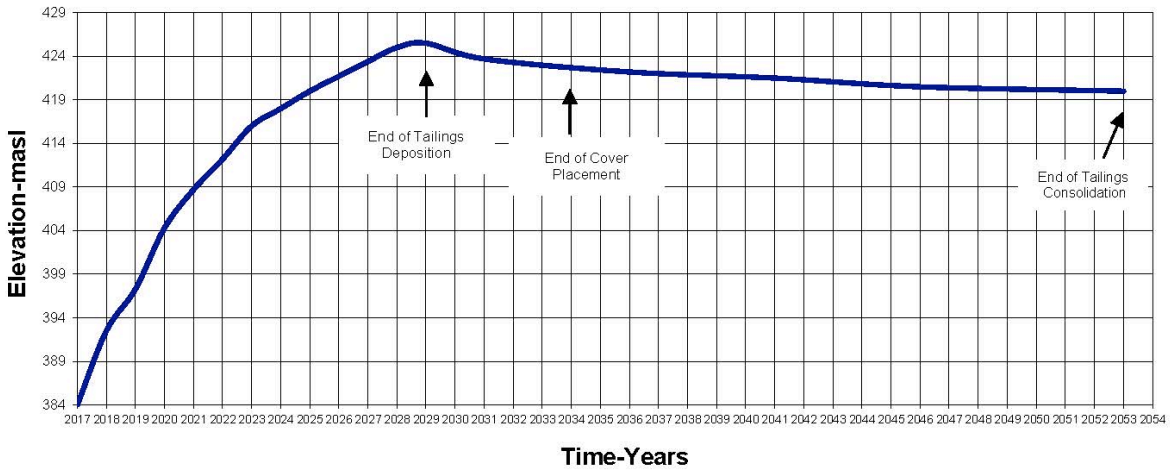


Figure 7. Predicted tailings elevations- proposed in-pit TMF – Rabbit Lake

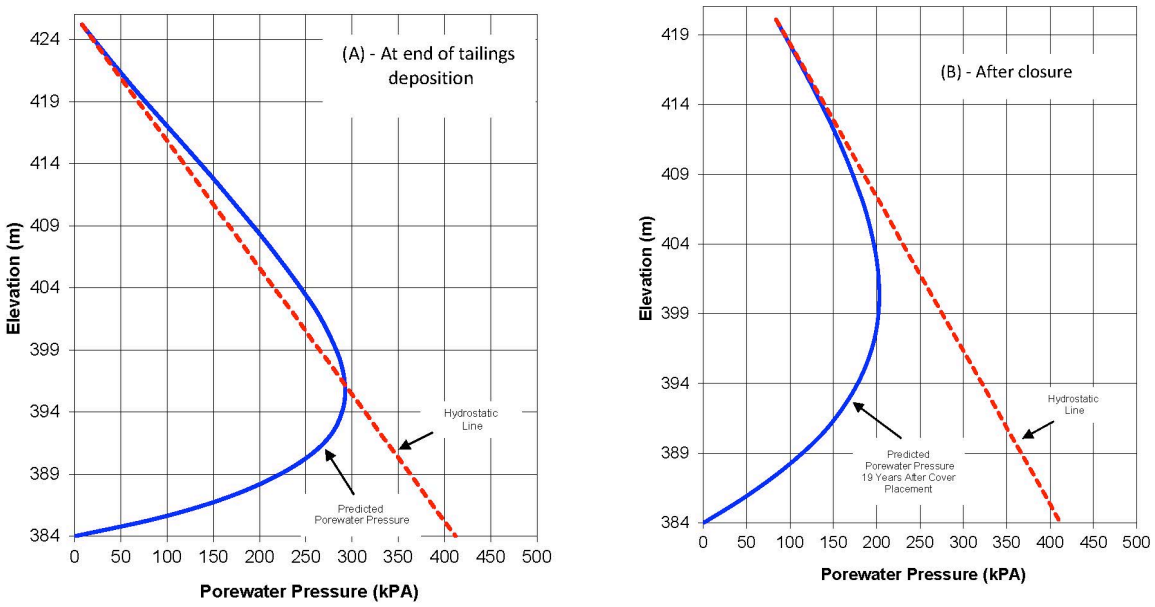


Figure 8. Predicted pore water pressure distributions -proposed in-pit TMF – Rabbit Lake

7 ACKNOWLEDGEMENTS

The authors are grateful to Cameco Corporation for encouragement and permission to publish data presented in this paper.

8 REFERENCES

Clifton 1988. Preliminary geotechnical characterization of uranium mill tailings, Cigar Lake, Saskatchwan. (File 5329), June 30, 1988.

Mittal, H.K. 1993. Laboratory test results and geotechnical design, Deilmann Pit TMF. A report prepared by H.K. Mittal and Associates Ltd. November 15, 1993. Deilmann EIS (Appendix C).

Mittal, H.K., Holl, N. & Landine, P.G. 2000. Two uranium tailings management facilities. *Uranium 2000;Proc. intern. symp. on the Process Metallurgy of Uranium*, Saskatoon, 9-15 September 2000. Saskatchewan, Canada.

Mittal, H.K. & Landine, P.G. 2013. Experiences relevant to ERCB Directive 074. *Tailings and Mine Waste*, Banff, 3-6 November 2013. Alberta, Canada.

NUTP. 1987. National uranium tailings program consolidation of uranium mill tailings – final report – Part B (field investigations – Rabbit Lake). February 1987. DSS File No. 15 SQ-23241-5-1708.

Dry stack tailings: some ideas

Jack A Caldwell
Robertson GeoConsultants, Vancouver, BC, Canada

Colleen A Crystal
SLR Consulting, Irvine, California, United States of America

ABSTRACT: Filter-pressed tailings are generally a fine silt to sandy silt sized rock-flour material placed and compacted at 80 percent solids by weight, or geotechnical moisture content of 15 to 23 percent. While not necessarily "dry" by geotechnical moisture content definitions, they are of significantly lower moisture content than paste, thickened, or conventional tailings. They may be transported from the filter press via conveyors and/or in conventional trucks. Accordingly there is considerable flexibility in the transport and placement methods and in particular in the final geometry of the dry stack that may be formed with the tailings. This is a major advantage when setting out to construct dry stacked monoliths that are stable and that are designed to become new topographic landforms of long durability in the surrounding landscape.

In this paper, the following issues that pertain to the design, construction, operation, and closure of stacks of filtered tailings are considered:

- When, how and why is cement added to the filtered tailings?
- At what moisture contents will the tailings be distributable, compactible, and trafficable?
- What is the optimum stack geometry in different topographies?
- How will the stack perform in the long term after closure?

1 INTRODUCTION

Filter pressed tailings are formed by removal of water from the fluid-like tailings either by belt filters, drum filters, vacuum filtration, and/or pressure filtration. In general pressure filtration achieves a lower moisture content, higher percent solids by weight than the other methods noted. In terms of standard Unified Soil Classification or ASTM System (USCS), the resulting material is generally a silt, to sandy silt with trace clay, but can include a significant percentage of clay (up to 20 to 30 percent), depending on the ore properties. At 80 percent solids by weight, filter pressed tailings achieve a moisture content above the optimum geotechnical moisture content for best compaction. Depending on the filtration method and achievable moisture content, the filtered tailings may be transported to the tailings disposal facility by conveyors, trucks, or a combination of both and compacted. The resulting facility is sometimes called a dry stack tailings management facility, or just dry stack. In this paper, we refer to filter-pressed, placed and compacted tails as dry-stacked or simply "stacked" tailings, or "the stack". The term stack is appropriate for the tailings may be placed to any desired geometry.

Common sense and responsible engineering dictate that the stack be stable. That is so basic a requirement that we do not address it further in this paper. Suffice it to say that if the native foundation soils on which you wish to establish your stack are not strong enough to support the desired geometry, you must either find another site or improve the foundations.

The side slopes of the stack must be flat enough to be statically stable during and after construction. The sideslopes must also be stable in the event of the maximum credible earthquake

(MCE)---for such an earthquake will occur sometime during the life of the stack, the design life for practical purposes in this paper being defined herein as the time it takes for the stack to either return to the sea by erosion or be subjected to the next ice-age.

You may persuade folk of the truth: the dry stack is not a rigid structure and deformation will occur in even moderate earthquakes. All you strive for as an engineer is acceptable, repairable deformation that does not threaten the facility, life-safety, or the environment. That is one of the major advantages of dry stacks of filter-pressed tailings: if designed and managed properly, deformation in an MCE seismic event does not necessarily mean a flow liquefaction failure; there is no dam impoundment or embankment to breach and no fluid tailings to flow miles down the valley. That is not to say that poorly placed dry-stacked tailings, well wet of optimum, in a poorly managed facility, or with poor foundation conditions will not be subject to unacceptably large deformations in the event of static or seismically induced slope instabilities.

The basics now being out of the way, we can say what we address in this paper. We focus on some topics not, to our knowledge, discussed in detail in the literature. This includes these questions:

- When, how and why is cement added to the filtered tailings?
- At what moisture contents will the tailings be placeable, compactible & trafficable?
- What is the optimum stack geometry in different topographies?
- How will the stack perform in the long term after closure?

The ideas we raise in this paper are just that: ideas. They are based on a few case histories we have worked on, and projects we would like to have worked on. We have read the literature and base our discussions on the excellent papers out there. But we quote none of them. We respect and applaud the experienced authors of the literature on filter-pressed dry-stack tailings facilities. We draw on their ideas and successes. We encourage more from them and other practitioners on this topic as more and more owners and engineers turn to dry-stacking.

Dry stacking is not a panacea for all ills, nor is it the appropriate or best solution for all projects in all environments. It has some severe limitations, placement difficulties, and generally significantly higher costs. The ideas put forth in this paper are ours and ours alone, and we take full responsibility for them. Our challenge is to others to critique, add to, and hopefully to continue to advance the state of the practice building on what we and others who have practiced in this field and written on the topic write.

2 CONVEYANCE

Filter pressed tailings may be conveyed to the stack by trucks or conveyors. Once at the stack, the tailings may be spread by the truck, the conveyor end point, or a stacker. If the tailings are readily traficable (see next section) then all that is involved is for the truck to dump the tailings as close as possible to their ultimate location. From there a bulldozer may spread them.

Two interesting approaches to transporting and distributing filtered tailings are shown in Figures 1 and 2. In the first instance, a rock “Christmas tree” is constructed of one-meter lifts of rock. The heavy trucks ride on the rock, and dump their load to the side from where it may be spread by bulldozers. In the second instance, a jackable header atop of which is a conveyor belt may be used to move the filter pressed tailings to a dump location from which they may be further spread by bulldozers.

3 PLACEMENT, COMPACTION & TRAFICABILITY

In theory, if the tailings moisture content is near the optimum compaction moisture content, the tailings will be trafficable. This is true for light construction equipment but may not be true for the heavy equipment needed to economically transport the tailings to the place where they are dumped to be spread and compacted.

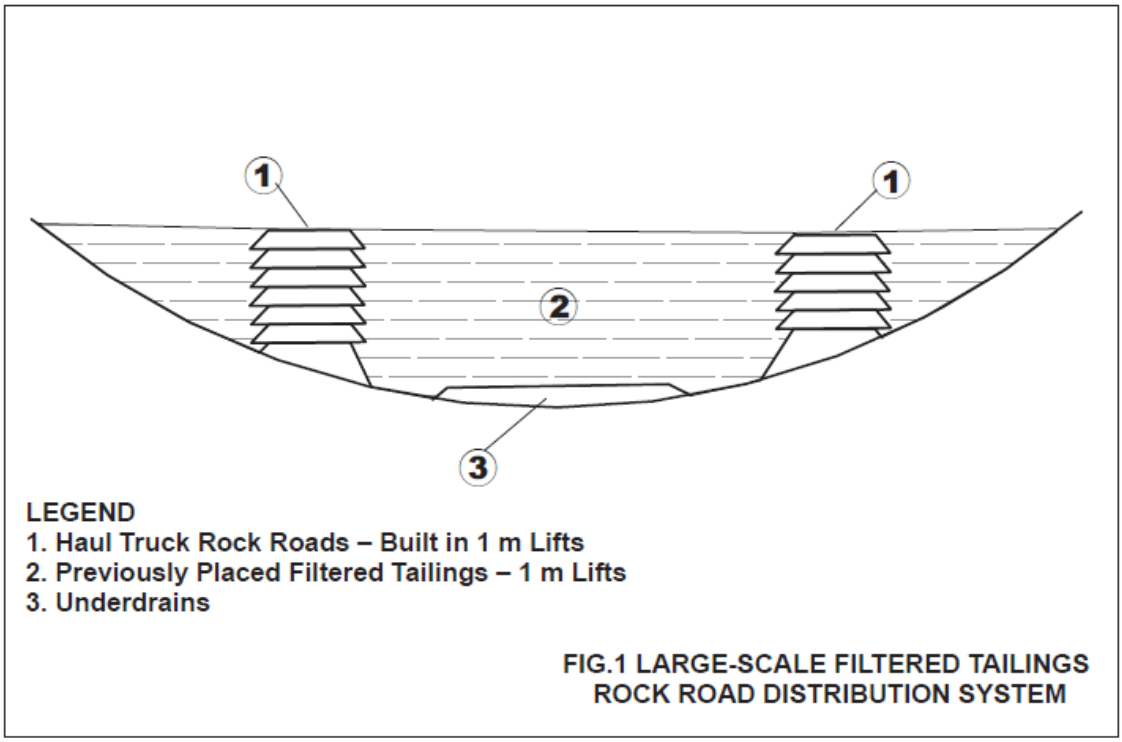


Figure 1. Large-scale filtered tailings rock road distribution system.

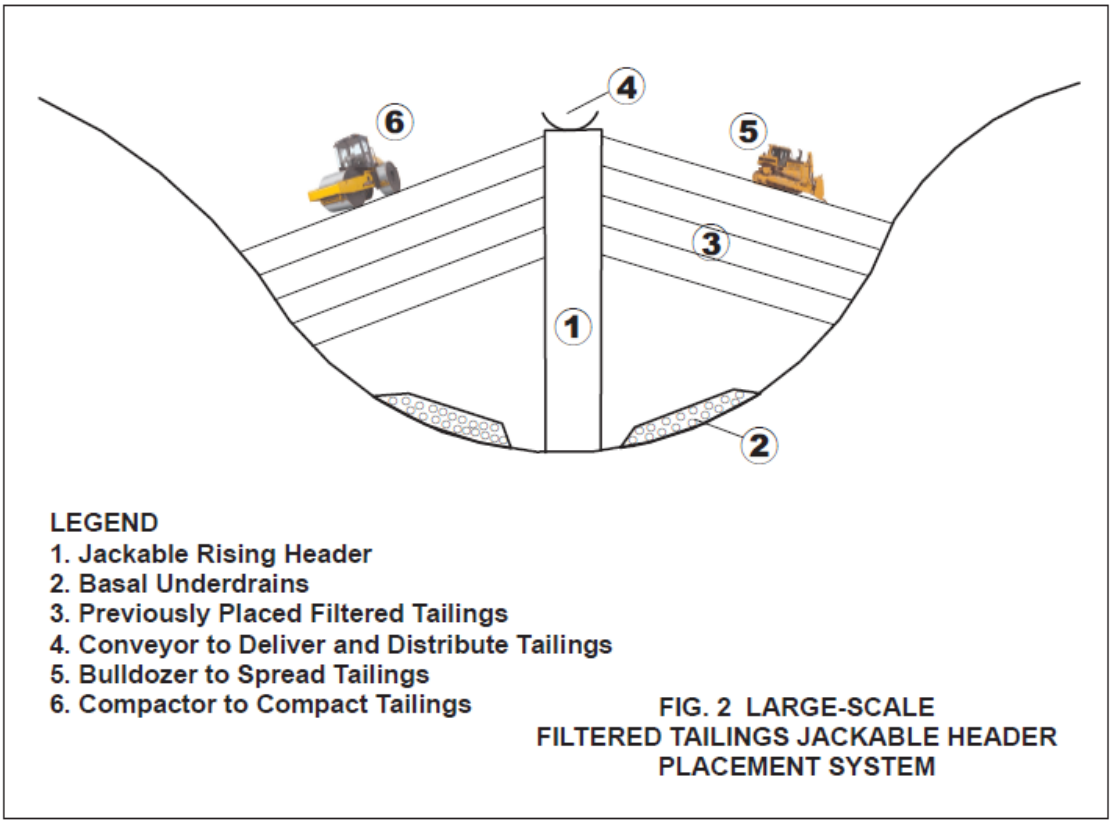


Figure 2. Large-scale filtered tailings jackable header placement system.

Keep in mind that trafficability is not a bearing capacity issue; except when the equipment is not moving. Most often the dumping & spreading equipment is moving. Then trafficability is a shearing issue. The wheels or tracks of the equipment are shearing the tailings as the wheel or track slides over the upper surface of the tailings. There may be some passive pressure issues too: if the wheel or track sinks or depresses the tailings, a bow wave develops ahead of the wheel or track and energy is expended in pushing against this bow wave.

There is much literature on trafficabilty: consult it and pay no attention to bearing capacity theories. It all boils down to the shear strength of the tailings. If they are wet and sloppy, the equipment will slide and sink into the tailings. You get nowhere.

The solutions include:

- Establishing a maximum achievable density criterion that provides for the required strength for stability of the proposed geometry: we are not building airport runways here and 95% Modified Proctor is not necessarily needed. Establish a good understanding of your standard proctor curve and at what range of moisture contents you can achieve a reasonable compaction for the material at hand.
- Lighter Equipment. A SnowCat is great; it has power, yet low track pressure. If it can handle snow it can probably handle wet tailings. But its capacity is limited and they are expensive.
- Cement Addition. This reduces the tailings moisture content. And, if the tailings are placed after the cement has been able to increase the material's strength, you may have sufficient shear strength to distribute, spread, and compact the tailings.
- Rock Plating. Use light equipment to form a rock plating over previously-spread tailings. Place a thick layer of rock and let the distribution equipment ride over this. It is all a matter of road design---see the literature on the topic; it is extensive.

For tailings that are not too wet (i.e. less than 4 to 6 percent above optimum, or thereabouts); the best way to compact is with the 20 ton trucks wheel loading themselves: establish traffic control with cones, flagging whatever and have trucks following each other over sequential sections as they dump. You'll get more bang for the buck than with tracked dozers, vibratory rollers and the like. You will want to borrow from the landfill industry's "daily cover" approach and make sure the last lift of the day is smooth-drum rolled so as to shed water and limit infiltration, particularly in wet climes. Just make sure that you're ripping it first thing before tying-in subsequent lifts. You don't want cold-joints and particularly not preferential seepage paths for whatever water may seep out of the tails themselves under consolidation loading.

Figures 3and 4 show possible alternative approaches to dealing with the trafficability issues associated with filtered tailings of moisture content not immediately able to support heavier equipment. Tailings relatively close to optimum moisture content may be dumped and spread as shown in Figure 3: the truck approaches the dump face over previously placed tailings; the tailings are dumped; the bulldozer spreads; and a compactor compacts to form a surface suitable for the trucks to dump another lift. In Figure 4 the following is done: The truck dumps relatively wet tailings; a bulldozer pushes waste rock from the other side to in effect fill the space between individual piles thereby creating a trafficable surface. This is akin to codisposal practices.

4 OPTIMUM GEOMETRIES

If the site is flat, you may place the filtered tailings to any stack geometry consistent with stability. Surface water management is a simple matter of diverting adjacent runoff around or away from the stack. Some provision has to be made to control incident precipitation on the top and sides of the stack. Keep the top topography as a bowl of sufficient size to hold incident probable maximum precipitation. Or provide penstocks or a spillway to one side. Sediment paddocks at the toe of the slope will control sideslope runoff and erosion.

If you have to place the filter-pressed tailings in a valley, you have to choose between what we call down-valley or up-valley placement.

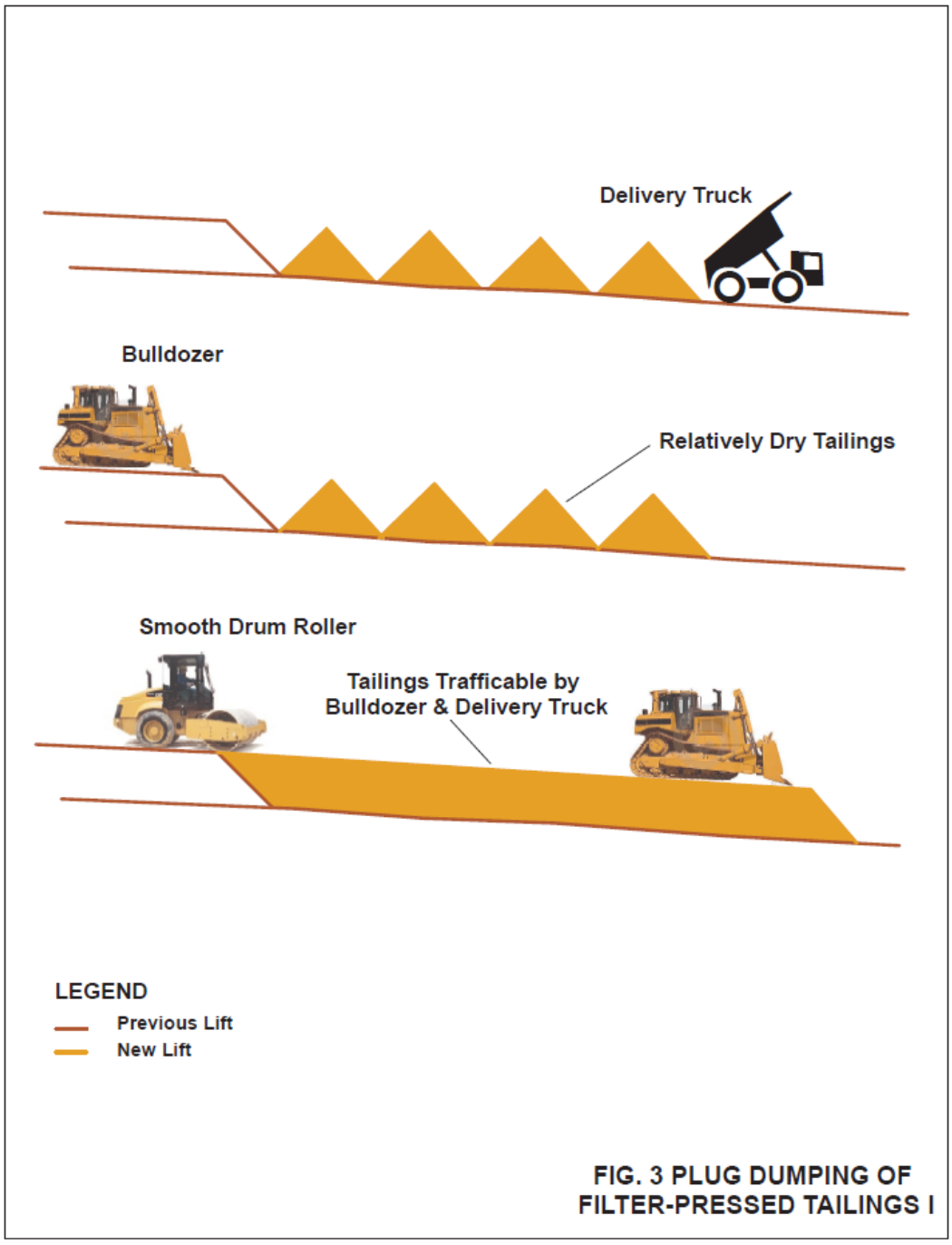


Figure 3. Plug dumping of filtered-pressed tailings I.

The advantages of down-valley placement include ease of control of surface water. By starting at the head of the valley, you do not have to divert much upgradient runoff water around the growing stack. It is of course desirable to divert upgradient runoff around and away from the stack. But is you are placing the closure cover as the stack grows, it may be possible to allow excess runoff the pass over the cover without much ado.

Conversely it you select an up-valley configuration, you will have to make much provision to divert or deal with upgradient runoff. Diversion works help. But it is seldom possible to provide for the truly big storms. You must configure the upper surface of the growing stack to impound excess runoff and runon. This means the top surface, or top deck as it is often called,

must slope back from the crest to the back of the valley, and the resulting volume must be sufficient to impound the probable maximum runoff without overtopping the crest of the pile.

A desirable detail is this: place rock berms on sideslopes (Figure 5). They provide secure volume to place new tailings, and they provide good erosion control in the event of overtopping and big storms. If you place some soil with or over the outer surface of the rock berm, you may establish vegetation as part of ongoing reclamation.

This is all easy if the tonnages are small—say in the region of 1,000 to 5,000 tons a day. All you need is: a few trucks to transport the tailings; a bulldozer to spread rock to make access road; another bulldozer to spread the tailings; compactor to densify the tailings; and a smooth-drum roller to create a low permeability surface that limits infiltration.

The problems arise when your project involves upwards of 100,000 tons a day. Now is time to think of conveyor transport. Maybe a conveyor system on a jackable header that rises as the elevation of the upper surface of the tailings rises (Figure 2.). Alternatively consider construction of Christmas-tree rock roads within the body of the tailings (Figure 3.)

Approaches that we have heard of that do not work include dumping the filtered tailings from a high rock embankment and letting the tailings fall by gravity down the slope. Or pushing the tailings down the slope with bulldozers. Of course it is prudent to get gravity to help spread the tailings. But you have a trafficability issue regardless. And the downslope distance may be great. We can envisage this working for tailings that are close to optimum moisture content, where the size of the facility is limited, and where gravity is powerful. Afterall, this approach is used for cyclone tailings underflow. Indeed there are many case histories of embankment construction using cyclone tailings underflow. We need to think harder about these successes and apply them to high-volume filter-pressed tailings facilities.

5 CEMENT ADDITION

The tailings are the result of facts and processes beyond the control of the stack designer. The ore and it inherent variability dictate the fundamental nature of the tailings particles. The grind the process engineer dictates to get the most gold, silver, copper, or other valuable material being mined, dictates the size and gradation of the tailings. The ability of the filter equipment manufacturer to squeeze water out of the fluid-like tailings dictates the moisture content of the tailings as received by the stack operator.

Thus the question arises: do we need to add cement to the filtered tailings?

In theory it is easy to answer the question: if the filtered tailings are too wet to conveniently compact and they will not drain readily, better be prepared to add cement.

Keep in mind that cement added to tailings has two very different results:

- In the first instance the cement (or lime) acts simply to reduce the overall moisture content on the mass.
- In the second instance and over time, the cement acts to increase the strength of the mix.
- If the moisture content of the just-filtered tailings is too high to compact conveniently, then you must find a way to allow the tailings to stand under cover until they drain naturally to a convenient compaction moisture content or you must add cement to dry the tailings. It is an economic comparison.

In practice, ore variability, filtering variability, and the passage of dry and wet seasons means that sometimes you will need to add cement and at other times you will not. It all depends, as they say. Thus prudence dictates that provision be made to add cement when needed. Write an Operating Plan that sets strict guidelines for when to add and when not to add cement.

An alternative to adding cement to moisture condition the tailings is to pass the as-filtered tailings through an asphalt drier. This is practical only at operations of low volumes, but it may be economic: do the calculations.

If you anticipate adding cement to moisture conditions the tailings, test in the laboratory. It is a simple matter to mix various percentage of cement to varying moisture-content tailings and record the resulting decrease of moisture content and the resulting optimum moisture content for best compaction.

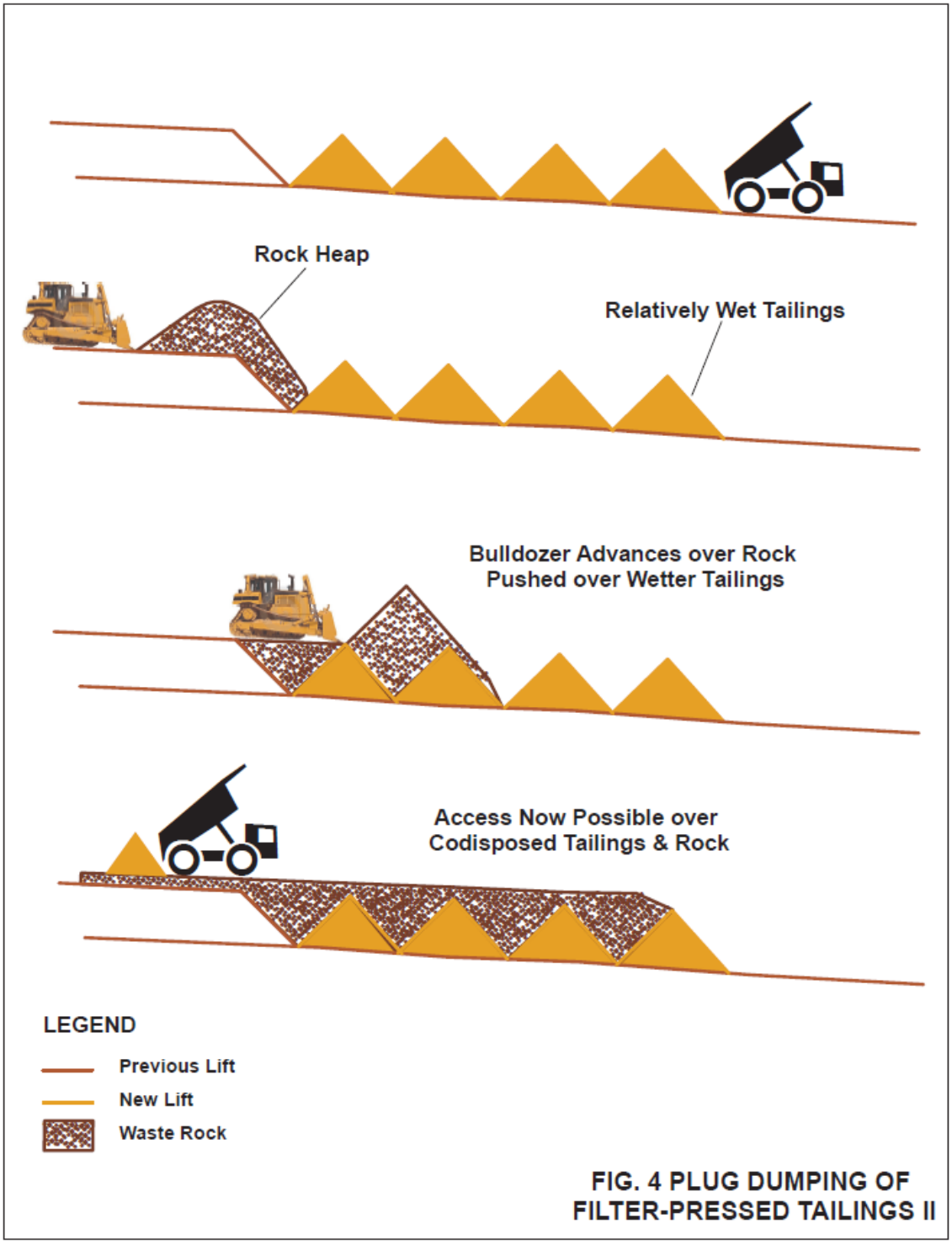


Figure 4. Plug dumping of filter-pressed tailings II.

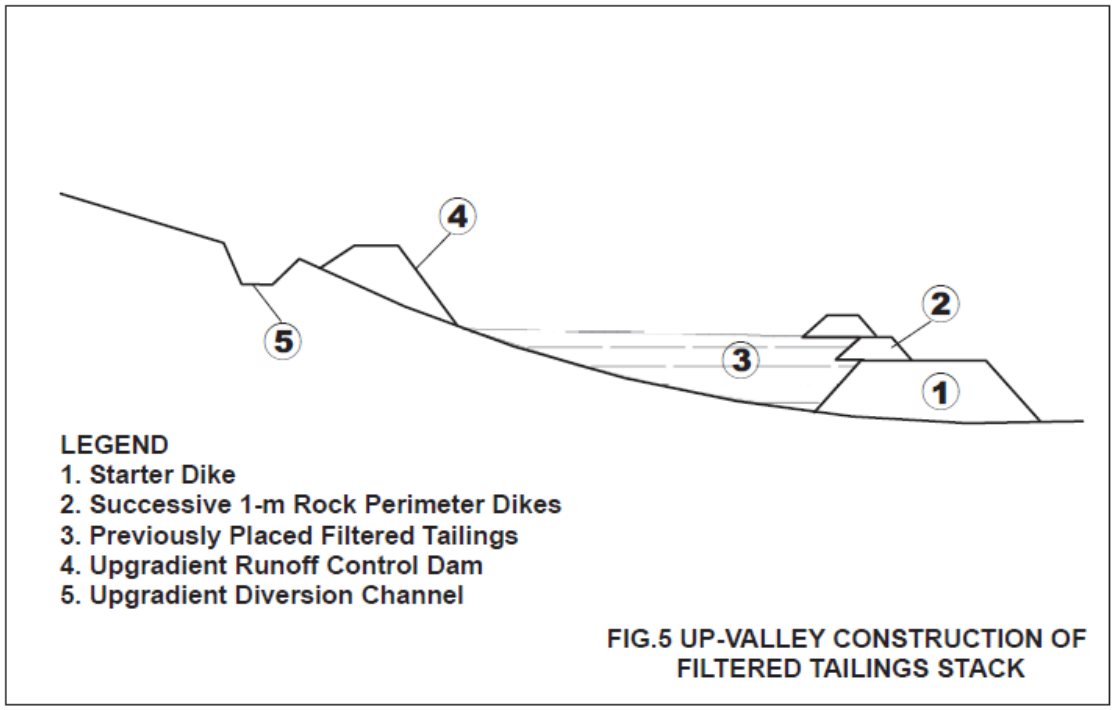


Figure 5. Up-valley construction of filtered tailings stack.

6 LONG-TERM PERFORMANCE

As with any tailings facility, we are terra-forming new topographic forms when constructing a filter-pressed, tailings dry-stack. The layout of the facility must blend with the topography of the environment and hence be stable, geomorphically, in the long term. This can be done. Evidence is the Chahokia Mounds of East St, Louis, Illinois. Constructed of uncompacted soil, they have been stable for 1,000 years and promise to last at least another thousand. There is much natural climax vegetation. There are some erosion gullies. We could preclude formation, in the long term, of such gullies by suitable shaping and construction of rock-line down-swales.

7 COST

Depending on location, grind and a multitude of other operational costs guesstimated dry stacking can be cost effective or not: one operation the authors are aware of has dry-stacking costs hovering in the $6.00 per tonne (ore processed). For other operations, in Northern Canada, projected pre-feasibility level dry-stacking costs are estimated to on the order of $2.00 per tonne (of ore) higher than conventional wet tails. The former of the costs quoted costs do not include capital costs of filtration plant, the latter difference between wet and dry does reflect the difference in capital costs for the filtration plant as well as other operational costs. Costs above do not include cement addition, which can be up to a further $3.00 per tonne (or more) extra for 2% cement. Extremely fine grinds (for example for rare earth tailings) may require more cement. Closure costs for dry-stacking can be far less particularly if closure is progressive.

8 CONCLUSIONS

Filter pressing and construction of a stack can be one of the most expensive ways to manage tailings, particularly where environmental conditions make placement and compaction a challenge. At least as far as operating cost are concerned. Lots of energy is required to filter the tailings and transport them to the stack. Lots of energy and expensive equipment is needed to distribute, spread, and compact the tailings. Money must be spent on provision of surface water management facilities.

Yet there are advantages. You can undertake progressive reclamation, and reduce your closure bond. There is no perpetual active operation, monitoring and maintenance. You can walk away if you do it right.

You can be proud that you have made a new topographic form that will blend with the environment, be a new topographic form, and probably last as long as the surrounding hills and valleys.

Tailings Facilities

Field deformations compared to a numerical model for a staged centerline raise – Cerro Corona Tailing Storage Facility, Perú

Charlie Krautmann, Fernando Torres & Walter Vela Amoros
MWH Perú S.A., Cajamarca, Perú

Sam Abbaszadeh
MWH Americas, Tempe, AZ, USA

Javier Gutierrez
Gold Fields La Cima, Lima, Perú

ABSTRACT: Gold Fields La Cima's (GFLC) Cerro Corona Tailing Storage Facility (TSF) includes a centerline rockfill dam that has been in operation since 2008. The dam has a low permeability core with transitional filters on its downstream side and supporting rockfill both upstream and downstream of these zones. To monitor deformations of the dam throughout operation and closure, GFLC implemented an instrumentation program in 2012 that includes twelve inclinometers on both the downstream and upstream sides of the core. Additional instrumentation was installed to monitor displacements as well as validate inclinometer data and provide further insight for deformation interpretation. Due to the centerline design, the dam is limited to annual staged raises to maintain upstream slope stability which is supported by the consolidated, sub-aerial tailing beach. In October 2012, a nine meter raise was completed over a six month period to elevation 3755 masl; providing a dam height of approximately 125 meters. This paper describes the measured deformations of the dam with focus on the recent raise. Furthermore, the nine meter raise of the dam is simulated using a finite difference modeling tool, FLAC, to calculate the deformations induced by recent construction. The numerical analysis deformations are then discussed and compared to measured field deformations.

1 INTRODUCTION

1.1 *Project Overview*

Gold Fields La Cima S.A.A. (GFLC), a subsidiary of Gold Fields Limited, owns and operates the copper and gold bearing Cerro Corona mine. Average grades of ore include 1.0 gram per tonne of gold and 0.5% copper. The diorite porphyry deposit has an estimated gold equivalent mineral reserve of 5.2 million ounces and has been in production since 2008. The life of mine is anticipated to continue through 2028. Since 2006, MWH has been providing design and construction support services to GFLC. The mine is located in the Northern Highlands region in the province of Cajamarca, Perú, approximately 615 kilometers north-northwest of Lima. By road, the mine is approximately 80 kilometers from Cajamarca.

1.2 *Dam Design*

The mine property lies within a 540 hectare area. Due to the small size of the property, the engineering team was challenged to exploit tailing storage space within two valleys that report to the offsite Tingo River. In order to maximize dam efficiency and tailing storage capacity, a centerline constructed rockfill dam with a low-permeability core zone has been implemented for the Tailing Storage Facility (TSF). The TSF dam crosses both the Aguilas and Gordas valleys and its downstream toe is dictated by the Tingo River. Each valley also contains a secondary seep-

age collection system between the toe of the dam and the Tingo River. The design consists of starter dams in both valleys that reach vertical heights of 80 meters and a centerline construction method to bring the ultimate dam height to 175 meters.

Figure 1 illustrates a typical section of the proposed ultimate TSF dam in the Aguilas valley. Above elevation 3732 masl, the design is based on centerline construction. The centerline design concept relies on support from the sub-aerial tailing beach on the upstream portion of the dam to resist driving forces into the pond. The current crest elevation is 3755 masl.

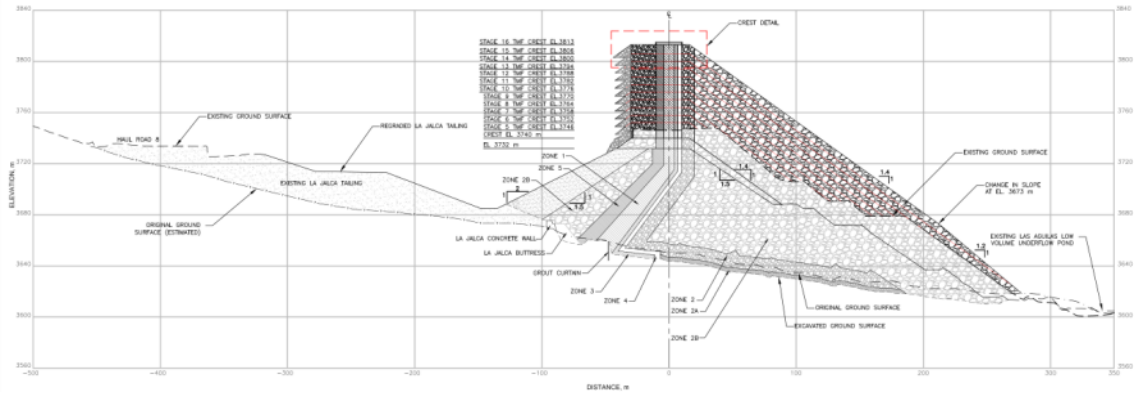


Figure 1. Typical Section of the Ultimate TSF Dam Design (Aguilas Valley)

1.3 *Construction Sequencing*

The design parameters for the dam include a two (2) meter freeboard between the crest of the dam and the surface of the pond after the occurrence of a Probable Maximum Flood (PMF) which is equivalent to 1.6 meters of vertical elevation. Therefore, the minimum vertical distance between the pond and the TSF crest at any given time is the design freeboard plus the PMF (ie. 3.6 meters). Considering slope stability requirements for the upstream face of the dam, the maximum freeboard has been calculated to be approximately nine (9) meters. A construction schedule which generally consists of annual six (6) meter raises has been developed for the TSF considering the rate of rise of the tailing material. To-date, the Aguilas section has been constructed in four discrete raises including the starter dam as shown in Table 1.

Table 1. Aguilas Dam Staged Construction Completed To-Date

Stage	Description	Completion Date
1	Starter Dam to 3732 masl	April 2010
2	Extension of Starter Dam to 3740 masl	December 2010
3	Centerline Raise to 3746 masl (6 vertical meters)	December 2011
4	Centerline Raise to 3755 masl (9 vertical meters)	October 2012

1.4 *Materials*

Brief descriptions of the distinct zones of the dam are provided in Table 2.

Table 2 - Material Properties for Static Analysis

Zone	Material	Description
Zone 2C	Upstream Rockfill	Uncompacted, Dirty Rockfill wedge on top of Subaerial Tailing Beach
Zone 2B	Upstream Rockfill	Compacted, Rockfill Column for Upstream Support
Zone 5A	Low Permeability Core	$K \leq 10^{-6}$ cm/s, Material with Sulfur Limitations
Zone 1	Low Permeability Core	$K \leq 10^{-6}$ cm/s, Material with Sulfur and Copper Limitations
Zone 3	Filter	Crushed, processed, washed and screened filter
Zone 4	Drain/Filter	Crushed, processed, washed and screened filter and chimney drain
Zone 2/2B	Downstream Rockfill	Compacted, Clean Rockfill for Downstream Support

Materials are presented from the upstream face (TSF pond) through the downstream shell. It should be noted that Zones 2 and 2B (rockfills), are placed in one meter lifts, compacted by a 19 tonne vibrating compactor that performs 6 cycles. Active sluicing of the rockfill has taken place during the dry season (May - September) while heavy rainfall in the wet season provides lubrication to the rockfill. Water in the amount of 5-10% the rockfill volume has been added before compaction.

2 INSTRUMENTATION CAMPAIGN

2.1 *Instrumentation Overview*

Since 2009 and in between the construction season for a staged raise of the dam, survey prisms have also been installed on both the upstream and downstream crest of the rockfill to monitor surface deformations. Prior to the 2011/2012 instrumentation program, the survey prisms provided the only information regarding horizontal and vertical displacements although proved challenging to monitor for continuous periods of time. Due to encroaching tailing levels, priority remained in continually raising the dam with minimal instrumentation until 2011/2012.

During 2011 and 2012, an extensive instrumentation program was executed throughout the TSF dam to better monitor its performance and deformations overtime. The program included installation of inclinometers, Casagrande piezometers, vibrating wire piezometers, magnetic settlement (extensometers) rings, settlement cells, and accelerometers both upstream and downstream of the low permeability core. MWH committed to maintain the integrity of the low permeability core thus instrumentation was installed in the upstream and downstream rockfill.

2.2 *Inclinometer II-1d Horizontal Deflections*

A total of 12 inclinometers were installed in the dam. Six inclinometers were installed in the upstream rockfill and the other six were installed in the downstream rockfill. The upstream inclinometers mirror the centerline core of the dam and remain 'floating' in the rockfill and are not anchored into bedrock to avoid crossing through the low permeability core of the starter dams. The maximum depth of the upstream inclinometer is 22 meters. The downstream inclinometers were installed downstream of the core at identical stations as the upstream points, although unlike the upstream points they continue to bedrock, some reaching 125 meters depth.

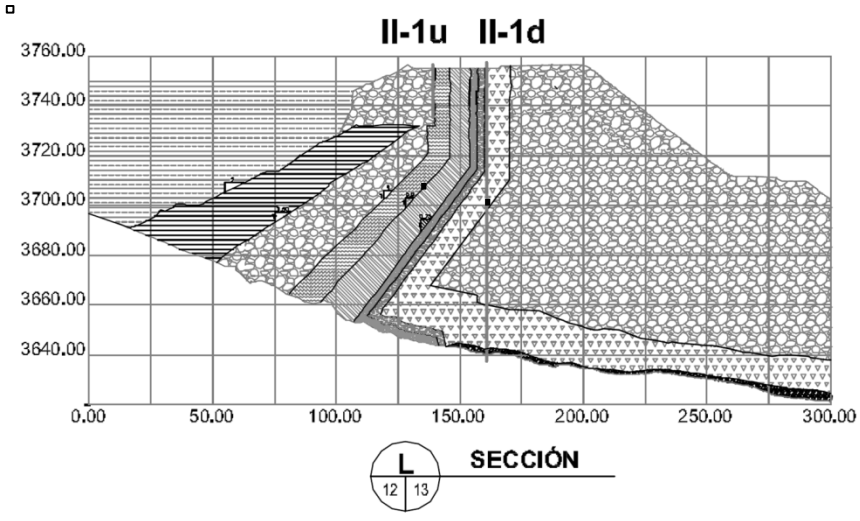


Figure 2. Cross Section of the Upstream (II-1u) and Downstream (II-1d) Inclinometers (Aguilas Valley)

To simplify the comparison of the two-dimensional (2-D) deformation model with the inclinometer displacements, inclinometer II-1d (downstream) was selected to represent the field deformations. II-1u, the mirror of II-1d on the upstream side of the core, remains suspended in the upstream rockfill and is 22 meters deep. Measured displacements in the inclinometers upstream of the core are considered relative as they are unanchored. Cumulative displacement graphs for inclinometers make the assumption that the lowest point is fixed and all displacements are summed starting at the bottom (fixed point) and moving up to the top of the casing. Inclinometer II-1d was installed along the deepest section of the Aguilas Valley and is anchored a few meters into bedrock as shown in Figure 2. II-1d is 125 meters deep.

Inclinometer II-1d has been monitored since October 2012. Records are provided through June 2013, representing nine (9) months of data. Survey measurements have generally been recorded on a bi-weekly basis. The inclinometer casing is surveyed every 50 centimeters (0.5 meters) although to reduce data scatter in the graph, readings were selected every five to nine meters. Figure 3 provides the horizontal displacement profile for the most recent profile recorded on June 6th, 2013. The profile represents movements along the A-axis which illustrates deflections in the upstream and/or downstream direction (approximately North-South for II-1d). Positive deflections are shown to the right (north & downstream) and negative deflections to the left (south & upstream). Axis B which considers lateral deformations along the alignment of the dam are not presented because the numerical model is two-dimensional and can only calculate displacements along Axis A.

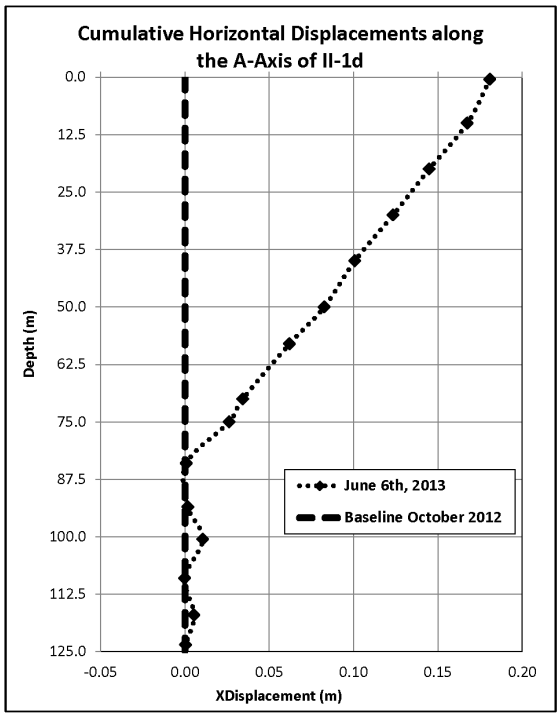


Figure 3. Cumulative Displacement Profile A-axis for Inclinometer II-1d

On surface, the inclinometer has deflected approximately 0.18 meters to the north (downstream). Displacements appear to originate at a depth of 80 meters and propagate upwards linearly. Below 80 meters depth, minimal displacements are recorded in both the upstream and downstream directions.

2.3 *Survey Prism & Extensometer Displacement Results*

Surface survey prisms have been installed along the upstream and downstream crest of the dam in-between construction activities to monitor horizontal and vertical displacements. Previous years have provided limited monitoring periods although the monitoring this past year started in

October 2012 and continued for approximately six months through March 2013. Two survey prisms, P_20 and P_22, were installed within 50 meters of inclinometer II-1d along the downstream rockfill crest of the dam. Due to construction activities in the area, the prisms were removed in March 2013 to commence the subsequent staged raise of the dam. Figure 4 represents the horizontal deflections incurred along the downstream crest. Both prisms show predominantly horizontal deflections in downstream (North) directions with prism P_22 displacing 0.17 meters and P_20 displacing 0.16 meters.

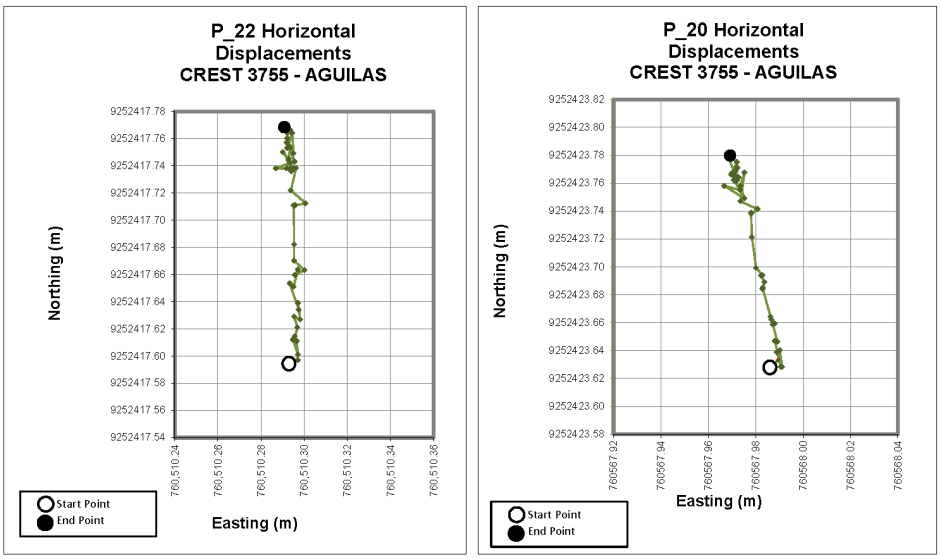


Figure 4. Survey Prisms P_22 & P_20 Horizontal Deflections

To verify settlements along the crest of the dam as well as monitor vertical settlements within the rockfill column of the dam, extensometers were installed on the outer casing of the inclinometers on a nine meter interval. Similar to the survey prisms, they have been surveyed on a bi-weekly basis and a few selected extensometer results are shown in Figure 5. The results present vertical displacements at distinct depth intervals along inclinometer II-1d. The results are plotted with the downstream crest survey prisms P_20 and P_22.

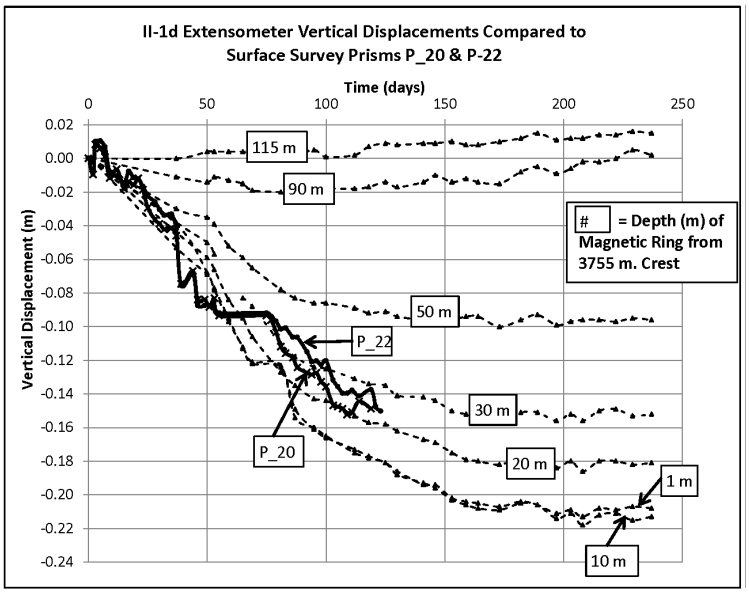


Figure 5. Field Data for II-1d Extensometer & Surface Survey Prism Vertical Displacements

2.4 *Interpretation of Instrumentation Deformation – Recent Staged Raise*

Over a nine month monitoring period of the most recently constructed raise of the dam, Stage 4, survey prisms installed along the downstream crest of the dam have deflected 0.16 to 0.17 meters in the downstream direction versus inclinometer II-1d which measures 0.18 meters in the same direction. On average, 0.17 centimeters of the dam crest has deflected downstream or per unit height 0.14% over a 9 month period. To construct Stage 4, the majority of additional material placed occurred on the downstream side of the dam. With continually rising tailing and pond levels on the upstream side of the dam and the additional material on the downstream section, horizontal deflections are expected to primarily occur in the downstream direction. Deflections decrease with depth because the effect of the additional load added during construction of Stage 4 reduces with depth. Additionally the deeper rockfill from previous construction stages has had more time to consolidate so less deflection occurs at deeper parts of the dam.

Vertical deformations on the crest of the dam coincide when comparing survey prisms with the extensometer installed at one meter depth. Both prisms settled approximately 0.14 meters over a period of 120 days although a few weeks of data were lost during relocation. This may be noted between 55 and 75 days where settlements for the prisms are horizontal. The uppermost extensometer at one meter depth settled 0.18 meters in a similar period of time and mirrored the prisms through 50 days of record when the survey prisms were repositioned. The extensometer continued settling for another two months to a maximum of 0.22 meters. The past two months of data show a tapered settlement rate in the upper sections of the rockfill while the deep sections of the rockfill appear to be heaving although in small increments (0.01 to 0.02 meters). Crest settlements per unit height are approximately 0.18% over a 9 month period.

Vertical settlements are the largest in the upper section of the rockfill that was most recently placed and most susceptible to the overburden pressures associated to additional loads. Deeper sections decrease in settlements as they have been settling over larger periods of time. Point to point contact of grains has increased overtime at depths due to consolidation confining pressures while void ratios have diminished therefore yielding less vertical displacements. Dascal (1987) suggested that downstream horizontal deflection could reach 1.5 to 5.0 times the settlement value. Currently the deflection values are 0.77 times the settlement value which may be associated to the effect of impounding the tailing pond as it is a slow, continuous process versus a rapid filling sequence experienced at most dam sites.

3 FINITE DIFFERENCE DEFORMATION MODELING

3.1 *Modeling Methodology*

A two-dimensional (2-D) static deformation model of the Aguilas dam section was created to estimate the vertical and horizontal deformations induced by construction of the Stage 4 raise. The objective of the numerical model is to compare its deformation results with field data in order to better estimate future displacements.

The computer program FLAC (Fast Lagrangian Analysis of Continua) was used in the analysis. FLAC is a 2-D explicit finite difference program for geotechnical and other applications developed by Itasca (2011). In a typical analysis, an idealized cross-section is divided into zones and nodal points in an analogous manner to the finite element method. FLAC uses the Lagrangian formulation of momentum equations (Newton's second law of motion) and, thereby, inherently accounts for the mass conservation law and allows elements with fixed masses to translate, rotate, or deform in space.

To build a representative deformation model, it is essential to appropriately define the stress-strain characteristics of the materials used for construction. The hyperbolic stress-strain relationship proposed by Duncan et al. (1980) is used in the model. In general, hyperbolic stress strain relationship accounts for the most important characteristics of soil stress-strain behavior including inelasticity, stress dependency and nonlinearity. More details of the hyperbolic stress-strain relationships used for each material are provided in the following section.

3.2 *Model Input Parameters and Geometry*

As mentioned before, the reliability of the displacements estimated by the numerical model largely depends on the selected stress-strain relationship for the material. Duncan et al. (1980) suggested the following equation to estimate the bulk modulus of the material as a function of minor principal stress, σ_3:

$$K = K_b P_a \left(\frac{\sigma_3}{P_a}\right)^m \quad (1)$$

Where K_b is the bulk modulus number, P_a is the atmospheric pressure and m is the bulk modulus exponent. K_b and m are both dimensionless so P_a, K and σ_3 all have the same units. Duncan et al. used a large variety of data from theses, research reports, engineering reports, and published papers and compiled a database to estimate K_b and m for over 80 soils. This database is mainly organized based on the gradation of the material, but there are additional characteristics such as compaction, initial void ratio and relative density that can also be used to make an appropriate estimate of K_b and m. For the modeling presented in this paper, the particle size distribution curves were used for the rockfill, core and filter materials to estimate the values of K_b and m parameters. The selected values are shown in Table 3.

Table 3. Estimation of the Bulk Modulus Number and Exponent

Material	**K_b**	**m**
Rockfill	100	0.34
Filter	360	0.57
Core	210	0

Table 4 summarizes the material properties used for the model. The properties were developed through a series of laboratory experiments as well as published literature and engineering judgment. Note that the effect of tailing and bedrock material properties is negligible on the displacements of inclinometer II-1d. The stress-strain relationship for these two materials was defined based on the shear modulus (G), based on laboratory data and engineering judgment

Table 4. Material Properties for Numerical Modeling

Material	**Unit Weight (kN/m^3)**	**Bulk Modulus, K (kPa)**	**Poisson's Ratio**	**Shear Strength (Degrees or kPa)**
Tailing	16.6	-	0.3	$\phi' = 20$
Rockfill	24.0	$2{,}089 \times (\sigma_3)^{0.34}$	0.36	$1.9323 \times (\sigma'_v)^{0.894}$
Core	21.0	210,00	0.37	$1.51 \times (\sigma'_v)^{0.894} \leq 431.3$ kPa
Filter	19.0	$2{,}608 \times (\sigma_3)^{0.57}$	0.35	$\phi' = 34$
Bedrock	21.0	-	0.3	N/A (Elastic)

ϕ' – Effective friction angle in degrees; σ'_v – Vertical effective stress in kPa; ; σ_3 – Minor principal stress in kPa

The model geometry, shown in Figure 2, was used for numerical modeling. The centerline rockfill dam was modeled in FLAC 2D software to estimate the horizontal and vertical displacements induced by construction of Stage 4. First, each stage was modeled incrementally and reached static equilibrium before the next stage of construction is simulated. After Stage 3 was modeled and reached static equilibrium, all displacements were set to zero before modeling the construction of Stage 4. Therefore, displacements given by the model are only induced by addition of Stage 4 and its associated overburden pressure. In the field, however, it is difficult to distinguish between the displacements induced solely by the addition of Stage 4 and those due to the previous construction stages. This difference could be a source of differences between the field and model displacements.

3.3 *Model Results and Interpretations*

Various stress-strain models are available in FLAC. The Elastic and Mohr-Coulomb models in FLAC were used for this analysis. Details of these models are provided by Itasca (2011). For the

results presented in this paper, the elastic model was used for all the material listed in Table 4 during the first set of iterations until the initial stresses are estimated. The Mohr-Coulomb model was then used for all material except bedrock for final static equilibrium.

Figure 6 illustrates both the horizontal and vertical displacement profiles from the numerical model that correspond to inclinometer II-1d. The model suggests that the horizontal displacements are primarily downstream deflections. At depths of 80 meters and below, little to no displacements are presented while in the upper 12.5 meters a total of 1.2 meters of horizontal displacement is estimated in the downstream direction or 0.96% deflection per unit height. Minor horizontal displacements in the upstream direction are noted below 80 meters.

Modeled vertical displacements near the surface are 1.6 meters or 1.28% per unit height and decrease with depth until it reaches zero at depth 112 meter. Lawton and Lester (1964) developed the following relationship for estimation of the settlement in rockfill dams after evaluating 11 dams using a best fit analysis:

$$s = 0.001H^{3/2} \tag{2}$$

Where s = total settlement and H = height of the dam in meters. Using Equation 2 for the current Cerro Corona TSF dam, the total settlement is 1.4 meters which is within 12.5% of the estimated settlement from the model. Lawton and Lester (1964) showed that the error in this equation is ±30% of settlement predicted.

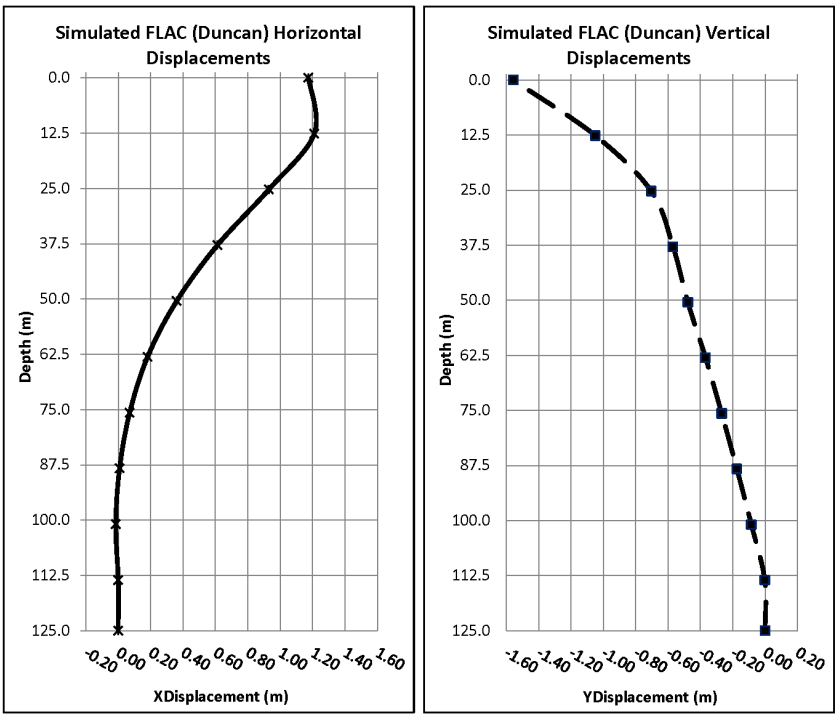


Figure 6. II-1d Horizontal (Left) & Vertical (Right) Displacements from FLAC Model Results

4 INSTRUMENTATION MEASUREMENTS COMPARED WITH FLAC MODEL & OTHER ROCKFILL DAMS FROM LITERATURE

Both vertical and horizontal displacements produced by the numerical model are considerably larger than the field-measured values. However, the model reports the final deformation values and the field measurements only correspond to a nine month period. Figure 7 compares the modeled displacements versus field measurements. Field horizontal displacements on the crest of the dam average 0.17 meters in the downstream direction or 0.14% per unit height. The modeled horizontal displacement on the surface is 1.2 meters in the same direction or 0.96% per unit

height. This suggests that the horizontal displacements measured in field to-date are about 14% of the total horizontal displacements estimated by the model.

Field vertical displacements near the surface average 0.22 meters of settlement or 0.18% per unit height while the modeled value is 1.6 meters or 1.28% per unit height. Similar to the horizontal deformations, to-date only 14% of the vertical displacements estimated by the model have been measured in the field.

Both field and modeled deformations follow the same trends and appear to converge and approach zero at similar points. Horizontal displacements approach zero at approximately 80 meters for both field data and modeling results. Vertical displacements approach zero at 90 meters and 112 meters depth for the filed data and model, respectively.

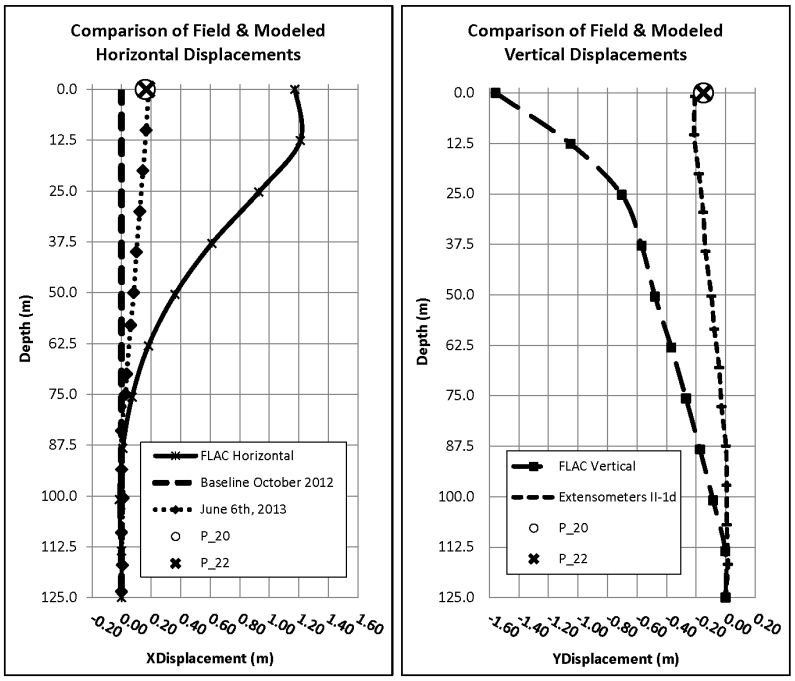


Figure 7. Field & Numerical Model Results for Horizontal and Vertical Displacements

Clements (1984) studied post-construction deformations of 68 rockfill dams throughout the world and although different construction methods and geometries were used, a few have been selected to compare crest settlement and deflections over a nine month period of time. Both sloping and central core dam geometries were selected as Cerro Corona's starter dam has a sloping core and the centerline design section is most closely related to a central core concept.

5 CONCLUSIONS AND RECOMMENDATIONS

Deformation curves calculated by numerical modeling illustrate similar displacement profiles to field measurements but with a different scale. Although a time component is not included in the model, only nine months of field data was available and is considered limited as the rockfill continues to deform. While a separate study suggests that rockfill dams reach maximum deformations 24 to 30 months post-construction (Dascal 1987), it can be concluded that field measurements for Cerro Corona's TSF dam have demonstrated two successive components of settlement. Initial measurements demonstrate rapid rates of settlement immediately post-construction for approximately 150 days and then a more long-term, creeping settlement ensues.

This study is considered preliminary and further modeling and interpretations should be conducted to better understand the deformations of the dam in both the horizontal and vertical directions. Modeled settlements correlate with an empirical equation developed from post-construction settlements by 11 rockfill dams. Also, the unique design and geometry of Cerro

Corona's TSF dam appears to be deforming similar to a sloping and central core rockfill dam. The field monitoring has confirmed that assumption. Based on the current field records, displacement data from historical dam records, and the modeling results, the following general conclusions and recommendations can be made for future studies and considerations:

1. A time–dependent model should be developed to better understand the progression of the ultimate deformation with time.
2. Previous studies that monitored crest settlements and deflections of rockfill dams suggest that the existing measured values are within reasonable ranges to-date although should be continually monitored.
3. The configuration and geometry of the dam is unique and survey prisms only provide small periods of time to monitor surface deformations. Due to an average annual six meter raise of the dam, it should be considered critical to continually maintain inclinometer and extensometer readings to evaluate the deformations over time.
4. Valley geometry may influence settlement along the dam alignment and create an arching effect over the deeper section of fill. Both upstream and downstream inclinometers should be evaluated near the abutments to verify if arching is occurring.

Table 5 – Comparison of Crest Settlements & Deflections of Rockfill Dams 9 Months Post-Construction

Name	Type	Height (m)	Crest Settlement / Unit Height, %	Crest Deflection / Unit Height, %	Construction Method & Remarks
Cerro Corona TSF	Sloping Core/Central Core	125	0.18	0.14	1 m. lifts, 19 tonne vibrating compactor w/ 6 cycles, 5-10% rockfill volume of water sluicing, flooding during construction & continually rising
Brownlee	Sloping Core	122.4	0.23	-	Coarse rock dumped. Fine rock 45 cm. lifts – 3 passes 50 ton roller, flooding during construction
Scammonden	Sloping Core	70	0.13	-	1 m. lifts, 11.5 ton vibrating compactor w/ 5 passes or 6 passes of two 5 ton rollers
Trangslet	Sloping Core	125	0.18	-	2-3 m. lifts U/S, sluicing & compaction; 20 m. lifts D/S, no sluicing
Gepatsch	Central Core	153	0.45	0.13	2 m. lifts; 4 passes with 8.6 ton vibrating roller
Muddy Run	Central Core	76.2	0.30	-	0.3-1 m. lifts with vibrating roller
El Infiernillo	Central Core	148	0.15	0.04 (Upstream)	< 1 m. lifts, 4 pass with D8 tractor, no sluicing
Akosombo	Central Core	112.8	-	0.25	1.8 m. lifts, 4 passes with 4 ton vibrating layer, some sluicing

Note: All data apart from Cerro Corona from Clements (1984).

6 REFERENCES

Clements, Ronald P. 1984. ¨Post-Construction Deformation of Rockfill Dams.¨ *Journal of Geotechnical Engineering,* ASCE, 110(7). 821-840.

Dascal, Oscar. 1987. ¨Postconstruction Deformations of Rockfill Dams.¨ *Journal of Geotechnical Engineering.* ASCE, 113(1), 46-59.

Duncan, J. M., Byrne, P., Wong, K. S. and Marby, P. 1980. ¨Strength, Stress-strain and Bulk Modulus Parameters for Finite Element Analysis of Stresses and Movements in Soil Masses.¨ Report No. UCB/GT/80-01. *Geotechnical Engineering, Department of Civil Engineering. University of California, Berkeley*. August 1980.

ITASCA, 2000. Fast Lagrangian analysis of continua (FLAC), Version 4, User's Guide. *Itasca Consulting Group, Inc*., Thrasher Square East, 708 South Third Street, Suite 310, Minneapolis, Minnesota.

Lawton, F.L., and Lester, M.D. 1964. ¨Settlement of Rockfill Dams.¨ Presented at the May 1964 *Eighth International Congress on Large Dams*, held at Edinburgh, Scotland, Vol. III, pp. 599-613.

Liquefaction assessments of tailings facilities in low-seismic areas

Holly Rourke & Caroline Holmes
SRK Consulting, Perth, WA, Australia

ABSTRACT: It is widely recognised that piezocone (CPTu) testing is a valuable technique for identifying the in situ engineering properties of tailings for use in stability and liquefaction assessments. Numerous empirical procedures have been developed to relate the results of piezocone testing to liquefaction potential. Appropriate assessments are particularly important for upstream raised tailings facilities which have an inherently higher risk of failure due to liquefaction following seismic events. This paper evaluates two commonly used procedures developed by Robertson (2010), and Idriss & Boulanger (2008) for determining liquefaction potential. These procedures calculate the factor of safety against liquefaction by comparing the cyclic resistance ratio (CRR) to the seismically induced cyclic stress ratio (CSR). During the design of an upstream raise to a tailings facility in Western Australia, it was found that Robertson's approach leads to improved estimates of the CRR by considering the influence of fines content. Idriss & Boulanger's recommendation of a cut-off value for earthquake magnitude scaling factors and magnitude-dependent stress-reduction coefficients offers a more conservative estimate of the CSR, particularly where the design earthquake magnitude is less than 7. The case study identified a gap between the methodologies for assessing the liquefaction potential for tailings facilities in areas with low seismicity that requires further research.

1 INTRODUCTION

Piezocone (CPT_u) testing is recognized as a valuable technique for identifying the in situ engineering properties of tailings. Continuous measurements enable profiling of the entire depth of tailings and foundation while identifying subtle changes in stratigraphy. The CPT_u is particularly useful for evaluating the potential for soil liquefaction which requires a strong understanding of the soil stratigraphy and in-situ properties of the tailings.

Numerous empirical methods have been developed to relate the results of field CPT_u testing to liquefaction potential. Most methodologies assess liquefaction potential by comparing an estimation of a seismically-induced cyclic stress ratio (CSR) to the cyclic resistance ratio (CRR) of the material. For the purposes of this paper, two commonly used procedures developed by Robertson (2010), and Idriss & Boulanger (2008) will be compared through the assessment the liquefaction potential for the design of an upstream raise to an existing tailings storage facility (TSF) in Western Australia.

2 METHODOLOGIES FOR ASSESSING LIQUEFACTION POTENTIAL

2.1 *Overall approach*

Both the Robertson and Idriss & Boulanger methods evaluate liquefaction potential using a de-

terministic relationship expressed as a Factor of Safety (FoS). The FoS is defined as the ratio of CSR to CRR calculated for a magnitude 7.5 earthquake, and scaled to the design earthquake by a magnitude scaling (MSF) factor, as summarised in Equation 1 below:

$$FoS = \frac{CRR}{CSR} \times MSF \tag{1}$$

No liquefaction is expected when FoS is greater than 1, and a material is deemed potentially liquefiable when FoS is less than 1.

2.2 *CSR and stress reduction coefficient, r_d calculation*

Both methods calculate CSR based on the simplified approach, originally proposed by Seed and Idriss (1971), as shown in Equation 2 below:

$$(CSR)_{7.5} = \frac{\tau_{av}}{\sigma'_{vo}} = 0.65\left(\frac{\sigma_{v0} a_{max}}{\sigma'_{vo}}\right) r_d \tag{2}$$

where τ_{av} is the average cyclic shear stress, σ_{v0} is the total vertical overburden stress, σ'_{v0} is the effective vertical overburden stress, a_{max} is the maximum horizontal acceleration of the ground surface, and r_d is a stress reduction factor. The constant 0.65 factor is used to convert the peak cyclic shear stress ratio to a cyclic stress ratio that is representative of the most significant cycles over the full duration of loading (reference). The calculation of r_d differs between the Robertson and Idriss & Boulanger methods. The former estimates r_d using depth-dependent relationships (Equation 3), whereas the latter expresses r_d as a function of both depth and earthquake magnitude (Equation 4).

$$r_d = 1.0 - 0.00765z \quad \text{(if z < 9.15 m)} \tag{3a}$$
$$= 1.174 - 0.0267z \quad \text{(if 9.15 m < z < 23 m)} \tag{3b}$$
$$= 0.744 - 0.008z \quad \text{(if 23 m < z < 30 m)} \tag{3c}$$
$$= 0.5 \quad \text{(if z > 30 m)} \tag{3d}$$

$$\ln(r_d) = \alpha(z) + \beta(z)M \quad \text{(if z ≤ 34 m)} \tag{4a}$$
$$\alpha(z) = -1.012 - 1.126\sin\left(\frac{z}{11.73} + 5.133\right) \tag{4b}$$
$$\beta(z) = 0.106 + 0.118\sin\left(\frac{z}{11.28} + 5.142\right) \tag{4c}$$
$$r_d = 0.12\exp(0.22M) \quad \text{(if z > 34 m)} \tag{4d}$$

where z represents the depth below surface. The implication on the overall factor of safety against liquefaction is described later in the paper.

2.3 *CRR calculation*

Both methods express CRR as a function of the CPT_u cone resistance, q_t, where the CRR-q_t relationship is derived from historical cases of liquefaction occurrences. The Idriss & Boulanger method has been developed for clean, cohensionless soils with fines content (FC) below 5%. For a known FC, the method provides a fines correction. This correction becomes constant for FC values greater than 35%. The Robertson method adjusts the measured CPT_u cone resistance by a correction factor, K_c that accounts for the effect of both fines content and plasticity of the material. Both methods employ an iterative approach to determine CRR. A summary of the calculation procedure is shown in Figures 1 and 2 that follow.

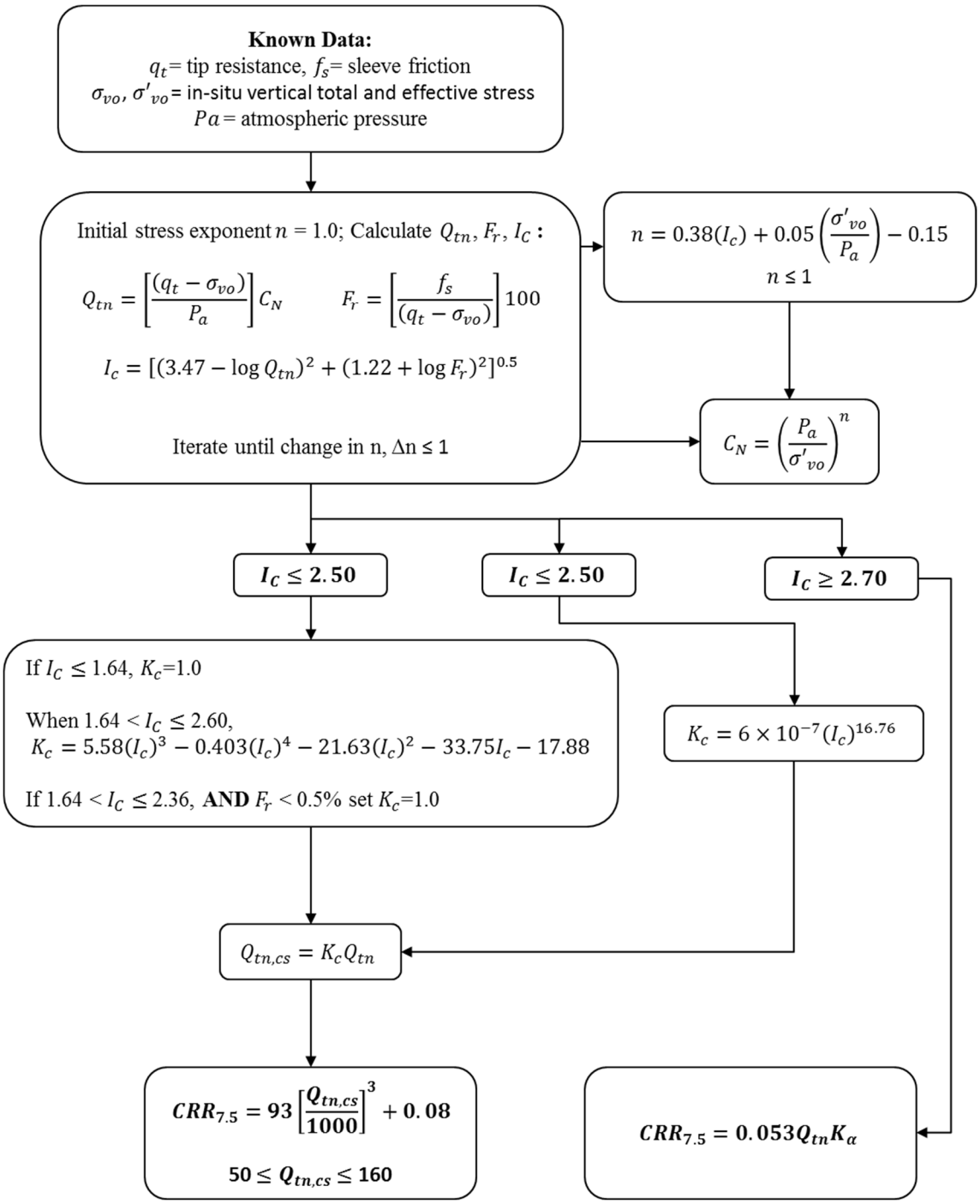


Figure 1. Flow chart to determine $CRR_{7.5}$ after Robertson 2009

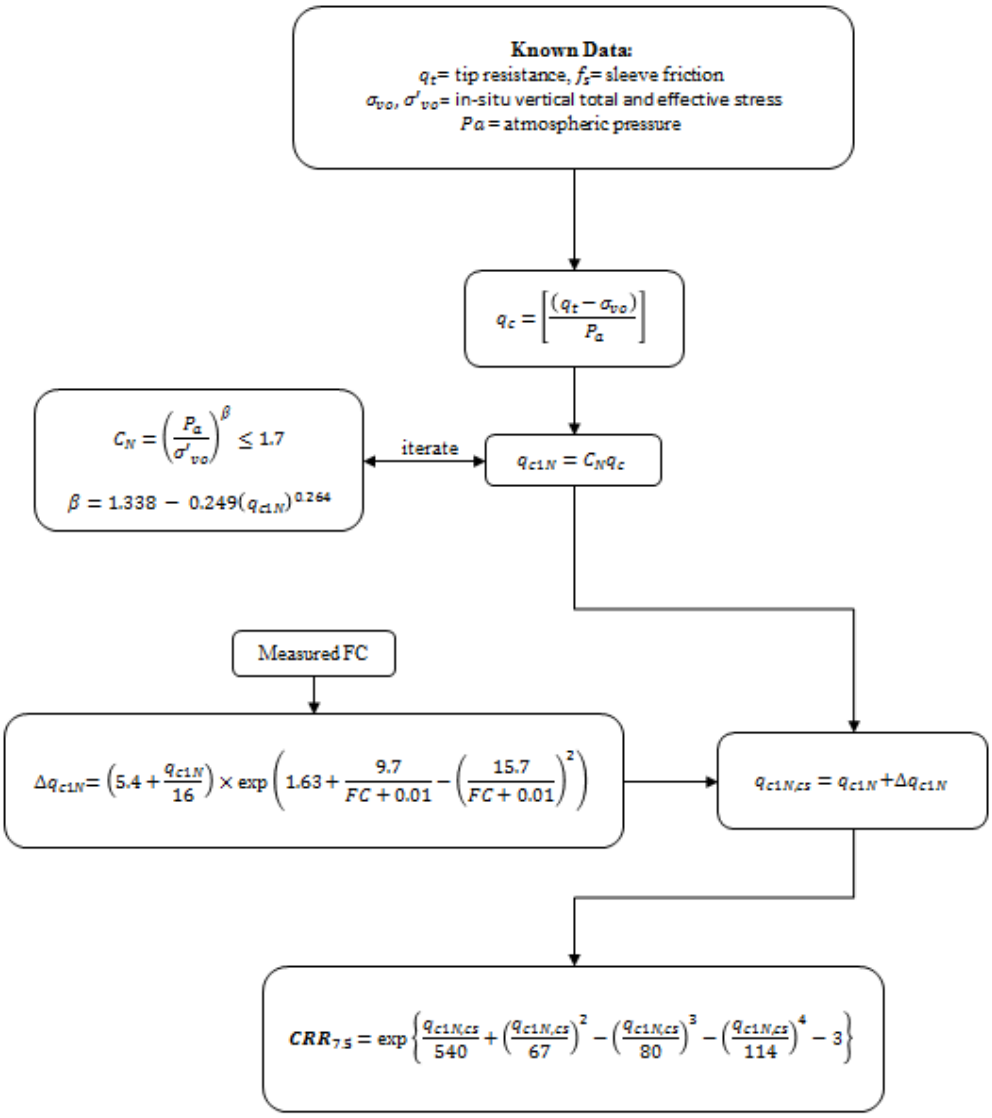


Figure 2. Flow chart to determine $CRR_{7.5}$ after Idriss & Boulanger 2008

2.4 *Magnitude scaling factor, MSF*

The MSF is used to scale the CSR estimated for a magnitude 7.5 earthquake to the design earthquake magnitude. The Idriss & Boulanger method used to calculate MSF is shown in Equation 5, and the Robertson method is shown in Equation 6. Idriss & Boulanger limit MSF to a maximum value of 1.8 for earthquake magnitudes less than 5.25.

$$MSF = 6.9 \exp\left(\frac{-M}{4} - 0.058\right) \leq 1.8 \quad (5)$$

$$MSF = \frac{174}{M^{2.56}} \quad (6)$$

MSF and r_d must be determined using consistent methodology. Idriss & Boulanger's magnitude-dependent r_d will decrease with reduced design earthquakes and the associated MSF will increase. Robertson's r_d is not related to earthquake magnitude and the total earthquake effect is represented in the MSF.

3 CASE STUDY

3.1 *General*

The TSF presented in this case study is a ring-dyke facility with tailings deposited through perimeter spigots. The TSF is located in the Yilgarn region of Western Australia and stores tailings from a nickel-sulphide operation. An upstream raise utilising *in-situ* tailings as the primary construction material was designed to accommodate the tailings production for the remaining life of mine. The potential for liquefaction of the embankment raise foundation was a key consideration for the design and a liquefaction assessment was carried out to confirm the suitability of an upstream raise.

3.2 *Seismic Setting*

There is limited information on seismic activity for the TSF site on which to base the a_{max}. The Earthquake Hazard Map of Western Australia (2003) presented in AS1170.4 (2007) recommends acceleration coefficients of between 0.08 and 0.09 g which corresponds to an event with a 1 in 500 annual exceedence probability.

A review of regional seismic events using data from the Geoscience Australia online Earthquake Centre (http://www.ga.gov.au/earthquakes/home.do) was undertaken to determine the magnitude and frequency of previous earthquake events in the region. The database was analysed for seismic events within the time period 1900 to 2012, and within a 300 km^2 radius of the project site. The results are presented in Figure 3.

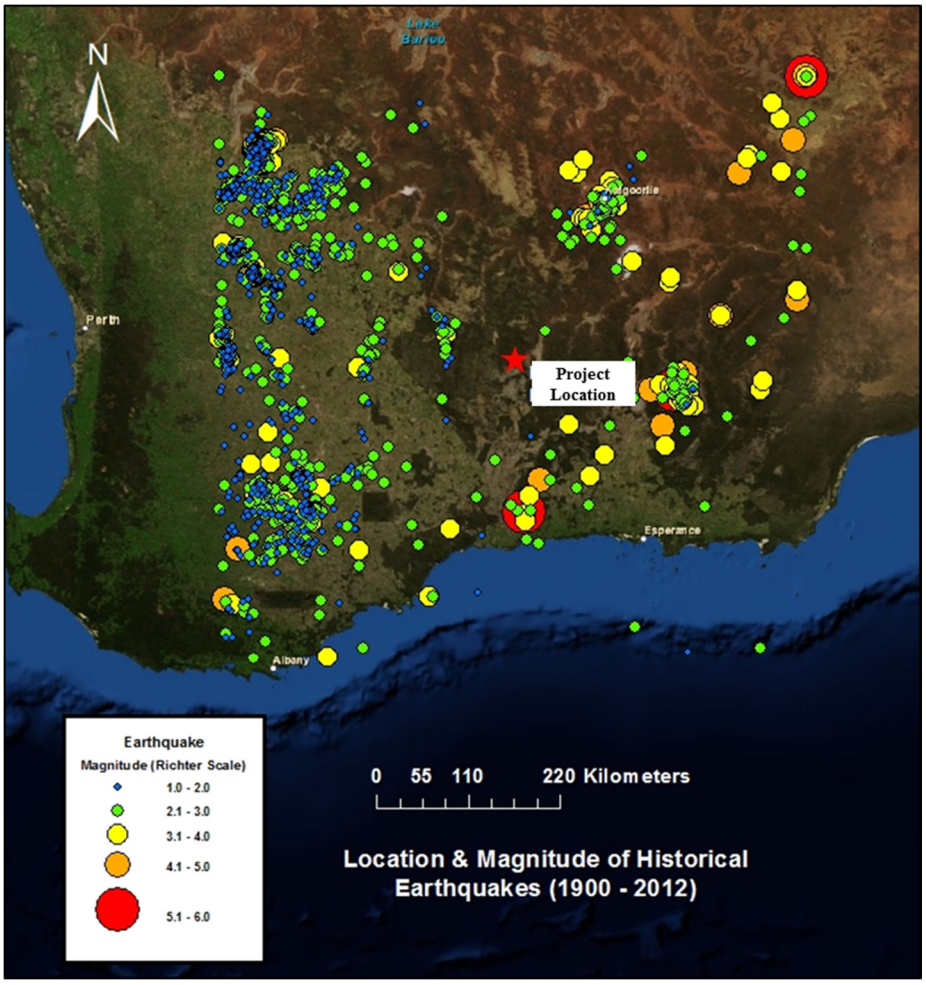


Figure 3. Location and magnitude of earthquakes near the project site.

The Richter magnitudes vary between 1.0 M and 5.6 M. Historical earthquake occurrences are clustered in two areas, around 200 km NE and approximately 175 km E of the project site. There are numerous earthquake occurrences to the west of the project site, though most of these earthquakes are of magnitude 3.0 M or less. The closest recorded seismic event, with a magnitude of 2.6 M, occurred at a distance of 43 km from the project site in April 2009.

In the absence of a site-specific seismic study the design earthquake magnitude was conservatively adopted as 5.0 M.

3.3 *Results of the liquefaction assessment*

Two CPT_u tests were undertaken in 2012, with CPT-1 tested on the tailings beach approximately 8 m from the existing embankment crest and CPT-2 tested 20 m further down the beach. The results of the liquefaction assessment for the two test sites are shown in Figure 4 below.

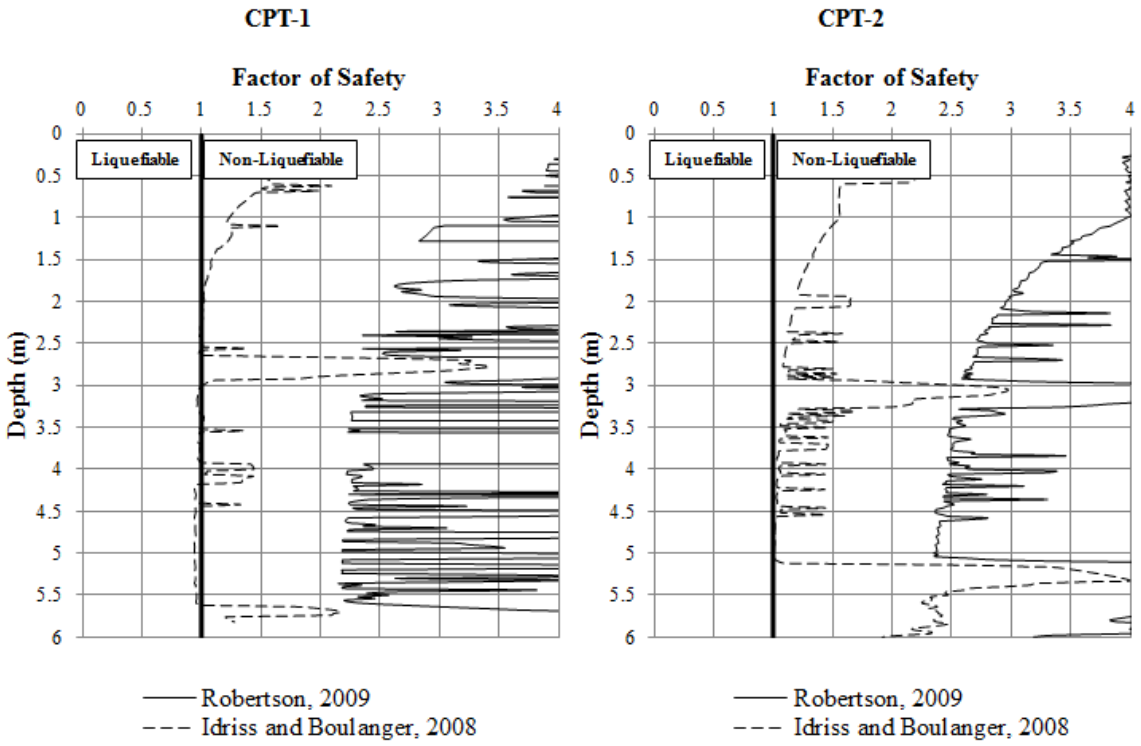


Figure 4. Results of the liquefaction assessment expressed as factors of safety

It can be observed that the Robertson method results in a significantly higher estimate of the FoS, generally 2 to 2.5 times the FoS determined using the Idriss & Boulanger method. Therefore the outcome of the liquefaction assessment is sensitive to the method selected for the analysis.

Despite using different relationships to determine r_d, the relatively shallow depth of the TSF and low seismic parameters result in similar r_d values which in turn yield comparable CSR estimates for both methods. The difference in FoS is therefore attributed to the variations in the CRR and MSF relationships. In low-seismic areas the difference is dominated by MSF and the CRR has a small contribution.

3.4 *CRR calculation comparison*

The range of CRR values calculated using both the Robertson and Idriss & Boulanger methods are shown in Table 1. The Robertson method consistently results in higher estimates of CRR.

Table 1. Range of CRR values calculated by Robertson and Idriss & Boulanger methods

Method	Highest CRR	Lowest CRR	Median CRR
Robertson	0.19	0.06	0.08
Idriss & Boulanger	0.08	0.05	0.06

The CRR determination is largely dependent on the measured cone tip resistance, corrected for atmospheric pressure and *in-situ* vertical total and effective stresses. The Robertson method includes a correction for the combined influence of particle size and plasticity which accounts for the higher calculated values of CRR. Numerous studies have identified these two parameters as key criteria for evaluating liquefaction potential.

A limited sampling program was carried out at the same time as the CPT_u probing, with samples taken approximately 0.5 m below the surface. Six samples were tested for particle size distribution (PSD), three samples were taken next to CPT-1 and three samples next to CPT-2. The results of the PSD testing showed no evidence of segregation between the two test areas, and the average fines content from all four tests provides a good correlation to the apparent fines content determined through the Robertson method (Table 2).

Table 2. Comparison of apparent fines content to laboratory-tested fines content

Test Location	Apparent Fines Content	PSD Fines Content
CPT-1	62 %	63%
CPT-2	65%	

The full PSD curves of the samples were compared to Ishihara et al.'s 1980 envelope of tailings susceptible to liquefaction (Fig 6).

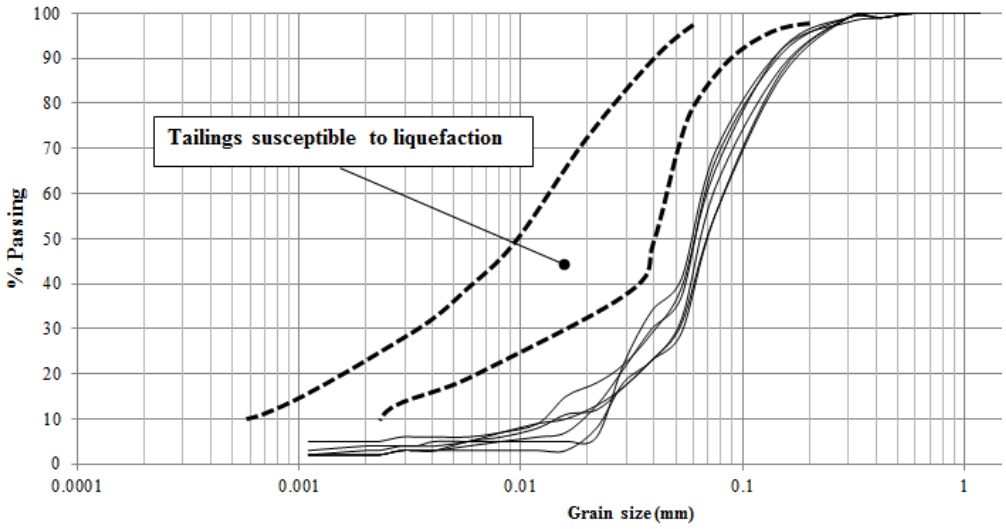


Figure 5. Tailings samples plotted against tailings liquefaction envelope after Ishihara, 1980.

On the basis of PSD alone, the tailings are expected to be non-liquefying suggesting that CRR values calculated using the Idriss & Boulanger method may be conservative. There are no plastic or liquid limit tests available to confirm this hypothesis on the basis of plasticity; however the tailings are classified as being non-plastic.

Direct comparisons cannot be made between the Idriss & Boulanger and Robertson methods as the overall CRR calculated is largely dependent on how the normalization of q_c for total and effective stresses and influence of fines is carried out (see Figures 1 and 2).

Idriss & Boulanger's method has been largely developed from SPT data, which may further contribute to the difference in CRR values. A 2010 study by Seed performed a comparison with Idriss & Boulanger's 2008 SPT and CPT-based methods. Although these methods were devel-

oped to be compatible, Seed states that the CPT correlation is approximately 35% more conservative than the SPT-based correlation for q_c values less than 50kPa (Seed, 2010). Another study (Liao, 2010) discovered further discrepancies between the CPT and SPT-based methods for tip resistances in the range of 50 kPa ≤ q_c ≤ 150 kPa, but in this case the SPT-based method was found to be more conservative. Idriss & Boulanger's fines correction requires known fines content from adjacent samples or, when samples are not available, relies on determinations from other methods. It is understood that rigorous sampling helps calibrate and improve the accuracy of CPT methods; however the need for sampling reduces some of the main advantages of the CPT (principally continuous data and speed) over other methods such as the SPT.

3.5 *MSF calculation comparison*

The MSF was found to be the dominant parameter for influencing FoS. The MSF relationship to earthquake magnitude is shown in Figure 6 for both the Robertson and Idriss & Boulanger methods using Equations 5 and 6. The Idriss & Boulanger MSF is limited to 1.8 for earthquake magnitudes less than 5.25 M.

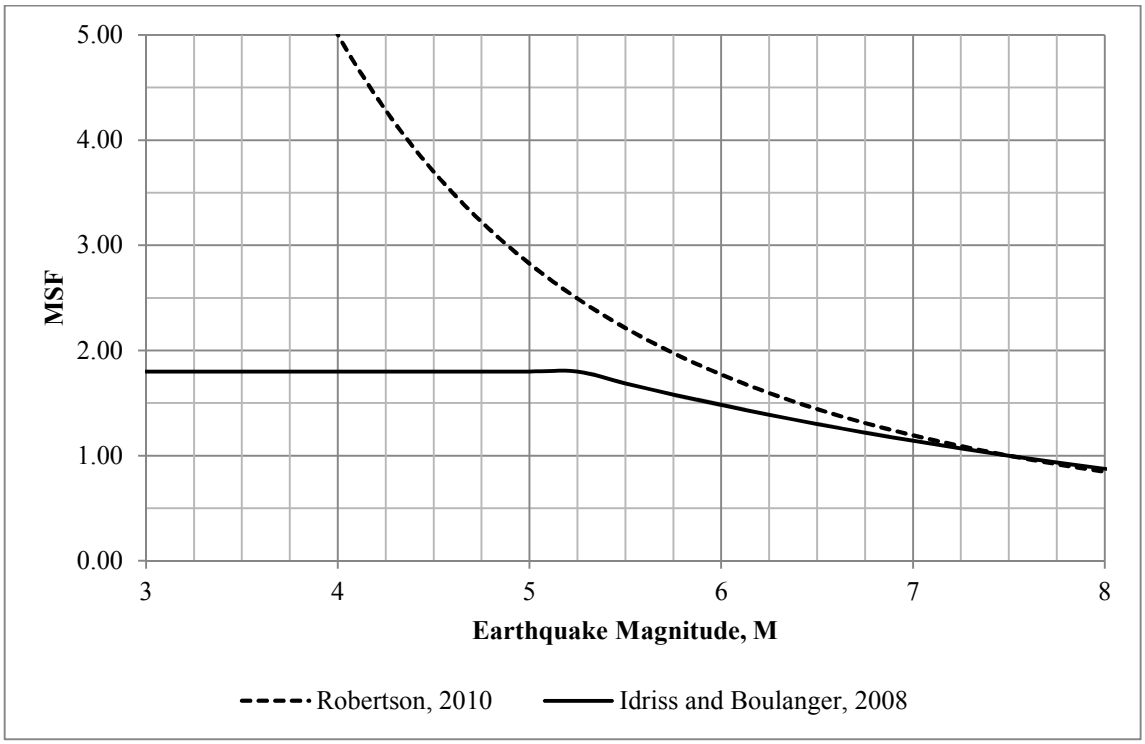


Figure 6. MSF comparison

For earthquake magnitudes 7.0 M or greater, both methods produce similar MSF values. As the earthquake magnitude decreases below 7.0 M, the difference between methods increases, with Robertson's method yielding larger MSF values. Applying the Robertson method in low-seismic areas will result in proportionally large MSF fluctuations for small changes in earthquake magnitude. As the MSF has a substantial influence on the overall FoS against liquefaction, Robertson's MSF relationship appears overly optimistic relative to the Idriss & Boulanger method, especially for areas where no site-specific seismic study has been undertaken to confirm the design earthquake.

4 SUMMARYOF RESULTS

A simple sensitivity analysis found MSF to have the greatest influence on FoS in the case study. The MSF is also the parameter with the least amount of confidence because it is exclusively dependent on the design earthquake magnitude. Using the Robertson method, increasing the design earthquake to 6 M decreases the FoS by 37% and decreasing the design earthquake to 4 M increases the FoS by 77%. For this case study, the Robertson method of calculating CRR is thought to provide an adequate representation of the fines influence, however his MSF relationship gives large variations for small changes to the earthquake magnitude. As a result, the Robertson method appears more suited to sites within medium-to-highly seismic areas. The fines correction by Idriss & Boulanger only considers fines content determined through laboratory testing or empirically using relationships derived by others, instead of the overall material behavior and is therefore only suitable for evaluating clean sands.

5 CONCLUSIONS

In the case study, the Robertson method resulted in significantly higher estimates of FoS than the Idriss & Boulanger method consistently across the entire profile; however this may not necessarily be the case for different projects. In general, the Robertson method is thought to provide a better representation of the effect of fines on soil behavior than the Idriss & Boulanger method. The Robertson method is preferable as it is not dependent on adjacent sampling and considers both f_s and q_c measurements to account for both particle grading and plasticity influences. The disadvantage of the Robertson method is the large fluctuations of MSF with small changes to the design earthquake affecting the overall FoS. Therefore the Robertson method appears more suitable for evaluating sites with silty and clayey material subject to medium to strong earthquake ground motions and the Idriss & Boulanger method is more suited to sites with clean sands subject to any earthquake magnitudes.

Each method has been developed with interdependencies within parameters and with the intention that all parameters be calculated using consistent methodology. Therefore the applicability of each method should be carefully assessed before use in a liquefaction assessment.

The case study identified an information gap between the methods that resulted in large variations of FoS. More research and site-specific test data is needed to adequately assess liquefaction potential, especially for tailings in low-seismic areas. When there is a discrepancy between reputable methods and site-specific data is scarce, general practice is to adopt the more conservative approach. Great benefits to cost and time savings could be achieved through a reduction to over-conservative designs by refining the methods to suit tailings facilities in low-seismic areas.

6 REFERENCES

Dillion, M.J. & Wardlaw, H.J. 2010. Strength and liquefaction assessment of tailings. *Mine Waste 2010, Perth, Australia*: 347-360.

Idriss, I.M. & Boulanger, R.W. 2008. *Soil liquefaction during earthquakes*. Oakland: Earthquake Engineering Research Institute.

Ishihara, K. et al. 1980. Cyclic strength characteristics of tailings materials, soils and foundations. 20(4).

Liao, J. 2010. Comparison of three procedures for soil liquefaction evaluation. *Annual Technical Conference, Kleinfelder Consultants, Denver, 19-20 February 2010.*

Olson, S.M. & Stark, T.D. Yield strength ratio and liquefaction analysis of slopes and embankments. *Journal of Geotechnical and Geoenvironmental Engineering*. 129(8):727-737.

Robertson, P.K. 2010a. *Guide to Cone Penetration Testing.* Signal Hill: Gregg Drilling & Testing Inc.

Robertson, P.K. 2010b. Evaluation of flow liquefaction and liquefied strength using the cone penetration test. *Journal of Geotechnical and Geoenvironmental Engineering*. 136(6):842-853.

Robertson, P.K. & Wride, G.R. 1998. Evaluating cyclic liquefaction potential using the cone penetration test. *Canadian Geotechnical Journal* 35: 442-459.

Seed, R.B. 2010. *Technical review and comments: 2008 EERI Monograph: Strength and liquefaction assessment of tailings.* Berkeley: University of California at Berkeley.

Seed, R.B. et al. 2003. Recent advances in soil liquefaction engineering: a unified and consistent framework. *26th Annual ASCE Los Angeles Geotechnical Spring Seminar. Long Beach, California, 30 April 2003.*

Youd, T.L. & Idriss, I.M. 2001. Liquefaction resistance of soils: summary report from the 1996 NCEER and 1998 NCEER/NSF workshops on evaluation of liquefaction resistance of soils. *Journal of Geotechnical and Geoenvironmental Engineering*. 127(4): 297-313.

Zhang, G., et al. 2002. Estimating liquefaction-induced ground settlements from CPT for level ground. *Canadian Geotechnical Journal*. 39:1168-1180.

Factual and foreseeable reliability of tailings dams and nuclear reactors: a societal acceptability perspective.

Franco Oboni & Cesar Oboni
Oboni Riskope Associates Inc, Vancouver, British Columbia, Canada

ABSTRACT: This paper compares the "historic" rate of failure (major accidents only) of tailings dams and nuclear reactors world-wide to well known, previously published acceptability criteria and codes. It then attempts a comparison of these two very different industries (nuclear vs. mining) from a quantitative risk evaluation point of view showing unexpected results. The paper then shows that the mining industry as a whole has considerably progressed in reducing the rate of dam failures from the 1970 to date. Three questions are asked: 1) Is it sufficient? 2) Is it sufficient from the perspective of present and future societal acceptability? 3) Do common practice risk assessments offer enough depth of analysis with respect to modern requirements? To answer these questions, the authors suggest a simplified model for long-term risk evolution of tailings dams with particular emphasis on post-production – closure – long-term dam life. The paper shows how a generic modern "excellent quality" dam probability of failure can be estimated, as well as how the initial probability of failure will evolve during the dam life as care and monitoring are released (in view of closure), and during the closure phase until, for example, the first Maximum Design Earthquake. The paper is written in non-scientific language to broaden the audience beyond the engineering community.

1 INTRODUCTION

This paper compares the "historic" rate of major accidents (failure) of tailings dams and nuclear reactors world-wide to previously published acceptability criteria and defines the long-term evolution of the risks (major accidents) generated through the life of a tailings dam (TD), with particular focus on the post-production phases/closure. In contrast to hydro dams that would typically be breached at the end of their production life, the closure phase is the longest phase for TD. A TD's life can be summarized as follows (M.B. Szymanski, M.P. Davies, 2004): Production (tailings disposal); Transition (preparation for the closure phase which may include flushing out contamination); Long-term treatment (dam operation continues in the sense of regulated water levels); Closure (dam is no longer operated in the sense of regulated water levels), likely more than 1,000 years. For the purpose of this paper, we will summarize the phases as follows: Production as the phase with the highest monitoring and care, Transition and Long-term treatment as phases during which monitoring and care are gradually reduced, and Closure as the phase during which the dam is "abandoned". Major hazard hits may occur during any of these phases.

A TD's probabilities of failure and those generated by major nuclear reactors' accidents to date are empirically estimated, and both are compared to societal and technical acceptability thresholds to understand if present and foreseeable performances are aligned with expectations. Risk is often modeled as the expected value of an undesirable outcome by combining the prob-

abilities of various possible events and an evaluation of the corresponding harm into a single consequence value. Accordingly, in this paper, the risk is defined as the product of the probability of failure by the related consequences expressed in casualties, leaving aside all other environmental and physical direct or indirect consequences, for the sake of simplification.

- As a first step the paper examines real life failure data (Fig. 1) for the world-wide and US TDs portfolio in an attempt to define a "base value" of the rate of failure p_f (annual probability of major accident), then an "excellent" TD rate of failure p_f.
- The second step encompasses the definition of a simplified model for the evolution of the probability of failure p_f of a TD over time, including the long-term post-production "era". In today's world, civilian/industrial facilities are generally designed to last for 50-100 years save, for example, spent nuclear fuel disposal sites. Some former mining sites (uranium tailings, arsenic disposals, etc.) are calling for "perpetual care", very much like nuclear fuel disposal. Perpetual care design means ensuring somehow survival for repeated major hazards hits, etc., certainly for more than the "classic 1,000 years". For example, the need to account larger exposure periods for TDs has been recognized in the New Zealand Dam Safety Guidelines (NZSOLD, 2000).
- Third, we compare risks generated under various conditions to different published acceptability thresholds and discuss the implications.

The simplified models used through this paper for TDs focus on major events and use approximations: they are geared toward defining an order of magnitude of the long-term risk evolution of a generic dam undergoing variation of the standard of care, during and after the mine closure, and when hit by a major hazard. This discussion could be expanded to cover various Maximum Design Hazards but it should not be relied upon for specific assessments; only a third party, i.e. not performed by the design team, quantitative risk assessment should guide specific sites' decisions to avoid biases and prejudices (F. Oboni, C. Oboni, S. Zabolotniuk, 2013).

A generic well-designed, built and monitored "excellent" dam is used as Base Case Study (BCS), where "excellence" is defined by compliance with modern TDs codes for critical, high consequences dams (ANCOLD, 2011). The BCS p_f is estimated using the "SLM" (F. Silva, T.W. Lambe, W.A. Marr, 2008) semi-empirical relationship with the classic Factor of Safety (FoS) (Fig. 2). The first step is to define the "Category" (I to IV) of the structure under examination by examining sequentially Design, Construction and Operations aspects of the slopes.

Within the frame of a specific and detailed analysis for a site specific quantitative risk assessment, probabilistic slope stability methods should be used to define the probability of failure of a particular dam.

2 HISTORIC FAILURES RATES

2.1 *Tailings Dams and Hydro Dams*

USCOLD (1994), UNEP (1996, 1998) studies have shown that Slope Instability is the highest cause for TDs failures (Fig. 1), followed by earthquake, overtopping and "unknown" (ICOLD, 2001). Following Davies & Martin (M. P. Davies, T.E. Martin, 2000; N. Lemphers, 2010) there were more than 3,500 TDs (of various kinds and construction type, with at least 50% of the upstream design) around the world. (For the US (See *1 in the Literature) we consider the total number of TDs at 984). In absence of more accurate data, and more particularly, on the evolution of this number, we will consider in this paper a portfolio of 3,500 dams globally and 1,000 dams for the US alone. Portfolios are assumed constant over the years but, as we will see later, even if that assumption was wrong by one order of magnitude, which is very difficult to believe, there would be no significant alterations in the conclusions of this paper.

From UNEP (1998) world data we read that there were 44 TDs failures in the decade around 1979 and 7 in the decade around 1999. From US sources, 984 TDs 984 (See *2 in Literature), the chronology of major failures (from 1960) gives a total of 28, with 7 failures in the decade around 1979 and 8 failures in the decade around 1999).

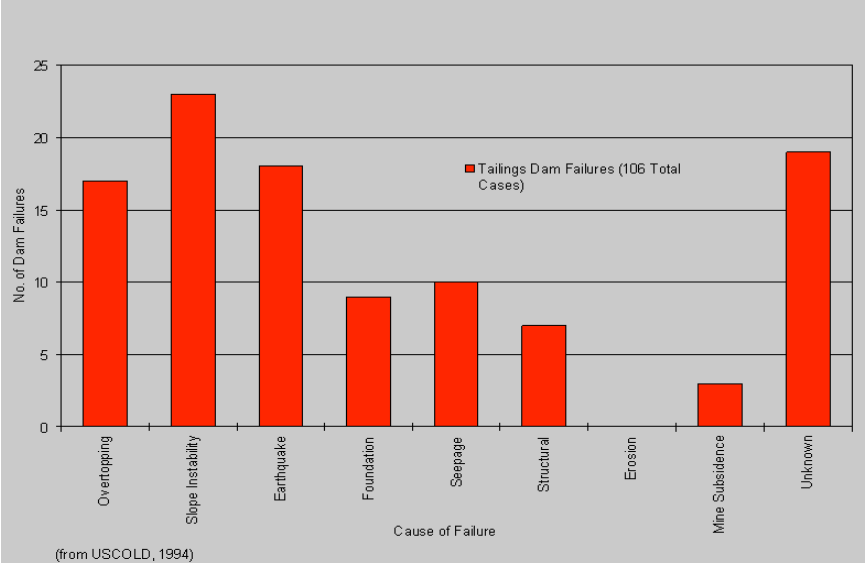


Figure 1. Causes of Failure of Tailings Dams, Number of Occurrences over a Total of 106 Recorded by USCOLD, UNEP up to 1994.

Where	When (decade)	p_f	Approx p_f	Verbiage for p_f
World-wide	Around '79	44/(3,500*10)	10^{-3}	One in one thousand
World-wide	Around '99	7/35,000	$2*10^{-4}$	Two in ten thousands
US	Around '79 & Around '99	7 or 8/(1,000*10)	$7 \text{ or } 8*10^{-4}$	Seven or eight in ten thousands

2.1.1 *Annual Probability of Failure vs. Factor of Safety*

As slope instability is the greatest source of TDs failures (Figure 1), for the sake of simplification, this paper looks only at this particular failure mode. The proposed methodology could, however, easily be expanded to cover other failure modes.

The SLM methodology examines sequentially the following *aspects* of the Design (D1 Investigation, D2 Testing, D3 Analyses and documentation) and Construction "CO" as well as Operations and Monitoring "OM" of embankments and slopes to determine the Category for a structure. Each aspect is described by various detailed specifications. The less stringent the specifications, the lesser the quality of the considered structure; thus, SLM defines four Categories ranging from I (Best) to IV (Poor). Experience shows that structures with high failure consequences are generally designed, built, and operated in such a way that they fall in Category I. Of course, if a structure has received little or no engineering it will fall in Category IV. Accordingly SLM's Category I has OM described as "complete performance program including comparison between predicted and measured; no malfunctions; continuous maintenance" whereas a Category IV will have "occasional inspection, no field measures". We will assume in this paper that Category I OM applies to Production Phase (undergoing full monitoring), and Category IV OM to Closure Phase with "abandonment" (no monitoring).

Figure 2 shows the FoS-p_f relationship for the four categories. If we go back to the rate of failure p_f empirical estimates (Section 2.1) for TDs = 10^{-3} to $2*10^{-4}$ (we will not mention the US value as it lies within that range) and assume that the average original FoS was in the area of 1.3 (ANCOLD, 2011), we would come to the conclusion that TDs are generally Category I or slightly inferior structures.

The statement above is in good agreement with the common understanding and empirical knowledge that TDs are generally of "lesser quality" than hydro dams. Indeed, if we consider

the hydro dam failures in the decades around 1989 and 1999 and evaluate p_f as we did for TDs, based on an "average number of dams" of 30,000, we get $p_f = 3*10^{-6}$ to 10^{-5}, values which are compatible, considering usual FoS, with a Category I (three failures in a million to one failure in one hundred thousand dams per year). By using the SLM methodology, we can estimate the p_f of an "excellent" TD at 10^{-5} to 10^{-6} as "excellence" would mean "top of the class" Class I structure, well engineered, undergoing serious QA/QC, with a minimal FoS of 1.4-1.5. Should inspections become occasional, measurements/monitoring not be performed, the probability will raise to $6*10^{-5}$. Interestingly, many different industries around the world consider values below 10^{-6} to 10^{-5} (below one in one hundred thousand to one in a million) as the boundary of what is humanly credible (meaning that below that range of probability any lay person or expert would imagine that an accident is "incredible").

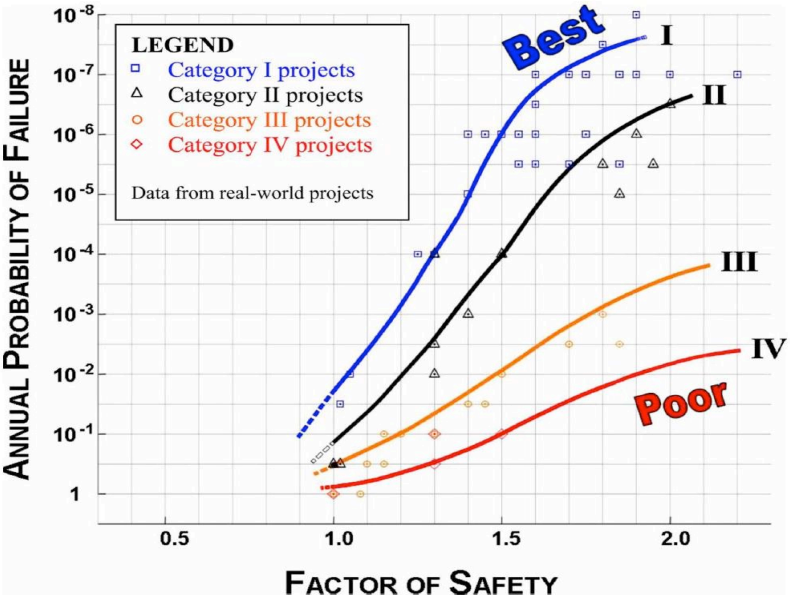


Figure 2. Annual Probability of Failure vs. Factor of Safety following Silva, Lambe, Marr (SLM) (F. Silva, T.W. Lambe, W.A. Marr, 2008) methodology.

In case of partial fulfillment of a Category's qualifications, the original SLM paper suggests to interpolate values (on Fig. 2) after defining weights for the specifications/Categories. Thus a stepped increase of the probability of failure is suggested if one of the *aspects* is gradually worsened for a dam belonging to a specific Category.

In the case of TDs, it is possible to "simulate" long-term complete abandonment. Thus the p_f could actually reach the value of the lower Category IV (and even higher). For example, if we look at the case of OM standards phased release from Category I (operational life) down to IV (long-term closure), the probability of failure will increase each time the OM standard attains a lower category. Interestingly, for initial FoS in the 1.3 to 1.5 range, the difference between Category I (we are assuming that the dam under examination is initially an "excellent" structure) and II varies respectively between 1.5 and 2 orders of magnitude: for FoS=1.5, $p_{fCatI}=10^{-6}$, with possible increase to 10^{-4} and higher if the same structure falls in total neglect.

2.1.2 *P_f with Seismic Event*

Following ANCOLD (2011) an "excellent" TD should be designed to remain serviceable under Operating Basis Earthquake (OBE), i.e. to undergo limited damage/deformation repairable without significant service disruptions (this moves the structure from Category I to Category II-III following SLM). Therefore p_f will increase from 10^{-6} to 10^{-4} or higher under OBE if the initial FoS is still attained (no expected liquefaction, well-drained structure, no change in shear strength).

In case the post-seismic shear strength would be lower than pre-seismic values, then ANCOLD 2011 declares an acceptable minimum Fos=1.1 and therefore the p_f could increase to $1.25*10^{-2}$ or higher. Of course this is again quite simplistic, insofar we are considering "a single earthquake" instead that the whole set of aftershocks on a weakened or damaged structure.

Under Maximum Design Earthquake (MDE) damage will be more extensive and disrupt operations, but the structural integrity of the dam needs to be maintained and uncontrolled release of tailings/water should not occur. MDE for Significant Consequence Dams should be those with an Annual Exceedance Probability (APE)=1/100=10^{-2}; APE=1/1000=10^{-3} for High & Extreme Consequences dams (ANCOLD, 2011). Thus we can estimate that after a MDE the dam could fall down to Category III during operations, and most likely Category IV or higher during the very long closure phase, during which the occurrence of at least one MDE is almost certain to occur.

Such low "acceptable" FoS and respective high p_f will lead to deformations and other defects of the dam which will be weaker when the next seismic event occurs, but more importantly an increase of risks. If we use the SLM suggested interpolation technique, if after an OBE the dam does not undergo routine maintenance and has uncorrected malfunctions, the probability of failure will rise significantly. After multiple hits, or if the first hit provokes severe damages equivalent to the cumulated damage of several quakes, we could see a possible post-seismic increase to $p_{fCatIPS}=1.2* 10^{-1}$ and higher if the dam has fallen in total neglect.

2.2 *Major Nuclear Accidents*

As of February 2, 2012, 435 nuclear power plant units with an installed electric net capacity of about 368 GW were in operation in 31 countries and 63 plants with an installed capacity of 61 GW under construction in 15 countries. The cumulative nuclear reactor operating experience amounted to 14,745 years by February 2012 (See *3 in the literature).

To date, the world has seen the occurrence of a number of major nuclear reactors accidents (rated 5 and above on the International Nuclear Event Scale by the International Atomic Energy Agency). For Fukushima we consider one accident (although more than one reactor was involved) to ensure the list is made of "independent" accidents. The reason Level 5 and higher is selected lies in Level 4 definition as "Accident with local consequences" which might not be comparable to a TD major failure discussed in the prior sections. Finally, to counter any possible comments depicting the nature of Fukushima quake magnitude and resulting tsunami as "exceptional", we note that:

a) in many areas of the world, seismic potential was/is poorly understood and therefore many structures were/are under-designed,
b) it is difficult, if not impossible, to structurally upgrade a working reactor,
c) power plants' risk assessments apparently focused on the safety of the nuclear reactor, but often underestimated the impacts and consequences on its environment and ancillary structures/ equipments.

Assuming seven accidents, the "historic" world average rate of Scale 5+ accidents is: 7/14,745 total operating time= $4.75*10^{-4}$ Scale 5+ accident/annum.

Level 5	Level 6	Level 7
Accident with wider consequences	**Serious accident**	**Major accident**
Chalk River (1952) Windscale (1957), Lucens (1969), Three Mile Island (1979)	Kyshtym (1957)	Chernobyl (1986) Fukushima (2011)

3 FAILURE RATES VS. HISTORIC AND ANCOLD ACCEPTABILITY THRESHOLDS

Figure 3 displays acceptability criteria developed independently by various authors over a peirod of more than forty years, together with some examples of industrial, transportation and dams accidents dating back to the 1960s (G. Morgan, L. Lave, 1990, R.V. Whitman, 1984, ANCOLD, 2003). Among these accidents, depicted as "bubbles" to include scatter of data, it is of particular interest to observe the "(hydro) dams bubble". If we compare these to the values defined in Section 2, we notice immediately that world-wide (but, surprisingly, not so much in the US) the situation has improved considerably with the p_f of TDs creeping down to values similar to those of hydro dams in the 1960s, and hydro dams lowering their p_f by one order of magnitude.

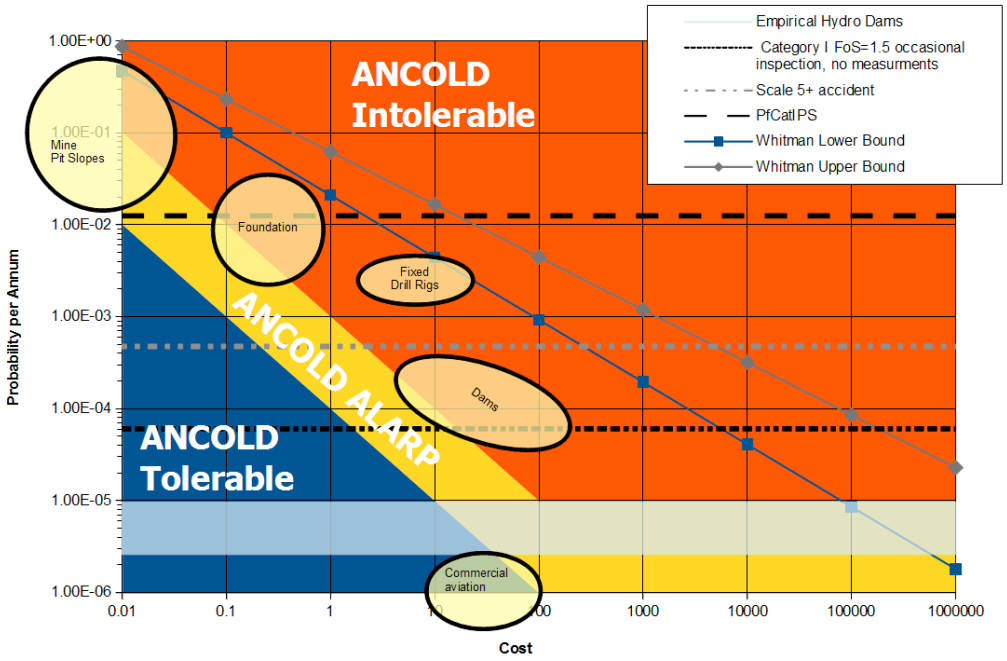


Figure 3. A probability (vertical)-Consequence (Horizontal) graph showing p-C "bubbles" from various industrial, transportation and dams accidents in the 1960s (R.V. Whitman, 1984 & G. Morgan, L. Lave, 1990), Whitman tolerability curves (upper bound and lower bound) as well as the ANCOLD (2003) "acceptability zones" (Tolerable, ALARP, Intolerable). The horizontal lines correspond from bottom to top: to the p_f of a Category I dam with occasional inspections and no monitoring/measurements, to Scale 5+nuclear accidents (See Section 5), and a Category I dam under total neglect and after seismic events.

The recent ANCOLD 2003 acceptability criteria (Figure 3) are compatible with Comar, Wilson (Comar, 1987, Wilson & Crouch, 1982) and later criteria published in the field of chemical industry, such as those from Renshaw (Renshaw, 1990), who defined simple societal risk acceptability criteria expressed as probability of fatality of one individual per year of risk exposure. Many publications from reputable (governmental, research) sources point at a probability (of a casualty per annum) of 10^{-4} (similar to ANCOLD lower bound) as being the limit of "safe", however with a lower limit of 10^{-6} for unwillingly exposed public.

The p_f of:

- a Category I dam with occasional inspections and no monitoring/measurements,
- a Scale 5+nuclear accidents, and a
- Category I dam under total neglect and after a number of seismic hits

can be compared to ANCOLD and other published historic tolerability thresholds (Figure 3). It becomes immediately apparent that any accident with more than 1 to 15 casualties is considered intolerable by ANCOLD or other modern "technical" tolerability thresholds when paired with the selected cases' p_f,whereas historic societal thresholds would have been complied with.

4 COMPARING RISKS OF TWO VERY DIFFERENT INDUSTRIES

4.1 *Empirical probabilities of mishaps*

The Table below (Data from Section 2.1, 2.2) compares TD and nuclear 5+ accidents including occurrence decade and empirical rate of return.

Where	What	When (decade)	p_f	Approx. p_f
World-wide	TD	Around '79	44/(3,500*10)	10^{-3}
World-wide	TD	Around '99	7/35,000	$2*10^{-4}$
US	TD	Around '79 & Around '99	7 or 8/(1,000*10)	7 or $8*10^{-4}$
World-wide	Nuclear 5+ accidents	Since inception	7 Scale/14,745	$4.75*10^{-4}$

Despite the fact that nuclear industry is highly regulated, its safety record to date is far from optimal. One would like to see severe mishaps to be, as for hydro dams, border-line credible, but historic data unfortunately prove the contrary.

4.2 *Cost of Consequences*

In order to evaluate risks we need now to evaluate consequences using the selected metric, i.e. casualties. Even such a "simplified" metric is difficult to apply as there might be for nuclear accidents a long delay between exposure and health effects, as explained below.

4.2.1 *Nuclear*

In some class 5+ accidents the estimate of casualties has been equated to nil. It is not within the scope of this paper to discuss that evaluation.

According to a June 2012 Stanford University study by John Ten Hoeve and Mark Jacobson, the radiation released at Fukushima could cause 130 deaths from cancer (the lower bound for the estimates being 15 and the upper bound 1,100) and 180 cancer cases (the lower bound being 24 and the upper bound 1,800), mostly in Japan. Radiation exposure to workers at the plant was projected to result in 2 to 12 deaths. An additional approximately 600 deaths have been reported due to non-radiological causes such as mandatory evacuations. Evacuation procedures after the accident may have potentially reduced deaths from radiation by 3 to 245 cases, the best estimate being 28; even the upper bound projection of the lives saved from the evacuation is lower than the number of deaths already caused by the evacuation itself. We can assume based on these numbers that a class 5+ accident to date has caused between nil and a maximum of 3,500 casualties, with a "best estimate" at 890 casualties.

4.2.2 *Dams*

If we look at the history of TD accidents (221 accidents: USCOLD, 1994; UNEP, 1996; 2001) in terms of victims, we record a few accidents with approximately 260 casualties (2008, Taoshi, Linfen City, Xiangfen county, Shanxi province, China; 1985, Stava, Trento, Italy). In 1966, the Mir mine disaster in Sgorigrad, Bulgaria, killed 488 people. In 1965, the El Cobre New Dam in Chile killed more than 200 people. Very few cases killed around 100, and most cases had 1-15 casualties. This leaves us with a minimum of nil, a maximum of ~500, and an expected value of ~80 casualties.

If we look at Whitman tolerability thresholds, most of the recent (1999) TD failures fall within societal acceptability lower bound, unlike the more ancient ones or US failures. However, should a TD failure result in a number of casualties greater than 1000, we should expect a very serious re-think of the industry world-wide similar to the one that the nuclear industry has just

seen. Should a TD be abandoned and undergo in the long run a number of natural hazards hits, the risks will become socially intolerable even if there are less than ten casualties.

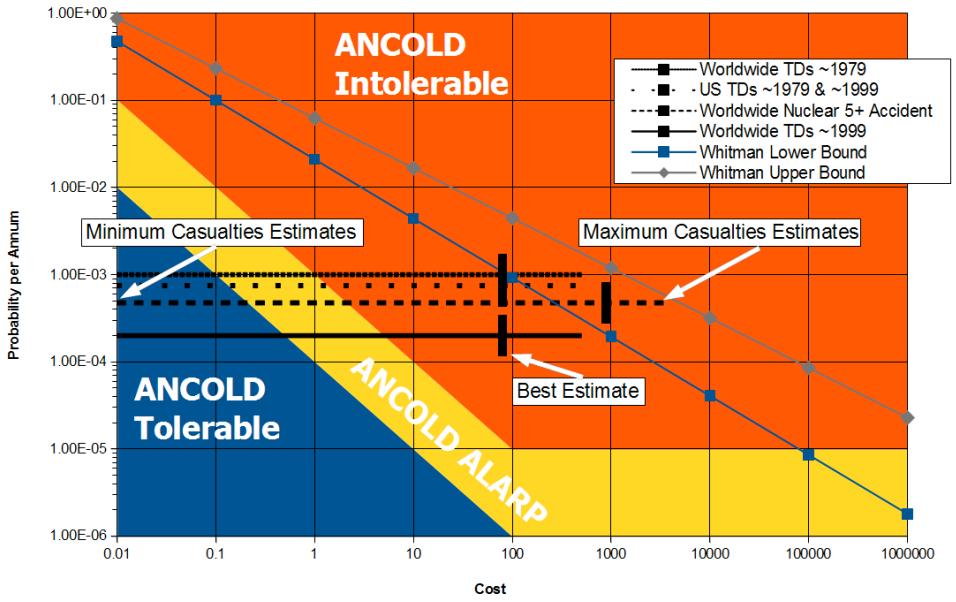


Figure 4. Same pf-C (Casualties) diagram as in Fig. 3, but "historic bubbles" have been removed and Casualties Estimates for TDs' and Class 5+ nuclear accidents have been added.

4.3 *Risks and their Evolution*

These results lead to the following set of conclusions:

a) Unless a TD is built as a Category I geo-structure, then is highly monitored and maintained, the ANCOLD tolerability guidelines suggest no one should ever be exposed to it.

b) unless a TD is designed, built and cared for like a hydro dam, which means "at perpetuity" high-level monitoring and care (TD cannot be breached, unlike hydro dams) no residents should be allowed downstream of the structure (this paper does not consider environmental damages), within reach of possible run-out from a breach, to ensure ANCOLD compliance.

c) risk assessments have to be sufficiently sophisticated to allow p_f estimates compatible with the ANCOLD tolerability thresholds.

d) Standard practice matrix-based risk assessments (F. Oboni, C. Oboni, S. Zabolotniuk, 2013, C. Oboni, F. Oboni, 2012) cannot be used as they lack the necessary finesse and resolution and could actually severely mislead TD owners/operators to the point of exposing them to severe liabilities.

5 CONCLUSIONS

Fukushima, with a "best estimate" casualties count at ten times the average of past TD accidents and the specter of radiations, brought the Japanese nuclear industry to an immediate halt and caused a very serious re-think of the industry world-wide. No TD failure has yet created such a socio-political shift. However, in the present climate of social awareness and social licensing to operate, should a severe accident happen anywhere in the world, we could expect "industry-wide" repercussions of some kind as failure will be deemed socially intolerable. To give an example of such repercussion, following the 2010 British Petroleum/Deepwater Horizon oil spill in the Gulf of Mexico, President Obama issued a moratorium on offshore drilling that halted

work on 33 exploratory drilling rigs in the Gulf of Mexico. The ban was lifted in October 2010 but, by February 2011, no one had received a permit to drill because those applying had to prove the ability to contain a spill.

Perpetual care design means ensuring survival for repeated major hazards hits, thus design criteria should be more stringent for the closure phase than for the production phase, especially if the consequences of dam failures will increase because of population, land-use, etc.

Especially in the case of TDs located in areas where demographic pressure leads to settlements in the downstream areas, social and legal consequences of a failure will dramatically increase. This will particularly be the case if the methodologies used to perform the risk assessments prove to be in disconnect with the needs of our modern society.

REFERENCES

ANCOLD, International Commission on Large Dams, 2003, Australian National Committee. Guidelines on risk assessment

ANCOLD, Guidelines On Tailings Dams Planning, Design, 2011, Construction, Operation And Closure, Draft-

M.P. Davies, T.E. Martin, January 2000, Upstream Constructed Tailings Dams- A Review of the Basics, Tailings and Mining Waste, Balkema Publishers

Dams Safety Committee, June 2012, DSC, DSC3F, Tailings Dams, New South Wales

ICOLD, 2001, Tailings Dams: Risk of Dangerous Occurences (Lesson Learnt from Practical Experience, bulletin 121

N. Lemphers, Oct. 12, 2010, Could the Hungarian Tailings Dam Tragedy Happen in Alberta?, www.pembina.org

G. Morgan, L. Lave, 1990, Ethical considerations in risk communication practice and research, Risk Analysts 1o, 355- 358-

NZSOLD, 2000, New Zealand Society on Large Dams, New Zealand Dam Safety Guidelines.

Oboni, F., Oboni, C., Is it true that PIGs fly when evaluating risks of tailings management systems? Short Course and paper, Tailings and Mine Waste '12, Keystone Colorado

Oboni, F., Oboni, C., Zabolotniuk, S., 2013, Can We Stop Misrepresenting Reality to the Public? CIM 2013, Toronto

F. Silva, T.W. Lambe, W.A. Marr, December 2008, " Probability and Risk of Slopes Failures", JGGE, ASCE

M.B. Szymanski, M.P. Davies, 2004, Tailings Dams Design Criteria And Safety Evaluations At Closure, BC Mine Reclamation Symposium,

UNEP, 1996, Environmental and safety incidents concerning tailings dams at mines: results of a survey for the years 1980-1996 by the Mining Journal Research Services, Report prepared for United Nations Environment Programme, Industry and Environment, Paris

UNEP, 1998, Case Studies on Tailings Management, United Nations Environment Programme, International Council on Metals and the Environment, November, ISBN 1-895720-29-X

UNEP, 2001, Tailings Dams - Risk of Dangerous Occurrences, Lessons learnt from practical experiences, Bulletin 121, Published by United Nations Environmental Programme Division of Technology, Industry and Economics (DTIE) and International Commission on Large Dams (ICOLD), Paris, 144 p.

USCOLD,1994, Tailings Dam Incidents, U.S. Committee on Large Dams (USCOLD), Denver, Colorado,

R.V. Whitman, 1984, Evaluating calculated risk in geotechnical engineering. J. Geot. Engineering, 110, 2

*1 http://www.wise-uranium.org/mdaf.html

*2 http://www.wise-uranium.org/mdaf.html

*3 http://www.euronuclear.org/info/encyclopedia/n/nuclear-power-plant-world-wide.htm

Tailings facility failures in 2012

Jack A Caldwell
Robertson GeoConsultants, Vancouver, BC, Canada

ABSTRACT: In 2012, the failure of at least three tailings facilities was reported on the internet. Near failures of other tailings facilities also made news. This paper collates publically available information about the 2012 tailings failures and examines the failures in the light of engineering and geotechnical perspectives as compared to the focus of popular news reports. The facilities that failed that are examined in this paper include: the HB Mine, Salmo BC tailings facility; the Philex Padcal Dam failure in Indonesia; and the Gullbridge Tailings Dam failure in Newfoundland. The author has no personal knowledge of any of these failed facilities, but draws instead on public reports and professional experience in discussing the perpetually fascinating and perplexing issue of continued failure of mine tailings facilities.

1 INTRODUCTION

There were three well publicized tailings facility failures in 2012: two in Canada and one in the Philippines. In this paper are summaries and discussions of the failures. The information in this paper is from publically available sources. I have no first-hand information about these failures. The approach used in this paper is to quote from web postings that were available as the failures occurred. This provides a real-time, yet unusual perspective; how people saw events as they occurred.

Reporting on the causes and subsequent action has dried up - possibly the lawyers have got control of the situation and the flow of information has been stemmed. Thus all that is left to us as engineers seeking to learn is the web and its raw footage. I have not been able to get any official statement from any of those involved in the failures. I trust they will bear with me in this paper which is prepared in the hope of advancing the practice of engineering as it relates to tailings facilities. I am truly sorry if any are offended by what I write; in response I ask only that they publish definitive accounts that may supersede this paper.

Because I quote accounts from the web that appeared as events unfolded, I am not always able to provide references in the best technical paper tradition. Many of the websites have simply disappeared. For those that are still there I provide the standard link. But there is no guarantee they will still be there when you seek them. The only justification I can give for this unusual approach is that I believe it is valuable to share these stories with the profession.

The approach that I adopt in this paper is as follows:

- First, I summarize the plot in my own words to tell you what I think happened.
- Second, I quote from the web in order to give you the basis of what I think happened and to enable you to make your own decisions.
- Third, I note a few lessons learnt, in the hope that they help.

In the second section on quotes from the web, my approach is unusual: I repeat only what was readily available on the web. This approach to "research" illustrates the power and limitations of

modern media: the immediate information; the limited perspective of the reporters; the power of those involved to craft the story; the suppression of nasty outcomes by those seeking to protect their reputations and liability; and the complete absence of learned engineering evaluation and analysis. This is a story of how the lawyers control the flow of information, so as best to protect the organizations responsible, and limit the truth to only that which the public accepts with equanimity.

I have learnt from these stories, and I hope you can too. At the least they provide information, insight, and the opportunity to work to preclude their repeat in the future.

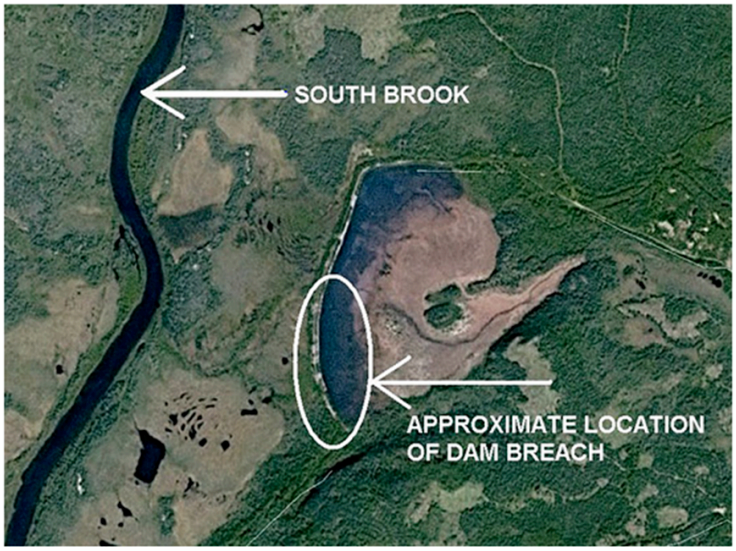
2 GULLBRIDGE MINE, NEWFOUNDLAND, CANADA

2.1 *Plot Summary*

The old Gullbridge mine tailings facility in Newfoundland is the responsibility of local government. Observations indicate potential problems. A respected consulting firm, Stantec, issues a report on the safety of the facility and concludes they cannot tell what is going on because of poor construction records, copious vegetation, and a lack of geotechnical data. They recommend a full investigation. But the local authorities delay, preferring to spend money on inexpensive reports in preference to expensive physical action. The dam fails and tailings spill into the downgradient wetland. Now they are fixing the failure.

2.2 *The Site*

Here is a picture of the Gullbridge tailings dam, showing the area of failure on December 17, 2012.



2.3 *Web Reports*

The Newfoundland and Labrador Department of Environment and Conservation (2012) reported:

> At 7:45 am on Monday December 17, the tailings dam at the former Gullbridge copper mine, central Newfoundland failed while work was under way to stabilize it. The failure resulted in a breach of the 7 m high dam approximately 25 m wide. The dam was impounding mine tailings that were partially covered by water forming a tailings pond. As a result of the failure, the pond drained completely over the next few hours, and a small amount of the tailings escaped. Small quantities of tailings pond water continue to flow from the breach.

The Telegram (2012) gives the most comprehensive report that I can find. Apparently an engineering report prepared about a year prior to the failure resulted in a total lack of action and, as predicted by the report, the dam failed. *The Telegram* reports:

> The tailings dam at the former Gullbridge mine site has collapsed, according to a news release from the departments of environment and conservation, and health and community services. The news release states:
>
> The area of the failure is approximately 50 metres wide and the full height of the dam.
>
> Residents of South Brook are being advised not to drink the water or to use it for consumption, washing food or brushing teeth, as the town's main water supply is 20 kilometres downstream from the site. Washing clothes, handwashing, bathing and washing dishes are considered safe, but further precautions may be necessary.
>
> "Our town water comes from a well, but if the water levels in the river are high enough, then there could be some cross-contamination," Mills said. "We're waiting for formal testing to take place."

The following is from KAIROS Canada (2012) on the failure:

> The provincial environment minister, Tom Hedderson, told CBC that the boggy terrain between the tailings pond and the water supply would help: "There is 400 metres of bog between the dam and the river, and that's where most of the tailings have ended up. It's fortunate in a way, because that becomes a natural filter."

All told the story has an immediate happy "ending:" The government of Newfoundland and Labrador lifted restrictions on water use for a north coast town. The town's water supply is about 26 kilometres away from the dam, and the province's Environment Department said the bog absorbed most of the runoff. The department says in a news release that lab results taken from the town's water supply indicate that it has not been contaminated.

Here is what little I could find out about the mine:

1967 — First Maritimes begins running mining and milling facility at site, sold later same year to K.C. Irving and becomes Gullbridge Mines Ltd.
1971 — Mine closes. About 2.8 million tonnes of copper ore produced during mine life.
1996 — Department of Natural Resources finds a washout in area of wooden "decant," meant to prevent dam overtopping. Repairs made, metal culverts installed.
1999 — Rehabilitation work at site includes demolition of buildings and sealing underground shafts. No documentation available.
2009 — Province commits to dealing with immediate needs at abandoned and orphaned mine sites. Includes addressing tailings dam at Gullbridge.
June 10, 2010 — Staff members with Department of Natural Resources conduct site visit, take photos of a crack/shallow failure in dam.
Nov. 2010 — Repairs made to culvert area, and a decision made that decided culverts would be replaced following year.
Nov. 29, 2010 — Site inspection completed by staff with Stantec (professional consulting services company) for report to provincial government.
March 2, 2011 — Stantec inspection report filed.
June 11, 2011 — Stantec site visit for more detailed Dam Safety Review.
Oct. 26, 2012 — Detailed Dam Safety Review filed with Department of Natural Resources.
Dec. 17, 2012 — Tailings dam failure. Water advisory issued for South Brook.

2.4 *The Stantec 2011 & 2012 Reports*

On March 2, 2011, Stantec issued a report on their dam safety review of the facility that failed about eighteen months later. Here are their findings—repeated verbatim from their report:

- The slopes and crest of the Gullbridge tailings dam were very densely vegetated along the length of the dam. Vegetation coverage was approximately 50-60% along the crest, 75-90% along the downstream slope, and 30% along the upstream slope. As such, it was difficult to observe and evaluate the condition of the dam shell.

- Ice-jacking and/or shelling was observed at the crest and upstream slope area, and differential elevation was also apparent.
- Some erosion and shallow slope failures were noted where the dam shell material was exposed on the downstream slope. The shallow slope failures are believed to be in the same location as the cracks shown in thephotographs recorded on June 10, 2010.
- Since the construction history of the dam is unknown (i.e. if the dam is of rolled-earth cutoff construction, or if there is a rolled-earth core with dumped rock shells (slopes)), it is difficult to determine the cause of the failure shown in the photos. Further, the presence of significant vegetation on the adjacent downstream slope prevented a detailed assessment of the area below these cracks. Given the age of the structure and condition of the remainder of the dam, it is anticipated that these are relatively shallow "sloughing" failures. Further assessment of this area is required once the vegetation is removed.
- Evidence of seepage at the downstream toe was observed at one location, but was difficult to observe elsewhere due to vegetation and the boggy conditions along the downstream toe over most of the dam length.
- Two (2) 900 mm culverts form the discharge outlet for the tailings pond. The culverts bottoms were severely eroded (rusted) on the upstream side. Due to the severe erosion of the culverts, flow through and erosion of the dam structure is occurring underneath the culverts. It is understood that DNR intends on replacing the culverts in the year 2011.
- Potentially acid generating (PAG) material was also observed in the dam embankment near the outlet upstream.
- Materials washed downstream from a relatively recent failure of the dam at the culvert (outflow) locations were observed and the repair area was also evident. Upon consultation with DNR, it is understood the area was repaired in November 2010, and that these materials are the result of the erosion from this repair and a washout of the original decant structure in 1996.
- A beaver house was observed, located approximately 40-50 yards from the southwest end of the dam. Beaver activity was also observed across the dam.
- Two (2) potential historical discharge locations were observed on the upstream side in the form of a standpipe and old wood frame, and a minor inlet/channel with some timber.

Stantec recommended that a $152,500 detailed dam safety inspection be undertaken. Work they recommended included: removal of vegetation; detailed survey and bathymetry; geotechnical investigation; borehole installation; hydrological assessment; tailings characterization; and dam safety review. They said that an order of magnitude estimate for the cost of remedial works would be about $235,000.

How much of the recommended work was undertaken, I cannot establish. A Stantec report dated December 12, 2012 states:

> "At the request of the Newfoundland and Labrador Department of Natural Resources (NLDNR), Stantec Consulting Ltd. (Stantec) carried out a supplemental geotechnical and hydrotechnical assessment for the tailings dam at the former Gullbridge Copper Mine in central Newfoundland. This review was initiated as a result of NLDNR revising the Dam Hazard Classification of the tailings dam from Low to Significant. Specifically, the purpose of this study was to determine if the change in classification had any impact on the recommended remedial measures for the Gullbridge Dam rehabilitation as provided in the Tender Documents issued by Stantec dated August 9, 2012."

It appears something was being done - at least recommendations were in the works. But before anything was done, on December 17, 2012 the dam failed as described above. Nature moved faster than those responsible. The picture below shows remedial works being constructed: a berm to contain spill and sediment and provide for repair of the failure zone.

2.5 *Lessons Learnt*

Gullbridge is a typical example of local authorities taking over a tailings facility without making the mine close it or even document how it was built. The local authorities appear not to have had the capacity to manage the facility. They engaged reputable consultants but failed to act on their advice, and appear to have stalled in order to minimize expenditure.

The fact is it is expensive to maintain so-called closed tailings facilities. It takes expertise and experience to look after closed tailings facilities. And even the best consultants are cowed by clients who do not want to spend money, regardless of how dire the situation.



3 PHILEX MINE, PHILLIPINES

3.1 *Plot Summary*

A tailings pond in the Philippines at Philex Mining Corporation's Padcal gold mine is discovered to be leaking on August 1, 2012. Philex suspends its operations in order to investigate the source of the leak. The company deploys cleanup crews to remove chemicals and sediments discharging into the river nearby. The tailings failure was said to have been caused by heavy rains. However, I believe the spill resulted from failure of the penstock.

The mine is owned by a Hong Kong mining company and they have done a superb job of controlling the flow of information about what happened. The authorities have fussed and fumed, but to no avail. It seems the penstock is now plugged and mining and tailings disposal continues apace.

3.2 *Web Reports*

TechnoMine (2012) reports that Fay Apil, acting MGB Cordillera [a government agency] director, said that they inspected the mine's tailings dam at 5:30 p.m. Friday and did not detect signs of the breach. The leak may have burst from a break in the dam's penstock, the gateway which discharges rainwater that collects on the surface of the tailings pond, she said.

Here is a brief statement from the web about the failure of the Philex tailings facility. It is part of a statement by a Phillipine senator, Sen. Osmeña, in a document issued by the Cordillera Peoples Alliance [an activist group.]

> In August 2012, the TP3 collapse released 20 mmt of mine tailings into the Agno. The Philex (TP3) failure is one of biggest mining disasters in the country.
>
> 20 mmt roughly translates to 400,000 metric tons/day, assuming 50 days since the first leak on August 1, 2012. The Philex minespill is 47 times the garbage generated in Metro Manila

(at 8,500 metric tons/day) and 12.5 times larger than the Marcopper tragedy in Marinduque. 20 mmt is equivalent to 20 billion kilograms, and, if one was to dump all these in one hectare of land or open space, the mine tailings would be 800 meters thick. And this is probably the very amount that went to the San Roque Dam downstream of the Agno in Pangasinan.

The collapse and failure of Philex's TP3 wrought serious devastation and destruction to indigenous peoples of Itogon and Tuba in Benguet and in the peasant and goldpanning communities of San Nicolas and San Manuel in Pangasinan.

The Agno River is historically polluted with the mine tailings of Philex since its operations in 1958, as it was only in 1967 that its Tailings Dam 1 operated. Its Tailings Pond 2 collapsed in 1992, resulting to the release of 80 million metric tons (mmt) of tailings.

Many reports appeared on the web subsequent to the failure. None gave an account of what caused the failure. On my blog, I THINK MINING, which is about things mining, I wrote: "None really gets to the nub of what is going on. There are vague statements on failure, seepage, sediments in rivers, non-toxic discharges, and penstock failures. My first take is that seepage occurred at penstocks and water and sediments flowed into river."

Here is a statement from a blog called A Cynic Meets Hope (2012) that supports this opinion:

…The Mines and Geosciences Bureau (MGB) has earlier reported that on August 1, 2012, TP3 suffered a tailings spill where the tailings breached the lower portion of Penstock A and discharged tailings into the Balog River, a tributary of the Agno River. This was followed by three more major occurrences of tailings leaks up to August 30. The Environmental Management Bureau (EMB)-CAR estimated the volume of tailings discharged from August 1-14 at 6 million metric tons.

Other reports tell of trying to plug the penstock leak with cement and an old school bus thrown down the sinkhole that formed in the impoundment as a result of spilled tailings.

Here from Google Earth is a picture of the mine, showing the various tailings impoundments. The facility that failed is towards the bottom right of the picture.

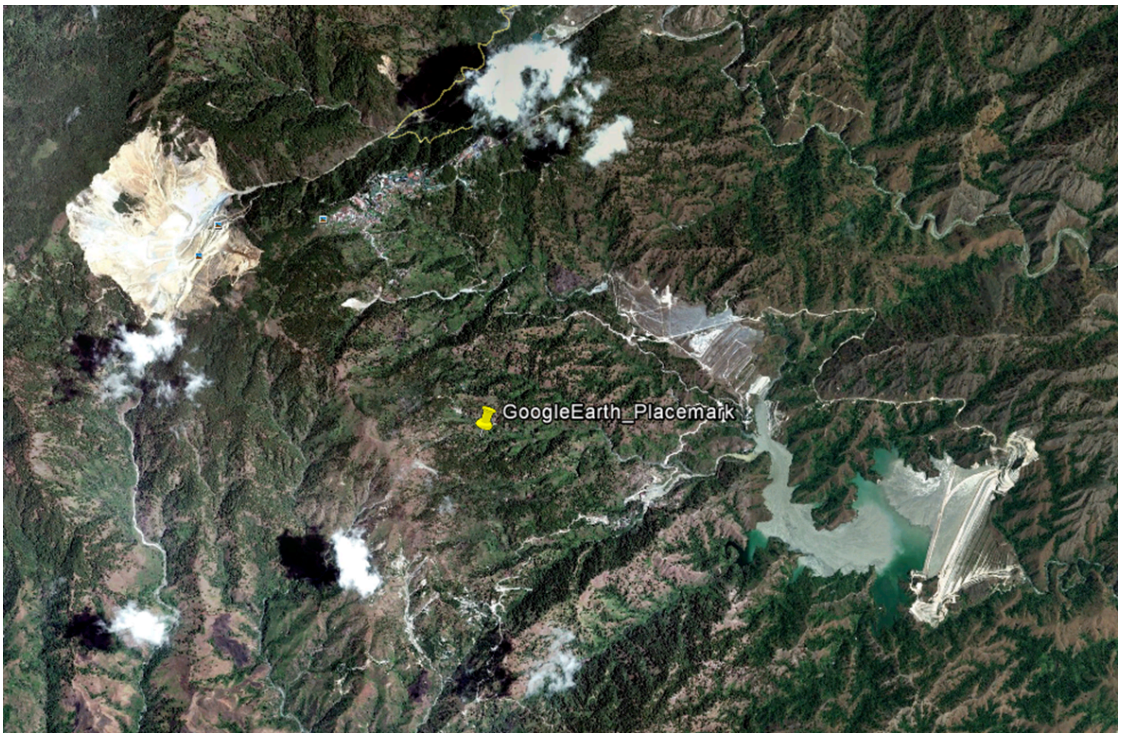
At the time of writing this paper, I found and copied the following news report (but it appears that it can no longer be opened):

NATIONAL POWER Corp. (Napocor) wants Philex Mining Corp. to pay over P6 billion in compensation and penalties over last year's Padcal tailings pond leak, which allegedly damaged a watershed and led to generation losses.

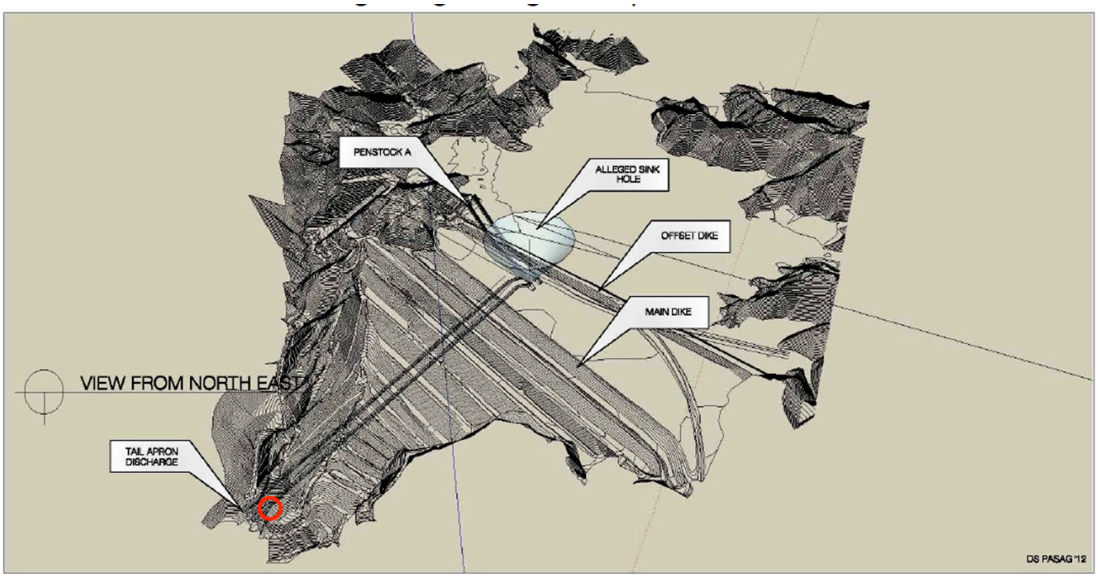
In a May 10 letter to Philex President Eulalio B. Austin, Jr., Napocor Vice-President Melchor P. Redulme claimed that tailings leak had affected the San Roque Watershed Reservation, over which the state-owned power firm has jurisdiction.

A total of 13,513,507 cubic meters of waste was said to have been deposited in the San Roque Multi-Purpose Facility's reservoir, which "reduced the volume of water to be used for power generation."

"The dislodged volume of water could have converted an annual equivalent energy of 4,820,000 kWh (kilowatt-hours), which according to our engineers accounts to P6,266,000.00 per year while the mine tailings are not removed ..." Mr. Redulme added.



At the time of the failure, I found the following figure on the web - I cannot now find it again to reference the source.



Also I found this picture of the sinkhole on the surface of the impoundment.

3.3 *Lesson Learnt*

This failure proves yet again that penstocks should not be used. I believe the root cause of the Bafokeng tailings dam failure was penstock failure; nobody agrees with me, but I walked the site longer and harder than anybody else. The new Bafokeng tailings dam (which I designed) has an old crumbling penstock and in spite of many pleas they will not block it up. Concerns that a barge and pipes will be stolen and the additional cost of pumping prompt them to continue to let gravity move the supernatant water.



This failure also proves that the size and public pronouncements of the mining company are vain hot-air when it comes to the tailings facility. The penstocks had leaked for weeks before the main event; yet nobody did anything. And prior to the event, the government was supine. After the event, the government is grousing, suing, and making noise. We will see what happens.

4 HB MINE, SALMO, BRITISH COLUMBIA, CANADA

4.1 *Plot Summary*

The mine closes and very intelligently gets the local authorities to take over the site as a landfill. It appears the landfill folk in the local authorities engineering group did not understand tailings. Environmental groups warn of the dangers, but nobody hears them. It rains a lot, and piping and leaks are observed. The earth dam sloughs; a sinkhole develops; tailings move out into the environment; it will now cost almost a million dollar to fix; and the taxpayer pays.

4.2 *Web Reports*

Here is the text of the first report that I read (Castlegar, 2012):

> The Regional District of Central Kootenay (RDCK) Emergency Operations Centre is working with various agencies to ensure public safety for travelers and area residents in response to concerns about sloughing and seepage from a tailings pond.
>
> The tailings pond has been impacted by heavy rainfall yesterday and ongoing creek/stream inflows. Some sloughing of the earthen dam was observed yesterday and there is ongoing seepage from sections of it. The tailings pond is located east of Highway 3 and 6, and south of Emerald Road, near Salmo driving south towards the Kootenay Pass summit.
>
> The Regional District purchased the former HB Mine property as part of its central landfill area in 1998.
>
> Residents who could be affected by a structural failure impacting the highway and properties below the site have been notified by the RCMP. Currently flaggers are positioned on the highway as a precautionary measure.
>
> Geotechnical engineers have installed three pumps to decrease the level in the tailings pond as a first step. Additional larger diameter pumps and siphoning hoses are en route to continue to reduce water levels. An outlet channel is also being deepened. Several excavators are on site and will work at in-filling areas of seepage when they are able to be deployed safely.
>
> Environmental monitoring and reporting is ongoing and 24 hour security has been implemented at the site. The weather forecast is favorable – with little or no precipitation forecast – and geo-technicians and engineers on site indicate the area is gradually getting drier. This should permit additional remediation planning and on-site work to proceed over the next few days.

By way of background, I found this earlier report expressing concern about possible failure of the facility (I can no longer find the website from which I downloaded the following):

The purpose of this report is to compile a general inventory and brief history of the historical mines, tailing piles, and ponds in the Salmo River Watershed. We have broken the watershed down into specific areas in which there was dense mine development. Each area is discussed and the major producing mines and mills and significant tailing piles are located. These areas include some of the tributaries of the Salmo River as well as the river itself.

We have prepared maps in order to give a visual perspective of the density of mines in each area. It is necessary to say that these maps are in no way exhaustive, there were at one time in this valley, around the turn of the last century, some 600 operating mines. The Salmo Watershed Tailings and Mine Locations map on the next page illustrates all of the mines and tailings that we could look at in yellow and the tailing piles of priority concern to the health of the Salmo River, in red.

The tailing piles were prioritized by their visual size and proximity to water courses. The tailings of priority concern are significantly large and directly adjacent to the Salmo River. The other tailings that we looked at were visible by helicopter or by vehicle when exploring these old mining roads.

We would like to stress that it is probable that the tailings these mines have produced may continue to have significant impact on our precious waterways. It is for this reason we are trying to identify areas of concern. We hope that each one of these areas will receive further attention in order to recruit them back toward naturally functioning ecosystems.

An explanation of the milling processes includes flow charts to show which part of the mineral extraction process the mine waste comes from and why. Common environmental hazards due to the mineral extraction process such as acid mine drainage and metal toxicity are also discussed.

The two main areas of concern that we were able to identify are the Yankee Girl Tailings located at the tributary of the Salmo River and Wildhorse Creek, and the Wesko tailings from the Center Star mine located near the confluence of the Salmo River and Ocsar Creek. These two tailings locations are by no means the only locations that we hope community action can help deal with in the near future. Other locations in the Sheep and Wildhorse Creek watersheds deserve our consideration.

Here is a report (from a website no longer available) that puts a different spin on what is happening. Here they talk of washing away of the embankment, not merely too much water. This shows just how difficult it is to get an objective story on the malfunction of even a tiny old tailings dam. So much for the theory that modern practice precludes such events.

The Regional District of Central Kootenay (RDCK) Emergency Operations Centre said in a release that they are working with various agencies to ensure public safety for travelers and area residents. The tailings pond, which is an area of refused mining tailings from an old zinc and lead mine, was impacted due to the water, and some sloughing of the earthen dam was seen on Tuesday. The RDCK also said there is "ongoing seepage from sections of it."

Then this rather cavalier statement from the *Vancouver Sun* (again the link I have produces a message of no longer available).

The Regional District of Central Kootenay issued the declaration for the Nelson-Salmo area over concerns that part of the retaining wall for the old Hudson's Bay mine tailings pond had been washed away by heavy rains. Bill MacPherson of the regional district's emergency operations centre said Wednesday that engineers were working on plans to shore up the dam. He said rumours the dam could collapse were exaggerated. "That's obviously a worst-case scenario and that's not where it's at right now," said Macpherson. "It's dependent on the weather and the weather is favourable."

Finally this from HQKootenay.com:

So far so good. The draw down of water from the compromised Tailings Pond near Salmo is continuing and there have been no breaches to report. RDCK Emergency Operations Spokesman Bill Macpherson says more larger pumps were expected to be on site. He says those are likely installed or being installed and Teck has also provided siphoning hoses to help draw the water down in the pond. He says with the improving weather conditions they should be moving heavy equipment in soon to shore up the retaining walls. The heavy rains

compromised the pond which contains toxic tailings from an old mine and the fear was it could burst and wash over Highway 3.

On 10 July, 2012 the *Globe and Mail* reported as follows:

> Heavy rainfall and a sinkhole contributed to the partial failure of an earthen dam in the Kootenay region, say local officials. The dam on the site of an old Hudson's Bay lead-zinc mine south of Salmo, B.C., is part of the retaining wall for the mine's tailings pond. Community officials declared a local state of emergency last week after the dam began to leak. "The sinkhole in combination with heavy rains, caused the slough, the failure, and then the subsequent seepage," said Bill Macpherson, a spokesman for the regional district. Mr. Macpherson said officials found the sinkhole on the inside of the dam, near the centre of the structure, after draining down the pond. The sinkhole was found about 1.8 metres below the normal high water mark, and regular inspections would not have revealed it because of its location and depth, said a statement from the district. Mr. Macpherson said the leaks have now been stopped, and officials are building up the face of the dam with rock, earth and fill. "The whole area's drying up, so it's certainly improved from what it was," he said.

4.3 *The Aftermath*

Here is all I can find about what was done after the failure (my original link no longer responds):

> More than $800,000 was spent on emergency work to stabilize the tailing pond at the HB Mine site near Salmo.
>
> The site was under a state of emergency from July 3 to 25, after heavy rains caused a sinkhole to form on the underwater wall of the earthen dam, causing some sloughing and seepage along the slope. High capacity pumps were brought in to reduce the water level behind the dam while repair wok got underway.
>
> Regional District of Central Kootenay, owners of the HB Mine property, co-ordinated the emergency response, but the bill will be covered by the province.
>
> Jim Gustafson, RDCK chief administrative officer, said the same is true for all the environmental disasters that resulted in states of emergency this summer.
>
> "Whether it's the minor slide in Thrums, the flooding around Kootenay Lake, the massive landslide in Johnson's Landing - it all follows the same process," he explained. "Once a state of emergency is declared, we plan the mitigation in conjunction with the province ... and they approve what sounds reasonable."
>
> At the HB Mine site, the bulk of the emergency funds were spent on reconstruction of the failed part of the dam, as well as paying someone to monitor the dam 24/7 for three weeks, and to keep two flaggers on standby near the highway below, so they could immediately stop traffic if the structure did fail.
>
> With the state of emergency lifted, the burden of paying for ongoing work at the dam has shifted back to the RDCK. Gustafson said there is still periodic pumping and monitoring needed at the site. As well, he expects consultants will be needed to help the RDCK plan for the future of the site, which may include the decommissioning of the dam.
>
> "The next phase is to do an assessment of the site and make a determination of how to manage the area behind the dam, with or without water and how to manage tailings and all other impacts associated with that site," he said.

4.4 *Lessons Learnt*

The taxpayer pays again! As good a lesson as any.

Sometimes environmental groups know or have more insight than local landfill engineers, who are probably afraid to speak up even if they do know.

I heard somewhere that Teck helped with repairs. Bravo the BC mining industry, which can hardly afford another black eye. Maybe we should let a group of smart mining tailings engineers advise local governments on closed tailings facilities for which they have responsibility.

5 CONCLUSIONS

Tailings dams fail. The failure rate in 2012 was average. The causes are ill-informed responsible parties; too little funding; arrogance on the part of regulators; cowardly consultants; and complacent public and politicians.

We may conclude that the three 2012 tailings failures that became public (there were surely others not made public) can be attributed to the Black Swan. They were not acts of God; they were not force majeure; they simply were not foreseen or anticipated by the honest folk responsible.

In hindsight it is easy to be critical. However, there but for the grace of God go I. Be aware and ever vigilant if you deal with a tailings facility, open, operating, or closed.

6 REFERENCES

A Cynic Meets Hope (2012) At this link: http://cynicmeetshope.wordpress.com/2012/10/04/philex-mine-spill-results-of-cso-investigation-released/

Castlegar (2012) News Report at this link: http://castlegarsource.com/news/update-tailings-pond-19830#.Ua1WGZ1rbIU

Globe and Mail (2012) At this link: http://www.theglobeandmail.com/news/british-columbia/mines-leaky-dam-blamed-on-heavy-rain/article4401820/

HQ Kootney (2012) At this link: http://hqkootenay.com/home/news/v/Local/79838/Work-Continues-at-Tailings-Pond-Near-Salmo

KAIROS Canada (2012) http://www.kairoscanada.org/sustainability/tailings-ponds-a-toxic-legacy-for-south-brook-2/

Newfoundland and Labrador Department of Environment and Conservation (2012) At this link; http://www.env.gov.nl.ca/env/waterres/southbrook/gullbridgedam.html

Stantec (2011) Dam Safety Review Various Mine Sites, Former Gullbridge Copper Mine NL. March 2, 2011.

TechnoMine (2102) At this link: http://technology.infomine.com/articles/1/8499/tailings.failure.philex/local.perspective.on.aspx

The Telegraph (2012) At this link http://www.thetelegram.com/News/Local/2012-12-17/article-3141752/Update%3A-Tailings-dam-collapses-at-former-Gullbridge-mine-site/1

Dams

Dams and Liner Systems

State of practice dynamic analysis of a rock fill dam subjected to high seismic earthquake conditions

Amanda L. Dolezal, Jorge L. Castillo & Allan J. Breitenbach
Ausenco, Denver, CO, United States

ABSTRACT: This paper presents the state of practice dynamic analyses for a geomembrane lined large rock fill dam located in a high seismicity zone in southern Mexico. The Maximum Credible Earthquake (MCE) was considered in the design for long term closure seismic event greater than 8.0 Magnitude.

The dynamic analyses were conducted as non-linear two-dimensional analyses using the Fast Lagrangian Analysis of Continua (*FLAC*) computer code. The dam was modeled considering the UBCHYST nonlinear hysteretic damping, response analysis program developed at the University of British Columbia for predicting the amount of deformation movement in the dam fill for a given design earthquake peak ground acceleration intensity and duration.

The results of the state of practice dynamic analyses indicate that dam crest deformation movements can be controlled and diminished by substituting high strength non-plastic rock fill materials with well compacted cohesive granular soils in the top crest area section of the embankment.

1 INTRODUCTION

A downstream rock fill dam was designed for a new tailings storage facility (TSF) located in a high seismicity zone of Mexico. Compacted downstream rock fill dams have been constructed in seismic areas of South and Central America since 1996 due the large number of upstream method dam failures (both static and dynamic). Rock fill dams have been shown to be the most stable type of dams in high seismicity regions of the world for water reservoirs and mine tailings storage.

The 70 m high dam will be constructed primarily of rock fill material in a single phase with allowance for additional downstream construction raises as needed for gold tailings storage within a composite geomembrane lined impoundment. The crest section of the dam will be constructed with a 7 m wide crest and 7 m deep zone of cohesive clayey gravel fill. The material properties of the clayey gravel fill were varied in order to determine the relationship between cohesive gravel fill versus non-cohesive compacted rock fill deformation movements within the crest section of the dam under high seismic loading conditions.

The dam dynamic stability analyses were conducted using the state of practice Fast Lagrangian Analysis of Continua (*FLAC*) computer modeling program.

2 SITE CONDITIONS

2.1 *Location and Regional Seismic Hazard*

The TSF is located in southern Mexico, in the central part of the State of Oaxaca. A seismic hazard study was previously conducted and the site was found to be in a very high seismic hazard zone. Based on published global seismic hazard maps (GSHAP), the peak ground acceleration (PGA) values expected at the site range from 0.48 to 0.51g for 475 year return period. The Maximum Credible Earthquake (MCE) was considered as the seismic design event for operations into long term closure with MCE PGA determined to be 0.56g.

2.2 *Groundwater Considerations*

The rock fill dam is founded on sedimentary/volcanic rock. The exploration boreholes developed in the area indicate that the ground water is deep within the impoundment site. In addition, the tailings impoundment will be fully lined with a composite geomembrane/GCL liner system. Therefore, the dam and foundation are anticipated to remain unsaturated throughout operations to closure.

3 MODEL DETAILS

3.1 *Geometry*

A cross section was developed for the most critical maximum section of the rock fill dam to use for the dynamic stability modeling. The critical cross section used in the model is shown on Figure 1.

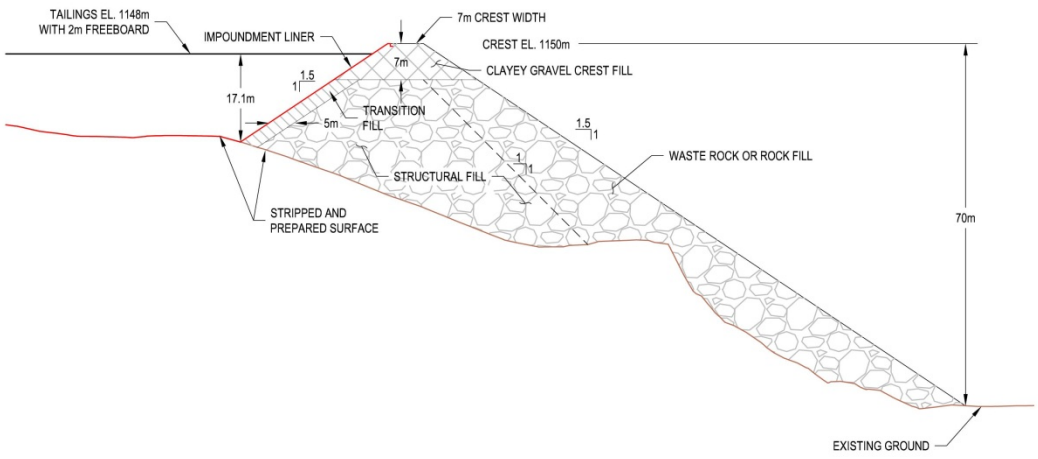


Figure 1. Ultimate Dam Cross Section Modeled in FLAC

The rock fill dam will be 70 m high (measured from the dam crest to the downstream toe) with a 7 m wide crest at El. 1150 m. The embankment will be constructed primarily of rock fill material in a downstream construction fashion. A 5m wide zone behind the upstream face of the dam will be constructed with transition fill material and covered with a composite geomembrane and geosynthetic clay liner (GCL) system. The crest of the dam will be constructed of a 7 m thick zone of clayey gravel fill extending from the upstream face through the entire dam to the downstream face. The maximum tailings elevation will be at 1148 m allowing for 2 m of freeboard.

3.2 *Material Properties*

For the static analyses portion of the FLAC model the dam fill properties were modeled using linear behavior in order to simplify the model. The analysis incorporates Mohr-Coulomb failure criterion. Effective stress properties were utilized for the analysis. The material properties adopted to use on the dynamic analyses are given in Table 1.

Table 1. Material Properties

Material Description	Moist Unit Weight (kN/m^3)	Mohr Coulomb Cohesion (kPa)	Friction Angle (Degrees)
Bedrock	26	4000	36
Clayey Gravel Crest Fill	23	Varied from 15, 30, and 50	38
Transition Fill	18.5	0	38
Structural Fill	23	0	Varies with depth from 44.5 to 36.2
Waste Rock or Rock Fill	23.3	0	Varies with depth from 51.5 to 46.0
Tailings Modeled as liquid pressure	17		
Rockfill / Bedrock Interface		0	40

The soil and rock fill static properties adopted were based on the values obtained from published literature and previous experience with similar materials (Hunter, et al, 2003; Bowles, 1996; Kulhawy, 1998). The tailings were assumed to be fully liquefied at zero strength in a seismic event and were modeled as an applied pressure to the upstream face of the dam. This neglects the shear strength of the tailings prior to the onset of liquefaction as well as the nominal post-liquefaction shear strength and adds conservatism to the results.

Shear strength properties for the bedrock and transition zone were estimated from experience with similar materials on previous projects. The shear strength properties of the rock fill were modeled as a function of effective vertical stress (Leps, 1970).

Based on observed rock core samples taken from onsite boreholes in non-ore materials, two separate rock fill strengths were used to model the dam fill materials. For the structural fill within the upstream and central portions of the dam, the selected rock fill strength for design was based on the "low density" rock fill from Leps chart with no assumed cohesion. The strength used for the waste rock or rock fill placed on the downstream face of the dam were considered a median relationship between "average rock fill" and "high density" rock fill from Leps graph with no assumed cohesion.

The material properties of the crest portion of the dam was varied in order to determine the optimal material properties if the crest fill materials to reduce the amount of displacement and deformation experienced within the crest of the dam. The fill material used to construct the crest of the embankment will be placed seven meters thick; compacted at 1.5H:1V both upstream and downstream. A base case was performed for this analysis that assumed the crest portion of the embankment will be constructed of the same waste rock or rock fill placed on the downstream face of the dam and was assigned the same material properties described above based on the "average rock fill" and "high density" rock fill from Leps graph with no assumed cohesion.

Based on previous construction experience, the material type of the crest portion of the dam was changed to a clayey gravel fill for the remainder of the trials in this analysis. The strength properties for the clayey gravel fill was based on the material encountered onsite at possible borrow areas. The cohesion of the clayey gravel fill was varied from 15kPa, 30kPa and 50kPa throughout the trials in order to examine the differences in displacement and deformation experienced within the crest portion of the dam with these varying levels of cohesion. The friction

angle of the clayey gravel fill was kept constant at 38 degrees throughout all trials in this analysis.

An interface between the rock fill dam base and the foundation was also applied to the model. This interface was given a friction angle of 40 degrees. Keys will be developed into the foundation during construction, prior to the rock fill being placed on top of it. The keys will help to prevent some slippage along the interface between the dam and the foundation. Due to the large difference in scale of the keys in relation to the overall dam, the keys are not directly incorporated into the geometry of the cross section modeled in FLAC.

4 NUMERICAL MODELING APPROACH

The static and the dynamic analyses were performed using a finite difference technique-based computer code, FLAC (Fast Lagrangian Analysis of Continua) Version 6.0 computer program developed by Itasca Consulting Group Inc. (2008). FLAC generates the equations of motion in finite difference form over a mesh covering the modeled section and solves the equations in explicit form in the time domain using very small time steps. The small time steps allow accurate modeling of the non-linear inelastic stress-strain behavior. The mesh size for the FLAC model was selected to provide accurate seismic wave transmission.

The static analysis was conducted primarily to establish the state of stress following construction prior to earthquake loading. The pre-earthquake stress condition within the dam is represented by the mean effective stress (σ'_m) calculated for each element of the model grid as shown in Equation 1 below:

$$\sigma'_m=(\sigma'_{xx}+\sigma'_{yy}+\sigma'_{zz})/3 \quad (1)$$

As described later, the mean effective stress is used in calculating the confining stress dependent shear modulus at each point and time during the dynamic analysis. The associated inelastic dynamic displacements are modeled as the ground motion proceeds, and the displacement field is predicted directly in the modeling approach adopted.

4.1 *Damping*

Dynamic response of earth and rock fill structures is very dependent on the amount of energy dissipated internally by the fill during shaking. This mechanism of energy dissipation is commonly referred to as "damping". The magnitude of damping is reflected in, and is proportional to, the “area” enclosed by the stress-strain hysteresis loop for a complete loading-unloading cycle, which in turn depends on the fill type, and increases with the level of shear strain.

There are two basic approaches to model or incorporate damping in dynamic analyses: 1) equivalent viscous damping, and 2) hysteretic damping. A system in which the damping at any instant is proportional to the velocity of motion is said to possess viscous damping. This model does not produce realistic response of earth structures, nor does it account for the permanent displacement due to the inelastic behavior of the material. In a hysteretic damping model, damping is proportional to displacement, but in phase and velocity. For seismic loading of earth structures, a hysteretic model of damping seems to be more realistic. Accordingly, for the current analysis, the hysteretic damping approach was adopted by incorporating into FLAC, a state of the art hysteretic damping subroutine UBCHYST developed at the University of British Columbia (E. Naesgaard and P. Byrne, 2011). UBCHYST is meant to be used with highly permeable granular soils and non-saturated granular soils.

The UBCHYST subroutine allows for modeling the nonlinear and inelastic stress-strain response of soil directly in the dynamic analyses. This is achieved by treating the material damping and tangent modulus term as a function of the level of stress and strain reached at each point in the time and space, and keeping track of whether the loading or unloading is taking place. Such response, including the phenomenon of “size of stress-strain loops vary with strain level”,

is very similar to that observed in cyclic loading laboratory tests at very low strain levels (e.g. 0.0001 to 0.01 percent strain), and a small amount of viscous damping, generally in the range of 1 to 12 percent, is added to match the measured response.

4.2 *Shear Modulus*

Generally the secant shear modulus is defined in terms of the small-strain amplitude shear modulus (G_{max}) and the variation of normalized shear modulus at any strain level (G_{sec}/G_{max}) with the shear strain amplitude. The secant shear modulus reduces as the shear strain amplitudes increase.

The shear modulus is strongly influenced by three main factors: 1) the confining pressure, 2) the strain amplitude, and 3) the void ratio. An empirical, but convenient relationship between the shear modulus and the confining pressure developed for cohesionless soils given below in Equation 2 (Seed and Idriss, 1970) was used in the dynamic analysis:

$$G_{max} = 21.7K_{2,max} * Pa * \left(\sigma'_m\right)^{1/2} \quad (2)$$

Where, the mean effective confining stress σ'_m and the maximum Shear Modulus G_{max} are in kPa units and the influence of the void ratio and the strain amplitude is reflected in the soil modulus coefficient $K_{2,max}$. According to Byrne (2013) for loose and dense rock fill, the value of $K_{2,max}$ varies from 100 to 160. For the analysis of the rock fill tailings dam, the maximum recommended $K_{2,max}$ value of 140 was adopted for the compacted rock fill.

4.3 *Model Calibration*

The hysteretic damping model was calibrated to match the laboratory test data for gravel and rock fill using a single element simulation in FLAC. Due to the large diameter of the test specimens and expensive laboratory facility required, there are limited investigations of the shear modulus and damping ratios presented in the form of the stress-strain loops for coarse gravel and rock fill materials.

Accordingly, for gravel and rock fill applications, an indirect method of verification and model calibration has been adopted. Stress-strain loops for gravel and rock fill were produced using a simple hysteretic total-stress constitutive model (UBCHYST). The hysteretic damping model calculates the tangent shear modulus (G_t) as a function of the peak shear modulus (G_{max}) multiplied by a reduction factor that is a function of the developed stress ratio and the change in stress ratio to reach each failure (E. Naesgaard and P. Byrne, 2011). The tangent shear modulus is calculated as follows in Equation 3:

$$G_t = G_{max} * \left(1 - \left(\frac{\eta_1}{\eta_{1f}}\right) * R_f\right)^n * Mod1 \quad (3)$$

Where:
η_1 = Developed stress ratio
η_{1f} = Change in stress ratio
n = Calibration factor (typically 2 to 4 for rock fill)
R_f = Calibration factor (typically 0.70 to 0.98)
Mod1 = Reduction factor for first-time or virgin loading

To calibrate the modulus reduction and damping, data are typically adjusted by the exponent "n" and/or "R_f". Calibration trials were made for the cases where the tangent shear modulus is calculated with exponents "n" of 2, 3, and 4. The value of "n" equals 4 was found to be the best fit to the rock fill laboratory shear data, and then the "R_f" factor was varied to further calibrate the model. The "R_f" factor was initially set at its maximum value of 0.98 for the calibration trials where the "n" factor was adjusted. Once "n" was set to 4, the "R_f" factor was then set at its

minimum value of 0.70 for the next calibration trial and then "R_f" was varied within this range until a reasonable fit to the rock fill shear data was established.

It is not practical to compare the rock fill stress-strain loops calculated by FLAC to stress-strain loops obtained from laboratory testing due to the laboratory limitations in testing large rock fragments in a rock fill. Hence to calibrate the model G_{sec}/G_{max} and damping, calculations from the stress-strain loops were compared to curves normally used for either the equivalent viscous damping or equivalent linear approach published in the technical literature.

The hysteretic model modulus results provide a reasonable fit to the published modulus data when the "n" factor exponent of 4 and the "R_f" factor of 0.91 are considered. Figure 2 shows the G_{sec}/G_{max} curves used for calibration as well as the model results, which are shown as brown triangles (Δ).

Damping calculated using the hysteretic model does provide a good match to the published damping data for the low range of shear strain (0.0025% to 0.01%) for rock fill and gravelly soils as shown on Figure 3. However, for high shear strain range (0.025% to 0.1%) the calculated damping appears to provide a suitable match to the back-calculated damping values determined through actual measurement of rock fill embankment response during earthquakes (Iwashita et al, 1995).

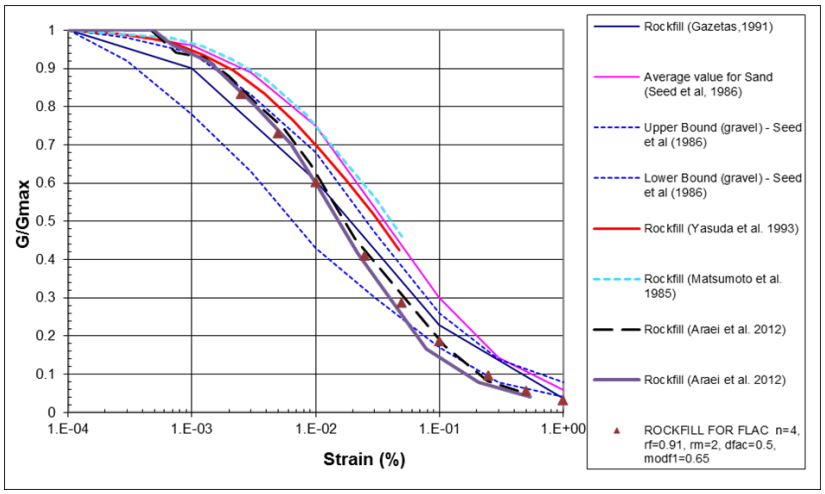


Figure 2. Published G_{sec} / G_{max} vs. Stress-Strain Curves Compared with Selected Rock Fill Curve (from calibration)

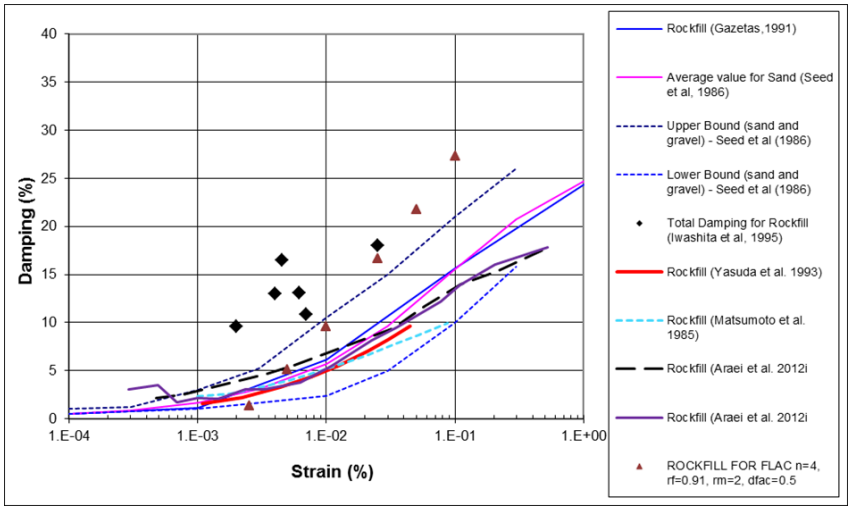


Figure 3. Published Damping vs. Stress-Strain Curves Compared with Selected Rock Fill Curve (from calibration)

4.4 *Earthquake Ground Motion*

As shown in the seismicity hazard study previously performed for the site, the controlling MCE for the current analysis was taken as a large magnitude intraplate event (Ms 8.0) at a source-to-site distance of 35 km resulting in 0.56g peak horizontal ground acceleration.

For the dynamic analysis a suite of three or more earthquake time-histories that correspond to the design earthquake are required as the input ground motion. These records should be selected on the basis of the duration of the event, tectonic setting (subduction zone thrust faulting versus shallow crustal faults), source-to-site distance, frequency content, and local site conditions. Generally, a suite of earthquake time-histories selected on the above-mentioned basis, are used to impart some sort of randomness to the input ground motion and avoid potential bias in the results due to any one of those time-histories in particular.

A total of four earthquake time-histories were selected, modified in the frequency domain to obtain a better fit to the spectra design, and applied to the model as seismic load for dam dynamic analyses. This technical paper only shows the results of the Caleta del Campo N00W earthquake time-histories from a 19 September 1985 Mexican earthquake, which induced the largest displacement into the model.

The acceleration record used for the dynamic analyses of the rock fill dam is based on the acceleration measured at rock outcrops during the seismic event. The accelerations measured at the rock outcrops are not appropriate to apply directly to the base of the FLAC model since some of the propagating waves will be transferred upwards and the remaining will be transferred downwards. Therefore, in order to determine the appropriate reduction factor to apply to the input acceleration record, an analysis was performed on just the bedrock foundation portion of the model to determine the level of amplification of the waves as they transfer through bedrock with these particular material properties.

5 RESULTS AND FINDINGS

The displacement experienced in the horizontal and vertical directions as well as the peak acceleration measured at several points within the dam were measured for each trial performed. The upstream crest, mid-crest and downstream crest of the dam were monitored throughout all the trials for displacement experienced under the seismic loading conditions. The results of the trials and recorded measurements can be seen in Table 2.

Table 2. Results of Dynamic Stability Analyses

Fill Type	Crest Cohesion (kPa)	Acceleration (g)		Upstream-Crest Displacement (m)		Mid-Crest Displacement (m)		Downstream-Crest Displacement (m)	
		Mid-Height Dam	Mid crest	X Disp	Y Disp	X Disp	Y Disp	X Disp	Y Disp
Non-Cohesive Compacted Rock Fill	0	0.59	0.80	1.20	0.30	1.90	1.70	4.00	2.80
Cohesive Granular Fill	15	0.54	0.78	1.00	0.55	1.20	0.70	2.25	1.20
	30	0.78	0.55	0.95	0.45	0.90	0.60	1.15	0.60
	50	0.69	0.51	0.90	0.45	0.90	0.50	1.10	0.55

The base case trial (non-cohesive compacted rock fill at the crest zone) showed the largest displacements measured within the crest of the dam, where the downstream crest of the embankment experiences 4.0 m of displacement in the horizontal direction and 2.8 m in the vertical direction and a crest acceleration of 0.80g. The trial assuming 15 kPa cohesion within the clayey gravel shows considerably less displacement at the downstream crest in both the horizontal and vertical directions, measuring 2.25 m and 1.20 m, respectively. Figures 4 through 6 depict the FLAC output results for modified Caleta del Campo N00W time-history considering 15 kPa cohesion within the clayey gravel fill.

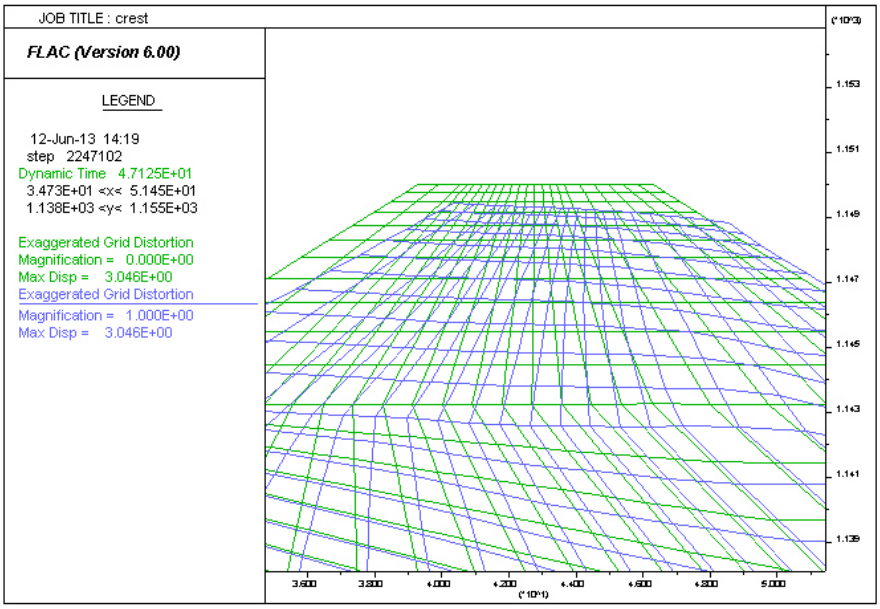


Figure 4. Deformed Grid at Crest

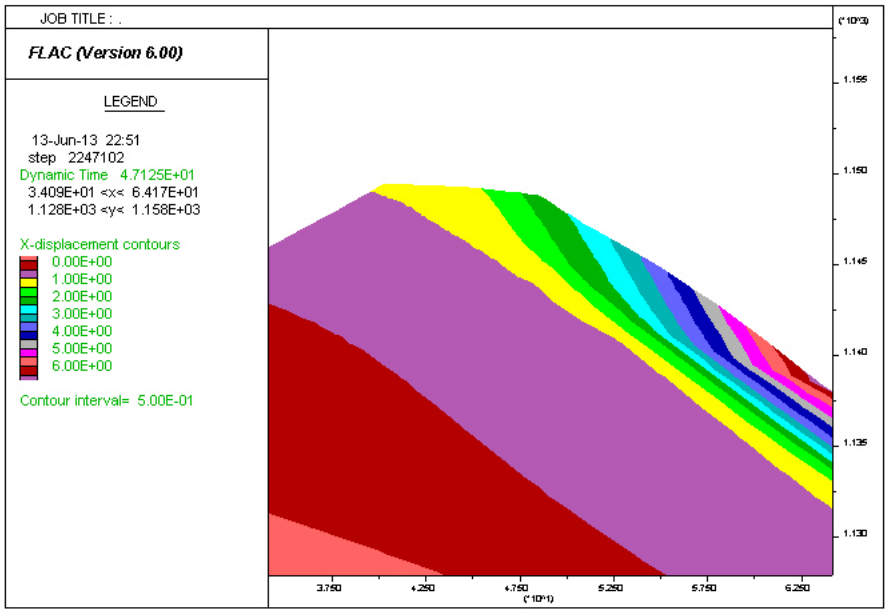


Figure 5. Horizontal Displacement

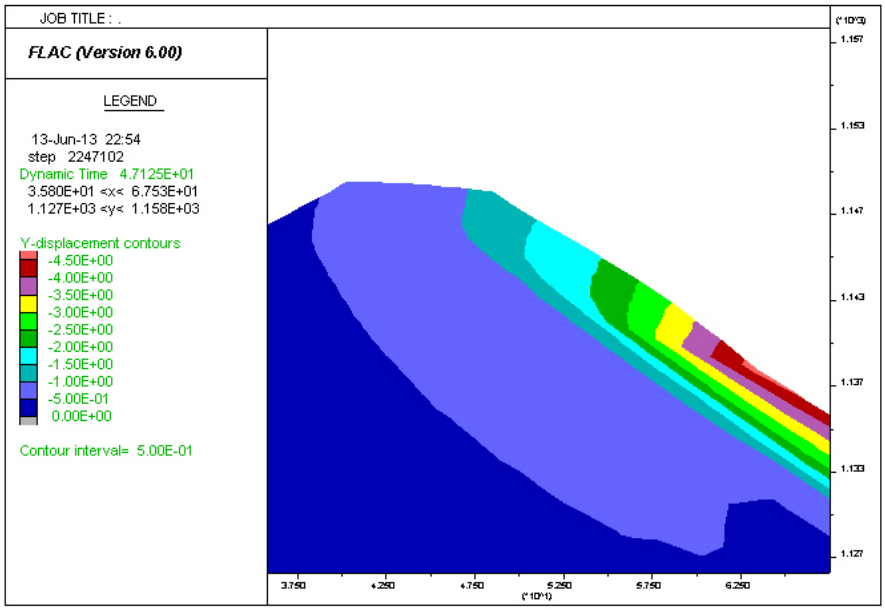


Figure 6. Vertical Displacement

The downstream horizontal crest displacement continues to decrease as the cohesion of the clayey gravel fill is increased. This trend was also observed in the displacement measured at the upstream and mid-crest locations. At these locations the displacement measured in the upstream and mid-crest portions of the dam decreased as the amount of cohesion within the clayey gravel fill increased.

6 CONCLUSION

In order to estimate the potential effects of strong earthquake ground motions on a large rock fill dam in Southern Mexico at closure of the facilities, a state of practice nonlinear dynamic analyses was performed using FLAC, which can predict permanent inelastic deformations in the dam fill structure. In addition, the top section of the dam was modified from a compacted non-plastic rock fill to a compacted cohesive granular fill to reduce the amount of crest deformation movement during a severe earthquake event.

The results of the FLAC analyses demonstrate that the rock fill dam is stable at the seismic loading considered for the MCE of Ms = 8.0 earthquake directly beneath the rock fill dam site, provided that cohesive well compacted fill is placed in the top section of the dam.

Permanent MCE displacements of the dam crest are consistent with empirical data. However, the level of deformation indicates that significant cracking and slumping at the edge of the embankment crest could occur, but that adequate freeboard would remain to prevent uncontrolled release of tailings or water from within the impoundment. These results are consistent with ICOLD guidelines (Wieland, 2005), which indicate that "significant structural damage is accepted" for MCE ground motions although no uncontrolled release form the reservoir shall occur.

Based on the results of these dynamic stability trials, the optimal material properties for the crest portion of the dam were determined to have clayey gravel with a minimum cohesion of 15 kPa. The results show that using clayey gravel fill with 15 kPa or above for the crest of the embankment will help to limit the amount of displacement and deformation within the crest under seismic loading conditions.

7 REFERENCES

Bowles, J. (1996). "Foundation Analysis and Design". McGraw-Hill Companies, Inc.

Byrne, Peter (2013). Professor Emeritus at the University of British Columbia, Civil Engineering Department. Personal communication.

Hunter G. & R. Fell. (2003). "Rockfill Modulus and Settlement of Concrete Face Rockfill Dams. Journal of Geotechnical and Geoenvironmental Engineering.

Itasca (2008). "Fast Lagrangian Analysis of Continua", Version 6.0. Itasca Consulting Group, Inc.

Iwashita, T.et al. (1995) "Dynamic Deformation Characteristics of Rockfill Materials from Laboratory Test, In-Situ Test and Earthquake Motion Analysis." Proceedings of the 3rd International Conference on Recent Advances in Geotechnical Earthquake Engineering and Soil Dynamics, St. Louis, Missouri, April 2-7.

Kulhawy, F. (1998). "Manual on Estimating Soils Properties for Foundation Design". Prepared for Electric Power Research Institute. Research Report 1493-8.

Leps, T.M. (July 1970). "Review of Shearing Strength of Rockfill", Journal of Soil Mechanics and Foundations Division, ASCE, Volume 96, No. SM4, pp. 1,159 to 1,170.

Naesgaard, E. and Byrne, P. (April 2011). "Hysteretic Model for Non-liquefiable Soils (UBCHYST5d)". UBCHYST5d Memo.

Seed, H. B., & Idriss, I. M. (1970), "Soil moduli and damping factors for dynamic response analysis", Report No EERC 70-10, Earthquake Engineering Research Center, University of California, Berkeley, California.

Wieland, Martin, 2005; "Review of seismic Design Criteria of Large Concrete and Embankment Dams." Presented at the 73rd Annual Meeting of ICOLD, Tehran, Iran, May 1-6, Paper No. 012-W4.

age length is 240 mm.

Seismic deformation analysis of Cerro Corona tailings dams

S. Abbaszadeh, C. Weber, E. Rondinel-Oviedo, & P. Corser
MWH Americas, USA & Peru

R. Hadidi
GeoPentech, Santa Ana, CA, USA

J. Gutierrez
Gold Fields Limited, Peru

ABSTRACT: The Cerro Corona gold and copper mine is located in the Cajamarca district of Peru and owned by Gold Fields La Cima. Tailing produced by the processing plant is stored in the Tailing Storage Facility, located just northwest of the plant site and includes several dams. To support future mining operations, the dams will be raised, the tallest to an ultimate height of 170 meters. The dam is a centerline construction with a central low permeability core and transitional filters located on its downstream side, with supporting rockfill both upstream and downstream of these zones. The integrity of the dam and its core under earthquake loading were of particular concern during the design of the dam. This paper presents a summary of seismic analysis of the dam performed to address this concern. The mine is located in a seismically active zone with a history of significant earthquake events. A site-specific seismic hazard analysis was conducted and two design earthquakes were identified: a M8 intraslab event with a PGA of 0.55 g at a distance of 75 km, and a M9.2 interface event with a PGA of 0.29 g at a distance of 118 km, for which design ground motions were developed for use in the deformation analysis. The seismic deformation of the dam under the postulated ground motions was then evaluated using a two-dimensional nonlinear time domain analysis. General analysis approach is discussed and the detailed results of the seismic analysis for the most critical section are presented.

1 INTRODUCTION

Gold Fields La Cima S.A.A. (GFLC), a subsidiary of Gold Fields Limited, owns the Cerro Corona mine, a copper mine with significant gold content. The mine is located in northern Peru in the Region of Cajamarca, approximately 760 km north-northwest of Lima and 80 km by road from the city of Cajamarca, as shown in Figure 1. The deposit is a diorite porphyry with an average grade of 1.0 gram per tonne of gold and 0.53% copper. The mine has gold-equivalent mineral reserves of 5.2 million ounces and has been in production since 2008, producing about 300,000 gold-equivalent ounces a year.

Tailing produced by the Cerro Corona processing plant is stored in the Tailing Storage Facility (TSF), located just northwest of the plant site, covering the Las Aguilas and Las Gordas valleys. MWH has been contracted by GFLC to develop designs for the TSF. Currently, a new mine plan is being considered that would expand the life of mine to 16 years (through 2029) and reserve to 130 Million tonne (Mt). The main challenge was that the mine site was very constrained with very limited space for construction of a TSF dam of this capacity. After evaluating different alternatives to support the new mine plan, MWH conceptually proposed and developed a design for a TSF centerline dam with a central low permeability core and transitional filters located on its downstream side, with supporting rockfill both upstream and downstream of these zones. The proposed TSF dam had an ultimate crest elevation of 3815 masl (meters above sea level) and maximum height of about 170 meters. This dam is likely one of the highest dams of its kind. The upstream stability of the low permeability core, which was required to protect a

nearby river, was of major concern. To increase the upstream stability of the core, a wide layer of rockfill was included on the upstream of the core. Detailed static and seismic analyses were performed to confirm the upstream stability of the core.

Corser and Rogers (2011) discussed the static analyses used to size the upstream rockfill. The objective of this paper is to present the seismic deformation evaluation of the main dam (constructed across Las Aguilas valley) at the TSF under postulated design ground motions. The seismic deformation analyses presented in this paper are the result of collaboration between MWH and GeoPentech. Although not presented in this paper, dams constructed over adjacent valleys have also been analyzed using a similar approach.

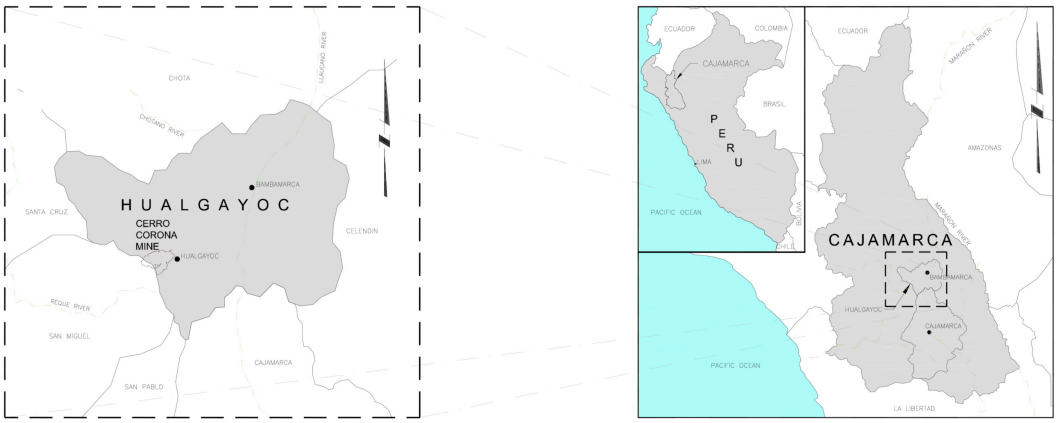


Figure 1. Plan View of the Cerro Corona Mine Location

2 MATERIAL PROPERTIES

A summary of the material properties, developed through a series of laboratory tests as well as published literature and judgment, are provided in Table 1. Drained material properties are used to estimate in-situ stresses prior to shaking (i.e. static), and undrained properties used to characterize the materials during the shaking that are both shown in Table 1.

Table 1. Material Properties for Static and Seismic Analyses

Material	Unit Weight (kN/m^3)	G_{max} (kPa)		Poisson's Ratio		Shear Strength (Degrees or kPa)	
	Static and Seismic	*Static*	*Seismic*	*Static*	*Seismic*	*Static*	*Seismic*
Tailing	16.6	$1{,}200 \times (\sigma'_v)^{0.77}$	$25 \times S_u$	0.3	0.45	$\phi' = 20$	$0.03 \times \sigma'_v$
Rockfill	24.0	$40{,}072 \times (\sigma'_v)^{0.5}$	$40{,}072 \times (\sigma'_v)^{0.5}$	0.36	0.36	$1.9323 \times (\sigma'_v)^{0.894}$	$1.9323 \times (\sigma'_v)^{0.894}$
Core	21.0	$17{,}000 \times (\sigma'_v)^{0.5}$	$17{,}000 \times (\sigma'_v)^{0.5}$	0.37	0.45	$1.51 \times (\sigma'_v)^{0.894} \leq$ 431.3 kPa	$0.168 \times \sigma'_v + 42.8$
Filter	19.0	$17{,}418 \times (\sigma'_v)^{0.5}$	$17{,}418 \times (\sigma'_v)^{0.5}$	0.35	0.35	$\phi' = 34$	$\phi' = 34$
Volcanic Breccia	20.0	375,000	375,000	0.3	0.3	$9.0384 \times (\sigma'_v)^{0.716}$	$9.0384 \times (\sigma'_v)^{0.716}$
Bedrock	21.0	2,242,000	2,242,000	0.3	0.3	N/A (Elastic)	N/A (Elastic)
La Jalca Tailing	20.0	998,980	998,980	0.3	0.3	$\phi' = 27$	$0.4 \times \sigma'_v$

ϕ' – Effective friction angle in degrees; σ'_v – Vertical effective stress in kPa; S_u – Undrained Shear Strength

2.1 *Shear Strengths*

The shear strength of the rockfill material was characterized using a relationship developed by Leps (1970), which relates the friction angle to confining stress. The drained and undrained

shear strengths for the core material were selected based on the results of consolidated-undrained (CU) triaxial testing. The undrained shear strength was reduced by 20% to account for potential strength loss during a seismic event. The shear strength for the filter and transition materials located just downstream of the core was based on published strength values for similar materials and is characterized by an effective friction angle of 34 degrees.

The drained and undrained shear strengths for the impounded tailing material were developed using cone penetration test (CPT) data collected during a geotechnical investigation performed on the tailing beach. For the static deformation analysis, the impounded tailing was assigned an effective friction angle of 20 degrees which represents the long-term drained strength of the material. For the seismic deformation analysis, the impounded tailing was assumed to have liquefied. This is a conservative assumption as liquefaction typically occurs towards the end of shaking or after the shaking has stopped. The impounded tailing was assigned an undrained shear strength ratio of 0.03.

2.2 *Dynamic Properties*

The dynamic properties of the embankment fill and foundation materials were developed for use in the seismic deformation analysis and based on field investigation data, published empirical relationships, published values for similar materials, and engineering judgment.

A geophysics investigation was performed on the in-place TSF embankment materials for the Las Gordas and Las Aguilas portions of the dam. The geophysics investigation included both multi-channel spectral analysis of surface waves (MASW) and seismic refraction methods. The MASW test method provides the shear wave velocity with depth at a single point whereas the seismic refraction provides p-wave velocity with depth along a line. The data from both methods were ultimately used to estimate the maximum shear modulus (G_{max}) for the embankment fill materials. Equation 1 shows the relationship between the shear wave velocity and G_{max}:

$$G_{max} = \rho \times v_s^2 \quad (1)$$

where ρ is the density of the material and v_s is the shear wave velocity.

Both data sets were used in the development of G_{max} for each fill material, but in order to use the seismic refraction data, it had to be converted from p-wave velocity to shear wave velocity. The p-wave velocity (v_p) was converted to shear wave velocity (v_s) using a v_p/v_s factor estimated based the assigned value of Poisson's ratio for each material (Table 1).

The MASW and seismic refraction data were compiled for each material and plotted with depth (Figure 2). The maximum shear modulus (G_{max}) relationship with effective vertical confining pressure was developed for the each of the materials based on the shear wave velocity data obtained from the geophysics investigation.

2.3 *Modulus Reduction and Damping Curves*

The modulus reduction and damping curves for the rockfill and filters were estimated using a methodology developed by Menq (2003), which develops curves based on the median particle size (D_{50}) and the coefficient of uniformity (C_u) of a granular material. Gradations for the rockfill and filters obtained as part of the construction quality assurance program were used to estimate the D_{50} and C_u values. A C_u value of 55 was estimated for the rockfill along with an average D_{50} value of 95 mm. A C_u value of 21 was estimated for the filter and transition zone along with an average D_{50} value of 2.2 mm. The modulus reduction and damping curves for the rockfill and the filters were developed for a range of confining pressures: 50 to 1,600 kPa. The curves are shown in Figure 3.

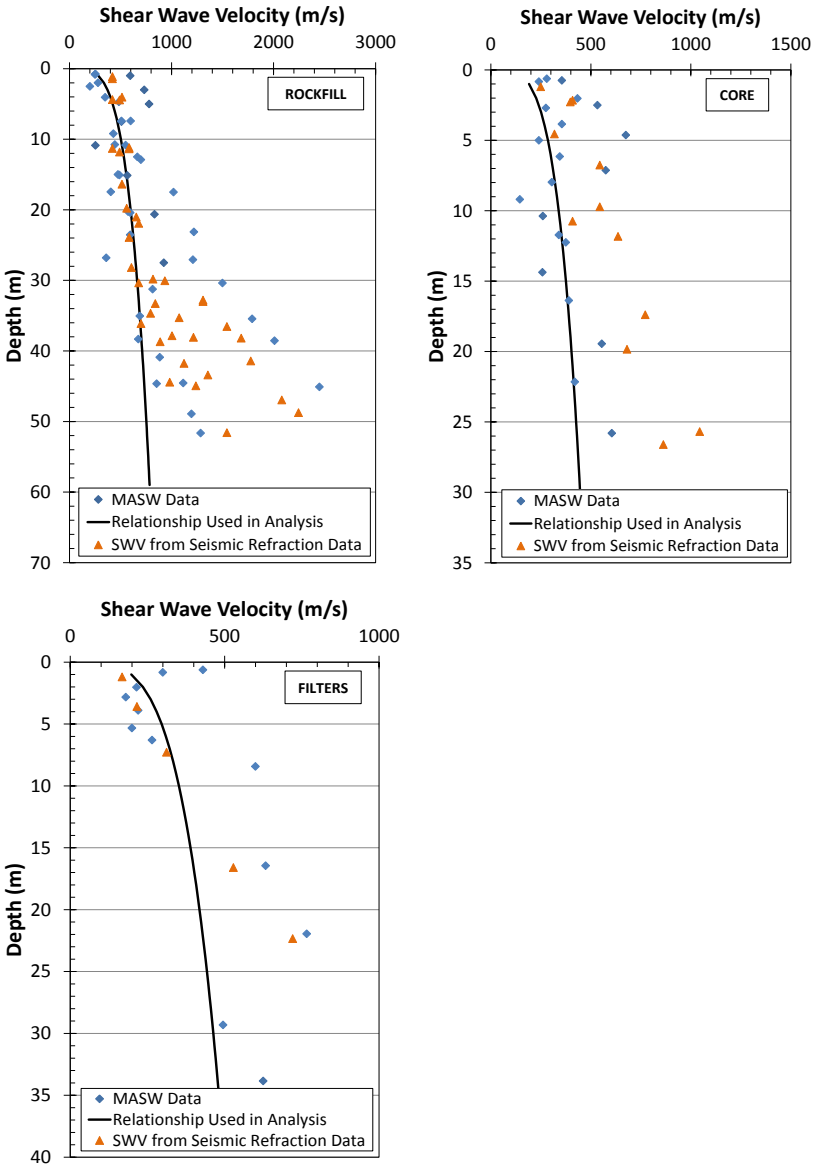


Figure 2. Measured and Estimated Shear Wave Velocity with Depth for Rockfill, Core and Filter Materials

Modulus reduction and damping curves were estimated for the core materials using the methodology developed by Darendeli (2001) for an average plasticity index of approximately 15. The modulus reduction and damping curves for the core were developed for a range of confining pressures: 25 to 1,600 kPa. The curves are shown in Figure 3.

The tailing was modeled as a liquefied material in the seismic deformation analysis and it was assumed that the liquefied tailing had a constant maximum shear modulus (G_{max}) (i.e. G/G_{max} = 1). Also, it was assumed that the liquefied tailing would have 2% Rayleigh damping for all cyclic shear strains. Similar assumptions were applied to the bedrock and volcanic breccia.

2.4 *Site-Specific Seismic Hazard Assessment*

A site-specific seismic hazard assessment (SHA) was performed for the Cerro Corona mine site, which included a deterministic seismic hazard analysis (DSHA) and a probabilistic seismic hazard analysis (PSHA). The SHA is based on a seismotectonic model and source characterization of the region surrounding the mine site. The seismotectonic model identifies four general seismic sources in the site region: subduction zone earthquakes originating at the Nazca-South

America plate interface (interface earthquakes), earthquakes originating within the subducting Nazca plate (slab earthquakes), shallow earthquakes in the overriding South America plate (crustal earthquakes) and background seismicity. Each of the source zones was characterized to establish input parameters for the seismic hazard analyses.

Confining Pressures

Based on the results of the SHA, two seismic scenarios were recommended for design:

- Interface: a maximum M_w 9.2, a closest distance of about 118 km and depth of 35 km, a PGA of 0.29 g, and a spectral acceleration at 1 second of 0.26 g.
- Slab: a maximum M_w 8.0 and a closest distance of about 75 km and depth of 75 km, a PGA of 0.55 g, and a spectral acceleration at 1 second of 0.35 g.

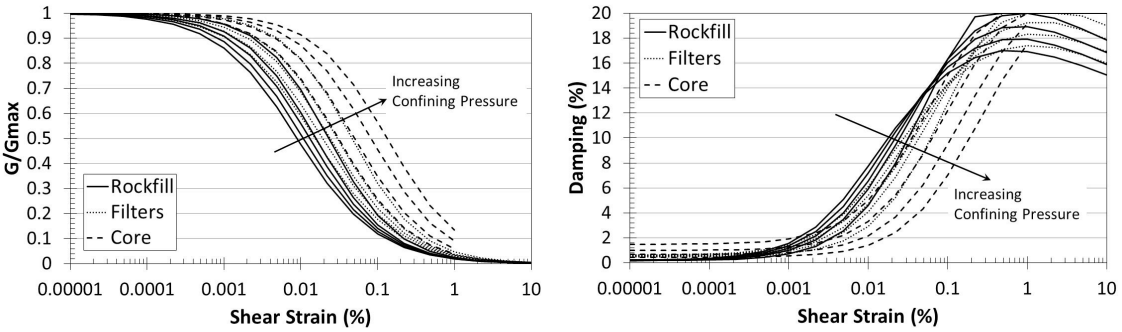


Figure 3. Modulus Reduction and Damping Curves for Rockfill, Core and Filter Materials for Varying

2.4.1 *Ground Motion Time Histories*

Acceleration time histories were developed for each of the design scenarios for use in the seismic deformation analysis. A total of six spectrally matched time histories were used in the deformation analysis. A summary of the time histories considered in this analysis is included in Table 2. The design response spectra at 5 percent damping for the interface and slab events are shown on Figure 4.

Table 2. Summary of Time Histories Selected for Deformation Analysis

Ground Motion	Design Scenario	PGA (g)	Arias Intensity (m/s)	Equiv No. of cycles	Duration 5-75% (sec)	Duration 5-95% (sec)
INT1	Interface	0.28	3.46	96	54	78
INT2	Interface	0.29	5.04	115	60	101
INT3	Interface	0.29	2.46	55	27	41
SLB1	Slab	0.54	11.7	96	40	64
SLB2	Slab	0.54	6.52	66	12	35
SLB3	Slab	0.51	5.09	54	13	18

3 SEISMIC DEFORMATION ANALYSIS

3.1 *Analysis Methodology*

The seismic deformation of the dam under the postulated ground motions was evaluated using a two-dimensional nonlinear time domain analysis, which accounts for the nonlinear response of the materials in the model. The material characterization and site-specific SHA used in this analysis are discussed in Section 2.

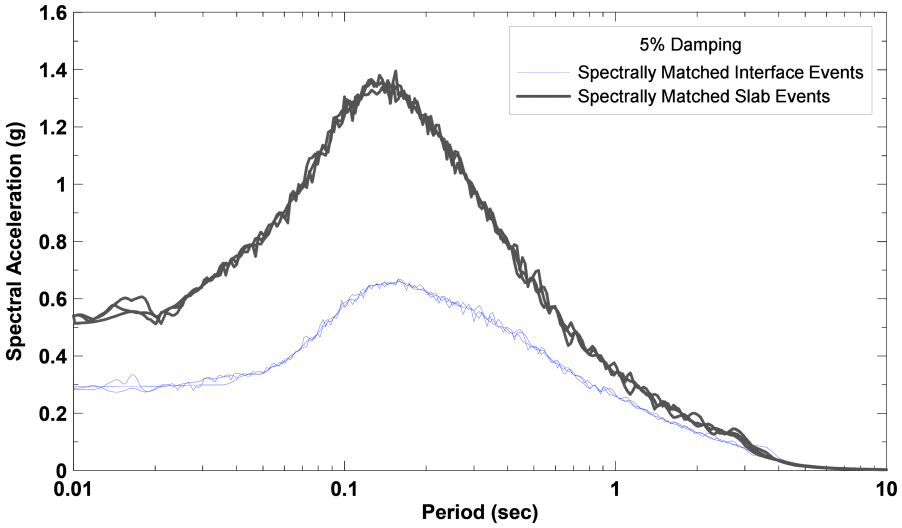


Figure 4. Response Spectra for the Interface and Slab Time Histories used in the Seismic Deformation Analysis

The computer program FLAC (Fast Lagrangian Analysis of Continua) was used in the analysis. FLAC is a two-dimensional explicit finite difference program for geotechnical and other applications developed by Itasca (2011). In a typical analysis, an idealized cross-section is divided into zones and nodal points in a way analogous to the finite element method. FLAC uses the Lagrangian formulation of momentum equations (Newton's second law of motion) and, thereby, inherently accounts for the mass conservation law and allows elements with fixed masses to translate, rotate, or deform in space. The analysis input motion is specified at the base of the analysis section, approximately incorporating the effects of a compliant boundary representing the bedrock in the analysis.

Various stress-strain models are available in FLAC. The Mohr-Coulomb model and the elastic model in FLAC were used for the analysis presented in this paper. Details of these models are provided by Itasca (2011). For all the results presented in this paper, the elastic model was used for the bedrock and, depending on the analysis being performed (static or seismic), either the Mohr-Coulomb model or the elastic model was used for all the other materials. In particular, the Mohr-Coulomb model was used for the embankment fill and tailing materials in the seismic deformation analyses.

The Mohr-Coulomb model consists of elastic-perfectly-plastic stress-strain relationships. Therefore, the materials are elastic before yielding. To make the elastic portion of the analysis reasonable, an equivalent-linear analysis is performed on a two-dimensional model of the dam using the computer program QUAD4MU (Idriss, 1973, updated version dated 2003) to obtain the strain-compatible shear modulus and Rayleigh damping values for the postulated shaking conditions. The analysis results from QUAD4MU provide the basis for the strain-compatible shear modulus and damping values to be used in the elastic portion of the Mohr-Coulomb model in the FLAC analyses. These assignments of modulus and damping are done such that the computed response spectra of corresponding selected points of the analysis sections from QUAD4MU and FLAC analyses are reasonably compatible. The "perfectly-plastic" portion of the Mohr-Coulomb model is specified as the appropriate shear strength of the material.

3.2 *Analysis Section and Discretization*

Three sections of the dam at the Cerro Corona TSF were selected for analysis. The locations of these sections are shown in Figure 5, and are referred to as the Las Aguilas Section, the Las Gordas Section, and the La Hierba Section. As mentioned earlier, this paper only presents the results for the Las Aguilas section. This particular section represents the maximum section of the dam.

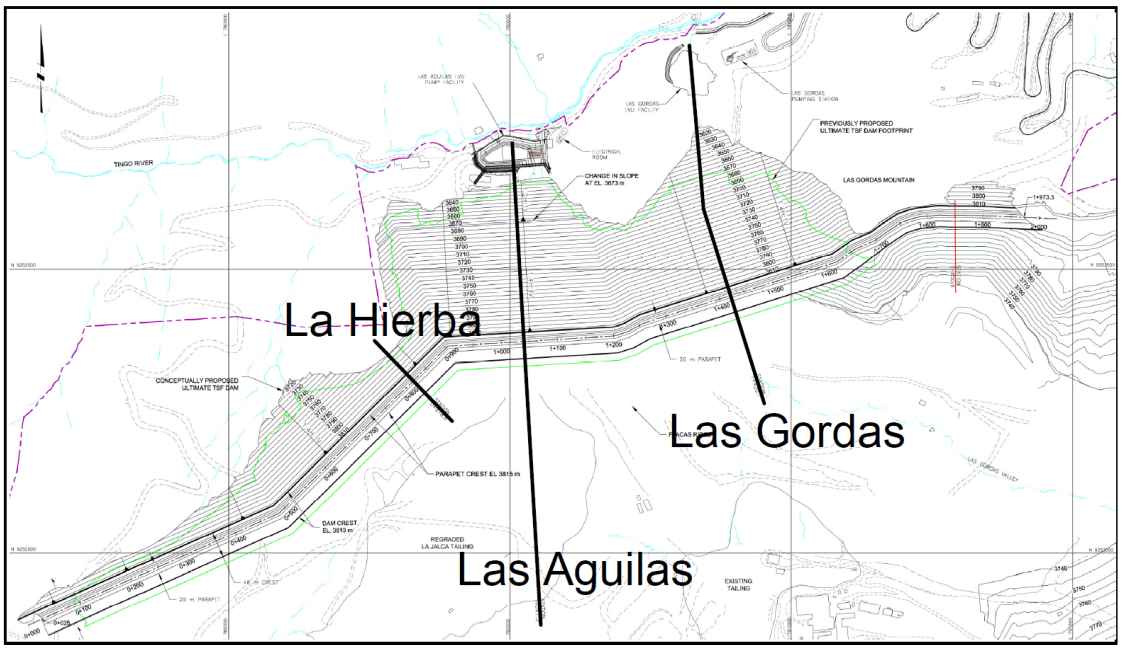


Figure 5. Plan View of the Selected Sections for Deformation Modeling Analyses of Cerro Corona TSF Dam

For the Las Aguilas Section, two different geometries of the section were analyzed: one corresponding to the full (ultimate) design height of the dam which is at 3815 m (crest at 3813 m with 2 m parapet wall) and one corresponding to an intermediate stage with the crest elevation at 3776 m. In this paper, only results for the full height configuration are presented. The full height geometry is shown in Figure 6. Idealized stages of construction used in the analysis to compute pre-earthquake static effective stress conditions in the analysis sections are also shown with dashed lines on Figure 6.

The mesh for the model was generated to: (1) allow appropriate dynamic wave propagation in the system; (2) reduce kinematic constraints provided by the linear elements used in FLAC; and (3) control numerical problems introduced by element shapes.

The tailing was discretized to account for the loading imposed by the tailing material on the dam. The bedrock was discretized for the purpose of providing a compliant base that would appropriately and adequately allow the incoming seismic waves to be introduced into the analysis section and absorb the seismic waves passing out of the analysis section.

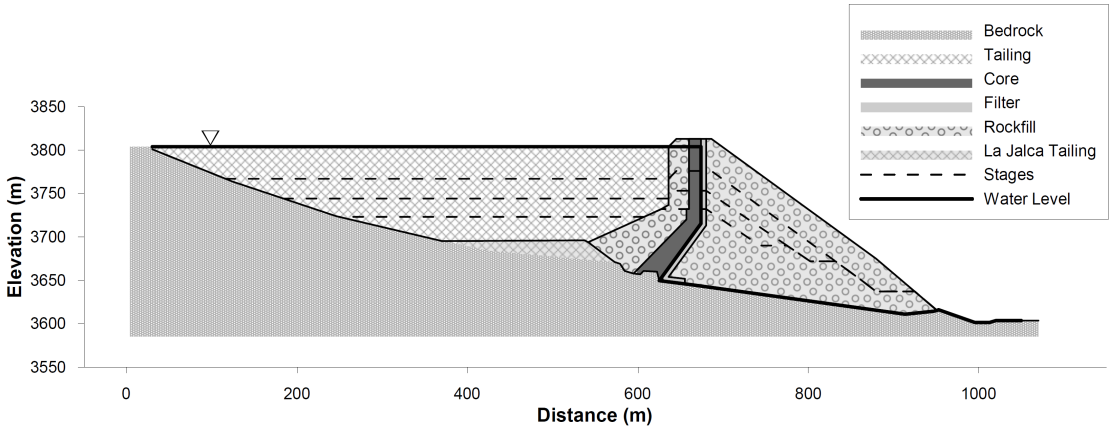


Figure 6. Finite Difference Numerical Modeling Using FLAC 2D: Las Aguilas Section

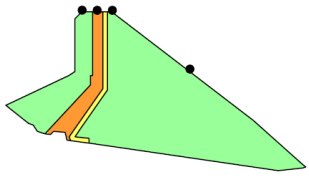
3.3 *Results and Discussion*

The FLAC seismic deformation analyses were performed using the positive and negative polarities for each of the six input ground motions (or a total of 12 different time histories, or cases). In Table 3, results of the Las Aguilas analyses are summarized in terms of permanent seismically-induced displacements (horizontal and vertical) at the end of shaking for four different points along the crest and downstream slope. These points are upstream edge of the crest, top of core zone, downstream edge of the crest, and middle of downstream slope, as shown on the small graphic below the table.

Table 3. Seismically-Induced Deformations for Las Aguilas Full-Height Section

Motion	Polarity	Displacements (m)							
		Upstream Crest		Mid Crest		Downstream Crest		Mid Slope	
		Hor.	Vert.	Hor.	Vert.	Hor.	Vert.	Hor.	Vert.
SLB1	Positive	-0.1	0.2	1	2.2	2	1.1	1.4	0.8
	Negative	-0.1	0.2	0.9	2.3	1.8	0.8	1.2	0.7
SLB2	Positive	0.2	0.1	0.6	1.2	0.8	0.3	0.8	0.5
	Negative	0.1	0.1	0.7	1.2	1.1	0.5	0.8	0.5
SLB3	Positive	0.3	0.1	0.7	1	1.3	0.6	1	0.6
	Negative	0	0.1	0.8	1.1	1.3	0.6	1	0.5
INT1	Positive	-0.2	0.1	0.1	1.2	0.1	0	0.2	0.1
	Negative	-0.1	0.1	0.2	1.2	0.2	0	0.2	0.1
INT2	Positive	0.1	0.1	0.1	1.1	0.2	0	0.2	0.1
	Negative	-0.1	0.1	0.2	1	0.3	0	0.2	0.1
INT3	Positive	0	0.1	0.2	0.8	0.2	0	0.2	0.1
	Negative	-0.2	0.1	-0.1	0.9	0	0.1	0.1	0

Notes:
Downstream movements are indicated with a positive number.
Settlements are indicated with a positive number.



Only the analysis results for the SLB1 input motion of the full height geometry that gave the highest crest displacement are presented in this paper as the key example of the results.

Figure 7 presents the input time histories and response spectrum for the SLB1 design motion. Figure 8 compares the response spectra of acceleration time histories computed at three points (i.e. upstream and downstream edges of the crest, and mid-height of downstream slope) using both equivalent linear QUAD4MU and equivalent linear FLAC, where no yielding is allowed in any of the zones (i.e. elastic response) and the modulus reduction and damping part of the FLAC analysis were assigned based on the results of the QUAD4MU analysis. Figure 8 indicates that the seismic responses of the FLAC analysis section induced by the SLB1 input motion appear reasonable for the purposes of calculating the seismic displacements.

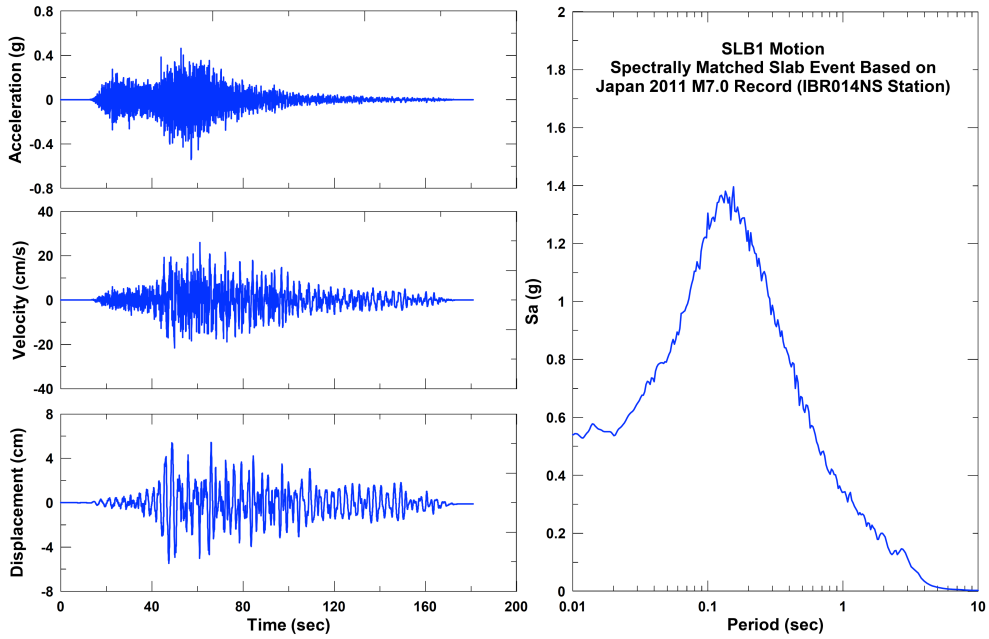


Figure 7. SLB1 Time Histories and Response Spectrum

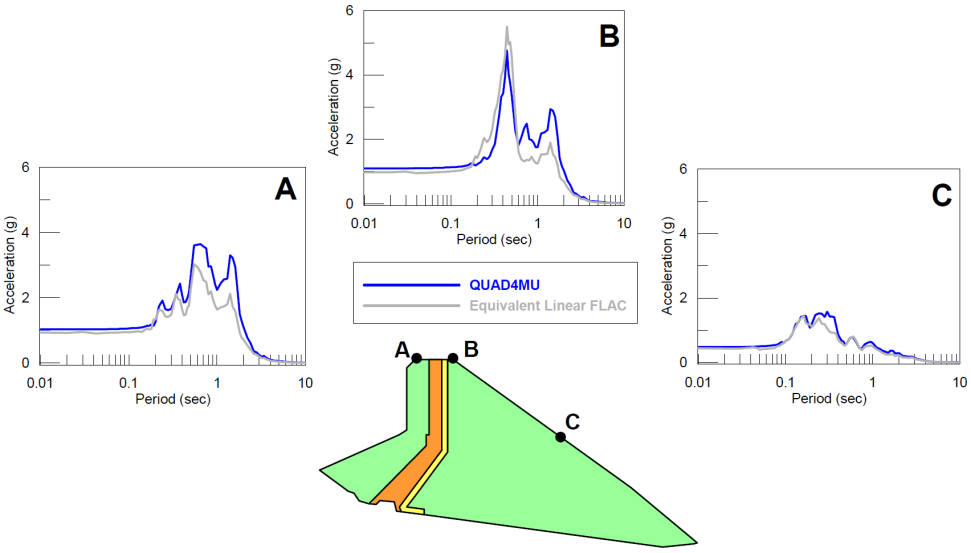


Figure 8. Response Spectra Comparison at Various Points: FLAC versus QUAD4MU

Figure 9 shows the seismic displacement contours for the SLB1 case; seismic displacement vectors with numbers corresponding to the computed seismic displacements in meters are also shown for four points (i.e. upstream crest, top of core, downstream crest and near middle of the downstream slopes). The calculated seismic displacement values are not large, but there is a general trend of seismically-induced movements in a downstream direction. Additionally, the core is settling about 2 meters as a result of the movement of the upstream and downstream rockfill in opposite directions. This type of settlement in the core can likely be repaired after the earthquake.

Figure 10 shows time histories of seismic displacements (horizontal) at the three selected points on the surface of the embankment, all for the SLB1 case. This figure illustrates how the post-earthquake permanent displacements have been accumulated throughout the duration of shaking. The combination of the results shown on Figure 9 and Figure 10 provides an appreciation of the computed seismic deformations within the embankment for this case.

Based on the analysis results for the full height Las Aguilas section (Table 3), the displacements under slab events are higher than those under interface events.

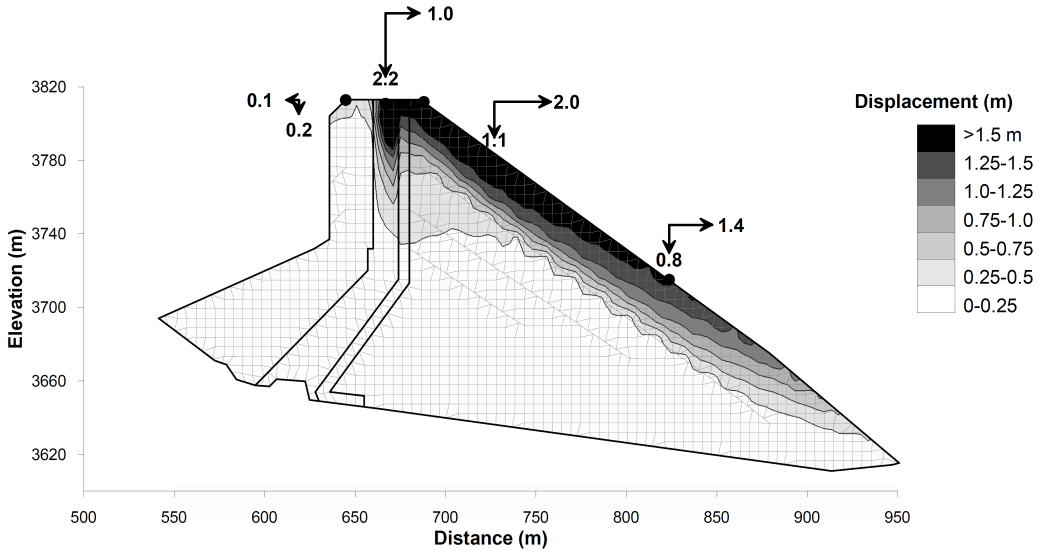


Figure 9. Calculated Displacements at the end of shaking for Las Aguilas Full Height Section

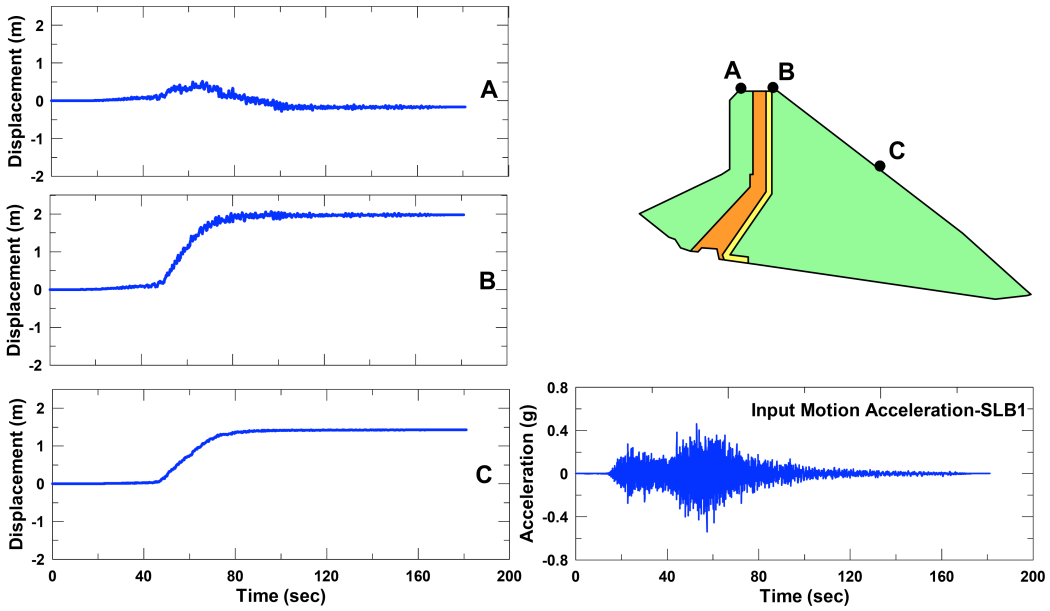


Figure 10. Calculated Displacements Time Histories Las Aguilas Full Height Section

4 CONCLUSIONS AND RECOMMENDATIONS

To support the new Cerro Corona mine plan, MWH conceptually proposed and developed a design for TSF centerline dam with a central low permeability core to protect the nearby river. With maximum height of 170 meters, the proposed TSF dam is likely one of the highest centerline dams. The upstream stability of the low permeability core was of major concern. To increase the upstream stability of the core, a wide layer of rockfill was included on the upstream of the core. Detailed static and seismic analyses were performed to support this design.

This paper presented the seismic deformation analyses performed to support the proposed centerline TSF dam design. The rationale and methodology behind the development of the material properties and time histories used as input for the models were also discussed.

A total of three sections were analyzed under the postulated seismic loading namely: Las Aguilas, Las Gordas and La Hierba sections. However, this paper only presented the results for the Las Aguilas section with full height configuration which was the highest of the three. Las Aguilas section was analyzed for six different input motions (three slab events and three interface events). These input motions were developed specifically for the Cerro Corona site.

Based on the results of the seismic analyses, the following conclusions can be made:

- Generally, the slab events resulted in larger displacements compared to the interface events. This was expected because the response spectra for the slab events were higher than that of the interface events.
- The combination of the Las Aguilas full-height section with SLB1 motion exhibited the largest displacements among all the modeled sections. The nature of the movements was primarily downstream with some settlement in the core. The maximum horizontal and vertical displacements of the dam were both calculated to be around 2 meters.
- The upstream and downstream rockfill exhibited movements in opposite directions that caused the core to settle about 2 meters, which is considered repairable should it occur.
- Because the values of seismic displacements induced by the evaluated events are relatively small and the dam is designed with a minimum of two meters of freeboard, the likelihood of total loss of freeboard, significant cracks forming in the crest and other areas, as well as loss of stability is considered low under the postulated design condition.

5 ACKNOWLEDGEMENTS

The authors would like to thank the Cerro Corona Mine and Gold Fields La Cima S.A.A. for the permission to publish this study. We also express our appreciation to the entire Cerro Corona team, whose collaboration and efforts have been fundamental to the success of this project.

6 REFERENCES

Corser P. and Rogers J. 2011. Design, Construction and Operation of a Centerline Rockfill Tailing Dam with Low Permeability Core Zone. *Proceedings Tailings and Mine Waste 2011: Vancouver, BC*, November 6 to 9, 2011.

Darendeli, M.B. 2001. *Development of a New Family of Normalized Modulus Reduction and Material Damping Curves*, PhD Dissertation, University of Texas at Austin.

Idriss I.M., Lysmer J.L., Hwang R., and Bolton Seed H. 1973. *Quad-4: A Computer Program for Evaluating the Seismic Response of Soil Structures by Variable Damping Finite Element Procedures*, EERC Report 73-16. Berkeley: University of California, Berkeley.

ITASCA, 2000. Fast Lagrangian analysis of continua (FLAC), *Version 4, User's Guide*. Itasca Consulting Group, Inc., Thrasher Square East, 708 South Third Street, Suite 310, Minneapolis, Minnesota.

Ladd, C. 1991. Stability Evaluation During Staged Construction. *Journal of Geotechnical Engineering*, 117(4).

Leps, T. 1970. Review of Shearing Strength of Rockfill. *Journal of the Soil Mechanics and Foundations Division*, 96(SM4): 1159 – 1170.

Menq, F. 2003. *Dynamic Properties of Sandy and Gravelly Soils*, PhD Dissertation, University of Texas at Austin.

Bituminous geomembrane failure at a co-disposal tailings storage facility

Philip Addis & Brian Andruchow
Golder Associates Ltd, Mississauga, Ontario, Canada

Irwin Wislesky
Golder Associates Ltd, Calgary, Alberta, Canada

ABSTRACT: The staged construction of a co-disposal facility (CDF) at a copper/gold mine located in the tropics has recently been completed. The mine produces two streams of tailings as a result of processing sulphide ore (copper) and oxide ore (gold/silver), which are thickened prior to deposition in the CDF. The tailings are potentially acid generating and metal leaching, as is a portion of the mine rock, both of which are managed within the CDF. The CDF embankments were constructed with compacted layers of non-acid generating waste rock sourced from the mine's open pit. The CDF floor and upstream embankment slopes were initially lined with compacted clay, transitioning to geosynthetics for the latter stages of construction due to a shortage of suitable on-site clay borrow material. Initially, the compacted clay was replaced with a 4.8 mm thick oxidized bituminous geomembrane liner, of which approximately 6,000 m^2 was installed on the upstream slopes of the embankment. A large portion of the bituminous geomembrane remained exposed to the elements during deposition of tailings into the CDF. Several months after installation of the bituminous geomembrane, water began to seep out of the CDF embankments at a rate of approximately 22 m^3/h. The exposed bituminous geomembrane was inspected and it was apparent that a large scale failure of the liner had occurred. This paper looks at possible reasons for the failure and the remediation work undertaken.

1 INTRODUCTION

The Cerro de Maimon project is located in the Dominican Republic approximately 75 km northwest of the capital city of Santo Domingo. It is near the town of Maimón in the Monseñor Nouel province. The open pit copper/gold mine has been operational since 2007 and has 6 Mt of proven reserves. There are two basic ore types, a surficial oxide ore and a sulphide ore, which are processed on-site into gold-silver doré and copper concentrate, respectively. The projected mine life at start-up was 9 years, however, exploration activities have resulted in expanded ore reserves. The tailings from process circuits are combined prior to deposition in the CDF, and are both potentially acid generating (PAG) and metal leaching. A portion of the mine rock is also PAG.

2 SITE DESCRIPTION

2.1 *Climatic Data*

The climate data used to represent the Cerro de Maimon project site is from the Falcondo Mine located 9 km north of the site. The Cerro de Maimon site is characterized as a maritime cli-

mate. The average annual temperature is 25.5ºC and ranges from 24ºC to 27ºC. The mean monthly maximum temperature is 34ºC (June) and the mean monthly minimum temperature is 18ºC (December). The average relative humidity is 80%. The average annual precipitation and evaporation are 2,012 and 1,710 mm, respectively. The dry period typically occurs between December and March. Hurricane season normally runs from June to November.

2.2 *Co-Disposal Facility*

Staged construction of the CDF was completed in 2012. The CDF can be described as a side hill site with embankments constructed with compacted non acid generating waste rock on three sides, the fourth side is a natural slope. The CDF was initially developed in three cells to facilitate co-disposal of the tailings and PAG waste rock (Li et. al., 2011). Stage 1 construction consisted of Cells 1 and 2 to a crest elevation of 150 m (vertical height of approximately 30 m), the upstream slopes and base were lined with compacted clay and a downstream toe berm was constructed to improve the overall stability. Stage 2 construction consisted of Cell 3 to a crest elevation of 150 m, of which the base and west slope were lined with compacted clay and the base was covered with a layer of PAG waste rock for erosion protection; the upstream slopes on the north and east sides of Cell 3 were lined with a bituminous geomembrane; and the south embankment was unlined as it was an internal embankment shared by Cell 2. Stages 3 and 4 of the construction raised the embankments in a downstream direction to a final elevation of 169 m. The three cells were then combined into one facility as the division embankments became flooded.

The tailings from both the oxide and sulphide circuits are pumped together as slurry to the thickening plant, where the slurry is thickened to approximately 56% solids (by mass). Overflow from the thickener is recovered for re-use in the milling process. The thickened tailings are pumped to the CDF via a 150 mm nominal diameter HDPE deposition pipe. There are multiple discharge pipes into each of the CDF cells to aid in beach slope development, although only one pipe is active at a time. The CDF also receives PAG waste rock, which is delivered by trucks, dumped, and spread out on the tailings beach by a bulldozer. Water decanted from the CDF, and all contact water (i.e. surface water generated over modified ground) are directed to the contaminated water collection pond (CWCP) located just downstream of the CDF. Water entering the CWCP is treated to remove cyanide, and is provided with sufficient residence time to settle out solids prior to entering the reverse osmosis water treatment plant. Discharge from the reverse osmosis water treatment plant is routed through a polishing pond prior to environmental discharge.

3 MATERIAL DESCRIPTION

Bituminous geomembrane products have been used extensively in Europe since the early 1970s, and to a lesser extent in Africa and North America. They have been used as liners and caps for solid and liquid waste storage facilities, for water storage as dam and canal linings, and as ditch liners in transportation projects and below railway ballast.

The advantages of bituminous geomembranes include:

- Bituminous geomembranes can be installed in cold weather, according to Breul (2008), with manufacturer claims that the lower bound installation temperature is -25°C for the elastomeric bitumen geomembranes and 5°C for the oxidized bitumen geomembranes.
- Bituminous geomembrane mass per unit area is greater than a HDPE or LLDPE geomembrane and hence it is less susceptible to wind uplift.
- The lower co-efficient of expansion on bituminous geomembranes ensures minimal folds and therefore better contact with subgrade, compared to HDPE or LLDPE.
- Bituminous geomembranes have good puncture resistance.
- Bituminous geomembranes are more elastic compared to HDPE.

In general, material supply costs for bituminous geomembranes are higher than HDPE or LLDPE geomembranes; however, the overall system costs can be less if the costs of subgrade preparation and cover material are taken into consideration. The bituminous geomembranes manufacturer claims that bituminous geomembrane liners do not require subgrade preparation

(i.e. placement of sand or fine gravel as bedding) that is as stringent as HDPE or LLDPE. Bituminous geomembranes have a long history of use below railway ballast, which is typically 38 mm crushed stone aggregate, which indicates their excellent puncture resistance.

A bituminous geomembrane can be considered to be a composite liner as it is made up of layers of different materials. A 4.8 mm thick oxidized bituminous geomembrane liner was specified for the Cerro de Maimon project, consisting of the following:

- a non-woven polyester geotextile with a mass per unit area of 300 g/m^2;
- a 50g/m² glass fleece reinforcement;
- a bituminous mastic consisting of a oxidized bitumen Penetration Grade 100 and filler.
- a Terphane film bonded to the underside when the membrane is hot; and
- a coating of fine sand on the upper surface,

Each component has a defined purpose: the geotextile provides the primary strength and important puncture resistance; the glass fleece reinforcement provides stability during fabrication and contributes to the strength of the geomembrane; the bituminous mastic provides the water retention capabilities; the Terphane (polyethylene cepthalene) film prevents penetration of the membrane by plant roots; and the sand coating increases the frictional resistance on slopes. In addition to the specified bituminous geomembrane, rolls of the 5.6 mm thick oxidized bitumen as well as the 4.8 mm thick elastomeric bitumen geomembrane were also delivered to site, due to a shortage of elastomeric bitumen stock at the production plant. Prior to installation, the manufacturer confirmed the received materials were compatible.

4 DESCRIPTION OF BITUMINOUS GEOMEMBRANE INSTALLATION

The CDF has embankments constructed with layers of compacted waste rock hauled from the open pit with 50 tonne trucks. The rockfill lifts had a maximum uncompacted thickness of 0.4 to 1.0 m, depending on the material type and quality (thicker lifts for coarser material). Construction material had to be approved prior to placement. Boulders greater than 1 m in diameter were rejected and pushed to the side of the embankment for collection and dumping in the waste rock dumps, or for use in specialized construction items such as sediment traps. Compaction of the dam fill was achieved by six passes with a vibratory smooth drum roller. Compaction efforts for each lift were checked with a nuclear densometer and areas identified with low compaction were required to have additional compaction prior to lift approval. Trimming of the upstream dam slope to 1.5H:1V (34 degrees) was carried out with an excavator, generally after the rockfill had been raised 2 to 3 m. During slope trimming the surface was also prepared for interfacing with the liner. This involved scraping the surface smooth by excavator bucket and placing fines in locations where voids or excessively coarse material was present. The placing of material was generally done by hand and tamped down. The surface finish was somewhat iregular but a 540 g/m^2 non-woven needle punched geotextile was installed as a cushion layer between the subgrade and the bituminous geomembrane. The minimum crest width of the embankments was 10 m which provided sufficient space for the bituminous geomembrane to be installed from the top downwards. The maximum slope length was 25 m.

A total of approximately 6,000 m^2 of bituminous geomembrane was installed on the north and east upstream slopes of the Cell 3 containment dams. Personnel from the bituminous geomembrane manufacturer were brought to site from April 18 to 23, 2010, to train a local contractor on proper liner installation methods and quality control requirements. During this period approximately 2,000 m^2 of liner was installed. No concerns with the installation or subgrade preparation were expressed while the liner manufacturer's representatives were on-site. The liner installation was completed in entirety by May 3, 2010. The bituminous geomembrane was installed with the sandy textured side facing down and the Terphane film facing up. This was to improve the frictional resistance of the bituminous geomembrane on the slope and was an amendment discussed with and approved by the manufacturer. Full-time supervision of the liner installation was provided by Golder Associates Ltd.. Seaming was achieved using a blow torch and a minimum overlap of 200 mm was provided. Quality control involved testing a destructive seam sample at 1,000 m intervals, vacuum box testing every 30 m of seaming, and ultransonic testing of the seams every 300 m. A 1x1 m anchor trench with a 1 m runout was provided at the crest of the

embankment. At the toe of the slope the bituminous geomembrane was tied into the clay-lined base with an anchor trench.

5 FAILURE AND INSPECTION OF BITUMINOUS GEOMEMBRANE

5.1 *Tailings Deposition*

Tailings deposition in Cell 3 began on June 12, 2010. On July 1 extensive seepage was observed at the toe of Cell 3. Test results of the seepage indicated it likely originated from within Cell 3, and was not groundwater. The seepage water was clear and no tailings or other fine particles were observed which would indicate particle migration within the dam. The seepage reported to a natural depression, which was immediately dammed off to prevent discharge to the environment. All seepage from Cell 3 was collected and pumped to the CWCP for treatment/storage. The rate of seepage was estimated at 22 m^3/h. Following identification of the leak, tailings deposition was redirected to Cell 2, and a decant pump provided to draw down the water level inside Cell 3.

5.2 *Visual Inspection*

After the water level within Cell 3 was drawn down, a visual inspection of the in-situ liner was carried out along the North and East Dams of Cell 3, with a representative from the liner manufacturer on September 10, 2010. The inspection was completed when the weather was a mix of sun and cloud, with a maximum ambient air temperature of 37°C at 2:30 pm. The following observations were made:

- The primary sources of the leak were three holes, varying in size, which occured in the vicinity of each other at the centre of the North Dam (see Figure 1). The largest was a near vertical tear estimated to be 1.5 m long by 0.1 m wide (see Figure 2).
- Complete and partial seam failures were observed along many of the panels above and within the water draw down zone (see Figure 3), although primarily below the maximum water level. Failing seams had poor tensile strength and could be pulled open by hand. Failure of the seams appeared to have no correlation to the coarseness of the subgrade material, as they were widespread and occurred in locations where the liner subgrade was fine grained.

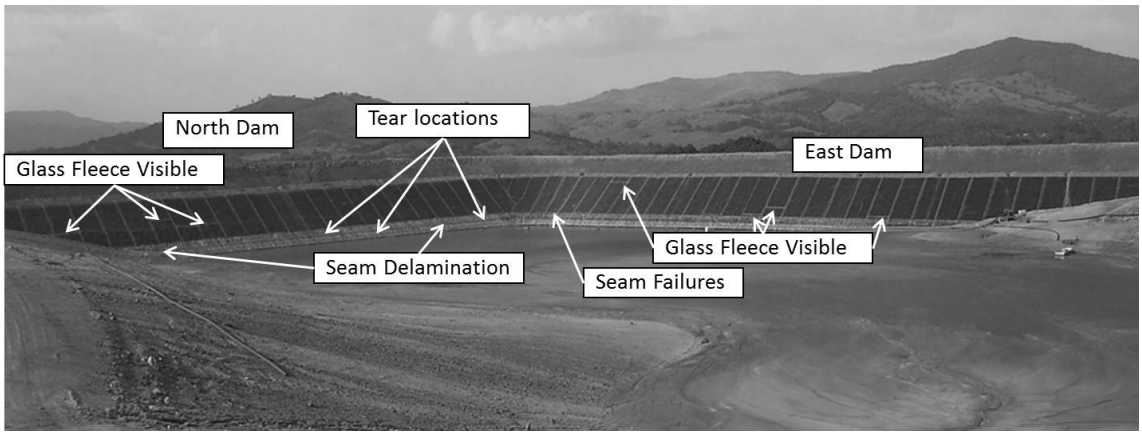


Figure 1. Locations of geomembrane failures



Figure 2. Tear Failure on North Dam



Figure 3. Seam Failure

- In addition to the failures, the bituminous geomembrane showed numerous signs of distress including delamination, surface deformation, concentric stress circles, cracking, and melted bitumen dripping down the face of two panels.
- The underlying cushion geotextile was largely intact but the heat from seaming the geomembrane panels resulted in the melting of the geotextile in a number of places.



Figure 4. Melted Bitumen on Geomembrane Surface

6 ON-SITE TESTING OF BITUMINOUS GEOMEMBRANE

6.1 *Thermal Imaging*

Thermal imaging of the in-situ geomembrane was captured using a FLUKE Ti25 thermal imaging camera (thermal sensitivity ≤0.1ºC). The thermal imaging was carried out in the heat of the day around 3:30 pm when the ambient air temperature was 37ºC. The thermal images showed a range in surface temperature from 69.3ºC to a maximum of 86.2ºC with most of the liner above 75ºC.

In addition to the above testing, temperature measurements were taken of the surface of samples of the bituminous liner exposed to sunlight on a sunny day. One sample was black (natural) and the other was spray painted white. In general the surface temperature of the black liner was about 20 degrees C hotter than the white liner.

6.2 *Ultrasonic Seam Testing*

Ultrasonic testing of several seams on the North Dam was carried out by the manufacturer's representative to confirm that overlapping panels had sufficient contact and did not contain air voids. An Epoch XT unit was used, and it confirmed that intact seams were installed free of air pockets, although they could still be pulled apart by hand. This indicates that the ultrasonic testing of seams is only suitable to determine if there is complete contact of the same panels, but does not indicate a tensile strength.

6.3 *Tensile Strength Testing*

In an attempt to obtain an understanding of the failure mechanism involved, on-site tensile strength testing of seven samples of the bituminous geomembrane was carried out under various temperatures and environmental exposure conditions. The Cerro de Maimon site did not have a materials testing laboratory or equipment used in typical tensile tests, so a digital crane hoist (accuracy ±0.2 kg) with vice grips was used. The testing involved connecting the liner to the digital crane hoist and applying a tensile force. Test strips were brought to temperature in an oven, with temperature readouts during testing provided by an infrared thermometer. All samples

tested had a width of 50 mm and a length of approximately 300 mm. The strips were tested in a cross-width direction. Test strips 1, 2, 5 and 6 were sourced from the same seam/panel, which had never been exposed to process water and was installed over a smooth clay subgrade. Test strips 3 and 4 were taken from a new roll of 4.8 mm thick oxidized bituminous geomembrane on-site; this material had never been exposed to UV radiation or temperatures exceeding ambient. Test strip 7 was taken from the North Dam within the recent water draw down zone. The specimens were cut to size, heated in an oven on-site for about 30 minutes, their temperatures checked with an infrared thermal gun, and then tested.

The results of the tensile strength tests on the non-seamed bituminous geomembrane are presented in Table 1.

Table 1. Testing of Non-seamed Bituminous Geomembrane.

Test No.	Material Source	Temperature at Test Start (ºC)	Tensile Loading at Failure (kg)	Tensile Strength (kN/m)
1	New	31	102	20.0
2	New	60	82	16.1
3	North Dam above water line	27	93	18.2
4	North Dam above water line	58	87	17.1

The tensile loading was recorded in kg, and converted to tensile strength in kN/m. Although the testing was not in accordance with a standard ASTM test method, the tensile strength calculated for Test 1 does indicate a good correspondence with the materials tensile strength of 21 kN/m (cross-width direction) as provided in the manufacturer's data sheet with test methods ASTM D7275 and ASTM D4595. Tests 1 and 2 show the effects of temperature on virgin material which had never been exposed to solar radiation or temperatures above ambient. Exposure to elevated temperatures for under 30 minutes resulted in a strength loss of 20%. The results from Tests 3 and 4 show that an increase in temperature of just over thirty degrees to 58ºC has a minimal effect on the behaviour of the specimen.

The effects of elevated temperatures are more noticable in the seams than on the non-seams, as indicated by the results in Table 2.

Table 2. Testing of Seamed Bituminous Geomembrane.

Test No.	Material Source	Temperature at Test Start (ºC)	Tensile Loading at Failure (kg)	Tensile Strength (kN/m)	Failure Location
5	North Dam above water line	27	62	12.2	Seam
6	North Dam above water line	70	20	3.9	Seam
7	North Dam below water line	66	24	4.7	Seam

From Test 5 it is evident that repeated heating and cooling of the liner to temperatures at or near the bitumen softening point results in permanent strength loss which is most evident in the seams, even after the liner is cooled to ambient temperature. During installation, shear tests were performed on several seam samples and all passed (i.e., failure did not occur in the seam but in the liner material adjacent to the seam). The seam on Test Strip 5 failed at 61% of the tensile strength of the Test Strip 1 (virgin material) at a similar temperature.

The reduction in tensile strength of the seams is even more pronounced if the material is tested at an elevated temperature. This is evident from Tests 6 and 7 which were both sampled from the North Dam. A temperature increase of 43ºC caused Test Strip 6 to fail at 31% of its ambient temperature strength. Test 7 was performed on liner which had been submerged during pond filling and only recently re-exposed to elevated temperatures due to water draw down in Cell 3. A temperature increase of 39ºC caused Test Strip 7 to fail at 39% of its ambient temperature strength.

7 DISCUSSION ON FAILURE MECHANISM

The scale and number of failures, as well as the visible signs of distress in the geomembrane indicate that the integrity of the liner was severely compromised. The evidence of dripping bitumen from two areas indicates that the liner temperature was near to or at the bitumen softening point. The testing on-site indicates that even short-term exposure to elevated temperature reduces tensile strength, particularly at the seams.

The upstream slope of the Cell 3 embankment is 34 degrees. The reported interface friction angle between a bituminous geomembrane and rolled sand/crushed gravel is 40 degrees. In this instance however, a non-woven geotextile separated the bituminous geomembrane from the subgrade. The critical interface for frictional resistance is therefore either the geotextile/bituminous geomembrane or the geotextile/subgrade. From Golder's in-house testing database, typical interface friction angles for geotextile/gravel or sand can vary from 25 to 40 degrees. The interface friction angle for the geotextile/bituminous geomembrane is likely to be lower, due to the relatively smooth surface of the geomembrane The slope angle is therefore close to, or greater than, the critical interface friction angle, and there is therefore minimal frictional resistance provided by the slope. This results in the full length of the geomembrane on the slope being placed in tension when it is loaded at the toe. The locations of the concentric stress circles and delamination were not limited to one portion of the slope and this appears to confirm that a large portion of the geomembrane was under tensile loading.

The failure mechanism therefore appears as follows. The geomembrane was installed on a relatively steep slope and anchored at the toe and the crest. It was exposed to a number of heating and cooling cycles with the temperature reaching near to the melting point of bitumen. This reduced the geomembranes' ability to act as a composite material. A tensile load was induced in the geomembrane, firstly due to its self-weight and then due to the deposition of tailings at the toe. The roughness of the subgrade induced localized stress points on the geomembrane. The geomembrane then failed in a number of places with the seams, in particular, being a weak point.

It should be noted that this application of a bituminous geomembrane differs from that of a canal lining or heap leach pad. In a canal lining application there is minimal tensile loading. In a heap leach application, the loading is primarily compressive and the liner is usually covered with a drainage layer to collect the leached run-off.

In this application it appears that the liner failed due to a combination of weakening by heat and tensile stress.

8 MANUFACTURER'S RESPONSE

The response from the manufacturer on the failed liner was provided in a letter dated September 24, 2010 to Golder Associates Ltd. and the client. The manufacturer's analysis concluded that the failure was due to bad support; the presence of a large quantity of sharp stones and the complete lack of soil compaction was identified as the main cause. Any other consideration (e.g., temperature) was not considered relevant, and all tensile strength testing (discussed under Section 6.3) completed on-site was considered irrelevant as the methodology did not follow ASTM procedures. The manufacturer claims that the product has been installed in many different countries and, in particular, in hot countries (30°C to 35°C, and sometimes more than 40°C) without incident. For many of these sites, long-term feedback had been received. The manufacturer proposed that the liner should be cut away in the failure areas, the subgrade improved and the liner patched, and continued to recommend the product for future use at the site.

9 REMEDIATION

Due to the extensive nature of the failure, and on Golder Associates Ltd.'s recommendation, the client replaced the bituminous geomembrane with a single side textured 1.5 mm HDPE geomembrane and a 500 g/m^2 nonwoven needle punched geotextile. Installation of the new liner system required that all tailing impounded against the failed bituminous liner be removed and

sufficient working area at the toe be exposed such that the HDPE liner could be properly connected to the Cell 3 floor. Access dykes were pushed out into Cell 3 along the dam upstream slopes, and the tailings residing between the access dyke and bituminous liner removed by excavator. Access dykes to facilitate tailings excavation were constructed of weathered PAG waste rock, which was challenging due to the high silt content and subsequent moisture sensitivity (resulting in physical instability) of the material.

The bituminous geomembrane was either left in place (if adequate protection for the HDPE was provided) or cut away, the subgrade improved by providing a 100 mm thick sand bedding layer placed over the trimmed waste rock surface, and the liner installed. All subsequent phases (a total of approximately 90,000 m^2) used the same lining system and construction was completed in October 2012. Since installation of the HDPE liner, no seepage out of the CDF has been observed.

10 CONCLUSION

The following conclusions are made regarding the use of bituminous geomembranes at the Cerro de Maimon mine:

- Ambient temperatures of 37ºC can result in geomembrane temperatures as high as 86.2ºC. This appears to be at or near the softening point of the bitumen.
- A combination of heat and tensile stress appear to be the primary cause of the bituminous geomembrane degradation and failure.
- An uneven subgrade may have contributed to the failure by inducing local stress points, but failures were also observed in areas with a smooth subgrade. In addition, the underlying geotextile appeared to be intact, which indicates that the bituminous geomembrane had not suffered a puncture failure.
- The testing of bituminous geomembrane seams should not be confined to ultrasonic tests.

It is recommended that extensive long-term testing is undertaken on bituminous geomembranes to assess the impact of heat and/or ultraviolet radiation on the liner integrity. Bituminous geomembranes are often marketed as an alternative to HDPE geomembranes, but they have not been subjected to the same degree of testing. There are no standardized specifications from the Geosynthetic Research Institute for bituminous geomembranes as there are for supply and seaming of other lining materials (GM13, GM17 and GCL3 for supply, and GM19 for seaming). If bituminous geomembranes are to replace HDPE or LLDPE geomembranes in waste containment applications, they should be subjected to the same internationally recognized, standardized testing procedures. This will enable the design engineer to make an informed choice.

11 REFERENCES

Li, A., Andruchow, B., Wislesky, I., and Olson, E., (2011). Field testing of Co-Disposal Techniques for Acid Generating Tailings and Waste Rock at Cerro de Maimon Mine. *Tailings and Mine Waste* 2011, Vancouver.

Geosynthetic Research Institute (GRI). Test Method GM13. Standard Specification for Test Methods, Test Properties and Testing Frequency for High Density Polyethylene (HDPE) Smooth and Textured Geomembranes.

Geosynthetic Research Institute (GRI). GRI Test Method GM17. Test Methods, Test Properties and Testing Frequency for Linear Low Density Polyethylene (LLDPE) Smooth and Textured Geomembranes

Geosynthetic Research Institute (GRI). GRI-GCL3. Standard Specification for Test Methods, Required Properties, and Testing Frequencies of Geosynthetic Clay Liners (GCLs).

Geosynthetic Research Institute (GRI). GRI Test Method GM19. Standard Specification for Seam Strength and Related Properties of Thermally Bonded Polyolefin Geomembranes

Breul, B., Huru, M., and Palolahti, A., (2008). Use of Bituminous Geomembrane (BGM) Liner for Agnico-Eagle Mine in Kittilä (Finland), Proceedings of EuroGeo4, paper number 245.

ASTM D7275. Standard Test Method for Tensile Properties of Bituminous Geomembranes (BGM).

ASTM D4945. Standard Test Method for Tensile Properties of Geotextiles by the Wide-Width Strip Method.

Subaquatic repairs of a hdpe liner system by using an asphaltic base geosynthetic material at "El Valle –Boinas" mine, Asturias, Spain

S. Castro Tejerina & K. Sánchez Arrótegui
Golder Associates Global Ibérica S.L.U, Madrid, Spain

ABSTRACT: As part of restart operations at "El Valle-Boinás" gold mine in Asturias, Spain, the Tailing Management Facility (TMF) associated to the treatment plant which presented various defects on its liner system were requested by the authorities to be fixed in order to obtain the necessary authorizations to operate and manage the installation; the mine owner held this engineering group to find a technical solution to fix the liner system.

The TMF was used during a previous closure time to manage the water runoff from the open pit and rainfall water, such volume of water prevented to use traditional methods for fixing the HDPE system.

As a technical solution for the defects found, it was proposed to use an asphaltic base geosynthetic material with a density higher than 1 g/cm^3 and adhesive, which allow each different surface to be glue underwater by a process named vulcanization an also seal the joins.

The solution apply had fixed the defects and had achieved the authorities request to obtain the authorization to operate and manage the TMF.

The article will also describe the results obtain after 5 weeks of installing the solution proposed.

1 INTRODUCTION

"El Valle-Boinás" gold mine is located in the north of Spain, in Asturias province on its Occidental side. The mine Project has a benefit plant and the produce tailings, will be storage on a TMF built for this purpose.

Previously to initiate the mining activities, the owner of the project carried out various tasks to adequate the storage area in order to obtain the authorization to operate and manage the facility. At the time start the permitting process, the storage facility was exclusive fill with runoff water from the open pit were the facility is located and rainfall water.

During the permitting process, the authorities carried out various site visit and requested that additional works were developed to ensure that the facility accomplish all the environmental requirements, which included the correct impermeabilization of the facility.

Previous episodes indicated the existences of defects on the liner, at the moment those were located below the water level. The owner request to an engineering group to search for a viable solution which will fix the defects found.

2 SOLUTION APPLIED

Due the fact that the defects were located below water level, it was impossible to use the custom techniques to fix a HDPE system, this issue lead the search to new solutions and defined the searching parameters, which are describe below:

- The material choose need to be glue to an existing HDPE material, taking into account that the join could not be done using heat;
- the proposed material should present the same properties, in terms of chemical and physic-mechanical resistances, as the existing material and;
- material and installation methodologies should granted the impermeabilization of the TMF.

After the searching process concluded a company with experience of using an asphaltic base geosynthetic material was approached.

The solution presented to the owner consisted in, using an asphaltic base geosynthetic material and its chemical union to the HDPE by a process named vulcanization using an adhesive capable to work under water and ensuring the sealing between surfaces.
This solution covered the prior requirements and allowed to fix the defects founded.

3 METHODOLOGY FOLLOWED

To install and fix the defect founded it was prepared a worked methodology between the engineering, the manufacturer and the owner which is describe in the following sections

3.1 *Initial review*

Previously to initiate the fixing activities it was carried out an inspection of the areas where was considered the existence of defects in the impermeabilization system.

This task was performed by a scuba diver team, which located the defect underwater, indicating the deep and the approximate size. While on surface the defect were topographic marked, in this way the defect were precisely marked.

This review was done in sections of 2-3 meters and was defined two types of defects depending on size and geometry. It was named “breaches” those defects bigger than 20 cm with a longitudinal geometry, including those with a L setting; in the other hand were named “leakage” those defects no higher than 10 cm with a circular or semicircular geometry.

During the initial review were found 13 “breaches” and 19 “leakage” in two areas of 130 and 250 linear meters.

3.2 *Repairing*

To repair the defects founded during the initial review, it was proposed the following methodology:

1) The scuba driver will relocated the defects according with available data from the initial review.
2) Will delimiting the area leaving 1 m on each side of the axis in where the defect is located by using two master ropes.
3) The scuba driver will reconfirm the deep of the defects located during the previous review and will left a distance of 0.5 m (min) below defect location; this will be use to define the length of the geosynthetic piece of material up to it final position, which will be located a minimum distance of 0.5 m from the head of the slope.
4) On surface a point mark will be done at the define length and a central axis will be trace to center the piece of material.
5) While the material it is cut and prepare (see following points) a scuba driver will clean the slope face to ensure the correct vulcanization process of the product.
6) Material preparation: Once the defect is located, the measurement will be transfer to the piece of material already cut.
7) Surrounding the defect will place a thick and abundant cord of adhesive, attending to site engineer criteria to ensure the maximum seal of the defect (see figure 1 and 2).
8) On the perimeter of the piece and up to the water level will be place a finer cord which purpose is to avoid possible undesired movements of the piece (see figure 1and 2).

9) Once the piece is ready, it will be center on the sign already made, the area should be clean and the adhesive applied. The piece will be fixing to the berm mechanically by using a thread bar (30 x 30 x 30 on a U form).
10) The scuba dive will clean the area once again while step 9 is occurring.
11) The piece mechanically fix will be slide down the slope and the scuba dive will be place it properly.
12) Finally the operative on surface along with the scuba dive will place a certain amount of sandbags on the axis of the defect, one of the sandbag have to be on top of the defect, and on the perimeter of the piece.
13) The sandbag schemes propose will remain in place at least 4 weeks, to ensure the chemical vulcanization process between the different products.
14) The mechanical fixes will be seal by welding a piece of geosynthetic material on top of the thread bar, by using this will be ensure that no infiltration will pass through this point. The dimension of the fixes and the sandbags lines can be modify according with the dimension of the piece and are left to the site engineer criteria.

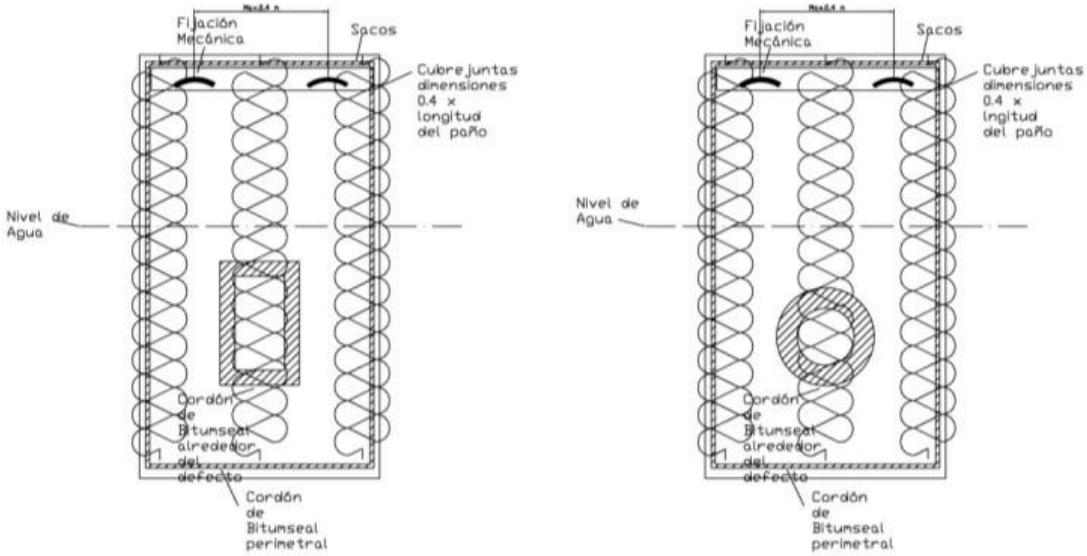


Figure 1. Material piece configuration

According with the methodology describe above, was fixed 100% of the defects detected. Following a serial of pictures showing the reparation process are presented

3.3 *Further actions*

Once the Works were done after 5 weeks an inspection was carried out to verify the status of the repairs.

The objective of the inspection was to verify that the sealing and the joins between the materials were produced as was expected, and also to ensure that the defects repaired did not presented any failure that will lead to a poor sea of the defect.

A scuba team performed an inspection of the repairs according with the following criteria already establish:

- The sandbags maintain the same position.
- There are not roughnesses on the cloth surface placed.
- The cloth was seal, there were no miss joins between materials.
- There were not lateral displacements.

The inspection carried out showed that 100% of the defects were without any roughness, seal and without lateral displacement. Only to mention that a line of sandbags were out of place due the welding of the mechanical fixation.



Figure 2. Geosynthetic cloth ready to be place



Figure 3. Axis of the defect marked on the Berm.



Figure 4. Mechanical fixation of the geosynthetic cloth



Figure 5. Final result of a repaired defect.

4 CONCLUSIONS

After all the work developed can be conclude the following:

- It is possible to repair defects on a HDPE liner under water.
- The joins between geosynthetic material from different origins it possible throughout chemical process (vulcanization).
- The. Durability and guarantees of the material are maintained along the time.
- Hydrostatics pressures generated by the water help to fix the cloth to the slope face.

5 ACKNOWLEDGEMENT

The authors, would like to express their gratitude to the site property for it authorization to present the this article and also to the opportunity to develop the Project together.

Mining

Mine Water Treatment

Coal mine effluents: tackling the selenium issue

Lukas Ryan Moore & Jean Robert Durand
Kemira Minerals and Metals, Atlanta, GA, USA

ABSTRACT: Mining is essential to our modern way of life. Whether for energy (oil, uranium, and coal), or construction (metals and minerals), mining affects us all. However, mining is a potential source of environmental contamination to the most vital fluid, water. Contaminated mine water has become an increasing concern, making the treatment of such water critical and mandatory. Selenium is an element of concern in mine effluents that often effects coal explorations and processing facilities. A technology has been developed and evaluated on the mine effluent obtained from a typical coal mining operation in Western Canada. This technology successfully reduced selenium concentration in the mine effluent from 545 ug/L to below 5 ug/L. An evaluation of dosage demand and process limitations, including temperature, ion sensitivities, and flocculation were explored.

1 INTRODUCTION

There is no question that man is dependent on fossil fuels. Of the fossil fuels, coal is the most plentiful. The Raw Material Data Base (RMD) states that 7,695 Mt of coal was mined in 2011, of which ~14% was produced in North America (Figure 1). (RMD, 2013) At the current rate of consumption it is predicted that the planet can sustain another 190 years before the coal deposits have been depleted. (Meegoda, 2011) Coal-related activities and the growth of such activities have caused significant environmental challenges, associated with both the water (process, runoff, etc.) and the solids (fly ash, boiler slag, coal stockpiles, etc.). The air and water contaminants resulting from coal-related activities include oxides (such as SOx, NOx, SeOx), mercury and more.

Selenium has surfaced in recent decades as a major impurity of concern in the mining and utilization of fossil fuels due to its toxicity and level of bioaccumulation. If left untreated, selenium can pose a significant threat to aquatic life (Lenz, 2009). The National Primary Drinking Water Standard is 50 ug/L for total selenium and the National Fresh Water Quality Standard is 5 ug/L for total selenium (EPA 2001; EPA 2011). British Columbia has placed a standard of 2 ug/L for total selenium.

Coal, for example, has been reported to contain 0.4-24 mg/L selenium prior to processing or usage (Lemly, 2004; Vesper, 2008). (Table 1) During coal processing/usage, selenium may become further concentrated as seen in the fly ash (0.2-500 mg/L). As with coal, oil is also a source of selenium contamination. Crude oil can contain levels of selenium between 500-2000 ug/L, while oil shale has been reported to contain levels between 1.3-5.2 mg/L. Refinery waste water has been reported with levels of selenium contamination as high as 75 ug/L. Such mining and industrial activities have led to an increase in selenium contamination in the aqueous biota,

hence the need for removal from coal mine related effluents. Selenium discharge limits are becoming enforced on the state level as restrictions on discharge are surfacing on NPDES permits (National Pollutant Discharge Elimination System). For example, West Virginia has announced limits of 4.7 ug/L monthly average discharge and an 8.2 ug/L maximum daily discharge (Harrison, 2010).

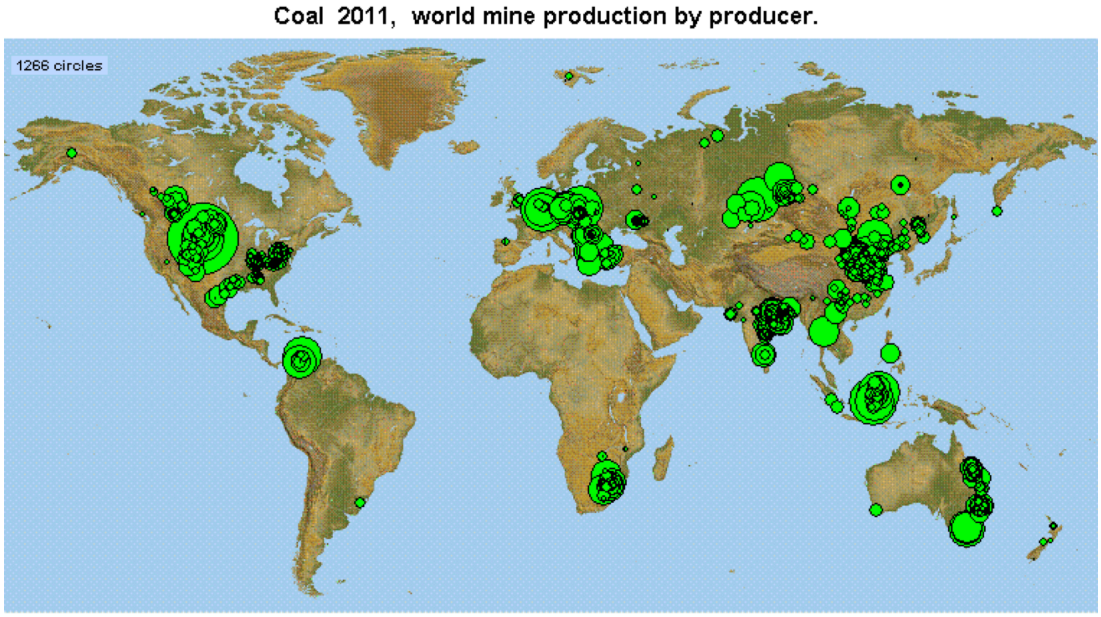


Figure 1. Global production of coal in 2011

2 RESULTS AND DISCUSSION

2.1 *Selenium Containing Coal Mine Effluent*

Raw water was obtained from a coal mine in Western Canada. Run-off from the mine site yields selenium concentrations of 545.6 ug/L and sulfate concentrations of 1052 mg/L (Table 2). The selenium species was discovered to be > 99% selenate. As this mine site is in Canada, seasonal sensitivities such as temperature and variations in competing ion concentrations must also be considered. The site requested a chemical means to achieve < 5 ug/L selenium in the discharge to accommodate the limits stated on the permit.

2.2 *Selenium Treatment*

A process was designed for the treatment of selenium from mine effluents (Figure 2). The initial step is a pH adjustment, if necessary. A proprietary, experimental treatment (E-4863) is dosed and allowed to mix for a controlled time, which in most cases required 2-5 minutes. The treated water is then transferred into a clarifier where a flocculant is dosed and allowed to settle for 10 min. At this point a filtration step may be applied, thus providing water with < 5 ug/L selenium and sludge that can be maintained in a land field or a tailings facility depending on the leaching characteristics.

Table 1. An example of the selenium concentrations found during the mining, processing and usage of coal.

Material/Waste	Selenium Concentration
Earth's Crust	0.2 mg/L
Surface Water	0.2 ug/L
Coal	0.4-24 mg/L
Coal Storage Pile (Leachate)	1-30 ug/L
Coal Cleaning (Process Water)	15-63 ug/L
Coal Cleaning (Solid Waste)	2.3-31 mg/L
Coal Cleaning (Solid Waste Leachate)	2-570 ug/L
Coal Burner Ash (Bottom Ash)	7.7 mg/L
Precipitator Ash (Fly Ash)	0.2-500 mg/L
Scrubber Ash (Fly Ash)	70-440 mg/L
Fly Ash (Leachate)	40-610 ug/L
Flue Gas Desulfurization (Process Water)	1-2700 ug/L
Flue Gas Desulfurization (Sludge)	0.2-19 mg/L
Boiler Cleaning Water	5-151 ug/L
Coal Ash Slurry	50-1500 ug/L
Ash Settling Ponds	87-2700 ug/L
Ash Pond Effluents	2-260 ug/L
Ash Disposal Pit (Leachate)	40-950 ug/L
Coal Gasification (Solid Waste)	0.7-17.5 mg/L
Coal Gasification (Solid Waste Leachate)	0.8-100 ug/L
Gasification (Solid Waste Leachate)	0.8-100 ug/L
Coal Liquifaction (Process Water)	100-900 ug/L
Coal Liquification (Solids Waste)	2.1-22 mg/L

Table 2. Raw water analysis

IC Analysis	Concentration (mg/L)	ICP Analysis	Concentration
Fluoride (mg/L)	2	Copper (µg/L)	ND
Chloride (mg/L)	9	Arsenic (µg/L)	ND
Sulfate (mg/L)	1052	Selenium (µg/L)	546
Bromide (mg/L)	2	Cadmium (µg/L)	1
Nitrate (mg/L)	299	Sodium (mg/L)	3
Phosphate (mg/L)	ND	Magnesium (mg/L)	198
Conditions		Aluminum (mg/L)	ND
pH	7.75	Calcium (mg/L)	59
Turbidity (NTU)	1.02	Manganese (mg/L)	3
Total dissolved solids (mg/L)	1393	Iron (mg/L)	120
Total Organic Carbon (mg/L)	< 5	Strontium (µg/L)	225
Conductivity (uS/cm)	2090		
Total suspended solids	4		

ND- none detected with IC unit with a detection limit of 1 mg/L.

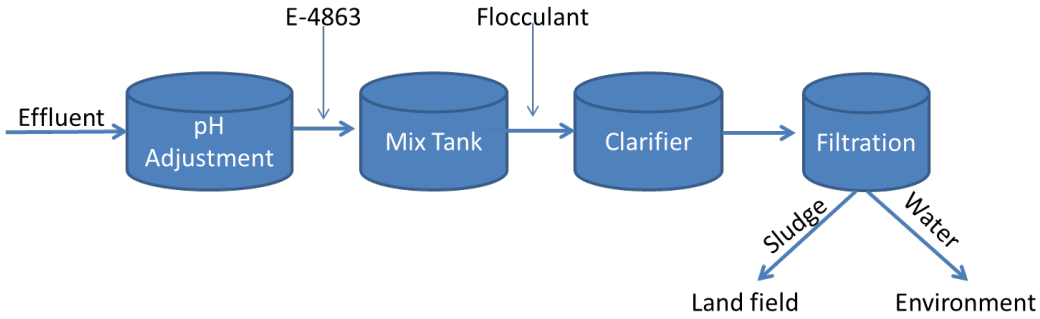


Figure 2. General treatment scheme for selenium removal using an experimental technology (E-4863)

E-4863 was evaluated towards the above mentioned water with the goal of obtaining a reduction in selenium concentration from 546 ug/L to < 5.00 ug/L. (Figure 3). 89% removal can be reached if the dosage is increased to 4000 mg/L in just 1 minute of resident time. The treatment kinetics were explored by considering the effect of treatment dosage as a function of time (Figure 4). At 2000 mg/L E-4863 61% of the selenium is removed during the first minute at which time the rate of removal decreases to 10% of that remaining for both 5 and 10 minutes of contact. While at a treatment dosage of 4000 mg/L 89% of the selenium is removed during the first minute with a total of 98% removal of selenium being observed after 10 minutes of resident time. It is also observed that increasing the treatment dosage to 6000 mg/L will allow for 98% removal in 1 minute, thus the removal kinetics are definitely influenced by treatment dosage.

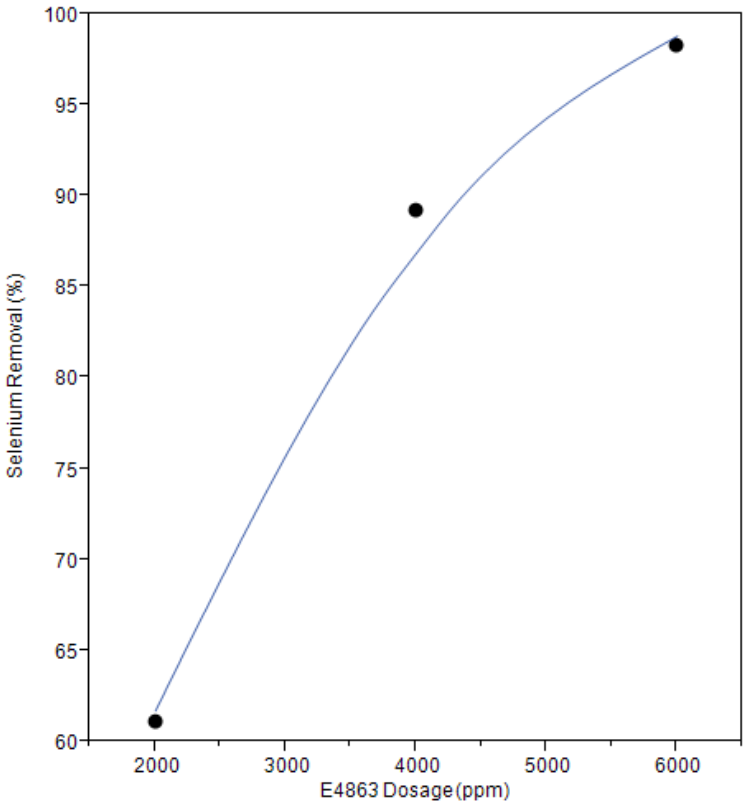


Figure 3. E-4863 dosage demand towards selenium removal (first minute)

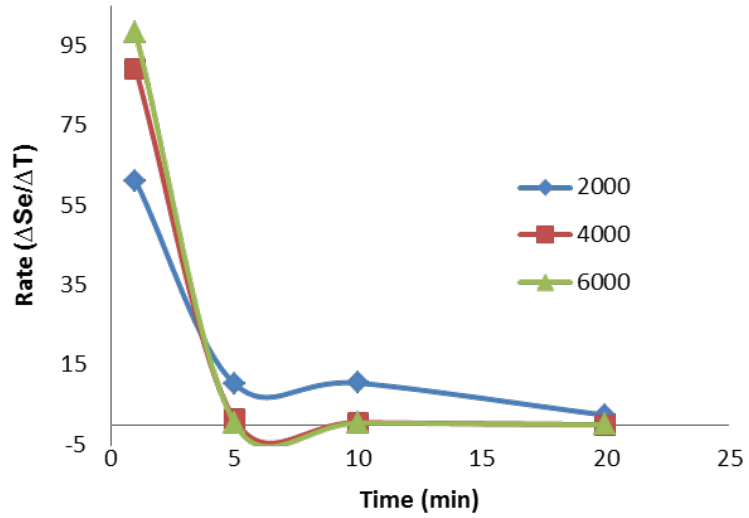


Figure 4. E-4863 selenium removal kinetics. (Calculated by the difference in selenium concentration divided by the change in time)

As selenium is of concern in coal mines both in the warmer Southeastern USA as well as the cooler regions of Canada seasonal sensitivities as a function of removal inhibition need to be understood. The dosage demand of E-4863 was evaluated as a function of temperature (Figure 5). The optimal temperature is at 25 °C where 83% removal is obtained at a dosage of 2000 mg/L E-4863, which can be increased to 96% removal by increasing the dosage to 4000 mg/L. However, an inhibitory effect is observed at temperatures less than 10 °C as a dosage of 6000 mg/L E-4863 is required to achieve 94% removal.

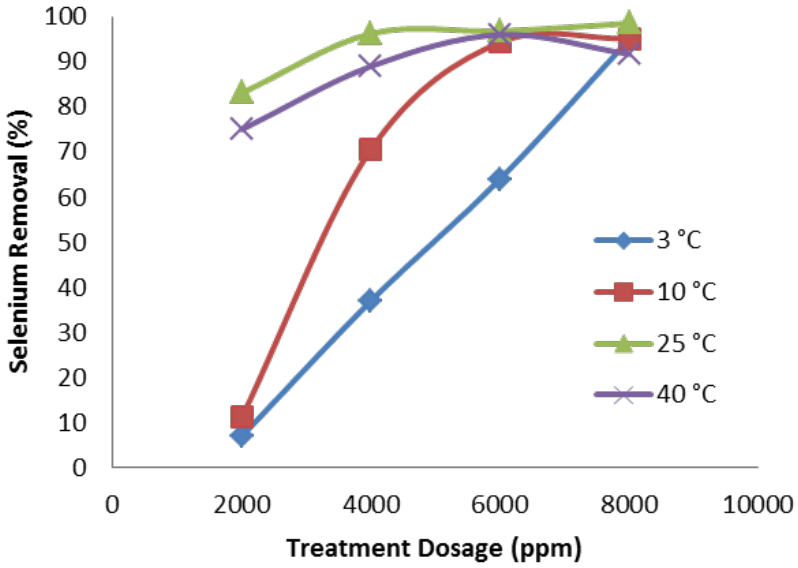


Figure 5. E-4863 dosage demand as a function of temperature sensitivity towards selenium removal

Understanding ion sensitivity of the treatment is critical when trying to expand the selenium removal to alternate mines. Anions would be the more likely to decrease the selenium removal efficiency through competing ion effects, thus oxyanions (sulfate) and halides (chlorides) were evaluated at varying concentrations (Figure 6). Applying 3500 ppm E-4863 while increasing the chloride concentration from 2200 mg/L to 4078 mg/L does not appear to have an inhibiting effect as 99% removal is still obtained even at the higher concentration. However, sulfates do appear to pose a substantial inhibiting effect as the removal is decreased from 98% at 956 mg/L sulfates to 81% at 5080 mg/L sulfates. Increasing the E-4863 dosage does help alleviate this inhibitory effect.

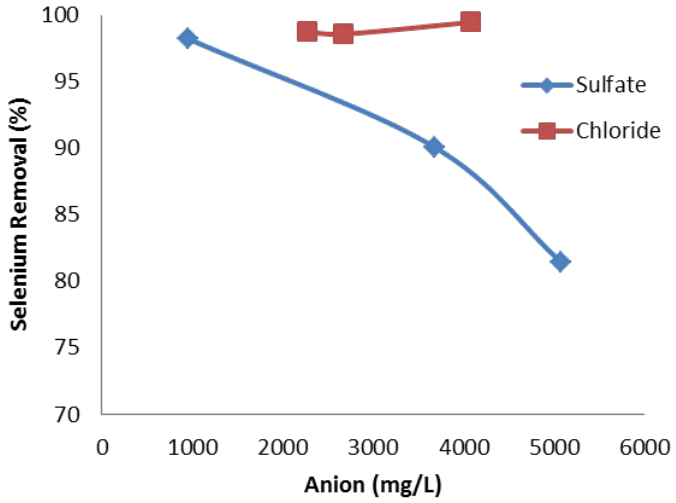


Figure 6. Ion sensitivity of treatment efficiency on selenium removal

2.3 *Sludge Dewatering*

It is obvious that the selenium removal can be accomplished to the desired < 5 ug/L criterion; however, it is only the first step in the water treatment process. Sludge dewatering and removal are critical steps of the treatment process. The application of an incorrect flocculant may lead to decreased throughput due to slow settling rates or poor dewatering. A series of flocculants ranging in charge and molecular weight were evaluated and particle size distribution of resulting flocs was measured. (Figure 7 & 8) This evaluation was performed both in-line and off-line to evaluate the floc stability. When the floc was prepared off-line, meaning outside of the particle size analyzer, one can conclude easily that a cationic flocculants could be problematic or at least require a more mechanical force for dewatering since 88% of the generated flocs are less than 100 um and with a wide particle size distribution. The three modes could represent a mechanical decomposition of the floc. Most of the anionic flocculants generate flocs with particle size that are 50% more than 100 um. As the flocculant charge is increased the resulting particle size distribution broadens. Furthermore, 75% of the floc generated from the non-ionic flocculant has a particle size greater than 100 um. In line flocculation (Figure 8) supports the hypothesis that nuetral floculants yield more stable, i.e. larger flocs.

The dewatering properties of the sludge generated are important to understand when considering storage capacity for the tailings facilities. The dewatering of the sludge generated from selenium removal with E-4863 followed by flocculation via a series of flocculants was measured using a capillary suction time (CST) (Figure 9). The CST is the time interval it takes an aqueous solution to traverse between two radial positions in a filter paper under the influence of capillary suction. A low CST value implies good sludge dewatering; i.e. the water from the sludge releases quickly with little impediment. When evaluating the flocculant charge, it was found that charge did not significantly affect the dewatering rate as all flocculants evaluated yielded a CST

of 25-32 seconds at a dosage of 5 ppm. However, increasing the flocculant dosage to 25 ppm significantly improves the dewatering as the CST can be decreased to 13 seconds. A treatment that was evaluated in the absence of a flocculant yielded a CST of 321.1 seconds, thus suggesting significantly slower dewatering for non-flocculated sludge.

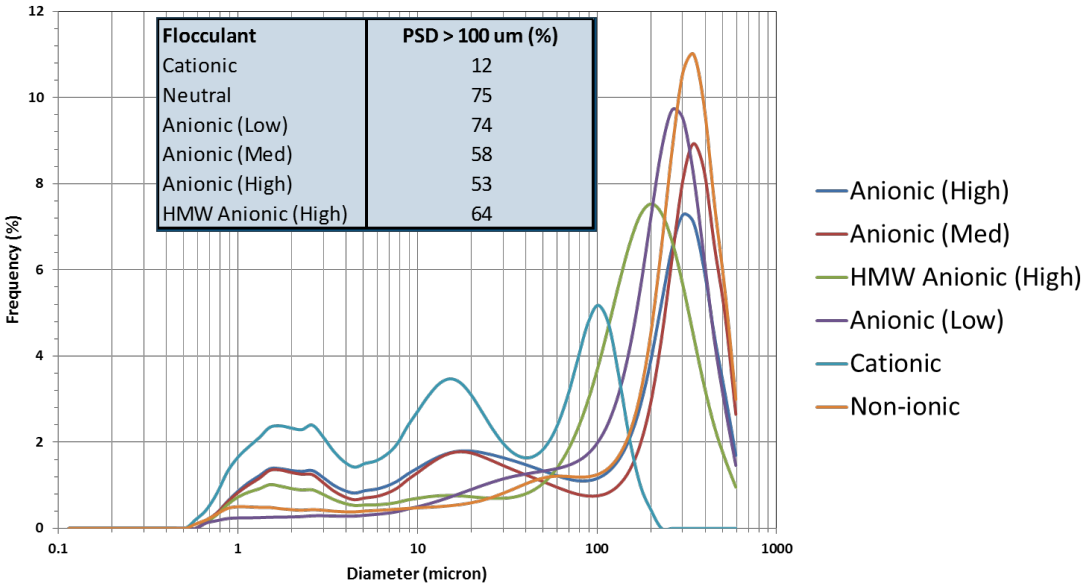


Figure 7. Effect of flocculant charge and molecular weight on the sludge particle size distribution (Off-Line Flocculation)

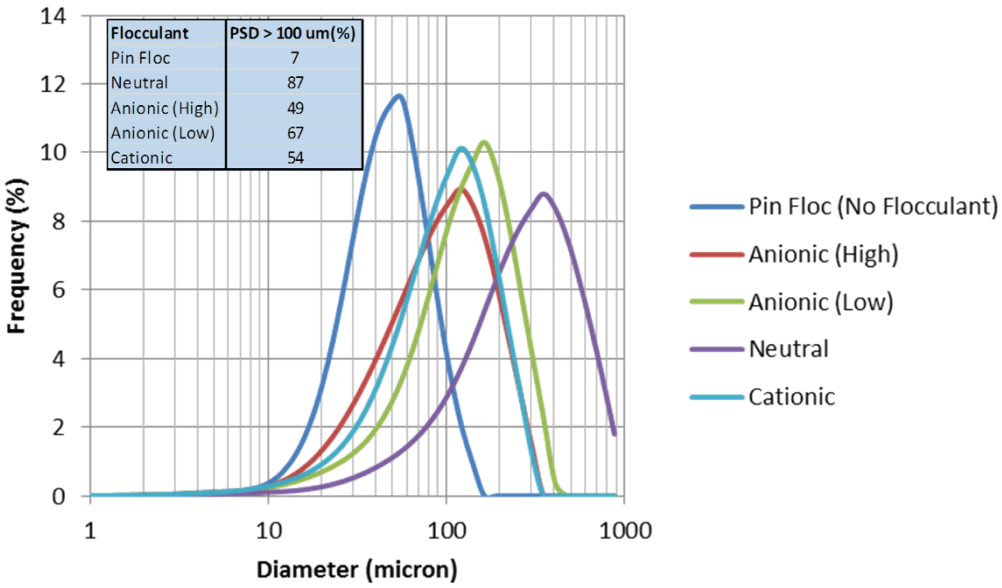


Figure 8. Effect of flocculant charge on the sludge particle size distribution (In-Line Flocculation)

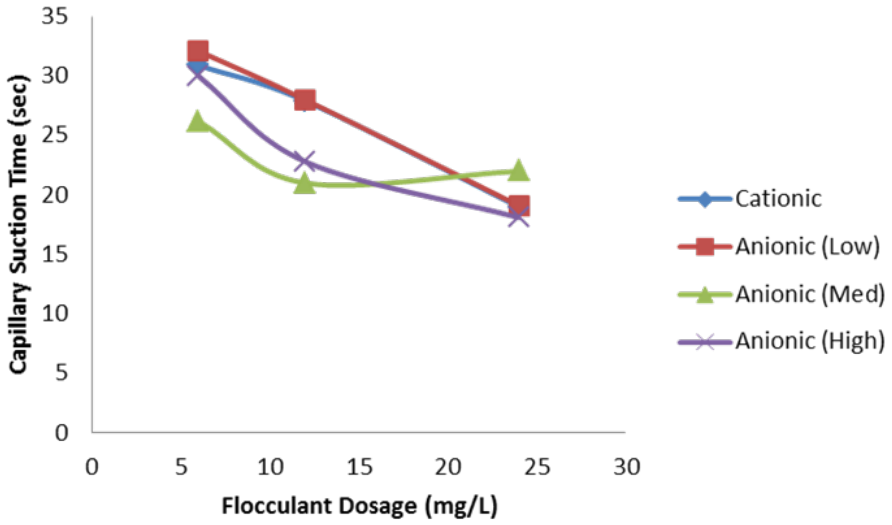


Figure 9. The effect of flocculant charge/dosage on dewatering time (CST)

When the sludge was dewatered using a filtering system, it was discovered that there was not a substantial difference in the selenium removal efficiency when filtered through 0.22 um membrane or sand as both generated > 98% removal under the optimal conditions. In an ideal system, filtration would not be required, but rather the sludge is allowed to settle in a clarifier and the selenium free water is collected in the overflow.

In such a system, the overflow clarity must also meet the permitted discharge criterion, which may vary from state to state; but is typically between 20-40 mg/L as a monthly average is permitted. Generally, a total suspended solids (TSS) level between 40-80 mg/L is cloudy and considered dirty if 150 mg/L is exceeded. To evaluate supernatant clarity, the TSS levels were measured 10 minutes after the flocculant addition and initial mixing. (Figure 10) Most of the flocculant systems evaluated produced an effluent with a TSS < 20 mg/L. There is a strange anomaly observed with a decrease in performance at 12 mg/L of the medium charged flocculant when applied, but repeated experiments confirmed that trends are reproducible.

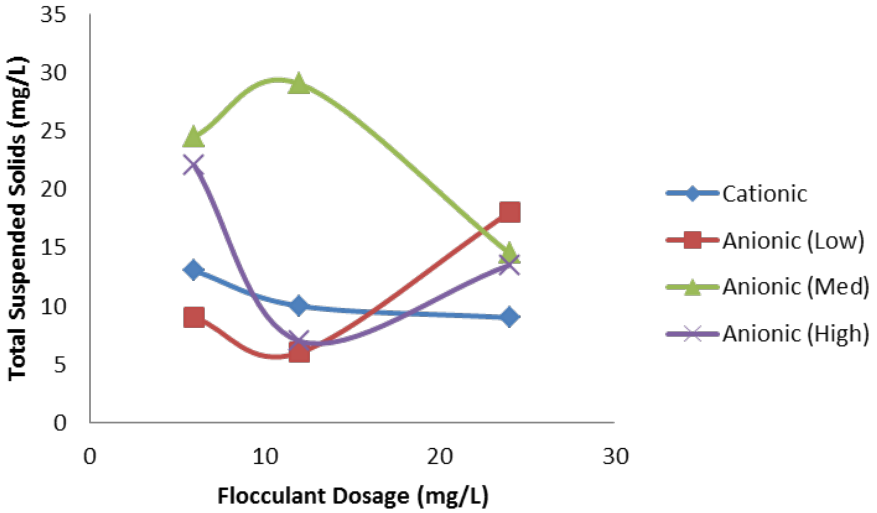


Figure 10. The effect of flocculant charge/dosage on the overflow water clarity (TSS)

3 CONCLUSIONS

A water treatment scheme was developed for the removal of selenium from mine produced effluents. This treatment involves a novel technology that was applied as a viable process for selenium removal from process water that was obtained from a coal mine in Western Canada. It was concluded that a dosage of 4000 mg/L E-4863 would yield ~90% removal of the selenium within the first minute of resident time, which can be increased to 98% if the resident time is increased to 10 minutes. Higher dosages yield corresponding improvement in removal efficiency and treatment times. Though high levels of removal can occur over a broad temperature range (3-40 °C) it required a higher dosage as the water temperature decreased. It was also concluded that elevated levels of sulfates could pose an inhibitory effect at lower dosage of E-4863, but could be overcome with an increase in treatment dosage. Post treatment with a low charged anionic flocculant provides the most optimal sludge handling conditions when considering sludge dewatering (CST), overflow quality (TSS), .and yields the most narrow particle size distribution of the sludge generated.

4 EXPERIMENTAL

4.1 *Treatment Process*

A solution of 300 mL raw selenium contaminated water was transferred to a beaker that is equipped with magnetic stirring capabilities. After comparing magnetic stirring versus overhead stirring with blades and with paddles, there was no noticeable dependence of the removal efficiencies on the stirring mechanisms. After a controlled mix time, the water was transferred to a settling tank where it could be combined with a flocculant (Kemira) to increase settling rates. The filtrate was transferred through a Millipore membrane filter (pore size of 0.45 µm, unless otherwise stated), which gave a clear, visibly solid-free water sample for ICP. E-4863 is a novel technology invented by Kemira.

4.2 *Instruments*

4.2.1 *Ion Determination*

The inductively coupled plasma mass spectrometer (ICP-MS) was an Agilent 7700x equipped with a He collision cell to remove polyatomic isobaric interferences. Samples were introduced to the nebulizer spray chamber by an ASX-500 series autosampler. The average of six replicate measurements were recorded. The isotope selected for Se determinations was m/z 78, while that used for arsenic was monitored at m/z 75. The MassHunter (version A01.02) data acquisition parameters were: RF Power 1550, RF Matching 1.80, Sampling depth 8.0, Carrier Gas 0.45, Nebulizer pump 0.10, S/C temp 2, Dilution Gas 0.65, extract1 0, extract2 -160, Omega Bias -90, Omega Lens 8.0, cell entrance -30, cell exit -60, deflect 0.0, plate bias -60, collision cell He 5.0, Oct Bias -18, Oct RF 180, energy discrimination 4. To mitigate the inherent variability of atmospheric pressure ionization sources (e.g. suppression or signal enhancement due to matrix effects) as well the variability associated with the autosampler, the calibration model for this study was an internal standard method. The detector response for the analyte signal was normalized versus the detector response of the internal standard prior to concentration determination. The internal standard was continuously introduced via a peristaltic pump and mixed with the sample prior to reaching the nebulizer. The internal standard was germanium (Ge) monitored at m/z 72. Quantitative elemental analyses of trace elements were conducted on a Bruker S4 Explorer wavelength-dispersive X-ray fluorescence spectrometer. Element distributions of selenium before and after treatments were used for qualitative and quantitative analyses of chemisorption of the contaminant species on inorganic polymeric solid sorbent. Headings

4.2.2 *Speciation*

Analyses were carried out by Southern Research Institute via UHPLC-ICP-MS.

4.2.3 Dewatering (Capillary Suction Timer)

Capillary suction time (CST) method was used to measure the time interval it takes an aqueous solution to traverse between two radial positions in a filter paper (Whatman No. 40, 9 cm) under the influence of capillary suction, as described in Standard Method APHA 2710 G. CST measurements were carried out using a CST instrument from Venture Innovations Inc. (California, USA).

4.2.4 Particle Size Distribution

Malvern Mastersizer S. was used to measure the particle size. The samples were run at 1600 rpm. The method applied a 3THD presentation which used a refractive index of 2.5935 (an estimate of the refractive index of the sample material), and imaginary refractive index of 0.1000 (accounts for any absorbance), and a refractive index of 1.3300 (refractive index of water, your dispersant fluid) for the calculations.

4.2.5 Overflow Clarity (Total Suspended Solids)

Analysis was carried out on a Hach DR/890 datalogging colorimeter.

5 REFERENCES

ATSDR, 2011. Agency for Toxic Substances and Disease Registry, The Division of Toxicology ToxFAQs. http://atsdr.cdc.gov/tfacts92.pdf (accessed April 2011).

EPA, 2011, National Recommended Water Quality Criteria. http://water.epa.gov/scitech/swguidance/standards/current/index.cfm (accessed May 2011).

EPA, 2001*, Selenium Treatment/Removal Alternatives Demonstration Project*; Mine Waste Technology Program Activity III, Project 20; MSE Technology Applications, Inc.: Butte, MT. EPA/600/R-01/077.

Harrison, T; Sandy, T.; Leber, K.; Srinivasan, R.; McHale, J.; Constant, J. 2010, Characterization and Treatment of Selenium in Water Discharged from Surface Coal Mining Operations in West Virginia*, SME Annual Meeting,* Preprint 10-142.

Lemly, A. D., 2004, Aquatic selenium pollution is a global environmental safety issue. *Ecotoxicology and Environmental Safety*, 59, 44-56.

Lenz, M.; Lens, P. N. L., 2009, The essential toxin: The changing perception of selenium in environmental sciences. *Science of the Total Environment,* 407, 3620-3633.

Meegoda, J. N.; Gao, S.; Al-Joulani, N. M. A.; Hu, L., 2011, Solid waste and ecological issues of coal to energy. *Journal of Hazardous, Toxic, and Radioactive Waste, ASCE*, 15, 99-107.

RMD, Raw Material Database, 2011 global production of coal, accessed 2013

USGS. United States Geological Survey. Mineral Commodity Summaries-Selenium 2007. http://minerals.usgs.gov/minerals/pubs/commodity/selenium/.

Vesper, D. J.; Roy, M.; Rhoads, C. J. 2008, Selenium distribution and mode of occurance in the Kanawha Formation, Southern West Virginia, U.S.A. *International Journal of Coal Geology*, *73*, 237-249.

Metal chelation: addressing the concerns of nickel in effluents

Laura Ann Sanders, Lucas Ryan Moore & Jean Robert Durand
Kemira Minerals and Metals, Atlanta, GA, USA

ABSTRACT: Metal contaminants such as nickel, mercury, lead and copper are of concern in mining effluent waters due to their negative effects on aquatic systems, including being readily adsorbed and bio-accumulating in animals and plants. This problem has received considerable attention in recent years as discharge criteria are more tightly regulated. A range of chemical and physical treatment technologies are available to remove contaminants such as soluble metallic salts, however, because of the complex variations in coordination properties across the periodic table, removal of these dissolved species can present a problem. Chelants are chemicals that form complex molecules with certain metallic ions, which can be tailored to allow for successful complexation with specific metallic families of interest as well as to provide a control over the solubility of such complexes. A chelant treatment package was developed to successfully remove nickel from mine effluents to below the site specific discharge criterion of 500 ppb. This evaluation explores a wide range of process variations such as pH, temperature, treatment dosage, and removal kinetics.

1 INTRODUCTION

The pollution of water resources due to the contamination from metal ions has recently caused worldwide concern (Rao et al, 2007). Metal ions of interest include, but are not limited to, nickel, mercury, lead, and copper, and are readily adsorbed and bio-accumulated by animals and plants. Nickel is an abundant element and occurs in nature in a wide variety of minerals, namely those containing large amounts of iron and magnesium. It is found in soils, waters, and foods, and generally occurs most frequently in combination with sulfur, arsenic and antimony (NPI, 1999). Nickel is an important metal in that it is resistant to corrosion and oxidation in both air and water. Therefore, nickel is used in a variety of applications, such as the manufacture of nickel-cadmium batteries, steel coatings, and in nickel and other metal-based alloys (Health Canada, 1994).

Nickel, in dissolved and particulate forms, enters the aquatic environment in variety of ways, including through effluents and leachates, as well as through atmospheric deposition after release from anthropogenic sources (Health Canada, 1994). Most industrial sources of nickel in effluents include those from nickel mining, smelting and refining, metal plating, gold mining, iron, and steel processing. Nickel concentrations in mining effluents are regulated by site-specific criteria.

Under the Clean Water Act, the EPA sets national technology-based pollutant limits for wastewater discharges from mining (EPA, 2011). Discharges from mining must meet best available technology/best practicable technology (BAT/BPT) limits for inorganic contaminants including cadmium, copper, lead, mercury, nickel and zinc.

The fate of nickel in the aqueous systems is determined by physical and chemical interactions. These include complexation, precipitation/dissolution, adsorption/desorption, and oxidation/reduction. Under normal conditions, nickel is associated with abundant iron and manganese particles which precipitate and absorb free nickel ions (NPI, 1999). This process occurs both in aqueous systems and in soils and sediments where iron and manganese are available, particularly serpentine soils where nickel concentrations may range from 1000 to 6000 mg/kg dry weight (Rajapakshaa et al, 2012).

There are a number of nickel removal technologies available to date for application in mining effluents. Methods being used include chemical precipitation, ion-exchange, adsorption, membrane filtration, and electrochemical treatment technologies (Fu et al, 2011). Each method has their own advantages as well as limitations in applications where metals removal is involved.

Chemical precipitation is effective and generally the most widely used metals removal process in the industry (Ku et al, 2001). It is achieved by either chemically altering the solvent matrix to either decrease or diminish the solubility of the substance or by conversion of the substance to an insoluble form (Britannica 2012A). The most widely used chemical precipitation techniques for precipitation of nickel are precipitation by hydroxides, sulfates or carbonates. Nickel can be removed by precipitation as hydroxide at pH ranging from 10-11 (Armenante, 1997).

Coagulants and sequestering agents can also be applied to achieve chemical precipitation. Coagulants are substances that cause particles, colloids, or dissolved contaminants in aqueous solutions to destabilize, forming small suspended aggregates (Britannica, 2012B). Ferric salts are sometimes used for applications involving metals such as chromium, copper, lead, zinc and nickel, to some extent, with the aid of an anionic polymer. This removal technique is less effective for nickel removal because nickel requires a pH of greater than 11 for effect removal from the aqueous phase (Johnson et al, 2008). Sequestering is the ability of a molecule to remove or separate metal ions from solution (Britannica 2012C). Typically, these agents are organic ligands which coordinate or complex to a metal ion. The processes of coagulation or sequestering of metal ions are generally followed by a process known as flocculation, where particle size of the precipitate increases and settling rates are improved. This is accomplished by the use of high molecular weight anionic polymers.

In metal contaminant removal by sequestration, it is important to understand the metal-ligand stability and interactions occurring. Predictions can be made to tailor a ligand towards a specific family of metals based on its physical properties, such as charge, size of the metal radius and hard/soft acid/base chemistry. The key to a successful precipitation lies in the ligand's ability to remain complexed, thus becoming labile only when desired.

Chelation is the ability of a single ligand or sequestering agent to coordinate to a single metal ion by two or more ligation sites (Moore et al, 2013). A chelating ligand, having more than one ligation site, has much stronger coordination strength than a monodentate ligand with only one ligation site (Clapp et al, 2006). Therefore, chelants can be used in chemical precipitation methods where a chelant forms a stable complex with a metal ion and the flocculant can help to cluster those newly formed complexes. This paper explores the use of a chelant, manufactured by Kemira, towards the removal of nickel from a mine effluent to below the site specific discharge criterion of 500 µg/L.

2 RESULTS AND DISCUSSION

A mine in North America operates a flotation process which functions to concentrate nickel. During this process, some levels of nickel remains in the gangue. This gangue moves to a separate plant where it is processed for other metals. During this process, nickel is lost to the effluent in levels approaching 0.2%. Water was obtained from this process and stored in a cooler at 1°C prior to use. Water analysis was carried out as it is important to understand the other ions present in the water. These ions can potentially act as either competing ions (sulfates, nitrates, etc.) for the treatment or provide an alternative coordination possibility for the contaminant itself. The raw water (untreated effluent) contained sulfate levels of 1526 mg/L, calcium levels of 7135 mg/L and a total dissolved solids (TDS) concentration at 2670 mg/L, as shown in Table 1. This

water also contained 1698 µg/L of nickel which needed to be reduced to 500 µg/L or less. This was a site specific regulation.

Table 1. Raw water analysis.

IC Analysis	Concentration	ICP Analysis	Concentration
Flouride (mg/L)	ND	Copper (µg/L)	377
Chloride (mg/L)	421	Arsenic (µg/L)	2047
Sulfate (mg/L)	1526	Selenium (µg/L)	545
Bromide (mg/L)	ND	Cobalt (µg/L)	199
Nitrate (mg/L)	ND	Sodium (µg/L)	853
Phosphate (mg/L)	ND	Magnesium (µg/L)	8649
Conditions		Aluminum (µg/L)	88
pH	8.2	Calcium (µg/L)	7135
Turbity (NTU)	5.0	Zinc (µg/L)	56
Total dissolved solids (mg/L)	2670	Iron (µg/L)	430
Hardness (as $CaCO_3$)	53.4	Nickel (µg/L)	1698
Conductivity (uS/cm)	3.85	Barium (µg/L)	48
Total suspended solids	31.5		

A chelant, KemMet 1140, was designed with a superior ability to remove select metal ions from aqueous systems and was evaluated in the above mentioned effluent to remove nickel to below the desired 500 µg/L discharge criterion. Figure 1 shows the process of the treatment using KemMet 1140. This treatment could either be continuously fed or applied via a batch process. This single stage treatment takes place in a mixing tank containing the process water, followed by transfer to a gravity settling tank. Once the solids have settled, they may be discharged to a tailings containment facility and the decontaminated process water may be discharged or undergo further treatment, if necessary. Faster solids/liquid separation is generally accomplished by the addition of common organic flocculants.

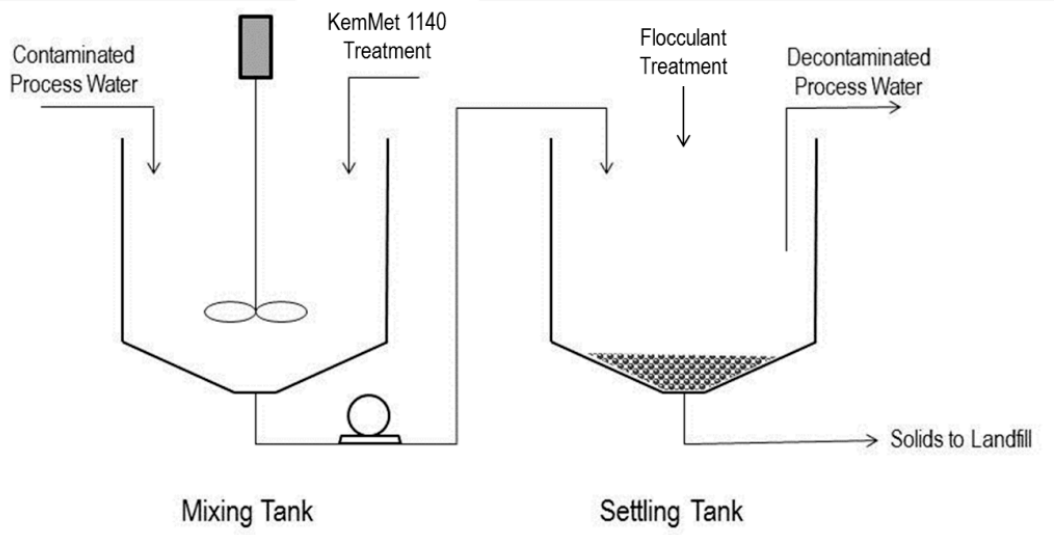


Figure 1. Schematic representation of water treatment in this work.

A Treatment dosage of KemMet 1140 was evaluated for the efficiency of nickel removal applying 0.625, 1, 10, 50, 100 and 200 mg/L treatment dosage (Figure 2). At treatment dosages of 0.625 and 1 mg/L, the discharge criterion of 500 µg/L was not met, but treatment dosage at 10 mg/L resulted in <100 µg/L nickel remaining in solution. The treatment range between 1 and 10 mg/L could be further narrowed down to reduce treatment dosage necessary for proper nickel removal in the future.

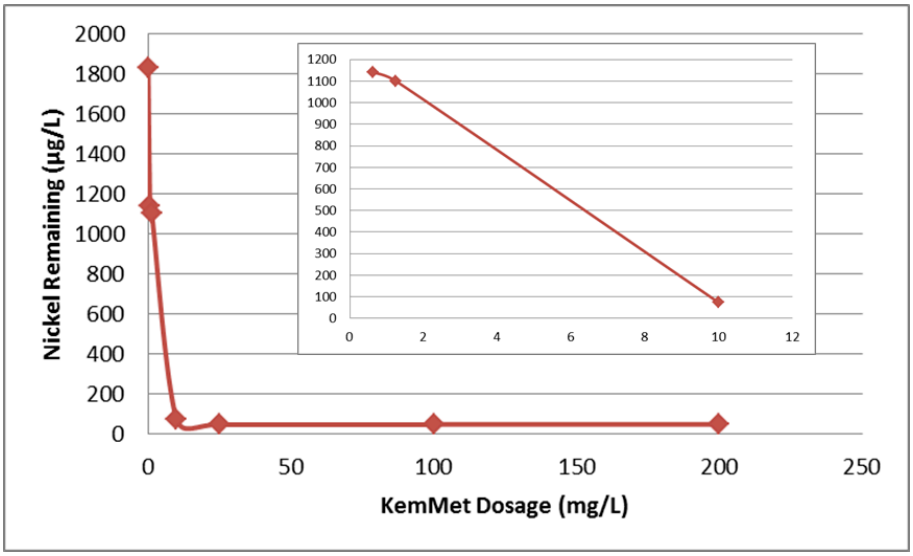


Figure 2. Effect of KemMet 1140 on nickel removal.

A good understanding of process limitations is necessary when transferring this technology to other mine sites. The first evaluation for process limitations involved monitoring the effect of pH on nickel removal by KemMet 1140. Dosages of 25, 100 and 200 mg/L KemMet 1140 were evaluated at 27°C for various pH's (Figure 3). The KemMet 1140 performance was consistent at 27°C when evaluated over a pH range of 5 to 10.5, but there appeared to be a loss in performance at pH 3. At pH 3 higher treatment dosage showed slight improvement in performance. At only 25 mg/L dosage, less than 50 µg/L nickel remained in solution for all pH's evaluated, except for that of pH 3.

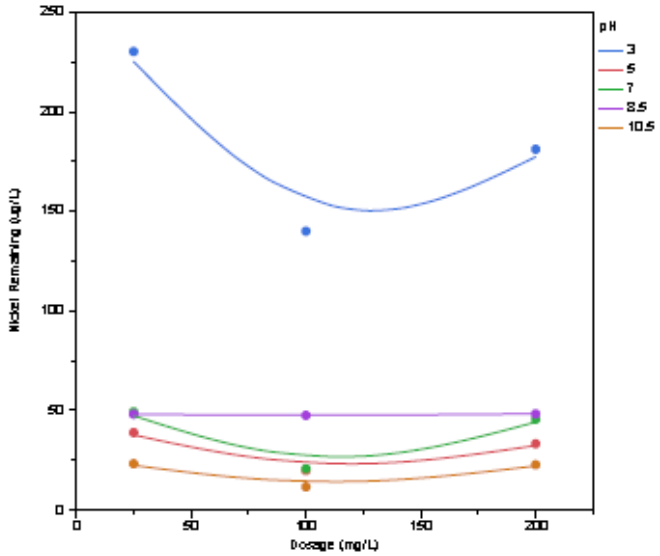


Figure 3. Evaluation of KemMet 1140 over a broad range of pH's at 27°C

To further evaluate process limitations, dosages of 25, 100, and 250 mg/L KemMet 1140 were evaluated at three different pH's and three different temperatures (Figure 4). In each condition evaluated, less than 500 µg/L nickel remaining was reached. Nickel remaining in solution reached less than 50 µg/L at all temperatures and dosages evaluated at pH 5 and 7. There was a loss in performance at pH 3 as previously noted. Lower temperatures improved performance at this pH.

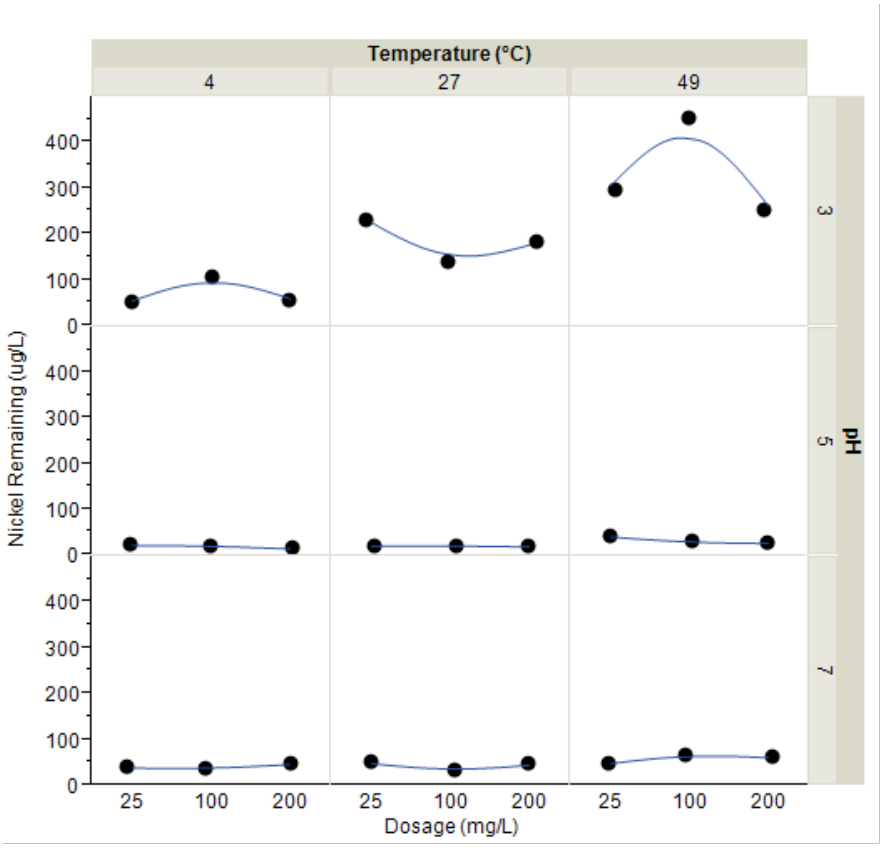


Figure 4. Evaluation of KemMet 1140 over a broad range of process conditions.

The mine site that was studied has observed a seasonal inconsistency in the nickel removal process throughout the year with their current method of precipitating nickel hydroxide. The site currently adds lime to their effluent to adjust pH, thereby reducing nickel concentration in solution. To simulate the seasonal sensitivity of this precipitation mechanism, the pH was adjusted while controlling the temperature at 4°C and 27°C (Figure 5). Less than 500 µg/L nickel remained in solution at 27°C when pH was adjusted to 9.5 with sodium hydroxide. The best removal was seen at pH 10.5 at 27°C, where 15.9 µg/L nickel remained but at lower temperatures, nickel removal performance decreased and the nickel remaining in solution was >200 µg/L. These results showed that while pH can be adjusted to remove nickel, without chelation treatment, it is very dependent on temperature for optimal removal of nickel. This phenomenon was observed to be much worse in actual practice at the treatment plant onsite as 500 µg/L was not met during the winter months.

Another process limitation that is often of concern is treatment time. At both 4 and 49°F, nickel removal was evaluated with 100 ppm of treatment at pH 8.5 (Figure 6). At both temperatures examined, 95% removal was observed within the first minute of treatment with KemMet 1140. Nickel content remaining in solution reached approximately 60 µg/L after treatment for 1 minute and maintained nickel content of 60 µg/L in solution over 10 minutes of treatment. This supports that rapid removal could occur once treated with KemMet 1140, removing concerns of time limitations from the chelation/precipitation process.

Often, chemical precipitation methods work well for metals removal but a drawback of the method is sludge volume and stability. In a test where 500 mL mine effluent water was treated with 25 mg/L KemMet 1140, a dry cake with a mass of 0.013 g was formed which was 0.003% of the original sample amount (Figure 7). Therefore, sludge volumes of this small amount should not be of concern to operators at the mine site.

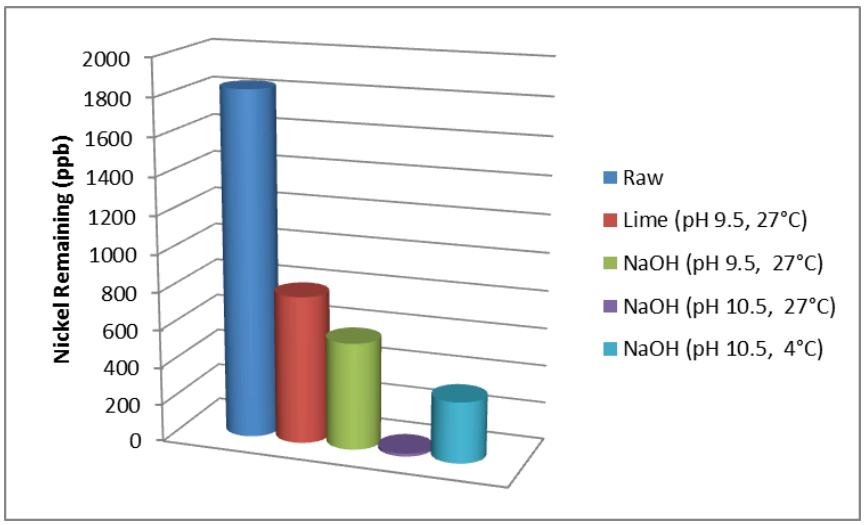


Figure 5. Effect of various hydroxide precipitation conditions on nickel removal.

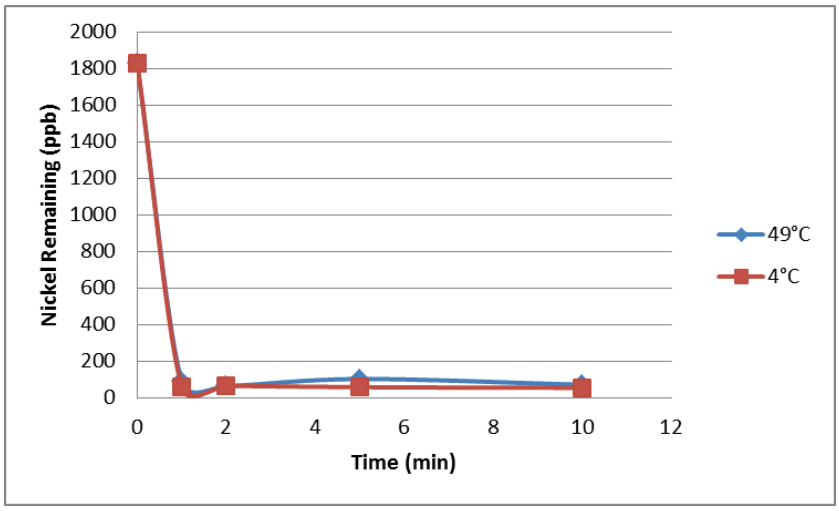


Figure 6. Effect of treatment time on nickel removal at 4 and 49°C.

3 CONCLUSIONS

The required discharge criterion was met under various processing conditions established during lab scale evaluations. To examine seasonal sensitivities which are currently observed, the effect of temperature on nickel removal was studied. Results suggested that over a range of temperatures between 4 to 49°C, nickel removal efficiency was not negatively affected as long as the pH was maintained above 3. KemMet 1140 yield optimal performance at both pH 5 and pH 7. At dosages as low as 10 mg/L, less than 100 µg/L nickel remained in solution. The effects of pH on nickel removal, as nickel hydroxide, without added chemical reagents were examined and it was found that the removal efficiency was highly affected by temperature, thus would explain the seasonal sensitivities observed during the current treatment process. Future work would include field evaluations at the mine site for nickel removal by KemMet 1140.

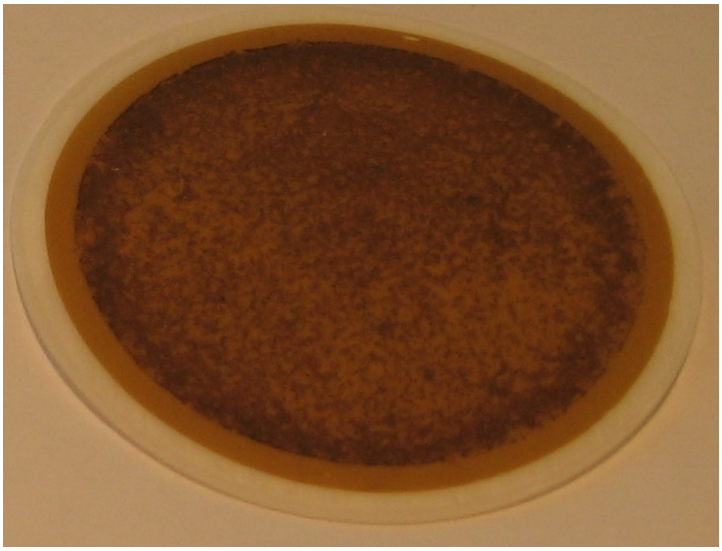


Figure 7. Sludge volume as a result of KemMet 1140 treatment.

4 EXPERIMENTAL

4.1 *Materials*

KemMet 1140 and Superfloc A130HMW (anionic flocculant) are manufactured and sold by Kemira. The flocculant is sold as a solid material and was prepared by dissolution in DI Water to 0.25% solids in solution before adding to nickel containing mine water.

4.2 *Procedure*

A sample of 500 mL of supplied mine water was added to a 600 mL beaker equipped with magnetic stirring. The pH was adjusted to the desired range using diluted nitric acid or 10% sodium hydroxide. Once the experiment-desired pH and temperature was reached and controlled, the KemMet 1140 was added using a 100-1000 µL precision pipette equipped with disposable pipette tips. At the end of the two minutes agitation, flocculant (Superfloc A130HMW) was added and allowed to agitate at the same speed for 5 minutes. The precipitate was allowed to settle for 10 minutes prior to filtering through a 0.45 µm Millipore filter. The filtrate was then submitted for ICP to obtain nickel analysis.

4.3 *Instrumentation*

In this study, a Thermo Scientific ICP-AES system model iCAP 6500 equipped with a charge injection device detector and a CETAC ASX-520 autosampler was used for determination of nickel species in water samples. Low detection limits (10 µg/L for nickel) were achieved by preconcentration of 100 mL aqueous samples. Quantitative elemental analysis of trace elements was conducted on a Bruker S4 Explorer wavelength-dispersive x-ray fluorescence spectrometer.

5 REFERENCES

Armenante, P.M. (1997) http://cpe.njit.edu/dlnotes/CHE685/Cls06-2.pdf (Accessed May 2013).

Clapp, L.A., Siddons, C.J., VanDerveer, D.J., Reibenspies, J.H., Jones, S.B., Hancock, R.D. (2006) The Amide Oxygen Donor. Metal Ion Coordinating Properties of the Ligand Nitrilotriacetamide. A Thermodynamic and Crystallographic Study. Dalton Transactions, 16, 2001-2007.

Encyclopedia Britannica A. http://www.britannica.com/EBchecked/topic/108784/chemical-precipitation; (Accessed May 2013).

Encyclopedia Britannica B. http://www.britannica.com/EBchecked/topic/637296/water-supply-system/286122/Coagulations-and-flocculation (Accessed May 2013).
Encyclopedia Britannica C. http://www.britannica.com/search?query=sequestering+agents (Accessed May 2013).
Fu, F., Wang, Q., (2011) Removal of Heavy Metal Ions from Wastewaters: A Review, Journal of Environ-mental Management, 92, 407-418.
Health Canada (1994) http://www.hc-sc.gc.ca/ewh-semt/pubs/contaminants/psl1-lsp1/compounds_nickel_composes/compounds_nickel_composes_2-eng.php (Accessed January 2013).
Johnson, P.D., Girinathannair, P., Ohlinger, K.N., Ritchie, S., Teuber, L., Kirby, J., (2008) Enhanced Removal of Heavy Metals in Primary Treatment Using Coagulation and Flocculation, Water Environment Research, 80, 5, 472-479.
Ku, Y., Jung, I.L. (2001) Photocatalytic Reduction of Cr (VI) in Aqueous Solutions by UV Irradiation with the Presence of Titanium Dioxide. Water Res., 35, 135-142.
Moore, L.R., Durand, J.R., Strickland, F. (2013) Copper Removal from Mine Effluents-From Lab to Field Evaluations, Mine Water and the Environment
National Pollutant Inventory (NPI), 1999, www.npi.gov.au/substances/nickel/references.html (Accessed May 2013)
Rao, G.P., Lu, C., Su, F., (2007) Sorption of Divalent Metal Ions from Aqueous Solution by Carbon Nanotubes: A Review. Separation and Purification Technology, 58, 224-231.
Rajapakshaa, A.U., Vithanage, M, Oze, C, Bandara, W.M.A.T., Weerasooriya, R. (2012) Nickel and manganese release in serpentine soil from the Ussangoda Ultramafic Complex, Sri Lanka; Geoderma, 189-190, 1-9.
US Environmental Protection Agency, (2011) Ore Mining and Dressing Preliminary Study Report EPA-820-R-10-025, http://water.epa.gov/lawsregs/lawsguidance/cwa/304m/upload/orereport.pdf (Accessed May 2013).

Mine water treatment with geotextile tube system at Goldex Mine (Val d'Or, Qc, CANADA)

Jocelyn Douhéret
ASDR Environment, Malartic, Quebec, CANADA

Andy Lister
Tencate, Toronto, Ontario, CANADA

ABSTRACT: AGNICO Eagle operates Goldex Mine an underground gold mine in Val d'Or (Qc, CANADA) since April 2008. In 2009, Goldex decided to better handle mine water which was formerly directed to sumps. Solids from sumps were daily emptied mobilizing a full time scoop tram. Furthermore, water from the sumps was abrasive causing slurry pumps renewal. A pilot test using a geotextile tube started in January 2010. High TSS mine water was conditioned in line with a coagulant and a floculant prior dewatering with a geotextile tube. As results were convincing an automatic system was installed to feed two geotextile tubes in sequences. Mine water average flow is about 60 m3 per hour with a 4 000 mg/L TSS level. Clean water comes out of the bags at a 10 mg/L TSS level. Once a geotextile tube is full, solids are removed by a scoop tram and reprocessed in the ore treatment process.

1 INTRODUCTION

AGNICO Eagle has been operating the Goldex underground Gold Mine in Val d'Or (QC, CANADA) since April 2008. The Mine is located in a semi-urban location at the west end of Val d'Or, QC. (Population 45 000).



Picture 1. Goldex Mine in Val d'Or.

In 2009, Goldex decided to better handle mine water. Mine water was formerly directed to sumps. Solids from sumps were regularly emptied mobilizing a full time scoop tram. Furthermore, water from the sumps was highly abrasive causing frequent slurry pumps renewal.

The gold mine extracts 8500 tons of ore per day. The Lowest level of the underground mine is situated at 2500 ft beneath the surface. Ore is extracted from the bottom of the gold reef.

Mine water comes from water infiltration at the surface as well as from the reef itself. This natural water is composed of 80% Mine Water. The water is also used for underground operations such as rock crushing, machinery cleaning as well as dust control. Mine water runs along the gallery eroding the mine shaft and transporting a high level of suspended solids. This water is collected in a sump located at the very bottom of the mine (level 76 under ground level).



Picture 2. Sump collecting Mine Water



Picture 3. Sump pump

Mine Water is then pumped to the surface using high power pumps and booster pumps. This Mine Water is extremely abrasive, which increased the maintenance costs on the pumps. a. In addition the Mine Water was not clean enough to meet the discharge criteria into the local water course. Quebec regulation, Directive 019 from the Ministry of Environment, lists discharge criteria as shown in Table 1.

Table 1: Discharge Criteria under Quebec Regulation

PARAMETER	Monthly Average Concentration	Maximum Concentration
Arsenic	0,2 mg/l	0,4 mg/l
Copper	0,3 mg/l	0,6 mg/l
Iron	3 mg/l	6 mg/l
Nickel	0,5 mg/l	1 mg/l
Lead	0,2 mg/l	0,4 mg/l
Zinc extractible	0,5 mg/l	1 mg/l
Cyanures	1 mg/l	2 mg/l
Hydrocarbons (C10-C50)	----------	2 mg/l
TSS	15 mg/l	30 mg/l

Solids at the bottom of the sump were removed daily by a scoop tram dedicated to this full time.



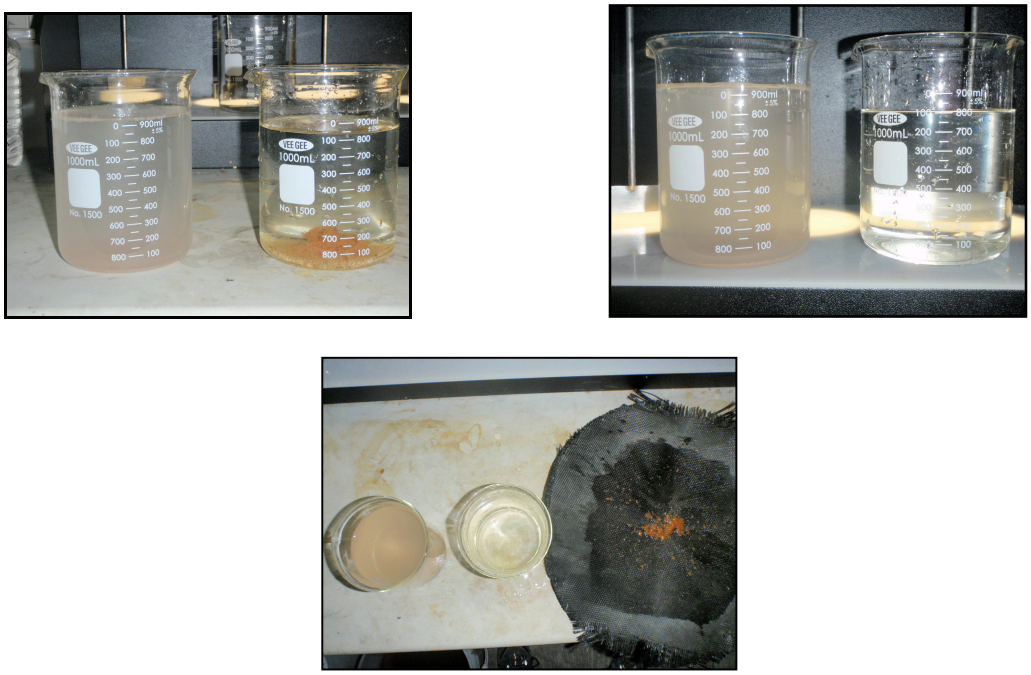
Picture 4. Scoop Tram

With the above factors in mind, Goldex Mine decided to find a better solution to manage their mine water. Goldex Mine had one goal:

- Reduce mine water management cost by
    - Reusing water
    - Obtaining dryer solids

2 PROPOSED SOLUTION AND PILOT TEST

A Rapid Dewatering Test (RDT) with a woven geotextile tube was conducted. The purpose of the RDT test is to identify the appropriate polymers, their dosage rate and the effectiveness of the woven geotextile. The chemical conditioning consisted of using a coagulant first to precipitate dissolved ions followed by a flocculant to create a strong flock that would allow the water to be released from the sediments and subsequently filter through the geotextile tube.



Picture 5. Chemical conditioning results

A pilot test was then proposed. The process consisted of:

- Constant Agitation of the slurry in the Sump
- Pump the Mine Water to the treatment station
- Coagulant injection
- Floculant injection
- Static Mixer, mixes both coagulant and flocculant
- Treated mine water pumped to a geotextile tube
- Clean water is collected and recycled to the crusher

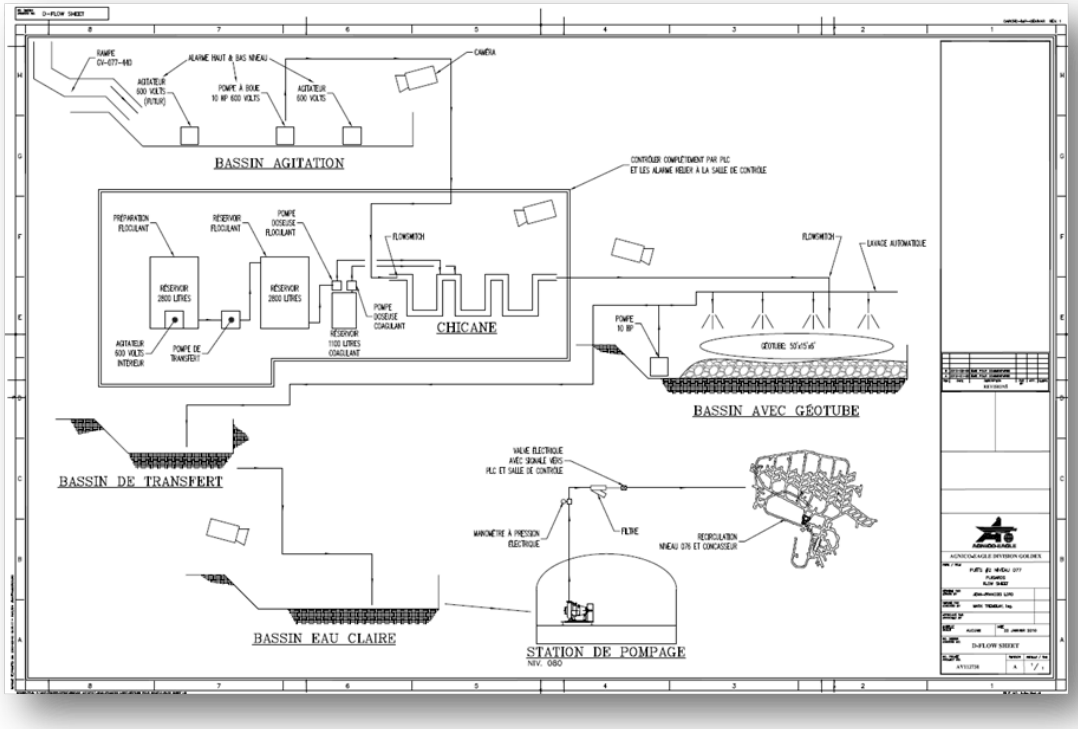


Figure 1: Principles of the process

A pilot test using a geotextile tube started in January 2010. High TSS mine water of 4000mg/l was conditioned in line with a coagulant and flocculent prior to pumping to the geotextile tube which was located in a nearby gallery (See Figure 1, Principles of the process). The dimensions of the geotextile tube were 30ft (9.14m) circumference X 50 ft(15.2m) long.



Picture 6: Chemical conditioning unit



Picture 7: Geotextile tube in a gallery

Water coming out of the geotextile tube was extremely clean with a TSS of 10mg/l.



Picture 8. Clean water

3 UNDERGROUND OPERATION

With the positive results of the pilot test an automatic polymer feed system was installed to feed in sequence two 30 ft (9.14m) circumference x 50 ft(15.2m) long geotextile tubes.

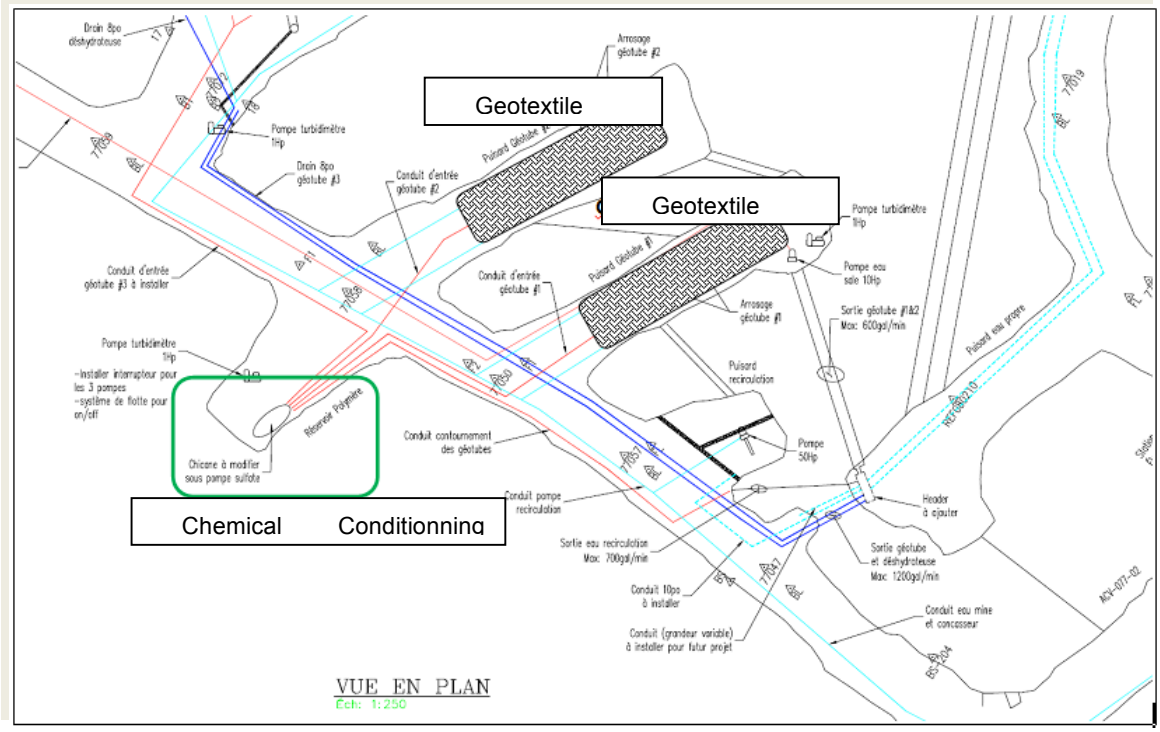


Figure 2. Installation Plan

A more sophisticated and fully automated treatment unit was installed to ensure proper chemical conditioning of Mine Water prior to filtration and dewatering by the geotextile tube.



Picture 9. Polymer preparation unit



Picture 10. Chemical dosing and mixing unit

Mine Water is pumped 40 minutes per hour at an average flow rate about 60 m3 per hour with a TSS level around 4 000 mg/L. Clean water comes out of the bags at a TSS level around 10 mg/L.

A sprinkler system was installed to spray water on the geotextile tube to prevent clogging. Clean water coming out of the geotextile tube is used for crushing operation as well as equipment cleaning.

The geotextile tubes are filled 40 minutes every hour, 24 hours a day, 7 days a week during weeks. Solids are retained in the geotextile tubes. A complete fill cycle lasts approximately 1 month at which time the geotextile tubes are full holding 65 m3 of solids. The solids are then removed by the scoop tram and reintroduced into the ore treatment process. Table 2 shows performances of the geotextile tube solution regarding water treatment and solids dewatering.



Picture 11. Sprinkler System

Table 2: Performances of the geotextile tube solution

Parameters	Raw Water	Clean Water	Dewatered Solids
TSS Level (mg/L)	4000	10	n/a
Turbidity (NTU)			n/a
% solids	1 to 0,25	0,001	65
Specific Gravity (metric Tons/m3)	1,6	1,0	3,5

4 CONCLUSION

Geotextile tube solution with proper chemical conditioning allows for better Mine Water management.

Low maintenance clear water pumps then replaced the former slurry pumps. Clean water is re-used for mine operation and reduces the environmental impact of the mine on the local environment. The geotextile tube system also replaced a full time scoop tram with driver. Solids are removed once a month and follow the same mill process as ore extracted from the reef.

Using the geotextile tube solution, Mine water management costs were reduced by more than 50% compared to the previous manner.

Titanium dioxide mediated removal of benzene-like compounds from wastewater and industrial effluent

Stuart Linley & Frank Gu
Department of Chemical Engineering and Waterloo Institute for Nanotechnology, University of Waterloo, Waterloo, Ontario, Canada

ABSTRACT: One of the largest problems emerging in the water treatment industry today is the presence of persistent benzene-like compounds. Benzene, toluene, phenol, naphthalene, and xylene are some of the major byproducts from refining crude oil and can be found in the effluent of such operations in concentrations of up to several thousand ppm. Current, traditional water treatment methods are incapable of removing these compounds to safe levels and novel treatment methods are required if this water is to be remediated; treatment methods that must be capable of removing or destroying these pollutants at the molecular level. Titanium dioxide has long been known as a strong photo-oxidative catalyst under UV light, producing radical oxygen species in water which have proven effective in removing a number of organic contaminants. Our recent research into TiO2's efficacy on realistic water contaminants has shown capability of removing 70-80% of benzene, ethyl-benzene, toluene, and xylenes in a period of only 2 hours. Combination of TiO2 with new nanomaterials and subsequent optimization of this platform will produce a treatment that is recyclable, economic, and simple to deploy, providing a viable solution for these persistent, hazardous contaminants in the near future.

1 INTRODUCTION

One of the greatest environmental concerns of the current day is the contamination of large volumes of wastewater and groundwater by the chemical and oil industries. Some of the major causes for concern are aromatic compounds such as benzene, xylene, ethylbenzene, and toluene (BTEX compounds) which find significant application in industrial processes, are present in high concentrations in fossil fuels, and are increasingly being found as sources of groundwater contamination (Lin et al. 2009; Jo et al. 2008; Mazzeo et al. 2010). These compounds exhibit high volatility and are soluble enough in water to be recognized as a significant concern for groundwater aquifers(Anneser et al. 2008). By being partly dissolved in non-aqueous phase liquids, the contaminants are easily and quickly transported with groundwater to create contaminant plumes stemming from underground pipeline or storage leaks, improper waste disposal, or accidental incidents such as spills (Jo et al. 2008),(Anneser et al. 2008). This is a serious environmental concern due to the highly toxic nature of BTEX compounds which are known to exhibit carcinogenic and genotoxic effects as well as posing significant non-carcinogenic threats such as adverse effects on the liver, kidneys, central nervous system, and respiratory system (Cho et al. 2008; Hinwood et al. 2007; Ramírez et al. 2012; Murata et al. 1999).

While there are significant environmental issues surrounding contamination due to BTEX compounds, there are also many other hazardous by-products and wastes from the chemical and petroleum industries which pose similar ecological hazards. One of the primary examples of this which is of particular relevance to the Canadian petroleum industry is the presence of naphthenic acids in oil sands process water. Naphthenic acids are aliphatic or alicyclic carboxylic acid petroleum hydrocarbon derivatives which are found commonly in petroleum reserves and oil sands (Qi et al. 2004; Tomczyk et al. 2001; Clemente & P. M. Fedorak 2005). Naphthenic acid (NA) tainted process waters from oil sands petroleum extraction are held in tailing ponds with NA concentrations ranging between 20-120 mg/L (Clemente & P. M. Fedorak 2005). Studies have shown that naphthenic acids are acutely toxic to numerous organisms including plants,

fish, and bacteria with the potential for bioaccumulation, and thus these tailings wastes pose a serious environmental threat (Clemente & P. M. Fedorak 2005; Madill et al. 2001; Scarlett et al. 2012). While oil sands companies are required to maintain a zero discharge policy, the process waters are ultimately expected to be released back into the environment or be naturally reclaimed, requiring the naphthenic acid concentrations to be significantly reduced or eliminated (Scott et al. n.d.; Clemente & P. M. Fedorak 2005).

Various solutions for remediating process tainted waters and industrial effluent have been proposed with promising results, particularly the biodegradation of BTEX compounds and naphthenic acids (Lin et al. 2009; Mazzeo et al. 2010; Clemente & P. M. Fedorak 2005), (Toor et al. 2013). While good removal efficiencies are observed for biodegradation techniques, the process is often slow, requiring days to years of treatment time. Furthermore, it has been found that even with long bacterial residence times, the persistent chemicals are not completely removed from the contaminated site (Toor et al. 2013). Other issues associated with biodegradation is bacterial specificity towards certain compounds and the necessary conditions required for bacterial biodegradation, for example anaerobic or aerobic (Farhadian et al. 2008). Ideally, the solution to treating these problems is one that can address multiple contaminant species and completely remove the contaminants in a short amount of time.

Titanium dioxide photocatalysis has long been known as a promising method for treating a wide range of organic contaminants in an aqueous phase (X. Chen & Mao 2007; Chong et al. 2010; Zainal et al. 2005). Ultraviolet light is absorbed by the material, generating highly oxidative electrons and reductive holes. These electrons and holes interact with oxygen species, water, or the contaminants themselves to induce the degradation or complete mineralization of organic species in water. Furthermore, the TiO_2 catalyst has the potential of indefinite reusability if an appropriate support structure is chosen, for example, immobilization on magnetic nanoparticles allows simple recovery and redeployment of the catalyst (Liu et al. 2011; Linley et al. 2013; Leshuk et al. 2013). Some recent, preliminary findings indicate that TiO_2 photocatalysis is an ideal mechanism for removing even high concentrations of a variety of ecologically relevant materials including BTEX compounds and naphthenic acids. We anticipate that a TiO_2 based industrial effluent remediation strategy would be an efficient, effective methodology for addressing the concerns raised by the presence of these by-products and their effect on the environment.

2 EXPERIMENTAL

2.1 *Photocatalysis of Methylene Blue*

A 5 mg/L Methylene blue (Met-B) solution containing 0.1 mg/mL catalyst particles was made up by adding 6.25 mg/L Met-B stock solution to amounts of 1 mg/mL catalyst particle suspension and Millipore DI water. The as-prepared solution was then placed in the dark for 30 minutes to allow adsorption of organic species to the surface of the catalyst. After the adsorption period and after every 15 min of UV exposure, a 1 mL aliquot was drawn from the solution and placed in the dark. Once all aliquots were collected, they were centrifuged for 10 min at 15000 rpm to remove all catalyst and their colour was assessed by a spectrophotometer (BioTek Epoch).

2.2 *Methylene Blue Recyclability Study*

This study was performed as described in a previous work (Linley et al. 2013). Briefly, a 1 mg/L Methylene blue solution containing 0.2 mg/mL catalyst particles was prepared. The solution was exposed to UV light for 30 min, after which a 1 mL aliquot was taken, centrifuged at 15000 rpm for 10 min, and assessed by a spectrophotometer (BioTek Epoch). After each 30 min trial, the particles were magnetically separated, the treated water decanted, and new 1 mg/L methylene blue solution was added to the beaker.

2.3 *Photocatalysis of Benzene*

A 1 mg/mL solution of benzene was prepared in Millipore DI water and P25 commercial TiO_2 particles were added such that the catalyst concentration was 1 mg/mL. The solution was then placed in the dark for 30 min to allow contaminant adsorption to occur. After this period, and after every 15 minutes of UV exposure, a 1 mL aliquot of solution was drawn and stored in the dark. After 1 hour exposure time, the aliquots were centrifuged at 15000 rpm for 10 min to remove all catalyst particles and assessed by a spectrophotometer (BioTek Epoch).

2.4 *Photocatalysis of BTEX Contaminated Industrial Wastewater*

Industrial waste effluent was obtained from a local polymer synthesis company and placed in a separatory funnel for 1 week to allow the aqueous and organic phases to separate. The aqueous phase was extracted and filtered using coarse filter paper and a Buchner funnel to remove any solids. Some of this sample was extracted and stored in 40 mL EPA septa vials to use as control samples. Wastewater to be treated was mixed with P25 commercial TiO_2 such that the final concentration of TiO_2 was 10 mg/mL in solution. This solution was exposed to UV radiation for a set amount of time. After UV exposure, samples were centrifuged at 4000 rpm for 20 minutes to remove catalyst particles. The treated water was decanted and stored in 40 mL EPA vials before being sent to an external facility for analysis. Methods of F1-BTEX analyses conform to validation outlined in the "Alberta Environment Draft Addenda to the CWS-PHC,
Appendix 6, Validation of Alternate Methods".

2.5 *Photocatalysis of Naphthenic Acid*

A 50 mg/L solution of naphthenic acid was prepared by adding 60 mg/L naphthenic acid stock solution to appropriate amounts of 1 mg/mL P25 commercial TiO_2 solution and Millipore DI water such that the final concentration of P25 was 0.1 mg/L. The prepared solutions were placed in the dark for 30 min to allow adsorption of naphthenic acid to the catalyst surface to occur. After dark adsorption, samples were placed under UV radiation for a pre-determined amount of time. After UV exposure, samples were centrifuged at 4000 rpm for 20 min to separate catalyst particles and the treated solution was weighed and decanted into a separatory funnel for naphthenic acid extraction. To extract naphthenic acids from water, DCM was added to the solution in a 1:2 ratio, shaken for 5 min, then extracted to a 40 mL vial. This process was repeated once. After 40 mL DCM had been extracted from the separatory funnel, the solution was dried under forced air. A known volume of DCM was then added to the vial to concentrate the extracted naphthenic acids. FTIR analysis was performed in DCM using an FTIR liquid cell with KBr windows.

2.6 *Transmission Electron Microscopy*

The catalyst particles were analyzed with a Philips CM-10 transmission electron microscope (TEM). Samples were prepared by placing 5 μL of aqueous solution containing particles on Formvar-carbon coated 100 mesh copper TEM grids (Canemco) and allowed to dry overnight in a covered Petri dish.

3 RESULTS

A number of trials have been performed to test the ability of titanium dioxide to address a variety of organic contaminants including organic dyes, BTEX compounds, and naphthenic acids. One of the major benefits of using TiO_2 as a catalytic platform is its ability to be reused indefinitely, a property which can be examined through performing consecutive photocatalytic tests using a single catalyst sample.

3.1 *Titanium Dioxide Efficacy on Organic Dyes*

One of the simplest methods of assessing the ability of a catalyst sample to remove organic species from water is to perform the test using a coloured organic contaminant. Methylene blue (Met-B) is a heterocyclic aromatic compound with a peak light absorbance at approximately 668 nm, making it relevant to the degradation of aromatic BTEX compounds and simple to detect. Met-B itself is a common contaminant in the wastewater effluent of many textile factories, giving it environmental relevance as well. Figure 1 demonstrates the ability of TiO_2 photocatalysts to quickly and effectively remove methylene blue from solution. The initial concentration of the Methylene blue was 5 mg/L, and the catalyst concentration is 0.1 mg/mL in each case. Each sample is mixed in the presence of Met-B for 30 min prior to UV-C exposure to allow adsorption equilibrium to be attained. Once the particle solution is exposed to UV-C radiation, photocatalysis occurs and the Met-B is degraded *in situ*. From these results, it is apparent that TiO_2 based catalysts can be effectively employed to degrade organic contaminants in various nanophase dispersions without reduction in photocatalytic efficiency. P25 is a commercial photocatalyst with an average particle size of ~20 nm while the magnetic photocatalyst is TiO_2 anchored on a magnetic core with an average particle size of ~500 nm. The different particle morphologies can be seen in Figure 2.

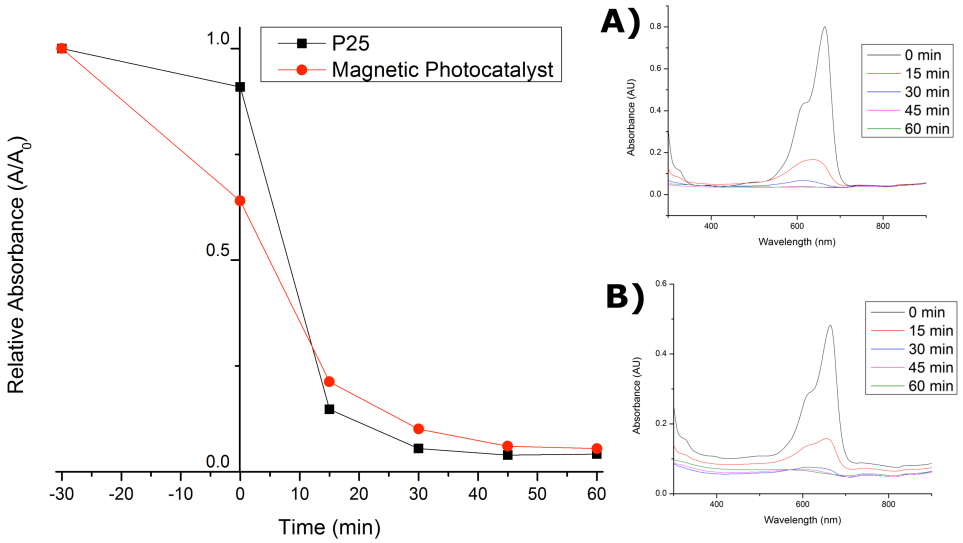


Figure 1. The graph on the left demonstrates the removal of methylene blue from solution relative to the initial solution concentration. Time to the left of the y-axis indicates time prior to exposure in which methylene blue could be adsorbed to the catalyst surface. Insets **A)** and **B)** show the spectrum of methylene blue treated overtime by P25 and magnetic photocatalyst, respectively. [Methylene blue] = 5 mg/L, [catalyst] = 0.1 mg/mL in all cases.

The ability for TiO_2 to be anchored onto a support structure such as a magnetic nanoparticle highlights its versatility and potential to be applied in treatment scenarios where the catalyst must be completely recovered from solution and can even be re-used. We have demonstrated the ability of magnetic based TiO_2 catalysts to be recycled and provide consistent treatment for methylene blue in a previous study (Linley et al. 2013). The recyclability study shown in Figure 3 demonstrates how TiO_2 can be easily recovered from solution and redeployed into a new batch of contaminated water. The methylene blue (1 mg/mL) was removed quickly over the course of each 30 min trial with a small reduction in efficiency. The efficiency of the TiO_2 could be restored by exposure to UV radiation for an extended period of time. This treatment provided the energy necessary to degrade any contaminants adsorbed to the TiO_2 surface, freeing up more active sites for catalysis, which allowed efficient degradation of the contaminant on the subsequent trial.

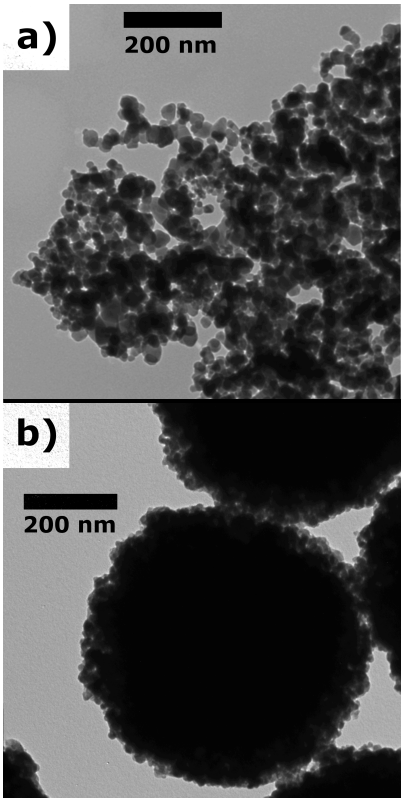


Figure 2. Comparison of the morphologies of P25 commercial TiO_2 (a) and TiO_2 anchored on a magnetic particle substrate (b). Despite the large particle size difference, photocatalytic efficiency remains relatively unhindered and the magnetic particles boast the capability of simple, fast separation.

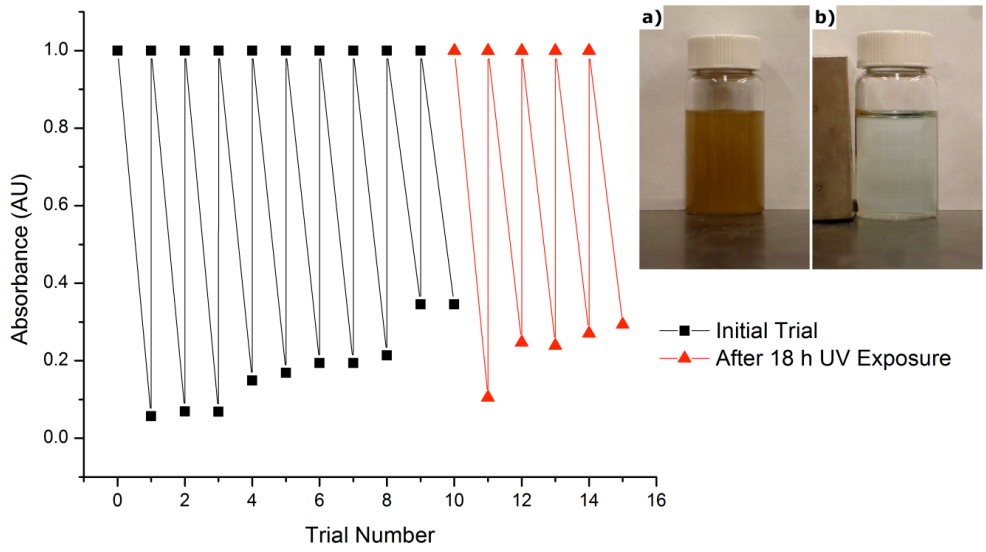


Figure 3. Taken from Linley et al. *ACS Applied Materials & Interfaces*, vol. 5, no. 7, pp. 2540–2548, Apr. 2013. This figure demonstrates the recyclable property of titanium dioxide nanomaterials by displaying the endpoint absorbance of Met-B samples after 30 min UV exposure in the presence of catalyst. After one trial, the catalyst is recovered and used in the next trial with new Met-B. The inset shows the magnetic photocatalyst before (a) and after (b) 1 min exposure to a magnet.

The ability of TiO_2 nanomaterials to quickly remove organic dyes such as methylene blue from aqueous solutions provides a good indication of the material's ability to treat similar organic compounds such as BTEX and also demonstrates its ability to be reused for multiple treatment cycles.

3.2 *Titanium Dioxide Treatment of BTEX Compounds*

Titanium dioxide's excellent efficiency in degrading methylene blue is a good indicator that its photocatalytic treatment properties will carry over to numerous other organic compounds, particularly those with an aromatic type structure. In order to test this, aqueous samples of benzene were assessed by a similar spectrometric method. After these tests proved successful, industrial waste effluent containing high concentrations of BTEX compounds was obtained and tested under varying parameters. The initial benzene spectrometric tests were performed by adding P25, a commercial TiO_2 photocatalyst (1 mg/mL) to an aqueous solution of benzene (1 mg/mL), exposing the slurry to UV radiation for set durations, and then observing the solution's light absorbance in the UV range. The results of this test can be seen in Figure 4.

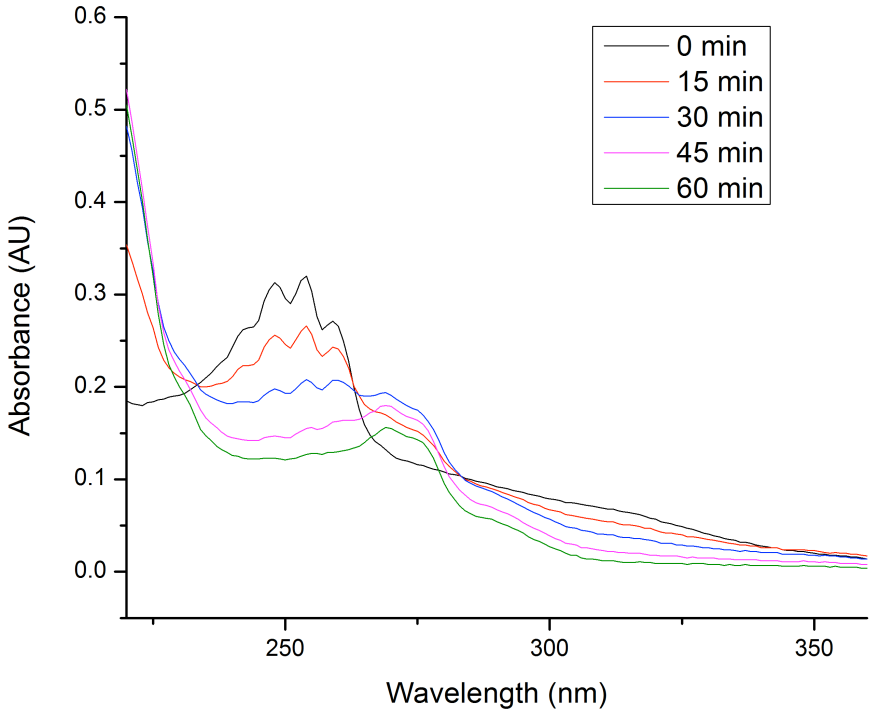


Figure 4. UV/Vis spectrum of benzene solution after various exposure times in the presence of P25, a commercial TiO_2 photocatalyst. The triple peak appearing around 250 nm corresponds to benzene and its intensity is decreased with longer UV exposure.

The results shown in Figure 4 demonstrate the removal of benzene from an aqueous solution over the course of an hour as the result of TiO_2 photocatalysis. Benzene has a characteristic triple UV absorbance peak observed close to 250 nm with individual peaks observed at approximately 249, 254, and 260 nm. Over the course of the test, these peaks are removed, indicating the degradation of benzene. However, the appearance of a broad peak between 270 nm and 280 nm, and the increased UV absorbance at ~220 nm suggest that UV absorbing degradation byproducts are being formed over the course of the reaction. Studies on the pathways of benzene degradation have confirmed that under oxidative conditions, oxygen can be added to benzene to transform it to phenol, then catechol, or transform it to muconaldehyde through a parallel route

(Yoshida et al. 2008; Zhang et al. 1995; Bui et al. 2011; Bui et al. 2010). The UV/Vis absorption spectrum of catechol is a broad peak appearing from 270-280 nm, and the appearance of a similar peak in Figure 4 can be attributed to the formation of catechol. Similarly, it is known that conjugated dienes have UV absorbance peaks close to 220 nm. Muconaldehyde contains such a structure, and the increase of absorbance towards the lower end of the spectrum can be attributed to the formation of this compound. These by-product compounds are known to be susceptible to photocatalytic oxidation by TiO_2, ultimately mineralizing the contaminant to produce CO_2 (Bui et al. 2011). This demonstrates the capability of TiO_2 to effectively degrade benzene in an aqueous environment, indicating that it is a good candidate for catalyzing BTEX removal from wastewater.

BTEX contaminated wastewater was obtained from a local company specializing in polymer synthesis. The aqueous phase of the effluent was separated and extracted, filtered by a coarse filter in a Buchner funnel to remove any solids, and then mixed with TiO_2 and subjected to UV irradiation. The concentration of contaminants was measured at an external facility. The results after 2 h UV exposure to 10 mg/mL P25 commercial TiO_2 can be seen in Figure 5.

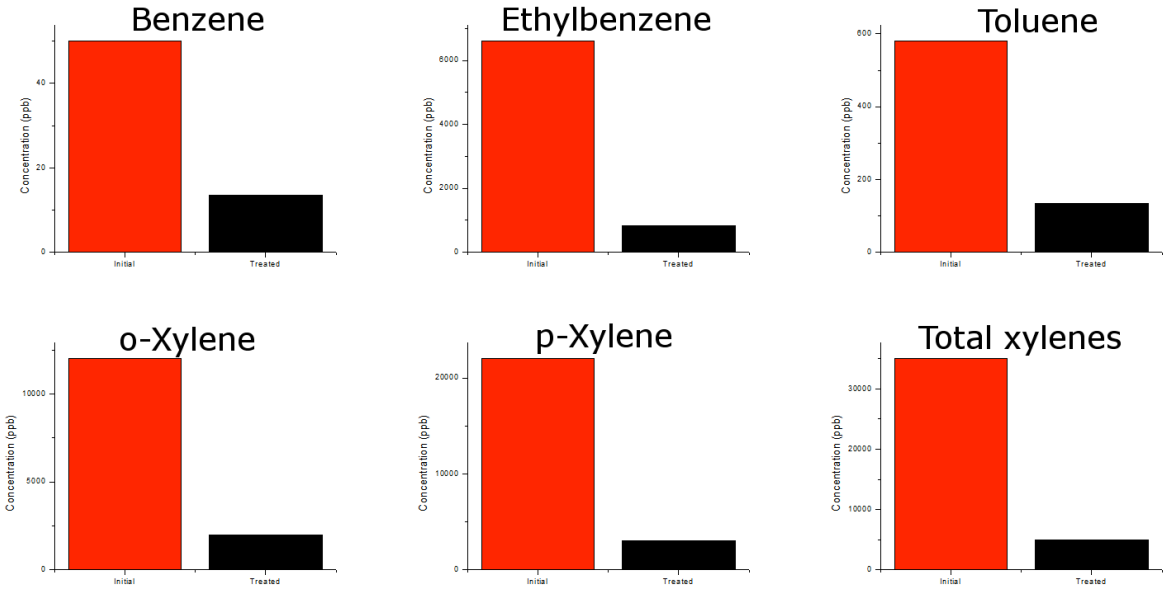


Figure 5. The left bar in each panel displays the concentration of the contaminant prior to UV exposure. The bar on the right displays the concentration after 2 h exposure to UV radiation in the presence of 10 mg/mL P25. Average removal for all compounds is 80.7%.

The data from Figure 5 shows that TiO_2 photocatalysis has the ability to effectively treat high concentrations of BTEX compounds in a very short period of time. Most notably, the concentration of xylenes in the aqueous sample is reduced from 35,000 ppb to 5000 ppb within the duration of the test, a reduction of 85.7%. Overall, the average removal for BTEX compounds within 2 h is 80.7%. Given longer test periods, it has been found that greater degrees of removal can be achieved. Given a 16 h test period using the same concentrations, 98.5% of xylenes are removed, down to 150 ppb, and benzene is reduced below its detectable limit. It is anticipated that a major inhibitor to catalytic performance of TiO_2 particles is the adsorption of degradation by-products to the catalyst surface, most notably catechol (Bui et al. 2010). This could partially explain why the remaining 150 ppb xylenes are not removed. In practice, this catalytic inhibition could be addressed by performing UV treatments on the particles in the absence of contaminants to allow the radical species to interact with the adsorbed contaminants without the sites being taken up by new organic species, as seen in Figure 3. These preliminary results clearly demonstrate the versatile nature of TiO_2 as a catalyst capable of addressing this class of compounds in wastewater. Additionally, TiO_2 photocatalytic treatment is a quick process, and multiple treatments could be performed in a short time to ensure complete removal of contaminants. Finally,

the catalyst can be easily regenerated if activity is decreased due to the occlusion of surface sites by degradation by-products.

3.3 *Titanium Dioxide Treatment of Naphthenic Acids*

The ability of TiO_2 to treat water contaminated by naphthenic acids was assessed using a similar test to those described above. P25 commercial TiO_2 was suspended in a volume of aqueous naphthenic acid solution such that the concentration of TiO_2 was 0.1 mg/mL and the concentration of naphthenic acids was 50 mg/L. The solution was then exposed to UV light in predetermined increments over the course of 30 min. Naphthenic acid presence was assessed by observing the intensities characteristic peaks from FTIR. The results of this test can be seen in figure 6.

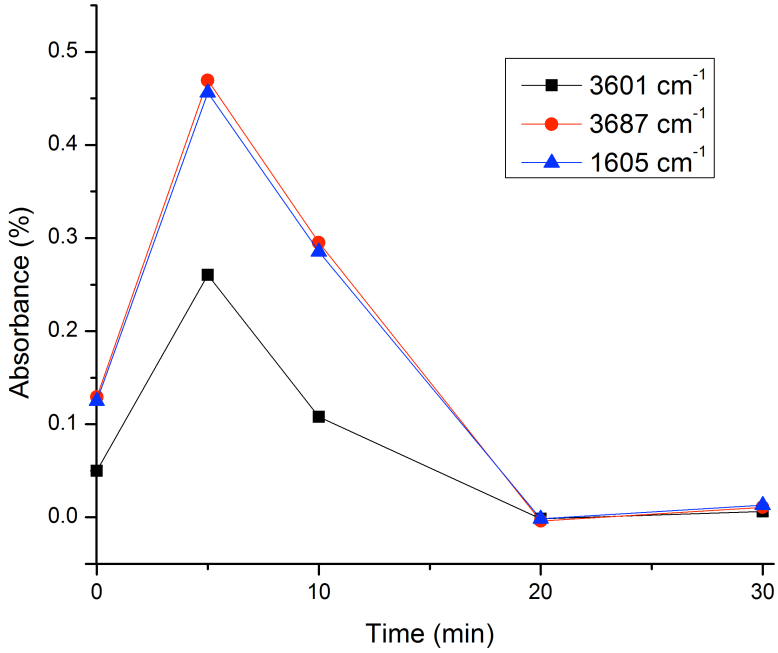


Figure 6. FTIR peak heights after different exposure times of 50 mg/L aqueous naphthenic acid solution to UV light in the presence of 0.1 mg/mL P25 TiO_2. The increase after 5 min can be attributed to the formation of compounds with a greater number of oxygen groups and the decrease after 10 min corresponds to their removal, presumably through mineralization to CO_2.

The data displayed in Figure 6 indicates the FTIR absorbance of peaks at 1601 cm^{-1}, 3601 cm^{-1}, and 3687 cm^{-1} for samples exposed to 0.1 mg/mL P25 over varying amounts of time. It is anticipated that the peak at 1601 cm^{-1} corresponds to a C=O carbonyl stretch peak which may be shifted toward 1600 cm^{-1} if present in a conjugated chain. It is possible that the alkane chain of the naphthenic acid could have this structure introduced via photo-oxidation from the reactive oxygen species produced in water and direct reduction of the carbon chain by photo-active holes from the TiO_2. The peaks at 3601 cm^{-1} and 3687 cm^{-1} are thought to correspond to –OH stretching peaks and long range H-bonding associated with such groups. In the initial stages of the treatment process, large amounts of oxygen groups may be added to the contaminant, increasing the presence of these FTIR peaks. After 20 minutes of the catalytic degradation process, the contaminant may be broken down to smaller constituents such as CO_2 and the previously observed peaks disappear. This indicates that TiO_2 is an appropriate catalyst for dealing with a large range of hazardous organic contaminants, including naphthenic acids which are a significant environmental hazard resulting from the oil-sands extraction process.

4 CONCLUSIONS

The preliminary data collected on TiO_2 photocatalysis of environmentally relevant contaminants indicates that TiO_2 is an excellent candidate as a catalyst for wastewater treatment for a number of reasons. First, it has excellent versatility in the sense that it is effective on a number of hazardous organic compounds, including BTEX and naphthenic acids, two contaminants which are pervasive in wastewaters from the oil industry. Second, TiO_2 photocatalysis is a very efficient process, with treatment times for even high concentrations of contaminants within the span of a few hours. Furthermore, any loss in catalytic efficiency associated with the occlusion of catalytic sites can be mitigated by UV treatment in clean water. In this way, wastewater could be potentially be treated quickly by exposure to multiple TiO_2 treatments and the catalyst could be recovered and regenerated. Finally, TiO_2 has the ability to be anchored to functional supports such as magnetic particles without any significant loss in catalytic efficiency. This enables simple recovery and reuse of the catalyst, providing an economic and environmental advantage to using such a technology. It is anticipated that TiO_2 photocatalysis may be a potential solution for removing hazardous organic contaminants including BTEX compounds and naphthenic from industrial wastewater streams that may be implementable in the near future.

5 ACKNOWLEDGEMENTS

We would like to thank the Natural Sciences and Engineering Research Council of Canada (NSERC) for funding this research.

6 REFERENCES

Anneser, B. et al., 2008. High-resolution monitoring of biogeochemical gradients in a tar oil-contaminated aquifer. *Applied Geochemistry*, 23(6), pp.1715–1730.

Bui, T.D. et al., 2010. Lowering of photocatalytic activity of TiO2 particles during oxidative decomposition of benzene in aerated liquid. *Applied Catalysis B: Environmental*, 94(1-2), pp.186–191.

Bui, T.D. et al., 2011. Two routes for mineralizing benzene by TiO2-photocatalyzed reaction. *Applied Catalysis B: Environmental*, 107(1-2), pp.119–127.

Chen, X. & Mao, S.S., 2007. Titanium Dioxide Nanomaterials: Synthesis, Properties, Modifications, and Applications. *Chemical Reviews*, 107(7), pp.2891–2959.

Cho, I.-H. et al., 2008. Risk assessment before and after solar photocatalytic degradation of BTEX contaminated groundwater at a gas station site in Korea. *Environmental Progress*, 27(4), pp.447–459.

Chong, M.N. et al., 2010. Recent developments in photocatalytic water treatment technology: A review. *Water Research*, 44(10), pp.2997–3027.

Clemente, J.S. & Fedorak, P.M., 2005. A review of the occurrence, analyses, toxicity, and biodegradation of naphthenic acids. *Chemosphere*, 60(5), pp.585–600.

Farhadian, M. et al., 2008. In situ bioremediation of monoaromatic pollutants in groundwater: A review. *Bioresource Technology*, 99(13), pp.5296–5308.

Hinwood, A.L. et al., 2007. Risk factors for increased BTEX exposure in four Australian cities. *Chemosphere*, 66(3), pp.533–541.

Jo, M.-S. et al., 2008. An analysis of synergistic and antagonistic behavior during BTEX removal in batch system using response surface methodology. *Journal of Hazardous Materials*, 152(3), pp.1276–1284.

Leshuk, Tim et al., 2013. Mesoporous Magnetically Recyclable Photocatalysts for Water Treatment. *Journal of Nanoscience and Nanotechnology*, 13(4), pp.3127–3132.

Lin, C.-W. et al., 2009. Microbial communities and biodegradation in lab-scale BTEX-contaminated groundwater remediation using an oxygen-releasing reactive barrier. *Bioprocess and Biosystems Engineering*, 33(3), pp.383–391.

Linley, S., Leshuk, Timothy & Gu, F.X., 2013. Synthesis of Magnetic Rattle-Type Nanostructures for Use in Water Treatment. *ACS Applied Materials & Interfaces*, 5(7), pp.2540–2548.

Liu, H. et al., 2011. Synthesis of TiO2/SiO2@Fe3O4 magnetic microspheres and their properties of photocatalytic degradation dyestuff. *Catalysis Today*, 175(1), pp.293–298.

Madill, R.E.A. et al., 2001. Preliminary risk assessment of the wet landscape option for reclamation of oil sands mine tailings: Bioassays with mature fine tailings pore water. *Environmental Toxicology*, 16(3), pp.197–208.

Mazzeo, D.E.C. et al., 2010. BTEX biodegradation by bacteria from effluents of petroleum refinery. *Science of The Total Environment*, 408(20), pp.4334–4340.
Murata, M., Tsujikawa, M. & Kawanishi, S., 1999. Oxidative DNA Damage by Minor Metabolites of Toluene May Lead to Carcinogenesis and Reproductive Dysfunction. *Biochemical and Biophysical Research Communications*, 261(2), pp.478–483.
Qi, B. et al., 2004. Study on Distribution and Composition of Carboxylic Acids of Bohai Crude Oil in China. *Petroleum Science and Technology*, 22(3-4), pp.463–473.
Ramírez, N. et al., 2012. Chronic risk assessment of exposure to volatile organic compounds in the atmosphere near the largest Mediterranean industrial site. *Environment International*, 39(1), pp.200–209.
Scarlett, A.G. et al., 2012. Predicted toxicity of naphthenic acids present in oil sands process-affected waters to a range of environmental and human endpoints. *Science of The Total Environment*, 425, pp.119–127.
Scott, A. et al., Ozonation of oil sands process water removes naphthenic acids and toxicity. *Chemosphere*, 71(1), pp.156–160.
Tomczyk, N.A. et al., 2001. On the Nature and Origin of Acidic Species in Petroleum. 1. Detailed Acid Type Distribution in a California Crude Oil. *Energy & Fuels*, 15(6), pp.1498–1504.
Toor, N.S. et al., 2013. Degradation and aquatic toxicity of naphthenic acids in oil sands process-affected waters using simulated wetlands. *Chemosphere*, 90(2), pp.449–458.
Yoshida, H. et al., 2008. Photocatalytic hydroxylation of aromatic ring by using water as an oxidant. *Chemical Communications*, (38), p.4634.
Zainal, Z. et al., 2005. Removal of dyes using immobilized titanium dioxide illuminated by fluorescent lamps. *Journal of Hazardous Materials*, 125(1-3), pp.113–120.
Zhang, Z. et al., 1995. Studies on pathways of ring opening of benzene in a Fenton system. *Free radical biology & medicine*, 18(3), pp.411–419.

Mine Waste Management

The evolution of coal mine waste management practices in Western Canada

F. Claridge, W. Funk, & L. Martin
WorleyParsons Canada, Burnaby, British Columbia, Canada

ABSTRACT: The perspective on mine waste management practices has been evolving over the past decade to account for major shifts in mine economics, social awareness, growing knowledge of the effects of mining on the environment and, an increasingly stringent regulatory environment. One response from these drivers is the desire to reduce or even eliminate the need for long term water treatment following mine closure.

The paper provides examples of modifications to waste management practices at coal mining operations in western Canada, including measures that are currently being researched for reducing the release of selenium and other mineral constituents. Using a broad sustainability-based lens, it discusses the pros and cons associated with potential measures to deal with this issue. These include covers, water diversions, subaqueous deposition, creation of biologically active dump environments and water treatment.

1 INTRODUCTION

A recent consideration for operators and regulators of metallurgical coal mines in western Canada is the recognition of the damaging effects of selenium in the environment - especially, the watersheds influenced by these mine operations. This awareness has driven a regulatory-inspired industry response to examine current mine planning and spoiling practices along with other measures to manage the release of bio-available selenium into the environment. The objective of this paper is to provide an overview of the selenium management strategies broadly under consideration by the metallurgical coal operators. Its purpose is to identify the design characteristics of an“ideal” waste rock storage dump based on recent learnings while considering its environmental, social and economic (triple bottom line) effects.

2 BACKGROUND

2.1 *Physical, Geochemical and Environmental*

Selenium, an element which is present in minute quantities throughout the Earth’s crust, is located immediately beneath sulphur on the periodic table and behaves similarly, oxidizing and leeching out of waste rock dumps in a fashion analogous to acid rock drainage. When free oxygen is present, selenium oxidizes and becomes water soluable and bioavailable. The presence of free water in the dumps therefore acts both to promote oxidation, by transporting free oxygen into the dump, and to transport the oxidized, water soluable-bioavailable selenium oxides out of the waste dump into the local watershed.

Selenium is a curious element; essential for animal life as a micronutrient, it becomes toxic in elevated concentrations. Fish, amphibians and birds are all considered sensitive to elevated selenium concentrations. Selenium is commonly associated with coal deposits, present in both the coal itself and in sedimentary rock overburden.

Given that selenium accumulates in vegetation, its presence in elevated concentrations in the western Canadian coal deposits and immediate overburden rock is thought to be related to the Mississippian Era swamps, present along the old continental margin of western North America that spawned the formation of the coalfields.

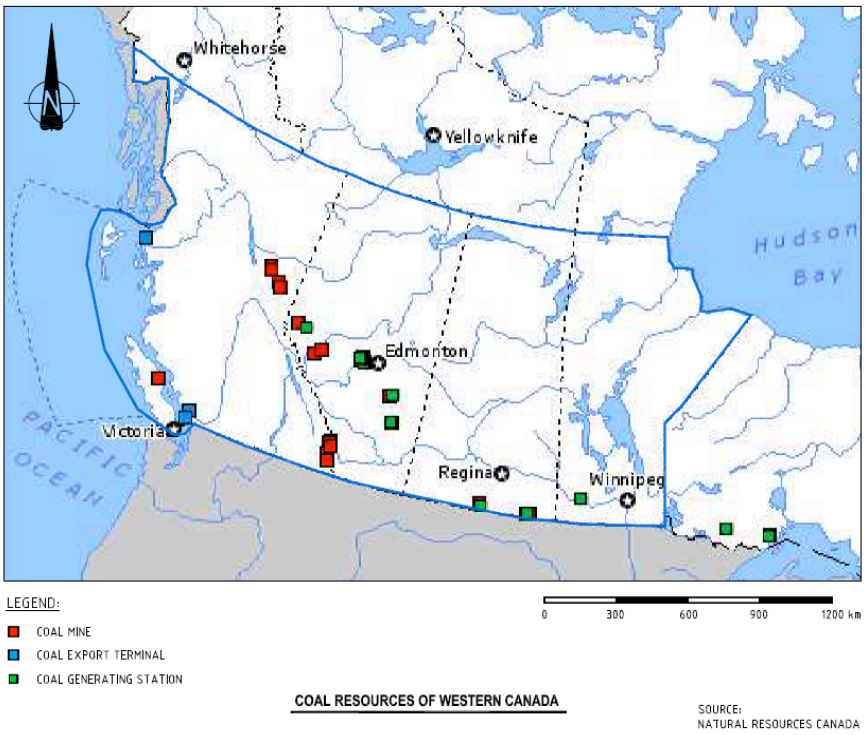
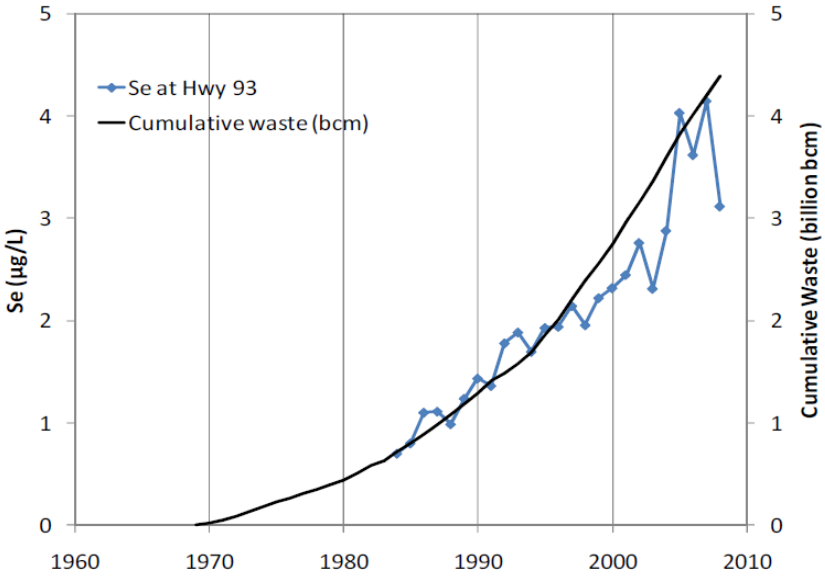


Figure 1. Coal Resources of Western Canada

All of the currently operating western Canadian coal mines are open pit mines, located in the Rocky Mountains (see Figure 1). Strip ratios are typically on the order of 8 to 12 (cubic meters of waste rock to strip per tonne of raw coal). Therefore, the recent mining practice (from 1970 on) has favored what is essentially mountaintop mining, with the waste rock being dumped off the side of the mountain or hill into adjacent valleys in large, top-down angle of repose dumps. Many of these valley bottoms contain creeks and streams; however, the coarsest fraction of the waste rock typically segregates to the base of the dump during initial placement, these dumps often include, either by design or accident, a rock drain. The large coarse rock in these drains promotes a high porosity and the buried watersheds often continue to flow relatively unimpeded beneath the waste rock dump.

As the waste rock in the majority of these mines is Non Potentially Acid Generating (NPAG), the practices of top down spoiling and cross-valley fills were not considered problematic and water quality issues historically revolved around the concentrations of calcite and nitrate in the watersheds downstream of the waste rock dumps. However, in 1995, elevated concentrations of selenium were detected during a routine water quality assessment in support of a mine effluent permit amendment (MacDonald & Strosher 1998). Routine sampling detected concentrations of 25 µg/L below the mine and less than 1 µg/L above the mine. This finding triggered a revisiting of historical water quality samples from the mouth of the Elk River, 65 km downstream of the Southeast British Columbia coalfields and it was quickly discovered that selenium concentrations had been on the rise in the Elk River for the better part of two decades. Since that point, selenium concentrations have continued to increase and, more alarmingly, the concentrations are

increasing exponentially more or less in direct correlation to the total volume of waste rock deposited into the Elk River watershed (Swanson, et. al 2010).



Correlation between Concentration of Selenium in the Elk River at Highway 93 and Waste Rock Volume

Figure 2. Selenium Concentrations in the Elk River (from Swanson, et. al 2010)

This trend of increasing selenium concentrations in SE British Columbia has caused delays to expansion projects at the mines and is now threatening their continued operation under current mining practices. In response, the operators have begun investing significant resources into attempting to halt the increase in selenium concentrations in the watershed, and hopefully reverse it.

Similar issues with elevated selenium have now been detected in metallurgical coal operations in northeast British Columbia (BC) and northwest Alberta (AB).

2.2 *Sustainability and Metallurgical Coal*

As metallurgical coal operations grapple with the increasingly important regulatory mandate to manage the selenium associated with their operations they must balance their management responses with a broad spectrum of triple bottom line consideration. The Strategic Advisory Panel on Selenium Management in their 2010 report (Swanson et. al, 2010) identified several dozen triple bottom line and technical considerations developed from a series of stakeholder engagements in southeast BC and northwest AB. In essence, these considerations compel the operators to consider the capital and operational expenses of these selenium management responses and their potential efficacy relative to the short and long term impacts on community and environmental wellbeing. It was widely recognized by the stakeholder contributing the SAPSM Panel review that it was not in the communities' (society's) interest to adopt strategies that force coal operations to the economic margin. At the same time, the increasing trend of selenium concentrations in the watershed had to be halted and reversed. This is not an intractable position but it does require the coal operations, their stakeholders and the regulators to identify and accept a series of environmental, social and economic trade-offs as they attempt to sustainably manage selenium.

3 VIRTUAL PROTOTYPE MODELING

There are two approaches available for selenium management: preventing the release of selenium from waste dumps or treating the water downstream of the dumps to remove the selenium. In general, the first approach comprises measures employed to prevent water and oxygen moving through the interior of the dumps; the second involves construction of either active or passive water treatment facilities. The first approach is still relatively immature. It has not been employed on a wide scale in the prevention of selenium release and, while the theories behind it are sound and relatively well understood, it remains commercially unproven. The second approach is further along in the Research and Development curve and, to date, it has been favored by the mine operators in western Canada.

3.1 *Water Treatment Measures*

Water treatment measures comprise techniques used to remove selenium from impacted surface water flows. Installed at the base or downstream of a waste rock dump, these measures can be divided into two groups: active treatment and passive treatment.

3.1.1 *Active Treatment*

To date, active treatment has received the most attention from mine operators in western Canada. At least one mine has completed an active treatment trial, another is underway and a large scale water treatment plant is in the advanced stages of design. Three mechanisms are possible for active water treatment: physical processes (filtration, reverse osmosis, etc.), chemical treatment (precipitation, cementation, etc.) and biologic processes (Nitrogen and Selenium Management Program 2007). Biologic processes work due to the fact that selenium is a sulphur analogue; sulphur reducing microbes can also utilize selenium in their metabolism, reducing the oxidized selenium to an insoluble form.

All of these technologies use some form of reactor process, requiring a large industrial scale facility, are electrical power intensive and produce a selenium rich sludge that must be properly disposed. In short, not only do they require a large capital investment, the mine operator must then finance their continued operation for at least the life of the mine and, in all probability, for a significant period beyond mine closure perhaps for decades. The size of the plant is in direct proportion to the volume of water that must be treated; for some of the larger watersheds in British Columbia where active treatment is being considered, construction costs are anticipated to be on the order of $50,000,000 to $80,000,000 Canadian with ongoing operational costs of $2,000,000 to $5,000,000 CDN per year.

Despite the high and ongoing cost, the advantage of these systems is that the processes involved are relatively well understood, commercially proven and have a high degree of certainty regarding the reduction of bioavailable selenium in the watershed. To some degree they are also modular. Consequently, treatment trains can be added or deleted as selenium concentrations change with time. Most importantly, the active treatment facilities begin working as soon as the plant is brought online.

3.1.2 *Passive Treatment*

In a passive treatment system, a reactor is not used. Impacted water is sequestered in a large lagoon, constructed wetland or covered engineered cells and biologic treatment through microbial action or algae sequestration is utilized to remove selenium from impacted water. The obvious advantage to this system is that once constructed and well established, the ongoing operating costs of the system are lower than in an active treatment system. Disadvantages to passive treatment systems include the large amount of land required for the lagoon, wetland or treatment cells, the potential for these systems to become an attractive nuisance for birds, amphibians and mammals and most importantly, the difficulty in establishing a sustaining system with a controlled, low selenium concentration output.

Passive treatment systems for the management of selenium currently sit on the research and development spectrum rather than that of their commercially proven alternative (i.e., active water treatment systems).

3.1.3 *Saturation Zones*

Under the right conditions, certain bacteria will utilize dissolved selenate (Se[VI]) in their metabolism, reducing Se[VI] to selenite (Se[IV]) and then to elemental selenium (Se[0]), which precipitates out of solution (Maiers, et. al 1988). As this reaction is relatively unenergetic, microbes will typically utilize other energy sources, such as carbon or nitrates before moving on to reduce the selenium. As well, anoxic or low oxygen environments tend to work better for encouraging the growth of selenium reducing microflora. Once appropriate conditions are established, selenium reduction occurs relatively rapidly; on the order of days to weeks.

If dump water was forced to percolate slowly through a saturation zone, oxidation of mine waste and bacterial action would slowly deoxygenate the water. This should create conditions favorable for establishment of a suitable selenium reducing microbe community within the dump, in essence turning the dump itself into a passive treatment system. It is thought that residency times on the order of 6 months are necessary to first deoxygenate the dump water and then allow for microbial selenium reduction.

Saturated conditions can be created at the toes of existing dumps relatively easily by constructing an impoundment and backing dump water into the mass of waste rock. An illustration of a conceptual design is presented in Figure 3. By calculating an accurate water balance for the dump, the impoundment can be sized properly to ensure an appropriate residency time. This approach also has the benefit of allowing for the construction of an engineered outlet for the dump water; regular sampling of the dump water at the outlet would allow for diversion of water to secondary treatment facility if necessary. Notably, saturation zones currently are not commercially proven in metallurgical coal sector of western Canada; indeed, they will require both research and development and a thorough understanding of the geological and hydrogeological conditions at each site for which they are considered.

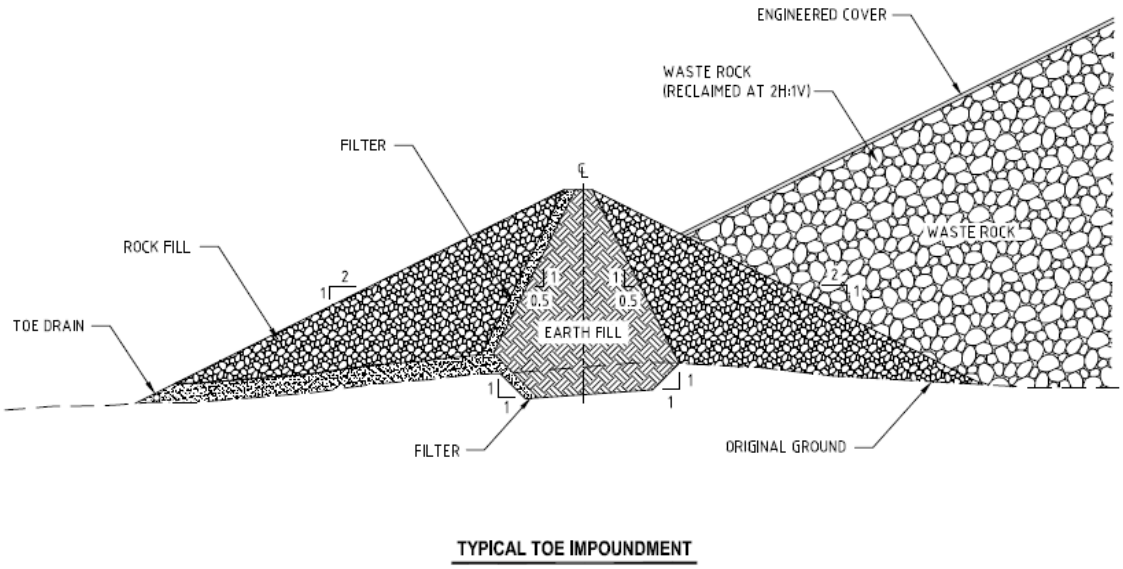


Figure 3. Typical TOE Impoundment

3.2 *Selenium Prevention*

Selenium prevention measures work by inhibiting the oxidation of selenium present in the host rock, the transport of the oxidized selenium out of the dump by surface water or both, by controlling water and oxygen flux through the dump.

Selenium prevention measures are currently in research and development phases and will require several years of investigation to demonstrate their selenium management efficacy.

3.2.1 *Sub Aqueous Sequestration*

Sub aqueous sequestration works by submerging waste rock in still water. The limited amount of dissolved oxygen in the water is consumed by oxidation and, at that point, further selenium production by oxidation stops. The best opportunity to employ this technique is by backfilling waste into open pits that partially flood at mine closure, although a good understanding of groundwater flows through the flooded dump is necessary to adequately characterize the system. The advantage to this technique is that once permanently flooded, the rock is expected to stop producing selenium. The disadvantage is that rehandling of waste may be necessary to maximize the backfilling of spoil.

3.2.2 *Dump Covers*

Dump covers work by constructing a low permeability cap on a waste rock dump, stopping infiltration of precipitation into the dump. In theory, this produces a dry dump environment, and selenium, while it may oxidize out of the waste rock, is prevented from leaching out of the dump. While the theory is simple, the practice of constructing adequate dump covers to prevent Acid Rock Drainage (at mines with this issue) has proven somewhat problematic in practice. It should also be pointed out that, while a dump cover may not be able to completely eliminate a selenium problem, by reducing the volume of precipitation entering a dump they can reduce the volume of impacted water flowing out of a dump requiring further treatment.

Current cover practice has gained much from advances in the field of unsaturated soil mechanics. State of the practice covers are highly engineered structures, incorporating multiple materials to produce capillary breaks within the cover and designed to allow for rapid establishment of vegetation. The field of dump cover design continues to evolve and mature and dump covers will undoubtedly play a major role in selenium control and mitigation in the future. Typical conceptual designs for dump covers, including those of a geosynthetic membrane are illustrated in Figure 4.

3.2.3 *Surface Water Management*

Proper management of surface water flows around waste rock dumps is a crucial item in any selenium management plan. The goal is to limit selenium contact with mine-affected water (i.e., keeping clean water clean) while limiting the volumes of selenium-affected water requiring treatment (of any sort). Surface water management typically takes the form of surface water diversion ditches around the waste rock dumps, although tunnels beneath or around dumps are also possible. On their own, surface water diversions are not expected to significantly reduce selenium release from waste rock dumps. However, when combined with dump covers they can help create a significantly drier dump environment. Most importantly, a good surface water management system has the potential to significantly reduce the volume of selenium impacted water requiring treatment.

3.2.4 *Waste Concentration*

Waste concentration works by limiting the number of watersheds impacted by waste rock dumping. While not necessarily reducing selenium release on its own, this technique can significantly limit the volume of water becoming selenium impacted and requiring treatment. For operating mines, waste concentration involves transporting waste rock to pre-existing dump locations instead of forming new waste rock dumps as mine development proceeds.

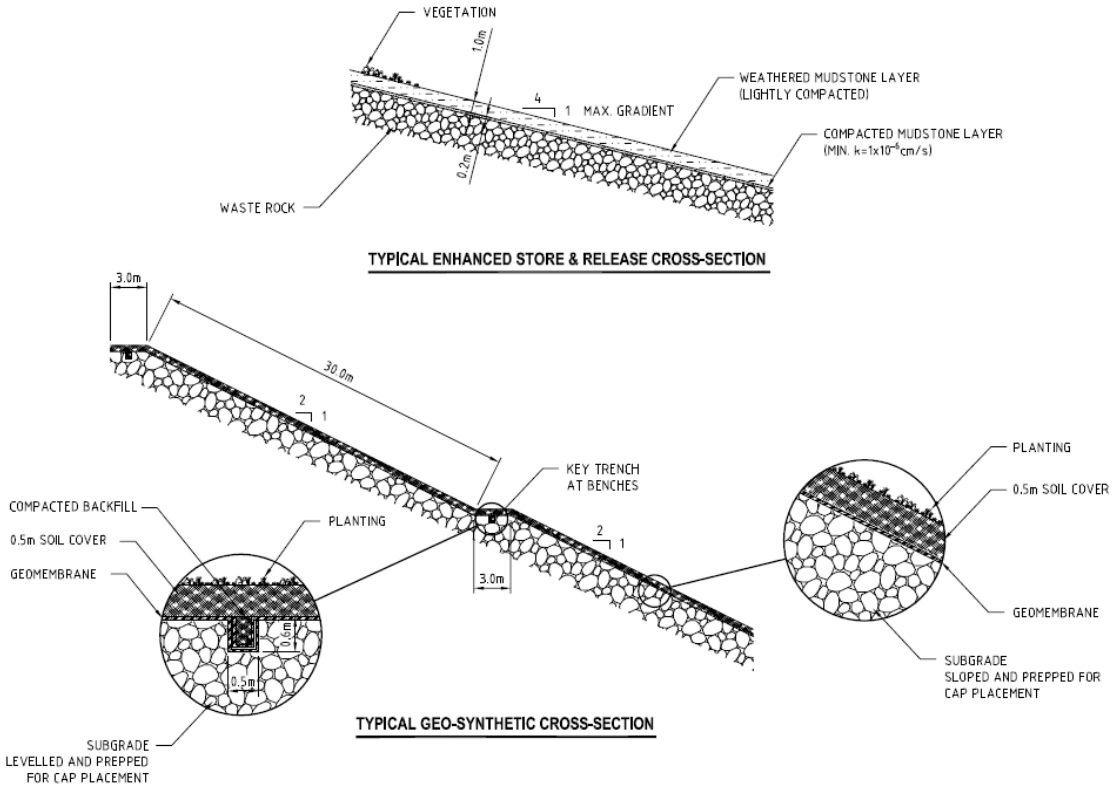


Figure 4 Typical Geo-Synthetic Cross-Section

3.2.5 *Dump Construction*

The majority of dumps constructed at the western Canadian coal mines are top-down, valley-fill dumps. These dumps are formed by free dumping waste rock off the side of hills or mountains where mining is occurring into the adjacent valleys. Waste rock dumps formed in this fashion are highly segregated, with coarse waste at the bottom and toe of the dump and finer waste at the top, and form at the angle of repose of the waste rock, with a Factor of Safety against instability of 1. As well as being difficult to reclaim, vegetate and cap, such dumps are also prone to instability, failure, debris runouts and ongoing settlement. Large fissures in the dump platforms are commonplace and these act as conduits, transporting oxygen and water deep into the dump.

An alternative form of dump construction is the bottom-up dump, where waste is dumped in thin, horizontal lifts from the base of the dump upwards. Multiple selenium management advantages accrue from this methodology. The thin lifts promote a more homogenous, dense structure, retarding the entrance of free oxygen and water to the dump. An additional benefit rests in an idea currently under research - that such dumps can enhance selenium reduction through microbial control (Swanson et. al, 2010). The dump stability is virtually assured, thus eliminating dump failures, excessive settlement and fissure formation. Finally, bottom-up dumps facilitate progressive reclamation and vegetation of the dump face during mine operation, again reducing the ingress of precipitation and oxygen into the dump. A conceptual cap design for a bottom-up is illustrated in Figure 5.

The downside to the bottom-up dump, at least in the context of western Canadian mountaintop mining, is that they are more expensive than the conventional top-down angle of repose dump, requiring extra haul distances to transport the waste down to the dump platform in trucks or conveyors.

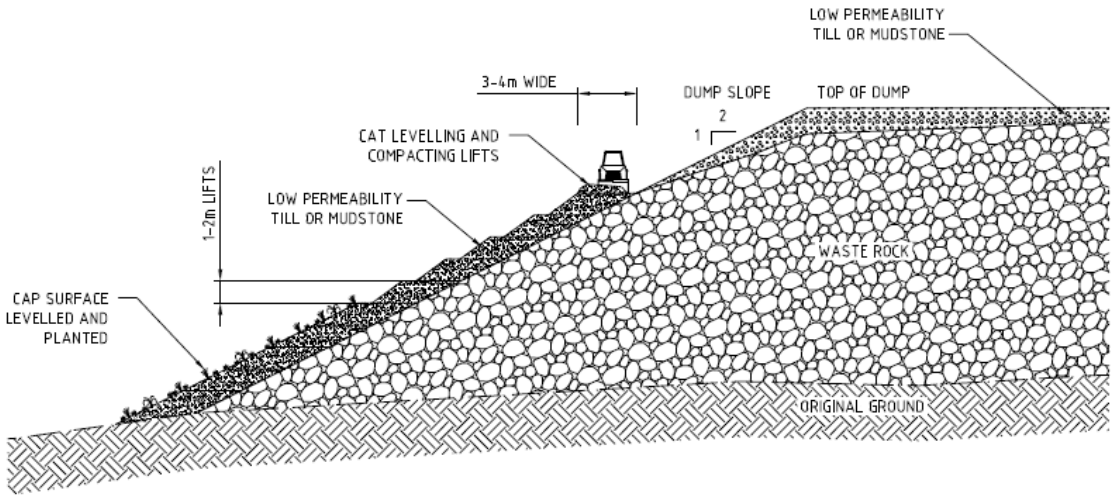


Figure 5 Low Permeability Bottom-UpCap

3.3 *The Ideal Dump Design*

3.3.1 *Design Considerations*

Given the various options described above, one can envision the ideal ex-pit waste rock dump from a selenium management point of view. It is located at, or at close as practical, to the head of a watershed. This reduces the amount of surface and ground water that could potentially enter the dump. Any surface water flows above the dump are picked up by diversion ditches and routed around the dump. The dump itself is constructed in bottom-up fashion out of a series of thin lifts (5 - 15 meters thick), with the exposed dump face having a gentle gradient, 2 or 3 horizontal to 1 vertical. This allows for the dump face to be progressively reclaimed as placement proceeds, with an engineered, vegetated cover. Precipitation and snow melt on the surface of the dump is routed into engineered gullies and channels, helping to remove it from the surface of the dump before it can pool and soak into the waste rock. The downstream toe of the dump incorporates a low-permeability clay core, forming a dyke to backup dump water inside the waste rock. A grout cutoff wall or curtain may be present beneath. The dyke includes an engineered outlet at a prescribed elevation, producing sufficient residency time to allow for biologic selenium reduction for any remaining, selenium impacted water flowing out of the dump.

3.3.2 *Sustainability Considerations*

From a triple bottom line perspective, the "ideal dump design" does not account for capital or operating expenses, state of knowledge re. potential and probable selenium reduction efficacy, research and development and construction time horizons or the potential environmental and social benefits and costs that might accompany it. Indeed, although posited in this paper as "ideal" a series of operational, economic and physical conditions may be required (e.g., haul distances and grade financially favor bottom up, there is sufficient spoil area to accommodate the spoil angles, site-wide water balances are known and hydrological conditions are well understood etc.).

That said, the "ideal dump design" could become an effective component of a portfolio of selenium management solutions that are required to stabilize and reverse the selenium loading trends observed in the watersheds affected by western Canadian metallurgical coal operations.

As currently available technologies become increasingly marginally ineffective and inefficient the "ideal" dump design alongside the other selenium management options noted above will need to be deployed to ensure that the affected watersheds provide environmental, social and economic value (referred to as fishable, drinkable and swimmable by the stakeholders consulted by the SAPSM).

3.4 *Concluding Perspective*

Future practices for mine waste disposal must take into account the release of what were formerly considered trace or even in former times non-measurable mineral constituents on the aquatic environment. Measures adopted for controlling constituent releases, including those described in this presentation, must be effective – not only during the operational life of the mine, but for decades or even centuries thereafter.

A set of possible modifications to the traditional manner of waste disposal at mountainous mine sites in western Canada has been described in this paper. In determining which measures merit the most attention for application, both short term capital and operational costs must be taken into account and compared with forecast long term costs and possible savings in post operational maintenance of water treatment facilities, as well as the ultimate sustainability of the potential interventions.

4 REFERENCES

Maiers, D. T., P. L. Wichlacz, D. L. Thompson, and D. F. Bruhn. 1988. Selenate reduction by bacteria from a selenium rich environment. Appl. Environ. Microbiol. 54:2591-2593.

McDonald, Leslie E., Strosher, Mark M. 1998. Selenium Mobilization from Surface Coal Mining in the Elk River Basin, British Columbia: A survey of Water, Sediment and Biota, Min. Env., Lands and Parks Kootenay Region, Cranbrook, British Columbia.

Orange County Nitrogen and Selenium Management Program (NSMP) 2007.

Swanson, et al. The Strategic Advisory Panel on Selenium Management (SAPSM). Report to Teck Coal Limited, June 30, 2010.

Treatment options for selenium control in mine-site runoff

David A. Jackson
WorleyParsons, Victoria, BC, Canada

Alex Timmis & Allan Bronsro
WorleyParsons, Vancouver, BC, Canada

ABSTRACT: This paper presents a basic methodology for developing water treatment plans that will help address the selenium control challenges at mine sites in a cost-effective manner. This starts with understanding the mine site water - selenium balance and minimizing the requirement for "active" treatment (use of mechanical systems), which tends to be more cost-intensive than certain other "passive" mitigation measures. A wide range of passive and active treatment methods are surveyed and the methods that are ready for practical application, such as biological de-nitrification are described and compared on the basis of configuration, operational requirements, scalability and implementation challenges. Rule of thumb costs are presented. Finally, the options for permanent disposal of selenium residuals are discussed and important considerations in selenium management are highlighted.

1 BACKGROUND

Selenium in stormwater runoff is a prominent current issue for coal and phosphate mining operations in West Virginia, Idaho, western Canada and an emerging issue for many other mining projects across North America. Selenium is liberated from waste rock during mining operations and is considered to have deleterious effects on certain aquatic organisms during their reproductive stage, at concentrations as low as 1 or 2 ppb. Runoff from mining operations can often have Se concentrations in excess of 100 ppb. Selenium is commonly associated with coal deposits, present in both the coal itself and in sedimentary rock overburden. Management of selenium can have major cost and approval implications for a project and water management plans need to carefully consider the constraints associated with selenium control.

Selenium is located immediately beneath sulphur on the periodic table and behaves similarly in a mining context. It leeches out of waste rock dumps in a manner similar to acid rock drainage and in the process is oxidized to selenite and selenite, becoming bioavailable. The flux of free water in the dumps provides the oxygen for these processes and transports the mobilized selenium oxides out of the dump and into watersheds. Selenite is amenable to removal by various precipitation processes whereas options for removal of the fully oxidized selenate (the more common species in runoff) are much more limited.

2 UNDERSTANDING THE PROBLEM – WATER BALANCE, MINE PLANNING AND THE ENVIRONMENTAL CONTEXT

The water - selenium management plan for a mine site should be developed in concert with the mine plan. The potential costs associated with water and selenium management (projected to be

in excess of 100 million for some coal mine sites) are of such a magnitude that accommodations in the mine plan to moderate these costs need to be considered. A thorough hydrologic / hydrogeological understanding of the mine site is fundamental and can be used in concert with variants of the mine plan to develop year-by-year water balances with seasonal water flows and selenium and nitrate concentrations for each affected catchment and watershed. Understanding groundwater flows on the mine site at a detailed level is important. Infiltration from rock dumps drainage channels and ponds can bypass the runoff collection and treatment systems and has been noted as contributing to significant selenium levels in creeks in dry "no flow" conditions.

A geochemical model that relates mine activity (principally the volume of exposed waste rock) to the amount of Se release allows one to test different mine plan / water management scenarios. Predicting Se loading from waste rock varies with dump area, depth, volume, location and is site specific. It is generally agreed that there is a delay between waste rock placement and Se release – somewhere between 1 and 3 years. Site specific hydrology data and contaminant sampling data may be inserted into a model such as GoldSim to predict selenium release over the mine life. Unfortunately, there is little data available on how the rate of selenium release changes through the decades of mine life and afterward. Consequently, these forecasts entail significant uncertainties and will have to be tuned as the mine operation proceeds.

The regulatory context for selenium discharge from mine sites is complex and evolving, with potential inclusion of coal mines into the Metal Mining Effluent Regulation (MMER) and possible listing of selenium as a contaminant. Concurrently, water quality guidelines for Se are being developed by CCME and the Province of BC. The MMER is understood not to apply after mine operations are ceased, rendering the site under the jurisdiction of the Fisheries Act with its ambiguous prohibition on "deleterious substances". An environment assessment process (and / or the application of any of the mentioned regulations and guidelines) may result in site water quality performance objectives for a mine site that could include multiple in-stream Se effluent concentration targets for certain sampling points in various affected catchments or watersheds. Despite the regulatory uncertainty, some means must be found to establish effluent selenium targets for design purposes. If necessary, a range of values can be investigated. The time dimension of effluent selenium limits is a major consideration. A 10 ppb limit on a 30-day rolling average basis is much less onerous than a 10 ppb "not to exceed" grab sample basis, since the former allows some flexibility to adapt to changing site water flows and concentrations and will typically result in a reduced treatment plant size compared to the "not to exceed" basis.

During the operating phase of the mine, nitrate is usually present with selenium and in concentrations that are typically orders of magnitude greater. The nitrate is predominantly derived from the use of explosives in the mining operations and therefore will diminish rapidly when operations cease, whereas selenium release will persist for many decades. Nitrate concentration is often the primary size-determining variable for selenium treatment systems because of the fact that (as explained below) essentially all nitrate must be removed before selenium removal can be effected. Therefore, in situations where selenium discharge targets require active treatment, regulatory requirements relating to nitrate may not be of great consequence for treatment system costs. In contrast, any requirement to provide removal of sulphate as well as selenium and nitrate can have huge implications for the cost of treatment, as discussed in Section 5.

Mines that are located at the highest elevations of watersheds (a common situation for western Canadian coal mines) have a more challenging selenium management situation since the dilution capabilities of local water courses will be low or non-existent. This location factor can easily make the difference between needing active treatment or not.

3 MINIMIZING THE PROBLEM WITH BEST MANAGEMENT PRACTICES AND WATER MANAGEMENT DESIGN

The cost of selenium and water management can be moderated by minimizing the volumes of incident rainwater, surface water and groundwater that could be exposed to contaminant sources (principally waste rock) and subsequently require treatment. Selenium contamination that will require active treatment for removal is to be particularly avoided to the extent possible due the high capital and operating costs of this type of treatment compared to primary treatment (sedimentation optionally assisted by chemical addition).

Figure 1 is a simplified depiction of water / selenium interaction on a mine site and the means by which the requirement for active treatment of selenium may be minimized. Clean water diversion (structures to avoid contact between clean runoff and groundwater with waste rock) is well established and widely practiced. Where diversion around a valley-located waste rock dump is impractical, capturing upslope runoff and pipelining it through the dump may be. Clean water diversion combined with partial or full rock dump covers can dramatically reduce the water flux through rock dumps and consequently the release of selenium. Of course, rock dump covering, while excellent from the viewpoint of leachate control, entails geotechnical, logistical and material handling challenges that may limit its applicability to a given site.

Any selenium-bearing waste rock that experiences a flux of water in an aerobic environment will tend to leach selenium. The levels of selenium mobilization for some affected waters may be such that primary treatment (sedimentation optionally assisted by chemical treatment) may meet discharge standards. Storage, blending and timed release may also help maximize the volume of water that may be released without selenium treatment. In other cases, some form of selenium removal is required. This can include internal passive, external passive and active treatment methods. While internal passive systems are typically constructed with considerable equalization / storage capacity, external passive and active systems are very sensitive to peak flows and it is necessary to optimize equalization capacities and discharge strategies to moderate capital costs for these more expensive facilities. For example, it is typically cost-prohibitive to treat the peak flow during the freshet; and the selection of an appropriate treatment design flow rate depends on the interaction between the water balance, the engineered water management facilities (ponds and pumping systems), and the permitted discharge criteria.

Modelling has shown that 'active' water management –storing Se rich water and releasing during higher flow events - can be beneficial. Conversely, storage and release of 'clean' water during low flow periods can provide some benefit. Generally, the period immediately following the start of freshet is challenging to control (high flow and relatively high concentration). In a "top of watershed" setting, Se rich runoff from the mine site may increase before the flows in receiving creeks swell, resulting in temporarily higher Se concentrations in the creeks. In these situations, having storage capacity available in the sedimentation ponds at the start of the freshet can help avoid selenium discharge exceedences.

4 INTERNAL AND PASSIVE TREATMENT OPTIONS

It is not practical to totally eliminate water - waste rock contact at a mine site. For example, recently produced waste rock cannot be immediately covered and covering may be economically non-viable in some circumstances. In these cases, it may be possible to condition the contact water within the rock dump, prior to release of the contact water into the environment. One promising general approach is to establish a saturated zone at a strategic location within a rock dump where reducing conditions will be maintained and where selenium mobilization through oxidation can be prevented or reversed. Variants of this approach include "in-pit subaqueous sequestration", "saturated toe zone " (Claridge et al, 2011) and "saturated pit backfill" (Martin, 2013). These systems would be designed such that essentially all contact water within a rock dump would have to traverse the saturated zone before release to the environment. The saturated zone (essentially a buried pond) would be much smaller than the total volume of the contributing rock dumps. Field testing of the concept (Martin, 2013) showed that an annualized average hydraulic residence time of 145 days was more than adequate to reduce both selenium and nitrate to very low levels. The data suggested that considerably smaller hydraulic residence times might also be effective. Many questions remain regarding the practicalities of design and long term performance of the concept, however, this internal, passive method for selenium control deserves further investigation.

5 ACTIVE TREATMENT OPTIONS

This section addresses "active" methods that can be employed to remove nitrate and selenium from contact water. These are distinguished from the passive methods described above in that

they are mechanical in nature and can be operated to respond to changing treatment conditions. Active selenium removal methods are many and varied. Several technology survey articles and reports have been prepared which compare and contrast available methods. The most comprehensive survey and the one most relevant to the mining industry was prepared by the North American Metals Council (NAMC, 2010) and recently updated (NAMC, 2013 and Sandy, 2013).

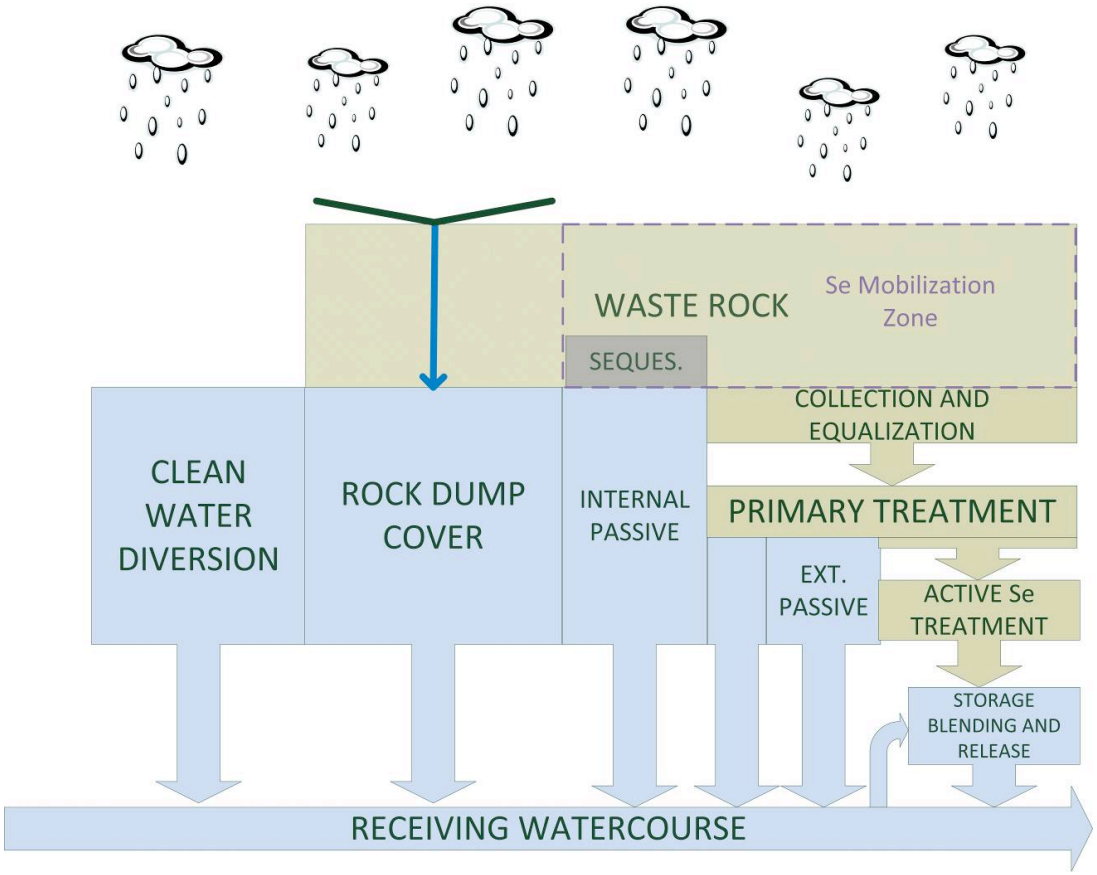


Figure 1. Simplified Depiction of Selenium Control Measures at a Mine Site

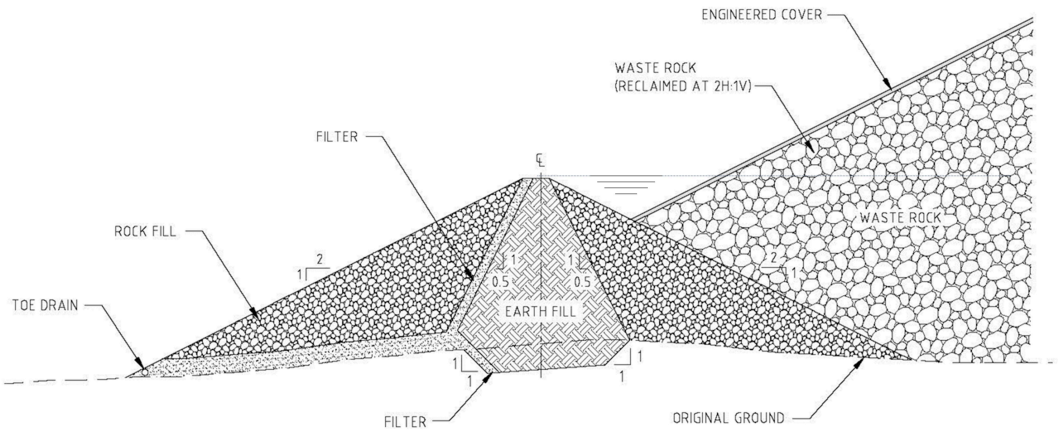


Figure 2. Simplified Depiction of a Saturated Toe Zone Impoundment

In comparison with more established selenium removal applications such as treatment of flue gas desulphurization (FGD) water, Mining Influenced Water (MIW) applications in Canada are characterized by high flows, low temperatures, relatively low selenium concentrations and stringent effluent discharge limits. For these applications, the methods that have been implemented to date for large scale mining runoff applications are almost exclusively based on attached growth biological treatment. Fundamentally, this is because selenate, being the dominant species encountered, is resistant to chemical precipitation methods and must be reduced before it can be removed. Chemical reduction of selenate is difficult and expensive, however, certain bacteria that are also responsible for de-nitrification have enzymatic mechanisms that can accomplish this task relatively easily.

5.1 *Systems Based on Biological Reduction*

Attached growth biological treatment systems use a media as a support structure and surface for the growth of a biofilm (complex colony of micro-organisms) including the facultative heterotrophs that reduce nitrate to nitrogen gas and reduce selenate and selenite to elemental selenium. The insoluble selenium is precipitated to combine (and be removed) with the biological solids (biosolids, or sludge) that is a byproduct of any biological treatment process. The reduction process requires an electron donor supplied as the carbon within organic sources such as methanol or molasses. The stoichiometric ratio of electron donor to electron acceptors (nitrate and selenate) must be carefully controlled to maintain appropriate oxidation-reduction (redox) conditions.

The redox profile for biological reduction reactions is well established. Important features of this profile relevant to selenium removal are as follows:

a) Nitrate reduction (denitrification) must be essentially complete before selenate can be reduced.
b) Selenate reduction occurs at redox values of approximately 112 to 450 mV (2 to 8 pE), in the anaerobic region.
c) More strongly negative redox encourages perchlorate reduction (if present) and sulphate reduction, producing H_2S.

In MIWs, nitrate content will typically be several orders of magnitude greater than the selenium concentration so that variations in nitrate concentration can have a major influence on biological selenium reduction. MIWs also typically contain sulphate and conversion to H_2S is possible, however, this is undesirable from the viewpoint of safety and biotoxicity. Although sulphate can theoretically be removed with biological reduction, in practice, the cost of incremental electron donor, the complexities of handling H_2S production and biotoxicity concerns render this impractical. If sulphate removal is required, substantial additional physical-chemical treatment facilities will be required.

5.2 *Comparing Available Biological Reduction Systems*

Three types of attached growth biological systems have been applied to selenium removal applications, namely Static Bed Biofilters (SBBs), Fluidized Bed Reactors (FBRs), and Moving Bed Bioreactors (MBBRs). They are chiefly distinguished by media type and motion (or lack thereof) within the reactors. In all three technologies, selenium will accumulate within, and be removed with, biosolids, however there are major differences in how this removal is effected. In terms of level of experience in selenium treatment applications, SBB would be first, followed by FBR and MBBR.

Figure 3 is a simplified comparative schematic of how the three technologies would be implemented in a typical mine setting. It is clear that much of the infrastructure will be common to the three systems. For example, primary treatment, equalization and filtration will be required regardless of the system selected in order to moderate flows and the levels of suspended particulate in the runoff. All systems require the addition of a carbon source and nutrients to support the biological process and all generate biosolids that must be properly disposed of. Although other methods may be considered, the schematics assume that the biosolids (which will contain nearly all of the selenium) will be dewatered to produce a “dry cake” sludge product for disposal at a secure landfill, to minimize the opportunity for selenium remobilization. Consequently, bio-

solids thickening and dewatering equipment is common to the three systems. It is also likely that the systems will require aerobic biological post-treatment to both consume residual soluble organic matter and increase dissolved oxygen levels. Finally, these systems typically do not guarantee performance for temperatures below about 10C so heating may be required, depending on local seasonal conditions. Since heat fuels represent a high cost, heat integration is included to minimize this cost.

The SBB employs a media that (at least in normal operation) remains immobile. In contrast, the media in both the FBR and MBBR are in constant motion. In the case of the FBR, as represented by the Envirogen FBR process, a media consisting of sand or activated carbon is fluidized (kept in suspension) by the vertical flow of water in the cylindrical reactor. A variable recycle is employed to maintain a relatively constant velocity and bed expansion. In the MBBR process, the media consists of plastic "biomass carriers" approx. 1 – 3 cm in diameter that are shaped to provide a large surface area for biofilm growth. The biomass carriers are kept in suspension by fluid motion induced by a low speed impeller.

The SBB process is a semi-continuous flow through process whereby the bioreactor serves to accumulate and store biosolids as well as effect the biochemical reactions. For example, GE's ABMet processs which has several full scale installations for treatment of selenium in MIW, is a conventional downflow activated carbon biofilter with periodic degassing and backwash. In a manner very similar to the common Biological Aerated Filter (BAF) process, the bioreactor must be periodically taken off-line and backwashed to strip out the accumulated biomass. The backwash must be thickened and dewatered.

The FSB and MBBR systems are flow-through, steady state processes with a continuous entrainment of biological solids in the treated effluent stream, requiring unit operations downstream of the reactors to remove solids from the full process flow. These solids must be separated from the effluent, thickened and dewatered. In this respect, they differ from the SBB which discharges biosolids only in the backwash mode. In normal operation, effluent from the SBB does not require subsequent solids removal step. Given the turbulent nature and media collisions within the FBR and MBBR, the effluents may contain very fine particulate (including colloidal fractions) that is difficult to separate with conventional solids separation equipment and more advanced equipment such as ultrafiltration may be required to consistently achieve very low selenium target values (less than 10 ppb).

Another area of difference is the semi-batch nature of SBB operation compared with flow-through steady state operation of the FBR and MBBR. Each SBB biofilter will be backwashed on a regular basis (perhaps daily). Each backwash dramatically changes the biomass content and therefore the microbial population of the reactor. A freshly backwashed reactor may be less efficient and require its effluent to be re-processed in a "ripe" reactor for a period of time. There is also a question as to whether the steady state nature of the FBR and MBBR allows them to adapt more precisely and consistently to the particular characteristics of the influent. In the FSB and MBBR systems, there is a vigorous biomass control, a relatively constant sludge age (average residence time of biomass) and a high intensity of activity due to the high mass transfer kinetics (particularly so for the FBR). Gases generated in the process (which could include N_2, H_2S or even methane) are quickly stripped out of the systems and do not accumulate. In the SBB system, there will be noticeable changes in the microbe assembly between backwash cycles. Also, gases will tend to accumulate between backwashes and could cause channelling or episodic release (bubbling) both of which could affect performance. In cases of high nitrate loading, gas purging cycles may be required in addition to the normal backwash cycles.

The requirement to heat effluent is a major cost factor. Any substantial differences between the processes in tolerance for low temperatures would be a significant consideration. Indications are that FBR and SBB systems can perform at temperatures below 10C, however comparative data is scarce.

Hydraulic Retention Time (HRT) is an important variable for all three technologies. Excessive HRT can shift the redox toward a more negative region. Insufficient HRT can result in incomplete reduction. Since flows can vary dramatically seasonally at mine sites, the ability to adapt to changing flows is an important consideration. The SBB system addresses flow variations by employing multiple parallel modules, which can be used on an "as required" basis but with some serious constraints, namely that several weeks of acclimation would be required for the addition of a bioreactor, so that it must be done on a planned basis and not in response to

short term runoff conditions. Similarly, once a bioreactor is taken offline and idled for several weeks, it cannot be immediately brought back online.

The FSB maintains a constant HRT for each bioreactor and a dedicated recycle flow is adjusted as required to maintain this, however long term operation at low flows would require modules to be shut down. Based on experience in other applications, MBBRs are expected to be tolerant of wide variations in flow, however, there is limited practical experience in selenium applications to support this supposition.

The foregoing discussion illustrates that the FSB and MBBR have a lot of similarities. The FSB is among the most volume-efficient bioreactor types available and can be expected to require less HRT than the SBB or MBBR for a given application. For FBR and MBBR, the principal tradeoff is between the reactor size and the mechanical and operational simplicity. Due to its simplicity, the MBBR may be more amenable to implementation in a distributed treatment scenario, where smaller plants are located at several sites, provided that a workable solids collection system can be developed.

5.3 *Comparative Costs of Active Treatment Systems*

Table 1 provides indicative capital and operations and maintenance (O&M) costs for the three types of active treatments systems described herein, based on recent work by NAMC (NAMC, 2013). These are indicative costs only but are meant to include roughly the scope of facilities depicted on the process schematic that is downstream of the sedimentation / equalization facilities. A flow rate of 3800 m3/day is assumed.

Table 1. Notional Costs of Several Types of Active Treatment Systems - 3800 m3/day (700 USgpm)

Type	Capital	O&M
FBR	30	1.7 - 2.0
SBB	37	1.7 – 2.0
MBBR	25	1.7 – 2.0

*Capital is Total Installed Cost in millions of US$. O&M in US$ million/yr

It should be noted that the variations in costs indicated above are well within the accuracy of the estimate (+100%, - 50%) and no conclusions can be drawn regarding which technology would be most cost-effective for a particular application. Economies of scale can be expected to vary between the technologies and the ranking of costs could be different at higher flow rates. Each case would need to be investigated in detail to select the most cost-effective technology.

6 CONCLUSIONS

A range of options is available for selenium control at mine sites. The cost of active selenium treatment is such that methods to minimize the volume of contact water requiring active treatment should be investigated and employed where practical. These methods include well-established practices such as clean water diversion, known effective but potentially costly methods such as waste rock covers and novel passive methods such as in-pit subaqueous sequestration where the costs and long term performance are not well understood.

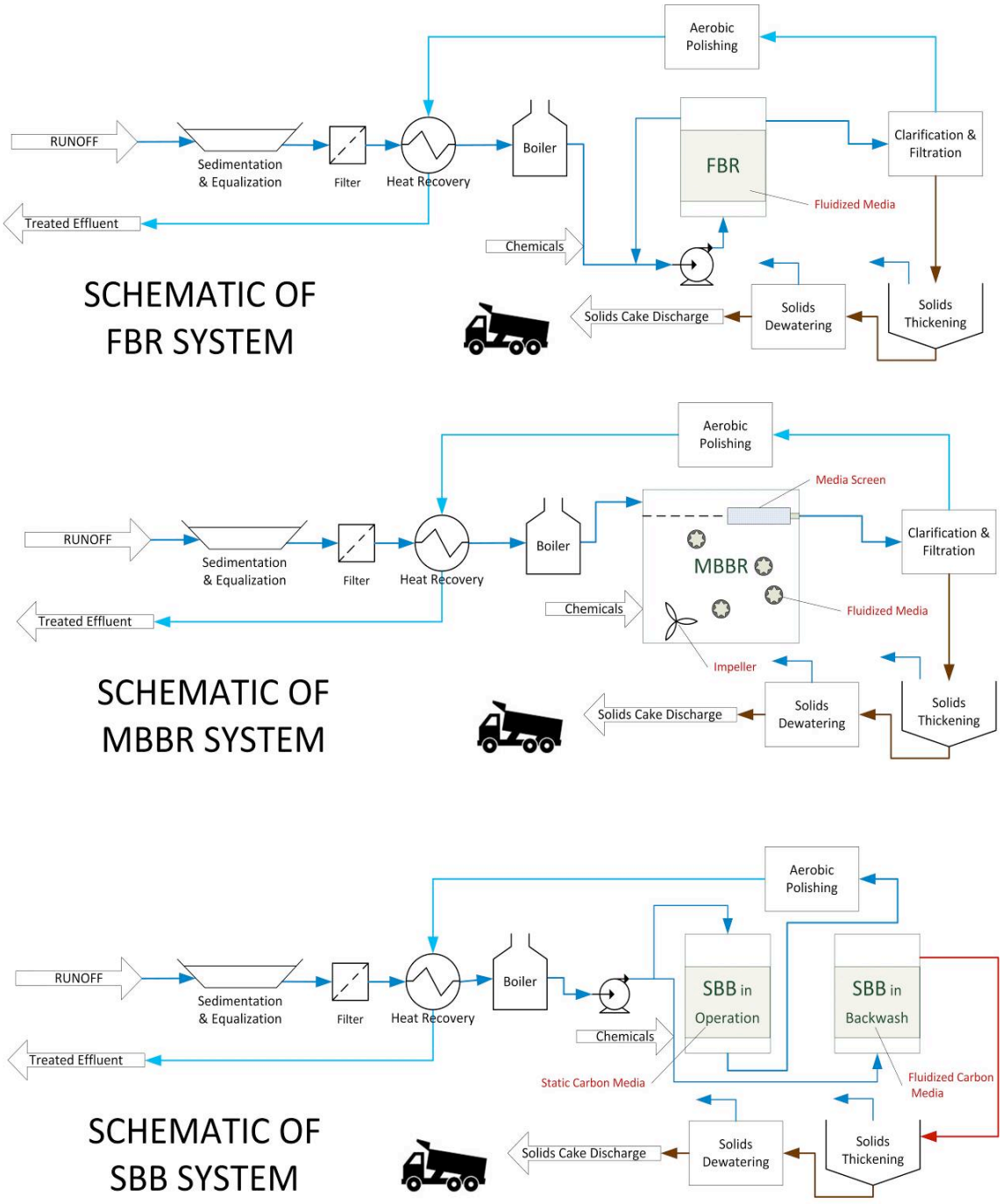


Figure 3. Process Schematics for Several Active Treatment Systems for Selenium Removal.

7 REFERENCES

North American Metals Council (NAMC) 2010 *Review of Available Technologies for the Removal of Selenium from Water.*

North American Metals Council (NAMC), 2013 *Review of Available Technologies for the Removal of Selenium from Water - Addendum.*

Claridge F, Funk W, Martin L., 2011 *The Evolution of Mine Waste Management Practices in Western Canada* WorleyParsons Canada Services Ltd.

Martin, A. 2013 *Assessment of Selenium Attenuation in Saturated Pit Backfill*. Presentation at NAMC-Selenium Working Group Meeting, June 20, 2013, Vancouver, BC, Canada
Sandy, T 2013. *NAMC Whitepaper Report Addendum*. Presentation at NAMC-Selenium Working Group Meeting, June 20, 2013, Vancouver, BC, Canada

Water quality guidelines for metals

Sushil Dixit, Tamzin El-Fityani & Doug Spry
National Guidelines and Standards Office, Emerging Priorities Division, Environment Canada, Gatineau, QC, Canada

ABSTRACT: The National Guidelines and Standards Office of Environment Canada has developed and/or is developing a number of water quality guidelines (WQGs) for the protection of aquatic life for metals. The approaches considered for guideline development, that is, species sensitivity distribution (SSD), single factor adjustment equations, multiple linear regression (MLR) and biotic ligand model (BLM) are discussed in detail along with their application to specific metals. The WQGs for aquatic life provide benchmarks for the quality of the ambient environment. Where the WQG is met there is low likelihood of adverse effects to aquatic life. WQGs are increasingly being used to aid in pollution prevention by providing targets for acceptable environmental quality, in evaluating the significance of concentrations of substances currently found in the environment, and as performance measures of the success of risk management activities.

1 INTRODUCTION

The potential for ecological effects of metals is related to the duration of exposure of the specific metal form and its concentration in the environment. In terms of persistence of the available form of metal, measures that require attention are complexation, precipitation, mineralization and transformation rates. Complexation with dissolved organic carbon and suspended solids in surface waters and binding with settled solids and sulfides in sediments are some of the key processes that control metal persistence and resulting exposure levels in aquatic ecosystems (Di-Toro et al. 2001). Metals have a rapid turnover rate in the water column and the residence time in water column is directly related to the fraction of the metal that is sorbed to particles (Nriagu et al. 1996). Diffusion and settling are the two main processes for removing metals from the water column (Di Toro et al. 2001). Plankton are widely considered as one of the most important factors controlling the residence time of metals in the water column (Twiss et al. 2005).

Water Quality Guidelines (WQGs) for the protection of aquatic life have a long history in Canada and are developed and published by various Canadian jurisdictions. In 1987, the Canadian Council of Resource and Environment Ministers (CCREM) published the national Canadian Water Quality Guidelines (CWQGs) by compiling available federal (Canadian, US) and provincial WQGs. The Canadian Council of Ministers of the Environment (CCME) took on this responsibility when it was formed in 1996 to provide an intergovernmental forum in Canada that focuses on environmental issues of national and international concern. It is comprised of all levels of the government including environment ministers from federal, provincial and territorial governments. Since 1987, over 200 water quality guidelines have been developed through CCREM/CCME. The updated "Protocol for the Derivation of Water Quality Guidelines for the Protection of Aquatic Life" (CCME 2007) offers significant advances in developing WQGs, and

includes significant changes to previous protocol such as the use of species sensitivity distributions (SSDs) and accounting for unique properties of contaminants that influence toxicity. Special attention in the new protocol is given to toxicity modifying factors and bioavailability.

Environment Canada (2013) has recently developed Federal Environmental Quality Guidelines (FEQGs) that provide benchmarks for the quality of the ambient environment. The development of FEQGs is the responsibility of the Federal Minister of Environment under the *Canadian Environmental Protection Act, 1999*. FEQGs are developed as an adjunct to the risk assessment/risk management of priority chemicals identified in the Chemicals Management Plan (CMP) and other federal initiatives. The FWQGs are intended to protect all forms of aquatic life for indefinite exposure periods and this objective is in line with the guiding principle of the CWQGs, that is, to protect all forms of aquatic life and all aspects of the aquatic life cycles, including the most sensitive life stage of the most sensitive species over the long term, from the negative effects of exposures to substances via the water column (CCME 2007). Similar to CWQGs, FEQGs are based on the toxicological effects or hazards of specific substances or groups of substances and do not take into account analytical capability or socioeconomic factors. Where the FEQG is met there is low likelihood of adverse effects on the protected use (e.g., aquatic life or the wildlife that may consume them). The use of FEQGs is voluntary unless prescribed in permits or other regulatory tools.

The derivation of a WQG begins with a broad overview of a substance's use pattern, its environmental fate and behaviour, and a detailed evaluation of available aquatic toxicological information for the substance. The compilation and evaluation of relevant toxicological data require an in-depth search of the toxicological literature and this step forms the backbone of a guideline derivation. Individual toxicological studies are evaluated against a standard set of acceptability criteria (Klimisch et al. 1997) before the data are included in guideline derivation. Using the selected toxicological database, the WQG values are obtained by applying the SSD or safely factor approach (for details see CCME 2007). SSDs acknowledge that sensitivity to toxic compounds differs among species due to physiology, morphology, life history, behavior, etc.

The use of SSD has become common in ecological risk assessment and environmental quality guidelines development. SSD represents the variation in sensitivity of species to a substance where the distribution can be a parametric function, such as a triangular, normal or logistic distribution, or a non-parametric function (Posthuma et al. 2002). Mathematically, SSDs can be used to estimate the proportion, fraction or percentile (p) of species potentially affected at given concentrations of a chemical in an environmental medium. In practice, these percentiles are used to set environmental threshold values such as a hazardous concentration for 5% of the species (HC_5), which would protect 95% of the species included in the distribution (Aldenberg and Slob 1993; Aldenberg and Jaworska 2000; Wheeler et al. 2002a,b). The HC_5 is the preferred protection level (Aldenberg and Slob 1993; Posthuma et al. 2002; OECD 1992; CCME 2007). As implemented by CCME, the curve is based on no effect values and no safety/uncertainty/application factor is used.

Once the WQG has been determined, a factsheet and/or detailed technical report is prepared containing information about the environmental fate and behaviour of the substance, its use in Canada, the toxicological data found and used, and how the WQG was derived. Before publication these documents undergo internal and external peer review process.

2 CANADIAN WATER QUALITY GUIDELINES FOR METALS

Canadian WQG values and associated details for selected metals are available from the CCME (http://ceqg-rcqe.ccme.ca). In this presentation our focus is to discuss WQGs for metals that are recently developed and/or being developed by the National Guidelines and Standards Office of Environment Canada in collaboration with CCME and other partners. Specific examples of long-term (i.e., chronic) WQGs for uranium, cobalt and cadmium are presented here in detail.

3 WATER QUALITY GUIDELINE FOR URANIUM

The long-term WQG for uranium was published by CCME (2011) and summary details are presented here. Uranium is a naturally occurring metal that is radioactive in nature and can occur in three isotopic forms of distinct radioactive properties (ATSDR 1999). Although uranium has chemical properties of elemental metal, it is not found in elemental form in nature, but exists in ~155 minerals, including oxides, phosphates, carbonates, vanadates, silicates, arsenates and molybdates (CCME 2011). Naturally high concentrations of uranium ore deposits found in Canada, including Saskatchewan and Ontario, are mined in the past and present (Environment Canada and Health Canada 2003) and are mainly used as a fuel. Details on the environmental fate, behaviour and toxicity to aquatic organisms are presented in CCME (2011). In addition to altering environmental fate and behaviour, water chemistry (e.g., pH, hardness, organic matter) can influence the toxicity of uranium to aquatic organisms.

The evaluation of long-term uranium chemical toxicity data (radiochemical toxicity is much lower than chemical toxicity and was not considered) for aquatic biota identified that among fish species, rainbow trout (*Oncorhynchus mykiss*) was most sensitive. Among the more sensitive invertebrates and plants, amphipod (*Hyalella azteca*) and green algae (*Pseudokirchneriella subcapitata*) were the most sensitive to uranium toxicity, respectively. Because at this time there is insufficient information available to quantify the influence of toxicity-modifying factors for uranium, they could not be taken into account during the guideline derivation.Abstract frame

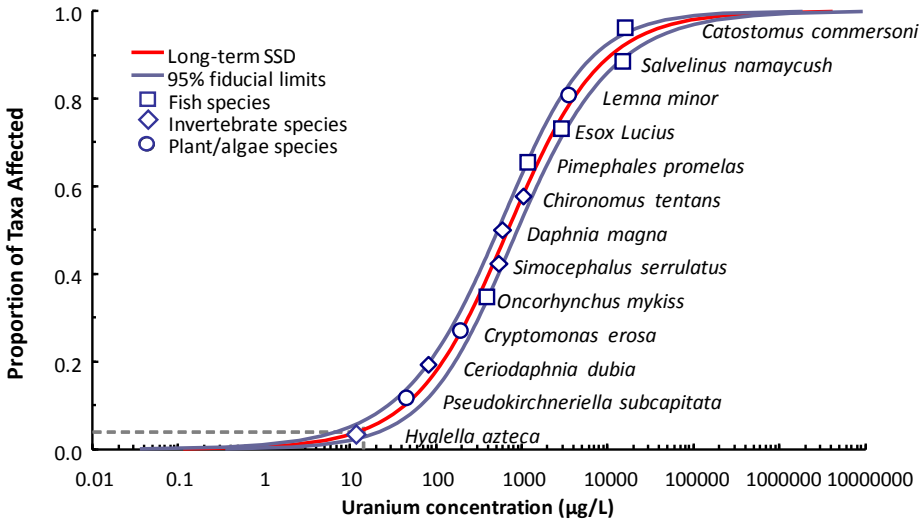


Figure 1. Long-term SSD showing the toxicity of uranium to fresh water aquatic species (Source: CCME 2011).

The long-term WQG for uranium for the protection of aquatic life was developed following the CCME protocol (CCME 2007) protocol and toxicity data for 13 species were used in the derivation of the guideline using the SSD approach. In SSDs, each species that has suitable toxicity data is ranked according to sensitivity, and its centralized position is determined using the Hazen plotting position. Amongst the models tested, the logistic model provided the best fit (Figure 1). The 5th percentile on the SSD is 15 µg/L and this value is the long-term freshwater WQG for uranium (CCME 2011).

4 WATER QUALITY GUIDELINE FOR COBALT

The long-term WQG for cobalt was developed this year and the details presented here are from Environment Canada (2013) publication. Cobalt is a naturally occurring element released to the environment from anthropogenic sources such as burning of fossil fuels, sewage sludge, phos-

phate fertilizers, mining and smelting of cobalt-containing ores and industrial processes using cobalt compounds (Hodge and Dominey 2001; IPCS 2006). Cobalt is used in pigment manufacturing, chemical and alloy production, and in the manufacture of rechargeable batteries (ATSDR 2004; CDI 2006; Environment Canada 2009). The majority (99%) of the cobalt manufactured in Canada is exported and in 2006 upwards of 22 million kg was imported in products such as cobalt chloride, cobalt sulphate, and sulphuric acid cobalt salts (Environment Canada 2009). Cobalt chloride and cobalt sulphate are highly soluble, and are almost always in the dissolved form. Cobalt binds strongly with sediments and suspended particulate matter, suggesting that cobalt will remain for the most part in bottom sediments after depositing there. Text and indenting
All text, figures, tables, etc. should fit exactly in the type area of 15 × 24 cm (5.91" × 9.52"). All text should be typed in Times New Roman. All text is 11 pt on 12 pt line spacing except for the paper title (16 pt on 18 pt), author(s) (12 pt on 13 pt), affiliation(s) (10 pt on 11 pt) and the small text in tables, captions and references (10 pt on 11 pt). All line spacing is exact. Never add a line space between lines or paragraphs.

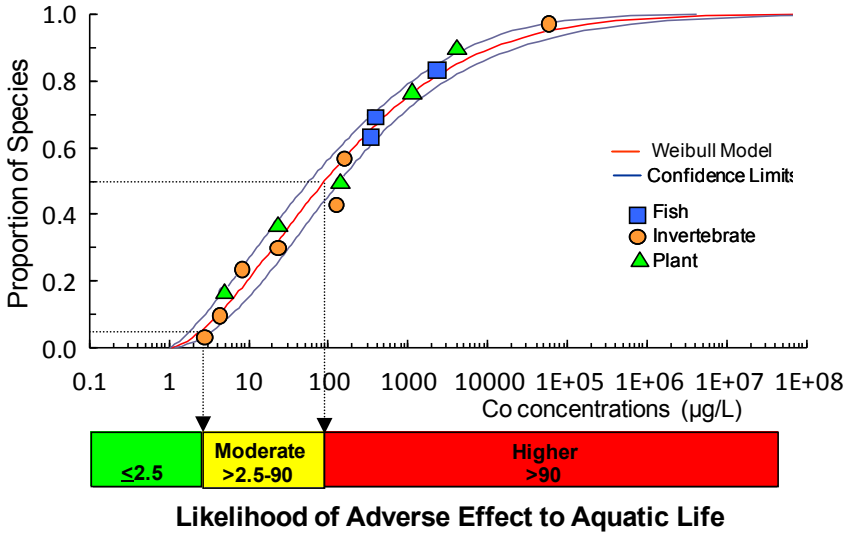


Figure 2. Long-term SSD for aquatic cobalt toxicity data and associated effect levels for aquatic life (source: Environment Canada 2013).

Long-term toxicity data for three fish, seven invertebrates and five plant/algae species were included in the development of the WQG for cobalt (Figure 2). Invertebrates were more sensitive to cobalt than fish; however, the sensitivities do overlap among taxa. Among invertebrates, *Hyalella azteca* was the most sensitive species, while the rotifer *Philodina acuticornis* was the least sensitive. The most sensitive fish and plant species were zebrafish (*Brachydanio rerio*) and duckweed (*Lemna minor*), respectively (Environment Canada 2013). The least sensitive fish and plant species were the rainbow trout (*Oncorhynchus mykiss*) and green algae (*Chlamydomonas acidophila*), respectively. Toxicity of cobalt can be influenced by the water chemistry (Government of Canada 2011), however, toxicity data could not be standardized because the required data were not available.

Following the CCME protocol (CCME 2007), several cumulative distribution functions were fit to the data using the SSD approach and the Weibull model provided the best fit for these data. The 5th percentile is 2.5 µg/L (Figure 2) and is considered as the Federal Water Quality Guideline (FWQG) for aquatic life. The FWQG represents the concentration below which one would expect either no, or only a low likelihood of adverse effects on aquatic life. In addition to this guideline, two additional concentration ranges are provided for use in risk management. At concentrations between the 5th and 50th percentile of the SSD (2.5-90 µg/L) there is a moderate likelihood of adverse effects to aquatic life. Concentrations greater than the 50th percentile (>90 µg/L) have a higher likelihood of causing adverse effects (Environment Canada 2013).

5 WATER QUALITY GUIDELINE FOR CADMIUM

The long-term WQG for cadmium is being developed by the National Guidelines and Standards Office of Environment Canada for the CCME. The details presented here are from the draft version released for the public review in October 2012. Cadmium occurs naturally in the environment and is typically found in rocks as a minor constituent in mineral sulphides. Because cadmium is mainly recovered as a by-product from the smelting of zinc, its production in Canada is based on the level of zinc production (Nriagu 1980). For the Canadian ore a range of 0.001% to 0.067% recoverable cadmium by weight were reported (Brown 1977). Nickel-cadmium batteries, pigments, coatings, stabilizers in plastics and synthetic products, and alloys are the major industrial uses of cadmium (NRCan 2005).

In natural waters cadmium may exist in a range of chemical species that have a major role in geochemical and biochemical processes. Water hardness, alkalinity, pH and dissolved organic matter can influence the toxicity of cadmium to aquatic species. Alkalinity generally covaries with hardness, and hardness has been shown to be a better predictor of aquatic toxicity than alkalinity (USEPA 2001). CCME (2012) evaluated the influence of toxicity modifying factors on cadmium toxicity to aquatic species and concluded that hardness was the only toxicity modifying factor for which the draft guideline could be adjusted due to data availability. Based on hardness-toxicity data, empirical relationships were developed and used to calculate a hardness-toxicity slope of 0.83 which is applicable across species. This slope was then used to develop a hardness adjustment equation that can be applied to standardize endpoint values to a common water hardness.

Following the CCME protocol (CCME 2007) toxicity data for 36 aquatic species were used in the derivation of the draft long-term cadmium guideline. All data points included in the SSD were adjusted to a standard water hardness of 50 mg/L as $CaCO_3$ equivalents using the hardness adjustment equation. Species were ranked according to adjusted effect concentration and their positions were determined on the SSD (Figure 3). The log-logistic model provided the best fit among the models tested and the 5th percentile value is 0.09 µg/L. This HC_5 value at 50 mg/L hardness, along with the hardness-toxicity slope of 0.83, were used to derive a guideline equation into which users can enter the water hardness of the site under consideration to derive a site-specific guideline. Thus, the long-term draft cadmium guideline is derived from an equation with water hardness rather than being a single value. The equation to derive the WQG for cadmium is: $WQG = 10^{\{0.83(\log[\text{hardness}]) - 2.46\}}$. Where the WQG is expressed in total cadmium concentration (µg/L) and hardness is measured as $CaCO_3$ equivalents in mg/L.

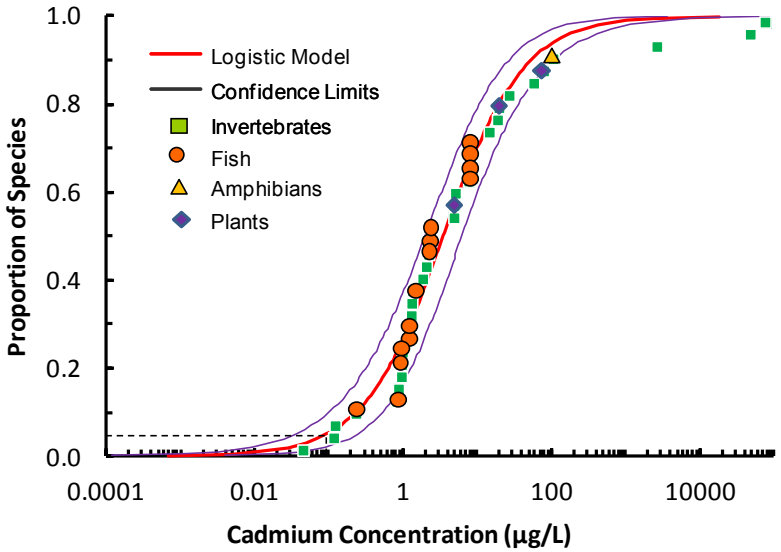


Figure 3. Long-term SSD showing the toxicity of cadmium to fresh water aquatic species normalized to 50 mg/L hardness (Source: CCME 2012).

6 ONGOING WATER QUALITY GUIDELINES WORK

The National Guidelines and Standards Office is at various stages of developing WQGs for silver, chromium, copper, iron, manganese, lead, vanadium and zinc. The approaches used in developing these WQGs include methods discussed above for cadmium, cobalt and uranium. Additional approaches, such as step-wise multiple linear regression (MLR) and biotic ligand model (BLM) are also being evaluated for the WQGs development.

Step-wise MLR analysis has recently been used in WQGs development (Esbaugh et al. 2011, 2012). In conducting a step-wise MLR analysis, the independent water chemistry parameter that explains the greatest amount of the variance in the dependent variable (i.e., toxicity value) is considered first. If the relationship between this independent variable and the dependent variable is not significant, the modeling process is complete and no model is developed. If the relationship is significant, the variable is retained and the independent variable that explains the highest proportion of the remaining variance is entered next. If this second variable does not explain a significant additional percentage of the variance, the variable is removed and the final model contains only the first independent variable that was entered. If the variable is retained, the independent variable explaining the next greatest proportion of remaining variance is entered, and so forth. Environment Canada is examining the use of the MLR approach for the development of guidelines for lead and iron.

The BLM is a multi-parameter model that can be used to adjust for multiple toxicity modifying factors at the same time. The model considers the effects of dissolved metal concentrations on toxicity as well as competitive interactions of metals with organic and inorganic ligands that affect metal speciation and hence availability (Di Toro et al. 2001; Santore et al. 2001). Worldwide efforts to-date have resulted in the development of short- and/or long-term models for metals such as copper, manganese, nickel and zinc (e.g., USEPA 2007; ECI 2008; UKTAG 2012. Environment Canada is also studying the BLM approach for developing the site-specific WQGs for copper.

7 CONCLUSIONS

Traditionally, approaches used in developing WQGs for metals considered parsimonious methods, however, advances have been made in incorporating toxicity modifying factors in guideline development. Consistent with approaches used internationally, EQGs developed under CCME and CMP for data-rich substances have adopted the SSD approach in characterizing ecological effects. Rather than relying on information from a single sensitive species, SSD uses data for multiple species representing a variety of taxa and ideally a variety of functional roles within the ecosystem. The approach acknowledges that sensitivity to toxic compounds differs among species.

The WQGs for aquatic life are recommendations of the toxicity threshold and allow flexibility in their application. They are not absolute limits nor are they the only way to derive targets or benchmarks for risk management. It is emphasized that WQGs, which apply to the ambient environment are not effluent limits or “never-to-be-exceeded” values but may be used to derive them. The WQGs developed both by CCME and Environment Canada can serve three important functions: first, they can be an aid to prevent pollution by providing targets for acceptable environmental quality; second, they can assist in evaluating the significance of concentrations of chemical substances currently found in the environment (monitoring of water, sediment and biological tissue); and third, they can serve as performance measures of the success of risk management activities.

The WQGs developed for metals are highly applicable to the metal mining sector for risk assessments. Because the aquatic toxicity of metals is strongly dependent on physical and chemical characteristics of the exposure water, a careful consideration of the bioavailability and toxicity of specific metals to aquatic organisms under site-specific conditions is recommended.

8 REFERENCES

Aldenberg, T. & Slob, W. 1993. Confidence limits for hazardous concentrations based on logistically distributed NOEC toxicity data. *Ecotoxicol. Environm. Safety* 25: 48-3.

Aldenberg, T. & Jaworska, J.S. 2000. Uncertainty of the hazardous concentration and fraction affected for normal species sensitivity distributions. *Ecotoxicol. Environm. Safety* 46: 1-18.

ATSDR. 1999. Toxicology profile for uranium. U.S. Department of Health and Human Services Atlanta, GA.

ATSDR (Agency for Toxic Substances and Disease Registry). 2004. Toxicological Profile for Cobalt. Department of Health and Human Services, ATSDR. Available from: http://www.atsdr.cdc.gov/toxprofiles/tp33.html

Brown, D. H. 1977. Cadmium. *In* Canadian minerals yearbook. Ottawa, Mineral Resources Branch, Energy, Mines, and Resources Canada.

Di Toro, D.M., Allen, H., Bergman, H., Meyer, J., Paquin, P. & Santore, R. 2001: "A Biotic Ligand Model of the Acute Toxicity of Metals: I. Technical Basis". *Environmental Toxicology and Chemistry* 20: 2383-2396.

Government of Canada. 2011. Screening Assessment for the Challenge - Cobalt (Elemental cobalt), Chemical Abstracts Service Registry Number (CAS RN) 7440-48-4; Cobalt chloride, CAS RN 7646-79-9; Sulfuric acid, cobalt (2+) salt (1:1) (Cobalt sulfate), CAS RN 10124-43-3; Sulfuric acid, cobalt salt (Cobalt sulfate), CAS RN 10393-49-4. Report prepared by: Environment Canada, Health Canada, Existing Substances Program. 124 pages. Gatineau, Quebec. Available from: http://www.ec.gc.ca/ese-ees/default.asp?lang=En&n=8E18277B-1

CCME (Canadian Council of Ministers of the Environment). 2007. A Protocol for the Derivation of Water Quality Guidelines for the Protection of Aquatic Life. In: Canadian Environmental Quality Guidelines, 1999, Canadian Council of Ministers of the Environment, Winnipeg. Available from: http://ceqg-rcqe.ccme.ca/

CCME (Canadian Council of Ministers of the Environment). 2011. Canadian water quality guidelines for the protection of aquatic life: Uranium. In: Canadian environmental quality guidelines, 1999, Canadian Council of Ministers of the Environment, Winnipeg.

CCME (Canadian Council of Ministers of the Environment). 2012. Canadian Water Quality Guidelines: Cadmium. Draft Scientific Criteria Document for Public Review. Canadian Council of Ministers of the Environment, Winnipeg.

CDI (Cobalt Development Institute). 2006. Cobalt Fact Sheet 8: Electronics. Surrey, United Kingdom.

ECI (European Copper Institute). 2008. European Union risk assessment report on copper, copper(II) sulfate pentahydrate, copper(I) oxide, copper(II) oxide, dicopper chloride trihydroxide. Voluntary risk assessment.

Environment Canada. 2009. Data for Batch 10 substances collected under the Canadian Environmental Protection Act, 1999, Section 71: Notice with respect to certain Batch 10 Challenge substances. Data prepared by: Environment Canada, Existing Substances Program.

Environment Canada. 2013. Canadian Environmental Protection Act, 1999: Federal Environmental Quality Guidelines – Cobalt. http://www.ec.gc.ca/ese-ees/default.asp?lang=En&n=92F47C5D-1

Environment Canada and Health Canada. 2003. Priority Substances List Assessment Report: Releases of Radionuclides from Nuclear Facilities (Impact on Non-human Biota). Her Majesty the Queen in Right of Canada (Environment Canada).

Esbaugh A.J., Brix, K.V., Mager, E.M. & Grosell, M. 2011. Multi-linear regression models predict the effects of water chemistry on acute lead toxicity to *Ceriodaphnia dubia* and *Pimephales promelas*. *Comp Biochem Physiol Part C* 154: 137-145.

Esbaugh, A.J., Brix, K.V., Mager, E.M., De Schamphelaere, K. & Grosell, M. 2012. Multi-linear regression analysis, preliminary biotic ligand modeling, and cross species comparison of the effects of water chemistry on chronic lead toxicity in invertebrates. *Comp Biochem Physiol C* 155:423-431.

Hodge, F.G. & Dominey, L. 2001. Cobalt and cobalt alloys. Kirk-Othmer Encyclopedia of Chemical Technology,

IPCS (International Programme on Chemical Safety). 2006. Cobalt and inorganic cobalt compounds. Geneva (CH): World Health Organization. (Concise International Chemical Assessment Document 69). Jointly sponsored by the United Nations Environment Programme, the International Labour Organization, and the World Health Organization, and produced within the framework of the Inter-Organization Programme for the Sound Management of Chemicals. Available from: http://www.inchem.org/documents/cicads/cicads/cicad69.htm

Klimisch, H.J., Andreae, M. & Tillmann, U. 1997. A systematic approach for evaluating the quality of experimental toxicological and ecotoxicological data. Regul. Toxicol. Pharmacol. 25: 1–5.

Nriagu, J.O. 1980. Production, uses and properties of cadmium. In: *Cadmium in the Environment* (J.O. Nriagu, ed.), Wiley, New York, Vol. 1, pp. 36-70.

Nriagu, J.O., Lawson, G., Wong, H.K.T. & Cheam, V. 1996. Dissolved trace metals in Lakes Superior, Erie and Ontario. *Environ. Sci. Technol*. 30: 178187.

NRCan (Natural Resources Canada). 2005. Mineral and metal commodity reviews, cadmium. http://www.nrcan.gc.ca/mms/cmy/content/2005/15.pdf

OECD. 1992. Report of the OECD workshop on the extrapolation of laboratory aquatic toxicity data to the real environment. OECD Environment Monographs 59. OECD, Paris, France.

Posthuma, L, Suter, G.W. II & Traas, T.P. (eds). 2002. Species Sensitivity Distributions in Ecotoxicology. Lewis Publishers. Boca Raton. 587 *pp*.

Santore, R.C., Di Toro, D.M., Paquin, P.R,, Allen, H.E. & Meyer, J.S. 2001. Biotic ligand model of the acute toxicity of metals. 2 Application to acute copper toxicity in freshwater fish and *Daphnia*. *Environ Toxicol Chem* 20: 2397–2402.

Twiss, M.R., Gouvêa, S.P., Bourbonniere, R.A., McKay, R.M.L. & Wilhelm, S.W. 2005. Field investigations of trace metal effects on Lake Erie phytoplankton productivity. *J. Great Lakes Res* 31: 2168–179.

UKTAG. 2012. Development and use of the manganese bioavailability assessment tool *(Draft)*. Water Framework Directive - United Kingdom Technical Advisory Group (WFD-UKTAG), Edinburgh, UK.

USEPA (United States Environmental Protection Agency). 2001. Update of ambient water quality criteria for cadmium. Washington, D.C., Office of Water.

USEPA. 2007: Aquatic Life Ambient Freshwater Quality Criteria - Copper 2007 Revision, Office of Water, Washington, DC, EPA-822-R-07-001.

Wheeler, J.R., Grist, E.P.M., Leung, K.M.Y., Morrit, D. & Crane, M. 2002a. Species sensitivity distributions: data and model choice. *Marine Pollut. Bull.* 45: 192-202.

Wheeler, J.R., Grist, E.P.M., Leung, K.M.Y., Morrit, D., Sorokin, N., Rodgers, H., Toy, R., Holt. M., Whitehouse, P. & Crane, M. 2002b. Freshwater to saltwater toxicity extrapolation using species sensitivity distributions. Environ. Toxicol. Chem. 21: 2459-2467.

Development of an integrated mine waste management plan for the metates gold-silver project, Durango and Sinaloa States, Mexico

William A. Cincilla
Chesapeake Gold Corp, Centennial, Colorado, USA

Allan Breitenbach, & Joel Carrasco
Ausenco, Greenwood Village, Colorado, USA

ABSTRACT: Chesapeake Gold Corp. is currently advancing it's 100% owned Metates gold-silver project to the full feasibility stage. Over the anticipated 25-yr project life, approximately 1.2 billion tonnes of waste rock (almost 75% of which is classified as acid-generating (AG) or potentially acid-generating (PAG)) and 700 million tonnes of flotation tailings will be produced and managed together in an integrated waste management storage facility (ISF). Tailings will be delivered to the ISF at a nominal daily rate of 103,000 tonnes. The waste management plan in its current form evolved since it's early design stages from conventional slurry disposal in a hydraulic impoundment along with separate mine waste rock disposal, through various alternatives, where a wide range of geotechnical , geochemical , operational and closure variables were systematically evaluated. The plan was developed with technical support from a multi-disciplinary team of experts, and incorporates thickening and filtration of the flotation tailings slurry to produce a low-moisture-content waste stream that is amenable to direct co-disposal with AG and PAG waste rock placed within a stable shell constructed of non-AG waste. The result was a management system that greatly reduces or eliminates the potential for acid generation, reduces overall project water consumption by as much as 60%, and provides the basis for a sustainable long-term reclamation and closure plan when compared to more conventional approaches. This paper presents details of the design constraints, performance criteria and test work, methods and operational strategies that formed the foundation of the current plan

1 INTRODUCTION

1.1 *Project Location and Description*

The Metates Project is located in northwest Mexico in the northwestern part of Durango State, some 160 km northwest of the city of Durango and 175 km north of the coastal resort city of Mazatlan**.** Topography in the area is mountainous with elevations in the general region ranging from 620 meters in the west near the village of San Juan de Camarones to 2,300 meters along the ridge line to the southeast. Elevations in the immediate Metates Project area range from 650 to 1,180 meters in the general area of the concentrator site.

The climate is highly variable (from subtropical to temperate) because of the property's location and elevation extremes. The dry season is generally from October through May, and the wet season from June through September. Approximately two-thirds of the average of 1,420 mm of annual rainfall at the Metates site occurs during the monsoonal wet season. During May and June, temperatures can reach 40°C at the lower elevations, and during December and January, sub-zero temperatures and snow can be expected at higher elevations.

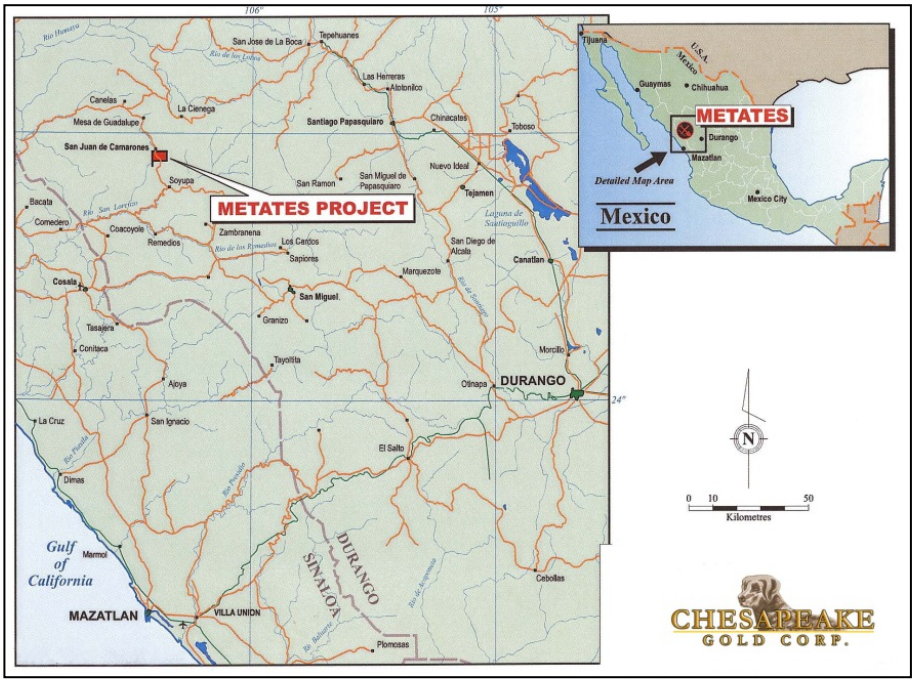


Figure 1. Metates Site Location Map

1.2 *Mineral Reserve and Mine Schedule*

The Metates mineral reserve amounts to 1.15 billion ore tons at 0.50 g/t gold, 14.2 g/t silver, and 0.165% zinc. Contained metal amounts to 18.5 million ounces of gold, 526.1 million ounces of silver and 4.2 billion pounds of zinc. The final pit design is based on a floating cone run at $1200 per ounce gold and $24 per ounce silver. Five mining phases have been established to mine the pit from the initial starter pit to the final pit limits. Total mine material is 1.15 billion tons for an overall waste to ore ratio of 1.01 to 1, with low grade considered as ore.

The annual waste rock delivery schedule was developed with tonnages segregated by rock type. Sulfur assays were carried out for all ore and waste samples that were used in assembly of the ore reserve estimates. This allowed for waste rock scheduling to be integrated with the overall waste management plan (discussed in greater detail in Section 2).

The Metates mine will operate for a total o f 19 years at a nominal daily ore production rate of 120,000 tonnes. A low-grade ore stockpile will be mined, beginning near the end of Year19, with the processing operations continuing until Year 25. Flotation tailings from the processing of the low-grade stockpile will be used to partially backfill the lower portions of the open pit, which will eventually become a pit lake that will remain a stable hydraulic sink in perpetuity. (M3, 2013).

1.3 *Process Operations*

Roughly 50% of the gold and silver in Metates ore is locked up in pyrite and other sulfides, As a result, the sulfides must be concentrated and oxidized before cyanide leaching. Grinding and concentration of the ore is done near the mine site at Metates.

From the run of the mine, the ore is crushed and ground to 80% finer than 212 microns through two primary crushers (60in x 89in gyratory), two semi-autogenous grinding (SAG) mills (40ft x 24ft) and four ball mills (24 ft x 37.5 ft). Flotation is done with a single rougher stage to produce a concentrate that contains about 92% of the gold, 88% of the silver, 89.3% of the zinc, and 91% of the copper. The project mass pull into the concentrate is 15%. The concentrate is thickened and then pumped downhill from a single pump station (about a 750 m drop in elevation) some 127 km to Ranchito for acid pressure oxidation and cyanidation.

Acid pressure oxidation will be performed in five autoclaves (AC), each with a 5.6 m inner shell diameter and 44.5 m tangent-to-tangent length. Operating parameters are 220°C, 60 minutes, and an O_2 overpressure of 700 kPa. The AC discharge will be cooled by flashing, and then pumped to four stages of counter current decantation (CCD) wash to rinse the slurry of as much free acid and dissolved iron as possible. The rinsed slurry will then undergo lime boil for 2 hours before leaching by cyanidation. Gold and silver in solution are then recovered by filtration and Merrill-Crowe zinc precipitation. The gold and silver precipitate is then smelted and cast into doré bars. Gold and silver recovery during POX and cyanidation is projected to be 98% and 87%, respectively. About 1 % of the metals are expected to be lost during filtration and zinc cementation. The overall process flowsheet is shown on Figure 1-2.

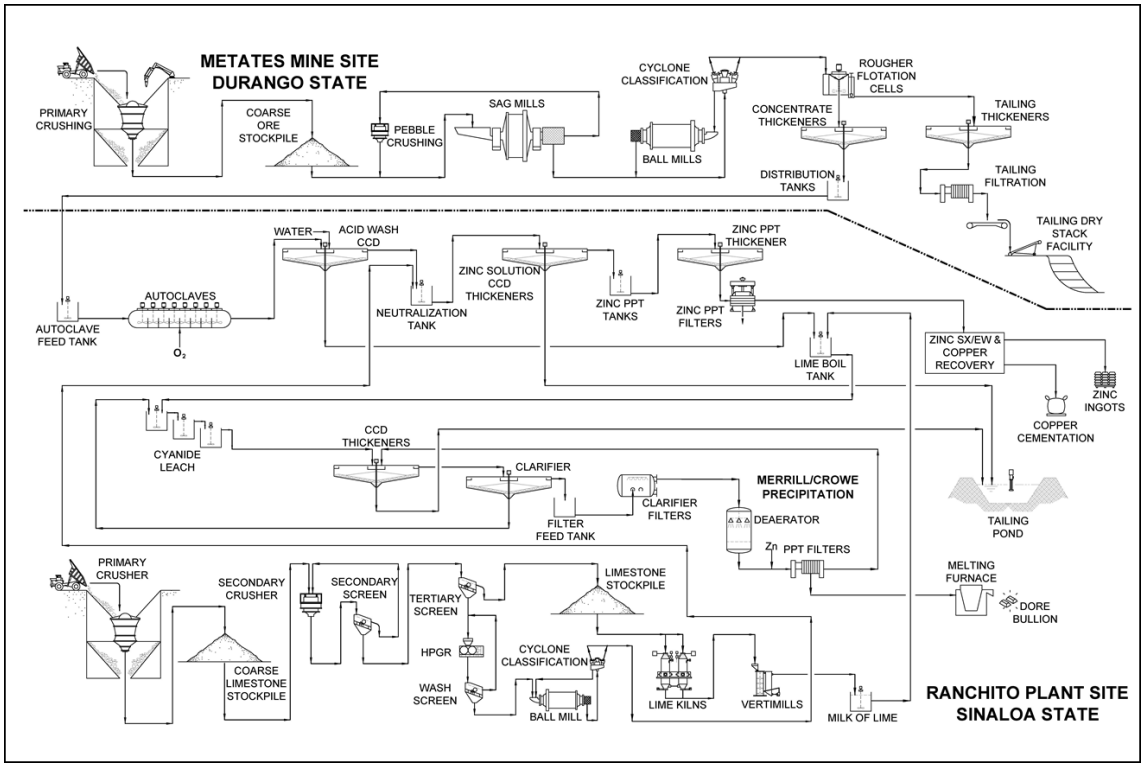


Figure 2. Generalized Processing Flowsheet of the Metates Project

2 THE EVOLUTION OF WASTE MANAGEMENT PRACTICE AT METATES

2.1 *Background*

Over the course of the past four years, the Metates project has undergone significant changes, not only in terms of the selection and optimization of metallurgical processes, but for critical work elements such as water supply and sourcing, waste management and closure and reclamation. As the process flowsheet was optimized, two major factors emerged as the major drivers for development of waste management alternatives: water; and the limitations imposed by the rugged topography in the areas adjacent to the Metates mine and mill site. More than 15 alternatives were analyzed over the course of 48 months, and gradually a preferred alternative emerged that incorporated nearly all of the major objectives of the program:

1) Maximizing the utilization of mine waste rock
2) Maximizing the conservation of water resources
3) Limiting the impact areas of the overall waste management program; and
4) Integrating Design-for-Closure Concepts into the overall scheme

The issue of water conservation was elevated to prime status based on several contributing factors, among them, the cost, availability and acquisition of the required water resources. The

Metates flotation plant will operate at a nominal daily ore throughput of 120,000 tonnes and requires large amounts of fresh water. In addition, a large volume of water was required for transport of sulfide concentrate via a 127-km pipeline from the Metates mine and mill site, to the Ranchito metal processing operations plant. This offsite transfer of water from the system was a contributing factor that re-emphasized the need for water conservation at Metates and was a major force in efforts to reduce consumptive water use in both the processing and waste handling operations.

The earliest alternatives that were incorporated in to the Preliminary Economic Assessment (PEA) (M3, 2010) involved separate management systems for waste rock and flotation tailings. Waste rock was placed in dumps adjacent to the Metates open pit, while flotation tailings were cyclone, with the coarse sand fraction being employed as upstream embankment fill for a hydraulic impoundment. As characterization test work on waste rock and flotation tailings became available, there was a gradual shift in design philosophy that favored the co-disposal of waste rock (much of it classified as PAG or AG) and the relatively sulfide-free coarse flotation tailings.

In the final analysis, the decision was made to move completely away from any tailings management alternatives that did not incorporate complete dewatering. A full range of alternatives for tailings dewatering were analyzed and costed, and pressure filtration was selected as the best alternative.(Paterson & Cooke, 2013a) Pressure filtration applications in fine process tailings has been limited and plagued with typically higher operating and capital costs compared to other methods. In the case of the Metates process, the tailings are relatively coarse (target P80 is 65 microns) and as a result excellent filtration results were obtained during the supporting testing program and alternatives evaluations. The resulting design included F.L. Smidth "Colossal" filters capable of processing the nominal 102,000 tonnes per day of flotation tailings. The resultant material is anticipated to have a terminal moisture content of approximately 16% and as a result conventional large-scale stackers and conveyors were integrated into the placement schemes.

2.2 *Waste Characterization*

There are two main waste streams from mining and mineral processing operations at the Metates site:

- Acid-generating or potentially acid generating (AG or PAG waste) and Non-acid-generating (NAG) waste rock; and,
- Bulk flotation tailing having functionally minimal or no acid-generating potential.

A comprehensive characterization program was carried out for waste rock and tailings at Metates.(InterraLogic, 2013a) This program included geochemistry, humidity cell testing and follow-on analyses such as acid-base accounting and acid generation potential classifications for all major material types. Table 1 illustrates the relative quantities and classification of the different waste types that have been integrated into the management strategy. The following is a summary of the general findings of the characterization test work carried out to date:

2.1.1 *Waste Rock*

- Pyrite (sulfide sulfur) was present in all samples except some of the rhyolites
- Significant siderite was present in samples, indicating that neutralization potential (NP) values based on Sobek methods may underestimate the NP and that oxidizing methods (e.g., net acid generation (NAG) testing using hydrogen peroxide) are likely more representative of actual NP
- Andesite is considered not potentially acid generation (non-PAG) with significant NP (as dolomite) and low to moderate sulfur content
- Basal conglomerate and rhyolite samples are also considered non-PAG, with both low NP and low sulfur content
- Lutite-arenite, intrusives, and conglomerate samples were generally considered PAG
- Metals leaching was highly variable across lithology types; however was fairly well (inversely) correlated with effluent/rinseate pH

2.2.2 *Whole Tailings*

- At a presumed mixture of 60% CH-A and 40% CH-I, humidity cell test (HCT) results indicated circumneutral pH during the entire test period of 58 weeks with low sulfate, zero to low acidity, and zero to low alkalinity
- Paste pH is slightly acidic at 5.3 and NAG pH is acidic at 3.75
- Net neutralization potential (NNP) was -2.6 and the NP:AP ratio (NPR) was 0.5 which would be considered PAG by definition, but the material is low in total sulfur which would more realistically categorize this material as "Uncertain" or Inert
- Kinetic NAG (KNAG) tests conclude that based on specific analysis methods, lag time could be as little as two months for CH-A before the material becomes acidic but at least a year for the blended CH-A/CH-I
- Rinse tests (SPLP) do not show any significant metals leaching
- Stage 2 tailings feed and underflow samples showed circumneutral paste pH
- Feed tailings and underflow tailings samples were in the PAG category according to ABA work, with NNP of -5.1 and -7.8 respectively and NPR of both samples of 0.4.
- Both samples were very low in sulfur having 0.32 (feed) and 0.54 (underflow) total sulfur. The majority of this sulfur is sulfide.
- Testing sulfur speciation of successive feed, overflow and underflow of the flotation tailings showed that total and sulfide sulfur generally increased slightly with successive processing.
- Multi-element analyses by aqua regia show this material is elevated in 9 metals over crustal abundances (at least three times crustal abundance) including sulfur.
- HCT results indicate both the feed and underflow tailings show elevated to circumneutral pH, measurable alkalinity and no acid generation during the testing. No significant amount of metals was released from the HCTs.

Table 1. Summary of Ore and Waste Generation

Mined and Processed Materials	Tonnage (kt)	ercent of Total Mined	Percent of CDF Material
Ore (Low and High Grade)	1,148,861	50%	
Waste Rock	1,157,954	50%	54%
Total Waste and Ore Mined	2,306,815	100%	
Flotation Tailings	976,532		46%
Total Tails + Waste Rock	2,134,486		100%

Waste Rock Types		Tonnage (kt)	Percent of Total Waste
PAG	Intrusive Waste	38,030	3%
	Sedimentary Waste	776,894	67%
	Total PAG Waste	814,924	70%
Non-PAG	Basal Conglomerate Waste	4,546	0%
	Andesite Waste	138,010	12%
	Rhyolite Waste	62,978	5%
	Rhyolite Talus Waste	137,478	12%
	Total Non-PAG Waste	343,012	30%
Total Waste Rock		**1,157,954**	100%

2.3 *Geotechnical Site and Material Characterization*

Ausenco (Ausenco, 2012) conducted a geotechnical site investigation of selected areas at the Metates site between June 2011 and February 2012. This initial investigation included 12 seismic refraction profile lines totaling 10,055 m, excavation of 32 test pits, 14 geotechnical boreholes, field hydraulic testing, and soil sampling. Auger drilling was performed on the overburden materials while wire line coring was used throughout the rock portions of the boreholes. The locations of the boreholes and test pits fall into three general areas on the Metates site, including the water storage reservoir and dam, the ISF site and the plant site. Other testing included field permeability in critical foundation areas of the ISF. The site investigations were focused on the foundation areas for the ISF and included detailed geologic mapping. These areas are predominantly underlain by shale and sandstone formations that were found suitable for supporting the downstream and upstream containment portions of the ISF facility.

The plant site is underlain by variable strength tuff and rhyolite rock, which is encountered at or near the surface. Some excavation and replacement with compacted granular structural fill is recommended for uniform load support for the critical structure locations. Groundwater was not encountered to the maximum depth investigated (40 m).

Geotechnical testing was also carried out on samples of flotation tailings. The results were applied to a range of preliminary stability analyses for both static and pseudo-static conditions and integrated into the design of the ISF outer slopes, placement strategies and surface and groundwater management systems.

2.4 *Co-disposal of Waste Rock and Tailings*

Since the PEA, a wide range of potential waste management strategies have been evaluated, from conventional hydraulic impoundment of bulk and cyclone tailing in slurry form, to the current plan, which incorporates tailing thickening and filtration to produce a low-moisture-content material that is amenable to co-disposal along with the waste rock. This integrated approach to waste management was demonstrated to have significant long-term cost and environmental advantages over more conventional approaches, and allows for a reduction of approximately 60% in water consumption at the Metates operations. In combination, the net effect on the project is notable from the perspectives of decreased risk and improvements in overall environmental sustainability. The waste management plan for Metates meets or exceeds current best practice standards in the mining industry on an international basis.

Over the life of the mine, approximately 1.2 billion tons of waste rock (about 74% of which is classified as AG) and 700 million tons of dry tailing will be produced and managed in the Metates integrated waste management storage facility (ISF). Dry tailing will be placed at a nominal daily rate of 103,000 tons. During operating years 1-19, when the open pit mine is active, the dry, filtered tailing will be placed in the ISF. From years 20 – 25, previously stockpiled low-grade ore will be re-mined and processed, and the largest portion of the flotation tailing produced will be used to backfill the depleted open pit up to an approximate elevation of 860m. The dry-stack tailing will be placed predominantly within the central portion of the ISF. The outer perimeter of the ISF is constructed of bulk-fill waste rock that will serve as a large earth buttress and will be sequentially covered with low-permeability rock and soil to reduce infiltration in the outer slopes and allow for concurrent reclamation. The inert dry tailing will be placed in thick layers using a combination of large-capacity transport conveyors and mobile stackers to cover placed ARD waste rock in relatively rapid succession. Approximately 1% of the dry tailing will be placed using a small dedicated truck fleet that will service the needs of waste rock placement outside of the central bulk-fill zone as interim cover to greatly reduce or eliminate the potential for acid generation from exposed AG waste rock. Figure 2-1 illustrates the general configuration of the Metates ISF as it will appear in active operation during production year 3 as well as the mine and processing facilities and ancillaries.

Ausenco (Ausenco, 2012) describes the details of the design and costing of the integrated tailing and waste rock storage facility (ISF) for the Metates site. The facility will be constructed downhill and west of the open pit to contain the 2,134 Mt of waste rock and tailings generated at the Metates site. The controlled placement of waste rock around a perimeter buttress provides both uphill and downhill stable containment of the dry stack tailing in the interior of the ISF. .

Figure 3 is a generalized cross section through the ISF, illustrating the relative elevations and thicknesses of the waste rock and tailings fill zones.

Non-Acid Rock Drainage (ARD) generating waste rock will be placed in the valley bottoms, partially up the valley side slopes, and on the faces of the exterior slopes of the ISF. The bulk flotation tailing generated at the Metates site are dewatered in the Metates Filter Plant and delivered to a staging and transfer area via twin 100-m-long belt conveyors that discharge into chutes that feed either the main stacking system belt or the alternative truck load-out belt that is used as required for interim cover material for portions of the ARD waste rock disposal operations.

The dry stack tailing will be placed in the ISF together with mine waste rock excavated from the mine pit during mine year 1 through year 19, during which time approximately 714 million tons of dry stack tailing will be generated. The inert tailing will be placed primarily within the inner portions of the ISF via bulk dumping from the conveyor/stacker system to rapidly cover ARD waste rock. The ISF base case concept includes end dumping interior deep lifts of relatively dry ARD waste rock from benches in a downhill direction at angle of repose. The density of this consolidated waste rock and dry stack tailing material is estimated to be approximately 1.8 t/m^3.(Paterson & Cooke, 2013b)

A portion of the dry tailing (about 1% on a daily basis) is also used as interim cover for portions of ARD waste rock placed outside of this bulk placement zone in the pile, to minimize the potential generation of ARD on a daily operational basis. Tailings used for interim cover accounts for approximately 1% of the daily output from the tailing dewatering plant and is delivered to the ISF via trucks from the truck load-out conveyor and spread with dozers in 1 or 2 m thick layers as waste rock is being placed. The majority of the dry stack tailings from the low grade ore processing will be used to partially fill the mine pit to a suitable elevation with the remainder placed on designated areas of the final top surface of the ISF.

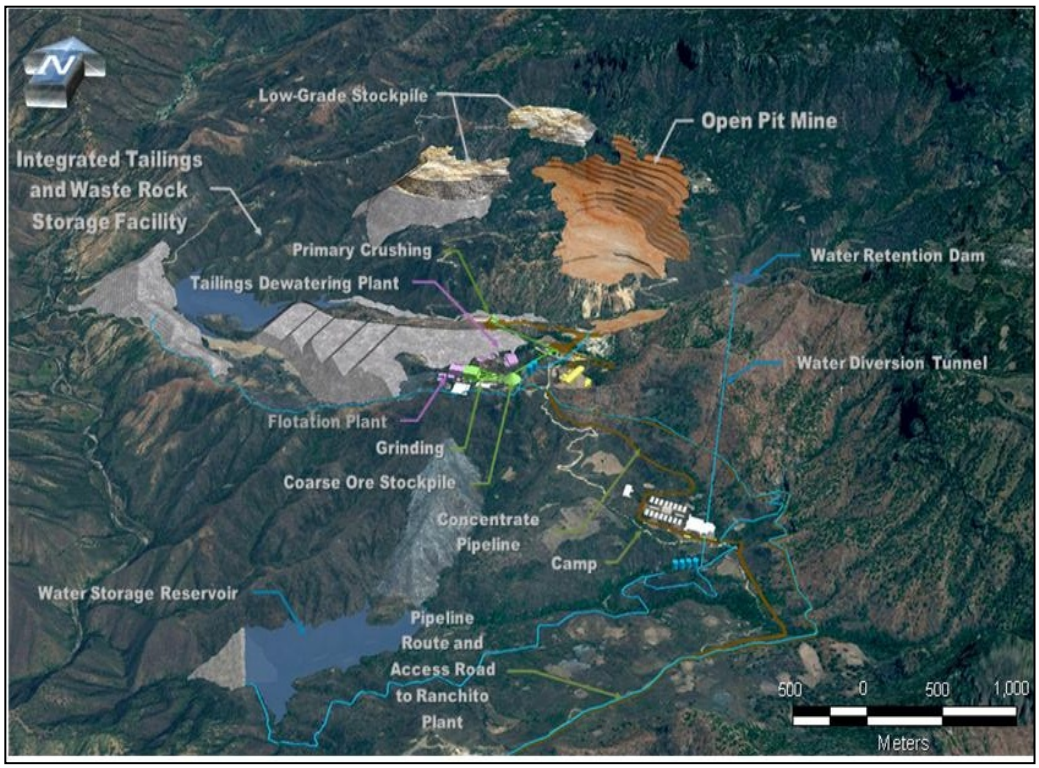


Figure 3. Metates ISF Development and Site Facilities – Production Year 3

3 RECLAMATION AND CLOSURE

Alternatives were developed and evaluated to manage waste rock and tailings during operation and closure at the Metates site(InterraLogic, 2013b). These included variations on the configurations, locations of the facilities, operational handling and segregation of wastes, pit backfill, and cover designs

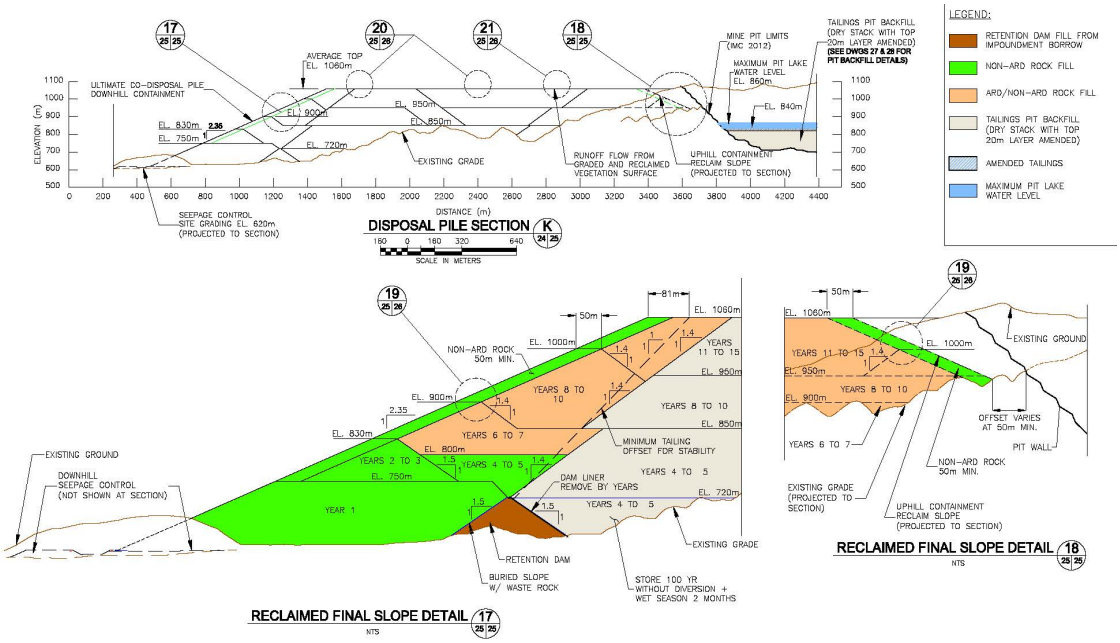


Figure 4. Generalized Section through the ISF at closure

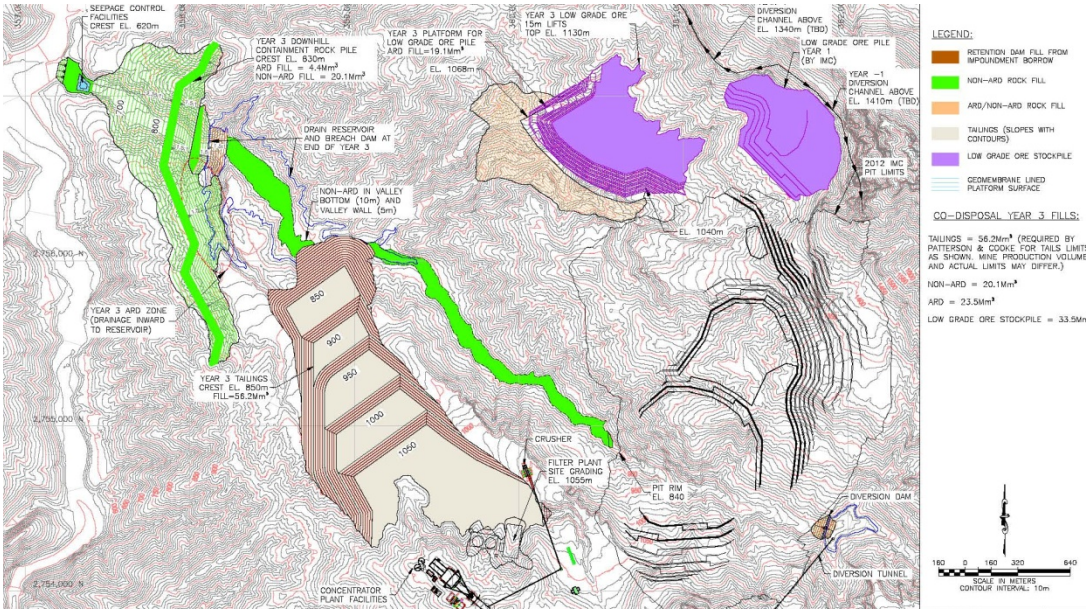


Figure 5. Metates IFS Plan – Operational Year 3

The Design-for Closure philosophy that formed the basis for the Metates ISF design involved the integration of operational management strategies for wastes that brought together the mine plan and water management plans in a manner consistent with minimizing exposure and weath-

ering of both waste rock and the tailings. By actively managing the placement of wastes during operations, water and oxygen ingress to acid generating wastes is limited, and the potential for release of impacted water is minimized. Several operational practices were identified including:

- Selective handling and encapsulation of PAG waste rock within inert waste rock "cells"
- Daily to weekly covering of reactive waste rock with low-sulfur, fine-grained, moist tailings
- Concurrent reclamation of the outer slopes to the extent practicable

The placement plan includes a rapid rate of rise such that any given placed waste rock or tailings material would be subsequently covered by the next lift of tailings within maximum of two weeks, and within less time than that under normal operations.

Concurrent reclamation is incorporated in these operational practices and includes actively implementing a broad strategy of reclamation during operation as opportunity allows. Concurrent reclamation will specifically target the outer slope of the ISF that includes the following components:

- 56m of encapsulation/cover material comprising 50m (width) of non-PAG waste rock, 5m (width) of shale/clay, and minimum 1m (thick) of low-sulfur tailings
- An overall 2.35:1 benched outer slope to manage clean runoff
- Outer benches constructed with non-PAG waste rock, graded into the hillside
- Revegetated outer slope using hydroseeding with lime/mulch/seed mixture

Final closure of the facility will include finalizing the concurrent reclamation of the outer slopes per the closure described above and construction of a final cover on the top surface of the facility with the following components:

- A cover system consisting of minimum 1m of low-sulfur tailings overlain by a minimum of 1m blended non-ARD rock and tailings
- Cap of 0.15m hydroseeded growth media amended with 5 percent bentonite
- Revegetated surface to enhance evapotranspiration and shed runoff
- Engineered channels to direct runoff away from the open pit
- Channel construction includes the same components of the standard cover plus an additional 5 percent (total of 10 percent) bentonite in the upper layer, plus rip rap for channel armoring.

Figure 6 is a rendering of the final, reclaimed configuration for the Metates site.

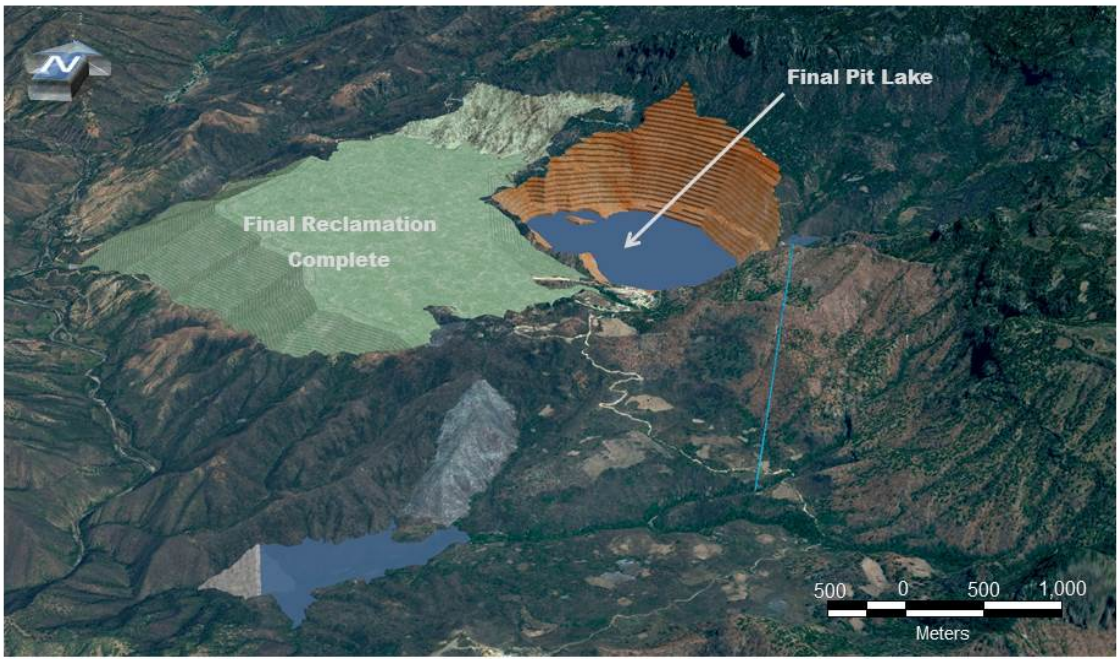


Figure 6. Post-Closure Conditions – Metates Site

At closure, the facility will be covered with an inert waste rock cover (including low-permeability shale on the slopes) plus low-sulfide tailings, robust soil, and growth media layers, and graded to collect and discharge non-contact surface water downstream. Any seepage water will be collected in the seepage control facilities and pumped back to the processing plant during operations, and collected for treatment and discharge post closure, as necessary. A pit lake will form in the post-mining open pit. The pit lake closure and management includes several key components to minimize impacts to the environment:

- Partially backfill the pit with low-sulfide tailing from the low-grade ore stockpile processing to an elevation below the long-term hydraulic sink elevation of the pit.
- Rapid fill of the pit by directing all runoff water from the upgradient catchment of the San Nicolas drainage into the pit.
- After rapid filling, upstream runoff will be directed away from the pit through the diversion tunnel, as necessary, to maintain a stable pit lake elevation above the backfill, but below the hydraulic sink elevation, ensuring a long term, shallow lake in the pit that can monitored and managed.
- The pit lake is expected to be a long-term passive hydraulic sink under average conditions based on the existing climate and hydrogeologic datasets.
- Lime will be added to the upper 20m of the tailing backfill to maintain an elevated pH in the lake and lake bottom sediments.

4 CONCLUSIONS

Metates is among the largest undeveloped gold an silver deposits in the world, with recoverable reserves of more than 18 million ounces of gold and over 500 million ounces of silver. Developing a waste management strategy for over 2 billion tonnes of waste rock (much of it acid-generating or potentially acid-generating) and flotation tailings was major challenge for Chesapeake Gold and its international team of consultants and advisors. Over the past 5 years, the Chesapeake team has advanced an integrated waste management program that applies large-scale tailings dewatering and waste rock co-disposal strategies that significantly reduce both short and long-term environmental risks, while controlling operational costs. Strong emphasis on water conservation resulted in a reduction of consumptive water use by over 60% when compared to more conventional management approaches.

The project is now advancing into full-scale feasibility and a number of key optimizations in waste management are being investigated including bulk mixing and concurrent dry stacking of tailings and waste rock, continued validation of ARD test work, and further improvement in the capital and operating cost profiles. Emphasis on water conservation and utilization is continuing as well as integration of the latest advances in dewatering technology in concert with some of the premier equipment manufacturers in the world.

5 REFERENCES

Ausenco, 2012, *Co-Disposal Base Case, Mine Pit Dewatering and Water Supply*, Greenwood Village, Colorado

InterraLogic, Inc, 2013a, *Baseline Geochemistry Report, Metates Project, Mexico*, Project No. 100023, Golden, Colorado

InterraLogic, Inc, 2013b, *Preliminary Feasibility Study Level – Reclamation Plan, Metates Project, Mexico, Project No. 100023,* Golden , Colorado

M3 Engineering and Technology Corporation, 2010, *Metates Gold-Silver Project, NI 43-101 Technical Report, Preliminary Economic Assessment*, Tucson, Arizona

M3 Engineering and Technology Corporation, 2013, *Metates Gold-Silver Project, NI 43-101 Technical Report, Preliminary Feasibility Study*, Tucson, Arizona

Paterson and Cooke, 2013a, *Metates pre-Feasibility Study, Metates Tailings Dewatering, Report No. CGM-5254 R07 RevA*, Golden, Colorado.

Paterson and Cooke, 2013b, *Metates pre-Feasibility Study Metates Tailings Dry Stacking Report No. CGM-5254 R01 Rev0,* Golden, Colorado.

Development of a mine site-wide water balance

M. Davis
MWH Americas, Inc., Fort Collins, Colorado, United States

Z. Zurakowski & T. Alexieva
MWH Americas, Inc., Denver, Colorado, United States

ABSTRACT: Water management is a key challenge for the mining industry. Proper mine site water management increases efficient usage of existing water supply, ensures sufficient storage availability, assists in managing discharge water quality, minimizes costs, and reduces risks. A site-wide water balance is an important decision making tool to assist mine managers to achieve these water management objectives. Water balance models can be simple or highly complex depending on site needs. Model requirements differ depending on the stage of operation and the types of facilities present. This paper presents an overview of the steps required for developing a mine site water balance focusing on tracking water quantity, and to a lesser extent, water quality. Case studies are included to illustrate uses and benefits of a mine site water balance.

1 INTRODUCTION AND OVERVIEW

1.1 *General*

Freshwater comprises 2.5 percent of the earth's water resources (UN-Water, 2006). Of that 2.5 percent, only a fraction is accessible for use. Freshwater is used primarily for irrigation for agriculture (approximately 70%). The remainder is used for industry (20%) and domestic use (10%) (WWAP, 2009). Competition for water exists at all levels and is forecast to increase as water demand grows globally (WWAP, 2012). Limited water resources for industry and increasing global population, as well as more focus on sustainability, highlight the importance of mine sites developing an effective water management strategy that includes minimizing water usage and the impact to the water supply of the surrounding communities.

Development of an accurate water balance model requires thorough understanding of all water related components at a mine site and their operation, and facilitates the preparation of an efficient water management plan by evaluating a range of operational scenarios, understanding the impacts of changes in the climate, changes in the properties of the water balance components, and opportunities of water recycling and reuse. Understanding the impact of water chemistry on the recovery process is also important and should be incorporated in the model.

1.2 *Regulatory drivers*

Regulatory drivers for mine site water management include various national, state and local laws that provide requirements for water discharge quantity and quality. Requirements vary depending on mine site location and corresponding government agency; however they all evolve towards stricter water use and discharge requirements in line with sustainability principles. In addition, many mine sites follow international best management practices such as those provided by the International Finance Corporation (IFC), International Council on Mining &

Metals (ICMM), International Cyanide Management Code for Gold Mining, and Global Reporting Initiative (GRI). These practices include adopting measures to reduce water usage and minimize impacts of water consumption on others, as well as developing effective water accounting procedures. GRI provides specific guidelines for sustainability performance indicator reporting including metrics for water usage, discharge, and impacts.

1.3 *Scope of paper*

This paper describes the main steps in developing a water balance model, which include: (1) outlining the water balance objectives, (2) selecting the water balance methodology, (3) defining the conceptual model, (4) collecting and evaluating model input data, and (5) developing and calibrating the model. It is important to note that this order for developing a water balance model is provided as a general guide and returning to previous steps may be necessary as part of the process. Case studies are discussed at the end of the paper.

2 OUTLINING WATER BALANCE OBJECTIVES

Defining the main objectives of a water balance is the key starting point to model development. Objectives can be driven by multiple factors ranging from regulatory compliance to internal reporting. It is important to note that objectives evolve over the mine lifecycle as water-risks/operational priorities change and incorporating flexibility in the model may be beneficial. For example, a simple spreadsheet model may suffice for the pre-feasibility stage of a design, but a more complex model with capability to evaluate various probabilistic scenarios may be necessary for final design. Using a simple version of a more complex model may allow for an easier transition to the model used for final design. The following lists provide some potential water management objectives that could be addressed by a mine water balance from development through mine reclamation and closure.

New mines

- Estimate quantity of water required for the operations
- Identify opportunities to reduce costs for water supply
- Evaluate opportunities for water reuse and recycling
- Define the quality of the output streams and evaluate the environmental impact
- Evaluate the impact of the project on water use for surrounding communities
- Estimate the energy required to extract, move and treat water

Operating mines

- Provide information for reporting requirements
- Evaluate the risks for insufficient water for the operations
- Evaluate the risks for excess water leading to stopping production due to a lack of storage capacity
- Evaluate the risk of discharge of contaminated water
- Evaluate the risk of tailing dam overtopping
- Identify and compare measures for risk reduction
- Identify opportunities to reduce operational costs
- Estimate water quantity required for an expansion
- Assess change in the water management due to an operational change

Mine closure

- Evaluate potential climate change impacts
- Estimate changes in water quality and quantity following closure
- Assess whether water treatment will be required
- Evaluate alternatives to reduce costs, liability and risks

3 SELECTING THE WATER BALANCE METHODOLOGY

3.1 *General*

Well defined objectives are important as they will be used to select the water balance model methodology. Some of the questions that need to be answered when deciding on the water balance methodology include the following:

- What is the phase of mine life being modeled and will this model predict future phases?
- Is a chemical mass balance required?
- Should the model be steady-state or dynamic? (Steady-state is for a single solution unchanging in time and dynamic is for a solution that will change in time)
- If the model will be dynamic, what time step should be used (daily, monthly, annual)?
- What is the quality of the input data available for the model development?
- Should the model be deterministic (repeatable solutions) or stochastic (random solutions)?
- Should the model allow for addressing changes to the operational practice, climate variations, impact of storm events, etc.?
- Will the model be used during the operations and who will use it?
- What software should be used?

The more questions are addressed prior to model development, the more efficient the modeling process will be.

3.2 *Water balance model software*

A number of software options are available to build a water balance model. The following subsections present a few of the common types of software used and discuss their capabilities.

3.2.1 *Microsoft Excel®*

Microsoft Excel is a readily available program that can create deterministic mass balance models for both steady state and dynamic solutions. Add-on programs, such as Crystal Ball and @Risk, are available which incorporate Monte Carlo simulations that can analyze risks and represent uncertainty. Microsoft Excel is compatible with Supervisory Control and Data Acquisition (SCADA) systems and data from a SCADA system can be exported directly into Microsoft Excel (a Windows-based SCADA server is required). Microsoft Excel has strong data formatting and display options. Macros can be created to automate tasks within the model.

Microsoft Excel has many benefits for building a simplified water balance. Microsoft Excel can also be used to develop large water balance models; however, as models become larger and more cumbersome, other programs may be more suitable. It can also be difficult to track what cells affect other cells when the system becomes large. Microsoft Excel also requires that unit conversions must be entered manually, which can easily lead to errors.

3.2.2 *Real time management software*

Real time management software, also called SCADA systems, is useful for real-time data processing and management during operations and are used for specific processes such as a concentrator at a process plant. Examples of SCADA system software include SysCAD, MetSim, and PI System. These systems provide historic data processing (mass and energy balances) and can be used for steady-state and dynamic simulations. Alarms can be created for mitigating risk. Disadvantages of using real time management software packages are that they are not very adaptable for site-wide water balance and generally do not have stochastic capabilities.

3.2.3 *Dynamic software*

Dynamic programs have the capabilities for developing dynamic and Monte Carlo simulations. Some software used to build water balance models in this framework include GoldSim, Stella, and MATLAB Simulink. These are highly graphical and object-oriented programs. This software can efficiently organize and manage complex systems. The programs are hierarchical and scalable, allowing for easily adding and managing complexity. The software is extensible and can be linked to other software including database software such as Microsoft Excel and Microsoft Access®. Dynamic software is less likely to be used for simple models that can easily be presented in a spreadsheet. Dynamic software disadvantages may include the cost of the program and that it does not link directly to SCADA systems.

3.3 *Chemical mass balance software*

If a chemical mass balance will be incorporated in the water balance, it is important to select software that will effectively model the situation. The Compendium of Tools for Watershed Assessment and TMDL Development (EPA, 1997) and Water Quality Models (WERF, 2001) are useful references for developing chemical mass balance models. Some software used for chemical mass balance models is listed below:

Steady-state & dynamic software

- PHREEQ-C – A program developed by the United States Geological Survey for speciation, batch-reaction, one-dimensional transport, and inverse geochemical calculations.
- Hydrological Simulation Program FORTRAN (HSPF) – This program simulates watershed hydrology/water quality for point/non-point loading.
- Generalized Watershed Loading Functions (GWLF) model. This model can be used to evaluate impact of land uses on watersheds. Model does not allow for toxin/metal loading.

Hydrodynamic software

- Water Quality Analysis Simulation Program (WASP) – This program can be used to evaluate fate and transport of pollutants in surface water bodies.
- Environmental Fluid Dynamics Computer Code (EFDC) – This is a hydrodynamic model that can be used to simulate aquatic systems in one, two, or three dimensions.
- CE-QUAL-W2 – This software is a two dimensional model that is useful for stratified water bodies like reservoirs.

Effluent mixing software

- Cornell Mixing Zone Expert System (CORMIX) – This software can be used for environmental impact assessment of regulatory mixing zones resulting from continuous point discharges.

3.4 *Sensitivity analyses*

Sensitivity analysis is a simple procedure to study the impact of a range of values an independent variable may have on the results of the water balance. It simulates the uncertainty of how independent input variables impact dependent output values.

Some examples of parameters for which sensitivity analyses are commonly performed include: (a) climate variables (extreme dry or wet climate conditions); (b) production rates; (c) underground mine dewatering rates; (d) hydrologic coefficients (i.e. runoff coefficients; wet beach, dry beach, and pond surface evaporation rates); (e) water quality concentrations (extreme high or low values). There are numerous other parameters that can be considered for sensitivity analyses and are dependent on the site being evaluated. Tornado charts can be used to present a comparison of the sensitivity of various variables to the water balance model in one chart.

3.5 *Deterministic versus probabilistic model simulations*

In most real-world systems many controlling parameters and processes are uncertain or stochastic. If input variables have uncertainty then the results will also have uncertainty. It is important to represent the uncertainty for decision making. Stochastic simulation is the process of representing the uncertainty of processes or events by describing model inputs as probability distributions. This is typically referred to as a Monte Carlo simulation. Each data set generated represents a potential realization of conditions impacting the water balance model and is used to generate model outputs. The results are presented as a distribution showing the probability in percentile (i.e. 5^{th} to 95^{th}) of occurrence.

4 COLLECTING AND EVALUATING THE INPUT DATA

A key part to model development is compiling pertinent water balance data and evaluating the suitability of the input data for the model. Overall information for the site, such as location of facilities, design criteria of key structures, and regulatory requirements, are important to include in data collection. Historical reports (i.e. hydrologic, hydrogeologic, geotechnical, design, operation manuals, etc.) can be useful references. In addition, aerial photographs and topographic maps provide information on historical operations at the site, location of facilities, runoff areas, and existing diversion channels. Additional examples of data types that may be collected for a site-wide mine water balance are provided in the following subsections.

4.1 *Climate and hydrologic data*

Site-specific climate data (i.e. precipitation, snow data, and evaporation) should be collected, if available. If site-specific data are unavailable or unreliable, data from regional stations in the vicinity of the site can be used if correlated properly to the site. Information to consider with climate data includes uncertainty, trends or cycles in the data, El Niño and La Niña phenomenon, and climate change.

Hydrologic data includes evaporation factors and runoff coefficients (i.e. for catchment areas, ponds, wet beach areas, and dry beach areas). This information is used for calculating water inputs from direct precipitation and runoff, in addition to evaporation losses.

4.2 *Water supply*

Water supply rates, storage components, restrictions, and permitting requirements can be collected for a water balance. Proposed changes to the water supply over time should also be included in the model. This may include changes in rates or type of water supply (i.e. wells versus water from a desalination plant). Data on the baseline chemical constituents of the water supply may be required if necessary to evaluate the impact on the loading to the mill.

4.3 *Mines and associated facilities*

Information needs to be collected on the mines at the site (i.e. open pit and underground mines), as well as associated facilities such as waste rock storage facilities and ore stockpiles. Some of the data that should be collected include:

- Mine plans (historical and future production schedules)
- Water requirements for drilling and dust control
- Runoff catchment areas and information on diversion channels
- Dewatering rates (historical and projected) and uses for water collected
- Groundwater inflow to underground mine (includes results of hydrogeologic models)
- Water quality and geochemistry data for mines, waste rock facilities, and ore stockpiles
- Plan for closure for the mines and stockpiles

4.4 *Process plant*

Process flow diagrams for the process plant and associated facilities can provide detailed information for each flow stream. Other data that can be collected for the process plant include:

- Historic and projected plant throughput rates
- Freshwater requirements for processing
- Other water requirements (i.e. potable water, dust control, etc.)
- Operating logic for key storage components and dimensions of storage facilities
- Ore moisture content
- Details on concentrators or cyclones, if present
- Concentrate production information
- Percent solids of tailing

4.5 *Tailing storage facility*

Data that can be collected for a tailing storage facility includes:

- Tailing properties (settled density, consolidation information)
- Percent solids of the tailing slurry from plant and from thickeners (if any)
- Seepage collection information
- Catchment area and diversion information
- Wet beach and dry beach estimates
- Storage capacity curve
- Freeboard requirements
- Reclaim pond information (i.e., minimum pond volume, normal operating volume, pumping rates, etc.)

4.6 *Heap leach facility*

Useful data to collect for heap leach facilities for the water balance includes:

- Average leach time and variations in leach time
- Leaching areas, loading schedules, and lift heights over time
- Solution application rates
- Initial, operational and residual moisture contents of ore
- Irrigation rates (historical and projected) and methods
- Rinsing schedule and application rates
- Water used for crushing and agglomeration
- Flow rates from leach pad

Evaluating the input data includes proving initial review to determine if there is data missing, additional data or explanation is necessary, or the correct data has been provided. If the data appears correct, the first question to ask is whether or not the data makes sense. If data gaps exist, data will need to be estimated using other data, calculations, or engineering judgement. Data can be calibrated against related data to determine if there are issues. Data evaluation is an on-going part of model development, as often development of the model can indicate an issue with data.

Some data issues, beyond missing information, include inconsistency, limited quantity, and poor quality. Data evaluation can also be an opportunity to identify areas where instrumentation is not working properly.

5 DEFINING THE CONCEPTUAL MODEL

Prior to developing the water balance model and following preliminary review of collected data, a conceptual model should be defined. The conceptual model is a flow diagram of the main

components for the model and should capture all key flows in the model. It is beneficial to have all parties involved review the conceptual model to minimize revisions during model development. Some components that can be included in a mine water balance are:

- Water supply
- Water storage facilities
- Drainage features (i.e. diversion channels, catchment areas, seeps, pump back systems, etc.)
- Underground mine
- Open pit mine
- Mill and process plant
- Process ponds
- Ore stockpiles
- Waste rock storage facilities
- Tailing storage facility (TSF)
- Heap leach facility
- Water treatment plant and other water treatment facilities

Figure 1 shows an example of a mine site-wide water balance and includes components that could be listed in a water balance for a new or existing mine.

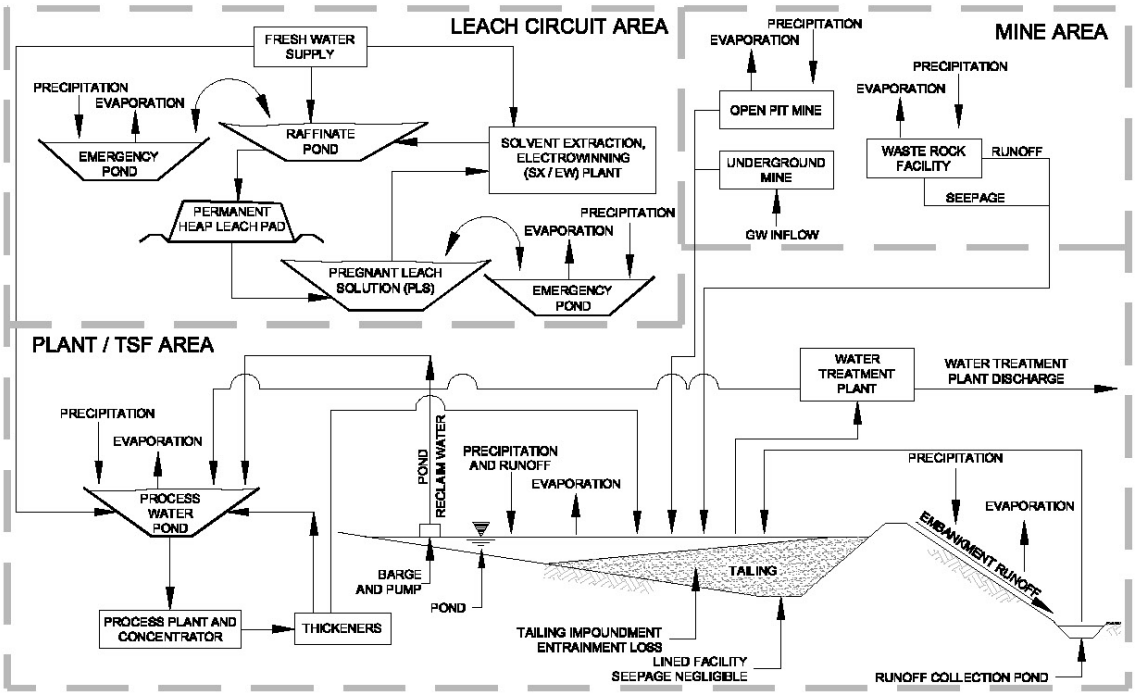


Figure 1. General Mine Site-Wide Water Balance Conceptual Model

6 DEVELOPING AND CALIBRATING THE MODEL

6.1 *Model development*

Models are usually constructed in a "top-down" manner to capture all the key aspects and inter-relationships between the mine components. At the top level are the main mine area components. The intermediate levels include the components and links between the main mine areas. The lower level of the model consists of all input data, assumptions, and calculations

within the individual components. The top level and some intermediate level information is illustrated in the conceptual model which should be used as the start of model development.

Once the model framework is built, incorporating the climate variables is a reasonable next step. Climate variables may consist of precipitation, evaporation, storm events, and snowmelt. Daily, weekly, or monthly precipitation and evaporation data can be used in the model. If sensitivity analyses will evaluate drier and wetter conditions, values used to represent these conditions can also be entered in the model. If the climate data will be evaluated stochastically, then a probability distribution will need to be fit to the climate data. This requires good quality and quantity of historical data. Permitting often requires the design and management of certain storm events (e.g. 24-hour, 100-year storm, Probable Maximum Precipitation, etc.) for different types of facilities. The storm events of concern can be incorporated in the model. In cold climates, modeling snowmelt is necessary, as well as consideration of surfaces which will freeze. A separate snowpack model may be developed.

The water balance of each main mine area should be added next. This will consist of calculating the water demands and losses at each major facility. If any variables will be modeled stochastically, a probably distribution will need to be fit to the data. As noted above, this requires good quality and quantity of data. If only a range of data is available and the distribution of the data cannot be well defined, a sensitivity analyses would be a better option to evaluate the variable.

An example of one mine component to model for the conceptual model in Figure 1 is the TSF. The TSF at a mine site is usually the biggest "consumer" of water, due to the losses to water trapped in the impounded tailing voids, evaporation and seepage. In dry climates the losses exceed inflows, causing a water deficit, and in wet climates runoff may exceed losses, causing a water surplus. Water inflows to the TSF include: (a) direct precipitation on the pond; (b) runoff from the catchment area, wet beach area, dry beach area, and collected from the embankment; (c) water in the tailing; (d) water from underground dewatering; and (e) open pit dewatering. Water outflows include reclaimed water to the process pond and decant water to the water treatment plant. Water losses consist of water entrained in the voids of the tailing, in addition to evaporation from the pond, wet beach, and dry beach areas. The change in water storage in the pond is equal to water inputs minus water outflows and water losses. The calculations for each variable would be defined in the model.

The remaining mine components are then defined and calculations for the links between model components are completed at the same time. All assumptions, input data, and references should be listed in the model.

6.2 *Model calibration*

Model calibration is usually performed for operating mines, where actual data is available. Once the model is developed, the simulated results from the model are compared with actual results for a specific calibration time period. A time period when operations were consistent or measured data is the most reliable are types of time periods to use for calibration. It is useful to have the time period also include seasonal affects. The model can be calibrated by achieving agreement (within an acceptable tolerance) between simulated and measured results by modifying uncertain parameters such as runoff coefficients, evaporation factors, etc. A model should be recalibrated when new measured data is available or new information has been provided for historical data that would change the calibration.

6.3 *Model results*

Model results include flow rates, storage volumes, water levels, and chemical mass concentrations. Results can be presented in tables, graphs, or text, depending on the objectives of the model. For example, if the objective is to provide data for reporting requirements, tables and charts showing the breakdown of water usage over time could be presented. If the objective

is to estimate the water quality of discharge, the result could include a table comparing model results to regulatory requirements.

7 CASE STUDIES

Case studies discussed in the following subsections indicate some uses for a site-wide water balance. Case studies were selected for a new mine, an operating mine, and for a mine in closure. Details of the case studies are not provided due to client confidentiality.

7.1 *New mine*

A deterministic spreadsheet water balance was developed for feasibility design of a new mine in Central America. The site climate is dry sub-tropical with a moderate wet season. Water balance objectives were to provide an estimate of fresh water make-up requirements for mine operations and estimate expected size fluctuations of the reclaim water pond at the TSF. Maximizing water reuse was a significant concern due to high costs for obtaining a permit for water supply wells. To assist with this requirement, it was planned that the reclaim water pond on the TSF would serve as a leveling reservoir to help reduce the fluctuation in the make-up water requirements during the wet and dry seasons. A relatively small pond was assumed for the initial years of operation to contribute to creating a tailing beach and encourage consolidation of the tailing. The results of the water balance provided an estimate of the variation of freshwater make-up requirements and reclaim pond storage over the life of the mine. Sensitivity analyses were conducted to evaluate the impact of extreme precipitation conditions (dry and wet) and variations in groundwater inflow to the mine (to be delivered to the TSF). The precipitation conditions had the most impact on the results, with an average 25 percent increase or reduction of freshwater make-up requirements.

7.2 *Operating mine*

A deterministic water balance was developed using GoldSim for an operating mine in South America. The site is in a desert climate. The model was initially developed as a tool for the mine during operations for tracking water quantity and metrics, but was later used to evaluate various components during operations and alternatives associated with expansion. One model analysis included evaluation of the mine pit lake water quality and quantity at closure. A geochemical investigation was conducted to assist with forecasting the drainage chemistry from the pit lake as a function of time. Inputs to the pit lake included direct precipitation, runoff from the pit walls and groundwater inflow. Losses from the pit lake are evaporation. Geochemical mass to the pit lake came from groundwater inflow and leaching of the pit walls. Mixing and reactive processes were modeled to occur within the pit lake, as well as flushing at the interface of the pit lake and pit wall. The model PHREEQ-C was used for the geochemical modeling at each time step and the results were set up to automatically import into GoldSim for the water balance model. The results provided estimates of changes in water storage and water quality over time. Sensitivity analyses were conducted to evaluate impact of the (a) range of values for the scaling factor (laboratory to field); (b) pit filling rate; (c) groundwater inflow rate, and (d) precipitation. The results of the sensitivity analyses showed the scaling factor had the most impact on the chemical mass balance results.

7.3 *Mine closure*

A deterministic spread water balance model was developed for a mine in closure in the United States. The site climate is semi-arid and the majority of runoff is from spring snowmelt. The objective of the model was to estimate water storage requirements during reclamation. The mine site includes two open pits that will be backfilled with waste rock during reclamation. All

contaminated water is collected on-site and stored in both pits prior to delivery to a water treatment plant for treatment and discharge. A predictive water balance model was developed based on historical operating conditions and worst-case storage requirements. Model analyses included evaluating variations in water storage under historic operating conditions and estimating storage requirements using the proposed water treatment plant capacity and operating schedule for a new plant. Sensitivity analyses were conducted for alternate water treatment plant operating schedules and plant capacities. The results were used for design of a new water storage facility.

This model was initially intended only for the analyses listed above. However, as the project progressed evaluation of new water management decisions were added to the list of objectives. The spreadsheet model was already large, so the model is in transition to use the GoldSim for future modeling efforts.

8 CLOSING

This paper presented the general method for developing a mine site-wide water balance and discussed each of the steps involved. Defining the objectives of the water balance and the conceptual model early in the process is important, as are the types of data collected and typical components included. Potential software programs were discussed, as well as details on the development and calibration of the models. Case studies presented illustrate potential uses for water balance models.

Reducing water usage and impacts to the water supply (quantity and quality) are important water management objectives of mines. A mine water balance is a useful tool to help meet these objectives as well as assist with making critical decisions throughout the life of the mine. It is expected that water balance models will become requirement for mine water management because of the increased demand on the existing water supply and emphasis on sustainability, resulting in more stringent regulatory requirements.

9 REFERENCES

United States Environmental Protection Agency (EPA). 1997. The Compendium of Tools for Watershed Assessment and TMDL Development. EPA Report 505-2-90-001, Office of Water Enforcement and Permits, Office of Water Regulations and Standards, Washington, D.C., USA.

UN-Water. 2006. Coping with Water Scarcity: A Strategic Issue and Priority for System-wide Action. UN-Water Thematic Initiatives. Geneva, UN-Water.

Water Environmental Research Foundation (WERF). 2001. Water Quality Models: A Survey and Assessment Project 99-WSM-5, Water Environment Research Foundation, Alexandria, VA, USA.

World Water Assessment Programme (WWAP). 2009. United Nations World Water Development Report 3: Water in a Changing World. Paris/London, UNESCO Publishing/Earthscan.

World Water Assessment Programme (WWAP). 2012. United Nations World Water Development Report 4: Managing Water under Uncertainty and Risk. Paris/London, UNESCO Publishing/Earthscan.

Mine Waste Modelling

Modeling of seepage through segregating waste rock

M. D. Fredlund & R. C. Thode
SoilVision Systems Ltd., Saskatoon, SK, Canada

ABSTRACT: Stratified layering occurs as a result of the manner in which waste rock is deposited over the face of the pile. The layer thickness and the saturated-unsaturated modeling parameters determine the underlying flow regime. This paper presents a summary of several models that were developed to investigate the processes that affect the flow within the Goat Hill waste rock pile. Reasonable flow parameters were developed based on four different modeling scenarios. The relative influence of each soil parameter and applied moisture flux on the overall flow regime was studied.

1 INTRODUCTION

Considerable segregation can take place in materials that are end-dumped onto a waste-rock pile. The process of creating a slope by dumping waste rock materials from the crest of the slope creates a multi-layer structure within the waste rock dump. The random dumping process can result in layers of fine and coarse materials coming to rest at roughly the angle of repose. This is similar to the stratification found in soil layers laid down by wind or water.

The waste rock at the Goat Hill North rock pile consists of multiple layers of fine and coarse materials. This paper presents the results of several multi-layer numerical models which were created to study the flow of water through the waste rock material.

2 OBJECTIVE

The objective of this numerical study is to investigate the possibility of relative preferential flow of water through the coarse and fine materials. Specific objectives include the following:

- Determination of the soil parameters that produce preferential flow in coarse and fine layers.
- Determination of the relative flows through coarse and fine layers.
- Estimation of saturation and volumetric water contents in the fine and coarse layers.
- To describe the change in the flow regime between a homogenous system and a multi-layered system.
- Determine the reasonable layer thickness which may be used in the further numerical modeling.

In order to achieve the above objectives, a multi-layer seepage modeling was used with seepage models at different model scales.

3 SEEPAGE MODELING

Primary seepage modeling was performed to determine the effects of various seepage model parameters on the flow of water through a multi-layer system. Due to the scale of the actual slope and the complexity of the geometry, three levels of model geometries were implemented in this study: i) a small sub-domain model, ii) a large sub-domain model, and iii) a full scale model (Figure 1). The following four sets of seepage models were implemented in this study:

- Set *P1*: Includes twelve computer runs on small sub-domain models with different soil parameters and applied surface fluxes. The series of computer runs were performed to determine the effect of soil parameters and surface fluxes on flow in the gravel and sand layers.
- Set *P2*: Includes 5 computer runs on small sub-domain models with different layer thicknesses to study the effect of the layer thickness on flow through the multi-layer system.
- Set *P3*: A large sub-domain model was performed to compare the small sub-domain results to the sensitivity to the size of the simulation model.

3.1 *Study effects of soil parameters and surface flux (P1)*

A series of small-scale steady-state models were run to study the effect of net surface flux and soil parameters on the flow of water in the waste rock slope. Details of the model geometry, soil parameters, boundary conditions, and model results are described in the following sections.

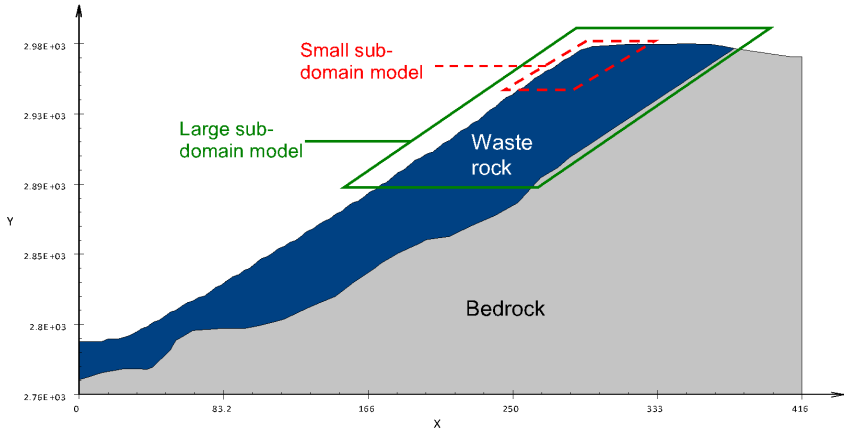


Figure 1. Schematic illustration of the full and 2 sub-domain models

3.1.1 *Model Geometry*

The small sub-domain model has 10 sandwich layers of sand and gravel (Figure 2). The thickness of each layer is 0.5 m. The surface layer of the model was assumed to be gravel. In order to avoid the concentration of water flow in the bottom layer (i.e., as described in the large-scaled transient model), a triangular soil region was added to the right side of the model. The triangular (i.e., blue) region can be either sand or gravel and the effect of soil type variation can be examined using this model.

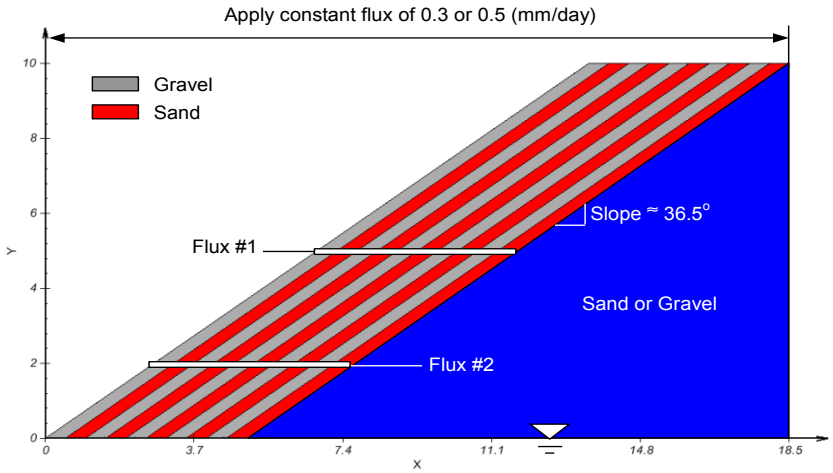


Figure 2. Geometry of the small sub-domain multi-layer model with layer thickness of 0.5 m.

3.1.2 *Soil Parameters*

There are three sets of soil parameters used in this modeling study:

i. Base case soil parameters.

ii. One standard deviation difference: In this case, an attempt was made to produce as much differential flow as possible. Soil parameters in the gravel and sand were changed such that gravel tended towards a coarser material and sand tended towards a finer material. The following four soil parameters were changed by one standard deviation for both sand and gravel: a) Saturated volumetric water content; b) Air-entry value; c) Saturated hydraulic conductivity; and d) Slope of the unsaturated hydraulic conductivity curve. The residual water content and residual soil suction were assumed to not significantly affect the flow of water in the soil.

iii. One standard deviation difference for the slope of unsaturated hydraulic conductivity: The slope of the unsaturated soil parameters was studied since this soil property has a significant effect on the flow of water in the soil. The slope of the unsaturated hydraulic conductivity for the gravel was chosen as the mean value plus one standard deviation, while the mean value minus one standard deviation was chosen for the sand.

Soil parameters for the sand and gravel for the three sets of model soil parameters are presented in Table 1. Plots of the soil-water characteristic curves, SWCCs, and the unsaturated hydraulic conductivity curves for the three sets of soil parameters are shown in Figure 3, Figure 4, and Figure 5, respectively.

Table 1. Summary of 3 sets of soil parameters for the gravel and sand

Soil parameters	Base case: mean soil parameters values for sand and gravel		One SD difference: Gravel towards coarse, sand towards fine		Only slope k_{unsat}: Gravel k_{unsat} slope+SD, Sand kK_{unsat} slope-SD	
	Sand	Gravel	Sand	Gravel	Sand	Gravel
θ_s	0.302	0.302	0.253	0.351	0.302	0.302
ψ_{ae}, AEV (kPa)	1.64	0.408	2.913	0.199	0.4087	1.64
θ_r	0.133	0.104	0.133	0.104	0.104	0.133
ψ_r (kPa)	31.33	2.2	31.33	2.2	2.2	31.33
k_{sat} (m/day)	1.469	7.1	0.369	143.84	7.1	1.469
Slope of k_{unsat}	2.83	2.83	1.863	3.797	2.83	2.83

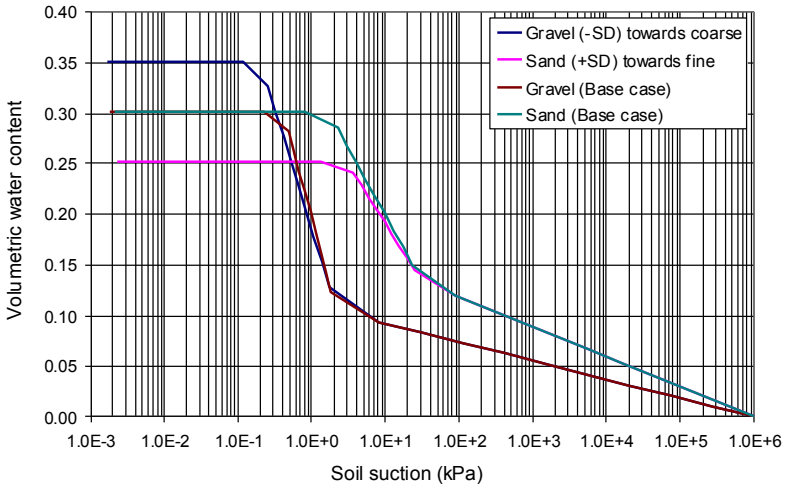


Figure 3. Soil-water characteristic curves for sand and gravel for modeling of the multi-layer system

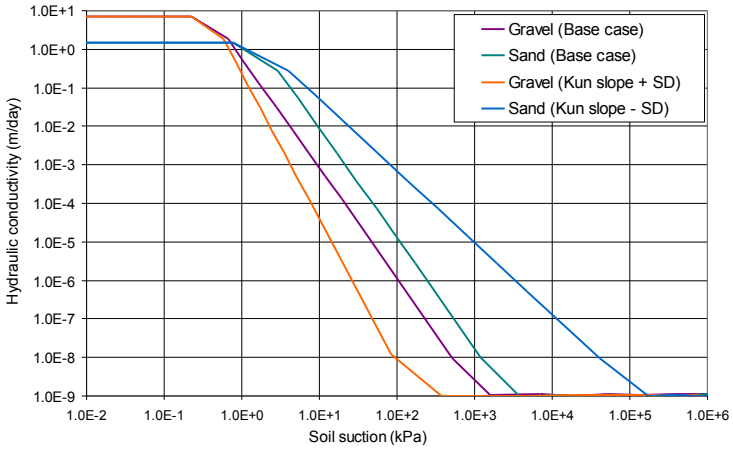


Figure 4. Unsaturated hydraulic conductivity functions for the sand and gravel for the base case and one standard deviation for all soil parameters

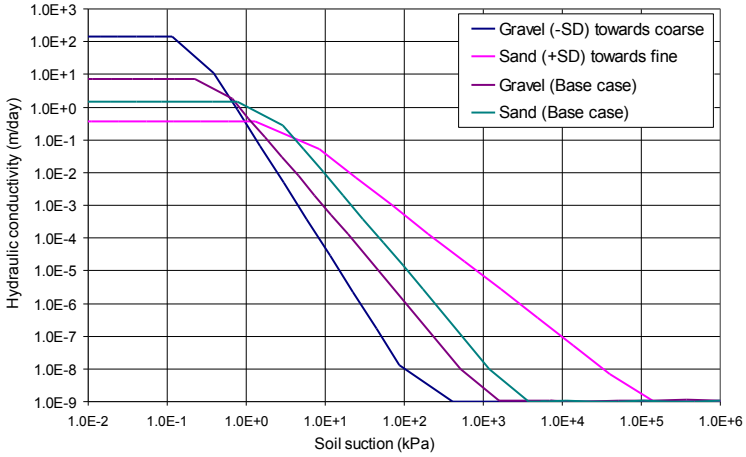


Figure 5. Unsaturated hydraulic conductivity functions for the sand and gravel for base case and one standard deviation for k_{unsat} slope.

There are three sets of soil parameters for gravel and sand; namely, two cases for soil parameters in the triangular region and two cases for surface flux (i.e., 0.3 mm and 0.5 mm), resulting in 12 computer runs for the small sub-domain multi-layer model.

3.1.3 *Initial boundary conditions*

A soil suction of 90 kPa was set for the entire soil model as the initial condition. A constant flux of either 0.3 mm or 0.5 mm of water was applied at the ground surface. The right edge of the model was set as a "no flow" boundary condition. The water table (i.e., pressure head = 0.0 m) was assumed to be at the bottom edge of the model.

3.1.4 *Results and discussion*

Two flux sections were added to the models to monitor the amount of water flowing through the sand and gravel layers (Figure 2). Flux sections #1 were used to measure the amount of water flowing through the sand and gravel layer at the middle of the model (i.e., elevation of 5.0 m). Flux section #2 was used to measure the amount of water flowing through the sand and gravel at an elevation of 2.5 m above the bottom of the model.

Plots of the pore-water pressures and degrees of saturation for various computer runs are shown in Figure 6 to Figure 15. In these computer runs, soil suctions in the model were in the range from 5 kPa to 90 kPa.

A summary of two flux sections for the twelve computer runs is presented in Table 2 and Table 3. The percentages of water flow through the five layers of sand and through the five layers of gravel at two flux sections were calculated for each run. The results showed that there is no preferential flow at the base case of soil parameters.

The comparison of the case of changing four soil parameters and the case of changing only the slope of the unsaturated hydraulic conductivity function showed that the slope of the unsaturated hydraulic conductivity function plays an important role in the distribution of the water flow in sand and gravel. When the slope of the unsaturated hydraulic conductivity curve in the gravel was decreased by one standard deviation and the slope of the unsaturated hydraulic conductivity curve of the sand was increased by one standard deviation, the amount of water flow in the sand was more than 94% of the total flow in the ten layers of gravel and sand.

The results also show that there is no significant difference in the preferential flow when the triangular section beneath the layers is comprised of either sand or gravel soil parameters.

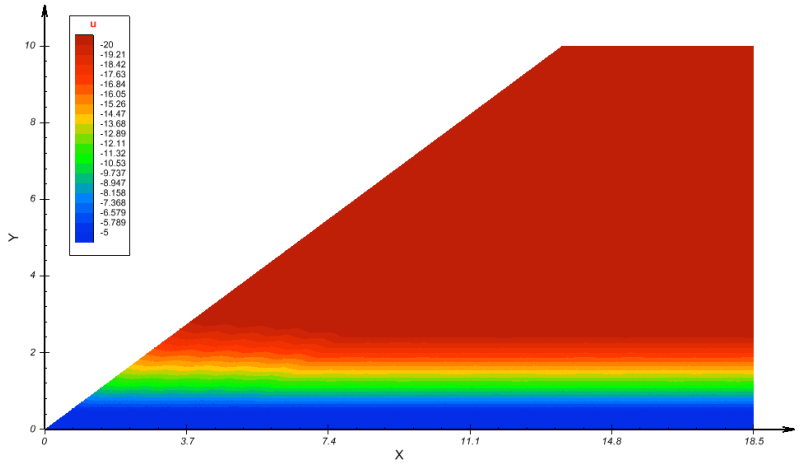


Figure 6. Pore-water pressure distribution in a small sub-domain multi-layer model for the base case of soil parameters, 0.3 mm surface flux and Sand parameters for the triangular soil region.

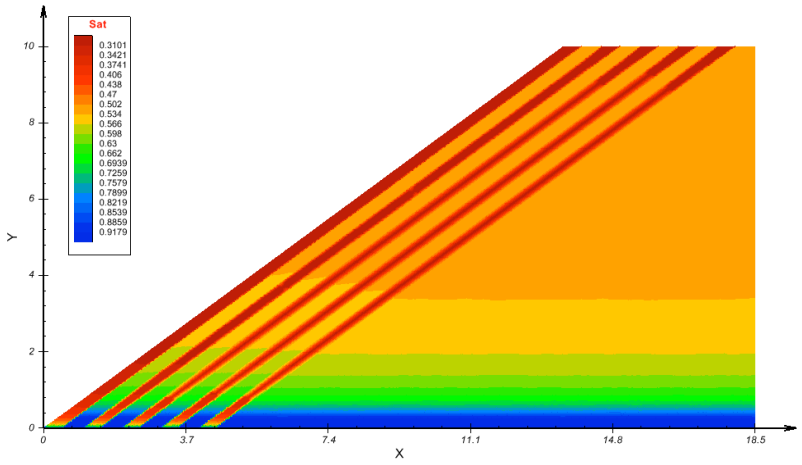


Figure 7. Degree of saturation distribution in a small sub-domain multi-layer model for the base case of soil parameters, 0.3 mm surface flux and Sand parameters for the triangular soil region.

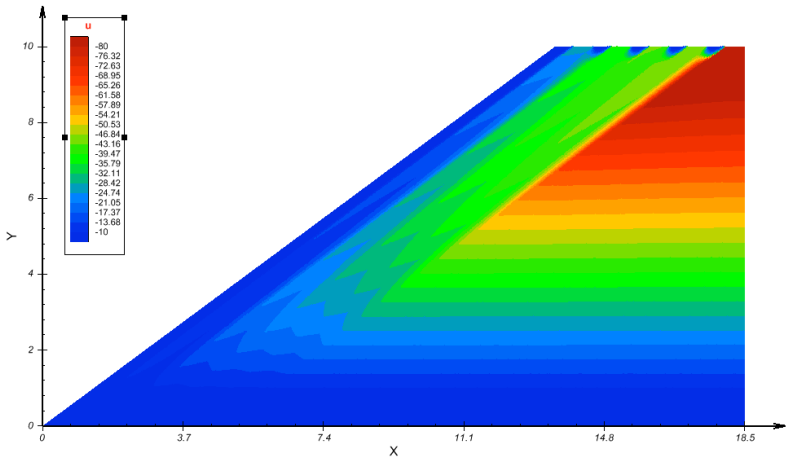


Figure 8. Pore-water pressure distribution in a small sub-domain multi-layer model for the case where the gravel tends towards a coarser material (one standard deviation) and the sand tends towards a finer material (one standard deviation), 0.3 mm surface flux and Sand parameters for the triangular soil region.

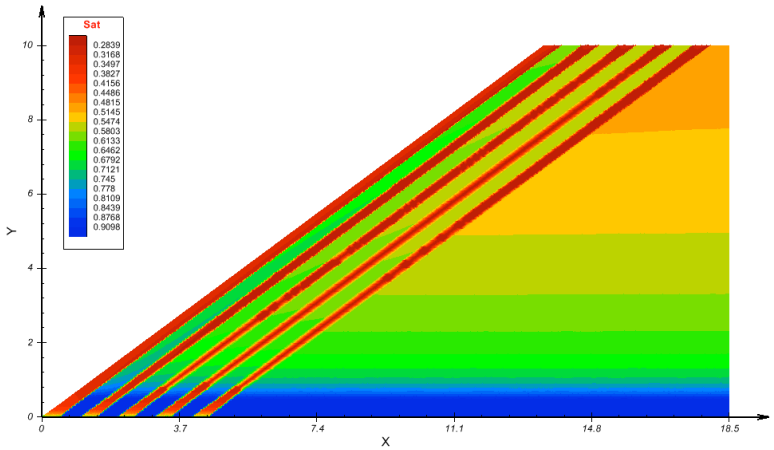


Figure 9. Degree of saturation distribution in a small sub-domain multi-layer model for the case where the gravel tends towards a coarser material (one standard deviation) and the sand tends towards a finer material (one standard deviation), 0.3 mm surface flux and Sand parameters for the triangular soil region.

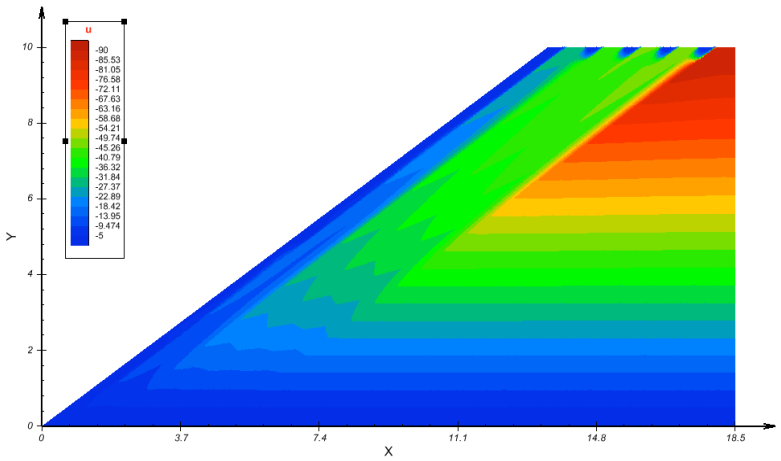


Figure 10. Pore-water pressure distribution in a small sub-domain multi-layer model for the case when using a slope of k_{unsat} of Gravel plus SD (one standard deviation) and a slope of k_{unsat} of Sand minus SD, 0.3 mm surface flux and Sand parameters for the triangular soil region.

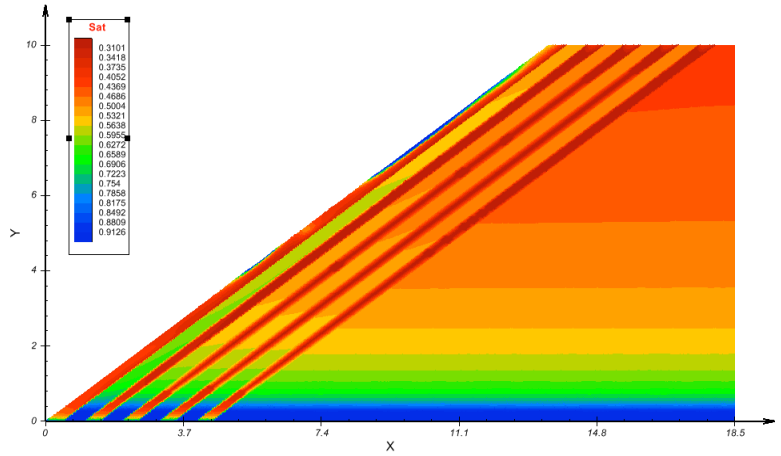


Figure 11. Degree of saturation distribution in a small sub-domain multi-layer model for the case when using the slope of k_{unsat} of Gravel plus SD (one standard deviation) and the slope of k_{unsat} of Sand minus SD, 0.3 mm surface flux and Sand parameters for the triangular soil region.

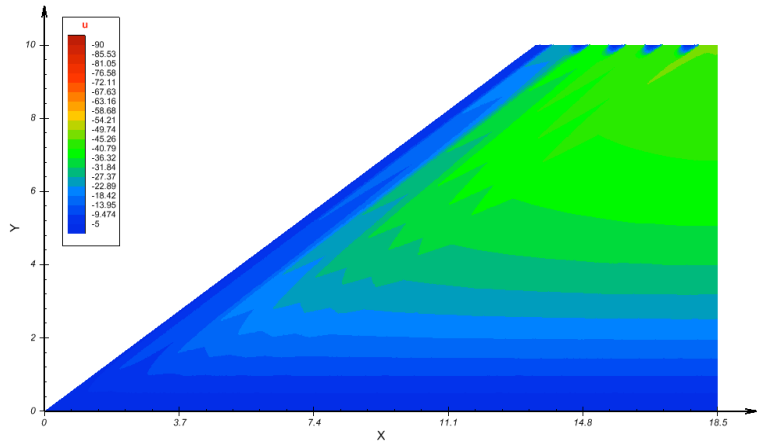


Figure 12. Pore-water distributions in a small sub-domain multi-layer model for the case when the gravel tends towards a coarser material (one standard deviation) and the sand tends towards a finer material (one standard deviation), 0.3 mm surface flux and Gravel parameters for the triangular soil region.

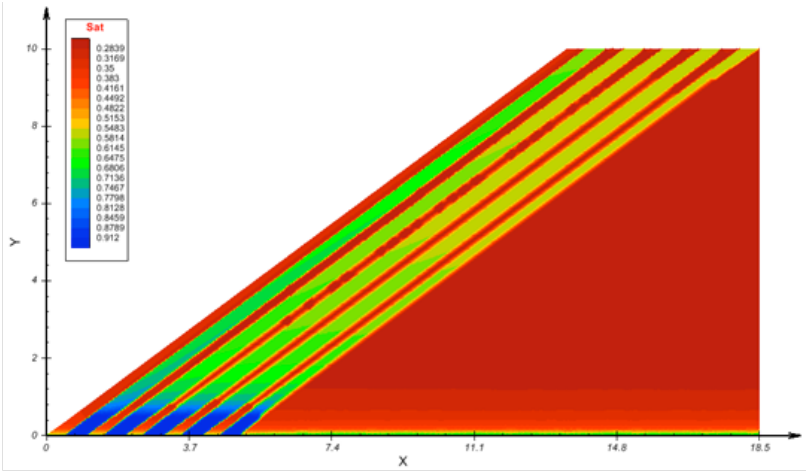


Figure 13. Degree of saturation distribution in a small sub-domain multi-layer model for the case where gravel tends towards a coarser material (one standard deviation) and the sand tends towards a finer material (one standard deviation), 0.3 mm surface flux and Gravel parameters for the triangular soil region.

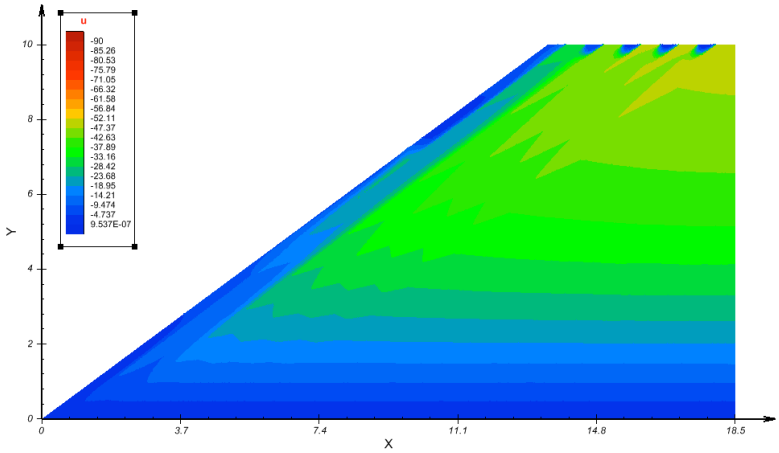


Figure 14. Pore-water pressure distribution in a small sub-domain multi-layer model for the case when using a slope of k_{unsat} of Gravel plus SD (one standard deviation) and a slope of k_{unsat} of Sand minus SD, 0.3 mm surface flux and Gravel parameters for the triangular soil region.

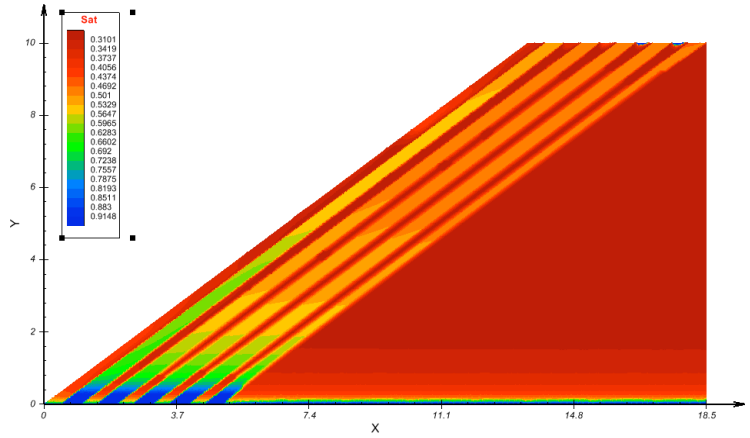


Figure 15. Degree of saturation distribution in a small sub-domain multi-layer model for the case when using a slope of k_{unsat} of Gravel plus SD (one standard deviation) and a slope of k_{unsat} of Sand minus SD, 0.3 mm surface flux and Gravel parameters for the triangular soil region.

Table 2. Modeling results for 6 computer runs with sand parameters in the triangular region

Flux	Soil	Percentage of flow in sand and gravel					
		Base case: mean soil parameters values for sand and gravel		One SD difference: Gravel towards coarse, sand towards fine		Only slope k_{unsat}: Gravel k_{unsat} slope+SD, Sand k_{unsat} slope-SD	
		0.3 mm	0.5 mm	0.3 mm	0.5 mm	0.3 mm	0.5 mm
#1	Gravel	47.94%	46.31%	4.57%	4.65%	6.53%	3.64%
	Sand	52.06%	53.69%	95.43%	95.35%	94.47%	96.36%
#2	Gravel	46.03%	45.04%	3.66%	3.76%	5.48%	6.00%
	Sand	53.97%	54.96%	96.34%	96.24%	94.52%	94.00%

Table 3. Modeling results for 6 computer runs with gravel parameters set for the triangular region

Flux	Soil	Percentage of Flow in sand and gravel					
		Base case: mean soil parameters values for sand and gravel		One SD difference: Gravel towards coarse, sand towards fine		Only slope K_{unsat}: Gravel k_{unsat} slope+SD, Sand k_{unsat} slope-SD	
		0.3 mm	0.5 mm	0.3 mm	0.5 mm	0.3 mm	0.5 mm
#1	Gravel	46.94%	44.32%	4.03%	4.18%	2.60%	4.36%
	Sand	53.06%	55.68%	95.97%	95.82%	97.40%	95.64%
#2	Gravel	44.58%	42.82%	3.37%	3.43%	1.48%	2.86%
	Sand	55.42%	57.18%	96.63%	96.57%	98.52%	97.14%

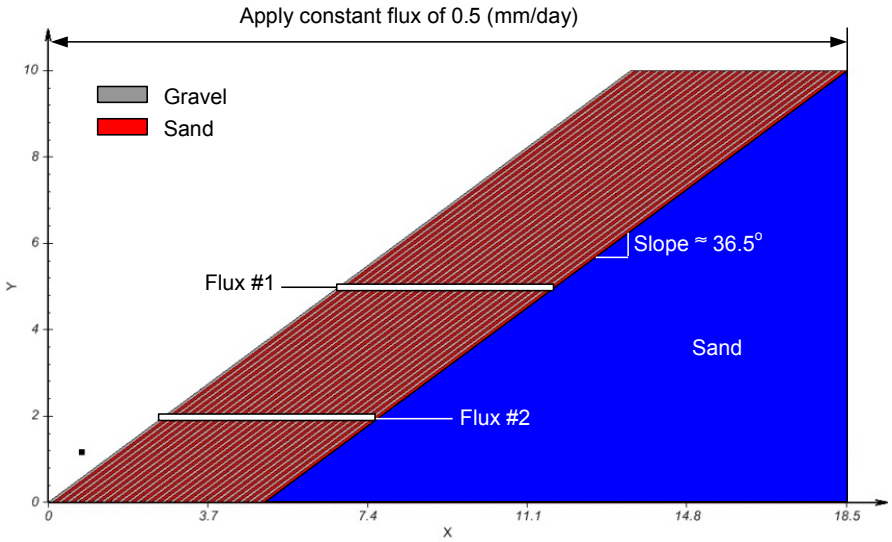


Figure 16. Geometry of the small sub-domain multi-layer model with a layer thickness of 0.1 m.

3.2 *Study effects of layer thickness (P2)*

The purpose of this section is to study the effect of the thickness of each soil layer on preferential flow in the gravel and sand layers. The model geometry, soil parameters, boundary condition, and simulation results are presented in the following sections.

3.2.1 *Geometry*

The geometry of the model is similar to that of the small sub-domain model. Five layer thicknesses were selected for this study: 0.1 m, 0.3 m, 0.5 m, 0.7 m and 1.0 m. The model geometry for the 0.5 m thicknesses is the same as presented in Figure 2. Model geometries for 0.1 m, 0.3 m, 0.7 m and 1.0 m thick layers are shown in Figure 16 to Figure 19.

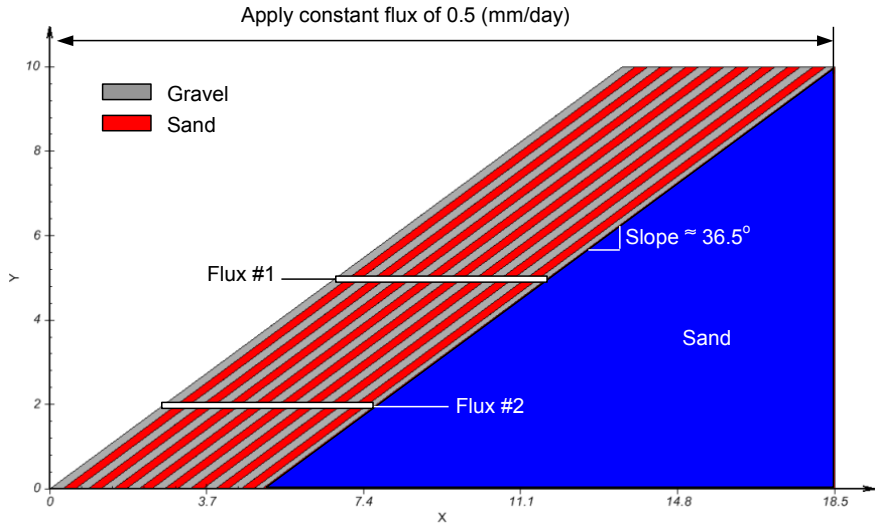


Figure 17. Geometry of the small sub-domain multi-layer model with a layer thickness of 0.3 m.

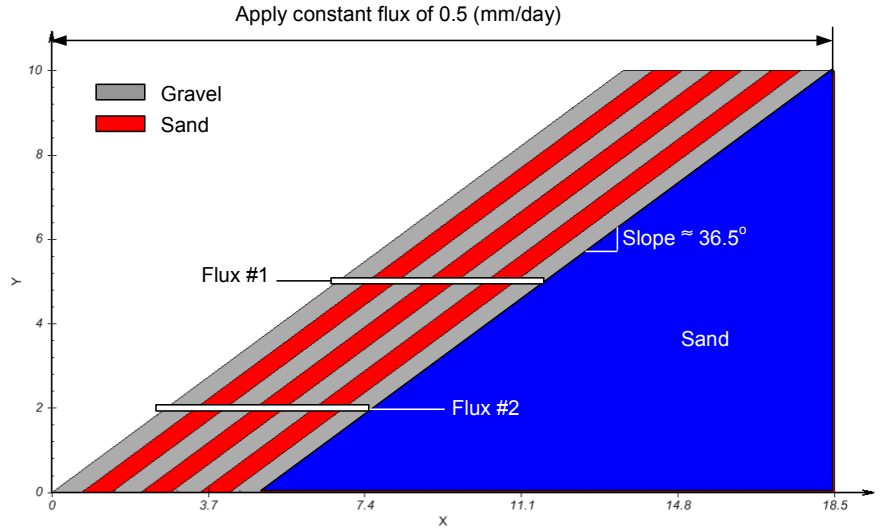


Figure 18. Geometry of the small sub-domain multi-layer model with a layer thickness of 0.7 m.

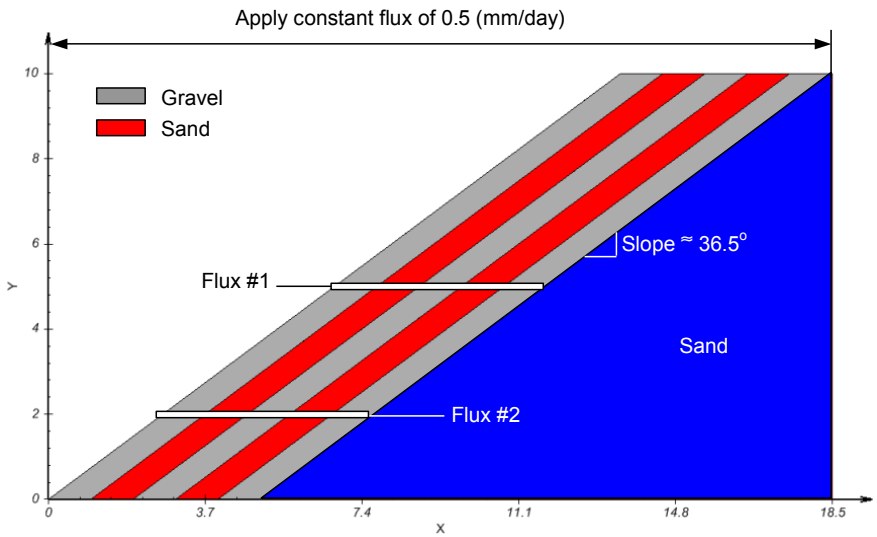


Figure 19. Geometry of the small sub-domain multi-layer model with a layer thickness of 1.0 m.

3.2.2 *Soil Parameters*

Soil parameters used in these model studies are the same as those used in the previous model study where the parameters of the gravel were one standard deviation towards a coarser material and the parameters of the sand were one standard deviation towards a finer material. Soil parameters for the gravel and sand are presented in Table 4.

Table 4. Soil parameters for the gravel and sand in the set of modeling *P2*

Soil parameters	One standard difference difference: Gravel towards coarse, sand towards fine	
	Sand	Gravel
θ_s	0.253	0.351
ψ_{aev}, AEV (kPa)	2.913	0.199
θ_r	0.133	0.104
ψ_r (kPa)	31.33	2.2
k_{sat} (m/day)	0.369	143.84
Slope of k_{unsat}	1.863	3.797

3.2.3 *Initial and boundary conditions*

Similar to the above model, a soil suction of 90 kPa was set for entire soil model as the initial condition. A constant flux of 0.5 mm of water was applied on the ground surface. The right edge of the model was set as a "no flow" boundary condition. The water table (i.e., pressure head = 0.0 m) was assumed to be at the bottom edge of the model.

3.2.4 *Results and discussion*

Similar to the previous set of seepage modeling (*P1*), two flux sections were added to the models to monitor the amount of water flowing through the sand and gravel layers (Figure 2). Flux section #1 was used to measure the amount of water flowing through the sand and gravel layers at the middle of the model (i.e., elevation of 5.0 m). Flux section #2 was used to measure the amount of water flowing in sand and gravel layers at an elevation of 2.5 m from the bottom of the model.

Simulation results are summarized in Table 5. The results show that there is a significant difference in the flow in the sand and gravel. The amount of water flowing in the gravel is significantly increased with the thicknesses of the soil layer, especially when the layer thickness is equal to 0.7 and 1.0 m. Preferential flow can be significantly affected by the layer thickness.

In the next set the multi-layer seepage models, a large sub-domain model was used with layer thicknesses of 2.0 m. The results are of value in verifying the above observation.

Table 5. Modeling results for the sub-domain model set *P2*

ID	Layer thickness (m)	Percentage of flow through sand and gravel			
		Flux #1		Flux #2	
		Gravel (%)	Sand (%)	Gravel (%)	Sand (%)
1	0.1	1.97	98.03	1.67	98.33
2	0.3	3.29	96.71	2.70	97.30
3	0.5	4.65	95.35	3.76	96.24
4	0.7	11.64	88.36	5.49	94.51
5	1	15.23	84.77	5.86	94.14

3.3 *Large Sub-domain Model (P3)*

The effect of the size of the model on the preferential flow in the gravel and sand is studied in this set of models. Model geometry, soil parameters, boundary condition, and simulation results are presented in the following sections.

3.3.1 *Geometry*

The large sub-domain model has a width of 90 m, a height of 100 m, and a slope of approximately 36.50. A total of 45 layers of soil with a thickness of 2 m/layer were used for the model. The surface waste rock layer was assumed to be a coarse material (gravel).

3.3.2 *Soil Parameters*

The soil parameters of the two soils used in this numerical analysis are the same as the "one standard deviation difference" values used in the Set *P2*. Details of the soil parameters for the sand and gravel are presented in Table 4.

3.3.3 *Initial and boundary conditions*

A soil suction of 90 kPa was set for entire model as the initial condition. As presented in the previous seepage report, the amount of water flow from waste rock into the bedrock was estimated to be insignificant (i.e., close to the crest); therefore, a "no flow" boundary condition was applied on the right edge of the model. A pressure head boundary condition of 0 kPa was applied on the bottom edge of the model.

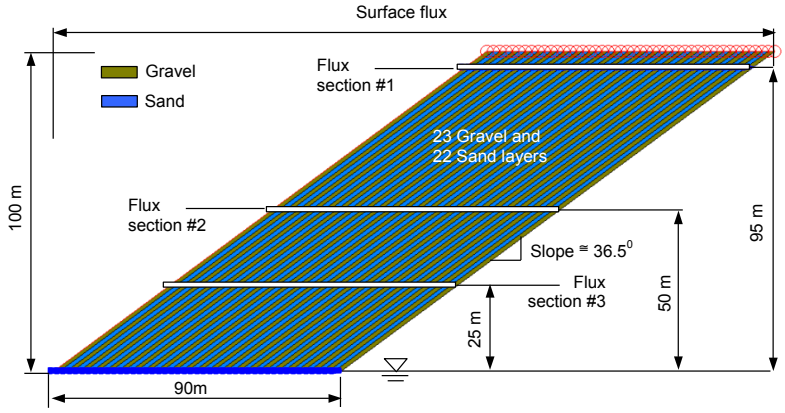


Figure 20. Geometry of the large sub-domain model

3.3.4 *Results and discussion*

Three flux sections were added to the model; namely fluxes #1, #2 and #3 (Figure 20). Flux sections #1, #2 and #3 have elevations of 95 m, 50 m and 25 m (i.e., referenced to the bottom of the model).

A summary of the simulation results is shown in Table 6. The results show that flow of water through the sand is significantly higher than flow through the gravel.

Table 6. Modeling results for the large sub-domain model (*P3*)

Flux	Percentage of flow through gravel and sand	
	Gravel (%)	Sand (%)
#1	2.41	97.58
#2	3.37	96.62
#3	3.83	96.17

3.4 *Summary and conclusions from primary study*

The primary study shows that the preferential flow in a multi-layer model is highly dependent on the soil parameters, particularly the slope of the unsaturated hydraulic conductivity curve. The thickness of each soil layer may not significantly affect the preferential flow in the soil.

A combination of the results from the small sub-domain model, large sub-domain model, and full-scaled model shows that the soil layer thicknesses and the scale of the model do not significantly affect the preferential flow through the materials involved.

The results also show that with an extreme set of soil parameters (i.e., soil parameters of the gravel being one standard deviation towards a coarser material and soil parameters of the sand being one standard deviation towards a finer material) there is almost no flow through the gravel.

4 CONCLUSIONS

The present study is useful in determining the reasonable variation of material parameters given the extensive field program executed in the present study. Conclusions for this study may be divided in to four categories associated with the specific purposes of the modeling performed.

4.1 *Modeling Set P1*

The purpose of the modeling study was to determine reasonable material parameters that would differentiate flow between the fine and coarse layers. A wide variety of grain-size distributions was measured in the field program. No distinctive categorization of a specific layer of coarse or fine material was identified in the field program. However, specific coarse layers were noted visually at the Goat Hill North site. Therefore professional judgement was used to identify reasonable soil parameters in the present study which will produce preferential flow.

The results of modeling Set *P1* is that it is shown that current base case Sand and Gravel soil parameters must be modified one standard deviation further apart from each other in order to produce reasonable preferential flow. The primary variable which produces the greatest sensitivity is the slope of the unsaturated hydraulic conductivity curve. When the mentioned statistical separation was used, the flow values were approximately 95% in the sand and approximately 5% in the coarse material. This differentiation produces a significant air volume in the coarse layer.

4.2 *Modeling Set P2*

Modeling of extremely fine layers in a full-scale model is computationally challenging. The thickness increase in the fine and coarse layers which could be reasonably assumed in the full scale numerical model without significant influence on the overall flow was studied. Coarse layers in the Goat Hill North rock pile were as thin as 10 cm. From the numerical modeling it was found that increasing coarse layers to a thickness of 1 m only increased the total flow in the coarse layers approximately 10%. Given that the reasonable error limit of the numerical model itself is 8% it is reasonable to conclude that this difference is acceptable.

4.3 *Modeling Set P3*

In the third modeling scenarios the upscaling of the small-scale models to a full-scale model was examined. From this model it can be seen that a 2 m size layering could be used while preserving the concept of primary flow through the fine material. This was verified using average flow applications.

5 REFERENCES

SoilVision Systems Ltd., 2006, Seepage Numerical Modeling Report, Molycorp Weathering Study, Phase I, November.

Numerical simulations of air convection cover for mine tailings of Lupin mine

Nam H. Pham & David C. Sego
University of Alberta, Edmonton, Alberta, Canada

ABSTRACT: Maintaining mine tailings in a frozen state is an important requirement for mine closure in permafrost regions. In a frozen state, the processes related to acid generation from the tailings cease or reduce to a minimum. Soil covers are often used to maintain or reduce temperature of tailings; however, only conductive heat transfer is utilized with these soil covers. In cold regions where the winter temperatures are cold and prolong, conduction is not efficient compared to convection. Natural air convection within a coarse rock cover results in a rapid cooling of the tailings. Therefore, when natural air convection is used in soil covers, which is called Air Convection Cover (ACC), for mine tailings, frozen conditions in tailings can be achieved much faster.

1 INTRODUCTION

Freezing of tailings deposits in continuous permafrost regions is very crucial as it reduces or eliminates the environmental problem of acid rock drainage (ARD). This is because under cold temperatures, the chemical and biological processes that create ARD are reduced and the frozen ground can limit the transport of pollutants (Jaynes et al. 1984). Without a cover on top of tailings, the active layer that forms in summer each year can create ARD and spread the pollutants to the surrounding area. Therefore, a soil cover on top of tailings is required to prevent the active layer forming in tailings. Soil cover is a multi-layer system in which there is at least one saturated layer. This saturated layer contains not only greater latent heat to prevent the penetration of active layer but also limits the transport of oxygen into tailings. The heat transfer mechanism through a soil cover is usually thermal conduction. However, if a soil cover contains a layer of coarse rock, heat transfer though this layer may involve both heat conduction and convection. Conduction dominates during summer and during winter natural air convection can be significant due to potentially unstable stratification of air within the rock cover involving heavy cold air sinking through warmer air at depth in the cover.

The effectiveness of air convection in highly porous media has been utilized in many engineering applications, specifically in geotechnical engineering for protection of road and railway embankments in permafrost region of northern Alaska and China as well as to eliminate ARD in the northern regions of Canada (Goering & Kumar 1996, Mu et al. 2010, Pham 2013, Pham et al. 2013). In order for natural air convection to take place, a non-dimensional Rayleigh number is determined based on the properties the porous media, air and the geometry of the examined domain must be above a certain value (Nield & Bejan 1999).

$$\mathbf{Ra} = \frac{\rho_a g \beta C_a K H \Delta T}{\mu \lambda} \quad (1)$$

where: ρ_a, β and μ are the air density, the coefficient of thermal expansion and the dynamic viscosity of air, g is the gravitational constant. C_a is the volumetric heat capacity of air; K is the air permeability of the porous media. H is the height of the porous layer, ΔT is the temperature difference between the lower and upper boundary of the porous layer, and λ is the bulk thermal conductivity of the media. For the case of a horizontal layer of porous media, the value of Ra at the onset of natural convection is $4\pi^2$ for closed top and bottom boundaries and 27.1 for the case of open top and close bottom (Nield & Bejan 1999). At larger values of Ra than the values at the onset, meaning air convection is stronger and multi cells may form vertically within the cover layer. At the onset, the air inside the porous layer changes from immobile to mobile. The streamlines of air particles forms convection cells, which transfers heat from the bottom warm layer to the cooler top layer. The higher the value of Ra, the larger the internal air velocity, more curvature of temperature contours and greater numbers of convection cells (Figure 1). This paper presents a numerical study for freeze-back of tailings at the northern Lupin mine with and without a coarse rock cover. In the covered cases, both conduction and convection types of cover system will be assessed.

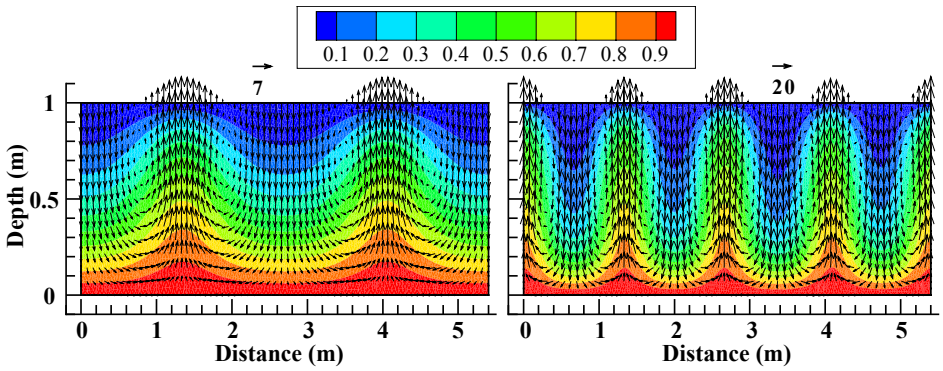


Figure 1. Nondimensional temperature contours and velocity vectors at Ra = 30 (A) and Ra = 60 (B).

2 SITE DESCRIPTION AND THERMAL PROPERTIES

2.1 *Site Description*

Lupin gold mine is located on the west shore of the Contwoyto Lake in the Northwest Territories about 80 km south of the Arctic Circle and 400 km northeast of Yellowknife. The mine is within the continuous permafrost regions with permafrost to a depth of 540 m (MEND 1.61.4 2004). Mean annual air temperature (MAAT) of −10.9 °C for the period between 1982 and 2006 (Environment Canada 2013) (Figure 2), corresponding to air freezing index, which is the summation of days having temperatures below 0 °C, (AFI) and air thawing index (ATI) of 4743 and 761 °C·days respectively.

At the mine site, tailings are stored in an area called the tailings containment area (TCA). TCA consists of 5 cells where tailings were deposited and the cells are separated by dykes (Figure 3). After individual cell reached capacity and a soil cover was constructed. The soil cover uses local, Esker material, and it is based on the saturated zone soil cover concept. This design concept includes two layers; the top layer is used to lower the evaporation of the bottom layer and the bottom layer to limit the influx of oxygen into the tailings. The thickness of the cover must be sufficient to contain the active layer during summer. This design has been applied to some cells at the site and the cover thickness is between 0.6 to 1.6 m (MEND 1.61.4 2004).

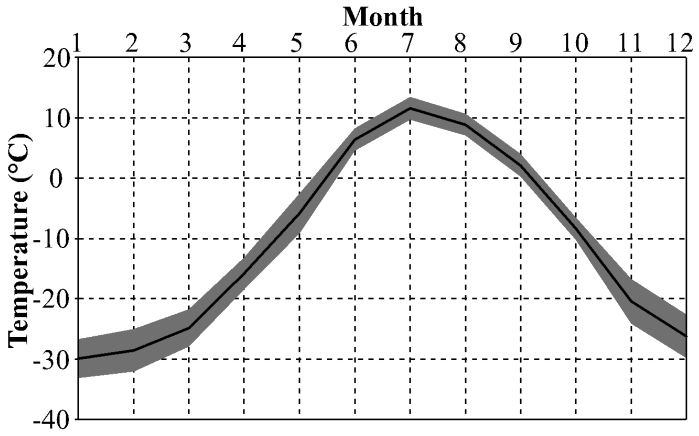


Figure 2. Monthly average air temperature at the site, the shaded area is one standard deviation from the average

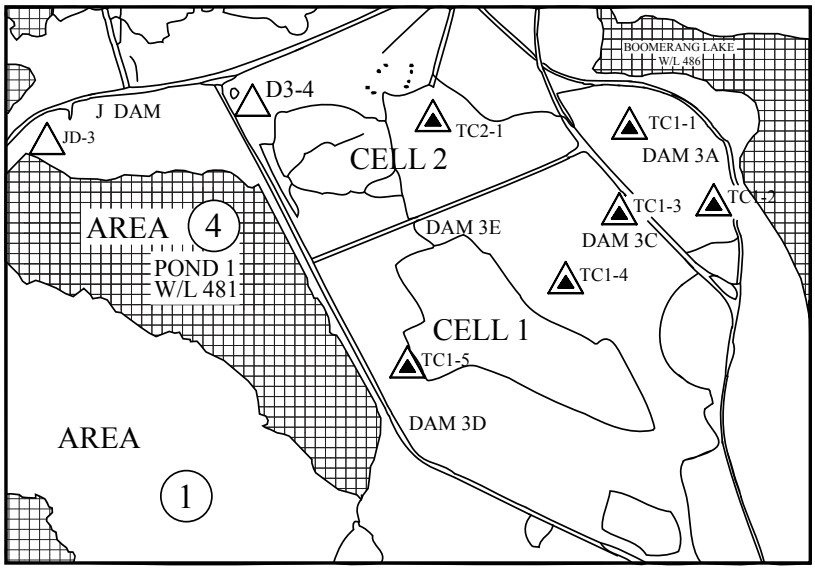


Figure 3. A protion of TCA with thermistors location (TC1-1 to TC1-5 and TC2-1).

2.2 *Thermal properties.*

Measurement of thermal conductivity of tailings was conducted by the University of Alberta and the results are plotted in Figure 4A (MEND 1.62.2 1998). This figure indicates an average for the tailings in frozen and thaw state of 2.8 and 1.7 W/(m·K) respectively. The existence of unfrozen water in tailings is indicated by Figure 4B and at a temperature of –10 °C the unfrozen water content is about 5%, which is about 10% that of thaw state (51%). Other thermal properties of tailings and thermal properties of other materials used in simulation are calculated based on a geometric mean (thermal conductivity) or volumetric mean (volumetric heat capacity) (Table 1). The latent heat released/absorbed by tailings is calculated by the difference in water content between frozen and thaw state. Other materials are assumed to undergo phase change at temperatures below 0 °C.

Table 1. Thermal properties of materials

Material	Latent heat (MJ/m^3)	Thermal conductivity (W/(m·K))		Heat capacity ($MJ/(m^3 \cdot K)$)	
		Frozen	Thaw	Frozen	Thaw
Tailings	161	2.80	1.70	2.47	3.48
Esker sand/gravel (Unsaturated)	50	1.27	1.55	1.91	2.23
Esker sand/gravel (Saturated)	100	2.06	3.04	2.23	2.86
Coarse rock	0	0.7	0.7	1.6	1.6

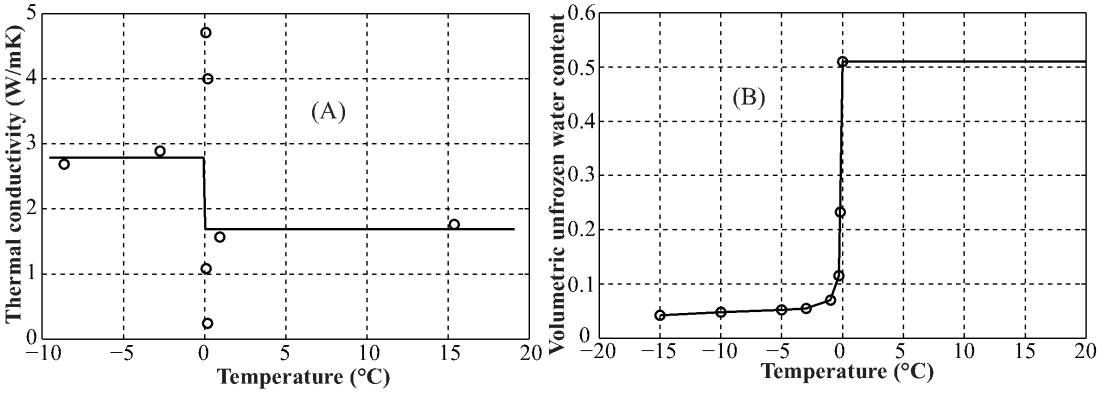


Figure 4. Thermal conductivity and unfrozen water content versus temperature (MEND 1.62.2 1998)

3 NUMERICAL RESULTS

3.1 *Initial and boundary conditions*

A uniform placement temperature of 7 °C was used for the entire thickness of 12 m as an initial temperature of tailings and this value is the average temperature during summer. The surface is subjected to varying air temperatures and other components such as radiation, wind, snow cover, moisture and surface's albedo. However, these processes are interacted and fluctuated drastically and they are difficult to simulate properly. Therefore, the n-factors approach was used (Andersland & Ladanyi 2004). Andersland & Ladanyi (2004) provided a list of n-factors for different soils and surface's conditions. The values of n-factors are then used to determine ground surface temperatures as boundary conditions at the surface and the procedure was reported by Lunardini (1981). It is reasonable to use thawing index, $n_t = 2.5$, and freezing index, $n_f = 0.9$ for tailings surface. With these values and air temperatures from Figure 2 results in a mean annual ground surface temperature (MAST) = –6.5 °C and an amplitude of ground surface temperature ($A_{surface}$) = 25.8 °C were obtained. Ground temperature at the bottom boundary was chosen to be equal with MAST = –6.5 °C and this value is similar to ground temperature measurement at 13 m depth (MEND 1.61.4 2004).

In the uncover case, the simulation was run for 10 years with the initial and boundary conditions stated above. For the covered cases, the initial temperatures used for the tailings was from year three of the uncover case and initially uniform temperature of the cover placed over these tailings was set to be 7 °C. In the cover cases, involving the conduction and convection, for the conduction covered cases including 12 m tailings and a soil cover layer between 1 to 2 m. The soil cover includes a fully saturated zone of esker sand and gravel of 0.4 m and an upper zone of the same material but at 50% saturation. In convective cover cases, the domain is 2D with 20 m width by 14 m (2 m cover plus 12 m tailings) or 15 m (3 m cover plus 12 m tailings) height.

Simulations were conducted by using a commercially available software, COMSOL multiphysic (COMSOL 2008).

3.2 *Conduction covers*

Field observation shows that 0.4 m Esker sand at the bottom of the cover was fully saturated (MEND 1.61.4 2004) and the zone above was 50% saturation. Without this cover, the active layer penetrates about 1.8 m into tailings (Figure5A) and it is similar for cases with soil covers up to 1.5 m thickness (Figures 5B, C). When the cover thickness increases to 2.0 m the active layer is about 1.5 m (Figure 5D). These results indicate that 2 m thick cover will be sufficient to limit the active layer within 2 m for 10 years. Thaw layers only exist from June to October and the remaining months, the entire profile is frozen.

Field results at Lupin show that with the cover thickness ranging between 0.6 and 1.6 m, the active layer varies between 1.2 and 1.8 m (Table 2). The greater the cover thickness, the deeper the active layer. This can be explained as the thin cover contains less latent heat therefore the active layer is restrained by the latent heat of the tailings beneath. With thicker cover, heat enters deeper into the cover and creates greater active layer. The main factor that controls the active layer is the thickness of saturation zone within the cover.

Table 2. Field results of active layer thickness (MEND 1.61.4 2004)

Thermistor	Cover thickness (m)	Active layer thickness (m)
TC1-1	0.9	1.5
TC1-2	1.2	1.7
TC1-3	0.6	1.2
TC1-4	0.6	1.7
TC1-5	1.6	1.8
TC2-1	0.9	1.8

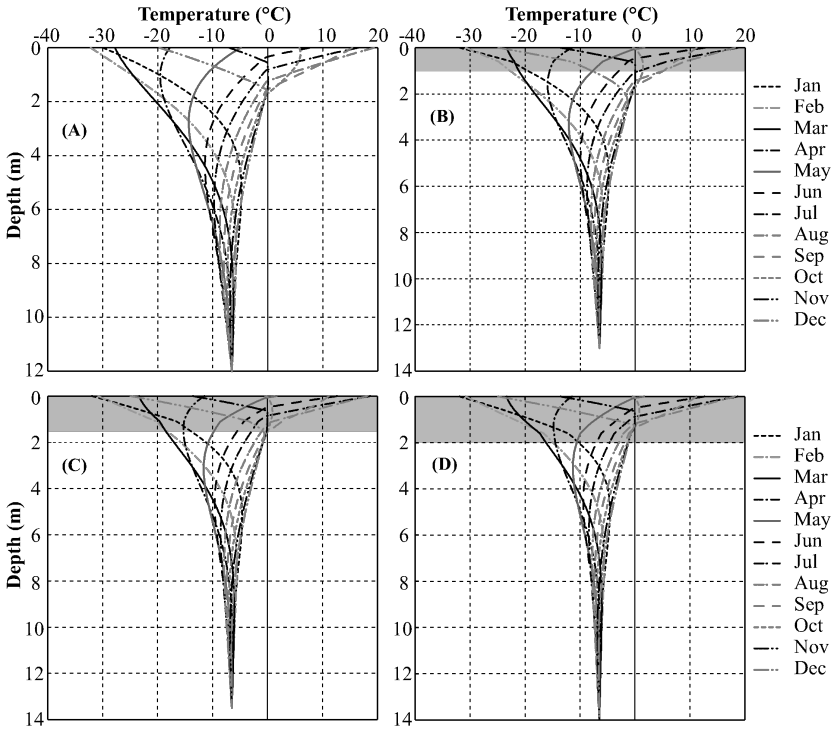


Figure 5. Conduction modeling: without cover (A), 1 m cover (B), 1.5 m cover (C) and 2.0 m cover (D). The shaded areas indicate cover thickness and crossing of the 0 °C line indicates thaw penetration.

As shown in Figure 6, at permeability ≥ 4×10^{-7} m^2 the active layer is about 1.8 m. Furthermore, temperatures within the air convection cover during winter are colder compared to the conduction cases (Figure 5). When the thickness of the cover is increased to 3 m, the active layer increases to 1.9 m (Figure 7). Ground temperatures within the cover and tailings are colder than for the cases of 2 m cover. According to the Eqn. 1, at the onset of air convection ΔT reduces to 5.2 °C for the 3 m cover. Similarly, to the conduction case, the thaw layer within convection cover is formed from June to October each year (Figures 6, 7) but it does not penetrate into the underlying tailings. It clearly shows that the trumpet curves of ground temperatures in the case of 3 m air convection cover produce colder temperatures (Figure 7).

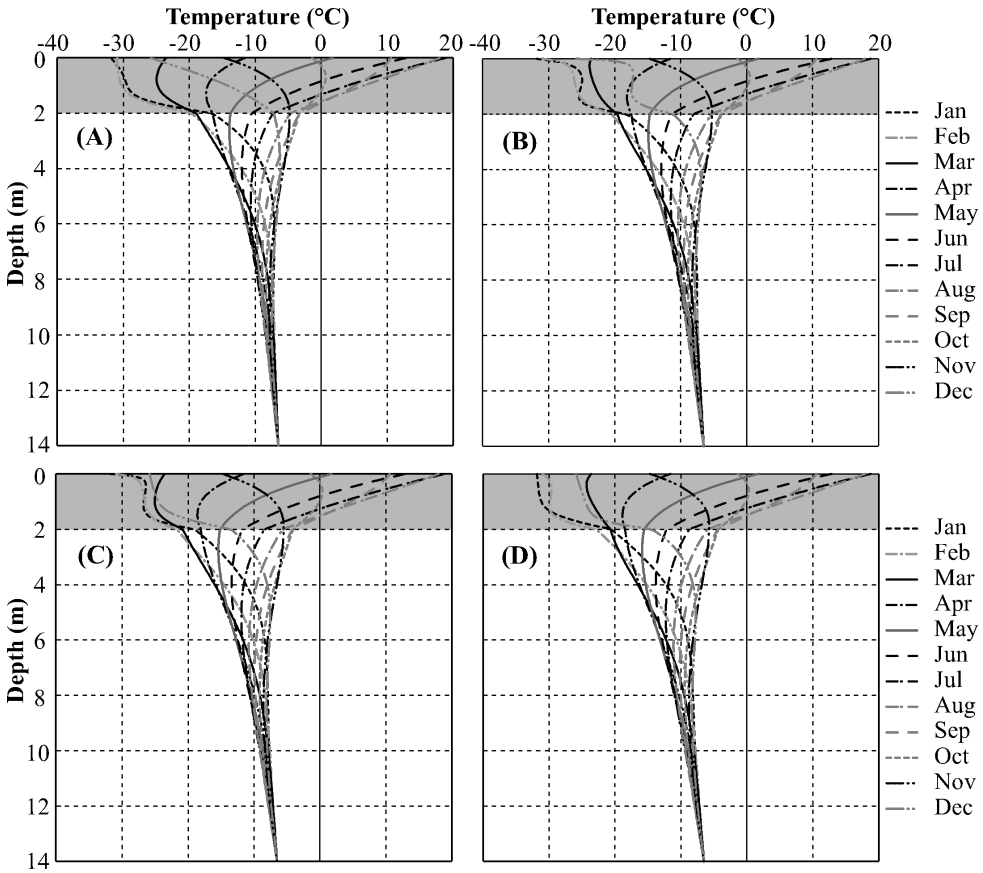


Figure 6. Air convection cover modeling with a 2 m cover and intrinsic permeability of: 4×10^{-7} m^2 (A), 6×10^{-7} m^2 (B), 8×10^{-7} m^2 (C) and 1×10^{-6} m^2 (D).

Ground temperatures at the surface of tailings are always below 0 °C for a cover thicker than 2 m. However, air convection cover produces colder temperatures for the same thickness (Figure 8A, B). In conduction case (2 m cover), ground temperatures vary between −1 °C and −16 °C, whereas at permeability ≥ 4×10^{-7} m^2, ground temperatures fluctuate between −3 °C and down to −23 °C at permeability 1×10^{-6} m^2 (Figure 8A). When the cover thickness increases to 3 m, minimum ground temperatures within the cover do not vary significantly (around −23 °C) but maximum ground temperatures changes to −7 °C from −3 °C (Figure 8B).

After about 1500 days, ground temperatures at 5 m below the surface of tailings reach steady state conditions from initially 0 °C (Figures 8C, D). In the conduction case, steady ground temperatures vary between −5.2 and −8.5 °C and with the 2 m convection cover, ground temperatures fluctuate between −8 and −12 °C (Figure 8C). When the cover thickness increases to 3 m, air convection is stronger and the active period is longer during winter. Therefore, ground temperatures are colder −10 and −13 °C (Figure 8D). Moreover, at a given thickness, the higher the permeability of the cover, the colder the ground temperatures within the underlying tailings.

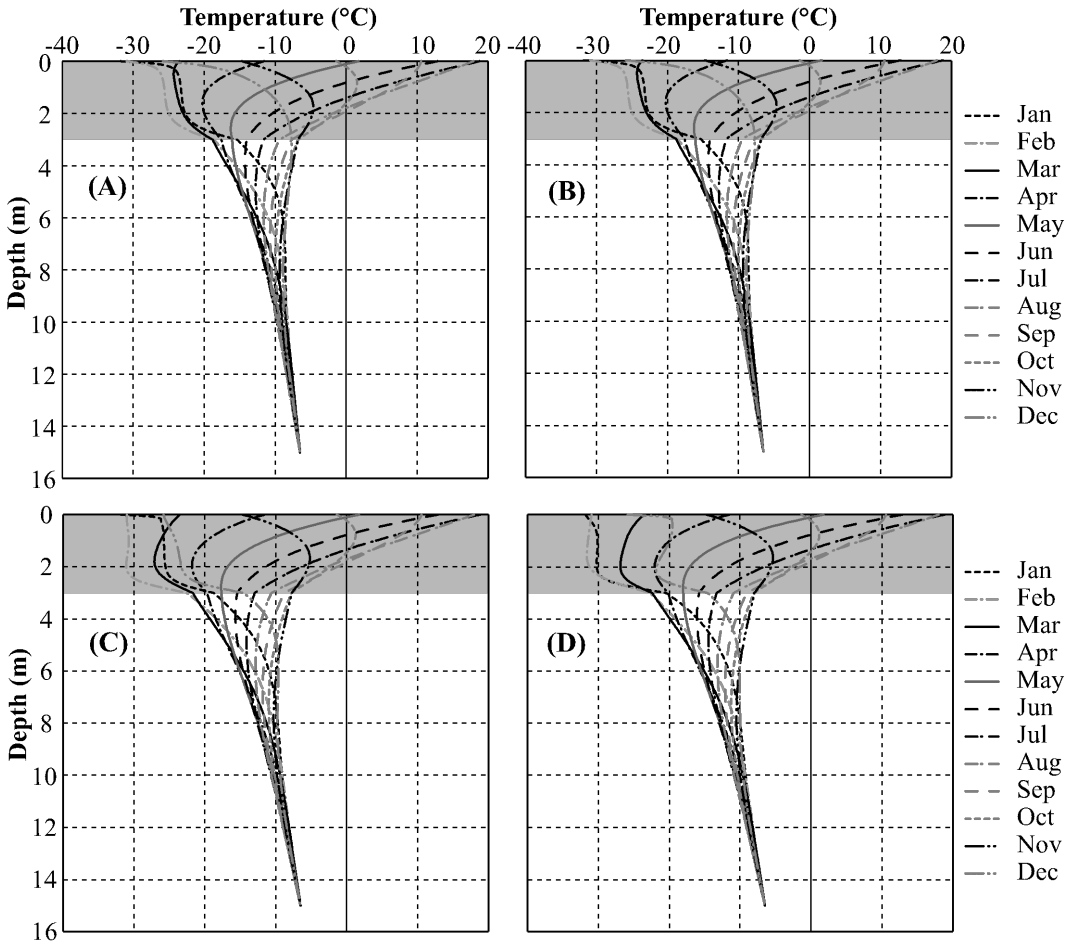


Figure 7. Air convection cover modeling with a 3-m thick cover and intrinsic permeability of: 4×10^{-7} m^2 (A), 6×10^{-7} m^2 (B), 8×10^{-7} m^2 (C) and 1×10^{-6} m^2 (D).

According to the Equation. 1, the strength of natural air convection in porous media depends on the geometry of the layer and the properties of air and porous material. However, most often the permeability, thickness and the temperature difference within the layer dominates other parameters as they can vary significantly and easily. Figure 9 shows the various stages of air convection in the covers. During January, the difference in temperature within the cover layer is largest, $\Delta T = 15$ °C, therefore, air convection is greatest within a year (Figure 9A). At this ΔT the value of Rayleigh number is 122 which is 4.3 times than Rayleigh number for onset. Convection cells are formed within the cover with spacing between warm flumes varies between 3 and 5 m and air velocity can reach 1×10^{-2} m/s. These cells extract heat from the surface of tailings and carry it up to the ambient cold surface. When surface temperature warms, air convection becomes weaker and then ceases.

As shown in Figure 9B, during April local air convection occurs at some depths near the base where temperature gradients are still sufficient. Air velocity is also much smaller about 7.5×10^{-4} m/s. In July, which is the warmest month and October, surface temperatures are higher than ground temperatures at the base of the cover. As a result, the favor conditions for natural convection are diminished and heat transfer is controlled by conduction through the coarse rock cover. Air velocity is small in the order of 10^{-5} m/s (Figures 9C, D). In December, air convection occurs at a temperature difference of 12 °C corresponding to Ra = 97.6. Therefore, air convection in December is lightly smaller than that of January (Figure 9E).

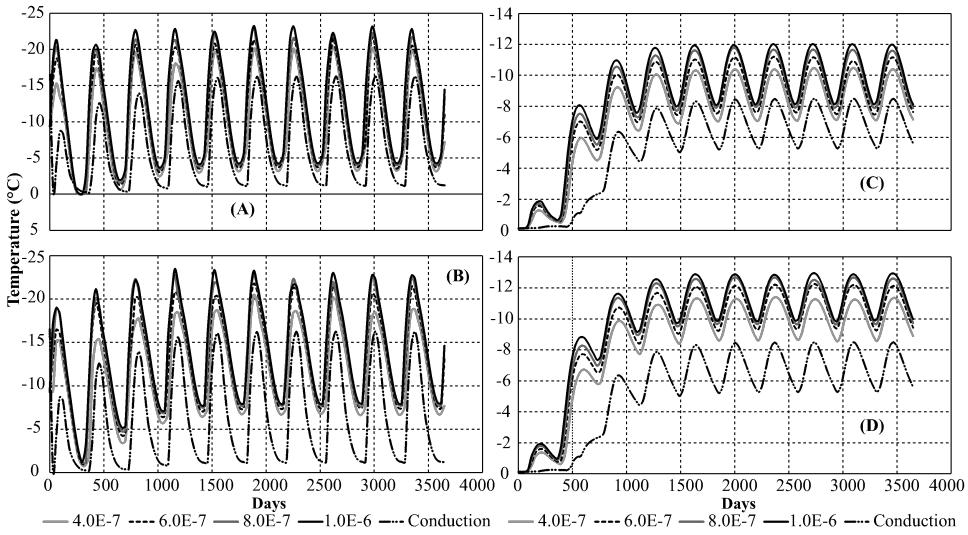


Figure 8. Ground temperatures at the surface and 5 m below surface of tailings in case of 2 m (A and C) and 3 m cover (B and D).

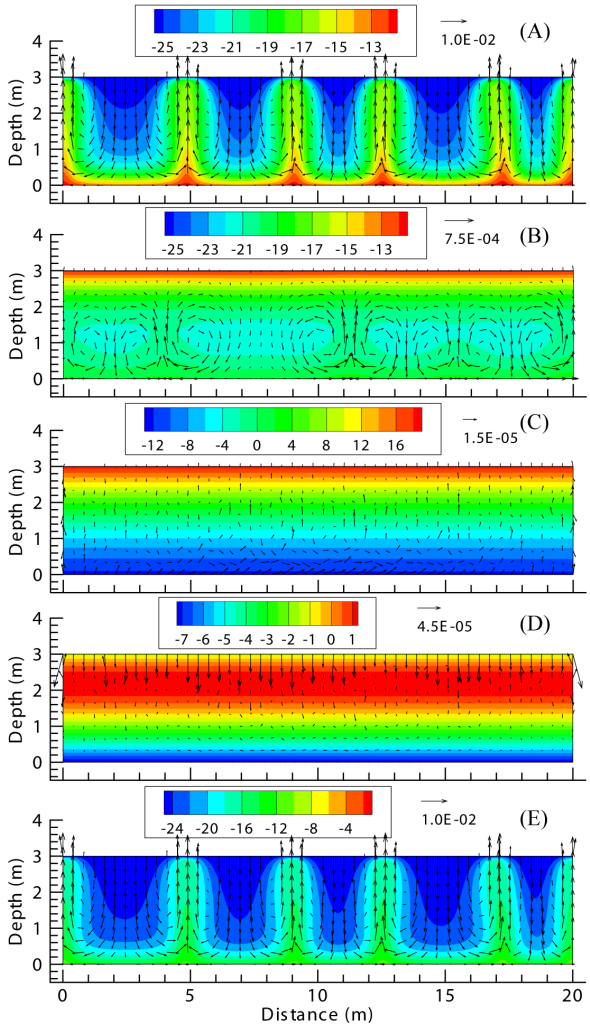


Figure 9. Temperature and air velocity vector within 3 m the cover with permeability of 6×10^{-7} m^2 at various months of year 10: January (A), April (B), July (C), October (D) and December (E).

4 CONCLUSIONS

Due to the cold climate at the Lupin site, numerical modeling shows that a 2 m thick esker sand layer with a 0.4 m saturated zone at its base is sufficient to maintain freezing conditions in tailings within 10 years of deposition. This result is confirmed by field data and a thaw layer only exists between June and October at a maximum depth of 1.5 m.

If the materials used to construct the cover layer are permeable enough, air convection can form during winter. Rayleigh number is used to determine the threshold for the onset of air convection. With a 2 m thick cover, air convection is sufficient to contain the active layer within the cover and reduces ground temperatures in the tailings to colder temperatures than without air convection. At a given site, increasing the thickness or permeability of the cover, natural air convection is stronger and active longer during winter. As a result, ground temperatures in underlying tailings are colder.

5 ACKNOWLEDGEMENTS

This research was made possible through funding provided by the NSERC Discovery Grant held by the senior author.

6 REFERENCES

Andersland, O.B. & Ladanyi, B. 2004. *Frozen Ground Engineering*. John Wiley & Sons.

COMSOL multiphysic 2008. *User guide 3.5a* .

Environment Canada 2013. Climate data online. *National climate data and information archive*.

Goering, D.J. & Kumar, P. 1996. Winter-time convection in open-graded embankments. *Cold Regions Science and Technology*, 24(1):57–74.

Jaynes, D.B., Rogowski, A.S., & Pionke, H.B. 1984. Acid mine drainage from reclaimed coal strip mines: 1. Model description. *Water Resour. Res.*, 20:233–242.

Lunardini, V.J. (1981). *Heat transfer in cold climates*. Van Nostrand Reinhold Company.

MEND 1.61.4 2004. Covers for reactive tailings in permafrost regions. *Mining Association of Canada-Mine Environment Neutral Drainage (MEND) Program*.

MEND 1.62.2 1998. Acid Mine Drainage behavior in low temperature regimes - Thermal properties of tailings. *Mining Association of Canada-Mine Environment Neutral Drainage (MEND) Program*.

Mu, Y., Ma,W., Liu, Y., & Sun, Z. 2010. Monitoring investigation on thermal stability of air-convection crushed-rock embankment. *Cold Regions Science and Technology*, 62(2-3):160–172.

Nield, D. & Bejan, A. 1999. *Convection in porous media*. New York: Springer.

Pham, N.H. 2013. *Heat transfer in waste-rock piles constructed in a continuous permafrost region*. PhD thesis, University of Alberta.

Pham, N.H. Sego, D.C. Arenson, L.U. Blowes, D.W. Amos, R.T. & Smith, L. 2013. The Diavik Waste Rock Project: Measurement of the thermal regime of a waste-rock test pile in a permafrost environment. *Appl. Geochem. (2013)*, http://dx.doi.org/10.1016/j.apgeochem.2013.05.007

Model analysis of differential settlement for a heap leach constructed on a mine waste storage facility

S. Abbaszadeh, N. Haws, S. Taylor
MWH Americas, Tempe, AZ, USA

C. Weber
MWH Americas, Denver, CO, USA

ABSTRACT: Existing mining facilities typically have fixed property boundaries, permit limits, or economic considerations that constrain the mining infrastructure to a limited area. Expansion projects at these mines often must fit into these fixed areas and compete with the space requirements of ongoing activities. An alternative for a facility expansion being developed at a copper and gold mine in South America is to locate a new gold heap leach on top of an existing waste storage facility. Because the waste facility was not originally constructed as a heap leach foundation, a concern is that the various types and depth of materials in the waste facility will have different settlement responses. Differential settlement beneath the leach pad could lead to (1) tears in the leach pad liner due to excessive liner strains and (2) poor drainage of pregnant leach solution due to reversal of gradient in the collection pipes. In this paper a series of possible differential settlement scenarios are simulated using the finite difference modeling software, FLAC. The location and extent of the differential settlement is what differentiates between these scenarios. The total differential settlement and the stresses and strains developed in the liner are calculated for each scenario. The modeling demonstrates strategies to mitigate the risk of differential settlement beneath the heap leach.

1 INTRODUCTION

Recent advancements in mining allow for mining resources today that were not possible to mine or process before. We now see mines and facilities located on mountains or in difficult terrains constrained by both property boundaries and topography. Expansion projects at these mines can be challenging due to the space restrictions.

An example is a mine in South America that needs to process a low grade gold ore stockpile through heap leaching. Due to space limitations, and to minimize the environmental disturbance, one of the few feasible options is to locate the leach pad on an existing waste storage facility (WSF). As the waste facility was not originally constructed as a compacted foundation, a concern is that the various types and depths of materials in the waste facility could have different settlement responses. Differential settlement beneath the leach pad could lead to (1) tears in the leach pad liner due to excessive liner strains and (2) poor drainage of pregnant leach solution due to reversal of gradient in the collection pipes.

The site is surrounded by sensitive environmental and social areas such as off-site rivers and streams that form headwaters to drinking water supplies for downstream communities. Discharges into these rivers and streams are controlled through strict environmental regulations, and the mine's social license to operated requires protecting these water sources. Karst voids are known to sometimes provide links to rivers, streams and groundwater so potential leakage of the cyanide heap leachate must be eliminated.

As a preliminary risk assessment, the authors evaluated potential differential settlement scenarios as a result of constructing a heap leach facility on the existing waste dump and the associated strains on the geomembrane liner. Our approach for this evaluation was to first develop simplified differential settlement scenarios that could potentially create excessive strains on the liner. We then used a finite-difference numerical model to simulate the differential settlement, under various mitigation strategies, and predict the liner strains. Based on the results from these analyses, the initial assumptions can now be modified to improve the liner design and optimize the costs.

2 HEAP LEACH PAD FOUNDATION DESIGN

Figure 1 shows the plan view of the WSF on which the heap leach will be constructed. The foundation of the leach pad will include the following components (from bottom to top):

- bedrock
- up to 50 meters of uncompacted and variable waste
- 5 meters compacted waste
- 0.6 m underliner material
- Geosynthetic Clay Liner (GCL)
- 80 mil linear low density polyethylene (LLDPE) geosynthetic liner
- 0.6 m overliner material
- 8 meter on-off heap

The purpose of the compacted waste is to provide a more rigid base to the leach pad and minimize, and/ or bridge, settlement. The overliner and underliner are to protect the liner from tears caused by sharp rocks or vehicle traffic. The geomembrane liner prevents leakage of process solution to the environment. The GCL provides a secondary layer of protection against leakage.

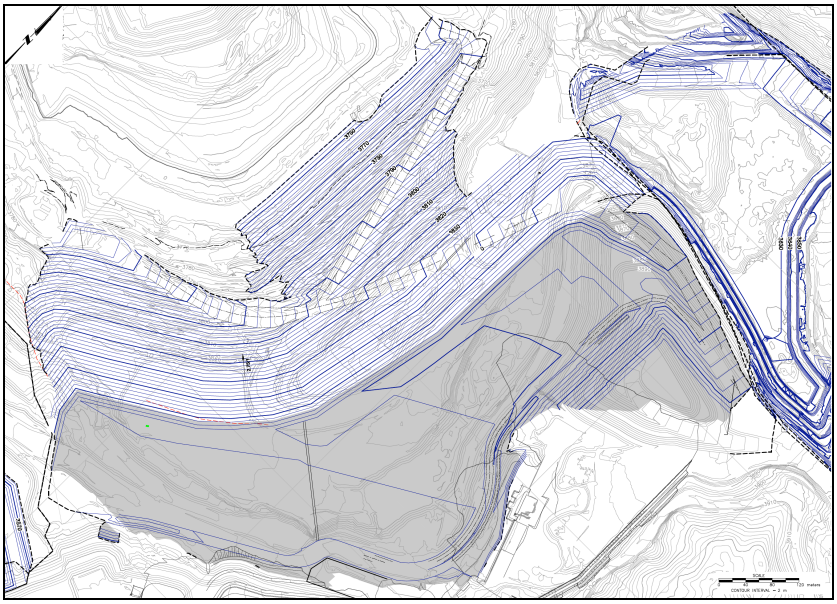


Figure 1. Layout of the Waste Storage Facility (WSF) as Foundation of the Heap Leach Pad

3 DIFFERENTIAL SETTLEMENT SCENARIOS

The impact of differential settlement on the geomembrane liner is sensitive to the length over which the differential settlement occurs. For example, differential settlement occurring abruptly over a short length will induce higher strains in a liner than the same amount of settlement over a longer length. Predicting the length over which differential settlement will occur can be difficult in a waste storage facility where the dumping sequence and variability of the waste proper-

ties is not well known. As a rigorous characterization of the waste storage facility was not practical, we used the little information on the waste dump that was available to develop several simplified scenarios under which differential settlement could occur. Our intent in developing these scenarios was that our assumptions not be directly supported by data would favor over-predicting the potential liner strains (i.e., conservative assumptions).

We developed three scenarios. The basic assumption for each scenario was that somewhere within the waste dump there is a 10 meter wide prism of soft waste material surrounded by less compressible waste material. The depth of the waste dump in the area of the soft waste material was assumed to be 50 meters, which is approximately the maximum thickness of the waste that exists underneath the proposed heap leach pad. Although the exact dimensions of the area over which differential settlement may occur are difficult to predict, these assumed dimensions are more than likely conservative, based on our knowledge of the proportion of soft material in the waste facility. Furthermore, the waste material is unlikely to abruptly change in compressibility as the waste is dumped in 1 to 2 meter lifts and having 10 meters of soft material with a depth of 50 meters requires that a 10 meter wide section of soft material be placed directly over previously placed soft material for at least 25 consecutive lifts, which is highly unlikely.

Figure 2 shows the 3 possible differential settlement scenarios evaluated in this study. The primary difference between these scenarios is the location and orientation of the soft (compressible) material and the existence of a layer to mitigate differential settlement. This layer was assumed to be a cap of compacted waste directly beneath the pad, or the pad overliner and underliner.

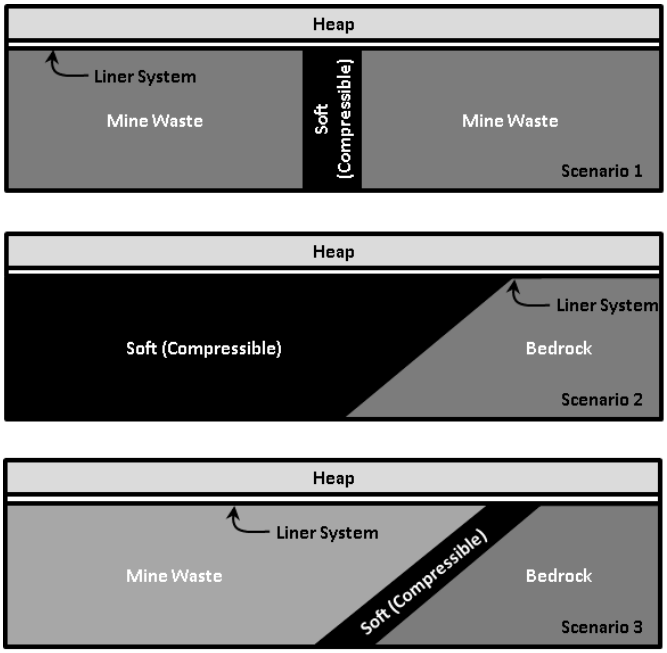


Figure 2. Different Scenarios Evaluated for Differential Settlement Analysis

Details of these scenarios are discussed below:

(1a) Leach Heap located over a 50 m deep and 10 m wide column of highly compressible (soft) material surrounded by less compressible waste material and with no compacted waste cap and no overliner/underliner.

(1b) Leach Heap located over a 50 m deep and 10 m wide column of highly compressible (soft) material surrounded by less compressible waste material and with a 0.6 m thick overliner, a 0.6 m thick underliner and a 5 m thick cap of compacted waste.

(2a) Leach Heap located partially over bedrock and partially over highly compressible (soft) material and with no compacted waste cap, and no overliner or underliner. The bedrock-waste interface is sloped so the thickness of the soft waste material varies throughout the leach heap from 0 to 50 meters.

(2b) Leach Heap located partially over the bedrock and partially over highly compressible (soft) material and with a 5 m thick cap of compacted waste, a 0.6 m thick overliner and a 0.6 m thick underliner. The bedrock-waste interface is sloped so the thickness of the soft waste material varies throughout the leach heap from 0 to 50 meters.

(3) Leach Heap located over a 10 m wide strip of highly compressible (soft) material bounded by the bedrock on one side and less compressible waste on the other side with no compacted waste cap, and no overliner or underliner.

4 NUMERICAL MODELING OF THE DIFFERENTIAL SETTLEMENT

The differential settlement of the heap was simulated using a FLAC 2D finite difference model. A sensitivity analysis was performed to determine the appropriate mesh size for each scenario. The bottom boundary of the model was fixed in both X (horizontal) and Y (vertical) directions and both sides of the model were fixed in the X direction and free in the Y direction to allow deformation. For Scenarios 2 and 3, the interface between the bedrock and the compressible material was modeled with consideration for the possibility of sliding of the compressible material relative to the bedrock.

The physical properties and strength parameters employed to model the strong and soft waste, heap, and bedrock material are shown in Table 1.

Table 1. Material properties used for the differential settlement FLAC modeling

Material	ρ (KN/m3)	ρ (kg/m3)	G_{max} (Shear Modulus in MPa)	K (Bulk Modulus in MPa)	Model	φ	c (kPa)
Bedrock	23	2345	2344	5080	Elastic	-	-
Heap Leach	15	1529	120	559	Mohr/Columb	24	9.5
Less Compressible Waste	20	2039	279	837	Mohr/Columb	27	9.5
Soft Waste (Highly Compressible)	20	2000	0.3	0.35	Mohr/Columb	27	9.5
Overliner/Underliner & Compacted Waste	20	2039	279	837	Mohr/Columb	27	9.5

The parameters for the soft waste material were set by "calibrating" Scenario 1 so that it had 80 centimeters of settlement after placing the 8 m heap overburden on top of the liner. The 80 cm settlement corresponds to the maximum expected consolidation of a 50 m deep column of the waste material due to the additional load exerted by placing the heap and a 5 m layer of compacted waste on top of it. This expectation is based on a consolidation calculation in accordance with one-dimensional consolidation theory. The properties used to calculate settlement are estimated from the weakest standard penetration test (SPT) blow count values of the waste storage facility (WSF) material.

One case of concern for differential settlement is when the soft material is placed next to bedrock the waste may slide against the bedrock as it settles, causing stress concentrations in the liner located on top of the waste/bedrock interface. This case was modeled in FLAC as Scenarios 2 and 3 to evaluate the potential displacements as well as the strains developed in the liner associated with this case. In Scenario 2, the entire mass of waste material was assumed to consist of soft waste. This scenario is highly unlikely because the properties of the soft material are calibrated based on the weakest material found on the previous SPT exploration of the WSF and is not representative of the entire mass of waste material. In Scenario 3, a 10 m wide strip of soft material is assumed to exist next to the bedrock. The properties of the soft material developed in Scenario 1 were used to represent the compressible material for Scenarios 2 and 3. The bounda-

ries selected for modeling of all 3 scenarios is shown schematically in Figure 3.

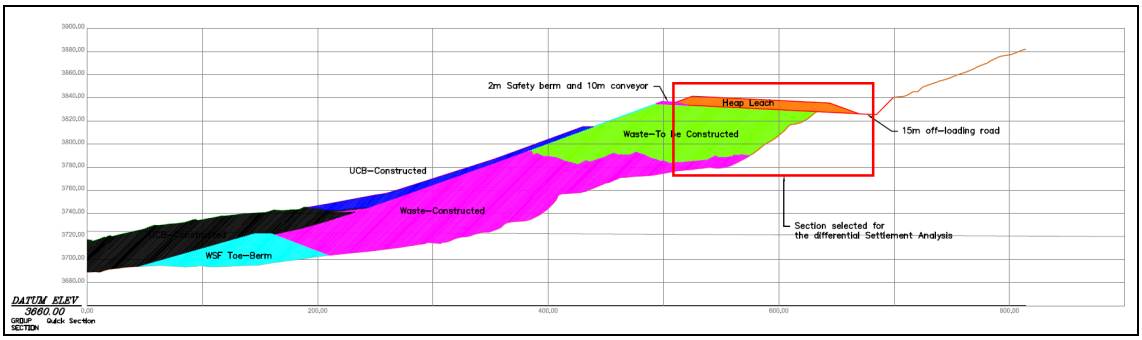


Figure 3. The model boundary selected for the differential settlement analysis

4.1 *Modeling Results*

The calculated maximum displacements and strains in the liner for each scenario are shown in Table 2. Results for each scenario are discussed in the following subsections.

Table 2. Summary of the maximum displacements and strains in the liner for different Scenarios

Scenario	*Max. Liner Settlement (cm)*	*Max. Liner Strain (%)*
1a	81.7	11.15
1b	0.47	0.02
2a	5.59	19.48
2b	4.95	7.06
3	8.17	14.33

4.1.1 *Scenario 1*

In Scenario 1a, the heap leach is modeled with 50 m of waste below the liner and an 8 m heap on top. As shown in Figure 4, a 10 m wide region of soft material with high compressibility is assumed in the middle of the pad in this scenario. The engineering properties of this material were adjusted such that, under the load of heap, the liner settles 80 cm, which is the expected total settlement due to the consolidation of a 50 m deep column of waste material. A sensitivity analysis was performed to determine the appropriate mesh size. In this process, the mesh size for the region of interest (in the middle of the model) was decreased until the results (e.g. liner strain) became independent of the mesh size. Figures 5 through 7 show the results for Scenario 1a (the calibration case). The maximum tensile strain developed in the liner due to the differential settlement for Scenario 1a is 11.15 percent (%).

The maximum liner tensile strain calculated by the FLAC model is higher than the maximum allowable strain for an LLDPE geomembrane liner for static loads which the authors estimated to be 7%. However, Scenario 1a does not include the overliner or underliner or the 5 meter compacted waste layer. The presence of these materials is expected to reduce the liner strains by providing reinforcement. The effect of inclusion of the overliner, underliner and the compacted waste layer is modeled in Scenario 1b.

Scenario 1b demonstrates that the overliner, underliner and compacted waste will significantly reduce the liner strains by supporting the liner and reducing the liner deformations associated with the differential settlement of a 10-m wide compressible waste column. The maximum liner tensile strain for Scenario 1b was determined to be 0.02 percent. This result suggests that in Scenario 1b the 5 meter compacted waste, 0.6 meter underliner and 0.6 meter overliner support the liner by spreading the soft waste deformation over a wider area, hence reducing liner strain. We performed a series of calculations to evaluate the potential for shear failure of the 5 meter compacted waste, and the results showed that the stresses induced in the compacted layer by settlement of the underlying waste do not exceed the compacted soil shear strength, which is consistent with the reported FLAC modeling results.

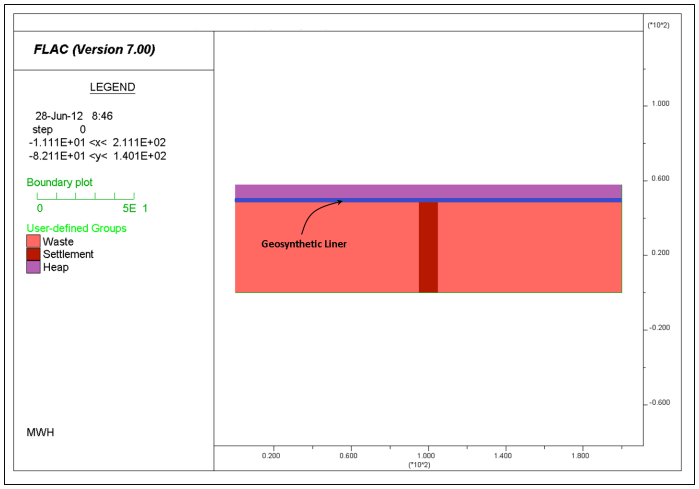


Figure 4. General view of the calibration case model (Scenario 1a) used for the differential settlement analysis

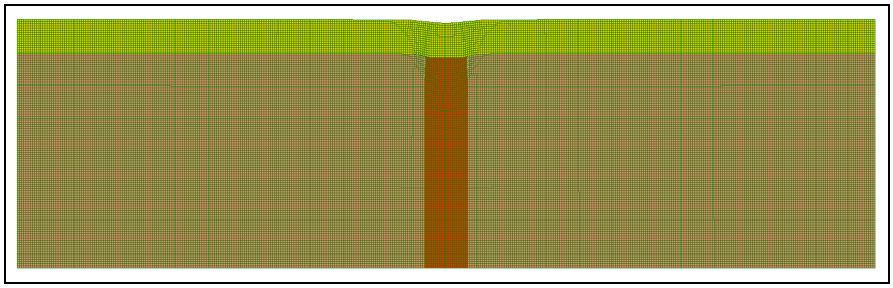


Figure 5. Deformed mesh after placing the 8 m heap for the calibration case (Scenario 1a)

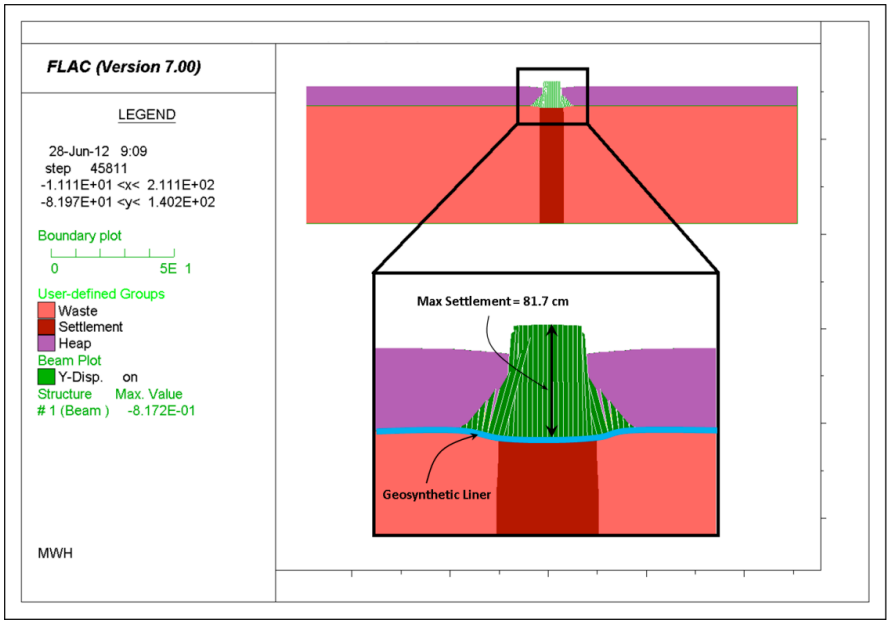


Figure 6. The maximum liner settlement for Scenario 1a

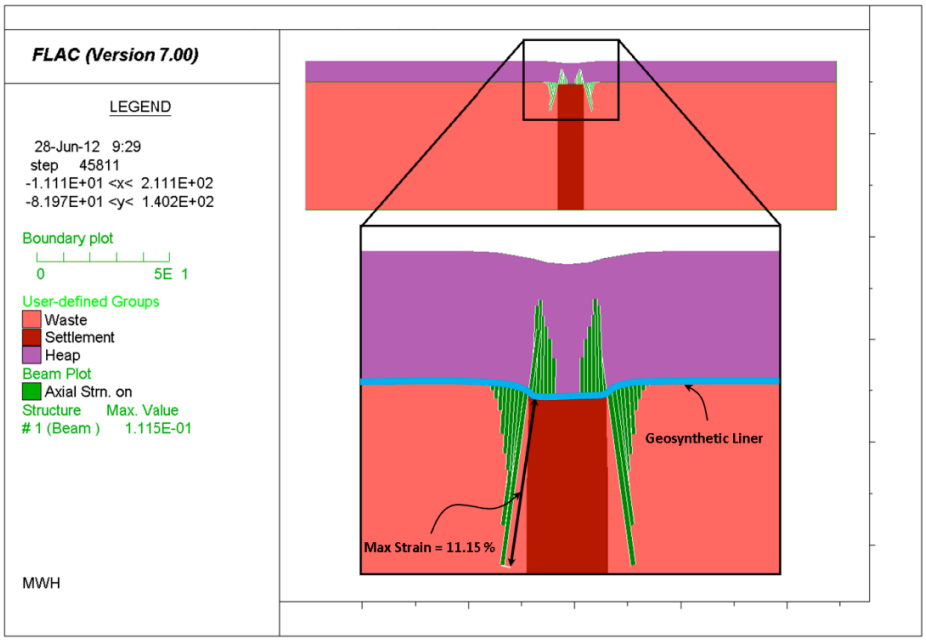


Figure 7. The maximum liner strain for Scenario 1a

4.1.2 *Scenario 2*

Scenario 2 simulates the conservative situation when all the waste consists of soft material; whereas, Scenario 3 assumes that only a 10 m band of waste adjacent to the bedrock is made of soft material. The maximum differential settlement for Scenarios 2 occurs near the waste-bedrock interface. Figure 8 provides the general geometry of Scenario 2a. Figures 9 provides the deformed mesh and Figure 10 illustrates the strain distribution of the liner for Scenario 1a. Similar to Scenario 1, once the 5 meter compacted waste cap, 0.6 m overliner and 0.6 m underliner layers were added, Scenario 2b, the maximum liner strain was decreased from 19.5% to 7%. Although this strain may seem marginal in comparison to the acceptable liner strain, it was considered acceptable due to the very conservative assumptions embedded into Scenario 2, including the majority of the heap leach foundation assumed to be compressible.

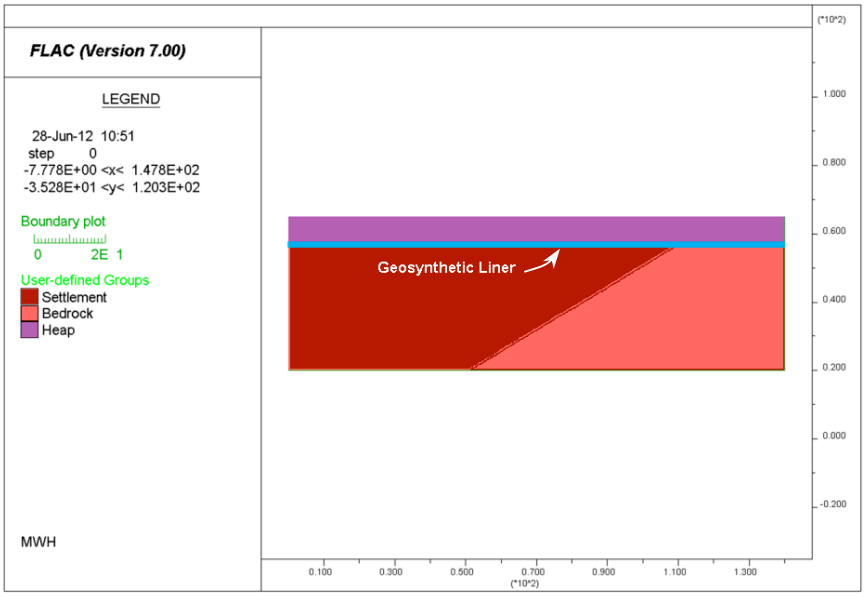


Figure 8. General view of Scenario 2a used for differential settlement analysis

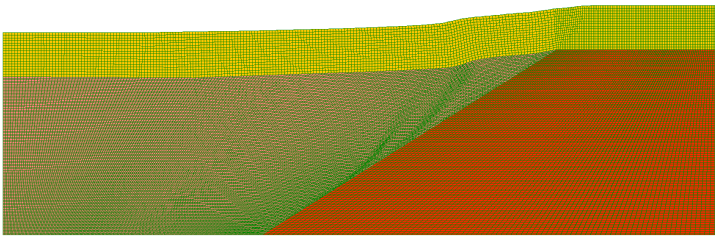


Figure 9. Deformed mesh after placing the 8 m heap for Scenario 2a

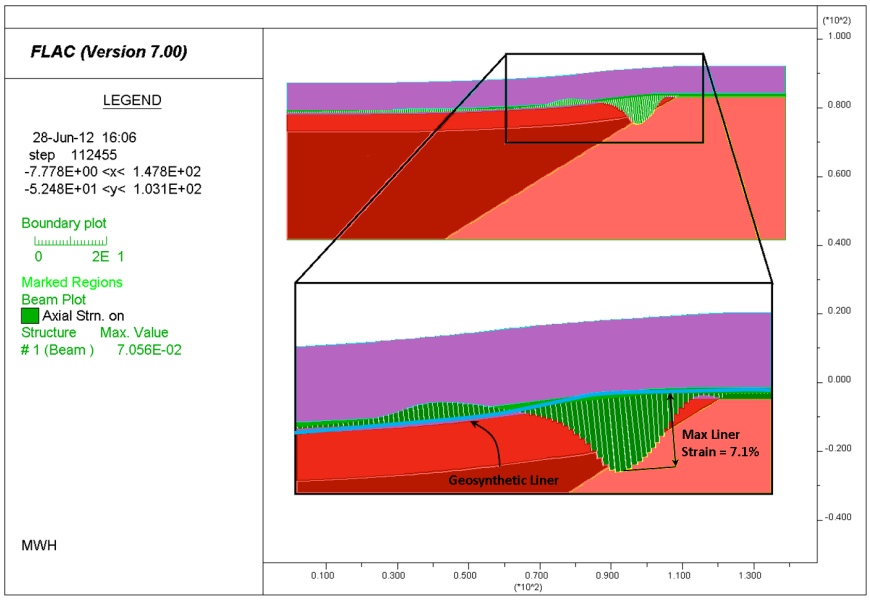


Figure 10. The maximum liner strain for Scenario 2a

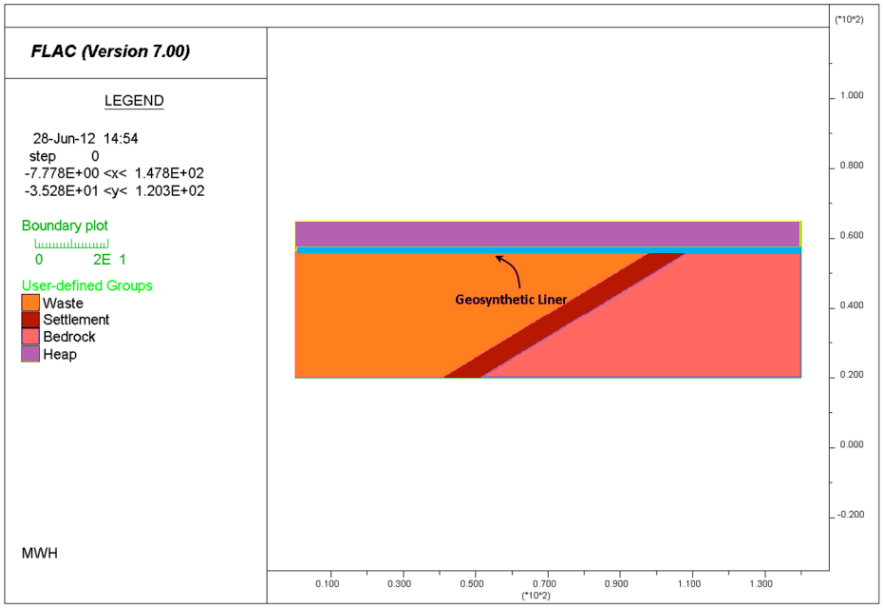


Figure 11. The maximum liner strain for Scenario 2b

4.1.3 *Scenario 3*

Scenario 3 is similar to Scenario 2 except instead of assuming that all the WSF consists of soft material, only a 10 m band of WSF adjacent to the bedrock is modeled as soft material. This is shown in Figure 12. The deformed mesh after construction of the 8 m heap and the calculated strains along the liner for Scenario 3 are shown in Figures 13 and 14, respectively.

Scenario 2a showed a higher maximum liner strain than Scenario 3. Therefore, only Scenario 2a was selected for further evaluation using a 5 m thick compacted waste cap, a 0.6m overliner, and a 0.6 m underliner. This evaluation was performed as Scenario 2b and the results shown in Figure 11. It is expected that adding the compacted waste and overliner/underliner layers to Scenario 3 would result in the maximum liner strains lower than that calculated in Scenario 2b (7%) and would be within the acceptable range.

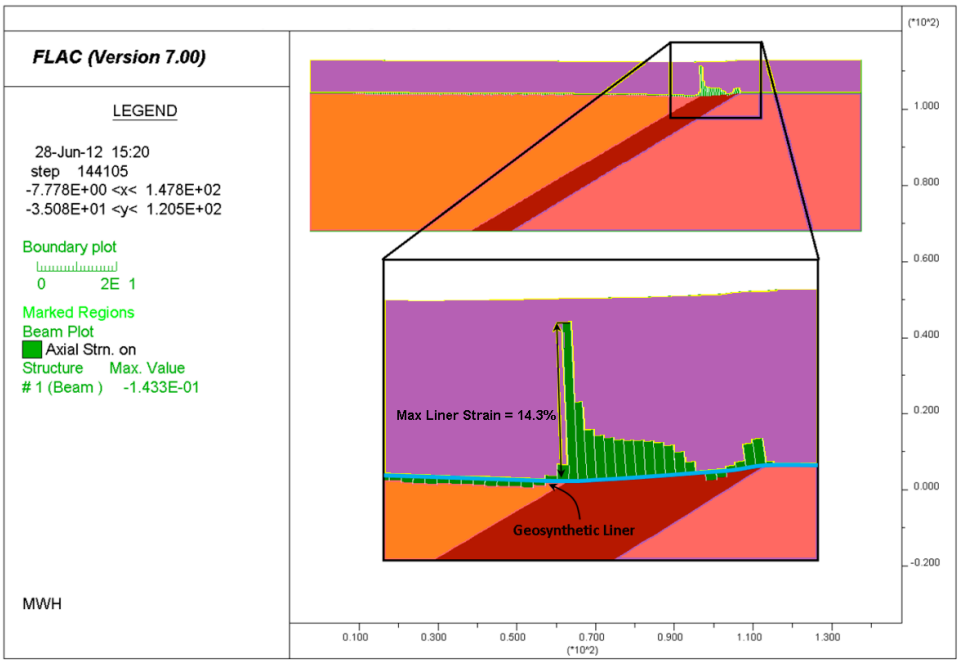


Figure 12. General view of Scenario 3 used for differential settlement analysis

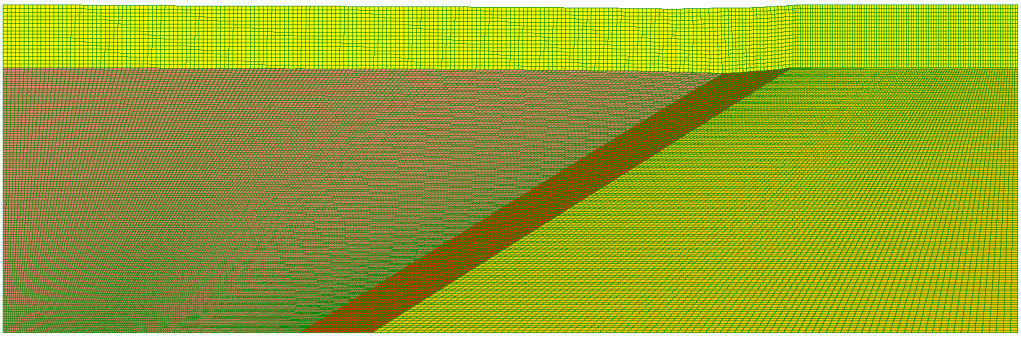


Figure 13. Deformed mesh after pacing the 8 heap for Scenario 3

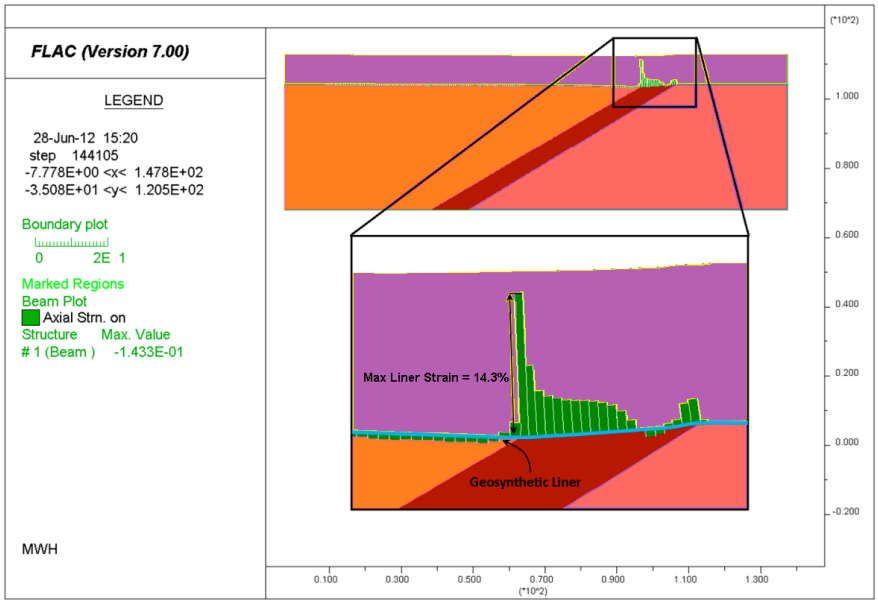


Figure 14. The maximum liner strain for Scenario 3

5 CONCLUSIONS

This paper presents the differential settlement modeling performed to evaluate the integrity of the proposed liner for a heap leach pad at a South American mine subject to differential settlement. First, a 50 m deep and 10 m wide column of soft waste was simulated in the middle of the waste deposit to determine the displacements and strains developed in the liner due to settlement of the soft layer after placement of an 8m high heap. The properties of the soft layer were chosen such that the final settlement in the absence of the underliner, overliner, and compacted waste layer considered in subsequent analyses was 80 cm, where 80 cm is the calculated total consolidation of the existing waste as a result of the additional load exerted by the heap. The maximum liner tensile strain due to this settlement was calculated as 11.1% without considering the 5 m compacted waste cap, 0.6 m overliner, or 0.6 m underliner. When these components were taken into consideration, the maximum liner tensile strain was reduced to 0.02%.

The second modeling case simulates another potential critical condition of differential settlement. In this case the soft waste material is located adjacent to the bedrock (i.e. adjacent to an incompressible material). The results from the analyses showed that the maximum liner tensile strain can become as high as 19% if the 5 m compacted waste and the overliner and underliner are not included in the simulation. However, by taking the 5 m compacted waste cap, 0.6 m overliner and 0.6 m underliner into consideration, the calculated maximum liner strain was reduced to 7.1% which is taken as the limit of acceptable tensile strains for an LLDPE liner.

Furthermore, Scenario 2b assumed that the entire WSF consisted entirely of soft waste material, which is a highly conservative assumption as the properties of the soft waste material are based on the weakest material found in the previous SPT exploration of the WSF, which is not representative of the entire WSF. Another conservatism used in this study is assuming a 50 meter deep soft layer in all the analyses. Fifty meters is the maximum depth of the waste under the leach heap, but most of the leach heap will be placed over waste with thickness less than 50 meters. Additionally, considering the fact that the waste materials are being placed in 1 to 2 meter lifts over a long period of time and in a large area, it is highly unlikely that soft material will be placed directly and repeatedly over soft material to build a continuous column of soft waste material that is 10 meters wide and 50 meters deep.

The results of the modeling showed the important role of the compacted waste cap, overliner, and underliner for reducing liner strains. This emphasizes the importance of the construction of a firm and well compacted foundation for the leach pad.

Based on the FLAC modeling of the settlement and the available data, our judgment, based

on conservative design criteria, is that as long as a competent foundation is provided, differential settlement of the underlying waste is not a threat to the integrity of the proposed heap leach pad liner on the WSF.

As the project moves into more detailed design, we will use the differential settlement model presented in this paper to optimize the cap thickness and location, any further waste characterization and the pad design details.

6 REFERENCES

ITASCA, 2000. Fast Lagrangian analysis of continua (FLAC), *Version 4, User's Guide*. Itasca Consulting Group, Inc., Thrasher Square East, 708 South Third Street, Suite 310, Minneapolis, Minnesota.

Cadwallader, M. W. 1987. Small Mines Development in Precious Metals 1987 . Chapter 23 - Low Cost Processing For Precious Metals Recovery. ISBN: 0-87335-069-3

Covers and Closure Planning

Distributed temperature observations reveal the scale of spatial variability in unsaturated soil covers

L.K. Tallon & M. O'Kane
O'Kane Consultants Inc, Saskatoon, Saskatchewan, Canada

B.C. Si
Department of Soil Science, University of Saskatchewan, Saskatoon, Saskatchewan, Canada

S.L. Barbour
Department of Civil and Geological Engineering, University of Saskatchewan, Saskatoon, Saskatchewan, Canada

ABSTRACT: Unsaturated reclamation soil covers are designed under the assumption of homogeneous, one-dimensional behaviour across the entire spatial extent. This assumption is rarely, if ever, tested. The costs associated with measuring water content often preclude intensive monitoring to verify soil cover homogeneity. Distributed Temperature Sensing (DTS) is an emerging technology that uses fibre optic cables and a laser reader to measure temperature every metre at ranges up to thousands of metres. Applying this technology to monitoring of reclamation soil covers allows for an investigation of the spatial and temporal scales of variation. Cover systems at uranium and oil sands mines were instrumented with a DTS system. An investigation of temperature variability using geostatistical techniques revealed that cover physical properties had a strong influence on the scales of variation.

1 INTRODUCTION

Mining companies are required to reconstruct functioning landscapes that reproduce the associated functions of natural watersheds as a precondition for operation (Carey, 2008). The industry has extensively used engineered soil covers to achieve this condition (Nicholson et al., 1989; Yanful, 1993). Current soil cover design methods attempt to optimize key vadose zone processes such as maximizing evapotranspiration and minimizing net percolation in a subsection of designs known as Unsaturated, Evapotranspirative (ET) or Store and Release covers. (McGuire, et al., 2009; Blight and Fourie, 2005; Albright, et al., 2004; Hauser, et al., 2001; Khire, et al., 1997). The dynamics of these cover systems is governed by the physical properties of the cover material and the coupled heat and mass transfer within the cover itself and between the cover and the atmosphere (Kelln et al., 2008).

The current state of practice for cover design involves the construction of small test covers with localized soil profile monitoring of suction, water content, and temperature. Performance monitoring centers on reducing the net annual percolation below the cover into the waste to an acceptably small percentage of precipitation input (Scanlon et al., 2006). Monitoring data are interpreted using one-dimensional numerical models to simulate field water and energy dynamics. One-dimensional analyses have been found to be inadequate in predicting percolation and runoff when they are extrapolated to the field scale (Ogorzalek et al. 2008; Bohnhoff et al. 2009; McGuire et al. 2009). Furthermore, in the soil science discipline it has long been accepted that a full characterization of the spatial variability of certain soil parameters will lead to a more complete understanding of the system (Oliver, 1987). A well-characterized system optimizes what is known as the scale triplet of spacing, extent, and support (Blöschl and Grayson, 2000). By optimizing the triplet a balance is struck between capturing small-scale variability, covering large spatial extents, and sampling a volume that is not so large as to artificially smooth the data

(Blöschl and Grayson, 2000). Despite the recognition that spatially distributed measurements of various performance parameters is important, there remains a paucity of data on the subject, especially with regards to unsaturated soil covers.

Distributed temperature sensing (DTS) is a system that precisely measures temperatures at high spatial and temporal resolutions (Tyler et al., 2009). A DTS system uses a high-powered laser to interrogate a fiber-optic cable. The backscattering of the light pulse is partitioned into a wavelength of the incident light, and wavelengths that are slightly above and below the incident wavelength. The latter two wavelengths are known as the Stokes and Anti-Stokes wavelengths, and the ratio of the two are temperature sensitive. The utility of a DTS system lies in the optimization of the scale triplet. Spatial resolutions are as high as 1 m while extending up to 5000 m. Temporal resolution can be as high as every 30 seconds, depending on the integration time of the signal. In this way, a cover system can be instrumented with a fiber-optic cable and can be monitored for temperature every meter for thousands of meters every 30 seconds.

Soil temperature is an important variable of interest in mine reclamation, albeit one that is most often overlooked in favor of soil water content. Soil temperature is a key state variable in the surface energy balance and is linked to the soil water balance through the latent energy term. Fluctuations in soil temperatures are governed by soil physical and thermal properties, the partitioning of radiation at the surface, and the volume of water in the subsurface (Hillel, 1998). Given the ease with which temperature is measured with a DTS system, the spatial distribution of temperatures in covers systems warrants further investigation.

Distributed temperature sensing has recently been used in the earth sciences, particularly in the area of stream hydrology (Selker et al., 2006a,b). The method has also been applied as a means of estimating water content through thermal diffusivity (Steele-Dunne et al., 2010; Rutten et al., 2010; Krzeminska et al., 2011). While inferring soil water content by passively monitoring thermal diffusivity has showed initial promise, the technique suffers from a non-unique relationship between diffusivity and water content (Steele-Dunne et al., 2010). The uncertainty involved in inferring soil water content from thermal properties may make the technique unsuited to examining the spatial variability of cover systems.

Spatial variations in soil temperature have been investigated previously. Vauclin et al. (1982) examined the spatial structure of soil temperature and found it to be well correlated with soil water content. Mohanty et al. (1995) found that spatial correlations will change based on soil physical properties. Interestingly, it was found by Mohanty et al. (1998) that soil temperature will vary temporally in hysteretic loops with minimum temperature variances occurring at the point of daily temperature minimum. Soil temperature demonstrates spatial and temporal structure and can be used to examine the scales of variability in reclamation cover systems.

The implicit assumption in the design of unsaturated soil covers is that disturbance of the cover materials in cover construction will serve to homogenize the cover, thus obviating the need for investigating spatial variability of cover soil parameters. However, this assumption has never been tested. Given the lack of data existing for the mining industry, further investigation into the spatial scales of cover system variability is warranted. The objective of this study was to i) investigate the utility of intensive temperature monitoring in unsaturated soil covers using a DTS system; and ii) to provide a preliminary assessment of the spatial variability of temperature as it relates to physical parameters in unsaturated soil systems.

2 MATERIALS AND METHODS

2.1 *Study Area*

A field experiment was conducted at a uranium mine in northern Saskatchewan, Canada, from August 20 to 28, 2011. The study area was a waste rock dump on which a cover system had been constructed two months prior to commencing the field study. The cover system consisted of a 1 ha plateau and a 0.5 ha slope. The plateau area had a 2% south facing slope and the slope faced north at 25%. The cover system was constructed to a nominal thickness of 1 m using fine sand salvaged from a local drumlin. Average sand, silt, and clay content were 94, 5, and 1%, respectively, with an average bulk density of 1.55 g cm^{-3}.

2.2 *Climate*

Climate at the site was classified as continental. Thirty year climate normals indicated mean January and July air temperatures of -23 and +16 °C, respectively. Thirty year mean annual precipitation was 481 mm (Carey et al., 2005).

2.3 *DTS System*

An Oryx DTS-SR (Sensornet, UK) was used for the field experiment. The Oryx was field deployable and had a measurement range up to 5000 m with a 1 m measurement resolution. Temperature resolution was 0.05 °C with a 60 s integration time. Measurements were calibrated by reserving a 50 length of cable to be kept in an ice bath. The temperature along that 50 m portion was calibrated against a pair of PT-100 platinum thermistors. The DTS system was powered by deep cycle batteries that were charged with a solar panel array.

The fiber-optic cable installed at the site was the Sensornet DamSense cable (Sensornet, UK). The DamSense cable was 5.5 mm in diameter and was rated for accurate temperature measurements from -55 to +85 °C.

2.4 *Cable Installation*

A 500 m fiber-optic cable was installed in a linear transect that was excavated into the existing cover system. The transect extended for 65 m on the plateau and 35 m down the slope. Cable was installed at 90, 50, 10, and 0 cm. Note that the 0 cm cable was laid on the surface and was only covered with enough material so as to not be directly exposed to the atmosphere.

The installation process proceeded as follows: a trench was excavated with an excavator. Once the proper depth was reached, the cable was laid out by hand and protected with a layer of cover sand. The trench was then backfilled until the next depth was reached, at which point the process repeated. In this way, the cable was extended in one continuous length and wrapped back on itself to proceed to the next depth.

2.5 *Data Collection*

Spatially distributed temperature measurements were taken with the DTS system every 20 minutes with a 60 s integration time for the duration of the field experiment. Soil temperature data were complimented by climatic data from an automated meteorological station 20 m from the transect. The meteorological station collected data on air temperature and humidity, wind speed and direction, and all-component radiation.

2.6 *Data Analysis*

The spatial structure of soil temperature data along the transect was analyzed using semivariograms (Isaaks & Srivastava, 1989). Temperature data were aggregated across all days to form a single minimum and maximum temperature dataset for each individual depth. Aggregated semivariograms were calculated using (Si et al., 2007):

$$\gamma(h) = \frac{1}{2N(h)} \sum_{k=1}^{N(h)} [T(x_k) - T(x_h + h)]^2 \quad (1)$$

where N is the number of pairs at lag distance, h, $T(x_k)$ is the measured soil temperature at location x_k, and $T(x_k+h)$, the soil temperature at location x_k increased by h lags. Semivariograms were then fit with a spherical model (Si et al., 2007):

$$\gamma(h) = c_0 + 1.5\frac{h}{\alpha} - 0.5\left(\frac{h}{\alpha}\right)^3 \quad (2)$$

where c_0 is the nugget, or the extrapolated semivariance at lag = 0, and α is the range, or the lag at which the semivariance reaches a plateau and becomes constant. The semivariance at which the range is reached is known as the sill. A spherical model can be combined to form nested models in the case of a semivariogram that displays more than one obvious structure.

Spatial dependence provides an indication of the distance at which any particular measurement remains similar to another measurement. For example, in a field that exhibits high spatial dependence, the degree of similarity between two points depends greatly on how proximal they are to each other. At low spatial dependencies, two measurements can be located large distances apart and still be similar. Spatial dependence describes how much two points being similar depends on the distance between those points. Spatial dependence is calculated as the ratio of the nugget to the sill. Spatial dependence <25% is considered strong, values between 25 and 75% are considered moderate, and spatial dependencies > 75% are indicative of little to no structure (Si et al., 2007).

3 RESULTS

3.1 *Preliminary Data Analysis*

The field experiment was conducted in late August as air and soil temperatures were beginning to decline from their summer maxima (Fig. 1). Average air temperature was 15.6 °C and average soil temperatures were 13.9, 13.9, 15.7 and 14.6 °C at the 0, 10, 50, and 90 cm depths, respectively. The highest average soil temperature at 50 cm depth was indicative of the lag in temperature propagation with depth. Preliminary indications of spatial variability of soil temperature, as denoted by the coefficient of variation (CV = standard deviation / mean) demonstrated that variability decreased with depth. Soil temperature CVs were 29, 19, 5, and 2% at the 0, 10, 50, and 90 cm depths, respectively.

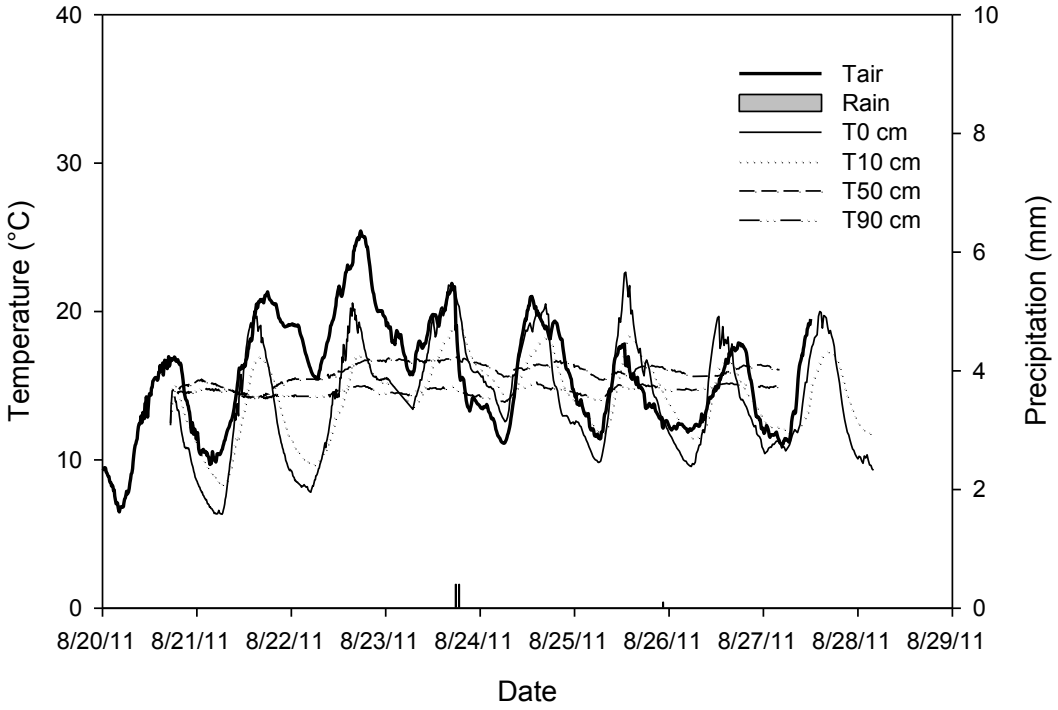


Figure 1. Meteorological and soil temperature data recorded during the field experiment.

Physical properties of the cover system were homogeneous across the entire transect (Fig. 2). Coefficients of variation for percent sand content and bulk density were 2.2 and 5.8%, respectively. The increased CV for bulk density was likely a result of the inherent difficulty in taking precise bulk density measurements in the field.

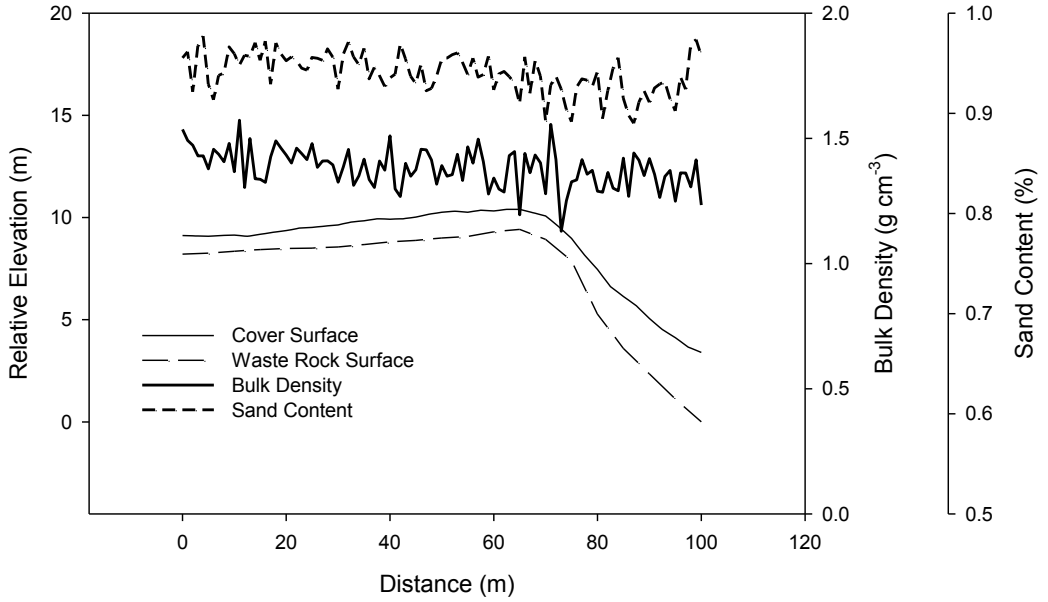


Figure 2. Spatial variation of bulk density, sand content, and relative elevation profile of the cover system experimental transect.

3.2 *Temperature Contours*

Cover system temperatures measured with a DTS system demonstrated homogeneity in both time and space (Fig.3). Cover system temperatures and qualitative indications of variability decreased between depths (Fig. 3 a, b, c, d). Within a given depth, the patterns of soil temperature did not show marked changes between days. Similar temperatures between days compared well with air temperature measurements, as no single day had substantially higher or lower air temperatures during the experiment. The majority of cover system temperature variation occurred within a given days as a function of transect distance. A zone of distinctly cooler temperatures consistently occurred from 65 to 100 m across each day during the experiment. This area corresponded to the slope area with a northern aspect.

3.3 *Semivariogram Analysis*

3.3.1 *Physical Properties*

Semivariograms of sand content and bulk density are indicative of a physically homogeneous cover system (Fig. 4). Neither semivariogram in Figure 4 reached a sill, or the point at which spatial autocorrelation is zero. The physical interpretation is that any measurement taken at any point on the transect is correlated with every other measurement, even at the maximum spatial extents. Therefore, a measurement taken at the origin of the transect is still spatially correlated to a measurement taken at the transect terminus. The bulk density semivariogram displayed the same behavior as that for sand content, albeit with a higher nugget value and greater dispersion of points. The higher nugget and greater dispersion is explained by the lower measurement precision of taking bulk density samples of a sand in the field.

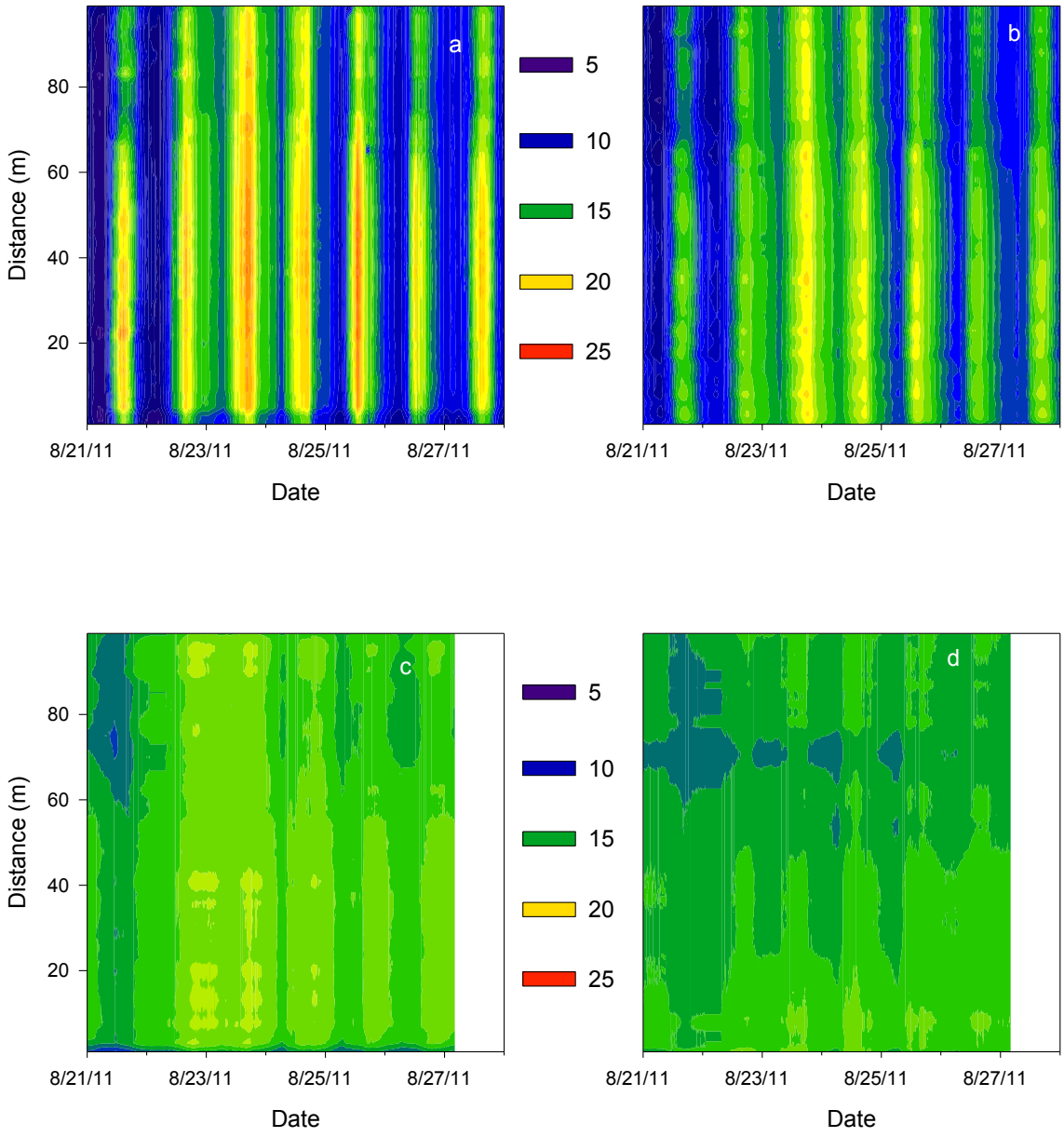


Figure 3. Distributed soil temperature values for the field experiment measured at a) 0, b) 10, c) 50, and d) 90 cm depths.

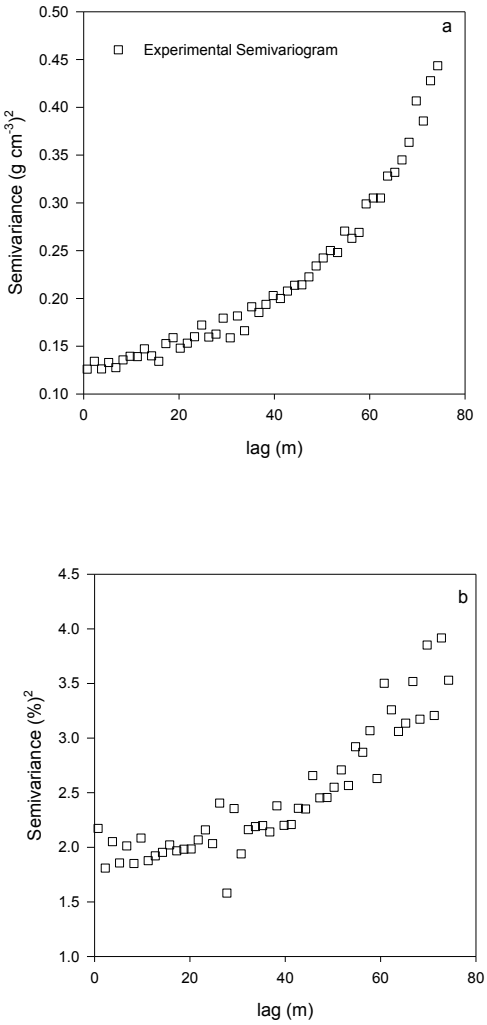


Figure 4. Semivariograms for a) percent sand content and b) bulk density.

4 DISCUSSION

Analysis of spatially distributed cover system temperatures revealed the spatial scales of variability at the field experiment. Initial analysis indicated a physically homogeneous cover system with low coefficients of variability. Temperatures monitored at a single point did not provide any indication of differential behavior at other locations. Spatially distributed temperatures demonstrated areas of distinctly different thermal behavior for each day of the field experiment. However, discussion of the differences remained qualitative unless more advanced data analysis techniques were applied.

Geostatistical analysis using semivariograms quantified what was seen qualitatively with temperature contours. Semivariograms for all depths reached a sill at short ranges from 2 to 28 m. Secondary structure was found at approximately 40 m for all depths. Although semivariograms do not convey any information as to the location of a certain process, the sharp division between plateau and slope allow some room for inference. The plateau extends a distance of 60 m and is south facing. The lack of vegetation or microtopography allows the plateau area to heat and cool as a distinct unit. Strong spatial dependencies at this scale mean that any measurement take on the plateau will be similar to another measurement taken at any other location on the plateau, even if they are separated by 60 m. For the slope, however, spatial dependencies were not as strong, and in some cases, two measurements could be separated by as little as 2 m before any autocorrelation was lost.

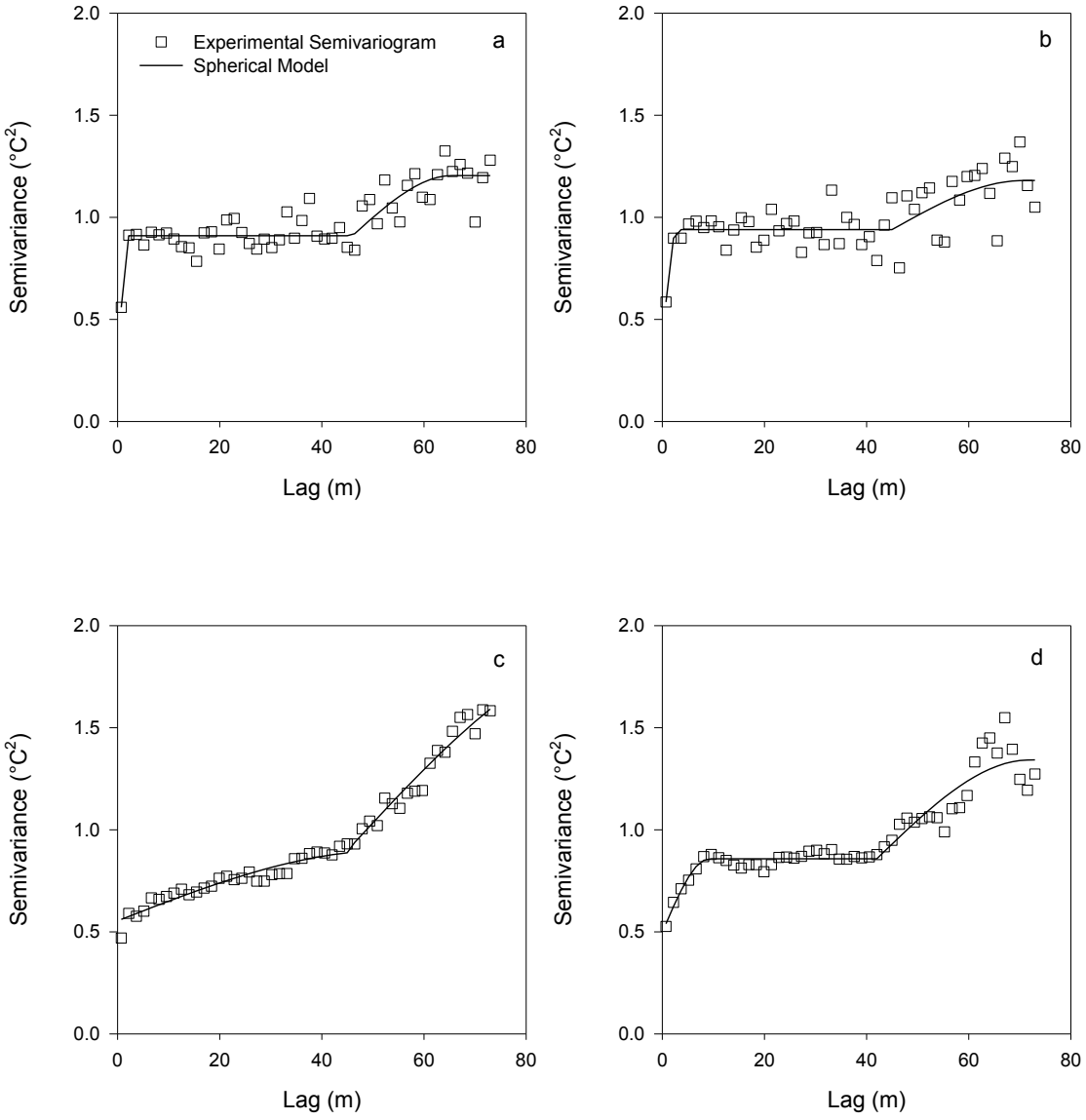


Figure 5. Semivariograms of minimum spatial temperature the experimental transect at a) 0, b) 10, c) 50, d) 90 cm.

5 SUMMARY

The field experiment presented above represents a fairly simplistic case: the borrow material was homogenized during salvage and placement, and the landform was designed to be devoid of topographical heterogeneity. The only major macroscopic difference in the cover system was the division of the system into plateau and slope areas. Clearly some difference between the plateau and slope would be expected. However, the salient point remains that any differences in performance or the effect of governing process would remain as speculation unless verified through spatially distributed monitoring as demonstrated. The techniques demonstrated in the current manuscript can be applied to larger systems designed with greater heterogeneity.

6 REFERENCES

Albright, W. H., Benson, C. H., Gee, G. W., Roesler, A. C., Abichou, T., Apiwantragoon, P., Lyles, B. F. and Rock, S. A. 2004. Field water balance of landfill final covers. J. Environ. Qual. 33: 2317-2332.

Blight, G.E., and A.B. Fourie. 2005. Experimental landfill caps for semi-arid and arid climates. Waste Manage. Res. 23:113-125.

Blöschl, G. and R. Grayson. 2000. Spatial observations and interpolation. p. 17-50. In Grayson, R. and G. Blöschl (eds.) Spatial patterns in catchment hydrology: Observations and modeling. Cambridge University Press, United Kingdom.

Bohnhoff, G.L., A.D. Ogorzalek, C.H. Benson, C.D. Shackleford, and P. Apiwantragoon. 2009. Field data and water-balance predictions for a monolithic cover in a semi-arid climate.

Carey, S.K. 2008. Growing season energy and water exchange from an oil sands overburden reclamation cover, Fort McMurray, Alberta, Canada. Hydrol. Process. 22: 2847-2857.

Carey, S.K., S.L. Barbour, and M.J. Hendry. 2005. Evaporation from a waste-rock surface, Key Lake, Saskatchewan. Can. Geotech. J. 42: 1189-1199.

Hauser, V. L., Weand, B. L., and Gill, M. D. 2001. Natural covers for landfills and buried waste. J. Envir. Engrg. 127(9): 768-775.

Kelln, C., Barbour, L. and Qualizza, C. 2008.Controls on the spatial distribution of soil moisture and solute transport in a sloping reclamation cover. Can. Geotech. J. 351-366.

Khire, M. V., Benson, C. H., and Bosscher, P. J. 1997. Water balance modeling of earthen final covers. J. Geotech. Geoenvir. Engrg. 123(8): 744-754.

Kellner, E. 2001. Surface energy fluxes and control of evapotranspiration form a Swedish Sphagnum mire. Ag. For. Met. 110: 101-123.

Krzeminska, D.M., S.C. Steele-Dunne, T.A. Bogaard, M.M. Rutten, P. Sailhac, and Y. Geraud. 2011. High-resolution temperature observations to monitor soil thermal properties as a proxy for soil moisture condition in clay-shale landslide. Hydrol. Process. DOI: 10.1002/hyp.7980.

McGuire, P.E., B.J. Andraski, and R.E. Archibald. 2009. Case study of a full-scale evapotranspiration cover. J. Geotech. Geoenviron. Eng. 135(3): 316-332.

Mohanty, B.P., W.M. Klittich, R. Horton, and M. Th. Van Genuchten. 1995. Spatio-temporal variability of soil temperature within three land areas exposed to different tillage systems. Soil Sci. Soc. Am. J. 59(3): 752-759.

Mohanty, B.P., P.J. Shouse, and M.T. van Genuchten. 1998. Spatio-temporal dynamics of water and heat in a field soil. Soil Till. Res. 47: 133-143.

Nicholson, R.V., R.W. Gillham, J.A. Cherry, and E.J. Reardon. 1989. Reduction of acid generation in mine tailings through the use of moisture-retaining cover layers as oxygen barriers. Can. Geotech. J. 26:1-8.

Ogorzalek, A.S., Bohnhoff, G. L., Shackelford, C. D., Benson, C. H., and Apiwantragoon, P. 2008. Comparison of field data and water-balance predictions for a capillary barrier cover. J. Geotech. Geoeng. 134(4):470-486.

Oliver, M.A. 1987. Geostatistics and its application to soil science. Soil Use Manage. 7: 206-217.

Rutten, M.M., S.C. Steele-Dunne, J. Judge, and N. van de Giesen. 2010. Understanding heat transfer in the shallow subsurface using temperature observations. Vadose Zone J. 9: 1034-1045.

Selker, J.S., N. Van De Giesen, M. Westhoff, W. Luxemburg, and M. B. Parlange. 2006a. Fiber optics opens window on stream dynamics. Geophys. Res. Lett. 33. doi:10.1029/2006GL027979.

Selker, J.S., L. Thévenaz, H. Huwald, A. Mallet, W. Luxemburg, N. Van De Giesen, M. Stejskal, J. Zeman, M. Westhoff, and M. B. Parlange. 2006b. Distributed fiber-optic temperature sensing for hydrologic systems. Water Resour. Res. 42 (12). doi:10.1029/2006WR005326

Steele-Dunne, S.C., M.M. Rutten, D.M. Krzeminska, M. Hausner, S.W. Tyler, J.S. Selker, T.A. Bogaard, and N.C. van de Giesen. 2010. Feasibility of soil moisture estimation using passive distributed temperature sensing. Water Resour. Res. 46: W03534, doi:10.1029/2009WR008272, 2010.

Tyler, S.W., J.S. Selker, M.B. Hausner, C.E. Hatch, T. Torgersen, C.E. Thodal, and S.G. Schladow. 2009. Environmental temperature sensing using Raman spectra DTS fiber-optic methods. Water Resour. Res. 45. W00D23, doi:10.1029/2008WR007052, 2009.

Yanful, E.K. 1993. Oxygen diffusion through soil covers on sulphidic mine tailings. J. Geotech. Eng. 119(8):1207-1228.

Case study: experimental cells complex in permafrost environment

J-F St-Laurent, Y. Jalbert, M. Paradis, A. Hébert
SNC-Lavalin inc., Québec, Québec, Canada

ABSTRACT: An Experimental Cells Complex (ECC) was built to support Raglan Mine current tailings stack facility reclamation cover concept. The ECC area is about 4,600 m^2 and is composed of four juxtaposed independent cells reproducing four distinct reclamation cover options. To understand the behavior of each cover in response to seasonal and hydrological variation, many physical properties were recorded and soil parameters were measured. A total of 18 thermistor strings, 43 unfrozen soil volumetric water content and suction sensors, 22 gaseous oxygen content sensors, and 12 tailings oxygen consumption tests stations were installed. Water/moisture behavior during the first year of data recording is presented in this paper. It is shown that soil water characteristic curve and soil freezing curve have been affected by field boundary conditions. This paper also presents the convective air flow impact over tailings temperature based on the first year collected data.

1 INTRODUCTION

The Raglan Mine property is located in the northern tip of the Ungava (Nunavik) Peninsula in the Province of Quebec, Canada (Nouveau Québec) north of the 61st parallel, as shown in Figure 1. The mine site is approximately 1,800 kilometres north of Montreal. Mean annual temperature on site, for the past 12 years, is about -9.3°C with a mean maximum value of 8.6°C during summer (July) and a mean minimum temperature of -26.2°C during winter (February). Snow accumulates on ground from mid-September to mid-June and air temperature is above 0^{o}C from July to September. The mean annual precipitation in this region increased between 1970 and 2005 from 560 mm to 620 mm (SLI, 2012).

Raglan Mine Tailings Storage Facility (TSF) is located on a local high ground approximately 2 km north-east of the accommodation and processing facility and is in operation since 1997. Filtered tailings produced by the milling operation have a grain size distribution corresponding to sandy silt (about 70% silt size). TSF current reclamation concept was designed to integrate tailings to permafrost conditions and keep them frozen during a warm year event with a recurrence of 1:100 years. This cover was designed as a walk-away solution which had the double function in the long term of providing an insulation cap and preventing TSF surface erosion what should limit any release of contaminant into the environment. Climate change issues and expected global warming raised concerns about the long term performance of this concept. To review and support the current TSF reclamation cover concept, an Experimental Cells Complex (ECC) was built in 2011/2012 to assess the reliability of four cover options. All concepts have

the objective to prevent environment contamination. Two concepts are using a thermal cover. One concept is using a low permeability layer (geomembrane) to stop water infiltration and the other one concept is using a thermal capillary barrier preventing water and oxygen infiltration and acting as heat damping layer. The ECC was designed to compare these four cover options and gain a better understanding of how these covers will react to site conditions by monitoring their behavior over a period of at least three years. Recorded data will also be used numerical model calibration purpose.



Figure 1. Site location

At this stage of the project, recorded data cover only one year of monitoring and it is too early to complete the concept selection. However, recorded data is used to improve our understanding of fundamental mechanism governing heat transfer, water transport/infiltration, oxygen variation, consumption and diffusion into the unsaturated cover material. This paper overviews mechanisms associated to water transport/infiltration and convective heat flow, provides a description of the ECC main design and characteristics and presents one year of selected data.

2 ECC DESCRIPTION

2.1 *Location and geometry*

As shown in Figure 2, ECC is located on the southwest side of the TSF near its southern corner. The ECC's upper 1/3 portion is located on the TSF's top 4% slope and its lower 2/3 part on the 5H:1V south-west face. The ECC was constructed in alignment with the slope. This configuration allows investigation of the effects of both slopes on the cover performance and provides maximum sun exposure. The ECC total length, width and area are roughly 61m, 76m and 4,600m^2 respectively. All cells have approximately the same dimensions, which have a horizontal surface length of 45m and a width of 15m. To reduce the influence that cells may have on each other (i.e.: boundary effect) and to allow stable and efficient construction process, an internal buffer zone of at least 2.5 m wide between each cell was implemented. An external buffer

zone of 2.0 to 5.0 m wide was implemented around the ECC. The thinnest cell was placed upwind to limit wind snow accumulation on the test pad surface.

2.2 *Cover options description*

As shown in Figure 3, Cell 1: Geomembrane Cover concept consists of a three layers design, including a geomembrane placed 0.4 m above tailings. The main objective of Cell 1 is to limit emission of contaminant by stopping water infiltration. Cell 2: Thermal Capillary Barrier concept is a three layer design, having a 0.5 m thick layer of 0-20 mm granular material mixed with powder bentonite (i.e.: the moisture retaining layer). The vertical hydraulic conductivity and suction distribution into that cell should limit vertical water and oxygen migration to the tailings, prevents tailings oxidation and limit the emission of contaminants. Also, once the moisture retaining layer will be saturated it should act as a heat dampening layer preventing the thaw of the tailings during the summer season. The moisture retaining layer was built by mixing 8% (w/w) of bentonite to the 0-20 mm material with an excavator. It was shown in laboratory testing, using thermo-gravimetric and relative density testing, that field samples had lost 1.5 to 2% of bentonite powder mass during cell construction (URSTM, 2012). It is then estimated that the moisture retaining layer contains $\pm$ 6% (w/w) of bentonite. This material was selected as fine material because no fine granular material is available on site. Cell 3: Base Case concept corresponds to the current two layer reclamation cover design. This concept consists of a 1.2 m thick 0-20 mm crushed rock layer under a 1.2 m thick layer of 0-600 mm. The objective if this concept is to integrate tailings into permafrost conditions. Tailings oxidation should then be limited as contaminant release. Cell 4: Modified Base Case – Convective Air Flow concept consists of a two layers design. Convective air flow into the coarser granular material should decrease tailings temperature and it was also assumed that during summer time, the cold air located at the base of the coarse granular material should act as insulation layer, protecting the frozen tailings from warmer temperature and limiting any contaminant release.

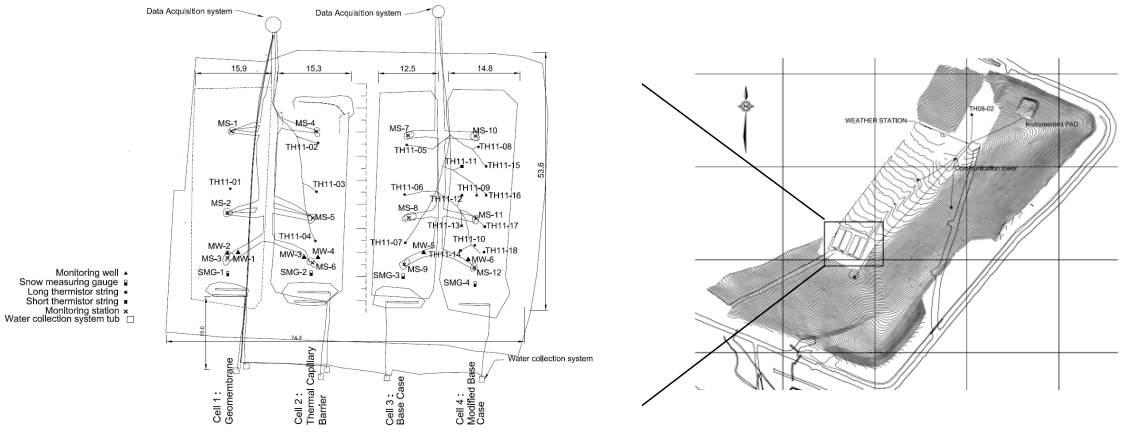


Figure 2. ECC layout and location

2.3 *Field instrumentation program*

To understand the behavior of each cover in response to seasonal and hydrological variation, numerous sensors were used to measure parameters at various locations along the slope. Collected data will also be used for numerical model calibration purpose. The instrumentation includes a weather station nearby the ECC, 18 thermistor strings, 43 unfrozen soil volumetric water content (UVWC) and soil suction or capillary pressure (CP) sensors, 22 gaseous oxygen content (OC) sensors, and 12 tailings oxygen consumption tests stations (OCT). Instrumentation was installed at strategic locations and depths inside and underneath each cover (Fig. 2, 3).

Also, monitoring wells, water collection systems and snow thickness measurement gauges were implemented to monitor water quality and establish water balance calculation.

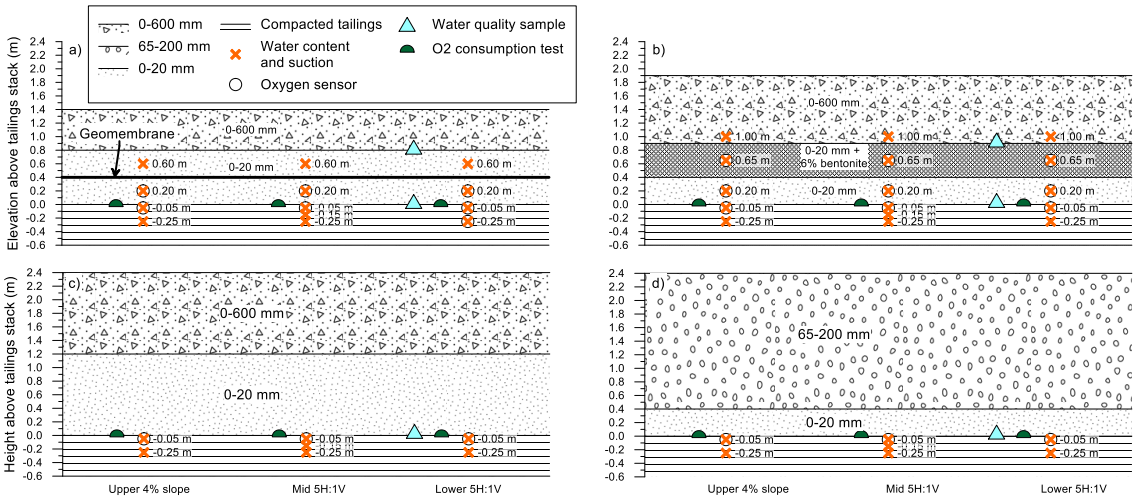


Figure 3. ECC concepts and instrumentations, a) Cell 1: Geomembrane cover, b) Cell 2: Thermal capillary layer cover, c) Cell 3: Base case cover, and d) Cell 4: Modified base case – Convective air flow cover.

Thermistor strings of 16 beads, down to a depth of 10 m into the tailings, are equally spaced and positioned along the central axis of each cell. Thermistor locations and beads depths are consistent from one cell to another in order to facilitate data analysis and comparison. About half of the 16 beads measure the temperature inside the cover and the other half measure tailings temperature. Eight (8) additional short thermistor strings, 2.4 m long, are positioned in cover of Cell 4 to monitor the convective air flow. These short thermistor strings, distributed in two rows parallel to the long axis of the Cell 4, are located within the coarse granular cover material. They are 2.5 m away from the cell centerline and equally spaced at 6.0m intervals.

During the ECC construction, excavated holes into frozen tailings were filled with fresh tailings, coming directly from the mill, to cover up sensors. All sensors and instrumentation are connected to a monitoring system having components certified to a temperature of -40°C.

Observed data shows that tailings temperatures recorded by the oxygen sensor are, most of the time, warmer than the temperature recorded by thermistor string at the same elevation (Fig. 4). Divergence between both sets of data is approximately +1 to +1.3°C, which corresponds to what is proposed by the sensor supplier (Apogee, 2013). The sensor warming tendency is due to the fact that Apogee sensors are equipped with a small heater, to prevent condensation on the oxygen porous membrane, hence affecting the temperature reading. The higher observed temperature is lower during winter time, and can be explained by the fact that the 74 mili-Watt (mW) drawn by the heater is not enough to warm the sensor by 1°C when the surrounding soil is cold (GKM, pers. comm.). However, this inaccuracy was neglected and oxygen sensor temperatures were used to correlate soil unfrozen volumetric water content, soil suction, soil oxygen content and tailings oxygen consumption tests because oxygen sensors are exactly at the same location and depth that other devices. In addition, the oxygen sensor warming effect must have impacted other recorded parameters, which have to be taken into consideration.

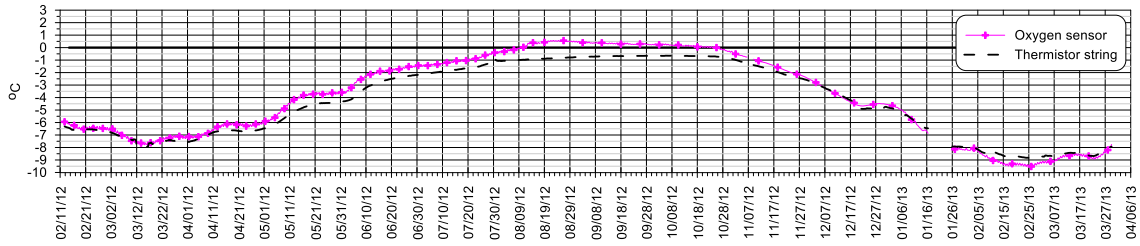


Figure 4. Oxygen sensor versus thermistor string recorded temperature, 0.05 m deep into tailings underneath Cell 1.

3 OBSERVED FIELD BEHAVIOUR

3.1 *Recorded soil unfrozen volumetric water content (UVWC)*

Changes in UVWC in response to rainfall for the 0-20 mm located above the liner (Cell 1), moisture retaining layer (Cell 2) and in the 0-20 mm layer of Cell 4 show similar characteristics. Monitored results of Cell 1 0-20 mm are presented in Figure 5.

Prior to the major rainfall at the end of June, 0-20 mm water content was nil. The significant water content increase at the end of June 2012, even if the soil temperature was below 0°C, is due to the fact that the ECC construction occurred in October the previous year and the soil pores were free of ice. Frozen soil hydraulic conductivity was then very high, allowing water to reach sensors without freezing. During that period, continuous rainfall kept the soil water content high, and the soil temperature was not low enough to freeze the water and decrease the UVWC into the 0-20 mm. MS03 lower values are associated to sensor initial calibration problem. No UVWC variation into the Cell 3 0-20 mm were recorded, due to the constant freezing conditions, water coming from rainfall did not reached the sensors.

Recorded water content variations through time in the moisture retaining layer of Cell 2 are shown in Figure 6. The water content of this layer is affect by rainfall, as observed into the 0-20 mm located above the geomembrane. However, the UVWC increase in the moisture retaining layer only started when the layer temperature reached 0°C. It is assumed that the strong UVWC variations at MS04 is associated to water accumulation on the cell flat surface at the end of summer 2012.

Since the change in UVWC and in soil suction through time for 0-20 mm located underneath the liner and moisture retaining layer show similar characteristics. Monitored results in Cell 1 are shown in Figure 7. The UVWC increased during the thaw process to reach a maximum value when soil temperature was at its maximum. Afterward, seepage or water/moisture suction by the bentonite layer above occurred, decreasing the 0-20 mm water content and increasing the soil suction. The recorded UVWC variations underneath the liner and moisture retaining layer is not affected by rainfall. When soil temperature dropped below 0°C, significant increase in suction occurred at MS03 due to water phase change.

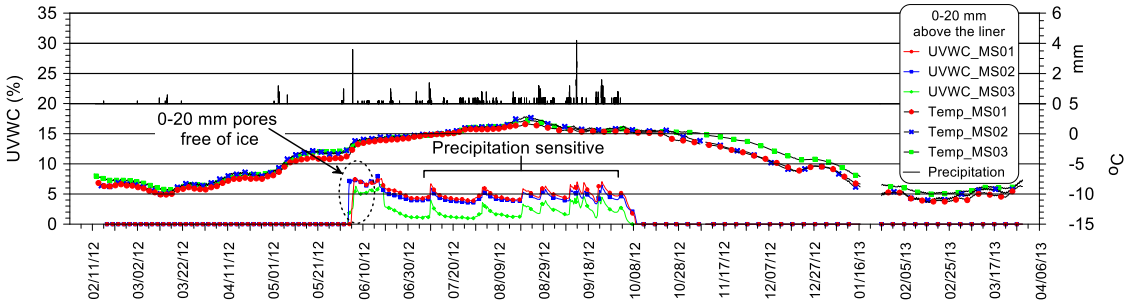


Figure 5. UVWC variation through time in cover 0-20 mm material above the Cell 1geomembrane

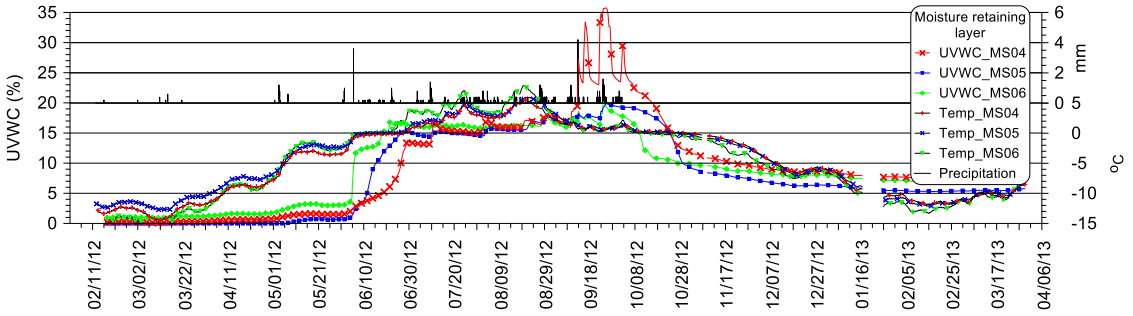


Figure 6. UVWC variation through time in the Cell 2 moisture retaining layer cover material

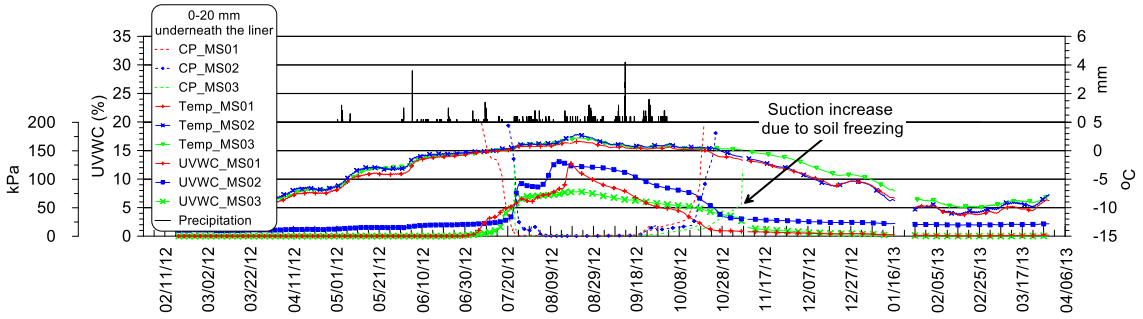


Figure 7. UVWC and soil suction variation through time in the 0-20 mm cover material underneath the Cell 1 geomembrane

As for overlying soils, the tailings UVWC increased during thawing to reach maximum value when their temperature was at its maximum. However, tailings UVWC variation under each cell did not show similar characteristics during summer time. Each cell presented different boundary conditions affecting tailings UVWC behavior. In this paper only tailings UVWC variation underneath Cell 1 is shown (Fig. 8). MS01 and MS03 (i.e.: up and down slope) UVWC were identical in July 2012, but behaved differently as time elapses. Up slope the water content decreased and down slope, it increased, to eventually decrease at the end of summer.

Based on the fact that both stations, MS01 and MS03, presented identical UVWC at the beginning of summer and tailings up slope dried out when the station located lower on the slope got saturated, it is postulated that seepage occurred in the tailings surface. This lateral water content variation was not observed underneath cells 2 and 3, even if tailings temperatures underneath Cell 2 are similar to the one recorded under Cell 1. Tailings UVWC underneath Cell 4 increased all summer long to reach very high value at the end of September. This increase is due to the coarse material extremely high hydraulic conductivity, allowing water to reach tailings.

Recorded values were used to establish soil water characteristic curves (SWC). As shown in Figures 9a, b the field 0-20 mm SWC do not match the laboratory curve determined be Coulombe (2012). The moisture retaining layer seems to affect the 0-20 mm SWC located above and below. For similar suction, water content in the 0-20 mm is higher in Cell 2 than in Cell 1. The bentonite content tends to absorb water and moisture, consequently increaseing the surrounding soil water content. It is interesting to notice the slope effect over the 0-20 mm SWC when the material is located underneath the moisture retaining layer, phenomenon not visible when only looking at the UVWC temporal distribution (Fig. 8). The 0-20 mm amended with bentonite field SWC (Fig. 9c) corresponds to what was found in laboratory (URSTM, 2013) with lower water content, probably due to field and laboratory conditions differing. In situ tail-

ings SWC are plotted in Figure 9d and are always lower than values found in the laboratory by Coulombe (2012).

Field soil freezing curves (SFC) were developed as shown in Figure 10. As for the SWC, the moisture retaining layer seems to affect the 0-20 mm SFC located above and below it (Fig. 10a, b). As presented by Koopmans & Miller (1966), soil unfrozen volumetric water content during freezing process are higher than what observed during thawing. However, when seepage occurs into soils during the summer time, modifying boundary condition, freezing curves can be observed below thawing curve, as shown in Figure 11, which is observed in 0-20 mm and tailings.

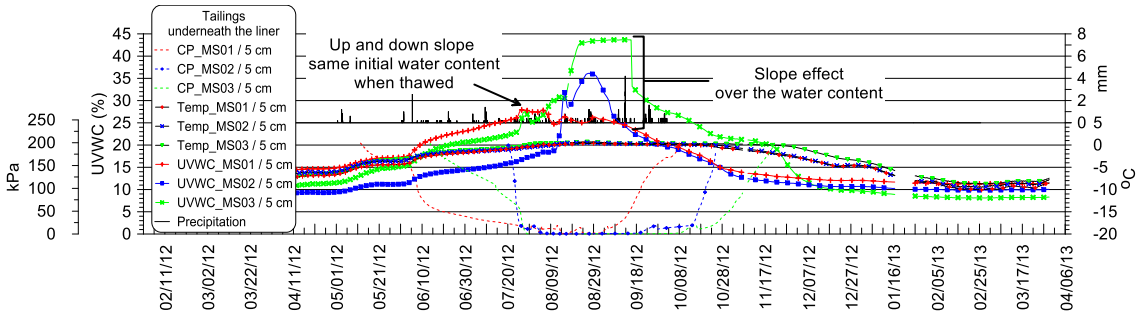


Figure 8. UVWC and soil suction variation through time in tailings underneath Cell 1 geomembrane

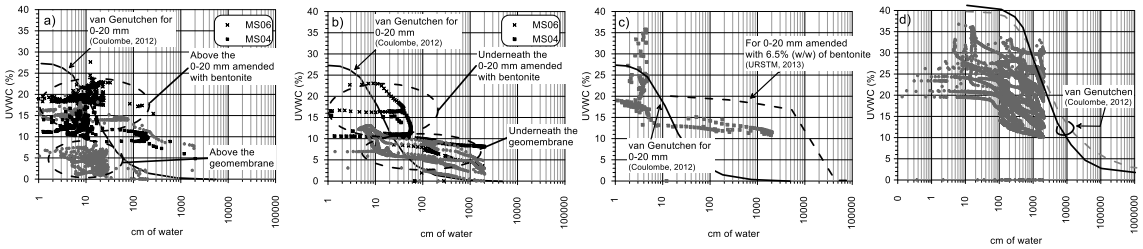


Figure 9. Field SWC, a) 0-20 mm above impervious layer, b) 0-20 mm below impervious liner, c) 0-20 mm amended with bentonite, and d) tailings

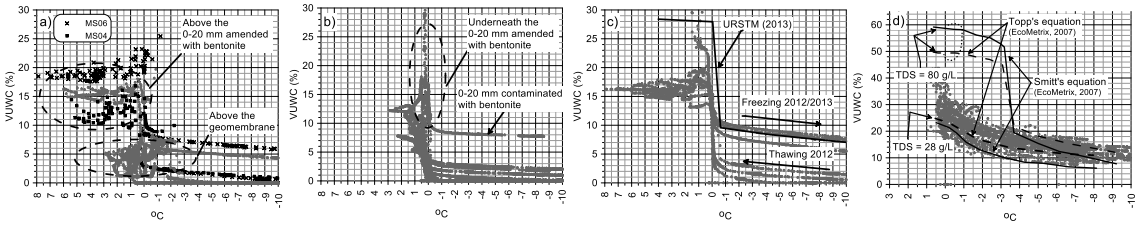


Figure 10. Field SFC, a) 0-20 mm above impervious layer, b) 0-20 mm below impervious liner, c) 0-20 mm amended with bentonite, and d) tailings

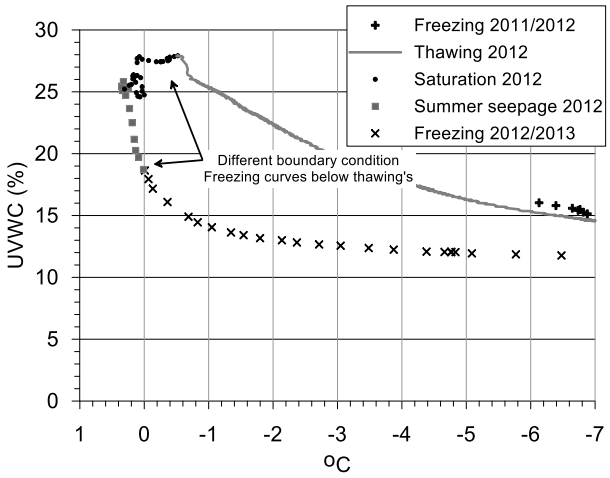


Figure 11. Tailings SFC hysteresis affected by seepage

As shown in Figure 10d, in situ tailings SFC are slightly above what was established by Ecometrix (2007) for fresh tailings having a pore water salinity of 28 g/L. As shown by Konrad & McCammon (1990), tailings low cooling rate will increase tailings pore water salinity at frost front. The increasing pore water salinity will have a tendency to move the SFC upward, as demonstrated by Ecometrix (2007) for tailings having a pore water salinity of 80 g/L. This phenomena that seems to be observed on tailings located underneath the ECC.

As presented by Ng et al. (2003), in situ measurement of volumetric water content, with sensors, differ from the one calculated using the measured gravimetric water content. They suggested that measured volumetric water content can only be interpreted as an indication of the variation tendency. Also, the above UVWC were estimated using the device supplier general calibration curve, what may gives erroneous values depending of soil. Laboratory testing to establish soil specific calibrations curves are currently ongoing. However, this calibration process will not modify the UVWC general variation trend, only values. Harrisson & Blight (2000) pointed out that in situ measured soil suction must be looked at as a direction (increase or decrease) and the magnitude of change should be looked at carefully because it does not have agreement between devices measuring in situ soil suction. Therefore, presented curves in this paper should then only be looked at as an indication of what is happening and should not be used as granted values.

3.2 *Heat transfert by convective air flow*

As presented above, 8 short thermistor strings are installed in the 65-200 mm material to record convective air movement through temperature variations. As shown in Figure 12, convective air flow uniformed the vertical temperature distribution in the coarse material and greatly decreases tailings temperature during winter time, down to a depth of 5 m (Fig. 13a).

The temperature reached in the 65-200 mm layer is about 4°C warmer than what observed in other cells at the same elevation from July to August. It is also possible to notice that the air temperature into the coarse granular material showed fluctuation, with smaller amplitude and frequency variation as we look lower inside the layer. These temperature fluctuations are associated to daily air temperature variations, and are attenuated as we look deeper into the layer. For the first year recorded temperature, cold air trapped at the base of the coarse granular material did not act as insulation layer as initially assumed by designer (Fig. 13c). The colder and denser air at the base of the 65-200 mm layer flew downward along the 5H:1V slope, as demonstrated numerically (Fig. 14). Air mass movement allowed warmer air to infiltrate into the coarse layer to warm the underlying material.

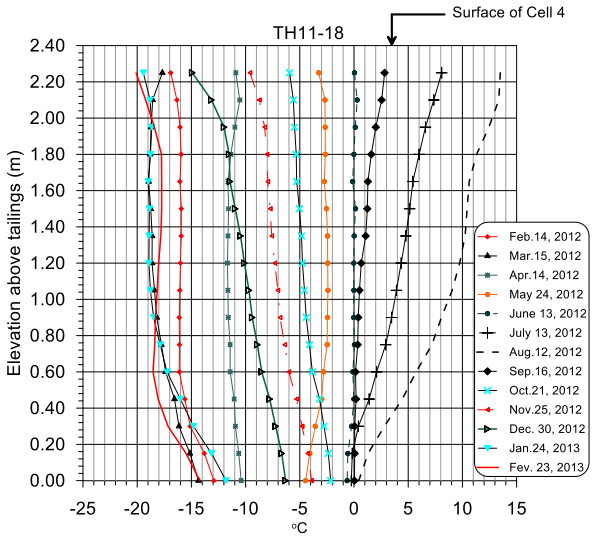


Figure 12. Temperature vertical distribution into the Cell 4 65-200 mm layer

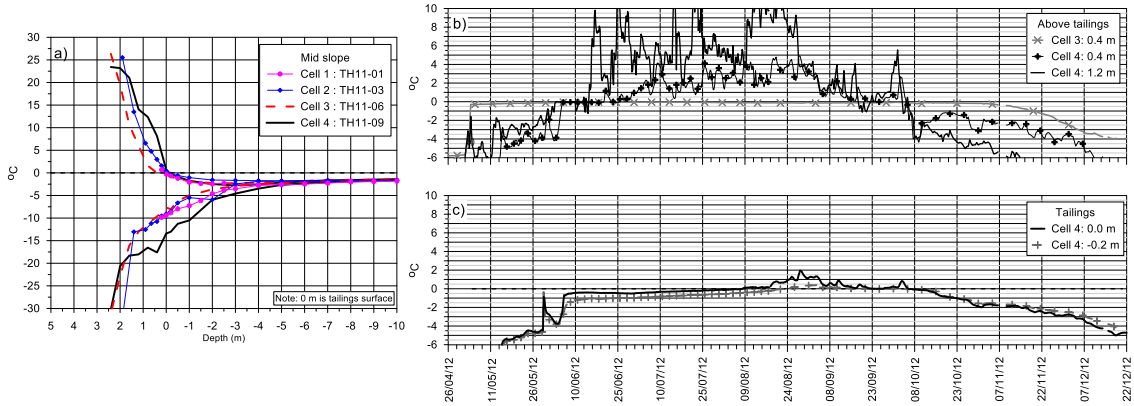


Figure 13. Convective air flow impact over a) soil vertical profile, b) 65-200 mm layer daily temperature distribution, and c) tailings surface daily temperature distribution

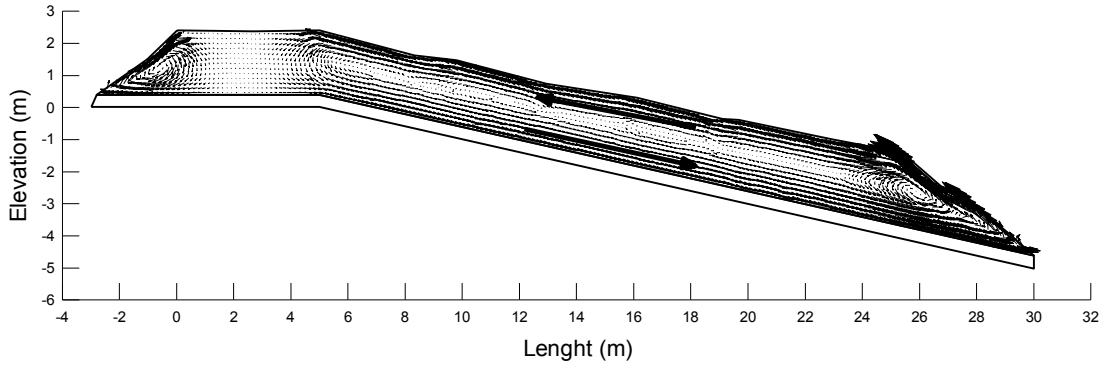


Figure 14. Air velocity vector into the 65-200 mm during summer time

4 SUMMARY AND RECOMMANDATIONS

Based on the first year field observations and associated interpreted results, the following observations can be drawn:

- Field recorded data are high quality informations, allowing to adequately interpret soil water/moisture variations through time and convective heat transfer.
- Sensors were able to measure in situ SWC and SFC hysteresis, showing than these soils characteristic curves are affected by boundary conditions and may vary through seasons.
- In situ 0-20 mm SWC above and below the geomembrane is different. The granular soil located underneath the impervious liner shows more suction than above, for identical water content. Also, the moisture retaining layer affected the surrounding 0-20 mm SWC.
- Moisture displacement, at the tailings surface, happens when appropriate conditions are encountered. Lateral moisture variations along the slope will influence boundary conditions throughout the year, affecting heat and moisture transfer.
- Convective air flow decrease tailings temperature during winter time. However, due to the TSF sloping face, the insulation property of this layer was not encountered during the first summer collected data. Cold air located at the coarse layer moved downward during the warm season.
- Tailings presented a wide distribution of SFC. Tailings SFC will be modified as tailings freezing occur, due to brine creation at the frost front. The increasing pore water salinity will tend to increase tailings unfrozen water content, influencing heat and water transfer.

Based on the one year recorded data, it is recommended to consider that SWC and SFC may be affected by site boundary conditions. Using unique SWC or SFC for one type of soil may lead to divergence between numerical results and observed behaviour as well as design problematics. If only laboratory SWC and SFC are available, it is suggested to conduct a sensitivity analysis to establish the impact of modified curves, by modifying the AEV and FPD as well as the curve shape. Also, it is suggested to consider that tailings SFC and associated freezing point vary through time and location, due to boundary condition changes, and the variability may be stronger where freeze and thaw cycles as well as seepage occurs.

It is important to point out that these observations are made with data collected over only one (1) year and that heat as well as water transfer affecting ECC behavior are still in a transitory state. At this state of the project, collected data can only be used to help understand heat and water transfer through materials and no conclusion can be drawn about the efficiency of each cover to prevent contaminant release.

5 ACKNOWLEDGEMENTS

Authors are grateful to Raglan Mine for permission to publish this material, especially to Kristan Straub and Joel Pagé. The authors would like to thanks GKM consultant who have been involved with the field work during ECC instrumentation and especially Jean-Marie Bréhé ing. who shared his knowledge with us. We also wish to acknowledge the assistance of Jean-Marie Konrad Ph.D and Denis Isabel Ph.D who have been involved with data interpretations. Thanks to Geneviève Cauchon-Voyer Ph.D. and Patrick Couture ing. for the paper review.

6 REFERENCE

Apogee Instrument. *apogee-oxygen-sensors-more-information.* Read, June 10, 2013, from http://www.apogeeinstruments.co.uk

Coulombe, V., 2012. Performance de recouvrements isolants partiels pour contrôler l'oxydation de résidus miniers sulfureux. Mémoire de Maîtrise, Université de Montréal, 250 p.

Golder, 2010. Final Cover of Tailings Storage Facility, Report number : 004-10-1221-0072 RPA Rev0. November 2010.

Harisson & Blight. 2000. Case study: Comparaison of in situ suction measurement. In H. Rahardjo, D.G. Toll and, E.C. Leong (eds), *Proc. Conf. Unsaturated Soils for Asia*, Singapore: 281-284, Rotterdam: Balkema.

Konrad, J.-M. & McCammon, A.W. 1990. Solute partitioning in freezing soils. *Canadian Geotechnical Journal* (67): 726-736

Koopmans, R.W.R. & Miller, R.D. 1966. Soil freezing and soil water characteristic curves. *Soil Science Society of America Proc*., 30: 680-685

Ng, C.W.W. & Pang, Y.W. 2000. Experimental investigation of the soil-water characteristics of a volcanic soil. *Canadian Geotechnical Journal* (37): 1252-1264è

URSTM. 2012. Estimation de la teneur en bentonite de mélanges gravier/bentonite, Rapport PU-2012-03-708. URSTM, Université du Québec en Abitibi-Témiscamingue.

URSTM. 2013. Travaux visant la détermination de propriété géotechniques pour différents matériaux, Rapport PU-2012-05-716. URSTM, Université du Québec en Abitibi-Témiscamingue.

SLI. 2012. Modélisation hydrologique des bassins versants de Katinniq et du parc à résidus, Étude sur la gestion des eaux. Rapport, 506051-0000-4HER-0003-00, 2012-02-01

Toward effective closure planning: from progressive reclamation to sustainable mining

G. McKenna, R. An, E. Scordo, & J. McGreevy
BGC Engineering Inc, Vancouver, BC, Canada

ABSTRACT: Mine closure planning is now a common activity and a regulatory requirement for most mines in Canada. A conceptual closure plan is developed as part of initial mine permitting and updated periodically. These plans form the basis for assessment of financial assurance. While the importance of closure planning is widely recognized, there are significant shortcomings with the current state of practice. These shortcomings include a general disconnect between most operations and their closure planning teams and fatal design flaws that do not come to light until later in the project. Typically, reclaimed landscapes do not meet regulatory expectations, even with viable closure plans. Fortunately, examples exist of successful elements of closure planning that offer effective strategies and techniques. This paper summarizes the current state of practice and provides guidance for practitioners, regulators, and stakeholders to produce effective closure plans.

1 INTRODUCTION

Mine closure planning is now common in Canada. Ideally, the closure plan will be aligned with the long-range mine plan, and will provide at least one viable path through the stages of mining: development/construction, operation and production, and reclamation/closure. Prior to mine development, a mine must submit a conceptual closure plan to regulators as part of the initial permitting process. The plan is updated whenever a significant change occurs to the mine plan, or in five or ten year increments. Calculations for financial assurance for mine closure and reclamation are based on the closure plan. Ideally, mine operations staff, stakeholders, and regulators can rely on the closure plan to inform strategies, decisions and actions in the field over the life of the mine.

Unfortunately, as described below, closure planning usually falls short of this ideal. The planning document is usually submitted as a regulatory requirement, but not implemented to its full potential. The document often carries little weight at the mine itself. For example, operations staff is often unaware of the closure plan's existence, crucial elements or details are not clearly communicated, or decision-makers at the mine overlook the plan (McKenna, 2002). However, mine operators could make adjustments that will make closure plans more effective. These adjustments can actually improve the bottom line and help the company meet its commitments to regulators and stakeholders. Creating, maintaining, and following a sound closure plan is an essential activity on the company's path to eventually relinquishing the land and its reclamation liability, the stated goals of most mines and the foundation of sustainable mining (Abbott and McKenna, 2012).



An effective closure plan can be defined as one that:

- Is developed with full participation of regulators and other stakeholders and sets out jointly developed goals, commitments, and plans.
- Is fully aligned with the long-range mine plan.
- Is detailed enough to support planners and designers in mining and progressive reclamation decisions.
- Provides a defendable basis for estimating reclamation and closure costs for financial assurance calculations.
- Identifies major uncertainties and threats to the plan and has an associated monitoring and adaptive management plan to manage these risks (with contingencies that are clearly defined).
- Provides a framework for decision-making by operations staff, regulators, and stakeholders.
- Fits within a regional context – it is aligned with other mines and adjacent land users.

This paper captures the current state of practice, including its strengths and weaknesses, and offers guidance on developing truly effective mine closure plans.

2 CURRENT STATE OF PRACTICE

Adopted by most mines in the 1970s, mine reclamation is a relatively new activity. At that time, it consisted of recontouring the land, adding a layer of top soil, and planting vegetation – typically with agronomic grasses for erosion control (e.g. Cummins and Given, 1973). Mines generally reclaimed progressively (as land becomes available). But even as these rudimentary practices were gaining favour, governments and operators were beginning to realize that more formal approaches to integrated planning and design would be required (e.g. US Department of the Interior, 1967). This need became more apparent as mines grew ever larger in size and as operators learned of the complexities involved in reclaiming such enormous landscapes. All the while, society's expectations that we would indeed reclaim these landscapes for specific land uses were also growing.

2.1 *Regulatory regime*

The current state of practice for closure planning is based on a framework developed almost 20 years ago by the Ontario Ministry of Northern Development and Mines (1996). This framework has been adapted for use in most jurisdictions (McKenna, 2002).

In Canada, each province has its own set of closure plan regulations and requirements. All provinces require the submission of a conceptual closure plan for most types of mines. Table 1 provides a list of the common requirements for closure plans submitted to regulators.

Table 1. Common elements of provincial closure and reclamation plan submission requirements

Requirement	Description
End land use objectives	The objectives for how the reclaimed land will be utilized, and how reclamation practices will achieve the land use objectives, must be clearly identified.
Tailings and mine waste	Plans for disposing of / or containing tailings and mine waste in a manner that minimizes the potential for metal leaching /acid rock drainage and other forms of contamination.
Infrastructure and equipment	Details to dismantle machinery, equipment and to decommission buildings, power lines, access roads, and other infrastructure.
Revegetation	All disturbed areas must be revegetated with a self-sustaining, succession-based cover of native seed mixtures and plant materials. Top soil management is crucial in successful revegetation.
Schedule	A schedule for implementing reclamation activities during and immediately following operations.
Reclamation cost estimate	A detailed cost summary associated with implementing the reclamation and monitoring activities.
Financial assurance	The amount and form of financial assurance.
Water management and treatment	Details for water management and treatment systems and re-establishment of water courses. The details include water treatment strategies, diversion of clean water, and plans for ultimate discharge.
Monitoring program	Details for monitoring for metal leaching/acid rock drainage, water quality, vegetation performance and subsidence during the operations and post-closure stage of mining.

Most closure planning documents share the same general table of contents:

1. Introduction
2. Predevelopment conditions
3. Mine operation practices
4. Landscape performance goals (and regulatory requirements)
5. Reclamation technologies and methods
6. Reclamation plans, balances, waste isolation methods
7. Long term monitoring and maintenance plans
8. Landscape performance prediction
9. Comparison of the performance prediction relative to the goals
10. Contingency plans
11. Schedules and costs
12. Financial assurance

Typically, the mines and their regulators come to an agreement on the table of contents at the start of the planning process. Further regulatory involvement may occur during preparation of the plan. Upon review of the submitted closure plan, regulators will sometimes request additional information / clarification from the mine (supplementary information requests). In some cases, the submission is formally approved by the regulator, but often its receipt is merely an acknowledgement that the mine has met an approval condition.

In British Columbia, the government requires the submission of an updated, detailed mine plan along with a detailed reclamation plan that outlines the objectives of the mine for the subsequent five years of operation. These plans must be submitted every five years throughout the operating life of the mine. The detailed five year reclamation plan includes information on vegetation development, soil conditions, land use objectives, natural plant succession and native plant species. These details must also be supported by research and maps. The five year reclamation plan is indicative of a plan for progressive reclamation.

Several jurisdictions require each mine to submit a schedule and plan for progressive reclamation. This includes British Columbia, Alberta, Saskatchewan, Nova Scotia, Yukon, the Northwest Territories and Nunavut. To the extent feasible, these plans provide details on how reclamation activities will occur during the life of the operation, given the mining and processing methods employed.

In Saskatchewan, government guidelines for the development of an operational decommissioning plan for mines suggest that mining facilities at project sites should be designed with closure in mind. The facilities within the mine should be designed to eliminate or at least minimize future impacts to the long term stability of the decommissioned infrastructure, such that the reclaimed area can be integrated into the surrounding environment. For the integration to occur as smoothly as possible, preference should be given to a system that allows for passive management in the post-decommissioning stages of the mine.

In both Saskatchewan and British Columbia, provincial guidelines recommend the use of an Ecological Risk Assessment (ERA) tool when developing an operational decommissioning plan. This tool advises using a source, pathway, and receptors framework. This approach is better aligned with the Environmental Impact Assessment process that occurs at the beginning of mining. The use of such a tool seems likely to become more common in the future.

Most mines in Canada are returned to wildlife habitat. Some are returned to industrial uses, others to recreational uses.

There is opportunity for the regulators in each province to review closure plan requirements in other parts of Canada (and internationally) and incorporate the most successful elements of regulations into their provincial requirements.

2.2 *Closure planning at the mines*

Closure planning efforts vary from mine to mine. Some plans are produced in-house by mine planners or reclamation specialists; others are done by engineering or environmental consultants to the mine.

Initially, the closure specialists provide input (usually in the form of constraints) into the long-range mine plan. The long-range mine plan is developed using these constraints, annually or every few years. A separate closure planning phase, which focusses on resloping, soil salvage, stockpiling, placement of coversoils, and revegetation, is developed as part of preparation of a closure plan for submission to regulators. Stakeholder consultation is typically ongoing throughout a mine's life, and closure planning is used as a central activity to communicate plans and accept input. The closure plan is typically several hundred pages in length, includes dozens of maps and illustrations, and can cost several hundreds of thousands of dollars to produce. The plan can take from 6 to 18 months to prepare.

The closure plans take into account the existing and proposed footprint (the lease / property / landscape scale) and can include anywhere from 5 to 20 mining landforms (such as dumps, tailings facilities, and mined-out pits). The closure water drainage system (the system of constructed surface-water creeks) and the related water quality usually feature prominently in planning, and drive much of the design.

Closure plans evolve over the life of the mine. The first conceptual closure plan is often overly optimistic and relies on unproven assumptions (such as the assumption that mine waste will be non-acid generating, or that passive water treatment measures will be effective at remediating poor mine effluent water quality). Reclamation research to address some of the outstanding issues usually begins at this phase. As mining progresses, subsequent plans are more detailed and reflect a better understanding of the water balance, geochemistry, and honour the performance of early reclamation efforts. Progressive reclamation allows mines to experiment and refine their reclamation efforts over the life of the mine.

As the end of production nears, most of the inactive areas will have been reclaimed (often 10-20% of the disturbance for metal mines, 60-80% for coal strip mines). Closure plans at this phase are detailed, and are often referred to as decommissioning plans. These decommissioning plans receive much higher levels of stakeholder and regulatory scrutiny, though at this point in the mine life options become limited. Instead of focusing on lofty goals, the decommissioning plans are generally focused on removal of infrastructure, establishing the surface water drainage system, and the design and construction of a water treatment facility to allow discharge of mine

water to the environment. These maps and plans tend to be in the form of detailed engineering drawings supported by schedules and budgets.

2.3 *Strengths, weaknesses, and opportunities for the current state of practice*

The strengths of current planning efforts include the practice of allowing the closure planners to influence the long-range mine plan, and ensuring such plans and designs account for closure. Mine plans are typically adjusted to meet corporate and regulatory goals and to take advantage of natural conditions (e.g., locating waste rock where effluent can flow naturally to the mined out pit for treatment and release). As well, mine plans identify research needs and tend to require that this research be carried out in a timely manner.

An additional strength of current planning is the obligation of operators to ensure their plans meet certain reclamation requirements (see Table 1). This obligation forces the mine and regulator to transparently examine each of the major elements of the landscape. It also ensures that definitions in the plan are commonly understood, and that the plan therefore provides a basis for concrete discussion and negotiation.

The general high quality of decommissioning plans indicate that mines and regulators can work together to provide useful closure plans. All staff remaining to decommission a mine quickly become closure planning and reclamation experts. Mines can take steps to create this situation before closure for major reclamation projects as evidenced by Suncor's strategy for its Pond 1 reclamation project (Russell et al, 2010).

The conceptual nature inherent to most closure plans can be both a strength and weakness. Often, little basis exists – especially at the start of a mine – for developing a detailed closure plan; there are simply too many unknowns. But even closure plans produced for mature mines can contain insufficient details to be of use to mine and tailings plans, and / or fail to prevent decisions that lead to excessive costs or result in some goals and regulations remaining unmet. The authors have experience being asked to provide engineering designs for specific landforms that are part of a closure plan that contains fatal flaws due to lack of detail. Renegotiating terms with stakeholders, First Nations, regulators, and those paying for closure under these conditions is usually upsetting.

Table 2 provides a list of the weaknesses with the current state of practice and some opportunities for improvement. The opportunities, many of which are being practiced or pioneered at operating mines today, are discussed further in Section 3.

3 MOVING TO EFFECTIVE CLOSURE PLANNING

This section provides techniques and strategies for moving beyond the current state of practice toward more effective closure planning (see list in Section 1), and recognizing the opportunities described in Table 2.

3.1 *Collaboration with regulators and stakeholders*

Ongoing closure planning presents a major opportunity for collaborative work between the mines, regulators and stakeholders. Genuine consultation and engagement include not only providing information on the anticipated impacts of a project, but also considering public comments, concerns and feedback (Saskatchewan Ministry of Environment, 2008). This process should not occur on a selective basis, but should be inclusive of all those directly affected by the project. The stakeholders will often include local First Nations and Metis, leaseholders, neighbours and nearby residents, local governments, local and regional business and service providers, non-government organizations and community groups. Stakeholder mapping is a simple tool to identify highly impacted and highly influential stakeholders.

Table 2. Some weakness and opportunities with the current state of practice for closure planning

Weakness	Opportunity
Closure plans are not detailed enough to highlight and avoid fatal flaws	Use fatal flaw analysis and other risk assessment tools to test the conceptual plan. Increase granularity of the plan and reassess risks.
Closure plans too closely reflect the expertise of the lead authors	Form a broad group of closure planners with various specializations. Use a truly independent review panel to review plans.
Plans are not well integrated with neighboring mines	Where other mines or industry are close by, establish joint working groups to plan along shared boundaries and for shared resources. Create joint detailed plans within 500m of any boundaries that are backed by legal agreements.
Plans tend to rely on a few overly optimistic assumptions	Carefully document all assumptions, and use risk assessment techniques to test them. Use a well-developed adaptive management program to deal with uncertainties. Develop and commit to realistic and timely contingencies.
Plans are not aligned with the mine plan, or quickly fall out of alignment	Create a single plan with different perspectives. Develop tools to keep the closure plan current.
Plans are overlooked by mine operations staff	Involve operations staff in the development of the plans. Ensure full alignment with mine plan. Communicate key design and planning factors with special tools.
Plans ignore climate cycles / climate change	Avoid precipitation estimates based on annual averages, or wet and dry years. Instead, run the period of record and synthetic data on a daily basis. Formally include climate change.
Tools for landform design are not all yet available	Develop focused university-based research programs at the watershed level to develop the technologies required. Implement a technical transfer program to translate findings into tools useful by practitioners at the mines and their expert consultants.
Following the plans does not yield custodial transfer	Build strong relations with regulators and stakeholders and keep the focus on the progressive reclamation and progressive signoff.
Plans fail to examine the transition to closure and the impacts on people and local communities	Work closely with specialists, regulators, and local communities to jointly develop long-term plans that consider the transition and post-closure periods.
Plans involving dozens of maps and hundreds of pages of text are poor communication tools	Develop better, more efficient communication tools that meet the needs of each “customer.”

Early consultation with stakeholders can minimize the disturbance to the surrounding communities and businesses, both physically and financially. Most closure decisions are made before the mining even starts, and most of these are irreversible. Each individual group may raise concerns regarding operations and closure that are specific to their needs. Early consultation with these groups will allow for more of these concerns to be addressed. Stakeholder consultation also lessens the likelihood that the local community will develop unrealistic expectations about the outcomes of the reclaimed land. Swanson et al. (2012) describe a case history regarding management of waters with elevated selenium derived from waste rock piles at Teck Coal’s operations in the Canadian Rockies. In this case history, decisions regarding selenium management were made jointly by mine management, regulators, and stakeholders – an outstanding example of true collaboration.

3.2 *Clear Definition of Closure Objectives*

Defining and reaching consensus on closure objectives at the outset is a central focus of closure planning, and critical to successful reclamation. Goals need to be specific enough to provide clear direction for planners and designers, but not so detailed or numerous that they collectively become unachievable.

The oil sands industry, for example, has made great strides in recent years to devise clear communication of goals. The Oil Sands Mining End Land Use Committee (1997) provides an example of end land use goals. The CEMA End Pit Lakes Guidance Document (CEMA, 2012) provides an example of selection of high level goals for end pit lake design and operation. The CEMA Landscape Design Checklist (CEMA, 2005) provides examples of more specific design goals for reclaimed landscapes. Shell Canada (2012) provides a good example of a compilation of the plethora of regulatory requirements for reclamation and closure of an oil sands mine. There are also numerous international publications on mine closure that provide frameworks for realistic goal-setting.

3.3 *Alignment with operations through a shared mine and closure plan*

The closure plan and the mine plan should be compiled into a single document, though written from different perspectives. The teams developing these documents need to become intimately familiar with the methods and constraints for each aspect of the plan.



Syncrude offers a successful example of alignment between closure and mine planning. Hachey and Lanoue (2011) describe the company's development of a shared topographic surface between mine planners and closure planners. Traditionally, a conceptual closure plan is presented in two dimensions (2-D) which tends to mask certain kinds of closure issues. Now, 2-D designs can be integrated into a continuous digital elevation model (DEM) to create a 3-D closure topographic surface. The site-wide 3-D surface includes design details for individual constructed landforms and provides a volumetrically accurate and operationally relevant representation of the closure landscape. A 3-D surface also offers regulators, miners and stakeholders a visual tool that can better align operational mine plans in order to create the ultimate closure surface. The surface can be updated within a few days of a suggested change.

The first step in developing an integrated surface is to identify the key geotechnical, hydrogeological and hydrological constraints for the mine and incorporate these constraints into closure planning (Hachey and Lanoue, 2011). Constraints include maximum allowable fluid elevations, dyke crests and channel inverts, and the location of a large scale surface drainage path. 3-D closure topography also provides the volumes of materials that will be required for the final landscape. This information is valuable throughout the operations stage, when decisions for material placement and soil salvage are made. The 3-D surface can also be used for site-wide hydrogeological and hydrological modeling to characterize conditions at closure and post-closure (Syncrude, 2011). Constraints are communicated through a laminated "constraint map" that graphically indicates the constraints and the reasons behind them. Constraint maps are posted in planning and operational areas and updated as new information and plans become available.

3.4 *Moving beyond conceptual plans*

Landform design is the interdisciplinary application of science and engineering to create anthropogenic landforms (McKenna, 2002). Landform design is generally practiced at the landform level – creating designs and construction drawings for individual dumps, tailings ponds, and end pit lakes (e.g. Russell et al, 2010). Effective closure plans divide the mining landscape into logical landform units (typically 10 to 20) and develop plans for each of these units, with a focus on topography, surface water and groundwater, soils, vegetation, and wildlife habitat. Each landform contributes to the overall success of the closure landscape. Often a clear drawing with a cross-section and a few pages of descriptive text provides sufficient detail in the closure plan to identify risks and provide direction to decision-makers. In particular, this level of design identifies critical elevations and material constraints that govern design and construction

of individual landforms. The closure plan allows landform designers to integrate their designs with those of adjacent landforms and leases. In subsequent stages of design, the level of effort required for a detailed design for an individual landform requires as much as a few thousand hours of multidisciplinary design and often some drilling or other field work.

3.5 *Technology selection*

Many of the decisions made before mining begins have huge impacts (positive and negative) on the success of the final closure landscape, such as selection of mining method (for instance, underground versus open pit) and tailings technologies. Such decisions need to be made within the context of sustainable mining (Abbott and McKenna, 2012). McKenna et al. (2012) provide an example of an extensive tailings technology evaluation project conducted from a sustainable mining point of view, which identified and ranked 101 tailings technologies and scored these technologies with several indicators with a strong focus in closure landscape performance.

3.6 *Identifying and reducing risk*

Numerous tools are available for risk assessment for closure plans. Two particularly useful ones are the Fatal Flaw Analysis (FFA) and Failure Modes and Effect Analyses (FMEA), as described by McKenna (2002) and MEND (2012). These tools transparently identify hazards and allow risk rankings to aid in the selection of mitigation measures.

As a risk reduction method, adaptive management has generally provided poor results for most applications (e.g. Allen et al, 2011). CEMA (2012) provides a revised framework for adaptive management modeled after Peck's (1969) observational method in geotechnical engineering. Properly applied, such an approach to adaptive management should prove an important tool for closure planning and risk management.

3.7 *Supportive research and development*

The technologies needed for the reclamation and closure of a mine site may not all be available when the first closure plan is designed. Outstanding technologies and risks should be identified in the closure plan, and a research and development program should be initiated that provides timely answers. It is often useful to conduct mine reclamation research using instrumented watersheds supported by laboratory scale research (McKenna et al, 2011; Pollard et al, 2012). Integral to this approach is a technology transfer program to ensure that the findings of this research are communicated and employed in closure planning, landform design, and reclamation operations.

Devito et al. (2012) provide an excellent example of technology transfer of reclamation research results from instrumented natural catchments in the boreal forest. MEND (2012) provides an excellent synthesis and guidance document for covers for cold regions – a good example of technology transfer and risk management. Similarly, the CEMA End Pit Lakes Guidance Document (CEMA, 2012) provides a good model of technology transfer in a text developed over a two-year period by an international, multi-disciplinary team.

3.8 *Landscape Integration*

Currently, reclamation and closure plans are completed for a single lease. Integration of the final reclaimed landscape into the surrounding environment is typically one of the ultimate goals of the closure plan. But how the actual integration process with the surrounding region will occur is still unclear. To better lay out this final process, the next step to successful reclamation is the development of integrated closure plans and eventually regional closure plans. Regional closure plans would be designed to integrate mining, planning and reclamation activities between neighboring operators. Ideally, regional closure landscapes will have landforms that contribute to surface water drainage plans. Competing operators would work together to create a single regional closure plan, where designs for similar landscapes can eventually be pieced together to meet closure goals everywhere in the landscape, overcoming inherent boundary issues.

Several issues would have to be addressed prior to the widespread adoption of a regional closure approach. These include: lease-boundary issues, varying mine development rates, operator risk tolerances, and buy-in by all operators. The development of a regional closure plan has yet to be achieved. The level of detail required to make such plans effective is unclear.

3.9 *Progressive reclamation and signoff*

Progressive reclamation (annual ongoing reclamation of mine areas as they become available) is common at most mines. Final signoff by regulators of reclaimed land is exceedingly rare (McKenna, 2002). Even rarer is annual, ongoing signoff (bond release, reclamation certification, relinquishment) of reclaimed mined lands, as practiced at the TransAlta coal mines located west of Edmonton (Mikalson, 1995). At these strip mines, the amount of land disturbed, reclaimed, and certified by regulators as reclaimed is about the same every year – a true demonstration of sustainability. This consistency also allows the mine and regulators to turn the reclamation signoff process into a routine activity, rather than making it a major event at mine closure when there are often competing agendas. It also permits them to evaluate reclamation activities and learn from their experience.

4 MOVING BEYOND THE CURRENT STATE OF PRACTICE

Abbott and McKenna (2012) redefine sustainable mining as the emergent outcome of doing the following seven things very well:

1. Engaging communities and earning trust
2. Exercising planning, decision-making, and design with flair
3. Executing promises operationally
4. Empowering employees
5. Efficiently managing resources
6. Exceeding shareholder expectations
7. Enhancing the environment

Effective closure planning is embodied in the second element listed above. Ideally, closure planning would start at the beginning of the exploration phase, and would involve building relationships with regulators and stakeholders, earning their trust, and taking care not to promise reclamation attributes that they cannot reasonably be sure of delivering should the mine go into production. Also, during development of the original long-range mine closure plan, there would be enough drilling, testing, planning, design, and foresight that basic elements of the plan would remain constant throughout the mine life and closure process. As a result, major changes to the plan would be very unlikely. Closure plans would focus less on the details of reclamation and more on creating useful watersheds for long-term sustainable uses, and sustainability would become a cornerstone of all strategies, decisions, and actions. Abbott and McKenna (2012) provide guidance to mines on how to implement sustainable mining within a three-year period, with an implicit challenge to closure planners to continue improving their practices in order to better facilitate this transition.

5 ACKNOWLEDGEMENTS

The work presented in this paper provides an update to Gord McKenna's 2002 PhD thesis at the University of Alberta prepared under the supervision of Drs Dave Sego and Norbert Morgenstern. The authors appreciate the support of our clients as well as all the regulators, operators, consultants and researchers that have contributed to the findings in this paper. Derrill Shuttleworth is thanked for the illustrations and Vanessa Mann and David Wylynko are thanked for their timely review and editing.

6 REFERENCES

Abbott, R and McKenna, G. 2012. Sustainable mining now: turning ideas and ideals into reality. Mine Closure 2012. Brisbane, 2012. Australian Centre for Geomechanics, Perth. p771-781.

Aboriginal Affairs and Northern Development Canada (AANDC). 2002. Mine Site Reclamation Policy for the Northwest Territories. < http://www.aadnc-aandc.gc.ca/eng/1100100036038/1100100036040#chp4>

Alberta Environment. 2006. Competencies for Remediation and Reclamation Advisory Committee: Recommendations Report. <http://environment.alberta.ca/documents/Competencies_Recommendations_Report.pdf>

Allen, C.R., J.J. Fontaine, K.L. Pope and A.S. Garmestani. 2011. Adaptive management for a turbulent future. J. Environmental Management 92: p1339-1345.

British Columbia Ministry of Energy and Mines. 2009. Guide to Processing a Mine Project Application Under the British Columbia Mines Act. < http://www.coalwatch.ca/sites/default/files/Guide-to-Processing-A-Mine-Project-Application-Under-The-British-Columbia-Mines-Act.pdf>

British Columbia Ministry of Environment. 2000. Environmental Risk Assessment: An Approach for Assessing and Reporting Environmental Conditions. <http://www.env.gov.bc.ca/wld/documents/era.pdf>

CEMA, 2012. Oil sands end pit lakes design guide. Cumulative Environmental Management Association, Fort McMurray. 434p.

CEMA-RWG Landscape Design Subgroup, 2005. Landscape Design Checklist. Cumulative Environmental Management Association, Fort McMurray. 8p.

Cummins, A.B., and Given, I.A., 1973. SME mining engineering handbook, Society of Mining Engineers of the American Institute of Mining Metallurgical and Petroleum Engineers Inc.

Cumulative Environmental Management Association (CEMA). 2005. Landform Design Checklist. <http://cemaonline.ca/index.php/administration/cat_view/2-communications/38-ldc>

Devito, K., Mendoza, C., Qualizza, C. 2012. Conceptualizing water movement in the Boreal Plains. Implications for watershed reconstruction. Synthesis report prepared for the Canadian Oil Sands Network for Research and Development, Environmental and Reclamation Research Group. 164p.

Energy, Mines and Resources of Yukon (EMR). 2006. Yukon Mine Site Reclamation and Closure Policy. <http://www.emr.gov.yk.ca/mining/pdf/mine_reclamation_policy_web_nov06.pdf>

Government of New Brunswick. N.d. Guide to the Development of a Mining and Reclamation Plan in New Brunswick. <http://www.gnb.ca/0078/minerals/pdf/Guide_Mining_Reclamation-e.pdf>

Hachey, L.M., and A.V. Lanoue. 2011. Use of Three-dimensional Topography as a Tool for Closure Integration at Syncrude Canada Ltd.'s Mildred Lake and Aurora North Leases. Proceedings of the 2011 Mine Closure Conference, Perth, p403-412. kubick, A.T., and McKenna, G.T., 2001, Stabilization of soft tailings: practice and experience, Eighth International Conference on Radioactive Waste Management and Environmental Management (ICEM'01): Brugge, Belgium, American Society of Mechanical Engineers.

Manitoba Industry, Trade and Mines. 2006. Manitoba Mine Closure Regulation 67/00: General Closure Plan Guidelines. <http://www.gov.mb.ca/iem/mrd/mines/acts/closureguidelines.pdf>

McKenna, G, Dawson, R, Hyndman, A, LeSueur, P, Sobkowicz, J. 2012. The Oil Sands Tailings Roadmap and Action Plan: Oil Sands Tailings State of Practice Overview. International Oil Sands Symposium, Edmonton.

McKenna, G, O'Kane, M, Qualizza, C. 2011. Tools for bringing mine reclamation research to commercial implementation. Proceedings Tailings and Mine Waste 2011. Vancouver.

McKenna, G. 2002. Sustainable Mine Reclamation and Landscape Engineering. PhD Thesis in Geotechnical Engineering, Depart of Civil and Environmental Engineering, University of Alberta, Edmonton, 660p.

MEND, 2012. Cold regions cover system design technical guidance document. Edited by O'Kane Associates Inc. Prepared on behalf of Aboriginal Affairs and Northern Development Canada (AANDSC) and MEND. Ottawa. MEND Report 1.61.5c. July 2012. 177p.

Mikalson, D.A., 1995, Principles and practices of sustainable development -- with TransAlta examples, in Singhal, R., ed., Mine Planning and Equipment Selection: Calgary, A.A. Balkema, p737-745.

Newfoundland and Labrador Department of Natural Resources. 1999. Guidelines to the Mining Act Part I: Format Requirements. <http://www.nr.gov.nl.ca/nr/department/guidelines.pdf>

Nova Scotia Environment. 2009. Guide for Surface Coal Mine Reclamation Plans. < http://www.gov.ns.ca/nse/ea/docs/EA.Guide-SurfaceCoalMineReclamation.pdf>

Oil Sand Mining End Land Use Committee, 1997, Oil Sand Mining End Land Use Committee Report and Recommendations: Fort McMurray, Alberta.

Ontario Ministry of Northern Development and Mines (OMNDM). 2012. Ontario Regulation 240/00: Mine Development and Closure Under part VII of the Act. <http://www.e-laws.gov.on.ca/html/regs/english/elaws_regs_000240_e.htm#BK15>

Ontario Ministry of Northern Development and Mines, 1996. Rehabilitation of mines: Guidelines for proponents, Ontario Ministry of Northern Development and Mines, Sudbury. 1v

Peck, R.B. 1969, Advantages and limitations of the observational method in applied soil mechanics, Milestones in Soil Mechanics -- The First Ten Rankine Lectures. Institution of Civil Engineers, Edinburgh. p263-279.

Pollard, J., McKenna, G.T., Fair, J., Daly C Wytrykush, C., and Clark, J., 2012, Design aspects of two fen wetlands constructed for reclamation research in the Athabasca oil sands, Mine Closure 2012: Brisbane, Australian Centre for Geomechanics, p815-829.

Quebec Ministry of Natural Resources. 1997. Guidelines for Preparing a Mining Site Rehabilitation Plan and General Mining Site Rehabilitation Requirements. <http://www.mrn.gouv.qc.ca/english/publications/mines/environment/guianmin.pdf>

Russell, B., McKenna, G., Leblanc, M., Wells, P.S. and Anderson, B. 2010. Design and construction of the reclamation surface for the first oil sands tailings pond. Mine Closure 2010, 23–26 November. Viña del Mar, Chile, Australian Centre for Geomechanics, Perth, p563–574.

Saskatchewan Ministry of Environment. 2008. Guidelines for Northern Mine Decommissioning and Reclamation. <http://www.environment.gov.sk.ca/adx/aspx/adxGetMedia.aspx?DocID=e28770f9-33f5-4dfe-bc33-c2a255111b47&MediaID=1611&Filename=Northern+Mine+Decommissioning+and+Reclamation+Guidelines.pdf&l=English>

Shell Canada Ltd. 2012. Muskeg River Mine Operation Integrated CC&R Plan. Report prepared for Alberta Environment and Water, December 31, 2011. Shell Canada Ltd, Calgary.

Swanson, S., Abbott, R., Funk, W., Kirk, L., McKenna, G., Ohlendorf, H., and Sandy, T., 2011, Building stakeholder engagement in sustainable solutions- the strategic advisory panel on selenium management. Mine Closure 2011. Lake Louise, Canada, Australian Centre for Geomechanics, p189-196.

Syncrude Canada Ltd. 2011 Mine Reclamation Plan and Life of Mine Closure Plan: Mildred Lake and Aurora North. Report prepared for Alberta Environment and Water, December 31, 2011. Syncrude Canada Ltd, Fort McMurray.

US Department of the Interior, 1967. Surface mining and our environment: a special report to the nation. United States Department of the Interior, Washington, DC, 124p.

Regional mine closure plans - the next improvement in closure planning

J. McGreevy, G. McKenna, R. An, & E. Scordo
BGC Engineering, Vancouver, British Columbia, Canada

ABSTRACT: Closure planning is now a routine activity at most mines. But for mining regions with several (sometimes hundreds) of mines, there are shortcomings with the present focus on individual lease/landscape scale of closure planning. Many of these shortcomings can be addressed through creation of regional mine closure plans. There is both an opportunity and a need for regional closure plans for mining regions to allow mine operators and their regulators to meet their sustainable mining goals.

This paper focuses on ways that practitioners and regulators can implement a regional closure plan framework. It provides the initial outline of a regional closure plan, and a five year plan to develop one. Efforts and challenges are highlighted, along with the potential benefits. Examples of successful accomplishment of many of the elements that will support developing regional closure plans are presented.

1 INTRODUCTION

Today, mine closure planning is a common activity for most mines. Closure plans include mine and reclamation designs at the lease/landscape scale – the area disturbed by an individual mine operation. Within the confines of the mine property, the plans consider geotechnical stability, surface water and groundwater issues, soils, vegetation, and often wildlife habitat. These plans cover an area of several square kilometers, or even tens of square kilometers.

These lease/landscape closure plans include five to 20 mining landforms. For example, they will have sections on waste rock dumps, tailings ponds, diversion dams, and mined out pits, as well as details on the reconstructed drainage system of creeks, wetlands, and pit lakes that connect these landforms. These water bodies are, in turn, connected to the regional natural surface water network.

The closure landscapes sit within a larger region that could be defined by jurisdictional (governmental) parameters or by physical, ecological, or even cultural attributes. Some regions contain several mines, while others have dozens or even hundreds. In fact, mining (active or historical) can sometimes be the defining feature of a region all together.

However, given their varied ownership, the planning for each mine within a region often occurs in isolation. This paper proposes greater integration and more successful reclamation through the development of regional mine closure planning – a hallmark of the burgeoning concept of sustainable mining.

The reasoning for this proposition is readily apparent. There are many natural and cultural processes acting at a regional level. For example, the surface water network operates at a regional level, while many animal habitats cover large portions of a region. As well, infrastructure (roads, powerlines, government services) is often managed at a regional scale. Numerous small mines, or a few large mines, can have an enormous impact on all of this activity within a region (e.g. MAC, 2012; Bowman and Baker, 1998; USEPA, 2012).

Often, reclamation activities are complicated by the way mining areas are designated. Individual mine properties are typically defined by historical claim staking activities or legal administrative boundaries (e.g. township and range) rather than by boundaries designed for specific orebodies, or by watersheds. This fragmentation can represent a significant drawback to successful reclamation; regional cooperation can go a long way to reversing that shortcoming. In regions with multiple mines, opportunities to develop regional closure plans abound. Indeed, taking advantage of such opportunities is a necessity if these areas are to achieve successful reclamation.

This paper explores opportunities and challenges for regional closure planning. Despite a recent focus on closure planning and sustainable mining (e.g., MAC, 2011), reclamation literature in Canada is limited. Therefore, the concepts described here are based primarily on the authors' experience with closure planning for the oil sands region of northeastern Alberta, Canada, and experience and literature of other mining regions internationally. Regional closure planning heralds multiple benefits. It can allow for better governance at a regional level, better integration between mines and with the surrounding landscapes, and ultimately better environmental performance at lower costs for the mine operators.

This paper builds on two earlier works. Gunnett (1975) discusses the potential for enhanced reclamation through regional mine planning. Bowman and Baker (1998) set out a conceptual framework of regional reclamation planning in order to capture the broader "shadow" effects of mining. The regional frameworks and experiences from the Athabasca oil sands are referenced frequently in this document, as learnings from these reclamation efforts are generally applicable to most mining regions.

2 SPATIAL SCALES FOR MINE CLOSURE PLANNING

An improved understanding of mine closure planning can be derived by first defining several spatial scales with respect to mining (see Table 1 and Figure 1). The scales are based on principles of landscape ecology (e.g. Forman, 1995).

Table 1. Nested spatial scales for mine reclamation design and planning

Scale / size	Mining example	Mine planning / design
Microsite 0.1 to 1m^2	A boulder, pothole, or log in the reclaimed landscape	Field fit
Patch 0.1 to 1km^2	Reclamation area (slope or plateau) with a consistent reclamation prescription	Annual reclamation design / plan
Landform 1 to 25km^2	Individual dump, tailings pond, mined out pit	Landform design, watershed design
Lease/ landscape 100 to 1000km^2	Mine property	Mine closure plan
Region 50,000 to 100,000km^2	Mining district, geographic region	Regional land use plan, regional mine closure plan

McKenna et al. (2013, this volume) describe the current state of practice for mine closure planning. Most jurisdictions require mines to submit closure plans as part of the initial permitting process before mining begins. Environmental impact assessments are also done at this lease/landscape level, and typically include cumulative impacts and socioeconomic impacts within the region.

Closure plans for new and old mines alike are updated and submitted to the regulator periodically (usually every five to ten years). The first plans are very conceptual in nature, while subsequent plans have additional detail as mining and progressive reclamation is completed (MAC, 2011). In time, detailed decommissioning plans are drafted as the orebody is exhausted.

Typically, the design of individual mining landforms is drawn largely from a mining and geotechnical engineering perspective, with some input by biologists, hydrogeologists, geochemists, and reclamation specialists envisioning extended closure planning activities. Such work is usually done under the banner of a dump design or dam/tailings facility design. Ideally, these designs will be written to support the goals and constraints imposed by the lease/landscape closure plan. Often, substantial regrading and other changes are required to close and reclaim these mining landforms.

Progressive reclamation typically occurs over the life of the mine (usually decades, sometimes a century or more). Reclamation activities can be undertaken on an annual basis, covering portions of a landform at a time, and can be thought of as occurring at the "patch" scale.

The mine closure plans generally accommodate water flows from upstream watersheds, and shed water (of a certain quality and quantity) to downstream watercourses. This is one of the main ways mine closure plans honour regional aspects.

A typical table of contents for a lease/landscape closure plan (McKenna, 2002) includes:

- Introduction
- Predevelopment conditions
- Mine operation practices
- Landscape performance goals (and regulatory requirements)
- Reclamation technologies and methods
- Reclamation plans, balances, waste isolation methods
- Long term monitoring and maintenance plans
- Landscape performance prediction
- Comparison of the performance prediction relative to the goals
- Contingency plans
- Schedules and costs
- Financial assurance

Broad regional planning is typically a provincial or state government activity, often focused on economic development and resource management. Three documents for the oil sands region provide useful study:

- The Oil Sands End Land Use Committee (1997) set out target end land uses for the region and highlighted the need for regional coordination.
- The Fort McMurray-Athabasca Oil Sands Subregional Integrated Resource Plan (IRP) was developed by governments and First Nations, industry, and interest groups to address issues of interest (Government of Alberta, 2002). It sets out resource management intents, broad objectives, and broad guidelines generally and more specifically for each of 12 focus areas (mineral and surface material resources, forest resources, settlement, access and infrastructure, agriculture, recreation and tourism, water resources, fisheries, wildlife, ecological resources, historical resources, population health).
- More recently, the. Lower Athabasca Regional Plan (Government of Alberta, 2012) was issued to complement the IRP. It is both broader and more explicit in setting out a vision, planning, outcomes, monitoring, and guidance for decision-makers. Adopting an implicit sustainability framework, it sets out a 10 or 50 year horizon in the area of growth, community development, and environmental health. Oil sands mining, the major economic driver in the region, is but one part of the overall framework. Explicit considerations of mine closure are limited to protection of sensitive areas, progressive reclamation and environmental protection. But the plan sets out regional items that the mine closure plans will need to consider.

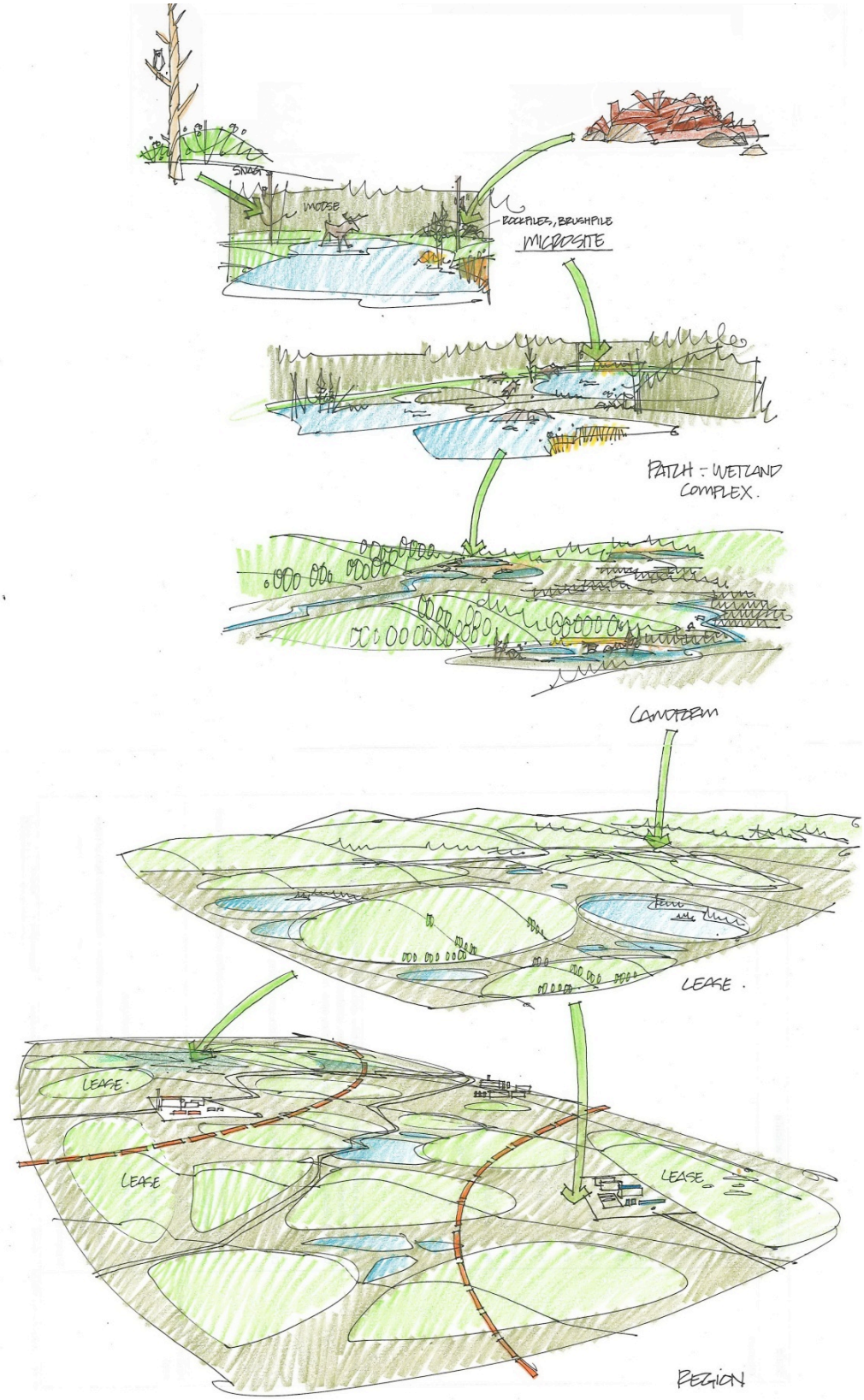


Figure 1. Conceptual drawing of each spatial unit nested within larger regional reclamation.

The oil sands benefit from the work of a regional multi-party stakeholder group which makes recommendations on the management of cumulative effects of regional development on air, land, water and biodiversity. The Cumulative Environmental Management Association (CEMA) has over 50 member organizations who sit in four caucuses: Aboriginal, Government, Non-Government Organizations and Industry. The organization produces, among other things, technical guidance documents related to oil sands reclamation. These documents assist with planning and design in the areas of soils, vegetation, wetlands, and end pit lakes.

In 2012, CEMA produced one of the first reclamation design documents that explicitly considers regional planning for reclamation in the oil sands. The document, called the End Pit Lakes Guidance Document (CEMA, 2012), describes the regional geography, the main high-level goals for end pit lakes (water flow management, water quality, bioremediation of process-affected waters and storage of tailings, sustainable aquatic ecosystem), and other uses such as fisheries, economic development, and greenhouse gas elimination. It notes that the region could eventually contain 30 end pit lakes, prioritizing – among other considerations – interconnected waterways and drainage. Assuming the oil sands lake end pit lake technology proves successful, the opportunity to turn the post mining area into a major tourism / recreational area would benefit local populations long after mining ceases.

3 WHEN TO DEVELOP A REGIONAL CLOSURE PLAN

Producing regional closure plans makes the most sense where mines are in close enough proximity to one another to have cumulative effects on the regional watersheds, wildlife, or human populations. There are literally hundreds of mining regions worldwide. In western Canada alone, examples include placer mining along Yukon Rivers, the Athabasca Basin uranium mines, the Athabasca Oil Sands, salt and potash mines in Saskatchewan, and coal fields in Northern BC, Southeastern BC, the Rocky Mountain foothills, and the southern Saskatchewan interior plains. A few examples of mining regions that would benefit from regional closure planning are explored below.

In Alberta, a regional closure plan for the oil sands region makes sense, since most mines share, among other things, orebodies, watersheds, stakeholders, contractors and consultants, and public infrastructure. As well, they generally rely on a trained pool of workers from the city of Fort McMurray and other local communities. All communities in the region will be affected by mine closure, and many will make use of the reclaimed post-closure landscape and surrounding environment (Government of Alberta, 2012).

Similarly, the five large coal mines in the Elk Valley of southeastern British Columbia are all in the Elk River watershed and are managed jointly by a single owner (Teck Coal) with respect to economic, environmental, and social benefits. A regional closure plan would benefit long-term planning here as well (Swanson et al., 2012). Indeed, such efforts are now underway.

The uranium mines in the Athabasca Basin are much more spread out; most of the active mines are relatively small and located tens of kilometres apart. But these mines share infrastructure and a workforce pool, and exert a tremendous impact on the region economically. Therefore, a regional closure plan in this area would make sense. Perhaps some of the more distant mines might have the option of joining the planning efforts.

In some cases, sharing of information and technology and joint planning regionally may be viewed as violating national competition laws. COSIA (Canada's Oil Sands Innovation Alliance) has worked to carefully define which areas are competitive (for example, oil sands extraction technology) and which areas can be collaborative, such as in environmental research and development (see Lewis, 2011). Regional collaborative initiatives would need to be transparent and meet competition rules.

In short, regional planning would be recommended in areas where resource extraction, the environment, or social benefits within a region would be impacted. Given the effort required for regional planning, one would want to establish the benefits before committing to the development of a regional plan.

4 THE OPPORTUNITY OF REGIONAL CLOSURE PLANNING

To help improve on existing practices and as a means of highlighting the case for regional planning, Table 2 examines some of the weaknesses and opportunities in the present approach of lease/landscape scale mine closure planning.

Table 2. Some weaknesses and opportunities with the current state of practice for closure planning.

Shortcomings of only designing at the lease / landscape level	Opportunities for regional planning
Some wildlife species operate at regional scales not dealt with well at lease/landscape planning levels	Habitat consideration for some animals (especially large mammals) is regional in nature. Regional closure planning is the right scale to examine and optimize habitat. Regional and lease-scale reclamation planning allows for creation of wildlife travel corridors between adjacent mines to allow large mammals transit (e.g., De La Mare, 2006).
Stakeholders don't have time to invest in all closure planning activities for areas with multiple mines	Much stakeholder input can be provided at the regional level and influence regional plans. The ELU Committee, IRP, and LARP provide examples of regional consultation. A standing committee on regional closure planning would provide a good venue for stakeholder interaction.
Cumulative effects is generally a regional activity	Cumulative effects work is common now in most mining regions and indeed extends to other land disturbances such other industry, infrastructure, and municipalities. Regional closure planning is a good way to address many cumulative effects.
Mine closure impacts local populations, especially multiple mine closures	Mining activity varies with commodity prices. Mine closure is particularly difficult on local populations, even more so when multiple mines close at the same time. Regional mine closure planning would allow better management of these changes. For example, mining and reclamation by various operators minimized impacts on the Muskeg River watershed (Alberta Environment, 2008).
Missed opportunity for shared research and monitoring	There are potential efficiencies in reclamation and other environmental research and local and regional monitoring. Regional closure planning, and associated collaboration, would help. As the use of LiDAR topography and remote sensing become more common, there are economies of scale that are available.
Lack of formal sharing of reclamation experience and planning technology between mine operators	Ongoing regional closure planning offers the opportunity to learn from progressive reclamation. In the case of end pit lakes, where international experience has been difficult to predict (McCullough, 2011), sharing of regional pit lake performance between operators is critical for risk management.
Duplicative development of regional climate, surface water and groundwater models. Overlap in management.	Groundwater remains a major issue at many mines and mining regions. Groundwater flow regimes are often regional and require regional modeling. Sharing geologic information and regional groundwater (and surface water) modeling is a major opportunity. Shared infrastructure (roads, powerlines, tailings pipelines, emergency services, contractor and camp facilities) would help improve bottom lines and enhance cooperative reclamation activities.
Lack of sharing of tailings and waste disposal facilities and reclamation material	Most mines attempt to operate independently. But there are major regional opportunities for joint disposal of wastes (e.g. Hardy Associates and Monenco Engineering 1978), use of another mined pit for tailings disposal, shared reclamation stockpiles, shared drainage systems, and regional landfills. Staged mining could allow an operator's old inventory of process-affected water to be used by a new mine, and its mined out pit as an initial tailings pond for the new mine.
Duplication of water treatment facilities	Water treatment facilities for post-closure discharges could be centralized, taking advantages of economies of scale and reducing post-closure "sprawl" of maintenance intensive activities across the region.

5 SAMPLE REGIONAL MINE CLOSURE PLAN

Following is a suggested initial table of contents of a regional mine closure plan. It builds on the work of Bowman and Baker (1998), and the format of a lease/landscape closure plan. It draws from the tables of contents of the oil sands IRP and LARP discussed above, and attempts to address the opportunities listed in Table 2.

- Introduction
  - Purpose of the plan
  - Planning process and participants
  - Definition of the region and the mines
  - Regulatory details
  - Major regional issues
  - Vision for the region
- Geography
  - Climate
  - Physical geography
  - Human geography (settlements, infrastructure, other activities / industries)
- Mining activities
  - Mining techniques
  - Planning techniques
  - Closure and reclamation
  - Schedule
- Regional goals for the closure landscape
  - Resource extraction goals
  - Land use goals
  - Landscape performance goals (post reclamation)
  - Societal goals (managing expansion, maturing, and contraction of populations)
- Closure and reclamation plans
  - For each mining operation
  - Along shared boundaries
  - Integration with other industries
  - Integration with the natural environment
- Expected regional reclamation performance
  - Geotechnical
  - Surface water
  - Ground water
  - Soils
  - Vegetation
  - Wildlife
  - End land uses
  - Socioeconomic
  - Assessment of planned integration and future opportunities
- Expected performance and residual risks assessment
- Adaptive management framework including long term monitoring and maintenance
- A forward look at the next plan

The regional plan would build on lease/landscape closure plans. Like the IRP and the LARP, it would need to be kept to a modest length (<50 to 100 pages) with a few key landscape maps from each operation and a few regional maps that focus on regional issues. The ongoing planning process will prove more important than the plan itself, but the preparation of periodic plans will be a central focus for the group. Dynamic, interactive plans might be a better format than traditional bound reports and maps.

6 CHALLENGES TO REGIONAL PLANNING

Regional mine closure planning requires great effort. Multi-disciplinary teams from each mine will need to work together under strong direction. Many of the issues will require high-level

management negotiations. While much of this work is already occurring today, the extent of the full commitment required of senior staff to long-term planning and negotiations (most which will be ongoing over decades, in some cases more than a century) is daunting. Representatives of mine management, technical staff, stakeholders, and regulators (and their advisors and consultants) tend to remain in their positions for only a few years. Consequently, regional teams will have a steady change of participants, necessitating extensive training and record keeping.

Polluter pays legislation is often interpreted as limiting the ability of each mine to handle one another's wastes (e.g. McKenna, 2002). This greatly restricts opportunities for comingling and shared facilities. Room may exist to amend policies and legislation that stand in the way of solutions that benefit the environment.

Mines start up and wind down in dramatically different stages, often apart by several decades. New entrants may feel restricted by the previous activities by others, or may be perceived as getting a "free ride" by established operators. During their initial permitting process, new entrants may promise more than can be reasonably delivered. Issues of fairness need to be carefully managed. Methods to deal with the time element will need to be developed and practiced.

Mine plans and lease-scale closure plans change relatively frequently with changes in ownership, commodity prices, and ongoing ore-body drilling. Maintaining a coherent regional plan with constantly changing mine plans will be extremely difficult, and may require changes to mine practices, such as accelerating the timeline for the delineation of the orebody (Abbott and McKenna, 2012).

Clearly, the benefits of an ongoing regional closure planning process will need to outweigh the costs. Strong leadership by industry and regulatory agencies will be key.

Remediation plans for historical mining districts highlight some of the complexities. For example, the clean-up of the Silver Valley Mining District near Coeur d'Alene in Idaho is a sobering case history (USEPA, 2012). Hundreds of small abandoned mines and a few large mines, mills, and tailings deposits present health and safety hazards to local residents. Developing a regional remediation plan took nearly 30 years. The clean-up is expected to cost $635 million and take an additional 30 years to complete. Many of the reclamation and decontamination solutions are suboptimal for both cost and for the environment. The process is made more complicated by legal issues, especially related to the history of ownership of the individual mines over the last century, and by the effort required to coordinate dozens of key stakeholder groups. Clearly, the sites would have benefited from a comprehensive regional closure plan before mining had begun. But at that time, even mine reclamation was waiting to be invented.

7 PRODUCING THE FIRST REGIONAL CLOSURE PLAN FOR YOUR REGION

Table 3 provides a five year schedule for producing a region's first closure plan. These steps are adapted from Bowman and Baker (1998), and updated with the authors' recent experience.

None of these activities is entirely novel. But merging these activities into a workable process remains to be achieved. Despite lacking a formal plan for regional planning, the oil sands operators and regulators have recently completed most of the tasks in Year 1 and Year 2 and all operators submitted strong closure lease/landscape plans at the end of 2011, including electronic copies in a common GIS format.

With strong leadership and commitment, a mining region can embrace this new direction. Although the region's first regional closure plan will prove difficult to devise, the mines, their stakeholders, and regulators will reap more benefits with each passing year. In time, it will be difficult to imagine a busy mining region that lacks this type of planning integration, as sustainable mining increasingly becomes standard industry practice.

Table 3. Five years to a regional closure plan

Date	Activities
Year 1	• Commit to ongoing closure planning, that is well-funded with wide participation. • Identify the mining region boundaries and identify all historical and active mining and mine projects that are likely to proceed. • Schedule a common date for submission of the next lease/landscape closure plans for the end of Year 3. • Create a team and a framework for regional closure planning. The team will include representatives from each mining company, stakeholders, regulators, and First Nations. • Establish an independent review team. • Develop a concise list of agreed upon land uses.
Year 2	• Agree on common definitions for reclamation and synchronize the development of lease closure plans using common GIS polygons and definitions, common or compatible mine planning software, a survey grid (most plans use UTM coordinates now). • Develop a concise list of closure planning and landscape performance goals including full listing of all related regulations, government policy, and agreements with stakeholders. Conduct a review of environmental impact assessments for the mining and other industrial projects for shared data, issues, and commitments. • Identify opportunities for regional collaboration, with a focus on lease boundaries for adjacent mines. • Catalog regional plans for other industries, infrastructure, and municipal projects.
Year 3	• Prepare and submit or share lease/landscape closure plans for individual mines, with a focus on regional and lease boundary issues. • Create an effective adaptive management program (see CEMA, 2012, Appendix D).
Year 4	• Compile plans and develop regional basis. • Affirm regional goals. • Begin the regional closure plan collaboratively.
Year 5	• Finish first draft of the regional closure plan. • Vet the plan with all participants. • Initiate a new monitoring and mitigation plan as part of adaptive management. • Continue to reclaim progressively. • Set a schedule for annual review of the regional closure plan and start preparing for the next regional closure plan five years hence.

8 ACKNOWLEDGEMENTS

Many of the learnings presented are based discussions and ideas from regulators, mine operators, stakeholders, and consultants working on closure and reclamation plans in the Athabasca Oil Sands over past 20 years. Table 1 is adapted from unpublished work with Jason Fisher and Brian Eaton of Alberta Innovates Technology Futures. Illustrations are provided by Derrill Shuttleworth. David Wylynko of West Hawk Associates is thanked for editing the manuscript.

9 REFERENCES

Abbott, R and McKenna, G. 2012. Sustainable mining now: turning ideas and ideals into reality. Mine Closure 2012. Brisbane, 2012. Australian Centre for Geomechanics, Perth. p771-781.

Alberta Environment, 2008. Muskeg River interim management framework for water quantity and quality: Management guidance for aquatic components of the Muskeg River watershed. Government of Alberta. June 2008, Edmonton. 99p. www.environment.gov.ab.ca/info/library/7951.pdf

Bowman, B., and Baker, D. 1998. Mine Reclamation Planning in the Canadian North. Report prepared for the Canadian Arctic Resources Committee.79p.

CEMA, 2012. Oil sands end pit lakes design guide. Cumulative Environmental Management Association. Fort McMurray. 434p.

CEMA-RWG Landscape Design Subgroup, 2005. Landscape Design Checklist. Cumulative Environmental Management Association. Fort McMurray. 8p.
De La Mare, C. 2006. Wildlife corridors expected to play a greater role in oil sands planning. Oil sands Review. November 2006. http://www.airwaterland.ca/article.asp?id=7455
Forman, R.T.T., 1995, Land mosaics: the ecology of landscapes and regions. Cambridge University Press, New York. 632p.
Government of Alberta, 2002. Fort McMurray-Athabasca Oil Sands Subregional Integrated Resource Plan. Alberta Environment and Alberta Sustainable Resource Development Publication No: I/358. http://srd.alberta.ca/LandsForests/LandusePlanning/IntegratedResourcePlans.aspx. 67p.
Government of Alberta, 2012. Lower Athabasca Regional Plan (LARP): 2012-2022. Government of Alberta. Edmonton. https://landuse.alberta.ca/RegionalPlans/LowerAthabascaRegion/Pages/default.aspx 98p.
Gunnett, J.W. 1975. Regional Aspects of Mine Planning to Increase Production and Enhance Reclamation: Third Symposium on Surface Mining and Reclamation, Oct 21-23, 1975 National Coal Association. Washington DC.
Lewis, J. 2011. Does collaboration undercut innovation in the oil sands? Alberta Oil Magazine. June 01, 2011. http://www.albertaoilmagazine.com/2011/06/good-co-op-bad-co-op/
MAC (Mining Association of Canada), 2011. Towards sustainable mining – mine closure framework. Mining Association of Canada. Ottawa. http://www.mining.ca/site/index.php/en/towards-sustainable-mining/performance-measures-a-protocols.html. 1p.
MAC (Mining Association of Canada), 2012. 2012 Facts and Figures of the Canadian Mining Industry. Ottawa. 140p
McCullough, C.D. 2011. Mine Pit Lakes: Closure and Management. Edited by C. McCullough. Australian Centre for Geomechanics, Perth. 183p.
McKenna, G. 2002. Sustainable mine reclamation and landscape engineering. PhD Thesis in Geotechnical Engineering, Department of Civil and Environmental Engineering, University of Alberta, Edmonton, 660p.
McKenna, G, An, R, Scordo, E, McGreevy, J. 2013. Toward effective closure planning: from progressive reclamation to sustainable mining. Tailings and Mine Waste 2013. November 3-6, 2013. Banff.
Oil Sand Mining End Land Use Committee, 1997. Oil Sand Mining End Land Use Committee Report and Recommendations. Oil Sands Fort McMurray, Alberta. 48p.
RM Hardy & Associates Ltd, and Monenco Consultants Ltd, 1978. Athabasca tar sands off-lease tailings disposal study: interim report: Calgary, R.M. Hardy & Associates Ltd. and Monenco Consultants Ltd. Calgary. 115p.
Swanson, S., Abbott, R., Funk, W., Kirk, L., McKenna, G., Ohlendorf, H., and Sandy, T., 2011, Building stakeholder engagement in sustainable solutions- the strategic advisory panel on selenium management. Mine Closure 2011. Lake Louise, Australian Centre for Geomechanics, Perth. p189-196.
USEPA, 2012. Interim Record of Decision Amendment, Upper Basin of the Coeur d'Alene River, Bunker Hill Mining, and Metallurgical Complex Superfund Site. United Stated Environmental Protection Agency Region 10. Seattle. August 2012. http://yosemite.epa.gov/r10/cleanup.nsf/sites/bh+rod+amendment#RODA. 488p.

Post-closure land-uses in the Athabasca Oil Sands area

Kelly Nelson Doran
Harvard University Graduate School of Design – Department of Landscape Architecture, Cambridge, Massachusetts, USA

ABSTRACT: Existing oil sands reclamation is primarily focused on the physical and environmental rehabilitation of post-extraction sites. In contrast, there is relatively little dialogue about the long-term socio-economic impact of mine closure and potential future uses of the Athabasca Oil Sands Area. Relative to other forms of mining oil sands reclamation and closure practices have a unique ability to plan for a wide range post-extraction land-uses. Recognizing this opportunity, this paper asks the question: After extraction, what are the oil sands? With a regional population estimated to reach approximately 250,000 people, the long-term viability of alternative urban, industrial and recreational land-uses requires exploration. With this in mind, future reclamation and closure efforts could serve to design and develop landscapes capable of sustaining new economies. This paper examines regional issues surrounding reclamation, the province's land-use plans for the AOSA, and related best-practice closure planning to inform a series of development scenarios for future oil sands land-uses.

1 INTRODUCTION

"Alberta is a global leader in the innovative, responsible, and collaborative development of oil sands. The benefits of development continue to support clean, healthy, and vibrant communities for Albertans and future generations." (Alberta 2009).

Oil sands reclamation and closure must begin addressing the region's long-term social and economic land-use planning needs to create a landscape capable of sustaining future generations. By stipulating that the Athabasca Oil Sands Area's (AOSA) surface mineable region return to pre-development conditions—that of a remote, largely uninhabited boreal forest—current closure planning policy and practice fails to address the urban, social, and ecological transformations underway.

The AOSA has become urbanized. The constant construction of pipelines, runways, highways and housing over the past two decades has irreversibly connected Fort McMurray and the entire AOSA with national and international flows of investment and exchange. The remote region's rapid growth has demanded (and will demand further) public and private investment into transportation and municipal service infrastructure to support an ever expanding urban footprint. Future expansion of these infrastructures will create even greater connection with the region's previously remote landscape, allowing for a greater diversity of access, ownership, and use of the AOSA. A region almost entirely dependent on long-haul imports for their existence could

reclaim with various forms of production—agricultural, industrial, and recreational—to support current and future populations.

Driving this urban expansion is an unprecedented era of socio-economic change. Having grown from roughly 50,000 to 125,000 over the past 20 years, the area's population is projected to exceed 225,000 by the year 2040 (Alberta 2011). A sustained influx will further change the region's already altered demographic and socio-economic makeup. As projects increasingly move from construction to production they attract, and often require, an older, more educated and permanent workforce. The long-term employment offered by operations results in long-term investment into housing, community and the future of the region. By no means a new phenomenon in the Canadian context, the existing mono-industrial make-up of the AOSA will require strategies for economic diversification in order to create a sustainable community.

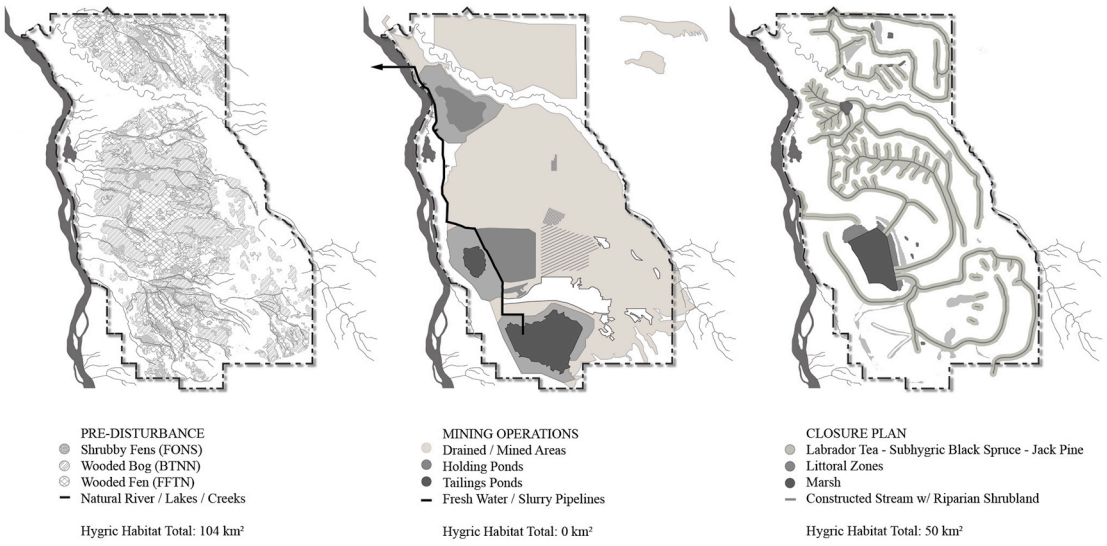


Figure 1. Overview of the Suncor Millennium Mine Pre-Disturbance and Post-Closure Hygric Conditions

Ecologically, existing reclamation policies targeting the return of local boreal forest ecosystems prescribe the construction of upland forests, wetlands and storage lakes in place of a complex ecologic fabric of fens, bogs, and peat lands (Rooney, Bayley et al. 2011). Under this mandate, the capacity of reclamation to produce "equivalent land-use capability, optimizing the value of the watershed, timber, wildlife habitat, fish habitat, recreation potential or other resources" is severely hindered by the topographic reality of the mining process (Suncor 2009). Operating across natural watershed boundaries, habitats, migration routes, and flyways - existing mining practices necessarily require operations to transform their entire lease. As evidenced by the Suncor Millennium closure plan, operations are set to completely reshape the original topography to create a landscape of hydrological control; initially a riverine landscape, the lease is designed to become an endorheic assemblage of marshes, littoral zones, and shrub lands (Suncor 2009). Recognizing this fundamental change as an unprecedented opportunity to engineer new ecologies, reclamation could engender new and economically sustainable uses.

It is clear that the region's entire ecosystem—which the patterns of extraction, reclamation, and urbanization are intrinsically a part of—is undergoing a radical and irreversible transformation. Moreover, this system's present form is ultimately unsustainable in the long-term. The industry primarily supporting the growth of the region will inevitably cease to provide when oil sands extraction ramps down. To create a truly sustainable landscape, closure planning needs to create new ecological situations, provide for a wider range of programmatic possibilities, and recognize the unique potential oil sands reclamation offers for new land-uses (Berger 2008).

2 EXISTING AOSA LAND USE PLANNING

2.1 *Land Use Plans*

The region's future post-closure land-uses will largely be determined by the Province. Beyond the existing closure requirements outlined in the Environmental Protection and Enhancement Act and the Public Lands Act, and land-use guidelines outlined in the Municipal Government Act, the Alberta Land Stewardship Act and the Land-use Framework, Alberta's position towards future Crown and private land-use has recently shaped two plans addressing the AOSA directly: the Lower Athabasca Regional Plan (LARP) and the Comprehensive Regional Infrastructural Sustainability Plan (AOSA CRISP).

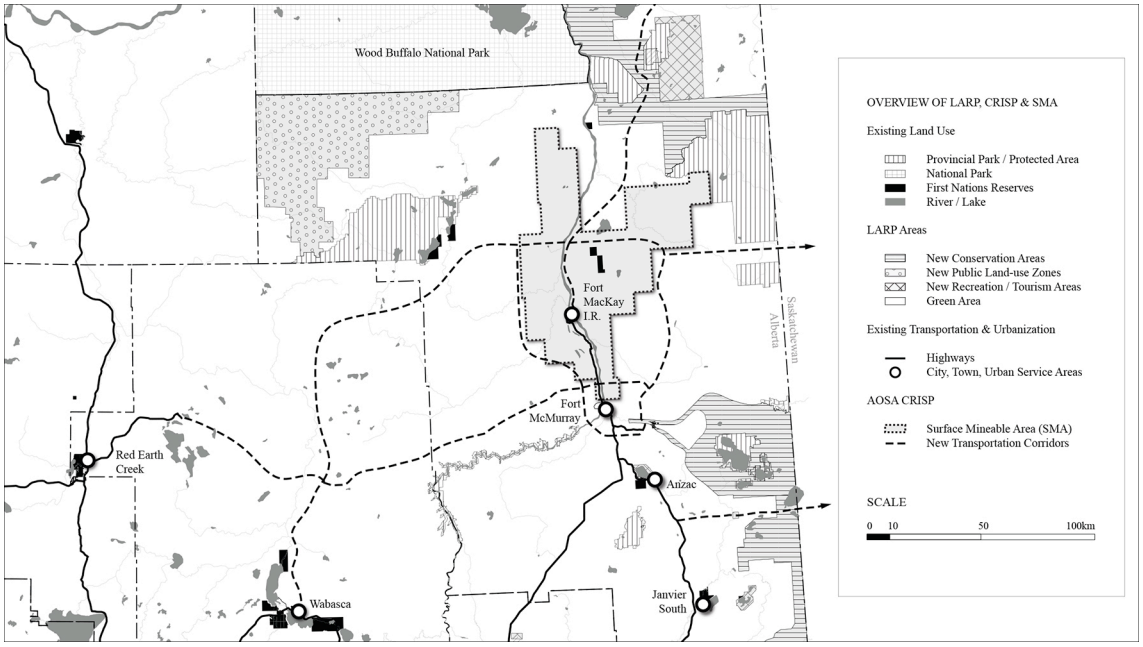


Figure 2. Composite map of LARP and CRISP focused on the SMA.

2.2 *The Lower Athabasca Regional Plan (LARP)*

The LARP outlines a set of strategic directions for the region to "achieve robust growth, vibrant communities and a healthy environment over the next 50 years" to be implemented by provincial, municipal and aboriginal authorities (Alberta 2012). The LARP's *Strategic Plan* identifies the need to further develop a diversified economy that relies on energy, forestry, agriculture, tourism, recreation, mineral extraction, and technological and environmental innovation. Particular to the ecological and social impacts of the oil sands, the Plan has highlighted that "Alberta's intentions and expectations around environmental and social outcomes need to be clearer, so that those who operate on the landscape can co-ordinate, innovate and succeed in creating a balanced set of economic, environmental and social outcomes for the region"(Alberta 2012). To achieve this the LARP calls for an improved integration of industrial activities, the creation of new interconnected conservation areas, the inclusion of aboriginal peoples in land-use planning, the management of biodiversity , and for both a reduction in active land disturbances and timely reclamation of disturbed lands. Specific to the future uses of disturbed, post-mining areas the Plan states that:

"Reclaimed lands will be used to help achieve the region's desired economic, environmental and social outcomes based on the region's evolving needs. As oil sands resources are recovered and the lands are reclaimed over time, opportunities will arise to reconnect lands to help achieve regional objectives relating to biodiversity, recreation and forestry."

The majority of the AOSA's surface mineable area (SMA) falls within the designated 'Green Area' which the LARP has identified as needing "an integrated, watershed-based *landscape*

management plan." Such a plan would inform future land-uses directly by establishing the set of landscape values, models, implementation and policy tools, environmental monitoring and data collection, a tailings management framework and progressive reclamation strategy prescribed. A landscape management plan, together with the LARP's future iterations (it being subject to revisions on 5 year intervals), would be well-suited to direct and coordinate the implementation of alternative land-uses across the AOSA.

2.3 *The Comprehensive Regional Infrastructure Sustainability Plan*

Supporting the LARP, the AOSA CRISP outlines a set of guidelines for the long-term development of transportation, water and wastewater, education and health care infrastructures (Alberta 2011). A 30-year plan, phased across four stages, links infrastructural needs to the oil sands industry's projected production and employment figures. Flexible and responsive to fluctuation rates, the CRISP's monitoring framework is designed to identify where and when increased demand will occur to guide future spending. The success of the plan relies on the alignment and implementation of the Plan by a range of stake-holders: multiple Government of Alberta departments, all levels of government, and the oil sands industry.

Significant to future land-uses of the AOSA, the CRISP identifies a series of transportation corridors that would establish new connections across the SMA. These corridors, set to encircle and bisect the area, would create greater public access to all mining project locations in the short-term and to their reclaimed lands in the long-term. Along these new corridors the Plan proposes the phased implementation of additional health care, education and water and waste water treatment facilities, upgrades to public and private airports and urban growth areas to support anticipated population growth. Focused primarily in and around Fort McMurray, this infrastructural spending would serve to permanently bond the landscape of the oil sands to Alberta's third largest urban centre.

Additionally, the Plan calls for new inter-regional highway connections across to northwestern Alberta via Red Earth Creek, northern Saskatchewan and other oil sands plays, and to the Northwest Territories via the Athabasca Valley. New year-round vehicular networks, in combination with existing social, aerial and nautical networks, would reposition the AOSA's SMA as a central figure in a new regional geography. No longer remote, the Plan positions Fort McMurray and a reclaimed oil sands area to become a productive and diversified service-providing centre for Canada's growing sub-arctic communities.

3 MODEL POST-RECLAMATION LAND USE PLANNING FRAMEWORKS

"Changes begin in people's minds. People's perceptions – their way of seeing Lusatia – must be changed so that they can see new possibilities and opportunities. The transformation of the Lusatian landscape will take decades – but the IBA's philosophy is to create the future rather than simply waiting for it."(IBA 2013)

The ongoing transformation, recultivation and reprogramming of lignite mines in western Germany's Lusatian region – a landscape that has undergone a century of topographic alteration - is a significant precedent for the oil sands. The Internationale Bauausstellung Fürst-Pückler-Land's (IBA) project team composed of multiple levels of government, energy industry representatives, local research institutions and the public has produced a long-term regional reclamation and redevelopment strategy for an area roughly ¼ the size of the AOSA's SMA. The IBA's mission to combine creative and technical innovation, to draw attention to the region, and to create new industrial and economic opportunities through the recultivation of the landscape has created a series of projects that exploit the opportunity of designing a landscape from the ground up.

The IBA project area encompasses roughly 1,000 square kilometers of former open cast mine sites surrounding the towns of Cottbus and Seftenburg in eastern Germany. Large-scale open-cast mining first developed the region's shallow lignite formations at the turn of the century. The region's proximity to Berlin, Leipzig and Dresden made it the primary source of both energy extraction and production from the 40's onward for the former German Democratic Republic. Progressive reclamation had kept pace with extraction until an era of rapid mine expansion

in the 1970's. Thirty years of the production-reclamation gap produced an enormous area of unattended, non-reclaimed, underutilized, quasi-wild landscape of lakes, emerging forests, grasslands and dunes. In 1994 regional planning authorities, having recognized that the scale of this new landscape required "a detailed strategy over and above community boundaries", commissioned the IBA to prepare a feasibility study intended to "shape (a) new post-mining landscape." Following the success of the study, the 'Lusatia Charter' was signed by representatives from local and federal government, industry, science and research institutions to support the project through the a joint commitment to dealing with post-mining landscapes.

Under the umbrella of the "Regional Planning Group Lusatia-Spreewald", the IBA established the public-private framework to effectively coordinate and execute a series of 30 projects. Each project addresses elements of adaptive re-use, economic development and diversification, afforestation and agriculture, recreation and tourism, and renewable energy production. The projects fall under one of seven classifications of reuse related to site-specific reclamation and redevelopment issues: *new territory, border landscapes, urban landscapes, transitional landscape, energy landscapes, waterscapes* and those of *industrial heritage*. *New territory* projects capitalize on the opportunity to fundamentally redesign surface mines via the composition of soil, relief, vegetation, circulation and the positioning of landmarks. Given the proximity of Poland to the project area, *border landscape projects* attempt to foster cross-border landscape initiatives to extend reclamation as a means to create cross-border tourist initiatives. *Urban landscape* projects highlight the re-use of worker housing through their disassembly and conversion into new, large-scale developments for new users. Indicative of the IBA's philosophy of creating vs. waiting, *transitional landscapes* program interim uses for the often wild, forbidden zones of ongoing reclamation. Energy landscape projects wed the growing roles of renewables with sparsely populated areas to create models for layering different energy sources on reclaimed sites. Capitalizing on the archipelago of pit lakes created by mining, *waterscape* projects support IBA's rebranding of the mine-scape as a lake area for tourism and economic development. Finally, as an anchor of the European Route of Industrial Heritage *industrial heritage projects* celebrate the distinctive scales, technologies and operational methods of lignite surface mining.

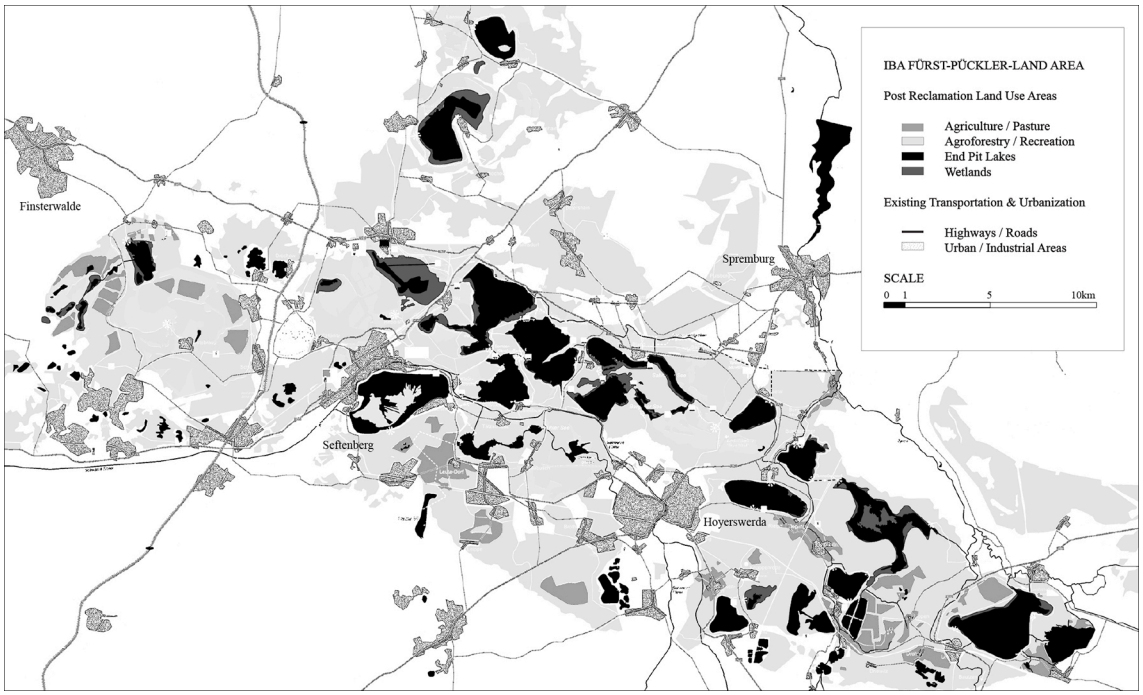


Figure 3. Overview of IBA Project Area

Of particular relevance to the future of the AOSA are projects that specifically address reclamation and recultivation as a means of generating economic diversification and new forms of renewable energy. Building on the regional tradition of energy generation and supply the *Wel-*

zow Energy Landscape project works hand-in-glove with ongoing lignite mining to forma landscape tailored to a varied mix of renewable energy production. The IBA's interest in the productive potentials of the post- mining landscape represented an opportunity for agriculture, forestry, science, engineering, and landscape architecture to collaborate, to experiment, to employ new methods in establishing soils and vegetation, and to develop innovative land use concepts for wide expanses of reclaimed lands.

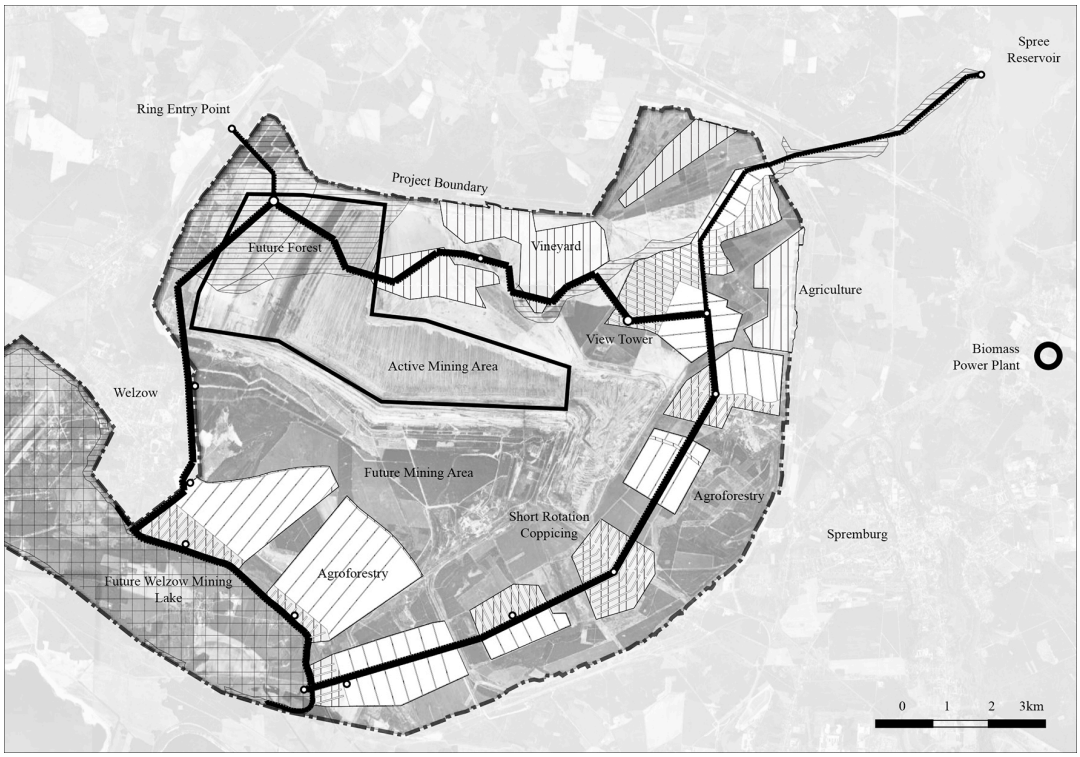


Figure 4. Composite of IBA's "Energy Ring" plan with aerial image of active mine extents (2011).

An 'energy ring' organizes the area by connecting a project's active programs - overburden stockpiling, surface mining, reclamation, soil farms, test-plots, tree nurseries, agroforestry plots, agricultural fields, impoundment lakes, overlooks, etc. - via a twinned pedestrian/vehicular loop (IBA 2010). This ring has allowed for a variety of species, cultivation methods and harvesting techniques to be tested simultaneously and proximately. This unique R&D environment allowed surface mine operators to work with a biomass company and researchers at Brandenburgische Technische Universität to develop and assess 10 years of fast-growing species across 170 hectares of reclaimed land (Kaschel, Friedricj et al. 2013). Based on the success of the project, the IBA launched a public awareness campaign and a touring exhibition to promote the exchange of experience and knowledge with applicable sites across the EU. More locally, the project has expanded; beyond its original boundary there are plans to acquire other reclamation sites and layer existing biomass production sites with wind and solar generation. Intended to serve as a "long-term productive and practical laboratory" for energy production and information, the Welzow project illustrates the potentials of a transformed energy region

Equally relevant to the future of the SMA is the series of *waterscape* projects that both adapt and anticipate the recreational and urban development potentials offered by the constellation of 30 end pit lakes. Under the IBA's leadership these projects have established a larger landscape park that has been rebranded as the Lausitzer Seenland (Lusatian lake region). The Seenland, miles for the Baltic coast, has attracted new users and investment to what is now Germany's most modern water tourism region.

Each lake's unique age, size, shape, depth, ecology and proximity to urban and industrial areas created a range of aquatic identities and functions. Based on these criteria the IBA has selected an initial cross sample of See's to be accessed and programmed as the first wave of the

park's master plan. Similar to the energy ring, the new Sees are connected to each other and the region through a network of recreational paths. To promote aquatic species movement and water circulation, a series of canals are to be constructed to develop the region's emerging ecology. This new network also serves to rejuvenate former industrial sites and worker housing communities by bringing new users to underutilized infrastructures.

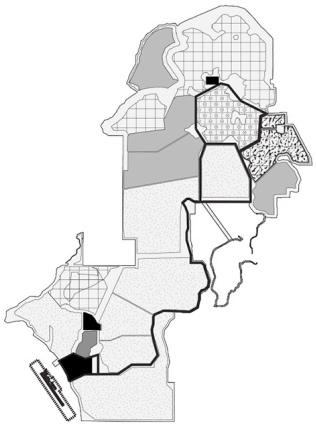


Figure 5. Aerial view of Lusatia area end pit lakes with adjacent housing development

Beyond adapting existing lakes, the IBA project also has the foresight to anticipate the creation of future water bodies. With active mining set to unearth a huge trench at the edge of Cottbuss, the city commissioned a design competition to provide a landscape development plan for a lake 20 years from creation. Coined "Cottbuser Ostsee", (Cottbuss' Baltic) the region's soon-to-be largest water body (1,900 ha) will emerge next to the region's largest community. To initiate the project a recreational route that simultaneously inscribes the perimeter of the lake while creating visual access to ongoing mining operations creating the new landform has been constructed. The new parkway gives residents access to a set of viewing towers overlooking the otherwise flat landscape, as well as seasonal toboggan runs that slide into the dry bed of the future lake. Perhaps most forward-looking of all, the future location of the City's new beach and harbor, currently at the edge of the mine, plays host to the Ostseefest: an intentionally premature gathering to celebrate the embodied potential of its yet-to-be reclaimed landscape.

4 AOSA ALTERNATIVE LAND USE SCENARIOS

Shell's Jackpine mine serves as the case study site for various land use scenarios. At just over 200 square kilometers, the mine's total disturbance area occupies a space comparable to major Albertan provincial parks, University of Alberta field research stations and forestry lease areas, while providing a contiguous landmass capable of connecting and supporting multiple uses (Shell 2012). The mine's existing progressive reclamation and closure plan, which intends to divide the site into 22 discrete cells over the next four decades, is ideal for a wide range of future users to progressively occupy parts of the site while operations are ongoing. Moreover, the relative uniformity of each cell's size and shape will allow models of occupation to be developed, tested and replicated over time. The uniform south-to-north sequence of overburden removal, stockpiling, mining, tailings disposal and progressive reclamation also permits the certification and/or handover of reclaimed lands to occur at a safe distance from ongoing operations.

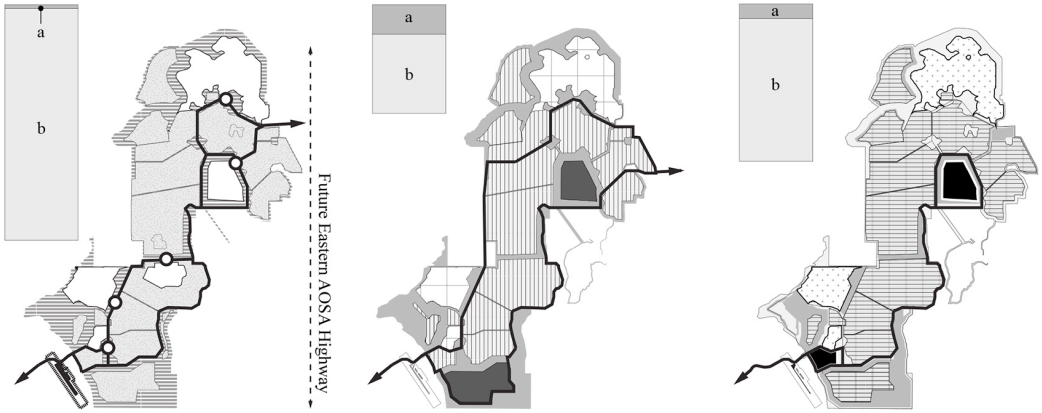


Jackpine 2050 Closure Plan

- Reclamation Soil
- Overburden Disposal Area
- Sand Tailings
- Fluid Tailings
- Centrifuge Cake
- Mining Areas
- Facilities & Circulation

Total Distubance Area : 209.9 km²

Figure 6. Shell Canada's Jackpine Mine Closure Plan (2050)



Scenario 1 : Jackpine Park

- Recreational Lakes
- Programmable Park Cells
- Program Hubs
- Parkway Loop & Airfield
- Perimeter Forest

Programmatic Area Comaparison
a. McDonald Island : 1.2 km²
b. Lesse Slave Lake PP : 77.7 km²

Scenario 2 : Agroforestry / Biomass

- Biomass Production Fields
- Research Plots
- Perimeter Forest Growth
- Marshlands
- Energy Ring

Programmatic Area Comaparison
a. U of A EMEND Project : 10 km²
b. U of A George Lake Station : 48.56 km²

Scenario 3 : Rangelands / Agriculture

- Flat Organic Soils
- Sloped Sandy Soils
- Water Supply / Fish Farms
- Stockyards
- Internal Circulation

Programmatic Area Comaparison
a. Syncrude Bison Area : 5.0 km²
b. U of A Kinsella Station : 48.5 km²

Figure 7. Future Land Use Scenarios for Shell Canada's Jackpine Mine

The post-closure landscape offers a variety of topographic and edaphic opportunities and constraints for future development. Much of the site is planned to be underwater; three large end pit lakes are planned across the site covering an area of roughly 30 square kilometers with a total developable, designable perimeter of roughly 60 kilometers of lake edge. Dedicated to a variety of disposal areas, the majority of the lease will be relatively flat requiring a cover design that in-

corporates soil and slope specification. The perimeter dykes of these areas – built primarily of clean sandy fill – provide a range of solar exposures and soil characteristics suited for new occupations and constructions. Finally, the areas housing the mine's facilities provide service infrastructures that could be piggy-backed, extended or reincorporated into future uses.

4.1 *Scenario 1: Recreation + Research*

To satisfy the "growing demand for quality lake-based recreation provides opportunities" that support a regional tourism economy and diversify its economic base this scenario establishes a series of autonomous recreational and research cells that collectively establish a larger park (Alberta 2012). The topography of elevated mounds, high ridges, excavated end pit lakes and yet-to-be determined cover of Jackpine's post-mining landscape is ideal for recreational programs. New lookouts, embankments and slopes shaped by disposal create new vistas across the lease and SMA. Conversely, the 3 excavated end pit lakes provide multiple depths of water suitable for a variety of riparian ecologies and recreational activities (McKenna, Hrynyshyn et al. 2012). Borrowing from Lusatia, boat launches, campsites, developable housing sites and other program hubs could be connected by a multimodal trail network that follows the former road network of mining operations to connect cells to each other. Located an hour's drive from Fort McMurray between highway 83 and a future eastern route, and serviced by its own airstrip, Jackpine is close enough to serve as a day excursion for locals or a weekend retreat for those further afield.

With a land area roughly that of Elk Island Provincial Park, Jackpine is also sufficiently large to house a diverse set of research and ecological management zones next to active recreational zones. Tailings disposal facilities and ODA's could take on distinct land forms and soils to engender a variety of habitats and uses. In initial stages the establishment of field stations, nurseries and breeding grounds in the southern edge of the park would create the seedlings, species and know-how required to recultivate and grow the park over time. Cells designated as conservation zones could permit seasonal uses (hunting, fishing, etc.) to aid in the monitoring and collection of data required for certification. To organize these regimes of research and recreation, long-term local employment opportunities – specifically for the First Nations communities in close proximity – would be created through the incorporation of a post-closure park.

4.2 *Scenario 2: Agroforestry and Biomass Generation*

The establishment of agroforestry and biomass production would convert a lease's ability to produce energy from finite to renewable and serve to further diversify the region's established forestry industry. Building upon post-reclamation ecology research underway in the region, such a program would serve to diversify research beyond restorative - towards a set of engineered ecologies able to sustain future energy economies. Learning from the Welzow project - establishing a research and development working group now would support Jackpine's progressive reclamation and certification. Likewise, by "getting in on the ground floor", future operators and research institutions would have the unique ability to test and tune the grade and soil cover of their entire operation.

Because biomass production – in the form of fast growing woody plant crops – requires substantial amounts of water an oil sand lease is well suited to take them on. As seen elsewhere in Alberta, these crops can play a secondary role in an operation's (or community's) wastewater treatment processes as bio-accumulators. When employed in concert with an agroforestry regime – where crops are interspersed among plantings of slower growing, more permanent species – biomass harvesting practices would also aid in the development of a reclaimed site's soil composition. Finally, given the seasonal nature of biomass harvesting – the spaces of production could be supported by recreational and livelihood programs operating throughout the rest of the year.

4.3 *Scenario 3: Rangelands*

AOSA's long standing reliance on imported foodstuffs could be offset and reversed; the one-way traffic of refrigerated trailers could become a two-way exchange along Highway 83 via a

rangeland based agricultural economy developed across the SMA. Developing commercial rangelands on the Jackpine lease would expand 40-fold upon the wood bison program initiated by Syncrude to help an expanding local appetite. By redefining certification requirements and encouraging land management practices that consider biological diversity and agricultural productivity, the Province could create the necessary conditions for an agricultural industry to emerge (Fuhlendorf and Engle 2001).

Rangelands that are graded, planted and periodically burned to create a landscape tailored for wood bison would serve a dual purpose as a biological repository for other native species. By capitalizing on the cellular and sandy composition of the lease, the Jackpine site is well suited to be converted into a series of distinct grazing cells, each capable of sustaining individual herds. The non-orthogonal, non-quarter-sectioned, and relatively large size of these cells allow for a grazing behavior that encourages plant growth, soil development and ecological heterogeneity (Fuhlendorf and Engle 2001). Designing the landform and soil cover of each cell to encourage the development of watering holes and wind breaks would further facilitate migratory grazing patterns while providing sheltered rest areas. In seasonally dry periods the lease's hydrological security (in contrast to operations in southern Alberta) could be drawn upon to water herds. As a composite of multiple rangelands the entire Jackpine lease could be managed as a larger range, allowing for a schedule of prescribed burning, flooding, calving and culling.

5 CONCLUSION

As McKenna identified a decade ago - the greatest challenge in determining post reclamation land use is "setting and achieving land use targets in a sustainable manner" (McKenna 2002). Given the future transformation and occupation of the AOSA, land use targets that promote the creation of sustainable landscapes should account for a variety of future productive uses. "Original and post-reclamation land-uses will not necessarily be identical", nor should they be (Suncor 2009). Future reclamation, by definition, will promote the reordering of new landscape and ecological situations. These new conditions are the ideal grounds to help develop and diversify the future socio-economic make-up of the region. The reclamation of Alberta's oil sands is an unprecedented opportunity to construct an entire region from the ground-up, one designed to sustain generations to come.

6 REFERENCES

Alberta, G. o. (2009). Responsible Actions: A Plan for Alberta's Oil Sands.

Alberta, G. o. (2011). Comprehensive Regional Infrastructure Sustainability Plan for the Athabasca Oil Sands Area.

Alberta, G. o. (2012). Lower Athabasca Regional Plan 2012-2022.

Berger, A. (2008). Designing the reclaimed landscape. London, Taylor & Francis.

Fuhlendorf, S. and D. Engle (2001). "Restoring heterogeneity on rangelands: Ecosystem management based on evolutionary grazing patterns." BioScience **51**(8): 625-632.

IBA (2010). Biomass on recultivated stockpiles. Großräschen, IBA Fürst-Pückler-Land GmbH.

IBA (2013). "IBA Fürst-Pückler-Land ". from http://www.iba-see2010.de/en/verstehen/konzep.html.

Kaschel, A., et al. (2013). Biomass production on hard coal mining dumps in Zwickau and Lugau-Oelsnitz, Central Europe Programme.

McKenna, G. (2002). Sustainable mine reclamation and landscape engineering. Department of Civil and Environmental Engineering. Edmonton, University of Alberta**:** 400.

McKenna, G., et al. (2012). End pit lake guidance document, Cumulative Environmental Management Association.

Rooney, R., et al. (2011). "Oil sands mining and reclamation cause massive loss of peatland and stored carbon." Proceedings of the National Academy of Sciences of the United States of America **109**(13).

Shell (2012). Jackpine Mine Expansion Project Joint Review Panel Suppliemental Information Request, Shell Canada Limited.

Suncor (2009). Tailings Reduction Operations Application.

Acid Mine Drainage

Co-disposal of coal/biomass fly ash and reactive mine tailings under neutral and acidic conditions

Kevin Penney
AMEC Environment & Infrastructure, St. John's, NL, Canada

Eltayeb Mohamedelhassan
Lakehead University, Thunder Bay, ON, Canada

ABSTRACT: This study investigated the co-disposal of reactive mine tailings (RMT) and coal/biomass fly ash (CBFA) to examine the chemical composition of its leachate. CBFA and RMT were blended at various proportions in addition to 100% CBFA and RMT controls. Kinetic column tests conducted in the laboratory simulated their co-disposal when permeated under neutral and acidic conditions. Properties monitored included leachate pH, leachate metal concentrations, and hydraulic conductivity. Under neutral conditions the addition of CBFA to RMT resulted in an increase in leachate pH, a reduction in the concentrations of heavy metals, and a minimal change in hydraulic conductivity. When permeated under acidic conditions using acid mine drainage (AMD), the addition of CBFA also resulted in an increase in leachate pH and reduction in heavy metals concentrations. It was noted that that the hydraulic conductivity of the blend permeated with AMD decreased with the increase of CBFA.

1 INTRODUCTION

The disposal of sulfide-bearing mine tailings in surface facilities is a major environmental concern due to the possibility of AMD production by the mine tailings. Prevention, control and treatment of AMD are major challenges to the mining industry. Conventional active remedial approaches to AMD include collection and treatment, which often require ongoing operation and maintenance. Passive approaches, such as co-disposal, can provide cost effective in situ means to treat the AMD.

Coal fly ash (CFA) is the by-product of coal incineration at terminal power generation facilities. It is an alkaline waste material that also poses challenges for its disposal. CFA leachate often has a high pH and contains elevated concentration of heavy metals, aluminum, and other elements.

The use of CFA, either by itself or amended with other materials (e.g. mine tailings, soil, and bentonite) for treating and/or containing AMD has been investigated in laboratory kinetic column tests (e.g. Xenidis et al., 2002; Shang et al., 2006; Wang et al., 2006; Yeheyis et al., 2007; Perez-Lopez et al., 2007; Penney et al., 2009a; Penney et al., 2009b). These studies showed that CFA can substantially increase the pH of AMD from acidic (pH < 4) to alkaline (pH > 7), and reduce the concentration of heavy metals in the effluent. A decrease in hydraulic conductivity was also observed when higher percentages of CFA were used in the column pack.

This study was conducted to investigate their potential to be disposed together (by mixing) to reduce their leachate's effects on the environment. CBFA and RMT were blended at various proportions (5/95, 10/90, 20/80, 33/67, and 50/50% (CBFA/RMT) by mass) in addition to 100% CBFA and 100% RMT as controls. Kinetic column tests were conducted in the laboratory to

simulate their co-disposal when permeated under neutral (distilled water) and acidic conditions (AMD). Properties monitored included hydraulic conductivity, leachate pH, and metal concentrations in the leachate.

2 MATERIALS AND METHODS

2.1 *Coal Biomass Fly ash*

CBFA was obtained from the Atikokan Thermal Generating Station, in Atikokan, Ontario, Canada, during a 16 % (by mass) wood biomass burn with lignite coal. Major CBFA constituents reported as oxides are silica (SiO_2), aluminum oxide (Al_2O_3), calcium oxide (CaO), sodium oxide (Na_2O), and iron oxide (Fe_2O_3). CBFA contains heavy metals (zinc, lead, copper, nickel, and chromium) at concentrations of a few tens of grams per tonne (see Table 1 below). Acid based accounting (ABA) by the Modified Sobek Method (BC-MEMPR, 1989) indicates a net neutralizing potential (NNP) of 298 tonnes $CaCO_3$/1000 tonnes.

Table 1. Compositions of CBFA and mine tailings

Component	Mine Tailings (%)	CBFA (%)	Element	Mine Tailings (g/t)	CBFA (g/t)
SiO_2	31.7	45.2	Ag	<2	<2
Al_2O_3	8.06	21.5	As	<30	<30
Fe_2O_3	42.3	4.04	Ba	300	3900
MgO	2.97	2.51	Be	0.64	4.2
CaO	3.58	13.6	Cd	<2	<2
Na_2O	1.31	7.33	Co	190	16
K_2O	0.97	0.73	Cu	1200	41
TiO_2	0.59	0.95	Li	<5	16
P_2O_5	0.11	0.62	Mo	<5	10
MnO	0.11	0.02	Ni	4900	27
Cr_2O_3	0.04	0.01	Pb	<100	48
V_2O_5	0.03	0.03	Sr	130	3300
SO_4	1.22	0.2	S	136000	<100
LOI[1]	6.53	0.36	Zn	180	53

Note: [1] Loss on ignition

Grain size analysis in accordance with ASTM D422 (2007), shows that CBFA consists predominately of particles in the silt size range (~84%) with traces of sand (~10%) and clay (~6%) sized particles. The specific gravity measured by ASTM D854 (2006) is 2.42. The liquid and plastic limits (ASTM D4318, 2005) could not be measured on particles smaller than 75 µm, indicating that the CBFA is non plastic.

2.2 *Reactive Mine Tailings*

Fresh mine tailings were obtained from Vale, Sudbury, Ontario, Canada. The tailings were kept in plastic buckets under a layer of water and below 4°C until their use in the column tests. Major constituents reported as oxides in the tailings are Fe_2O_3, SiO_2, Al_2O_3, CaO, and MgO. A large concentration of sulphur (136,000 g/t) is associated with sulphide and sulphate minerals. The most abundant heavy metals are nickel and copper with concentrations in the thousands of grams per tonne (see Table 1 above). ABA indicates a NNP of -416 tonnes $CaCO_3$/1000 tonnes, which corresponds to a strong acid generating capacity.

Grain size analysis shows that mine tailings predominately contain particles in the silt size range (~80%) with some sand (~10%) and clay (~10%) sized particles. The tailings specific gravity is 3.58. Liquid and plastic limits could not be measured on particles smaller than 75 µm, which indicates that the mine tailings are non plastic.

2.3 *Synthetic AMD*

A synthetic AMD solution was prepared in the laboratory. Its composition and pH is representative of a typical field AMD (see Table 2 below). Dissolved concentrations of nickel and copper (the two most abundant heavy metals in the tailings) were 2 and 1.3 mg/L, respectively, in the synthetic AMD.

Table 2. Composition of synthetic AMD solution

Element/Parameter	Concentration (mg/L)[1]	Element/Parameter	Concentration (mg/L)[1]
pH	2.8		
Aluminum	10	Sodium	30
Arsenic	0.01	Magnesium	23
Barium	0.04	Nickel	2
Calcium	170	Sulfur	300
Chromium	0.005	Silica	0.7
Copper	1.3	Strontium	0.1
Iron	40	Lead	0.04
Potassium	14.5	Zinc	2.5

Note: [1] except pH, shown values were highest concentrations encountered

2.4 *Kinetic Column Tests*

Laboratory kinetic column tests were carried out to study the effects of AMD flow on the hydraulic conductivity and effluent composition of various mixtures of RMT amended with CBFA. The columns were constructed of either 50 mm or 75 mm inside diameter clear acrylic tubing. Inert materials (nylon, vinyl, PVC, and stainless steel) were used as tubing, fasteners, collection containers, etc. The mixtures used as column packs were thoroughly mixed in a bowl to ensure homogeneity. The mixture was prepared at ~2% wet of optimum using distilled water and placed in the column in three equal layers. A moisture content of 2% wet of optimum achieves minimal hydraulic conductivity while nearly maximizing the density. Each layer was rodded 25 times with a 10 mm diameter plastic rod. After rodding, the sides of the column were tapped to remove air bubbles. Next, the top surface of the pack was trimmed and covered with a porous fabric and an acrylic porous plate. Upon final assembly, the pack was confined by applying a confining load to the top plate to prevent uplift under hydrostatic loading.

Under neutral condition the columns were continuously permeated with distilled water. For acidic conditions the columns were first permeated with distilled water, to establish the reference hydraulic conductivity, and subsequently switched to synthetic AMD. Equilibrium was achieved within 10 continuous pore volumes (PV) of distilled water flowing through the columns. Column tests where ran for at least 70 PV using either distilled water or AMD as the permeation fluid.

The concept of continuous pore volumes (PV) which is the total volume of leachate flowing through the sample divided by the initial pore volume of the sample, allows comparing results from test columns having different initial pore volumes. During the tests, effluent samples were collected, weighed, time recorded, and the hydraulic head measured. The hydraulic gradient was adjusted throughout the tests to allow for the collection of an acceptable volume of effluent (30 ml or more) in a reasonable time period (1 to 2 days). All effluent samples were analysed for pH. Select effluent samples were acidified to pH < 3 with nitric acid and analysed for elemental composition by inductively coupled plasma – atomic emission spectrometry (ICP-AES). Effluent metal concentrations were compared to Environment Canada Metal Mining Effluent Regulations (EC-MMER, 2003).

3 RESULTS AND DISCUSSION

3.1 *Hydraulic Conductivity*

Hydraulic conductivity results for the five mixed CBFA / RMT, 100% CBFA, and 100% RMT control packs are presented in Figure 1. Hydraulic conductivity ranged from 4.5x10-6 cm/s to 1.1x10-5 cm/s initially and from 3.0x10-6 cm/s to 1.3x10-5 cm/s at termination of the test (70 PV). The hydraulic conductivity was predominantly constant for all columns with the exception of a slight reduction in hydraulic conductivity observed in the CBFA control from the start of the test to 20 PV (4.5x10-6 cm/s to 3.0x10-6). This reduction was possibly due to pozzolanic and hydration activities of the CBFA (Pandian, 2004). The hard brittle consistency of the CBFA pack observed during removal from the column at termination of the test supports this assumption.

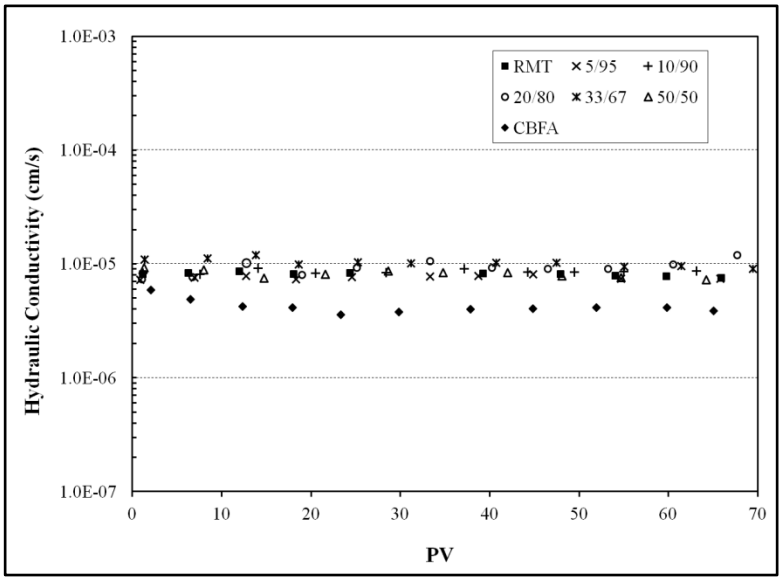


Figure 1. Hydraulic conductivity versus PV (permeated with distilled water)

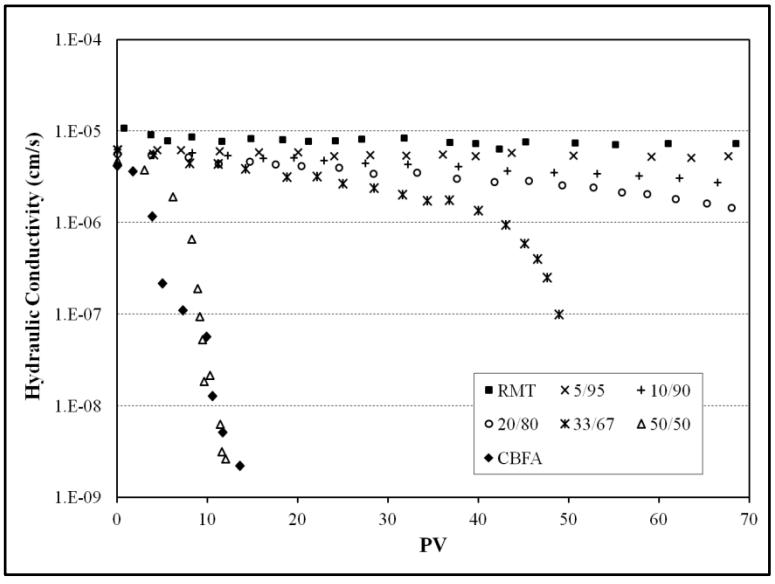


Figure 2. Hydraulic conductivity versus PV (permeated with AMD)

Hydraulic conductivity results for the five CBFA / RMT mixtures and the RMT and CBFA columns when permeated with AMD are presented in Figure 2. Hydraulic conductivity ranged from $4.2x10^{-6}$ cm/s to $1.1x10^{-5}$ cm/s for columns permeated with distilled water. Upon permeating with AMD, the hydraulic conductivity of all columns decreased.

The number of progressive pore volumes of AMD required for achieving a given reduction in hydraulic conductivity was inversely proportional to the fly ash content of the column pack. The hydraulic conductivity of the mine tailings control column only decreased slightly when permeated with AMD. By contrast, the hydraulic conductivity of the 50/50 CBFA/tailings mixture and 100% CBFA column decreased by nearly 2000 times to $2.6x10^{-9}$ cm/s and $2.2x10^{-9}$ cm/s, respectively, in less than 15 PV of AMD permeation.

3.2 *Effluent pH*

Effluent pH results for the five mixed CBFA / RMT along with the 100% CBFA and 100% RMT control packs when permeated with distilled water and AMD are presented in Figures 3 and 4, respectively.

As shown in Figure 3 an increased in pH was observed with an increase in CBFA content when permeated with distilled water. The effluent of all the CBFA and RMT mixtures and the 100% CBFA columns remained alkaline (8.5 > pH > 11.9) throughout the tests, while the pH of the mine tailings control was predominantly neutral (6.5 > pH > 7.5). The optimum pH buffering was observed with the addition of as low as 20% CBFA (i.e. similar pH values for 20% to 100% CBFA). A study by Shang et al. (2006) found that the alkaline leachate from coal fly ash was effective in buffering the pH of the underlying acidic mine tailings pore water.

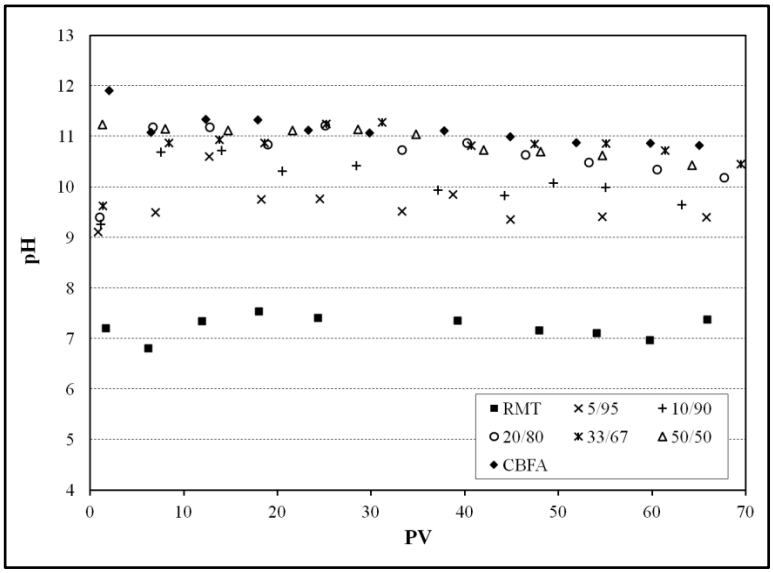


Figure 3. Effluent pH versus PV (permeated with distilled water)

The 5%, 10%, 20%, and 33% CBFA packs permeated with distilled water had a lower initial pH (8.5 > pH > 9.6) before reaching a maximum pH (10.7 > pH > 11.2). This lower initial pH was likely due to the reaction of the lower percentages of CBFA with the mine tailings during mixing. An odour and discolouration (yellow tint) was observed in the leachate collected during the initial 5 PV of permeation. The odour and discolouration corresponded with elevated sulphur and potassium concentrations in the leachate and the recorded low dissolved oxygen values in the leachate. The 50% CBFA amended mine tailings pack behaved similarly to the 100% CBFA pack, with an initial maximum pH (pH 11.2 and 11.9, respectively) which decreased linearly with continued permeation (pH > 10.3 at termination of the test). The RMT control fluctuated between pH 6.5 and pH 7.5 throughout the test which was similar to the pH of the distilled water used as permeation. The similarity between the pH of the mine tailings effluent and the distilled

water permeate is likely due to the non-oxidizing conditions within the column test (i.e. continuously submerged in water) and low concentrations of soluble minerals in the RMT at neutral pH.

Effluent pH results for all columns when permeated with AMD are shown in Figure 4. The effluent of the column containing 100% RMT remained slightly alkaline or neutral (7.8 > pH > 6.8) during the first 25 PV of AMD permeation. Afterwards, the effluent pH dropped and stabilized in a lower range (6.2 > pH > 5.8) until approximately 65 PV. This pH trend is consistent with the buffering effects of calcite dissolution (7.5 > pH > 6.5) followed by siderite dissolution (6.3 > pH > 4.8) (Bowles et al. 2003). This is further supported by the calcium and iron concentrations shown in Figure 5 of the 100% RMT leachate when permeated with AMD. Further permeation by AMD caused the effluent pH to decrease even more as neutralizing minerals became depleted in the column.

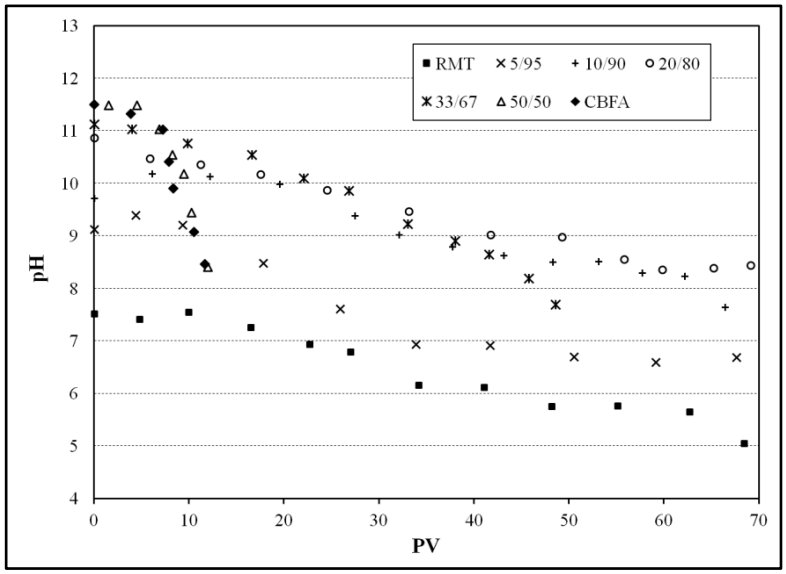


Figure 4. Effluent pH versus PV (permeated with AMD)

The effluent pH of all columns containing CBFA remained alkaline throughout the tests. A slight increase in effluent pH was observed during the initial distilled water permeation and up to 5 PV of AMD permeation for columns which contained 5%, 10%, and 20% CBFA by mass. This was followed by an approximately linear decrease in effluent pH during the next 25 to 30 PV. Afterwards, the effluent pH kept decreasing at a reduced and less regular rate.

By contrast, the effluent pH of the columns containing 33% and 50% CBFA and the CBFA control column were highest (pH>11) at the beginning of the test. The trends in effluent pH for both columns followed that of their hydraulic conductivities (compare Figures 2 and 4). The effluent pH decreased linearly during the first 40 PV of AMD permeation for the 33% CBFA column and 5 PV for the 50% CBFA and the CBFA control columns, and at an accelerated rate thereafter. The low pH values measured near the end of the tests (down to pH ~ 8) are likely an artifact of the sample collection method and do not reflect the true effluent pH. As the hydraulic conductivity decreased, the time interval required to collect a sufficient volume of leachate sample for analysis increased to several days. Since the effluent samples were exposed to the atmosphere, reaction of hydroxide ions with atmospheric CO_2 caused a sharp decrease in pH and the precipitation of calcium carbonate in the collection cylinder, which appeared as a white coating on the cylinder walls.

Metal mining effluent regulations for pH set the pH between 6 and 9 for EC-MMER (2003). The effluent of all CBFA amended tests were higher than the minimum regulatory pH of 6, however the maximum regulatory pH limit of 9 was exceeded initially by all CBFA amended columns.

3.3 *Effluent Composition*

The range of dissolved concentrations of major elements in the columns effluent are shown in Tables 3 and 4 for distilled water and AMD permeation respectively. Where applicable, these elements are compared to the EC-MMER (2003) mine effluent regulations (shown in Tables 3 and 4). Many of the elevated concentrations were observed at the beginning of the tests and are likely due to chemical reactions between the CBFA and mine tailings during mixing.

Table 3. Effluent analyses for CBFA / RMT mixed kinetic column tests permeated with distilled water.

Element	EC-MMER Guideline	100% RMT	10% CBFA 90% RMT	20% CBFA 80% RMT	50% CBFA 50% RMT	100% CBFA
Aluminum	na	0.02 – 0.11	2.50 – 14.75	9.12 – 18.88	13.25 – 33.87	12.56 – 361.10
Arsenic	0.5	nd – 0.132	nd – 0.020	nd – 0.014	0.009 – 0.023	nd – 0.023
Calcium	na	10.2 – 547.7	20.2 – 486.9	38.3 – 118.3	38.6 – 144.3	14.9 – 149.8
Chromium	na	nd – 0.002	nd	nd – 0.001	0.001 – 0.002	0.011 – 0.420
Copper	0.3	nd – 0.008	nd	nd – 0.007	nd – 0.011	nd – 0.007
Iron	na	0.011 – 0.552	0.003 – 0.026	0.004 – 0.065	0.004 – 0.604	0.001 – 0.253
Potassium	na	3.5 – 121.0	3.9 – 160.3	3.7 – 136.7	3.2 – 53.9	0.4 – 26.7
Magnesium	na	0.303 – 89.600	0.013 – 0.208	0.012 – 0.061	0.002 – 0.431	0.001 – 0.198
Sodium	na	2.5 – 145.4	9.0 – 769.3	8.9 – 1349.0	10.2 – 938.2	10.1 – 292.4
Nickel	0.5	0.001 – 0.559	nd – 0.103	nd – 0.093	0.001 – 0.039	nd – 0.016
Sulphur	na	4.7 – 943.9	9.5 – 1533.0	10.8 – 2512.0	11.3 – 834.7	1.1 – 508.1
Silica	na	2.19 – 2.84	2.26 – 4.36	1.96 – 4.35	0.85 – 5.28	0.11 – 6.53
Lead	0.2	nd – 0.028	nd	nd	nd – 0.014	nd – 0.010
Zinc	0.2	0.003 – 0.058	0.003 – 0.164	0.001 – 0.203	0.003 – 0.033	0.009 – 0.065
pH	na	6.5 – 8.5	9.2 – 10.7	9.4 – 11.2	10.1 – 11.2	10.6 – 11.9

Notes: Concentration in mg/L unless otherwise specified
na - no guideline provided.
nd - readings were below the minimum detection concentration of the icp standard.
Results for 5%CBFA/95%RMT and 33%CBFA/67%RMT are not presented.

Overall the effluent of the CBFA amended RMT when permeated with distilled water met the mine effluent guidelines for heavy metals. In contrast, the RMT control experienced higher concentrations of nickel that exceeded the 0.5 mg/L EC-MMER (2003) regulation. Concentrations exceeding regulations occurred in the initial 4 PV of permeation.

When permeated with AMD, the column containing only RMT did not meet the metal mining effluent regulations for pH and nickel. By contrast, columns amended with CBFA met all the applicable effluent guidelines with the exception of elevated pH during the initial PVs of AMD permeation (see 3.2 above). The reductions in heavy metal concentrations were not correlated with the percent CBFA in the columns: all columns containing CBFA performed equally well overall. Elevated concentrations of potassium and sodium are likely due to dissolution of K-jarosite and Na-jarosite minerals at a high pH.

Figure 5 below shows the evolution of calcium, sulphur, and iron concentrations in the effluent of the RMT column. The graph shows the relative concentration as a ratio (C/Co) of effluent concentration (C) to the AMD concentration (Co). A ratio below or above unity indicates an accumulation or depletion, respectively, of the element in the column. Calcium and sulphur concentrations were higher (C/Co > 1) than the synthetic AMD concentrations throughout the test for calcium and for the first 20 PV for sulphur. This indicates the probable dissolution of gypsum, calcium carbonate, and calcite in the RMT. The iron concentration in the effluent was much lower than in the synthetic AMD (Fe = 40 mg/L) for the first 30 PV, which indicates that iron was precipitating in the control column (C/Co <1). Afterwards, the iron concentration increased to more than 100 mg/L, coinciding with a drop in effluent pH below 6.2 and the dissolution of iron precipitates and siderite.

Table 4- Effluent analyses for CBFA / RMT mixed kinetic column tests permeated with AMD

Element	EC-MMER Guideline	100% RMT	10% CBFA 90% RMT	20% CBFA 80% RMT	50% CBFA 50% RMT	100% CBFA
Aluminum	na	0.024 - 0.215	1.35 - 10.19	1.77 - 11.56	11.36 - 34.61	5.7 - 46.54
Arsenic	0.5	0.002 - 0.023	0.002 - 0.024	0.005 - 0.021	0.004 - 0.015	0.004 - 0.024
Calcium	na	175.8 - 565.5	262.3 - 320.5	81.3 - 301.8	7.8 - 159.0	38.1 - 232.0
Chromium	na	< 0.0019	<0.0015	<0.0010	<0.0018	0.045 - 0.164
Copper	0.3	0.0006 - 0.046	0.0003- 0.002	0.0004 - 0.001	0.0006 - 0.0042	0.0007 - 0.005
Iron	na	0.1 - 105.2	0.011 - 0.274	0.005 - 0.110	0.012 - 0.267	0.007 - 0.117
Potassium	na	26.2 - 37.0	20.1 - 22.5	14.6 - 23.2	15.2 - 31.6	5.51 - 9.41
Magnesium	na	13.16 - 32.38	0.079 - 1.960	0.020 - 0.613	0.003 - 0.151	0.01 - 0.08
Sodium	na	6.8 - 34.3	59.3 - 63.5	72.6 - 84.3	47.4 - 209.3	41.9 - 109.7
Nickel	0.5	0.022 - 1.207	0.001 - 0.014	0.003 - 0.009	0.001 - 0.009	0.0002 - 0.003
Sulphur	na	274.6 - 662.9	256.0 - 298.7	187.9 - 311.5	26.2 - 121.5	5.1 - 78.8
Silica	na	2.11 - 7.79	2.73 - 4.81	2.61 - 16.35	0.88 - 7.23	2.49 - 13.92
Lead	0.2	nd	nd	nd	nd	nd
Zinc	0.5	0.023 - 0.070	0.004 - 0.030	0.004 - 0.033	0.018 - 0.034	0.010 - 0.039
pH	6.0 – 9.5	5.1 - 7.7	7.6 - 10.9	8.2 - 11.0	8.4 - 12.0	8.0 - 11.0

Notes: Concentration in mg/L unless otherwise specified
nd - readings were below the minimum detection concentration of the icp standard.
Results for 95%RMT/5%CBFA and 67%RMT/33%CBFA are not presented.

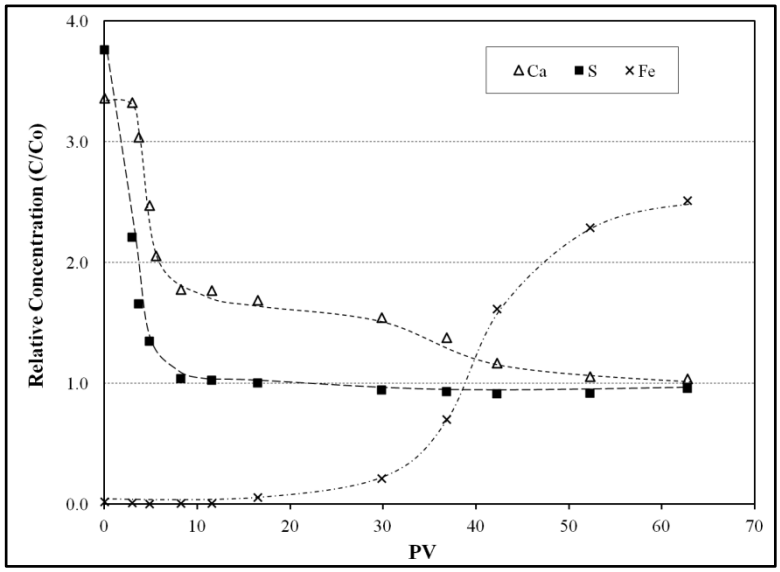


Figure 5. Relative concentrations of calcium, sulphur and iron in the effluent of the RMT column versus PV of AMD permeation

The evolution of calcium, sulphur, and iron concentrations in the effluent of the column containing 33% CBFA (by mass) is shown in Figure 6. Columns amended with different percentages of CBFA demonstrated similar trends. By contrast with the RMT, the calcium and sulphur concentrations were lower than in the synthetic AMD until 13 nPV of AMD permeation for calcium and through the test for sulphur. This net accumulation of calcium and sulphur (as sulphate) in the column was likely caused by the precipitation of gypsum, which then contributed to the large drop in hydraulic conductivity. The concentration of iron in the effluent remained well be-

low that in the synthetic AMD throughout the test, which indicated that iron also precipi tated in the column.

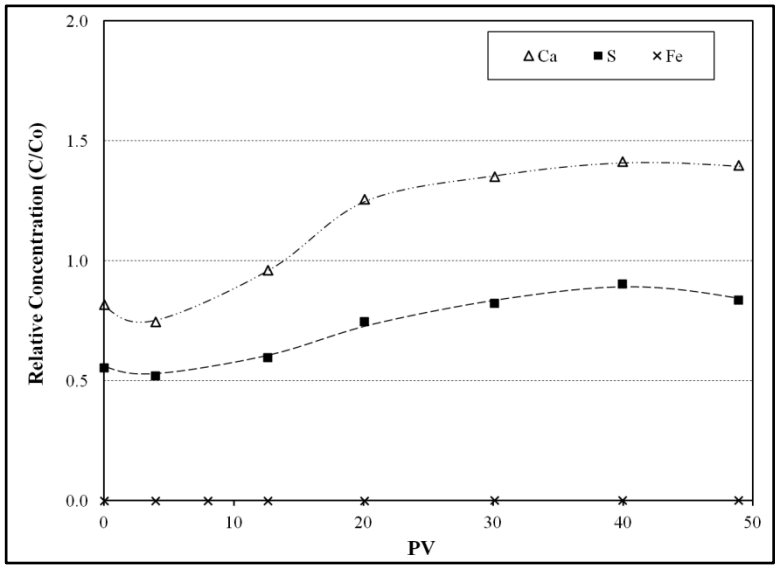


Figure 6. Relative concentrations of calcium, sulphur and iron in the effluent of the 33% CBFA / 67% RMT column versus PV of AMD permeation

Dissolved aluminum concentrations were lower than 1 mg/L in the RMT control column effluent but reached elevated levels (>10 mg/L or C/Co>1) in the effluent of all columns containing fly ash (See Figure 7). These concentrations decreased below unity (C/Co=1) as more AMD flowed through the columns. The elevated aluminum concentrations are attributed to the dissolution of Al-containing phases in the fly ash and high pH levels in the leachate. Aluminum concentrations in the effluent of a column containing 100% fly ash permeated with pure water ranged from 10 to 50 mg/L for more than 40 PV (not shown).

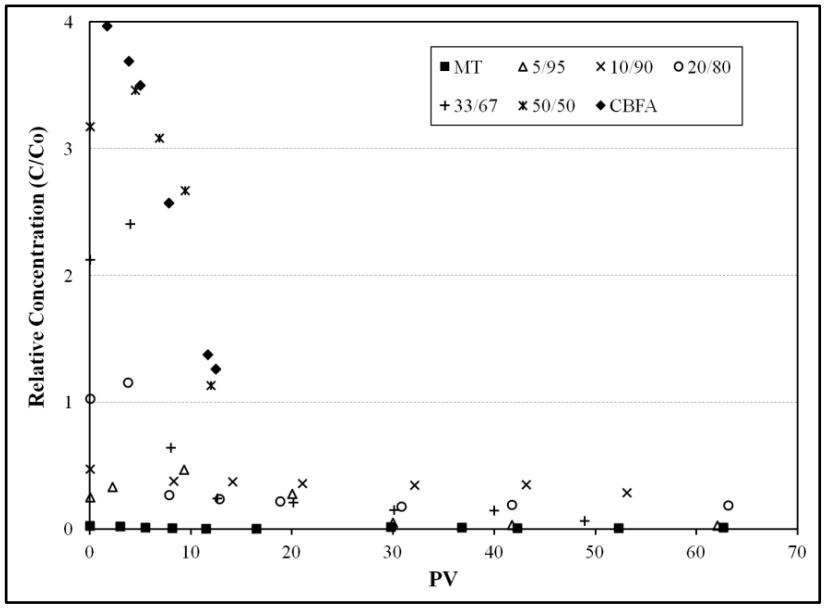


Figure 7. Relative concentrations of aluminum versus PV of AMD permeation

4 CONCLUSION

Kinetic column tests showed that amending RMT with CBFA was effective in reducing the concentrations of heavy metals and increasing leachate pH when compared to the RMT alone. The amended mixtures were effective in treating AMD even at low percentages. This is advantageous given the volume of RMT produced compared to CBFA. The reduction in hydraulic conductivity when permeated with AMD has the added benefit of reducing the flow of water through the tailings disposal area, thereby reducing the potential for the formation of AMD and dissolution of heavy metals. While the concentrations of heavy metals regulated by EC-MMER are below the regulatory guidelines, other elements such as iron and aluminum should be considered due to their effects on the environment at elevated concentrations.

5 REFERENCES

American Society for Testing and Materials (ASTM) D422 – 63, 2007. Standard Test Method for Particle-Size Analysis of Soils. ASTM International, West Conshohocken, PA.

American Society for Testing and Materials (ASTM) D854 – 06, 2006. Standard Test Methods for Specific Gravity of Soil Solids by Water Pycnometer. ASTM International, West Conshohocken, PA.

American Society for Testing and Materials (ASTM) D4318 – 05, 2005. Standard Test Methods for Liquid Limit, Plastic Limit, and Plasticity Index of Soils. ASTM International, West Conshohocken, PA.

Blowes, D., Ptacek, C., and Jurjovec, J., 2003b, Chapter 5 – Mill tailings: hydrogeology and geochemistry, *Environmental Aspects of Mine Wastes, Vol 31*: Mineralogical Association of Canada, Vancouver, BC.

British Columbia Ministry of Energy Mines and Petroleum Resources (BC-MEMPR) 1989. Draft acid rock drainage technical guide. *British Columbia Acid Mine Drainage Task Force,* Victoria, BC.

Environment Canada Metal Mining Effluent Regulations (EC-MMER) 2003. Environment Canada Status report on water pollution prevention and control under the metal mining effluent regulations. Ottawa. http://www.ec.gc.ca/nopp/docs/rpt/waterpollution/mining2003 /en/c2.cfm (accessed February 2009).

Pandian, N. 2004. Fly ash characterization with reference to geotechnical applications, *Journal Indian Institute Science* 84: 189-216.

Penney, K., Mohamedelhassan, E., and Catalan, L. 2009a. Utilization of coal/biomass fly ash in reactive barriers for treating acid mine drainage. *In* Proceedings of the IASTED International Conference on Environmental Management and Engineering (EME 2009), Banff, Canada, July 2009, pp. 67-73.

Penney, K., Mohamedelhassan, E., and Catalan, L. 2009b. Utilization of coal/biomass fly ash and bentonite as a low permeable barrier for the containment of acid mine drainage. *In* Proceedings of the 62nd Canadian Geotechnical Conference & 10th Joint CGS/IAH-CNC Groundwater Conference, Halifax, Canada, September 2009, pp. 867-874.

Perez-Lopez, R., Nieto, J. and & Ruiz de Almodovar, G. 2007. Utilization of fly ash to improve the quality of the acid mine drainage generated by oxidation of a sulphide-rich mining waste. *Chemiosphere,* 67: 1637-1646.

Shang, J., Wang, H., Kovac, V. and Fyfe, J. 2006. Site specific study on stabilization of acid-generating mine tailings using coal fly ash. *Journal of Materials in Civil Engineering*, March/April: 140-151.

Xenidis, A., Mylona, E. and Paspaliaris, I. 2002. Potential use of lignite fly ash for the control of acid generation from sulphidic wastes. *Waste Management,* 22: 631-641.

Yeheyis, M., Shang, J. and Yanful, E. 2007. Beneficial utilization of coal fly ash as acid mine drainage barrier. *In* Proceedings of the 60th Canadian Geotechnical Conference & 8th Joint CGS/IAH-CNC Groundwater Conference, Ottawa, Canada, October 2007: pp 1494-1499.

Mobilization of arsenic under reducing conditions: a case study from the Delnite mine tailings site

D. Paktunc, Y. Thibault & B. Tisch
Canmet MINING, Natural Resources Canada, Ottawa, ON, Canada

ABSTRACT: In order to assess the integrity of the tailings at the Delnite mine site with respect to the stability of arsenic and evaluate options for developing closure plans and long-term management of the tailings, field studies involving a biosolids-cover test plot and laboratory column-leaching experiments were undertaken. Arsenic is predominantly hosted by goethite in the oxidized portion of the tailings, and by arsenopyrite and pyrite in the unoxidized lower portions. The oxidized tailings are dominated by As^{5+} species tied to goethite whereas the As^{1-} species within arsenopyrite and pyrite are dominant in the unoxidized tailings. The tailings samples below the biosolids-cover have As^{3+} which increases in proportion towards the cover. This observation is independently confirmed by the column leaching experiments in that biosolids-cover caused the transformation of As^{5+} species to As^{3+} in the oxidized tailings. TCLP tests from the oxidized portions of the uncovered tailings indicate that As is effectively stabilized by goethite. In contrast, the tailings immediately below the biosolids cover have significantly elevated As in the TCLP extracts suggesting that the As^{3+} species formed under reducing conditions are highly mobile.

1 INTRODUCTION

The Delnite mine is a former gold mine owned by Goldcorp Inc., near Timmins, Ontario, operated for 27 years before its closure in 1971. There are about three million cubic meters of tailings impounded in an area of about 27 ha with an elevation of 3 to 10 m above the surrounding terrain (Blowes 1990; Jambor et al. 1991). As part of the Green Mines Green Energy initiative at CanmetMINING, field test plots utilizing a papermill biosolids cover were established in 2008 with the purpose to test the ability of the biosolids in supporting crops which can be used as feedstock for biofuel production as a closure option (Tisch et al. 2012). In order to assess the impact of reducing conditions imposed by the biosolids cover on the geochemical stability of the tailings, the tailings were sampled in 2010 and 2011. The samples were characterized to determine the mineralogical and geochemical conditions across the oxidation front to depths of about 6 meters and assess the effects of the oxidation and reducing conditions on the stability of the arsenic carriers in the tailings. In addition, the mine tailings were subjected to a column-leaching experiment to simulate the reducing conditions for a period of 5 years. The residual tailings from the column leaching experiments were characterized to determine the speciation of arsenic.

2 METHODOLOGY

The Delnite mine tailings were sampled along six holes to a depth of 4 to 6 meters depths. Two of the holes were drilled at the biosolids-covered test plots. Cores of 76 cm in length were taken by a Pionjar-type portable drill using a split-spoon core barrel. The samples were split in two-halves along the core, divided into 38 cm sections and packed in ice in a cooler prior to shipping to the laboratory in Ottawa.

The samples were air-dried, homogenized and split into four fractions through a set of riffles. One fraction of each sample was pulverized for chemical and X-ray diffraction analyses. Another fraction, as received, was set in epoxy for polished section preparation and Teflon sample holders for synchrotron X-ray absorption spectroscopy characterization. Another unprocessed fraction of each sample was used in leaching tests.

The samples were analyzed by ICP-AES, LECO and ion chromatography techniques for Si, Al, Fe, Mn, Mg, Ca, Na, K, As, P, S, SO_4 and CO_2 concentrations. The X-ray diffraction patterns were collected using a RIGAKU D/MAX 2500 rotating-anode powder diffractometer with monochromatic CuKα radiation at 50 kV, 260 mA, a step-scan 0.02°, and a scan rate at 1° per minute in 2θ from 5 to 70°. The polished sections were studied by optical microscopy, scanning electron microscopy (SEM) and electron microprobe (EPMA) techniques. For the leaching tests, a modified version of the USEPA's Toxicity Characteristics Leaching Procedure (TCLP) (USEPA 1992) was employed. In this test, 10 g of sample was contacted by 200 mL of distilled water for 20 hours. The solutions were filtered through 0.45 μm filters and the leachates were analyzed for As, Fe and Ca. The pH of the solution was not buffered due to the carbonate-rich nature of the tailings.

Column-leaching experiments involved 3 treatments run in duplicate, each containing 25 cm of oxidized tailings underlain by 60 cm of unoxidized tailings. Columns were constructed of clear lexan tubing (25.4 cm ID) with a drainage fitting at the base and a 1L graduated cylinder mounted to the side of the columns. The design allowed sample collection and maintaining water levels within the columns. Approximately 250 ml of distilled water was added to the top of the columns on a weekly basis. For the first 12 months, the columns were sampled from the bottom of the columns on a monthly basis, with the sampling frequency dropping to quarterly thereafter.

3 RESULTS AND DISCUSSION

3.1 *Mineralogical and geochemical observations on field samples*

Bulk chemical compositions of the samples are given in Table 1. The tailings samples are rich in Si, Al, Fe, Mg, Ca and CO_2 concentrations. Total Fe concentrations, expressed as FeO, range from 6.6 to 10.5 wt%. Sulphide S concentrations are variable between 0.51 and 2.44 wt%. Sulfate concentrations are generally low varying from 0.01 to 0.43 wt% (average 0.15 wt%) with an outlier value of 1.36 wt% near the top portion of one of the borehole samples. Arsenic concentrations of the tailings vary from 789 to 4030 ppm.

Mineralogical composition of the tailings samples from the Delnite site are relatively uniform with quartz, dolomite, chlorite, plagioclase, tourmaline, mica, magnesite and pyrite. Siderite is present in trace to minor quantities. Talc is present in trace to minor quantities in some of the samples. Variations in the quantities of the major minerals with depth are also limited.

The tailings samples from the uncovered portion of the impoundment down to about 1 m depth contain pyrite, pyrrhotite and arsenopyrite particles with oxidation features including secondary Fe(III)-oxyhydroxide rims. Although the As contents of pyrite and pyrrhotite are low (i.e. <1 wt%), the Fe(III)-oxyhydroxide rims typically contain significant concentrations of arsenic ranging from 1.1 to 6.0 wt% As_2O_5. The rims also contain variable levels of Ca, S and Si. Below the oxidation front at 1.5-2.0 m depth, the sulphide mineral particles have pristine surfaces.

The tailings below the biosolids cover are broadly similar in terms of their mineralogical

compositions to their counterparts from the uncovered tailings. One difference is that the sulphide particles in the tailings below the cover do not have secondary Fe(III)-oxyhydroxide rims. Only a few sulphide particles with secondary rims were noted in the deeper portions of the oxidized tailings with As, Ca, S, and Si concentrations comparable to those of the uncovered tailings. Below the oxidation front, the sulphide particles do not have secondary oxidation rims.

3.2 *Speciation of Arsenic by X-ray Absorption Near Edge Spectroscopy (XANES)*

The topmost samples from the uncovered tailings area are dominated by the absorption edge at ~11873 eV which is indicative of the As^{5+} species. Underlying samples representing unoxidized tailings at about 1 m depth and lower display a second absorption edge at about 11867 eV indicating the presence of As^{1-} species that are typical of arsenopyrite or arsenian pyrite (Paktunc 2008). These findings confirm the mineralogical observations in that As is essentially tied to the secondary oxidation products (i.e. goethite) in the oxidized tailings and that pyrite and arsenopyrite are the dominant carriers in the unoxidized tailings. Least-squares fitting of the XANES spectra indicate that more than 82% As is tied to sulphide minerals in the unoxidized portions of the uncovered Delnite tailings. Sulphide minerals form between 2 and 64% of the total As in the oxidized portions of the tailings. There is no evidence for the presence of As^{3+} species in the exposed tailings samples.

The tailings samples immediately below the biosolids-cover have a third As species at about 11869.5 eV indicating the presence of As^{3+} in addition to As^{5+} and As^{1-} (Figure 1). Trivalent As represented by tooeleite ($Fe_6(AsO_3)_4SO_4(OH)_4 \bullet 4H_2O$) in the least squares fitting forms about 10 % and 46 % of total As. The reason for the lower amount of As^{3+} in one of the borehole samples is probably due to mixing with the underlying tailings along the rather wide sampling interval (i.e. 0.3 m). The tailings samples from the unoxidized portions are dominated by As^{1-} species as in sulphide minerals forming between about 70 to 93% and 58 to 91% of the total As along the two boreholes.

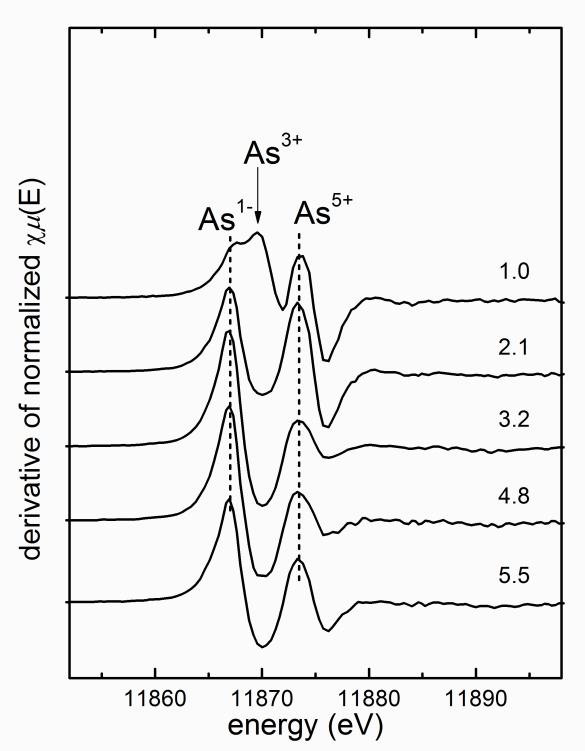


Figure 1. Derivative of normalized As K-edge XANES spectra of the biosolids-covered tailings as observed along one borehole; Numbers next to spectra are sample depths in meters; spectra shifted in absorbance values for display purposes, vertical scale remains uniform for all the samples.

Preliminary results from the residue of the column-leaching experiments indicate gradual increases in the proportion of As^{3+} species towards the biosolids cover. It appears that reduction occurred near the biosolids-tailings interface progressively impacting down to 30 cm depth for the column with 1 m biosolids cover (Figure 2).

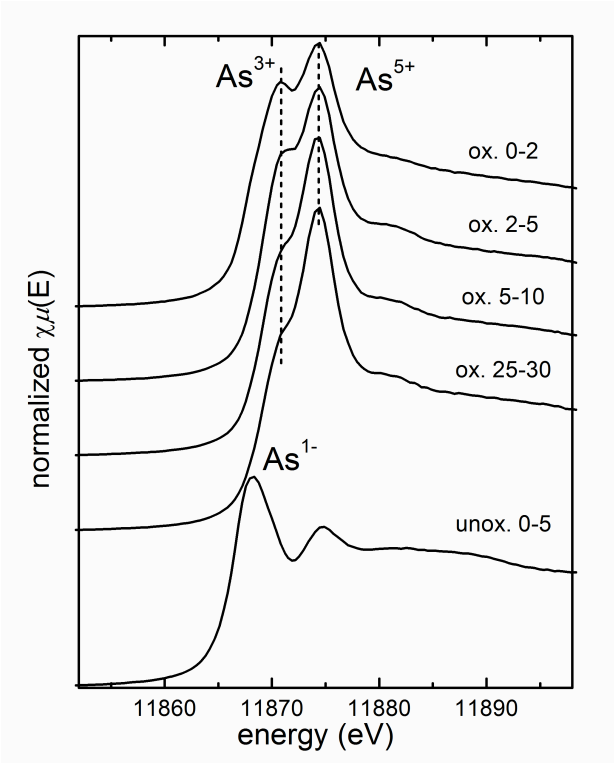


Figure 2. Normalized As K-edge XANES spectra of tailings residue from column-leaching experiment with 1 m biosolids cover. ox.: oxidized tailings; unox.: unoxidized tailings; Numbers next to spectra are sample depths in cm; spectra shifted in absorbance values for display purposes, vertical scale remains uniform for all the samples.

3.3 *TCLP tests on field samples*

Arsenic concentrations in the TCLP extracts from the oxidized portions of the uncovered tailings are low ranging from 0.5 to 5.7 µg/L. These are comparable to the pore water As concentrations of less than 50 µg/L for the oxidized tailings (Blowes 1990). In contrast, the underlying unoxidized tailings have higher As concentrations in the TCLP extracts with values reaching to 630 µg/L.

The samples immediately below the biosolids-cover have elevated As in the TCLP extracts (i.e. 3090 and 4067 µg/L) in accordance with the earlier results based on shallow cores from the Delnite site (Paktunc 2013). The deeper samples have As concentrations in the TCLP extracts that are similar to those of the uncovered tailings.

4 SUMMARY AND CONCLUSIONS

In the oxidized tailings which is about 1.5 m thick, As is predominantly hosted by Fe(III)-oxyhydroxides and to lesser extent by relict arsenopyrite and pyrite. All the sulphide particles show clear signs of oxidative dissolution. Electron microprobe analyses indicate that goethite has 0.7 to 3.9 wt% As. In the unoxidized tailings, the dominant As carriers are arsenopyrite and pyrite. Pyrite has up to about 1 wt% As.

XANES results indicate that the oxidized tailings are dominated by the As^{5+} species whereas the unoxidized tailings by the As^{1-} species. These findings confirm the mineralogical observa-

tions in that As is essentially tied to Fe(III)-oxyhydroxides in the oxidized tailings and to arsenopyrite and arsenian pyrite in the unoxidized tailings. There is no evidence for the presence of As^{3+} species in the exposed tailings samples. The tailings samples immediately below the biosolids-cover have As^{3+} in addition to As^{5+} and As^{1-} indicating the influence of the biosolids on reducing the As species and confirming the earlier findings by Paktunc (2013).

Arsenic concentrations in the TCLP extracts from the oxidized portions of the uncovered tailings are low whereas the unoxidized tailings have higher As concentrations with values reaching to 630 µg/L. The samples immediately below the biosolids cover have significantly elevated As in the TCLP extracts (i.e. 3090 and 4067 µg/L) in accordance with the earlier results based on shallow cores from the Delnite site (Paktunc 2013). These results indicate that biosolids cover caused the mobilization of As as the As^{3+} species. Higher As leaching from the unoxidized tailings appears to be controlled by the stability of the sulphide hosts. It appears that As is effectively stabilized by goethite in the oxidized tailings and sulphide hosts, arsenopyrite and pyrite in the unoxidized tailings.

5 ACKNOWLEDGEMENTS

The contributions of the following are acknowledged: Sarah Barabash and Mike Venhuis of Ecometrix during collecting the core samples, Ted MacKinnon for sample preparation, Judith Price for polished section preparation, Derek Smith for X-ray powder diffraction analyses, Erika Revesz for the synthesis of tooeleite and Analytical Services Group of CANMET for bulk chemical analyses and extraction tests.

6 REFERENCES

Blowes, D.W. 1990. The geochemistry, hydrogeology and mineralogy of decommissioned sulphide tailings. A comparative study. Ph.D. thesis, University of Waterloo.

Jambor, J.L., Blowes, D.W. & Owens, D.R. 1991. Mineralogy of tailings from Delnite Mines, a former gold producer near Timmins. CANMET, Mineral Sciences Laboratories Division Report MSL 91-26 (IR), 58p.

Paktunc, D. 2013. Mobilization of arsenic from mine tailings through reductive dissolution of goethite influenced by organic cover. Applied Geochemistry (in press).

Paktunc, D. 2008. Speciation of Arsenic in Pyrite by Micro-X-Ray Absorption Fine-Structure Spectroscopy (XAFS). *Proceedings of the Ninth International Congress for Applied Mineralogy*, Brisbane, QLD, AusIMM, 155-158.

Tisch, B., Hargreaves, J., Beckett, P., Lock, A., Spiers, G., Fyfe, J., Lanteigne, L. & Sulatycky, T. 2012. Post-mining agriculture for biofuels on mine tailings: An overview of results from the Green Mines Green Energy (GMGE) initiative. In W.A. Price, C. Hogan, G. Tremblay (eds), *Proceedings of the 9th International Conference on Acid Rock Drainage*. May 20-26, 2012, Ottawa, Ontario, Canada.

USEPA 1992. Toxicity characteristics leaching procedure. Method 1311. Revised 1992, 35pp.